

AD-758 126

AERODYNAMICS OF ROTARY WINGS

**Advisory Group for Aerospace Research and
Development
Paris, France**

February 1973

DISTRIBUTED BY:

NTIS

**National Technical Information Service
U. S. DEPARTMENT OF COMMERCE
5285 Port Royal Road, Springfield Va. 22151**

1

AGARD-CP-111

AGARD-CP-111

AD 758126

AGARD

ADVISORY GROUP FOR AEROSPACE RESEARCH & DEVELOPMENT

7 RUE ANCELLE 92200 NEUILLY SUR SEINE FRANCE

AGARD CONFERENCE PROCEEDINGS No. III

on

Aerodynamics of Rotary Wings

Reproduced by
NATIONAL TECHNICAL
INFORMATION SERVICE
U S Department of Commerce
Springfield VA 22151



NORTH ATLANTIC TREATY ORGANIZATION



DISTRIBUTION AND AVAILABILITY
ON BACK COVER

This document has been approved
for public release and sale by the
Department of Defense.

NORTH ATLANTIC TREATY ORGANIZATION
ADVISORY GROUP FOR AEROSPACE RESEARCH AND DEVELOPMENT
(ORGANISATION DU TRAITE DE L'ATLANTIQUE NORD)

AGARD Conference Proceedings No.111
AERODYNAMICS OF ROTARY WINGS

**Papers and discussions from the Fluid Dynamics Panel Specialists' Meeting
held in Marseilles, France, 13-15 September 1972.**

THE MISSION OF AGARD

The mission of AGARD is to bring together the leading personalities of the NATO nations in the fields of science and technology relating to aerospace for the following purposes:

- Exchanging of scientific and technical information;
- Continuously stimulating advances in the aerospace sciences relevant to strengthening the common defence posture;
- Improving the co-operation among member nations in aerospace research and development;
- Providing scientific and technical advice and assistance to the North Atlantic Military Committee in the field of aerospace research and development;
- Rendering scientific and technical assistance, as requested, to other NATO bodies and to member nations in connection with research and development problems in the aerospace field;
- Providing assistance to member nations for the purpose of increasing their scientific and technical potential;
- Recommending effective ways for the member nations to use their research and development capabilities for the common benefit of the NATO community.

The highest authority within AGARD is the National Delegates Board consisting of officially appointed senior representatives from each member nation. The mission of AGARD is carried out through the Panels which are composed of experts appointed by the National Delegates, the Consultant and Exchange Program and the Aerospace Applications Studies Program. The results of AGARD work are reported to the member nations and the NATO Authorities through the AGARD series of publications of which this is one.

Participation in AGARD activities is by invitation only and is normally limited to citizens of the NATO nations.

The material in this publication has been reproduced directly from copy supplied by AGARD or the author.

Published February 1973

629.7.026.5:629.7.015.3



Printed by Technical Editing and Reproduction Ltd
Harford House, 7-9 Charlotte St, London. W1P 1HD

AGARD FLUID DYNAMICS PANEL OFFICERS

CHAIRMAN: Professor Dr L.G.Napolitano
University of Naples, Naples, Italy

DEPUTY CHAIRMAN: Professor Dr D.Küchemann
Royal Aircraft Establishment, Farnborough, Hants, UK

PROGRAMME COMMITTEE MEMBERS

Mr P.F.Yaggy (Chairman)
US Army Aeronautical Research Laboratory
Moffett Field, California 94035, USA

M. l'Ingénieur Général Pierre Carrière
avenue de la Division-Leclerc
Châtillon-sous-Bagneux, France

Professor Norman Ham
Massachusetts Institute of Technology
Cambridge, Massachusetts 02139, USA

Dr Jeffrey P.Jones
Westland Helicopters Ltd
Yeovil, Somerset, UK

Dr Ing. B.Laschka
Messerschmitt-Blkow-Blohm GmbH (U.F.)
Ottobrunn bei München, Germany

M. le Professeur Jacques Valensi
Université d'Aix-Marseille, 1, rue Honnorat
13 - Marseille, France

FOREWORD

The Meeting was held to provide a forum for presentation and discussion of research performed to obtain a more complete understanding of the fluid dynamics of rotary wings, and methods for calculation and analysis of the aerodynamics and dynamics of rotary wing systems. The objectives of the Meeting were to survey the status of the technology, including recent advances, and to indicate need for further research.

Twenty-five papers were presented at the Meeting, which consisted of six sessions, considering the themes of Rotors' Wakes, Rotors in Hover and at High Advance Ratio, Rotor Unsteady Airloads, Rotor Airfoils, Rotor Configurations, and Noise, followed by a round-table discussion reviewing all the material presented. Aspects discussed within the main themes included recent work on calculation of rotor wake characteristics and inflow distribution; factors affecting performance at hover and high advance ratio, and techniques for their improvement; description of analytical methods for calculating rotor unsteady aerodynamics; experimental results for unsteady airloads; current and future trends in rotor blade airfoil design and rationale for parametric trade-offs; experimental results of noise measurements on rotors in flight and methods of noise calculation; recent rotary wing applications.

By invitation of the French National Delegates to AGARD, the Specialists' Meeting, recorded in this document, was held at the Centre Nationale de la Recherche Scientifique, Marseilles, from 13 to 15 September 1972.

CONTENTS

	Page
AGARD FLUID DYNAMICS PANEL OFFICERS, PROGRAMME COMMITTEE AND FOREWORD	iii
	Reference
<u>SESSION I -- ROTOR WAKES</u>	
ROTOR WAKES -- KEY TO PERFORMANCE PREDICTION by M.C.Cheney and A.J.Landgrebe Prepared comment -- J.P.Jones	1
AN ACTUATOR DISC THEORY FOR ROTOR WAKE INDUCED VELOCITIES by R.A.Ormiston	2
THE STRUCTURE OF THE ROTOR BLADE TIP VORTEX by C.V.Cook	3
A VORTEX-WAKE ANALYSIS OF A SINGLE-BLADED HOVERING ROTOR AND A COMPARISON WITH EXPERIMENTAL DATA by R.B.Gray and G.W.Brown	4
<u>SESSION II -- ROTORS IN HOVER AND AT HIGH ADVANCE RATIO</u>	
ROTOR EN VOL STATIONNAIRE ET A GRAND PARAMETRE D'AVANCEMENT par J.Soulez-Lariviere Prepared comment -- R.Hirsch	5
COMPOTEMENT D'UN ROTOR AU-DELA DU DOMAINE DE VOL USUEL A LA GRANDE SOUFFLERIE DE MODANE par M.Lecarme	6
AERODYNAMIC FACTORS INFLUENCING OVERALL HOVER PERFORMANCE by E.A.Fradenburgh	7
THE ROTOR IN AXIAL FLOW by H.F.Zimmer	8
THE DEVELOPMENT OF AN EFFICIENT HOVERING PROPELLER/ROTOR PERFORMANCE PREDICTION METHOD by D.C.Gilmore and I.S.Gartshore	9
<u>SESSION III -- ROTOR UNSTEADY AIRLOADS</u>	
A SUMMARY OF CURRENT RESEARCH IN ROTOR UNSTEADY AERODYNAMICS WITH EMPHASIS ON WORK AT LANGLEY RESEARCH CENTER by J.F.Ward and W.H.Young, Jr Prepared comment -- W.Johnson	10
CALCUL ET MESURE DES FORCES AERODYNAMIQUES SUR UN PROFIL OSCILLANT, AVEC ET SANS DECROCHAGE par J. J.Philippe et M.Sagner	11
EFFORTS AERODYNAMIQUES SUR UN PROFIL D'AILE ANIME D'UN MOUVEMENT HARMONIQUE PARALLELE A L'ECOULEMENT DE TAMIS par J.Valensi, J.M.Rebont, J.Renaud et G.Vingut	12
A COMPRESSIBLE UNSTEADY AERODYNAMIC THEORY FOR HELICOPTER ROTORS by C.E.Hammond and G.A.Pierce	13

SESSION IV – ROTOR AIRFOILS

SOME ASPECTS OF THE DESIGN OF ROTOR AIRFOIL SHAPES by G.Reichert and S.N.Wagner Prepared comment – F.X.Wortmann	14
RECENT DEVELOPMENTS IN ROTOR BLADE STALL by W.J.McCroskey	15
THE DERIVATION AND VERIFICATION OF A NEW ROTOR PROFILE ON THE BASIS OF FLOW PHENOMENA; AEROFOIL RESEARCH AND FLIGHT TESTS by H.H.Pearcey, P.G.Wilby, M.J.Riley and P.Brotherhood	16
THE EFFECT OF PLANFORM SHAPE ON THE TRANSONIC FLOW PAST ROTOR TIPS by W.F.Ballhaus and F.X.Caradonna	17

SESSION V – ROTOR CONFIGURATIONS

A SUMMARY OF WIND TUNNEL RESEARCH ON TILT-ROTORS FROM HOVER TO CRUISE FLIGHT by Ph.Poisson-Quinton and W.L.Cook	18
RECENT DEVELOPMENTS IN CIRCULATION CONTROL ROTOR TECHNOLOGY by R.Williams	19
SOME OBJECTIVES IN APPLYING HINGELESS ROTORS TO HELICOPTERS AND V/STOL AIRCRAFT by H.Huber	20
AERODYNAMICS OF HELICOPTER COMPONENTS OTHER THAN ROTORS by A.Bosco	21

SESSION VI – NOISE

FUNDAMENTAL CONSIDERATIONS OF NOISE RADIATION BY ROTARY WINGS by M.V.Lowson	22
WAKE CHARACTERISTICS OF A TWO-DIMENSIONAL ASYMMETRIC AEROFOIL by I.Kavrak	23
MESURES DE BRUIT D'HELICOPTERES EN VOL par F.N.D'Ambra, J.-P.Dedieu et A.Julienne	24
THE NOISE CHARACTERISTICS OF A LARGE "CLEAN" ROTOR by J.W.Leverton	25

APPENDIX A – DISCUSSIONS**APPENDIX B – TRANSCRIPT OF THE TAPE OF THE ROUND TABLE DISCUSSION HELD AFTER THE PRESENTATION OF PAPERS****APPENDIX C – A SELECTION OF AGARD PUBLICATIONS IN RECENT YEARS**

ROTOR WAKES - KEY TO PERFORMANCE PREDICTION

Anton J. Landgrebe* and Marvin C. Cheney, Jr.**

United Aircraft Research Laboratories
East Hartford, Connecticut 06108, USA

SUMMARY

The history of helicopter performance prediction methods and the influence of rotor wakes are traced from the simple momentum techniques used in the early years of propellers and rotors to the current state-of-the-art computer programs simulating the rotor's complex vortex structure. Early methods became inadequate as disc loadings increased and wake effects became increasingly important, particularly for hovering and low forward speed conditions where the tip vortex could induce stall at critical points on the blades. Analytical and experimental techniques are described which define the geometry of the vortex field of a hovering rotor and its effect on rotor performance. It was concluded that the most important factor which influences the prediction of hover performance was the interference caused by the tip vortex during its first revolution. Integrated performance in forward flight was generally not sensitive to variable inflow; however, when combined with unsteady airfoil data, variable inflow produced significant effects on blade torsional responses.

NOTATION

AR	Blade aspect ratio, R/c
b	Number of blades
c	Blade chord, ft
\bar{c}	Blade chord nondimensionalized by R
C_L	Rotor lift coefficient, $\text{lift}/\pi R^2 \rho (\Omega R)^2$
$C_{L_{TIP}}$	Blade section lift coefficient near blade tip
C_M	Section pitching moment coefficient, $\text{moment}/\frac{1}{2} \rho U^2 c^2$
C_N	Section normal force coefficient, $\text{force}/\frac{1}{2} \rho U^2 c^2$
C_{PF}	Rotor propulsive force coefficient, $\text{force}/\pi R^2 \rho (\Omega R)^2$
C_Q	Rotor torque coefficient, $\text{torque}/\pi R^3 \rho (\Omega R)^2$
C_T	Rotor thrust coefficient, $\text{thrust}/\pi R^2 \rho (\Omega R)^2$
F	Distance from axis of rotation to blade section nondimensionalized by R
R	Rotor radius, ft
U	Resultant blade section velocity, ft/sec
V	Free-stream velocity, knots
V_z	Induced velocity at blade in axial direction, positive up, ft/sec
z	Axial coordinate measured normal to tip-path plane nondimensionalized by R
Z_G	Distance between the center of the rotor hub and ground, ft
α	Section angle of attack, deg
$\dot{\alpha}$	Rate of change of section angle of attack, radians/sec

*Supervisor, Rotary Wing Technology

**Chief, Aerodynamics Section

α_{TPP}	Tip path plane angle of attack, positive nose up, deg
Γ	Local blade circulation (equal to $\Omega R F c c_1/2$), or strength of vortex element in wake, ft^2/sec^2
θ_1	linear built-in twist rate, positive when tip pitch greater than root pitch, deg
θ_{75}	Blade collective pitch measured at the 0.75R radial station, deg
μ	Advance ratio, $1.69V/\Omega R$
ρ	Air density, slugs/ ft^3
σ	Rotor solidity, $bc/\pi R$
ψ	Blade azimuth position, deg
ψ_w	Wake azimuth position, azimuthal degrees between vortex element and blade from which it originated, deg
Ω	Rotor angular velocity, rad/sec

1. INTRODUCTION

The problem of accurately predicting the flow field and associated performance of a lifting rotor continues to restrict designers in their efforts to provide improved blade designs for helicopters. Methods for determining rotary-wing inflow and performance were originally developed for propellers and have evolved over the last one-hundred years. Following the early development of the simple actuator disc and blade element-momentum methods, emphasis was placed on the development of vortex theory. This resulted from the demands for more precise prediction of rotor performance, structural limitations, vibrations, stability and acoustic characteristics. The progress of vortex methods has largely paralleled the progress in the development of high-speed computers. The simple vortex theory approaches have been superseded by complex wake modeling techniques for predicting the instantaneous rotor flow field. This would not have been possible without the current advanced state of computer technology.

The prediction of the instantaneous flow field for the rotor is complicated by the following factors: (1) the geometry of the vortex system generated by the rotor (rotor wake) is considerably more complicated than that of a fixed wing wake and (2) unsteady flow effects must be considered since the loading on the blades varies with time even when the helicopter is in steady forward flight. Some of the principal assumptions limiting the accuracy of rotor inflow methods have been associated with the geometry of the wake and the neglect of unsteady aerodynamic effects. Generally, the rotor wake geometry was prescribed in advance as a classical geometry consisting of undistorted skewed helical vortex filaments. However, it is well-known from flow visualization results that the actual wake geometry differs significantly from the classical model. Recent efforts at the United Aircraft Research Laboratories (UARL) have concentrated on the development of an analytic method for predicting the effects of distorted wake geometry and unsteady aerodynamics on rotor performance.

The primary objectives of this paper are to (1) review the history of methods for determining rotor inflow emphasizing the wake models employed, and (2) describe results from methods developed at United Aircraft which demonstrate the influence of wake geometry and unsteady aerodynamics on rotor inflow and performance for hovering and forward flight conditions.

2. SURVEY OF ROTOR INFLOW METHODS

The intent of this survey is to present a brief history of the methods and the technical approaches used along with a fairly comprehensive list of references. Although, the literature has been carefully searched for the references presented herein, no claim is made for completeness. The references are mainly limited to those describing theoretical rotor inflow and wake methods. Selected propeller methods, which are adaptable to helicopter rotors, are also referenced. Completely experimental studies and studies directed at understanding the fundamentals of the problem are generally not included. Since a general description of each method is beyond the scope of this effort, emphasis, for the vortex methods, has been placed on indicating wake models used. More complete descriptions of selected references may be found in Refs. 1 through 5. In general, emphasizing the wake, each method may be characterized by selecting the applicable combination from the following major descriptive categories.

1. Rotor or propeller theory
2. Hover (static thrust) or forward flight
3. Momentum or vortex theory

4. Type of wake model in vortex theory

- a. Simplified (vortex cylinder etc.) or complex (helical vortex filaments) wake model
- b. Undistorted or distorted wake
- c. Theoretical or empirical wake model

References representing nearly all combinations within the above categories are presented below.

2.1 Inflow methods based on momentum theory

Rotary-wing momentum theory was originated by Rankine (1865, Ref. 6) and Froude (1889, Ref. 7). Simple momentum theory is based on the assumption of a uniformly loaded actuator disc and results in a uniform inflow distribution at the rotor or propeller which is assumed to have an infinite number of blades without tip losses. Removal of the constant inflow assumption was achieved to a limited extent by the introduction of blade element-momentum theory by Drzewiecki (1892, Ref. 8), Reissner (1910, Ref. 9), and Glauert (1926, Ref. 10; 1927, Ref. 11). In blade element-momentum theory, as applied to the hovering condition, the radial variation of inflow is found by neglecting contraction of the wake and considering the rotor disc to be divided into concentric rings. Through strip analysis the elemental thrust produced by each ring element is determined in terms of the inflow velocity at the rotor. By equating this to the overall momentum change in the air flow through each annulus, and assuming that the inflow velocities are constant around any ring, the inflow at each element can then be determined. In Ref. 10, Glauert provided a simple linear representation of the fore-aft variation of inflow over the rotor for forward flight conditions. Mangler and Squire (1953, Ref. 12) developed a modified actuator disc theory to predict the rotor inflow variation with azimuth. Recently, Wood and Hermes (1969, Ref. 13) developed a forward flight, variable inflow theory based on blade element-momentum theory and an empirical relation for induced flow build-up on a blade. However, most current forward flight momentum methods used in rotor design are based on the constant inflow assumption.

2.2 Inflow methods based on undistorted wake geometry

To solve the inflow problem in a more refined manner as required for accurate blade airloads calculations, the rotor wake must be analyzed. Simple vortex theory describes the wake by a semi-infinite cylindrical vortex sheet which is emitted from the blade tips (Fig. 1a). This implies an infinite number of blades, uniform blade loading, and neglects wake contraction. The rotor inflow due to the cylindrical vortex sheet is solved through use of the Biot-Savart law and by representing the sheet as a uniform distribution of an infinite number of vortex rings of infinitesimal thickness which are located in planes parallel to the rotor disc. The constant (hover) or mean (forward flight) induced velocity resulting from this theory, which was first developed by Knight and Hefner for the propeller static thrust condition (1937, Ref. 14), has been shown to be equivalent to that obtained from momentum theory. Coleman, et al. (1945, Ref. 15) developed a method to calculate the fore-aft variation of rotor inflow produced by the skewed elliptical wake cylinder for forward flight conditions. This method was later expanded on by Castles and DeLeeuw (1954, Ref. 16) and Castles and Durham (1956, Ref. 17) to result in methods for predicting the induced velocity distribution for the longitudinal and lateral planes of symmetry of the rotor, respectively. Heyson and Katzoff (1957, Ref. 18) removed the uniform loading assumption from the above approach by modeling the wake as a number of parallel and concentric vortex cylinders (Fig. 1b), the intensities and dimensions of which correspond to the prescribed pattern of the loading. The sum of the superimposed induced velocity fields of the individual vortex cylinders yield the overall inflow field of the radially nonuniformly loaded rotor. As described in a series of NACA reports, Heyson continued to refine this approach and finally included a nonuniform azimuthwise vorticity distribution (1960, Ref. 19). An earlier attempt at predicting the inflow variation with azimuth, using vortex theory, was developed by Drees (1949, Ref. 20). Two other vortex theories based on an infinite number of blades are those of Wang Shi-Tsun (1961, Ref. 21) and Baskin (1960, Ref. 22) in which the vortex rings that had previously been used to represent the vortex cylinder are replaced by vortex lines and a layer of dipoles, respectively.

Due to the inherent limitation of the above methods using vortex cylinders, which is that time-averaged rather than instantaneous induced velocities are predicted, these methods are not adequate for providing accurate variable inflow distributions for the determination of the fluctuation of the blade airloads. To solve for the variable inflow for a finite number of blades using vortex theory, the wake from each blade must be considered. Goldstein (1929, Ref. 23) derived a vortex theory for propellers with finite numbers of blades. Goldstein solved the problems of the flow attributable to a set of semi-infinite, equidistant, coaxial, helicoidal surfaces, each one representing the vortex sheet emanating from a blade (Fig. 2). Goldstein's solution was developed using Betz's optimum loading condition (1919, Ref. 24); that is, it neglects the slipstream contraction and hence refers rigorously only to a lightly loaded propeller. The basic assumption of the Goldstein theory is that the velocity field of the vortex system at a large distance from the propeller is equivalent to the potential field of the rigid helicoidal surfaces. This is rigorously correct only for propellers where the circulation along the blades is such that the flow in the wake is identical with the potential flow of such a set of equidistant coaxial helicoidal surfaces. The Goldstein analysis as extended by Lock (1932, Ref. 25) has been applied to the hovering condition for helicopter rotors. The primary limitations, the assumptions of a non-contracting wake and a small ratio of wake displacement velocity to propeller advance velocity, were not important to the original development which was intended for propellers operating in axial flight.

However, even with their limitations recognized, the Goldstein-Lock and blade element-momentum analyses, until recently, represented the state-of-the-art for routine calculation of rotor hover performance.

Due to the complexity of the induced velocity calculations associated with a spiral wake system in forward flight, these calculations had to await the availability of the digital computer. A computer method by Willmer (1963, Ref. 26) replaced the undistorted spiral wake from each blade by a simplified model. He assumed that only those parts of the wake which are near to the reference blade are important. To these he applied his "rectangularization" principle which consisted of straightening out those parts of the wake near the blade and making the mathematical simplification of integrating to infinity since the outer parts of the straightened wake could be assumed to have little effect. Thus the wakes of all blades are divided in parts (rectangular sheets) and placed in their appropriate positions according to the mean flow velocity through the disc and the number and relative positions of the blades that shed them. Using an extension of Glauert's lifting line theory, the inflow solution is reduced to a system of simultaneous equations. These are solved on a digital computer and the results have shown considerable improvement over the simpler theories that preceded it. A variation of Willmer's method was developed by Molyneux (1962, Ref. 27) in which the rectangularized sheets in the far wake are replaced by a line of doublets whose strength is the integral of the doublet distribution across the span of the sheet. One shortcoming of Willmer's method is the neglect of the time-wise variations of vorticity in the wake. That is, the shed vorticity, which is defined as the vorticity which leaves the blade due to timewise changes of circulation, and the corresponding changes in strength of the trailing vorticity (vortices emitted normal to the blade span to blade radial circulation variations) are neglected. Loewy (1957, Ref. 28) had earlier used a simplified two-dimensional representation of the shed vorticity to investigate the flutter characteristics of an oscillating rotary wing airfoil. This problem was also treated by J. Jones (1965, Ref. 29), who developed a method for determining the influence of the shed wake at an actuator disc (infinite number of blades) for low speed conditions. R. Miller in a series of publications (1962, Ref. 30; 1964, Refs. 3, 31, 32) accounted for the shed vorticity through use of Theodorsen type lift deficiency functions. A simplification to the spiral wake, developed by R. Miller (1964, Ref. 31), is characterized by the feature that the helical vortex lines departing from the blade are replaced at specific points by their tangents (infinite straight filaments). A similar wake representation is used in the methods of Harrison and Ollerhead (1966, Ref. 33), Fuhr and Kussman (1970, Ref. 34), and W. Jones and Rao (1971, Ref. 35).

One of the first methods using helical vortex filaments to represent the undistorted wake of a rotor is that of Castles and Durham (1959, Ref. 36). Undistorted filaments are used to represent the tip vortex spiral from each blade. The vorticity shed from the inboard portion of the blade is represented by a central straight vortex line along the axis of the wake. Nondimensionalized induced velocities for specific points are tabulated as a function of number of blades, wake axial velocity, and radius of the point. A similar wake model was used in a method by N. Miller, Tang, and Perlmuter (1968, Ref. 37). R. Miller used the spiral undistorted wake model, which he termed a "rigid wake", as an alternative to his simplified straight vortex filament approach described above. The undistorted or "rigid wake" assumption means that the in-plane wake coordinates (in planes parallel to the tip path plane) are determined simply by the rotor rotational and translational velocities and the axial coordinates (normal to the tip path plane) are determined by a mean flow velocity which is generally the momentum inflow value. Piziali and DuWaldt (1962, Refs. 38, 39) modeled the undistorted wake from each blade by a mesh of segmented vortex filaments (Fig. 3). Each segment is straight and of constant vortex strength. However, the strengths of the various segments vary in accordance with the variation in the azimuthwise and radial variation of the blade bound circulation. The segmented trailing vortex filaments emanate from each of the end points of the blade lifting-line segments. The segmented shed vortex filaments intersect the trailing filaments in a manner such that the segment end points of both are coincident. In this manner, the changes in, and the effects of, trailing and shed vorticity are simultaneously computed. In a similar manner, Madden (1967, Ref. 40) extended the method of R. Miller to include the effect of both azimuthwise and radial variations of wake trailing circulation strength by representing the trailing vorticity by several spiral vortices emanating from the blade and divided into finite straight line segments. However, he retained a two-dimensional lift-deficiency type formulation for the shed wake influence. Scully (1965, Ref. 41) has noted possible refinements to R. Miller's approach. Sogel (1966, Ref. 2) expanded the method of Piziali and DuWaldt to the transient condition by allowing the mean inflow, which establishes the axial position of the rigid wake, to vary with time in accordance with the transient momentum changes. He included only the trailing wake contribution, since he considered the shed wake effect as second order. Davenport (1964, Ref. 43) and Balcerak (1967, Ref. 44) expanded the techniques developed by R. Miller and by Piziali and DuWaldt for an undistorted wake to the tandem rotor application. Ichikawa (1967, Ref. 45) used an undistorted vortex sheet approach to develop a unique linear theory for the blade spanwise lift distribution in which he deduced a closed form lifting-line type solution from a lifting surface theory by mathematical approximation. Several propeller performance theories that use an undistorted wake have been summarized by Wu (1965, Ref. 2). Three other propeller theories that are also based on an undistorted wake geometry are those of Nelson (1964, Ref. 46), Hough (1967, Ref. 47), and Mandl (1967, Ref. 48).

2.3 Inflow methods based on a theoretical distorted wake geometry

It was recognized by the earlier proponents of the rigid wake model (e.g., R. Miller, Ref. 32, Piziali, Ref. 50) that the sensitivity of blade inflow and associated airloading to wake distortions could be significant. The requirement for an improved wake geometry model was also concluded at the

United Aircraft Corporation in a series of unpublished applications of the methods of Piziali and DuWaldt, Willmer and Miller by Arcidiacono and Landgrebe and in a later study in which they cooperated with Carlson and Hilzinger (1965, Ref. 49) to couple the variable inflow solutions to a Sikorsky Aircraft aeroelastic blade response program.

R. Miller (1964, Ref. 31) established the concept of a "semi-rigid" wake. A semi-rigid wake geometry results by replacing the constant axial velocity (normal to the tip path plane) of the rigid wake with the instantaneous axial velocity of each vortex element occurring at its generation at the blade. Although this results in a distorted spiral wake, changes in the vortex element velocities with time, due to interaction with the wake and blades, are neglected. Piziali (1965, Ref. 50) also included a provision for a semi-rigid wake. In addition, he refined his wake model to approximately account for the roll-up of the spiral wake surface by truncating the mesh of trailing and shed vortex elements behind the blade at a prescribed wake azimuth and by providing thereafter for two concentrated vortex filaments to represent a rolled-up tip vortex and root vortex. Brandt (1962, Ref. 51) and Ham (1963, Ref. 52) applied R. Miller's method using a semi-rigid wake to investigate wake effects on rotor blade airloads for low speed flight conditions. A comparison of the semi-rigid wake geometry with results from an experimental program showed major discrepancies between the semi-rigid and measured wake coordinates which Ham concluded could be significant if accurate blade airloads are to be predicted.

In recent years the requirement for an improved distorted wake model has been recognized. Several methods for predicting a more realistic wake geometry have been developed in the past seven years. These range from simplified methods, such as methods in which (1) the wake is approximated by vortex rings or vortex tubes or (2) the rotor is represented by an actuator disc, to more complex methods in which the distorted wake geometry is predicted through calculation of the mutual interaction of the wake filaments emitted from each blade.

The first of the simplified methods was that of Brady and Crimi (1965, Ref. 53) in which the contracted wake of a static propeller, in and out of ground effect, is calculated by a time-step procedure employing vortex rings of constant circulation strength. Trenka (1966, Ref. 54) used the results of this method to establish the contraction and spacing of a mesh of discrete segments similar to Piziali's wake representation for the purpose of predicting the performance of VTOL propellers. Greenberg and Kaskel (1968, Ref. 55) combined an actuator disc model of a hovering rotor with a wake comprised of a distribution of equal strength vortex rings over the slipstream surface boundary. From applications of this approach, they concluded that the streamline pattern is virtually independent of thrust coefficient. This result was later questioned on the basis of experimental results obtained at United Aircraft (1971, Ref. 56). Theodorsen (1969, Ref. 57) extended his early propeller theory to obtain a solution for the wake contraction and associated performance of static propellers and hovering helicopter rotors with optimum loading. Following the unsuccessful application of a semi-empirical wake model (1965, Ref. 58) and a complete continuous vortex sheet deformation approach, Erickson (1969, Ref. 59) developed a method for the static performance of a VTOL propeller in which he specifies the wake contraction based on the method of Greenberg and Kaskel, and calculates the pitch of the trailing vortex sheets by iterating on the axial positions and velocities at prescribed field points. A method for low speed forward flight conditions was developed by Joglekar and Loewy (1970, Ref. 60) in which the rotor is assumed to be an actuator disc and the corresponding distortions of the tip vortex filaments are used to establish the wake geometry for use in Piziali's airloads program (Ref. 50). Vaskin (1966, Ref. 61) uses a distorting vortex tube of uniform circulation to obtain an approximate representation of the distorted wake of a rotor in forward flight. An approximate solution for the wake downstream of a rotor, where the wake rolls-up into two concentrated counter-rotating vortices similar to a fixed wing wake, was developed by Levinsky (1970, Ref. 62). For the wake close behind the rotor he used inclined actuator disc theory applied to a combination of an infinite number of ring vortices of elliptical cross section and an infinite number of ring vortices and sources directed parallel to the axis of the elliptical cylinder. For the far wake he used a single horseshoe vortex divided into numerous straight, viscous core segments.

The more complex distorted wake methods are all characterized by the representation of the wake from each blade by segmented vortex filaments which are allowed to freely distort until a converged wake results. The wake geometry method developed by Landgrebe at the United Aircraft Research Laboratories is described in a series of references (1969, Ref. 63; 1971, Refs. 56, 64, 65, and 66; 1972, Ref. 67). The wake model is composed of a finite number of discrete vortex filaments from each blade. The straight vortex elements are free to convect at a velocity equal to the sum of the free stream velocity and the velocity induced by the trailing and bound vorticity. The influence of the shed vorticity on the wake distortions is assumed negligible since its intensity is small in comparison to the trailing vortex strength. However, the influence of the shed wake directly behind each blade is included empirically in the airloads calculation through the use of unsteady two-dimensional airfoil data. Several modes of operation have been provided in the computer program for this method. The most complex mode, and also the most costly, is to allow all the wake elements to interact freely with the intent of calculating all the wake features including the rolling-up of the tip vortex and the distortion of the wake (vortex sheet) emitted from the inboard region of the blade. The computer requirements and costs are normally prohibitive for this mode of operation so various alternatives have been provided. The selection of these alternatives is usually determined by the accuracy required and the flight condition of interest (hover or forward flight). One alternative mode consists of grouping the vortices from each blade into (1) a strong, rolled-up tip vortex filament, and (2) several weaker trailing vortex filaments representing the inboard vortex sheet (Fig. 4). The complete mutual interaction of these vortices may be calculated, or

the geometry of the inboard vortices may be prescribed and the distortions of the tip vortex computed.

The computation of the wake geometry is accomplished by the following procedures:

1. The circulation strength in the wake is estimated from a previous solution of the bound circulation distribution on the blade (lifting line).
2. An initial wake geometry is specified.
3. The classical Biot-Savart law is applied to compute the velocities induced by each vortex segment in the wake at the end points of the assigned distorting segments.
4. These velocities are integrated over a small increment in time to define a new wake geometry.
5. Steps (3) and (4) are repeated, alternately, until a converged wake geometry corresponding to the initial estimate of blade bound circulation is obtained.
6. A new estimate of the blade bound circulation distribution is computed using the calculated wake.
7. Steps (2) through (6) are repeated, iterating until a compatible wake geometry-circulation solution is obtained.

The wake geometry method has been coupled with a circulation analysis and an aeroelastic blade response analysis so that a consistent wake geometry, rotor inflow distribution, and airload distribution may be iteratively computed (Fig. 5). The method is applicable to both steady-state hovering and forward flight conditions, and it is currently being extended for transient conditions and to include a lifting surface representation for the blades. In order to avoid prohibitive computation costs, the far wake model for hovering flight may be represented by helical filaments and, unlike the near wake, this far wake region is constrained from distorting freely. Another option in the method for reducing computer costs is to consider the lesser induced effects at each wake point in approximate form. By selecting a bounding displacement velocity induced by a single wake segment at each segment end point considered, a grouping of all segments into a near and far wake region is achieved for each end point. The near wake region contains the segments which make a substantial contribution to the displacement velocity at the segment end point. Thus, this contribution is calculated anew for each time step in the iteration loop. The displacement velocities induced by the segments of the far wake region are recalculated only at selected time steps. Their summation yields the combined influence of the far wake region on the segment end point, which is kept constant for the selected interval (generally, calculation of the displacement velocities due to the far wake during the first time step is sufficient). A similar wake geometry method was developed by Crimi (1966, Ref. 68). This method differs from the above mainly in the following manner: (1) the wake consists only of tip vortex filaments, (2) a near and far wake provision is not included, (3) refinements for the hover condition are not included, and (4) fuselage interference effects on the wake are calculated. A third method, which is also similar to the above in the basic technical approach, is that of Scully (1967, Ref. 69). Scully's wake model consists of distorting segmented tip vortex filaments and nondistorting inboard filaments. Rather than start the interaction procedure with an assumed initial wake model, Sadler (1971, Ref. 70) developed a method to predict the wake geometry by a process similar to the start-up of a rotor in a free stream. An array of distorted, discrete trailing and shed vortices is generated as the blade proceeds in time. The "free wake analysis" developed by Clark and Leiper (1969, Ref. 71), limited to hovering rotors, is a spatial analysis rather than the previous temporal analyses. That is, rather than computing the wake velocities and associated wake geometries for a series of time steps, the segmented trailing wake is allowed to move freely through a computed velocity field to establish a wake pattern. Similar near wake geometry results from this spatial method and Landgrebe's temporal method are shown in Ref. 65.

2.4 Inflow methods based on prescribed empirical wake geometry

Concurrent with the rotor inflow methods based on a theoretical wake geometry, other methods have been developed based on empirical wake models. Most of these methods are directed toward the rotor hover condition in that this condition is the one most influenced by wake distortion effects and it is the simplest one for obtaining experimental flow visualization data.

Gray (1955, Ref. 72; 1956, Ref. 73) developed a semiempirical method for the wake of a single bladed rotor based on experimental wake geometry data obtained from smoke-visualization tests. He postulated the wake as a rolled up tip vortex filament and a separate inboard vortex sheet (Fig. 6). Although this method was relatively advanced for its time, it was necessary for Gray to make several simplifying assumptions, since this was prior to the availability of high-speed computers. Gray's approach was later expanded for propellers by Gartshore (1966, Ref. 74). Rorke and Wells (1969, Ref. 75) modified momentum theory to include the effects of the prescribed near wake by adding a wake-induced "interference" velocity distribution to the adjusted momentum inflow. Magee, Maisel and Davenport (1969, Ref. 76) developed a semiempirical method for prescribing the wake and computing the performance of a hovering rotor. The degree and rate of wake contraction are determined from the ring vortex model of Ref. 53 and the axial wake coordinates are based on a "slipstream acceleration parameter" which was partially based on

experimental data and synthesized to provide correlation for several rotors and propellers. Seed (1967, Ref. 77) used a prescribed slipstream profile, based on experimental observations, and a semiempirical relation for the spiral pitch to calculate the performance of a rotor with circulation control by blowing. He found that his prescribed wake model provided better correlation than his "continuous deformation model" in which the spiral wake form is allowed to deform within a specified wake contraction boundary.

The requirement for a method employing an accurate prescribed wake model obtained from experimental wake data was concluded by Jenney, Olson, and Landgrebe (1968, Ref. 78) who found that the rapid contraction of the slipstream under a hovering rotor places the vortex system sufficiently close to the rotor blades that it causes significant changes in the radial distributions of induced velocities which can result in a loss in hover performance. A method based entirely on an empirical wake was developed by Landgrebe (1971, Ref. 56; 1972, Ref. 67) at the United Aircraft Research Laboratories for hovering rotors with any number of blades. The method, entitled "The UARL Prescribed Wake Hover Performance Analysis", was derived to compute the blade circulation and inflow distribution and the corresponding rotor performance based on a prescribed wake geometry. Generality regarding the specification of the geometry was maintained in the computer analysis to permit the evaluation of a wide variety of wake geometry models. Sample computer plots are shown in Fig. 7 for a typical experimental wake (far wake instability neglected) and a classical wake model. Each blade is represented by a segmented lifting line, and the wake is represented by a finite number of segmented vortex filaments trailing from the blade segment boundaries. The blade and wake characteristics are assumed to be independent of azimuth position. The program is divided into three parts. The first transforms the wake geometry input to wake coordinates. The second contains the computation of the wake influence coefficients at the blades as defined by the Biot-Savart law and the numerical procedures for solving the circulation matrix and associated induced velocity distribution. In the third part, performance characteristics are computed. Conventional strip theory based on two-dimensional airfoil data is assumed applicable to compute the rotor performance characteristics. The method was successfully applied at UARL following the experimental acquisition of systematic model rotor hover performance and wake geometry data which were generalized to facilitate the rapid estimation of wake geometry for a wide range of rotor designs and operating conditions. The method is currently in use at Sikorsky Aircraft and the U. S. Army Aviation Materiel Research and Development Laboratory, and has accurately predicted the hover performance of a wide range of full-scale helicopter rotors. This prescribed wake analysis was successfully applied to predict propeller performance by Ladden (1971, Ref. 79) based on generalized propeller wake data. Gilmore in Part II of the same reference presented an extension of Gartshore's semiempirical approach.

For forward flight conditions, Tararine (1960, Ref. 80) empiricized an analytical wake model based on tip vortex flow visualization data obtained using smoke techniques in a wind tunnel. Isay (1971, Ref. 81) developed a simplified vortex model for the analysis of the flow at the rotor based on a prescribed trapezoidal flow distribution in the wake. Landgrebe and Bellinger (1971, Ref. 64) modified the UARL aeroelastic performance method, described previously, to include a prescribed wake option for forward flight conditions, and have prescribed the experimental wake patterns of Lehman (1968, Ref. 82) which were obtained from photographing tip vortex bubble patterns of a model rotor in a water tunnel.

2.5 Recent emphasis in inflow studies

In addition to refining the wake geometry models, recent emphasis has been placed on more accurate analytical simulation of blade-vortex interference. Several studies have been conducted to investigate improved representations of the blade and the wake (particularly, the tip vortex). These studies include the following areas:

1. Representation of the blade by a lifting surface instead of a lifting line (e.g., Refs. 83 through 85),
2. Details of blade-vortex interaction (e.g., Refs. 86 through 89), and
3. Studies of vortex structure and stability (e.g., Refs. 90 through 92).

Although significant progress has been made in these areas, continued studies are required to improve our understanding of the complex rotor problem and to apply the new knowledge and analytical techniques to rotor inflow methods.

3. RESULTS OF RECENT STUDIES CONDUCTED AT UNITED AIRCRAFT

For several years, investigations have been conducted at the United Aircraft Research Laboratories to experimentally examine specific effects of blade parameters and wakes on rotor performance and to develop methods to predict those effects. Many of these efforts considered hovering flight since this remains the most important asset of the helicopter. The work, in addition to the forward flight and unsteady flow effects presented later, have been supported, to a large extent, by the U. S. Army Air Mobility Research and Development Laboratory and the NASA Langley Research Center.

3.1 Hovering flight

There have been a variety of techniques devised to improve the efficiency of rotors in hover. These include twist, planform taper, thickness taper, root cutout, camber, and blade tip sweep. These parameters generally affect the thrust characteristics at a given power and, of course, the objectives have always been to increase thrust at a given power. The objective of increasing maximum thrust for a given rotor size was not rigorously pursued during the years of the reciprocating engine since installed power was generally insufficient to reach maximum thrust conditions. However, with the advent of the turboshaft engine, and the corresponding improvement in power to weight ratio, stall-associated problems rather than power limits often have limited performance.

Initial performance methods could not predict these stall effects and as a result new high performance helicopter designs did not achieve their expected performance levels. In many cases these reductions in maximum thrust reached levels as high as 10 percent, which seriously compromised payload capabilities. This reduction in actual lift compared to lift predicted using classical methods is demonstrated in Fig. 8. Here experimental results are shown for model rotors having two and six blades and compared to theoretical results of the Goldstein-Lock and momentum analyses. This figure demonstrates the good correlation for the 2-bladed rotor and the poor correlation for the 6-bladed rotor. These results, and additional results obtained for other blade configurations (Ref. 56) provided evidence that the discrepancy was related, at least in part, to the failure of the analyses to simulate the change in blade aerodynamics caused by the increase in solidity (higher number of blades). Programs were undertaken at United Aircraft to identify the mechanisms causing these discrepancies and to provide the technical base from which improved performance methods could be developed. Initial research efforts were directed at experimental measurements of the wake geometry, particularly the strong tip vortex, and the effects of various blade design parameters on wake geometry. Data were obtained on 4-ft model rotors by emitting smoke thru the rotors and visualizing the vortices. As shown in Fig. 9, it is possible to locate the core center of the tip vortex relative to the blade tip as well as the cross section of the inboard vortex sheets. Another important wake characteristic is evident from the photographs of Fig. 9. This is the vertical spacing between adjacent vortex cores relative to the vertical spacing between the first (uppermost) vortex and the blade passing above it. The spacing between cores is significantly greater than that between the first vortex and following blade demonstrating the increased transport velocity of the tip vortex after the passage of the following blade. Examination of sequential photographs revealed that the vertical velocity of the tip vortex consists of two distinct constant values. In the region between the generation of the vortex and the passage of the adjacent following blade there is no strong downwash influence present and the rate is relatively low. The passage of the following blade then imparts a large downward momentum producing the resulting geometry shown in Fig. 9. The radial velocity, on the other hand, does not experience a distinct change due to a blade passage, but instead exhibits an initially high value and then approaches zero exponentially. This radial component of velocity was found to be relatively insensitive to all design parameters investigated and was dependent primarily upon disc loading. The effects of increasing solidity on vortex geometry is revealed from Fig. 9 where the 8-bladed rotor is shown to place the trailing tip vortex very close to the following blade. As a result of the interference produced by the high induced velocities of the tip vortex, local stall could be produced for an 8-bladed rotor whereas such stall could be avoided for a rotor having fewer blades. However, at constant disc loading and solidity interference is relatively insensitive to number of blades. This represents the major requirement in predicting the performance of a rotor in hover -- the ability to define the position of the tip vortex and the induced velocity field around it. The influence on the tip vortex location and induced angle of increasing the number of blades is also illustrated in Figs. 10 and 11. For a fixed blade loading and chord, the radial and vertical locations of the tip vortex below the following blade are shown for 2-, 3-, 4-, 6-, and 8-bladed rotors. As shown in Fig. 11, the angle induced at the blade increases significantly as the vertical displacement decreases. For higher loaded rotors it is obvious that severe stall could be produced which would significantly reduce performance over that predicted using classical methods. This becomes an important consideration when the maximum lift capability of an existing rotor is increased by adding one or more blades. Such a configuration change could not achieve the increased lift expected unless the effects described above are accurately modeled. It should be noted that the effects of increased number of blades are less serious when the chord is reduced to maintain constant solidity. Under these conditions, if a reduction in chord accompanies an increased in number of blades, the reduction in vortex strengths compensates the reduction in vertical displacement.

The effects due to vortex interference on radial distribution of angle of attack and loading are shown in Fig. 12. Here the distributions predicted for a model rotor operating below stall ($C_T/\sigma = 0.07$) are presented for the distorted wake and classical wake methods. The most notable difference is over the tip region where angle of attack and loading excursions of the distorted wake method reach levels approximately 50 percent higher than those of the undistorted wake methods. To avoid premature rotor stall caused by tip disturbances of the type shown in Fig. 12, some recent rotor designs have incorporated a finite reduction in blade angle near the tip to obtain a more nearly uniform angle of attack distribution. This ensures that a greater span of blade can more nearly achieve its lift potential.

Additional rotor design parameters such as tip speed, blade twist, aspect ratio, planform taper, and camber have been experimentally investigated at United Aircraft (Refs. 56 and 93) to determine their effects on performance and wake characteristics. It was found that the wake geometry was insensitive to independent variations in tip speed, aspect ratio, and camber, at least over the range of variables tested. The influence of number of blades is limited to establishing the wake azimuth angle where the tip

vortex passes below the adjacent downstream blade at which point the vertical velocity increases significantly. The effect of camber was, as expected, to increase the maximum rotor thrust due to the increased $C_{l_{max}}$ of the cambered section. Blades having planform taper at zero twist were found to stall at a considerably lower thrust coefficient than constant chord blades of equivalent blade area. Although only limited flow visualization data have been obtained for the tapered blade rotor, preliminary results indicate that the initial vertical velocity of the tip vortex is much reduced over that of the constant chord rotor. As a result, greater interference effects are produced on the following blade causing premature tip stall. It is speculated that the tip circulation strength, which is the primary source of the initial downwash velocity, is lower due to the reduced blade chord. As a result of tip stall, much of the inboard blade area, which is considerable in light of the taper effects, does not nearly reach its full lift potential. Of course, large values of negative twist should accompany taper in order to place the inboard sections at more favorable L/D levels and, in fact, it seems reasonable to expect that a tapered blade should require greater twist than a constant chord blade of equivalent area. This appears warranted since for equivalent areas, the tip chord of the tapered blade is less than that of the untapered blade and, assuming no twist, would be subjected to tip stall at a lower thrust level.

Results of the UARL Prescribed Wake Analysis described earlier are compared to experimental results in Fig. 13. The wake used to generate these results was estimated from flow visualization photographs where the accuracy in reading coordinates is approximately 1/2 percent of the radius. The sensitivity of performance to the tip vortex position is demonstrated in Fig. 13 where the tip vortex is displaced this amount (1/2 percent R) further from the rotor. The important conclusions that have resulted from these investigations are that knowledge of the strength and position of the tip vortex of highly loaded multi-bladed rotors is extremely important and that performance prediction methods must accurately simulate this geometry if reliable performance estimates are to be expected.

3.2 Wake stability characteristics

Indications from the many flow visualization investigations conducted at United Aircraft, primarily with model rotors as reported in Ref. 56, are that the helical tip vortex is relatively stable and repeatable in the region below the hovering rotor extending down to approximately 20 percent of the radius. This region is, of course, the most important regarding performance and fortunately produces a generally steady aerodynamic environment at the blades. However, as the helix progresses downstream it takes on a more random behavior and eventually an apparent instability. Whether the tip vortex undergoes a form of viscous dissipation (decay) or vortex breakdown (bursting) as characterizes certain fixed wing tip vortices is conjecture at this time. However, results indicate a definite departure from the classical concept of a smoothly contracting wake below the rotor. Evidence of this is shown in Fig. 14, in which the fourth vortex cross section proceeds to travel radially outward (note particularly the photographs for $\psi = 60$ and 120 deg) until it is no longer visible. Although it is recognized that a small perturbation such as a small amount of ambient wind or a slight blade-out-of-track may be necessary to precipitate the instability, this is believed to be an academic consideration since full-scale rotor operation is certainly subject to greater disturbances than those present under controlled laboratory conditions.

Wake stability was found to increase with decreasing wake azimuth, ψ_w . For example, the repeatability of the tip vortex position beneath the following blade ($\psi_w = 360$ deg/b) was within ± 1 percent of the radius. More photographic examples and a more complete discussion of the unstable nature of the far wake are presented in Refs. 56 and 67. Evidence of far-wake instability for a small-scale propeller with two blades is discussed in Ref. 91. It is mentioned therein that the instability was characterized by axial but not radial oscillations of the tip vortex in the far-wake region. This differs from the observations of the model rotor tip vortices which exhibited substantial radial as well as axial movements.

The implications of this far wake instability on rotor performance and vibration have not yet been confirmed; however, it is believed that under steady hovering flight conditions the disturbances in the far wake are sufficiently removed from the rotor plane so as not to significantly affect its aerodynamic environment. The unsteady effects of the far wake are expected to play a more important role when considering acoustic phenomena, the effects of wake impingement on fuselage and tail surfaces, and the problems associated with slung loads.

3.3 Forward flight

Applications of the wake methods to the forward flight case have shown rotor performance for conventional helicopter flight conditions to be considerably less affected by the wake. In forward flight, with forward tilt of the rotor disc, the blades are moving away from the wake, therefore feeling less of its influence. As in the hover condition, the wake elements become distorted as a result of interactions with other elements in the wake. These distortions are similar to those produced by a fixed wing, as depicted schematically in Fig. 15. Shown is the general "rolling up" characteristic produced at the lateral extremities of the wake with the rolled-up portions growing in size as they proceed downstream. These large downstream distortions, however, do not significantly influence the flow field at the rotor. A more quantitative representation of the tip vortex geometry obtained from Ref. 64 is presented in Fig. 16. Here, theoretical results are presented for a 2-bladed rotor, and the wakes are shown for both the classical helical shape (undistorted) and the more realistic distorted wake. The planform view indicates relatively small differences in the tip vortex geometry, particularly over the

important near wake region; however, the profile views show significant differences. A comparison of the axial tip vortex coordinates for a model rotor predicted by the theory of Ref. 63 and obtained from the experimental results of Ref. 82 is presented in Fig. 17. Although the geometric differences between the distorted and nondistorted wakes are significant and generate great academic interest, it has been found that they are generally not important differences when it comes to the determination of rotor performance and certain other rotor characteristics for conventional forward flight conditions. (This cannot be generalized, however, to include flight conditions which place portions of the wake in the plane of the rotor, for example during maneuvers.) In fact, for many flight conditions, simple constant inflow theory predicts generally the same integrated performance as the variable inflow theories.

A comparison from Ref. 66 of the predicted performance using constant inflow, undistorted wake variable inflow, and distorted wake variable inflow with full scale experimental results is presented in Fig. 18. The results indicate only minor differences over the conditions investigated and relatively poor correlation with the test data. It will be shown later that improved correlation is achieved when unsteady aerodynamic effects are included.

It is interesting to note that the integrated performance results of Fig. 18 remain relatively unchanged between the three analytical results, yet the calculated inflow over the disc and the azimuthal distribution of angle of attack and loading contain considerable variations which must be simulated to accurately predict nonperformance rotor characteristics such as noise, stresses, vibration, and control loads. These variations are exemplified in Figs. 19, 20, and 21, where results were calculated using UAC blade response and variable inflow analyses. Figure 19 shows a typical inflow velocity map (induced velocity produced at the blade location during each revolution) demonstrating the highly variable character of the inflow, particularly over the outer region on the retreating side where the strong tip vortex induces large downwash velocities. Considerably lower velocities are induced on the advancing blade where a weaker tip vortex is produced as a result of the reduced lift over the advancing blade tip region. The two pockets of upwash shown in the two forward quadrants are produced by the passage of tip vortices from previous blades similar to the vortex passage shown in Fig. 19. The azimuthal variation in section angle of attack at the 75 percent radial station is shown for the constant and variable inflow cases in Fig. 20. The maximum excursions of 1 to 2 deg of the variable inflow curves from the constant inflow curve are attributable directly to tip vortex passage effects and occur on the advancing blade at approximately 130 deg and on the retreating blade over a region from 240 deg to 330 deg. Although the retreating blade disturbances appear greater than those on the advancing blade, the actual loading disturbances are less due to the reduced dynamic pressure on the retreating blade. The azimuthal variations in loading for the 75 percent station are shown in Fig. 21 where the relatively small advancing blade angle-of-attack disturbances shown on Fig. 20 translate into large loading disturbances. The effects of wake distortions are shown in Figs. 20 and 21 to increase the peak disturbances over those of the undistorted case. It should be noted again, however, that although the variable inflow theories generate significant differences in loading distribution compared to the constant inflow case, the integrated performance shows negligible differences. One should expect this when considering the basic characteristics of vortex interference phenomena; for flight conditions below stall, that is when the blade sections are operating on the linear portions of their lift curves, and assuming steady-state airfoil data, the interference produced by a vortex should generally induce upwash and downwash on adjacent sections of the rotor disc. The net effect should be one of cancellation which is evident in Fig. 21 where an increased loading at one azimuth position is generally accompanied by an unloading at an adjacent azimuth position.

The following comments summarize the forward flight wake characteristics which have been revealed through research conducted at United Aircraft.

1. Wake geometry in forward flight is primarily determined by number of blades and the following parameters: advance ratio, μ , rotor angle of attack, α , and thrust coefficient, C_T .
2. Rotor wake effects on blade airloading generally decrease with increasing advance ratio, increasing rotor angle of attack, and decreasing number of blades.

Increasing the advance ratio reduces the number of blade-vortex intersections by displacing the wake downstream from the rotor. Increasing the rotor angle of attack increases the axial spacing between the wake and the rotor by providing an additional component, $V \sin \alpha$, to the wake axial transport velocity relative to the rotor disc. Decreasing the number of blades reduces the number of blade-vortex intersections by reducing the number of tip vortices in the wake. In addition, for rotors with fewer blades the vortices from the previous blades have more time to move further beneath a blade due to the increased blade spacing. The effect of rotor thrust level is more complex in that it tends to increase wake effects by increasing the rotor-wake axial spacing. In addition to the reduction of wake effects due to these blade-wake geometry considerations, advance ratio and angle of attack influence the proportion of the wake induced velocities to the total induced velocities at the blades. An increase in either of these parameters leads to an increase in the axial velocity component, $V \sin \alpha$, which contributes to the total inflow. An increase in this inflow component decreases the significance of the wake induced velocities. At moderate to high flight speeds (hereafter referred to as $\mu > 0.1$) this component is typically greater than half of the total inflow. Also, as advance ratio is increased, blade flapping velocities become an increasingly greater proportion of the total inflow.

3. For moderate to high speed flight, the wake deflection angle is the predominant factor in determining the significance of wake effects. For most conventional helicopter conditions where the rotor supports the total gross weight and provides the total propulsive force, the rotor is normally tilted over at an angle of attack which results in a wake deflection angle of sufficient magnitude to reduce the wake sensitivity. However, wake effects can be anticipated as being very significant for helicopters with auxiliary propulsion for which the rotor tilt may be such as to result in wake deflection angles approaching zero.

4. For low speed flight ($\mu \sim 0.1$), the sensitivity to wake effects is stronger because of the low magnitude of the flight velocity components, $V \cos \alpha$ and $V \sin \alpha$, which limit the extent to which the wake is transported downstream and in the axial direction resulting in a greater number of blade vortex-intersections closer to the rotor. In fact, tip vortices pass above the blades for some low speed flight conditions. The typical "roughness" experienced by aircraft flying in this low speed range is attributed to wake effects on the vibratory response of the rotor blades.

5. In addition to the factors mentioned above, wake effects on rotor forward flight performance are less than wake effects on hover performance due to the fact that, unlike the hovering rotor wake, in forward flight the tip vortices do not continuously pass beneath the tip region of the following blades. The hovering rotor generates approximately $1/4$ to $1/3$ of its lift over the outer 10 percent of the blades. The passage of a tip vortex close to the blade in this tip region has been shown to significantly influence the tip airloading and, thus, the integrated rotor performance. In forward flight, the vortices do not continuously pass under the blades in the predominant loading regions. In fact, for rotors with low numbers of blades flying at high advance ratios there are no blade-vortex intersections for a large extent of the blade azimuth travel. In addition, the local vortex induced effects on performance tend to cancel for intersections at the inboard portion of the blade because of the equal and opposite velocities induced on opposite sides of the vortex.

3.4 Wakes and unsteady aerodynamics

The primary frequency content of the constant inflow loading curve shown on Fig. 21 is two per rev (2P); however, higher frequencies are introduced when variable inflow effects are included such as the 5P frequency contained in the variable inflow results shown in Fig. 21. These higher frequency components become particularly important when considering other rotor characteristics such as vibration, noise, and control loads. Exciting frequencies due to variable inflow effects (5P, for example) often coalesce with certain fundamental blade frequencies and, therefore, excite vibratory modes which would not otherwise be excited with constant inflow. Additionally, wake effects coupled with unsteady airfoil data produce important results which could not be predicted without simulating each of these phenomena. Unsteady aerodynamic effects are characterized by significant departures from the classical quasi-steady airfoil data, as shown in Fig. 22 (Ref. 95). Here the normal force and pitching moment are shown at one Mach number for both nose up (positive $\dot{\alpha}$) and nose down (negative $\dot{\alpha}$) pitching velocities and compared with steady state values. It is apparent that the forces and moments produced by an oscillating airfoil are extremely sensitive to the rate of change of angle of attack in addition to the absolute angle.

The impact of unsteady aerodynamics is felt primarily in two areas. The first is in performance where the lift overshoot shown by the positive $\dot{\alpha}$ curve in Fig. 22 directly affects the lift capability of the retreating blades of a rotor in forward flight. The apparent delay in stall results from the retreating blade increasing in angle of attack as it approaches its minimum dynamic pressure position thereby experiencing the favorable lift characteristics shown by Fig. 22. Precipitous stall to below the steady state value is avoided for many flight conditions because the blade moves into a more favorable angle of attack environment while undergoing its negative angle of attack change. An example of the effects of unsteady aerodynamics on performance is shown in Fig. 23. The full scale test results which were presented in Fig. 18 and compared to variable inflow theory are now compared to theory including unsteady aerodynamics. Improved performance correlation is indicated. The increased lift over that of the classical theory shown at the higher angles is attributable to two changes occurring on the rotor. The first is the direct increase in lift of the retreating blade due to the higher lift coefficients produced by the unsteady effects (Fig. 22), and the second is the higher advancing blade lift which accompanies the increment in lift of the retreating blade. This is simply a result of the trim requirement that the advancing and retreating blade flapping moments be equal. In addition, it's expected for most conditions that the advancing blade lift increment would be greater since its center of pressure is more inboard and requires higher lift to balance the retreating blade lift moment.

The influence of the combined effects of variable inflow and unsteady aerodynamics is significant in evaluating vibration and control loads. This is demonstrated in Fig. 24 where experimental blade root torsional moments, which are directly relatable to control loads, are compared to analytical torsional moments assuming unsteady aerodynamics with and without variable inflow. It is apparent that improved correlation is achieved when variable inflow is included. Although results assuming steady aerodynamics are not presented in Fig. 24, comparisons with the test data were made and showed poor correlation. The need for both unsteady aerodynamics and variable inflow to achieve the higher harmonic response present in the test data becomes more apparent when referring back to Fig. 20. Here the high frequency content of the section angle of attack (and its first derivative) is evident. As described earlier, the variable inflow effects were responsible for the high frequency content of angle of attack. However, the steady airfoil pitching moment data are essentially insensitive to high frequency angle of attack variations

below stall. It thus becomes apparent that variable inflow is required to produce the variations in angle of attack, and unsteady aerodynamic airfoil data are required to allow the blade to respond to these variations. Studies are continuing at United Aircraft to correlate other dynamic characteristics of rotors, such as airframe vibrations and noise, and it is believed the potential for improvements in these important areas has been significantly advanced with the addition of variable inflow and unsteady aerodynamics.

4. CONCLUDING REMARKS

Rotor inflow methods have advanced from the early momentum and vortex theories based on an infinite number of blades, to complex wake models in which the vorticity from each blade is analytically represented. The wake representations used in the inflow methods have progressed from undistorted to distorted wake models. The distorted wake models are either calculated by iterative procedures, in which the self-induced effects of the wake structure are included, or prescribed using empirical wake data. In addition to refining the distorted wake geometry, recent emphasis has been on lifting surface techniques, improved analytical simulation of blade-vortex interaction, and improved definition of the structure and stability of the blade tip vortex.

Experimental investigations employing model rotors and flow visualization techniques have revealed important wake characteristics of rotors in hovering flight. These characteristics, departing significantly from classical concepts of wake structure, have been found to strongly influence rotor performance. For example, the axial velocity of an element of the tip vortex from one blade is substantially constant prior to its passage beneath the following blade at which point the velocity increases to a new value. The initial velocity varies linearly with blade loading, and the secondary velocity varies as the square root of disc loading, in a fashion similar to the momentum inflow velocity. Accurate simulation of these wake parameters, particularly the initial vortex velocity, has been shown to be necessary to ensure reliable performance predictions.

In forward flight, the extent to which the wake influences rotor airloads and performance varies considerably with the parameters defining the rotor operating condition. In particular, wake effects generally decrease with increasing flight speed and nose down angle of attack. For forward flight conditions where the wake passes close to the rotor, accurate prediction of the wake distortions near the blades is required for establishing rotor stresses and vibration characteristics. The combined effects of variable inflow and unsteady aerodynamics significantly improve the calculation of blade torsional responses in forward flight. The improvements are related to the higher frequency content of blade section angle of attack produced by the variable inflow, and the resulting oscillatory pitching moments produced by the unsteady pitching moment data.

REFERENCES

1. Kussman, A., Survey of Different Models for Computing the Flow of a Lifting Rotor, Deutsche Luft- und Raumfahrt, DRL Mitteilung 70-19, Dec. 1970.
2. Wu, T. Y., Some Recent Developments in Propeller Theory, Office of Naval Research, U. S. Dept. Navy, Report No. 97.6, Feb. 1965.
3. Miller, R. H., Theoretical Determination of Rotor Blade Harmonic Airloads, Massachusetts Institute of Technology, TR 107-2, Aug. 1964.
4. Gessow, A., Review of Information on Induced Flow of a Lifting Rotor, NACA TN 3230, Aug. 1954.
5. Gilmore, D. C., An Evaluation of Methods for Predicting the Performance of Propellers Operating at Zero Advance Ratio, McGill Univ. (Montreal), Technical Note 67-2, Apr. 1967.
6. Rankine, W. J., On the Mechanical Principles of the Action of Propellers, Trans. Inst. of Naval Architects, Vol. 6, 1865.
7. Froude, R. E., On the Part Played in Propulsion by Difference of Fluid Pressure, Trans. Inst. of Naval Architects, Vol. 30, 1889.
8. Drzewiecki, S., Bull. de l'assoc. technique maritime, 1892.
9. Reissner, H., Zeitschrift für Mathematik, Vol. 1, 1910.
10. Glauert, H., A General Theory of the Autogyro, Aeronautical Research Council (Great Britain), R&M No. 1111, 1926.
11. Glauert, H., On the Vertical Ascent of a Helicopter, Aeronautical Research Council (Great Britain), R&M No. 1132, 1927.
12. Mangler, K. W. and Squire, H. B., The Induced Velocity Field of a Rotor, Aeronautical Research Council (Great Britain), R&M No. 2642, 1953.
13. Wood, E. R. and Hermes, M. E., Rotor Induced Velocities in Forward Flight by Momentum Theory, AIAA/AHS VTOL Research, Design, and Operations Meeting, AIAA Paper No. 69-264, Feb. 1969.
14. Knight, M. and Heber, R. A., Static Thrust Analysis of the Lifting Airscrew, NACA TN 626, Dec. 1937.
15. Coleman, R. P., Feingold, A. M., and Stempin, C. W., Evaluation of the Induced-Velocity Field of an Idealized Helicopter Rotor, NACA WR L-126, June 1945.
16. Castles, W. and DeLeeuw, J. H., The Normal Component of the Induced Velocity in the Vicinity of a Lifting Rotor and Some Examples of Its Application, NACA TR 1184, 1954.
17. Castles, W. and Durban, H. L., Distribution of Normal Component of Induced Velocity in Lateral Plane of a Lifting Rotor, NACA TN 3841, Dec. 1956.
18. Heyson, H. H. and Katzoff, S., Induced Velocities Near a Lifting Rotor With Nonuniform Disc Loading, NACA TR 1319, 1957.
19. Heyson, H. H., Equations for the Induced Velocities Near a Lifting Rotor With Nonuniform Azimuthwise Vorticity Distribution, NASA TN D-394, 1960.
20. Drees, J. M., A Theory of the Airflow Through Rotors and Its Application to Some Helicopter Problems, J. Helicopter Assoc. (Great Britain), Vol. 3, No. 2, July-Sept., 1949.
21. Wang Shi-Tsun, Generalized Vortex Rotor Theory, Problems of Helicopter Rotor Aerodynamics, U.S.S.R., 1961. (See also, Mil, M.L., Helicopters, Calculation and Design, NASA TT F-494, Sept. 1967.)
22. Baskin, V. E., Induced Velocities of a Propeller Exposed to Flow at an Angle to Its Axis, Report at the All-Union Congress on Theoretical and Applied Mechanics, Moscow, 1960. (See also, Mil, M.L., Helicopters, Calculation and Design, NASA TT F-494, Sept. 1967.)
23. Goldstein, S., On the Vortex Theory of Screw Propellers, Royal Society Proceedings, Vol. 123, 1929.
24. Betz, A., Screw Propellers With Minimum Loss of Energy, Nachrichten der K. Gesellschaft der Wissenschaften zu Göttingen, 1919.
25. Lock, C. N., Application of Goldstein's Airscrew Theory to Design, Aeronautical Research Committee (Great Britain), R&M No. 1377, Nov. 1930.

26. Willmer, W. A. P., The Loading of Helicopter Rotor Blades in Forward Flight, Aeronautical Research Council (Great Britain), RM No. 3318, 1963.
27. Molyneux, W. G., An Approximate Theoretical Approach for the Determination of Oscillatory Aerodynamic Coefficients for a Helicopter Rotor in Forward Flight, Aeronautical Quarterly, Vol. 13, Aug. 1962.
28. Loewy, R. G., A Two-Dimensional Approximation to the Unsteady Aerodynamics of Rotary Wings, *Jl. Aeronautical Sciences*, Vol. 24, No. 2, 1957.
29. Jones, J. P., An Actuator Disc Theory for the Shed Wake at Low Tip Speed Ratios, Intl. Automotive Engineering Congress, SAE Paper 960G, Jan. 1965.
30. Miller, R. H., On the Computation of Airloads Acting on Rotor Blades in Forward Flight, *Jl. American Helicopter Society*, Vol. 7, No. 2, April 1962.
31. Miller, R. H., Rotor Blade Harmonic Air Loading, *AIAA Jl.*, Vol. 2, No. 7, July 1964.
32. Miller, R. H., Unsteady Air Loads on Helicopter Rotor Blades, *Jl. Royal Aeronautical Society*, Vol. 68, No. 643, April 1964.
33. Harrison, J. M. and Ollerhead, J. B., The Nature of Limitations Imposed on the Performance of a Helicopter Rotor, *Jl. Sound Vib.*, Vol. 3, No. 3, 1966.
34. Funr, J. W. and Kussman, A., Calculation of the Induced Distribution of Velocity of a Rotor in Steady Forward Flight, *Deutsche Luft- und Raumfahrt, DLR-Mitteilung* 70-22, March 1970.
35. Jones, W. P. and Rao, B. M., Tip Vortex Effects on Oscillating Rotor Blades in Hovering Flight, *AIAA Jl.*, Vol. 9, No. 1, Jan. 1971.
36. Castles, W. and Durham, H. L., The Computed Instantaneous Velocities Induced at the Blade Axes by the Skewed Helical Vortices in the Wake of a Lifting Rotor in Forward Flight, Georgia Institute of Technology, ASTIA AD-210613, 1959.
37. Miller, N., Tang, J. C., and Perlmuter, A. A., Theoretical and Experimental Investigation of the Instantaneous Induced Velocity Field in the Wake of a Lifting Rotor, USAAVLABS Technical Report 67-68, Jan. 1968.
38. Piziali, R. A. and DuWaldt, F. A., Computation of Rotary Wing Harmonic Airloads and Comparison With Experimental Results, Proceedings 18th Annual Forum, American Helicopter Society, May 1962.
39. Piziali, R. A., Daughaday, H., and DuWaldt, F. A., Rotor Airloads, Proceedings CAL/TRECOM Symposium, June 1963.
40. Madden, P. A., Angle-of-Attack Distribution of a High Speed Helicopter Rotor, *Jl. American Helicopter Society*, Vol. 12, No. 2, 1967.
41. Scully, M. P., Approximate Solutions for Computing Helicopter Harmonic Airloads, Massachusetts Institute of Technology, TR 123-2, 1965.
42. Segel, L., A Method for Predicting Non-Periodic Airloads on a Rotary Wing, *Jl. Aircraft*, Vol. 3, No. 6, 1966.
43. Davenport, F. J., A Method for Computation of the Induced Velocity Field of a Rotor in Forward Flight, Suitable for Application to Tandem Rotor Configurations, *Jl. American Helicopter Society*, Vol. 9, No. 3, July 1964.
44. Balcerak, J. C., A Method for Predicting the Aerodynamic Loads and Dynamic Response of the Rotor Blades of a Tandem-Rotor Helicopter, USAAVLABS Technical Report 67-38, June 1967.
45. Ichikawa, T., Linear Aerodynamic Theory of Rotor Blades, *Jl. Aircraft*, Vol. 4, No. 3, May-June 1967.
46. Nelson, D. M., A Lifting-Surface Propeller Design Method for High-Speed Computers, U. S. Naval Ordnance Test Station, NAVWEPS Report 8442, June 1964.
47. Hough, G. R., A Numerical Study of the Fluctuating Flowfield of a Uniformly Loaded Propeller, *Jl. Aircraft*, Vol. 4, No. 1, Jan.-Feb. 1967.
48. Mandl, P., Analytic Determination of the Axial Velocity Through a Propeller Moving Perpendicular to Its Axis, Specialists Meeting of the Fluid Dynamics Panel of AGARD on Fluid Dynamics of Rotor and Fan Supported Aircraft at Subsonic Speeds, Göttingen, Sept. 1967.
49. Carlson, R. G. and Hiltzinger, K. D., Analysis and Correlation of Helicopter Rotor Blade Response in a Variable Inflow Environment, USAAVLABS TR 65-51, 1965.
50. Piziali, R. A., Method for the Solution of the Aeroelastic Response Problem for Rotating Wings, *Jl. Sound and Vibration*, Vol. 4, No. 3, 1966.
51. Brandt, D. E., Investigation of Rotor Blade Dynamics During Equilibrium Transition Flight, M.S. Thesis, Massachusetts Institute of Technology, June 1962.
52. Ham, N., An Experimental Investigation of the Effect of a Non-Rigid Wake on Rotor Blade Airloads in Transition Flight, Proceedings CAL/TRECOM Symposium, Vol. I, June 1963.
53. Brady, W. G. and Crimi, P., Representation of Propeller Wakes by Systems of Finite Core Vortices, Cornell Aeronautical Lab. Report No. BB-1605-S-2, Feb. 1965.
54. Trenka, A. R., Development of a Method for Predicting the Performance and Stresses of VTOL-Type Propellers, USAAVLABS Technical Report 66-26, June 1966.
55. Greenberg, M. D. and Kaskel, A. L., Inviscid Flow Field Induced by a Rotor in Ground Effect, NASA CR-1027, May 1968.
56. Landgrebe, A. J., An Analytical and Experimental Investigation of Helicopter Rotor Hover Performance and Wake Geometry Characteristics, USAAMRDL Technical Report 71-24, Eustis Directorate, U. S. Army Air Mobility Research and Development Laboratory, Fort Eustis, Va., June 1971.
57. Theodoresen, T. T., Theory of Static Propellers and Helicopter Rotors, 25th Annual Forum, American Helicopter Society, No. 326, May 1969.
58. Erickson, J. C., Ladden, R. M., Borst, H. V., and Ordway, D. E., A Theory for VTOL Propeller Operation in a Static Condition, USAAVLABS Technical Report 65-69, Oct. 1965.
59. Erickson, J. C., Theoretical and Experimental Investigations of V/STOL Propeller Operation in a Static Condition, USAAVLABS Technical Report 69-55, Oct. 1969.
60. Jorglar, M. and Loewy, R., An Actuator-Disc Analysis of Helicopter Wake Geometry and the Corresponding Blade Response, USAAVLABS Technical Report 69-66, Dec. 1970.
61. Vaskin, V. E., Motion of a Three-Dimensional Diffusing Vortex Tube in an Incompressible Viscous Fluid, *Soviet Physics*, Vol. 10, No. 12, June 1966.
62. Levinsky, E. S. and Strand, T., A Method for Calculating Helicopter Vortex Paths and Wake Velocities, Air Force Flight Dynamics Laboratory, Technical Report AFFDL-TR-69-113, July 1970.
63. Landgrebe, A. J., An Analytical Method for Predicting Rotor Wake Geometry, *Jl. American Helicopter Society*, Vol. 14, No. 4, Oct. 1969.
64. Landgrebe, A. J. and Bellinger, E. D., An Investigation of the Quantitative Applicability of Model Helicopter Rotor Wake Patterns Obtained From a Water Tunnel, USAAMRDL Technical Report 71-69, Eustis Directorate, USAAMRDL, Dec. 1971.
65. Clark, D. R. and Landgrebe, A. J., Wake and Boundary Layer Effects in Helicopter Rotor Aerodynamics, AIAA 4th Fluid and Plasma Dynamics Conference, AIAA Paper No. 71-581, June 1971.
66. Bellinger, E. D., Analytical Investigation of the Effects of Blade Flexibility, Unsteady Aerodynamics, and Variable Inflow on Helicopter Rotor Stall Characteristics, NASA CR-1769, Sept. 1971.
67. Landgrebe, A. J., The Wake Geometry of a Hovering Helicopter Rotor and Its Influence on Rotor Performance, 28th Annual Forum, American Helicopter Society, May 1972. (Also, to be published in *AHC Jl.*, Oct. 1972.)
68. Crimi, P., Prediction of Rotor Wake Flows, CAL/USAAVLABS Symposium Proceedings, Vol. 1, June 1966.
69. Scully, M. P., A Method of Computing Helicopter Vortex Wake Distortion, Massachusetts Institute of Technology, ASRL TR 138-1, June 1967.
70. Sadler, S. G., A Method for Predicting Helicopter Wake Geometry, Wake-Induced Flow and Wake Effects on Blade Airloads, 27th Annual Forum -- American Helicopter Society, Preprint No. 523, May 1971.
71. Clark, D. R. and Leiper, A. C., The Free Wake Analysis - A Method for the Prediction of Helicopter Rotor Hovering Performance, 25th Annual Forum of the American Helicopter Society, Preprint No. 321, May 1969.
72. Gray, R. B., On the Motion of the Helical Vortex Shed from a Single-Bladed Hovering Helicopter Rotor and Its Application to the Calculation of the Spanwise Aerodynamic Loading, Princeton Univ. Aero Engineering Dept. Report No. 313, Sept. 1955.
73. Gray, R. B., An Aerodynamic Analysis of a Single-Bladed Rotor in Hovering and Low Speed Forward Flight as Determined From Smoke Studies of the Vorticity Distribution in the Wake, Princeton Univ. Aero. Engineering Dept. Report No. 356, Sept. 1956.
74. Gartshore, I. S., An Application of Vortex Theory to Propellers Operating at Zero Advance Ratio, McGill Univ. (Montreal), Technical Note 66-3, June 1966.

75. Rorke, J. B. and Wells, C. D., The Prescribed Wake-Momentum Analysis, Proceedings Third CAL/AVLABS Symposium, Vol. I, June 1969.
76. Magee, J. P., Haisel, M. D., and Davenport, F. J., The Design and Performance Prediction of Propeller/Rotors for VTOL Applications, 25th Annual Forum, American Helicopter Society, No. 325, May 1969.
77. Seed, A. R., Rotor Induced Flow, Specialists Meeting of the Fluid Dynamics Panel of AGARD, Fluid Dynamics of Rotor and Fan Supported Aircraft at Subsonic Speeds, Göttingen, Sept. 1967.
78. Jenney, D. J., Olson, J. R., and Landgrebe, A. J., A Reassessment of Rotor Hovering Performance Prediction Methods, J1. American Helicopter Society, Vol. 13, No. 2, April 1968.
79. Ladden, R. M. and Gilmore, D. C., Advanced V/STOL Propeller Technology, Static Thrust Prediction Method Development, Air Force Flight Dynamics Laboratory, AFFDL-TR-71-88, Vol. II, Sept. 1971.
80. Tararane, S. and Delest, M., Experimental and Theoretical Study of Local Induced Velocities Over a Rotor Disc for Analytical Evaluation of the Primary Loads Acting on Rotor Blades, European Research Office, U. S. Dept. Army, Report No. DE 2012, Oct. 1960.
81. Isay, W. H., A Vortex Model for the Analysis of the Flow at the Rotor Blade of a Helicopter, Inst. of Ship Design, Univ. of Hamburg, Report No. 872, July 1971.
82. Lehman, A. F., Model Studies of Helicopter Rotor Flow Patterns in a Water Tunnel, 24th Annual Forum American Helicopter Society, Paper No. 207, May 1968.
83. Kerwin, J. E., The Solution of Propeller Lifting-Surface Problems by Vortex Lattice Methods, Ph.D. Thesis, Massachusetts Institute of Technology, 1961.
84. Cummings, D. E. and Kerwin, J. E., Propeller Wake Deformation Due to Instability of a Trailing Vortex Sheet, Proceedings Third CAL/AVLABS Symposium, Vol. I, June 1969.
85. Murray, J. C., A Computerized Design Method for Prediction of Propeller Static Performance, UARL Report for Air Force Aero Propulsion Laboratory (to be published).
86. Jones, J. P., An Extended Lifting Line Theory for the Loads on a Rotor Blade in the Vicinity of a Vortex, Massachusetts Institute of Technology, Technical Report 123-3, Dec. 1965.
87. Simons, I. A., Some Aspects of Blade/Vortex Interaction on Helicopter Rotors in Forward Flight, J1. Sound Vibrations, Vol. 4, No. 3, 1966.
88. Johnson, W., A Lifting Surface Solution for Vortex Induced Airloads and Its Application to Rotary Wing Airloads Calculations, Massachusetts Institute of Technology, ASRL TR 153-2, April 1970.
89. Adamczyk, J. J., Passage of an Airfoil Through a Three-Dimensional Disturbance, Ph.D. Thesis, Univ. of Connecticut, May 1971.
90. McCormick, B. W., Tangler, J. L., and Sherrieb, H. E., Structure of Trailing Vortices, J1. Aircraft, Vol. 5, No. 3, May-June 1968.
91. Chigier, N. A. and Corsiglia, V. R., Tip Vortices - Velocity Distributions, 27th Annual Forum American Helicopter Society, May 1971.
92. Rorke, J. B. and Moffitt, R. C., Wind Tunnel Simulation of Full Scale Vortices, 28th Annual Forum American Helicopter Society, May 1972.
93. Bellinger, F. D., Experimental Investigation of Effects of Blade Section Camber and Planform Taper on Rotor Hover Performance, USAAMRDL Technical Report 72-4, March 1972.
94. Tanner, W. H. and Wahfield, R. M., Vortex Field, Tip Vortex, and Shock Formation on a Model Propeller, Proceedings of Third CAL/AVLABS Symposium, Vol. I, June 1969.
95. Carta, F. O. and Niebanck, C. F., Prediction of Rotor Instability at High Forward Speeds, Vol. III, USAAVLABS Technical Report 68-18c, Feb. 1969.

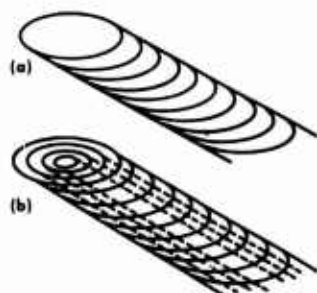


Fig. 1 Cylindrical Wake Model

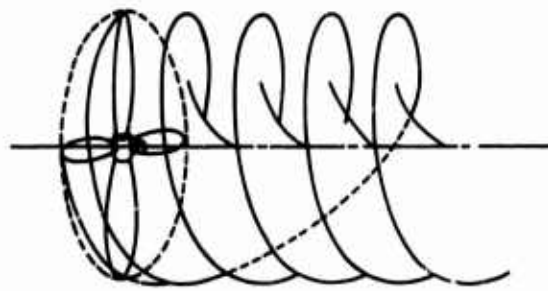
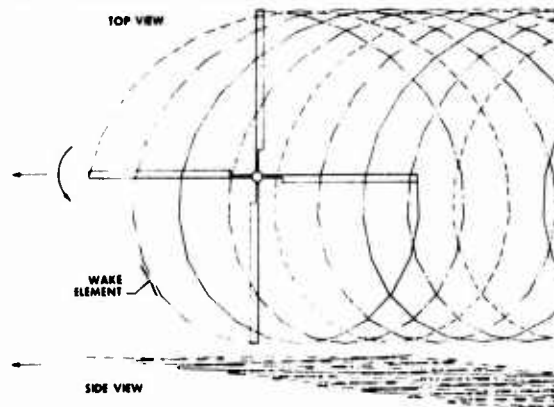
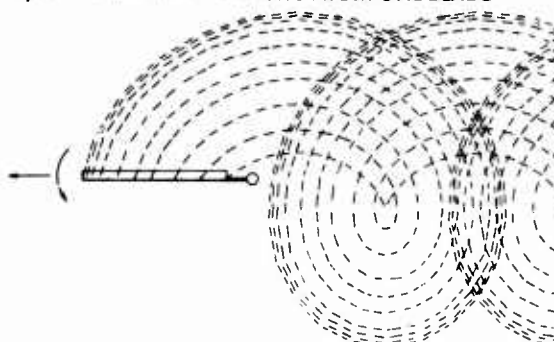


Fig. 2 Goldstein's Propeller Wake Model

a) TIP FILAMENTS FROM FOUR BLADES



b) ALL TRAILING FILAMENTS FROM ONE BLADE



c) SHED FILAMENTS FROM ONE BLADE

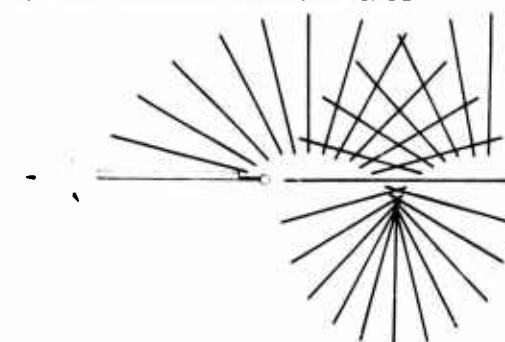


Fig. 3 Rotor Undistorted Wake Model

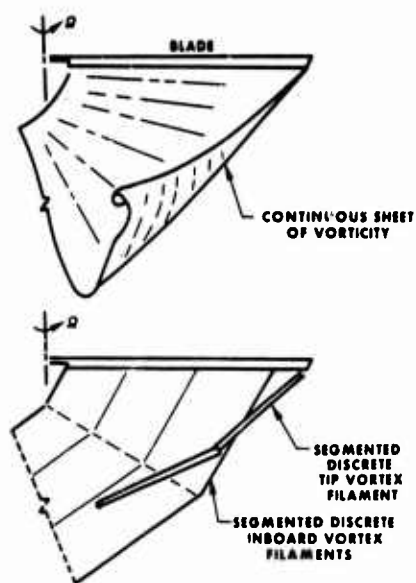


Fig. 1. Analytical Representation of Rotor Wake

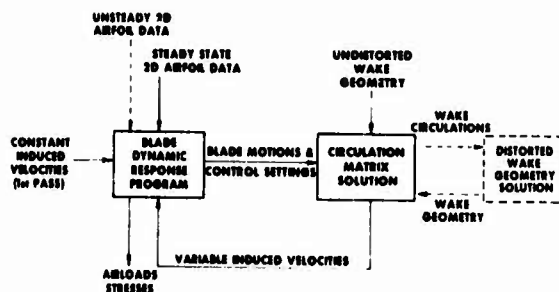


Fig. 5 UARL Rotor Aeroelastic Performance Method

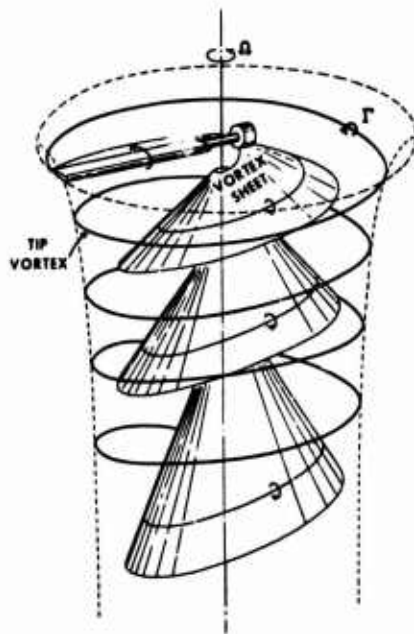


Fig. 6 Schematic of Hovering Rotor Wake Structure

EXPERIMENTAL WAKE CLASSICAL WAKE

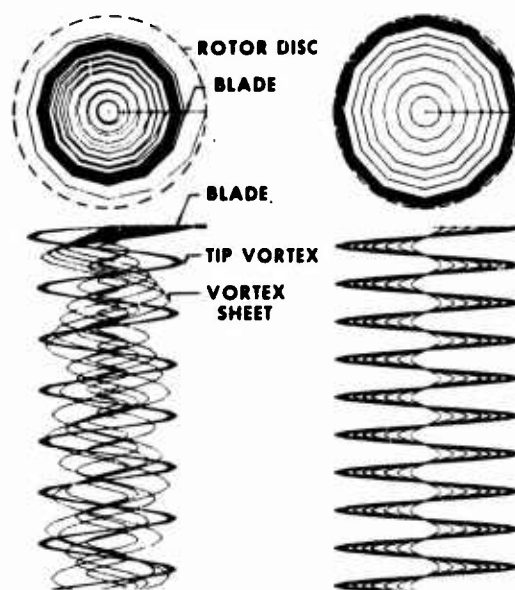


Fig. 7 Computer Wake Patterns for One Blade

EXPERIMENT

○ —

THEORY

□ — GOLDSTEIN-LOCK ANALYSIS

△ — MOMENTUM ANALYSIS

◇ — PRESCRIBED CLASSICAL WAKE ANALYSIS

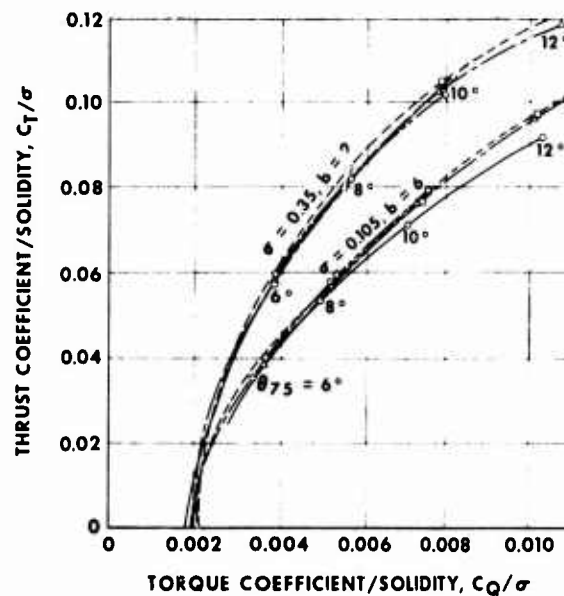


Fig. 8 Comparison of Results of Uncontracted Wake Analyses With Experimental Performance Results for Two- and Six-Bladed Model Rotors

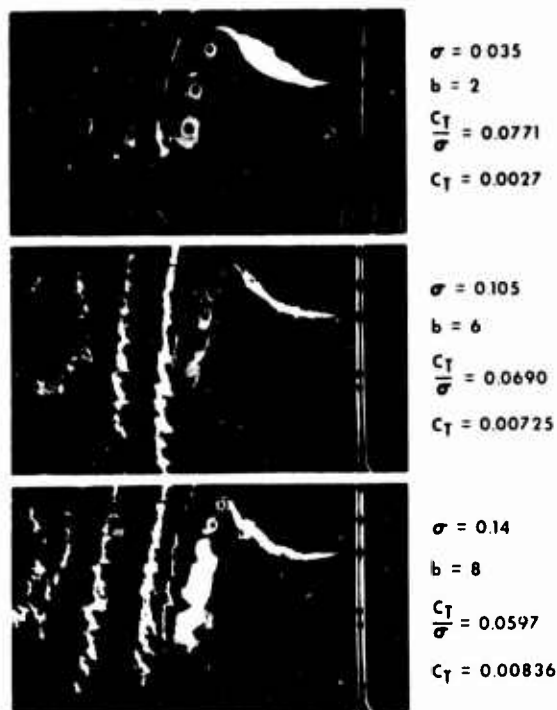


Fig. 9 Photographs Showing Effect of Number of Blades and Thrust Level on Wake Geometry

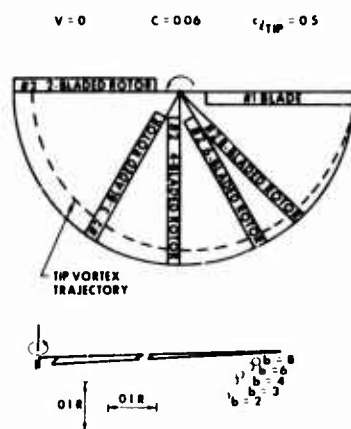


Fig. 10 Effect of Number of Blades on Tip Vortex Position Under Following Blade

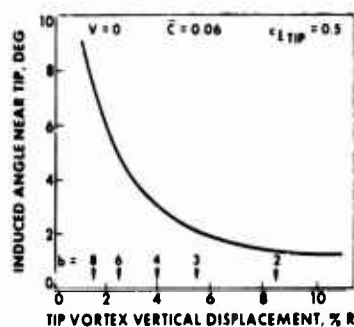


Fig. 11 Induced Angle Due to Blade-Vortex Interference

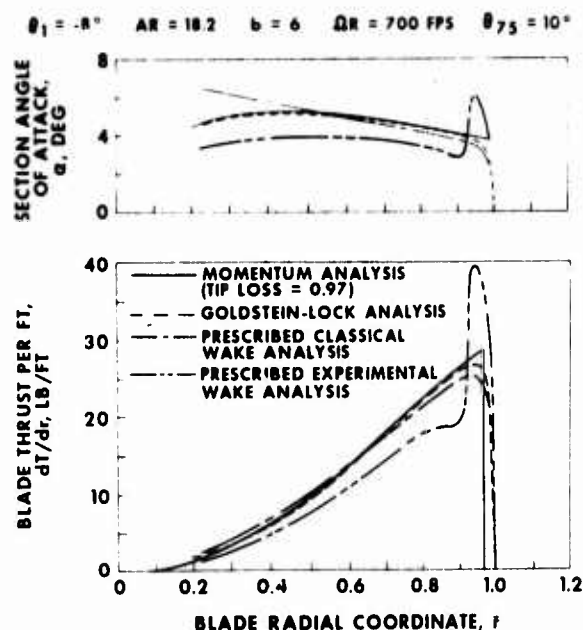


Fig. 12 Comparison of Model Rotor Blade Section Characteristics as Predicted by Various Analyses

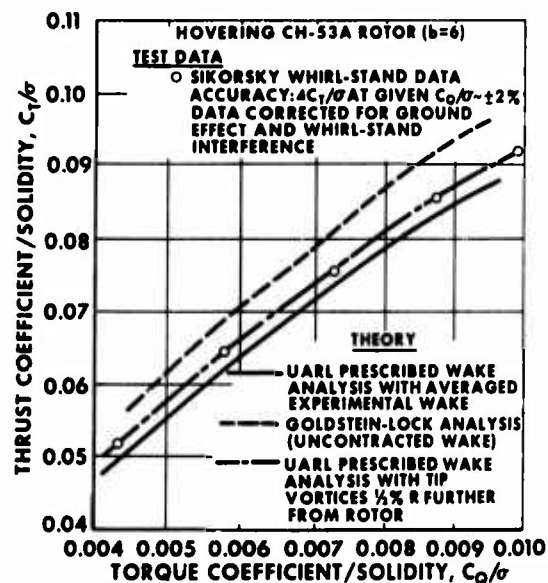


Fig. 13 Effect of Wake Geometry on Predicted Rotor Hover Performance and Comparison With Experiment

$$C_T/\sigma = 0.08$$

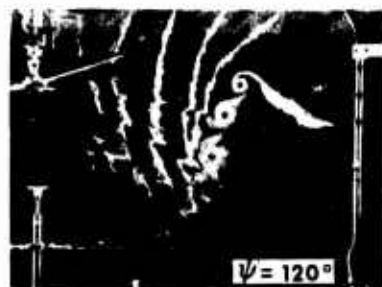


Fig. 14 Sequence of Photographs Showing Time History of Wake

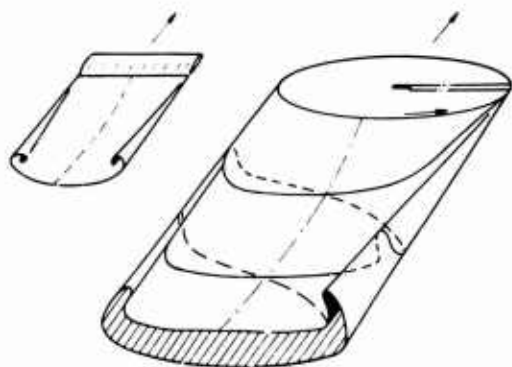


Fig. 15 Schematic of Rotor and Fixed-Wing Wakes

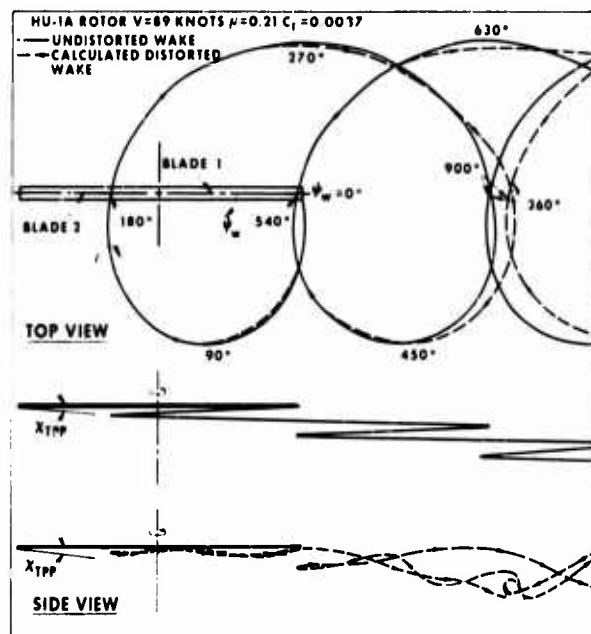


Fig. 16 Theoretical Wake Pattern From One Blade of a Rotor in Forward Flight

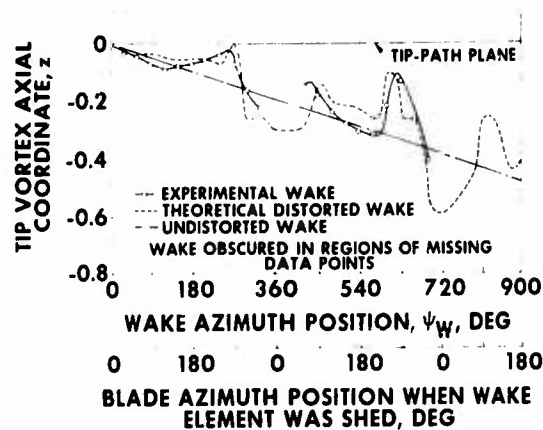


Fig. 17 Comparison of Experimental and Theoretical Wake Axial Coordinates
-- Model Rotor, Simulated 90 kt,
10,000 lb Lift

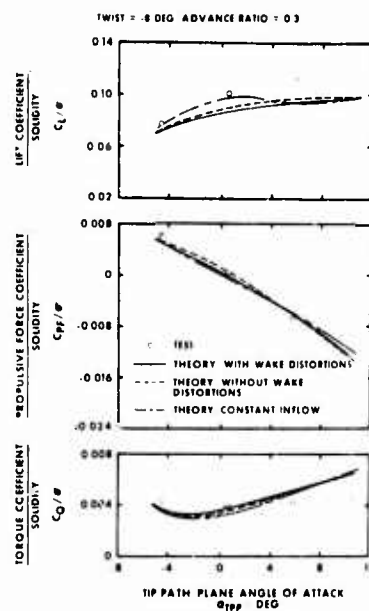


Fig. 18 Effect of Variable Inflow on Rotor Performance With Steady Aerodynamics

POSITIVE UPFLOW NORMAL TO TIP PATH PLANE IN FT/SEC
 $\theta_{75} = 8 \text{ DEG}$
 $\theta_1 = -8 \text{ DEG}$
 $V = 117 \text{ KNOTS}$
 $\alpha_{TTP} = -5.1 \text{ DEG}$

NOTE: INDUCED VELOCITY FOR CONSTANT INFLOW CONDITION = -4.2 FT/SEC

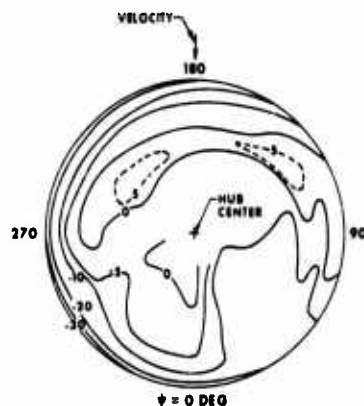


Fig. 19 Induced Velocity Distribution Based on Distorted Wake

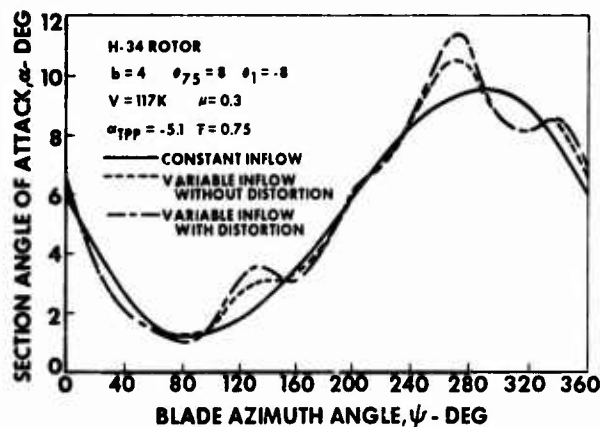


Fig. 20 Effect of Variable Inflow on Blade Section Angle of Attack

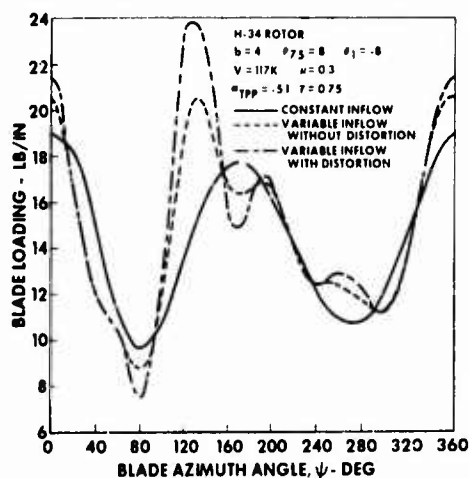


Fig. 21 Effect of Variable Inflow on Blade Section Loading

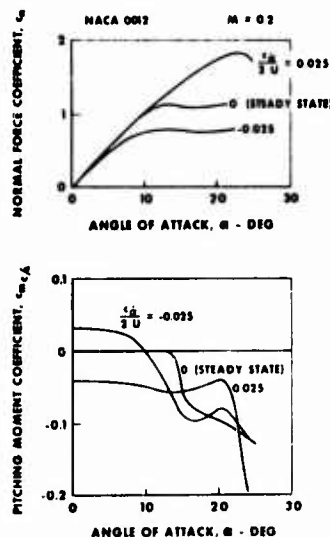


Fig. 22 Sample of Generalized Unsteady Data

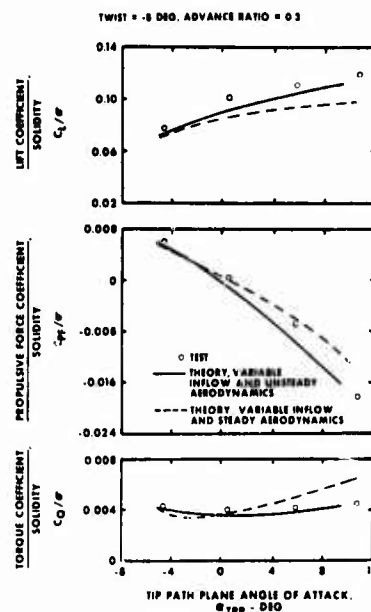


Fig. 23 Effect of Unsteady Aerodynamics on Rotor Performance

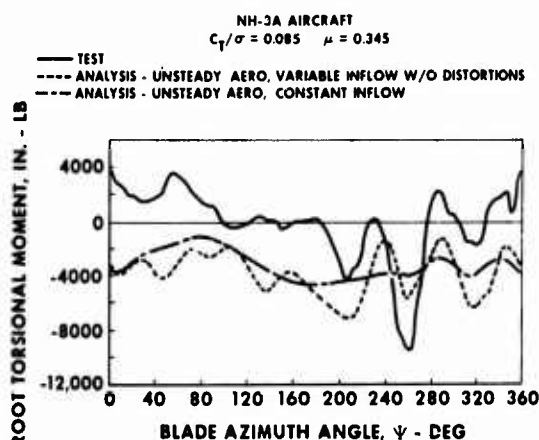


Fig. 24 Effect of Unsteady Aerodynamics and Variable Inflow on Blade Torsional Moments

POSITIVE UPFLOW NORMAL TO TIP PATH PLANE IN FT/SEC

$$\begin{aligned}\theta_{75} &= 8 \text{ DEG} \\ \theta_1 &= -8 \text{ DEG} \\ V &= 117 \text{ KNOTS} \\ \sigma_{TPP} &= -5.1 \text{ DEG}\end{aligned}$$

NOTE: INDUCED VELOCITY FOR CONSTANT INFLOW CONDITION = -4.2 FT/SEC

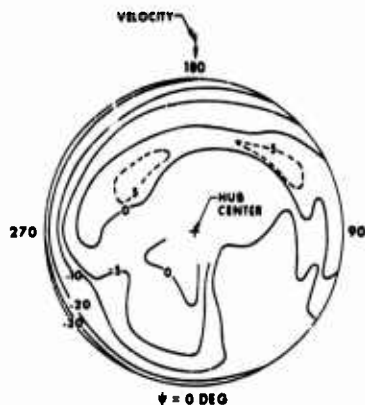


Fig. 19 Induced Velocity Distribution Based on Distorted Wake

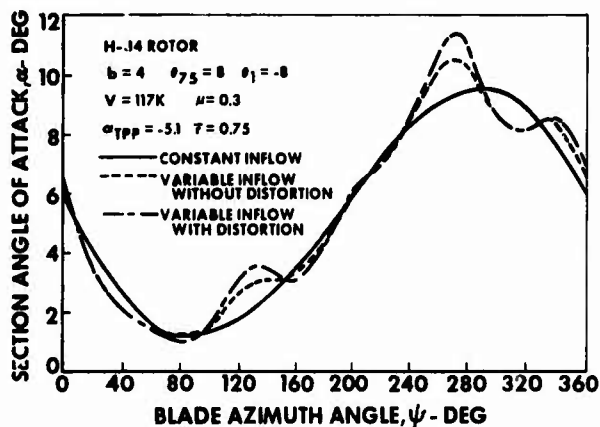


Fig. 20 Effect of Variable Inflow on Blade Section Angle of Attack

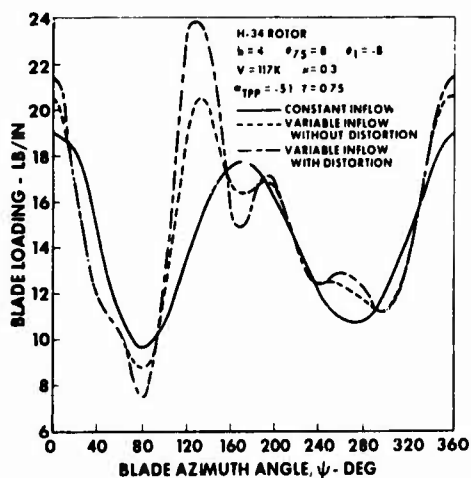


Fig. 21 Effect of Variable Inflow on Blade Section Loading

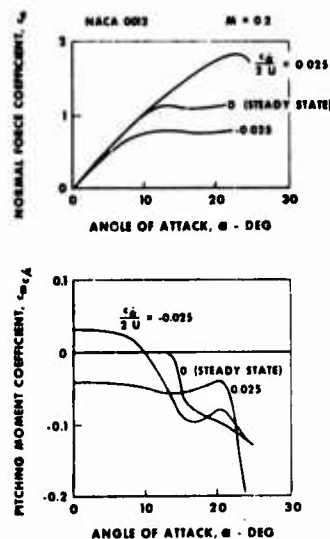


Fig. 22 Sample of Generalized Unsteady Data

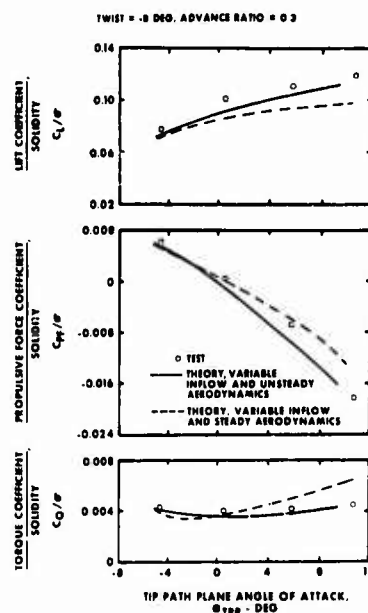


Fig. 23 Effect of Unsteady Aerodynamics on Rotor Performance

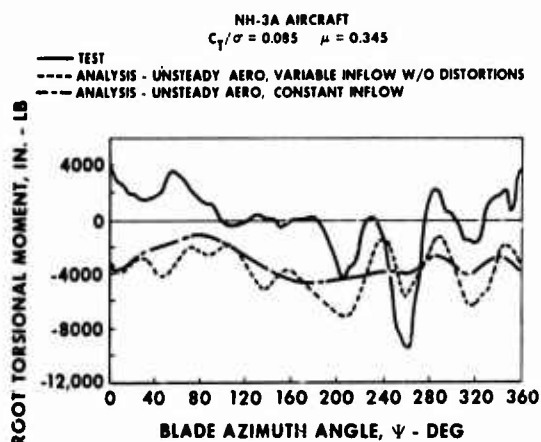


Fig. 24 Effect of Unsteady Aerodynamics and Variable Inflow on Blade Torsional Moments

Prepared Comments on Paper 1

by
J.P. Jones
Westland Helicopters Ltd
Yeovil, Somerset, UK

My first task is to congratulate Mr Landgrebe and Mr Cheney on their excellent paper. They have provided a comprehensive review of a difficult subject and their bibliography will be an indispensable source of reference for many years. And of course the authors themselves have made a considerable contribution to the subject. Therefore I hope they will not object if, in order to promote specialist discussion now and perhaps to give a lead to the later round table discussion, I question their paper in detail and what they are doing in principle.

One of the items which worries me is the treatment of vorticity. The Biot-Savart law is assumed, although the fluid is certainly compressible and it is often necessary to resort to some computing tricks, such as a finite core size or a limiting velocity, to make the wake patterns converge.

I was struck by (Section 2.5) the slight emphasis given to blade-vortex interaction and lifting surface theories, even though the interference between one vortex and a succeeding blade is the essence of the hover problem. Also could not this interaction be a source of the blade pitching moments?

Despite your claims in the paper I don't think that the combination of variable inflow and non-steady aerodynamics really explains the differences between the measured and calculated torsional moments which are shown in Figure 24. It is a step in the right direction but the remaining errors in amplitude and phase are large and, I suspect, the mean values are of opposite sign. I would suggest that some other phenomenon is present, perhaps an unusual dynamic response or inaccurate measurement.

Turning now from the details to the matter of principle I think it would be well to try to establish, during this meeting, just what the future of rotor wake studies should be. The authors have made it clear that the biggest influence on performance occurs in the hover and that in forward flight the wake mainly affects vibration and noise. (Even this cannot be clearly demonstrated; noise is determined by harmonics very much higher than the fifth and a study of a high speed helicopter has shown that the important vibration is largely unaffected by inflow variations.)

It may be therefore that there is little more to come from further, deeper studies of the wake.

Perhaps I should say that I am not playing devils advocate. I have a personal liking for this branch of the subject which is absorbing and should have special place for helicopter engineers because it has done more than anything else to start off and maintain a fundamental interest in rotor aerodynamics. But I sometimes feel that resources of money and intellect may be wrongly allocated to such studies. By the end of the meeting I would like to be convinced one way or the other.

AN ACTUATOR DISC THEORY FOR ROTOR WAKE INDUCED VELOCITIES

by

Robert A. Ormiston
U. S. Army Air Mobility R&D Laboratory
Ames Directorate
Moffett Field, California 94035, USA

SUMMARY

A general actuator disc theory is presented for predicting the time-averaged downwash distribution, and steady state force and moment response characteristics of helicopter rotors in forward flight. Particular attention is given to a proper definition of the rotor potential flow problem. The formulation of the theory is conceptually based on classical fixed-wing lifting-line theory to enhance its versatility and provide insight about the complex physical features of the rotor downwash distribution. The method of solution expresses the rotor downwash in a Fourier series where the coefficients are given as a summation of influence functions. It is shown that the rotor wake vorticity can be assumed to lie in a flat planar wake for a wide range of flight conditions, thus simplifying the Biot-Savart integration for the downwash. The vorticity elements in the flat planar wake are decomposed into simple circular and linear elements to further simplify the integrations. The quantitative results presented are preliminary and are limited to the downwash and influence functions for each element of vorticity for a specified rotor circulation distribution. The downwash distributions are then superimposed to illustrate the variation of downwash with advance ratio for uniform rotor circulation. The results show nonuniformities and lateral asymmetries of the downwash that were not revealed by previous analyses.

NOTATION

a	two dimensional lift curve slope	U_P, U_T	blade velocity components, Eq. (5)
a_n, b_n	blade flapping coefficients	$U_{c_i}^n, U_{s_i}^n$	cosine downwash influence functions, Eq. (13)
A_{c_n}, A_{s_n}	circulation integrals, Eq. (18)	V	velocity
b	number of blades	$V_{c_i}^n, V_{s_i}^n$	sine downwash influence functions, Eq. (13)
B_{c_n}, B_{s_n}	circulation integrals, Eq. (22)	w	induced velocity normal to disc
c	blade chord, per blade	x, y	rotor coordinates, Fig. 9
C_T, C_l, C_m	thrust, roll, and pitch moment coefficients	α	rotor shaft or airfoil angle of attack
$C_{c_i}^n, D_{c_i}^n$	downwash integrals, Eq. (18)	β	rotor blade flapping angle
$E_{c_i}^n, F_{c_i}^n$	downwash integrals, Eq. (34)	γ	lock number, $\rho acR^4/I$
I	blade flapping inertia	$\gamma_c, \gamma_s, \gamma_l, \gamma_r$	wake vorticity elements
I_{c_n}, I_{s_n}	circulation integrals, Eq. (25)	$\Gamma, \Gamma_{s_n}, \Gamma_{c_n}$	harmonics of bound circulation
K_o, K_{c_1}, K_{s_1}	downwash constants	η	dimensionless lateral coordinate, y/R
K_β	blade flapping spring constant	$\theta, \theta_o, \theta_s, \theta_c$	blade angle, collective and cyclic pitch
l	lift per unit length	$\lambda, \lambda_{c_n}, \lambda_{s_n}$	dimensionless induced velocity $\lambda = w/R\Omega$
L, M	rotor roll and pitch moment	μ	advance ratio, $\mu = U_\infty/R\Omega$
p	dimensionless flap frequency	ξ	dimensionless longitudinal coordinate, x/R
r	rotor radial coordinate	ρ	air density, dimensionless radial coordinate, r/R
R	rotor radius	σ	rotor solidity, $bc/\pi R$
T	rotor thrust	ϕ	induced angle of attack $\phi = U_I/U_T$
u^n, v^n	downwash coefficients, Eq. (12)	$\phi_{s_n}(\rho), \phi_{c_n}(\rho)$	circulation distribution functions, Eq. (10)
U_∞	free stream velocity		

χ wake skew angle
 ψ rotor azimuth angle

Ω rotor angular velocity
 $(-)$ nondimensionalized by $R\Omega$ for velocities,
 $abcR\Omega$ for circulation

1. INTRODUCTION

The problem of theoretically calculating the downwash distribution of helicopter rotors in forward flight continues to be an important focus for rotary-wing research, particularly as advanced rotor types are introduced and flight speeds increase. Notwithstanding the sophistication of present numerical techniques for predicting the complex rotor downwash field, a need exists for simpler but rigorous analytic techniques which will aid in understanding and interpreting the complex relationships between rotor circulation, downwash, and blade motion. In particular, the steady-state force and moment response characteristics of hingeless rotors are strongly influenced by the lower harmonics of nonuniformities in the downwash distribution. A natural approach is to apply the highly successful concepts of classical fixed-wing lifting-line theory to the helicopter rotor, but, somewhat surprisingly, this has not been fully attempted to date. Therefore, the present paper seeks to arrive at an appropriate problem definition, tailored to the prediction of rotor downwash and response characteristics, and provide an appropriate theory for treating this problem.

2. DISCUSSION OF THE PROBLEM

A general actuator disc theory must include a certain minimum number of factors to adequately represent the important physical processes which influence the rotor downwash distribution. The basic problem is to properly relate the bound circulation distribution at the rotor disc to the velocity field induced by that bound circulation and its associated wake vorticity. Equally important for actual rotors is the inclusion of rotor blade flapping motion dynamics. This implies that the theory must address simultaneous solutions of the appropriate equations governing these three unknown quantities, the circulation distribution, downwash distribution, and the blade flapping motion. The independent variables are configuration parameters such as blade planform geometry and twist, collective and cyclic pitch, shaft angle of attack, and advance ratio. Rotor thrust coefficient must be included for low advance ratios as it influences the wake skew angle.

Inherent in this problem definition are approximations which are acceptable within the limits of application of the theory, i.e., determination of rotor forces and moments required for basic performance and control analyses. The actuator disc replaces the actual rotor blades with an infinite number of blades which distribute the bound circulation continuously over the rotor disc. Although the vortex wake of actual rotors consists of a sheet of vorticity for each individual blade which rolls up into a viscous-core tip vortex, the wake vorticity of the actuator disc is continuously distributed within the volume of fluid which has passed through the rotor disc, and wake distortion due to the effects of self-induction is ignored. The general actuator disc theory can therefore be characterized as a rotor potential flow theory where certain restrictions are applied to the wake configuration. A skewed cylindrical region is most commonly used for the wake vorticity, although a flat planar wake may also be appropriate for certain operating conditions. The rotor circulation and downwash are related to one another by invoking the lifting-line assumption and neglecting the unsteady aerodynamics of the near shed wake. This is consistent with actuator disc theory since as the blade number becomes infinite the chord length vanishes and hence the reduced frequency ($k = \omega c / 2v$) also vanishes. Except for predicting detailed rotor blade airloads, vibrations, and acoustic properties, these approximations are not unreasonable and a general actuator disc theory should be capable of yielding highly accurate results for rotor response.

Conceptually, the general actuator disc problem defined above is a direct counterpart for rotary-wings of Prandtl's classical lifting-line theory for finite span fixed wings. The similarity of the various elements can best be

illustrated by the diagrams in Fig. 1 which trace the sequential relationship of circulation, vorticity, and downwash. Except for the existence of blade motion, the actuator disc problem contains elements identical to finite-wing lifting-line theory. They are complicated, however, by the periodic relative velocity experienced by the rotor blade in forward flight, and the increased complexity of the wake vorticity distribution caused by the circular motion of the rotor blades and the azimuthal and radial gradients of bound circulation.

The primary advantage of classical lifting-line theory derives mainly from its ability to provide insight and understanding about the effects of wing configuration on the spanwise loading and downwash and the wing induced drag. It is also a simple and versatile tool for calculating finite-wing characteristics, and many results can be generalized in terms of basic configuration parameters like aspect ratio and taper ratio. It is felt that these features are equally important for rotary wing analyses and that a generalized actuator disc theory would be highly useful.

Present techniques for computing the induced velocity field of helicopter rotors rely almost exclusively

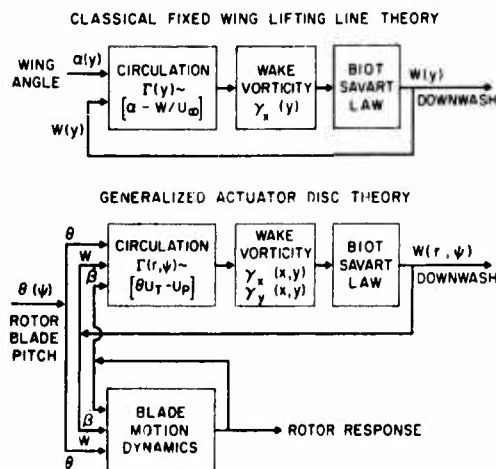


Figure 1. Corresponding potential flow problems for fixed and rotary wings.

on discrete vortex filament methods which are based on extensive digital computation (ref. 1-4). These techniques are necessary when detailed aerodynamic, vibratory, and acoustic results are required and they include the mutual interaction of the circulation distribution, downwash, and blade motion. However, because of the extensive numerical computations involved, they afford only limited physical insight, and lack the versatility of simpler methods. Therefore, they are not fully justifiable for predicting basic rotor response characteristics. These drawbacks can be partly attributed to the use of discrete vortex filaments for the wake in contrast to the continuous vorticity of classical lifting-line theory. It is felt that to obtain comparable simplicity and insight, a continuous wake method such as actuator disc theory must be used. A concise comparison of traits of the two analysis techniques is presented in Table 1.

Table 1. Comparison of two conceptual approaches to the rotor potential flow/response problem.

Characteristic \ Approach	Actuator disc continuous wake	Finite element, discrete vortex filaments
Wake geometry	Skewed cylinder or flat planar	Determined by mutual self induction
Range of applicability	Rotor forces and moments	Rotor forces, moments, blade loads, vibration, acoustics
Complexity, computation requirements	Low to moderate	High
Versatility, insight	High	Low

The solution for the present general theory is based on expanding the unknown variables in appropriate Fourier series in the blade azimuth angle, and solving the resulting equations using the harmonic balance method. That is, the coefficients of each of the sine and cosine harmonics for each equation are collected and equated, yielding a set of linear algebraic equations. Fundamental to this approach is expressing each Fourier harmonic of the downwash distribution as a linear combination of all the Fourier harmonics of the circulation distribution. The coefficient of each circulation harmonic is therefore an influence function [of the rotor radius] of the downwash distribution. The influence functions are determined by application of the familiar Biot-Savart law to the wake vorticity generated by individual harmonics of the circulation distribution. The resulting downwash distribution is then Fourier analyzed to obtain the influence functions. After determining the rotor circulation distribution from the harmonic balance method, the downwash distribution is obtained by appropriately weighting and then superimposing the various influence functions. The rotor response forces and moments may be obtained from either the blade motion or integration of the circulation distribution.

The major attraction of this approach is that the most difficult part of the problem, the Biot-Savart integral equation, can be solved independently for a series of rotor circulation distributions to yield the corresponding downwash influence functions. These functions need only be evaluated once, and the downwash for any rotor or flight condition may be obtained by merely solving the relatively simple harmonic balance equations. The influence functions themselves will also provide detailed insight into the structure of rotor downwash by identifying the specific contributions from each type of circulation distribution. While not a primary rotor response characteristic, the induced drag of helicopter rotors is an intriguing aerodynamic problem. Because of the continuous nature of the vorticity and downwash distributions of a combined actuator disc, lifting-line formulation, it should be feasible to rigorously investigate rotor induced drag characteristics. Although the elegance of the induced drag relations for fixed-wing lifting-line theory, in particular the minimum drag criterion, may not be attainable for the rotating wing, it may be possible to develop some useful analytical relationships to guide efforts for drag reduction.

Although the definition of the present actuator disc problem is relatively straightforward, being a natural extension of classical lifting-line theory to rotary wings, previous actuator disc theories have not usually been addressed to the general problem. Principally, the work of refs. 5-7 has been restricted to determination of the downwash in the longitudinal and lateral planes of symmetry of the rotor, for azimuthally constant circulation. Results for the entire rotor disc are presented in ref. 8. However, the contributions of certain wake elements are not included in the downwash. An azimuthally varying circulation distribution is extensively treated in ref. 9, however, results are restricted to the lateral plane of symmetry and again certain contributions to the downwash were not included. When viewed in the framework of the general actuator disc problem, these results represent a first step in determining the required influence functions, since the downwash contribution from all elements of the wake vorticity is required on the entire disc before the Fourier analysis can be performed. A limited number of other methods, refs. 10-11, based on, or similar to, actuator disc theory have been published, but for various reasons they do not fully satisfy the above problem definition.

The solution of the elementary rotor blade flapping equation for rotor response is traditionally carried out by harmonic balance assuming a uniform distribution of induced velocity. As an extension of these methods, several efforts have been made in refs. 12-14 to incorporate certain arbitrarily specified downwash distributions. Although quite versatile, these approximate methods are not derived from a rational simplification of a rigorous formulation of the rotor potential flow problem. Therefore, it is hoped that the present definition of the general actuator disc theory will provide a sound basis for generating future approximate techniques.

3. EFFECTS OF NONUNIFORM DOWNWASH ON HINGELESS ROTOR RESPONSE

The cantilevered blades of hingeless rotors are capable of transmitting bending moments to the rotor hub, resulting in substantial rotor moment responses to control inputs. These hub moments then create large azimuthal nonuniformities of the rotor downwash which have significant first harmonic content. An approximate treatment of this problem is given in ref. 13 where the nonuniform downwash was expressed by the first harmonic terms of a Fourier series.

$$\lambda = \lambda_0 + \lambda_c \cos \psi + \lambda_s \sin \psi \quad (1)$$

The downwash components λ_0 , λ_c , and λ_s were derived in terms of the rotor thrust and moments using simplified momentum and vortex theories. For example, in forward flight, the derivatives of the inflow components with respect to the rotor thrust and moment coefficients obtained from momentum theory were expressed as

$$\begin{Bmatrix} d\lambda_0 \\ d\lambda_c \\ d\lambda_s \end{Bmatrix} = \frac{1}{\mu} \begin{bmatrix} 1/2 & 0 & 0 \\ 0 & -3/2 & 0 \\ 0 & 0 & -3/2 \end{bmatrix} \begin{Bmatrix} dC_T \\ dC_l \\ dC_m \end{Bmatrix} \quad (2)$$

The simple diagonal form of the matrix expresses the direct correspondence between the distribution of rotor forces and downwash which is characteristic of momentum theory. The influence of flight condition is evident in the inverse

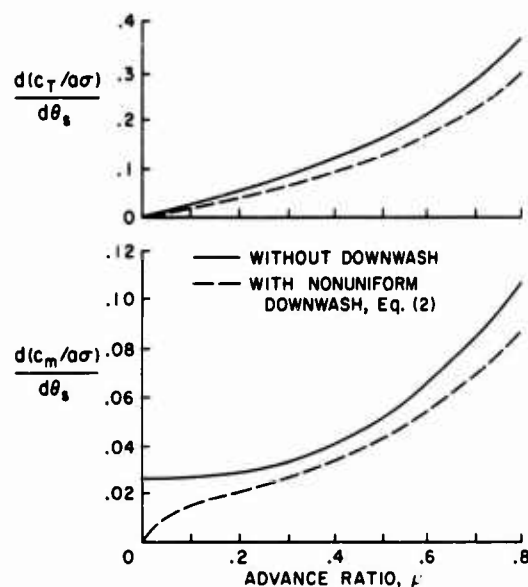


Figure 2. Typical effects of downwash on hingeless rotor response characteristics, $C_T = 0$ (from ref. 13).

variation of downwash with advance ratio. At higher velocities therefore, the downwash produced by the reaction of a given rotor force or moment is diminished. Rotor response characteristics including this downwash equation were investigated in ref. 13 using a linear harmonic balance technique to solve the blade flapping equation, including the effects of reversed flow. An example of these results using the first elastic flap bending mode are given in Fig. 2. Two response derivatives, rotor thrust and pitching moment due to longitudinal cyclic pitch versus advance ratio, for the non-lifting rotor condition ($C_T = 0$) are shown. In this condition the moment response vanishes in the limit as $\mu \rightarrow 0$, because Eq. (2) implies that infinite downwash would be required to support a finite moment. In other words, at $\mu = 0$, the downwash produced by a moment is always sufficient to cancel out that moment. For advance ratio greater than zero, the effect of downwash is to reduce the rotor response. This reduction decreases for the moment derivative as μ increases but only up to a point. Beyond that, ($\mu \sim 0.4$) it increases again. For the thrust derivative, the effect of downwash increases uniformly with advance ratio. These results are a contradiction of the intuitive basis on which many researchers disregard nonuniform downwash effects at high advance ratio. Even though the inverse variation of downwash with advance ratio in Eq. (2) supports this reasoning, the increasing sensitivity of hingeless rotor response at high advance ratio is of greater importance and therefore the downwash cannot be neglected.

Additional results in ref. 13 provide extensive correlation with experimental data and confirm that the simple downwash theories generally yield the proper qualitative results for most of the response derivatives. How-

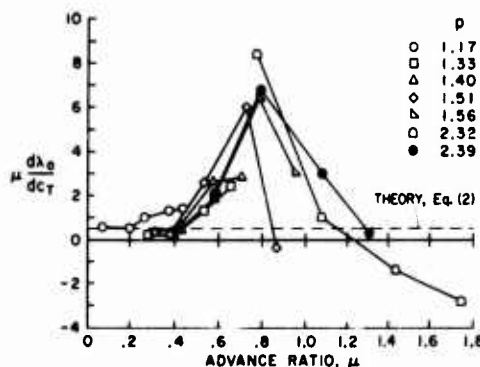


Figure 3. Comparison of simple downwash theory with experimental data (from ref. 13).

ever, in terms of desired quantitative accuracy, they are not considered wholly adequate. As a means of checking the downwash theory directly, an attempt was made to derive, from the experimental data, the relationship between downwash components and the rotor thrust and moments. This led to solution of an inverse problem and yielded empirical inflow derivatives in a form suitable for direct comparison with Eq. (2). One of the derivatives, $d\lambda_0/dC_T$, is shown in Fig. 3. At low advance ratio, it confirms the simple theory, but a striking departure occurs which peaks for advance ratios near 0.8. Although the reason for this phenomenon is not certain, the peaking at $\mu = 0.8$ implies that it may be related to the reduction in average blade dynamic pressure on the retreating side of the rotor disc which is also a maximum near this advance ratio.

The lack of detailed understanding of the nature of the rotor downwash distribution, and accurate means to

calculate its effect on rotor response characteristics provides a strong impetus for improving the aerodynamic potential flow theory of helicopter rotors. The results presented above should be particularly amenable to investigation by the general actuator disc theory presented herein.

4. DERIVATION OF THE THEORY

The general actuator disc theory rests on the solution of two simultaneous equations. The first one expresses the relationship between the bound circulation and the induced velocity while the second relates the blade dynamics to imposed aerodynamic flapping moments. The former is derived from the Kutta-Joukowski theorem, $l = \rho V \Gamma$, and steady thin airfoil theory $c_l = a\alpha$. Since $\alpha = \theta - \phi$, we have the fundamental equation of lifting-line theory.

$$\Gamma = \frac{abcV}{2} (\theta - \phi) \quad (3)$$

For rotating wings, the component of V normal to the blade span is taken, and ϕ is defined in terms of the relative velocity of the blade perpendicular to the plane of rotation. Applying the usual small angle approximations yields

$$\bar{\Gamma} = \frac{1}{2} (\theta \bar{U}_T - \bar{U}_P) \quad (4)$$

where

$$\bar{U}_T = \rho + \mu \sin \psi, \quad \bar{U}_P = \lambda + \rho \dot{\beta} / \Omega + \mu \beta \cos \psi + \mu \alpha \quad (5)$$

The rotor blade pitch angle is given by the usual relation for collective pitch, and lateral and longitudinal cyclic pitch respectively

$$\theta = \theta_0 + \theta_c \cos \psi + \theta_s \sin \psi \quad (6)$$

The downwash associated with the rotor potential flow field is contained in Eq. (5), and denoted by λ .

The equation for the blade dynamics is obtained from the integrated flapping moments.

$$I \ddot{\beta} + (I \Omega^2 + K_\beta) \beta = R^2 \int_0^1 l(\rho) \rho d\rho \quad (7)$$

The flapping deflections of an elastic blade have been approximated by a single rigid body degree of freedom, rotation about a centrally located hinge. A spring element K_β is used to simulate the elastic restraint of hingeless rotor configurations, and determines the dimensionless flapping frequency, $p = \sqrt{1 + K_\beta / I \Omega^2}$. For hingeless rotors, p is a fundamental parameter which specifies the relative stiffness of the rotor. It has a significant influence on the magnitude of rotor moment response and the degree of coupling between the pitch and roll axes of the rotor. The importance of the actual elastic bending degrees of freedom is discussed in ref. 13, and if required they could easily be incorporated in Eq. (7). The aerodynamic lift in Eq. (7) is obtained from the Kutta-Joukowski theorem yielding,

$$\ddot{\beta} / \Omega^2 + p^2 \beta = \gamma \int_0^1 \bar{\Gamma} \bar{U}_T \rho d\rho \quad (8)$$

A more customary form of this equation is obtained by substituting in Eq. (4) for $\bar{\Gamma}$.

$$\ddot{\beta} / \Omega^2 + p^2 \beta = \frac{\gamma}{2} \int_0^1 \text{sgn}(\bar{U}_T) (\bar{U}_T^2 \theta - \bar{U}_P \bar{U}_T) \rho d\rho \quad (9)$$

Although the first equation eliminates the complication of integrating the aerodynamic flap moment in the reversed flow region ($\bar{U}_T < 0$) since $\text{sgn}(\bar{U}_T)$ is a function of ρ , it cannot yield a solution for the fundamental harmonic of blade flapping when $p^2 = 1$, i.e., for articulated rotors. Since we are primarily interested in rotor blades with elastic flapping restraint, we will proceed with Eq. (8) and return to the articulated rotor configuration below.

The two Eqs. (4) and (8) together with the Biot-Savart law for the downwash are used to solve for the three unknown quantities, $\bar{\Gamma}(\rho, \psi)$, $\beta(\psi)$, and $\lambda(\rho, \psi)$. This system of linear integro-differential equations with variable coefficients is solved most easily by expressing the dependent variables in appropriate Fourier series in ψ , and then resorting to the harmonic balance technique to obtain the Fourier coefficients. For the circulation and flapping angle we have

$$\bar{\Gamma} = \bar{\Gamma}_0 \phi_0(\rho) + \sum_{n=1}^{\infty} \left(\bar{\Gamma}_{cn} \phi_{cn}(\rho) \cos n\psi + \bar{\Gamma}_{sn} \phi_{sn}(\rho) \sin n\psi \right) \quad (10)$$

and

$$\beta = a_0 + \sum_{n=1}^{\infty} (a_n \cos n\psi + b_n \sin n\psi) \quad (11)$$

The downwash is given in similar fashion, however, each harmonic is written as a linear combination of all the harmonics of the circulation series. The coefficients of each circulation harmonic are termed downwash influence functions and these are obtained from the Biot-Savart law, which will be discussed below.

$$\lambda = u^0 + \sum_{n=1}^{\infty} (u^n \cos n\psi + v^n \sin n\psi) \quad (12)$$

where

$$\begin{aligned} u^0 &= U_o^0(\rho) \bar{\Gamma}_o + \sum_{i=1}^{\infty} \left[U_{c_i}^0(\rho) \bar{\Gamma}_{c_i} + U_{s_i}^0(\rho) \bar{\Gamma}_{s_i} \right] \\ u^n &= U_o^n(\rho) \bar{\Gamma}_o + \sum_{i=1}^{\infty} \left[U_{c_i}^n(\rho) \bar{\Gamma}_{c_i} + U_{s_i}^n(\rho) \bar{\Gamma}_{s_i} \right] \\ v^n &= V_o^n(\rho) \bar{\Gamma}_o + \sum_{i=1}^{\infty} \left[V_{c_i}^n(\rho) \bar{\Gamma}_{c_i} + V_{s_i}^n(\rho) \bar{\Gamma}_{s_i} \right] \end{aligned} \quad (13)$$

The influence function $U_{c_i}^n(\rho)$ represents the n th cosine harmonic of downwash resulting from the wake vorticity associated with the i th cosine harmonic of the bound circulation distribution. Similarly, $V_{s_i}^n(\rho)$ denotes the n th sine harmonic of downwash associated with the i th sine harmonic of circulation.

Equations (10) through (12) are first substituted in the circulation Eq. (4). Since the Fourier series expressions for the dependent variables are not expanded in the blade spanwise coordinate, ρ , the circulation equation can only be satisfied in an average integrated sense. This is accomplished by weighting Eq. (4) by ρ^2 and integrating from the blade root to tip as follows

$$\int_0^1 \bar{\Gamma} \rho^2 d\rho = \frac{1}{2} \int_0^1 [\theta \bar{U}_T - \bar{U}_P] \rho^2 d\rho \quad (14)$$

After substituting in the series expressions, the coefficients of each sine and cosine harmonic on each side of Eq. (14) may be equated. This harmonic balance technique then yields the following series of linear algebraic equations.

$$(A_o + C_o^0) \bar{\Gamma}_o + \sum_{i=1}^{\infty} (C_{c_i}^0 \bar{\Gamma}_{c_i} + C_{s_i}^0 \bar{\Gamma}_{s_i}) + \frac{\mu}{12} a_1 = \frac{1}{8} \left(\theta_o + \frac{2}{3} \mu \theta_s - \frac{4}{3} \mu \alpha \right) \quad (15)$$

$$C_o^1 \bar{\Gamma}_o + A_{c_1} \bar{\Gamma}_{c_1} + \sum_{i=1}^{\infty} (C_{c_i}^1 \bar{\Gamma}_{c_i} + C_{s_i}^1 \bar{\Gamma}_{s_i}) + \left[\frac{\mu}{12} (2a_o + a_2) + \frac{b_1}{8} \right] = \frac{\theta_c}{8} \quad (16)$$

$$D_o^1 \bar{\Gamma}_o + A_{s_1} \bar{\Gamma}_{s_1} + \sum_{i=1}^{\infty} (D_{c_i}^1 \bar{\Gamma}_{c_i} + D_{s_i}^1 \bar{\Gamma}_{s_i}) + \left[\frac{\mu b_2}{12} - \frac{a_1}{8} \right] = \frac{1}{8} \left[\theta_s + \frac{2}{3} \mu \theta_o \right]$$

$$n = 2, \infty$$

$$\begin{aligned} C_o^n \bar{\Gamma}_o + A_{c_n} \bar{\Gamma}_{c_n} + \sum_{i=1}^{\infty} (C_{c_i}^n \bar{\Gamma}_{c_i} + C_{s_i}^n \bar{\Gamma}_{s_i}) + \frac{1}{4} \left[\frac{n}{2} b_n + \frac{\mu}{3} (a_{n-1} + a_{n+1}) \right] &= \begin{cases} -\frac{\theta_s}{12}, & n = 2 \\ 0, & n > 2 \end{cases} \\ D_o^n \bar{\Gamma}_o + A_{s_n} \bar{\Gamma}_{s_n} + \sum_{i=1}^{\infty} (D_{c_i}^n \bar{\Gamma}_{c_i} + D_{s_i}^n \bar{\Gamma}_{s_i}) + \frac{1}{4} \left[-\frac{n}{2} a_n + \frac{\mu}{3} (b_{n-1} + b_{n+1}) \right] &= \begin{cases} \frac{\mu \theta_c}{12}, & n = 2 \\ 0, & n > 2 \end{cases} \end{aligned} \quad (17)$$

where

$$A_{()} = \int_0^1 \phi_{()} \rho^2 d\rho, \quad C_{()} = \frac{1}{2} \int_0^1 U_{()} \rho^2 d\rho, \quad D_{()} = \frac{1}{2} \int_0^1 V_{()} \rho^2 d\rho \quad (18)$$

If the circulation series is truncated for $n > N$, then $2N + 1$ equations are obtained. It should be noted that the circulation equation could be satisfied without the integral averaging if the dependent variables were expanded in a doubly infinite series of both independent variables. Alternatively, a collocation method could be used to satisfy the circulation equation at a finite number of arbitrary radial locations. Note that the ρ^2 weighting function is equivalent to a single point collocation at $\rho = 0.75$ for radially constant circulation and downwash proportional to radius.

The differential Eq. (8) for blade dynamics is similarly converted into a series of linear algebraic equations which may be used to solve directly for the flapping coefficients (a_n, b_n) in terms of the harmonics of the rotor circulation.

$$a_o = \frac{\gamma}{2} \left(\bar{\Gamma}_o A_o + \frac{\mu}{2} \bar{\Gamma}_{s_1} B_{s_1} \right) \quad (19)$$

$$\left. \begin{aligned} a_1 &= -\frac{\gamma}{p^2-1} \left(\Gamma_{c_1} A_{c_1} + \frac{\mu}{2} \Gamma_{s_2} B_{s_2} \right) \\ b_1 &= -\frac{\gamma}{p^2-1} \left(\mu \Gamma_o B_o + \Gamma_{s_1} A_{s_1} - \frac{\mu}{2} \Gamma_{c_2} B_{c_2} \right) \end{aligned} \right\} p^2 \neq 1 \quad (20)$$

$$\left. \begin{aligned} a_n &= -\frac{\gamma}{p^2-n^2} \left[\Gamma_{c_n} A_{c_n} + \frac{\mu}{2} \left(\Gamma_{s_{n+1}} B_{s_{n+1}} - \Gamma_{s_{n-1}} B_{s_{n-1}} \right) \right] \\ b_n &= -\frac{\gamma}{p^2-n^2} \left[\Gamma_{s_n} A_{s_n} + \frac{\mu}{2} \left(\Gamma_{c_{n-1}} B_{c_{n-1}} - \Gamma_{c_{n+1}} B_{c_{n+1}} \right) \right] \end{aligned} \right\} p^2 \neq n^2 \quad (21)$$

where

$$B_{()} = \int_0^1 \phi_{()} \rho \, d\rho \quad (22)$$

These relations are a less restrictive generalization of results which may be found in ref. 2. A significant result of Eq. (20) is that the first harmonic flapping coefficients and thus the moment response of a hingeless rotor is independent of circulation harmonics higher than the second, therefore, accurate rotor moment predictions should be obtained by truncating third and higher harmonics of the bound circulation. It should be noted that this conclusion neglects the indirect effect (via the circulation equation) of the higher circulation harmonics on the first two circulation harmonics. As noted above, a_1 , b_1 cannot be defined by Eq. (8) for articulated rotor blades but the following relations regarding the first two circulation harmonics are obtained. These result from the physical fact that the first harmonic aerodynamic flapping moment of a centrally hinged rigid blade must vanish.

$$\Gamma_{c_1} = -\frac{\mu}{2} \frac{B_{s_2}}{A_{c_1}} \Gamma_{s_2}, \quad \Gamma_{s_1} = -\mu \frac{B_o}{A_{s_1}} \Gamma_o + \frac{\mu}{2} \frac{B_{c_2}}{A_{s_1}} \Gamma_{c_2} \quad (23)$$

These relations show how the first sine and cosine harmonics of bound circulation are related to the zeroth and the second harmonic in the case of an articulated rotor and are a generalization of results presented in ref. 10.

The steady thrust and moment response of the rotor may be determined by appropriate integration of the aerodynamic loading over the rotor disc.

$$T = \frac{\gamma \Gamma_o^2 b}{R} \left[\Gamma_o B_o + \frac{\mu}{2} \Gamma_{s_1} I_{s_1} \right], \quad M = -\frac{\gamma \Gamma_o^2 b}{2} \left[\Gamma_{c_1} A_{c_1} + \frac{\mu}{2} \Gamma_{s_2} B_{s_2} \right], \quad L = -\frac{\gamma \Gamma_o^2 b}{2} \left[\mu \Gamma_o B_o + \Gamma_{s_1} A_{s_1} - \frac{\mu}{2} \Gamma_{c_2} B_{c_2} \right] \quad (24)$$

where

$$I_{()} = \int_0^1 \phi_{()} \, d\rho \quad (25)$$

Note that the moments are simply proportional to the first harmonic flapping coefficients a_1 , b_1 . In fact, they may be equivalently written as

$$M = -\frac{bK\beta}{2} a_1, \quad L = -\frac{bK\beta}{2} b_1 \quad (26)$$

The simultaneous harmonic balance equations from the circulation and blade flapping equations may be solved using Cramer's rule. This procedure will be illustrated for a first approximation to the solution, i.e., retaining only first harmonic ($N=1$) Fourier coefficients for radially constant circulation. In matrix form, then, the three circulation Eqs. (15) and (16) become

$$\begin{bmatrix} (A_o + C_o^o) & C_{c_1}^o & C_{s_1}^o \\ C_o^1 & (A_{c_1} + C_{c_1}^1) & C_{s_1}^1 \\ D_o^1 & D_{c_1}^1 & (A_{s_1} + D_{s_1}^1) \end{bmatrix} \begin{Bmatrix} \Gamma_o \\ \Gamma_{c_1} \\ \Gamma_{s_1} \end{Bmatrix} + \frac{1}{8} \begin{bmatrix} 0 & 2/3 \mu & 0 \\ 4/3 \mu & 0 & 1 \\ 0 & -1 & 0 \end{bmatrix} \begin{Bmatrix} a_o \\ a_1 \\ b_1 \end{Bmatrix} = \frac{1}{8} \begin{bmatrix} 1 & 0 & 2/3 \mu & -2/3 \mu \\ 0 & 1 & 0 & 0 \\ 2/3 \mu & 0 & 1 & 0 \end{bmatrix} \begin{Bmatrix} \theta_o \\ \theta_c \\ \theta_s \\ \alpha \end{Bmatrix} \quad (27)$$

and the three blade dynamics Eqs. (19) and (20) become

$$\begin{Bmatrix} a_o \\ a_1 \\ b_1 \end{Bmatrix} = \gamma \begin{bmatrix} \frac{1}{3p^2} & 0 & \frac{\mu}{4p^2} \\ 0 & \frac{1}{3(p^2-1)} & 0 \\ \frac{\mu}{2(p^2-1)} & 0 & \frac{1}{3(p^2-1)} \end{bmatrix} \begin{Bmatrix} \Gamma_o \\ \Gamma_{c_1} \\ \Gamma_{s_1} \end{Bmatrix} \quad p \neq 1 \quad (28)$$

These 6 simultaneous equations in 6 unknowns may then be solved directly. Note that θ_o , θ_s , θ_c , and α are independent control variables. If we write Eqs. (27) and (28) in concise notation

$$[A] \{\Gamma\} + [B] \{\beta\} = [C] \{\theta\}, \quad \{\beta\} = [D] \{\Gamma\} \quad (29)$$

Solving for the circulation vector $\{\Gamma\}$ in terms of the control vector $\{\theta\}$ we have

$$\{\Gamma\} = [E] \{\theta\}, \quad \text{where } [E] = [A + [B] [D]]^{-1} [C] \{\theta\} \quad (30)$$

The matrix $[E]$ represents the derivatives of each circulation harmonic with respect to each control variable, or

$$[E] = \begin{bmatrix} d\bar{\Gamma}_o/d\theta_o & d\bar{\Gamma}_o/d\theta_c & d\bar{\Gamma}_o/d\theta_s & d\bar{\Gamma}_o/d\alpha \\ d\bar{\Gamma}_{c_1}/d\theta_o & d\bar{\Gamma}_{c_1}/d\theta_c & d\bar{\Gamma}_{c_1}/d\theta_s & d\bar{\Gamma}_{c_1}/d\alpha \\ d\bar{\Gamma}_{s_1}/d\theta_o & d\bar{\Gamma}_{s_1}/d\theta_c & d\bar{\Gamma}_{s_1}/d\theta_s & d\bar{\Gamma}_{s_1}/d\alpha \end{bmatrix} \quad (31)$$

Therefore, with the circulation harmonics determined, the appropriate weighting of the influence functions in the superposition Eq. (12) yields the downwash distribution. For the flapping coefficients Eq. (29) is used.

$$\{\beta\} = [D] [E] \{\theta\} \quad (32)$$

Finally, the rotor thrust and moments may be determined from Eqs. (24) or (26).

We will now briefly examine the method of solution for the articulated rotor. The alternate form of the blade flapping Eq. (9) will be used, reversed flow effects will be ignored, and only the first harmonic coefficients will be retained. This yields the following matrix equation where $p^2 = 1$.

$$\begin{bmatrix} 1 & 0 & 0 \\ \frac{\mu}{6}\gamma & 0 & \frac{\gamma}{8}(1+\frac{\mu^2}{2}) \\ 0 & \frac{\gamma}{8}(\frac{\mu^2}{2}-1) & 0 \end{bmatrix} \begin{Bmatrix} a_o \\ a_1 \\ b_1 \end{Bmatrix} + \gamma \begin{bmatrix} C_o^o + \frac{\mu}{2}F_o^1 & C_{c_1}^o + \frac{\mu}{2}F_{c_1}^1 & C_{s_1}^o + \frac{\mu}{2}F_{s_1}^1 \\ C_o^1 + \frac{\mu}{2}F_o^2 & C_{c_1}^1 + \frac{\mu}{2}F_{c_1}^2 & C_{s_1}^1 + \frac{\mu}{2}F_{s_1}^2 \\ D_o^1 + \mu E_o^o & D_{c_1}^1 + \mu E_{c_1}^o & D_{s_1}^1 + \mu E_{s_1}^o \\ -\frac{\mu}{2}E_o^2 & -\frac{\mu}{2}E_{c_1}^2 & -\frac{\mu}{2}E_{s_1}^o \end{bmatrix} \begin{Bmatrix} \bar{\Gamma}_o \\ \bar{\Gamma}_{c_1} \\ \bar{\Gamma}_{s_1} \end{Bmatrix} = \frac{\gamma}{8} \begin{bmatrix} 1+\mu^2 & 0 & \frac{4}{3}\mu & -\frac{4}{3}\mu \\ 0 & 1+\frac{\mu^2}{2} & 0 & 0 \\ \frac{8}{3}\mu & 0 & 1+\frac{3}{2}\mu^2 & -2\mu^2 \end{bmatrix} \begin{Bmatrix} \theta_o \\ \theta_c \\ \theta_s \\ \alpha \end{Bmatrix} \quad (33)$$

$$\text{where } E_{()}^{()} = \frac{1}{2} \int_0^1 U_{()}^{()} \rho \, d\rho, \quad F_{()}^{()} = \frac{1}{2} \int_0^1 V_{()}^{()} \rho \, d\rho \quad (34)$$

With only the first harmonics of circulation retained, Eq. (23) yields the following

$$\bar{\Gamma}_{c_1} = 0, \quad \bar{\Gamma}_{s_1} = -\mu \frac{B_o}{A_{s_1}} \bar{\Gamma}_o \quad (35)$$

Using these relations, the circulation harmonics may all be written as functions of $\bar{\Gamma}_o$, thus the matrix of downwash coefficients becomes a simple column vector where the elements will be defined as K_o , K_{c_1} , K_{s_1} respectively. Since Eq. (19) is valid for a_o when $p = 1$, we may determine $\bar{\Gamma}_o$ in terms of a_o

$$\bar{\Gamma}_o = \frac{a_o}{\gamma K}, \quad \text{where } K = A_o - \frac{\mu^2}{2} \frac{B_o B_{s_1}}{A_{s_1}} \quad (36)$$

We are now able to eliminate $\bar{\Gamma}_o$ from Eq. (33) and determine the flapping coefficients in closed form.

$$a_o = \frac{\gamma}{8} \frac{[(1+\mu^2)\theta_o + \frac{4}{3}\mu(\theta_s - \alpha)]}{[1 + (K_o/K)]} \quad (37)$$

$$a_1 = \frac{1}{(\frac{\mu^2}{2} - 1)} \left[\frac{8}{3}\mu\theta_o + \left(1 + \frac{3}{2}\mu^2\right)\theta_s - 2\mu^2\alpha - \frac{8K_{s_1}a_o}{\gamma K} \right] \quad (38)$$

$$b_1 = a_c - \frac{8 a_o}{\left(1 + \frac{\mu^2}{2}\right)} \left[\frac{\mu}{6} + \frac{K_{c1}}{\gamma K} \right] \quad (39)$$

Except for the effects of downwash which are condensed in K_o , K_{c1} , K_{s1} , these results are identical to the elementary expressions given in ref. 15. (In the notation of ref. 15 the coefficients given here would be a_o , $-a_{1s}$, and $-b_{1s}$ respectively.)

They also indicate that relatively simple approximate analytic expressions for rotor flapping response including the effects of nonuniform downwash may be obtained. Furthermore, within the constraints of actuator disc theory, these expressions can be obtained from a rational theory derived from first principles. The influence of the downwash due to wake vorticity is completely contained in the constants K_o , K_{c1} , K_{s1} , therefore, the effects of any wake geometry assumptions will be reflected in them.

It is interesting to note one additional piece of information from the second form of the blade flapping Eq. (9). Examination of the harmonic content of the aerodynamic flapping moment shows that the first harmonic terms, which determine the thrust and moment response of the rotor, are not affected by downwash harmonics higher than the second. Thus, only the first two harmonics of downwash need be retained for prediction of the rotor thrust and moment response. Like the similar conclusion noted earlier regarding truncation of the circulation series, we are neglecting here the secondary effects which may be produced by the circulation equation.

5. THE WAKE VORTICITY DISTRIBUTION

Of central importance to the general theory developed above is the determination of the downwash at the rotor disc corresponding to each of a series of bound circulation functions. This is accomplished by integration of the wake vorticity according to the Biot-Savart law. But first we must determine the distribution of vorticity in the wake. Vorticity is deposited in the wake by the bound circulation, which, in accordance with Helmholtz' theorem, generates trailing and shed elements of vorticity in proportion to the radial and azimuthal gradients of bound circulation respectively. The vorticity deposited in the wake is convected away from the rotor by the resultant fluid velocity. Since this velocity is determined in part by the spatial distribution of the wake vorticity, a direct analytic solution for both the downwash and wake vorticity is virtually impossible to obtain.

In specific cases, however, approximations to the convection velocity may be used to avoid this difficulty and also improve the utility and versatility of the theory. Specifically, in the case of actuator disc theory, it is customary to assume the convection velocity to be the vector sum of the free stream velocity and the mean downwash velocity. This then leads to a skewed cylindrical region of vorticity originating at the rotor disc, where the trailing and shed vorticity elements appear as skewed helical and radial lines respectively, as shown in Fig. 4(a). The skew angle is given by

$$\chi = \tan^{-1} \frac{\mu}{\lambda_o} \quad (40)$$

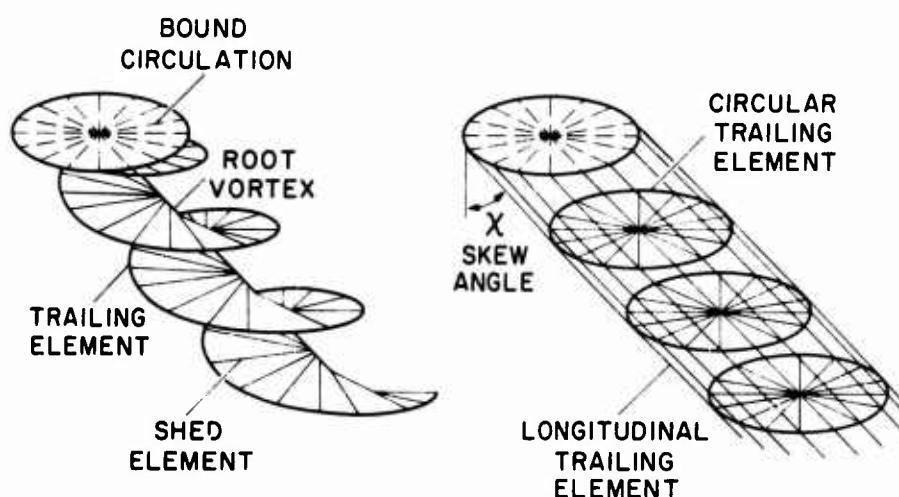


Figure 4. Skewed wake used for actuator disc theories,
a) actual trajectories of wake vorticity elements,
b) equivalent simplified wake system.

It has been known that the helical trailing wake elements could be decomposed into a simpler equivalent pattern consisting of circles and straight line elements which is shown in Fig. 4(b). This wake geometry was used for the downwash calculations presented in refs. 5-7 and 9. As discussed above, these results were generally restricted to the lateral and longitudinal planes of symmetry and not all of the vorticity elements which contribute to the rotor downwash were treated.

A further simplification of the rotor wake geometry is valid if certain relatively mild restrictions on the rotor operating condition are accepted. At low rotor thrust or high forward velocity, the downwash becomes small in comparison to the free stream velocity and the wake skew angle approaches 90° . This leads to the limiting case of a flat, planar wake where the vorticity lies in the plane of the rotor disc and extends infinitely far downstream of the rotor. Under these conditions, the wake for a rotating wing is equivalent to the conventional fixed-wing wake geometry. It should be noted that for lifting rotors operating at very low advance ratios, however, the flat planar wake (and to some degree even the skewed cylindrical wake) is completely invalid, but for moderate thrust levels over a fairly wide range of advance ratios it can be expected to give quite reasonable results. The major benefit of the flat planar wake geometry is the simplification of integrating the wake vorticity according to the Biot-Savart law. Furthermore, the wake skew angle is eliminated as a variable.

The restrictions imposed by the assumption of a flat planar wake may be estimated to first order by using the results of refs. 5 and 9 which present calculations of some important downwash properties in terms of wake skew angle. Two of these are chosen as criteria for estimating permissible deviations in wake skew angle. The first is the longitudinal gradient of downwash at the rotor center for a uniform circulation distribution, from ref. 5.

$$\frac{1}{\lambda_0} \frac{d\lambda}{d\xi} (\xi = 0) = \tan \frac{\lambda}{2} \quad (41)$$

The second property is the downwash on the lateral axis ($\psi = 90^\circ$) for a sinusoidal variation of radially constant circulation taken from ref. 9. Both of these are plotted as a function of wake skew angle in Fig. 5(a). The permissible skew angle deviation for a 10% error in these two quantities is noted on the figure. The wake skew angle may be related to advance ratio for any given value of rotor thrust coefficient by means of simple momentum theory for downwash

$$\lambda = C_T \sqrt{2/\lambda^2 + \mu^2} \quad (42)$$

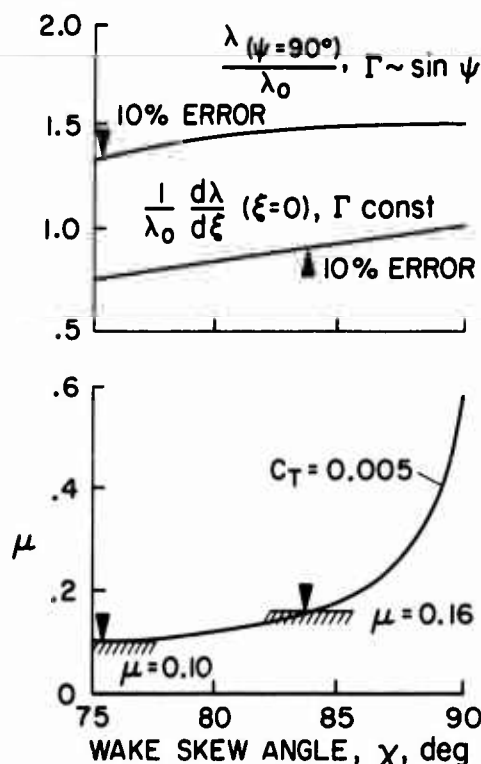


Figure 5. Validity of the planar wake configuration, a) selected downwash criteria; b) resulting minimum advance ratio limit for 10% allowable error in downwash.

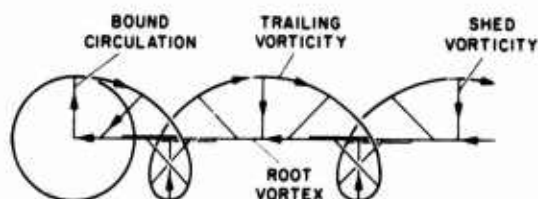


Figure 6. Schematic of constituent elements of vorticity in wake for the flat planar configuration.

This relation is plotted in Fig. 5(b) for a thrust coefficient representative of a lg flight condition. In this way, the above wake skew angle deviations may be translated into the minimum permissible advance ratio for the flat planar wake. As shown in Fig. 5(b) the corresponding advance ratios are 0.10 and 0.16. These results mean that the approximate flat planar wake is justifiable for conventional helicopter rotors over a significant range of rotor flight conditions. For substantially unloaded, reduced tip speed rotors of future advanced compound rotorcraft, the flat planar wake would be fully acceptable with essentially negligible error due to wake skew angle deviations.

We will return now to the determination of the wake vorticity distribution, restricting attention to the flat planar wake. As in the case of the skewed cylindrical wake, the elements of vorticity in the flat planar wake may be decomposed into simpler constituent elements. The basic elements of vorticity are again illustrated in Fig. 6 for the flat wake. For clarity, discrete trailing and shed vortex filaments from a single bound circulation element are shown. The root vortex is included for generality but only exists for arbitrary circulation distributions which are finite at the rotor center. The arrows indicate the circulation direction; the right hand rule defines the direction of rotation of the induced velocity. Note that the shed vortex filaments imply continuously increasing bound circulation.

The decomposition of the spiral trailing vortex element into simple circular and linear elements may be easily demonstrated geometrically. In Fig. 7, the spiral trailing tip vortex filaments of two successive bound circulation filaments are traced as they are generated by alternate incremental rotations and translations of the rotor. In this way, the circular and linear portions of the spiral are easily visualized. Furthermore, the contributions of additional spirals from other bound circulation filaments can be seen to form complete circles and continuous linear elements. In the limit as infinitesimal increments are taken, the trailing wake forms a continuous distribution of circular and longitudinal elements of vorticity.

In a similar manner, it may be shown that the radial shed vorticity elements can be represented by successive circles distributed behind the rotor disc, with the shed vorticity oriented on the radii of the circles.

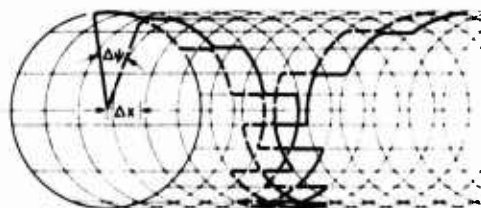


Figure 7. Decomposition of spiral trailing vorticity element into equivalent circular and longitudinal elements.

One final step in decomposing the wake vorticity elements is to resolve the circular and radial elements into their orthogonal x and y components. The wake vorticity is then in a form directly amenable to the Biot-Savart integrations. These components are shown schematically in Fig. 9 in relation to the rotor coordinate system. It is convenient to define specific regions of the wake which are labelled in the figure. These are the front half, region ①, and the rear half, region ②, of the rotor disc, and wake behind the rotor, region ③. The wake in regions ① and ② will also be referred to as the interior wake, while region ③ will be called the exterior wake. Note the positive sign conventions for the orthogonal wake vorticity components.

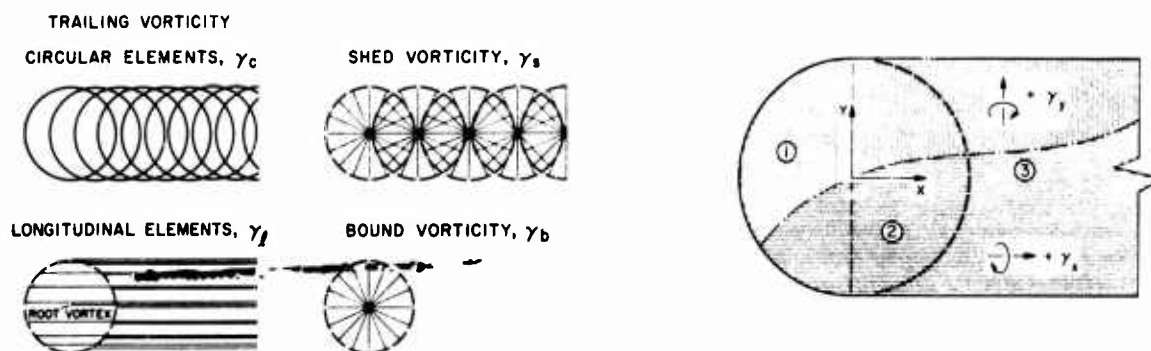


Figure 8. Schematic of each decomposed constituent element of vorticity in flat planar wake.

Figure 9. Boundaries of vorticity of flat planar wake, rotor coordinate system, wake regions, and orientation of positive vorticity components.

5.1 Differential Wake Vorticity Elements. With the wake vorticity broken into the various elements discussed above, it is appropriate to now derive the relations for their strength in terms of the bound circulation gradients. This process may be broken down into three steps. First, the differential trailed and shed circulation deposited from a specific radial location of the rotor is determined, according to Helmholtz' theorem. Second, the spatial distribution of this differential wake circulation is defined giving the differential circulation per unit distance, or the differential wake vorticity. Third, the contributions from all radial locations are integrated for the final wake vorticity.

5.1.1. Different Circulation in Wake — Consider first the trailing vorticity deposited from radius r by a rotor blade having angular velocity Ω , shown in Fig. 10. According to Helmholtz' theorem, the trailed circulation in the annulus of width dr is proportional to the radial gradient of bound circulation but it will also increase continuously as the blade rotates. Therefore, the infinitesimal rate of change of circulation is proportional to time and radial differentials and is therefore second order. Similar reasoning applies to the differential shed circulation of Fig. 10. Thus, for the actuator disc we have,

$$d^2\Gamma_t(r, \psi) = \frac{\Omega dt}{2\pi} \frac{\partial \Gamma}{\partial r}(r, \psi) dr, \quad d^2\Gamma_s(r, \psi) = \frac{\Omega dt}{2\pi} \frac{\partial \Gamma}{\partial \psi}(r, \psi) d\psi \quad (43)$$

Note that the positive vector quantities for these differential circulation elements are indicated in Fig. 10.

5.1.2. Differential Wake Vorticity — We now consider the differential vorticity due to the circular and longitudinal elements of the trailing spiral wake. The incremental angular rotation $d\psi$ and translation dl of the rotor in a time increment dt together with the associated differentials of trailed circulation are shown in Fig. 11. (Note the similarity with Fig. 7). The strength of the circular and longitudinal elements $d^2\Gamma_c$ and $d^2\Gamma_l$ are equal to $d^2\Gamma_t$ given by Eq. (43). As mentioned above, the circular element may be resolved into x and y components which are also shown in Fig. 10 and are equal to $d^2\Gamma_t$. Since vorticity is defined as circulation per unit length, the components of vorticity trailed from radius r at a lateral distance y in the wake are

$$d\gamma_{c_x} = \frac{d^2\Gamma_c}{dy} \frac{x}{dl}, \quad d\gamma_{c_y} = \frac{d^2\Gamma_c}{dl} \frac{y}{dl}, \quad d\gamma_l = \frac{d^2\Gamma_l}{dy} \quad (44)$$

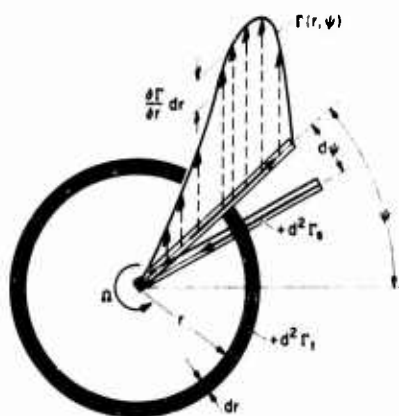


Figure 10. Differential circulation shed and trailed from rotor.

where $dl = U_\infty dt$, $dx = -y d\psi$, $d\psi = \Omega dt$, and $dy = \sqrt{r^2 - y^2} d\psi$. Note that dy_{c_x} must be multiplied by the ratio dx/dl because the vector $d^2\Gamma_{c_x}$ extends only over the dx portion of the length dl . We now have,

$$\begin{aligned} dy_{c_x}(y, r) &= -\frac{\text{sgn}(y)}{2\pi\mu R} \left[\frac{\partial \Gamma}{\partial r}(r, \psi) \right] \frac{y}{\sqrt{r^2 - y^2}} dr \\ dy_{c_y}(y, r) &= \frac{\text{sgn}(x)}{2\pi\mu R} \left[\frac{\partial \Gamma}{\partial r}(r, \psi) \right] dr, \quad dy_{c_t}(y, r) = -\frac{1}{2\pi} \left[\frac{\partial \Gamma}{\partial r}(r, \psi) \right] \frac{dr}{\sqrt{r^2 - y^2}} \end{aligned} \quad (45)$$

The sgn functions reflect the change in vector orientation of the differential circulation around the azimuth. The use of x appearing in these equations refers to the x location on the rotor disc where the element of vorticity originated. These expressions give the differential wake vorticity at a lateral position y due to trailing circulation deposited from radius r . A significant characteristic of the wake vorticity is revealed in these equations. The vorticity due to the circular element of trailing circulation is inversely proportional to advance ratio, while the longitudinal element is independent of μ . The former variation reflects the increased spacing between successive circles deposited at time intervals dt as the rotor translation velocity increases. The significance of this result is that it gives some insight into the effects of advance ratio on the variation of wake vorticity and hence rotor downwash.

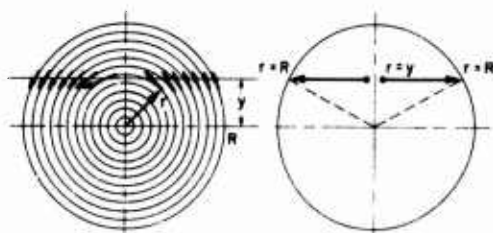


Figure 12. a) Radii contributing to vorticity at point y in external wake, b) schematic of integration path.

doubling or cancelling the wake vorticity, depending on the sign of the integrand. Then for region ③, Eq. (45) yields

$$\gamma_{\textcircled{3}}(y) = 2 \int_y^R dy_{\textcircled{3}}(y, r) dr, \quad \text{or } \gamma_{\textcircled{3}}(y) = 0 \quad (46)$$

Consider next a point in region ① of the interior wake. Again, the circular trailed vorticity elements for all radii are shown in Fig. 13(a). Since we are now fixed in the rotor disc x, y coordinate system, these are circular elements which were shed by the rotor at its present position. (Previously deposited circular elements have been swept behind the rotor a distance $x = U_\infty t$ and for clarity are not shown in Fig. 13(a).) Circular elements of $r \geq \sqrt{x^2 + y^2}$ will pass over the point $-x, y$ as they are swept rearward and thereby contribute to the vorticity. However, those of $r < \sqrt{x^2 + y^2}$ will be swept behind the rotor without passing over the point of interest and clearly will not contribute to the vorticity. Therefore, the appropriate limits of integration are $\sqrt{x^2 + y^2} \leq r \leq R$ which are also diagrammed in Fig. 13(b). Similar reasoning applies for vorticity in region ② and we have

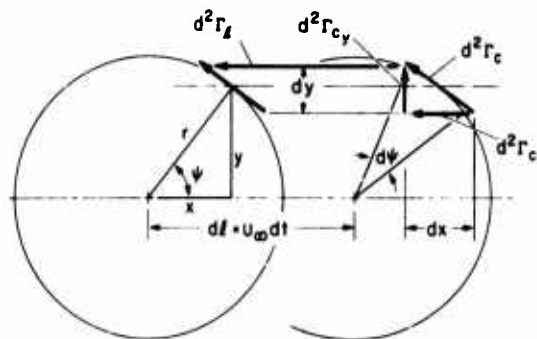


Figure 11. Schematic of spatial distribution of differential circular and longitudinal circulation elements of trailing wake for successive incremental rotations and translations of the rotor.

5.1.3. Integrated Wake Vorticity — To account for the vorticity trailed from each radial location, Eq. (45) must be integrated over the rotor radius. The integration limits will depend, however, on the lateral position y if the point of interest is in the exterior wake and on both x and y if the point is in the interior wake. We will first consider points in the exterior wake, or region ③ in Fig. 9. The circular trailing vorticity elements for all radii are sketched in Fig. 12(a); only those circles where $r \geq y$ contribute to the vorticity at y . Therefore, the range of integration will be $y \leq r \leq R$. Furthermore, both the left and right portions of the circular elements contribute to the wake vorticity, requiring two integrations, the paths of these integrations are diagrammed in Fig. 12(b). These two integrations are generally equal in magnitude thereby

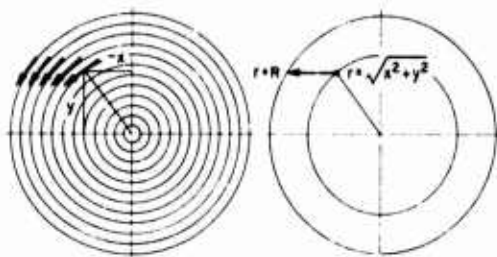


Figure 13. a) Radii contributing to vorticity at point $-x, y$ in region ① of interior wake, b) schematic of integration path.

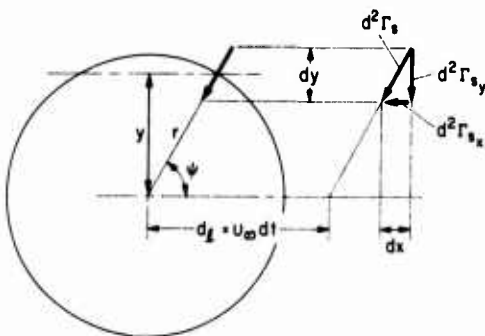


Figure 14. Schematic of spatial distribution of differential circulation elements of shed wake for successive incremental translations of rotor.

$$\gamma_{\textcircled{1}}(x, y) = \int_{\sqrt{x^2+y^2}}^R d\gamma_{\textcircled{1}}(y, r) dr,$$

$$\gamma_{\textcircled{2}}(x, y) = \int_r^R d\gamma_{\textcircled{1}}(y, r) dr + \int_{\sqrt{x^2+y^2}}^R d\gamma_{\textcircled{2}}(y, r) dr \quad (47)$$

The expressions for wake vorticity presented above were developed for the general case of a radially varying rotor circulation distribution. It is of interest to consider a special restricted case, that of radially constant rotor circulation. This implies that all trailing vorticity is shed at the rotor perimeter, i. e., as tip vortices. The above expressions for vorticity are then easily developed without the need for radial integration. Corresponding to Eq. (43) the differential trailing circulation is given by $d\Gamma_t(\psi) = \Gamma(\psi) \Omega dt/2\pi$. Then corresponding to Eq. (45) we have

$$\gamma_{c_x} = \frac{\Gamma}{2\pi\mu R} \frac{y}{\sqrt{R^2 - y^2}}, \quad \gamma_{c_y} = \frac{\Gamma}{2\pi\mu R}, \quad \gamma_t = \frac{\Gamma}{2\pi\sqrt{R^2 - y^2}} \quad (48)$$

These formulas are valid for the interior wake, in regions ① and ②. However, in the exterior wake they either double or cancel, depending on the azimuthal variation of rotor circulation.

We have now determined general relations for the vorticity due to the x and y components of the circular trailing vorticity and the longitudinal trailing vorticity element for a flat planar wake. We must now treat the resolved components of the shed vorticity elements. The differential circulation element $d^2\Gamma_s$ shed from radius r at a lateral point y and swept downstream a distance $d\ell$ in time increment dt is shown in Fig. 14. The resultant components of wake vorticity are

$$d\gamma_{s_x} = -\frac{d^2\Gamma_{s_x}}{dy} \left(\frac{dx}{dt} \right), \quad d\gamma_{s_y} = -\frac{d^2\Gamma_{s_y}}{d\ell} \quad (49)$$

Since $dx = \cos \psi dr$, $dy = \sin \psi dr$, $d\ell = U_\infty dt$ and $d^2\Gamma_{s_x} = d^2\Gamma_{s_y} = d^2\Gamma_s$ given by Eq. (43), we have

$$d\gamma_{s_x} = -\frac{1}{2\pi\mu R} \left[\frac{\partial \Gamma}{\partial \psi}(r, \psi) \right] \frac{d\psi}{\tan \psi} \quad (50)$$

During a differential rotation $d\psi$ for constant y , $\tan \psi dr = r d\psi$ and we have

$$d\gamma_{s_x} = -\frac{\text{sgn}(x)}{2\pi\mu R} \left[\frac{\partial \Gamma}{\partial \psi}(r, \psi) \right] \frac{dr}{r}, \quad d\gamma_{s_y} = -\frac{\text{sgn}(y)}{2\pi\mu R} \left[\frac{\partial \Gamma}{\partial \psi}(r, \psi) \right] d\psi \quad (51)$$

For $d\gamma_{s_x}$, the previously derived integration limits for r apply, however, it is advantageous to integrate azimuthally for $d\gamma_{s_y}$ due to its simpler form. The limits are $\psi_R \leq \psi \leq \psi_L$ in regions ① and ② where $\psi_L = \sin^{-1} y/\sqrt{x^2+y^2}$ and $\psi_R = \sin^{-1} y/R$. In region ③ the limits are $\psi_R \leq \psi \leq \pi - \psi_R$. Note that the shed wake vorticity components are inversely proportional to advance ratio, as were the circular elements of trailed vorticity.

The remaining elements of vorticity which can contribute to downwash are the bound circulation distribution, and a root vortex if present. The root vortex will be present if radial circulation distributions are used which are finite at the rotor center. Although physically unrealistic, this may occur for certain approximate circulation distributions. If so, the root vortex will be equal in strength to the integrated average of circulation around the azimuth for $r = 0$. This is just the total bound circulation strength Γ_0 of the rotor since harmonics of the circulation will not contribute to the root vortex.

The bound circulation will contribute to the rotor downwash if azimuthal harmonics are present. In this case, the vorticity is radially oriented and is simply the circulation divided by the angular distance at each radius. Thus $\gamma_b(r, \psi) = \Gamma(r, \psi)/2\pi r$.

To demonstrate the application of the vorticity relations derived above, some example results will be given. For a radially uniform circulation distribution having a mean and first harmonic sine and cosine variation, the associated contributions to the wake vorticity have been derived. These are given in Table 2 and illustrate some interesting features of the wake. Note that the rotor coordinates x, y, r have been made dimensionless by R becoming ξ, η, ρ . For many of the wake vorticity components, the vorticity is invariant with x except when crossing from the interior to the exterior wake where the vorticity either doubles in value or vanishes. In all cases, the vorticity is invariant with x in the exterior wake. Note that the shed vorticity does depend on x in the interior wake, but that on the lateral axis ($x = 0$) the vorticity is equal to 1/2 the value in the exterior wake (if finite). Furthermore, the change in vorticity from the value at $x = 0$ is either an odd or even function of x .

Table 2. Components of wake vorticity for radially constant, first harmonic rotor circulation distribution, $\Gamma = \Gamma_o + \Gamma_c \cos \psi + \Gamma_s \sin \psi$

Γ	Wake Region	Trailing Vorticity			Shed Vorticity		Bound Vorticity	Root Vortex
		Circular		Longitudinal				
		$2\pi R \mu \gamma_{cx}$	$2\pi R \mu \gamma_{cy}$	$2\pi R \gamma_\ell$	$2\pi R \mu \gamma_{sx}$	$2\pi R \mu \gamma_{sy}$	$2\pi R \gamma_b$	γ_r
Γ_o	①, ②	$\Gamma_o \frac{\eta}{\sqrt{1-\eta^2}}$	Γ_o	$\frac{\Gamma_o}{\sqrt{1-\eta^2}}$	0	0	$\frac{\Gamma_o}{\rho}$	Γ_o
	③	$\Gamma_o \frac{2\eta}{\sqrt{1-\eta^2}}$	0	$\frac{2\Gamma_o}{\sqrt{1-\eta^2}}$	0	0		$\eta = 0$ $0 \leq \xi \leq \infty$
$\Gamma_c \cos \psi$	①, ②	$-\Gamma_c \eta$	$-\Gamma_c \sqrt{1-\eta^2}$	$-\Gamma_c$	$\Gamma_c \eta \left(1 - \frac{1}{\rho}\right)$	$\Gamma_c \left(\sqrt{1-\eta^2} + \frac{\xi}{\rho}\right)$	$\Gamma_s \frac{\xi}{\rho^2}$	0
	③	0	$-2\Gamma_c \sqrt{1-\eta^2}$	0	0	$2\Gamma_c \sqrt{1-\eta^2}$		
$\Gamma_s \sin \psi$	①, ②	$\Gamma_s \frac{\eta^2}{\sqrt{1-\eta^2}}$	$\Gamma_s \eta$	$\Gamma_s \frac{\eta}{\sqrt{1-\eta^2}}$	$\Gamma_s \left[\sqrt{1-\eta^2} - \ln \left(\frac{1+\sqrt{1-\eta^2}}{ \eta } \right) + \operatorname{sgn}(\xi) \left[\frac{ \xi }{\rho} - \ln \left(\frac{ \xi +\rho}{ \eta } \right) \right] \right]$	$\Gamma_s \eta \left(1 - \frac{1}{\rho}\right)$	$\Gamma_c \frac{\eta}{\rho^2}$	0
	③	$\Gamma_s \frac{2\eta^2}{\sqrt{1-\eta^2}}$	0	$\Gamma_s \frac{2\eta}{\sqrt{1-\eta^2}}$	$2\Gamma_s \left[\sqrt{1-\eta^2} - \ln \left(\frac{1+\sqrt{1-\eta^2}}{ \eta } \right) \right]$	0		

6. INDUCED VELOCITY

The expressions for the various elements of wake vorticity enable the calculation of the rotor downwash using the Biot-Savart law. This is given in differential form in the following equation.

$$d^2 w(x_o, y_o) = \frac{1}{4\pi} \frac{\gamma_x(x, y)[y - y_o] + \gamma_y(x, y)[x - x_o]}{[(x - x_o)^2 + (y - y_o)^2]^{3/2}} dx dy \quad (52)$$

The double integration must be carried out over the entire wake region of Fig. 9. The order of integration in x and y depends upon convenience and also avoiding difficulties with singularities. Because of the relative simplicity of some of the expressions for vorticity, much of the integration may be carried out analytically, but in general, numerical integration will also be required. After the downwash distributions have been obtained, it is a relatively straightforward matter to Fourier analyze the results to obtain the downwash influence functions. Some results of this type will be presented below.

It is of some interest to discuss the relation between the symmetry properties of the wake vorticity and the downwash distribution. This is because the harmonic content of the downwash can be determined in part from its symmetry. As discussed earlier, only the first two downwash harmonics directly influence the rotor thrust and moment response. Therefore, the symmetry relations will enable certain information about the eventual influence on rotor response to be determined from the wake vorticity distribution alone.

We will consider briefly only one example, where the component of vorticity in the exterior wake is twice the value in the interior wake but otherwise only a function of y . We are interested in the symmetry of downwash with respect to the y axis, therefore the pairs of points on the lines $x = \pm x$ shown in Fig. 15. The vorticity in the interior

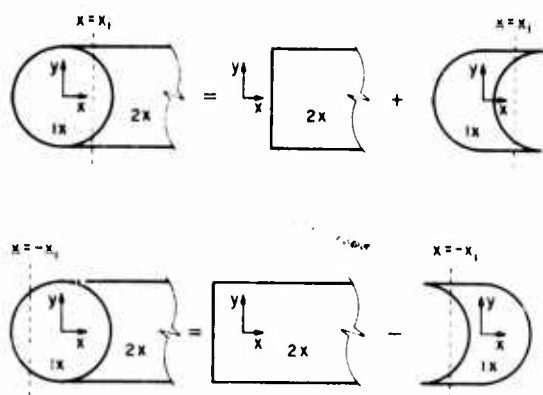


Figure 15. Geometric demonstration of symmetry relations of downwash.

Table 3. Downwash harmonics excluded.

	x axis	y axis
Downwash symmetric about axis	All sine harmonics	Odd cosine and even sine harmonics
Downwash antisymmetric about axis	All cosine harmonics	Even cosine and odd sine harmonics

parallel between the downwash of a fixed wing and the downwash on the lateral axis of a rotor. As shown above, when the x component of vorticity is independent of x within the interior and exterior regions, only the semi-infinite rectangular portion of the equivalent wake will contribute to downwash on the lateral axis. Since this is identical to the wake configuration of a fixed wing, the downwash will be identical for equivalent vorticity distributions.

7. QUANTITATIVE RESULTS

The present quantitative results are preliminary and are limited to the downwash influence functions for one rotor circulation distribution, that of uniform circulation. These results permit a graphic interpretation of the distribution of induced velocity on the rotor disc for each of the contributing wake vorticity elements. For uniform circulation, these elements consist of the two components of the circular trailing vorticity, γ_{cx} , γ_{cy} , the longitudinal trailing vorticity γ_l , and the root vortex, γ_r . These elements are given in Table 2. Both the vorticity and corresponding downwash distributions are shown in Fig. 16 in isometric plots. For the downwash of the longitudinal trailing vorticity and the root vortex the advance ratio was chosen to be unity. In this way the downwash distributions could be plotted with comparable vertical scales. All four are equal except the downwash of the root vortex which is reduced by 1/2. The vorticity elements, however, are not drawn to scale. The radii of the downwash plots are limited to $r/R \leq 0.95$ since for uniform circulation, the downwash generally becomes infinite at the rotor perimeter. For the same reason, the downwash of the root vortex singularity is truncated at $\psi = 0^\circ$ and for $r/R \leq 0.25$. These downwash distributions show the familiar fore-aft gradient on the longitudinal axis due to the circular trailing vorticity elements. Furthermore, the full azimuthal distributions presented here also reveal that significant nonuniformities are present at $\psi = 90^\circ$ and 270° due to the γ_{cx} vorticity component. Both the longitudinal trailing vorticity and root vortex are shown to produce laterally asymmetric downwash distributions which will be increasingly predominant at higher advance ratios. The lateral asymmetry for a uniform azimuthwise circulation distribution has not been evident in other actuator disc theories because these two vorticity elements are typically neglected. Figure 17 includes conventional plots of the downwash distributions and the corresponding influence functions. The downwash nonuniformities of the γ_{cx} vorticity component are manifest as odd cosine harmonic influence functions. The γ_{cy} component, in contrast, yields only a single influence function, the first cosine harmonic. Since the downwash of the γ_l and γ_r vorticity elements is antisymmetric about the x axis, only sine harmonic influence functions exist. Note that influence functions V_0^n for γ_r are equal for all n . Although these results are limited to the uniform circulation distribution, we now have an indication of the downwash on the entire disc, and a first set of downwash influence functions for the flat planar wake configuration.

A final figure is included to illustrate the total downwash due to the superimposed contributions of the various wake vorticity elements. For a specified uniform circulation distribution the total downwash will be uniquely determined by the advance ratio. Therefore, Fig. 18 depicts isometric plots for three advance ratios $\mu = 0.0, 0.25$, and 0.75 . The zero advance ratio case is idealized in that the flat planar wake is not valid for this condition. These plots depict the increasing asymmetry of the downwash as the advance ratio increases. The powerful influence of the root vortex is also evident. One example is shown for $\mu = 0.75$ in Fig. 18 which neglects the root vortex contribution. Physically this corresponds to the downwash produced by the tip vorticity trailed from the rotor disc perimeter. This figure indicates how the downwash gradients from two vorticity elements, γ_{cx} and γ_l are mutually reinforce and attenuate one another at $\psi = 90^\circ$ and 270° respectively. Thus at $\psi = 90^\circ$, for high advance ratios, the impulsive loads on the blade will be severe, especially since the velocity is greatest, whereas the reduced gradient and lower velocity

and exterior wake is labelled $1x$ and $2x$ respectively to represent the doubling factor. Now when the γ_x component of vorticity is invariant with x , the downwash induced at a point P by elements of the wake equidistant upstream and downstream of P will be identical. As a result, wake filaments extending upstream of P may be flipped over to coincide with equal length downstream filaments without changing the downwash at P . Using this basic procedure on the points at $\pm x$ yields the equivalent wake systems shown in Fig. 15. Thus the downwash is composed of two terms, one due to a double strength semi-infinite rectangular wake and the other due to an irregular shaped remnant. The remnant wake differs only in sign for the points $\pm x$ therefore its contribution is an odd function of x , or antisymmetric about the y axis. It is relatively simple to demonstrate that wake vorticity which is an even or odd function of y will produce a downwash distribution which is correspondingly an odd or even function of y . It may be shown that these symmetry characteristics lead to the exclusion of downwash harmonics shown in Table 3.

An example will illustrate these results. Consider the γ_{cx} component of vorticity for uniform circulation (see Table 2) which doubles in the exterior wake and is an odd function of y . The downwash will thus be symmetric about the x axis, and the remnant wake will produce a downwash contribution antisymmetric about the y axis. As a result, no sine or even cosine harmonic influence functions will exist. Similar relations may also be deduced for other components of vorticity and also for vorticity distributions which are functions of both x and y in the interior wake. The symmetry relations may be used to demonstrate an interesting

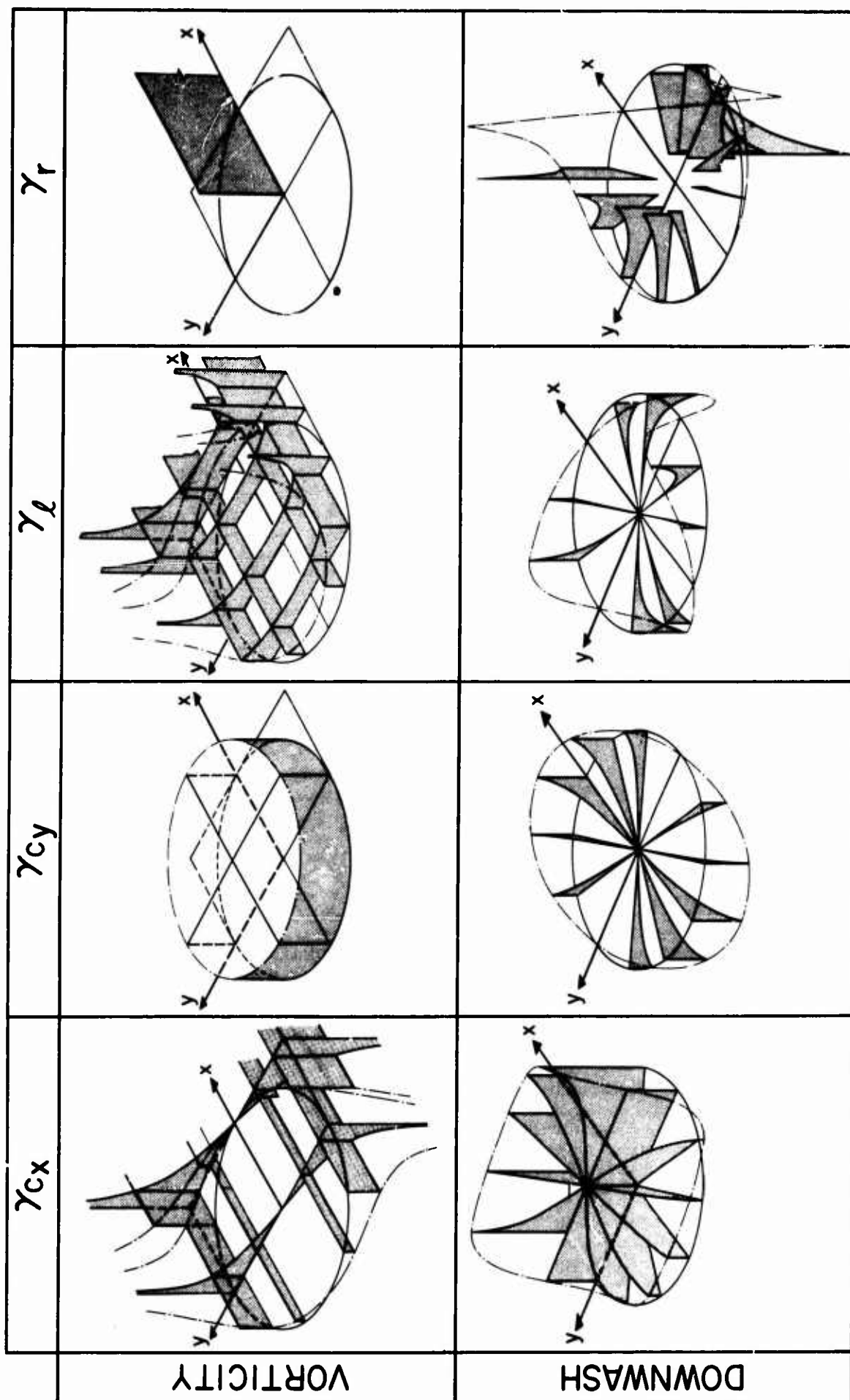


Figure 16. Isometric plots of vorticity and downwash elements for uniform circulation distribution.

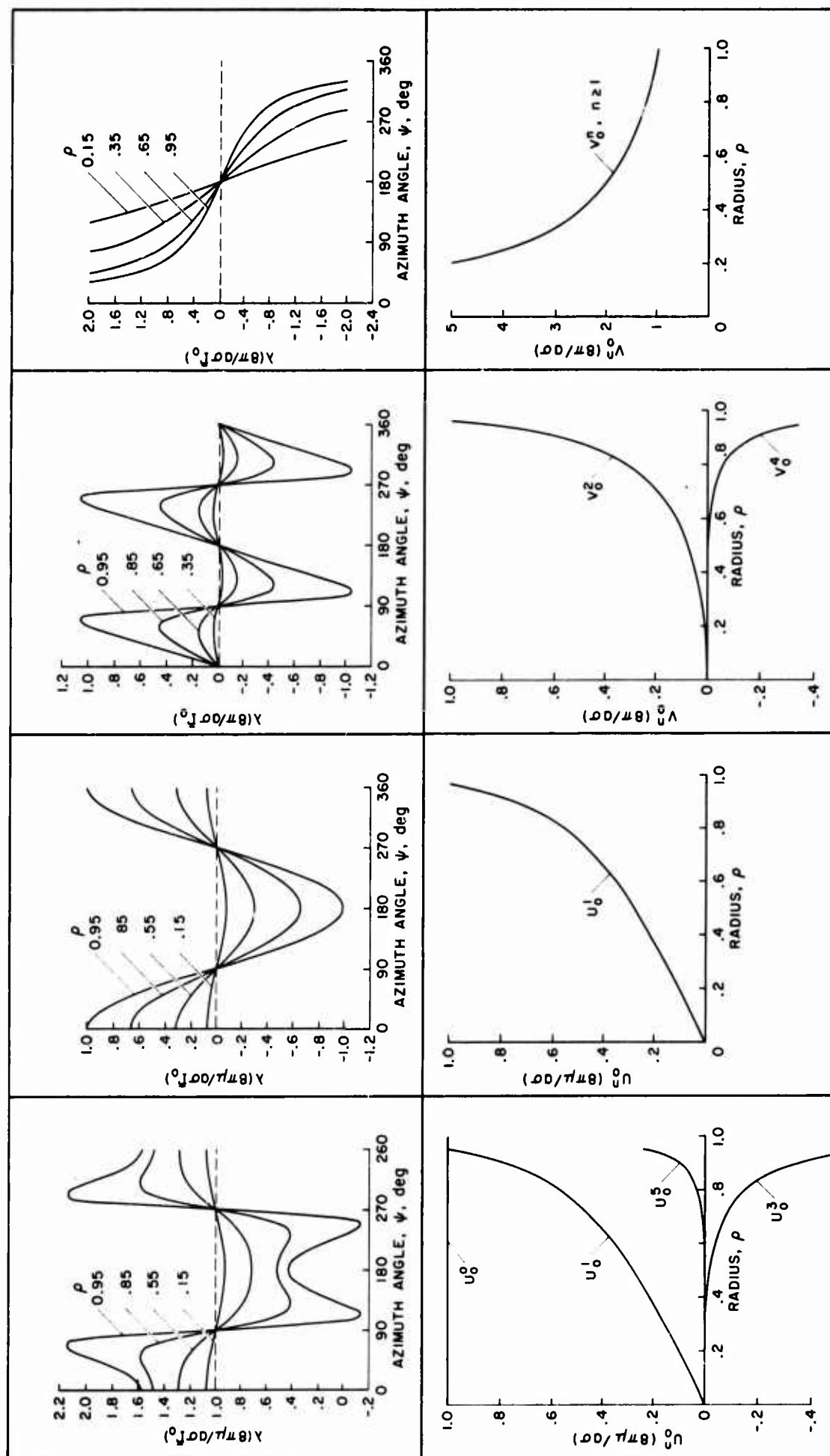


Figure 17. Downwash distributions and corresponding influence functions from vorticity elements of figure 16.

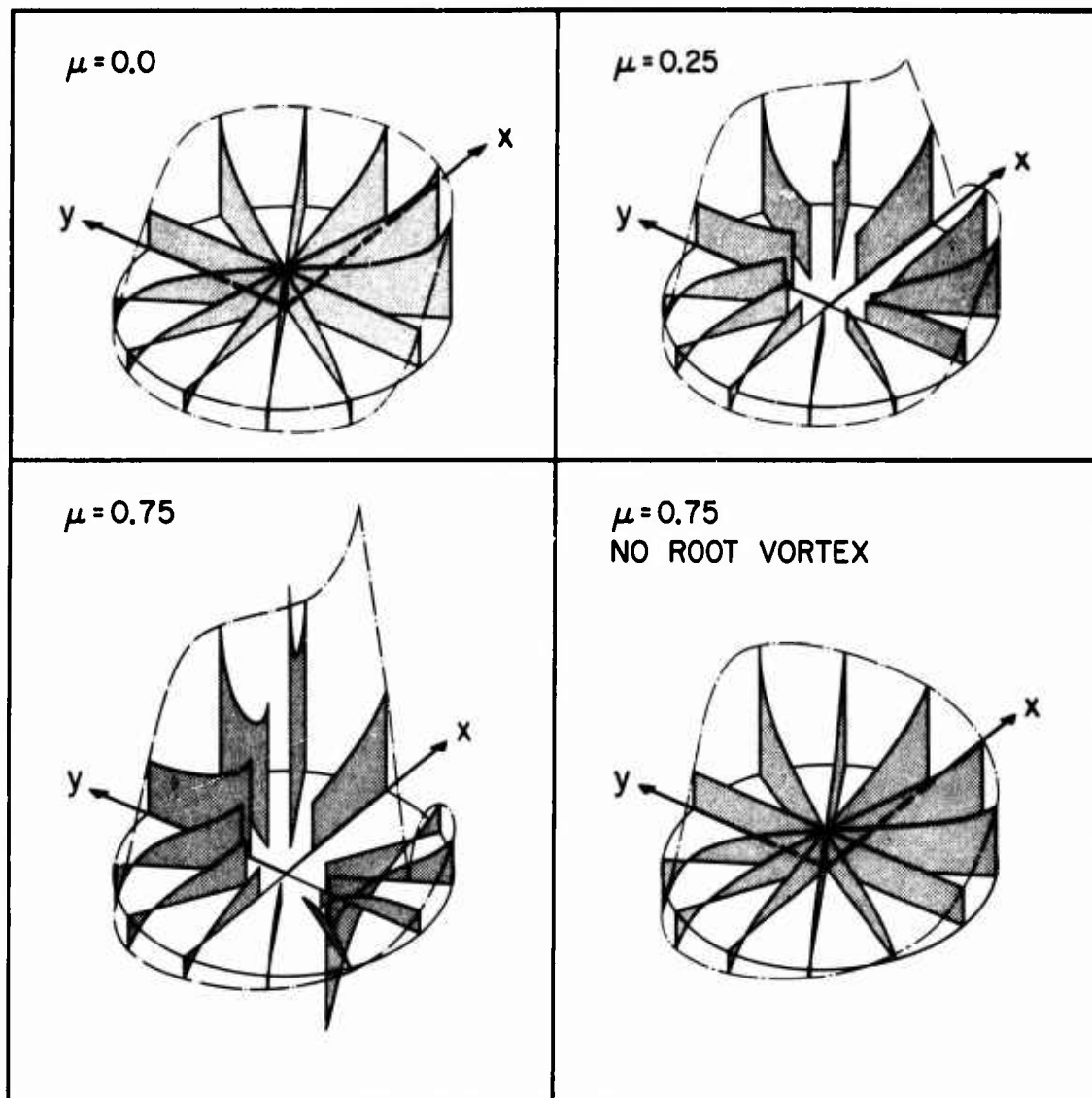


Figure 18. Variation of downwash distribution with advance ratio for uniform circulation.

at $\psi = 270^\circ$ combine to virtually eliminate the impulsive loading. Therefore retreating rotor blade problems due to the time-averaged downwash distribution are lessened in comparison to the advancing blade, a striking departure from the customary behavior of rotary wings.

8. CONCLUDING REMARKS

For rotors assumed to be characterized by an actuator disc, a proper definition of the rotor potential flow problem, for application to downwash and response predictions, has been proposed. An appropriate theory and method of solution are outlined which should be sufficiently simple and versatile to give a better understanding of the complex physical features and influences of the rotor circulation and downwash distributions. The important results obtained from the derivation and the numerical results will be noted below.

- 1) A simple, flat planar wake has been found to be a valid configuration for the wake vorticity down to advance ratios of around $\mu = 0.15$ for a nominal rotor thrust coefficient.
- 2) The rotor blade flapping equation reveals that only the second and lower harmonics of circulation or downwash directly influence the rotor thrust or moment. This implies that a reasonable approximation for the exact solution of the theory would be to truncate Fourier coefficients beyond the second harmonic.
- 3) Examination of the wake vorticity elements reveals that they fall into two groups, those whose strength varies inversely with advance ratio and those which are invariant.
- 4) The numerical downwash results show large gradients at the advancing and retreating azimuth locations and their variation with advance ratio. The longitudinal vorticity elements which are usually ignored are shown to cause significant lateral asymmetries in the downwash.

5) The uniform circulation distribution has undesirable characteristics evidenced in the infinite downwash at the rotor perimeter, and the discrete root vortex. The radial circulation distribution must be chosen to be zero at $r = 0$ and R to give realistic results.

6) Future efforts must obtain additional influence functions in order to use the present theory to predict rotor response.

9. REFERENCES

1. Crimi, P.: Theoretical Prediction of the Flow in the Wake of a Helicopter Rotor. Cornell Aero. Lab. Report No. BB-1994-S-1, September 1965.
2. Miller, R. H.: Rotor Blade Harmonic Airloading, AIAA Journal, Vol. 2, No. 7, July 1964.
3. Landgrabe, A. J.: An Analytical Method for Predicting Rotor Wake Geometry, Journal of the American Helicopter Society, Vol. 14, No. 4, October 1969.
4. Sadler, S. G.: A Method For Predicting Helicopter Wake Geometry, Wake-Induced Flow and Wake Effects on Airloads. Preprint No. 523, American Helicopter Society 27th Annual National Forum, Washington, D.C., May 1971.
5. Coleman, R. P.; Feingold, A. M.; and Stempin, C. W.: Evaluation of the Induced-Velocity Field of an Idealized Helicopter Rotor, NACA Wartime Report ARR-L5E10, June 1945.
6. Castles, W. and deLeeuw, J. H.: The Normal Component of the Induced Velocity in the Vicinity of a Lifting Rotor and Some Examples of its Application, NACA TR 1184, 1954.
7. Heyson, H. H. and Katsoff, S.: Induced Velocities Near a Lifting Rotor with Non-Uniform Disk Loading, NACA TR 1319, 1957.
8. Mangler, K. W.: Calculation of the Induced Velocity Field of a Rotor. Royal Aircraft Establishment Report No. 2247, February 1948.
9. Heyson, H. H.: Equations for the Induced Velocities Near a Lifting Rotor with Nonuniform Azimuthwise Vorticity Distribution, NASA TND-394, August 1960.
10. Drees, J. M.: A Theory of Airflow Through Rotors and its Application to Some Helicopter Problems, J. Helicopter Association of Great Britain, Vol. 3, July-September 1949.
11. Willmer, M. A. P.: The Loading of Helicopter Rotor Blades in Forward Flight, Royal Aircraft Establishment Report Naval 2-N-76935, No. 8, April 1959.
12. Bailey, F. J., Jr.: A Simplified Method of Determining the Characteristics of a Lifting Rotor in Forward Flight, NACA Report 716, 1941.
13. Ormiston, R. A.; and Peters, D. A.: Hingeless Rotor Response with Nonuniform Inflow and Elastic Blade Bending — Theory and Experiment, Paper No. 72-65, AIAA 10th Aerospace Sciences Meeting, San Diego, CA, January 1972.
14. Harris, F. D.: Articulated Rotor Blade Flapping Motion at Low Advance Ratio, Journal of the American Helicopter Society, Vol. 17, No. 1, January 1972.
15. Gessow, A.; and Myers, G. C. Jr.: Aerodynamics of the Helicopter, Macmillan Co., New York, 1952.

The Structure of the Rotor Blade Tip Vortex

by

C.V. Cook

Senior Research Engineer (Aerodynamics)

Westland Helicopters Limited
Yeovil England

SUMMARY.

The results of a set of experiments devised to measure the velocity distribution through a helicopter rotor blade tip vortex are presented. The experiments were conducted on a single full scale rotor blade operating at a representative tip speed on a whirl tower. The rotor was mounted in the inverted position (i.e. thrusting downward) to reduce the ground effects and produce a steady flow through the rotor. The vortex velocity distributions were measured for a range of vortex "ages" and a number of blade loadings, the highest of which was above that normally associated with a hovering rotor. A vortex 'age' range in terms of blade rotation of approximately 70° to 380° of azimuth was covered.

Flow visualisation using smoke was employed to determine the trajectory of the vortex and a hot wire anemometer to measure the induced velocities associated with the tip vortex.

NOTATION.

- $\delta(r)$ The vorticity function expressed in terms of the distance, r , from the axis of symmetry of the vortex.
 q_r Circumferential vortex induced flow.
 A^r The magnitude of the vorticity in the central region (vortex centre line to r_0)
 B, C Constants describing vorticity distribution outside central region ($r_0 - r_1$).
 r_0 Outer boundary of constant vorticity region.
 r_1 Outer boundary of vorticity distribution associated with the vortex.

1. INTRODUCTION.

The accurate prediction of rotor performance, rotor limit conditions, vibratory loads and the rotor noise are becoming an increasingly important requirement in the early stages of helicopter design. Reliable theoretical methods are essential in order to predict these parameters with the accuracy required by the designer. The precision with which these qualities may be determined relies upon a detailed knowledge of the aerodynamic loading on the rotor blade and how it varies around the disc. One of the most difficult features to determine in the estimation of the aerodynamic loading is the induced flow through the rotor. Many theoretical models of a helicopter rotor wake, in both hover and forward flight, have been developed in Europe, United States and the U.K., in an effort to improve upon the commonly used uniform induced flow-momentum theories. The majority of these models represent the rotor wake by a system of trailing vortices. They vary in complexity from the relatively simple concepts of Willmer, (1) who used a set of semi and doubly infinite vortex lines, to the more complex free-wake models such as those of Crimi, (2) Landgrebe, (3) and more recently Clark and Leiper (4). All these mathematical models, by necessity, make assumptions on the structure of the tip trailing vortex. Some methods assume a finite core size to the vortex, others limit the maximum velocities to some arbitrary figure. These assumptions have been necessary due to the lack of experimental information and may have been acceptable in the past, but as the wake models become increasingly more sophisticated the validity of the assumptions must be open to question. Such queries become particularly significant when considering wake deformation and the proximity of the trailing vortex to the following blades. The tip trailing vortices may lie within one chord's width of the blade throughout a large region of the helicopters flight envelope.

An experiment was carried out by Simons et al (5) where the velocity distribution through the vortices was measured on a model rotor using hot wire anemometry techniques. This experiment showed the techniques of using a hot wire probe to be possible, but the results are restrictive in application due to the small scale of the rotor and the low tip speed employed. An experiment was therefore devised to measure the velocity distribution through the tip vortex of a full scale rotor.

2. DESCRIPTION OF TEST FACILITY.

The experiment was carried out using a standard production blade mounted on a whirl tower (shown in fig.1), normally used for the balancing and tracking of production blades. The power supply was from a 400 h.p. electric motor, capable of running in either direction. The blade and hub were mounted in the inverted position and rotated in the opposite direction from standard, producing a rotor that thrusts downward. This method of mounting has a distinct advantage in that the ground effect is reduced and a far steadier flow through the rotor is produced on a tower whose height from ground level to hub centre is only 19 ft. A single blade was attached to the hub with a large counterbalance weight attached diametrically opposite to balance the centrifugal forces. The single blade and to some extent the presence of the ground produces a tip vortex path that remains 'below' the rotor disc for more than one revolution. This feature enabled the velocity measuring equipment to be positioned below the rotor and moved both radially and vertically with comparative ease. In addition the use of a single blade meant that high blade loadings could be obtained with the limited power available. The rotor was 28 ft. radius, with a blade chord of 1.367 ft, 8° overall washout and NACA 0012 section. The blade tip cap was similar in design to that of a standard Sikorsky S58 rotor blade, extending $6\frac{1}{2}$ inches beyond the spar at the quarter chord reducing to 1 inch at the trailing edge. A tip speed of 600 ft/sec. was used throughout the test program. The whirl tower had the facility to measure rotor thrust and power.

3. DESCRIPTION OF EXPERIMENT.

Success of the experiment relied on the steady nature of the flow through the rotor, absolutely still

air conditions and the ability to determine accurately the trajectory of the tip vortex. The requirement that the tip vortex centre should pass exactly through the probe meant that these features were essential.

3.1. Flow visualisation

The trajectory of the tip vortex was determined by taking a large number of 'still' photographs of the flow, made visible by injecting smoke into the rotor flow field. The smoke was generated by a commercial distress flare housed in a small container with a supply of compressed air. The smoke was piped to a five pronged rake mounted vertically, just above and outside the rotor disc. In this position the smoke becomes entrained in the tip vortex making the passage of the vortex clear over more than one revolution of the rotor. A set of photographs was taken using two hand operated cameras positioned in the disc plane and at right angles to the rake. The sequence of photographs in figure 2 show the passage of the tip vortex during one revolution of the rotor. (The photographs were not obtained during one revolution consequently they are not at equal time intervals). The photographs have been sequenced to give an indication of the progress of the vortex across the rotor disc. The rotor hub is to the left of the picture and the blade is advancing towards the camera.

A large number of these photographs were processed to obtain the path of the vortex during its period below the disc, an example of which is shown in figure 3. The scale of the photographs was obtained from the knowledge of the dimensions of the rake. Figure 3 also shows the position (below the blade) of the vortex from the preceding blade passage. It is interesting to note the rapid change of direction of the vortex from the predominately spanwise movement to a combined spanwise and vertical movement after the following blade has passed over the vortex, the change in direction being principally due to the presence of the 'new' tip vortex outboard. The presence of an axial velocity, along the vortex in the direction of rotation of the rotor can be observed from the photographs. The smoke entrained near the centre of the vortex is seen to move circumferentially around the rotor disc by a substantial amount during one revolution of the rotor. A crude estimate of the magnitude of the vortex axial velocity suggests that it is of the order of a tenth of the tip speed, but further detailed investigation would be necessary for a reliable estimate. Photograph 2 of the sequence shown in figure 2 shows the blade having just passed through the smoke trails leaving a distinct tip vortex, illustrating the very rapid rolling up of the trailing vorticity.

The trajectory of the tip vortex was determined by this photographic process for the five collective pitch settings used in the experiment to measure the vortex velocity distribution.

3.2. Velocity measurement

3.2.1. Instrumentation

The hot wire anemometer, used to measure the velocity distribution through the vortex, consists of a short piece of wire 5 microns in diameter and approximately 1/16th inch in length suspended between two prongs as shown in figure 4. The wire forms one arm of a bridge circuit and is heated by the current flowing in the bridge. This bridge is powered by a servo amplifier whose output voltage is controlled by the bridge unbalance and which maintains the probe resistance (and hence the probe temperature) very nearly constant.

Air flow reduces the temperature of the wire, which is sensed by the change in current flow due to the corresponding change in resistance, and is instantaneously corrected by the servo amplifier. Fundamentally, the power required to maintain constant temperature is monitored. As this output is non linear with velocity it is conditioned by a small battery powered analogue computer (Lineariser) having a transfer function such that the output voltage is proportional to flow velocity. The output from the lineariser is therefore amenable to quantitative assessment by recording on a U.V. or a magnetic tape recorder, or observation on an oscilloscope.

The 'electronic upper frequency' limit of the anemometer was found to be of the order of 90kHz. No direct frequency response measurements were made as the expected frequencies of flow fluctuations of interest in the experiment were far below this frequency. Each probe was calibrated individually against a pitot-static tube for a velocity range of 0 to 350 ft/sec.

The instrumentation used during the experiment included a long persistence scope which was used to monitor the output signal from the lineariser. A magnetic tape recorder with an upper frequency limit of 20kHz was used to record the signal. Analysis of the signal was carried out later by replaying the tape recorder at a reduced speed and reproducing the signal on a U.V. recorder. The reproduce speed of the tape recorder was reduced by a factor of 16 such that the 1200Hz galvanometer response was effectively increased to approximately 20kHz thereby maintaining the recorded bandwidth.

3.2.2. Experimental procedure

Having determined the trajectory of the tip vortex the probe could be positioned accurately below the rotor, recording the velocity distribution associated with the tip vortex as it passes over the probe. The axis of the probe was aligned normal to the rotor radius and parallel to the ground, i.e. with the axis of the sensitive element laying along the axis of the tip vortex. As the element is insensitive to velocities along its axis no rotor swirl components or axial velocities within the vortex would be measured. The velocities measured are only those in the plane normal to the axis of the wire and therefore will be the translational velocity of the tip vortex in spanwise and vertical directions (of the rotor) and the circumferential induced velocities associated with the vortex. Vortex radial flows are assumed small by comparison with the circumferential velocities. The translational velocity of the vortex over the probe was measured from a cine film of the smoke flow visualisation of the vortex. The movement of the vortex centre from frame to frame was determined and with the knowledge of the speed of the film the translational velocity of the vortex over the probe was obtained. This information enabled the time base of the recording of the vortex 'signal' to be converted to a distance base. Also the translational velocity of the vortex could be removed from the signal. Thus the circumferential velocity of the vortex alone could be deduced and its variation with distance from the vortex centre. Recorded on a separate channel was an

azimuth marker positioned to indicate when the blade was directly above the probe. The exact 'age' of the vortex in terms of how far the blade had progressed around the azimuth by the time the vortex was recorded could therefore be obtained. By varying the spanwise position of the probe a vortex 'age' range was obtained, ages between 70° and 380° of azimuth were found to be possible.

The output signal from the probe was displayed on a long persistence scope and although the vortices were immediately visible when the probe was mounted in the estimated path of the vortices the height of the probe had to be adjusted such that the maximum number of vortex centres passed through the probe. It was found that the path of the vortices tended to drift with time but when a good set was observed (determined by the maximum velocities) they were recorded on magnetic tape. It was not possible from observation of the scope to tell if the vortex core passed over the probe so reliance was made on observing the magnitude of the velocity peaks. Replaying the tape at a slower speed was the only way of telling whether the vortex centre had been intersected. This intersection was determined by comparing the minimum velocity within the vortex core with the mean translational velocity over the probe. When the two velocities were the same the core centre had been intersected, i.e. the condition of zero induced velocity associated with the vortex under consideration.

4. ANALYSIS OF RESULTS.

The hot wire probe measures velocities in a plane normal to the axis of the wire but cannot distinguish direction within the plane. The wire therefore records the vector sum of the vortex induced flow and the translational velocity of the vortex. In order to conduct any analysis of the vortex by the fixed hot wire approach, a number of assumptions on the relative magnitude and character of the flows must be made. They are:-

1. That the major components of the flow in the plane normal to the element are a circumferential velocity associated with the vortex and the translational velocity. No significant vortex radial velocities are assumed to exist when conducting the analysis.
2. The curvature of the vortex path is assumed to be small over the region where the vortex velocities are being measured.
3. The translational velocity is constant over the period when the vortex signal is being recorded.
4. The three above assumptions and the condition that the vortex centre passes exactly through the probe, are prerequisite for any analysis. Only under these conditions can the two velocities (the induced and the translational) be separated, the translational velocity being in a direction normal to the induced, can therefore be removed from the signal.
5. The recordings being time-based and not the measurement of the vortex velocities at an instant in time (or age) of the vortex means that any change in the structure of the vortex, such as roll-up, would be reproduced during the time taken for each vortex to effectively traverse the probe i.e. one side of the vortex would be younger than the other. However, it was argued that the characteristic time for traversal of the vortex was small in terms of its ageing. This feature was subsequently shown to be the case, even the vortices at widely differing ages (within the measured range) did not show any significant structural changes.
6. The measurements of induced flow, although only obtained in one horizontal plane through the vortex, were assumed to be representative of the flows in any radial section of the vortex, i.e. the vortex was assumed to be symmetrical and hence isolated; a requirement for any basic interpretation of the measurements. This assumption amounts to the fact that the vortex may be considered as an effectively fully rolled-up tip vortex.

Since it is only possible to interpret those recordings where the vortex centre passed through the probe, the method obviously produced a large amount of unusable information. However, it was found that with only about one minute of recording for each condition a sufficient number of vortices of good quality were obtained. In the majority of conditions at least 5 vortices were considered sufficiently good to analyse. A typical trace of one of these vortices is shown in figure 5. This figure shows the symmetry of the vortex and a well defined 'viscous' core, with the minimum velocity within the core of similar magnitude to the translational velocity of this vortex, indicating zero induced velocity associated with the vortex. (Remembering that the probe cannot distinguish the change in direction of the induced velocity as the vortex centre is crossed). The time base of the signal has been converted to a distance base to give an indication of the relative size of the tip vortex.

A certain amount of high frequency content to the signal was observed in the vicinity of the high induced velocities, the origin of which is as yet unknown but it is believed to be associated with the probe and possibly a motion of the wire produced by the high rates of change of air velocity. The possibility of it being turbulence was ruled out as the energy content was far too high. A lower frequency signal can also be observed in the high velocity region of the vortex which could represent the rolling up of the trailing vortex sheet. A similar observation was made by Kucheman (6) when analysing the structure of the leading edge vortex on a slender delta wing.

Figure 6 shows a sequence of vortices illustrating the regularity and degree of repeatability attainable. The line down the centre of the third vortex indicates that the viscous core was intersected. The small discontinuity in the region between the vortices is produced by the passage of the blade over the probe and can therefore be used to estimate the 'age' of the vortex.

In order to analyse the results and compare the differing test conditions the output velocity traces were curve fitted and the translational velocity component removed. The form of the curve fitting was based upon the estimated vorticity distribution within the vortex rather than the velocity profile, the form of the vorticity distribution being the easier quantity to manipulate although it was the velocity profile comparison that was used as the criterion for the quality of the fit. The type of function defining the vorticity distribution was determined by transforming the velocity distribution of a number of vortices into a vorticity distribution via the expression:-

$$\gamma(r) = \frac{q_r}{r} - \frac{dq_r}{dr} \dots\dots\dots (1)$$

(Assuming the vortex to be doubly infinite for the purposes of determining the core vorticity distribution which is valid when the core radius is small compared with the radius of curvature of the vortex). The function that was found to best fit the vorticity distribution outside the central region of the core was of the form:-

$$\frac{B}{(r+c)^N} \dots\dots\dots(2)$$

and within the central region a constant distribution of vorticity was assumed, due to the lack of detail on the trace and its small size. Defining a single function for the vorticity distribution was not found to be realistic due to the rapid 'fall-off' in vorticity at the edge of the central area. Thus the vortex is divided into three areas, the inner core (region 1) where the vorticity is constant (extending to r_0) the outer part of the core where the vorticity is of the form of equation 2 and outside the core where no vorticity exists (region 3).

Having defined the form of the functions describing the vorticity the equation giving the velocity distribution was obtained. The velocity at any radial point being:-

$$q_r = \frac{1}{r} \int_0^r \gamma(r) r dr \dots\dots\dots(3)$$

giving the expression for the velocity within the area of constant vorticity (region 1) vortex centre line to r_0 as:-

$$q_r = \frac{1}{2} A r \dots\dots\dots(4)$$

(where A is the magnitude of the vorticity)
and within the area containing the vorticity but outside r_0 (region 2, $r_0 - r_1$):-

$$q_r = \frac{1}{r} \left\{ \frac{A r_0^2}{2} + \frac{B}{(2-N)(1-N)} \left[\left\{ r(1-N) - C \right\} (r+C)^{1-N} \right]_{r_0}^r \right\} \dots\dots(5)$$

and outside the area containing the vorticity (region 3, $r_1 - \infty$) the expression becomes:-

$$q_r = \frac{1}{r} \left\{ \frac{A r_1^2}{2} + \frac{B}{(2-N)(1-N)} \left[\left\{ r(1-N) - C \right\} (r-C)^{1-N} \right]_{r_0}^{r_1} \right\} \dots\dots(6)$$

(where r_1 is the radius of the region containing the vorticity)

Using equations 4 and 5 the unknowns (A, B, C, N and r_0) were determined taking 9 point values of the velocity profile from the traces and using a least squares approach to obtain the best fit. All of the test conditions were analysed in this fashion. For each condition 9 point velocity values from each trace were measured and the unknowns A, B, C, N and r_0 obtained for the condition. The quality of the agreement between the original traces and the constructed line is shown in figure 7. Also shown is the distribution of vorticity within the core and the three regions described above.

5. DISCUSSION OF RESULTS.

Five thrust conditions were covered for a constant tip speed of 600 ft/sec. and for each thrust condition four radial positions of the probe were considered, giving an age range of approximately 70° to 380° . It was not possible however, to analyse some of these conditions, particularly the low pitch and early vortex age. The proximity of the probe to the blade leading edge precluded positioning the probe in the optimum position. Although high velocity peaks were recorded no well defined vortex cores were observed except for the higher loading case. Only the analysis of the good quality vortices have therefore been reproduced.

Figures 8(a) to (d) show the resultant analysis of the induced velocity distribution through the vortex for the differing ages and blade thrusts. All the traces are basically similar in form with the maximum velocities increasing with increasing blade lift, except for the highest blade loading condition where the peak velocity is greatly reduced and the viscous core diameter increased. The reason for this apparent discontinuity could be due to blade tip stall. A theoretical analysis using a contracting wake model (described in reference 7) suggests that the blade is on the point of stalling at a blade lift of approximately 3800 lb. This figure was determined by postulating that the blade section near the tip (95% radius) stalls at a similar lift coefficient to that occurring on a model of the section in a wind tunnel under two dimensional flow conditions. A similar value of blade lift was obtained from the reduction of flight test data from a Wessex undergoing high attitude hover tests.

Figures 9 through to 12 show some of the observed basic characteristics of the tip vortex and how they vary with blade lift and time. Figure 9 shows the vortex circulation measured from the traces by taking the velocity at the outer edge of the core. The outer edge of the core was readily observable on the majority of traces and was identifiable by a definite change in slope of the measured vortex velocity distribution. The curve outboard of this point obeyed the $1/r$ law, showing the flow to be irrotational. The core was also distinguishable by a sharp increase in the high frequency content of the signal. The circulation is plotted against total blade lift and is compared with the equivalent tip vortex strength for a theoretical constant spanwise blade circulation distribution. The circulation appears to be lower than might be expected considering that uniform spanwise circulation would under-predict the peak circulation near the tip. A similar observation was made by Dosanjh et al (8) who found that the measured circulation in the rolled up tip vortex behind a semi-wing mounted in a wind tunnel was only 58% of the expected value. A further indication of the difference between bound circulation and the circulation entrained in the tip vortex is found in the high loading case if the stalled condition of the blade tip is the cause of the growth of the tip vortex core. The C_u near the blade tip approaching this condition would be approximately 1.0 (before stall). The expected vortex circulation would be of a similar order to the bound circulation i.e. approaching 400 ft²/sec. The measured circulation, as shown in figure 9, never reaches half this value. A difference of this magnitude is unlikely to be attributable to inaccuracies in the equipment or the experimental process. Resolution of this apparent discrepancy can only be obtained by a more comprehensive investigation where the blade loading distribution is also measured.

The experimentally obtained band on the graph indicates the degree of scatter of the vortex signals and includes the effect of vortex 'age'. The effect of age on the circulation contained in the tip vortex has not been reproduced as the scatter from trace to trace was in most cases larger than the variation of the mean value with age. Therefore, within the experimental accuracy the total circulation in the tip vortex remained substantially constant over the age range covered. A similar conclusion was made regarding the size of the vortex, the variation with blade loading was observable but any variation with age was not. The variation in vortex diameter with blade loading is shown in figure 10, again the scatter band is quite large increasing with the higher loadings. The fact that the vortex size and the circulation do not change materially within the age range covered (within experimental accuracy) suggests that the roll up process can be considered complete by at least 70 degrees of rotation of the rotor.

The viscous core size, on the otherhand, did show a small but distinct change with vortex age, but no significant changes over the blade loading range, except for the highest loading case. The viscous core being defined for the sake of description by the distance between the velocity peaks (which is not necessarily the diameter of the constant vorticity region). The variation of viscous core size with vortex age is shown in figure 11, the difference in size between the lower loading conditions and highest condition being readily observable. The viscous core diameter was considerably smaller than expected, especially as the boundary layer of the blade would be expected to be turbulent at a Reynolds No. of 5.2×10^6 , based on tip speed and blade chord. A comparison was made between the measured velocity distribution and the theoretical distribution for a viscous vortex (9). A value of 10 times the laminar kinematic viscosity was used, as suggested by Newman (10) for conditions where the boundary layer is turbulent. This theory produced a velocity distribution with a viscous core approximately three times larger than measured and a velocity distribution that was underestimated outside the viscous core. The comparison indicated that significantly more vorticity existed outside the viscous core than has been observed by Newman and Dosanjh who also compared measured results from a wing mounted in a wind tunnel with viscous vortex theory.

Figure 12 shows the decay of the induced velocity peaks with vortex age for the five blade loading conditions. The velocity peaks are those obtained as a result of the curve fitting, not necessarily the peak velocity recorded on the trace which included some high frequency 'noise' near the peak. The peaks on the signal were of the order of 20 to 40 ft/sec. higher than the curve fitted values. At a blade loading of 3,750 lb. a higher degree of scatter was observed on the peak velocities than on the lower loading cases, a dashed line has therefore been used and indicates the higher velocity values obtained for each age condition.

The most commonly used representation of the tip vortex in theoretical rotor wake models is a vortex with uniform vorticity in the core, sometimes called the 'combined' or Rankine vortex. Using this representation a core size is normally postulated, which if chosen too small will produce extremely high induced velocities. A comparison between the observed vortex velocity distribution and a vortex with uniform vorticity, but having the same total circulation is shown in figure 13. Two 'combined' vortices are illustrated, one having the same maximum velocity as the observed vortex and the other with half the core size. Both vortices show that the combined vortex representation overestimates the induced velocities in the vicinity of the core by a substantial amount. The radial position of the peak velocity is also overestimated for any reasonable restriction on the maximum velocity.

6. CONCLUSIONS.

The observed structure of the rotor blade tip vortex indicates that the vortex can be assumed to be effectively rolled up by at least 70° of rotation of the rotor. The effective size of the vortex core was considerably larger than simple theories would suggest, but the viscous core was significantly smaller.

The velocity distribution through the vortex was unlike those observed in experiments on semi wings in a wind tunnel. The type of comparison obtained with the viscous vortex theory for the wind tunnel experiments by Newman and Dosanjh was not attainable with this experiment. The primary difference being the small viscous core size and 'fuller' velocity profile. Representation of the tip vortex by a Rankine or combined vortex would produce significant errors in the induced velocity within a 'half chord' radius of the centre of the tip vortex.

The circulation contained in the tip vortex was approximately half the value expected, based on the supposition that the rolled up vortex strength would be of a similar order to the peak circulation near the blade tip.

The results of the highest blade loading case showed a marked change in the vortex structure suggesting that the blade tip may have been in a high drag or stalled region. Should this suggestion be the case then it may be that at higher tip speeds when the strength and position of the shock wave on the aerofoil is dominating the drag characteristics a significant change in vortex structure may be produced.

The experiment, although primarily of an exploratory nature indicated the feasibility of using a hot wire anemometer to measure full scale rotor wake characteristics, although some refinements for more detailed work would be desirable.

7. REFERENCES.

- | <u>Author</u> | <u>Title</u> |
|-------------------|---|
| 1. M.A.P. Willmer | The Loading of Helicopter Rotor Blades in Forward Flight. Royal Aircraft Establishment (Bedford), Report No:NAVAL 2, April 1959. |
| 2. P. Crimi | Theoretical Prediction of the Flow in the Wake of a Helicopter Rotor. Cornell Aeronautical Laboratories. Report No.BB-1944-5-1. September 1965. |

<u>Author</u>	<u>Title</u>
3. A.J. Landgrebe	An Analytical Method for Predicting Rotor Wake Geometry. J. American Helicopter Society 14 (4), October 1969.
4. D.R. Clark & A.J. Leiper	The Free Wake Analysis: A Method for the Prediction of Helicopter Rotor Hovering Performance. J. American Helicopter Society 15 (1). January 1970.
5. I.A. Simons, R. Pacifico & J.P. Jones	The Movement, Structure & Breakdown of Trailing Vortices from a Rotor Blade. Presented to the CAL/USAA Avlabs Symposium in Buffalo, New York in June 1966.
6. D. Kückeman	'Turbulence' and Vortex Motions. Unpublished Procurement Executive, Ministry of Defence Report.
7. C.V. Cook	Rotor Performance Predictions in Hover. Research Paper 357 Westland Helicopters Ltd., Yeovil, England. November 1968.
8. D.S. Dosanjh, E.P. Gasparek & S. Eskinazi	Decay of a Viscous Trailing Vortex. The Aeronautical Quarterly May 1962.
9. H. Lamb	Hydrodynamics. Cambridge University Press, 6th Edition, 1932.
10. B.G. Newman	Flow in a Viscous Trailing Vortex. The Aeronautical Quarterly, May 1959.

8. ACKNOWLEDGEMENTS

The author wishes to acknowledge the assistance of his colleagues during the tests and in the analysis of the results, which were carried out under contract to the Ministry of Defence (Procurement Executive). He also thanks the MOD (PE) and Westland Helicopters Limited for permission to publish this paper, which nevertheless expresses the author's opinions, not necessarily coinciding with those held by these authorities.



FIG 1 - ROTOR WHIRL TOWER FACILITY

FLOW VISUALISATION
PROGRESS OF TIP VORTEX DURING
ONE ROTOR REVOLUTION



1.



2.



3.



4.



5.



6.



7.

FIG. 2

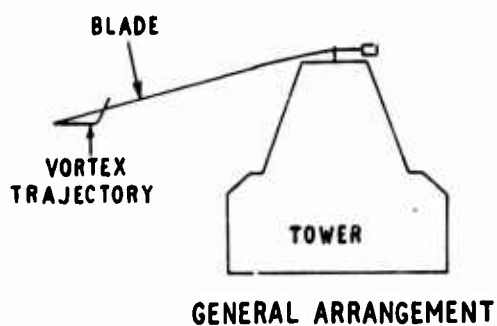


FIG. 3
TRAJECTORY OF BLADE
TIP VORTEX

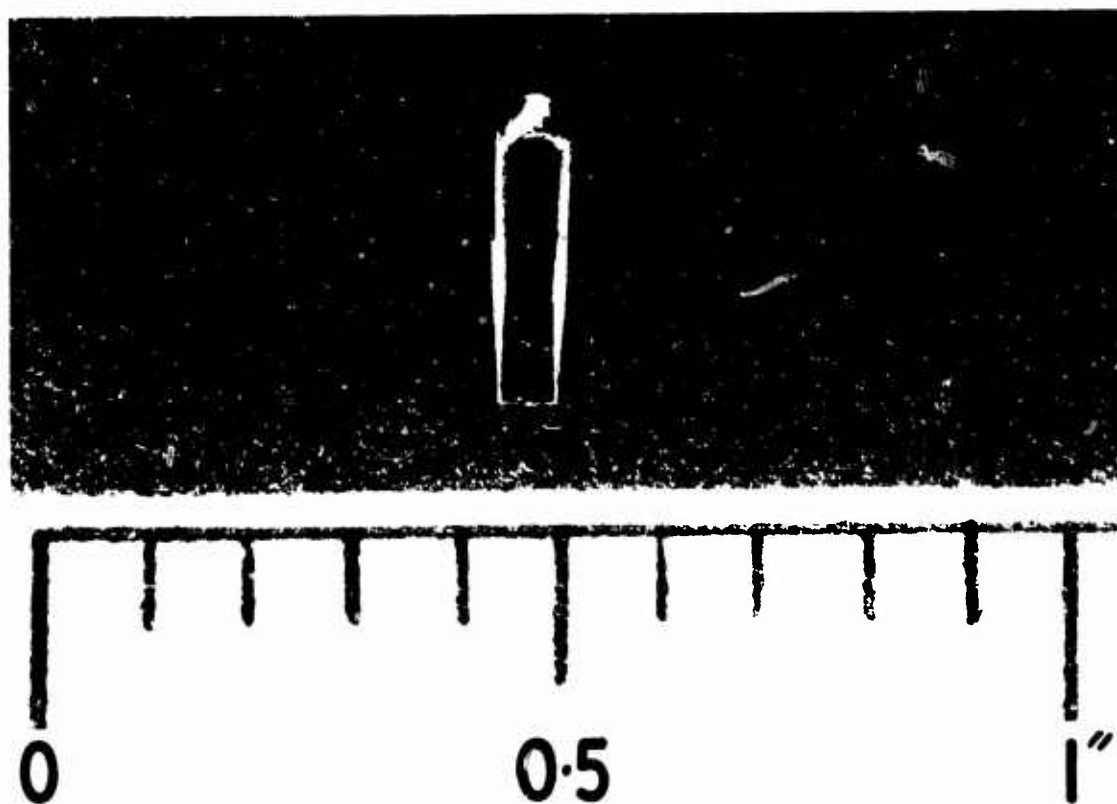
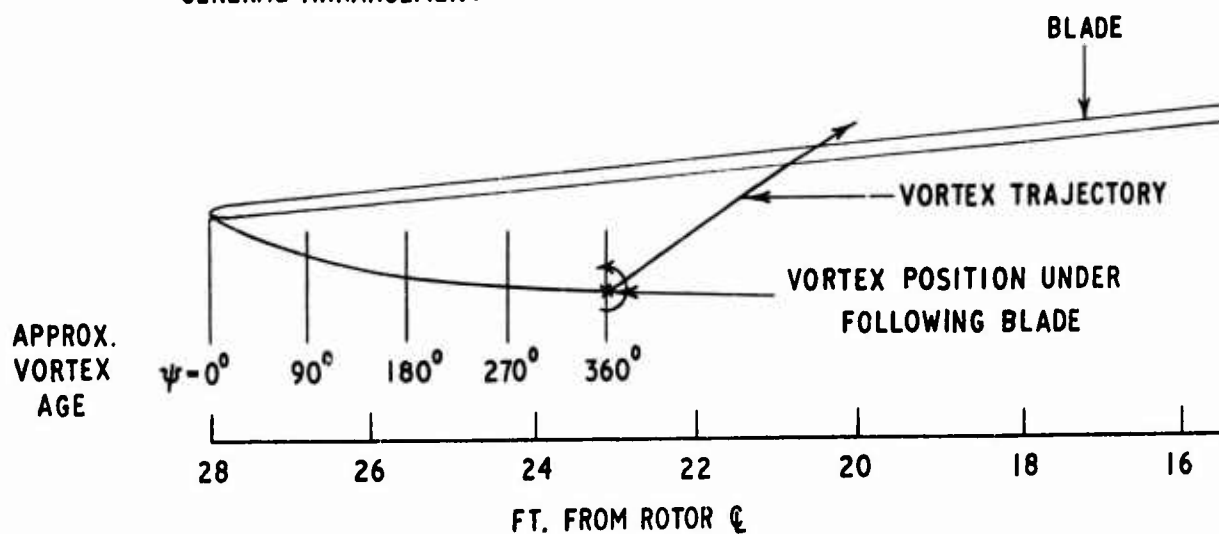


FIG. 4 HOT WIRE ANEMOMETER

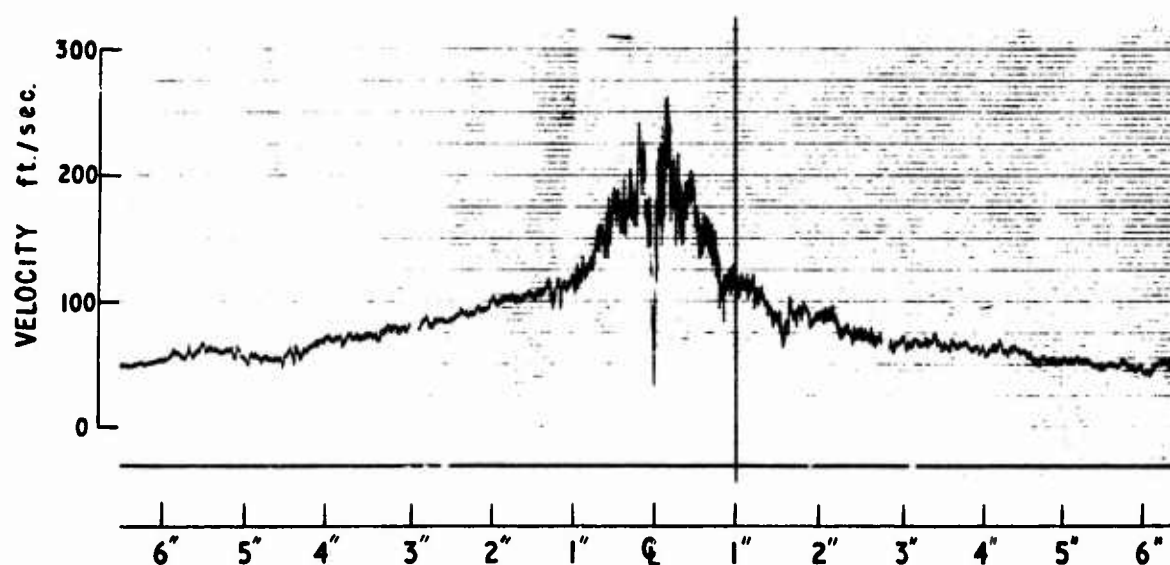


FIG.5-A TYPICAL TRACE OF THE VELOCITY DISTRIBUTION THROUGH A TIP VORTEX

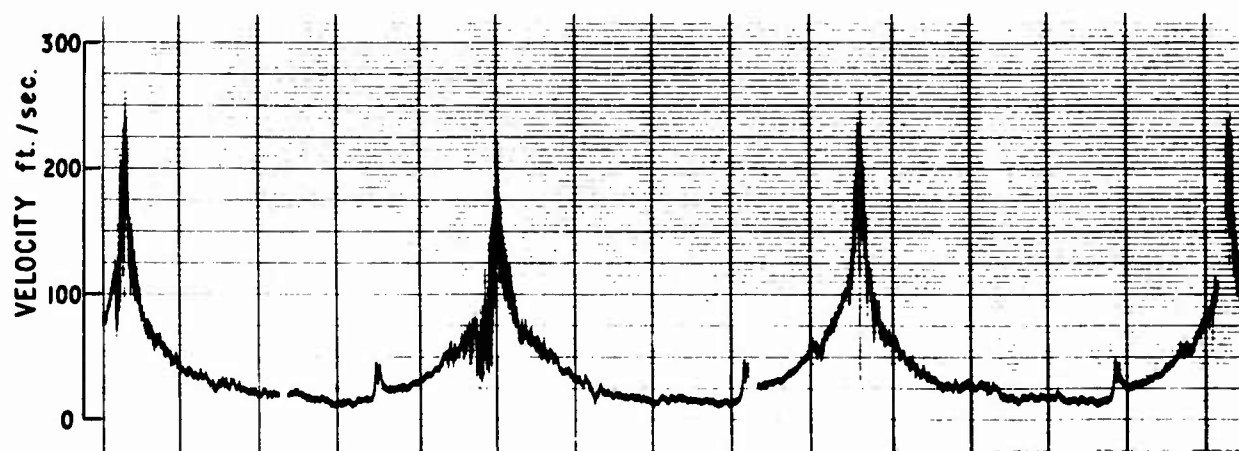
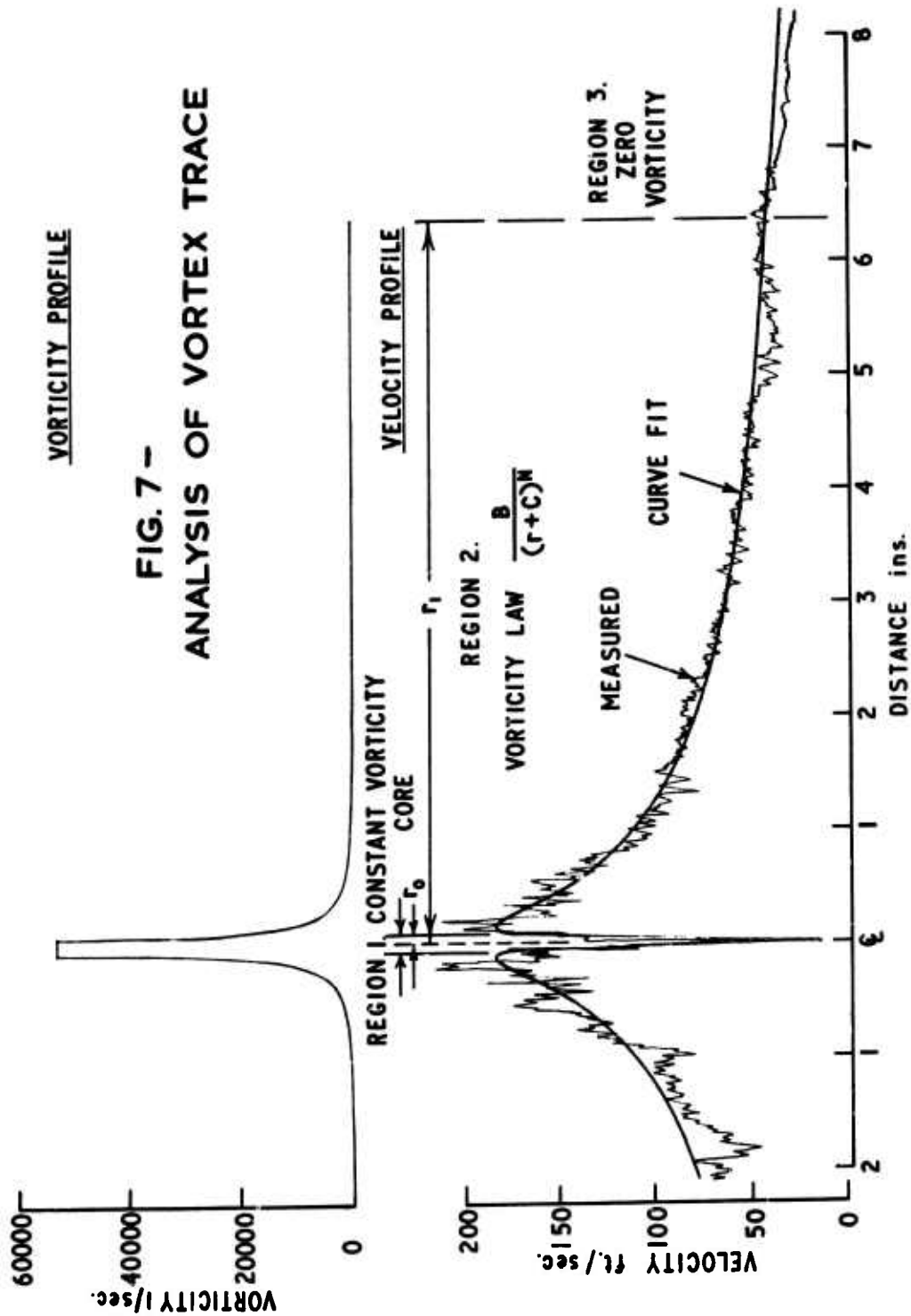


FIG. 6 - A SEQUENCE OF TIP VORTICES



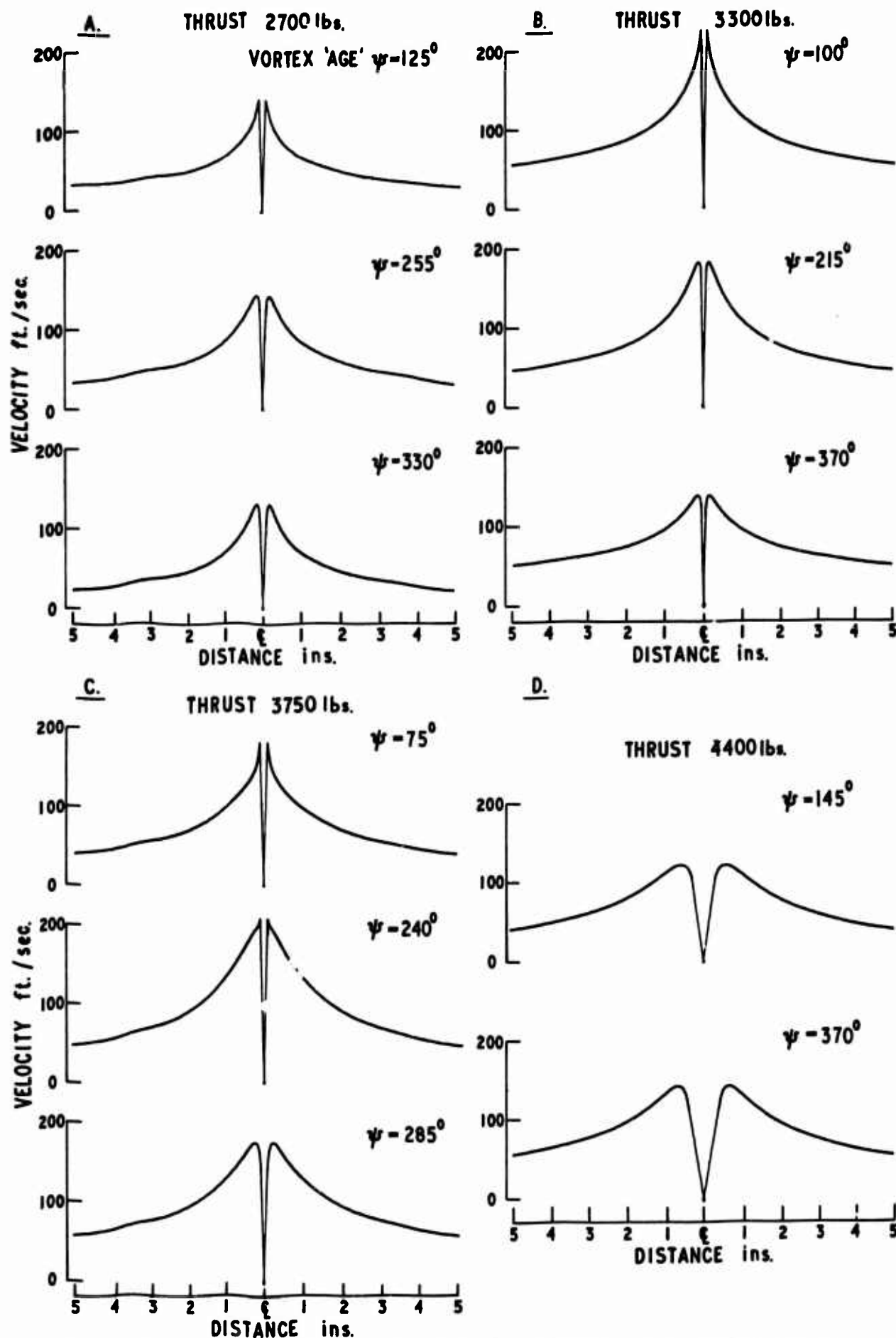
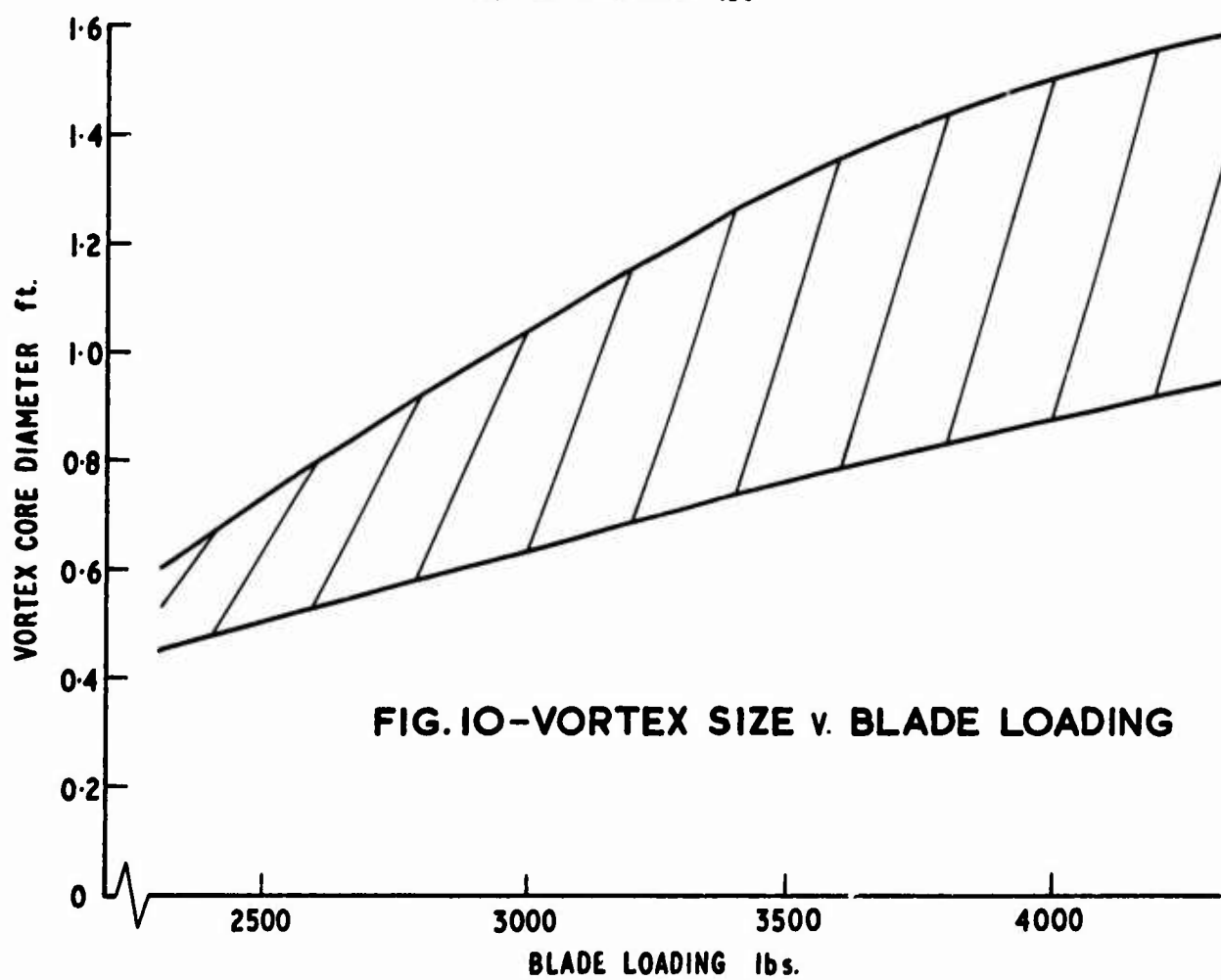
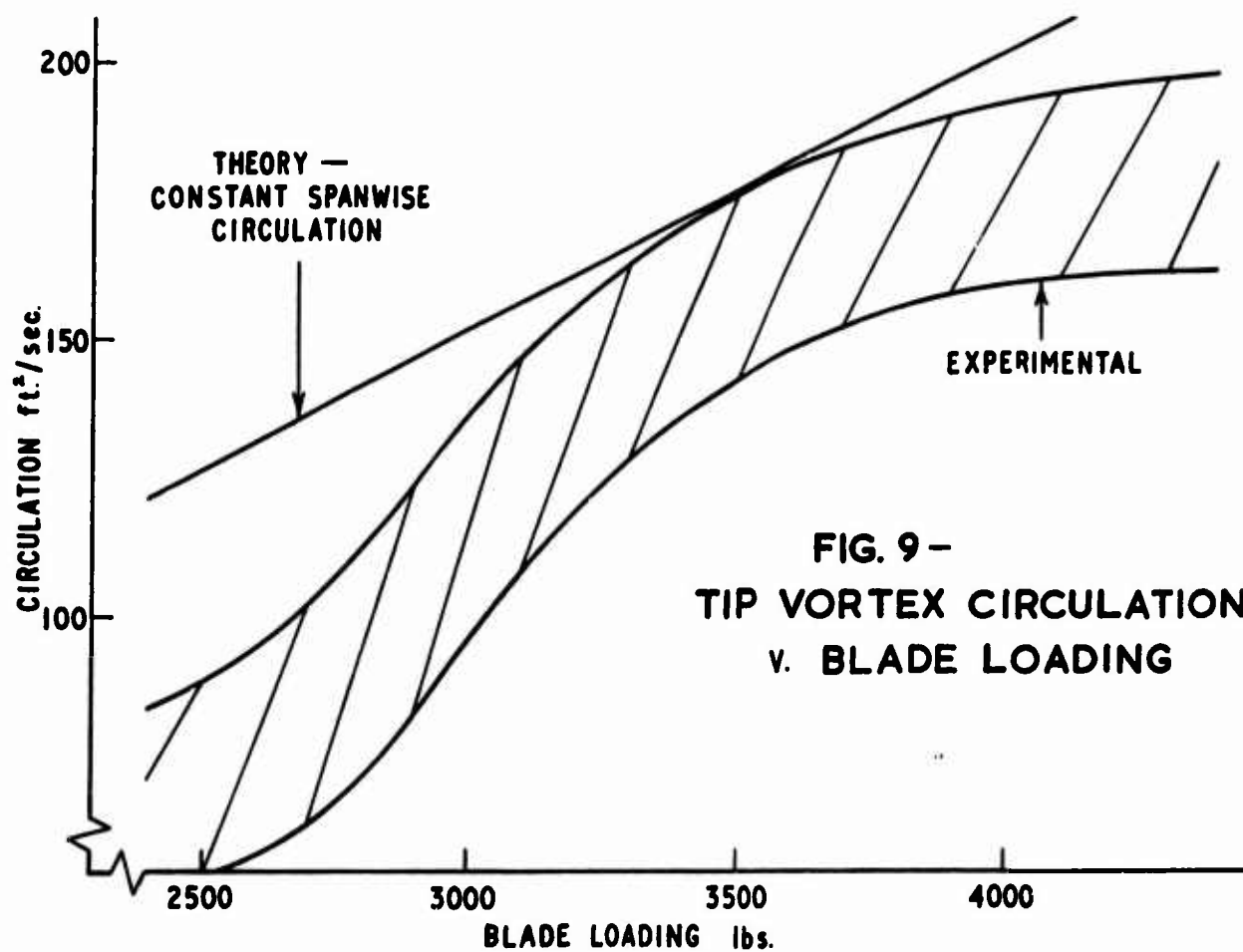


FIG.8-VARIATION OF VELOCITY DISTRIBUTION WITH TIME



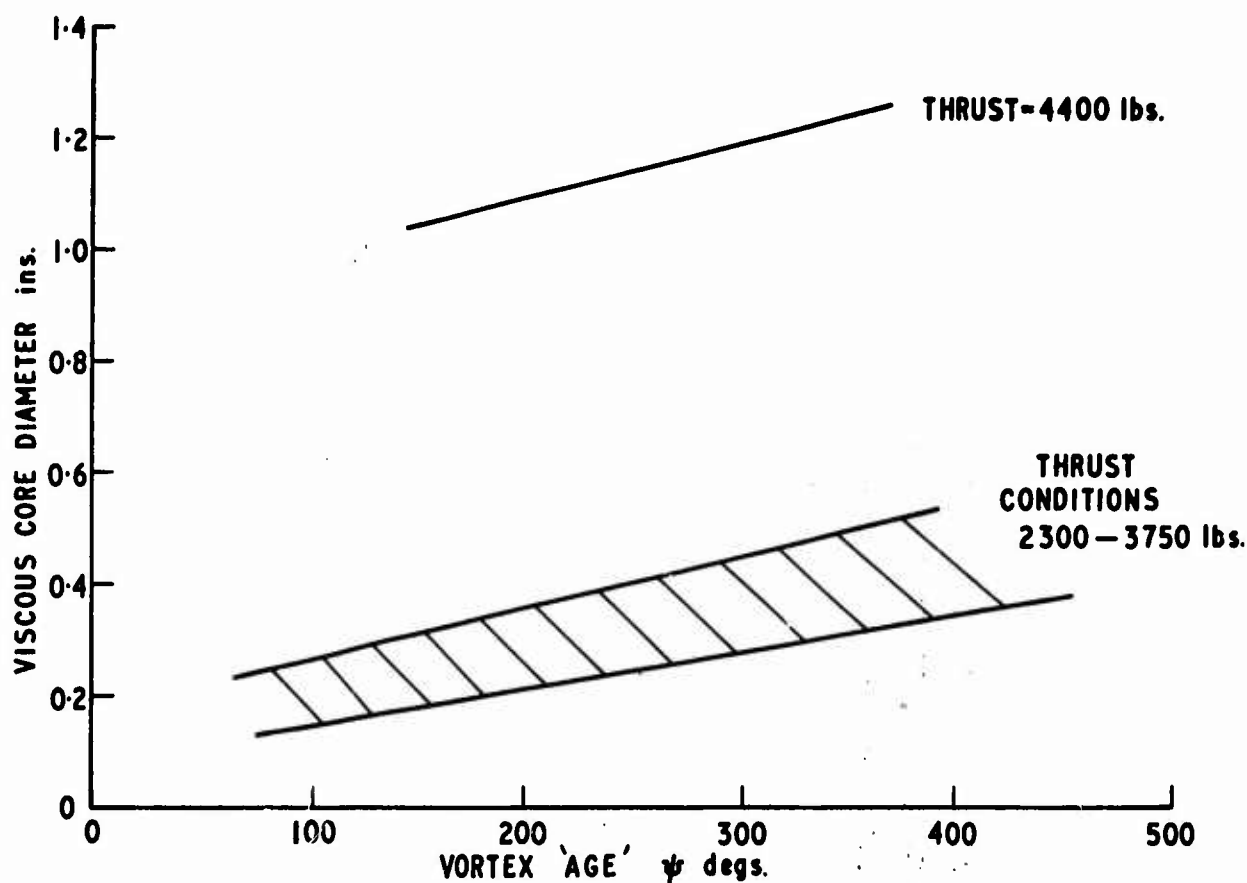


FIG. II - VISCOUS CORE DIAMETER v. VORTEX AGE

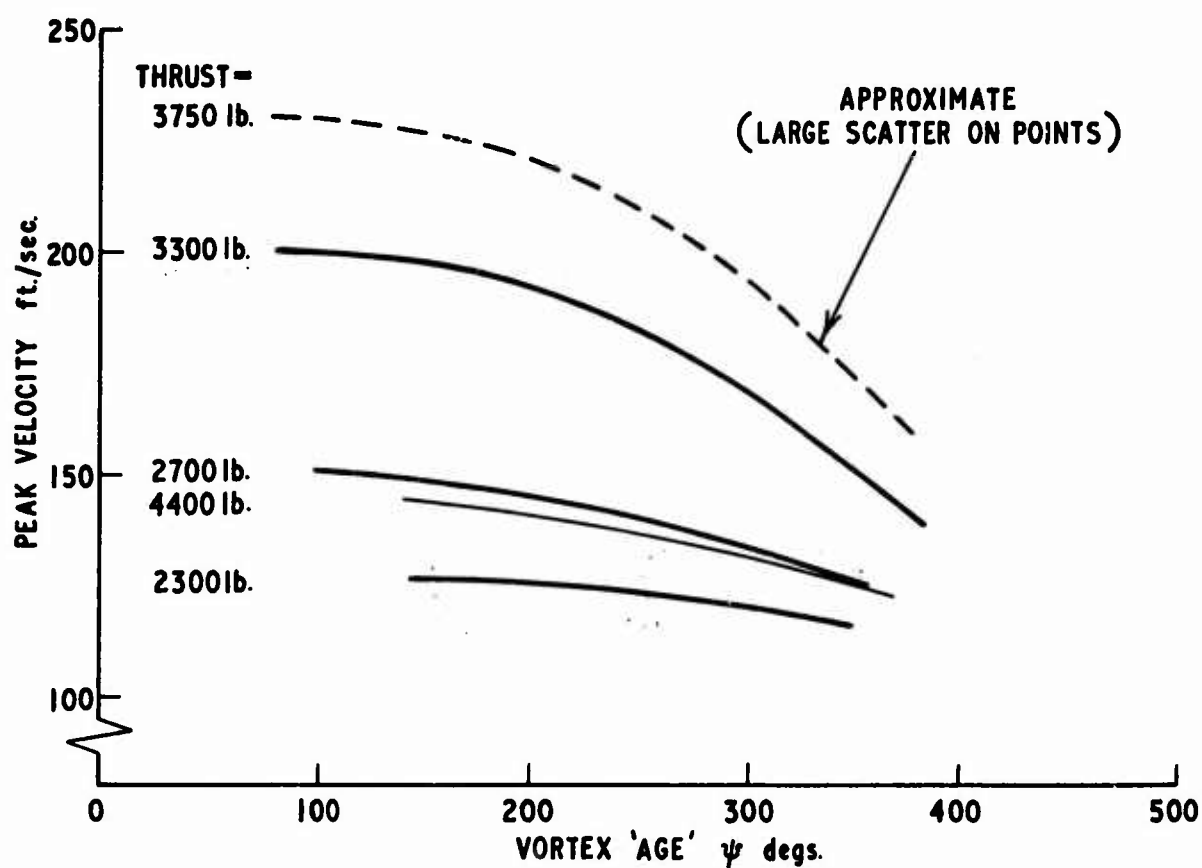
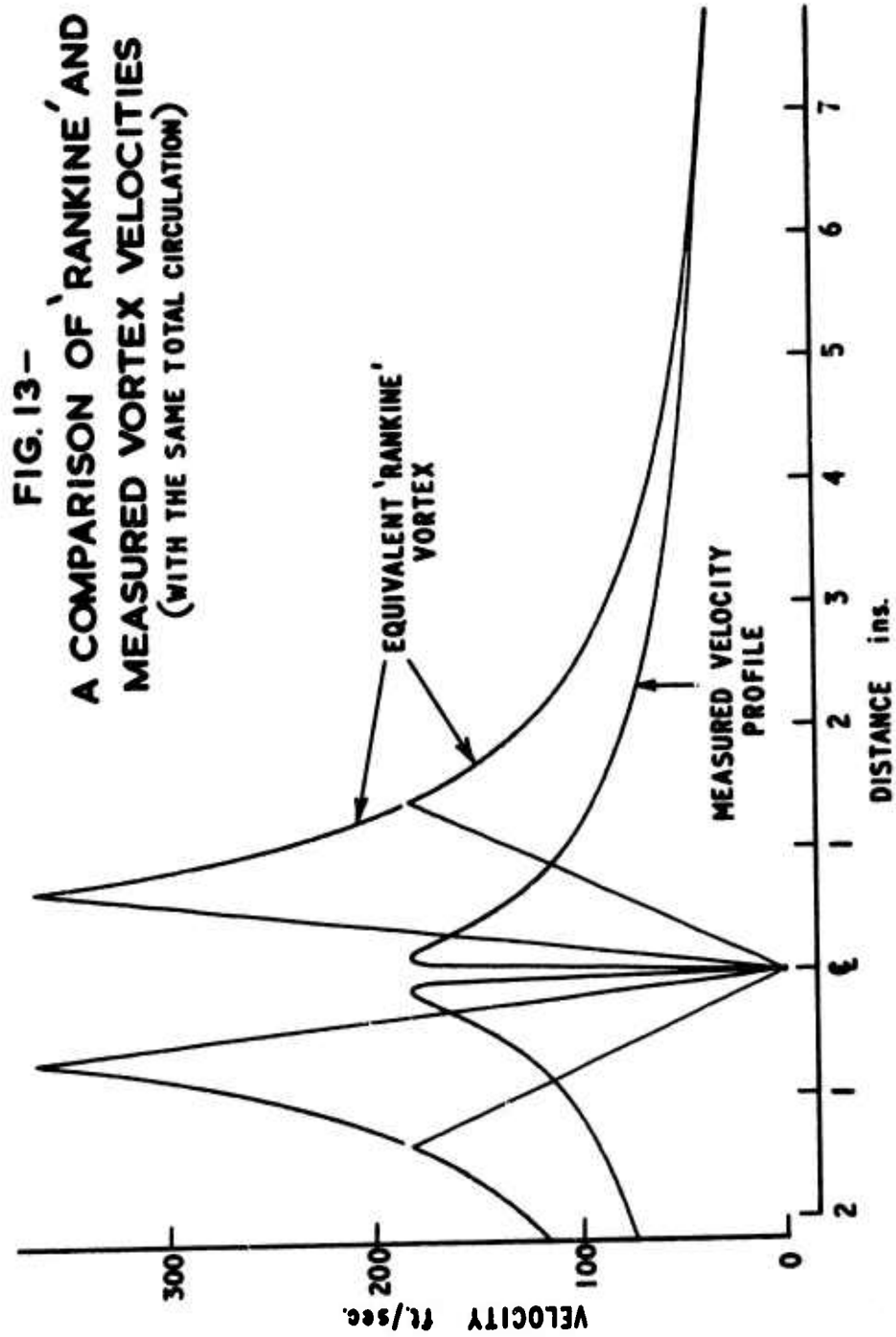


FIG.12 - PEAK VELOCITY TRENDS v. VORTEX AGE



A VORTEX-WAKE ANALYSIS OF A SINGLE-BLADED HOVERING ROTOR AND A COMPARISON WITH EXPERIMENTAL DATA

by

Robin B. Gray⁺ and George W. Brown⁺⁺
School of Aerospace Engineering
Georgia Institute of Technology
Atlanta, Georgia 30332

SUMMARY

A theoretical method is developed for determining the geometry and strength distribution of the vortex wake generated by a single-bladed hovering helicopter rotor. The analysis begins with a simple model of the ultimate wake geometry and then proceeds to establish the corresponding nondimensional tip-vortex strength. This simple vortex-wake model is adjusted by procedures that are based on the Biot-Savart law to obtain a first approximation for the tip-vortex geometry. Next, an estimate of the blade collective pitch angle is found from blade-element considerations. Then, a first approximation for the geometries and strengths of the vortex-sheet filaments that are shed from the blade trailing edge is determined by marching inboard from the blade tip. Thus, a simultaneous solution for the filament strengths is not required. Further adjustments to the wake geometry, the strengths of the inboard filaments, and the collective pitch are made until succeeding changes become acceptably small.

The results are in good agreement with experiment for the axial displacements of the tip vortex after one turn of the helix, for the blade collective pitch angle, and for the thrust coefficient. The axial displacement of the first turn of the helix and the rate of contraction of the wake is not as good. It appears that the wake model in this, as in other analyses, differs from the physical wake in certain important, but unknown, features.

RESUME

Une méthode théorique est développée pour déterminer la géométrie et la distribution de la force des tourbillons dans le sillage d'un rotor à une seule pale d'hélicoptère qui se balance dans l'air. L'analyse commence avec un modèle simple de la géométrie finale du sillage et puis procède à établir le coefficient du tourbillon de bout de pale. Ce modèle simple des tourbillons dans le sillage est ajusté par des procédés qui se basent sur la loi Biot-Savart pour obtenir une première approximation pour la géométrie du tourbillon de bout de pale. Ensuite, on trouve une estimation de l'angle du pas de la pale en considérant l'élément de la pale. Puis, on détermine une première approximation pour les géométries et les forces des filaments des tourbillons dans le sillage du tranchant traînant de la pale en marchant à l'intérieur partant du bout de pale. Aussi, une solution simultanée pour les forces des filaments n'est pas exigée. Encore des ajustements à la géométrie du sillage, aux forces des filaments intérieurs, et au pas sont faits jusqu'à ce que les changements successifs deviennent petits à un degré acceptable.

Les résultats s'accordent bien avec l'expérience pour le déplacement dans le sens de l'axe du tourbillon de bout de pale après une rotation de l'hélice, pour le pas de la pale, et pour le coefficient de la poussée. Le déplacement dans le sens de l'axe de la première rotation de l'hélice et la vitesse de la contraction du sillage ne se conforment pas si strictement avec les résultats expérimentaux. Il paraît que le modèle du sillage dans cette analyse, comme dans d'autres analyses, diffère du sillage physique quand il s'agit de certains aspects qui sont importants mais inconnus.

NOTATION

a	lift curve slope	K_2	axial displacement parameter of tip-vortex helix in ultimate wake
A	wake contraction ratio, R_w/R	r	length in radial direction
b	number of blades	R	rotor radius unless with subscript
c	blade chord length	T	rotor thrust
C	1 - A	u	with subscript, nondimensional induced velocity component, $u_r/RA\Omega$, etc.
C_T	tip-vortex strength coefficient, $\Gamma/4\pi R^2 A^2 \Omega$	u	u_r/C_T
C_{TB}	bound-vortex strength coefficient	u', v', w'	radial, tangential, and axial induced velocity components
C_{TF}	vortex-filament strength coefficient	U	velocity relative to blade element and perpendicular to blade span
C_T	thrust coefficient, $T/\rho\pi R^4 \Omega^2$	v	u_ψ/C_T
K_1	axial displacement parameter of first turn of tip-vortex helix		

⁺ Professor

⁺⁺ Graduate Research Assistant

w	u_z/C_T	ϕ, ϕ'	axial pitch angle of vortex, Figs. 1 and 3
x	nondimensional radius, r/RA	ψ	azimuth angle
x'	nondimensional radius of vortex element, r'/RA	ψ_0	azimuth angle between calculating point and first radial plane
z	nondimensional axial distance, Z/RA	ψ'	azimuth angle from reference point to vortex element
z'	nondimensional axial distance to vortex element, Z'/RA	Ω	blade angular velocity
Z, Z'	length in axial direction	Subscripts	
α_1	induced angle of attack at blade lifting line	a	with u and w: apparent induced velocity
β, β'	radial pitch angle of vortex, Fig. 3	B	bound vortex
Γ	tip-vortex strength	F_n	nth vortex filament
ϵ	nondimensional vortex core radius, ϵ'/RA	n	integer
ϵ'	vortex core radius	P	arbitrary point
θ	blade collective pitch angle	r, ψ, z	radial tangential, and axial components
λ_2	wake contraction parameter	t	tip vortex
ξ, η, z	Cartesian coordinate system	W	wake boundary defined by tip vortex
ρ	air density	∞	ultimate wake

1. INTRODUCTION

The primary objectives of this analysis are to develop a vortex-wake method for determining the hovering performance of a helicopter rotor without the degree of empiricism that is required in the prescribed-wake method and to achieve an elapsed computer time less than that required in the free-wake analyses that generate the vortex system from rest. The procedures to be used for generating the wake vortex system and relating the blade aerodynamic loading to the strengths of the trailing vortex filaments differ, in several respects, from those of both the prescribed-wake and the free-wake analyses. However, the numerical techniques used in programming the Biot-Savart law for the digital computer are essentially the same.

In the prescribed-wake analysis, the geometry of the wake vortex system near the rotor is determined from flow visualization studies. With the wake geometry known, the application of the Biot-Savart law and the blade-element theory to the system yields a set of simultaneous equations which are then solved for the blade bound-vortex strength distribution. The calculation of the thrust and power is straightforward. The computer time that is required for these calculations is relatively short. However, for a general application of the method, tables of experimentally determined geometric parameters describing the radial and axial coordinates of the vortex elements in terms of their azimuth positions from the blade must be available for a wide range of thrust levels and rotor configurations.

In the free-wake analysis, the complete vortex system is generated from rest with the initial filaments being constrained to follow a contracting path as they move down the wake. The Biot-Savart law is again used to determine the motion of the filaments and the filament strengths are related to the blade characteristics through the blade-element theory. The vortex filament strengths are found by solving the resulting set of simultaneous equations. The constraint on the wake is then relaxed and iterations are performed until the system converges to the free-vortex configuration. Therefore, a relatively large amount of computer time is required.

Both of these methods have been shown to yield good comparisons with experiment for overall performance. However, the free-wake analysis does not predict the initial tip-vortex geometry accurately. Furthermore, if the measured geometry is introduced as the initial condition for the free-wake analysis and if the iterations are allowed to proceed, the result is essentially the same as that which would be generated from rest. Since the physical wake is a free-vortex system, it would appear that there are omissions in its mathematical model which lead to a different configuration when the free-vortex condition is satisfied analytically.

In consideration of this problem and of possible ways of determining its causes, it appeared that an advantage would be realized if a procedure were developed which would proceed from the more important to the less important elements that contribute to the flow field. This marching process would isolate the various contributions and would permit analytical experimentation. A second consideration is that the method should be developed in terms of the quantities that are more easily measured in the laboratory. A third consideration is that the experience that has been gained over the years should guide the development. The procedures to be presented satisfy all of these requirements to some extent. In addition, a complimentary experimental program has been initiated which should provide further guidance toward improving the preliminary results.

A single-bladed rotor has been chosen for this development. This obviously reduces the complexity of

the vortex system and hence the numerical computations. From a consideration of previous results, it would appear that some of the problems are not associated with the number of blades. Thus a successful solution should be easily extended to multi-bladed rotors. However, in that case, a different problem arises which is not considered here and which becomes more severe with increasing numbers of blades. This is the interaction problem in which the aerodynamic loadings on following blades are modified by the close passage of the tip vortices shed from preceding blades.

In addition, the single-bladed rotor is more amenable to experimental investigation since it eliminates the necessity for constructing a model having exactly identical blades with the same aerodynamic load distributions, tip-vortex strengths, and wake geometries. Without this specification on multi-bladed models, the tip vortices from each blade will not follow identical paths but will interact to a greater or lesser degree. It is recognized that a theoretical analysis based on an invariant wake will be "ideal" in that helicopter rotors, in conjunction with existing environmental conditions, rarely achieve this effect. However, the availability of such an ideal analysis will provide a starting point for investigating the real case by perturbation techniques.

2. FIRST APPROXIMATION OF THE TIP-VORTEX GEOMETRY

It is assumed that the isolated, single-bladed rotor is hovering in a non-viscous, incompressible fluid which is at rest at infinite distances from the rotor hub except for points within the ultimate wake. The Helmholtz theorems are obeyed and the Biot-Savart law is applicable.

2.1 Simplified wake model

The initial blade and wake vortex configuration is very much simplified and is shown in Fig 1. Blade coning and flexibility are neglected which is reasonable for a counterweighted, see-saw blade of rigid construction. These effects may, however, be included at a later point in the analysis. The blade is replaced with a lifting line having constant circulation. A straight-line vortex of the same strength but negative in sign is placed along the axis of the system. A helical vortex, also of the same strength, is shed into the wake at the blade tip position. This helical vortex has a constant radius and a constant geometric pitch. The vortices have a constant-radius core which is assumed to rotate as a solid body. For some distance down the wake below the rotor plane, these shed vortices are not free but are bound to the spatial coordinates as described. This condition will, however, be relaxed.

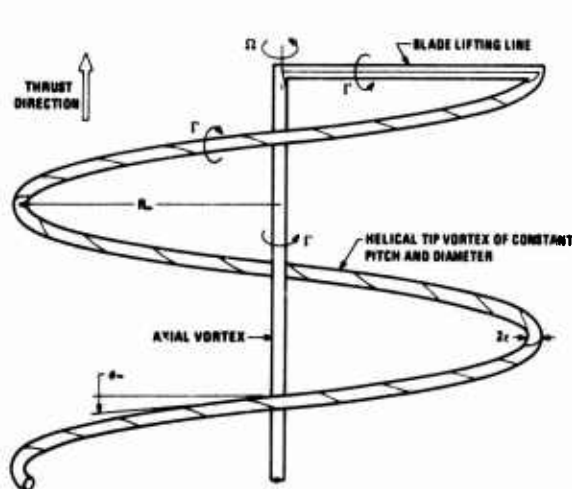


Figure 1. Simplified vortex model for a hovering, single-bladed rotor.

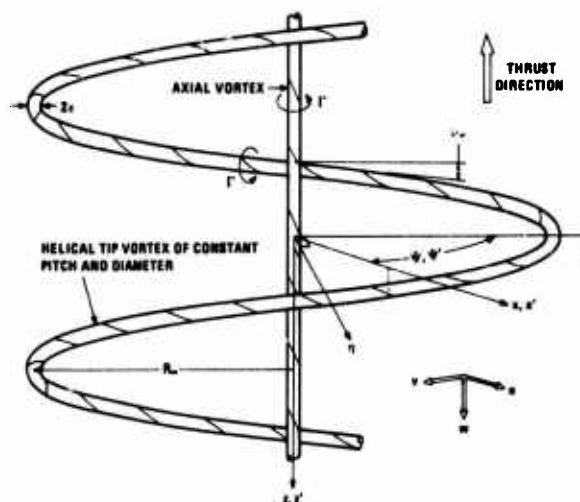


Figure 2. Simplified ultimate-wake vortex model for a hovering, single-bladed rotor.

The ultimate wake is then composed of two vortex filaments as shown in Figure 2. One lies along the axis of blade rotation which is also the axis of the vortex system. The other is a right circular helix representing the tip vortex. Here in the ultimate wake, these vortices are truly force-free.

2.2 Analysis

The induced velocity field is related to the vortex strength and geometry by the Biot-Savart law. From the general derivation given in Ref 1, the nondimensional radial, tangential, and axial induced velocity components are found to be respectively:

$$\frac{u_r}{C_T} = u = \frac{C_{TF}}{C_T} \int \left\{ x'^2 \tan \phi' \sin(\psi' - \psi) + [x' \tan \beta' \sin(\psi' - \psi) + x' \cos(\psi' - \psi)](z - z') \right\} \frac{d\psi'}{p^3}, \quad (1)$$

$$\frac{u_\psi}{C_T} = v = \frac{C_{TF}}{C_T} \int \left\{ x'^2 \tan \phi' [x - x' \cos(\psi' - \psi)] - [x' \tan \beta' \cos(\psi' - \psi) - x' \sin(\psi' - \psi)](z - z') \right\} \frac{d\psi'}{p^3}, \quad (2)$$

and

$$\frac{u_z}{C_T} = w = \frac{C_{TF}}{C_T} \int \left\{ x'^2 - xx' \cos(\psi' - \psi) - xx' \tan \beta' \sin(\psi' - \psi) \right\} \frac{d\psi'}{P^3}, \quad (3)$$

where

$$P^2 = x^2 + x'^2 - 2xx' \cos(\psi' - \psi) + (z - z')^2 + \epsilon^2. \quad (4)$$

The primed quantities represent the nondimensional coordinates and certain geometric angles of the center line of the rotational core of the vortex. The unprimed quantities represent the nondimensional coordinates of the point at which the induced velocity components are to be calculated. The introduction of the vortex core radius, ϵ , does not permit P to become zero. Hence the integrands remain finite everywhere and the points at which the velocities are calculated are approximately restricted to the surface of the vortex core. Unless otherwise noted, all lengths are made nondimensional by dividing by the ultimate wake radius and the velocities are nondimensionalized by dividing by the product of the ultimate wake radius and the rotor angular velocity. The tip-vortex strength coefficient is included in the definition of u , v , and w . It is noted that in the ultimate wake where $\tan \beta'$ is zero, the integrand of Eq (1) is an odd function of ψ' whereas those of Eqs (2) and (3) are even functions. Thus for the simplified model of Fig 2, the radial velocity of the tip vortex is identically zero and the values of the tangential and axial velocities are exactly twice those of the blade tip of Fig 1 if the effect of the lifting line is excluded.

In this method, the selection of a value of ϕ_∞ completely defines the nondimensional geometry of Fig 2 since $x' = 1$. The corresponding value of the tip-vortex strength coefficient is found from a consideration of the velocity diagram with respect to the blade of a point on the tip vortex in the ultimate wake. This diagram is similar to that of Fig 3a. Thus

$$C_T = \frac{\tan \phi_\infty}{w_t - (v_t - 2b) \tan \phi_\infty} \quad (5)$$

where b is the number of blades and v_t and w_t are found by numerically integrating Eqs (2) and (3) over the tip vortices from minus infinity to plus infinity. The term involving "b" accounts for the contribution of the vortex along the axis of the system. This value of C_T is held constant for the remainder of the procedures.

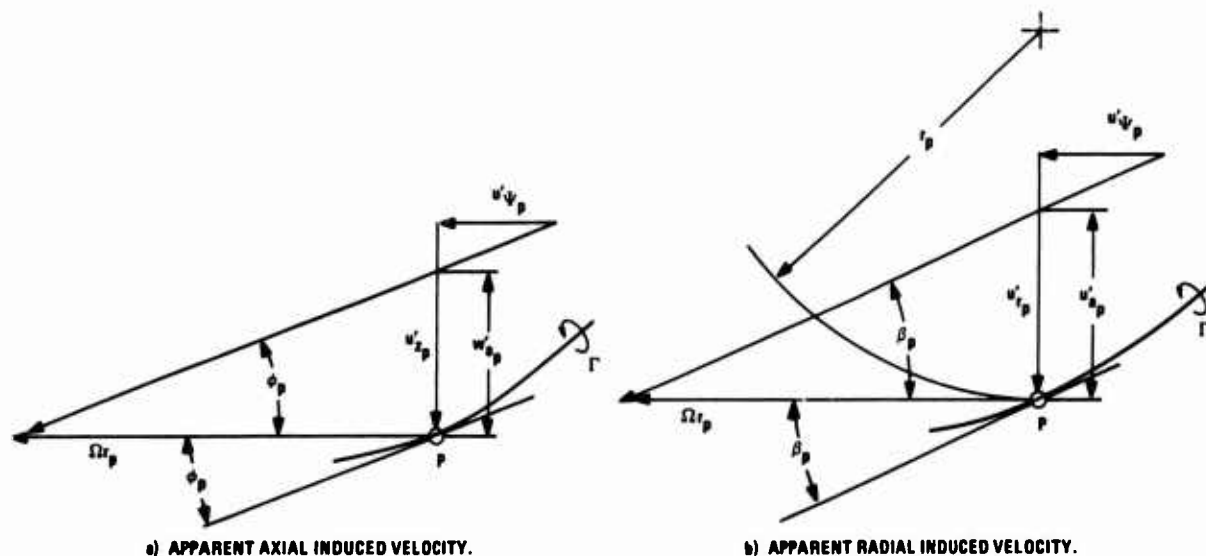


Figure 3. Velocity diagrams for determining the apparent axial and radial induced velocities at a point, P, on a vortex filament.

Before continuing with the determination of the flow field associated with the simplified wake model, several questions must be resolved. The first of these is concerned with the numerical procedures to be employed and with the expression of the theoretical results in terms that will be convenient for comparison with experimental results. In determining the motion of a vortex filament, the usual practice has been to identify a sufficient number of points along the vortex so that their displacement in the theoretical flow field will adequately define the vortex geometry as time progresses. The displacement of these points is three dimensional and therefore the three coordinates that define each point will vary with time. On the other hand and for the experimental case, it is convenient to observe the vortex motion in a radial plane. Here, the motion is two dimensional although the identity of the point under observation changes with time. Therefore, a definite advantage would be realized if the theoretical analysis were developed in a corresponding manner. Thus, the theoretical and experimental motions would correspond directly and the angular coordinates of the points at which the velocities were calculated could be fixed once and for all. The velocity components that are observed and calculated in these radial planes are given the name "apparent velocity components". The necessary relationships are found from a consideration

of the velocity diagrams at a point on the vortex filament. These diagrams are determined with respect to the blade and are shown in Figure 3. Thus, the apparent radial and axial velocity components are found to be respectively:

$$u_{aP} = \frac{u_P \left(\frac{x_P}{C_T} \right)}{\frac{x_P}{C_T} + v_P} \quad \text{and} \quad w_{aP} = \frac{w_P \left(\frac{x_P}{C_T} \right)}{\frac{x_P}{C_T} + v_P} \quad (6)$$

Here, u_P , v_P , and w_P are the radial, tangential, and axial induced velocity components that are associated with the entire vortex system. In a like manner, the radial and axial pitch angles of a filament are respectively:

$$\tan \beta_P = u_{aP} \left(\frac{C_T}{x_P} \right) \quad \text{and} \quad \tan \phi_P = w_{aP} \left(\frac{C_T}{x_P} \right) \quad (7)$$

A second question is concerned with the angular spacing of the radial planes that are described in the preceding paragraph. This spacing can not be determined a priori except that the planes should be more closely spaced in the immediate vicinity of the calculating point. Some experimentation is required in order that the contributions of the vortex elements to the velocity at a point will be adequately represented. An example will be given later in the paper.

A third question is concerned with the structure of the tip-vortex core. The representation used in Eqs (1) - (3) does not adequately describe the phenomenon and appears to underestimate the local self-induced effect. An approximate expression for this contribution is found by starting with the equation given in Ref 1 for the rate of advance of a vortex ring. There, the core is described as having a circular cross section and to be rotating as a solid body. In the present case, the contributions of small arc lengths of the helical filament on either side of, and adjacent to, the calculating point are desired. The circular arc that is equivalent to the helical arc is found by passing a circle through the calculating point and through the intersection points of the helix with the two adjacent radial planes. The vortex core between these two planes is assumed to have a circular cross section of radius, ϵ , and to be rotating as a solid body. Over the remaining length of the ring, the core is reduced to a line vortex. The desired contribution is then the difference between the result of Ref 1 for the complete ring and the integral of the Biot-Savart equation over the line vortex described above. The results for an arc of a helical vortex having a constant radius and a constant geometric pitch are

$$\Delta v_t = - \Delta w_t \tan \delta \quad (8)$$

$$\Delta w_t = \frac{2 \cos \delta}{P_L} \left\{ \ell_n \frac{4P_L}{\epsilon} - \frac{1}{4} - \frac{k^2 \sin \frac{\theta_0}{2} \cos \frac{\theta_0}{2}}{\left[1 - k^2 \cos^2 \frac{\theta_0}{2} \right]^{\frac{1}{2}}} - \ell_n \left[\frac{1 + \cos \frac{\theta_0}{2}}{\sin \frac{\theta_0}{2}} \right] + \cos \frac{\theta_0}{2} \right\} \quad (9)$$

where δ is the inclination angle of the circle with respect to the system axis

$$\tan \delta = \frac{y_0 \tan \phi_\infty}{\sin y_0}$$

y_0 is the angle between the calculating point and the first adjacent radial plane. The angular spacing of the radial planes is symmetric about the calculating point.

$$\sin \theta_0 = \frac{\sin y_0 \cos \delta (1 - \tan^2 \delta)}{1 + \cos^2 \frac{y_0}{2} \tan^2 \delta}$$

$2\theta_0$ is the arc length of the ring over which the core is assumed to extend.

$$P_L^2 = 4 \left(1 + \cos^2 \frac{y_0}{2} \tan^2 \delta \right)^2 + \epsilon^2$$

$$k^2 = 1 - \frac{\epsilon^2}{P_L^2}$$

Because of the approximations involved in the development of Eq (9), the incremental velocities become increasingly in error as the arc length of the helix, y_0 , approaches zero. This is due primarily to the behavior of the fourth term in this equation. On the other hand, as y_0 is increased, the representation of an arc of the helix by a circular arc becomes poor from the geometrical viewpoint. It appears that a value $y_0 \sim 6^\circ$ is acceptable. Additional work is required on this aspect as well as on the development of Eqs (8) and (9). The derivation of a similar set of equations for the general case is an exercise in geometry and will not be included here. It is to be noted that an increment to the radial induced velocity will appear in the general development.

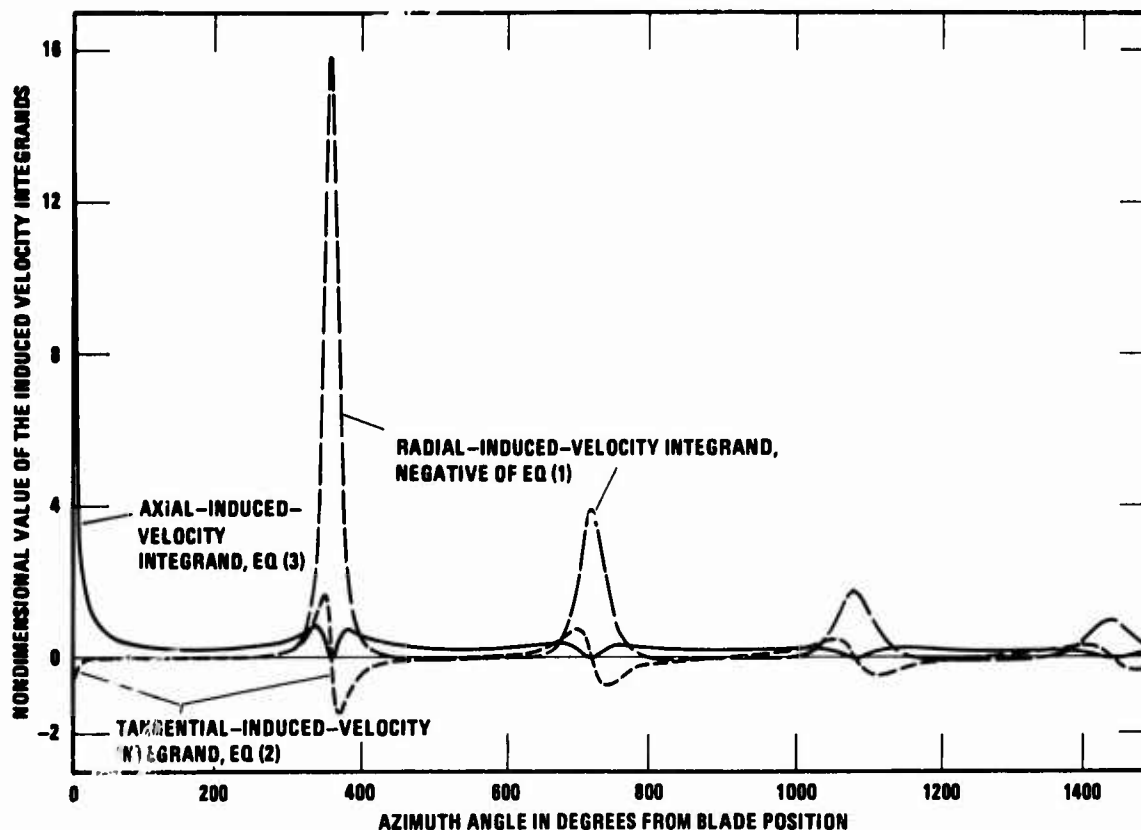


Figure 4. Azimuthal contributions of the tip-vortex elements to the induced velocity components as determined from the Biot-Savart law. The areas under the curves represent the tangential, axial, and negative radial induced velocity components at the blade tip for the simplified vortex wake model of Figure 1. $\tan\phi_\infty = 0.04$; $\epsilon R \approx 0.01$.

2.3 Flow field associated with the simplified wake model

Eqs (1) through (4) have been used to calculate the self-induced velocity components along the tip vortex of Figs 1 and 2 for several values of $\tan\phi_\infty$ and a ratio of core radius to rotor radius of 0.01. In order to determine a satisfactory angular spacing of the radial planes, the integrands of Eqs (1)-(3) were first computed for $\tan\phi_\infty = 0.04$ and plotted in Fig 4 as a function of azimuth distance from the blade position. This is a typical distribution and illustrates the necessity of having a close spacing in the vicinity of the point at which the velocities are calculated. The areas under the curves represent the velocity components so that for numerical integration, it appears that locating the radial planes at plus and minus 0.75° , 1° , 1.25° , 2° , 5° , 10° , 15° , 20° , 30° , 45° , 90° , and 135° , and at 0° and 180° would be satisfactory. If Eqs (8) and (9) are used with $\psi = 5^\circ$, then the first radial planes would be located at $\pm 5^\circ$ for the first turn but would need be located at $\pm 2^\circ$ (i.e. $\pm 358^\circ$ and $\pm 362^\circ$, etc.) for succeeding turns. When the calculating point is at the end of the helix, the increments given by Eqs (8) and (9) must be divided by two. The contribution of the first 5° of the helix to the axial velocity at the blade tip as found from Eq (3) is about 6 per cent of the total. For the same length, Eq (9) yields a contribution of about 9 per cent. The same comparisons exist for the ultimate wake. At both points, if the core radius is divided by two, the contribution is increased by about 28 per cent. The location of the calculation points is given in the next section.

The variation of the nondimensional self-induced velocity components along the tip vortex with azimuth distance from the blade position is shown in Fig 5. The effects of the lifting line and the axial vortex are not included at this point. The ultimate wake values were determined by an extrapolation process in which the turns of the helix were approximated by vortex rings. Note that for the greater part of each turn of the helix, the radial and tangential induced velocities are very nearly constant.

2.4 Displacement procedures for the tip vortex

It has been pointed out previously that the tip vortex of the simplified wake model in Fig 1 is not force-free but is bound to the specified coordinates. This condition is now relaxed and the tip vortex is allowed to displace according to the velocity field given in Fig 5. Again for the numerical procedures, a satisfactory number and distribution of radial planes must be established which will be favorable for the establishment of an acceptable displacement of the tip vortex when it is allowed to move under the action of the apparent radial and axial induced velocities. An inspection of the velocity variations of Fig 5 shows that the radial and tangential induced velocities are very nearly constant for a large part of each turn of the helix and, for approximately the same intervals, the slope of the axial induced velocity curve is also nearly constant. Thus, the same spacing of the radial planes that was given in Sec 2.3 should be satisfactory if the 0° reference plane is lined up with the lifting line. These planes also locate the calculating points for the procedures of Sec 2.3. Note that these planes are fixed to the system whereas the planes in Sec 2.3 are centered on the calculating point and are moved from point to point along the

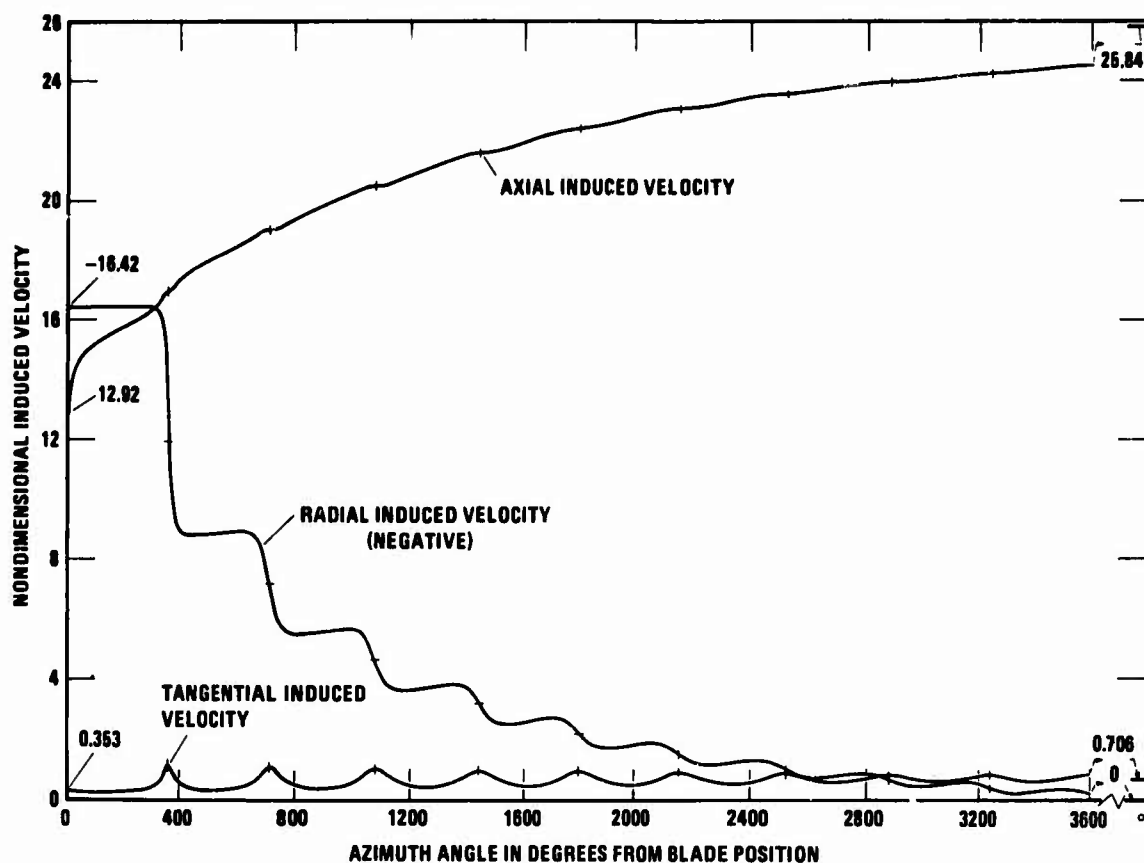


Figure 5. Nondimensional induced velocity components associated with the tip vortex only and at the tip vortex locus for the simplified vortex wake model of Figure 1. $\tan \phi_\infty = 0.04$; $C_T = 0.00156$; $\epsilon R \approx 0.01$.

filament as the velocity calculations proceed. For multi-bladed rotors, it is suggested that the radial planes be located by dividing the given azimuth angles that are greater than 5° by the number of blades and then eliminating those that are moved within the 5° arc. This distribution should be centered on each blade to complete the full circle of 2π radians. A similar distribution would determine the spacing of the planes with respect to the calculating points. This will require further investigation however.

The displacement of the tip vortex begins in the ultimate wake where the geometry and velocities are known and do not change with time (i.e. the tip vortex is force-free). For practical reasons, a limit must be established and this limit is set at 20 turns of the helix. The velocities will not be precisely those of the ultimate wake but the small errors should be acceptable. Hence, starting 20 turns down the helix from the rotor and designating this point as point "n", the apparent radial and axial induced velocities are determined by Eqs (6) using the extended data of Fig 5. Then, moving up the helix towards the rotor to the next radial plane and the (n-1) calculation point, the apparent velocity components are computed in a like manner. The averages of the components in the two planes are used to locate a new point of intersection of the helix with the (n-1) radial plane. This procedure implies a moving backward in time and if the reference coordinate system is attached to point "n" in the ultimate wake, the new location in the (n-1) plane is given by (Ψ measured from blade)

$$x_{n-1} = 1 + \frac{(u_{a_n} + u_{a_{n-1}})}{2} C_T (\Psi_{n-1} - \Psi_n)$$

and

$$z_{n-1} = \frac{(w_{a_n} + w_{a_{n-1}})}{2} C_T (\Psi_{n-1} - \Psi_n)$$

where $C_T(\Psi_{n-1} - \Psi_n)$ is the nondimensional time (negative) required for the blade to rotate through an angle equal to the angle between the two planes. A new intersection point of the tip-vortex helix with the (n-2) plane is determined in a similar manner. The process is repeated between each of the radial planes until the rotor plane is reached. The general expressions for the coordinates of the intersection in each plane are

$$x_{n-m} = 1 + \sum_n^{n-m} \frac{(u_{a_{n-m+1}} + u_{a_{n-m}})}{2} C_T (\Psi_{n-m} - \Psi_{n-m+1}) \quad (10)$$

and

$$z_{n-m} = \sum_n^{n-m} \frac{(w_{a_{n-m+1}} + w_{a_{n-m}})}{2} C_T (\psi_{n-m} - \psi_{n-m+1}), \quad (11)$$

where $1 \leq m \leq n$. When $m = n$, the rotor plane has been reached and the vortex geometry is referenced to the rotor plane by subtracting z_0 , which is a negative quantity, from the values obtained from Eq (11). The results of this first displacement for one case are shown in Figs 6 and 7. The effect of the lifting line is not included in this step. Its length is, however, increased in the radial direction so as to join the end of the tip vortex in its new location. It is interesting to note that the ratio of the new rotor radius to the ultimate wake radius is very nearly $\sqrt{2}$ which is the value predicted by the simple momentum theory. Inspection of Fig 7 indicates that the slopes of the axial and radial displacement curves undergo appreciable changes only in the immediate vicinity of azimuth angles from the blade position that are integer multiples of 2π . It is also seen that the wake has essentially contracted to its final value after about eight turns of the helix whereas the helix pitch angle is still increasing after ten turns.

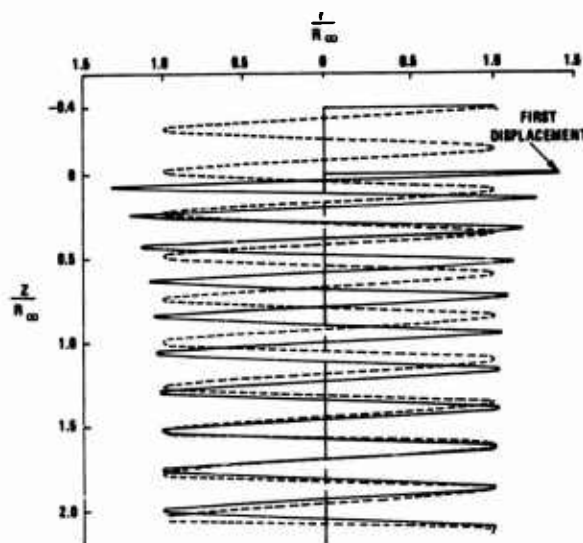


Figure 6.

Result of first iteration on tip vortex geometry. Dashed-line helix is the initial configuration of constant diameter and constant helix pitch angle. The solid-line helix is obtained after the first displacement based on velocity components associated with the dashed-line helix. (Single-bladed rotor; ultimate-wake helix pitch angle = 0.04 rad.)

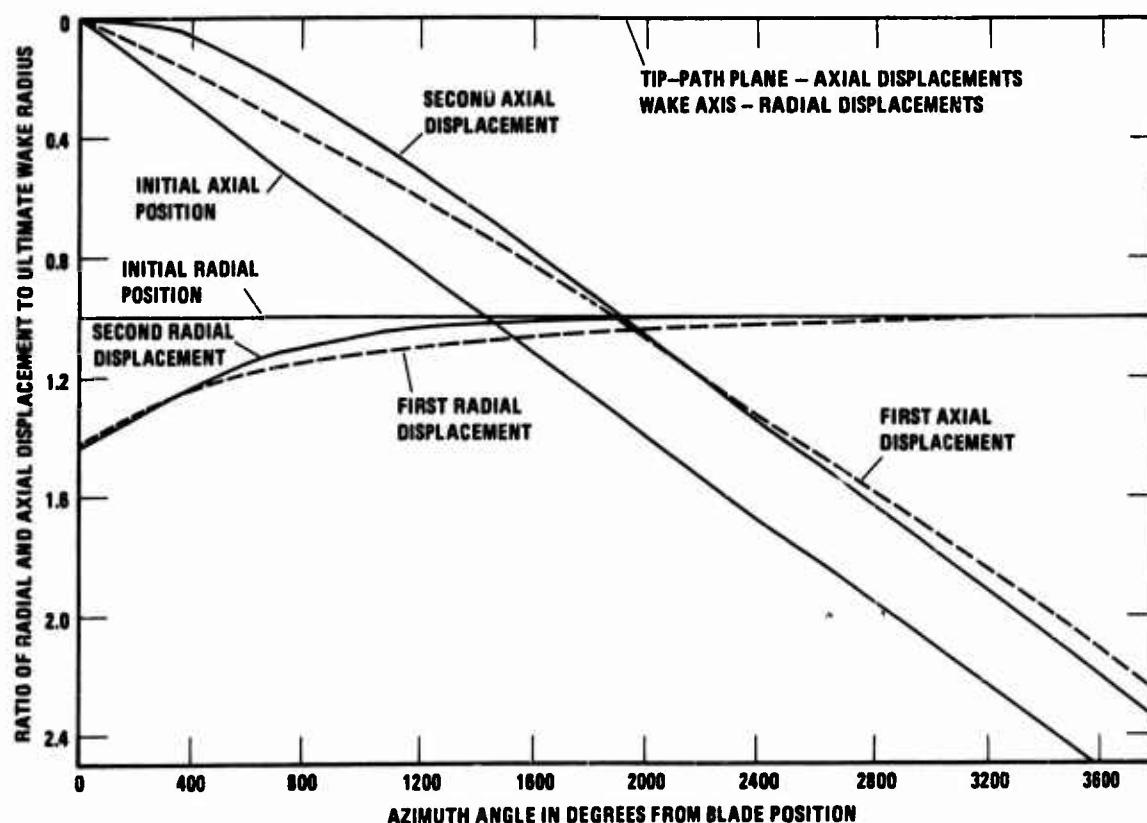


Figure 7. First and second, radial and axial displacements of the tip vortex for the simplified vortex wake model. $\tan \phi_w = 0.04$; $C_T = 0.00156$; $\epsilon R \approx 0.01$.

The three induced velocity components are computed as before at a number of points along the first displaced position of the tip vortex. The total values are determined which include the self-induced effect and the contributions from the extended lifting line and the axial vortex. The total apparent velocity components are calculated in each radial plane and a second displacement of the tip vortex is found according to the procedures described previously. This second displacement is also shown in Fig 7. It is seen that the rotor radius has increased slightly, that the wake has essentially contracted to its final value after five turns of the helix, and that the helix pitch angle has reached its final value after four turns.

Since the purpose of this section is to obtain a good approximation to the tip-vortex geometry, the procedures are terminated at this point. Additional iterations on the geometry will be performed after an approximate geometry and strength distribution has been obtained for the vortex sheet that is shed from the blade trailing edge.

3. FIRST APPROXIMATION FOR THE TRAILING-EDGE VORTEX SHEET

In order to proceed with the analysis, it is necessary to introduce the blade geometric characteristics. The quantities used are those for a model rotor for which measured tip-vortex geometries are available. The characteristics of this rotor are described in Sec 5. Also a different value of the ultimate-wake geometric pitch angle is used so that $\tan \phi_\infty = 0.07$ which corresponds to a $C_T = 0.00303$ for this model. Using the procedures of Sec 2, a tip-vortex strength coefficient is determined and an approximation to the tip-vortex geometry is computed. This coefficient remains constant throughout the analysis whereas further adjustments to the tip-vortex geometry will be made in Sec 4.

The vortex sheet that is shed inboard of the blade radial station at which the bound circulation is a maximum is replaced by ten vortex filaments. The procedure automatically locates these filaments so that they are more closely spaced over the radial intervals where the sheet strength is greater and vice versa. The accuracy of the filament geometries is not as critical as for the tip vortex. This assumes that they remain separate from, and inside the path of, the tip vortex. The effect of these filaments on the aerodynamic loading is more pronounced on the blade sections toward the blade root where the dynamic pressure is low so that the effect on the total thrust is small. Therefore, the procedures for developing the geometry of the trailing-edge filaments will be more approximate than that for the tip vortex.

3.1 First approximation of the blade collective pitch angle

The blade bound vortex strength coefficient is related to the blade characteristics through the Kutta-Joukowski theorem and the blade-element theory. Thus

$$\frac{C_{T_B}}{C_T} = \frac{acU}{8\pi R^2 A^2 \Omega C_T \cos \alpha_1} (\theta + \alpha_1) \quad (12)$$

This equation may be solved for θ so that

$$\theta = C_T \frac{C_{T_B}}{C_T} \left(\frac{8\pi R^2 A^2 \Omega}{acU} \right) \cos \alpha_1 - \alpha_1 \quad (13)$$

where

$$\alpha_1 = \arctan \frac{-u'_z}{\Omega r + u'_y} = \arctan \frac{-w}{\frac{x}{C_T} + v} \quad (14)$$

The induced angle variation in the vicinity of the blade tip is computed by Eq (14) using the induced velocity components associated with the axial vortex and the tip vortex in its second displaced position and for a given blade angular velocity. An example of this variation is given in Fig 8 for $\tan \phi_\infty = 0.07$ and shows that the magnitude of the induced angle is a minimum at $r/R = 0.89$. The blade bound vortex strength will be a maximum near this same point but its exact location will depend upon the distribution of the blade twist and chord length, upon the variation in the blade airfoil section characteristics, and upon the relative velocity, U . In terms of the nondimensional quantities,

$$U^2 = (RA\Omega C_T)^2 \left[\left(\frac{x}{C_T} + v \right)^2 + w^2 \right]. \quad (15)$$

An initial value of θ is obtained from Eq (13) by setting $C_{T_B}/C_T = 1$ and substituting the values at $r/R = 0.89$ for the other quantities. A somewhat better value of θ is obtained from Eq (12) by adjusting θ slightly and observing its effect on the radial variation of the bound vortex strength ratio. When this ratio reaches a maximum value of 1 at some radial station, then the necessary condition on the bound vortex strength is satisfied. Lacking a suitable model of the tip-vortex shedding mechanism, it is assumed that the vortex sheet that is shed from the blade outboard of this radial station immediately rolls-up to form the tip vortex. In the example of Fig 8, the condition is satisfied at $r/R = 0.905$ at which $\theta = 7.51^\circ$. This value is the first approximation of the blade collective pitch angle. Given the blade twist distribution, the usual reference pitch angle at the tip, at the $0.75R$, or at the blade root can be easily established.

3.2 Determination of the geometry and strength of the inner filaments

With the first approximation of the collective pitch angle now determined and for the computed

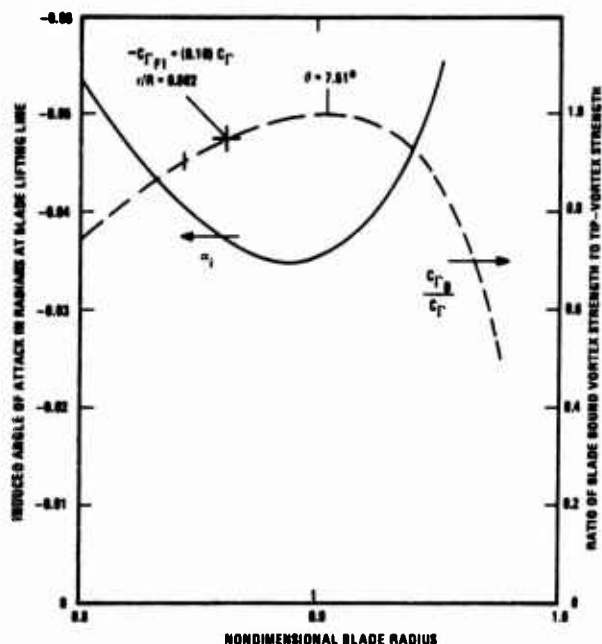


Figure 8. Location of spanwise station at which first inboard vortex filament is shed from blade trailing edge. $\tan \phi_\infty = 0.07$; $C_T = 0.004606$; $\epsilon R \approx 0.01$.

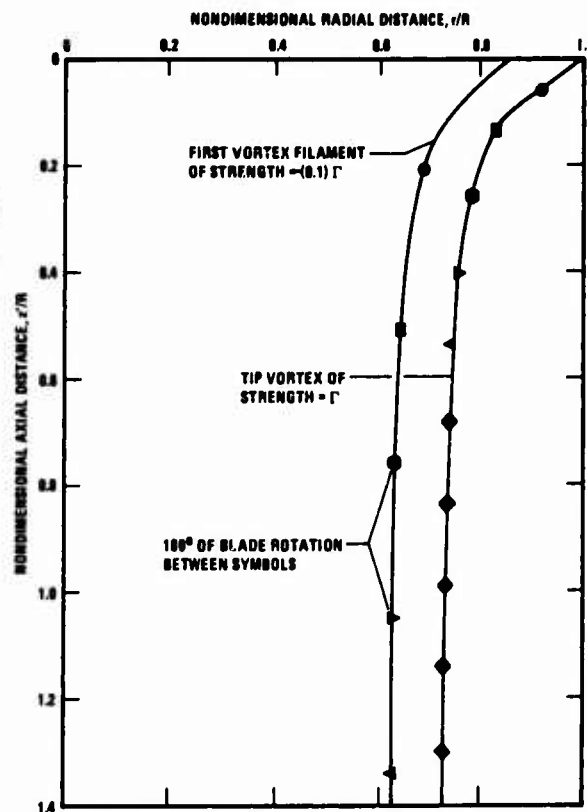


Figure 9. Axial displacement of first inboard filament with corresponding radial position proportional to local tip-vortex position. $\tan \phi_\infty = 0.07$; $C_T = 0.004604$; $\epsilon R \approx 0.01$.

values of the induced velocity components along the lifting line, the ratio of the blade bound vortex strength to the tip-vortex strength is calculated by Eq (12). The radial variation of this ratio is also plotted in Fig 8. The stations at which this ratio has the values 0.90 and 0.95 are located at $r/R = 0.843$ and 0.862 respectively. These points remain fixed for the succeeding calculations. A vortex filament of one-tenth the strength of the tip vortex but negative in sign is shed into the wake at $r/R = 0.862$. (It is to be noted that the strength of this filament will be allowed to vary from step to step in the procedure but its initial shedding point will not. Its strength will always be set equal to the negative of the difference between the tip vortex strength and the bound vortex strength at $r/R = 0.843$ which will be determined anew in each step). The strengths of the lifting line inboard of $r/R = 0.862$ and the axial vortex are reduced to $0.90C_T$ and $-0.90C_T$ respectively.

For the first approximation, the filament is constrained to move down the wake along a surface whose local radius is proportional to that of the surface described by the motion of the tip vortex. The constant of proportionality is the nondimensional point of origin of the filament which in this case is 0.862.

The procedure begins with the calculation of the apparent axial velocity at the blade trailing edge. This velocity has contributions from the tip vortex, the lifting line with its stepped circulation distribution, and the axial vortex at its reduced strength (negative with respect to that of the tip vortex). The axial position in the first radial plane is determined using an expression similar to Eq (11) except that the summation begins at the rotor plane instead of in the ultimate wake. The corresponding radial position is found by multiplying the radius of the tip-vortex surface at the same axial position by the proportionality constant. The self-induced effect is not included. The apparent axial velocity is then computed in the first radial plane and is used to find the axial coordinate in the second radial plane. The process is repeated until the "ultimate" wake of the tip vortex is reached. An example is given in Fig 9. The distance between symbols represents 180° of blade rotation. Corresponding points in time for the tip vortex and the first filament are indicated by the same symbol. The axial distance shown covers about two-thirds of the total distance that was computed.

The axial and tangential induced velocities that are associated with the tip vortex, the axial vortex, and the first filament are computed near the tip of the lifting line and the induced angle is determined. In this case, the difference from the distribution of Fig 8 are slight but the variation is plotted in Fig 10 for illustrative purposes. The location and value of the minimum magnitude of the induced angle has changed and this determines a new value of θ from Eq (13). As before, the bound vortex strength ratio variation is calculated and after several adjustments of θ , the necessary condition is satisfied as described in Sec 3.1. The resulting variation is also plotted in Fig 10. The bound vortex strength is now equal to the tip vortex strength at $r/R = 0.90$ for $\theta = 7.50^\circ$. The bound vortex strength is computed at $r/R = 0.843$ and the strength of the first filament is now set equal to the negative of the difference between the strength of the tip vortex and the bound vortex at this point. The origin of the first filament remains at $r/R = 0.862$.

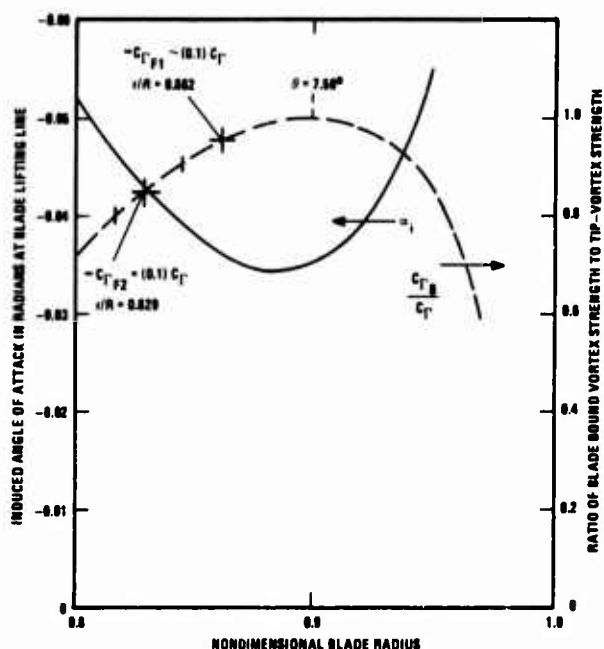


Figure 10. Location of spanwise station at which second inboard vortex filament is shed from blade trailing edge. $\tan \phi_{\infty} = 0.07$; $C_{\Gamma} = 0.004604$; $\epsilon R \sim 0.01$.

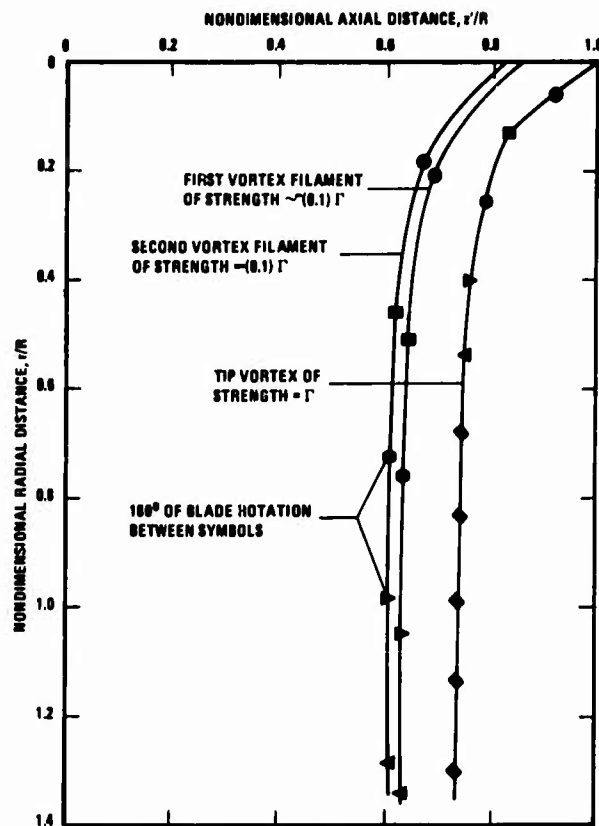


Figure 11. Axial displacement of second inboard filament with corresponding radial position proportional to local tip-vortex position. $\tan \phi_{\infty} = 0.07$; $C_{\Gamma} = 0.004604$; $\epsilon R \sim 0.01$.

The locations or the radial stations at which the bound vortex strength ratios are 0.80 and 0.85 are found to be $r/R = 0.818$ and 0.829 respectively. A filament is shed from the trailing edge at $r/R = 0.829$ whose strength is the negative of the difference in bound vortex strengths at $r/R = 0.843$ and 0.818 . The magnitude of its strength is very nearly one-tenth the strength of the tip vortex and is so designated in Fig. 10. Again the radial station of origin of this second filament is not changed in the succeeding iterations although its strength may be changed.

The intersection points of this second filament with the radial planes are located in the same manner as described for the first filament. However, the effect of the first filament is included in the computation of the apparent axial induced velocities that are used to locate these intersection points. In addition, the bound vortex strength is decreased at $r/R = 0.862$ by an amount equal to the strength of the first filament and at $r/R = 0.829$ by an amount equal to the strength of the second filament. The strengths of the remaining segment of the lifting line and the axial vortex are now 0.80 and -0.80 , respectively, of the tip vortex strength. The coordinates in the radial planes of the intersection points at intervals of 180° of blade rotation are shown in Fig. 11. Note again that the geometries of the first filament and the tip vortex are not changed from those which were determined previously.

The procedures that are described above are repeated step-by-step until the blade root is reached. At this point, any circulation that remains about the blade is assumed to be shed into the wake and the geometry of the corresponding filament is determined. As a result, the strength of the axial vortex is reduced to zero.

This completes the determination of the first approximation for the geometry and strength distribution of the trailing-edge vortex sheet. The sheet has been replaced by a number of vortex filaments whose geometry and strength are found by a process that marches inboard from the blade tip so that a simultaneous solution for these quantities is not required. The procedures automatically maintain the condition that the sum of the filament strengths must equal the strength of the tip vortex. The process is justified by the results which confirm the assumption that the effects of the inner filaments on the motions of the outer filaments are not appreciable. In this regard, computations show that the blade collective pitch angle remains essentially unchanged after several filaments are shed into the wake and this part of the procedures may be omitted beyond that point. However, it will be seen that further adjustments to the pitch angle will occur later in the analysis.

4. ITERATIONS ON VORTEX GEOMETRIES AND STRENGTHS

The wake vortices whose geometries and strengths were computed in Secs 2 and 3 are not force-free. The procedures for fulfilling this condition are essentially the same as those employed in the previous analyses that have been developed by other investigators.

4.1 First iteration on the inner filaments

The procedure begins with the calculation of the apparent axial and radial velocities at selected points along the position of the first filament that is shed inboard of the blade tip. These velocities contain contributions from the entire vortex system including the self-induced effect. The initial geometries and strengths are, of course, those determined in the preceding sections. The first displacements of the intersection points of this first filament with the radial planes are computed in the same manner as that for the tip vortex in Sec 2. After the new geometry is found, the collective pitch angle is adjusted and a new strength for the first filament is calculated.

The next step is to calculate the apparent axial and radial velocities at selected points along the position of the second filament. The difference here is that the new strength and geometry of the first filament are used. In a like manner and after a new filament geometry is found, the collective pitch angle is adjusted and new strengths for the first and second filaments are calculated. The bound vortex strength outboard of the point at which the filament is shed is also adjusted so that the system conforms to the Helmholtz theorems.

This procedure is repeated for each of the filaments that are shed from the blade trailing edge.

4.2 First iteration on the tip vortex.

The first iteration on the tip-vortex geometry is accomplished in a similar way. The apparent axial and radial velocities are computed for selected points along the position of the tip vortex. These include contributions from the tip vortex using the geometry found in Sec 2.4, from the inner filaments using the strengths and geometry found in Sec 4.1, and from the corresponding blade bound vortex strength distribution. The procedure for displacing the intersection points of the tip vortex in the radial planes is the same as described before. After a new geometry is found, the collective pitch angle is adjusted and a new distribution of the blade bound vortex strength ratio is computed by Eq (12). The nondimensional thrust loading can now be computed from

$$\frac{d C_T}{d(r/R)} = 4A^3 c_T^2 \left(\frac{C_{TB}}{C_T} \right) \left(\frac{x}{C_T} + v \right) . \quad (16)$$

This distribution is numerically integrated to give the thrust coefficient. Since the bound vortex strength ratio is a stepped function of radius and if the stations where the filaments are shed are taken as the calculating points, then the average value of this ratio should be used in the computation.

The calculations have not been carried beyond this point. The results that will be discussed in Sec 5 differ from the measured geometries in certain aspects which, it is believed, cannot be corrected by further iterations. It appears that the theoretical model differs from the physical model in certain important, but unknown, details. One area that is under investigation is the vortex core size and structure.

4.3 Further iterations on vortex strengths and geometries

Additional iterations can be performed using the procedures just described. The positions of the inner filaments are changed with adjustments to their strengths and to the collective pitch angle as required. The radial stations at which these filaments are shed and the tip-vortex strength coefficient are held constant. Then the tip-vortex position is adjusted with adjustments to the pitch angle following as necessary. This procedure may be continued until the changes in positions between successive steps become acceptably small. The rotor thrust and power are then computed using standard blade-element procedures.

5. COMPARISON OF PRELIMINARY RESULTS WITH EXPERIMENT

The procedures that are described in the preceding sections have not yielded an acceptable final geometry for the wake vortex system. The results that follow were obtained at the end of the computations that are described in Sec 4.2. No concentrated effort has been put forth to make the computing procedures more efficient. Each case that is presented has taken about 70 minutes on the CDC 6400 computer.

The calculated parameters are compared with the experimental results of Refs 2 and 3. The model rotor had the following characteristics:

No. of blades . . .	1	Airfoil section . . .	NACA 0015
Chord	15.24 cm (constant)	Radius	1.22 m
Twist	None	Tip geometry	Rounded half body of revolution
Solidity	0.040		

Fig 12 compares the measured and calculated nondimensional radial and axial displacements of the tip vortex for $\tan \phi_\infty = 0.07$. In this figure, the coordinates are referenced to the rotor radius and only cover the range of the experimental observations. The axial positions after one revolution of the blade compare favorably. In both sets of data, the axial position of the vortex oscillates about a line having a constant slope of approximately 0.07. The oscillations correspond to the close passage of the inner filaments and appear to be approximately 180° out of phase with each other. This is an inconsistency and will be investigated. For the first turn, the data comparison is not good. Although the axial displacements are very nearly linear during this interval, their slopes are appreciably different. In addition, the computed rate of contraction of the tip vortex is considerably less than the measured value. However, the computed contraction ratio after ten revolutions of the blade agrees very closely with that measured after three turns. These results are consistent with those published by other investigators and

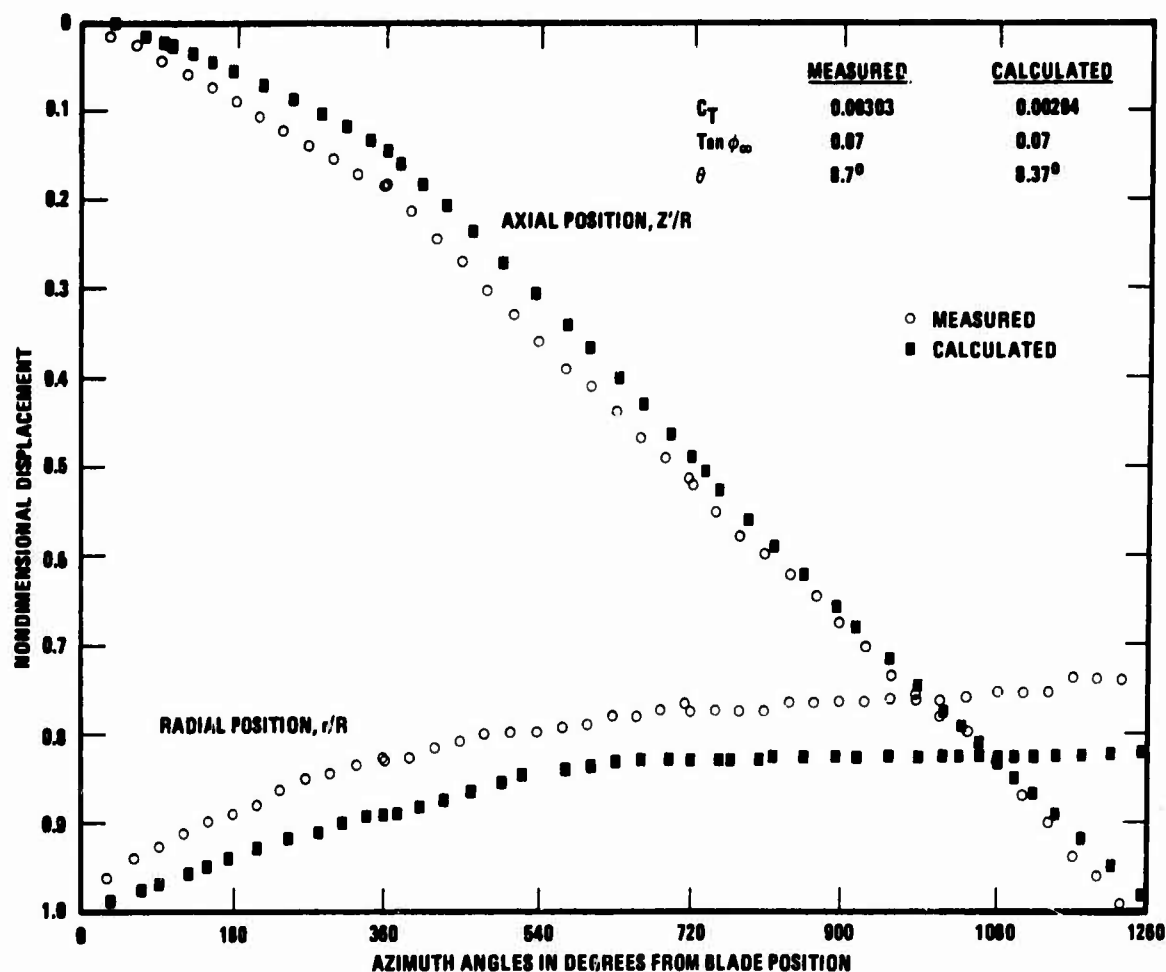


Figure 12. A comparison of measured and calculated nondimensional radial and axial displacements of the tip vortex.

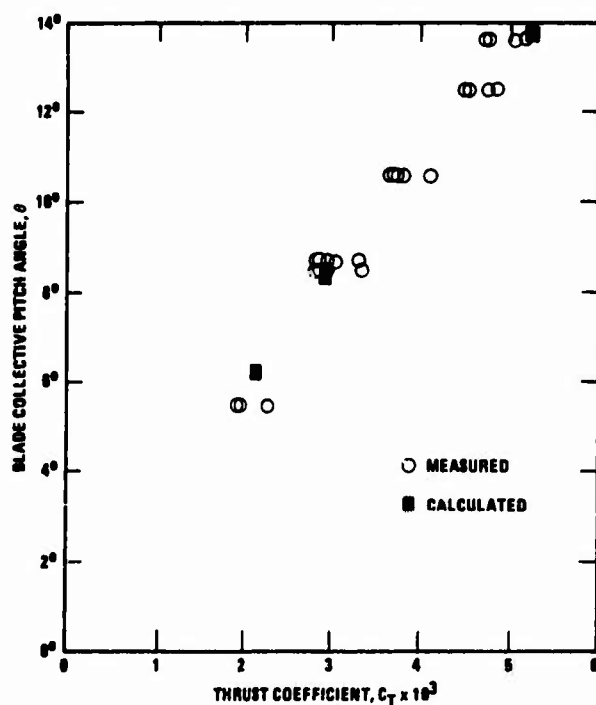


Figure 13. A comparison of measured and calculated collective pitch angles for a hovering, single-bladed model rotor.

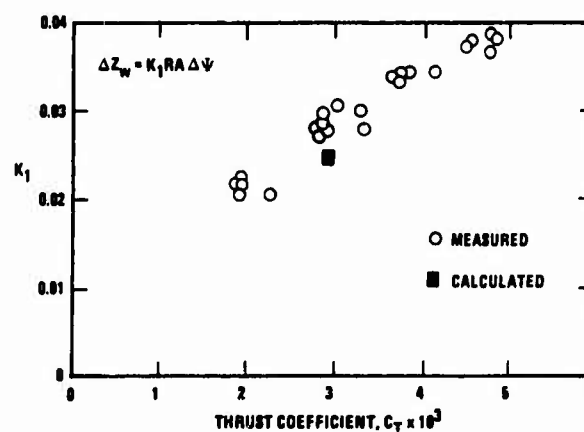


Figure 14. A comparison of measured and calculated values of the axial displacement parameter for the first turn of the tip vortex of a hovering, single-bladed model rotor.

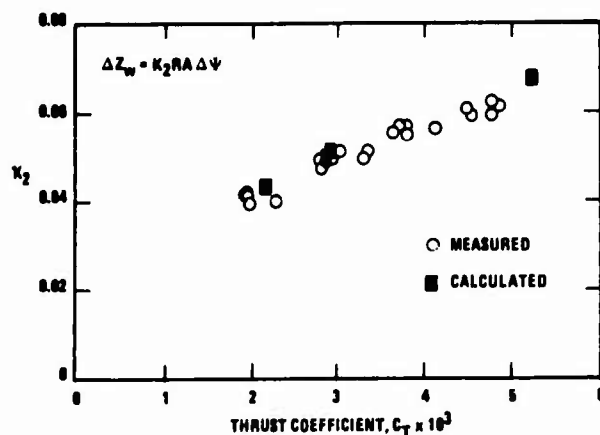


Figure 15. A comparison of measured and calculated values of the axial displacement parameter in the ultimate wake for the tip vortex of a hovering, single-bladed model rotor.

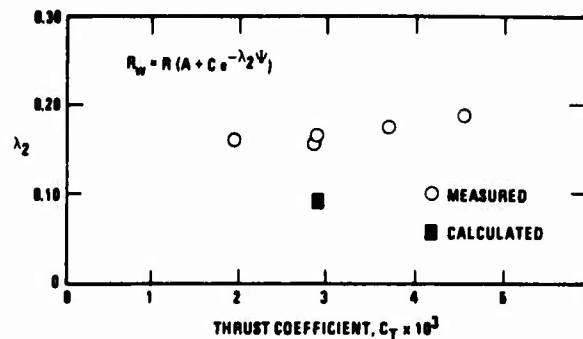


Figure 16. A comparison of measured and calculated values of the parameter describing the rate of contraction of the tip vortex of a hovering, single-bladed model rotor.

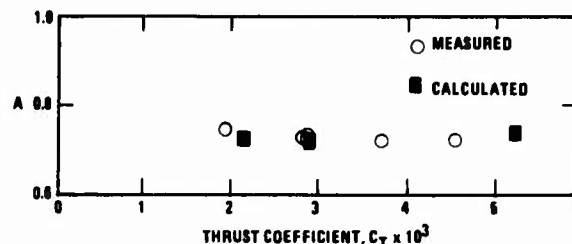


Figure 17. A comparison of measured and calculated values of the contraction ratio parameter for the tip vortex of a hovering, single-bladed model rotor.

seem to support the previous observation that important physical details have not been properly modeled.

Figure 13 shows the comparison of the calculated and measured values of the collective pitch angle. The calculated points fall within the range defined by experiment. The apparent scatter of the experimental data can be attributed to scale effects. The $3/4$ -radius Reynolds numbers for these tests were between 240,000 and 430,000. Two-dimensional data for the NACA airfoil show a decrease in lift-curve slope of about 10% over this range. For the calculations, $a = 5.73$ per radian.

Figs 14 - 17 present a comparison between the computed and measured geometric parameters as a function of thrust coefficient. The measured parameters are from Refs 2 and 3 and represent a good approximation of the experimentally observed tip-vortex geometry. However, they are to be viewed as average values since the objective of these tests was to determine a simple representation that would be suitable for performance prediction. As may be seen, the agreement is good for the contraction ratio and the axial displacement parameter in the "ultimate" wake while the agreement is not as good for the rate of contraction and the axial displacement parameter for the first turn of the tip-vortex helix.

6. CONCLUDING REMARKS

Theoretical procedures have been presented which permit the determination of the vortex geometry and strength distribution in the wake of a hovering rotor. The method begins in the ultimate wake and proceeds to establish the complete vortex system in a step-by-step process. This system is then allowed to displace as required until the force-free condition is fulfilled. The rotor performance is based on this final configuration.

The computed results compare favorably with experiment in some aspects but not in others. In this regard, it is consistent with the results of other investigators using other methods. It appears that certain important physical details of the system are not properly modeled.

7. REFERENCES

1. Lamb, H. Hydrodynamics. Sixth Edition, New York, Dover Publications, 1945. pp. 240-241 and 239-241.
2. Gray, Robin B. On the Motion of the Helical Vortex Shed from a Single-Bladed Hovering Model Helicopter Rotor and Its Application to the Calculation of the Spanwise Aerodynamic Loading. Princeton, N.J., Princeton University Aeronautical Engineering Department Report No. 313, Sept. 1955.
3. Gray, Robin B. An Aerodynamic Analysis of a Single-Bladed Rotor in Hovering and Low-Speed Forward Flight as Determined from Smoke Studies of the Vorticity Distribution in the Wake. Princeton, N.J., Princeton University Aeronautical Engineering Department Report No. 356, Sept. 1956.

ROTOR en VOL STATIONNAIRE et à GRAND PARAMETRE d'AVANCEMENT

par

J. SOULEZ-LARIVIERE

Adjoint pour la Recherche au Directeur

de la Division Hélicoptères

"AEROSPATIALE"

B.P. 888

13221 MARSEILLE Cédex 1

FRANCE

Résumé

Le rotor de l'hélicoptère a été le premier moyen technique qui ait permis d'accomplir le vol vertical. C'est d'ailleurs encore le plus efficace. L'exposé retracera la démarche historique qui y a conduit. Puis, en examinant les diverses limitations auxquelles il s'est heurté en vol stationnaire et en vol de translation, il énumérera les procédés envisagés pour l'améliorer.

En annexe, sera donné l'historique des méthodes de calcul des performances.

INTRODUCTION

1972, voilà une belle année où l'hélicoptère se porte bien si nous devons en juger par l'assistance nombreuse qui est venue à ce Congrès de Marseille, capitale française de l'hélicoptère. Et, cet optimisme nous porterait facilement à une attitude d'auto-satisfaction. Qu'ils sont loin les pionniers qui ont créé petit à petit l'hélicoptère d'aujourd'hui et que nous mépriserions facilement de n'avoir pas su construire les merveilleuses machines que nous produisons. Et quant à chacun d'entre nous ici, il pense avoir adapté sur ses hélicoptères tous les progrès possibles et imagine souvent mal quel progrès nouveau pourrait y être incorporé.

Ces deux attitudes sont évidemment inadmissibles, car ce sont nos devanciers qui nous ont permis de parvenir au point actuel et il ne faut pas que nous croyons que le progrès technique de la voilure tournante s'arrête à ce que nous savions en sortant de l'école ou aux améliorations que nous pouvions prévoir à cette époque.

Pendant que l'avion à voilure fixe connaissait le prodigieux progrès en vitesse et en distance franchissable, il restait congénitalement embarrassé de sa vitesse minimale de sustentation pour quitter ou rejoindre le sol, et l'intérêt considérable d'emploi que présente un domaine de vol qui inclut l'ensemble de la surface terrestre et non pas seulement quelques pistes bien choisies, pressait les chercheurs de trouver. Mais, le problème de vol immobile est autrement plus ardu que celui de la glissade sur l'air et il suffit de remarquer comme une mouette qui plane paisiblement sur ce port doit s'agiter fébrilement pour s'envoler et se poser, pour mesurer qu'il y a bien une différence de nature entre les deux problèmes.

Mon exposé n'a pas la prétention d'être une revue historique complète du rotor de l'hélicoptère, d'abord, parce que certains d'entre vous ici ont à ce sujet beaucoup plus d'expérience ou de connaissance que moi-même et que l'histoire complète du rotor d'hélicoptère nécessiterait un livre entier.

Je remercie M. Francis Maillard d'avoir bien voulu pour sa part se charger de dresser un petit historique (cf annexe) des perfectionnements successifs des méthodes de calcul de performance du rotor. Il a lui-même vécu toute cette période passionnante et parle de tout cela en témoin actif qu'il fut.

Par contre, j'essaierai de rappeler comment les différentes limitations rencontrées dans l'amélioration des hélicoptères se sont révélées et ont pu être progressivement éloignées ou supprimées. Et surtout, je voudrais insister sur le fait que l'hélicoptère est encore une technique en pleine jeunesse; que son évolution technique est loin d'être terminée et que les progrès considérables, encore possibles, devraient lui permettre de fournir à des utilisateurs de plus en plus nombreux, des services de plus en plus grands.

LE VOL STATIONNAIRE

C'est naturellement par ce point du domaine de vol que nous commencerons puisque c'est bien dans cet ordre que le problème a été abordé par les hélicoptéristes (à la différence des avionistes qui cherchent depuis dix ans à ajouter cette possibilité de vol vertical à des avions conçus pour le vol de croisière) : comment décoller et se maintenir en vol immobile ? Une première évidence s'impose : puisqu'il faut un déplacement relatif d'une surface par rapport à l'air pour générer des forces et puisque l'appareil est supposé immobile, il faut que des surfaces portantes se déplacent par rapport à l'appareil; comme par ailleurs, le seul mouvement que la technologie sait réaliser commodément est le mouvement de rotation uniforme, il faut faire tourner des ailes ou des pales autour d'un axe. Nous voici donc conduits immédiatement à l'hélice de Léonard de Vinci (qui n'est pas encore une voilure tournante), et, au début de ce siècle, tous les chercheurs et savants travaillent sur l'hélice.

Avant de regarder leurs travaux, arrêtons-nous un instant sur les autres, ceux qui choisissent des voies différentes. Que de projets avortés d'aérodynes à ailes battantes. Et pourtant, les oiseaux volent ainsi et parviennent à des performances de vitesse importantes, qui, transposées en similitude de Froude aux tonnages des machines actuelles, (rapport de vitesse = $\sqrt[6]{\text{rapport de masse}}$) sont de l'ordre de 500 km/h. Comment ferez-vous pour vous déplacer avec votre hélice à axe horizontal ?

Le pari technique du rotor d'hélicoptère se déplaçant dans son plan et soumis à d'atroces dissymétries paraît contre nature et détourne de lui de nombreux chercheurs qui veulent tenter du premier coup une synthèse entre les nécessités du vol stationnaire et du vol de translation. Mais les inventeurs d'ailes battantes ou tournantes autour d'autres axes que l'axe vertical, comme le cyclo-gyro, échoueront sur ce qui a été, est encore et restera longtemps le problème numéro un de toutes nos réalisations, la tenue en fatigue, les vibrations et l'aéroélasticité.

La raison qui a conduit la nature à choisir cette solution quatre fois (*) au cours de l'évolution, reside-t-elle dans des avantages spécifiques ou bien dans l'impossibilité biologique de faire autrement ?

On n'a pas encore tranché définitivement la question des avantages spécifiques de l'aile battante, mais si Oehmichen (**) avait penché pour le oui, Vance A. Tucker (***) semble avoir donné une grande probabilité au non, en analysant le bilan énergétique d'oiseaux dressés à voler en soufflerie. Il faut donc penser que la solution de l'aile battante a passé par la résolution du gigantesque problème de fatigue posé par le mouvement alternatif et que c'est dans la structure fibreuse et constamment renouvelée des os et des plumes vivantes qu'elle l'a été (il ne se pose réellement que pour les gros oiseaux en raison de la croissance des contraintes comme la racine cubique de la masse en similitude de Froude).

Revenons alors à cette hélice à axe vertical qui va nous permettre de réaliser un rêve si ancien : nous tenir en l'air immobiles où nous voulons.

La première limitation qui apparaît immédiatement est une limitation de performance. Pour enlever le moteur et sa transmission de mouvement, l'hélice elle-même et son pilote, il faut une poussée supérieure au poids et les hélices connues ne procurent pas cette poussée. Et la machine de Léonard de Vinci méconnaît une première loi fondamentale qui relie la poussée au diamètre. Il est inutile comme l'indiquent ses dessins de prévoir une surface de pale qui fasse deux fois le tour de l'hélice; ça n'est pas en augmentant cette surface de pale que l'on augmentera la poussée, mais bien en augmentant le diamètre. Froude, Renard, Bréguet établiront chacun leurs chiffres de qualité de l'hélice en air immobile; la poussée maximale d'une hélice par unité de puissance installée est liée à la charge de disque de façon inéluctable et le maximum que l'on peut en espérer fournit une référence commode de qualité, uniformément utilisée aujourd'hui,

$$M = \text{chiffre de Mérite} = \frac{F}{P} : \frac{F}{\sqrt{2\rho S}} < 1$$

Pour soulever l'hélicoptère, il va donc falloir apprendre à construire des hélices de grand diamètre. La liste est longue de ceux qui se lanceront dans des constructions d'appareils grandeur, mais la valeur des efforts à encaisser, de la force centrifuge, du moment d'encastrement, un devis de masse extrêmement précaire, ajouté à des problèmes de stabilité et de pilotage, qui sont en général à cette époque simplement escamotés, ne permettront que des expériences sans résultats pratiques. Et puis vient le premier miracle de l'hélicoptère, le rotor génial de La Cierva. Conscient de l'insuffisance des moteurs de son époque et de la trop grande complexité du problème, il renonce à l'hélicoptère à décollage purement vertical et munit ses avions d'une voilure autogire qui tourne en autorotation à la place de la voilure fixe. Les premiers modèles ont encore des pales haubanées pour encaisser le moment fléchissant et une aile auxiliaire avec des gouvernes classiques; mais, les machines marchent mal et roulent en raison de la dissymétrie aérodynamique. Alors La Cierva invente cette géniale articulation de battement qui résout tous les problèmes d'un coup et les vols du quatrième appareil, le C4, à la fin de 1922 marqueront la première étape capitale de l'histoire du rotor.

Structuralement, il n'y a plus de moment fléchissant et la force centrifuge qui ne pèse rien devient une amie en se chargeant de remplir la fonction de hauban; l'appareil ne roule plus puisque par une conjonction heureuse, la pale se trouve battre autour de son axe avec une fréquence qui est justement égale à la fréquence de rotation et que la phase de ce mouvement de battement s'ajuste d'elle-même à la phase de la variation de vitesse relative pour augmenter l'incidence de la pale qui recule et diminuer celle de la pale qui avance. Et, puisqu'il n'y a plus de moment transmis au mat, on peut le manoeuvrer facilement pour piloter l'appareil et supprimer ainsi l'aile et ses gouvernes.

Le second miracle sera l'oeuvre de Bréguet qui poursuit avec ténacité son projet d'hélicoptère à vol vraiment vertical. Abandonnant le rotor biplan qui lui avait permis de voler dès 1907, il reprend le rotor de La Cierva. Il trouvera le moyen d'articuler les pales suivant leur axe longitudinal pour commander le pas de façon cyclique (nouveau hasard heureux, la fréquence naturelle du mouvement est encore sensiblement égale à la fréquence de rotation du rotor), permettant de dissocier l'orientation du rotor nécessaire au pilotage et l'orientation de son axe, fixé cette fois-ci rigidement à l'appareil et à son moteur. Le gyroplane Bréguet-Dorand surpassera considérablement en 1936 tous les records d'hélicoptère et sera véritablement la première configuration comportant tous les organes de notre hélicoptère d'aujourd'hui.

Les rotors coaxiaux de Bréguet sont ceux qui se rapprochent le plus du schéma de Froude. Ce schéma bien connu idéalise le rotor sous forme d'un modèle de disque qui agit comme une pompe volumétrique en faisant subir à l'air qui le traverse une surpression Δp , Fig. 1. Si le nombre de pales est assez grand et si on prévoit deux rotors voisins tournant en sens inverse, il est facile de voir que cette assimilation est légitime; l'équation de Bernoulli en mouvement non permanent

$$\frac{P}{\rho} + \frac{1}{2} V^2 + \frac{\partial \varphi}{\partial t} = 0 \quad \text{Fig. 2}$$

montre bien que le potentiel créé par la circulation autour des pales Γ varie de façon brusque en dessous et en dessus du disque et que toutes les molécules d'air qui ont traversé le disque, même sans avoir touché les pales, sont soumises à ce gain de pression totale. Ce gain est constant si les pales sont à circulation constante et l'échappement tourbillonnaire se réduit à un débit $\frac{d\Gamma}{dt} = \frac{\Delta p}{\rho}$ en extrémité de disque, ce qui correspond, il est facile de le voir, à l'optimum de ce schéma et donne une vitesse induite constante égale à la moitié de la vitesse du souffle à grande distance.

(*) Les insectes, les ptérodactyles, les oiseaux et les chiroptères.

(**) Oehmichen. Nos maîtres, les oiseaux.

(***) The energetics of bird flight American Scientific. May 1969.

Les seules pertes par rapport à ce schéma sont les pertes de frottement sur les pales et pour les minimiser, il y a lieu :

- . de chercher des profils à grande finesse;
- . de choisir une forme en plan hyperbolique et un vrillage également hyperbolique;
- . de choisir une faible vitesse périphérique pour que l'angle moyen de sillage ne s'éloigne pas trop de 45° (suivant la théorie classique de l'hélice

$$\eta_p = \frac{\tan \beta}{\tan (\beta + \text{Arc } \tan \frac{1}{p})} \quad) \text{ Fig. 3}$$

Les rotors de Bréguet s'efforceront de remplir ces conditions à l'exception toutefois de la vitesse périphérique qui réagit directement sur le couple nécessaire à l'entraînement des rotors et donc sur la masse du réducteur principal.

D'autres dispositions de rotors seront essayées. Quelques mois après Bréguet (1938), Focke s'adjugera tous les records et traversera l'Allemagne avec un appareil à deux rotors latéraux. Puis Sikorsky trouvera la disposition monorotor à hélice anticouple qui se généralisera et s'est imposée jusqu'à nos jours à plus de 9 hélicoptères sur 10. Bell fera voler le premier hélicoptère à rotors en tandem. Vers 1950, l'apparition de la turbine à gaz, beaucoup plus légère, achèvera de donner à l'hélicoptère sa physionomie d'aujourd'hui, sans oublier le Fenestron de notre maison en 1970.

Ces diverses configurations qui suivent celles de Bréguet sont aérodynamiquement un peu moins bonnes puisqu'une partie de l'énergie est perdue par rotation de la veine d'air, et ceci modifie légèrement l'optimisation aérodynamique du disque sustentateur, en obligeant à ce que la circulation des pales et la portance s'annulent au centre du disque, mais compte tenu de la forte vitesse périphérique déjà nécessaire par ailleurs et de l'impossibilité pratique de donner aux pales une corde infinie en emplanture, cette perte est faible et de l'ordre de 7% (*). Quelques pertes (5%) également sont à attribuer au nombre de pales finies et à la perte induite en bout de pale(**).

Mais en fait, le problème de l'optimisation d'un rotor au point fixe est immoral, en ce sens qu'il faudrait se donner beaucoup de mal pour améliorer de quelque pour cent l'efficacité sustentatrice et réciproquement il est possible de faire subir à la configuration optimale beaucoup d'outrages sans que l'efficacité descende beaucoup.

Si on regarde les rotors d'aujourd'hui et qu'on les compare à ceux de Bréguet et aux hélices encore antérieures, on pourra être surpris de leur trouver peu d'avantages.

Une fois passé le cap du gyroplane de Bréguet, qui avait enfin permis de considérer le problème de la poussée en vol stationnaire comme résolu, on a au contraire assisté à une dégradation progressive des performances de qualité sustentatrice (chiffre de Mérite) des hélicoptères et de leurs rotors. La configuration avec rotor de queue est moins efficace que celle de Bréguet, mais nous savons qu'elle est plus légère à construire; la vitesse périphérique des pales a eu tendance à augmenter et la surface des pales à diminuer bien au-delà du compromis optimal, d'où un rendement propre guère meilleur que 0,7, mais c'est pour des impératifs de vol en translation; la forme en plan est devenue rectangulaire, car c'est la seule qui ait pu être fabriquée commodément; le vrillage est beaucoup trop faible parce qu'un vrillage trop élevé fatigue les pales en vol rapide; le profil n'est pas cambré parce que la cambrure donne des efforts dans les commandes de vol, etc... .

Tout ceci nous amène à ne pas être fiers du chiffre de Mérite des hélicoptères d'aujourd'hui, qui se situe tout compris entre 0,4 et 0,5.

En terminant ce rapide tour d'horizon des moyens utilisés pour le vol vertical, je dirai simplement un mot de la configuration de l'hélice carénée à laquelle j'ai consacré autrefois personnellement beaucoup d'efforts. L'hélice libre habituelle remplit deux fonctions simultanées : fournir à l'air qui la traverse l'énergie nécessaire pour provoquer le mouvement, et encaisser la force qui en résulte.

C'est cette double fonction qui entraîne que la surface efficace du jet à l'infini soit rigoureusement la moitié de celle du disque de l'hélice. N'est-il pas possible en séparant les deux fonctions précédentes, de les assurer mieux et d'échapper à cette fatalité ? La réponse est positive : en disposant des surfaces annulaires autour de l'hélice, on peut parvenir à guider la veine d'air à sa sortie et à lui imposer, par un angle de divergence aval important, n'importe quelle surface efficace à l'infini. En fluide parfait incompressible, il n'y a donc pas de limite supérieure au chiffre de Mérite, mais les limitations viennent d'autre part :

d'abord de la viscosité du fluide qui provoque les décollements de l'air dans la couche limite du diffuseur. Il est donc nécessaire d'organiser la régénération de cette couche limite et l'énergie ainsi dépensée fait que le chiffre de Mérite comporte une limite supérieure dépendant de la viscosité du fluide; ensuite, à un moindre degré, le débit à travers l'hélice est limité par la compressibilité, et ceci joue pour les très fortes charges de disques supérieures à 1000 ou 2000 kg/m².

Si l'on se contente d'une sortie cylindrique, le chiffre de Mérite rapporté à l'hélice avec la même référence que l'hélice libre, est limité par la valeur $\sqrt{2}$ et de façon pratique des chiffres de l'ordre de 1,1 ont pu être obtenus ($\sqrt{2} \times 0,7 \approx 0,8$).

Avec une sortie divergente à 45°, la Société Bertin a obtenu grâce à une stabilisation de soufflage du diffuseur, un chiffre de 1,7 ($\sqrt{2} \times 1,2$) en comptabilisant l'énergie de soufflage sans pertes de charge (Fig. 4). Avec cette même sortie, la Sté NORD-AVIATION a pu obtenir un chiffre proche de 1,4 ($\sqrt{2} \times 0,95$) en stabilisant la couche limite grâce à un tourbillon piégé entretenant par la rotation même de l'hélice, c'est-à-dire sans faire appel à aucune autre source. Mais, faire voler un avion à hélice carénée est d'un tout autre ordre de difficulté; sensibilité aux rafales, effet de sol néfaste, violent effet de tangage de la translation, traînée très élevée des carénages à grande vitesse. Le rotor libre de l'hélicoptère a peu à craindre pour le moment de cette concurrence.

(*) Shapiro. Principles of Helicopter Engineering.

(**) Sissing. B = 0,97

LE VOL EN TRANSLATION

Nous avons déjà dit comment La Cierva d'un coup avait inventé le rotor que nous connaissons aujourd'hui et que l'articulation de battement avait résolu génialement, à la fois des problèmes de légèreté structurale, de mécanique du rotor et de pilotage.

Bréguet, Focke, Sikorsky et les autres exploitèrent cette merveilleuse idée pour donner naissance à la forme classique du rotor articulé, qui est encore aujourd'hui complètement généralisée.

Comment alors vont apparaître les limitations de vitesse ? Sur les premières machines, ce sont manifestement des limitations de puissance et ceci sous la forme la plus simple qui soit, à savoir la traînée du fuselage.

En ce qui concerne le rotor lui-même, la mise en translation d'un disque sustentateur s'accompagne en effet d'un effet favorable sur la puissance nécessaire prise en compte dès 1926 par Glauert à l'occasion des calculs d'autogires, et il n'est que de regarder la fig. 5 pour le comprendre.

Alors, en effet qu'en vol stationnaire la portance est générée par l'accélération vers le bas de l'air qui a traversé le rotor et de lui seul, la mise en translation produit sur la veine tourbillonnaire un enroulement un peu analogue à celui de la nappe tourbillonnaire de l'aile, si bien que nous pouvons y distinguer trois catégories de molécules d'air :

- (1) . des molécules qui ont traversé le rotor et subi le saut de pression Δp ;
- (2) . des molécules qui passent suffisamment loin du rotor pour échapper complètement à son influence et retrouver à l'infini aval les mêmes pression et vitesse à l'amont et qui ne participent donc en rien à l'affaire ;
- (3) . des molécules qui, sans être passées dans le rotor, s'en sont approchées suffisamment pour être captées par les vitesses induites de l'enroulement tourbillonnaire.

Cette dernière catégorie de molécules augmente, tout compte fait, le débit d'air sur lequel s'appuie l'hélicoptère et produit donc une baisse de la puissance nécessaire au vol, si bien que l'hélicoptère qui a réussi à décoller, a ipso facto suffisamment de puissance pour atteindre des vitesses de 100 à 150 km/h.

Malheureusement, le fuselage d'un type cage à poule, que l'on a été contraint de construire, n'a rien de bien fin et constitue au départ la principale limitation. Même en 1970, il faut savoir que ces résistances passives, comme la tête du rotor, le moyeu, le moteur, le train, etc... sont encore plus coûteuses en puissance dissipée que tout le reste, y compris la nacelle des passagers. Mais là n'est pas le sujet et nous reviendrons au rotor (Fig. 6).

La première limitation en vitesse du rotor apparaît dans la limitation de portance de la pale reculante. Plus l'hélicoptère va vite, plus la pale reculante va doucement, et comme grosso modo il faut bien que cette pale porte sa part de l'appareil, (ne serait-ce que pour l'équilibre en roulis), voilà que cette limitation de vitesse minimale que l'on dénonçait sur l'avion à voilure fixe, réapparaissait comme limitation de vitesse maximale de l'hélicoptère. Mais, fort heureusement, de nombreux facteurs favorables vont faire que cette limitation, pendant de longues années, ne sera pas vraiment critique.

D'abord, la pale ne passe en position reculante que pendant un court instant et les décollements se manifestent dans ces conditions d'une façon beaucoup plus tardive que dans le cas d'écoulements permanents. Pour fixer les idées, un profil symétrique qui ne porte que $C_x = 1,2$ en régime permanent, dépasse 2 en régime transitoire. Bien qu'ignoré ou mal pris en compte, encore récemment, on peut affirmer que ce phénomène heureux a repoussé ipso facto d'au moins 50 km/h les limites d'apparition de décrochage et que, conclusion pratique pour les chercheurs d'aujourd'hui, les travaux futurs d'investigation sur de nouveaux profils ou de nouvelles configurations de rotor ont peu de sens s'ils ne cherchent pas dès le départ à cerner les phénomènes dans ces conditions transitoires.

Ensuite, le début de décrochage de la pale reculante n'est pas une limite infranchissable; il ne se traduit pas comme sur la voilure fixe d'une perte de manoeuvrabilité de l'appareil, mais seulement par des vibrations dans les commandes dues au recul du centre de poussée, ou par des contraintes accrues dans les pales. Par ailleurs, par raison de symétrie, la baisse de portance de la pale reculante amène une baisse de portance de la pale avançante dont l'extrémité peut même être déportée, et le déficit global est réparti sur les pales en positions AV et AR. La puissance nécessaire au vol augmente bien évidemment, mais ceci reste modéré et admissible jusqu'à un certain niveau de décollements. Il y a donc là une barrière, absolue bien sûr, mais qui apparaît progressivement.

Que faire pour aller plus vite ? une fois atteinte la limite de décrochage, il faut impérativement augmenter la vitesse périphérique, ceci va naturellement augmenter globalement la puissance perdue par la traînée propre des pales, mais laisser le décrochage s'instaurer coûterait encore plus cher en puissance et en limitations diverses. Mais en augmentant cette vitesse périphérique, nous atteignons la limitation de vitesse supérieure de la voilure fixe avec l'apparition sur la pale avançante, cette fois, des phénomènes de compressibilité (ondes de choc, bruit, augmentation de traînée). Si la tendance à partir de 1945 va être d'augmenter la vitesse périphérique, celle-ci sera presque stabilisée vers un peu plus de 200 m/s à partir de 1955.

Par rapport au rotor de 1950, le rotor de 1970 a gratté encore quelques points, par exemple :

- . en augmentant la surface des pales, ce qui retarde le décrochage de la pale reculante sans aggraver les phénomènes de compressibilité. Mais, ceci coûte cher en masse de pales et en traînée de profil;
- . en affinant les profils d'extrémité jusqu'à 6% d'épaisseur relative par exemple, pour permettre de tourner un peu plus vite;
- . en multipliant le nombre de pales et en mettant des servo-commandes pour réduire la gêne due aux vibrations;

mais tout ceci n'ira plus bien loin et nous pouvons conclure que la forme classique du rotor de l'hélicoptère, que nous connaissons tous aujourd'hui, est définitivement condamnée à ne pas dépasser des vitesses de l'ordre de 350 km/h, soit un paramètre d'avancement de l'ordre de 0,40.

Et après ?, donnerai-je tort à mon introduction et faut-il que les écoliers qui sortent de l'école, ou les futurs responsables qui n'y retourneront plus guère, s'imaginent que le progrès technique de l'hélicoptère a atteint son asymptote et qu'ils peuvent dormir tranquilles avec des idées bien en ordre pour le reste de leurs jours ? J'aurai la cruauté de les déromper et de leur affirmer qu'ils auront encore des efforts à faire pour assimiler et comprendre les développements considérables qui attendent la technique de la voilure tournante. Mais là, la variété des possibilités techniques m'interdit de jouer les prophètes et il va falloir que vous m'écoutez redire bien des choses que vous savez déjà sur les grandes classes de possibilités techniques qui sont offertes au rotor et que je reclasserai en trois catégories : hélicoptères purs, hélicoptères combinés, hélicoptères convertibles. Malheureusement, en raison de leur très grand nombre, je ne pourrai dire que quelques mots sur chacun.

LE ROTOR D'HELICOPTERE PUR A GRAND PARAMETRE D'AVANCEMENT

Si la barrière de compressibilité est bien absolue, celle du décrochage l'est moins. J'ai parlé de $C_x = 1,2$ tout à l'heure, alors que les valeurs déjà atteintes sur les ailes d'avion sont deux à trois fois celle-là et l'action sur la couche limite par aspiration, soufflage et par d'autres procédés peut élever encore ces valeurs. Je citerai les projets du NGTE, mais surtout les travaux de nos amis français Giravions-Dorand qui ont réussi, en France vers 1956 et depuis lors, dans les souffleries de Ames, de belles expériences avec un rotor à volet fluide (Fig. 7). Des finesses remarquables, supérieures à 12 ont été obtenues à des paramètres d'avancement proches de 0,5 sans vibrations gênantes et le rotor expérimenté a montré d'excellentes qualités beaucoup plus loin encore.

Il est malheureux que l'entraînement par réaction masque ces avantages par un rendement de propulsion très médiocre, mais ceci n'est peut-être pas rédhibitoire. En tous cas, des progrès sont certainement encore possibles de cette façon puisque nous sommes loin encore des possibilités maximales des profils.

LE ROTOR DERSCHMIDT (Fig. 8)

Il faut signaler cette tentative de nos collègues allemands vers 1960, de donner à la pale un mouvement de traînée de grande amplitude de façon à compenser en grande partie la dissymétrie fondamentale. Bien sûr, ce mouvement devra être accordé sur la fréquence du rotor, ce qui est possible en excentrant suffisamment l'articulation de traînée. De ce fait, la pale séjournera plus longtemps du côté avançant que reculant, mais comme la force de portance est proportionnelle au carré de la vitesse, il est possible grâce à une amplitude suffisante de compenser effectivement à la fois les deux facteurs. En fait, le procédé a échoué sur les problèmes de vibrations et de tenue à la fatigue qui sont notre pain quotidien d'hélicoptéristes.

LE ROTOR A B C (Fig. 9)

Cette voie fructueuse a été imaginée par la maison Sikorsky et fait l'objet de développements très importants. Vous savez tous que son principe est, revenant en arrière sur l'articulation de la Cierva, d'accepter de construire un encastrement complètement rigide et de neutraliser le moment de roulis généré par la dissymétrie de vitesse, en associant deux rotors coaxiaux tournant en sens inverse. Les pales peuvent alors s'éviter de modifier leurs incidences et garder celle de la meilleure finesse. Les difficultés pour un hélicoptère pur de cette formule sont dans le fait que le rotor rigide peut difficilement s'incliner par rapport à son axe pour assurer la propulsion de l'appareil et que même dans ce cas, la partie des pales reculantes proche du moyeu restera attaquée par le bord de fuite dans de mauvaises conditions.

En fait, l'application du rotor A B C ne se conçoit que dans la formule combinée dans laquelle une propulsion auxiliaire permet au rotor et à l'appareil de rester parfaitement horizontal.

L'HELICOPTERE COMBINE (Fig. 10)

Le premier appareil à voilure tournante de la Cierva était déjà un appareil combiné, c'est-à-dire qu'il combinait une voilure tournante pour le vol à faible vitesse, à une aile et une propulsion classique pour la grande vitesse.

Le principe de cette combinaison est assez naturel pour l'esprit surtout pour ceux qui ont une longue tradition d'hélicoptère derrière eux.

Si l'hélicoptère refuse de porter ou de propulser au-dessus d'une certaine vitesse, alors quel'avion à voilure fixe refuse au contraire de se sustenter au-dessous d'une autre vitesse, combinons les deux moyens et utilisons-les alternativement dans l'une ou l'autre des deux phases de vol.

Malheureusement, cette voie intuitive est très coûteuse.

D'abord sur le plan aérodynamique, nous avons déjà dit que vers 350 km/h, une fraction très importante de la puissance était dépensée à vaincre les résistances passives et que parmi celles-ci, le moyeu et la partie centrale des pales étaient responsables de beaucoup. Or, la puissance perdue par un $C_x S$ donné varie comme le cube de la vitesse. C'est-à-dire que pour aller plus vite, en gardant le rotor sous la forme où il a permis de décrocher l'appareil, il est nécessaire d'augmenter énormément la puissance, donc le poids et la consommation du moteur.

Par ailleurs, sur le plan structural, ajouter des propulseurs, des transmissions et une aile, ce n'est pas gratuit et cela se traduit par de la charge utile et de la rentabilité en moins.

En conséquence, dans tous les projets d'hélicoptères combinés que nous avons pu faire ou voir, la finesse généralisée se dégrade de façon catastrophique d'une valeur d'environ 4 à 5 pour l'hélicoptère pur à des valeurs à peine supérieures à 2. L'hélicoptère combiné est donc une manière chère d'obtenir de la vitesse. Est-ce à dire que cette voie soit sans intérêt. Absolument pas. D'abord parce que dans certains cas une vitesse élevée peut être absolument nécessaire dans une mission donnée et le client de la machine peut accepter d'en payer le prix. Et ensuite, parce que les inconvénients que j'ai signalés plus haut ne seront pas toujours infranchissables.

Pour diminuer la traînée des rotors à grande vitesse, on peut ralentir leur rotation, éventuellement songer à retractor leurs pales télescopiques (comme Bell l'a étudié) et finalement arrêter complètement le rotor et le replier à l'intérieur du fuselage. Si de telles opérations ne sont pas faciles, elles ne sont pas non plus impossibles et en fin de compte il s'agit de comparer le résultat final avec ce que l'on pourrait avoir par d'autres méthodes.

Par exemple, si on veut produire un avion supersonique capable de décollage vertical, on a le choix entre une solution de ce genre et une solution avec réacteurs de sustentation. Volume, masse, traînée de l'un et de l'autre système doivent être mis en comparaison et il serait bien difficile aujourd'hui de parier quelle est tous comptes faits la solution la plus économique.

HELICOPTERE CONVERTIBLE

L'hélicoptère convertible a été défini par l'organisation qui nous invite ici, comme un hélicoptère qui utilise des rotors à axes verticaux pour décoller et les fait pivoter de 90° pour les utiliser comme propulseur en translation.

Nous retrouvons là une idée extrêmement ancienne et qui répond à l'objection que devaient se faire vers 1900 les pionniers qui refusaient l'axe vertical de l'hélicoptère, responsable des dissymétries dont j'ai parlé, pour se lancer dans des aventures d'avion à ailes battantes.

Il suffit en effet de bien observer les oiseaux pour constater que, après avoir pris leur envol par un mouvement d'aile AV - AR, (l'aile attaquant l'air par l'intrados au cours du mouvement de retour), ils produisent ensuite une trajectoire de ce mouvement progressivement inclinée, pour finir à grande vitesse par un mouvement principalement de haut en bas. Si bien, que le rotor à axe horizontal, comme moyen de sustentation et de propulsion, ne date pas d'aujourd'hui.

Le meilleur historique en a été fait par le Pr Focke au cours de la 5ème conférence du Memorial de La Cierva. Rappelons les projets du Dr Vol Host vers 1940, puis le projet d'Heliconair qui fut développé au Brésil par le Pr Focke après la guerre et mené jusqu'aux essais d'un banc grandeur (Fig. 11), pour être repris ensuite par Curtiss-Wright et Hank Borst en 1960 (X-19) et plus récemment par le Dr Siegfried Gunter, Heinkel et VFW. Mais c'est à notre regretté collègue Lichten de Bell que revient le mérite d'avoir fait voler en 1958 l'appareil XV3. Aujourd'hui, tous ceux qui sont ici peuvent dire qu'ils travaillent à des projets de ce genre et nul doute que cet hélicoptère à rotor convertible marquera un progrès décisif analogue aux inventions de La Cierva et Bréguet.

Sur le plan technique, il bénéficie de tous les avantages de l'hélicoptère et garde une charge utile qui est sensiblement voisine, puisqu'il n'y a pas de parties importantes supplémentaires à prévoir. Quant aux limitations aérodynamiques, la conversion supprime définitivement la limitation de décrochage de la pale reculante et atténue la limitation de compressibilité sur la pale avançante, puisque l'addition de la vitesse de la pale et de celle du déplacement se fait quadratiquement et non plus arithmétiquement.

Le rotor convertible, bien que d'apparence extérieure assez semblable à un rotor classique, en diffère cependant notablement. D'abord son vrillage est beaucoup plus fort et ceci se comprend facilement. En effet, c'est au cas de translation qu'il importe d'adapter ce vrillage pour éviter que certaines parties de la pale propulsent pendant que d'autres traînent, ce qui dégraderait le rendement de façon inacceptable. La difficulté est alors d'éviter que les pieds de pale n'aient en vol stationnaire un calage trop élevé et ne décrochent prématurément. Mais ceci est faisable et, une fois obtenu conduit à des chiffres de Mérite en vol stationnaire au moins 1,5 fois ceux des hélicoptères actuels (0,75 contre 0,5) ou mieux.

M. Gilmore de Boeing affirme avec raison que l'hélicoptère convertible est le véhicule le plus efficace du monde en vol immobile.

Quant au comportement en translation, il retrouve malheureusement pour nous toutes les embûches du rotor classique, à savoir : fatigue, vibration, et aéroélasticité; mais cette fois avec la satisfaction de travailler pour un gain très important de vitesse et sans que la résolution de ces problèmes ne soit à priori plus difficile que sur un hélicoptère pur.

Au-delà de 750 km/h, à peu près, la limite de compressibilité devient absolue et d'autres solutions devront être imaginées.

L'hélice carénée munie d'une sortie variable (diffusion en vol stationnaire, contraction en vol de translation) pourrait là retrouver une place de choix jusqu'à la barrière du vol supersonique qui devra évidemment faire appel à d'autres techniques.

CONCLUSION

La voilure tournante qui nous permet aujourd'hui de construire et d'utiliser des appareils, capable d'une mobilité inconnue autrefois, est le fruit des travaux acharnés de tous nos devanciers et cet exposé n'aura pu en donner qu'un reflet bien fugitif. Mais, elle a encore devant elle des possibilités de développement considérable, notamment sous forme convertible. Nous savons que ces progrès seront une œuvre collective à laquelle chacun d'entre nous peut apporter une contribution.

Je souhaiterais que dans le cadre de cette organisation qui nous accueille aujourd'hui nous puissions provoquer les discussions fructueuses et, personnellement, en vous remerciant de m'avoir écouté pendant quelques instants, je suis prêt à répondre à vos questions.

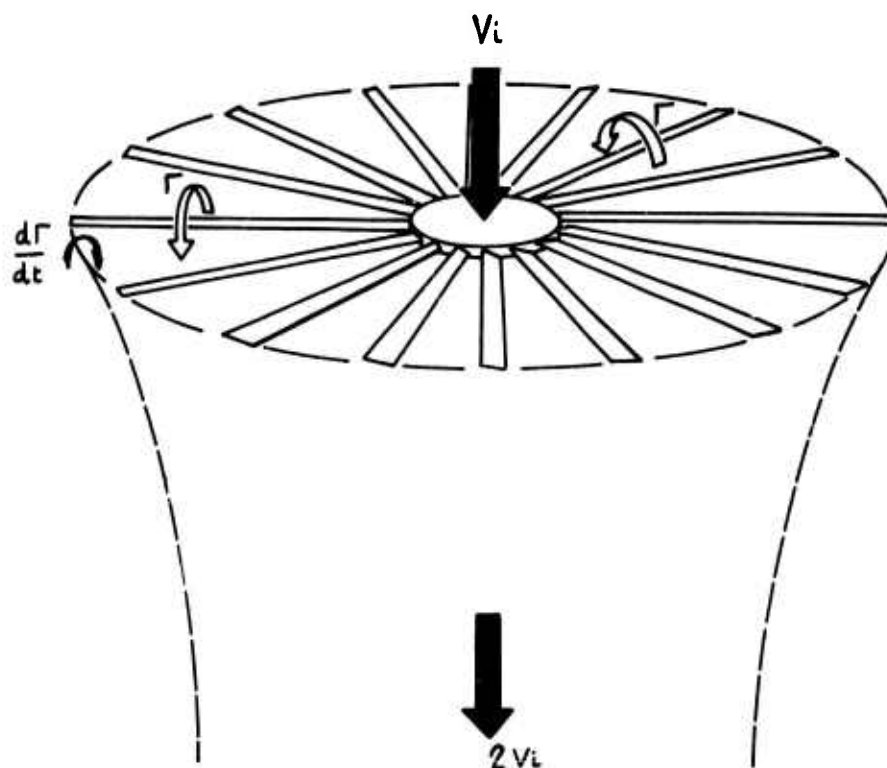


Fig. 1

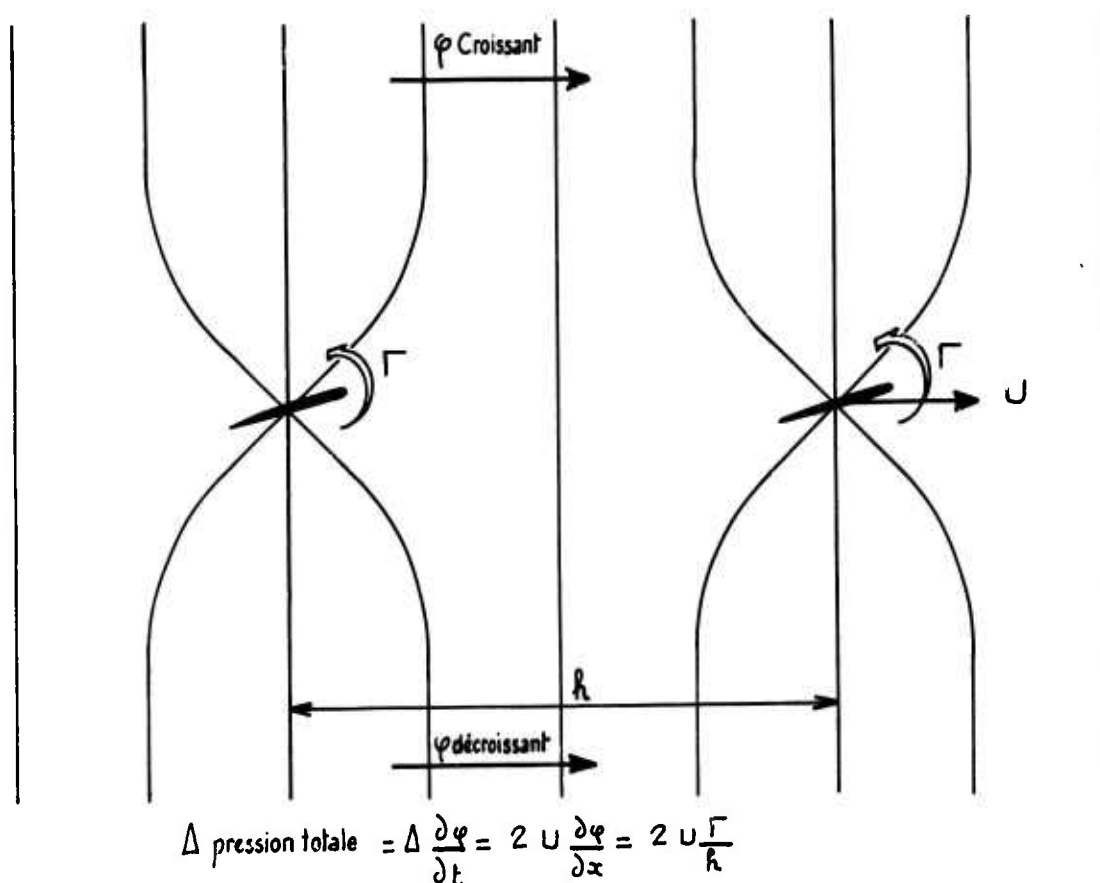


Fig. 2

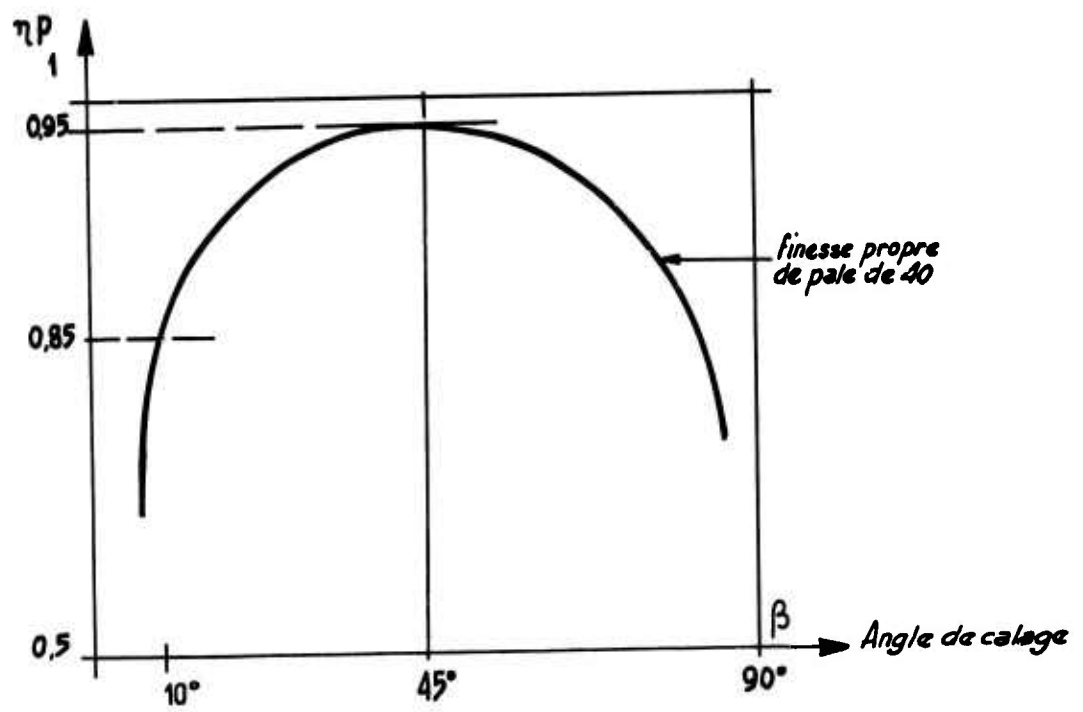


Fig. 3

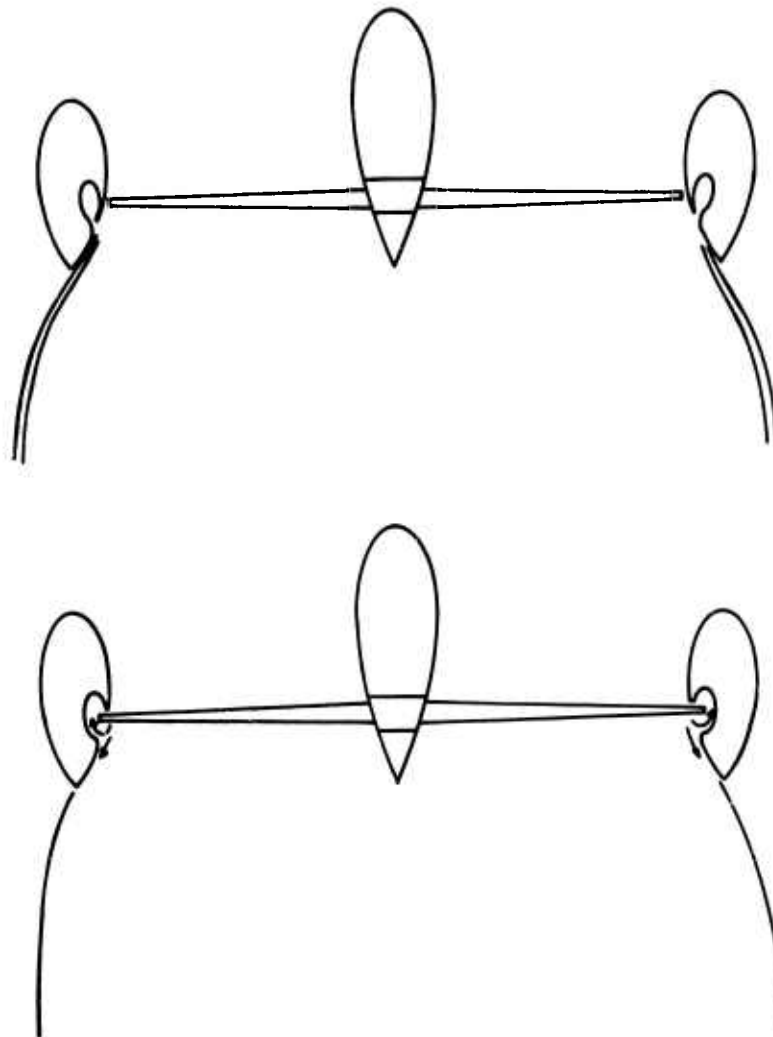


Fig. 4

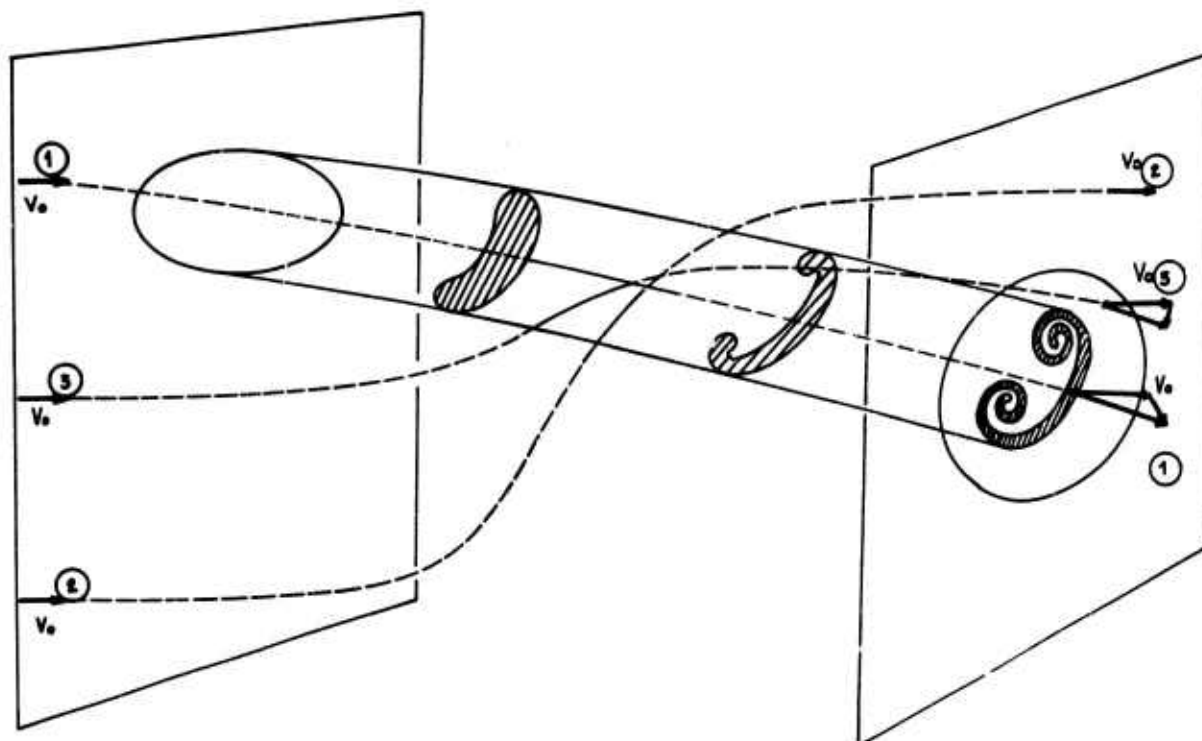


Fig. 5

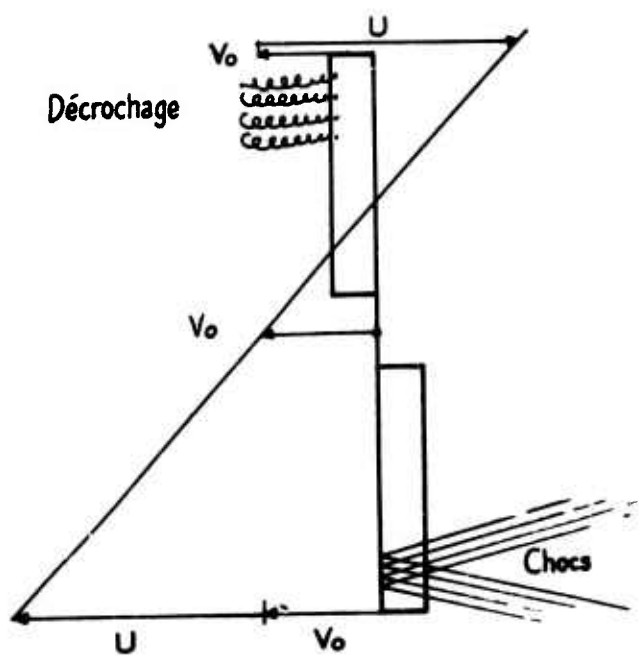


Fig. 6

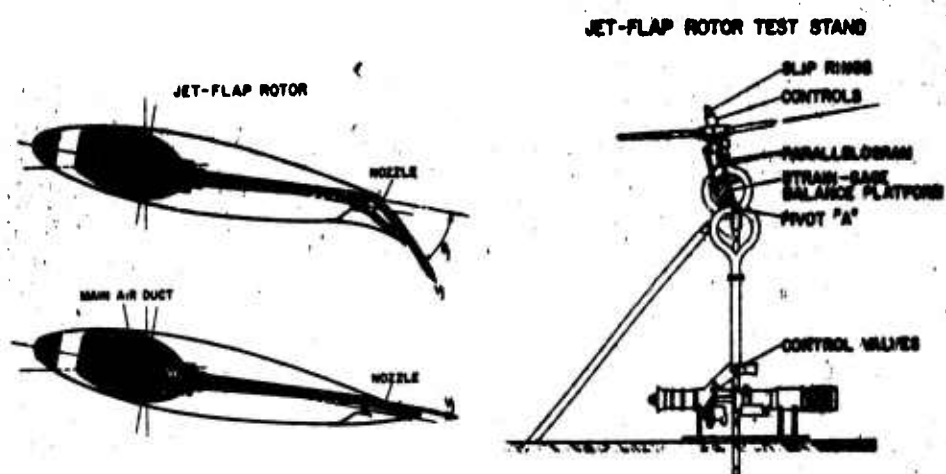


Fig. 7

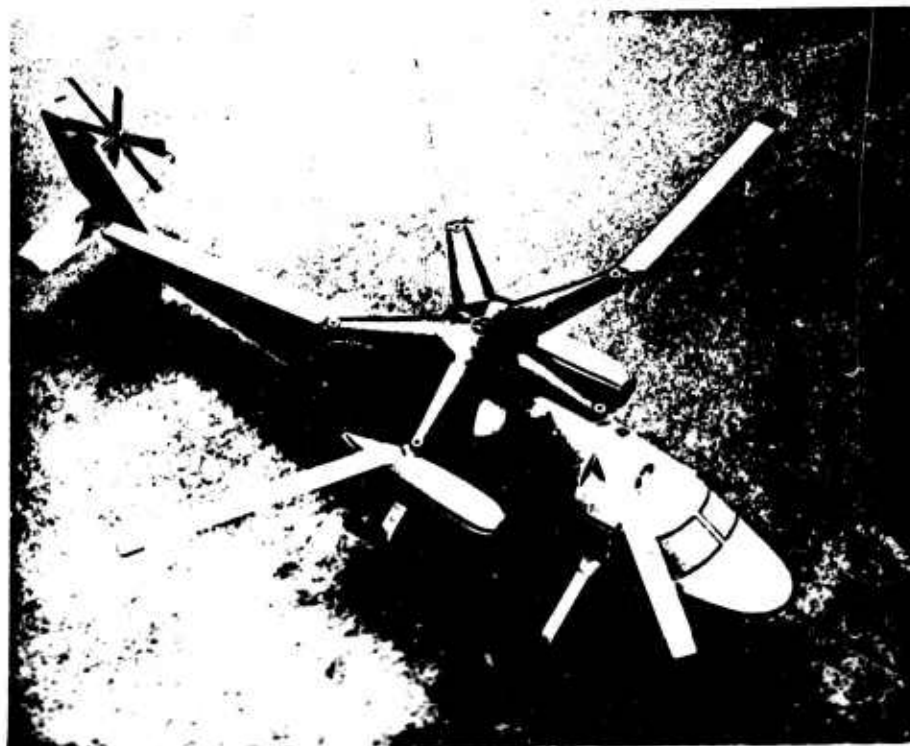


Fig. 8



Fig. 9



Fig. 10

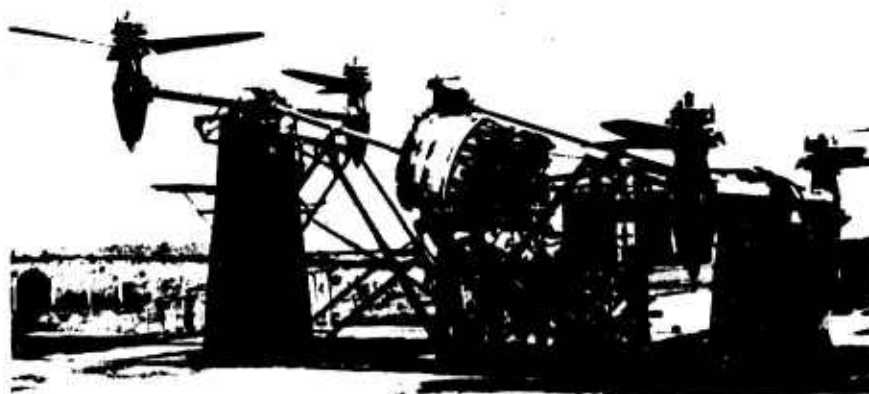
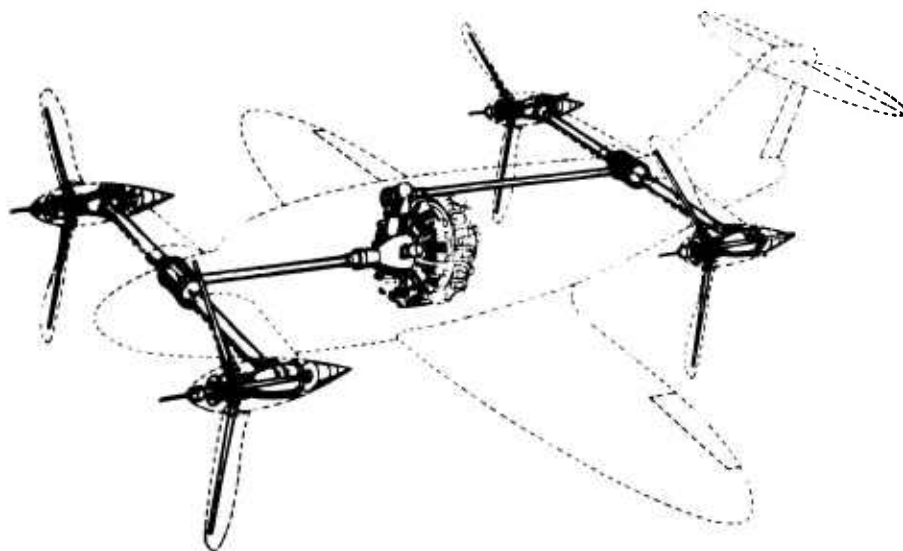


Fig. 11

HISTORIQUE DES METHODES DE CALCUL DE PERFORMANCE DES HELICOPTERES

par

J. SOULEZ-LARIVIERE et F. MAILLARD

Du fait de l'extrême variabilité, dans le temps et dans l'espace, des conditions de fonctionnement d'une surface élémentaire de pale d'un rotor, on rencontre sur celui-ci et à chaque instant à peu près tous les aspects possibles de l'aérodynamique.

Les vitesses peuvent être nulles, négatives ou positives jusqu'à atteindre Mach 1, les incidences faibles dans une partie de la pale atteignent 40° ; dans d'autres, les angles de dérapage peuvent aussi atteindre 90° . Toutes ces valeurs sont simultanément instantanées.

Chaque pale est théoriquement interactionnée par une infinité de sillages variables provenant des pales précédentes, ainsi que par les parties passives comme un fuselage ou le sol, activés comme une aile auxiliaire, ou dynamiques comme un système anticouple ou un jet propulsif.

Le problème du calcul de performances d'un hélicoptère est donc nécessairement très complexe. Il est donc normal qu'il n'ait pu être abordé d'entrée dans toute sa généralité et que les méthodes employées aient historiquement évolué dans le sens d'une sophistication de plus en plus poussée.

Négligeant les travaux fondamentaux communs à toutes les applications aérodynamiques, on constate que c'est à l'occasion de l'autogire que furent développées les premières méthodes valables.

C'est Glauert qui en 1926 (RM 1111) base sa méthode sur la constatation qu'en vol vertical un rotor se comporte comme le prévoit la théorie de Froude, et qu'en vol horizontal le flux moyen induit est le même que celui d'une aile ayant même sustentation que le rotor et dont l'envergure serait le diamètre du rotor.

Négligeant les variations locales de ce flux, il calcule alors la distribution d'incidence nécessaire à l'équilibre du rotor; puis, presumant que le terme passif C_{xp} du coefficient de traînée de profil peut être considéré comme constant ou être moyenné, il établit une méthode de calcul applicable aussi bien à l'hélicoptère qu'à l'autogire et permettant de calculer la puissance absorbée, dans l'hypothèse où les angles d'incidence et de dérapage restent partout faibles, et les vitesses radiales peuvent être négligées.

Dès le départ, cette méthode a permis, dans le cas des autogires lents et peu chargés, des prévisions satisfaisantes.

Cette méthode fut bientôt complétée par Goldstein, puis Lock (RM 1127) introduisit dans le calcul le premier harmonique de battement et Wheatley (NACA TR 487) le cercle d'inversion et le vrillage.

Ces méthodes purent s'appliquer à la fin des années 30 et dans l'immédiat après guerre à l'hélicoptère vrai qui faisait son apparition. Les auteurs, pour la plupart se contentèrent d'introduire des facteurs correctifs plus ou moins empiriques, ou de tenir compte de phénomènes précédemment présumés négligeables.

Ainsi furent introduits le rayon utile BR et une non-uniformité de la vitesse induite pour le calcul du flux (Sissingh) et l'écoulement radial fut pris en considération. Bayley (NACA TR 716) fait varier C_{xp} avec l'incidence locale. Wheatley, Glauert et Lichten introduisent des formes en plan non rectangulaires et le couplage pas-battement. Meyer le déport de l'axe de battement, Kissilovsky les profils évolutifs; Nicholsky, Mangler et Miller améliorent la définition du flux induit local; Jenkins tient compte des oscillations de traînée; Gessow (NACA TR 3366) suppose un C_z plafonné aux grands angles et prend en compte un pied de pale non aérodynamique; Zbrozek étudie l'effet de sol et Gabel l'influence des déformations élastiques des pales. Parallèlement au développement de ce qui peut être considéré alors comme une méthode classique, des francs-tireurs appliquent des méthodes originales.

A l'occasion du Gyroplane Bréguet, vers 1935, Devillers et Dorand créent une méthode basée sur la considération d'un nombre fini d'azimuts représentatifs des positions successives de pales, azimuts qui peuvent être étudiés de façon approfondie. Cette méthode préfigure celle qui sera développée dans les années 60 chez Sikorsky pour étudier, en même temps que les performances, les mouvements d'une pale articulée et flexible.

En 1945 Klemin présente (Aero Digest) d'une façon très claire, une méthode beaucoup plus empirique mais très souple, qui est celle du bilan. Quoique la mort de Klemin ait interrompu la publication de cette méthode avant qu'elle ne soit mise au point, elle a rencontré un grand succès tant à cause de sa simplicité que de la facilité avec laquelle on y introduit l'influence de phénomènes parasites de toute nature et des résultats très suffisants qu'elle permet d'obtenir dans la plupart des cas.

Dans les années 50, l'amélioration des performances, l'introduction de charges de disque et de pale élevées, l'adoption de hautes vitesses de rotation, et de puissances élevées, grâce en particulier aux turbines, révèlent que les méthodes de calcul deviennent insuffisantes à prévoir les performances dans les cas extrêmes.

Les phénomènes de compressibilité et de décrochage, en régime instationnaire, sont la cause de cette insuffisance.

Tanner (NASA CR 114) tient compte des phénomènes de compressibilité mais se limite à quelques cas particuliers de forme de rotor.

Tarzanin, chez Boeing-Vertol, et Harris (J. of AED) tiennent compte du caractère dynamique du décrochage et des interactions d'un écoulement radial avec le décrochage.

En France, Hirsch tente une synthèse en vue de tenir compte avec une meilleure précision que celle atteinte jusqu'ici, de l'ensemble des phénomènes.

Malgré l'ampleur des travaux effectués, il reste beaucoup à faire pour obtenir une méthode entièrement satisfaisante.

Certains phénomènes sont en pratique tout à fait négligés par les calculs actuels, par exemple :

- Mise en rotation par le couple moteur de la veine d'air traversant le rotor (effet facilement calculable, mais généralement modéré).
- Supplément de traînée induite sur chaque pale, dû à un effet d'allongement de la pale (cet effet dont l'importance fut exagérée par les auteurs jusqu'aux années 30, est au contraire à tort tout à fait négligé aujourd'hui).
- Centrifugation de la couche limite, travail de pompage correspondant, et interactions diverses liées à cette centrifugation.
- Interactions rotor-fuselage (mais on tient compte, conformément à la théorie du biplan, des interactions rotor-aile).

D'autres phénomènes sont traités de façon insuffisante :

- Variation du nombre de Reynolds le long de l'envergure et en fonction de l'azimut.
- Tous les phénomènes liés à l'instationnarité (en incidence, en vitesse, en pompage et en dérapage) et aux interactions de ces instationnarités.

C'est là un ensemble de phénomènes insuffisamment connus et qui exigera beaucoup d'études élémentaires préalables.

- Influence des sillages des pales sur les pales suivantes et spécialement des tourbillons marginaux (tant d'extrémités que d'implanture), mais aussi des nappes tourbillonnaires produites par les variations de circulation et des nappes ralenties dues aux traînées passives.
- Profil dynamique différent du profil géométrique (lié à l'instationnarité).
- Bordure du cercle d'inversion, où des incidences de $\pm 90^\circ$ sont rencontrées avec des vitesses non négligeables lorsque le disque a une forte incidence (vol à très haute vitesse, rotor délesté ou en cours de conversion).

Il peut sembler étonnant que tant de phénomènes importants étant plus ou moins inconnus ou négligés, les prévisions de performances se révèlent cependant à peu près satisfaisantes dans les cas normaux. Cela tient à deux choses :

. D'une part, ces phénomènes sont souvent d'une nature telle que leur influence est faible sur le bilan de puissance. Ainsi le tourbillon marginal émis par une pale et rencontrant la suivante, produit des effets du même ordre mais de signes contraires dans sa partie extérieure et sa partie intérieure. L'effet global sur la puissance est donc très faible, bien que la distribution des poussées et traînées soit gravement perturbée.

. D'autre part, ces phénomènes ne prennent toute leur importance que dans des cas extrêmes ; par exemple : charge de pale très élevée en ressource. Dans ce cas, il ne s'agit pas d'un cas de vol permanent et on ne demande généralement pas au calcul une grande précision.

Cependant il peut s'agir de cas qui peuvent définir une possibilité extrême très importante : par exemple survitesse possible en piqué, décélération en ressource ou quick stop, virage à grande vitesse et à ce point de vue il sera nécessaire de disposer de méthodes de prévisions correctes. En outre, seules de telles méthodes peuvent être utilisées si on veut s'en servir pour prévoir les efforts dans les pales, particulièrement dans les cas extrêmes qui sont nécessairement les plus utiles à connaître.

Il importe aussi de disposer de méthodes suffisamment exactes pour permettre de prévoir, non seulement les performances globales de la machine, mais aussi les variations que pourra provoquer telle ou telle modification constructive, variations qui devront pouvoir s'exprimer, soit en puissance absorbée dans un cas de vol donné, soit en recul des limitations pour une même puissance.

Reflexions Faisant Suite à l'Exposé de l'Article 5

par
R. Hirsch
Aérospatiale
Etablissement de Chatillon

L'exposé très exhaustif et de grande clarté que M. Soulez-Larivière a présenté se suffit à lui-même: il est en soi assez complet pour qu'il n'apparaisse réellement pas utile d'en commenter les différents paragraphes, ce qui reviendrait à les paraphraser.

Je me bornerai donc à émettre quelques remarques complémentaires sur deux chapitres que me tiennent à coeur:

- La prévision théorique du fonctionnement des rotors d'hélicoptères;
- La conception des rotors de "Convertibles" et les possibilités qui en découlent.

En ce qui concerne la 1ère question, nous en sommes à modéliser, assez complètement le fonctionnement des profils de pales à condition que ne se manifestent pas les combinaisons d'effets soniques et d'effets d'écoulements transverses en décrochage.

Sont actuellement pris en compte:

- Les effets d'induction d'un système tourbillonnaire en réseau de nappes hélicoïdes aplaies et déformées pour que figurent la contraction et la distortion du pas.
- Les effets instationnaires touchant le développement de la circulation et celui des champs de pression.
- Les effets de compressibilité infrasonique, y compris l'influence des délais de transmission de signaux d'induction.
- Les effets d'interactions tridimensionnelles entre profils.
- Les effets de non linéarité des lois de coefficients de portance des profils à l'égard de l'incidence variant de -180 à $+180^\circ$ dans le cercle d'inversion.
- Les effets de non linéarité dus aux battements vertical et horizontal et en chaque station azimutale aux déformations de flexion et de torsion de pales.

L'influence de chaque effet peut être ainsi pesée.

Les quelques diagrammes ci-joints permettent la comparaison entre essais à Modane et calculs - Leur concordance n'est bien sûr pas absolue, mais l'on peut considérer-qu'il est possible d'effectuer des prévisions convenables concernant les résultats à attendre de modifications de forme ou de structure de rotors en projets - *sur l'ensemble* (aérodynamique et mécanique) *de leur comportement*.

On pourrait même maintenant passer sur un plan rationnel analogue à celui mis en oeuvre pour les hélices, les problèmes d'optimisation des performances d'un rotor et essayer d'en déduire la forme de pale optimum à construire.

Ceci nous conduit à la deuxième question: la conception des rotors de convertibles.

Les phases fondamentales de fonctionnement de ceux-ci sont: le soulèvement - le vol à vitesse élevée toutes deux en configuration "axiale".

Nous savons depuis longtemps déterminer la forme de pale (forme en plan, vrillage, nature des profils) qui satisfaisant à certain conditions de compatibilité, permet d'obtenir une performance simultanément optimum en deux régimes de fonctionnement distincts. De nombreuses vérifications et applications ont permis d'affirmer cette technique. Ces méthodes d'optimisation ont été appliquées au problèmes des convertibles et l'on a constaté la possibilité, grâce à elles, d'obtenir, avec la même pale, des performances satisfaisantes en soulèvement (chiffre de mérite de 0,74 par exemple pour $D = 5,20$ m et 830 Kw) et à vitesse élevée effets de compressibilité inclus à 18 000 ft: rendement $\eta = 0,77$ à Mach 0,67, sous 630 Kw. Ceci s'obtient avec des charges au disque nettement supérieures à celles dont on use sur hélicoptères, mais encore faibles vis-à-vis de celles habituelles aux hélices.

Il en résulte évidemment que la poussée de soulèvement par unité de puissance est plus faible que celle obtenue sur hélicoptères: mais, compte tenu des besoins en puissance d'un tel appareil pour qu'il fonctionne aux vitesses de

croisière de 400 Kts, il n'y a pas là un handicap véritable. Les diagrammes et la photo ci-joints indiquent les résultats de mesure obtenus sur une maquette de rotor de 90 cm de diamètre.

La forme des pales issues de la double optimisation très élargies à leur embase, peut soulever des difficultés de réalisation. Il y a moyen de tourner la difficulté par aménagement d'un volet de courbure d'embase de pale tel que nous avons pu le proposer dès 1948 dans notre publication de l'époque*. C'est là une forme assez atténuée de la double pale Hamilton qui doit conduire à une réalisation relativement aisée.

De telles pales, beaucoup plus "consistantes" que celles des rotors de convertibles à faible charge au disque soulèveront des problèmes de tenue mécanique, en vibrations notamment, certainement plus faciles à traiter pourvu qu'on s'attache à créer pour elles une technologie adaptée.

Ainsi donc, je suis pour ma part persuadé qu'on a un intérêt évident *sur tous les plans*, à viser haut dans la performance à obtenir des convertibles -- et à cesser de se contenter d'en attendre un prolongement modeste du domaine des combinés.

En bref, et c'est simple-t-il la conclusion à retenir, il sera possible, avec des convertibles de la famille évoquée ici, *de disposer d'appareils ayant les performances de vitesse d'utilisation exigées pour les STOL actuellement en projet, tout en bénéficiant des avantages du décollage vertical.*

Je suis heureux que l'occasion m'ait été offerte de souligner ces remarques devant vous.

SYMBOLES

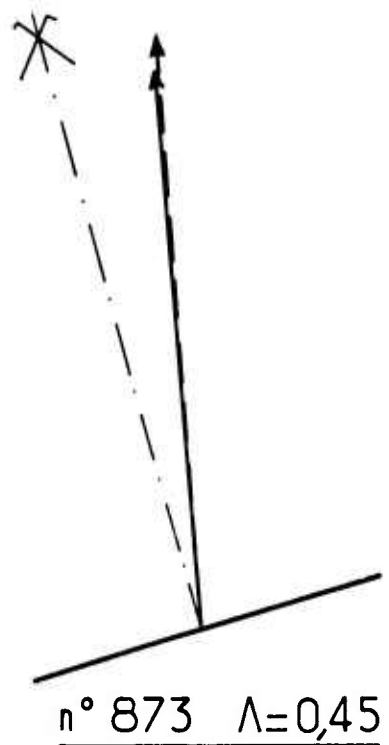
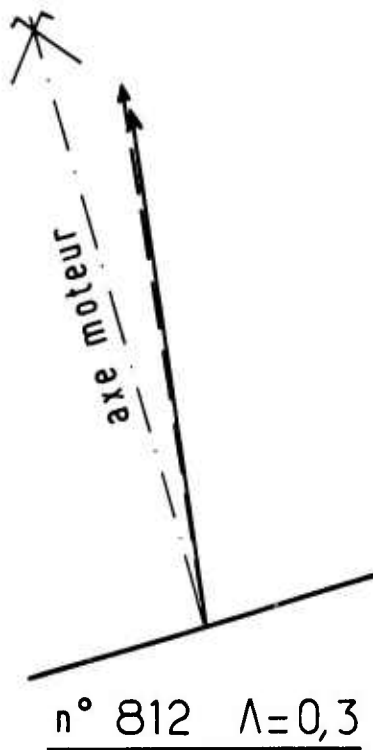
(Unités MKSA)

n	régime de rotation en tours/sec.
ρ	masse volumique de l'air
D	diamètre disque rotor
S	surface
U	vitesse périphérique
v	vitesse de translation
T	traction
W	puissance absorbée
Q	couple
R_z	portance globale référée à la vitesse d'entraînement
R_x	trainée globale référée à la vitesse d'entraînement
\hat{R}_z	charge aérodynamique locale d'un profil de pale
Λ	paramètre d'avancement $\frac{V}{U}$
ψ^*	azimut de la pale
$x = C_p$	coefficient de puissance $\frac{W}{\rho n^3 D^5}$
C_T	coefficient de traction $\frac{W}{\rho n^2 D^4}$

* R.Hirsch: Hélices optima simples et coaxiales. PST.225 -- T.II -- 1948.

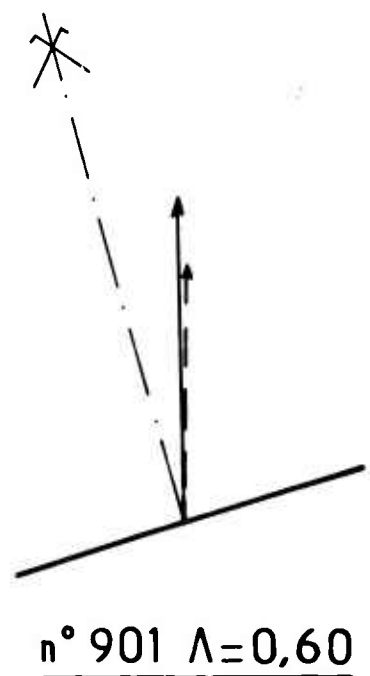
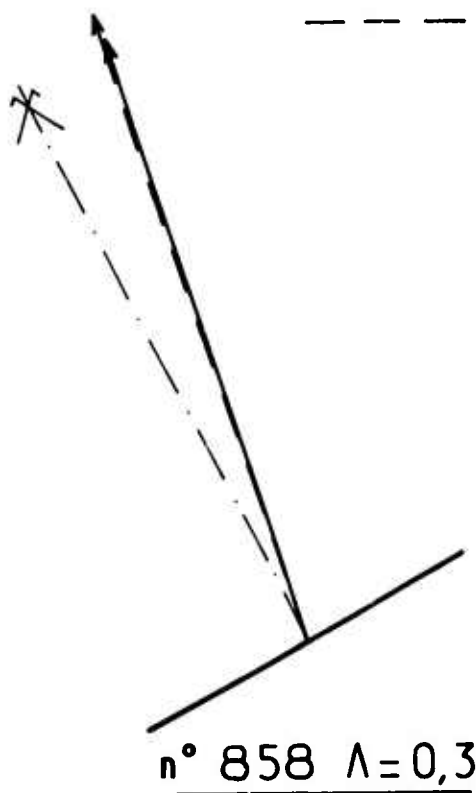
C_z	coefficient de portance	$\frac{R_z}{\rho/2 S U^2}$
C_x	coefficient de trainée	$\frac{R_x}{\rho/2 S U^2}$
C_{mnq}	coefficient de couple	$\frac{Q}{\rho/4 S U^2 D}$
$l \int_0^l \frac{\Delta p}{p_0} dx = P_m$	charge aérodynamique locale relative des profils de pale $\dot{R}z_1/p_0$	
$a_1^{(0)}$	élongation de la fondamentale de battement	
p_0	pression statique ambiante	

Position des résultantes aérodynamiques



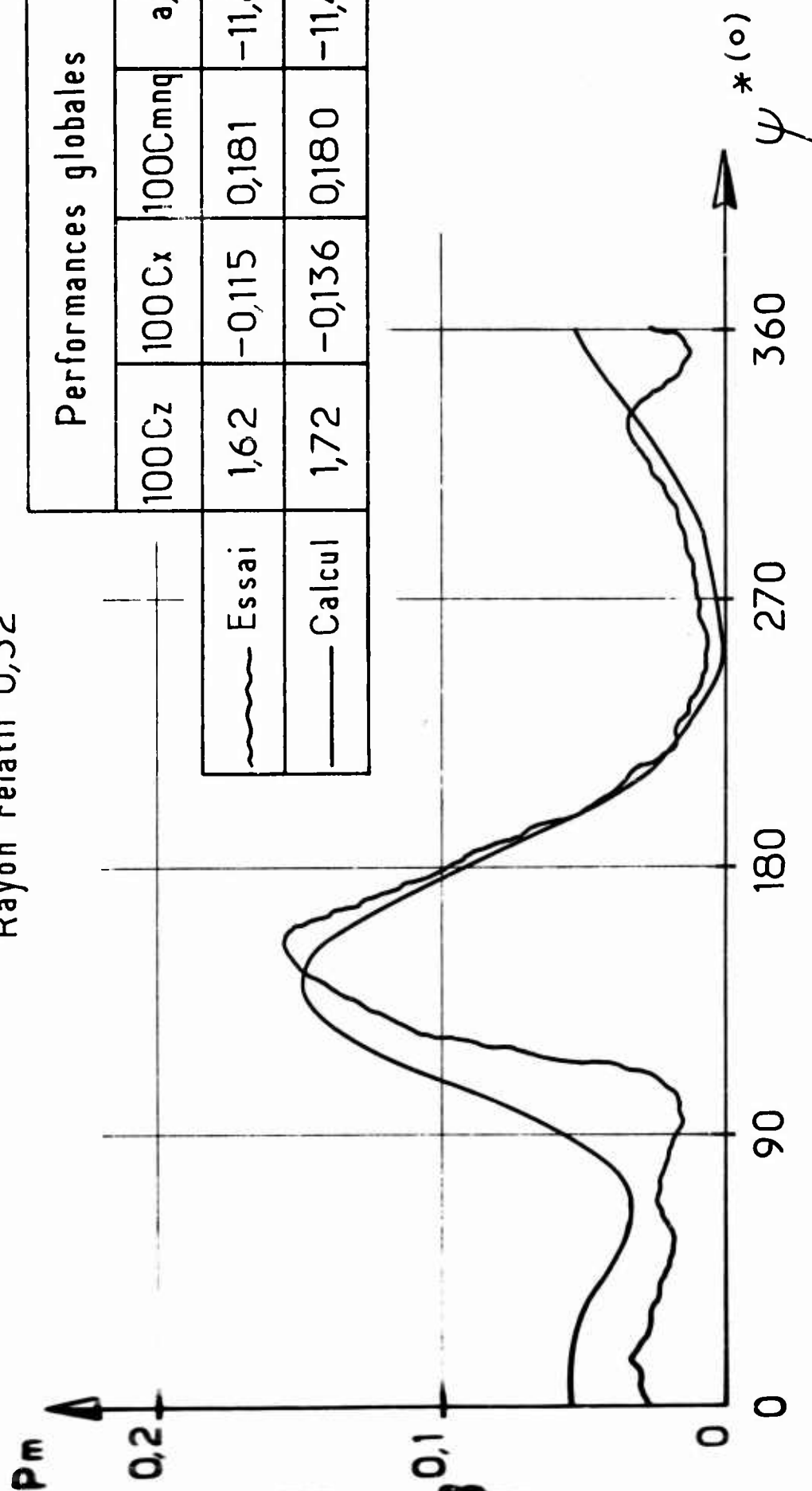
——— Essai (corrigé de l'effet de moyeu)

- - - - - Calcul



Charges aérodynamiques locales Pm dans le tour pour $\Lambda=0,45$

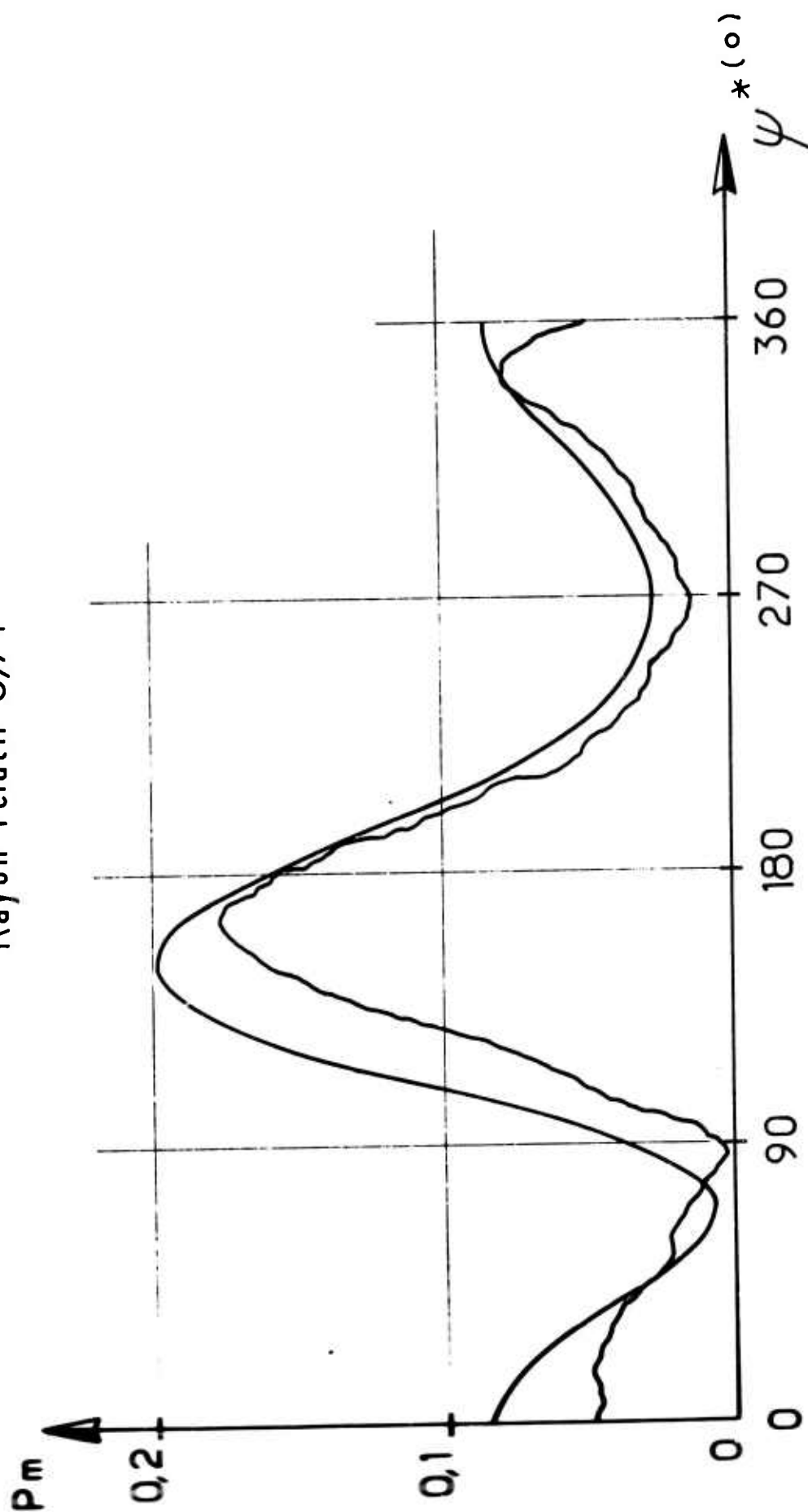
Rayon relatif 0,52



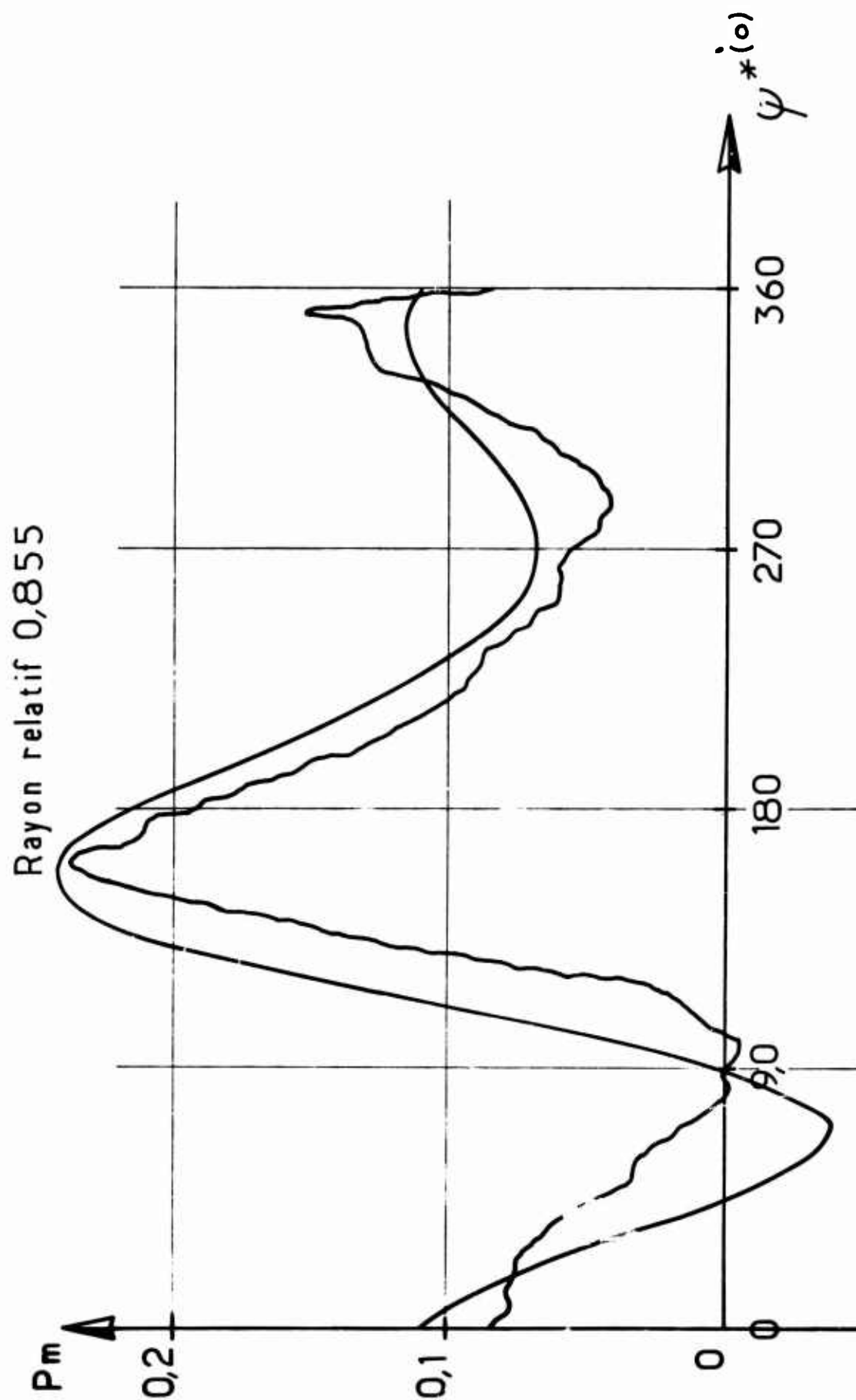
	Performances globales			
	100 Cz	100 Cx	100 Cmq	α_1 (°)
Essai	1,62	-0,115	0,181	-11,85
Calcul	1,72	-0,136	0,180	-11,46

Charges aérodynamiques locales P_m dans le tour pour $\Lambda = 0,45$

Rayon relatif 0,71

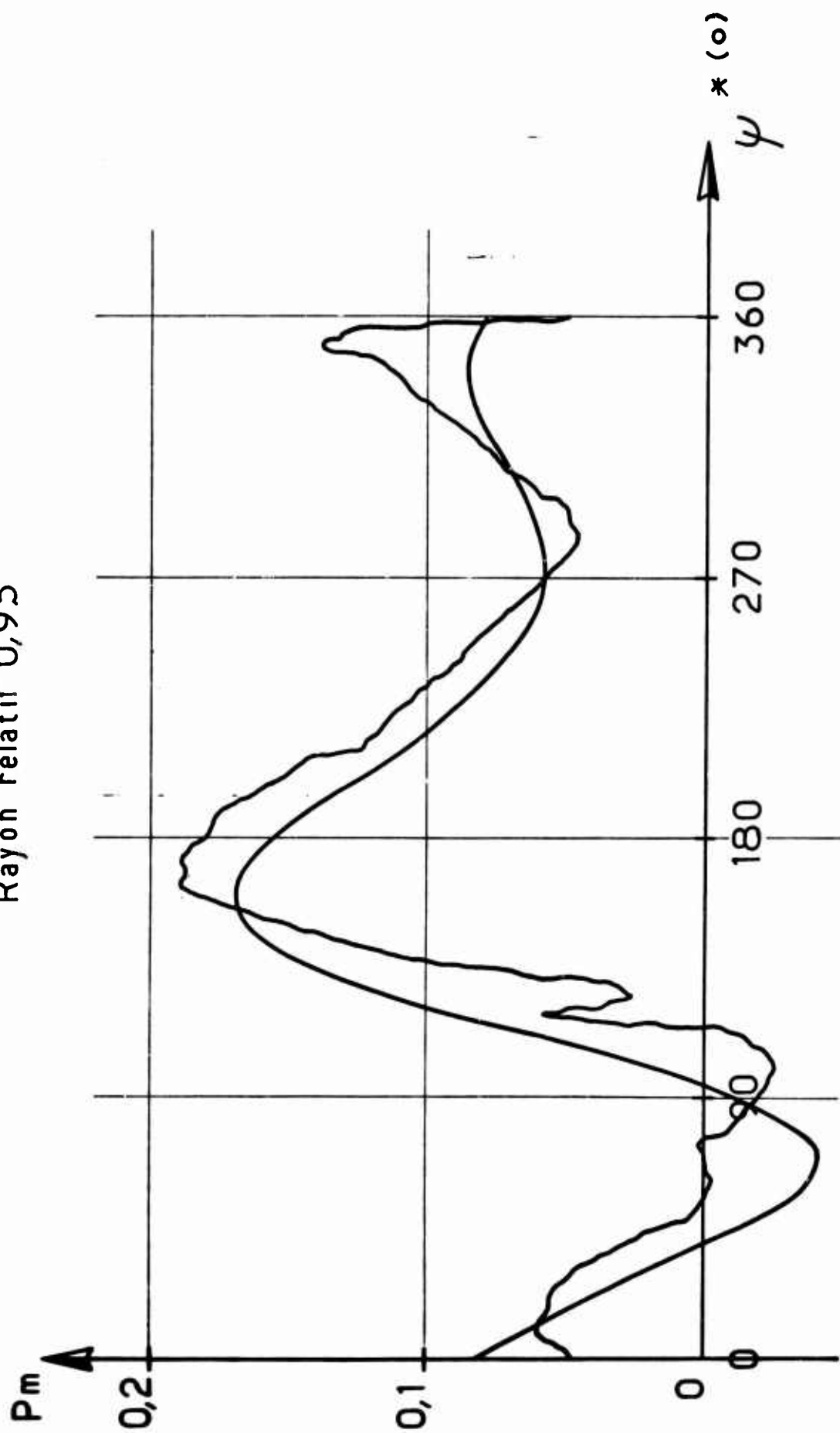


Charges aérodynamiques locales P_m dans le tour pour $\Lambda = 0,45$



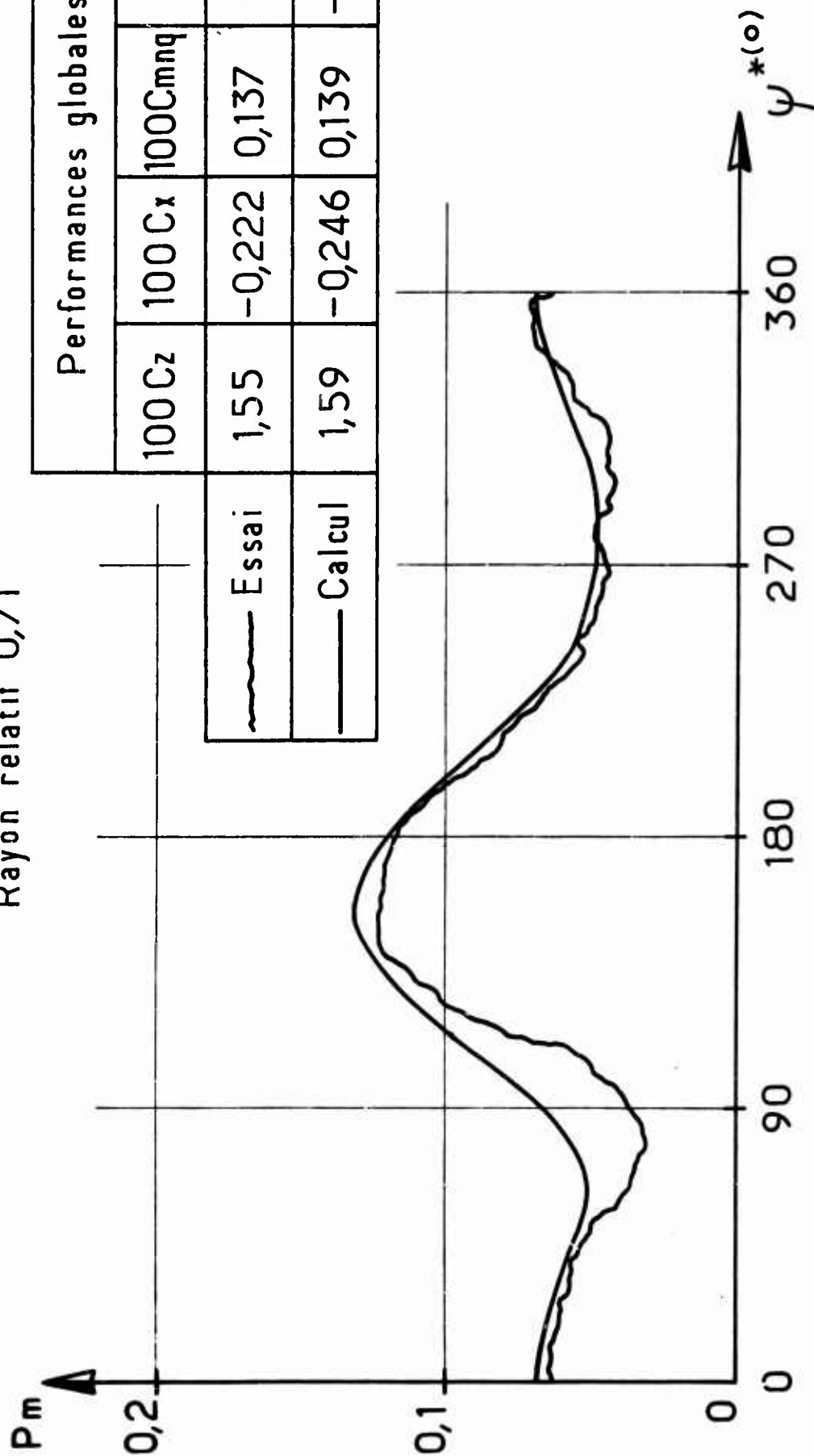
Charges aérodynamiques locales P_m dans le tour pour $\Lambda = 0,45$

Rayon relatif 0,95



Charges aérodynamiques locales Pm dans le tour pour $\Lambda=0,30$

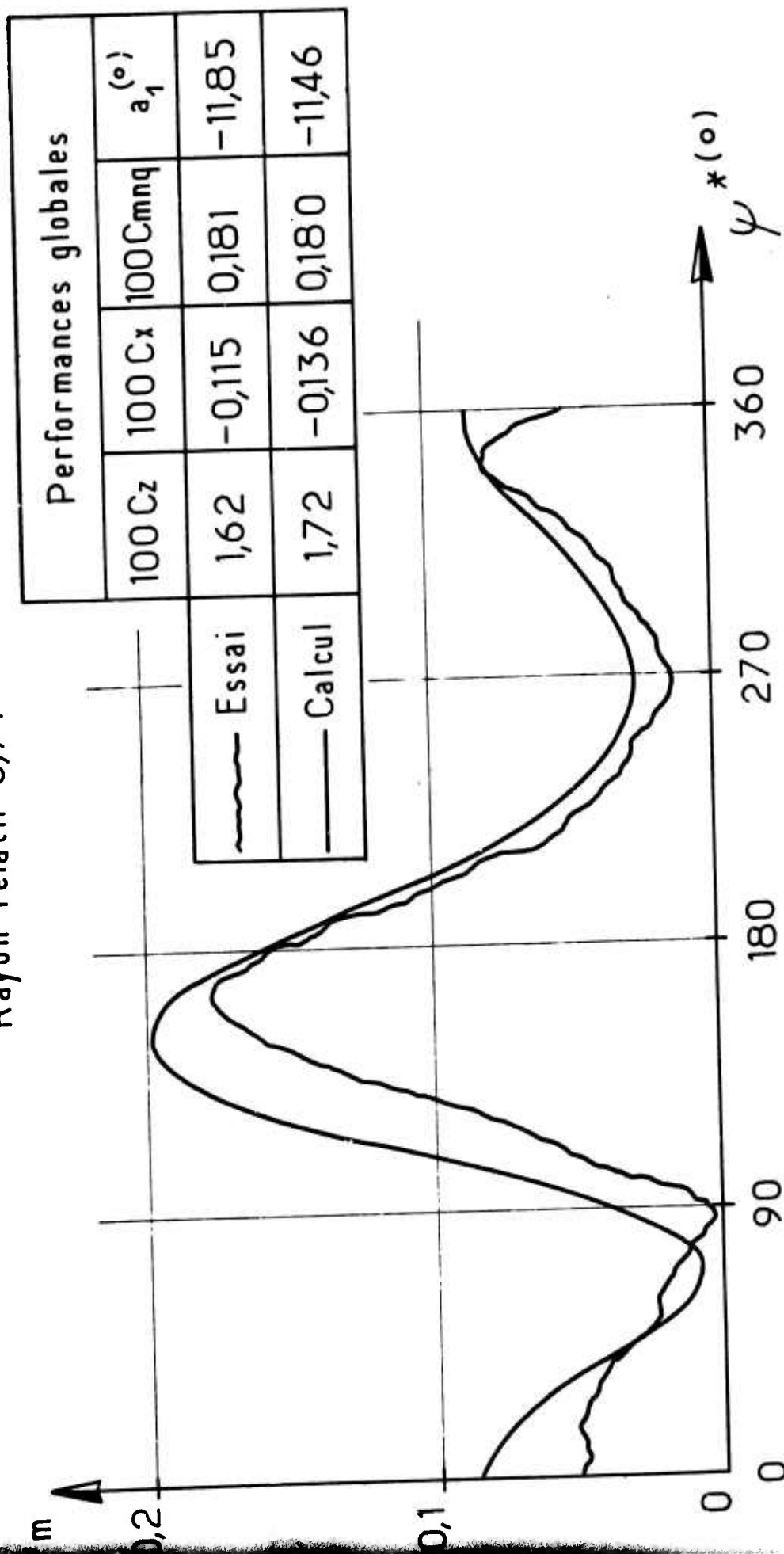
Rayon relatif 0,71



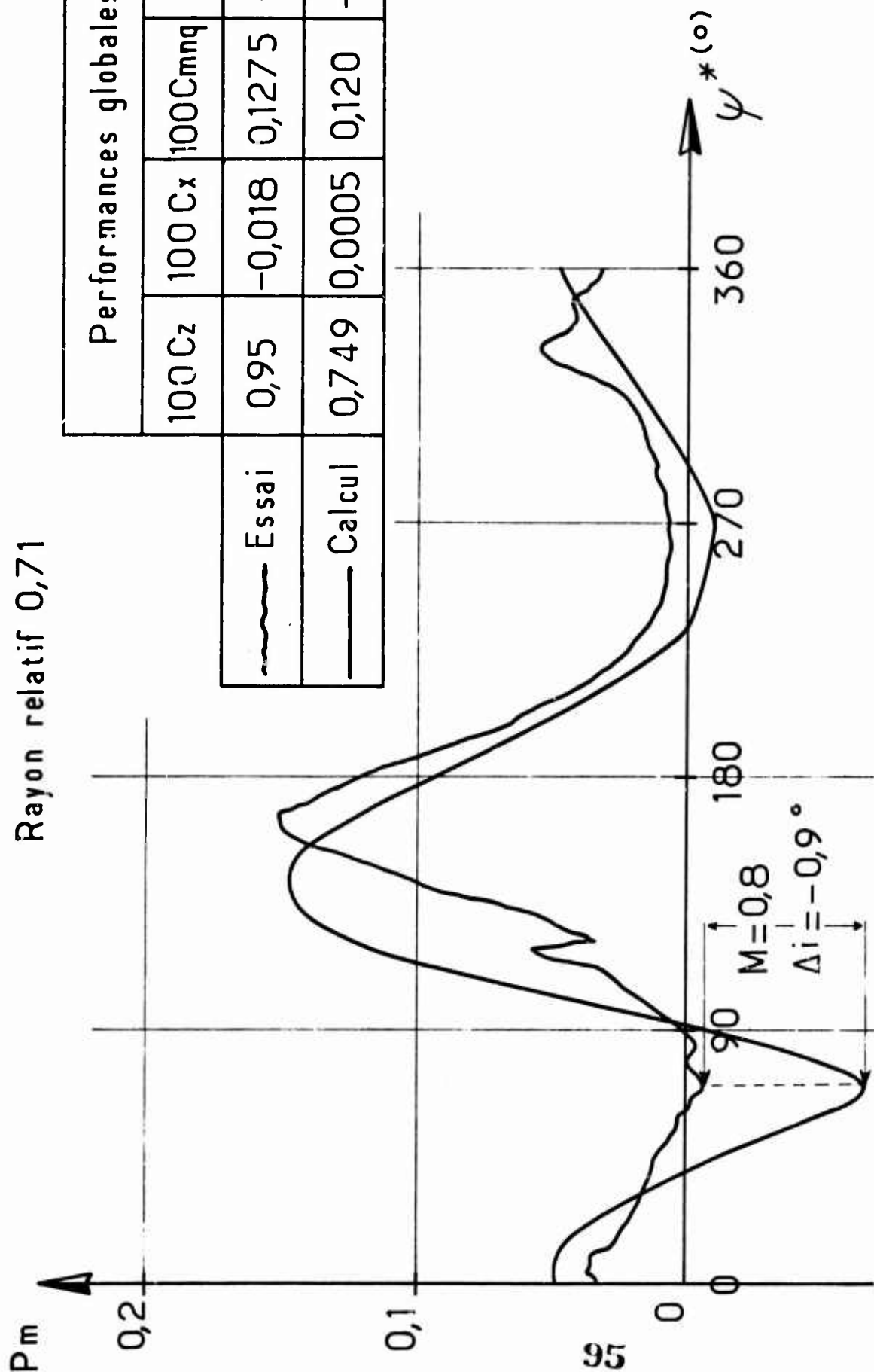
	Performances globales			
	100 Cz	100 Cx	100 Cmnq	$a_1^{(o)}$
Essai	1,55	-0,222	0,137	-7,5
Calcul	1,59	-0,246	0,139	-7,05

Charges aérodynamiques locales Pm dans le tour pour $\Lambda = 0,45$

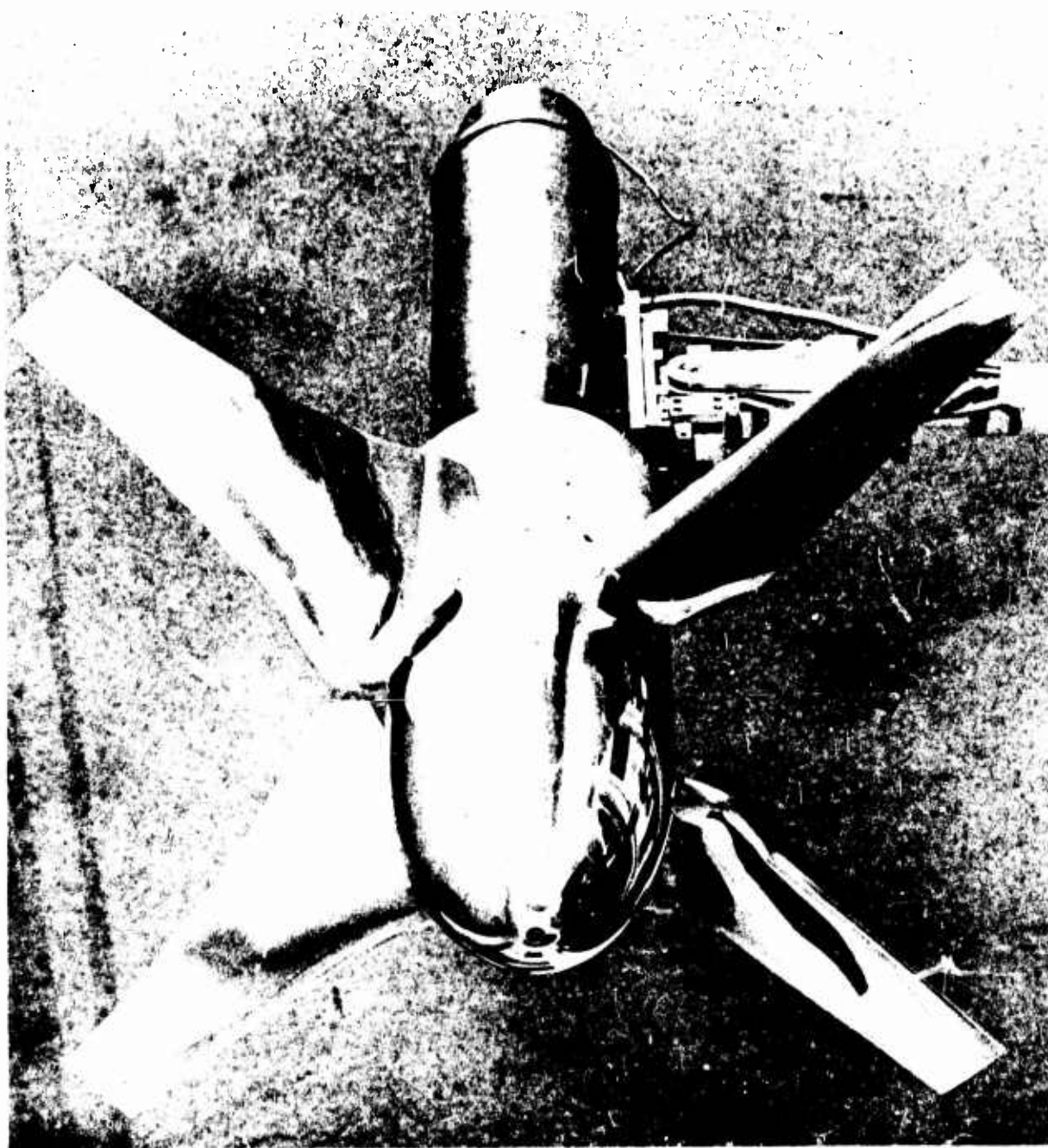
Rayon relatif 0,71



Charges aérodynamiques locales P_m dans le tour pour $\Lambda = 0,60$



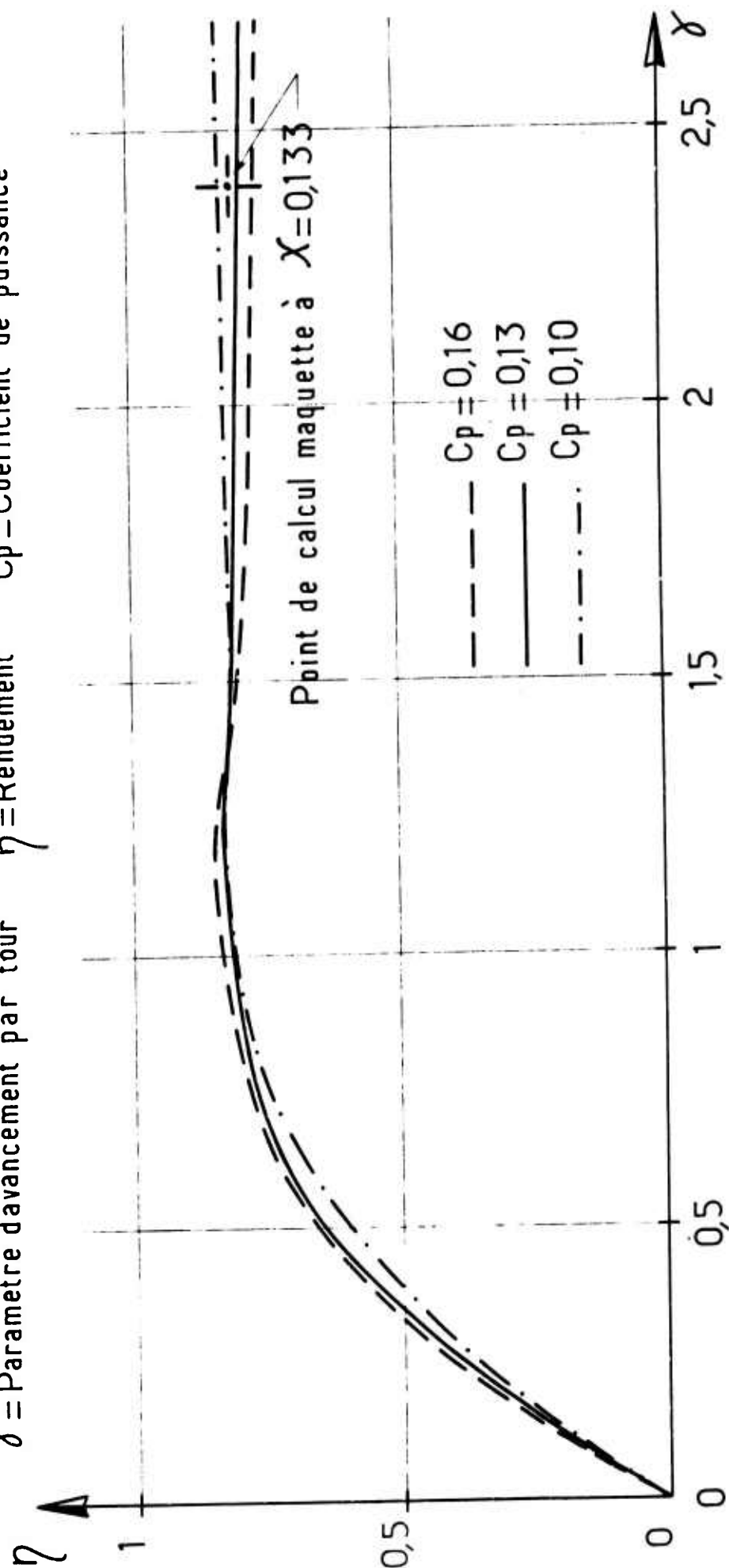
	Performances globales			
	100 Cz	100 Cx	100 Cmq	$a_1^{(o)}$
Essai	0,95	-0,018	0,1275	-10,3
Calcul	0,749	0,0005	0,120	-9,63



Rotor quadripale à double adaptation $\phi = 0,90m$

Essais en translation à S_2 de Saint-Cyr Rendement à $C_p = \text{Constante}$

χ = Paramètre d'avancement par tour η = Rendement C_p = Coefficient de puissance



Rotor quadripale à double adaptation $\phi = 0,90\text{m}$

Essais au point fixe à Chalais-Meudon

Coefficient de puissance $C_p = \frac{W}{\rho n^3 D^5}$

Chiffre de mérite $F_m = 0,798 \frac{C_p^{3/2}}{C_p}$

$\theta = \text{Calage à } 0,7 R$

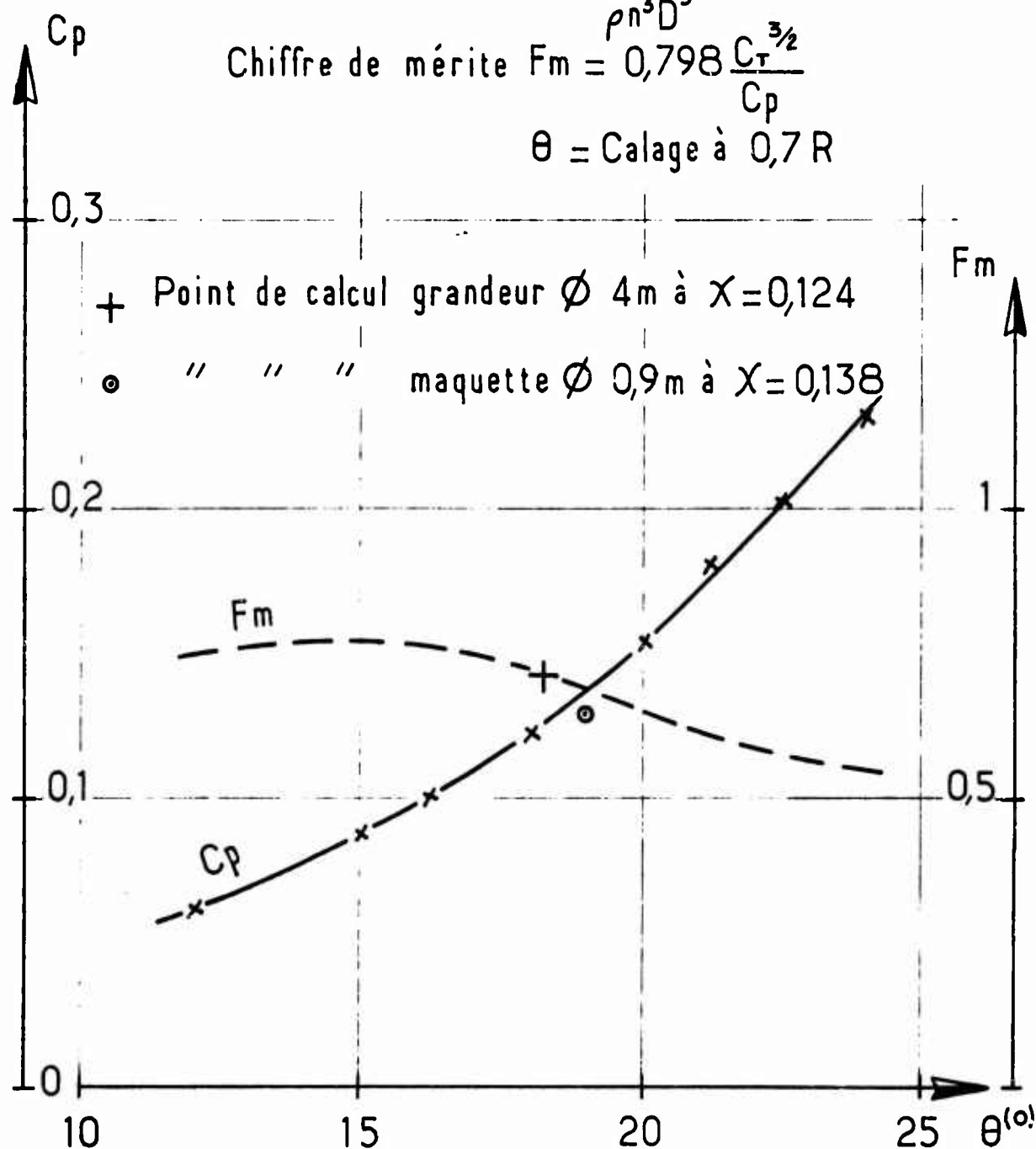
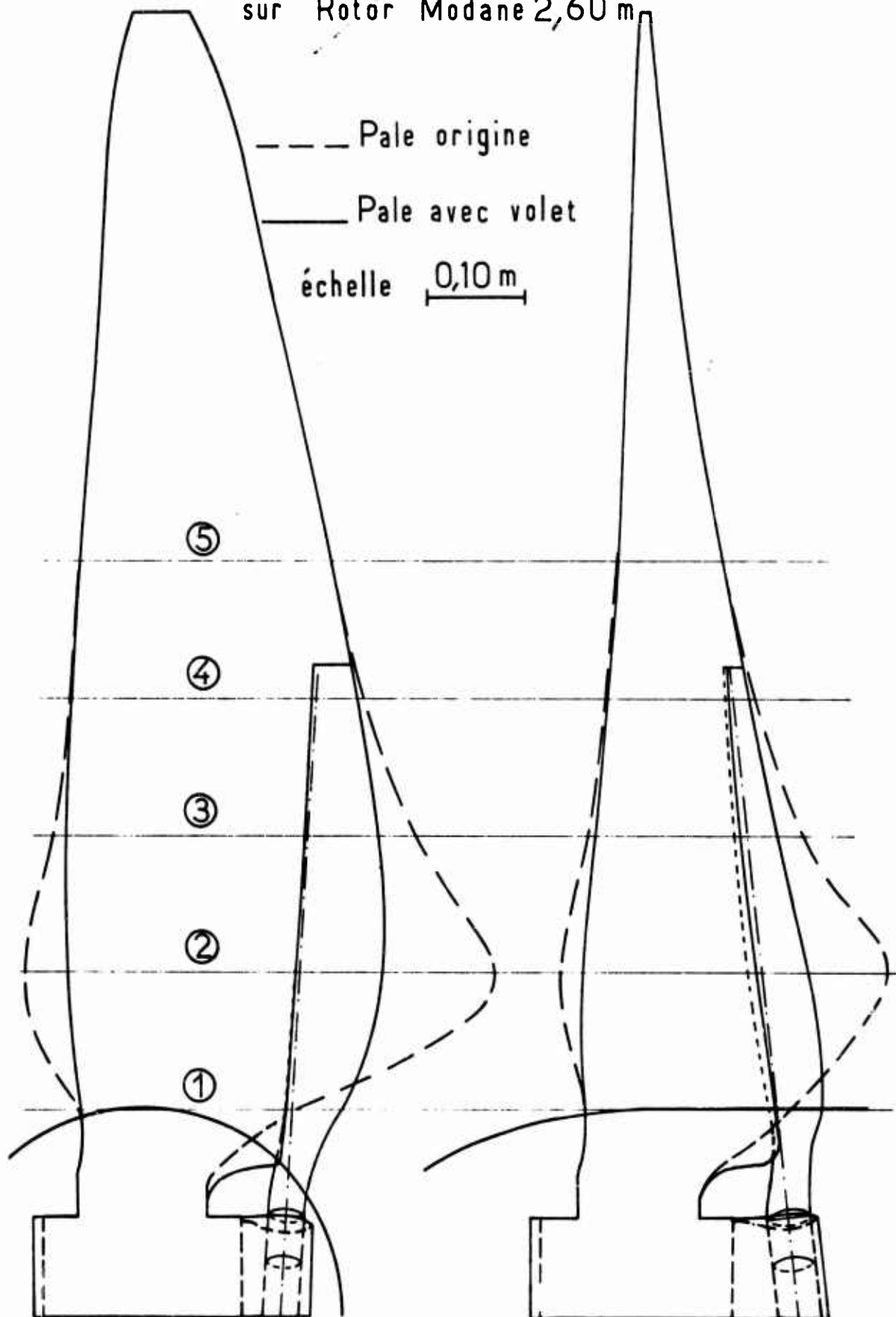
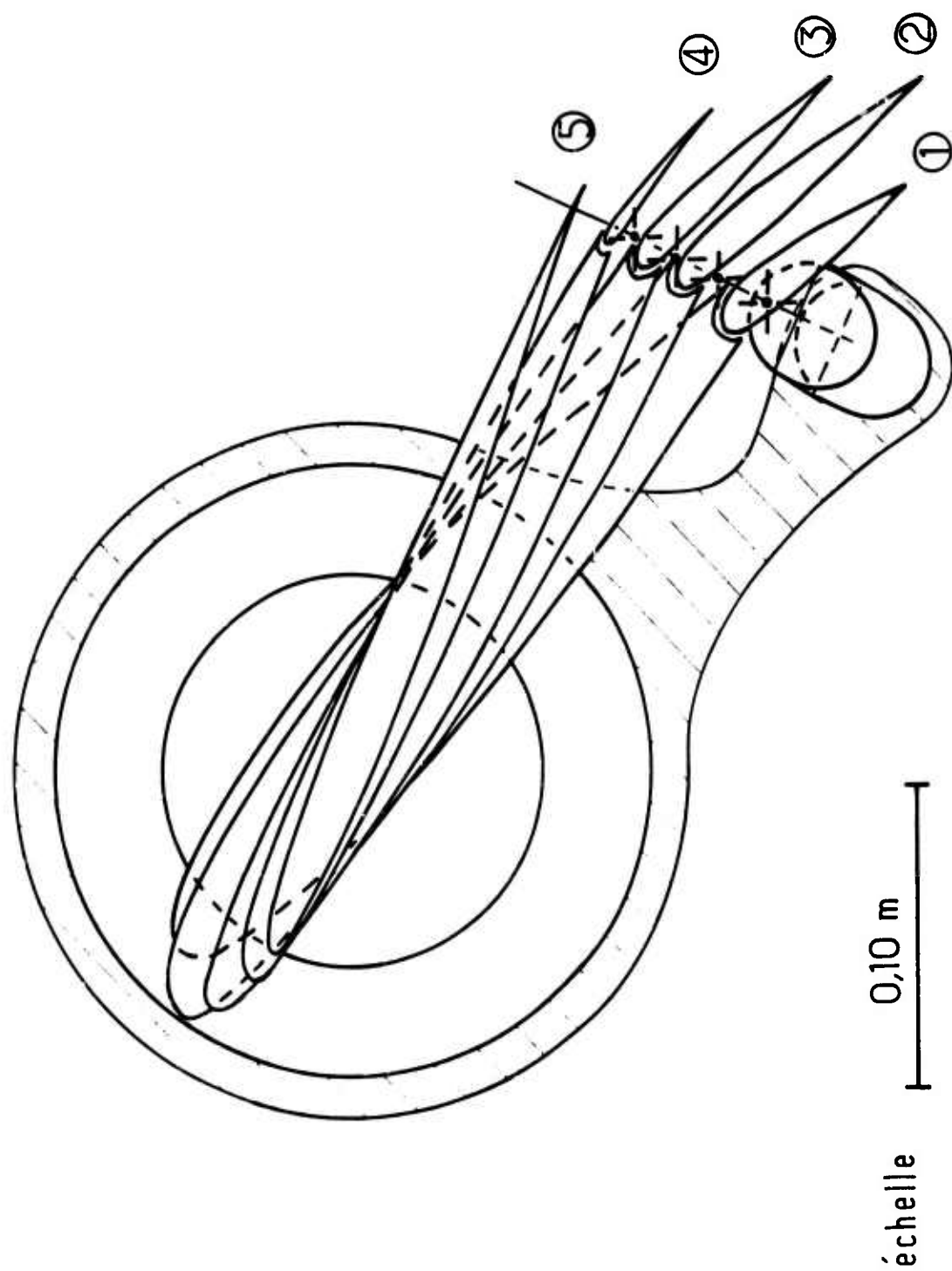


Schéma de principe d'un volet
sur Rotor Modane 2,60 m



Hélicographie rotor Modane 2,60m avec volet



COMPORTEMENT D'UN ROTOR AU-DELA DU DOMAINE DE VOL USUEL A LA GRANDE SOUFFLERIE DE MODANE

par

Michel Lecarme
Ingénieur de recherche à l'AEROSPATIALE
Division Hélicoptères
13221 Marseille Cedex 1
France

RESUME

Un rotor expérimental de 4,150 mètres de diamètre a fait l'objet de plusieurs campagnes d'essais à la Grande Soufflerie de l'ONERA à Modane. La raideur des pales et la puissance des moyens expérimentaux de la Soufflerie nous ont permis d'effectuer de nombreuses mesures et visualisations dans des configurations sévères et à des vitesses périphériques élevées.

Au cours de l'exploration des domaines d'essais de nos divers jeux de pales, nous sommes allés jusqu'au paramètre d'avancement 0,87 ; le décrochage de la pale reculante a été étudié pour de nombreuses valeurs des paramètres d'affichage : vitesse du vent, vitesse périphérique, inclinaison de l'arbre et pas général ; le moyeu actuel ne comporte pas de commande cyclique du pas.

Les limites d'utilisation d'un rotor conventionnel en paramètre d'avancement ont été précisées ; le développement du décrochage de la pale reculante est influencé par le cercle d'inversion et les interactions tourbillonnaires ; ce décrochage produit des perturbations d'autant plus importantes que le paramètre d'avancement est plus faible.

SUMMARY

Several series of tests have been performed on a 4.150 meter diameter experimental rotor in the ONERA large wind tunnel at Modane. The blades stiffness and available power of test equipment in this wind tunnel made a number of measurements and visualisations possible in somme severe configurations and at high tip speeds.

During the exploration of the test envelopes for our various sets of blades, a tip speed ratio of .87 was reached ; the retreating blade stall was studied at several values of pre-set parameters, such as : wind speed, rotor tip speed, rotor shaft tilt, and collective pitch. The present rotor head is not provided with cyclic pitch control.

Operating limits for a conventional rotor were determined in terms of tip speed ratio ; development of retreating blade stall is affected by the reverse flow area and vortex inter-actions ; this stall produces disturbances which increase as the tip speed ratio decreases.

NOTATIONS

R	Rayon du rotor (mètres)
r	Distance de l'axe du rotor d'un point de la pale (mètres)
\bar{r}	Distance relative = r/R
C	Corde d'une pale (mètre)
σ	Plénitude du rotor = $3 C/\pi R$ (rotor tripale)
V	Vitesse du vent (mètres/seconde)
v	Vitesse locale (mètres/seconde)
ω	Vitesse angulaire du rotor (radians/seconde)
U	Vitesse périphérique = ωR (mètres/seconde)
Λ	Paramètre d'avancement = V/U
α_Q	Inclinaison de l'arbre moteur par rapport à la verticale (degrés) positive vers l'aval
α_D	Incidence du rotor = inclinaison du plan décrit par les extrémités des pales par rapport à un plan horizontal (degrés), positive en cabré ; cet angle est défini dans l'approximation du premier harmonique de l'angle de battement
j	Angle d'attaque oblique (degrés), positif vers l'extérieur
ψ	Angle d'azimut de la pale (degrés), origine en position extrême aval ; le sens de rotation est le sens horloge vu de dessus
β	Angle de battement d'une pale (degrés) positif vers le haut
	$\beta = \alpha_0 - a_1 \cos \psi - b_1 \sin \psi - a_2 \cos 2\psi - b_2 \sin 2\psi$ etc...
a_1	Basculement longitudinal du rotor (degrés) $\alpha_D = \alpha_Q + a_1$
θ	Pas d'une pale à $\bar{r} = 0,75$ degrés
M	Nombre de Mach local
	Nombre de Mach en extrémité de pale avançante
ρ	Masse volumique de l'air (Kilog/mètre cube)
S	Surface balayée par le rotor (mètres ²) = πR^2
X	Traction ou traînée du rotor (Newtons), positive en traînée, dans le trièdre vent
Z	Portance du rotor (Newtons) dans le trièdre vent
\bar{X}	Abbréviation pour $100 f_x/\sigma = 100 X/1/2 \rho S U^2$
\bar{Z}	Abbréviation pour $100 f_z/\sigma = 100 Z/1/2 \rho S U^2$
	N.B. Notations de certains auteurs américains :
	$CXR/\sigma = -\bar{X}/200$ $CLR/\sigma = \bar{Z}/200$
p_0	Pression statique dans la veine (Pascals)
p	Pression statique locale (Pascals)
Δp	Pression différentielle locale = p intrados - p extrados au même pourcentage de corde (Pascals)

$\Delta p/p_0$	Pression différentielle relative
P_m	Charge aérodynamique locale sans dimension, intégration le long de la corde $\int_0^1 \frac{\Delta p}{P_0} d\left(\frac{x}{c}\right)$
	Rapport des chaleurs spécifiques de l'air (1,40)
C_N	Coefficient de portance normale locale = $2 P_m / \gamma M^2 = 1,43 P_m / M^2$
q	Pression cinétique (Pascals) = $1/2 \rho v^2$
$\Delta p/q$	Coefficient de pression différentielle = $\frac{\Delta p}{P_0} \frac{1}{P_m}$
Q	Pression cinétique maximale (Pascals), en extrémité de pale avançante
M_θ	Moment de battement en une section de la pale (mètres x Newtons)
\bar{M}_θ	Coefficient sans dimension de moment de battement = $M_\theta / \rho \omega^2 CR^4$
M_s	Moment de traînée en une section de la pale (mètres x Newtons)
\bar{M}_s	Coefficient sans dimension de moment de traînée = $M_s / \rho \omega^2 CR^4$
M_t	Moment de torsion en une section de la pale (mètres x Newtons)
\bar{M}_t	Coefficient sans dimension de moment de torsion = $M_t / \rho \omega^2 C^2 R^3$

N.B. Les caractéristiques de performances du rotor sont données moyeu exclus. Les coefficients de moments sont relatifs aux amplitudes (demi crête-à-crête), soit globales soit par harmonique.

1. INTRODUCTION

En 1970 et 1971, nous avons étudié à la Grande Soufflerie de Modane SI MA un rotor expérimental dans un domaine d'essai maximal, s'étendant aussi loin que nous le permettaient les limitations technologiques et vibratoires.

Nous avons effectué un grand nombre de mesures et de visualisations d'écoulement dans des configurations qui se situent au-delà de celles des vols actuels, notamment avec décrochage de la pale reculante et à des paramètres d'avancement très élevés, tout en ayant des vitesses périphériques réalistes.

Le domaine d'essai exploré s'étend du stationnaire jusqu'au paramètre d'avancement 0,87 ; nos moyens d'investigations consistèrent en pesées globales du rotor, mesures des contraintes des pales, mesures de pressions locales sur les pales, visualisations par fumée ou par fils de laine. Quelques configurations ont fait l'objet de mesures acoustiques.

2. MOYENS D'ESSAIS

Les moyens d'essais ont été décrits dans notre communication au 7ème Congrès de l'ICAS, à ROME, en 1970, reproduite dans la revue "l'Aéronautique et l'Astronautique" n° 25 de 1971.

Nous rappellerons que l'installation de la Grande Soufflerie de Modane est surpuissante, nous ne sommes limités ni par la vitesse du vent ni par la puissance disponible au rotor. L'inclinaison de l'arbre peut aller de -95° à $+25^\circ$; en particulier les essais en fonctionnement hélice sont possibles et le cas du stationnaire hors effet de sol peut être étudié avec une procédure ONERA permettant d'éliminer l'influence de la vitesse induite dans la veine par le rotor.

La veine d'expérience a un diamètre de 8 mètres et une longueur de 14 mètres.

Une balance à six composantes et un compteur situés sous le moyeu donnent les caractéristiques de performances du rotor. Un collecteur tournant de 111 pistes transmet à la chaîne de mesure les informations en provenance des pales : jauges de contrainte, angles de battement et de traînée, capteurs de pressions. La conduite des essais fait l'objet de précautions particulières : en dehors des surveillances de routine, 25 informations sont examinées en permanence par deux spécialistes et certaines d'entre elles sont enregistrées durant toutes les rotations.

3. CARACTERISTIQUES DES ROTORS

Les rotors essayés à ce jour sont des rotors tripales complètement articulés, de 4,150 mètres de diamètre ; le vrillage des pales est de quatre degrés par mètre, soit approximativement 8 degrés du centre rotor à l'extrémité des pales.

Le rotor 1 comporte plusieurs jeux de pales ne différant que par leurs équipements et leurs masses ; la corde est constante : 0,210 mètre et la plénitude est égale à 0,09664 ; le profil est le NACA 0012, symétrique.

Le rotor 2 comporte des pales à profil NACA 0012 muni d'une extension cambrée du bord d'attaque, la corde passant à 0,21525 mètre.

Nous n'avons pas cherché à réaliser un rotor semblable à un rotor réel ; nos pales sont denses (nombre de Lock faible) mais les fréquences propres relatives sont analogues à celles des pales élastiques, de sorte que nous avons des comportements vibratoires réalistes mais de faibles amplitudes, circonstance heureuse qui nous permet de tester des configurations très sévères inabordables par un rotor dynamiquement semblable à un rotor réel classique.

Le moyeu actuel ne comporte pas de commande cyclique du pas ; la variation d'incidence du rotor est obtenue par l'inclinaison de l'arbre ; pour simplifier le langage nous appellerons ce type de rotor : "rotor à basculement libre". Dans ces conditions il y a quatre paramètres d'affichage : la vitesse du vent, le régime du rotor, le pas général et l'inclinaison de l'arbre.

La commande cyclique du pas sera introduite en 1973.

4. LES GRANDS PARAMETRES D'AVANCEMENT

L'objectif des essais de 1970 était l'étude d'un rotor de vitesse périphérique usuelle : 200 mètres/seconde ; lorsqu'on augmente le paramètre d'avancement, les troubles transsoniques apparaissent : dégradation des performances et accroissement des vibrations ; dans ces conditions nous n'avons pas pu dépasser le paramètre d'avancement 0,60 ; quelques essais complémentaires à régime variable nous ont appris que l'influence de la compressibilité se faisait sentir à partir d'un nombre de Mach en extrémité de pale avançante 0,85 ; pour étudier en 1971 les grands paramètres d'avancement, nous avons donc diminué

le régime rotor de manière à rester en-dessous du seuil de compressibilité, tout en nous maintenant au-dessus de la limitation technologique inférieure (685 tours/minute, soit une vitesse périphérique 149 mètres/seconde). Nous sommes alors parvenus avec le rotor 1 à $\Lambda = 0,87$ et $U = 152$ m/s, et avec le rotor 2 à $\Lambda = 0,84$ et $U = 156,5$ m/s.

4.1. Réduction du domaine d'essais

Le domaine d'essais diminue régulièrement quand le paramètre d'avancement augmente. La figure 1 montre dans le diagramme portance/pas la grande différence des domaines réalisés avec le rotor 1 pour $\Lambda = 0,30$ et $\Lambda = 0,87$; aux petits pas nous sommes limités par les couples négatifs, un peu au-delà des autorotations, pour des raisons technologiques propres au Banc ; aux pas plus élevés, à $\Lambda = 0,30$, nous sommes limités par les vibrations des pales en traînée ; quand Λ augmente, une nouvelle limitation apparaît : les butées de battement, car le basculement longitudinal croît avec Λ ; d'autre part les vibrations augmentent et contribuent à la réduction du domaine expérimental.

Cette importante réduction du domaine est propre aux rotors à basculement libre ; il est probable qu'elle serait moins spectaculaire avec un rotor à basculement contrôlé par la commande cyclique de pas.

4.2. Pilotage du rotor

L'impression dominante de l'expérimentateur est la difficulté du pilotage du rotor aux grands paramètres d'avancement (au-delà de 0,60) ; indépendamment de l'ambiance vibratoire, qui sera examinée plus loin, cette difficulté provient de la susceptibilité du rotor au pas général (la dérivée $\partial \bar{Z} / \partial \theta$) et de l'espacement des montées en pas à l'inclinaison α_Q constante (la dérivée $\partial \theta / \partial \alpha_Q$), illustrée par la figure 2. Les changements d'inclinaisons α_Q doivent être entrepris avec précaution, avec manoeuvres alternées du pas, et à petits intervalles.

Quant à la susceptibilité au pas, nous pensons qu'un rotor à basculement libre deviendra impilotable vers un paramètre d'avancement égal à 1, car $\partial \bar{Z} / \partial \theta$ sera infini à α_Q constant.

Il est à noter que nos rotors étaient parfaitement stables dans tous les domaines à grands Λ , même en autorotation.

4.3. Performances

L'étude des performances de nos rotors aux grands Λ conduit à envisager deux domaines :

a) Les incidences rotoriques α_D négatives

Il devient de plus en plus difficile d'incliner le rotor vers l'amont (incidence α_D négative), comme le montre la figure 3, à cause de la grande importance du basculement longitudinal (dérivée $\partial z_1 / \partial \alpha_Q$).

La résultante des forces aérodynamiques, à peu près normale au disque aux faibles Λ , s'incline vers l'arrière, de sorte que même si l'on réussit à obtenir une incidence négative, on ne peut pas obtenir de traction valable : figure 4 ; à $\Lambda = 0,60$ le rotor n'est même pas capable de tirer son moyeu (dont le coefficient de traînée croît comme Λ^2).

b) Les incidences rotoriques α_D positives

Le basculement longitudinal a peu d'importance dans ces cas-là ; lorsqu'on représente, selon l'usage, les résultats moyeu exclus, on a la surprise de constater que la polaire d'autorotation est indépendante du paramètre d'avancement ; les lois de pas diffèrent légèrement. L'augmentation de traînée du rotor complet quand Λ croît, pour une portance donnée, est due au moyeu.

4.4. Vibrations des pales

Le comportement vibratoire de nos rotors aux grands Λ présente deux aspects :

- les amplitudes globales des vibrations de battement, traînée, et torsion augmentent considérablement avec Λ , comme le montre la figure 5 ; d'autre part, les vibrations croissant généralement avec la portance, la portance maximale utilisable diminue quand Λ augmente. Les courbes de la figure 5 ont été établies pour une portance faible de manière à ne pas faire intervenir le décrochage de la pale reculante.

- aux Λ modérés les essais sont parfaitement répétitifs, les raies non harmoniques faibles et rares, l'analyse de Fourier sur une période est valable ; aux grands Λ il n'en est plus de même, en particulier le rotor devient davantage susceptible aux résonances, et les harmoniques de rang supérieur à 4 ont une grande part d'aléatoire.

Nous donnons à titre d'exemples figures 6, 7 et 8 quelques analyses de Fourier sur une période ; nous ne pouvions pas effectuer des analyses sur un grand nombre de périodes, notamment des analyses spectrales habituellement faites sur des enregistrements de trois minutes, car nous étions constamment en conditions endommageantes, nous avions un grand nombre de points de mesures à faire dont la durée devait être minimale.

4.5. Écoulements sur la pale reculante

Les paramètres d'avancement élevés sont le domaine de l'attaque oblique, dont l'influence est importante dans la détermination théorique des performances et l'apparition du décrochage.

La figure 9 montre la différence des zones à forte attaque oblique entre $\Lambda 0,30$ et $\Lambda 0,70$. On peut séparer les effets de l'attaque oblique sur les écoulements en deux zones : la zone éloignée du cercle d'inversion et la zone proche de ce cercle. Loin du cercle d'inversion, il est bien connu que l'attaque oblique retarde le décrochage ; dans nos essais du rotor 1 équipé de prises de pression nous avons pu constater que le décrochage apparaît vers $C_N 1,2$ pour $\Lambda 0,30$ tandis qu'il faut monter à $C_N 1,7$ pour $\Lambda 0,60$. Mais dès que l'on s'approche du cercle d'inversion la situation est changée.

L'examen des résultats des prises de pression du rotor 1 et des visualisations d'écoulements sur le rotor 2 nous a montré que les perturbations en pale reculante près du cercle d'inversion apparaissent à des charges de plus en plus faibles quand le paramètre d'avancement augmente, et dès la portance nulle au-delà de $\Lambda 0,60$; dans le cas où nous avons la portance locale nous avons pu constater des perturbations analogues à celles d'un décrochage pour des portances locales faibles, et ces perturbations sont situées au voisinage du cercle d'inversion ; dans ces conditions la rotation du vecteur vitesse locale pour un point lié à la pale est très rapide et produit d'importants cisaillements dans la couche limite générateurs de turbulence. Lorsque les portances locales augmentent par accroissement du pas ces perturbations amorcent le décrochage proprement dit et il n'est pas possible de séparer les phénomènes ni de dire à partir de quelle valeur du pas le décrochage commence ; pour simplifier le langage nous dirons simplement qu'à partir de $\Lambda 0,50$ le rotor est toujours décroché, plus ou moins suivant sa charge ; nous examinerons plus loin si ce phénomène est important ou non.

Pour illustrer ce fait nous donnons figure 11 un schéma de l'écoulement dans la configuration suivante : $\Lambda 0,77$ $\alpha_0 - 8^\circ$ $\theta 6^\circ$, portance du rotor nulle (rotor 2) ; les symboles de visualisations sont expliqués figure 10 ; il y a deux zones de perturbations : l'entrée dans le cercle d'inversion et la zone intérieure aval soumise au sillage du moyeu ; dans une partie de la sortie du cercle d'inversion les fils sont centrifugés, indice d'une couche limite épaisse dont l'énergie turbulente est insuffisante pour agiter les fils.

Les visualisations par fils sont obtenues de la façon suivante : une tourelle mobile située à la partie supérieure de la veine comporte un appareil de photo et des lampes stroboscopiques dont le champ est dirigé par télécommande vers la position de la pale en azimut que l'on désire ; pour une position en azimut l'obturateur de l'appareil photo est ouvert pendant cinq éclairs successifs, déclenchés par l'azimut choisi, de sorte que l'on est renseigné sur l'agitation des fils ; ceux-ci sont collés en un point sur l'extrados d'une pale en deux lignes : 25 % et 60 % des cordes.

L'examen des visualisations par fils montre que la première partie de la pale reculante est plus perturbée que la deuxième partie ; nous pensons que ce fait est dû à deux causes :

- l'amont du disque est plus chargé que l'aval, phénomène particulier aux rotors à basculement libre et à faible nombre de Lock
- l'angle de la force centrifuge et du vecteur vitesse locale est plus grand en début de pale reculante qu'en fin de pale reculante, de sorte qu'avant l'azimut 270° le fil est attaqué de travers par le vent local, ce qui peut provoquer une turbulence dans la couche limite.

5. LE DECROCHAGE

Le décrochage des pales d'un rotor n'est pas un problème simple ; entre l'écoulement sain à faible sillage et le décrochage du type courant plan à grand sillage turbulent il existe des états intermédiaires difficiles à classer, compliqués par l'apparition de phénomènes tridimensionnels instationnaires. Certains troubles de comportement, tels que l'augmentation des vibrations de torsion qui accompagne souvent le décrochage, peuvent se manifester dans d'autres circonstances, ou bien ne pas avoir lieu alors que l'on constate par ailleurs que le décrochage existe ; nous verrons plus loin que l'importance d'une perturbation d'écoulement est essentiellement liée à la valeur de la pression cinétique locale.

5.1. Influence du décrochage sur les performances

La portance et la traction (ou la traînée) du rotor sont très peu influencées par le décrochage de la pale reculante ; par contre le couple moteur augmente, surtout aux incidences faibles du rotor, positives ou négatives. Il ne faut pas en conclure que nous ayons là un critère simple de décrochage, car chaque fois que ce décrochage a pu être localisé en pas nous avons constaté que la divergence du couple commençait plus tôt, d'une part à cause de l'augmentation de la traînée de profil en pale reculante d'autre part à cause de la divergence de traînée transsonique en fin de pale avançante, comme nous l'ont montré nos analyses de pressions locales. Ainsi au point fixe, le chiffre de mérite chute plusieurs degrés avant le début de décrochage, à la vitesse périphérique de 200 mètres par seconde, le dernier quart de la pale étant en fonctionnement supercritique.

Nous avons obtenu une manifestation spectaculaire de l'augmentation du couple avec le décrochage dans des conditions incompressibles avec un rotor de 1,5 mètre de diamètre à la Soufflerie de MARGNANE : au cours d'une mesure en autorotation à forte portance, chute brutale du régime et augmentation non moins brutale du basculement longitudinal ; il a fallu injecter immédiatement de la puissance au rotor. C'est pourquoi les essais d'autorotation à forte portance sont délicats.

5.2. Les pressions locales

Une version du rotor 1 était équipée de capteurs de pression différentielle et de pression absolue ; les résultats les plus intéressants et les plus fiables proviennent des capteurs de pression différentielle, répartis en quatre cordes.

Les enregistrements sur bande magnétique sont numérisés cent fois par tour, moyennés sur trois tours et mis sous la forme $\Delta p/p_0$; puis les charges locales P_m sont calculées pour chaque corde, le nombre de Mach local de référence $M = \frac{1}{\sqrt{\gamma}} (RU + V \sin \psi)$ où a est la vitesse du son dans la veine, et le coefficient de force normale $a C_N = 1,43 P_m/M^2$. L'étude des pressions locales est grandement facilitée par l'utilisation du coefficient de pression $\Delta p/q C_N$ que l'on calcule par la formule $\Delta p/q C_N = \frac{\Delta p}{p_0} \frac{1}{P_m}$, qui a l'avantage de ne faire intervenir aucune hypothèse sur les vitesses locales. En incompressible non décroché les répartitions des coefficients de pression le long de la corde se réduisent à une courbe unique qui nous sert de référence ; parallèlement à nos essais de rotors, les profils utilisés étaient testés à la Soufflerie S3 MA en courant plan dans les mêmes conditions de nombres de Mach et de nombres de Reynolds, de sorte que nous avons pu comparer les résultats en rotor tournant et en courant plan ; la plupart des désaccords ont pu être identifiés et expliqués.

Les pales munies de capteurs de pression avaient un équipement très sommaire en capteurs de contrainte, de sorte que nous avons limité leur utilisation au paramètre d'avancement 0,60, les paramètres d'avancement plus élevés conduisant à des problèmes vibratoires délicats. Jusqu'à $\Lambda = 0,60$ les phénomènes sont stables et répétitifs à deux exceptions près : le point fixe où se déclenche brusquement un flottement de torsion, et les inclinaisons très grandes de l'arbre vers l'amont où les vibrations divergent si l'on persiste dans le décrochage.

Les répartitions des pressions en corde qu'il est possible de tracer sont trop nombreuses, de sorte que nous avons utilisé un critère simple pour caractériser l'évolution des zones de décrochage en fonction des paramètres d'essais : la chute des coefficients $\Delta p/q C_N$ au voisinage du bord d'attaque, à 2,5 % et 6 % de la corde, car c'est à partir du bord d'attaque que le décrochage se développe. Nous donnons cette évolution figure 12 pour six cas, qui méritent quelques commentaires ; les tracés ne sont pas lissés ; des droites joignent les points de calcul (100 par tour) :

a) $\Lambda 0,30 \quad \alpha_Q - 8^\circ$

$\theta 7,8^\circ$: pas de décrochage, mais importante manifestation d'une interaction tourbillonnaire dont l'emplacement théorique est noté IT sur l'axe des azimuts. Les lignes pointillées sont les valeurs de $\Delta p/q C_N$ en incompressible non décroché.

$\theta 10,4^\circ$: décrochage sur la plus grande partie de la pale reculante ; la brusque remontée de $\Delta p/q C_N$ dans l'interaction tourbillonnaire est accompagnée d'une baisse importante du coefficient de portance.

b) $\Lambda 0,30 \quad \alpha_Q - 24^\circ$

L'interaction tourbillonnaire a disparu, l'inclinaison de l'arbre éloignant les tourbillons marginaux des pales ; au pas de 15° il n'y a pas de décrochage (il y a peut être une bulle de décrochage à 2,5 % pour l'azimut 280°) ; $\Delta p/q C_N$ à 2,5 % est plus élevé en pale amont parce que dans ce cas le profil est en configuration supercritique au voisinage de son C_N maximal ; le décrochage est nettement établi au pas de $16,5^\circ$.

Dans tout le domaine compris entre $\Lambda 0$ et $\Lambda 0,40$ l'apparition du décrochage (en montant le pas) est brutale, tout au moins pour le rotor 1.

c) $\Lambda 0,50 \quad \alpha_Q - 8^\circ$

Pour ce paramètre d'avancement il n'y a pas d'interaction tourbillonnaire possible en pale reculante ; les perturbations au voisinage de l'azimut 360° sont dues au sillage du moyeu, dont l'importance croît avec le paramètre d'avancement ; le décrochage est progressif à cause de l'influence du cercle d'inversion.

Nous donnons figures 13 et 14 quelques courbes de répartitions en corde ; les tracés n'ont pas la prétention d'être rigoureux car ils sont basés sur six capteurs, situés à 2,5 % 6 % 26 % 40 % 60 % et 80 %. Pour $\Lambda 0,50$ on voit nettement le déplacement de l'amont vers l'aval des bosses de pressions différentielles produites par le déplacement des tourbillons issus du bord d'attaque, caractéristique du décrochage instationnaire ; on voit aussi les valeurs élevées des coefficients de portance dues à la fois à l'attaque oblique et au caractère instationnaire de l'écoulement. Lorsque les Mach locaux sont faibles les valeurs des C_N ne sont pas précisées, un calcul simple d'erreur montrant qu'il n'est pas possible de le faire ; on peut cependant affirmer qu'elles sont très supérieures à celles du courant plan stationnaire.

Sur la figure 14 nous avons montré par un schéma qu'une interaction tourbillonnaire en fin de pale reculante vient compliquer les écoulements, relayée peu après le sillage du moyeu.

Tous les essais du rotor 1 muni de prises de pression ont été effectués à la vitesse périphérique 200 mètres par seconde ; au paramètre d'avancement 0,60 nous avions un nombre de Mach en extrémité de pale avançante égal à 0,96, avec une ambiance vibratoire et une ambiance sonore très élevées. Il est probable que nous avions également des décrochages derrière les chocs en pale avançante, mais nous manquons d'informations à ce sujet.

5.3. Influence du décrochage sur les vibrations des pales

Le comportement vibratoire d'un rotor décroché dépend essentiellement du paramètre d'avancement (pour un vrillage donné). On peut énoncer comme loi générale que le décrochage est d'autant plus dangereux que le paramètre d'avancement est plus faible ; le cas le plus critique que nous ayons rencontré est le point fixe, où le décrochage a déclenché brusquement un flottement de torsion accompagné d'un violent bruit de tambour ; pour notre rotor (le rotor 1) le décrochage est apparu vers $R 0,80$ dans les conditions locales du courant plan stationnaire, le caractère instationnaire du phénomène ne se manifestant qu'une fois les vibrations de torsion déclenchées, à la fréquence propre des pales ($4,5\omega$).

Aux faibles paramètres d'avancement jusque vers $0,50$, le décrochage se manifeste essentiellement par une augmentation plus ou moins brutale des vibrations de torsion en fréquences harmoniques du régime, notamment de rangs 1, 2, 4 et 5 ; une augmentation des vibrations de traînée apparaît souvent mais ce n'est pas une règle générale. Le rotor 1 décroche brutalement ; en même temps, comme nous l'ont montré des visualisations par fils, les vibrations de torsion augmentent brusquement. Le comportement du rotor 2, à bord d'attaque cambré, est plus compliqué ; aux faibles inclinaisons de l'arbre le décrochage est progressif et l'évolution des vibrations de torsion n'est pas simple ; aux grandes inclinaisons de l'arbre vers l'amont on retrouve le comportement du rotor 1 avec un décrochage se produisant à de plus grandes portances à cause de la cambrure.

Lorsqu'on augmente le paramètre d'avancement le décrochage devient de plus en plus progressif pour nos deux rotors ; nous attribuons ce fait au développement du cercle d'inversion et aux cisaillements de la couche limite qui l'accompagnent. D'autre part l'influence du décrochage sur les vibrations diminue jusqu'à disparaître, pour les raisons suivantes :

- l'ambiance vibratoire augmente avec le paramètre d'avancement, dès la portance nulle
- les pressions cinétiques diminuent en pale reculante
- les limites vibratoires ne nous permettent pas de pousser le décrochage jusqu'à ce qu'il rencontre des zones à fortes pressions cinétiques.

Nous donnons figure 15 trois exemples caractéristiques du comportement du rotor 2 :

- a) $\Lambda 0,30 \quad \alpha_Q - 8^\circ$; au pas de 8° quelques troubles d'écoulement apparaissent à 40% du rayon par interaction tourbillonnaire en fin de pale avançante ; au pas de $10,5^\circ$ ces troubles déclenchent un décrochage local en début de pale avançante ; les vibrations de torsion augmentent ; un nouveau phénomène apparaît, de légères perturbations en fin de pale reculante par interaction tourbillonnaire. Au pas de 12° les vibrations de torsion diminuent, pour une cause inconnue, puis augmentent brusquement ; au pas de 13° le décrochage est bien établi et occupe une zone très importante de la pale reculante, comme le montre la figure 16.
- b) $\Lambda 0,68 \quad \alpha_Q - 8^\circ$; au pas de 6° la portance est pratiquement nulle ; malgré la faible valeur du nombre de Mach en extrémité de pale avançante ($0,78$) les vibrations sont fortes ; les écoulements ne sont perturbés qu'à l'entrée dans le cercle d'inversion. Quand on augmente le pas, ces perturbations s'étendent lentement dans la première moitié de la pale reculante, mais au pas de 8° des troubles sérieux d'interaction tourbillonnaire apparaissent en fin de pale reculante dans une zone où les pressions cinétiques commencent à être notables, et c'est peut être là la cause de l'augmentation des vibrations de traînée, tandis que les vibrations de torsion plutôt sensibles au décrochage proprement dit augmentent peu. Au pas final de 10° le décrochage est important mais à l'intérieur d'une zone de faibles pressions cinétiques ; les limitations de vibrations de battement et de traînée nous empêchent d'augmenter davantage le pas.
- c) $\Lambda 0,40 \quad \alpha_Q 0^\circ$; c'est le seul cas que nous ayons rencontré où le décrochage à faible Λ est accompagné d'une augmentation faible des vibrations de torsion ; nous franchissons là deux autorotations l'une à $\theta 4^\circ$, l'autre à $\theta 6,5^\circ$ après la divergence du couple moteur.

On sait que dans les autorotations les charges aérodynamiques sont déplacées vers le centre du rotor par rapport aux configurations usuelles ; il en résulte des troubles d'écoulement prématurés dans cette zone mais de peu d'importance au point de vue vibratoire ; c'est nettement l'interaction tourbillonnaire de fin de pale avançante qui déclenche ces troubles ; le décrochage proprement dit n'apparaît que vers $\theta 7^\circ$, où les vibrations de traînée croissent très rapidement ; pour cette valeur du paramètre d'avancement, l'interaction tourbillonnaire de fin de pale reculante est réduite à une zone minuscule.

Les interactions tourbillonnaires jouent un rôle important mais seulement dans les cas où elles sont possibles, c'est-à-dire aux faibles incidences du disque. Aux fortes incidences positives ou négatives les trajectoires des tourbillons marginaux sont trop éloignées des pales pour que les vitesses induites par ces tourbillons soient notables.

Les conséquences des perturbations de la pale reculante ne se manifestent que pour des pressions cinétiques relatives q/Q supérieures à $0,2$; la figure 17 montre leurs répartitions pour $\Lambda 0,30$ et $\Lambda 0,70$; aux très grands Λ les troubles en milieu de pale reculante ont peu d'importance.

Pour terminer nous donnons figure 18 deux exemples de photographies de pale munie de fils, choisies parmi les 850 photographies exploitables que nous avons obtenues. La direction des fils est un équilibre entre l'influence du vent local et celle de la force centrifuge. La photographie supérieure montre, de l'intérieur vers l'extérieur, une petite zone saine, une zone décrochée sur un tiers de rayon environ, avec des courants de retour dans la couche limite, puis une zone saine jusqu'à l'extrémité. La photographie inférieure a la particularité assez rare de montrer un écoulement inverse sain sur la majeure partie du cercle d'inversion ; la zone de décrochage proprement dite avec courants de retour s'étend presque jusqu'à l'extrémité de la pale ; une grande partie du bord de fuite comporte une couche limite épaisse de faible énergie turbulente, les fils sont centrifugés.

6. CONCLUSION

La Grande Soufflerie de Modane permet d'effectuer des essais de rotors dans des conditions très sévères, limitées seulement dans la plupart des cas par la tenue des pales en fatigue ; notamment il est possible de faire des mesures à des paramètres d'avancement très élevés tout en ayant des vitesses périphériques réalistes.

Il est possible d'utiliser des rotors classiques à des paramètres d'avancement très élevés à condition de ne pas leur demander des efforts de traction, de maîtriser les problèmes vibratoires, et de diminuer la traînée des moyeux.

L'étude du décrochage de la pale reculante n'est pas simple, de nombreux paramètres intervenant et des phénomènes annexes apportant leurs propres perturbations. D'une manière générale on peut dire que les conséquences du décrochage sont d'autant plus graves que le paramètre d'avancement est plus petit. Aux paramètres d'avancement très élevés la pale reculante est toujours le siège de perturbations d'écoulement, qui ont une faible importance tant que les pressions cinétiques sont faibles.

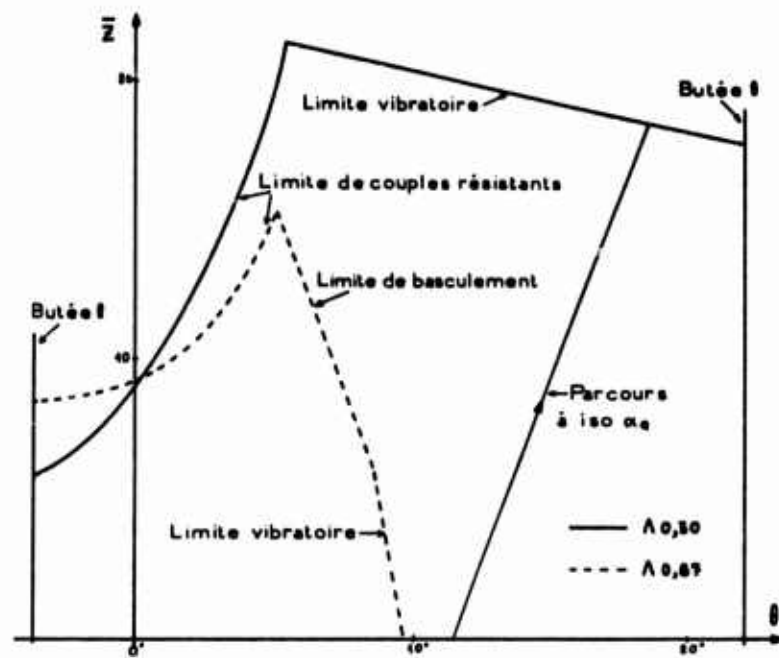


Fig. 1 DOMAINE DES ESSAIS, ROTOR 1 TEST RANGE, ROTOR N°1

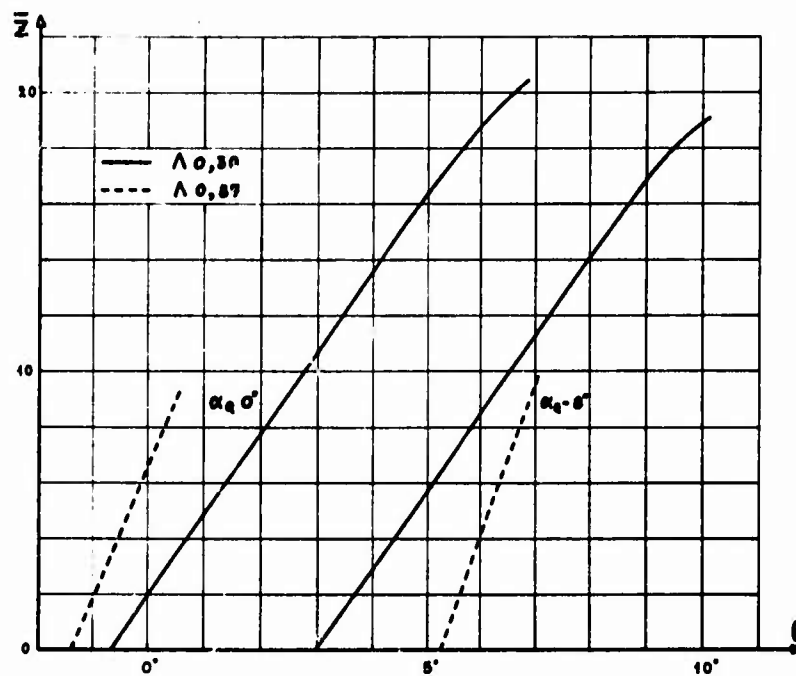


Fig. 2 INFLUENCE DU PAS PITCH INFLUENCE ON PERFORMANCES

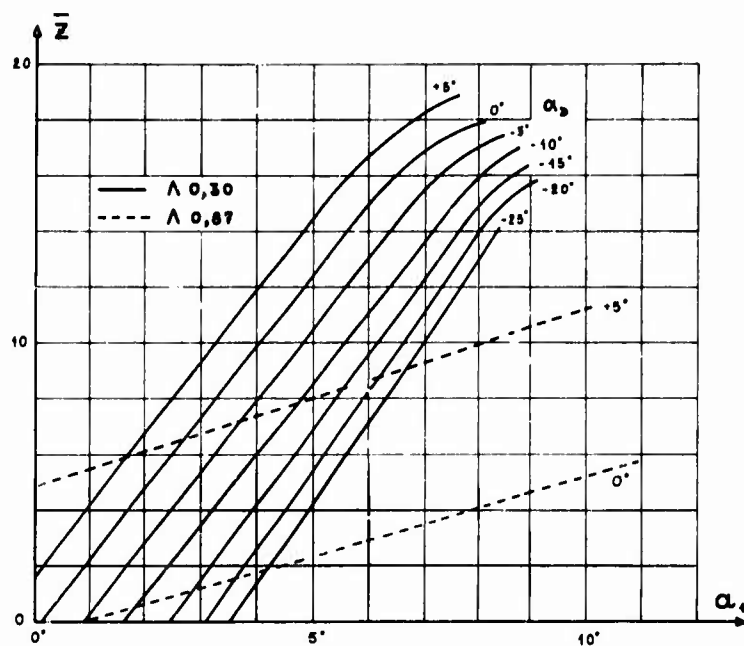


Fig.3 BASCULEMENTS ET INCIDENCES TIP PATH PLANE TILT AND ANGLE OF ATTACK

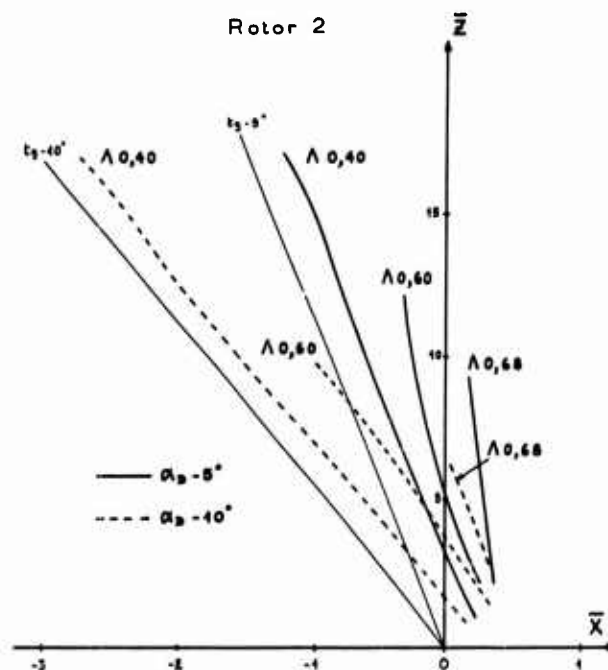


Fig.4 INFLUENCE DE Λ SUR LES TRACTIONS THRUST/ADVANCE RATIO

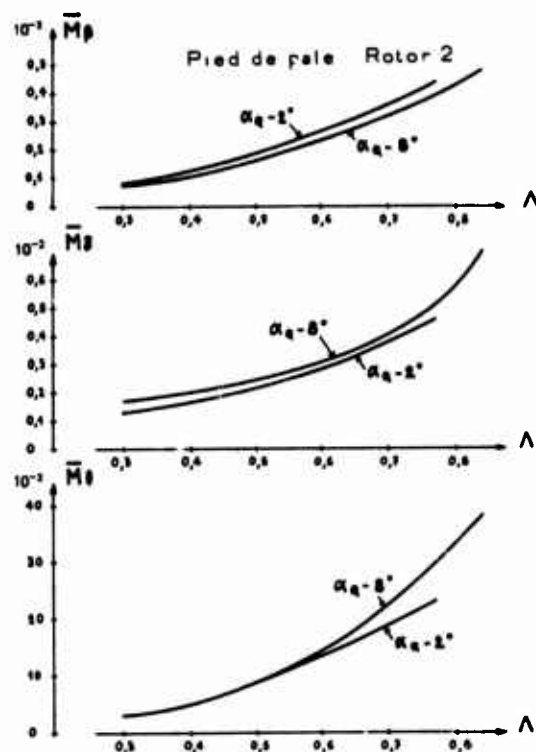


Fig. 5 INFLUENCE DE Λ SUR LES VIBRATIONS
VIBRATIONS/ADVANCE RATIO

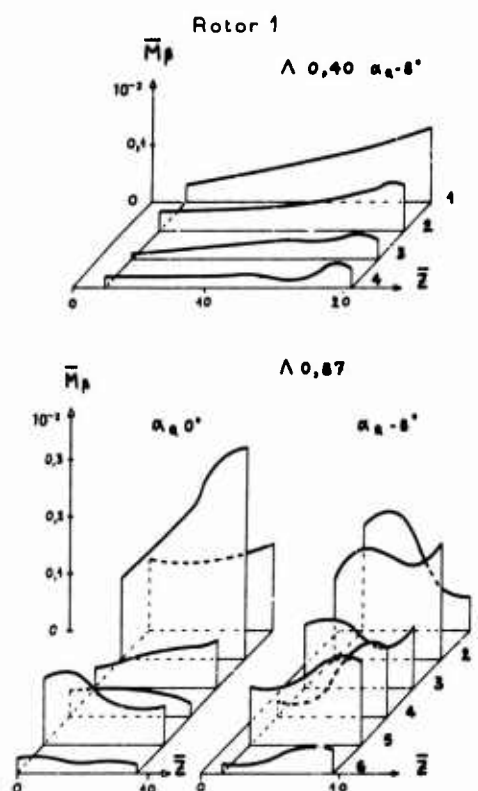


Fig. 6 HARMONICS DE BATTEMENT, ROTOR 1
FLAPWISE BENDING MOMENTS-FOURIER ANALYSIS

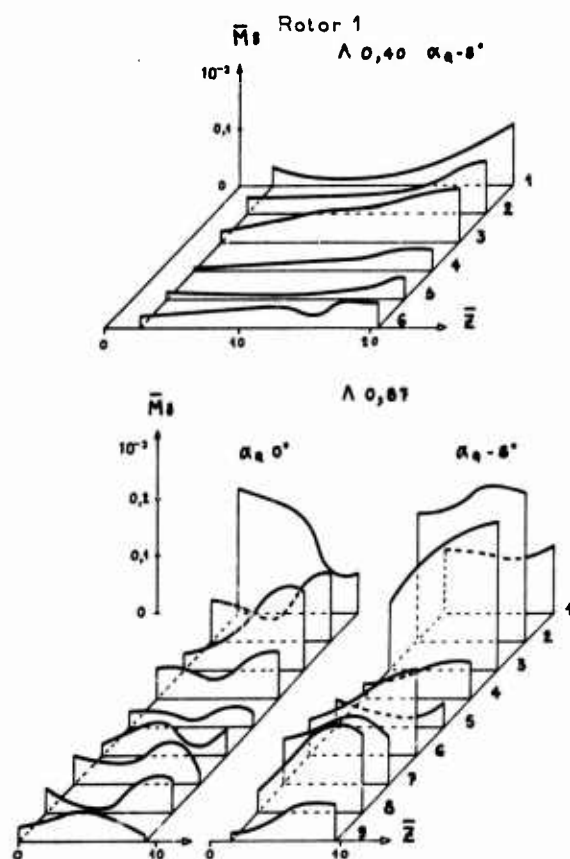


Fig. 7 HARMONICS DE TRAINÉE
CHORDWISE BENDING MOMENTS-FOURIER ANALYSIS

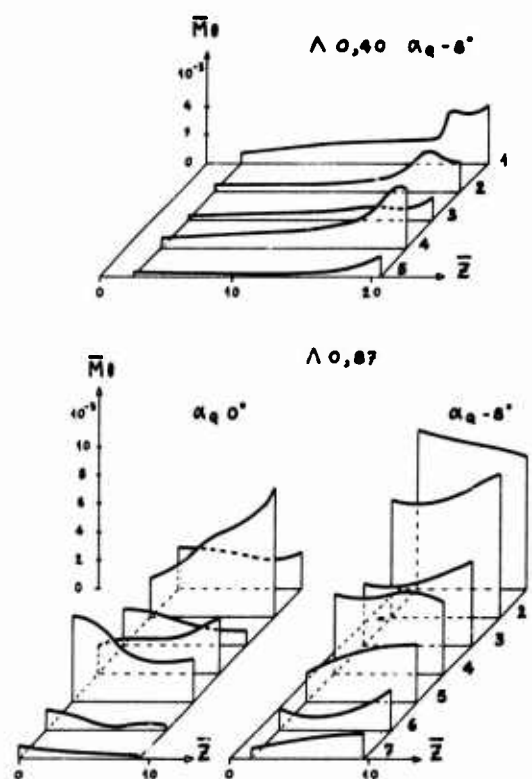


Fig. 8 HARMONICS DE TORSION
TORSIONAL MOMENTS-FOURIER ANALYSIS

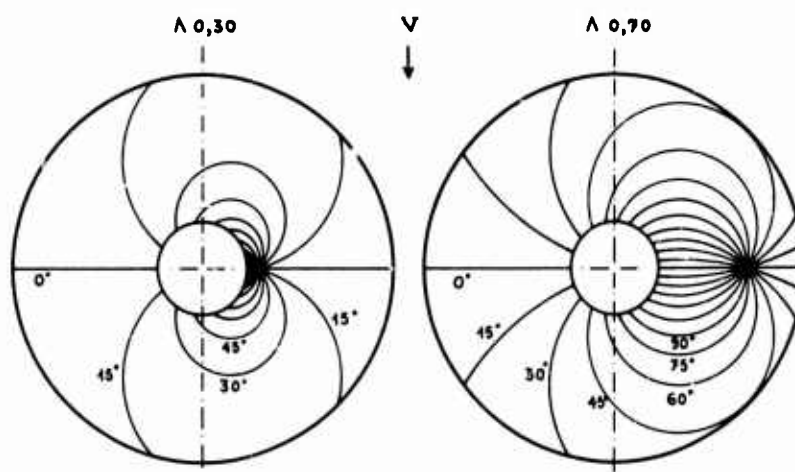


Fig.9 ATTAQUE OBLIQUE PATTERN OF EQUAL AIRFLOW YAWING ANGLES

- $\alpha_e - 8^\circ$ 86° ψ_{180° Rotor 2
- ✦ Fil stable
 - ✦ Fil légèrement agité
 - ✦ Fil très agité
 - ✦ Fil très agité sans position moyenne
 - ✦ Fil aval de direction très différente de celle du fil amont qui seule est représentée
 - ✦ " "
 - ✦ " "

Fig.10 SYMBOLES DE VISUALISATIONS
AIRFLOW VISUALIZATIONS-NOTATIONS

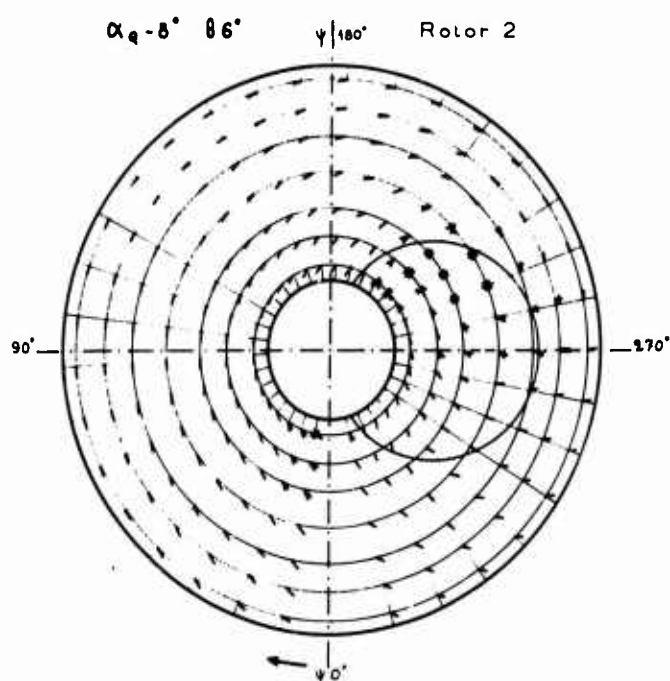


Fig.11 VISUALISATION Λ 0,77
VISUALIZATION-ADVANCE RATIO .77

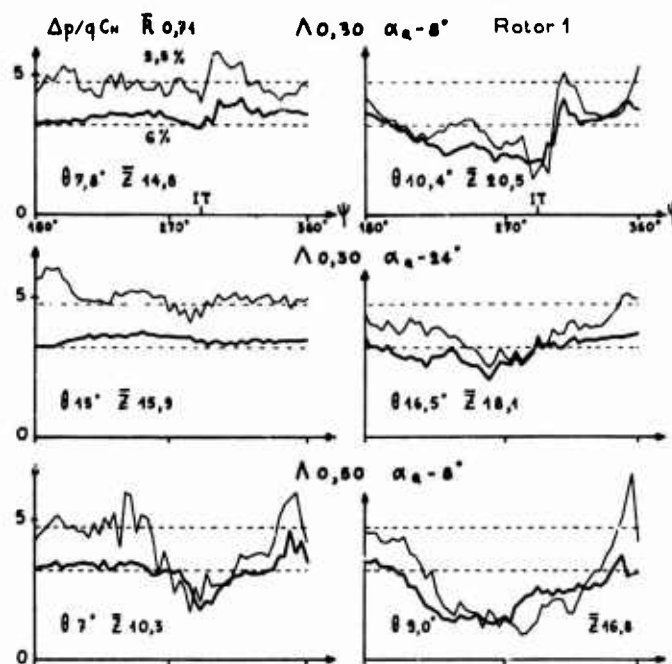


Fig.12 COEFFICIENT DE PRESSION EN PALE RECLANTE
PRESSURE COEFFICIENT ON RETREATING BLADE

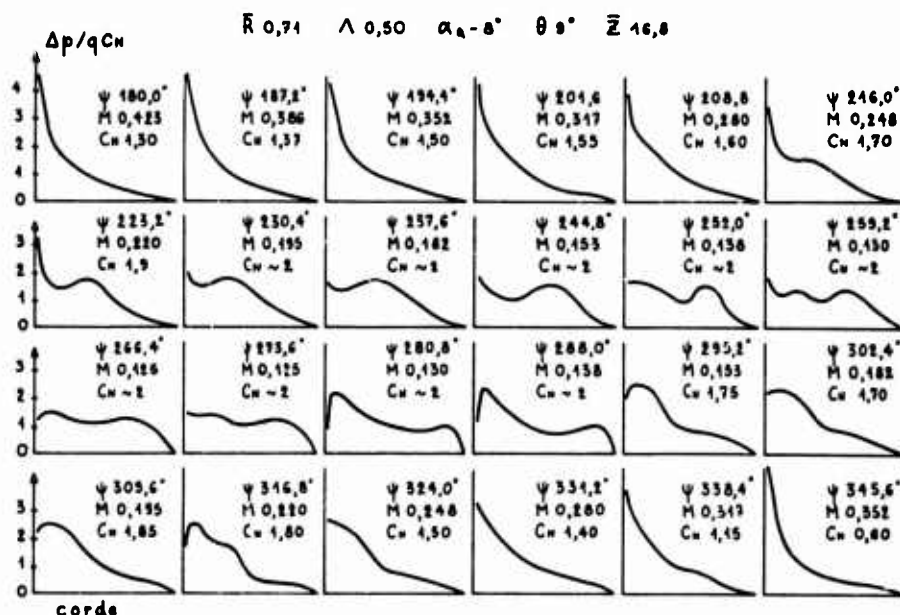


Fig.13 DECROCHAGE DE LA PALE RECLANTE, ROTOR 1
RETREATING BLADE STALL, ROTOR N°1

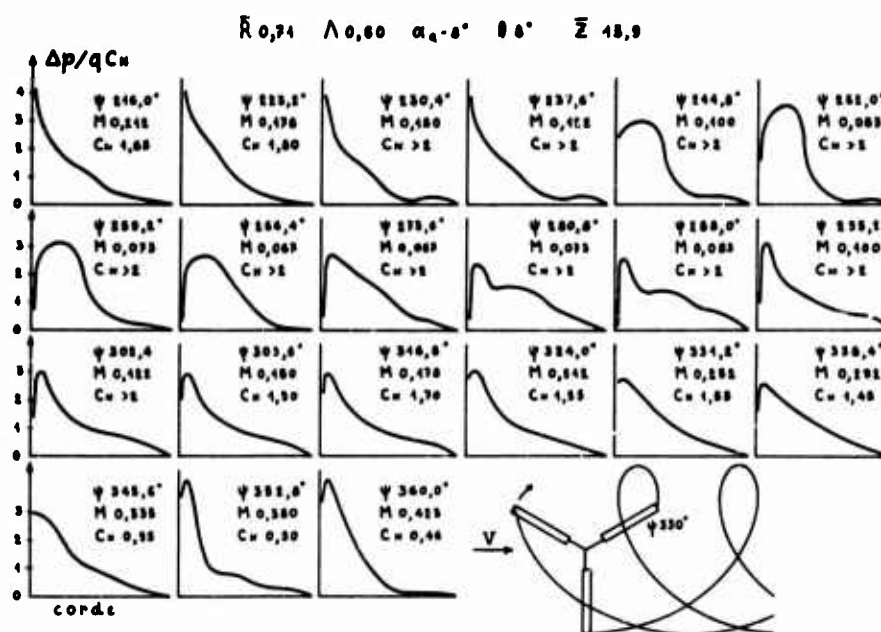


Fig.14 DECROCHAGE DE LA PALE RECLANTE, ROTOR 1
RETREATING BLADE STALL, ROTOR N°1

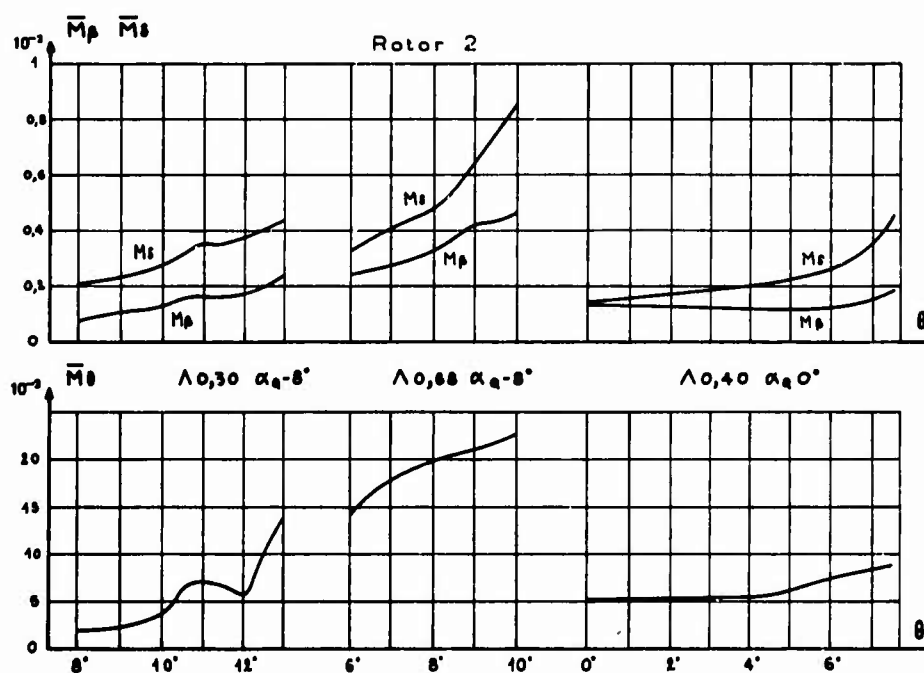


Fig.15 VIBRATIONS AU PIED DE PALE
ROOT BLADE VIBRATIONS

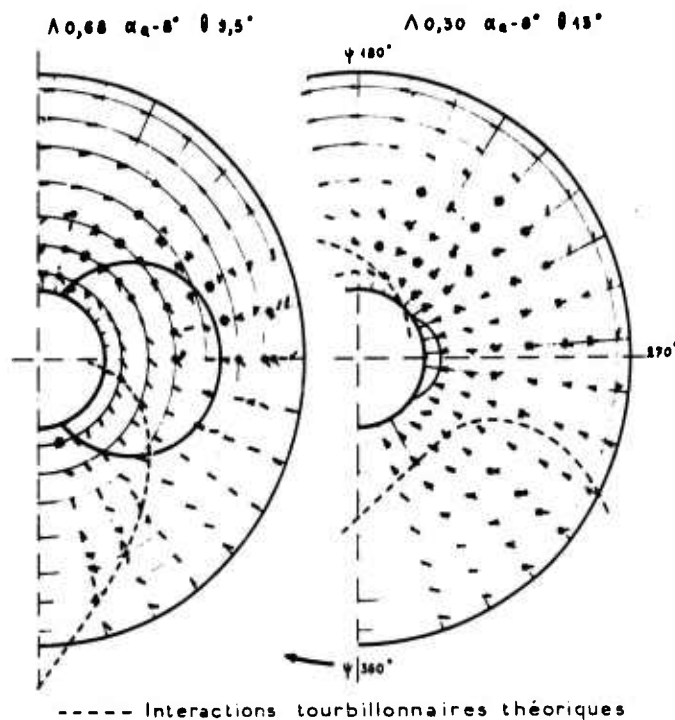


Fig.16 VISUALISATIONS DE DECROCHAGE, ROTOR 2
VISUALIZATIONS : STALL CONDITIONS, ROTOR N°2

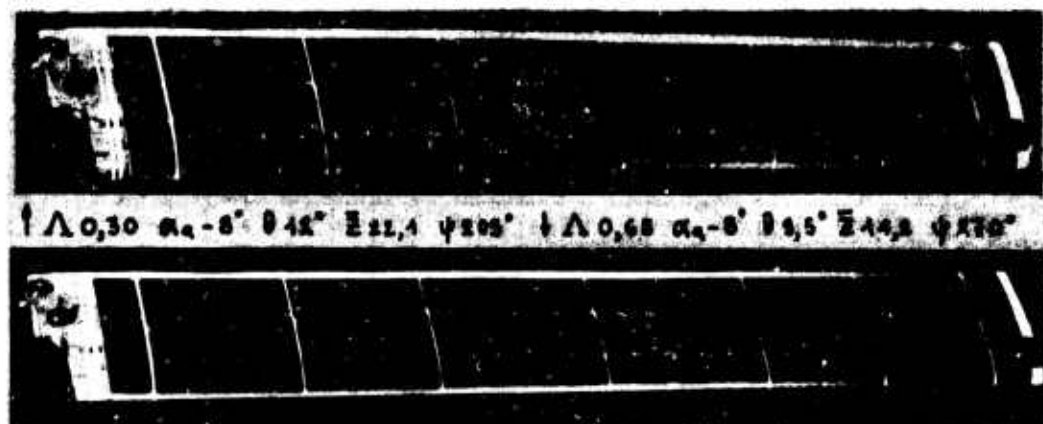
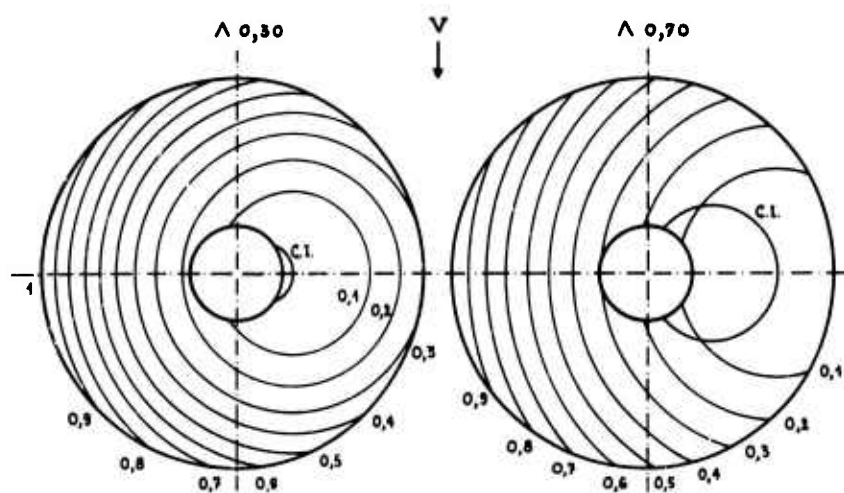


Fig.18 EXEMPLES DE PHOTOGRAPHIES

AERODYNAMIC FACTORS INFLUENCING OVERALL HOVER PERFORMANCE

by

Evan A. Fradenburgh
Chief of AerodynamicsSikorsky Aircraft
Division of United Aircraft Corporation
Stratford, Connecticut 06602
U. S. A.

SUMMARY

There are numerous aerodynamic factors and interrelationships which influence the hovering efficiency of a helicopter, but which are frequently neglected or inadequately treated. Analysis of isolated rotor performance and definition of wake structure and tip vortex characteristics are important subjects that are receiving a relatively high level of attention; this paper deals primarily with interference effects that should receive additional emphasis.

Some of the recent improvements in basic rotor design practice at Sikorsky Aircraft are described briefly, and results of several series of model rotor tests are discussed. Moderate values of blade root cutout are shown to have an unanticipated effect on hovering efficiency. A large root cutout decreases figure of merit of the rotor, but also reduces vertical drag of a typical airframe below the rotor, cutting the aerodynamic penalty to about half of what tests of the rotor alone would indicate. Tests of a tilt-rotor model show that, unlike the conventional single rotor helicopter configuration, the rotors do not benefit from a partial ground effect caused by the airframe in the rotor downwash field. The relationship of blade twist and ground effect is discussed, and the influence of ground proximity on vertical drag is presented. It is shown that net airframe vertical drag can be zero or negative when the aircraft is close to the ground. Additional systematic experimentation is clearly needed, as is the development of theory to cover the various relationships involved in overall hover efficiency.

SYMBOLS

b	Number of blades
c	Blade chord
C_D	Airframe vertical drag coefficient, $D/\pi R^2 \rho (\Omega R)^2$
C_Q	Rotor torque coefficient, $\text{Torque}/\pi R^3 \rho (\Omega R)^2$
C_T	Rotor thrust coefficient, $T/\pi R^2 \rho (\Omega R)^2$
D	Vertical download on airframe
M	Figure of merit, $.707 C_T^{3/2} / C_Q$
R	Rotor radius
r	Radial distance from center of rotation
T	Rotor Thrust
y	Distance below rotor
Z	Height of rotor above ground
$\theta_{.75}$	Collective pitch measured at three-quarters radius
λ	Hover inflow ratio, Induced velocity/ ΩR
ρ	Air density
σ	Rotor solidity, $bc/\pi R$
ψ	Azimuth angle, degrees
ΩR	Rotor tip speed

1. INTRODUCTION

The aerodynamic performance of a hovering helicopter is a much more complex subject than it was once considered to be. The traditional concept of hovering performance, used for the first quarter-century of helicopter development, was a highly simplified one. A few design variables, including rotor solidity, blade twist, and tip speed, were recognized as having a fundamental effect on hover figure of merit. These parameters plus the operational variables (altitude, temperature, gross weight range, etc.) were used to predict the basic hover performance, usually by classical or semi-empirical techniques. This performance was then corrected by 10 percent or so to account for tail rotor power, by 2 or 3 percent to account for transmission losses, and sometimes by a few percent to account for the vertical drag (aerodynamic download) on the fuselage caused by the rotor slipstream. This procedure provided an estimate of the overall aircraft hover performance. All too often, however, the measured hover performance was found to be something different.

In recent years much more sophisticated analyses have been developed to predict the performance of the isolated rotor. In particular the influence of the tip vortex has been recognized as a major factor. As illustrated schematically in Figure 1, the span load distribution of each blade is altered substantially by the presence of the trailing vortex from the preceding blade. Some of the initial work conducted in this area by Sikorsky Aircraft and United Aircraft Research Laboratories was reported in Reference 1. More recent and detailed investigations of rotor wake structure and performance effects are reported in References 2-4. Programs to define the basic characteristics of trailing vortices have been reported in References 5 and 6. There are current efforts to devise techniques for dissipating the trailing vortex, such as the air-injection method reported in Reference 7.

The subjects of wake structure, vortex characteristics, and effects on performance are receiving considerable attention at this time. On the other hand, there are a number of aerodynamic factors influencing hover performance which frequently are neglected or inadequately treated. The primary intent of this paper is to identify several examples of such factors, which warrant increased emphasis in the future.

2. AERODYNAMICS OF ISOLATED ROTORS

Rotor aerodynamic design variables are presented in Figure 2, divided into the traditional factors and some of the supplementary variables that are considered in modern analysis. Airfoil section and blade taper are shown in parentheses in the left-hand column, because although they have long been recognized as important design variables, there has been very little actual variation in these parameters until quite recently. Standard airfoils and constant chord have been the general rule. In modern blade designs, the airfoil sections are tailored specifically to meet design objectives. Not only are airfoil camber and thickness apt to be significantly different from traditional values but there is also frequently a spanwise variation of the airfoil section from root to tip, made possible by modern materials and fabrication techniques. Similarly, not only is blade taper now possible with economical construction methods, but arbitrary spanwise variations of chord may be considered, along with arbitrary blade twist distributions. Tip geometry has been recognized as having particular importance as a result of recent investigations of the structure of the rotor wake. The number of blades is recognized as having aerodynamic significance apart from the solidity consideration, because of effect of the number of blades on tip vortex structure. Special features or devices designed to influence the characteristics of the trailing vortex must also be considered as part of the rotor aerodynamic design. The extent of root cutout and spar shape have an impact on hover performance - an example of this effect is discussed in a following section. Finally, the blade structural dynamic properties, although not aerodynamic factors at all, interact so strongly with the aerodynamics under some circumstances that they are included in the list of design variables in Figure 2. The most common example of this interaction is the dynamic twisting of the blade, caused by aerodynamic torsional moments, which in turn changes the blade span load distribution and therefore performance.

One example of a recent Sikorsky rotor incorporating some of the newer design variables is shown in Figure 3. The Improved Rotor Blade or IRB, designed and developed for the CH 53 helicopter with support and active participation by the U. S. Naval Air Systems Command, has demonstrated significant performance advantages over the standard production blades. The IRB utilizes a hollow titanium spar and a molded fiberglass aerodynamic shell. It incorporates cambered blade sections, varying from 15 percent at the blade root to 9.5 percent thick at the tip. It has a high, nonlinear twist, with local variations near the tip to compensate for the angle of attack disturbance caused by the vortex from the preceding blade. The tip is also tapered to reduce the strength of the tip vortex and improve the spanwise loading distribution. This rotor has demonstrated substantial improvements in hovering performance over the standard production rotor system. It is also quieter than the standard rotor.

Another recent rotor design, shown in Figure 4, is that developed for the Sikorsky S-67 Blackhawk helicopter. The blades on this rotor incorporate a substantial tip sweep, combined with a twist change and an airfoil which varies from a symmetrical, 12 percent thick section at 95 percent radius to a cambered, 6 percent airfoil at the tip. These features are important factors in the good performance and low noise signature of this aircraft.

3. NET HOVER PERFORMANCE

Even with the refinements in the aerodynamics of rotors mentioned above, it is obviously not adequate to consider only the isolated rotor. The present concept of factors influencing net hover performance of the main rotor is shown in Figure 5. Not only are aerodynamic design of the rotor and operational variables considered, but the blade structural dynamics and the airframe design are also considered. The blade structure can influence the isolated rotor performance, as previously discussed, and the airframe design, in combination with the rotor aerodynamic design and operational variables, determine vertical drag (download on the airframe) and rotor thrust recovery (increase in rotor thrust at constant power due to the presence of the airframe). The isolated rotor performance, vertical drag, and thrust recovery determine the net rotor performance. Note that this diagram considers the main rotor only and that the tail rotor and transmission, etc., must still be considered for overall aircraft performance.

4. EFFECT OF ROOT CUTOUT

An example of some of the aerodynamic interaction factors mentioned will be described for a rotor having a large root cutout. One such rotor is the Sikorsky TRAC rotor system, which is a variable diameter, telescoping blade configuration under development for advanced VTOL aircraft, with support from the U. S. Army Air Mobility Research and Development Laboratories. This rotor has a blade physical arrangement which results in a root cutout of approximately 50 percent of radius when the blade is fully extended, as can be seen in Figure 6. The inboard half of the blade is an elliptical cross-section tube which is enclosed by the outer blade when the blade is retracted. The ellipse is 33 percent thick and has a chord of one-third that of the outer blade. There was concern that this large cutout might result in a substantial hovering performance penalty, and a series of tests of four-foot diameter rotors were conducted, under U. S. Air Force sponsorship, to establish the effect of root cutout. Results are reported in Reference 8. The test blades used in the investigation are shown in Figure 7. They included root cutout values, measured from the center of rotation, of 10 percent (minimum value), 25, 40, and 50 percent of radius. Typical test results are shown in Figure 8, which presents hovering figure of merit ratio (normalized to the 10 percent cutout value) as a function of percent cutout. The performance penalty at 50 percent cutout was about as predicted, ranging from about four to six percent at typical thrust coefficients and tip speeds. At lower cutout values an unexpected nonlinear variation was established, with significant performance losses which were not predicted by any of several theories used. In order to eliminate the possibility that differences in construction accuracy between the four sets of blades was causing the effect shown, the tests were repeated with a single set of blades, with root cutout successively increased by removing the inboard trailing edge, through the range from 10 to 50 percent cutout. Essentially identical results were obtained. It seems evident that the nonlinear behavior with cutout is associated with the changes in the downwash velocity distribution induced by the cutout, and possibly due to formation of a finite strength root vortex as well as the usual tip vortex. Flow visualization photographs, using smoke filaments ejected from the blades, show evidence of a finite strength root vortex for the 50 percent cutout case. The downwash patterns are different for the 10 percent and 50 percent cutout cases, as shown in Figure 9. These patterns, determined from the flow visualization studies, show that the large

cutout produces downwash flow which is farther outboard than for the conventional (minimum cutout) rotor. At high thrust, smoke emitted from the 50 percent spanwise station actually moves outboard as it flows down, in contrast to conventional behavior.

5. VERTICAL DRAG AND THRUST RECOVERY

As the large cutout rotor produces less lift and therefore less downwash near the center of the disk than the conventional small cutout rotor, it was reasoned that it should also produce less download (vertical drag) on that portion of the airframe inboard of 50 percent radius. To verify this hypothesis, a second series of tests were conducted, under U. S. Army sponsorship, to determine the differences in vertical drag and thrust recovery due to root cutout for several airframe configurations (Reference 9). A typical airframe model, representing a compound helicopter configuration, with fuselage and a wing having a span of 60 percent of the rotor diameter, is shown in Figure 10. The airframe download was measured simultaneously but independently of the rotor thrust and torque measurements. The measured values of vertical drag on this airframe, and similar measurements for the fuselage without wing, are shown in Figure 11 as functions of the net thrust coefficient-solidity ratio, $(C_T - C_D)/\sigma$. As can be seen, the vertical drag is reduced through use of the large cutout rotor, particularly for the winged configurations.

The effective vertical drag is actually less than the measured download, in most cases, because of a favorable interference effect of the airframe on rotor performance. This may be viewed as a partial ground effect and is referred to here as thrust recovery. The thrust recovery is defined in Figure 12 as the increase in thrust at constant power that the rotor experiences in the presence of the airframe, compared to the performance of the isolated rotor. This thrust recovery, expressed as a percentage of vertical drag, is shown in Figure 13 for the cases under consideration. For the fuselage model, the thrust recovery is slightly better with 50 percent cutout than with the minimum cutout, whereas with the wing, which has most of the additional area inboard of 50 percent radius, the thrust recovery is not as good. The net vertical drag, which is the difference between the airframe download and the thrust recovery, is presented in Figure 14. The net saving in vertical drag with the 50 percent cutout is not as large as the gross vertical drag reduction (Figure 11) but is still appreciable. In fact, the hover performance penalty for the large cutout, which amounts to four to six percent at typical thrust levels for the isolated rotor, is reduced to only two to three percent for the winged configuration when the net vertical drag savings are considered.

Hover performance and vertical drag are influenced by blade root cutout primarily because of the effect of cutout on blade span load distribution, which in turn affects rotor induced power and downwash near the root. It should be expected that any other rotor aerodynamic design variable which controls span load distribution might have similar effects. A second example of this relationship is provided by the use of blade twist to increase hover efficiency. Most helicopter rotors have a blade loading distribution which is too low at the inboard end to achieve the classic ideal of uniform disk loading. Increasing twist will usually improve the loading distribution and increase the hover figure of merit, at least for the isolated rotor. The higher downwash produced at the inboard end, however, can be expected to result in higher net vertical drags. This was illustrated by recent tests at Sikorsky Aircraft, where hover flight tests of a high-twist experimental rotor demonstrated an increase in useful lifting capacity of only two-thirds of the thrust increase demonstrated on the rotor whirl tower.

6. THRUST RECOVERY OF ASYMMETRICAL CONFIGURATIONS

All of the vertical drag model tests conducted by Sikorsky Aircraft for single rotor airframe configurations out of ground effect have shown thrust recovery effects, typically in the range of 20 to 50 percent of the vertical drag. These single rotor airframe models generally exhibit a substantial degree of polar symmetry, i.e. any area blockage under one portion of the rotor disk is more or less balanced by a similar area diametrically opposite. Thus the front of the fuselage tends to balance the rear of the fuselage, and a right wing panel tends to balance the left wing panel about the center of rotation. Tests of asymmetrical configurations, on the other hand, have not always shown favorable thrust recovery effects. One example of this was provided by a series of tests of tilt-rotor models. The tilt-rotor is a lateral twin rotor configuration, and although it is symmetrical with respect to the fuselage centerline, the area blockage is highly asymmetrical from the point of view of each rotor. One of the test models, which utilized an end plate as a reflection plane to simulate the presence of the second rotor, is shown in Figure 15. Measured vertical drag characteristics for this model out of ground effect are shown in Figure 16 for two wing flap conditions. Although the vertical drag forces were substantial, there was no measurable thrust recovery at high rotor thrust and actually a slight negative thrust recovery at low thrust. All of the tilt rotor configurations investigated showed generally similar results. Tests of the rotor with a reflection plane only showed no significant adverse interference for the rotor-to-rotor separation distance being simulated. Thus some peculiarity of the tilt rotor airframe configuration is responsible for the result.

For a while it was hypothesized that the lack of polar symmetry of the blocked area in the downwash flow of the rotor might be responsible for the lack of thrust recovery. This conjecture seemed somewhat reasonable considering that the rotor is articulated and therefore cannot support an unbalanced moment about the center of rotation. An interference in the downwash flow field might be supposed to cause the rotor to flap in such a manner as to cancel out any incremental lift. To check this idea, calculations were made for two simple cases with Sikorsky's Generalized Rotor Performance method, which accounts for the aerodynamics and dynamics of a freely-flapping rigid blade. An untwisted rotor at zero blade pitch was assumed, and the rotor inflow ratio, λ , was assumed equal to zero at all points except for a thirty degree sector of the disk in one case, and for two diametrically-opposite thirty degree sectors in the other case. In these areas an arbitrary inflow ratio of .02 was assumed, to represent an upward interference velocity in the plane of the disk caused by the airframe. If the hypothesis were correct, the symmetrical disturbance should produce a lift increment, whereas the unbalanced disturbance should produce none. Results of these calculations are presented in Figure 17. Time histories of blade flapping and thrust coefficient for one blade are shown for both the symmetrical disturbance (double pulse, with pulses centered about 90 and 270 degrees azimuth) and asymmetrical disturbance (single pulse

centered about 90 degrees azimuth angle). The calculations disproved the original hypothesis; the single pulse disturbance shows an integrated lift increment of exactly one-half that of the double pulse disturbance, rather than zero. The blades do flap to eliminate the unbalanced moment, but they do it in such a way that there is a positive lift increment on the half of the disk opposite the disturbance as well as directly at the disturbance.

The lack of thrust recovery of the tilt rotor models remains unexplained, but it is now believed that a partial recirculating downwash flow develops when both the flow blockage due to the wing and the reflection plane are present. This recirculation, which would not exist when either the wing or the plane of symmetry were absent, could cause an increase in the rotor induced power that would tend to cancel the beneficial thrust recovery effect. The test results are still believed to be correct and applicable to typical lateral twin rotor configurations.

Subsequent to the above test experience, Sikorsky has obtained test data on another asymmetrical configuration which does show the normal thrust recovery effect. This was a hover test of a full size tail rotor - vertical fin combination in which the rotor downwash was directed toward the fin rather than away from it. All of the area blockage was on one side of the rotor disk, but thrust recovery amounted to approximately 25 percent of the lateral fin drag, greatly decreasing the aerodynamic penalty of the blockage in the slipstream. This result provides a qualitative confirmation of the theoretical calculations described above. A positive thrust recovery effect should be considered as the normal situation for airframe components in the flow field of a hovering rotor whether the area blockage exhibits polar symmetry or not. It should be noted that this conclusion is not in agreement with earlier NACA studies, reported in References 10 and 11, where attempts to measure thrust recovery were generally unsuccessful. Obviously the influence of airframe components on the rotor will decrease as the distance between the two increases. This diminution of thrust recovery with increasing separation between rotor and airframe has been observed several times in various model tests.

7. GROUND EFFECT

The influence on hover performance of rotor proximity to the ground has long been recognized, but the phenomenon is not very well understood. Several peculiarities have been noted which as yet are not explained by theory. One example of this is the apparent influence of blade aspect ratio on the magnitude of thrust augmentation in ground effect. In a study conducted by Sikorsky Aircraft several years ago it was noted that low aspect ratio blades seem to have significantly higher augmentation ratios due to ground effect than high aspect ratio blades. This relationship was reported in Reference 12. Another unexplained phenomenon is the influence of blade twist on ground effect. Figure 18 presents hover performance data obtained in tests conducted at United Aircraft Research Laboratories on two model rotors which were identical except for blade twist. Some of these data were obtained in U. S. Army-supported tests which are described in Reference 3. For the out-of-ground-effect condition, high negative twist is beneficial at the higher thrust levels, as would be expected. With the rotor close to the ground, however, the lower twist rotor has substantially better performance throughout the usual range of thrust loadings. This effect is shown in a different manner in Figure 19, which presents thrust augmentation ratio (thrust in ground effect divided by thrust out of ground effect) as a function of height above ground.

As the thrust recovery aspect of vertical drag phenomena is presumed to be due to partial ground effect, it seems reasonable to assume that factors which influence the magnitude of ground effect, including blade aspect ratio and twist, would also influence the magnitude of thrust recovery. However, test data to verify this assumption are not available.

8. THE INTERRELATIONSHIP OF VERTICAL DRAG AND GROUND EFFECT

Because the downwash pattern below a hovering rotor is substantially altered by proximity to the ground, it is to be expected that vertical drag of airframe components will also be altered by ground effect. The change in downwash pattern is shown by the photographs in Figure 20 which show patterns of smoke introduced into the flow field just above the rotor. In ground effect, a dome-shaped region of low velocity air appears under the center of the disk, and the main downwash flow is pushed outboard. Static pressures in the flow field are also substantially altered, as described in Reference 13. Both the velocity and pressure fields will influence vertical drag. The interrelationship of ground effect and vertical drag is illustrated by test results obtained on a series of simple models below a rotor. The rotor is the same as that shown in Figure 20; it is two feet in diameter, with two untwisted blades of aspect ratio six. The vertical drag models included a cylindrical simulated fuselage with a diameter of 0.25 R and a length of 1.2 R (where R is rotor radius), a simulated wing with a chord of 0.2 R and a span of 1.6 R, and two flat disks having radii of 0.4 R and 0.6 R respectively. All models were symmetrically mounted under the rotor and the three flat configurations were 0.33 R below the rotor. The simulated fuselage was closer to the rotor; the top of the cylinder was .073 R below the rotor disk. Although these models do not represent any actual helicopter configuration, the trends of the data are generally representative of the aerodynamic interrelationships to be expected.

Typical results of the tests are presented in Figures 21-24. The collective pitch is constant (approximately 10 degrees) for all results shown. The measured rotor torque was also essentially constant within the accuracy of measurement for all conditions shown. The influence of height above ground and vertical drag configuration on rotor thrust at constant power is shown in Figure 21. A substantial ground effect exists for the isolated rotor; the rotor thrust coefficient - solidity ratio increases by approximately 35 percent as height is decreased from the out-of-ground-effect condition (assumed for $Z/R = 5$) to the lowest value ($Z/R = 0.45$). The presence of the vertical drag models increases the thrust (positive thrust recovery) at the out-of-ground-effect condition, but has very little effect on rotor thrust at the minimum height. It may be noted that in the vicinity of $Z/R = 1$ several of the models actually caused a negative thrust recovery, that is, the rotor thrust is less with the airframe components present than for the isolated rotor.

The thrust recovery, obtained from the differences in the curves of Figure 21, is shown in Figure 22 for the various vertical drag models. In each case the thrust recovery can be seen to drop substantially at rotor height ratios below 2.0, becoming negative for three of the models at $Z/R = 1.0$. At the lowest height the magnitude of thrust recovery is very small for all models.

The measured vertical drag values for the models are presented in Figure 23. These curves also exhibit a drop in value with decreasing Z/R , becoming negative for several models at the lowest rotor height. The 60 percent disk has a particularly large negative vertical drag (positive lift force) at minimum rotor height. Pressure measurements on the disk showed a substantial positive pressure on the lower surface and a surprisingly large negative pressure peak at the center of the upper surface. The negative pressure peak suggests the formation of a vertical standing vortex of substantial strength on the upper surface, as previously reported in Reference 14. A similar drop in pressure was noted on the ground directly under the center of the rotor when the rotor was mounted close to the ground but without vertical drag models.

The net vertical drag, which is the measured vertical drag minus the rotor thrust recovery, is presented in Figure 24. It can be seen that the net or effective vertical drag generally drops in ground effect, and can be substantially negative very close to the ground. The two disks, which show the largest negative drags, also exhibit a slight dip in the curve at a height-radius ratio, Z/R , of 2.0. Of all the models, the wing extends farthest out from the center of rotation into the higher velocity region of the downwash field. It exhibits an essentially constant net vertical drag with reducing rotor height down to one rotor radius, followed by a sharp drop to a near-zero net drag at the lowest height.

The final example of the complexity of vertical drag is presented in Figure 25 which shows additional test data on the effect of wing vertical location for the out-of-ground-effect condition. The apparent vertical drag (measured download divided by rotor thrust measured concurrently) is higher for the high wing position than for the low wing position. After accounting for thrust recovery, however, the effect is reversed; the net vertical drag (download minus thrust increase, divided by isolated rotor thrust at the same power) is higher for the low wing than for the high wing. This result seems qualitatively reasonable in view of the slipstream contraction which occurs below the rotor; the wing blocks a smaller percent of the slipstream when it is very near the rotor disk than it does in a low position where the slipstream is fully contracted.

9. CONCLUDING REMARKS

At the present time there is no theory which encompasses all or even most of the aerodynamic interrelationships considered herein. These factors can be studied with small models at moderate cost, with adequate accuracy and repeatability. The low Reynolds numbers of some of the flows involved, however, make direct application of the data to full size helicopters somewhat questionable. There needs to be a series of systematic experimental research programs on both small and large scale models to establish Reynolds number effects and to extend the fund of data available on the overall hovering efficiency of helicopters. Further, it is necessary to develop analytical models that will permit determination of vertical drag, thrust recovery, ground effect, etc., to give the designer the means of optimizing his aircraft without the necessity of long and costly experimental optimization programs.

There is an additional factor that needs emphasis. Up to this point the discussion has been limited to pure hover, in other words no horizontal velocity component due to either translation or wind is considered. Statistically, this is a rather rare event - the real "hover" situation involves advance ratios which are seldom below .01 and occasionally higher than 0.10. There is evidence, for example as discussed in References 1 and 15, that rotor hover aerodynamics are altered substantially at very low advance ratios. It is quite possible that rotor-airframe-ground interference relationships in general also are altered substantially at low speeds. There is very little useful experimental data on these relationships, and no established theories. It should be an objective to develop test data and theories for a continuous spectrum of operation from true hover up to high forward speeds. The rotor-airframe interference, which is primarily a performance consideration in hover, becomes primarily a stability and control consideration in cruise. A continuous theory is necessary to define the relative magnitude of these effects for any specified condition.

It is time to focus additional attention on the aerodynamics of hovering rotors in real environments: always in close proximity to an airframe, frequently in close proximity to the ground, and usually in variable winds which require continual corrective actions by the pilot.

10. REFERENCES

1. Jenney, D. S., Olson, J. R., and Landgrebe, A. J., A Reassessment of Rotor Hovering Performance Prediction Methods, Journal of the American Helicopter Society, Vol. 13, No. 2, April 1968, pp. 1-26.
2. Clark, David R., and Leiper, Albert C., The Free Wake Analysis, paper presented at the American Helicopter Society 25th Annual National Forum, Washington, D. C., May 1969.
3. Landgrebe, Anton J., An Analytical and Experimental Investigation of Helicopter Rotor Hover Performance and Wake Geometry Characteristics, USAAMRDL Technical Report 71-24, June 1971.
4. Landgrebe, A. J., The Wake Geometry of a Hovering Helicopter Rotor and its Influence on Rotor Performance, paper presented at the American Helicopter Society 28th Annual National Forum, Washington, D. C., May 1972 (Preprint No. 620).

5. Chigier, N. A., Sr., and Corsiglia, V. R., Tip Vortices - Velocity Distributions, paper presented at AHS National Forum, Washington, D. C., May 1971 (Preprint No. 522).
6. Rorke, J. B., Moffitt, R. C., and Ward, J. F., Wind Tunnel Simulation of Full Scale Vortices, paper presented at the American Helicopter Society 28th Annual National Forum, Washington D. C., May 1972 (Preprint No. 626).
7. White, Richard P. Jr., and Balcerak, John C., The Nemesis of the Trailed Tip Vortex - Is It Now Conquered?, paper presented at the American Helicopter Society 28th Annual National Forum, Washington D. C., May 1972.
8. Cassarino, Sebastian J., Effect of Root Cutout on Hover Performance, U. S. Air Force Technical Report AFFDL-TR-70-70, June 1970.
9. Cassarino, Sebastian J., Effect of Rotor Blade Root Cutout on Vertical Drag, U. S. Army AVLABS Technical Report 70-59, October 1970.
10. Makofski, R. A., and Menkick, G. F., Investigation of Vertical Drag and Periodic Airloads Acting on Flat Panels in a Rotor Slipstream, NACA TN 3900, December 1956.
11. McKee, J. W., and Naeseth, R. L., Experimental Investigation of the Drag of Flat Plates and Cylinders in the Slipstream of a Hovering Rotor, NACA TN 4239, April 1958.
12. Rabbott, J. P., Jr., Model vs. Full Scale Rotor Testing, paper presented at CAL/AVLABS Symposium on Aerodynamics of Rotary Wing and V/STOL Aircraft, Buffalo, New York, June 1969.
13. Fradenburgh, Evan A., Flow Field Measurements for a Hovering Rotor Near the Ground, paper presented at the American Helicopter Society Fifth Annual Western Forum, Los Angeles, California, September 1958.
14. Fradenburgh, Evan A., The Helicopter and the Ground Effect Machine, Journal of the American Helicopter Society, Vol. 5 No. 4, October 1960, pp. 26-28, 32.
15. Harris, Franklin D., Articulated Rotor Blade Flapping Motion at Low Advance Ratio, AHS Journal, Vol. 17 No. 1, January 1972, pp. 41-48.

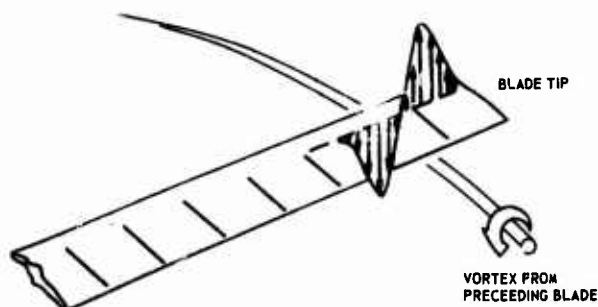


FIGURE 1 BLADE-VORTEX INTERACTION ON SPANWISE LOAD DISTRIBUTION

TRADITIONAL VARIABLES

DISK LOADING
SOLIDITY
OVERALL BLADE TWIST
TIP SPEED
(AIRFOIL)
(TAPER)

SUPPLEMENTARY VARIABLES

AIRFOIL SECTIONS (CAMBER, THICKNESS, SPAN DISTRIBUTION)
SPANWISE DISTRIBUTION OF CHORD
SPANWISE DISTRIBUTION OF TWIST
TIP GEOMETRY (SWEEP, ETC.)
NUMBER OF BLADES
SPECIAL FEATURES INFLUENCING VORTEX
CORE CHARACTERISTICS
ROOT CUTOUT AND SPAR CROSS SECTION
[BLADE STRUCTURAL DYNAMIC PROPERTIES]

FIGURE 2 ROTOR AERODYNAMIC DESIGN VARIABLES

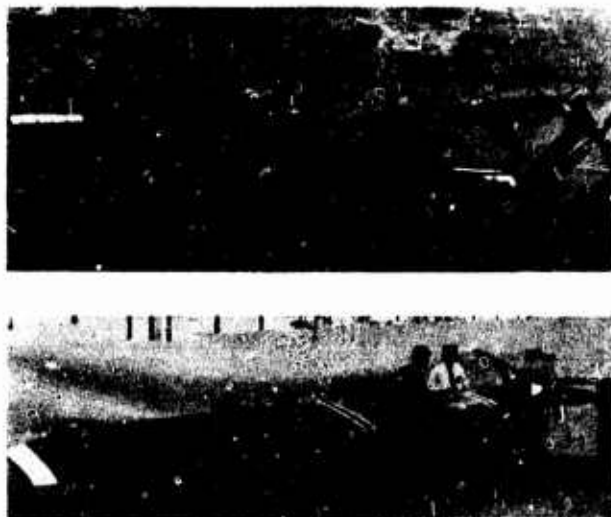


FIGURE 3 IMPROVED ROTOR BLADE ON CH53 HELICOPTER



FIGURE 4 SIKORSKY S-67 BLACKHAWK HELICOPTER

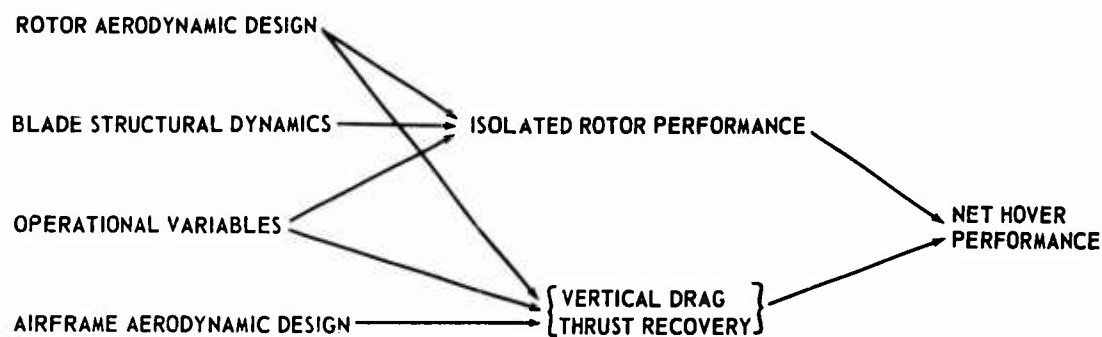


FIGURE 5 NET HOVER PERFORMANCE DIAGRAM FOR MAIN ROTOR



FIGURE 6 SIKORSKY TRAC TELESCOPING ROTOR CONFIGURATION



FIGURE 7 TEST BLADES FOR ROOT CUTOUT INVESTIGATION

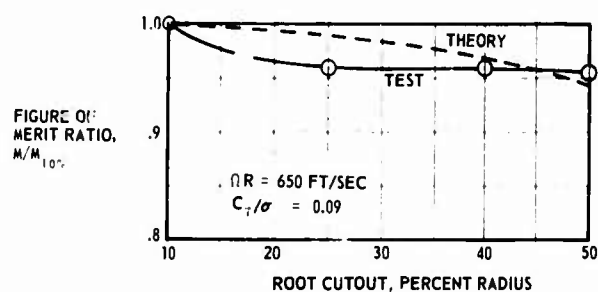


FIGURE 8 EFFECT OF ROOT CUTOUT ON HOVER FIGURE OF MERIT

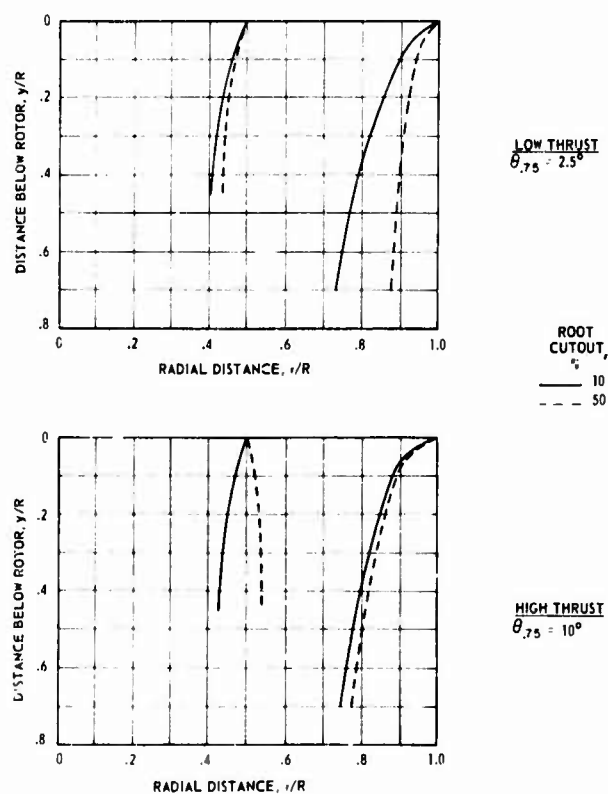


FIGURE 9 DOWNWASH GEOMETRY PATTERNS

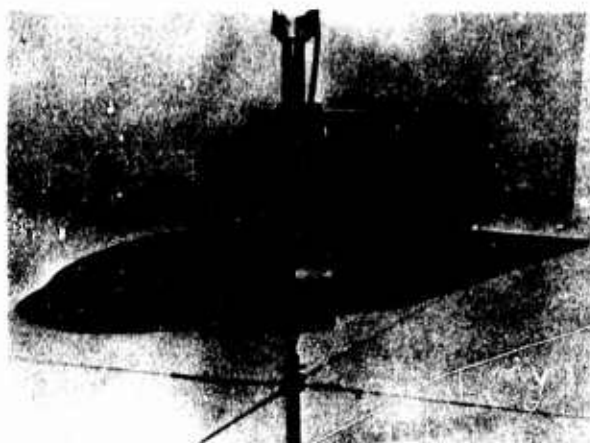


FIGURE 10 VERTICAL DRAG MODEL CONFIGURATION, FUSELAGE PLUS WING

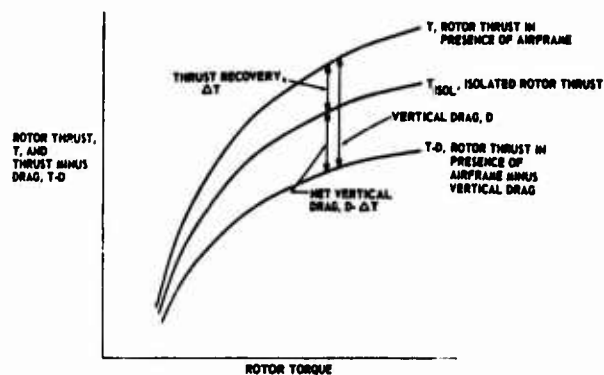


FIGURE 12 DEFINITION OF THRUST RECOVERY AND NET VERTICAL DRAG

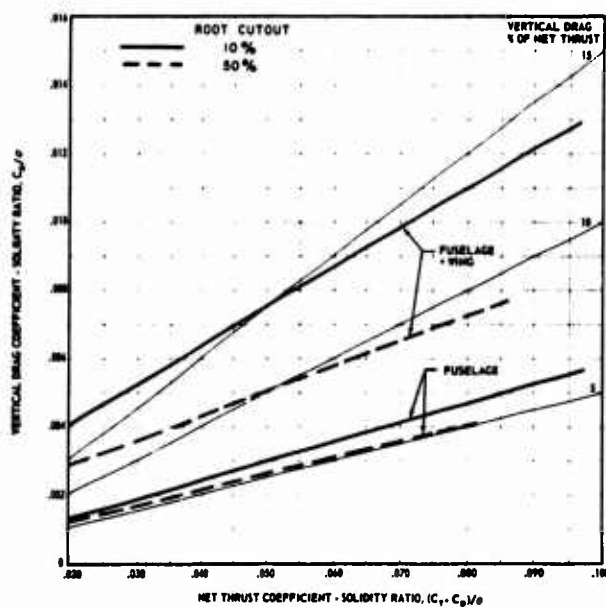


FIGURE 11 EFFECT OF ROOT CUTOUT ON AIRFRAME VERTICAL DRAG

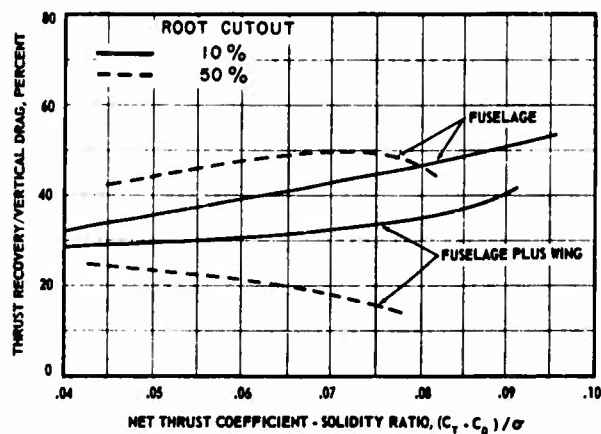


FIGURE 13 EFFECT OF ROOT CUTOUT ON THRUST RECOVERY

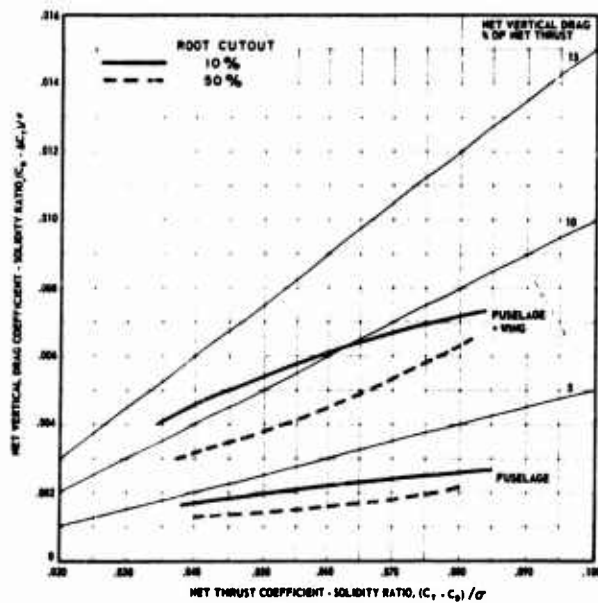


FIGURE 14 VARIATION OF AIRFRAME VERTICAL DRAG WITH NET THRUST

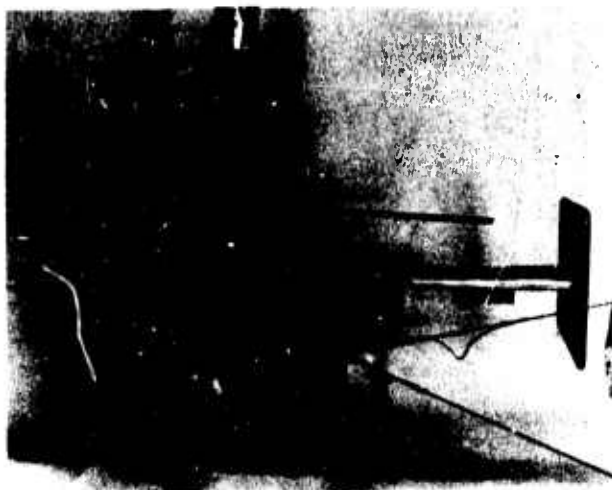


FIGURE 15 VERTICAL DRAG TEST, TILT ROTOR CONFIGURATION

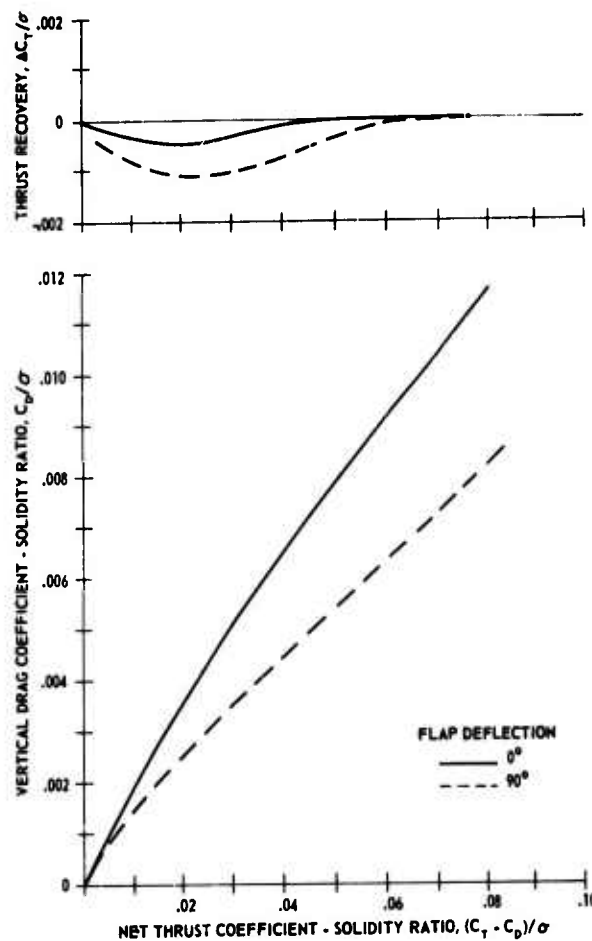


FIGURE 16 VERTICAL DRAG TEST RESULTS FOR TILT ROTOR CONFIGURATION

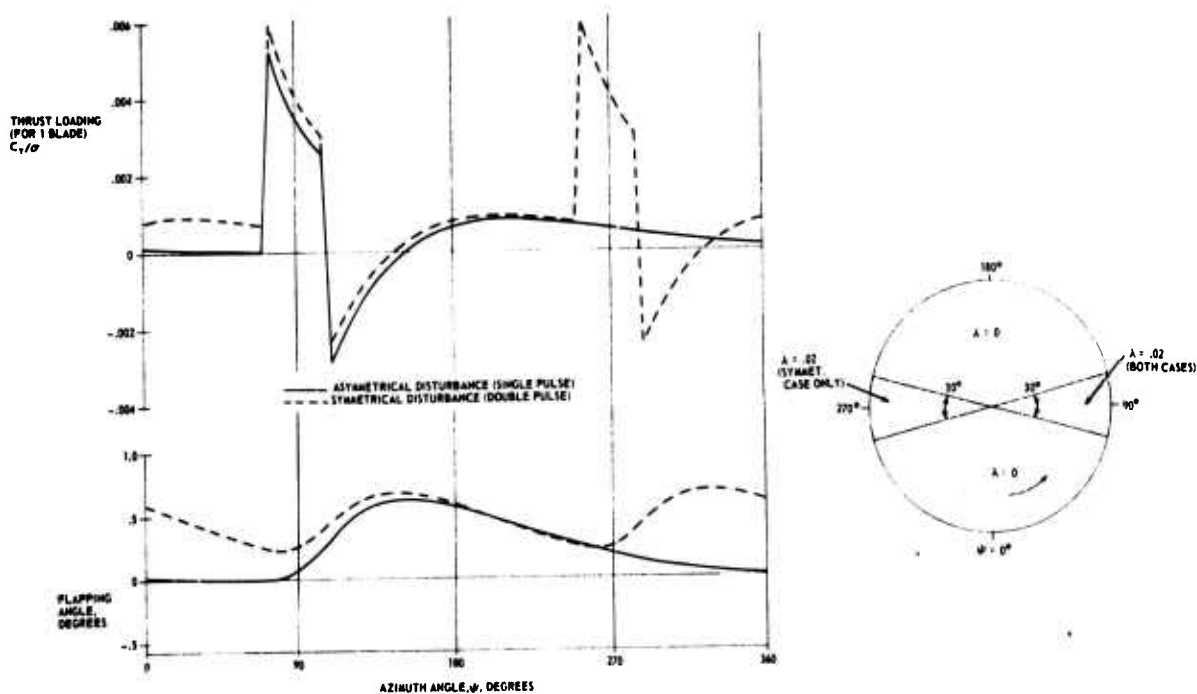


FIGURE 17 THEORETICAL CALCULATION OF ROTOR BEHAVIOR DUE TO INFLOW DISTURBANCE

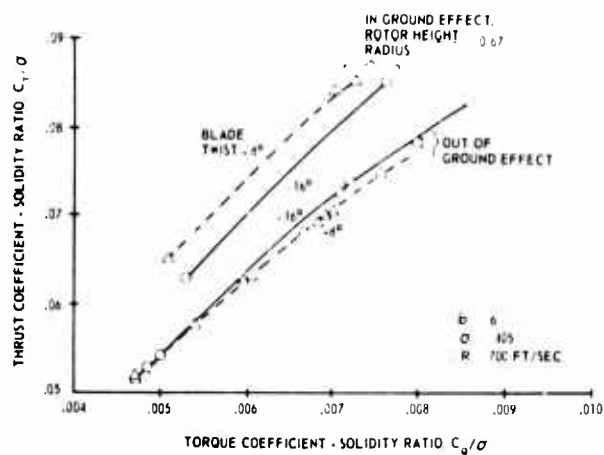


FIGURE 18 INFLUENCE OF BLADE TWIST ON GROUND EFFECT PERFORMANCE

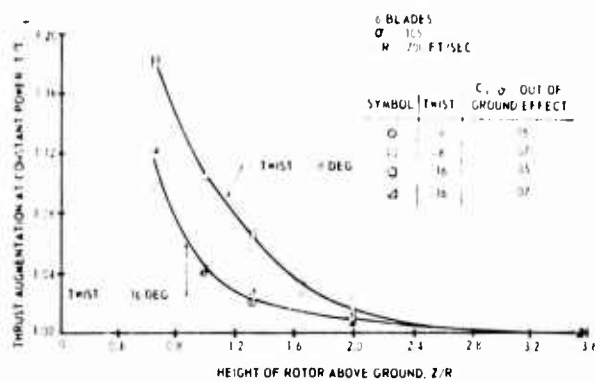
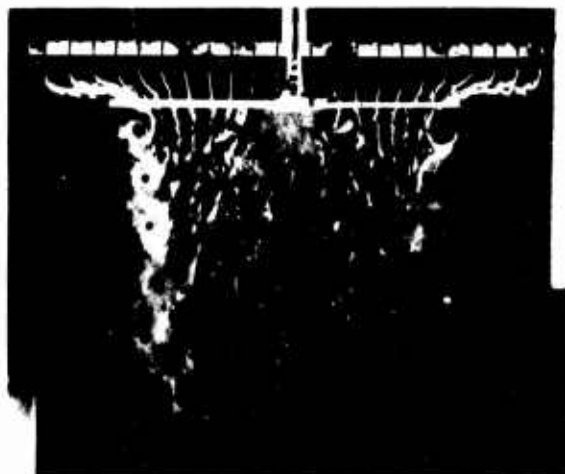


FIGURE 19 EFFECT OF BLADE TWIST ON THRUST AUGMENTATION IN GROUND EFFECT



ROTOR OUT OF GROUND EFFECT



ROTOR 1.0 RADIUS ABOVE GROUND

FIGURE 20 ROTOR DOWNWASH PATTERNS

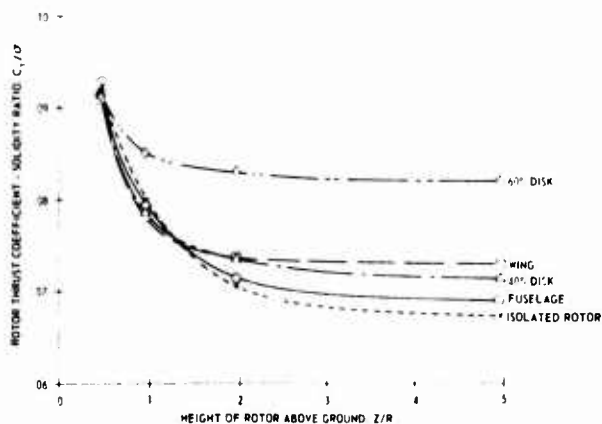


FIGURE 21 VERTICAL DRAG MODELS IN GROUND EFFECT - INFLUENCE ON ROTOR THRUST

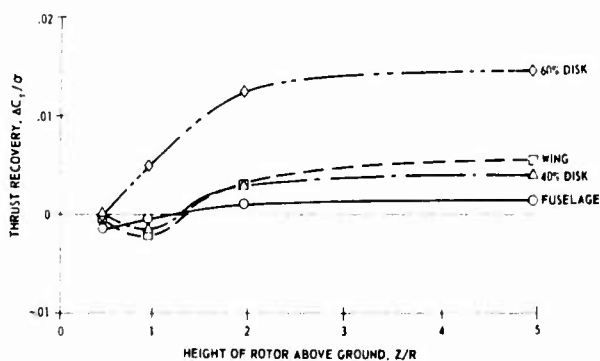


FIGURE 22 VERTICAL DRAG MODELS IN GROUND EFFECT - INFLUENCE ON THRUST RECOVERY

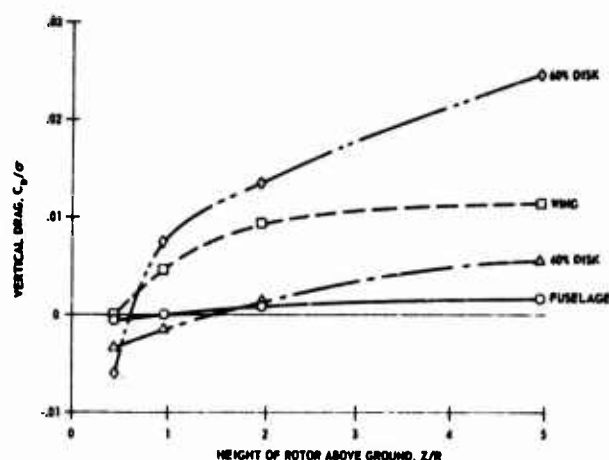


FIGURE 23 VERTICAL DRAG MODELS IN GROUND EFFECT - INFLUENCE ON VERTICAL DRAG

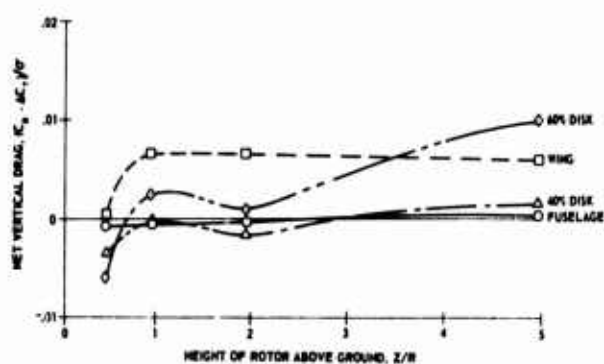


FIGURE 24 VERTICAL DRAG MODELS IN GROUND EFFECT - INFLUENCE ON NET VERTICAL DRAG

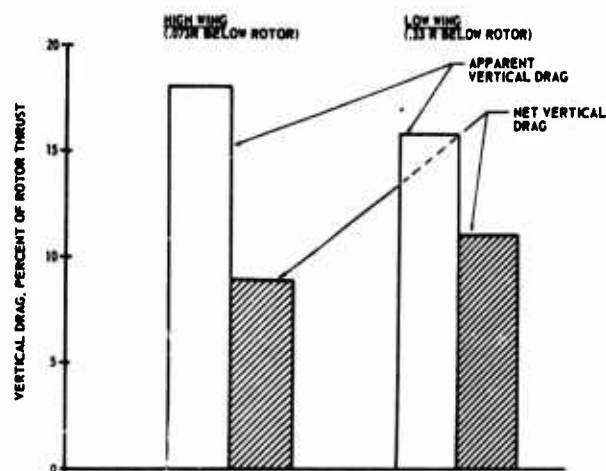


FIGURE 25 EFFECT OF WING VERTICAL LOCATION ON VERTICAL DRAG, OUT OF GROUND EFFECT

THE ROTOR IN AXIAL FLOW

by

Herbert Zimmer
DORNIER AG
Aerodynamics Departement
D-799 Friedrichshafen
Postfach 317
Germany

SUMMARY

The present study is concerned with the rotor in axial flow. It is possible to treat the whole practical region of advance ratios, beginning with large positive values (propellers) over small positive and negative values (helicopters) (part 1) up to large negative values (recovery rotor) (part 2).

Firstly a brief outline of the calculation methods is given. In the first part a vortex method is used, but in the second part a momentum - blade element method was applied on account of widely separated flow. Since these methods have to be used many times during a design cycle or during performance calculations it is important that they are as quick as possible to save computer calculation time.

Finally, a comparison with experimental data is performed for some cases.

LIST OF SYMBOLS

A	Rotor disc area	M	Rotor torque
Δ A	disc area element	Δ M	Torque of rotor blade element
Activity factor = $\frac{100.000}{16} \int_{0.2}^{1.0} \frac{c}{2R} \left(\frac{r}{R}\right)^3 d\left(\frac{r}{R}\right)$		m	Mass flow through rotor disc area element
b	Number of rotor blades	p	static pressure
c	Blade chord at radius r	p₁	static pressure on the upper side of rotor disc area element
c_D	Local blade section drag coefficient	p₂	static pressure on the lower side of rotor disc area element
c_l	Local blade section lift coefficient	p₀	atmospheric pressure
c_{l_i}	Blade section design lift coefficient	R	Total blade radius
c_{Li}	Integrated design lift coefficient = $4 \int_{0.2}^{1.0} c_{l_i} \left(\frac{r}{R}\right)^3 d\left(\frac{r}{R}\right)$	r	radius along blade
c_P Power coefficient = $\frac{0.5 \left(\frac{5HP1}{1000}\right)}{6 \left(\frac{[RPM]}{1000}\right)^3 \left(\frac{2R [ft]}{10}\right)^5}$		r_a	Radius of rotor area acting like an impermeable disc
c_T Thrust coefficient = $\frac{0.1515 \left(\frac{F [lb]}{1000}\right)}{6 \left(\frac{[RPM]}{1000}\right)^2 \left(\frac{2R [ft]}{10}\right)^4}$		r_i	Blade root
c_{WP} Pressure coefficient in turbulent wake behind fast descending rotor = $\frac{p - p_0}{\frac{\rho}{2} V^2}$		R_w	Radius of rotor tip vortex at azimuth angle ψ
Δ D	Drag of rotor blade element	V	Axial free stream velocity
F	Rotor thrust	V_d	Axial velocity through rotor plane = w _i - V
Δ F	Thrust of rotor blade element	V_R	Resulting velocity at rotor blade element
F.M.	Figure of merit = $0.798 \frac{c_T^{(1.5)}}{c_P}$	V_w	Axial velocity at end of wake core
h	Maximum blade profile thickness	v₀	Axial induced velocity at hovering for hypothetical rotor with uniform disc loading = $\sqrt{\frac{F}{2gA}}$
Δ L	Lift of rotor blade element	w_i	Axial induced velocity in rotor plane
		x, y, z	Rectangular coordinate system
		Z_w	Axial displacement of rotor tip vortex at azimuth angle ψ
		α	Rotor blade section effective angle of attack
		α_i	Local induced angle of attack
		β	Blade angle at radius r
		β₀	Blade angle at blade root
		δ	= arctan $\frac{V}{r \cdot \omega}$

$$\epsilon = \arctan c_l / c_D$$

$$\vartheta = \text{Inflow angle} = \arctan \frac{V_d}{r \cdot \omega}$$

$$\lambda_d = \text{nondimensional velocity through rotor plane} = V_d / v_\infty$$

$$\lambda_z = \text{nondimensional rate of descent} = V / v_\infty$$

$$\rho = \text{density of air}$$

$$\rho_0 = \text{sea level standard density}$$

$$\sigma = \rho / \rho_0$$

$$\psi = \text{Azimuth angle}$$

$$\omega = \text{Blade rotational speed} = \frac{2 \pi \text{ (RPM)}}{60}$$

1. HOVERING AND ASCENDING ROTOR (Helicopter, propeller)

This part, which is applicable to propellers and helicopter rotors, is valid in the whole positive advance ratio range over hovering flight up to very small negative values. The method is a vortex-line-blade-element-theory with vortex wake sheets of every blade consisting of several discrete vortices formed by straight line segments.

Especially for small advance ratios the blades of a rotor are operating in the vicinity of the wakes of the preceding blades, therefore a knowledge of the shape of these wakes is necessary to calculate the inflow and forces of the rotor. This is possible by the free-wake-analysis. But in this case no use was made of it, because the calculation time would be too high and because the aim of this study was the ability to take into account different conditions at the blade tips, as different blade tip shapes, radial blowing, tip jet drive.

1.1 THE CALCULATION METHOD

The basic shape of the blade wake vortex model is seen in Fig. 1. In the weakly loaded case the shed vorticity dissipates early, therefore the relatively short blade wakes. In the heavily loaded case, a rolling up of the vortex sheets takes place in general. But this process and the behaviour of the tip vortex is mainly a function of rotor geometry. This is shown by investigations in Ref. 1 and in Fig. 2.

Preliminary flow visualisations in the Dornier water channel (Ref. 7) also showed specific modifications of the tip vortex of a half wing model when altering the geometric wing tip shape. The main trends are also shown in Fig. 2: streamwise outer edges produce a high intensity tip vortex with small diameter. A drooped tip moves this vortex further outward than the not drooped case. Decreasing tip leading edge sweep-back below a certain limiting value ($\approx 60^\circ$) causes a decrease in tip vortex intensity and an increase in diameter. A pointed blade tip with 30° sweep-back showed no tip vortex. (compare with Ref. 11 for force measurements)

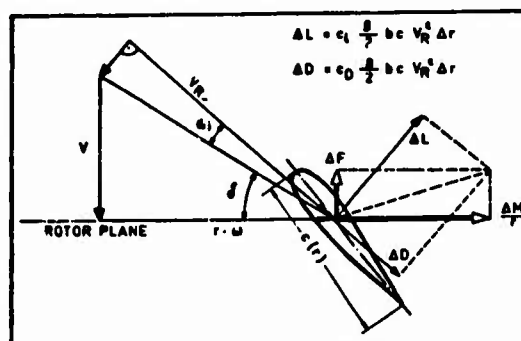
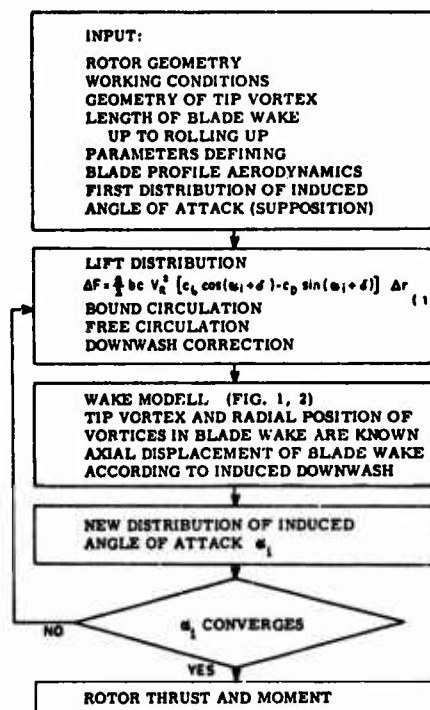
Observations described in Ref. 4 and also those of Dornier tip jet driven test rotors indicate, that the tip vortex follows the tip jet but dissipates early due to strong jet turbulence (Fig. 2).

On this basis a method was developed in which the geometric shape of the tip vortex and its length up to dissipation was prescribed according to the geometric properties of the rotor. Also the length of the several blade wakes up to rolling up is prescribed. The radial contraction of all elemental vortices in these wakes is assumed to be proportional to that of the tip vortex.

The axial position of the wake vortices however and consecutively the inflow angle and downwash distribution is found iteratively as the result of the induction of all vortices. The flow diagram of the computer program is seen in Fig. 0. An average example consumes about 15 sec CPU-time on an IBM/370-155 computer.

FIG. 0

FLOW DIAGRAM OF COMPUTER PROGRAM



1.2 CALCULATED EXAMPLES

The first example is the initial XC-142A propeller as shown in Fig. 3. According to Ref. 2 an extensive propeller research program was conducted because of the obvious static performance thrust deficiency encountered during flight tests. This case seemed to be of interest to check the present method. Because of the uncertainty concerning the drag-rise Mach number of the blade tip profiles two limiting values were taken. The measured values lie well between the calculated curves especially in the heavily loaded case.

In Fig. 4 the calculated performance of the original C-160 Transall propeller is seen. Measurements were not available, therefore a comparison with the brochure (Ref. 9) is made. The take-off performance according to the present method also shows a disagreement with Ref. 9 in the low-velocity and static case. This may be due to the strong blade-vortex interaction and the partly separated flow which is indicated by the thrust capacity in Fig. 4.

Fig. 5 shows the results of an alternative wood propeller design with several blade tip modifications which was chosen on account of structural reasons (Ref. 10). Measurements are not available because these results were used to modify the design. In the low speed range the propeller with swept tips shows the best performance.

As a final example, a Dornier tip-jet driven test rotor was chosen. In Fig. 6 the calculated downwash distribution in the rotorplane is compared with experiment. It can be concluded that the vortex model works also in this case. The measured rotor thrust in Fig. 7 however is higher than predicted. Possibly this is the influence of the dam surrounding the test rig. (Ref. 3). Further studies of this effect are running now.

2. DESCENDING ROTOR (Recovery Rotor)

The second part deals with the powered descending rotor - not with the windmill - for the aim of the present study was the calculation of a recovery rotor. Considering the complicated flow field of a descending rotor with extensive regions of separated flow (Fig. 8) a vortex theory seemed not to be valid. Therefore a special blade-element-momentum theory was developed.

2.1 THE IDEAL DESCENDING ROTOR

Fig. 9 shows the ideal descending rotor according to momentum theory in terms of nondimensional flow through the rotor plane against nondimensional sink rate. The theoretical flow fields are outlined together with a band of measurements. To describe these better, the following approach has been done:

2.2 FAST POWERED DESCENT

In this case the flow through the rotor plane is reverse, high angles of attack occur at the blades, and cause separated flow with constant pressure coefficient as depicted in Fig. 10. This flow is described by Eq. (5) which is also shown in Fig. 10. This equation leads to an ideal autorotation point at $\lambda_z = 2$. The rotor thrust in this case equals $\frac{1}{2} \pi R^2 V^2$ with atmospheric pressure in the rotor wake according to Eq. (4). That means the rotor acts like an impermeable disc with the drag coefficient 1.0. In order to make a more realistic approach with the actual disc drag coefficient the modification according to Eq. (6) has been introduced (Fig. 10 and 11). This model represents a decreasing portion to the impermeable rotor area, when the sink rate is increased. Beyond the sinkrate of 2.3 the flow through the whole rotor plane is again fully reverse.

Eq. (6) can not be solved for the result must be compatible with the blade-element representation according Eq. (7) in Fig. 11. The final solution of Eq. (8) is found iteratively.

2.3 THE VORTEX RING STATE

If the sink rate is decreased below the ideal autorotation value ($\lambda_z = 1.768$) the vortex ring state is entered. To calculate this flow, the approach of Ref. 5 was modified (Fig. 12). The basic considerations are as follows: The wake of a descending rotor behaves like a free jet. The area HIJ in Fig. 12 represents the loss free jet core. In the outside of line IJ the mixing zone begins with a practically constant static pressure. On the line IK there exists no axial velocity. Because this line contains the stagnation point of the onset flow it can be concluded that the static pressure there equals the total head of the onset flow. Experiments confirm this. Therefore the energy theorem can be written in the form given in Fig. 12. Again momentum theory and blade-element theory must be in accordance and Eq. (11) is solved iteratively. But a solution over the whole rotor disc area is found only in the static case. With increasing sink rate there exists an increasing rotor disc area, where Eq. (11) has no solution and when the ideal autorotation is reached there is no solution at all. This undefined rotor area is again replaced by a corresponding impermeable disc, so the flow field is similar to that depicted in Fig. 12.

2.4 CALCULATED EXAMPLES

The calculated performance of a recovery rotor in the region of high sink rates is given in Fig. 13. With the aid of results like this it is possible to establish a pitch schedule for a transition with constant power and RPM. A comparison with experiment throughout the whole transition range is shown in Fig. 14, which represents a quasi-stationary transition at a fixed pitch. Measured and calculated thrust and power agree fairly well from the vortex ring state up to a certain sink rate well beyond the ideal autorotation. Above this sink rate, however, the measured thrust is higher and the measured power is lower than the calculated values.

This behaviour cannot be explained by a lower than atmospheric pressure in the rotor wake using Eq. (4) nor with the blade profile polar curves according to twodimensional measurement.

But from preliminary flow visualisations according Fig. 15 there is some evidence for the existence of free vortices along the blade upper surfaces, which can in fact alter the twodimensional profile characteristics in a favourable direction. Fig. 15 gives also an impression of the selected layout of the recovery rotor. In the cruise condition the rotor is locked and operates as an empennage. For transition it is converted into a rotor with increased diameter due to the centrifugal force.

REFERENCES

- 1 J. Rorke, C. Wells:
The prescribed wake - momentum analysis
Proceedings Third CAL/AVLABS SYMPOSIUM
Aerodynamics of Rotary Wing and V/STOL
Aircraft.
VOL I: Rotor/Propeller Aerodynamics, Rotor
Noise, June 1969
- 2 M. H. Chopin:
Propeller Static Performance Tests for V/STOL
Aircraft. Part I
Technical Report ASD-TR-69-15
- 3 G. H. Timm:
Obstacle induced flow recirculation.
Boeing Scientific Research Laboratory Rep. 94
March 1965
- 4 J. Dunham:
Experiments towards a circulation controlled
lifting Rotor.
The Aeronautical journal of the Royal Aero-
nautical Society.
Jan./Febr. 1970
- 5 W. Castles:
Flow Induced by a Rotor in Power-on Vertical
Descent.
NACA TN 4330, July 1958
- 6 H. Zimmer:
Schuberhöhung an blattspitzengetriebenen Rotoren -
Theoretische Untersuchungen.
Unpublished Dornier-Report 71/33 B, Sept. 1971
- 7 H. Zimmer:
Über die Wirbelbildung an Tragflügeln großer Streck-
kung - Strömungsbeobachtungen im Dornier-Was-
serkanal.
Unpublished Dornier-Report 71/4 B, May 1971
- 8 H. Zimmer:
Ein Rotor im senkrechten Abstieg.
Unpublished Dornier-Report 3306.494.1/2, Oct. 1970
- 9 Hawker Siddeley Dynamics Limited
Performance of 18ft Diameter 4/8000/6 Propeller
for Rolls Royce Tyne Engines.
Performance Brochure No 255, April 1964
- 10 H. Zimmer:
Transall Propellerberechnung.
Unpublished Dornier-Report EA-101/2539, Sept. 1971
- 11 W. A. Spivey e.a.:
New insights into the Design of Swept-Tip Rotor
Blades.
26th. Annual National Forum of the A. H. S.
Washington D. C., June 1970

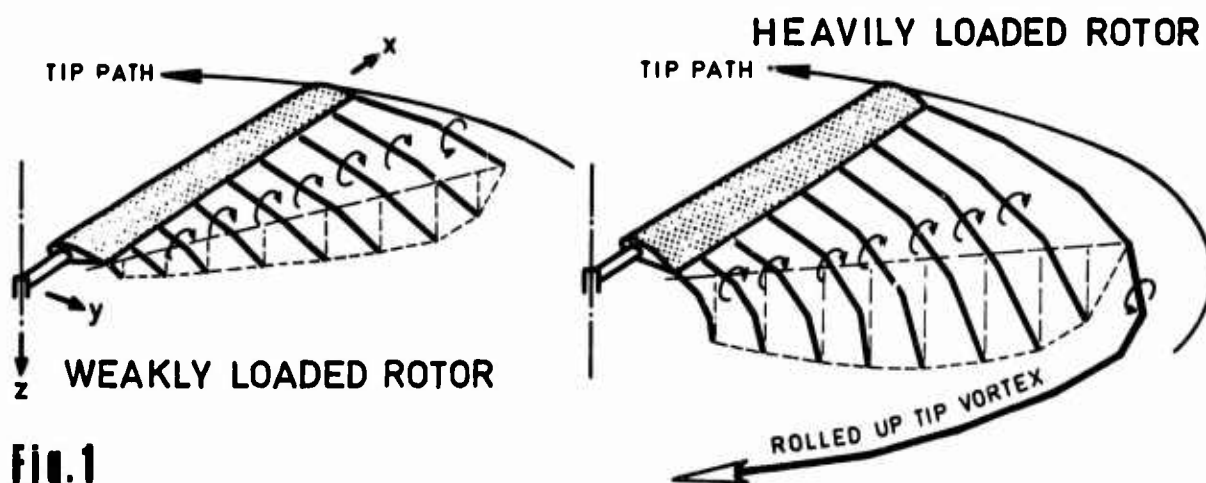
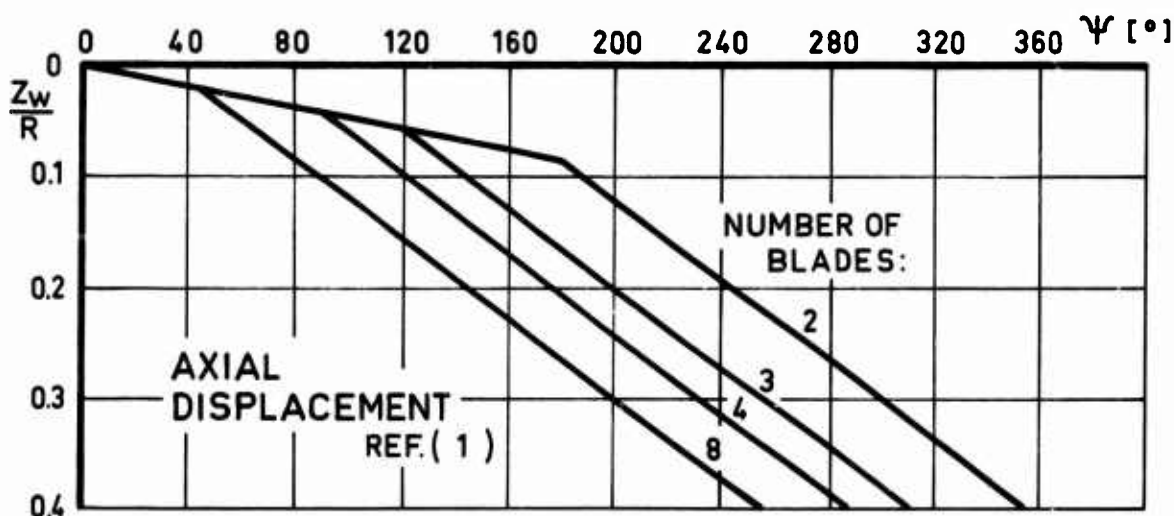


Fig. 1
VORTEX MODEL OF BLADE WAKE



RADIAL CONTRACTION
(INDEPENDENT OF
BLADE NUMBER)

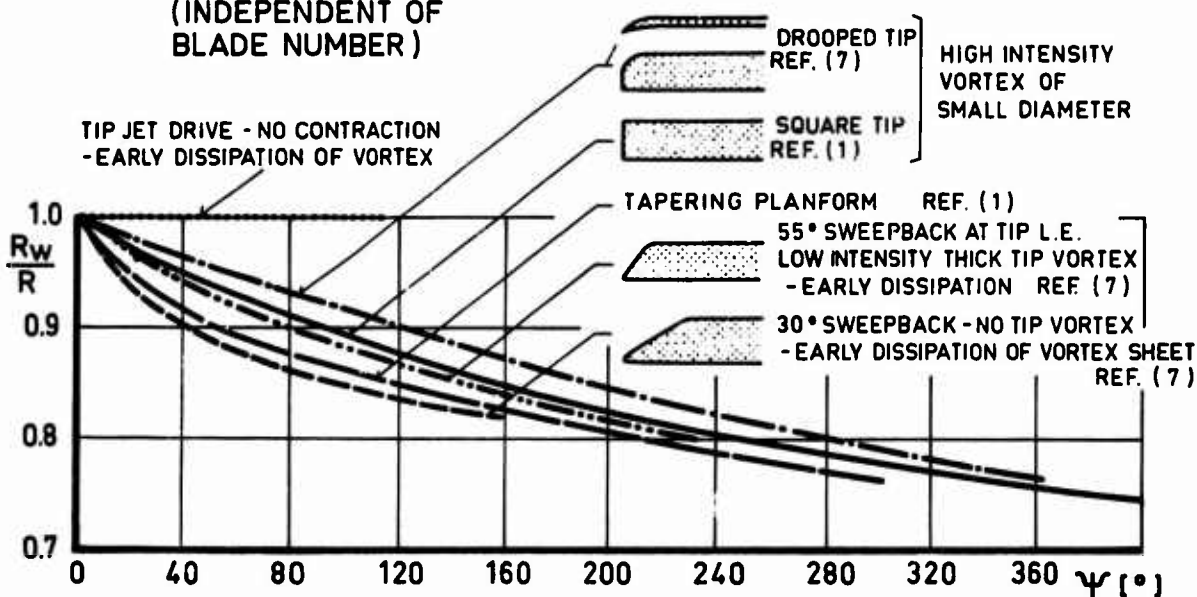


Fig. 2 **GEOMETRY OF ROTOR TIP VORTEX**

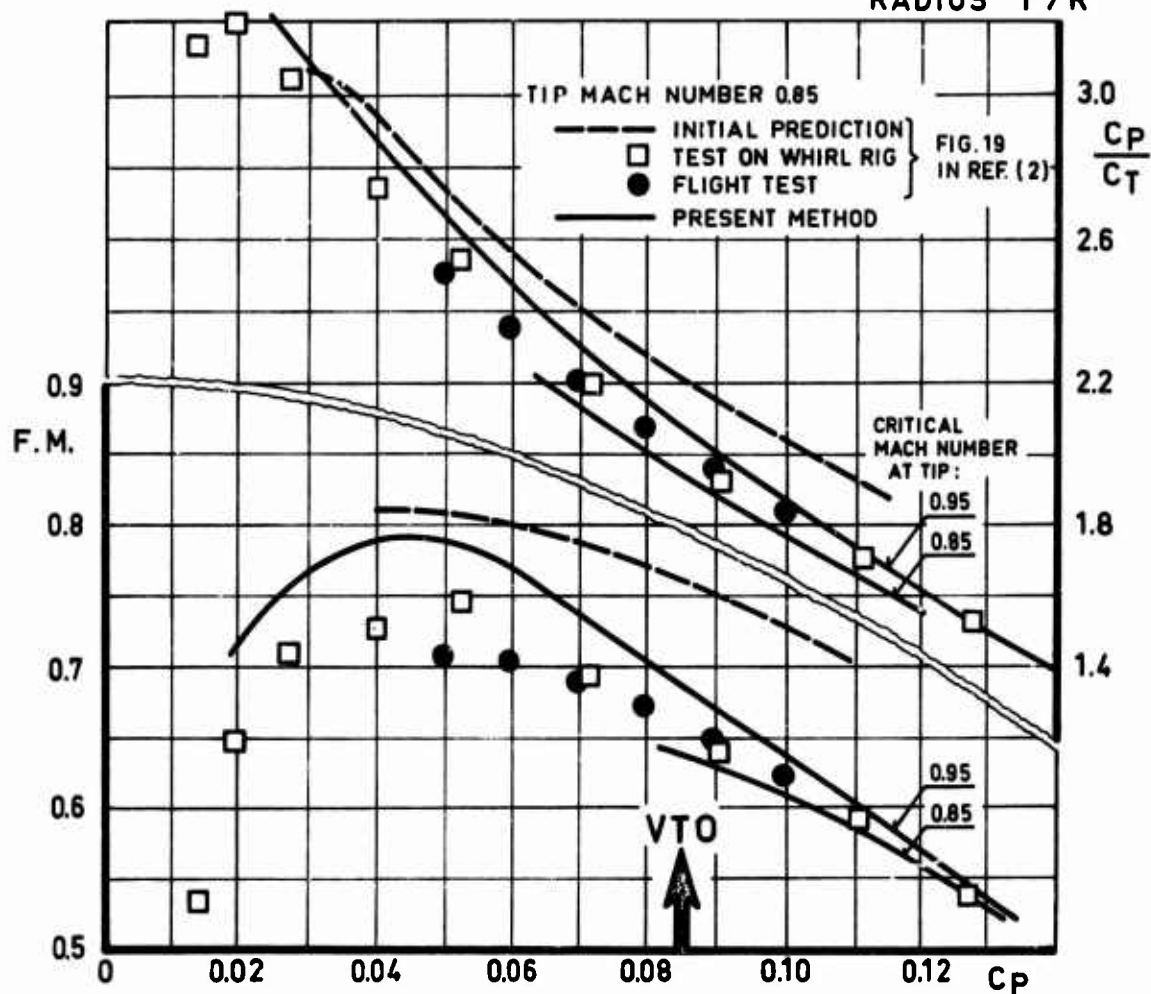
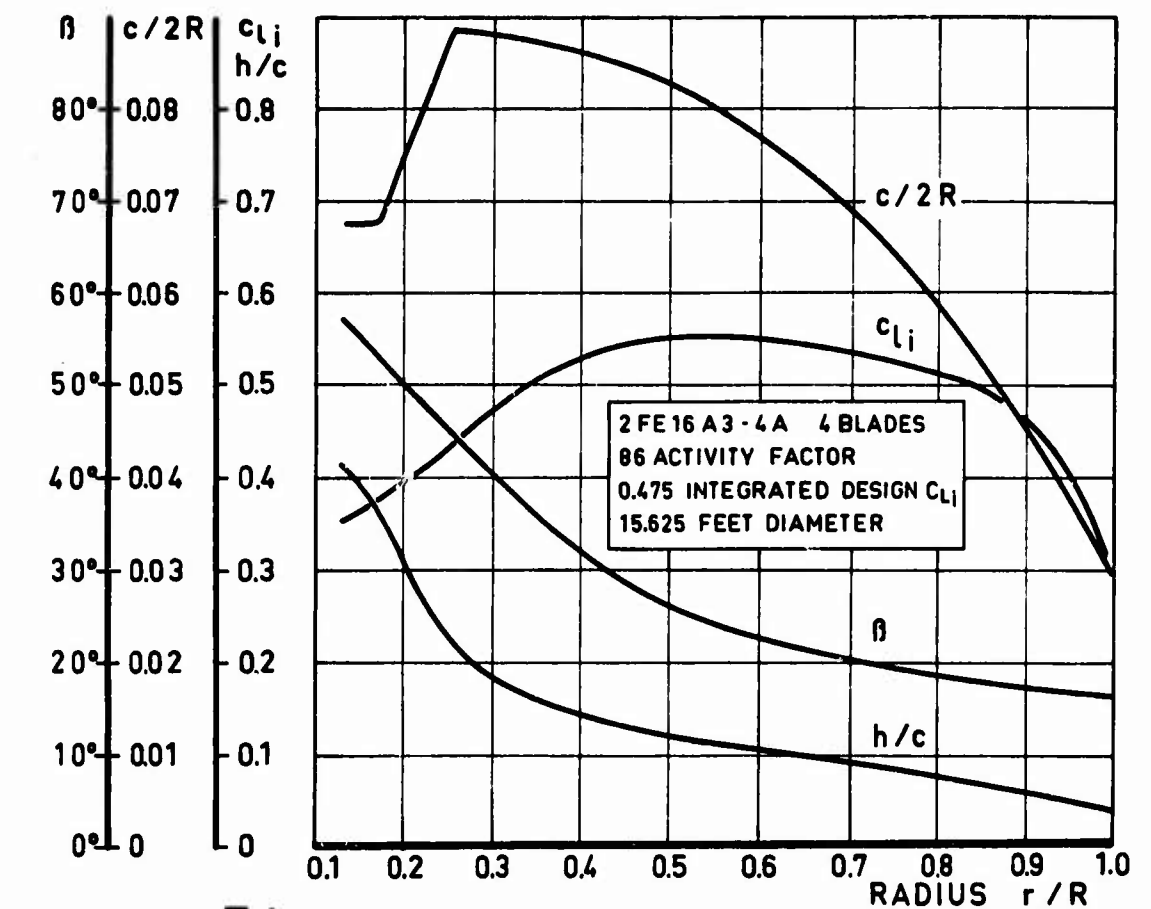


Fig. 3

INITIAL XC-142 A PROPELLER

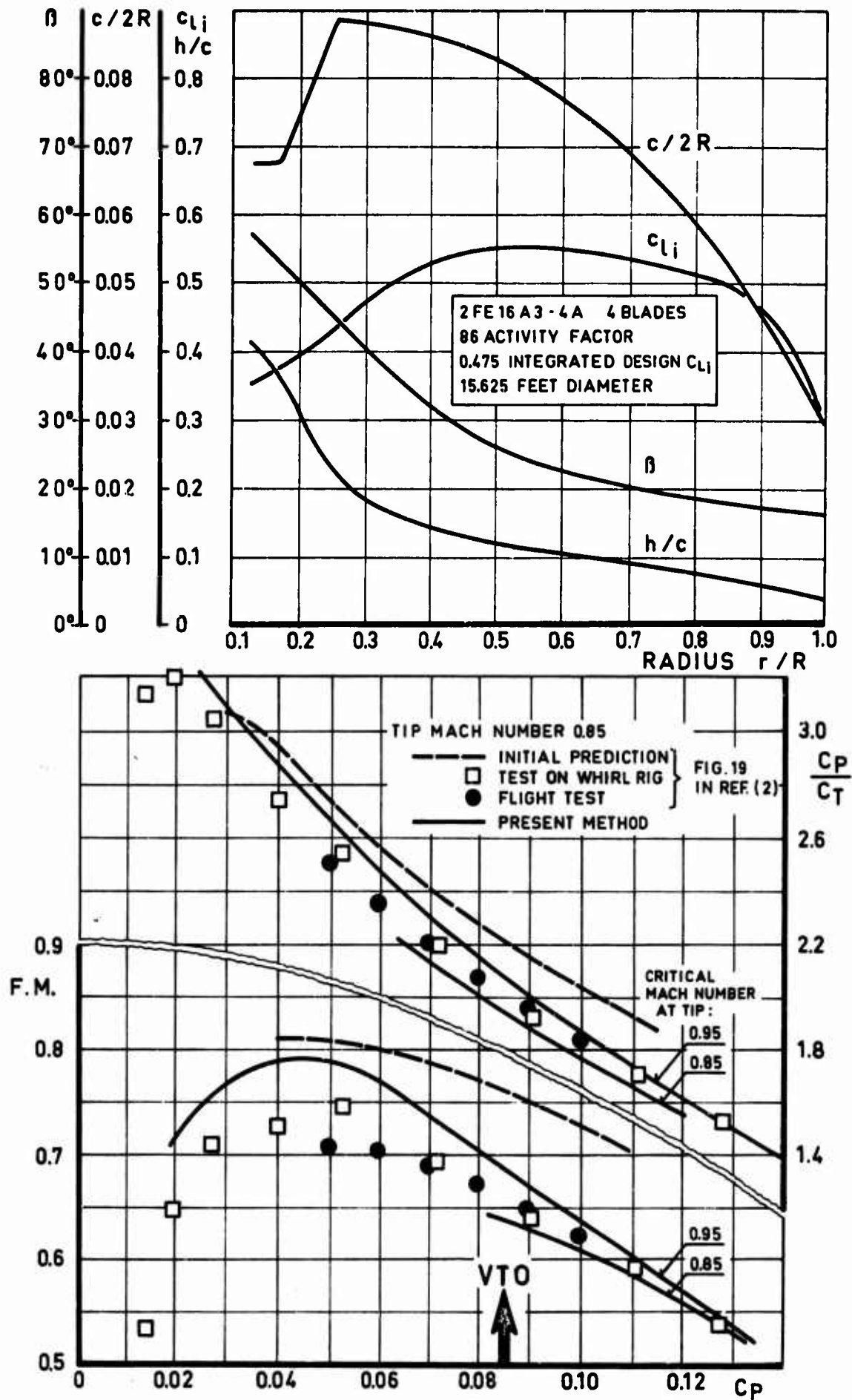


Fig. 3 INITIAL XC-142 A PROPELLER

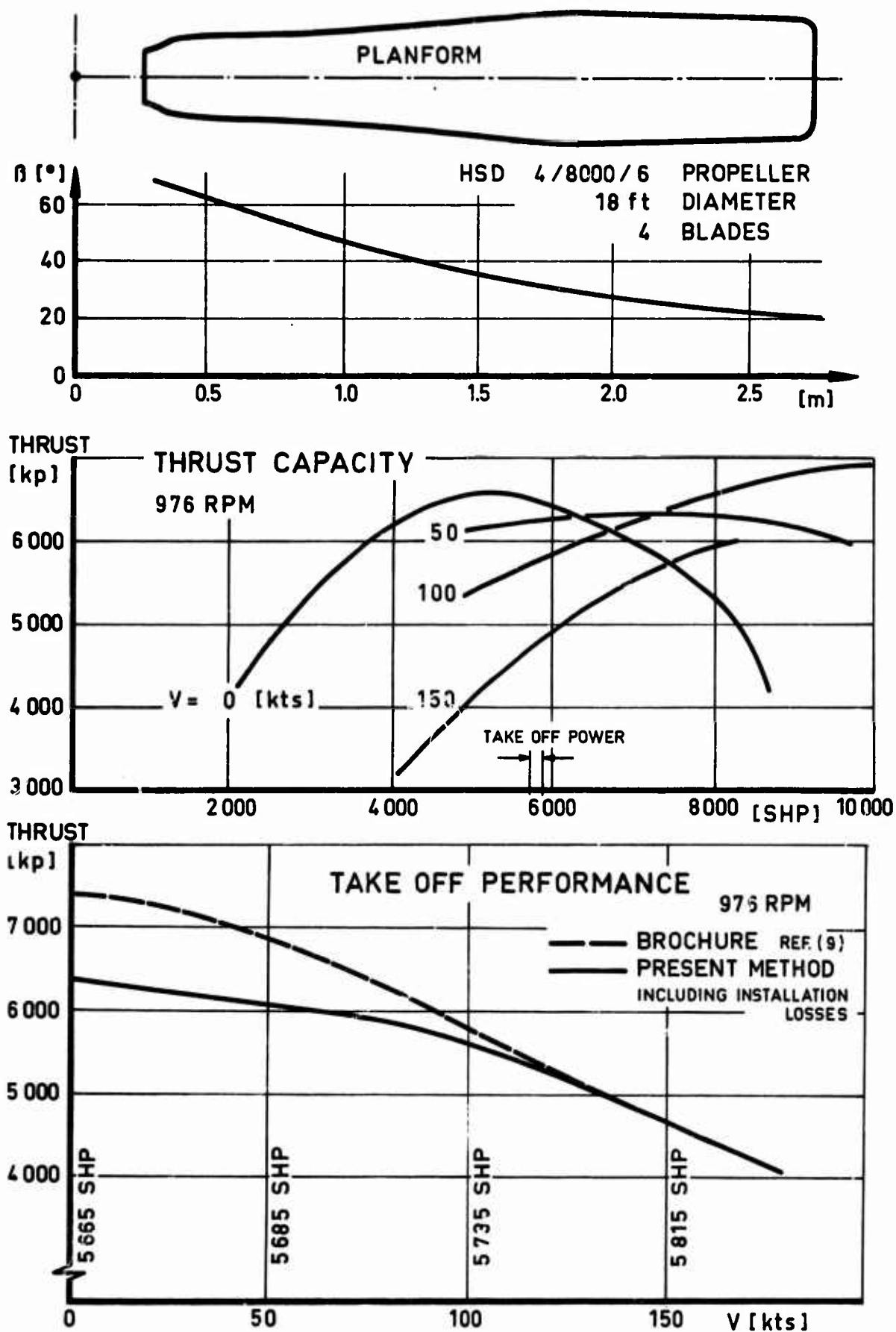


Fig. 4 C-160 TRANSALL METAL-PROPELLER

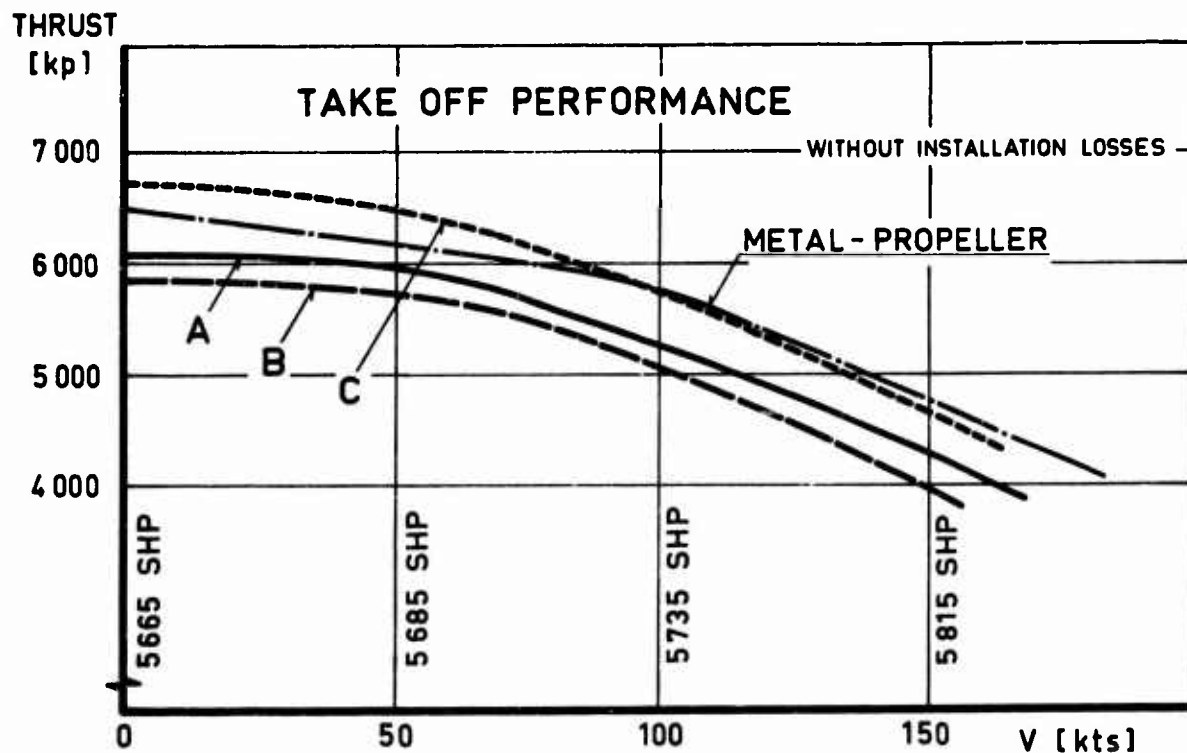
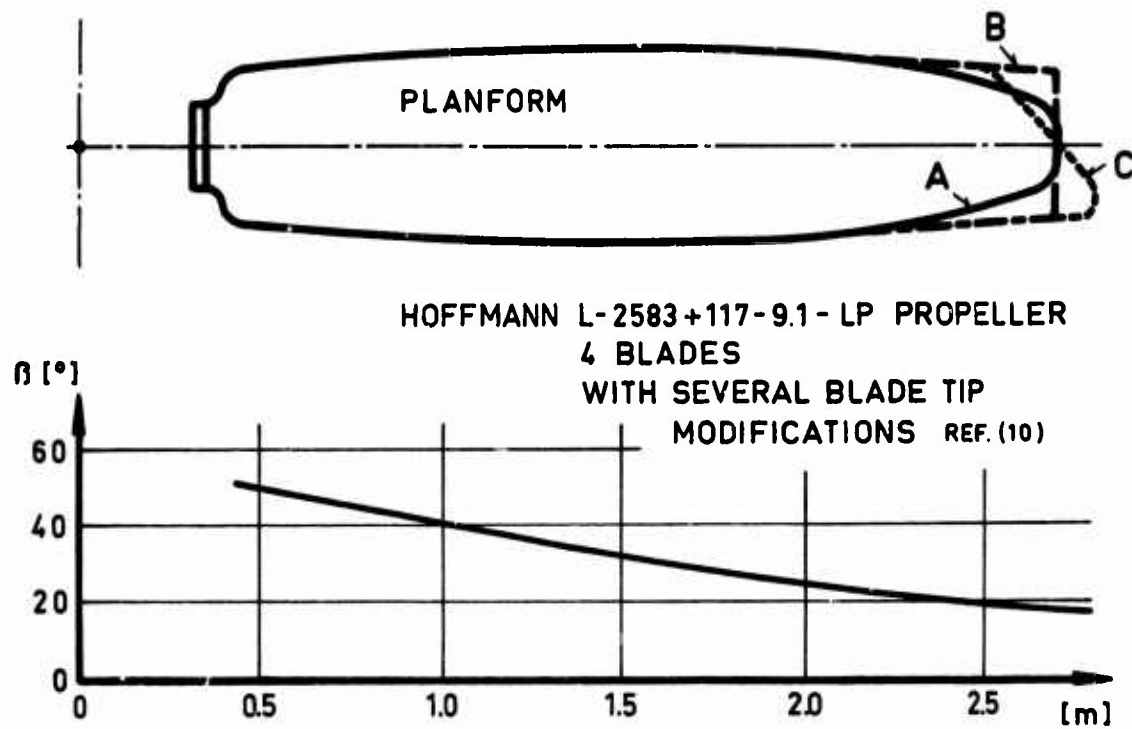


Fig. 5 C-160 TRANSALL WOOD-PROPELLER

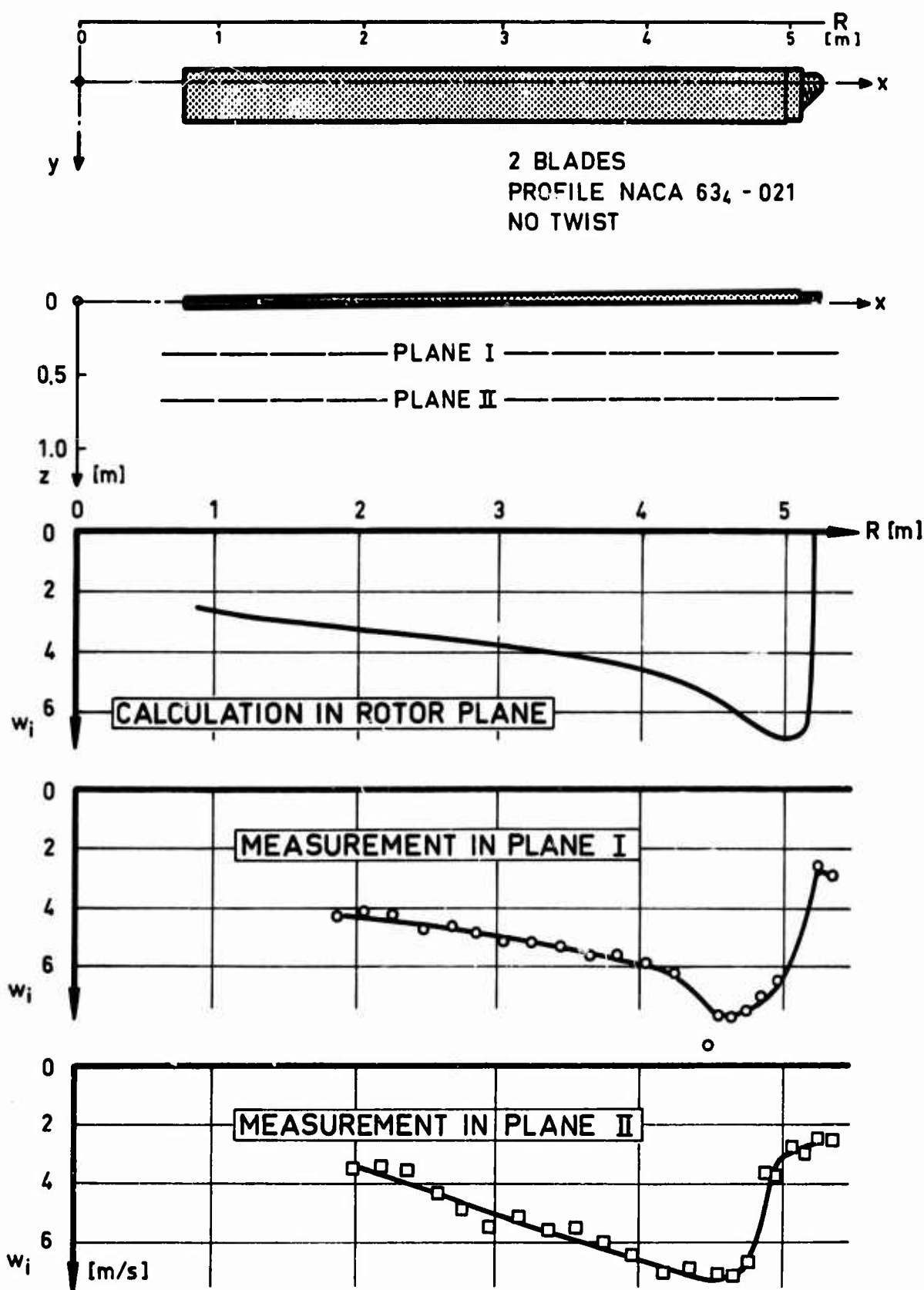


Fig. 6 TIP JET DRIVEN TEST ROTOR
a) DOWN WASH

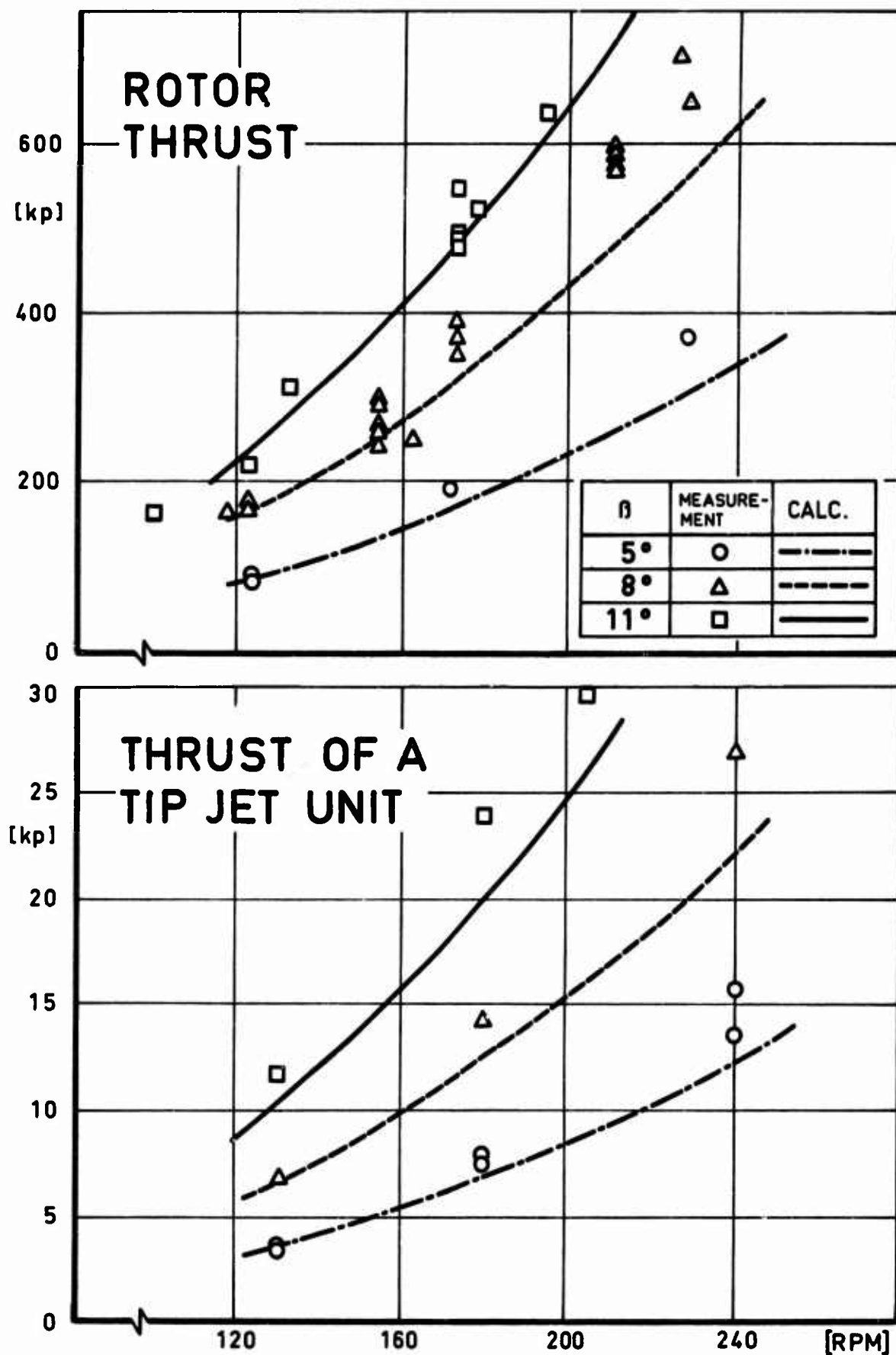
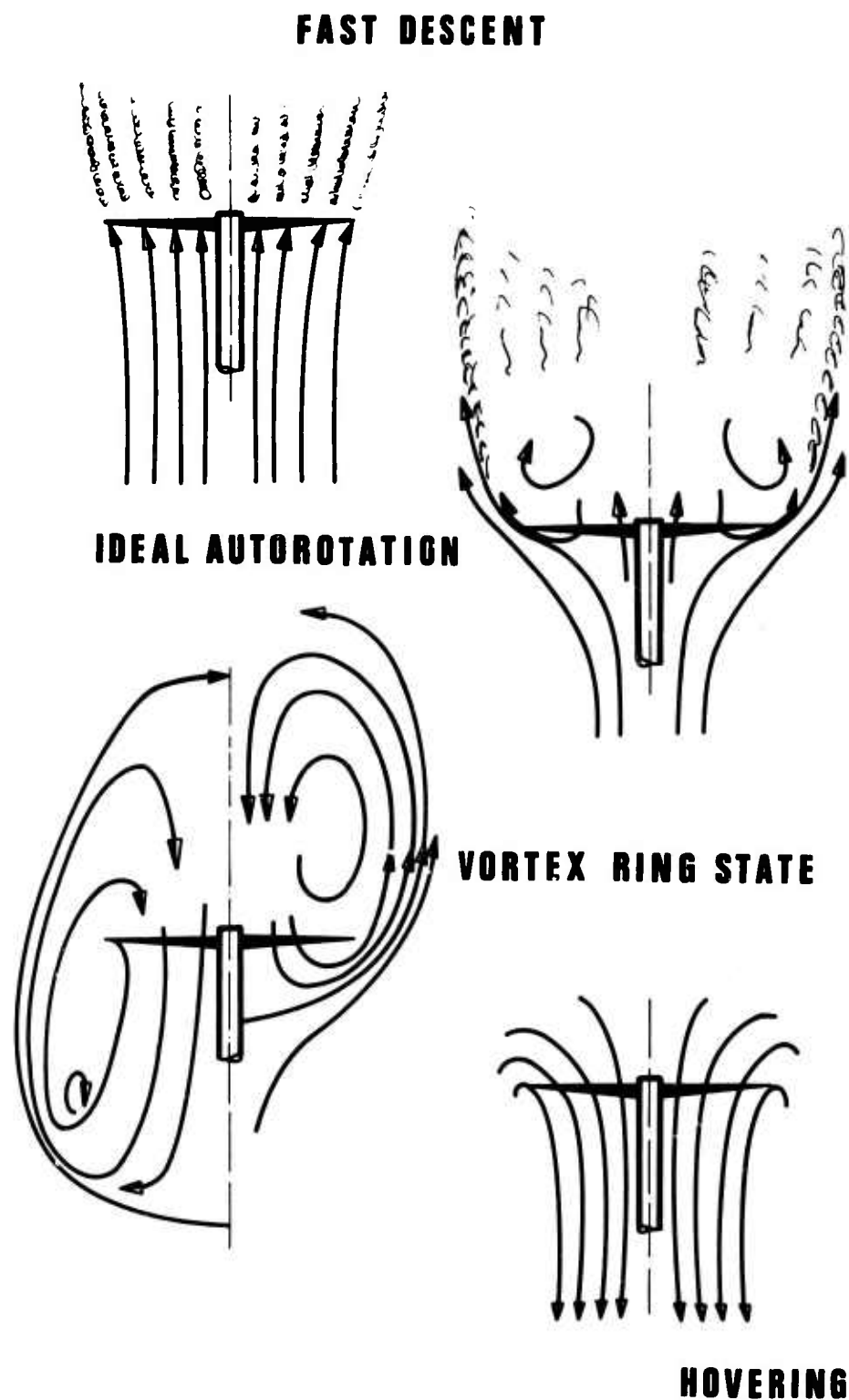


Fig.7 TIP JET DRIVEN TEST ROTOR
b) PERFORMANCE



**Fig. 8 RECOVERY ROTOR
TYPES OF FLOW DURING TRANSITION**

WINDMILLING

$$\lambda_d = \frac{\lambda_z}{2} + \sqrt{\left(\frac{\lambda_z}{2}\right)^2 - 1} \quad (2)$$

POWERED DESCENT

$$\lambda_d = -\frac{\lambda_z}{2} + \sqrt{\left(\frac{\lambda_z}{2}\right)^2 + 1} \quad (3)$$

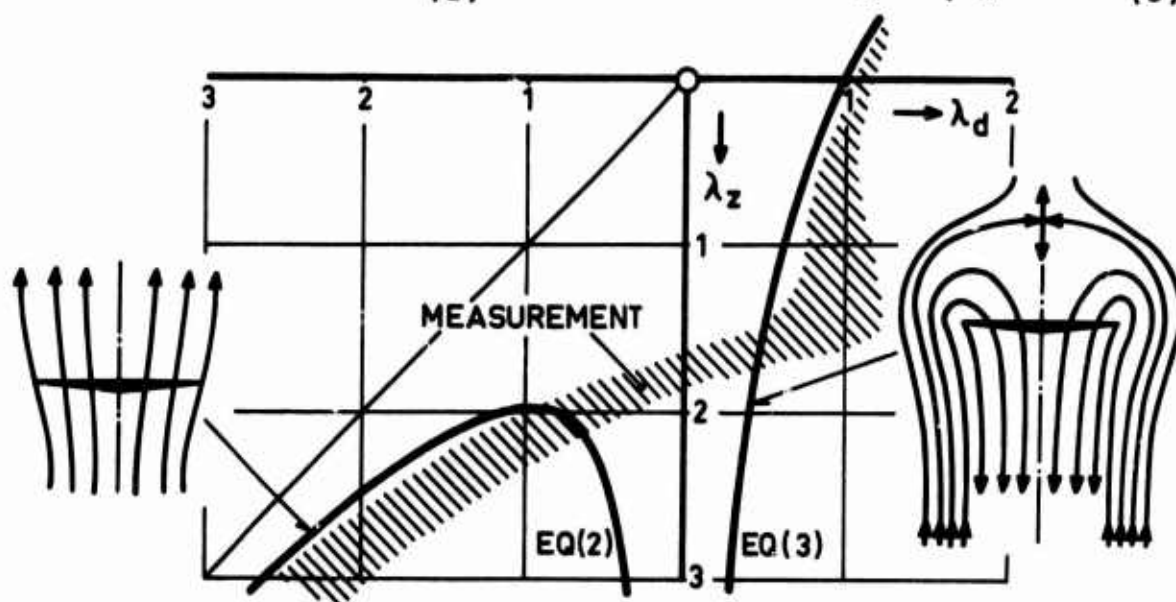
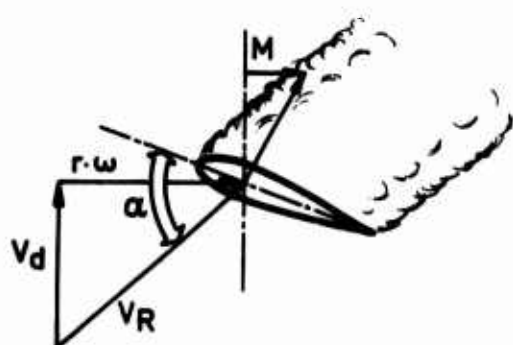


Fig. 9 IDEAL DESCENDING ROTOR



$$F = \frac{5}{2} \pi R^2 [V^2 (1 - c_{wp}) - V_d^2] \quad (4)$$

$$\lambda_d = \sqrt{\lambda_z^2 (1 - c_{wp}) - 4} \quad (5)$$

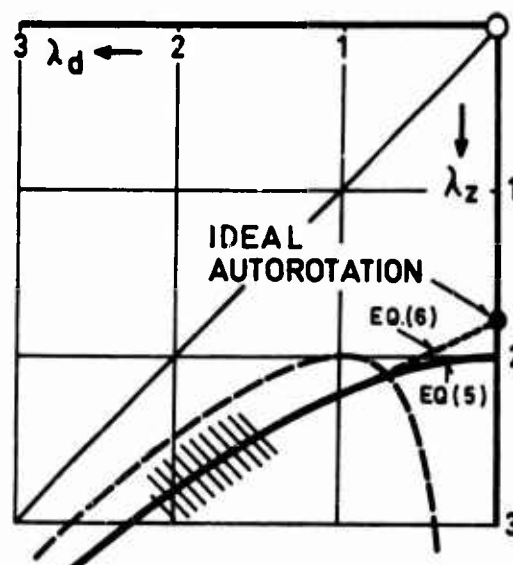
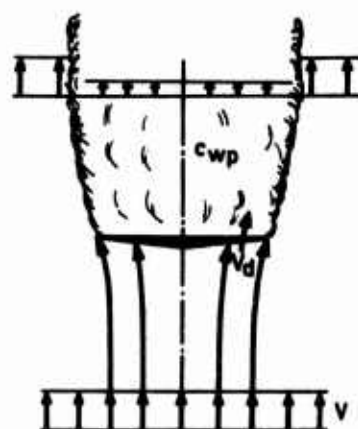
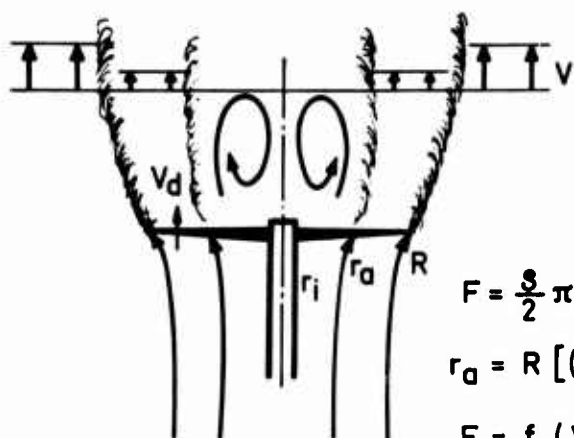


Fig. 10

«REAL» DESCENDING ROTOR

a) FAST POWERED DESCENT

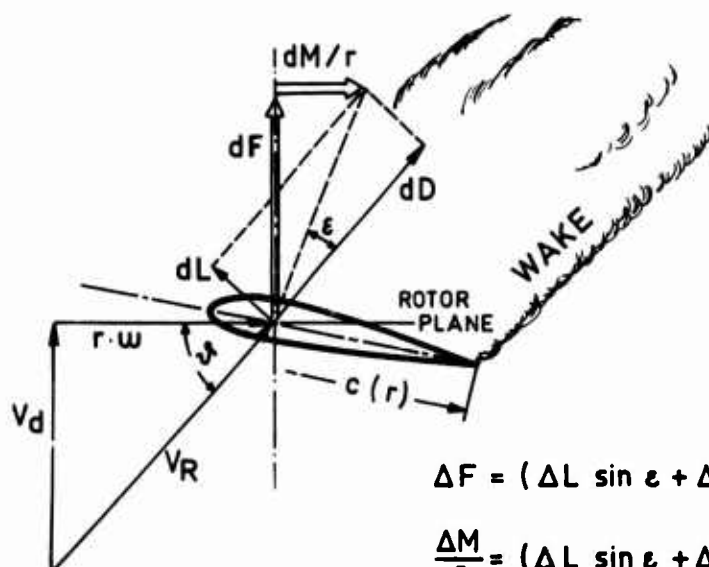


MOMENTUM THEORY

$$F = \frac{3}{2} \pi [V^2 (R^2 + 0.28 r_a^2 - 1.28 r_i^2) - V_d (R^2 - r_a^2)]$$

$$r_a = R \left[\left(1.8797 \frac{r_i}{R} - 1.8797 \right) \lambda_z - 3.3233 \frac{r_i}{R} + 4.3233 \right]$$

$$F = f(V, V_d, F) \quad (6)$$



BLADE ELEMENT THEORY

$$\Delta F = (\Delta L \sin \epsilon + \Delta D \cos \epsilon) \sin(\epsilon + \phi)$$

$$\frac{\Delta M}{r} = (\Delta L \sin \epsilon + \Delta D \cos \epsilon) \cos(\epsilon + \phi)$$

$$F = \frac{3}{2} b \int_{r_i}^R c (r^2 \omega^2 + V_d^2) (c_l \sin \epsilon + c_w \cos \epsilon) \sin(\epsilon + \phi) dr$$

$$F = g(V_d, \omega, \beta, F) \quad (7)$$

$$F = f(V, V_d, F) = g(V_d, \omega, \beta, F)$$

V, ω, β ARE GIVEN

$$F = f(V_d, F) = g(V_d, F) \quad (8)$$

Fig. 11 «REAL» DESCENDING ROTOR

b) FAST DESCENT UP TO IDEAL AUTOROTATION

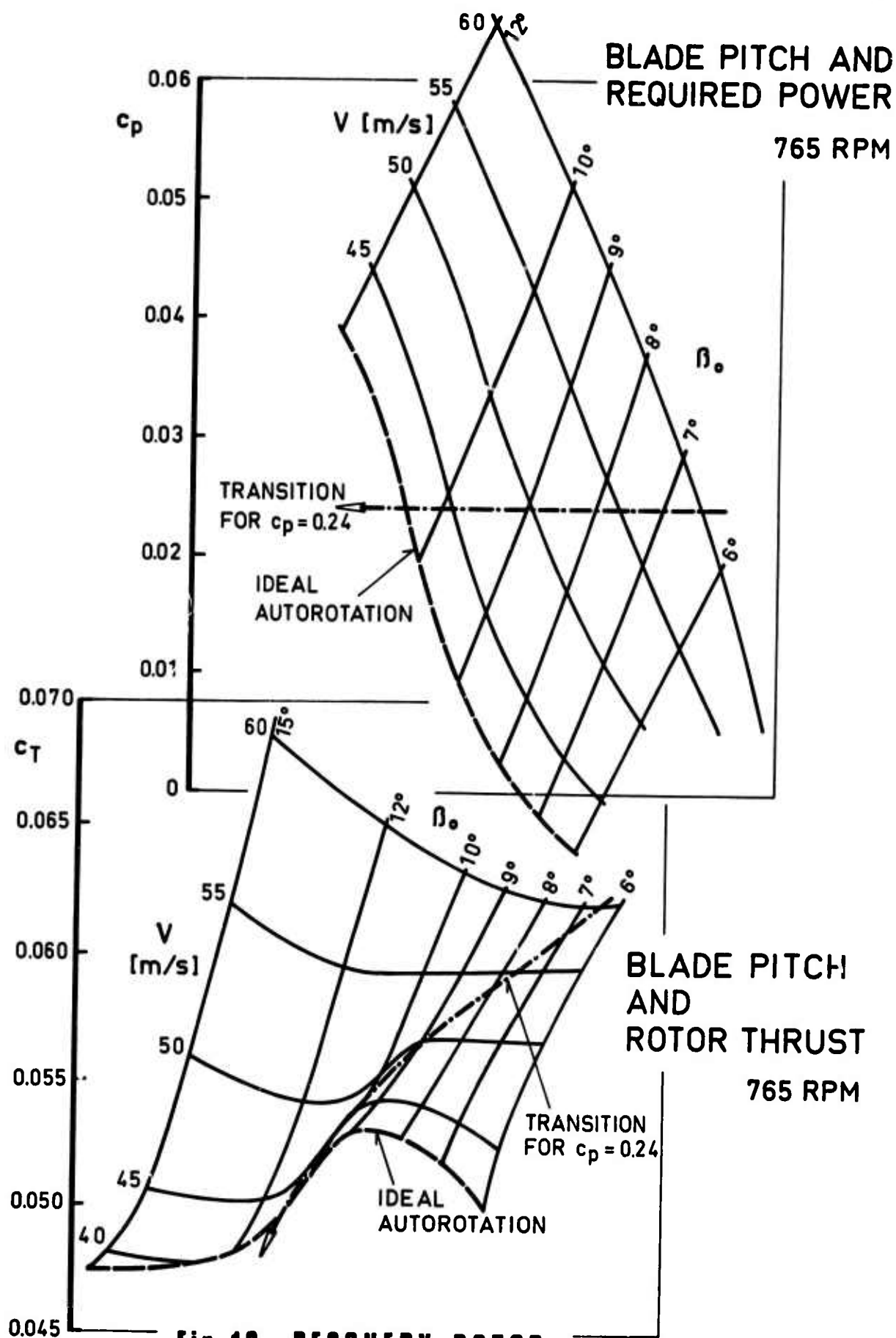


Fig. 13 RECOVERY ROTOR

a) THRUST AND POWER DURING TRANSITION

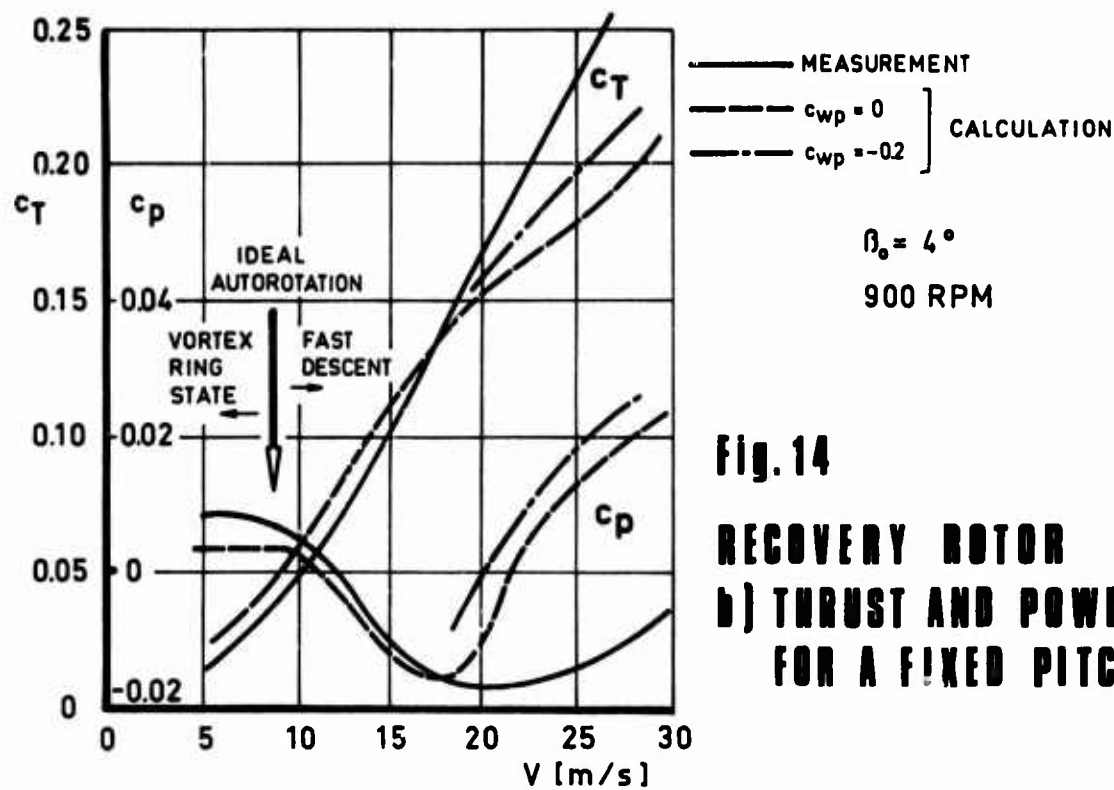
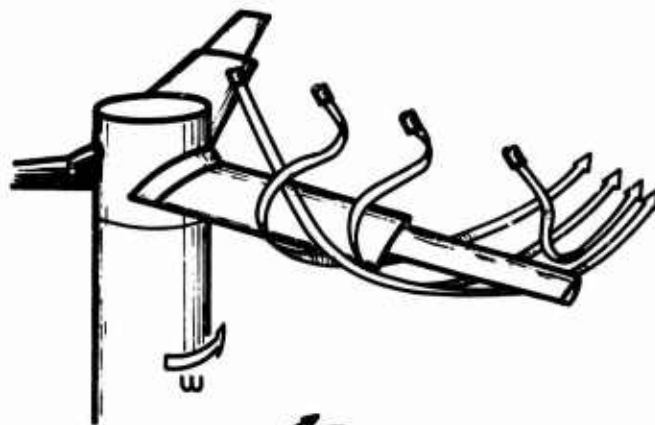


Fig. 14

RECOVERY ROTOR
b) THRUST AND POWER
FOR A FIXED PITCH



SMOKE FILAMENTS



TWO DIMENSIONAL

THREE DIMENSIONAL



Fig. 15

RECOVERY ROTOR
c) FLOW VISUALISATION

THE DEVELOPMENT OF AN EFFICIENT HOVERING
PROPELLER/ROTOR PERFORMANCE
PREDICTION METHOD

by

D.C. Gilmore** and I.S. Gartshore***

SUMMARY

This paper describes the development of a method for predicting the performance of heavily loaded propellers and rotors in steady hovering flight. The method has two particularly useful characteristics: 1) certain simplifying assumptions which allow consistency in the analytical model to be achieved with only a few small scale iterations and 2) a need for only a part of the wake to be specified.

The analytical model, built up from three basic elements, includes a single vortex filament shed from the tip of each blade, a vortex sheet shed inboard of the point of maximum bound circulation on each blade, and an outboard sheet rolling up to form the tip vortex at an arbitrary angle.

Roll-up angle affects the circumferential variation of induced velocity components but not their mean values. Application of the method to three propellers shows that accuracy of results is dependent upon realism of the assumed wake geometry.

The conceptual simplicity of the method and speed of computation make it a potentially useful tool.

** Mr. Gilmore is a staff aerodynamicist at Canadair Ltd.

*** Dr. Gartshore is associate professor of aerodynamics at the University of British Columbia

Notation

SYMBOL	DESCRIPTION	UNITS
A	Constant = $1/\sqrt{2} = .7071$	
A_z	Ultimate Wake Axial Velocity influence factor	
b	Blade Chord/Radius Ratio	
B	Number of Blades	
C	Tip Vortex Radial Contraction Distance/ R_{TIP}	
C_d	Local Drag Coefficient = $D / 1/2 \rho n^2 b R_{TIP}^2$	
C_l	Local Lift Coefficient = $L / 1/2 \rho n^2 b R_{TIP}^2$	
C_p, C_{PW}	Power Coefficient = Power/ $\rho n^3 D^5$	
C_T	Thrust Coefficient = Thrust/ $\rho n^2 D^4$	
C_Γ	Circulation Strength Coefficient = $\frac{1}{4\pi A} \times \frac{b C_{lu}}{2}$	
D	Diameter of Propeller	
e_1	Core Radius of Rolled-Up Tip Vortex and Inboard Sheet/ R_{TIP}^A	
e_3	Core Radius of Outboard Sheet Filaments/ R_{TIP}^A	
F	Azimuth Angle = $2\pi/B$	Radian
F.M.	Figure of Merit = $.798 C_T^{3/2} / C_P$	
k, k_1, k_2	Wake Pitch $dZ/d\psi, k_1$ is used for $0 \leq \psi \leq F$ and k_2 for $\psi > F$	Radians ⁻¹
P_1	Distance Between Element of Vorticity and Point of Interest in Flow Field	Ft
R	Radius, Distance to Radial Station	Ft
u	Total Velocity/ AR_{TIP}	
V	Induced velocity, also rotational velocity at R	Ft/sec.
v	Non-dimensional Induced Velocity = V/AR_{TIP}	
v'	Influence Coefficient in Biot-Savart Law	
x, r	Non-dimensional Radial Position = R/R_{TIP} also Cartesian Coordinate	
y	Non-Dimensional Cartesian Coordinate	
z	Non-Dimensional Axial Coordinate Used in Cartesian and Polar Coordinate Systems	
GREEK		
β, γ_5	Geometric Blade Angle at $x = .75$	
Γ	Circulation Strength = $4\pi A^2 n R_{TIP}^2 C_T$	Ft ² /sec.
λ	Radial Contraction Rate	Rad. ⁻¹
ϕ	Induced Angle = $\tan^{-1} (V_z / r^2 n^2 + V^2 \tan)^{1/2}$	
ψ	azimuth Angle Measured From Lifting Line	Radians
Ω	Rotational Speed	Rad./sec

SUBSCRIPTS

's'	Outboard Sheet Filament
'f'	Filament (especially in inboard sheet)
'm'	End of Filament i.e. where it intersects tip vortex
'o'	Tip Vortex; outboard sheet filament
r,x	Radial Direction
tan, ψ	Tangential Direction
TIP, T	Tip of Blade
y,z	Coordinate Directions

1. Introduction

Work in the last decade on helicopter and V/STOL aircraft has emphasized the need for detailed information on propellers or rotors at an early stage in design. While methods have been available to treat high advance ratio flight conditions (see ref. 1 to 11), as found in conventional propeller driven aircraft, the static thrust case and the low advance ratio condition (with either axial or oblique inflow) have very few design methods which allow predictions of detailed loading distributions to be made. The work described in this paper is aimed at the development and critical assessment of methods capable of predicting the performance of heavily loaded propellers and rotors in steady hovering flight.

The need for accuracy in calculations of VTOL rotor performance can be emphasized by noting that a 1% change in the lifting capability of a rotor, at a given power input, may mean a 10% change in payload for the aircraft, and perhaps the difference between profitable and unprofitable flight operation. A complete analytical prediction would also allow for an optimization of the blade geometry and operating conditions for a given mission requirement.

A review by the authors shows that analytical methods can be classed in one of three categories: 1) single point, 2) potential theory of rigid sheets, and 3) finite element vortex theories. All methods must have as their fundamental aim the prediction of flow conditions at the blade and a means of relating these to the load carried. Moreover, all must maintain consistency between conditions in the wake and those on the blade - this is the basic consistency relation.

Single point methods (1 to 7) require that one representative condition on the blade be related to a corresponding condition in the wake (typically velocity at a particular radius or mean velocity over the radius (13) neglecting the azimuthal variation of velocity). A wide variation in performance predicted from these is possible as shown in Figure 1.

Derivatives of theories (10, 11) in which the wake produced by a propeller in forward flight forms a rigid helical screw surface are classed in the second category. These offer a more realistic picture in that they account for a finite number of blades and maintain precisely the consistency between the assumed wake and blade loading but place restrictions on the velocity variations. The assumption of a rigid screw surface wake follows from the Betz solution (15) to the problem of the wake produced by a propeller with a minimum energy loss in forward flight (i.e. the optimum propeller). Application of the foregoing methods has indicated (17) that they are in general inaccurate and incapable of giving detailed loading information at low advance ratios, a flow region, admittedly, for which they were not designed. See, for example, Figure 2.

Recent efforts to develop theories applicable to low advance ratio operation of propellers and rotors have centred around increasing the accuracy in the modelling of propeller and wake. Flow visualization by Gray (12), Valensi (18) and lately by Adams (19) and Tanner (20) has revealed two basic features of the wake: a) the tip vortex shed from the blade near the tip which rolls up quickly and b) an inboard sheet with vorticity opposite in sense to that of the tip vortex and exhibiting no roll-up. Methods which include these flow features are grouped into the third category-finite element vortex theories. Here a further classification of methods can be made according to the amount of decoupling between blade loading and wake strength. Decoupling enables the consistency relation to be satisfied empirically and is used to reduce the magnitude of the computational effort.

The least decoupling is evidenced in methods (21, 22 and 23) in which the wake is allowed to align itself everywhere with the local flow. These produce the most consistent solutions and are capable of useful accuracy but at the expense of high computation times. At the other extreme (24, 25, 32), methods exist in which the wake is completely specified. These are useful if the wake geometry of an unknown design can be predicted reasonably well in advance. In between, are methods like (26) and (27). The former is concerned with comparing flow fields of a rotor in and out of ground effect while the latter can usefully predict only the inboard flow condition ($0.30 < R/R_p < 0.75$). Erickson (14, 28) tried with moderate success to use a continuous vortex sheet for the wake from each blade which could distort itself into alignment with the local flow within a specified axial variation of induced velocity. Gray (12) and later Gartshore (29) and Gilmore (31) using assumptions broadly based on flow visualization have developed a method in which the wake is partly decoupled - part of the wake is specified and the remainder is calculated.

A review, extension and evaluation of the present authors' partly decoupled model is given in later sections of this paper. In assessing the accuracy of the analytic models and assumptions, it is necessary to have accurate measurements of the mean and instantaneous velocities close to one or more propellers. These can be converted to local blade loadings using well-known strip theory, although the use of strip theory with two-dimensional aerofoil data is itself somewhat uncertain. An overall check on the accuracy can be made by measuring the total thrust and torque on the propeller and comparing these with integrated values of blade loadings calculated from measured inflow velocities.

Measurements of velocity near five propellers were used to evaluate the analytic prediction methods. In the case of the first three, designated as 1967, 1968 and HSD-9 propellers, mean velocities (averaged circumferentially) were measured at specified points in the propeller flowfield using a tuft to indicate direction and a pitot tube to measure velocity magnitude. Interpolation of measured values then gave the velocity components in the propeller plane. This process is called a "flow survey". In addition, the introduction of smoke into the flow used with stroboscopic lighting, provides visualization of the region near the propeller. For the remaining two propellers, direct measurements of the instantaneous velocity were made near the propeller plane using a single hot wire anemometer (30). The azimuthal variation of each velocity component was obtained from the measurements, to provide a further comparison with the results from the vortex wake models.

2.0 The Vortex Wake Model

This section describes the vortex wake models developed by the present authors and the calculation procedures which were used to predict performance of static thrust propellers. Three related models have been tested, as illustrated in figure 3: (a) the "simple" model in which each blade (represented by a lifting line) is assumed to shed a single vortex filament from the tip; (b) the simple model to which has been added an inboard vortex sheet shed from each blade at radii less than that where the maximum bound circulation occurs; and (c) a model in which each blade (again represented by a lifting line) sheds an inboard vortex sheet and an outboard vortex sheet which rolls up rapidly to form a tip vortex. The last model allows roll-up distance to be specified and the outboard sheet strength to be made consistent with the associated bound vortex strength at the blade.

While Gartshore (16) included an inboard sheet representation in his original model, its effect upon the induced field in relation to the tip vortex only was unknown. Calculations carried out by Clark and Leiper (22) on hovering helicopter rotors had suggested that the effect of the inboard sheet might be large under certain blade loading conditions. In addition, the neglect of the rolling up process in modelling the tip vortex of (16) was believed partly responsible for less than satisfactory agreement between measured and predicted performance.

The three basic wake features of the present authors' model, tip vortex, inboard vortex sheet and outboard vortex sheet, are described below.

2.1 The Tip Vortex

The tip vortex in the wake of a static thrust propeller can often be observed. From visualization using smoke and stroboscopic lighting its position may be approximately determined and represented by expressions of the form:

$$R_0 = R_{TIP} (A + C e^{-\lambda \psi_0}) \quad (1)$$

$$\frac{d\psi_0}{d\psi_0} = R_{TIP} k(\psi_0) \quad (2)$$

where: ψ_0 = azimuth angle defined as in Figure 9 with respect to coordinates fixed in space but instantaneously coincident with the blade plane such that $\psi_0 = 0$ is along the quarter chord of one blade.

R_{TIP} = blade radius

A, C, λ = constants

k = axial displacement function

z_0 = axial distance downstream

The tip vortex will have a constant strength if roll-up is not represented explicitly; its strength will vary if roll-up of the outboard vortex sheet is represented. The value of K appears to be approximately constant for $\psi_0 > 2\pi/B$, where B is the number of blades. After studying the flow visualization pictures for one propeller, the following form for K was assumed:

$$\begin{aligned} k &= k_2 (\psi_0 / [2\pi/B])^2 \quad \text{for } \psi_0 \leq 2\pi/B \\ k &= k_2 \quad \text{for } \psi_0 > 2\pi/B \end{aligned} \quad (3)$$

The reasons for choosing this form will be discussed later.

The tip vortex core, an often elusive quantity which is necessary to disguise one shortcoming of potential wake models is discussed in detail in (16). It is possible that this vortex core does not represent a real region which might be observed but rather denotes a region in which the potential model is grossly inaccurate. As such it should be considered as an empirical quantity, to be given a value which provides the most realistic results. As a general rule it appears plausible that the tip vortex core be about equal to the chord of the blade creating the tip vortex. This is not unreasonable since no lifting line theory representing the blade itself is likely to provide accurate information about the velocities in the wake less than one chord from the lifting line.

The strength of the tip vortex, once it is completely rolled up, has been made equal to the maximum bound circulation on the blades. This assumption was suggested by Gray (12) and is an extension of the usual lifting line theory of wings to the propeller case. No easy way of checking this assumption can be found; it is convenient and plausible however.

2.2 The Inboard Sheet

The second major feature of the wake of a propeller is the inboard vortex sheet. Vorticity shed inboard of the point of maximum bound circulation composes the sheet which, by contrast to the tip vorticity, does not roll up and is generally weaker in strength. The sheet is represented in the model by a number of discrete vortex lines or filaments. Assuming the effect of the sheet to be small its position in space has been fixed rather less exactly than was the case for the tip vortex. The position of a filament which was shed at $R = r \cdot R_{TIP}$ is:

$$R_f = r \cdot R_{TIP} (A + C e^{-\lambda g(z_f)}) \quad (4)$$

where

z_f = axial position of the filament

$$= R_{TIP} \int_0^{\psi} k(\psi_0) d\psi_0$$

$g(z_f)$ = value of ψ which makes filaments at z_f lie at the same relative radial positions as those at which they were shed.

$$\frac{dz_f}{d\psi} = R_{TIP} k_f(\psi)$$

k_f = pitch of filaments = constant. Presumably k_f varies for small z_f .

Following Gray's assumption (12) for the tip vortex, considered here to be somewhat too crude for the tip vortex but hopefully accurate enough for the inboard filaments representing the inboard vortex sheet, we assume:

$$k_f = k_1 = \text{const. for } \psi_f \leq 2\pi/B$$

$$k_f = 2k_1 \quad \text{for } \psi_f > 2\pi/B$$

Again, a vortex core must be assumed for the filaments representing the inboard vortex sheet, and again a value roughly equal to the mean chord of the blade appears appropriate.

2.3 Outboard Vortex Sheet

The vorticity which rolls up into the tip vortex must clearly be shed as a sheet; however, little is known about the roll-up process. Flow visualization pictures suggest that roll-up occurs close to the blade.

For computational simplicity the following assumptions were made: that the sheet can be represented by discrete filaments, and that vorticity shed from the blade outboard of the point of maximum bound circulation moves downstream with a characteristic radial contraction (outwards) until it meets the tip vortex. The characteristic contraction is equal to that of the most inboard filament, of the outboard sheet, which must intersect the tip vortex at a specified azimuth angle (the roll-up angle). Each filament upon meeting the tip vortex combines with it, changing the strength of the tip vortex. The position of an outboard sheet filament is:

$$R_e = r_e R_{TIP} (A + C e^{-\lambda_e \psi_e}) \quad (5)$$

If the filament intersects the tip vortex at R_{em}, ψ_r then

$$\lambda_e = -\ln \left[\frac{r_{em} - 1}{r_{en} - 1} \right] / \psi_r \quad (6)$$

$$\frac{d\lambda_e}{d\psi_e} = k(\psi_e) R_{TIP}$$

where:

λ_e = roll-up rate (characteristic contraction) of outboard sheet filament (rad⁻¹)

ψ_r = Roll-up angle - rad.

r_{em} = radius at which most inboard filament joins tip vortex

r_{en} = radius at which most inboard filament is shed from lifting line.

As roll-up angle decreases, the outboard filaments become more radially oriented and ultimately coincide with the bound vortex or lifting line when $\psi_r = 0$. This causes the effect of the outboard sheet to decrease and the model to approach the simpler lifting line and tip vortex representation. Various values of vortex core size for the filaments of the outboard vortex sheet have been tried but, again, a value of this quantity roughly equal to the blade chord is appropriate. In the calculation of the outboard vortex sheet position and effect, the tangential induced velocity V_ψ was neglected by comparison with the blade rotational velocity. This assumption could easily be improved, if required.

2.4 Basic Equations

The flow field is assumed to be potential, satisfying Laplace's Equation in three dimensions so that the influence of vortex elements in the field can be superposed. Once the geometry and strength of the trailing vortex filaments are known, the velocities at any point in the flow field can be calculated. In representing the vortex sheets, the filament circulation strengths are made equal to the difference in bound circulation on the lifting line between the shedding radial station and the next outboard station where the next filament is shed. Using the assumption of two-dimensionality at each radial station, the bound circulation from the Kutta-Joukowski rule is:

$$\Gamma_o = -\frac{1}{4\pi A} \cdot \frac{b C_L u}{2} \quad (7)$$

where:

Γ_o = bound circulation at radius r

b = chord to radius ratio

C_L = local lift coefficient

u = local total velocity = $[v_z^2 + (R\Omega + v_\psi)^2]^{1/2} / \Omega R_{TIP} A$

Considering a tip vortex element of circulation strength Γ_0 , a velocity is induced at a point r, ψ, z as given by the integral form of the Biot-Savart law (see ref. 16) which reduces here to:

$$\begin{aligned} v_r &= \Gamma_0 \int v_r' / P_i^3 d\psi_0 \\ v_\psi &= \Gamma_0 \int v_\psi' / P_i^3 d\psi_0 \\ v_z &= \Gamma_0 \int v_z' / P_i^3 d\psi_0 \end{aligned} \quad (8)$$

where:

$$\begin{aligned} v_r' &= v_x' \cos \psi_0 + v_y' \sin \psi_0 \\ v_\psi' &= -v_x' \sin \psi_0 + v_y' \cos \psi_0 \\ P_i &= [(x-x_0)^2 + (y-y_0)^2 + (z-z_0)^2 + e^2]^{1/2} \end{aligned}$$

and:

$$\begin{aligned} v_x' &= -\frac{dz_0}{d\psi_0} (y-y_0) + \frac{dy_0}{d\psi_0} (z-z_0) \\ v_y' &= -\frac{dx_0}{d\psi_0} (z-z_0) + \frac{dz_0}{d\psi_0} (x-x_0) \\ v_z' &= -\frac{dy_0}{d\psi_0} (x-x_0) + \frac{dx_0}{d\psi_0} (y-y_0) \end{aligned}$$

From equations (1), (2) and (3),

$$\begin{aligned} x-x_0 &= R \cos \psi - R_{TIP} (A + C e^{-\lambda \psi_0}) \cos \psi_0 \\ y-y_0 &= R \sin \psi - R_{TIP} (A + C e^{-\lambda \psi_0}) \sin \psi_0 \\ z-z_0 &= \begin{cases} z - \frac{k_z R_{TIP}}{F^2} \cdot \frac{\psi_0^3}{3} & \text{for } \psi_0 \leq 2\pi/B \\ z - k_z R_{TIP} \cdot \psi_0 & \psi_0 > 2\pi/B \end{cases} \end{aligned}$$

so that:

$$\begin{aligned} \frac{dx_0}{d\psi_0} &= -AR_{TIP} \left(\frac{R_0}{AR_{TIP}} \sin \psi_0 + \lambda \left(\frac{R_0}{AR_{TIP}} - 1 \right) \cos \psi_0 \right) \\ \frac{dy_0}{d\psi_0} &= AR_{TIP} \left(\frac{R_0}{AR_{TIP}} \cos \psi_0 - \lambda \left(\frac{R_0}{AR_{TIP}} - 1 \right) \sin \psi_0 \right) \\ \frac{dz_0}{d\psi_0} &= \begin{cases} k_z R_{TIP} \left(\frac{\psi_0}{F} \right)^2 & \text{for } \psi_0 \leq 2\pi/B \\ k_z R_{TIP} & \psi_0 > 2\pi/B \end{cases} \end{aligned}$$

Similar equations apply for the filaments representing the vortex sheets, the changes occurring only in the geometry of the filaments.

Numerical techniques were applied in the solution of equations (8) and the simplifications which were used in their application are described in the next section.

2.5 Approximations Used

In spite of the close specification of the wake by equations (1) to (6) it is not complete and several "free" constants remain to be fixed: A, C, k_1, k_2, λ

Since the tip vortex is assumed to leave the blade tip,

$$A + C = 1 \quad (9)$$

and from simple momentum models for propellers,

$$A = 1/\sqrt{2}$$

These assumptions are made, leaving k_1, k_2 and λ to be determined.

If one considers only the ultimate wake*, far from the propeller, the tip vortex has a helical shape of constant pitch and radius. Since the tip vortex is the dominant feature in the flow field, in the ultimate wake at least, we assume that it is the only part of the wake affecting its own position and motion. On this basis, the axial velocity of the helical vortex in the ultimate wake can be determined and hence its pitch can be found. The helix angle is equal to ϕ_1 where:

$$\phi_1 = \tan^{-1} (V_{z_0} / (R_0 \Omega + V_{\psi_0})) \quad (10)$$

is evaluated for $\psi_0 \rightarrow \infty$. Here V_{ψ_0} is the velocity of the filament in the direction of increasing ψ ; V_{z_0} , the velocity of the filament in the axial direction; Ω , the rotational velocity of the propeller, and AR_{TIP} , the radius of the tip vortex centreline in the ultimate wake. Since $k_2/A = \tan \phi_1$, from the geometry of the tip vortex, equation (10) allows a value of k_2 to be calculated from the velocities V_{z_0} and V_{ψ_0} .

In a similar fashion for the inboard sheet k_1 may be found by calculating the axial and tangential velocities in the ultimate wake at a radius occupied by one of the filaments. In this connection, since the tangential velocity term is always small compared with $R\Omega$, this part of the expression has been omitted, leaving

$$\frac{dz_f}{d\psi_f} = 2k_1 R_{TIP} = \frac{(V_z)_f}{\Omega} \quad (11)$$

evaluated where $\psi_f \rightarrow \infty$

To evaluate $(V_z)_f$, the velocities associated with or induced by the tip vortex and all filaments of the inboard vortex sheet at radii larger than that at which the one in question lies, are added.

The omission of all velocities associated with filaments inboard of the one under consideration follows the observation that the velocities induced by a helical vortex are usually much larger inside the helix than outside. In the limit, as the helix angle decreases to zero, this solenoidal approximation becomes exact, since the velocity then is zero outside the helix while it is non-zero and uniform inside.

The one remaining constant in equations (1), (4) and (5), λ , is found from the variation of radial position of the tip vortex with azimuth angle as determined from flow visualization pictures.

Several simplifications of the numerical procedure were used to shorten computing time. The velocity at the propeller plane associated with the ultimate wake tip vortex can be found with fair accuracy once and for all, by the following method. Since the ultimate wake tip vortex is a regular helix of constant pitch and radius the velocity associated with it will be nearly proportional to the circulation strength per unit length of cylinder. This would be exactly true for an infinite length of closely packed vortex rings, that is, in the limit when the helix angle goes to zero. Now the strength per unit length of one helical tip vortex is

$$\frac{d\Gamma_0}{dz} = \frac{\Gamma_0}{(2\pi AR_{TIP}) \frac{k_2}{A}} \quad (12)$$

where:

Γ_0 = the tip vortex strength

AR_{TIP} = radius of tip vortex in the ultimate wake.

If the velocities V_z are found for the tip vortex and divided by Γ_0/k_2 the resulting parameter

$$A_z = V_z / (\Gamma_0/k_2) \quad (13)$$

should be a constant for a fairly wide range of values of Γ_0 and k_2 , provided that Γ_0 and k_2 are consistent with each other. This assumption was checked for values of Γ_0 ranging over those expected in propeller calculations and was found to be reasonably correct (within a few percent in velocity V_z). Since the contribution to total V_z

* See comments in section 3.0 and 3.4 on the measured extent of the organized wake downstream of two propellers.

at the propeller from the ultimate wake (say for $z \geq \frac{1}{2} R_{TIP}$) is usually about 10% of the total, this error is small. Use of this approximation shortens computing time considerably. V_ψ cannot be found in this way with comparable accuracy but is small in any case, compared with ΩR_{TIP} .

For calculating the contribution to the velocities at the propeller plane from the inboard filaments in the far wake an identical scheme could not be adopted, since the helix angles of the inboard filaments in the ultimate wake are greater than are those of the tip vortex. In this case A_z was not assumed constant but was allowed to vary with helix angle of the vortex filament. It was assumed constant with radius, however, an assumption which when checked was found reasonably valid inside the filament helix radius. Again, calculating the contribution of the vortex filaments in the ultimate wake to velocities at the propeller plane by this method reduces computing time considerably.

The velocities in the ultimate wake associated with either the tip vortex or the inboard filaments may be calculated, once and for all, and a table constructed of values of A_z and k_z for this case, to be used for all subsequent calculations. This was done, again shortening computer time.

2.6.1 Results from Flow Visualization

Since the tip vortex is considered to be the dominant part of the flow field, it is important to locate it with fair accuracy. To do this, flow visualization photographs showing the vortex position for various blade azimuth angles were used to plot the vortex position. Three propellers were studied and are discussed below:

- 1) The 1967 propeller (4 blades) at 12° and 14° blade angle was studied. The tip vortex location is plotted in figures (4a) and (4b) as R_o/R_{TIP} and z_o/R_{TIP} against ψ_o .

There is a sudden change in axial location of the vortex when it passes beneath the next blade ($\psi_o \approx 90^\circ$). There appear to be further sudden jumps, of lower magnitude, at larger angles (about 230° and 320°, on the $\phi_{.75} = 12^\circ$ survey).

The radial contraction, while not well defined by the points, appears smooth. The tip vortex appears to stay near the propeller plane for the first 90°, then move away with nearly constant helix angle. These observations are reasonably well fitted by the equations (1) to (3) which are also represented on figures (4a) and (4b).

It is worth noting that for the first 90° the tip vortex lies less than one-half chord length below the propeller plane. This distance is certainly smaller than that for which lifting line theory is usually employed and provides cause for skepticism in the present calculation.

- 2) Data from the second propeller studied, the 1968 propeller, is presented in Figures (5) to (8) in the same form as that for the 1967 propeller.

The original version of the 1968 propeller, the 'A', at the 12° blade angle is shown in Figure (5). The circled points follow the normal radial contraction envelope shape within a 10% tolerance band, while the axial position increases gradually for $\psi < 90^\circ$ and then abruptly exhibits a jump in slope for $\psi \sim 90^\circ$ characteristic of four bladed propellers. A larger amount of scatter about the usual straight line variation is evident for the axial position. In addition, the first indication of a secondary, weak tip vortex, is shown by the crosses. Extrapolation of these points suggests that this weak vortex is shed from $R/R_{TIP} = 0.88$, a radius close to where a rather large change in slope of the radial distribution of blade angle occurs. The axial position of this secondary vortex at any azimuth always appears to be downstream of the strong tip vortex, and follows a similar variation.

Data from the "B" version of the 1968 propeller is plotted for 14° and 17° blade angle in Figures 6 and 7. The "B" blade geometry is noteworthy in that an even more abrupt slope change in blade angle distribution occurs for $.88 < R/R_{TIP} < 0.90$ than in the "A" version. There is presumably some correlation between the blade angle distribution and the double tip vortex feature, in view of the large undulations of both tip vortices radially and axially in Figure 6. These larger positional fluctuations imply more nearly equal strengths of the two vortices. The effect of increasing blade angle (or C_{μ}) tends to reduce the undulation amplitude, while the position of cross-over of both radial and axial coordinates does not appear from the available data to show any consistent variation with blade angle. Due to dispersal of the smoke in the flow visualization photos it is difficult to obtain data on the secondary vortex for $\psi > 90^\circ$.

- 3) The third propeller to which the method was applied was the HSD-9 propeller at 12° blade angle. The data from this propeller is plotted in Figure 8. Radial contraction and axial variation of the tip vortex position show no unusual properties.

2.6.2 Evaluation of Free Constants

From figures 4-8, values of the free constant λ were chosen to represent the three propellers. This data is included in Table (2-1). A simple polynomial (cubic) has been chosen for the relation between z_0 and ψ_0 for $\psi_0 < F$ and a linear relation for larger ψ_0 as in equation (3). The relation for z_0 (i.e. k) corresponding to $\psi_0 < F$ determines how far the tip vortex will pass under the succeeding blade. The actual vortex position could be found by iterative procedures, but such refinements are probably not worthwhile until other difficulties in applying the method are overcome.

Table 2-1

Propeller	λ	A	C	z_0
1967 $\beta_{.75} = 12^\circ$	0.40	.707	.293	1. Tip Vortex $\frac{dz_0}{d\psi_0} = \begin{cases} k_2(\psi_0/F)^3 & \text{for } \psi_0 < F \\ k_2 & \psi_0 > F \end{cases}$
1968-A $\beta_{.75} = 12^\circ$	0.48	.707	.283	2. Inboard Vortices $\frac{dz_1}{d\psi_1} = \begin{cases} k_2/2 & \text{for } \psi_0 < F \\ k_2 & \psi_0 > F \end{cases}$
1968-B $\beta_{.75} = 14^\circ$	0.51	.707	.273	
$= 17^\circ$	0.53	.707	.293	
HSD-9 $\beta_{.80} = 12^\circ$	0.50	.707	.293	k_2 chosen in program

3.0 Results and Discussion

3.1 Simplest Model

As already described, the simple model incorporates only a tip vortex, which leaves the blade at the tip and whose strength is equal (within 2%) to the maximum bound circulation on the blade. Conventional airfoil data was used in the strip theory necessary for converting velocities at the blade to forces and circulations on the blade. A constant drag coefficient of .01 was used, with one exception discussed separately. Before discussing the final results for forces, induced angles etc. on the blade, two particular observations are relevant:

- i) flow visualization pictures do not show vortices downstream of about $Z/R_{TIP} = .50$, their absence being consistent in all pictures.
- ii) flow surveys show that a tangential velocity exists behind the propeller of significant magnitude (20% of the local rotational blade velocity for small radii) and in the direction of rotation.

The first of these observations suggests a sudden rapid diffusion of tip vortices at some streamwise location. This may be due to vortex bursting, as suggested by some authors (34) or to an instability of the helical tip vortices. The latter can be investigated following the classical work of Levy and Forsdyke (35). They showed that a single helical vortex, of infinite extent in both directions and having a core radius 0.02 times the helix radius, was unstable to small disturbances for helix angles less than about $\tan^{-1}(0.3)$. This same critical helix angle also gave the condition for which the tangential velocity induced by the helix on itself was equal to zero, although Levy and Forsdyke point out that this fact may not be of general validity.

If we assume however that the helix angle for which the induced tangential velocity changes sign is equal or near to that value for which neutral stability occurs; present numerical values of tangential velocity for four helices can be used to estimate the stability of a four bladed propeller wake. Numerical integration shows that the tangential velocity of four helices on themselves is always positive, decreasing in magnitude as the helix angle decreases (as one would expect). This does not prove that the configuration is stable but suggests that it is.

The second observation clearly displays the deficiency of potential methods in defining the flow in the wakes of the blades, that is downstream of the propeller plane. The simple vortex wake model predicts tangential velocities which are positive for all radii when helix angles typical of those found in propeller wakes are used. In fact the blades have wakes (not vortex sheets only) which, through viscous action, drag fluid tangentially in the direction of rotation, that is they produce negative tangential velocity in the present notation (see figure 9). Hence we cannot expect an accurate assessment of the tangential velocities near the blades from the vortex wake consisting of a single filament shed at the tip,

particularly at inboard radii where the blade sections are thick and the blade wakes large. The resulting accuracy of the vortex wake method is, therefore, questionable regardless of the refinement of the vortex sheet configurations. This is an important observation, suggesting that potential models of any complexity are of limited accuracy and hence that the simplest models may be the most sensible.

Figures 10 and 11 show the power and thrust distribution on the blades of the 1967 propeller as calculated by the simple model and compared with values for a flow survey. The chord has been assumed to be zero at the tip to force values of lift and drag (thrust and power) to be zero there. Integrated values of thrust and power coefficients and figure of merit, are given below:

Table 3-I

1967 Propeller	C_T		C_P		FM	
	$\beta=12^\circ$	$\beta=14^\circ$	$\beta=12^\circ$	$\beta=14^\circ$	$\beta=12^\circ$	$\beta=14^\circ$
Direct Measurement	.1565	.1815	0.0600	.0755	.823	.817
Flow Survey + Strip Analysis	.1954	.2134	0.0660	.0815	1.048	.965
Vortex Wake Calc'n	.1615	.1880	.0684	.0840	.768	.757

Table 3-I shows that although the vortex wake simple model does not produce good agreement with thrust and torque, the figure of merit is not as far from the measured value as is the flow survey value.

It is of interest to see how accurately the simple vortex wake method can predict the percentage increments in thrust and torque which occur over a 2° change in blade angle. This is shown, again for integrated values of thrust and power, in Table 3-II.

Table 3-II

1967 Propeller	Change		% Change	
	C_T	C_P	C_T	C_P
Direct Measurement	.0250	.0155	16.0	25.9
Flow Survey + Strip Analysis	.018	.0155	10.0	21.8
Vortex Wake Calculation	.031	.0176	18.0	24.8

The simple vortex wake method predicts the percentage changes for the propeller with good accuracy.

Values of the calculated induced angle ϕ , which is used to determine the loading on the blades is shown in Figure (12) for the $\beta_{.75} = 12^\circ$ case. The calculated results can be compared with those from flow surveys of the propeller. The general trends of the calculated and measured results correspond, although the values of ϕ calculated inboard are too high, suggesting values of axial velocity which are too large or values of relative tangential velocity which are too small. Addition of inboard filaments, necessary for selfconsistency of the model, changes this picture, as described in the next section.

To evaluate the validity of comparisons of theory with flow survey measurements the azimuthal variation of axial velocity found from the simple vortex wake model was calculated. This variation for three radii, $R/R_{TIP} = .75, .85$ and $.95$ is plotted in Figure 13 where the experimentally measured average value is also shown. The calculated result shows that, in the tip region, the fluctuation of a tuft in a diametral plane (that is, neglecting tangential velocities) is about 9° at $R/R_{TIP} = .75$, 13° at $R/R = .85$ and 41° at $R/R_{TIP} = .95$. The experimentally determined average velocity near the tip is therefore very uncertain and comparison between the flow survey ϕ values and calculated values here is less valid than at the inboard stations.

Another comparison that may be made between the calculated and measured values is in the helix angle of the ultimate wake. This angle is calculated in the computer program once the tip vortex strength has been found by interpolating data relating tip vortex strength to ultimate wake pitch.

The wake pitch has also been measured from flow photography. The calculated location of the tip vortex is plotted in Figures 4a and 4b as Z_0/R_{TIP} versus ψ_0 .

If the radius of the helical wake were precisely specified the slope of the Z_0 versus ψ_0 curve would indicate the agreement in helix angle between observed and measured cases. The lines are reasonably close, lending credence to the analysis.

The effect of a change in drag coefficient from $C_d = .01$ to $.02$ is shown in Figure 10. As expected, the change raises the overall power distribution, particularly near the tip. No significant change in C_T was observed as a result of the change in C_d again as expected.

3.2 The Addition of the Inboard Sheet

The inboard vortex sheet is represented by a finite number of discrete filaments. The strength of these filaments has been determined from the bound loading in one of two ways:

- i. using velocities at the blade associated with the tip vortex only, to calculate the bound loading (called the "independent filaments" method).
- ii. using velocities at the blade associated with the tip vortex and all vortex filaments of the inboard vortex sheet originating outboard of the radius at which velocities are being calculated. This solenoidal type of approximation is discussed in section 2.4 and is called the "dependent filaments" method.

Because the bound vorticity increases with radius for small radii, the inboard vortex sheet consists of vorticity which is opposite in sign to that of the tip vortex. It therefore reduces the velocities over the inboard sections of the blade, correspondingly reducing the induced angles ϕ . The results for both methods are plotted in Figure 12.

It must be emphasized that the inboard vortex sheet filaments are assumed to affect only radii inboard of them as far as the velocity or loading is concerned, so that the tip region, outboard of $R/R_{TIP} = 0.80$ in this case, is completely unaffected by the inboard vortex sheet.

As can be seen from Figure 12, the addition of the inboard vortex sheet lowers the values of ϕ considerably, so that they become too low by comparison with the measured values.

Because the inboard vortex filaments reduce inboard values of ϕ , they increase local angles of attack and therefore increase the loading in the propeller. For $\beta_{75} = 12^\circ$ on the 1967 propeller the values of integrated thrust and power rise to $C_T = .198$ and $C_P = .073$, giving a figure of merit of .914. This is less satisfactory than the result obtained with no inboard filaments and suggests that if the inboard sheet is to be included, this strength must be more accurately found, perhaps by iteration.

It is perhaps encouraging that inclusion and omission of the inboard vortex sheet bracket the measured value of ϕ for the one case considered, suggesting that further iteration might produce fair agreement.

3.3 The Outboard Vortex Sheet

Since it is necessary, for self-consistency, to shed an inboard vortex sheet, it is also necessary to have an outboard vortex sheet. Hence for completeness an outboard sheet model was specified, as described in Section 2.3.

The model was developed in two parts:

- i. An uncontracting sheet in which filaments shed at the blade moved back at constant radius until each intersected the tip vortex path and
- ii. A model in which the sheet "roll-up" time could be arbitrarily specified, i.e. intersection of the most inboard filament of the sheet with the tip vortex could be specified.

In the case of the first model (i) only one application was tried, the 1967 propeller (4 blades) at 12° blade angle. The strengths of the outboard filaments representing the outboard sheet were specified by the bound vorticity on the blade as calculated from the simple model (tip vortex only). No attempt was made to make these filaments "inter-dependent" in the same way as was done with the inboard filaments. This would be possible through iteration, if convergence exists.

It is worth noting, from Figure 4a for example, that since the innermost filament is shed from $R/R_{TIP} = 0.85$, it joins the tip vortex in the present model at about $\psi = 100^\circ$, since it remains at constant radius. Thus it radically affects the blade following that from which it was shed. This length of roll-up, which is the physical phenomenon being represented, is thought to be unrealistic. Roll-up probably occurs in less than 90° . The smoke photographs do not show roll-up specifically, however, and little is known about this process. A more rapid roll-up, one that was completed in an azimuthal distance of less than $2\pi/B$ radians, would result in a much smaller difference between the simple model and that including the outboard sheet. This may explain in large measure, the fair agreement obtained with the simple model.

Results for the 1967 propeller, including the outboard and inboard vortex sheets, are plotted in Figure 14. The inboard vortex sheet was calculated assuming interdependent vortex filaments and assuming that the tip region could be represented adequately by the simple model. The outboard vortex sheet assumed that each vortex filament affected all points in the tip region, so that no solenoidal approximation was used in this part of the calculation. The final bound vorticity distribution, after re-calculation using the outboard vortex sheet, is no longer consistent with the assumption that the maximum bound vortex value is equal to the final tip vortex strength. Only one iteration of this outboard sheet model was completed.

The second outboard sheet model (ii) was applied to the 1967, 1968 and HSD-9 propellers. In this representation, the filaments composing the outboard sheet are postulated to move outwards exponentially with azimuth angle. Selection of the azimuth angle at which the sheet is fully rolled up fixes the position at which the innermost filament of the outboard sheet joins the tip vortex.

As applied to the 1967 propeller at 12° blade angle the outboard sheet (having a 15° roll-up angle) increased the induced angle distribution (by 1°) over the simple tip vortex plus inboard sheet model (See Figure 15). This gave a closer correlation with the derived induced angle from the flow survey. It must be emphasized however, that the flow survey measurements near the tip region are probably inaccurate, because of the large circumferential variations in velocity there. Assessment of axial and tangential velocities for the same propeller is shown in Figure 15. Axial velocity is qualitatively correct and tangential velocity only marginally so. This is partly due to the inability of the vortex wake program to account for the presence of viscous blade wakes and partly to numerical errors (round-off and truncation). However, overestimation of both axial and total tangential velocities at inboard radii has been partly self-cancelling resulting in generally good agreement of inboard ϕ values.

Figure 15 illustrates the effect of a change in roll-up distance from 15° to 50°. The largest effect occurs in axial velocity near the tip (a 25% change). Tangential velocity is affected by less than 1/2%. Qualitative agreement between azimuthal average axial velocity derived from the flow survey and the average axial velocity given by the vortex wake method is improved slightly at the higher roll-up angle.

Results of applying the complete vortex wake method to the 1968-A propeller at 12° blade angle are shown in Figure 17 and the 1968-B at 14° blade angle in Figure 18. The agreement in ϕ for all cases is not good. The degree of agreement in C_T , C_P and F_M between rig measurements and the theory is shown in Table 3-III.

Table 3-III

Propeller	β , 80	Test			Theory		
		C_T	C_P	F_M	C_T	C_P	F_M
1968 - A	12°	.1770	.0715	.828	.1676	.0677	.806
1968 - B	14°	.1530	.0610	.786	.1822	.0809	.769
"	17°	.1790	.0740	.819	.2135	.0971	.812

C_T and C_P were underpredicted consistently for each propeller in Table 3-III, substantiating; (a) the inability of the model to cope with the presence of a double tip vortex and, (b) the sensitivity of predicted performance to flow details in the tip region.

An attempt to iterate bound loading and outboard sheet filament strengths was made as follows:

For the i^{th} filament

$$C_{\Gamma_N}^{(i)} = \frac{C_{\Gamma_{N-1}}^{(i)} + C_{\Gamma_{N-2}}^{(i)}}{2} \quad (14)$$

where $N = 0, 1, 2$ etc. the number of successive approximations, $N > 2$

$C_{\Gamma_N}^{(i)}$ = Non-dimensional bound circulation of i^{th} radial station of outboard sheet (nth approximation)

Convergence was assumed complete when $C_{\Gamma_N}^{(i)}$ was within 2% of $C_{\Gamma_{N-1}}^{(i)}$

Figure 16 shows the successive loading changes in the tip region of the HSD-9 propeller at 12° blade angle and 60° roll-up. The loading $C_{\Gamma}^{(i)}$ usually converged in

less than 5 iterations. This is considered fortuitous and may, in large part, be due to the rather limited size of the outboard sheet.

While adding slightly to the complexity of the model, this iteration routine maintained self-consistency and resulted in improved predictions of the Figure of Merit. Table 3-IV compares the method with and without outboard sheet iterations.

Table 3-IV

HSD - 9 Propeller			
Blade Angle = 12°		Roll-up angle = 60°	
	C_T	C_P	FM
Measured	.2142	.1020	.776
Vortex wake (No iterations)	.2178	.1116	.727
Vortex wake (with iterations)	.2295	.1112	.789

To summarize, the model initially sheds a tip vortex, followed by the zeroth approximation of the outboard sheet which is assumed in all calculations to extend to the tip of the blade from the point of maximum bound circulation as found for the tip vortex above. Iterations are performed on the outboard sheet until strength convergence is achieved. Following this the inboard sheet is shed using the 'dependent filaments' scheme.

3.4 The Calculated Circumferential Variation of Velocity

Circumferential variations in velocity calculated from the present vortex wake model can provide some insight into:

- (a) probably accuracy of the flow survey (pressure probe)
- (b) the effect of roll up angle in the analytical model.

In addition to the usual flow survey velocity measurements, an attempt was made to measure the instantaneous velocities near two propellers using hot wire anemometers. The first propeller was a 65 AF design and the second, one of 120 AF. Both had integrated design lift co-efficients of 0.30, were 7 feet in diameter and were run in four bladed configurations.

The hot wire measurements (33) showed that a relatively small part of the wake contained clearly periodic velocities, as shown in figure 19. The average azimuthal variation of axial velocity in each wake was less than $\pm 10\%$, but because measurement accuracy was approximately $\pm 8\%$, definitive azimuthal variations of the wake velocity components were not obtained. Comparisons with the analytic model made in subsequent figures use mean values obtained from the flow surveys that is, from pressure probes.

The azimuthal variation of velocity at a particular R-Z position was calculated from the analytical model. No contribution from the bound vortices was assumed to be present for points lying within a specified small distance from the lifting line. All filaments shed into the wake were used to compute these velocities. The azimuthal mean values were computed from the following:

$$U = \sqrt{\frac{1}{N} \sum_{i=1}^N |U_i|^2} \quad (15)$$

where: U = Mean Azimuthal Velocity Component in any given coordinate direction - fps

U_i = Velocity at i^{th} azimuth station - fps

N = Total number of azimuthal stations used in obtaining the average

The pressure probes used in the flow surveys had negligibly small corrections for angles of attack (yaw and pitch) less than about 20° ; their response characteristics at larger angles were not considered in comparing the calculated and measured mean values of the velocity.

Figure 20 shows the predicted values of axial and tangential velocities with varying azimuth angles for the HSD-9 propeller. For comparison, two roll-up angles (30° and 60°) and the effect of the bound vorticity distribution are included as variables in the two sets of curves.

Roll-up angle, determining the extent and position of the outboard sheet, influences both the magnitude and phase of the axial velocity distribution especially near the tip. The bound loading contribution to axial velocity is symmetric about the R-Z plane lying mid-way between successive blades. As seen for $R/RTIP = 0.96$ the effect of adding this component is to increase the periodicity (or ratio of amplitude to mean value of the velocity variation). The comparison made in figure 20a between measured mean velocities and calculated mean values indicates better agreement as radius decreases (i.e. when periodicity is low). Near $R/RTIP = 0.96$ the agreement is poorest, suggesting greater sensitivity to the geometry of the trailing vortices, the probe response characteristics or the calculation procedure here than anywhere else.

The tangential induced velocity variation given in Figure 20b for three radial stations at the propeller plane indicates a much gentler azimuthal variation. The effect of roll-up distance is less than on the axial component, and the bound loading contribution is zero at all azimuth positions.

Comparison of calculated and measured mean values shows that the agreement worsens as the radius decreases, in contrast to the trend in the axial velocity case. This is likely due to both a) viscous effects which have not been included in the theory and b) use of the solenoidal approximation in the calculation procedure. The results above were obtained without iterating the strength of the outboard sheet.

3.5 Sensitivity to Core Size

A peculiarity associated with the model which was discovered when the inboard sheet was first added concerned the sizes of cores of trailing filaments. When the "dependent" filaments scheme was used the distribution of ϕ would experience wild oscillations with decreasing radius for what was considered to be realistic values of core size ($e \approx .01 R_{TIP}$). Only when core size was increased by at least an order of magnitude would these disappear. This although producing reasonable agreement (see Figure 11, for example) made the model physically less plausible due to the cores of adjacent vortices intersecting one another.

To try to reduce these large core sizes, another approach was tried, following Reference 22. The 'core size' term was removed from the Biot-Savart relations (putting $e=0$ in equation 8) and a new procedure instituted in which all filament elements lying within a specified distance of the point under consideration were not included in the calculation. Referred to as the "Sphere of rejection" criterion, its effect was to make the ϕ distribution for the 1967 propeller in Figure 21 less smooth, and for the smallest 'sphere' radius ($e = .01 R_{TIP}$) to increase the oscillatory variation of ϕ with radius. Since this method did not improve the problem of instabilities the original representation of core size was reconsidered. In the original representation, the Biot-Savart law is fundamentally violated since the $1/R^3$ term has been replaced by $1/(R^2 + e^2)^{3/2}$ where 'e' is the assumed vortex core radius. While preventing the appearance of singularities this modifies the magnitude of the induced velocity of a vortex from its centreline outwards for some distance, of the order of 10 core radii.

In an attempt to achieve the first aim of reducing core size to an acceptable level and, in addition to maintain plausibility, a third representation was tried which has been used exclusively since. Here the induced velocity is linearly scaled to zero with radius inside the core and retains the potential or $1/R^3$ form of the expression outside - the so-called 'solid body' representation.

In general, core sizes of the order of $0.10 R_{TIP}$ were required for the "solid body" representation of core when running the model with simple tip vortex and inboard sheet. The addition of the outboard sheet however, caused additional difficulty in that a particular ratio (nearly 1:1) was required to be maintained between outboard sheet core sizes (e_3) and inboard sheet core sizes (e_1). Results for the HSD-9 propeller are plotted as FM versus e_1 and e_3 in Figure 22. Figure of Merit appears to be sensitive to the value of e_3 , but for the present comparisons the values of e_1 and e_3 have both been made equal to $0.10 R_{TIP}$. This, or a similar assumption, is apparently necessary when using this vortex wake method.

4. Conclusions and recommendations

Various vortex wake representations have been explored and compared to observed flow visualization patterns and quantitative velocity measurements obtained from model propellers in the static thrust condition. From these comparisons, we conclude that:

- (a) Changes in performance can be predicted with reasonable accuracy for small changes in blade angle if the propellers considered (such as the 1967 blades) have wakes which do not contain unusual features.
- (b) Propellers (such as the 1968 blades) can create double tip vortices whose presence significantly complicates the wake and makes accurate performance predictions very difficult.

- (c) Increasing complexity of the analytical model, including both inboard and outboard vortex sheets does give improved prediction of the inflow angle (ϕ) at the propeller plane. Further iterations could create further improvements here in some cases at least.
- (d) Major difficulties in comparing measured and computed values of velocity at the propeller plane are the inability of a lifting line model to represent the flow near the real blade without ambiguity, and the presence in the real flow of wakes which cannot be represented by potential theory. These difficulties confuse comparisons of ϕ and may ultimately limit the usefulness of wholly potential calculations to represent a propeller in static thrust.
- (e) The effect of tip vortex roll-up distance upon performance for roll-up angles less than 60° is small in the analytical model but is significant in determining the azimuthal variation of axial induced velocity. If smoke or some other tracer could be injected into the wake from an actual propeller blade, the extent of the tip vortex (i.e. how far radially inboard the shed vorticity rolls up to form the tip vortex) and the rate of roll-up might be observed. The splitting into tip vortex and inboard sheet might be made more quantitative also.
- (f) Iterations performed upon the outboard sheet strength converged quickly for the case of the HSD-9 propeller at 12° blade angle and improved the predicted figure of merit. Convergence is strongly dependent upon core size assumed.
- (g) Physically high values of core size must be maintained for the current representation. The large core size acts to dampen the strengths of adjacent filaments resulting in smoother distributions of induced velocities. Alternative representations for the vortex core do not alter this conclusion significantly.
- (h) The calculated circumferential variation of velocity shows that the periodicity of the flow increases toward the tip as shown by experiment.

References

1. H.V. Borst, "A Short Method to Propeller Performance", Propeller Division, Curtiss-Wright Corporation, 1959.
2. Curtiss-Wright Corporation. "Calculated Performance...", Propeller Division, Ref. 60-4, 1960.
3. Rotol Ltd., "Charts for the Estimation of Performance of Propellers under Various Operative Conditions", Performance Office, Report No. 1164, 1959.
4. Rotol Ltd., "Choice of Propeller for the Canadair CL84", Performance Office Report No. 1243, 1960.
5. Hamilton Standard, "Generalized Performance of Conventional Propellers for VTOL-STOL Aircraft", Report No. HS-1829, 1958.
6. ANC-9 "Aircraft Propeller Handbook", 1956.
7. A. Gessow and G.C. Myers, "Aerodynamics of the Helicopter", 1952.
8. M. Knight and R.A. Hefner, "Static Thrust Analysis of the Lifting Airscrew", NACA TN-626, 1937.
9. S. Goldstein, "On the Vortex Theory of Screw Propellers", Proc. Roy. Soc. Vol. A-123, p. 440, 1929.
10. C.N.H. Lock, "Application of Goldstein's Theory to Design", ARC-R & M 1377, November 1930.
11. T. Theodorsen, "Theory of Propellers", New York, 1948.
12. R.B. Gray, "An Aerodynamic Analysis of a Single-Bladed Rotor...", Aero Eng. Dept. Report No. 356, Princeton University, 1956.
13. H. Glauert, "Elements of Aerofoil and Airscrew Theory", Cambridge, 1959.
14. J.C. Erickson, R. Ladden, H. Borst and D. Ordway, "A Theory for VTOL Propeller Operation in a Static Condition", USAAVLABS Technical Report 65-69, Ft. Eustis, Va., 1965.
15. L. Prandtl and A. Betz, "Vier Abhandlungen zur Hydrodynamik und Aerodynamik", Göttingen, 1927.

16. I.S. Gartshore, "The Application of Vortex Theory to Propellers Operating at Zero Advance Ratio", MERL Tech. Note 66-3, McGill University, 1966.
17. D.C. Gilmore, "An Evaluation of Methods for Predicting the Performance of Propellers Operating at Zero Advance Ratio", McGill University, MERL TN 67-2, April 1967.
18. J. Valensi, "Etude de l'Ecoulement de l'Air Autour d'une Helice", Publications Scientifique et Techniques du Ministere de l'Air No. 73, 1935.
19. G.N. Adams, "Propeller Research at Canadair Limited", Proc. of CAL/USAAVLABS Symposium on Aerodynamic Problems Associated with V/STOL Aircraft, Vol. I, Buffalo, N.Y., June 1966.
20. W.H. Tanner and R.M. Wohfeld, "Vortex Field, Tip Vortex, and Shock Formation on a Model Propeller", Proc. of CAL/USAAVLABS Symposium on the Aerodynamics of Rotary Wing and V/STOL Aircraft, Buffalo, N.Y., June 1969.
21. A.J. Landgrebe, "An Analytical Method for Predicting Rotor Wake Geometry", AIAA Paper 69-196, AIAA/AHS VTOL Research Design & Operations Meeting, February 1969.
22. D.R. Clarke and A.C. Leiper, "A Method for the Prediction of Helicopter Rotor Hovering Performance", Paper 321, 25th Annual National Forum Proc. AHS, May 14th - 16th, 1969.
23. M.P. Scully, "A Method of Computing Helicopter Vortex Wake Distortion", M.I.T. ASRL-TR-138-1, June 1967.
24. D.S. Jenny, J.R. Olsen, A.J. Landgrebe, "A Reassessment of Hovering Rotor Performance Prediction Methods", Paper No. 100, 23rd Annual National Forum, Proc. AHS, May 10th-12th 1967.
25. R. Piziali and F. Duwaldt, "Computed Induced Velocity, Induced Drag and Angle of Attack Distributions for a Two-Bladed Rotor - CAL Report, 1963.
26. M.D. Greenberg and A.L. Kaskel, "Inviscid Flow Field Induced by a Rotor in Ground Effect" - NASA CR-1027, May 1968.
27. M. Iwasaki et al, "Theoretical and Experimental Investigations of Prop Working at Static Condition", reprint from Reports of Research Institute of Applied Mechanics, Kyushu University, Japan, Vol. XVI, No. 52, 1968.
28. J.C. Erickson, Jr., "A Continuous Vortex Sheet Representation of Deformed Wakes of Hovering Propellers", Proc. of 3rd CAL/AAVLABS Symposium, June 18th-20th, 1969.
29. I.S. Gartshore, "Modifications and Applications of a Simple Vortex Wake Method for Predicting the Performance of a Propeller in Static Thrust", Canadair Report RAA 240-103, July 1969.
30. D.C. Gilmore, "The Performance of Propellers Operating at Zero Advance Ratio", M. Eng. Thesis submitted to Faculty of Graduate Studies and Research McGill University August 1967.
31. D.C. Gilmore "Investigation of a Vortex Wake Method for Predicting the Performance of a Propeller in the Static Thrust Condition", Canadair Report RAA-240-129, May 1970.
32. R. Ladden, "Static Thrust Prediction Method Development", Part I, Technical Report, AFFDL-TR-71-88, Vol. II, Air Force Systems Command, Wright-Patterson AFB, September 1971.
33. D.C. Gilmore and I.S. Gartshore, "Measurements of the Instantaneous Velocities in the Wakes of Two Propellers Operating at Zero Advance Ratio", unpublished work submitted to Therm Inc. under contract number TAR 849-2, Ithaca, N.Y., January 1967.
34. I.A. Simons, R.E. Pacifico and J.P. Jones, "The Movement, Structure and Break-down of Trailing Vortices from a Rotor Blade" - CAL/USAAVLABS Symposium Proceedings, Buffalo, N.Y. 1966.
35. H. Levy and A.G. Forsdyke, "Steady Motion and Stability of a Helical Vortex" - Proc. Roy. Soc. A-120 (1928).

Acknowledgements

The authors wish to acknowledge the assistance from a variety of sources. In particular, the U.S.A.F. Flight Dynamics Laboratory which sponsored the Propeller Technology Program is thanked for granting permission to publish some of the works performed during this program. Mr. Richard J. Hirt was program manager at AFFDL, Wright Patterson AFB. Mr. O.E. Michaelson and Dr. G.N. Adams are thanked for many helpful suggestions as well as the staff at Canadair who assisted in many ways with the flow surveys and report preparation. Lastly, credit is due to Drs. B.G. Newman, D.E. Ordway, J.C. Erickson and Mr. R. Ladden for providing helpful ideas.

FIGURE OF MERIT - FM

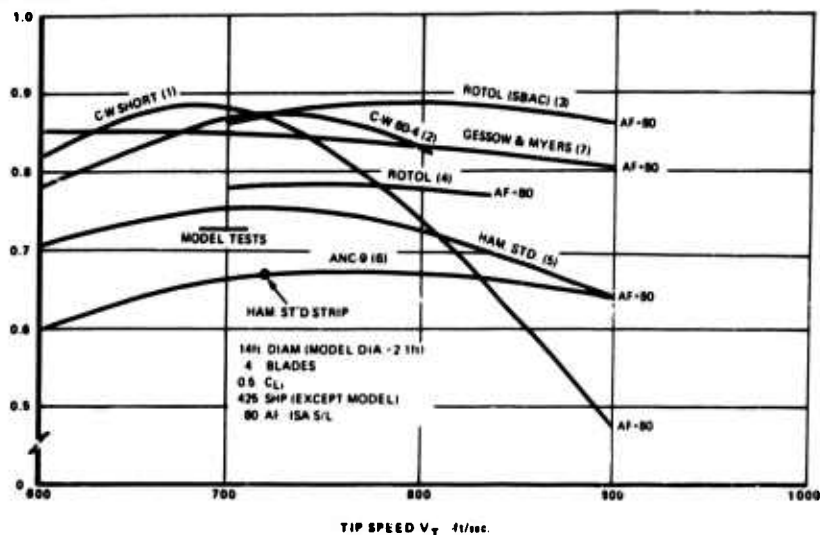


Figure 1 - COMPARISON OF SINGLE POINT METHODS

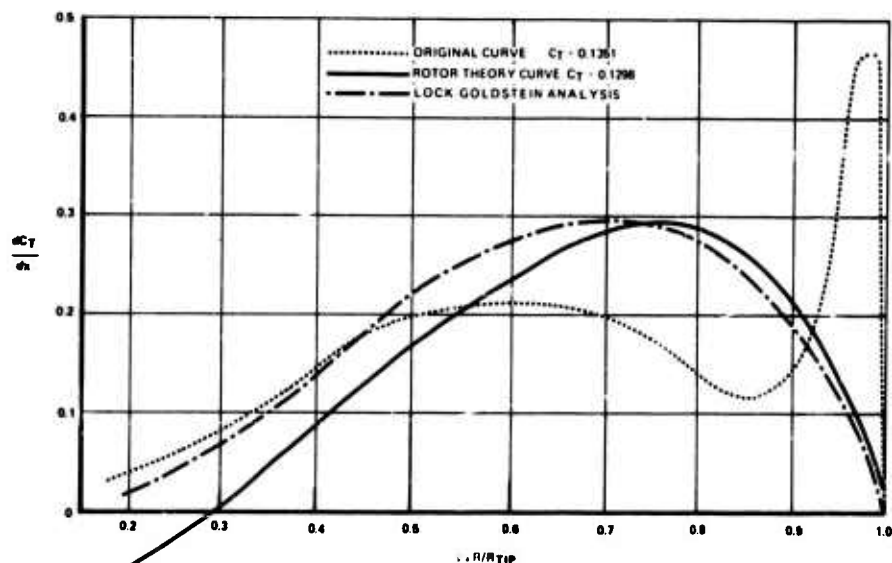
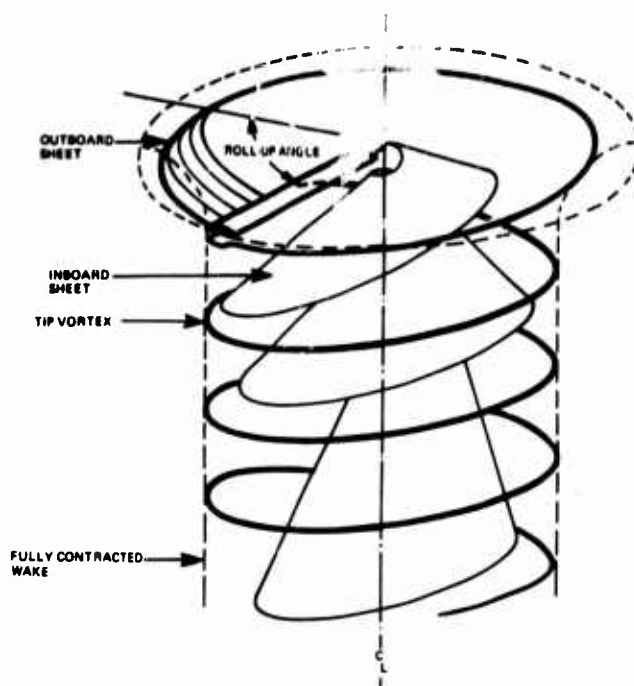


Figure 2 - ROTOR THEORY (8) & LOCK-GOLDSTEIN THEORY (10) COMPARED WITH STRIP ANALYSIS
(C.W. PHOP $\beta_{75^\circ-100^\circ}$)



MODEL 1) SIMPLE (TIP VORTEX ONLY)
 2) SIMPLE + INBOARD SHEET
 3) SIMPLE + INBOARD SHEET + OUTBOARD SHEET

Figure 3 - VORTEX WAKE MODELS

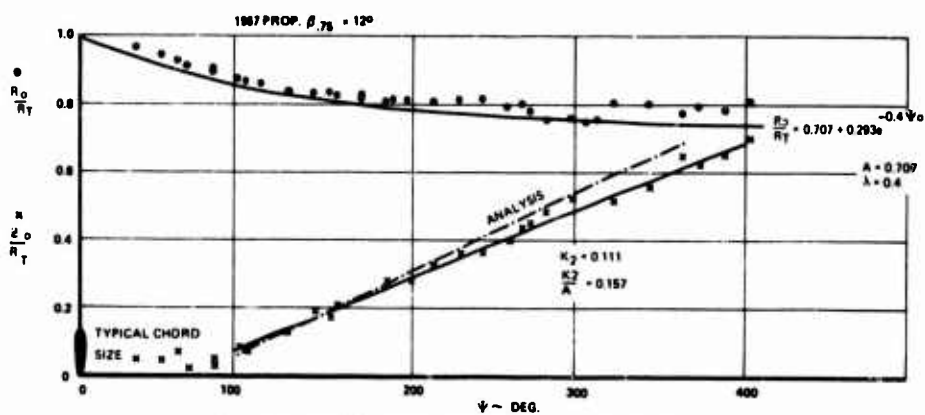


Figure 4a - TIP VORTEX COORDINATES (FROM SMOKE FLOW VISUALIZATION)

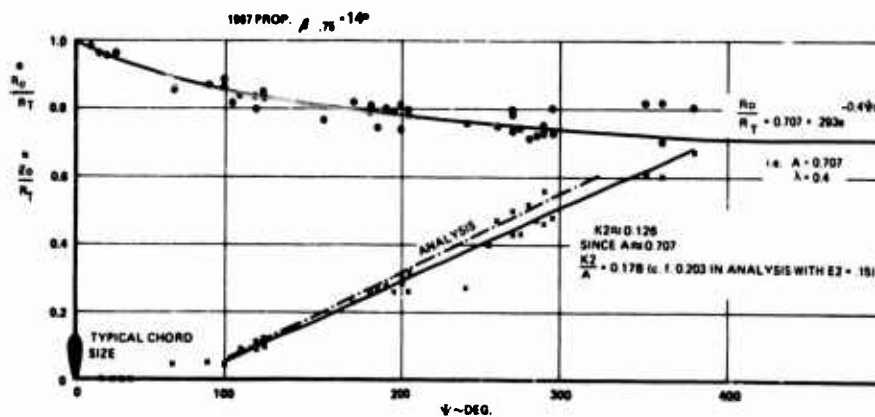
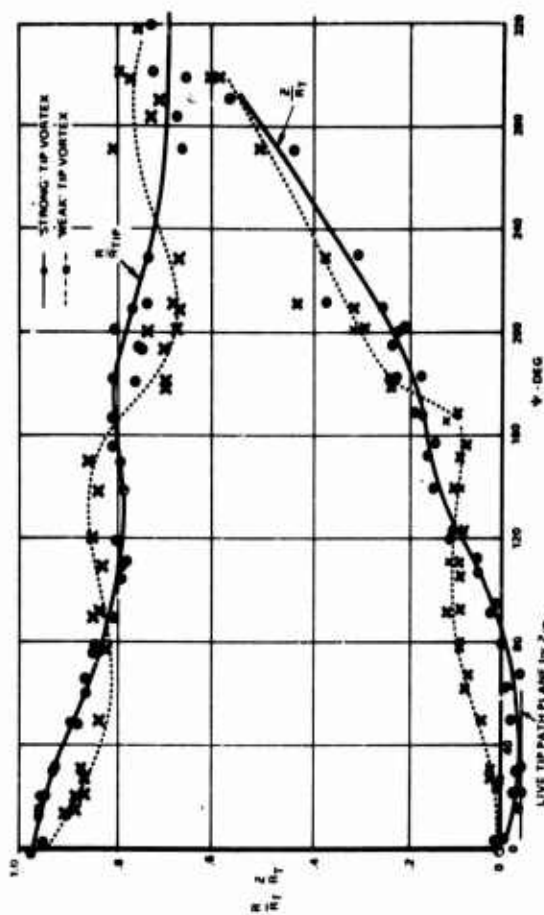
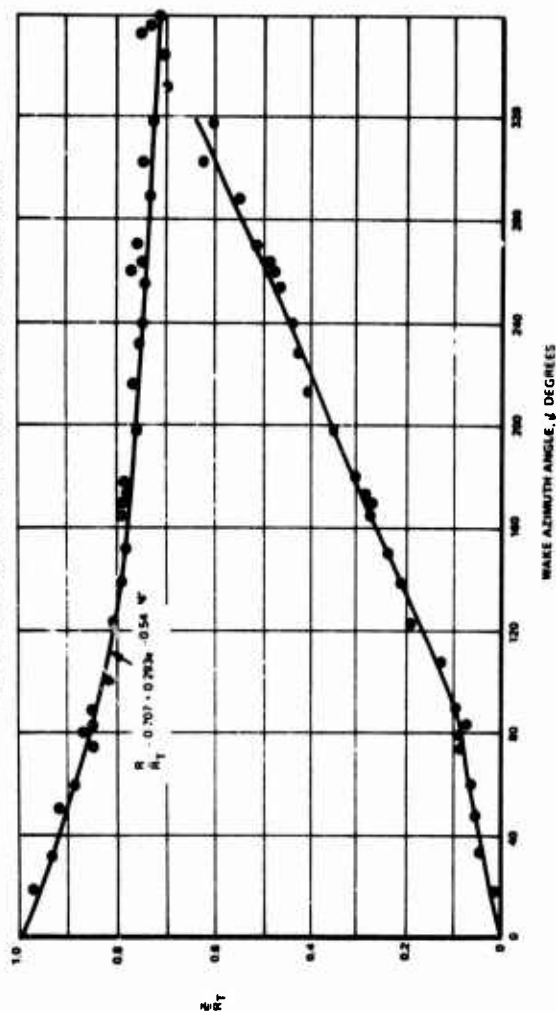
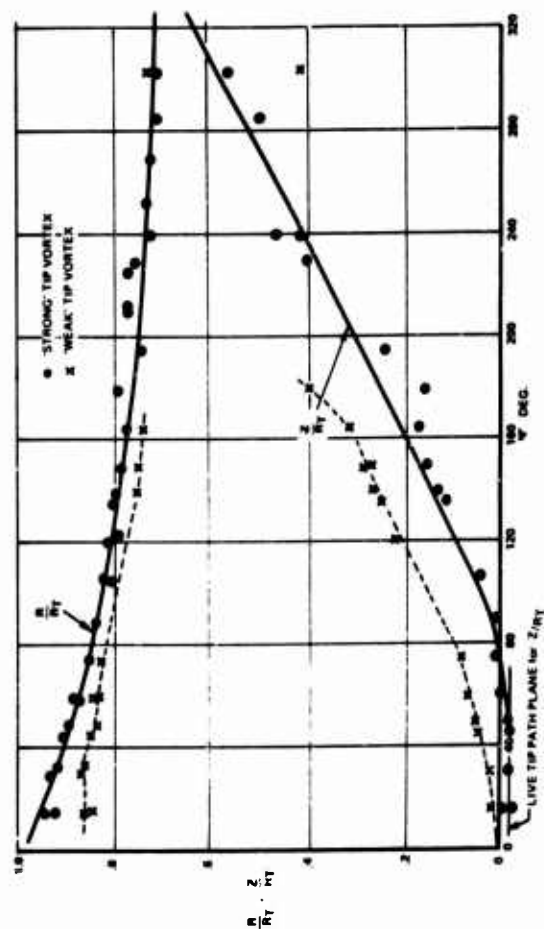
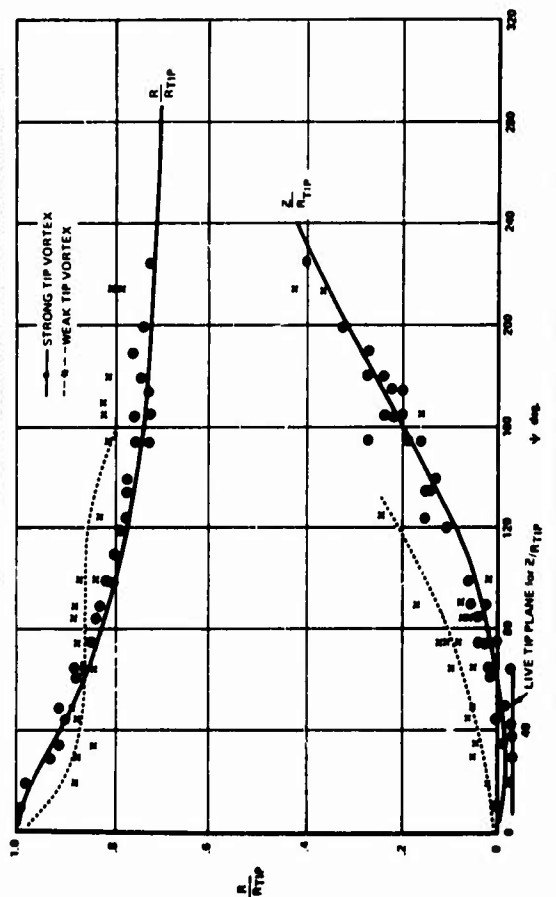


Figure 4b - TIP VORTEX COORDINATES (FROM SMOKE FLOW VISUALIZATION)

Figure 6 - "TIP VORTEX COORDINATES" 1988-B PROPELLER $\beta = 14^\circ$ Figure 8 - "TIP VORTEX COORDINATES" HSD-9 PROPELLER $\beta = 12^\circ$ Figure 5 - "TIP VORTEX COORDINATES" 1988-A PROPELLER $\beta = 12^\circ$ Figure 7 - "TIP VORTEX COORDINATES" 1988-B PROPELLER $\beta = 17^\circ$

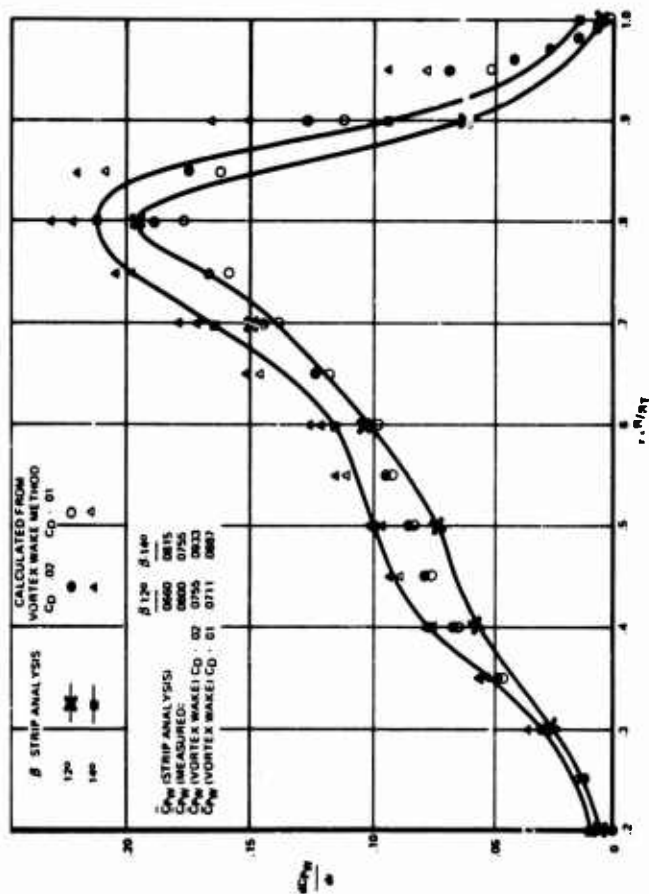


Figure 9 - COORDINATE SYSTEM USED IN WAKE DESCRIPTION

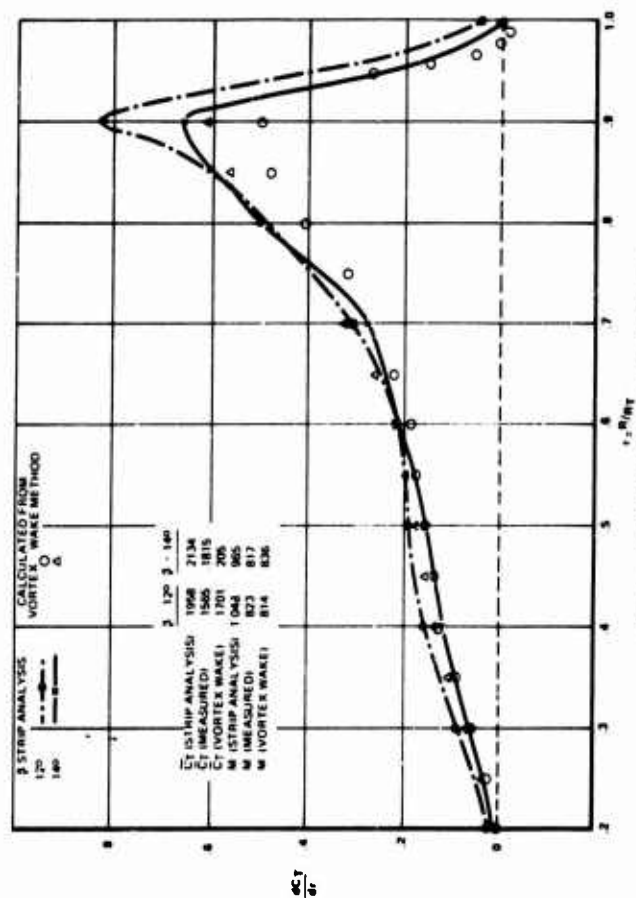


Figure 11 - THRUST DISTRIBUTION 1967 PROPELLER

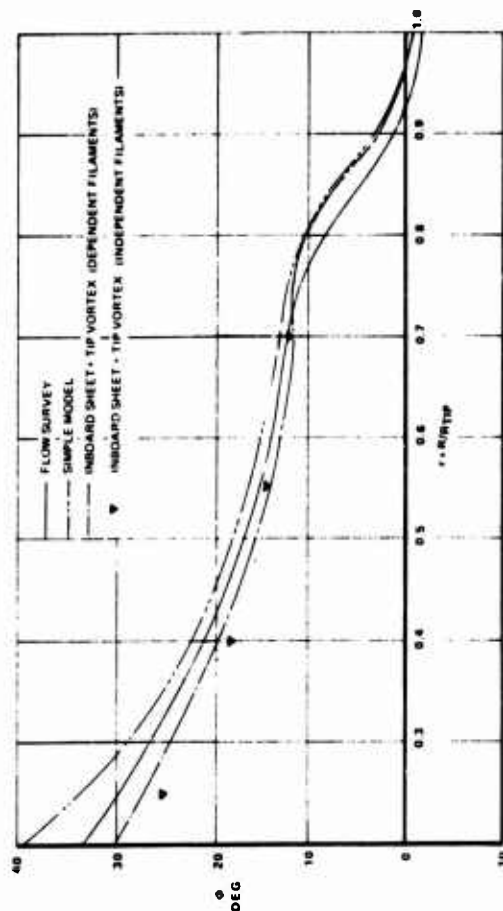
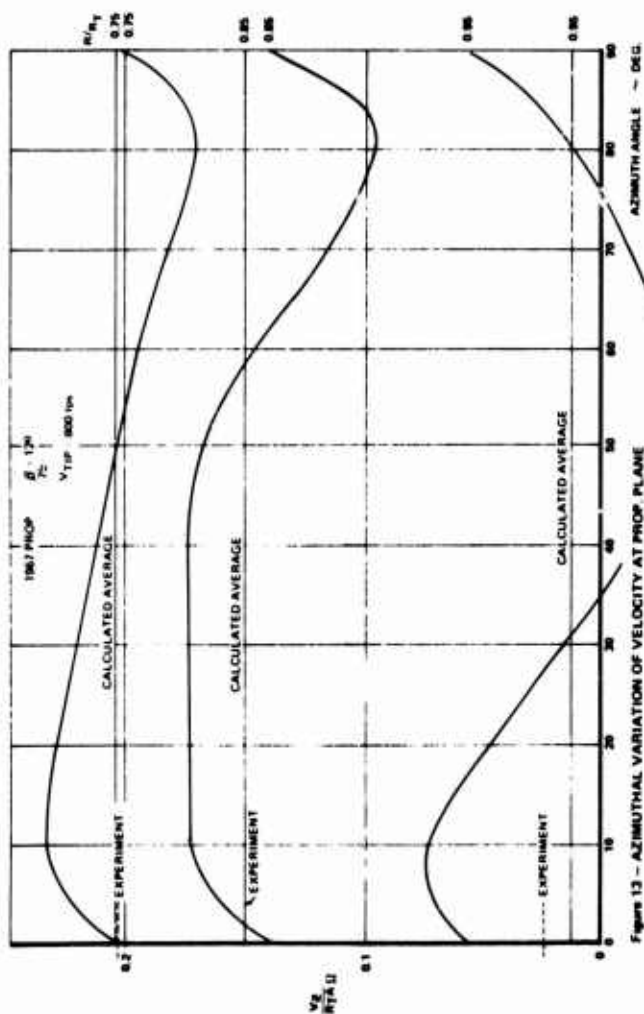
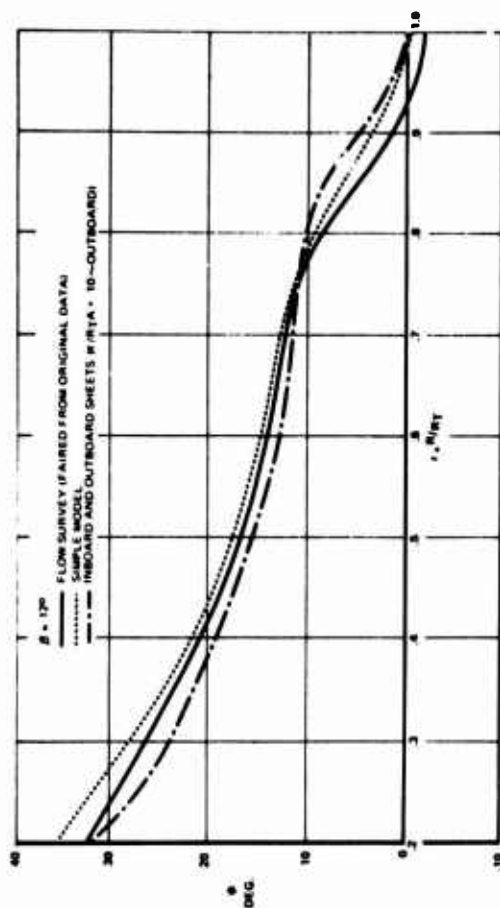
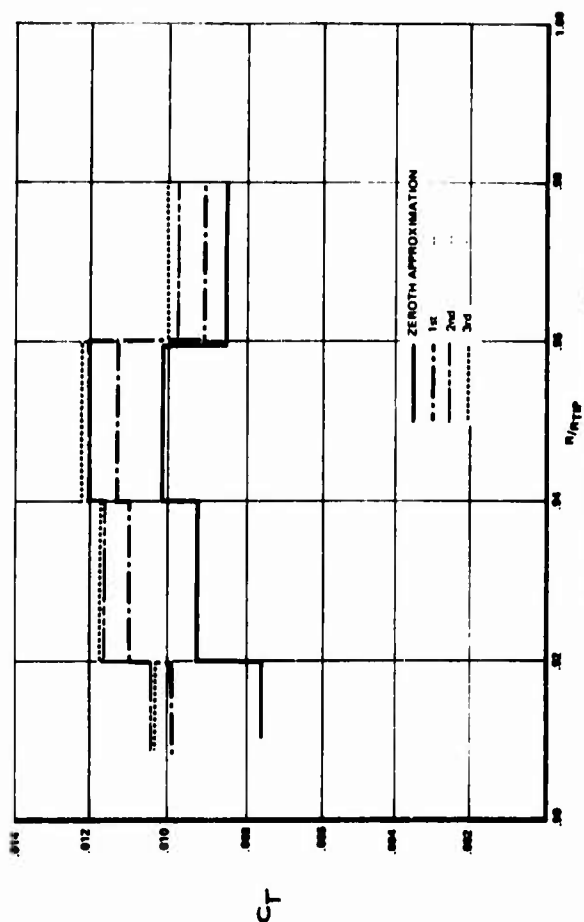
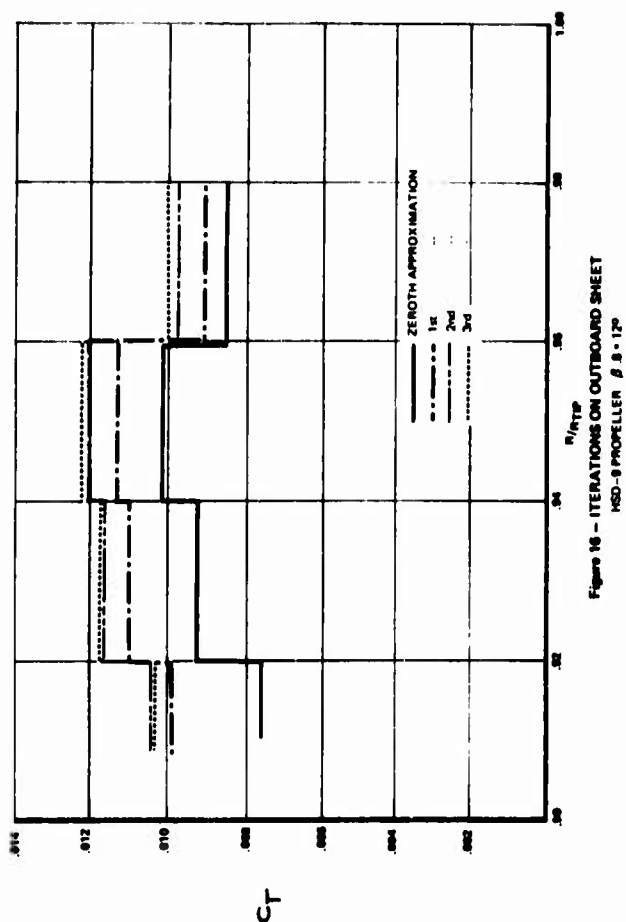


Figure 10 - POWER DISTRIBUTION 1967 PROPELLER

FIGURE 12 - INDUCED ANGLE DISTRIBUTION 1967 PROPELLER $\beta = 12^\circ$



163

Figure 14 - INDUCED ANGLE DISTRIBUTION 1967 PROPELLER $\beta = 75 - 120^\circ$ Figure 15 - INDUCED ANGLE DISTRIBUTION 1967 PROPELLER $\beta = 75 - 120^\circ$ Figure 16 - ITERATIONS ON OUTBOARD SHEET
 HSD-9 PROPELLER $\beta = 75 - 120^\circ$

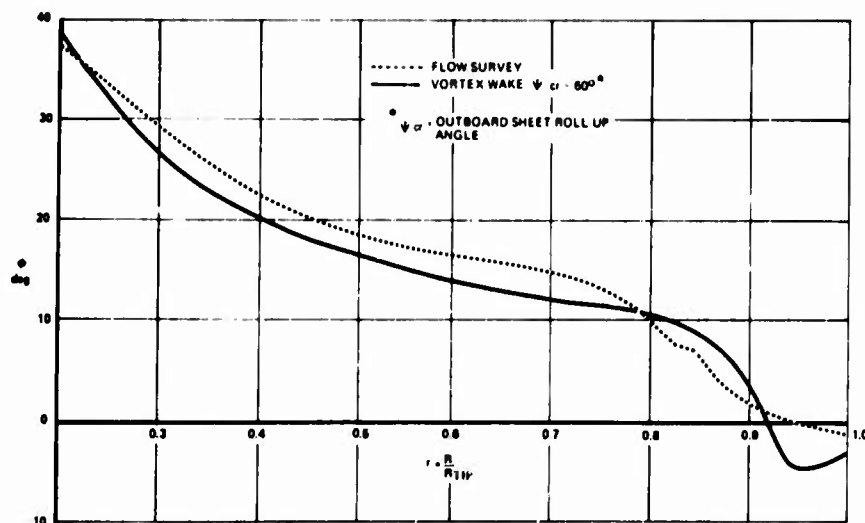
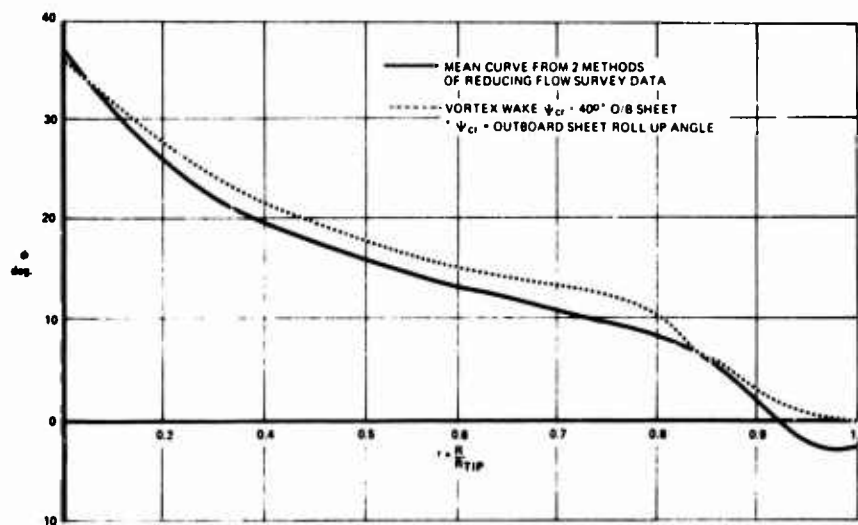
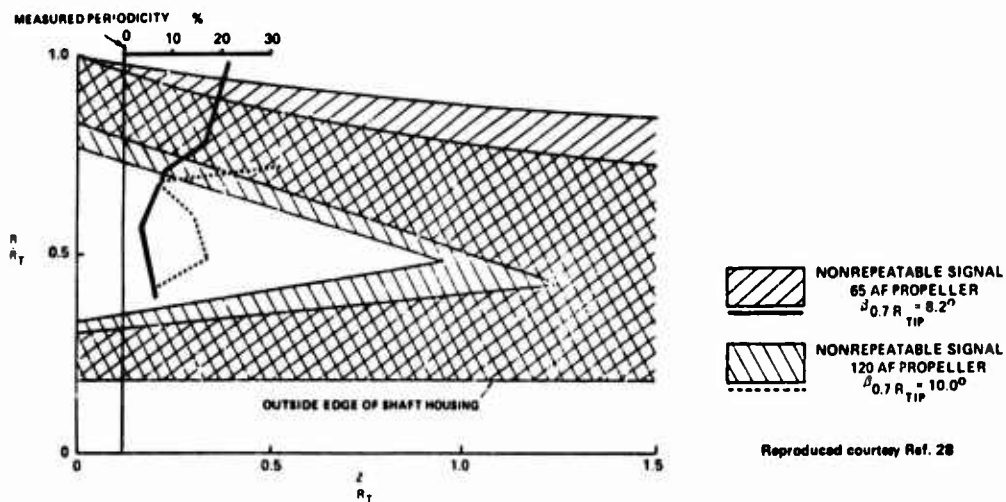
Figure 18 - INDUCED ANGLE DISTRIBUTION 1968 B PROPELLER $\beta = 14^\circ$ Figure 17 - INDUCED ANGLE DISTRIBUTION 1968 A PROPELLER $\beta = 12^\circ$ 

Figure 19 - REGIONS OF NON-REPEATING HOT WIRE SIGNALS FOR 2 PROPELLERS

Reproduced courtesy Ref. 28

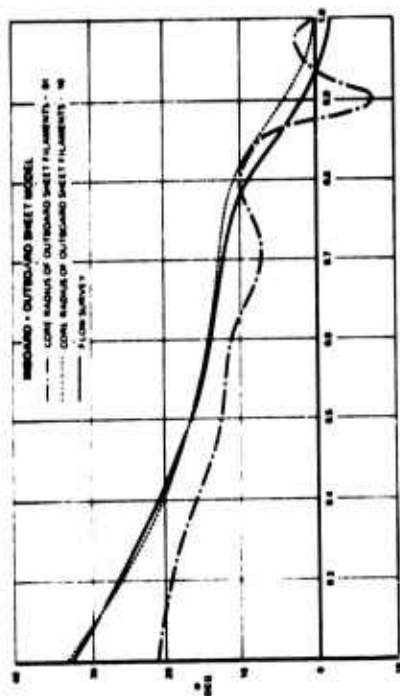


Figure 21 - REDUCED AMPLITUDE DISTRIBUTION 180 PROPPELLER 8 25-12P

A - 180°
 B - CORE RADIUS OF TIP WAVELENGTH, 180°
 C - CORE RADIUS OF TIP WAVELENGTH, 180°
 D - CORE RADIUS OF TIP WAVELENGTH, 180°
 E - CORE RADIUS OF TIP WAVELENGTH, 180°
 F - CORE RADIUS OF TIP WAVELENGTH, 180°
 G - CORE RADIUS OF TIP WAVELENGTH, 180°
 H - CORE RADIUS OF TIP WAVELENGTH, 180°
 I - CORE RADIUS OF TIP WAVELENGTH, 180°
 J - CORE RADIUS OF TIP WAVELENGTH, 180°
 K - CORE RADIUS OF TIP WAVELENGTH, 180°
 L - CORE RADIUS OF TIP WAVELENGTH, 180°
 M - CORE RADIUS OF TIP WAVELENGTH, 180°
 N - CORE RADIUS OF TIP WAVELENGTH, 180°
 O - CORE RADIUS OF TIP WAVELENGTH, 180°
 P - CORE RADIUS OF TIP WAVELENGTH, 180°
 Q - CORE RADIUS OF TIP WAVELENGTH, 180°
 R - CORE RADIUS OF TIP WAVELENGTH, 180°
 S - CORE RADIUS OF TIP WAVELENGTH, 180°
 T - CORE RADIUS OF TIP WAVELENGTH, 180°
 U - CORE RADIUS OF TIP WAVELENGTH, 180°
 V - CORE RADIUS OF TIP WAVELENGTH, 180°
 W - CORE RADIUS OF TIP WAVELENGTH, 180°
 X - CORE RADIUS OF TIP WAVELENGTH, 180°
 Y - CORE RADIUS OF TIP WAVELENGTH, 180°
 Z - CORE RADIUS OF TIP WAVELENGTH, 180°

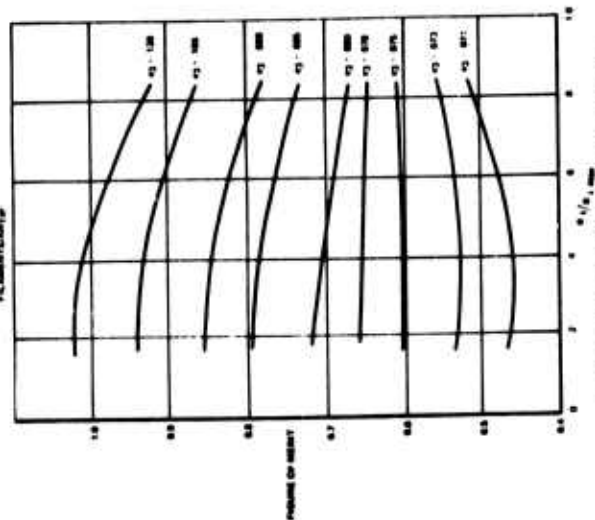


Figure 22 - SENSITIVITY OF FIGURE OF MERIT TO CORE SIZE

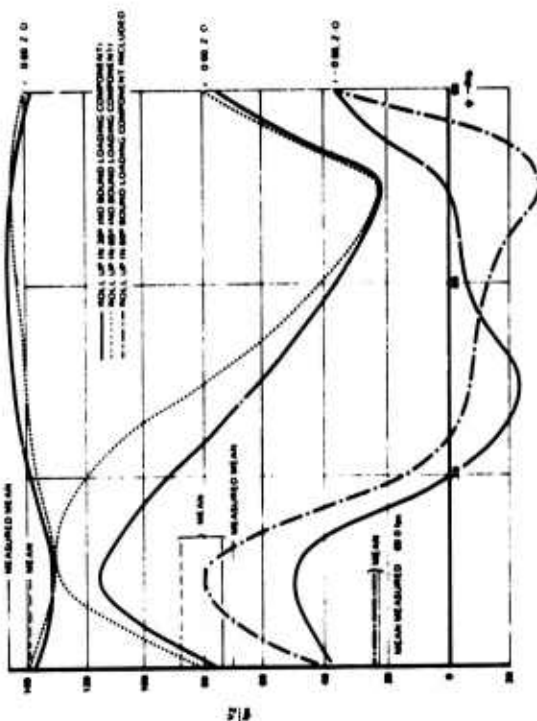


Figure 23 - AZIMUTHAL VARIATION OF ACTUAL VELOCITY AT PROP PLANE 180 PROP 8 25-12P

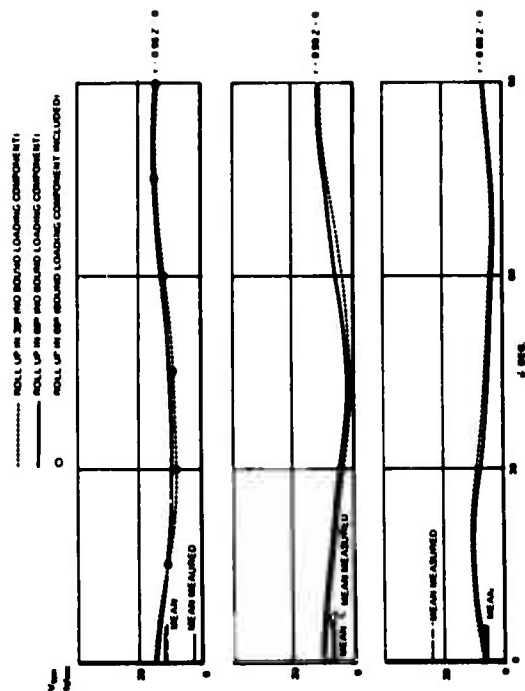


Figure 24 - AZIMUTHAL VARIATION OF TANGENTIAL VELOCITY AT PROP PLANE 180 PROP 8 25-12P

A SUMMARY OF CURRENT RESEARCH IN ROTOR UNSTEADY AERODYNAMICS
WITH EMPHASIS ON WORK AT LANGLEY RESEARCH CENTER

John F. Ward
Aero-Space Technologist

and

Warren H. Young, Jr.
Aero-Space Technologist
U. S. AAMRDL, Langley Directorate

NASA Langley Research Center
Hampton, Virginia 23365

SUMMARY

The unsteady aerodynamics of rotary wings presents a fascinating, yet formidable, challenge to the fluid dynamics researcher. The consequences of the unsteadiness in rotor aerodynamics are clearly evident in practically every aspect of rotorcraft technology. Most of the limitations of rotary-wing aircraft stem from the fact that the lifting system is subjected to unsteady airloads. These limitations include: vibration boundaries imposed upon level flight and maneuver performance; increased detectability due to rotor impulsive noise; rotor and airframe fatigue; and costly maintenance, repair, and replacement requirements. Therefore, the understanding, control and accurate prediction of the more significant unsteady aerodynamic phenomena can ultimately yield substantial benefits in improved rotary-wing aircraft.

This paper summarizes the basic unsteady aerodynamic environment of the rotor, discusses some of the observed trends in the state of the art, and sets forth some of the research needs that will require attention in the future. In addition, the paper presents a review of a number of research investigations underway at the Langley Research Center as part of a joint NASA/Army rotorcraft research program. The research investigations are directed toward achieving a better understanding of rotor unsteady airloads. Specifically, these investigations include research in rotor maneuver loads, level flight and maneuver wake prediction, tip-vortex flow, blade-vortex interaction, dynamic stall, transient Mach number airloads, and variable-geometry rotor research.

NOTATION

A	tip vortex mean-axial-velocity parameter (see Reference 16)
C, C_0	blade chord, meters
C_T	rotor thrust coefficient
C_Q	rotor torque coefficient
d	tip-vortex core diameter, meters
g, G	gravitational-acceleration constant, meters/second ²
r	blade radial station, meters
\bar{r}	tip-vortex radial coordinate
R	blade radius, meters
R_L	radius of lower blade set, meters
R_U	radius of upper blade set, meters
t	time, seconds
V, V_∞	free-stream velocity, meters/second
V_θ	tip-vortex tangential velocity, meters/second
x	distance aft from leading edge on airfoil, meters
\bar{z}_T	tip-vortex axial coordinate
ΔR	radius difference between upper and lower rotor, meters
$\bar{\Delta R}$	radius ratio, $\Delta R/R$
ΔZ	vertical spacing between upper- and lower-blade sets, meters
$\bar{\Delta Z}$	vertical-spacing ratio, $\Delta Z/R$
$\Delta \theta$	collective-pitch angle increment between upper- and lower-blade sets, degrees
$\Delta \psi$	azimuth increment of upper-blade set relative to lower-blade set, degrees
θ	blade pitch angle, degrees
μ	rotor-tip-speed ratio, $V/\Omega R$
σ	rotor solidity
ψ	blade azimuth position, $\psi = 0$ is aft, degrees
ψ_W	wake azimuth angle relative to upper blade, degrees
Ω	rotor rotational speed, radians/second

1. INTRODUCTION

By design, the helicopter rotor operates in its own turbulent wake. This results in a broad spectrum of unsteady airloads which excite the numerous dynamic-response modes of the flexible rotor and airframe. Understanding the source of these unsteady airloads and developing verified prediction methods, can have a very significant benefit on the ability to design improved rotorcraft. The state of the art in rotor unsteady airloads appears to be in a phase of detailed measurement, exploration, and attempts to devise workable mathematical models of some of the more significant unsteady aerodynamic phenomena observed in flight and wind-tunnel testing during the past decade.

The National Aeronautics and Space Administration and the United States Army Air Mobility Research and Development Laboratory are jointly engaged in a rotor research program at the Langley Research Center. This program includes in-house, grant, and contract investigations in the areas of rotorcraft aerodynamics, dynamics, stability and control, structures, and materials.

Following a brief assessment of the state of the art of rotor unsteady airload technology, this paper presents a review of a number of the current unsteady aerodynamics research investigations at the Langley Research Center. These investigations include maneuver loads, level flight and maneuver wake prediction, tip-vortex flow, blade-vortex interaction, dynamic stall, transient Mach number airloads, and variable-geometry rotor research.

2. ROTOR AERODYNAMIC ENVIRONMENT

2.1 The problem

There are numerous unsteady aerodynamic events that may occur in a single revolution of a helicopter rotor system operating at moderate to high forward speeds. The unsteadiness exists, to some degree, throughout the design operating envelope. The severity of the dynamic airloads associated with the unsteady aerodynamics depends upon the specific operating condition. Some of the more severe operating conditions are: maximum forward speed in level flight, maneuvering flight, rapid descents, and flared landings in ground effect. Rotor aerodynamics technology has been built on a foundation of blade-element theory, uniform inflow, and two-dimensional aerodynamics as a natural outgrowth of fixed-wing technology. However, the practical limitations of rotor operation are much more analogous to turbine engine/inlet matching aerodynamics (Reference 1) where the fundamental problem is one of dealing with extreme, time varying, three-dimensional distortions of the rotor inflow distribution.

Some of the more obvious unsteady, or transient, aerodynamic phenomena that contribute to rotor dynamic airloads are illustrated in Figure 1. The general categories of the flow shown in Figure 1 are: (1) stalled flow, (2) impulsive flow, (3) yawed flow, and (4) interference flow. Stalled flow includes airfoil dynamic stall and tip-vortex induced dynamic stall. A distinction is made here between airfoil and tip-vortex induced dynamic stall. Airfoil dynamic stall is associated with what has been referred to as stall flutter and it is sensitive to airfoil configuration changes. That is, airfoil modification has been shown to have a marked influence on the severity of stall flutter and the resulting oscillatory control-system loadings (Reference 2). A peculiar feature of this stall mechanism is the ability to distinguish between moment stall and lift stall during the initial stages of stall onset, as the blade moves through the retreating side of the rotor disk (References 3 and 4).

Tip-vortex induced dynamic stall is less sensitive to airfoil characteristics. The best airfoil cannot cope with some of the local angle-of-attack excursions induced by the passage of a tip-vortex filament in close proximity to the blade surface. Even in hovering flight the rotor performance is degraded by tip-vortex induced stall at the outboard blade sections (Reference 5). In forward flight maneuvers the blade-vortex interaction encountered in the aft portion of the rotor disk may cause high-frequency pitching-moment oscillations. Reference 6 indicates this blade-vortex dynamic stall may be a significant source of rotor vibratory load buildup during maneuvers.

Impulsive flow phenomena include blade-vortex interaction and transient Mach number effects. The impulsive airloads caused by blade-vortex interaction on the advancing side of the rotor disk result in the distinctive "blade slap" acoustic signature of some rotorcraft. In this case, the blade encounters a single vortex filament which causes extreme rates of change in airloading. This impulsive airload, which can occur simultaneously over large segments of the advancing blade, results in intense radiated noise in addition to the oscillatory structural loadings. The transient Mach number effects, which also occur on the advancing blade, include transient lift, drag, and pitching moments associated with the rapid movement of the shock wave over the upper surface of the blade. The interaction of the shock wave and boundary layer can also induce transient shock stall.

While there is still some question as to the significance of yawed flow in rotor aerodynamics, the extreme case of reversed flow is of concern when large inboard portions of the retreating blade are moving rapidly through 180° angle-of-attack changes and the aerodynamic center of the blade section is abruptly changing from the normal quarter-chord position to the three-quarter-chord position. This is of special concern for slowed, lifting rotors that are designed to operate at tip-speed ratios of one or greater.

Interference flow includes tail-rotor/main-rotor wake interaction, pylon-hub-engine exhaust interaction with the main and tail rotor, and wing-body interference. The significance of these aerodynamic interferences depends upon the specific rotorcraft configuration. However, in all cases these factors contribute to the difficulty of predicting the rotorcraft unsteady aerodynamic environment and the resulting dynamic airloads.

2.2 State of the art

The ultimate objective of rotor aerodynamic research should be to provide the rotorcraft designer with the analytical tools to develop and produce improved aircraft with a high level of confidence.

Figure 2, from Reference 7, illustrates this point by indicating the required capability in design analyses compared with the present capability. The figure includes both dynamics and aerodynamics because of the strong interaction between these two disciplines in rotorcraft design. In general, the present capabilities, and even the current efforts to provide improved analytical methods, are far short of the required capability. For the most part, verified design tools and meaningful design criteria do not exist in the area of rotor unsteady airloads. This situation exists because of the extreme complexity of both the rotor unsteady aerodynamics and the rotor and airframe dynamics.

Design of an entirely new rotor system cannot yet be classified as a science. It still retains many aspects of an "art," and the state of that art is such that rotorcraft tend to be evolved by small extrapolations in size and installed power. Manufacturers move in modest increments from one service-proven design to the next by exploring modifications of a basic rotor configuration. Paradoxically, there are wide variations in the basic designs of different manufacturers, which suggests that the necessity for relying heavily on empiricism, and trial and error has led different design groups down different paths. The present state of the art results in a hesitance on the part of the manufacturers to propose advanced concepts in aircraft design competitions. Likewise, it contributes to the user's reluctance to invest in the production of advanced designs even after investing heavily in the research and development of the advanced systems.

In the areas of rotorcraft aerodynamic and dynamic analyses the trend is toward the use of more complex computer programs to model the aeroelastic systems. While this is a natural tendency with the availability of digital computers having ever increasing capacity and computation speed, the point is being reached at which the analyst must observe the output of the computer much as a flight-test engineer observes the behavior of the actual aircraft. Since the computer model is approaching the complexity of the actual aircraft, a clear understanding of the "cause and effect" behavior of the aeroelastic mechanisms is lost in the computer. In any event, the burden is on the aerodynamicist to provide the proper input to the computer models. For example, the dynamicist and the acoustician are eagerly awaiting accurate unsteady airload inputs for their respective computer programs: the dynamicist - with the rotorcraft mass-elastic system well defined, and the acoustician - with the existing acoustic radiation theories ready to be applied.

In order to advance the state of the art to the proper level the unsteady aerodynamics technology must progress through the following steps:

- Identification of the problem
- Detailed measurement
- Mathematical modeling
- Verification of the math models
- Parametric studies
- Establishment of design criteria
- Development of accurate design methods

During the past decade rotor unsteady aerodynamics has moved from the first phase, problem identification, into a period of detailed measurement and mathematical modeling. Investigators are beginning to document, in detail, the rotor unsteady wake and boundary-layer flow. Mathematical models are also being developed in an attempt to duplicate the observed flow behavior. The principal areas of investigation include: hover, level flight and maneuvering wake-geometry prediction; tip-vortex flow; dynamic stall; and unsteady transonic flow.

There are a number of new trends in the manner in which investigators are dealing with rotor unsteady aerodynamics. Four of the more fundamental trends are:

1. There is tendency to deal more directly with transient and impulsive airloads rather than seeking methods to predict accurately individual harmonics of airloads from the steady to the 40th harmonic of rotor rotational speed.
2. Periodic rotor airloads have been demonstrated to be very repeatable for a given flight condition. While this is implicit in any attempt to correlate analytical and flight-test data, there had been frequent references in the past to the basic randomness of rotor airloads. This randomness is more directly associated with the variability of the rotor operating conditions.
3. There is increased concern over the validity of relating rotor-blade section aerodynamics to a local angle of attack which is poorly defined and frequently unknown in the unsteady wake environment.
4. There appears to be a trend away from a desire to amass great quantities of sinusoidal oscillating airfoil data. Research is now directed toward generalized theoretical and empirical methods that can be used to account for the effects of inflow unsteadiness on basic airfoil characteristics.

The above trends reflect the shift toward the detailed study of rotor unsteady flow. An example of the concern for more detailed investigation was noted in a specialists' meeting on the subject of dynamic stall held at the Langley Research Center in July 1971. This meeting brought together 50 investigators for 1 day to present and discuss their work and their ideas in the area of rotor dynamic stall. Some of the observations and recommendations resulting from the meeting are listed below.

1. Flow visualization documentation of rotor-blade dynamic stalling should be obtained to determine the role of vortex shedding in the actual dynamic stall of the retreating blade.
2. NASA/Army should review available dynamic-stall analyses, document them and pose a standard case for analytical correlation. Also, a standard dynamic-stall test case should be proposed so that a common test condition can be available for experimental and analytical correlation by all investigators.

3. Currently available dynamic stall C_n and C_m loops and free-wake analyses should be utilized to determine if the rotor tip-path plane position in space can be accurately predicted. If it cannot - determine why. Present testing indicates lateral flapping cannot be predicted accurately.

4. Two points of view can be taken with regard to dynamic-stall research:

a. Research oriented. - Study extreme cases of dynamic stall, and, after determining the basic mechanisms, interpolate back to stall onset and establish stall boundaries and stall margins.

b. Near-term design oriented. - Study the stall onset problem first, determine stall boundaries and means of delaying stall onset. After this has been achieved, proceed to a reassessment of the need for deep stall investigations.

5. The whole area of airfoil plunging should be reassessed. There are indications that this aspect of rotor dynamic stall may be as important as airfoil pitching motions.

6. Airfoil lift stall and moment stall should be considered as separate events - which may or may not happen simultaneously.

7. Consideration of C_n vs C_m loop characteristics may be useful in analyzing dynamic stall. Eliminating dependence on angle of attack, which is usually in doubt, may be helpful in correlating stall data from various sources.

8. A series of fundamental nonrotating blade tests should be conducted in order to build up to the complex rotating stall case in careful steps.

9. An investigation should be conducted to determine why some rotor systems are reported to be free of stall-flutter and dynamic-stall problems, and to determine whether it is a matter of definition or a fundamental rotor aeroelastic characteristic that is common to these rotor designs.

10. The influence of size on rotor dynamic-stall characteristics should be investigated. There appears to be some influence of size by way of stiffness, Reynolds number, number of blades, etc.

11. The role of the leading-edge shed vortex in the dynamic-stall mechanism should be explored. Is it an important mechanism, or is it a convenient analytical tool which has its counterpart in some flow visualization studies at low Reynolds number?

12. More emphasis should be placed on the short separation bubble at the leading edge of the airfoil. This bubble and its accurate analytical modeling are the key to the dynamic-stall process.

Similar recommendations for more experimental and analytical research effort would undoubtedly result from consideration of other aspects of rotor unsteady aerodynamics, such as, wake geometry, tip-vortex flow, and the development of suitable advanced airfoils.

2.3 Future research

In the future, emphasis should be placed on efforts to verify the mathematical models being developed. The many individual analytical tools will have to be combined and compared with data obtained from complete rotor systems. This verification process will require model-scale and full-scale rotor testing. At model scale it may be possible to avoid the usual difficulty of Reynolds number matching by conducting airfoil testing at the rotor-model scale. The analytical methods could then be verified by applying the model-scale airfoil data directly with the prediction of the model-rotor unsteady airloads and dynamic response. Ultimately, the development and verification of the analytical methods will also require full-scale rotor testing. Wind-tunnel testing of generalized rotor systems, which can be easily modified, will be essential. This type of capability is presently being developed at the Ames Research Center with the design and fabrication of a generalized rotor research system for use in the 40- by 80-foot wind tunnel. In addition, special flight research rotor test systems will also be required for the final verification of the analytical methods. Preliminary studies of such a rotor systems research aircraft are currently underway in a joint NASA/Army effort at Langley Research Center.

3. ROTOR UNSTEADY AERODYNAMICS RESEARCH AT LANGLEY RESEARCH CENTER

3.1 Research approach

The rotor unsteady aerodynamics research at the Langley Research Center is part of a cooperative-research program between the Langley Directorate of the United States Army Air Mobility Research and Development Laboratory and the Langley staff of the National Aeronautics and Space Administration. This joint program is, in turn, a part of an overall agreement between NASA and the United States Army Materiel Command which includes cooperative research programs at the Ames Research Center and the Lewis Research Center. The joint research effort was initiated in 1970 and involves the utilization of existing NASA research facilities and joint Army/NASA resources, such as: manpower, funding, research equipment, and flight-test aircraft. The research effort includes aerodynamics, dynamics, acoustics, structures, materials, and stability and control. In-house experimental and analytical investigations are complemented by supporting contract research as required. The following discussion presents a number of the research investigations in rotor unsteady aerodynamics currently underway as part of the joint NASA/Army rotorcraft research program.

3.2 Maneuver loads

There are severe limitations imposed upon helicopter maneuvering flight by unsteady aerodynamics. The limitations are reflected in a rapid increase in the magnitude of the rotor oscillatory control loads

and overall airframe vibration levels. The source of the problem is usually a buildup in the unsteady airloads induced by distorted wake flow, blade-vortex interaction, and dynamic stall. An example of how these factors interact to impose a limit on maneuvering flight was presented in Reference 6. This paper summarized a detailed review and analysis of H-34 helicopter rotor-blade differential pressure and structural load data for five maneuver-flight conditions. These maneuvers are indicated in Figure 3. For each case - four steady maneuvers and a single transient pullup maneuver - the maneuver was terminated when aircraft vibration levels increased to an unacceptable level. It was concluded from the analysis of the flight data that the probable cause of the maneuver limitation was a wake-induced buildup in the blade torsional degree of freedom response. The wake characteristic of primary importance was the helical pattern formed by the trailing vortices deposited into the fourth quadrant of the rotor disk during the maneuvers. Figure 4 indicates a typical trailed vortex pattern for the maneuver conditions investigated. The helical patterns formed by the trailed tip vortices are basically a function of rotor tip-speed ratio. In level flight the helical wake moves down and away from the rotor disk. However, in maneuvers the tip vortices come into close proximity with the rotor blades in the aft quadrants of the disk due to the changes in wake geometry caused by the blade lift variations and the maneuvering flight-path curvature. As a result, strong blade-vortex interaction can occur as indicated in Figure 4. The unsteady airloads induced by these blade-vortex interactions are shown in Figure 5. This figure presents time histories of the section aerodynamic pitching-moment coefficient at the 95% blade radius for one revolution of the rotor for a level-flight condition and a 1.5g transient maneuver condition. In contrast to the level flight case, the section pitching moment for the maneuver case indicates that local stalling is induced by the passage of the trailing tip vortices. The azimuth positions of the trailed vortex crossings, shown in Figure 4, are also indicated in Figure 5.

The important factors in the maneuvering flight unsteady airloads are wake geometry, tip-vortex flow, blade-vortex interaction, and dynamic stall. Each of these areas has been investigated in the Langley Research Center rotorcraft research program. Some of the highlights of these research efforts will be included in the following discussion.

3.3 Wake geometry

There is an increasing demand for more realistic analytical models for simulating rotor wake flow. The application of improved wake flow calculation methods is an important step in determining the blade unsteady airloads and dynamic response. References 8, 9, and 10 present a description of a rotor wake computer program which is now under development. Figure 6 illustrates the type of wake geometries that can be produced by the computer program. Basically, the rotor wake is calculated by a process similar to the startup of a rotor in a free stream. An array of discrete trailing and shed vortices is generated. Vortex strengths corresponded to stepwise radial and azimuthal blade circulations, and this array is limited to an arbitrary number of azimuthal steps behind each blade. The remainder of the wake model for each blade is an arbitrary number of trailed vortices. Vortex element end points are allowed to be transported by the free stream and vortex-induced velocities. Wake geometries, wake flows, and wake induced velocity influence coefficients for use in blade loads calculations are determined. Wake geometries can be calculated for various rotor configurations, including rotor systems having shaftwise separation, nonuniform azimuth spacing (as in Figure 6), counter-rotating blades, and rotors with blade length and other physical differences.

The computer program presented in Reference 10 also includes a blade loads program which allows the computation of the response of flexible rotor blades to the applied airloads. The wake geometry and blade response computer program was initially developed for level-flight conditions. It has recently been extended to handle steady-state maneuvers. In addition, the level-flight wake program is now being coupled to the rotor-blade/control-system dynamic-response computer program reported in References 11 and 12. A separate, but related, analytical investigation of the influence of blade flexibility, unsteady aerodynamics, and variable inflow on rotor stall performance characteristics is reported in References 13 and 14.

3.4 Tip-vortex flow

One of the primary ingredients of the rotor wake is the intense tip-vortex trailed from each rotor blade. In order to gain more understanding of the tip-vortex flow, a number of in-house and contract studies were initiated. The in-house effort was conducted using a small smoke tunnel to study the flow in the immediate vicinity of the tips of semispan wings. Figure 7 illustrates the basic tip-vortex formation mechanism for a conventional rotor-blade square tip shape. The formation can be considered in two phases. The first phase is the formation of a separation vortex along the streamwise edge of the tip. This vortex is much like the delta-wing leading-edge vortex in that it is formed by the separation of a vortex sheet from beneath the blade tip and reattachment of the sheet on the upper surface. The swirling flow formed by this process establishes the intense core of the tip vortex, with a core diameter of less than 1/10 of the tip-chord length. Downstream, behind the trailing edge, the vortex sheet shed from along the trailing edge is drawn around the separation vortex core to form the complete trailing-vortex system.

Following some additional flow visualization studies, reported in Reference 15, detailed tip-vortex-flow measurements were made using a three-axis hot-wire probe (Reference 16). This work was similar to the wind-tunnel investigation of Reference 17, and was done to determine scaling methods for simulating full-scale tip vortices. Figure 8 presents some of the results of this investigation. It was determined that all of the Mach number and Reynolds number data for vortex tangential velocities, axial velocities and core size could be collapsed onto curves which are functions of vortex age. If this correlating parameter can be shown to apply for vortex ages much larger than those of Reference 16, the results can also have significance with regard to the scaling of the fixed-wing trailing-vortex problem, which is now under intensive study by all segments of the civil aviation industry.

3.5 Blade-vortex interactions

The next phase of the investigation of rotor unsteady airloads was concerned with how the trailing tip vortices interacted aerodynamically with an airfoil. Experimental and analytical investigations were supported by grants to the Pennsylvania State University and Massachusetts Institute of Technology. The results of portions of these studies are presented in References 18 through 23. An example of the type of basic data obtained in these investigations is shown in Figure 9, taken from Reference 18. Figure 9 shows the variation of the section lift coefficient measured as the single-blade model cuts through the vortex center. Section lift coefficient peak-to-peak variations as high as 0.7 were measured in time intervals of 1 millisecond. This time interval corresponds to a blade translation distance of 1.15 chord lengths. Generally, the blade must move 8 to 10 chord lengths from the vortex before the influence is negligible. This will, of course, depend on the vortex dimensions and the orientation of the blade.

At the time of the original oral presentation of Reference 18, noise recordings and movies of the oscilloscope display of the pressure pulses caused by the blade-vortex interactions were presented. The correlation between the pressure-pulse signature and the blade "slap" noise was quite apparent. Since the original experimental work of References 18 and 19, additional testing and analytical correlation work has been done by Penn State and M.I.T. under various sponsors. Some of the results of this effort are presented in Reference 24 where very good analytical correlation is shown for the blade-vortex interaction impulsive noise measured with the Reference 18 model.

Besides the significance of the type of data shown in Figure 9 to the investigation of helicopter noise, these same data have important application to the unsteady airloads problem shown in Figure 5. In some situations the blade-vortex interaction will become severe enough to induce local-flow separation and result in dynamic stall. This likelihood is noted in the discussion of maneuver loads in section 3.2 of this paper. In order to investigate the dynamic-stall mechanism associated with blade-vortex interaction an analytical study was initiated. While the work was originally aimed specifically toward vortex-induced dynamic stall, it became apparent that the required analytical formulation contained all the ingredients of a general dynamic-stall analysis with vortex-induced dynamic stall as a special case.

3.6 Dynamic stall

The dynamic-stall analysis development is aimed at unsteady airloads research and design utilization, rather than helicopter performance prediction. The ability to predict the lift and pitching moment of new airfoils throughout the stall regime is a primary aim of the investigation. By including rotor dynamics, prediction of stall-flutter characteristics can be made. The dynamic stall induced by interaction with tip vortices of other blades can also be calculated by combining appropriate dynamic-stall subprograms with the rotor-free wake analyses.

Reference 25 presents the initial results of a dynamic-stall analytical method currently under development. This study has produced a theoretical model that predicts most of the features of dynamic stall qualitatively. The components of this incompressible, two-dimensional theory are shown in Figure 10. Below stall, the laminar separation point is followed by a separation bubble. After transition to turbulent flow, a reattachment region leads to a turbulent boundary layer. The viscous flow is solved by momentum integral techniques which require many empirical relations and outright assumptions. After stall, the separation region is assumed to be at constant pressure, and it is modeled by putting sources and sinks in the potential flow. The potential flow is a linear theory for a flat plate, but with a correction term to account for leading-edge radius. The vortices shed from the trailing edge are explicitly included, but the effect of the vortices shed from the leading edge is accounted for by the region of constant pressure.

The important sources of uncertainty in the present model are the expansion and contraction of the constant-pressure regions, the point of transition in the separation bubble, stall criteria, the pressure distribution near the leading edge, and the process of recovery from stall. The greatest asset of the model is the inclusion of the effect of the viscous regions on the potential flow. This strong interaction of viscous and potential flow is achieved by matching pressures. The results show that a weak interaction theory would be inadequate in the stall regions.

This model has made several significant contributions towards a better description of dynamic stall. It has been applied to the case of blade-vortex interaction discussed in sections 3.2 and 3.5. The response to the spacing of these vortices had been qualitatively defined. The analytical method is presently being applied to model the pitch-plunge stall flutter of an isolated airfoil. Further improvements will be made to the analytical model, and it will be incorporated into a helicopter performance program. Another achievement of this model is the integration of the essential components of dynamic stall. Boundary-layer experts should no longer ignore the strong interaction with potential flow. The ability of the potential-flow theory in representing an essential part of the problem is shown to be inadequate; elegant piecemeal analyses have been superseded by a less sophisticated, but more complete, model. The model also highlights several areas that are not well understood. The role of the separation bubble in transition and stall, the entire turbulence model in separated flow, and the process by which the airfoil unstalls are areas of ignorance.

A new model of dynamic stall is being developed, under a research contract by R. E. Olson and S. J. Shamroth of United Aircraft Research Laboratories. It will be designed to help remedy the major deficiencies of the theory of Reference 25 up to the stall point. It will later be extended to strong interaction so that the complete dynamic-stall loop can be calculated. The analysis will be valid for an airfoil of arbitrary shape with a distorted wake, but it will be limited to two-dimensional, incompressible flow. The components of the analysis are indicated in Figure 11. The regions of separated and stagnation point flow will be found by solving the unsteady Navier-Stokes equation by the method of Reference 26. In regions where it is obvious that the boundary-layer assumptions are valid, the Navier-Stokes equations will be simplified to parabolic form. The viscosity in transitional or turbulent flow

will be based on the turbulent kinetic energy as in Reference 27. Preliminary results show good agreement with experiment for transitional flow in a small separation bubble. The inviscid-flow solution of J. P. Giesing (Reference 28) will be utilized.

When the Navier-Stokes equations describe the flow near the body, there is no need to construct a preconceived model of the flow over the upper surface. If vorticity or stagnant flow passes over the upper surface, the solution will describe it. This advantage is purchased by greatly increased computational complexity. There is also a problem in setting the boundary between the viscous and inviscid flow. This will involve the stability and accuracy of the Navier-Stokes solution over large separated regions. A model for the relationship between the thick wake, the inviscid model of the wake, and airfoil circulation must be constructed. Another problem will be the calculation of the turbulent shear stresses in the separated regime.

3.7 Transient Mach number

H-34 helicopter rotor-blade pressure data (Reference 29) were reviewed in detail to determine the influence of transient Mach number on unsteady airloads. The data were obtained for selected, single rotor revolutions at a fixed tip-speed ratio - but with various advancing tip Mach numbers (that is, rotor operational advancing tip Mach number at $r/R = 1.0$ and $\psi = 90^\circ$). Typical time histories for the chordwise pressure transducers at the 95% radius station are shown in Figure 12. Both sets of data are at a tip-speed ratio, μ , of 0.28 and the same gross weight. The time histories on the left are for a rotor advancing tip Mach number of 0.74 and on the right for 0.82. The pressure pulse, which appears in the right hand traces for X/C values of 0.233 and 0.335, are the result of the transient shock front moving back and forth over the upper-surface pressure-transducer orifices. These pressure-pulse signatures, which are essentially superimposed on the basic pressure time histories at the left of Figure 12, changed in a logical fashion as the rotor advancing tip Mach number operating condition was varied while holding a constant tip-speed ratio.

The movement of the shock front at the 95% radius station is shown in the lower portion of Figure 13. The shock moves onto the blade at approximately 20° azimuth and appears to reach its most aft position at 100° azimuth. It then moves forward and off the blade leading edge at about 190° azimuth. While the precise start and stop of the shock movement is difficult to establish, the shock movement over the midchord region was clearly evident. The upper sketch in Figure 13 indicates the maximum aft excursion of the shock front over the outer blade surface determined from pressure-time histories at the 95%, 90%, 85%, and 75% radial stations. The maximum aft movement of the shock in this case occurred when the blade was at 100° azimuth position. The impulsive loading associated with the local transient Mach number variation causes a noseup blade torsional-moment response and a normal-force impulse of approximately 900 N (approximately 200 lbf) for a duration of less than 50 milliseconds. This introduces nonlinearities in blade pitch-control requirements and slight changes in rotor-trim requirements to accommodate the Mach number effects.

Additional transient Mach number data from flight tests of the CH-53 and NH-3 helicopters are currently being analyzed. This type of data has a number of important applications. Reference 30 presents transient Mach number effects as the source of rotor-blade self-excited oscillations at high subsonic Mach numbers. In addition, the H-34 airloads data indicate that any analytical treatment of rotor sound radiation must include the normal-force impulse in addition to the usual drag-rise considerations and the fact that the airfoil is accelerating at a speed near to, but less than, the speed of sound (Reference 31).

3.8 Tip shape

Various means of alleviating blade-vortex-interaction unsteady airloads are under study in the industry. These include reducing the intensity of the vortex during the formation stage by suitable tip-shape modifications, and inducing turbulent mixing and flow instabilities in the vortex flow so that rapid decay of the trailing-vortex system will take place. The latter approach is being investigated under Army, Navy and NASA sponsorship of research with the mass-injection blade-tip concept reported in Reference 32. Initial full-scale rotor testing of this active dissipation concept will be conducted on the whirl tower at Langley Research Center in the fall of 1972.

An alternate, passive approach for tip-vortex diffusion is to modify the formation mechanism in some manner by use of a special tip shape. A number of investigations of tip shapes have been underway throughout the industry. One of the shapes being investigated at the Langley Research Center is the ogee tip shape. A sketch of the tip-shape planform and the tangential velocity data from Reference 16 are presented in Figure 14. The tip thickness distribution is identical to the chord distribution, resulting in a fixed airfoil section over all but the extreme tip, where the airfoil section transitions to an elliptical shape. The square-tip data are repeated from Figure 8 for comparison purposes. The semispan wing tests were conducted using the same planform area for the square-tip wing and the ogee-tip wing. The maximum tangential velocities in the vortex core are reduced below those for a square tip by a factor of 4. The data also show that significantly more time is required for the vortex formed by the ogee tip to roll up completely and develop its maximum tangential velocity. The core diameter of the vortex from the ogee tip was substantially larger than that from the square tip and it was not well defined. In addition, the diffuse tip vortex of the ogee tip did not show any significant axial velocity trends. The formation process of the ogee-tip vortex is more analogous to the rollup of a trailing vortex sheet than to the formation of a conventional tip vortex. This suggests that the elimination of the separation vortex mechanism (Figure 7), which was the goal of the ogee-tip design, was substantially achieved. The concentration mechanism associated with the interaction of the intense core of the separation vortex and the vortex sheet shed from the trailing edge is no longer present. This allows a more gradual and diffuse rollup of the tip-vortex system. After correcting the lift-to-drag-ratio data for differences in aspect ratio, the ogee-tip wing had a slight (approximately 5%) improvement in efficiency over the square-tip wing.

A number of exploratory flow visualization studies have been conducted using the ogee tip shape on small-scale rotor models. Figure 15 shows some typical results of schlieren photography studies of a two-bladed, 0.4 m (1.3 ft) diameter, rotor model operating in a hover mode at a tip Mach number of 0.69. The intense tip vortex core helix can be seen for the square-tip model. The intensity of the tip vortex is considerably reduced for the ogee-tip model so that it is no longer visible in the schlieren photograph on the right of Figure 15.

A full-scale UH-1H helicopter two-bladed rotor system is presently being modified at the Langley Research Center to install the ogee tip shape. An exploratory flight test will be conducted to determine whether the reduction in tip-vortex intensity demonstrated in the wind-tunnel tip-shape tests and the model rotor schlieren studies, will actually result in a reduction in blade-vortex interaction unsteady airloads and blade-slap noise.

3.9 Variable-geometry rotor

A rotor concept that evolved from research into the problem of blade-vortex interaction is shown in Figure 16. The basic objective of the variable-geometry rotor is to gain some control over the way tip vortices and following blades interact aerodynamically and dynamically. The configuration is essentially composed of two co-rotating conventional rotor systems - one upper and one lower, with three or more blades each - that can be phased in azimuth position relative to one another. This phasing would ultimately be controlled in flight in order to achieve optimum phasing of blade forces at the hub, and to minimize the blade-vortex interactions for a given flight condition. The research investigation will include documentation of the influence of differential blade radius, differential collective and cyclic pitch, and vertical spacing in addition to the aerodynamic, dynamic and acoustic effects of azimuthal phasing between rotors. The analytical study of these rotor configurations utilizes the wake program discussed in section 3.3.

Some of the initial model test results are shown in Figure 17. Hovering performance and flow visualization tests were conducted using a 1.2 m (4 ft) diameter six-bladed rotor system. These tests were conducted at United Aircraft Research Laboratories with equipment similar to that used in the investigation of Reference 5. The results of the performance tests indicate that by changing from a conventional six-bladed configuration, with all blades in the same disk plane, to an arrangement where every other blade is raised vertically a distance of two chord lengths, the thrust is increased by approximately 7% at high-thrust conditions (or the torque is reduced by 11% for a fixed-thrust condition). Most of the performance increase resulting from vertical spacing was achieved with only one chord length vertical spacing. Increasing vertical spacing from one to two chord lengths and changes in azimuth spacing has secondary effects on the hover performance gains.

The aerodynamic mechanism involved in the performance increase is the manner in which the trailing tip vortices interact with each other and with the following blades. Figure 18 shows sample tip-vortex coordinates for the configuration that showed performance improvement in Figure 17. (Note that the blade vertical spacing depicted in Figure 18 is not to scale.) In a conventional six-bladed rotor, with all blades in the same disk plane, the tip vortex tends to trail back in the disk plane (see Reference 5) to the following blade and induce tip stalling at high thrust conditions. With vertical spacing between alternate blades, and a rotor phasing of 30° , the upper-blade tip vortex passes over the following blade and then is drawn down beneath the next blade pair as a result of interacting with the lower-blade tip vortex. The net result is a delay in the onset of tip stalling induced by blade - vortex interaction. Model tests are continuing with wind-tunnel tests, and plans call for conducting whirl-tower tests of a full-scale rotor to verify the model hover performance results.

The rotor systems currently under investigation are exploratory research rotors and, in some cases, may pose special hardware design difficulties in practical application. However, some of the more promising configurations will be selected for full-scale flight testing with the NASA/Army Rotor Systems Research Aircraft currently under development at the Langley Research Center. Preliminary design studies indicate that two, three-bladed, co-rotating rotors with vertical separation of one to two chord lengths and with in-flight control of azimuth phasing between rotors can be fabricated without difficulty.

3.10 Additional research

With the increased emphasis on civil and military helicopter utilization, Langley Research Center in-house rotorcraft research effort is expanding. While a major portion of the research summarized above has been accomplished with contract support, an increasing amount of in-house research is being initiated. Flight tests, whirl-tower tests, instrumentation development, airfoil development, wind-tunnel tests of rotor models and development of special research equipment are now being initiated with the availability of more NASA and Army manpower and funding.

Development of special rotor instrumentation has progressed to the flight demonstration phase. This system allows in-flight data acquisition of digitized, high frequency, rotor-blade pressure data which can be transmitted by a telemetry data link directly from the rotor hub to a ground station. Special schlieren, laser Doppler velocimeter, and hot-wire anemometry systems are being developed for application to wind tunnel and whirl tower rotor wake flow data acquisition. Research models under development include: (1) a general rotor-research model for use in the Langley V/STOL tunnel, (2) a general rotor stall-flutter model for use in the transonic dynamics tunnel, (3) a special model to study the isolated effects of yawing oscillation on airfoil unsteady aerodynamics, (4) an oscillatory wing model to study the dynamics of unsteady tip-vortex flow, and (5) a large scale airfoil pitching facility to simulate rotor airfoil angle-of-attack time histories and to investigate airfoil stall flutter. Wind-tunnel tests are continuing to study and document the tail-rotor aerodynamics (Reference 33). Research is also continuing in the area of airfoil noise generation for unsteady (Reference 34) and steady flow conditions.

Analytical studies planned will proceed to more sophisticated unsteady boundary-layer analyses for utilization in the dynamic-stall computer programs. In the area of fundamental fluid mechanics, a research grant has been initiated with Michigan State University to explore the application of Dr. Krzywoblocki's wave mechanics theory of turbulence (Reference 35) to the fundamental flow mechanisms encountered in rotor unsteady aerodynamics. If this work is successful, the wave mechanics theory of turbulence could have important and far reaching application to the general field of unsteady aerodynamics and turbulent flow.

4. CONCLUDING REMARKS

The state of the art of rotor unsteady airloads appears to have moved beyond the stage of problem identification and into a period of theoretical development, careful experimental documentation, and semi-empirical analytical modeling. The attention being given rotor unsteady aerodynamics by Government and industry researchers is increasing along with the general trend toward increased civil and military utilization of rotary-wing aircraft. However, there is a great deal to be accomplished before the required design analyses capabilities, such as generalized design methods and meaningful design criteria, are available to the industry as a whole. The next essential step in the development of these capabilities appears to be the careful experimental verification of the numerous, and increasingly complex, analytical tools that are being developed, and sometimes hastily implemented, as digital computers with ever increasing capacity and speed become available.

The joint NASA/Army rotorcraft unsteady airloads research program at Langley Research Center has been concentrated in the area of wake-geometry prediction, tip-vortex flow, blade-vortex interaction, dynamic stall, and transient Mach number investigations. Some methods for the alleviation of rotor unsteady airloads problems are being investigated, including tip-shape studies and variable-geometry rotor research. Additional efforts in instrumentation development, rotor model wind-tunnel tests, and exploratory flight testing are underway. Future plans call for development of special research rotors for investigating unsteady aerodynamics and verifying analytical methods in flight by utilizing the NASA/Army Rotor Systems Research Aircraft.

5. REFERENCES

1. Crites, R.
Czysz, P.
Lynch, F. R&D Pays Off for Inlet/Engine Matching. *Astronautics and Aeronautics*, vol. 10, no. 6, June 1972. pp. 64-67.
2. Benson, R. G.
Dadone, L. U.
Gormont, R. E.
Kohler, G. R. Influence of Airfoils on Stall Flutter Boundaries of Articulated Helicopter Rotors. AHS Preprint no. 621, American Helicopter Society, May 1972.
3. Ham, N. D. Review of MIT Research on Airfoil Dynamics Stall 1964 - 1971. ASRL TR 130-3, Massachusetts Institute of Technology, 1971.
4. McCroskey, W.
Fisher, R. K., Jr. Detailed Aerodynamic Measurements on a Model Rotor in the Blade Stall Regime. *Journal of American Helicopter Society*, vol. 17, no. 1, January 1972. pp. 20-30.
5. Landgrebe, A. J. The Wake Geometry of a Hovering Helicopter Rotor and Its Influence on Rotor Performance. AHS Preprint no. 620, American Helicopter Society, May 1972.
6. Ward, J. F. Helicopter Rotor Periodic Differential Pressures and Structural Response Measured in Transient and Steady-State Maneuvers. *Journal of American Helicopter Society*, vol. 16, no. 1, January 1971. pp. 16-25.
7. Tapscott, R. J. Rotorcraft Applications and Technology. *Proceedings of Conference on Vehicle Technology for Civil Aviation*, NASA SP-292, 1971. pp. 345-358.
8. Sadler, S. G. A Method for Predicting Helicopter Wake Geometry, Wake-Induced Flow and Wake Effects on Blade Airloads. AHS Preprint no. 523, American Helicopter Society, May 1971.
9. Sadler, S. G. Development and Application of a Method for Predicting Rotor Free Wake Positions and Resulting Rotor Blade Airloads - Model and Results. NASA CR-1911, 1971.
10. Sadler, S. G. Development and Application of a Method for Predicting Rotor Free Wake Positions and Resulting Rotor Blade Airloads - Program Listings. NASA CR-1912, 1971.
11. Piarulli, V. J. The Effects of Nonuniform Swash-Plate Stiffness on Coupled Blade-Control System Dynamics and Stability - Analysis and Application. NASA CR-1817, 1971.

12. Piarulli, V. J. The Effects of Nonuniform Swash-Plate Stiffness on Coupled Blade-Control System Dynamics and Stability - Computer Program Listing. NASA CR-1818, 1971.
13. Bellinger, E. D. Analytical Investigation of the Effects of Blade Flexibility, Unsteady Aerodynamics, and Variable Inflow on Helicopter Rotor Stall Characteristics. NASA CR-1769, 1971.
14. Bellinger, E. D. Analytical Investigation of the Effects of Blade Flexibility, Unsteady Aerodynamics, and Variable Inflow on Helicopter Rotor Stall Characteristics. AHS Preprint no. 520, American Helicopter Society, May 1971.
15. Piziali, R.
Trenka, A. An Experimental Study of Blade Tip Vortices. NASA CR-66860, 1970.
16. Rorke, J. B.
Moffitt, R. C.
Ward, J. F. Wind-Tunnel Simulation of Full-Scale Vortices. AHS Preprint no. 623, American Helicopter Society, May 1972.
17. Chigier, N. A.
Corsiglia, V. R. Tip Vortices - Velocity Distributions. AHS Preprint no. 522, American Helicopter Society, May 1971.
18. McCormick, B. W., Jr.
Surendraiah, M. A Study of Rotor Blade-Vortex Interaction. AHS Preprint no. 421, American Helicopter Society, June 1970.
19. Surendraiah, M. An Experimental Study of Rotor Blade-Vortex Interaction. NASA CR-1573, 1970.
20. Padakannaya, R. Experimental Study of Rotor Unsteady Airloads Due to Blade-Vortex Interaction. NASA CR-1909, 1971.
21. Walsh, R. G., Jr. Leading-Edge Pressure Measurements of Airfoil Vortex Interaction. ASRL TR 153-1, Massachusetts Institute of Technology, 1970.
22. Johnson, W. Application of a Lifting-Surface Theory to the Calculation of Helicopter Airloads. AHS Preprint no. 510, American Helicopter Society, May 1971.
23. Johnson, W. A Comparison Between Experimental Data and a Lifting Surface Theory Calculation of Vortex Induced Loads. ASRL TR 153-3, Massachusetts Institute of Technology, 1970.
24. Widnall, S. Helicopter Noise Due to Blade/Vortex Interaction. Journal of Acoustical Society of America, vol. 50, no. 1, July 1970. p. 345.
25. Crimi, P.
Reeves, B. L. A Method for Analyzing Dynamic Stall of Helicopter Rotor Blades. NASA CR-2009, 1972.
26. Briley, W. R. A Numerical Study of Laminar Separation Bubbles Using the Navier-Stokes Equations. Journal of Fluid Mechanics, vol. 47, no. 4, 1971. pp. 713-736.
27. McDonald, H.
Camarata, F. J. An Extended Mixing Length Approach for Computing the Turbulent Boundary Layer Development. Proceedings of the AFOSR-IFP-Stanford Conference on Computation of Turbulent Boundary Layers - 1968, Stanford, California, 1969.
28. Geising, J. P. Nonlinear Two-Dimensional Unsteady Potential Flow with Lift. Journal of Aircraft, vol. 5, March 1968. pp. 135-143.
29. Scheiman, J. A Tabulation of Helicopter Rotor-Blade Differential Pressures, Stresses, and Motions as Measured in Flight. NASA TM X-952, 1964.
30. Paul, W. F. A Self-Excited Rotor Blade Oscillation at High Subsonic Mach Numbers. AHS Preprint no. 228, American Helicopter Society, May 1968.
31. Lyon, R. H. Radiation of Sound by Airfoils that Accelerate Near the Speed of Sound. Journal of Acoustical Society of America, vol. 49, no. 3, March 1971. pp. 894-905.
32. White, R. P., Jr.
Balcerak, J. C. The Genesis of the Trailing Tip Vortex - Is It Now Conquered? AHS Preprint no. 624, American Helicopter Society, May 1972.
33. Boster, R. J.
Morris, C. E. K., Jr. A Note on Phenomenon Affecting Helicopter Directional Control in Forward Flight. Journal of American Helicopter Society, vol. 15, no. 4, October 1970. pp. 38-45.

- 34. Gray, R. B.
Pierce, G. A. Exploratory Investigation of Sound Pressure Level in the Wake of an
Oscillating Airfoil in the Vicinity of Stall. NASA CR-1948, 1972.
- 35. Krzywoblocki, M. Z. E. Wave Mechanics Theory of Turbulence. Tenth Symposium on Advanced
Problems and Methods in Fluid Mechanics, Proceedings, part 2,
Warsaw, Panstwowe Wydawnictwo Naukowe, 1972. pp. 365-390.

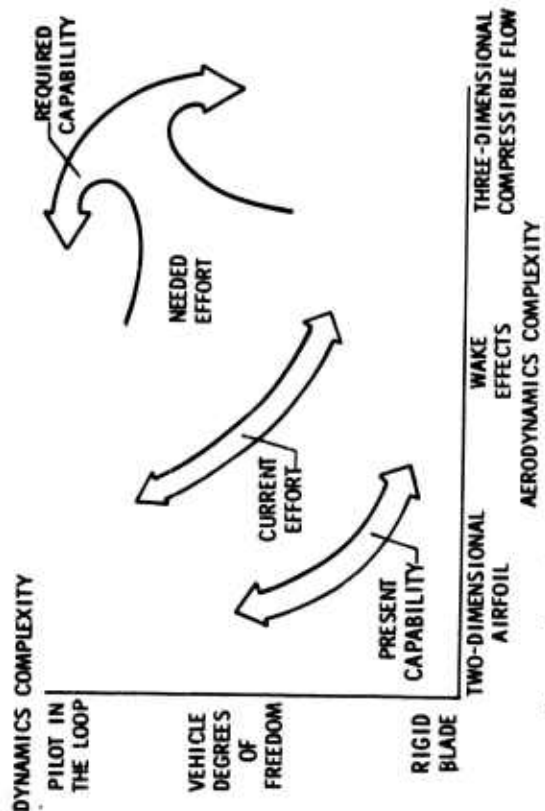


Figure 2.- Aerodynamic and dynamic considerations required in design analyses.

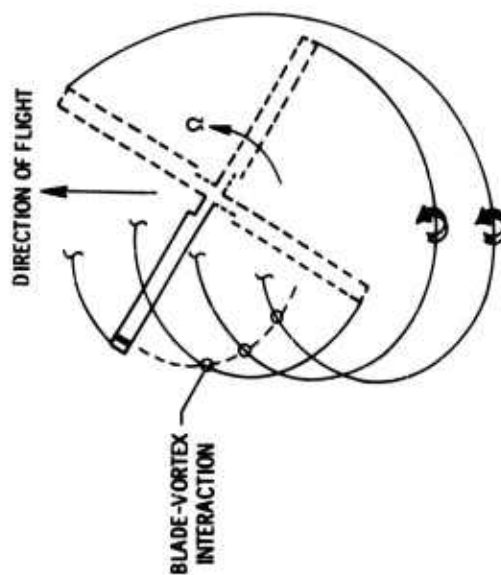


Figure 4.- Trailing tip vortex helical pattern at $\mu = 0.2$.

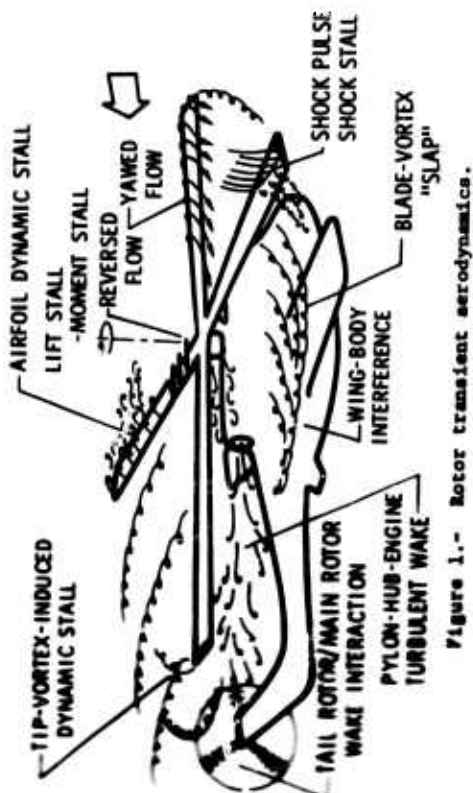


Figure 1.- Motor transient aerodynamics.

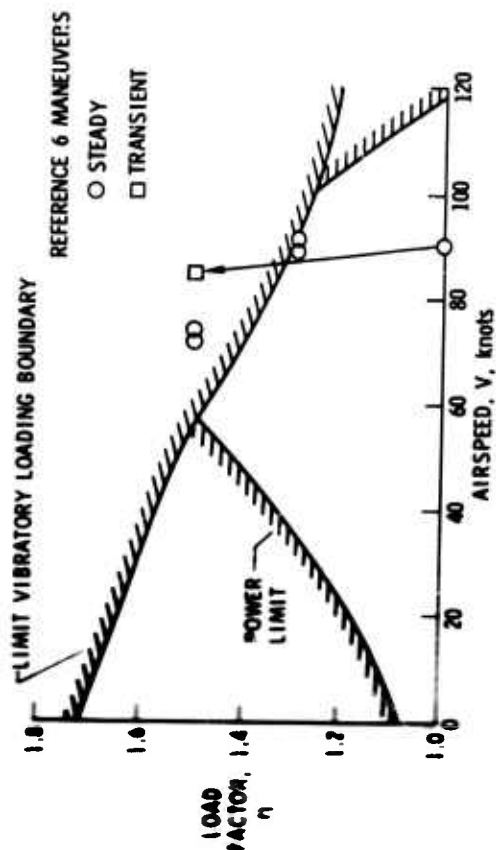


Figure 3.- H-34 maneuver loads envelope.

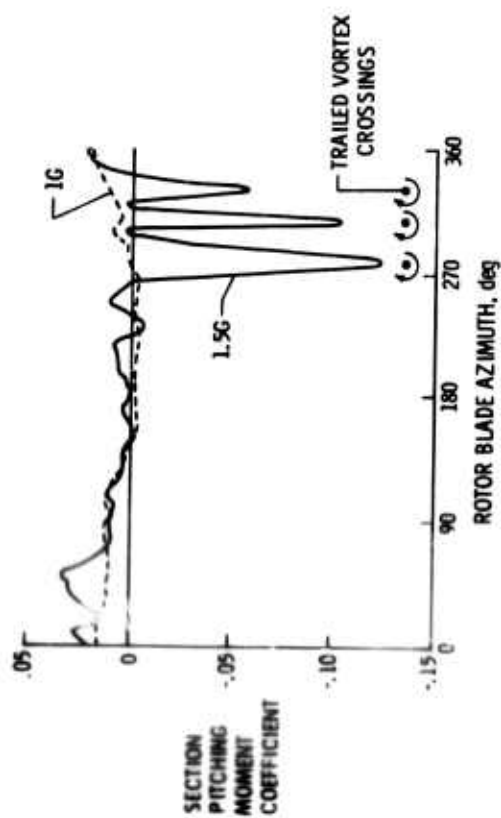


Figure 5.- Aerodynamic pitching moment coefficient
95-percent radial station, $\mu = 0.2$.

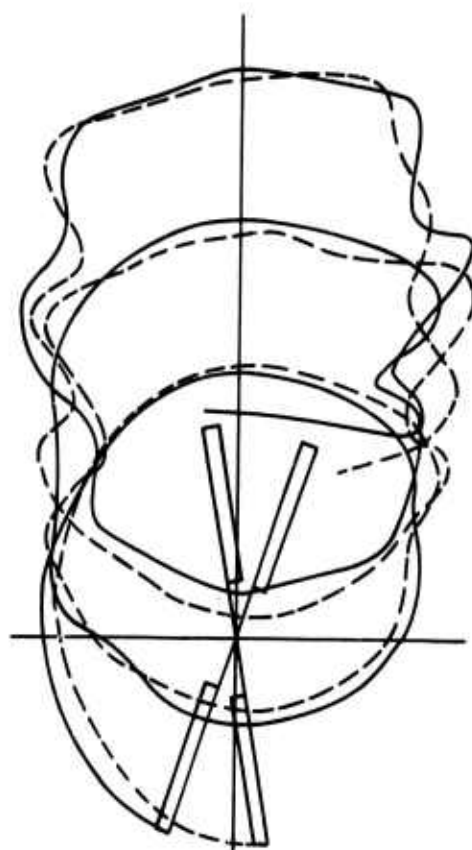


Figure 6.- Rotor wake geometry prediction computer
program output, $\mu = 0.1$.

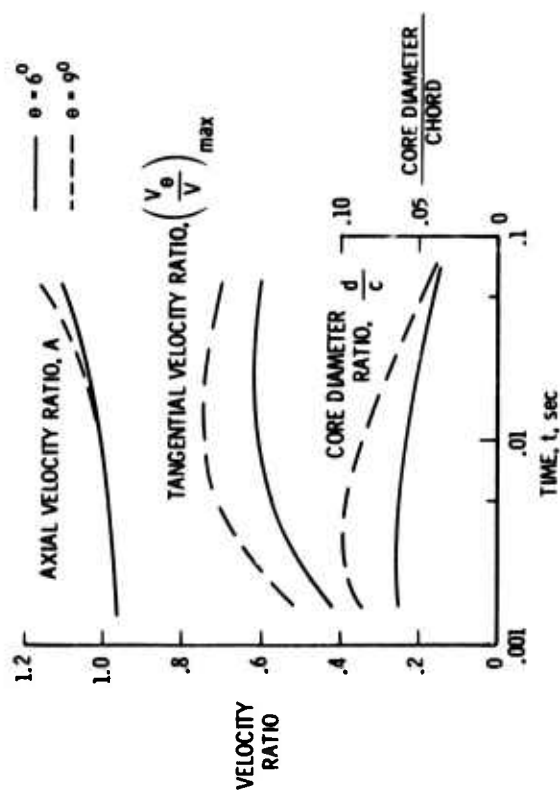


Figure 8.- Tip vortex flow characteristics.

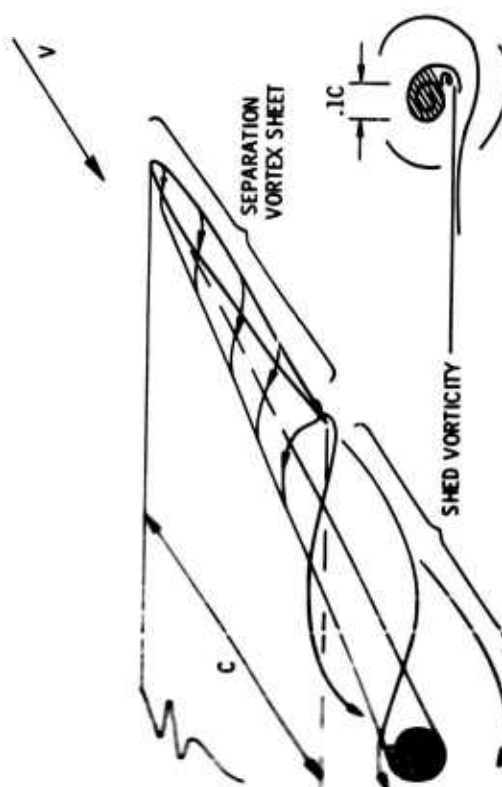


Figure 7.- Tip vortex formation mechanism.

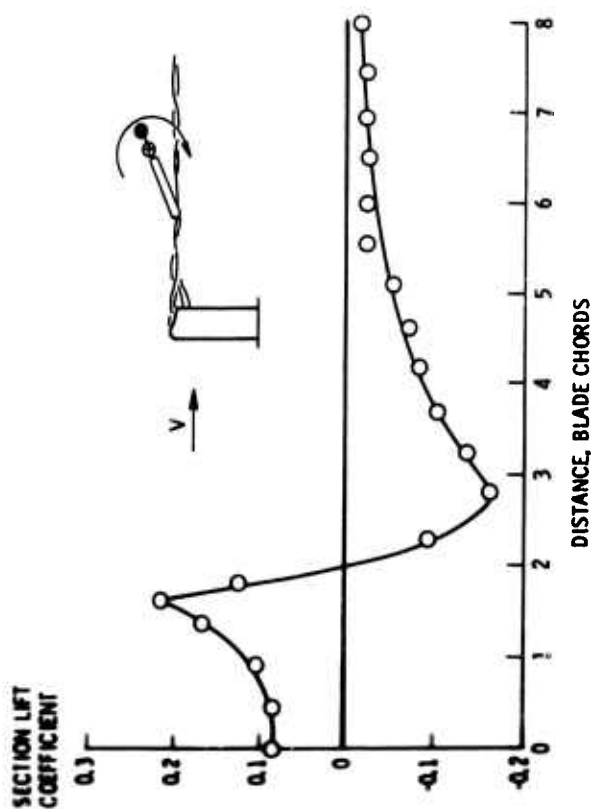


Figure 9.- Blade vortex interaction aerodynamics.

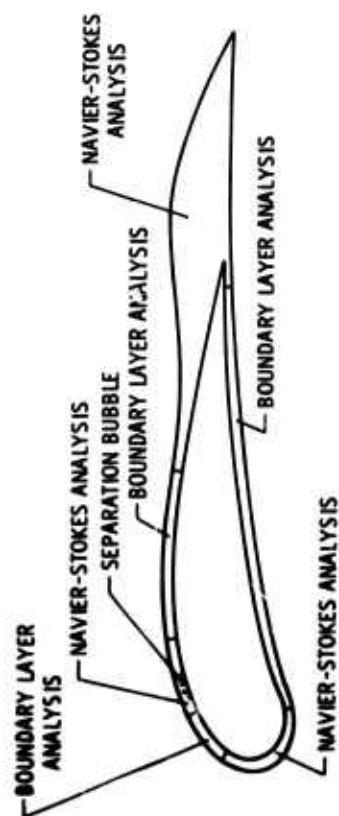


Figure 11.- Dynamic stall mathematical model.

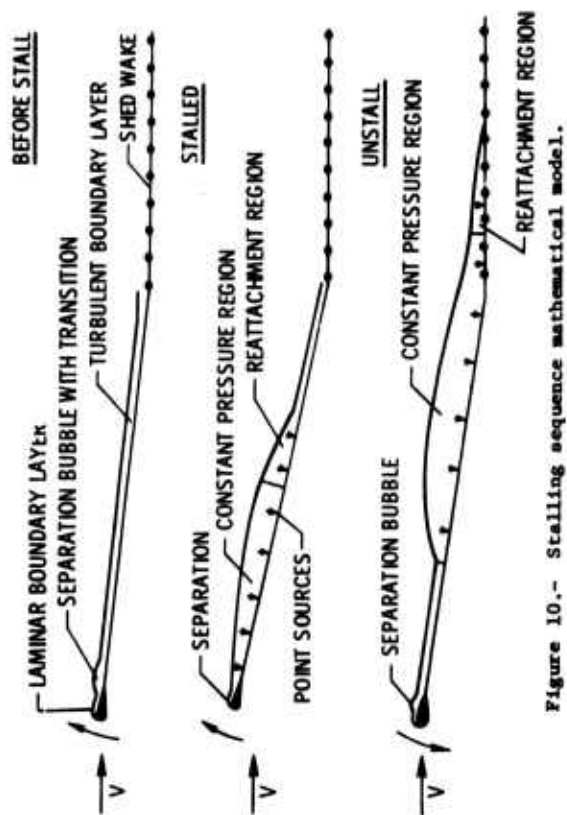


Figure 10.- Stalling sequence mathematical model.

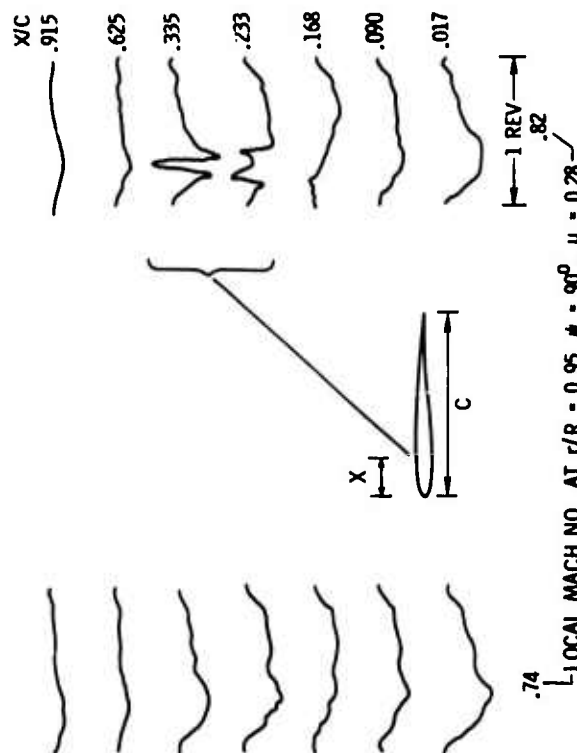


Figure 12.- H-34 blade pressure time histories.

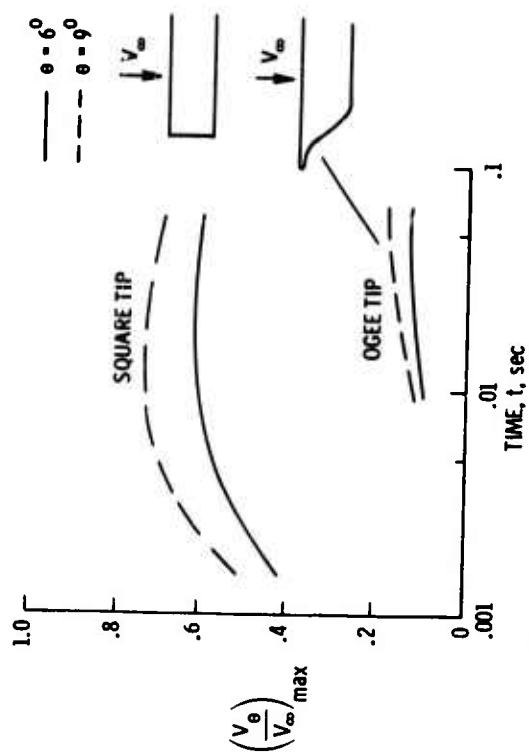


Figure 14.- Tip vortex tangential velocities.

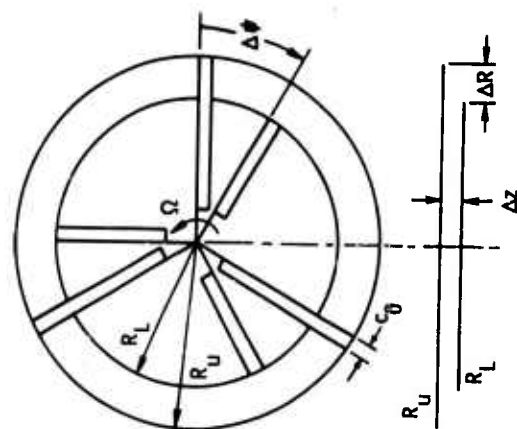


Figure 16.- Variable geometry rotor configuration.

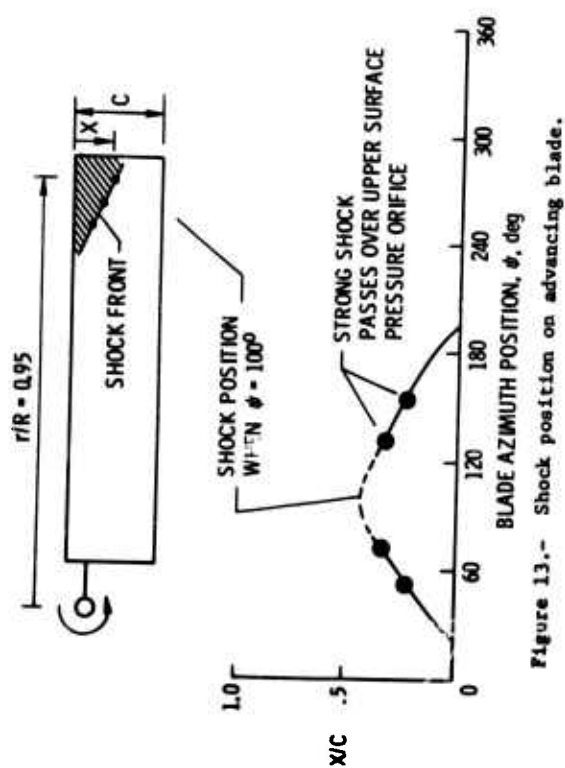


Figure 13.- Shock position on advancing blade.

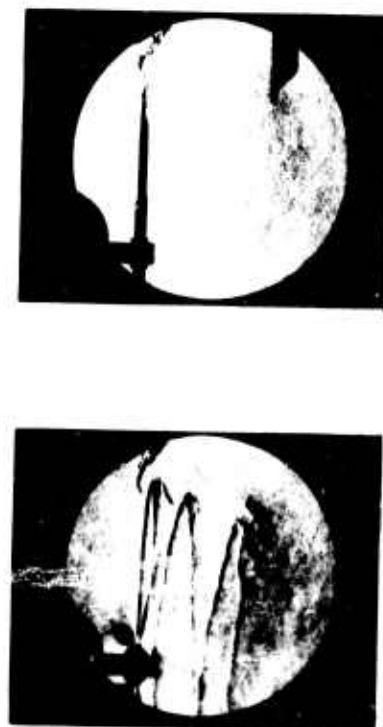


Figure 15.- Schlieren study of rotor wake flow.

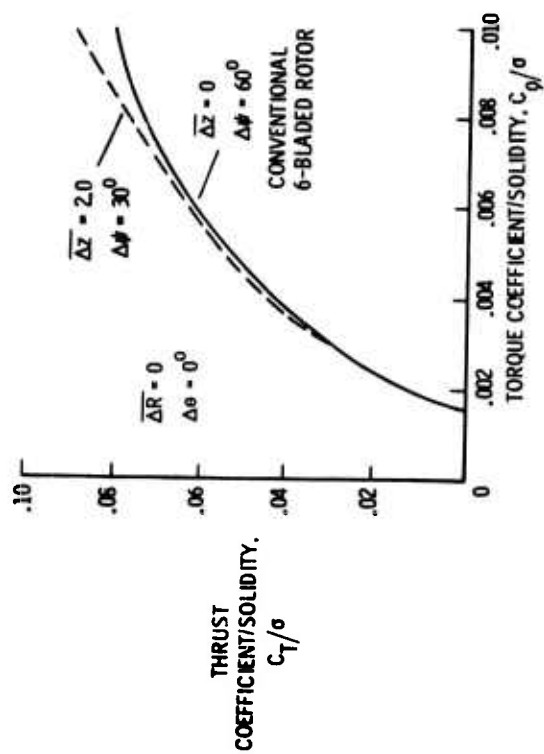


Figure 17.- Variable geometry rotor model hover performance.

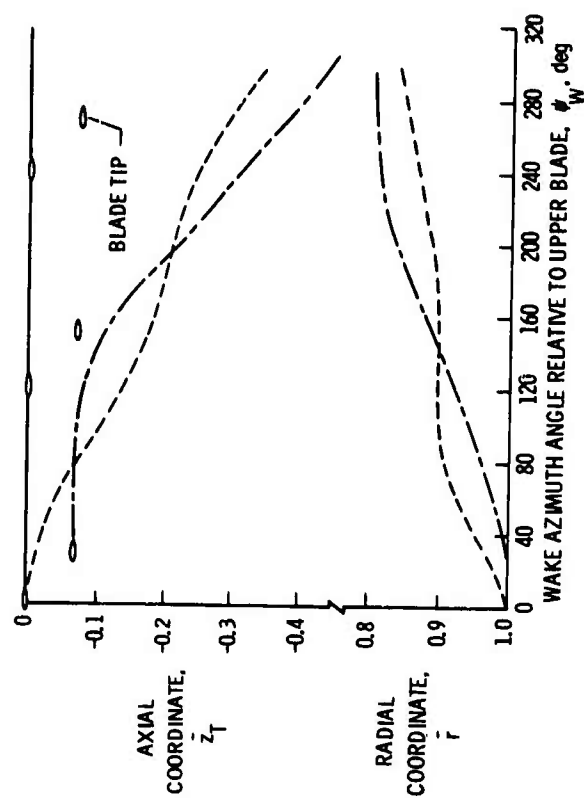


Figure 18.- Variable geometry rotor model tip vortex coordinates.

Prepared Comments on Paper 10

by

Wayne Johnson

US Army Air Mobility R & D Laboratory
Moffett Field, California

This article is a review of the theme paper on rotor unsteady aerodynamics, by John F. Ward and Warren H. Young, Jr. A specific point is to be made in the course of the review, a point about the direction rotary wing unsteady aerodynamic research is taking, and the direction it is suggested it should go.

The introduction gives the theme: "Understanding the source of unsteady airloads and developing verified prediction methods." The paper proceeds to discuss the problem in general, the status and direction of the state of the art, and then some examples of the work being done in this field, for example in dynamic stall, wake geometry, and blade/vortex interaction.

Consider Figure 2 in the paper, which is referred to in Section 2.2 on the state of the art. There is a feature of the figure which makes it very representative of the direction aerodynamic research is taking; the figure indicates the direction from present capability to current effort to needed effort is always toward more and more complex models. Perhaps it is only meant that more complex problems are to be considered, but what follows in the paper indicates otherwise. In the same section the paper points out a trend to more complex computer programs for aeroelastic problems, the trend being attributed to the availability of larger computers. No criticism of this trend is made really, although there is a tone of regret in the statement, rather it just points out that the theory output is becoming much like experimental data in terms of the reduction and interpretation required. There is another facet to this trend however: an inclination to always be putting the latest theory available from the state of the art into a computer program of ever increasing complexity, and giving no consideration to the other work required to extend the state of the art. What is missing is a consideration of extending the basic aerodynamic theory, the research base for the theory which must go into these programs. Much of the work building complex programs is being done in industry, where it is necessary and appropriate, and the resources for basic research limited; but the influence of this trend away from basic research also appears throughout the work on unsteady aerodynamics reported in the paper.

The important implication of this for unsteady aerodynamics is that it is the wrong kind of modelling to obtain the stated goals of increased understanding and verified prediction methods. The kind of modelling suggested takes whatever is available in the state of the art, in the basic disciplines of aerodynamics, dynamics, and structures, and builds a very complex and interactive structure, the attempt being to solve the complete problem of helicopter behaviour at once. This is an appropriate direction for industry, where what is desired is a design and development tool, and in fact currently most such programs are found in industry. However such a procedure cannot rise above its foundations in the basic theory; it is always limited by the development of the state of the art used as the base. This kind of modelling has had a great influence on the current approach to rotor aerodynamic problems. Much of the work concentrates on putting together the elements in the current state of the art in an attempt to solve these aerodynamic problems. Such a procedure is quite appropriate in putting together a model of the vehicle, for use in current design, aiming at a model that is the best possible within current levels of the state of the art. It must however fail in an attempt to model new aerodynamic problems, because the reason they are new is that the current state of art is not sufficient, and to handle them it is first necessary to build a new base in fundamentals for the mathematical model. That is what is not being done.

There is yet another implication in this trend. This kind of modelling is orientated toward putting together many pieces, then predicting the general influences on helicopter behaviour; as the paper puts it, there is then an increasing separation of cause and effect, by filtering through a big computer program. Again, the authors do not appear happy with this situation, but there is no real criticism of it. There is a criticism to make though: for work on the fundamental problems in rotor unsteady aerodynamics, this influence leads to some confusion of the aerodynamic phenomenon and its effects on the rotor. It leads to a tendency to consider prediction of the effects as verification of the model, and this again possibly precipitates a premature effort to put together a complex model before truly adequate and verified elements are available. The predictions of the effects on the helicopter are of course the goal, but it should be the last step, not the first. The first step must be attention to the aerodynamic phenomenon itself, to isolate it, study it, measure it; and for most of the problems confronting unsteady helicopter aerodynamics, this requires extensive basic research. It is not meant to imply that the study of possible effects using the current state of the art is not necessary, in fact it is extremely useful; but that is not to be viewed as basic research into the aerodynamic problems, that is required for true understanding and prediction capability, for it can never rise above the base on which it was built.

In the steps ascribed to the state of the art progression, it is mathematical modelling at which the trend reported in the theme paper and the direction advocated here diverge. The claim is made that in the last decade the problems in rotor unsteady aerodynamics have been identified. It is unlikely that all have indeed been found, that would imply a level of understanding far above current capability, but certainly some new and very interesting ones have appeared, and some detailed measurements are now being made of these aerodynamic phenomena. The

paper then states that "mathematical models are also being developed in an attempt to duplicate the observed flow behavior", but these attempts in many cases will not be successful in achieving the goals of understanding and predicting the phenomena, because of the lack of attention to the basic research which is required for a foundation for such theories.

Here then is the point this review is to make: influenced by the practice in the helicopter industry of constructing out of the state of the art more than more complex programs to predict helicopter behavior, theoretical work on the problems of rotor unsteady aerodynamics tends in many cases to follow a similar line, not giving attention to the basic research which is required before a new phenomenon may be adequately treated. The bulk of the theme paper is devoted to examples of current research in rotor unsteady aerodynamics, and these examples serve quite well also to illustrate the above statement.

First consider the results of the meeting on dynamic stall. There is a shift toward a more detailed study of the problem, as the paper recognizes. However, most of the suggestions are orientated toward the approach of trying to fit the experimental data with the pieces of the current state of the art; the implications of several of the points (1, 3, 6, 9, 11, 12) are of most interest when consideration is given to their sources. Points 9 and 10 are really the influences of rotor dynamics in the stall problem, not questions of the basic nature of dynamic stall as an aerodynamic phenomenon; this distinction is not made, and it reflects the confusion of the aerodynamic problem and its effects, a confusion which must be eliminated before progress can be made with either.

Section 2.3 on future research states that "emphasis should be placed on efforts to verify the mathematical models being developed. Many individual tools will have to be combined and compared with data obtained from complete rotor systems". The implication is that the state of the art of basic research is at a sufficient level to allow the construction of a mathematical model of the aerodynamic problems integrated into the complete system, and that the understanding of the problem has developed far enough that it is possible to check out the models of these aerodynamic phenomena through their effects on the entire rotor, i.e. filtered through all the other dynamic and aerodynamic characteristics of the rotor. The true level is far from that, for these are new problems which require additional basic research, which with the current directions will not be soon available. The problems in rotor unsteady aerodynamics discussed in the paper – notably wake geometry, vortex behavior, vortex/blade interaction, and dynamic stall – are new enough and complex enough that they will require considerable investigation as isolated phenomena first, before solutions are available for integration into general programs. In fact, even the basic elements of these problems may require additional study. A good example is dynamic stall; before even model problems, such as a two-dimensional oscillating airfoil, may be successfully attacked theoretically, study of even more basic areas such as leading edge separation bubbles and treatment of turbulence may be required. The emphasis on verifying the mathematical models with complete rotor systems shows the influence of the trend toward more complex prediction programs in the industry, and also the trend to look at the effects rather far removed from the causes. This influence is also shown in the view the paper takes of the rotor test system being built for the Ames Research Center 40- by 80-foot wind tunnel. According to the paper "development and verification of analytical methods will also require full scale rotor testing", and this rotor is to have that purpose. Certainly the rotor test system will be used for that when such methods become available; but as a researcher associated with the 40- by 80-foot tunnel, it is this author's observation that the real value of the rotor test system will be its flexibility as an experimental tool, for with the direction much current research on rotor aerodynamics is taking the analytical methods the paper envisions will not be around for a long time. It is doubtful if anything else may be expected of the flight rotor test system.

Consider Section 3.3 on wake geometry; the paper says "there is an increasing demand for more realistic analytical models for simulating rotor wake flow". However the work reported in the paper does not seem to really seek that. The efforts of Landgrebe and Scully have taken the basic idea – of calculating the self-induced distortion of the wake using potential flow induced velocity – quite far, but it is proving to be not sufficient by itself to improve airloads calculations. There is much more to be done now in terms of basic research, but there are few efforts to treat the more complex problems of wake geometry calculation. The purpose of the programs reported in the paper is not entirely clear, although they are evidently finding some good use in studying some unconventional vortex wake patterns (Section 3.9). What is clear is that this program in no way extends the basic theory – which is based mostly on just the Biot-Savart law, one of the oldest elements of aerodynamic theory. Fundamental investigations of particular value to helicopter problems would be work on the distortion of a vortex by a very close rotor blade or another vortex (so that viscous flow influences are important), and the prediction of the vortex geometry from the blade trailing edge to the encounter with the following blade (where a very high accuracy is required for good airloads predictions). Also important are questions of stability and steadiness of the vortex wake, especially in the rotary wing environment (the helical geometry and the many other vortices may be expected to have some influence). Such extension of the basic theory is what is necessary before returning to wake geometry calculations to try again for better results.

The vortex studies (Section 3.4) also illustrate the influence of the points of this review. Some excellent work on the fundamentals of vortex behavior is being done in helicopter engineering, especially detailed measurements of vortex characteristics. Interestingly, the impetus for the basic research going on now on vortex behavior and character in most cases comes not from helicopter engineering but rather from fixed wing engineering, particularly the wake turbulence problem. The result is that most attention is given to the fixed wing questions. For example,

theoretical work on the stability of tip vortex systems usually concentrates on the fixed wing configuration (two vortices behind a wing moving at a uniform velocity). The fixed wing case is the appropriate initial model to be studied even for rotary wings, but without a definite call from the helicopter industry for basic research the next step, to rotary wing studies, will not be taken with speed and resolution. In the example of tip vortex stability, the influence of the high curvature and all the other spirals needs to be investigated, especially for the forward flight case. Also, it will eventually be necessary to perform the measurements of the vortex characteristics behind the rotating wing; while that seems a very obvious next step, the considerations of a well defined program of basic research might lead to a different conclusion. For example, measurements of vortex characteristics behind a fixed wing with a bound circulation distribution more like that of a helicopter blade might be more appropriate first. The work being done now will be of considerable use to helicopter engineering, but unless some work specifically orientated to helicopter problems is done engineers will be faced with the usual uncertainties of transposing the fixed wing results to the rotary wing environment.

An interesting facet of the section on blade/vortex interaction (Section 3.5) is that some of this author's own work is being quoted. It is interesting because of what the paper does and does not say about the work and because the work had a definite influence on the ideas expressed here. This work (References 22 and 23 in the paper) chose a model for the problem (vortex/blade interaction), solved the model problem, verified it with some available experimental data, and then, only then applied it to the calculation of helicopter airloads. What the paper leaves unsaid is that the result of the last step was not at all satisfactory, although it at least gave one of the building blocks which will be required in the future to construct a theory that will give accurate airloads. Two impressions remain from the conduct and results of this work: developing a basic theory first can result in a tool that significantly affects the results of the mathematical model; and much more, very much more of this basic research is needed, in this one area alone. The basic research required is very much involved with problems of vortex character and behavior; for the vortex-induced airloads problem is just the other side of the problem of the distortion of a vortex by a nearby blade. A problem of immediate interest is the case of very small separation, when the viscous flow effects of both the vortex and wing, and the detailed geometry of the wing surface and vortex are possibly important. This problem has many complex ramifications, including vortex-induced stall, but by studying it in steps some useful progress should be possible. Also of interest is the problem of vortex-induced loads near the blade tip. Problems such as vortex distortion and vortex induced loads are in many aspects local aerodynamic phenomena, and as such are particularly adaptable to separate study (at least at first) using model problems.

Consider now Section 3.6 on dynamic stall. The work quoted (Reference 25) is one of the best examples in recent helicopter work of the inevitable fate of trying to solve these unsteady aerodynamic problems without an adequate theoretical base to build on. The description the paper gives of the work serves well to make this point. On the method of the dynamic stall theory it says "the viscous flow is solved by momentum integral techniques which require many empirical relations and outright assumptions", etc.; "the important sources of uncertainty in the present model are the expansion and contraction of the constant-pressure regions, the point of transition in the separation bubble, stall criteria, the pressure distribution near the leading edge, and the process of recovery from stall"; and "the role of the separation bubble in transition and stall, the entire turbulence model in separated flow, and the process by which the airfoil unstalls are areas of ignorance". The one thing the theory is quoted as showing is the importance of viscous/potential flow interaction in the airfoil aerodynamic behavior, especially at high angle of attack, but airfoil designers already knew that. There can be very little value in putting together a mathematical model with such shortcomings, shortcomings which must have been quite evident before the effort even started. Disregarding all these limitations, "further improvements will be made in the analytical model, and it will be incorporated into a helicopter performance program". So even now the thought is not to go back for the basic elements, rather to push on to integrate this program into still larger programs. Putting some semi-empirical theories of dynamic stall into rotor performance programs has been a significant achievement of the industry in the last years; but that did not solve the problem of understanding and predicting dynamic stall, and putting an entirely theoretical model into a performance program seems quite premature. But it was premature to even construct such a theory, for the required theoretical base for dynamic stall is far from available. The basic research that needs to be done in the field of dynamic stall may be seen in the limitations of the stall theories discussed in the paper; the research includes work on separation bubble character and behavior, stall criteria for airfoils (i.e. treatment of the breakdown of the boundary layer approximation), treatment of turbulence, and recovery from stall. Even static stall prediction is a difficult problem, so there is much to be done for dynamic stall. Of immediate interest for dynamic stall might be experimental and theoretical work on the separation bubble, particularly the transition point and turbulent recovery characteristics. So the amount of required basic research is quite tremendous, and the helicopter engineer will not be able to wait for other fields to provide it because much of the problem is unique to helicopters. The other dynamic stall efforts discussed in the paper appear to be much the same sort of thing, only more expensive. Again there is not the required basic research into the new problems of aerodynamics involved, but rather attempts to jump right into the complete solution. That solution often seems to involve now solving the complete unsteady Navier-Stokes equations, but even if that were done for the entire flow field it would not be an exact solution, of course, because of the problem of handling turbulence. Surely there is some modelling still possible, and at least some attempts should be made to find it, the reward in understanding and capability being so much greater than anything that can come out of such solutions as discussed in the paper.

The conclusion states that "the state of the art of rotor unsteady airloads appears to have moved beyond the stage of problem identification, and into a period of theoretical development, careful experimental documentation, and semi-empirical analytical modelling". Indeed several new and quite important problems have been singled out as most important for the current effort; and the experimental work seems to be doing well toward solving the problems in the ways it can. Much of the theoretical work however suffers from a lack of attention to the required basic research, and unless some changes occur another decade will see not new problems but these same old ones.

Much of the work described in the paper attempts to construct models of these new problems from the old state of the art, and this must inevitably fail. First it is necessary to build the new bases in aerodynamic theory required by these new problems, then it will be possible to build models that may be expected to more accurately handle the prediction of rotor behavior. What is needed is a new direction, a new orientation of helicopter research in these problems of unsteady aerodynamics. What has happened to require this change is that helicopter engineering has outrun the theoretical basis available to it from fixed wing work. An era has been reached where the aerodynamic basis available for the rotary wing is no longer adequate because helicopter engineering is now concerned with problems that are in many cases unique to the helicopter aerodynamic environment. The need now is for basic research into these problems, and it will not be possible to rely on fixed wing engineering to provide it. Then attention may return to integrating these problems into the model of the entire helicopter system. The real problem with the wrong direction is that it diverts very limited resources for research into areas which in some cases are simply dead ends, or at least much less useful than the basic research would be. The helicopter industry perhaps can not support all the basic research it needs, even just in the area of unsteady aerodynamics, for there are many complex and difficult problems involved. There is however always something that can profitably be done, and with limited resources it becomes even more important that the available effort is allocated in the most advantageous direction. It is desired to impress a new way of thinking about these problems, a new framework within which to formulate research programs, so that the best directions available may be found.

CALCUL ET MESURE DES FORCES AERODYNAMIQUES SUR UN PROFIL OSCILLANT
AVEC ET SANS DECROCHAGE

AERODYNAMIC FORCES COMPUTATION AND MEASUREMENT ON AN OSCILLATING AEROFOIL
PROFILE WITH AND WITHOUT STALL

par J.J. PHILIPPE - Ingénieur de Recherche à l' O.N.E.R.A.
M. SAGNER - Ingénieur à la Société BERTIN & Cie

SOMMAIRE

Afin de mieux connaître et prévoir les phénomènes instationnaires sur les pales d'hélicoptères, des recherches de base sur le calcul et la mesure des forces aérodynamiques sur profils oscillants ont été entreprises depuis quelques années en France. Les méthodes aussi bien expérimentales que théoriques mises au point à ce sujet font l'objet d'une présentation critique. Les problèmes posés par le décrochage instationnaire sont plus particulièrement développés. Les résultats obtenus jusqu'à présent concernent le profil NACA 0012 ; ils sont analysés en fonction de l'incidence moyenne, de l'amplitude des oscillations, de la fréquence réduite et du nombre de Mach. Les développements futurs prévus pour améliorer les mesures et les calculs, confrontés avec les résultats expérimentaux, sont également exposés.

SUMMARY

In order to know better and predict more accurately unsteady phenomena on helicopter blades, basic research work on computing and measuring aerodynamic forces on oscillating aerofoil profiles was started some years ago in France. The experimental as well as theoretical methods that have been developed are critically reviewed ; the problems brought up by unsteady stall are more particularly discussed ; the results obtained to date concern a NACA 0012 profile ; they are analyzed as a function of mean angle of attack, oscillations amplitude, reduced frequency and Mach number. Future developments anticipated to improve measurements and computing methods compared with experimental results are also reviewed.

NOTATIONS

α	incidence instantanée	
α_m	incidence moyenne des oscillations	
$\bar{\alpha}$	demi amplitude des oscillations	
f	fréquence des oscillations	
l	corde du profil	
s	abscisse curviligne	
V_0	vitesse de l'écoulement à l'infini amont	
k	$\pi \times f \times l / V_0$ = fréquence réduite	
M	nombre de Mach	
V	vitesse locale sur le profil	
C_z	coefficient de portance	} axes liés au vent
C_x	coefficient de traînée	
C_m	coefficient de moment de tangage	
C_{z1}	coefficient de force normale	} axes liés à la maquette
C_{x1}	coefficient de force axiale	
C_{m1}	coefficient de moment de tangage	
$ C_{z1} _1$	amplitude du 1er harmonique du coefficient de force normale	
$ C_{m1} _1$	amplitude du 1er harmonique du coefficient de moment de tangage	
$\varphi_{C_{z1} _1}$	phase du 1er harmonique du coefficient de force normale par rapport au mouvement d'incidence	
$\varphi_{C_{m1} _1}$	phase du 1er harmonique du coefficient de moment de tangage par rapport au mouvement d'incidence	
ΔK_p	coefficient de pression différentielle	

1. INTRODUCTION

L'évolution des hélicoptères vers des paramètres d'avancement élevés nécessite une connaissance et une prévision de plus en plus précises des charges locales instationnaires sur les pales. Dans une première approche, la loi de variation d'incidence d'une section de pale peut être simulée par le mouvement d'un profil en oscillations harmoniques de tangage. Ainsi apparaît naturellement l'intérêt de mesurer et de calculer l'ensemble des forces instationnaires dans ce cas simple. Cependant le problème se complique rapidement lorsqu'il s'agit de représenter fidèlement les conditions de vol des hélicoptères. En effet les variations d'incidence sont importantes et s'effectuent autour d'incidences moyennes élevées de sorte que, sur la pale reculante, les incidences locales peuvent être bien supérieures aux incidences de décrochage stationnaire des profils.

Les travaux menés dans le cadre des recherches de base sur profils oscillants dans ces conditions fait l'objet de la présente communication. Au point de vue expérimental, l'effort s'est cristallisé autour de la mise au point d'une méthode dynamométrique, permettant d'accéder au torseur complet des forces aérodynamiques et notamment aux traînées instationnaires. Ce travail entrepris par l'O.N.E.R.A., s'est poursuivi avec l'aide du S.T.Aé (Service Technique Aéronautique) en collaboration étroite avec la S.N.I.A.S. MARIGNANE (Division Hélicoptères) et le C.E.A.T. de TOULOUSE où se font les essais. L'étude théorique, a été confiée par la D.R.M.E. (Direction des Recherches et Moyens d'Essais) à la Société BERTIN, qui a commencé par les calculs sur profils en mouvement périodique quelconque en absence de décollement en s'appuyant sur les travaux de GIESING. Lorsque les incidences deviennent importantes, le cas beaucoup plus difficile à traiter, des configurations où apparaissent les décrochages instationnaires a été abordé en tenant compte des travaux de SARPKAYA et de HAM. Les résultats de calculs seront comparés aux valeurs expérimentales obtenus à TOULOUSE.

2. MESURES DES FORCES AERODYNAMIQUES SUR PROFILS OSCILLANTS

2.1. Méthode expérimentale

La figure 1 fournit un schéma de la maquette utilisée pour les essais de maquette de courant plan en oscillations harmoniques de tangage autour du quart de corde avant. Un dynamomètre trois composantes (a) mesure simultanément les forces normales, les forces tangentielles et le moments de tangage s'exerçant sur une tranche pesée centrale, isolée mécaniquement du reste de la maquette. Les forces d'inertie doivent être déduites de ces mesures afin d'obtenir les données aérodynamiques seules. Plusieurs solutions sont possibles. On peut soustraire les mesures d'essais en oscillations sans vent (où seules les forces d'inertie interviennent) de celles obtenues lors d'essais en oscillations avec vent. Cette méthode simplifiée n'est pas absolument correcte car elle suppose l'identité des mouvements de la tranche pesée en absence et en présence d'écoulement dans la soufflerie. C'est pourquoi un second dynamomètre trois composantes (b), inclus dans la maquette, avait été prévu pour agir en accéléromètre et mesurer des forces d'inertie proportionnelles à celles subies par la tranche pesée. Les forces d'inertie devaient être soustraites automatiquement de celles fournies par le dynamomètre principal, par l'intermédiaire d'un calculateur analogique. Mais cette solution s'est heurtée aux difficultés expérimentales suivantes :

- le dynamomètre correcteur d'inertie se trouve parfois excité à ses fréquences propres et les parasites ainsi créés sont si importants qu'il faut réduire notablement les gains d'amplification, ce qui enlève toute précision aux mesures ;
- l'emploi de filtres de haute précision sur l'ensemble des voies de mesure permet cependant son utilisation mais il apparaît alors d'autres facteurs parasites, en effet les mouvements de pilonnement de faible amplitude dus aux forces normales aérodynamiques instationnaires, entraînent de nouvelles forces d'inertie pour la tranche pesée, négligeables aux faibles fréquences d'oscillations mais notables aux fréquences élevées.

C'est pourquoi, le Service Recherches de la S.N.I.A.S. MARIGNANE a proposé d'améliorer prochainement la méthode actuelle par l'emploi de correcteurs d'inertie à 6 composantes, permettant théoriquement de corriger toutes les forces d'inertie.

Ce projet permettra d'affiner les mesures actuelles fournies par la méthode simplifiée qui, cependant, donnent satisfaction jusqu'aux fréquences de l'ordre de 12 Hz.

2.2. Acquisition et traitement des informations

La figure 2 en montre le schéma. Les mesures sont enregistrées sur bande magnétique analogique, puis numérisées toutes les millièmes de seconde. Une analyse harmonique sur ordinateur permet de les moyenner sur un nombre de périodes variable, limité à 5 actuellement. De ces informations, on déduit les coefficients sans dimension des forces aérodynamiques dans un trièdre lié à la maquette (forces normales, forces tangentielles et moments de tangage), puis par changement d'axes, les coefficients des forces aérodynamiques dans un trièdre lié au vent (portances et traînées).

Les prochaines campagnes d'essais seront améliorées en effectuant sur ordinateur des moyennes numériques sur un plus grand nombre de périodes, ce qui est nécessaire dans certaines configurations de décrochage particulièrement instables, où prédomine le caractère aléatoire des phénomènes à étudier.

2.3. Résultats obtenus sur le profil NACA 0012

Les résultats présentés ici proviennent des conditions d'essais suivantes :

- Profils NACA 0012 de corde $l = 0,4 \text{ m}$
- Nombre de Mach : $M = 0,2$; $M = 0,3$
- Fréquence des oscillations : $f = 4, 8, 12 \text{ Hz}$
- Amplitude des oscillations : $\alpha = \pm 3^\circ$; $\pm 6^\circ$ pour $f = 4$ et 8 Hz
 $\alpha = \pm 3^\circ$; $\pm 5^\circ$ pour $f = 12 \text{ Hz}$

- Incidences moyennes : α_m compris entre 0° et 16°

- Les fréquences réduites maximales sont donc :

$$k = 0,23 \text{ à Mach } 0,2$$

$$k = 0,15 \text{ à Mach } 0,3$$

La grande majorité des essais a porté sur des configurations où l'élongation d'incidence est imposée de part et d'autre des incidences de décrochage stationnaire du profil.

2.3.1. Influence de l'incidence moyenne et du nombre de Mach

L'examen des figures 3 et 4, où sont présentés les cycles obtenus à une même fréquence, permet de noter que :

- les portances instationnaires maximales sont bien supérieures aux valeurs stationnaires. Cet accroissement de portance diminue avec le nombre de Mach et passe par un maximum lorsque l'incidence moyenne croît ;
- les moments de tangage décrivent des cycles, dont l'instabilité varie progressivement avec l'incidence moyenne. Les cycles redeviennent stables aux incidences moyennes plus élevées ;
- l'amplitude des moments piqueurs maxima augmente avec l'incidence moyenne ;
- l'instabilité en tangage débute à une incidence moyenne d'autant plus faible que le nombre de Mach augmente.

Ces diverses conclusions confirment les résultats déjà mis en évidence par les travaux expérimentaux de DAVENPORT, LIIVA, CARTA et WINDSOR (Réf. 1 à 3) qui ont fait l'objet de maintes analyses détaillées (Réf. 4 à 8).

L'intérêt principal de la méthode dynamométrique est de fournir avec une précision satisfaisante les grandeurs aérodynamiques dans des axes liés au vent, notamment les traînées instationnaires pour lesquelles on ne disposait jusqu'à présent que de renseignements expérimentaux limités (Réf. 3 et 7). On peut ainsi montrer l'influence notable du nombre de Mach sur les cycles de traînée. Alors qu'à Mach 0,2 les traînées peuvent être, aux incidences élevées, inférieures aux traînées stationnaires (recul de la divergence de traînée), il n'est plus de même à Mach 0,3, où l'ensemble du cycle se trouve au dessus de la polaire stationnaire. L'effet de la compressibilité se fait sentir dès ce nombre de Mach, dès que les incidences sont élevées.

On note en effet que, pour $M = 0,3$, l'écoulement atteint $M = 1$ près du bord d'attaque pour une incidence stationnaire de 11° degrés.

2.3.2. Influence de la fréquence réduite et de l'amplitude

La figure 5 présente l'influence de ces paramètres. Elle confirme les lois simples déjà connues :

- les portances instationnaires maximales augmentent avec la fréquence réduite et avec l'amplitude ;
- les instabilités sont plus importantes à amplitudes faibles qu'à amplitudes élevées mais elles diminuent lorsque la fréquence réduite augmente.

Dans le cas de cycles stables, on remarquera figure 6 l'augmentation de la largeur des cycles de traînée avec la fréquence réduite. Lorsque celle-ci est suffisamment grande, des traînées instationnaires bien inférieures aux traînées stationnaires sont obtenues quand l'incidence décroît. Pour une même incidence moyenne, les incidences atteintes sont d'autant plus élevées que l'amplitude des oscillations est grande. L'influence de l'amplitude est donc importante comme le montre la figure 7. On notera également l'analogie de formes entre les cycles de traînées et de moments de tangage qui traduit essentiellement le fait que lorsqu'apparaît un décrochage, on a simultanément accroissement des moments piqueurs et augmentations de la traînée.

2.3.3. Problème de la détection de l'incidence locale

Dans ces essais, l'incidence imposée à l'ensemble de la maquette est mesurée avec précision. La fonction de transfert maquette-tranche pesée en absence d'écoulement est connue par une combinaison calculs-expériences. Cependant les moments de tangage aérodynamiques altèrent quelque peu le mouvement sinusoïdal pur fourni par le mécanisme d'oscillations. L'incidence géométrique réelle de la tranche pesée reste à déterminer d'une manière précise. Il est prévu, pour la suite des essais de calculer cette correction d'incidence à partir du moment de torsion réelle s'exerçant à chaque instant sur la tranche pesée.

2.4. Critiques et perspectives

En dehors des difficultés expérimentales signalées ci-dessus et des améliorations prévues, on doit signaler le caractère tridimensionnel des écoulements dans les configurations de décrochage, confirmé par l'examen des films de visualisation pris lors des essais à TOULOUSE. La figure 8 en montre un exemple. La méthode dynamométrique actuelle sera donc améliorée prochainement par un équipement de jauges câblées directement en forces et non en moments supposant l'hypothèse de symétrie de l'écoulement sur la tranche pesée.

Les résultats d'essais du profil NACA 0012 donnent l'évolution des grandeurs aérodynamiques en fonction du nombre de Mach, de l'incidence, de l'amplitude et de la fréquence réduite des oscillations. On s'efforce actuellement de les exprimer sous une forme analytique, permettant d'introduire ces données expérimentales dans les programmes de performances de rotors. Cet objectif a déjà fait l'objet de quelques travaux aux Etats-Unis (Réf. 8 à 10) qui en montrent tout l'intérêt.

3. CALCUL DES FORCES AERODYNAMIQUES SUR UN PROFIL EN ECOULEMENT BIDIMENSIONNEL, INCOMPRESSIBLE, INSTATIONNAIRE

L'intérêt de compléter l'expérience par le calcul est évident si l'on considère :

- le nombre des paramètres intervenant dans le problème ;
- la difficulté de représenter en soufflerie le mouvement complexe de l'élément de pale du rotor ;
- la nécessité d'utiliser des techniques expérimentales délicates et relativement complexes.

La méthode de calcul utilisée est valable pour un mouvement de forme quelconque, cependant l'application a été limitée au profil oscillant autour du quart avant.

3.1. Calcul sans décrochage

C'est un calcul numérique de fluide parfait incompressible non linéarisé. Dans le cadre de l'étude présentée il constitue simplement une étape nécessaire en vue du calcul du décrochage, il présente cependant un certain intérêt en soi pour l'étude des pales d'hélicoptères par les avantages qu'il a sur les méthodes linéarisées (THEODORSEN ...) :

- introduction des effets d'épaisseur qui permet de comparer différents profils au point de vue de la répartition des vitesses et de calculer des couches limites ;
- calcul de la traînée de pression. L'expérience montre que ses variations sont importantes ;
- détermination des harmoniques supérieurs à 1 et des effets non linéaires des superpositions de mouvements.

Le modèle de calcul très voisin de celui de GIESING (Réf. 11) comporte des singularités liées : segments de sources disposés à la paroi et tourbillons sur la corde, et des singularités libres : tourbillons émis près du bord de fuite dont on suit le mouvement pas à pas. On respecte à chaque instant la condition de tangence au profil, la conservation de la circulation globale et la condition de non-contournement exprimée sous la forme de l'égalité de vitesses extrados-intrados près du bord de fuite.

Le processus de calcul est le suivant :

- le profil est donné par ses cotes au besoin lissées numériquement ;
- le mouvement est donné dans le repère galiléen en principe il est périodique mais de forme quelconque ;
- les conditions initiales sont celles de l'écoulement permanent pour l'incidence de départ et le calcul est poursuivi jusqu'à l'obtention d'un cycle complet correspondant à la condition de périodicité (en général, un cycle et demi suffit).

Les résultats fournis sont : la répartition des vitesses et des pressions, le torseur des forces de pressions obtenu par intégration.

Un certain nombre d'améliorations apportées au principe de base ont permis de réduire le temps de calcul à 2' d'UNIVAC 1108 pour un profil donné en 48 points et un pas de calcul de 1/20 de période.

3.2. Calcul avec décrochage

3.2.1. Principe

Le modèle avec décrochage est dérivé du modèle précédent en introduisant une deuxième famille de tourbillons libres émis au voisinage du bord d'attaque et schématisant un décollement selon un procédé voisin de celui de HAM (Réf. 4)

En effet de nombreux travaux expérimentaux (de 12 à 16) aussi bien sur profil oscillant que sur le mouvement impulsif de cylindres ou de plaques ont mis en évidence l'existence, tout au moins pour le profil dans le cas du décrochage de bord d'attaque, d'un gros tourbillon prenant naissance près d'un point de décollement, qui grossit en se déplaçant le long de la paroi et finit par se détacher. Les propriétés particulières du décrochage dynamique peuvent être attribuées en grande partie à ce phénomène. Des études plus fines ont montré que ce décollement est constitué par une nappe tourbillonnaire émise à partir du point de décollement et s'enroulant sur elle-même. Un tel écoulement peut être schématisé dans un modèle de fluide parfait par une nappe de tourbillons libres ainsi que l'ont montré SARPRAYA (Réf. 17) pour le cylindre en mouvement impulsif et HAM (Réf. 4) pour le décrochage dynamique de la plaque plane. Les effets de viscosité se manifestent au niveau de l'émission de rotationnel au sein du fluide mais peuvent être négligés au cours de l'évolution ultérieure.

3.2.2. Description du modèle de calcul

Les éléments principaux en sont les suivants :

- un calcul de couche limite laminaire à partir de la répartition de vitesses instantanée par une méthode simple (Réf. 18) de régime permanent. Cette dernière hypothèse est justifiée dans le domaine des pales d'hélicoptère. Le calcul donne la position du décollement et les caractéristiques de la couche limite en ce point, par contre on ne peut pas l'utiliser comme critère de décollement vrai car le phénomène réel est plus complexe (bulbe court) ;
- un modèle d'émission de tourbillons au voisinage du décollement basé sur les hypothèses suivantes : (inspirées en partie de la Réf. 17)
 - . vitesse nulle au point de décollement
 - . débit de tourbillons égal au débit de rotationnel de la couche limite
 - . distance du tourbillon naissant à la paroi égal à l'épaisseur de déplacement de la couche limite
 - . trajectoire initiale des tourbillons faisant avec la paroi l'angle théorique de la ligne de séparation

laminaire au point de décollement laminaire (Réf. 19)

On notera que ce modèle définit le pas de calcul.

- le calcul de l'évolution des deux nappes de bord d'attaque et de bord de fuite. En pratique pour rendre le temps de calcul acceptable on utilise deux pas de temps. L'un très court pour suivre l'émission et l'évolution de tourbillons au voisinage du décollement dans le repère curviligne. L'autre plus long pour suivre l'ensemble du problème. Le calcul utilise également un procédé de coalescence des tourbillons.

3.2.3. Difficultés rencontrées

Critère de décollement : il est nécessaire d'introduire dans le calcul l'instant où commence l'émission des tourbillons libres car on a vu que le calcul de couche limite laminaire est inutilisable ; de la même façon la fin du décrochage devra être traduite par l'arrêt de l'émission.

En écoulement permanent on ne dispose pas actuellement de méthode simple pour prédire l'incidence de décrochage dans le cas de décrochage de bord d'attaque par éclatement de bulbe court.

En instationnaire il apparaît en outre un retard au décrochage dû à divers effets ;

- influence du mouvement sur la répartition de vitesse instantanée. En principe le calcul pourrait en rendre compte si on disposait d'un critère, en pratique dans le domaine des mouvements de pales d'hélicoptères cet effet reste faible ;
- effet de retard à l'apparition du décollement. Le problème commence à être abordé théoriquement pour le décollement laminaire, dans le cas du "bulbe court" il ne paraît pas accessible pour l'instant. Pour situer un ordre de grandeur on peut utiliser des résultats sur le mouvement impulsif de plaque elliptique : nous avons constaté (Réf. 15) un retard de la forme $\Delta t = k \frac{1}{\sqrt{\gamma}}$ avec k de l'ordre de 0,2 pour le mouvement transversal d'une ellipse de 20 % d'épaisseur ;
- délai de développement du sillage. En principe le modèle de calcul doit traduire le phénomène sans qu'il soit nécessaire d'introduire des données empiriques, on peut cependant agir sur certains paramètres du modèle d'émission pour ajuster le résultat.

Actuellement le problème du critère de début et de fin du décrochage n'a pas été résolu, nous avons prévu d'introduire dans le calcul soit l'incidence de décrochage en permanent soit l'instant déduit de l'expérience où apparaissent les perturbations des pressions et des forces, cette détermination restant imprécise. Certains expérimentateurs ont constaté l'apparition du décollement au voisinage de l'incidence maximale, des mesures plus fines seraient nécessaires. De plus l'exploitation du calcul permettra d'évaluer l'importance des différents termes et d'ajuster des critères plus élaborés.

Modèle d'émission de la nappe tourbillonnaire : le processus de création de rotationnel au sein du fluide parfait reste indéniablement très schématisé. En outre l'utilisation de deux pas de temps différents pour décrire les phénomènes locaux et l'écoulement d'ensemble et le schéma de coalescence des tourbillons paraissent avoir une certaine influence. Différentes tentatives ont été nécessaires pour obtenir une configuration de nappe réaliste.

Evolution de la nappe : des difficultés numériques sont apparues lorsque un tourbillon est très proche de la paroi. Elles sont liées à la discrétisation temporelle et à la discrétisation spatiale des sources sur le profil. Elle conduisent à adopter un pas de temps relativement faible d'où un temps de calcul assez long.

Condition à la pointe arrière : l'expression du non contournement en régime instationnaire et avec possibilité de recirculation à l'extrados présente des difficultés d'ordre théorique. Pour l'instant le procédé utilisé dans le modèle de calcul est très sommaire. Il se peut que des adaptations se révèlent nécessaires.

3.3. Résultats du calcul

L'exploitation a été limitée à un NACA 0012 oscillant autour du quart avant.

3.3.1. Calcul sans décrochage

Forme du sillage (figure 9). Dans le domaine des fréquences réduites de pales d'hélicoptères la nappe de bord de fuite présente une oscillation d'amplitude relative très faible mais pouvant dépasser une corde en valeur absolue loin du profil. Cet effet peut jouer un rôle dans les problèmes d'interaction pale-sillage.

Aux fréquences réduites très élevées la configuration devient complexe et le sillage est très épais.

Cycle $C_x(\alpha)$ (figure 10). On remarquera la forme du cycle de traînée à incidence moyenne très proche de l'expérience bien que le calcul ne tienne pas compte du frottement. Ce dernier est probablement faible par rapport à la traînée de pression. Le cycle présente des zones de C_x faiblement négatif et des valeurs maximales très importantes.

Premier harmonique de C_z et C_m (planche 11). Les résultats du calcul non linéarisé ne semblent pas apporter d'amélioration par rapport à la théorie linéaire. En fait la comparaison est rendue difficile du fait des écarts existant en stationnaire :

	$\Delta C_z / \Delta \alpha$	Position du foyer
- calcul non linéaire	6,92	26,4 %
- calcul linéaire	6,28	25 %
- expériences	5,9	26 %

On a tenu compte de cet écart pour le C_z en représentant $(|C_z|/\alpha) / (\partial C_z / \partial \alpha)$ pour les 3 évaluations mais pour le C_m on n'a pas pu apporter de correction simple aux résultats bruts.

On notera par contre la répartition de pression (planche 12) beaucoup plus proche de l'expérience que la théorie linéaire. Il reste un écart systématique inexpliqué sur le déphasage.

3.3.2. Cas du décrochage

Nous présentons (figure 13) quelques résultats montrant l'influence du mouvement sur la répartition des vitesses instantanées. On voit qu'il existe bien un effet dans le sens d'un retard au décollement et au recollement, mais cet écart est très faible dans le domaine des fréquences réduites usuelles de rotors. En l'absence de critère de décrochage valable même en permanent il n'a pas été possible de traduire cette influence en terme de retard. Nous indiquons également l'évolution du point de décollement laminaire donné par la méthode de THWAITES, on voit que pour $\alpha > 8^\circ$ celui-ci ne varie pratiquement pas. On attend des nouvelles techniques de mesures par film chaud, en cours de développement à l'O.N.E.R.A. à la suite des travaux de MC. CROSKY (Réf. 20 et 21), des renseignements valables sur la localisation et l'instant de formation et de disparition du décollement. En effet (figure 14) on distingue nettement sur l'oscillographe les écoulements laminaire, turbulent et décollé.

Une première tentative de calcul limitée à la phase initiale du décrochage, a été faite pour $\alpha = 12^\circ \pm 6^\circ$ et $k = 0,15$ en introduisant artificiellement le début du décrochage à $15,5^\circ$.

Les configurations successives obtenues pour la nappe tourbillonnaire (figure 15) sont assez réalistes bien que la hauteur de l'enroulement tourbillonnaire semble très importante. On observe l'apparition d'instabilités qui vont en s'amplifiant. Elles proviennent probablement d'un phénomène de couplage. La vitesse de propagation de l'enroulement est relativement faible. Les répartitions de pressions (figure 16) mettent également en évidence la propagation de perturbations constituées d'une zone de surpressions suivie d'une zone de dépressions que l'on retrouve qualitativement dans l'expérience, pratiquement seules les pressions extrados sont affectées ainsi que l'indiquent les résultats expérimentaux (Réf. 3).

Les premiers résultats obtenus sur la courbe de C_z semblent montrer une chute de portance dès l'émission de tourbillons, une partie de cet effet est cependant d'origine numérique, ensuite la portance se rétablit avec des oscillations à une valeur voisine de sa valeur sans décollement, le décrochage en portance ne se produirait que lorsque le bord de fuite est interactionné. Il semblerait donc que le terme prépondérant du "retard au décrochage" en C_z soit lié au délai de développement du sillage.

3.4. Critiques et perspectives

Les résultats présentés, qui ne constituent que les premiers tests de la méthode, montrent la possibilité de décrire de façon réaliste l'établissement du régime de décrochage de bord d'attaque. Indépendamment de la mise au point nécessaire et de difficultés ultérieures qui pourront apparaître on peut citer les points qui seront à améliorer :

Critère de décrochage. On peut tenter d'appliquer aux répartitions de vitesses les méthodes de prévision des décrochages de bord d'attaque (Réf. 22). On espère obtenir des nouvelles techniques par film chaud ou par visualisation des renseignements permettant d'élaborer des critères de décollement instationnaire.

Modèle d'émission. Le modèle utilisé comporte des hypothèses relativement arbitraires. Il paraît possible de l'améliorer pour obtenir de meilleurs résultats sans nécessairement introduire des paramètres empiriques. En particulier, des termes d'amortissement visqueux ont déjà été essayés.

Condition de bord de fuite. Une schématisation simplifiée du non-sourtoisement au bord de fuite acceptable en stationnaire ou sans décollement peut s'avérer insuffisante. Une expression plus physique de cette condition devrait être recherchée.

En plus de modifications visant à améliorer la validité du calcul, on peut envisager une extension de son domaine d'application dans les directions suivantes :

- extension au décrochage bord de fuite. Le cas semble se présenter dans plusieurs essais. Une adaptation de la méthode peut être tentée. Elle nécessiterait de disposer d'un critère de décollement turbulent valable.
- extension au compressible. Elle est difficile au stade actuel, cependant elle serait d'une grande utilité. Elle ne pourrait qu'être limitée à des nombres de Mach modérés.
- extension au tridimensionnel. Il est vraisemblable que le décollement réel sur les pales a un caractère tridimensionnel. On peut considérer le bidimensionnel comme une étape nécessaire dans la voie de cette extension. A priori elle ne paraît pas inaccessible compte tenu des résultats déjà obtenus sur le sillage de bord de fuite mais des ordinateurs de très grande capacité seront certainement nécessaires.

4. CONCLUSION

Les résultats obtenus sur le plan expérimental et théorique sont encourageants. La poursuite du travail demande, en particulier, une amélioration de la méthode dynamométrique en corrigeant de façon plus précise les forces d'inertie, et, dans les calculs, une introduction des critères de décollement instationnaire qui pourraient être définis à partir d'études théoriques et expérimentales sur les couches limites instationnaires.

En effet, l'étude des grandeurs aérodynamiques sur les profils en oscillations harmoniques de tangage paraît une étape indispensable pour aborder de façon réaliste les problèmes plus difficiles des écoulements instationnaires sur pales d'hélicoptères.

L'étroite collaboration établie entre les organismes de recherches, les constructeurs, et les services officiels doit permettre de mener cette étude dans les meilleures conditions.

BIBLIOGRAPHIE

1. L. GRAY, J. LIIVA, F.J. DAVENPORT - Two dimensional test of airfoils oscillating near stall - USAAVLABS - TR 68 13 A. 13 B - April 1968 Vol. 1 Summary and Evaluation of Results - Vol. 2 data report
2. F.O. CARTA - Experimental investigation of the unsteady aerodynamic characteristics of an NACA 0012 Airfoil - United Aircraft Research Laboratories Report M 1283 1 - August 1960
3. R.I. WINDSOR - Measurement of aerodynamics forces on an oscillating airfoil - USAAVLABS TR 69 - 98 - March 1970
4. N.D. HAM - Aerodynamic loading on a two-dimensional airfoil during dynamic stall - AIAA Journal Vol. 6 - N° 10 - October 1968
5. L.E. ERICSSON, J.P. REDING - Unsteady airfoil stall - NASA CR 66 - 787 - July 1969
6. P.F. YAGGI - Pure and compound helicopters - AGARD VKI Lecture Series on the Aerodynamics of V/STOL Aircraft - May 1968
7. J.J. PHILIPPE - Le décrochage instationnaire d'un profil-Aéronautique et Astronautique N° 27 (1971-3)
8. P.J. ARCIDIACONO, F.O. CARTA, L.M. CASELLINI, H.L. ELMAN - Investigation of helicopter control loads induced by stall flutter - USAAVLABS TR 70-2 - March 1970
9. F.D. HARRIS, F.J. TARZANIN, R.K. FISCHER - Rotor high speed performance, theory vs test - Journal of the American Helicopter Society - July 1970
10. E.D. BELLINGER - Analytical investigation of the effects of blade flexibility unsteady aerodynamics and variable inflow on helicopter rotor stall characteristics - NASA CR 1769 - September 1971
11. J.P. GIESING - Non linear two dimensional unsteady potential flow with lift - Journal of Aircraft Vol. 5 n° 2 - 1968
12. H. WERLE, C. ARMAND - Mesures et visualisations instationnaires sur les rotors - 6ème colloque d'aérodynamique appliquée AFITAE - TOULOUSE Novembre 1969 - TP ONERA N° 777
13. M. SCHWABE - Pressure distribution in a non uniform two-dimensional flow - NACA TM 1039 - 1943
14. T. SARPKAYA - Separated flow about lifting bodies and impulsive flow about cylinders - AIAA Journal Vol. 4 n° 3 - 1966
15. M. SAGNER, N. BAUDU - Champ aérodynamique instationnaire autour d'une plaque - Entropie n° 28 - 1969
16. D. PIERCE - Photographic evidence of the formation and growth of vorticity behind plates accelerated from rest in still air-Journal of Fluid Mechanics Vol. 11 Part 3 - 1961
17. T. SARPKAYA - An analytical study of separated flow about circular cylinders - A.S.M.E. Paper n° 68 FE. 15 - 1968
18. B. THWAITES - Approximate calculation of the boundary layer - Aeronautical Quarterly - Vol. 1 - Part 3 - Nov. 1949
19. K. OSWATITSCH - Die Ablösungsbedingung von Grenzschichten - IUTAM Symposium Freiburg - 1957
20. W.J. Mc. CROSKEY, R.K. FISHER - Detailed aerodynamic measurements on a model rotor in the blade stall regime - Journal of the American Helicopter Society - Jan. 1972
21. W.J. Mc. CROSKEY, E.J. DURBIN - Shear stress an flow angle measurements with heated films and wires - A.S.M.E. Paper n° 71 - WA / FE 17 - Nov. 1971
22. M. VINCENT DE PAUL - Prévion du décrochage d'un profil d'aile en écoulement incompressible - AGARD meeting on Fluid Mechanics on Aircraft Stalling - Lisbon, 25 - 28 April 1972

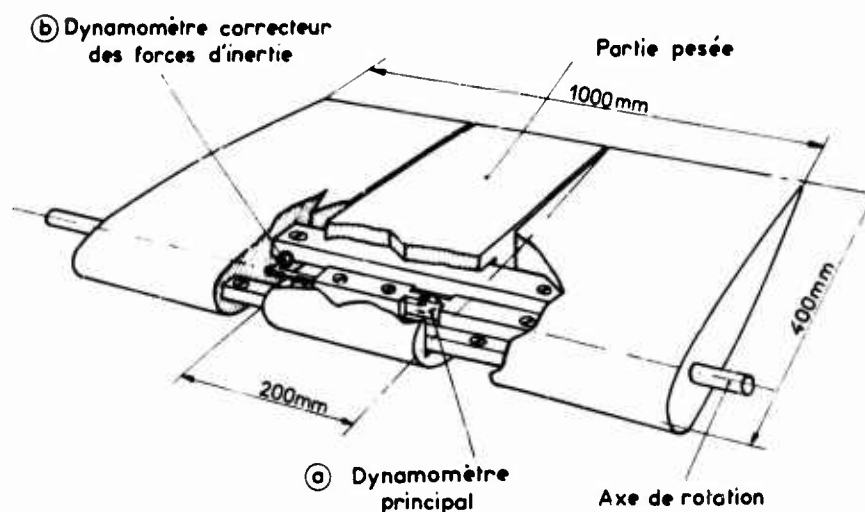


Fig. 1. SCHÉMA DE LA MAQUETTE POUR ESSAIS DE PROFILS EN OSCILLATIONS HARMONIQUES DE TANGAGE

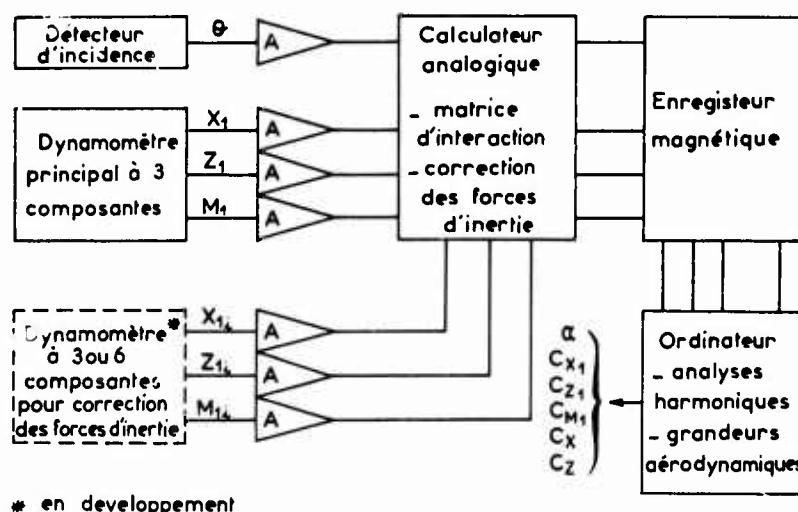


Fig. 2. ACQUISITION ET TRAITEMENT DES INFORMATIONS

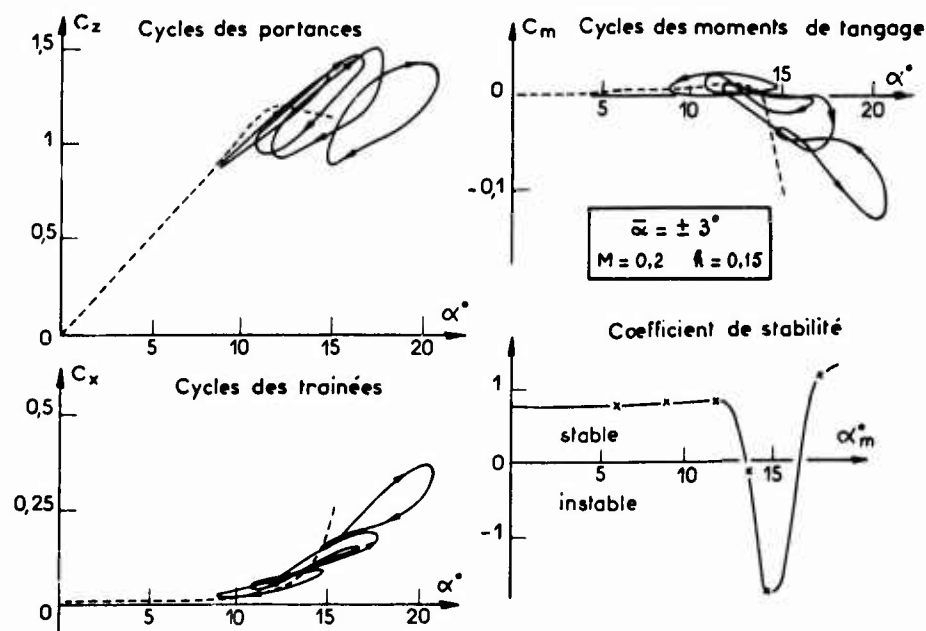


Fig. 3. EXEMPLE DE RÉSULTATS OBTENUS SUR LE PROFIL NACA 0012 A MACH 0,2

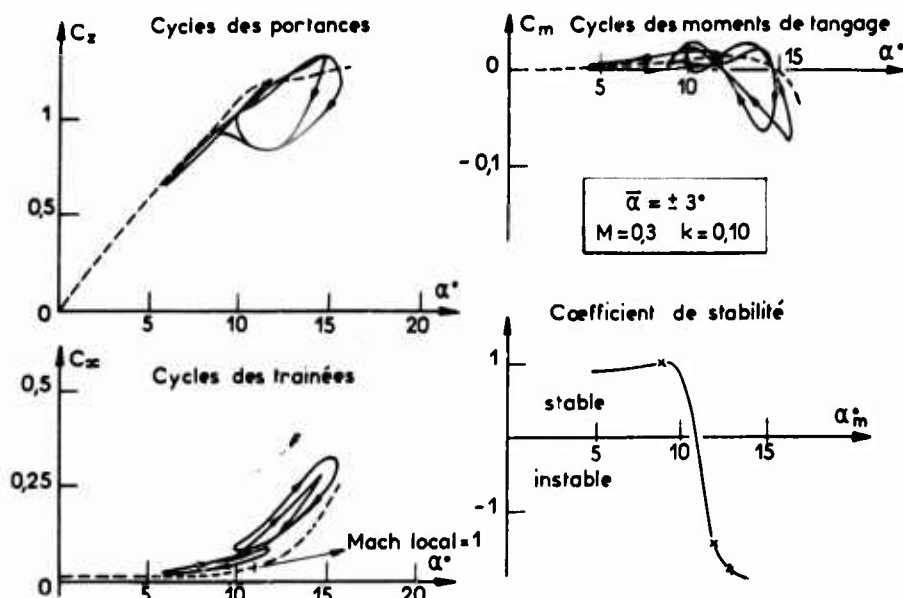


Fig. 4. EXEMPLE DE RÉSULTATS OBTENUS SUR LE PROFIL NACA 0012 A MACH 0,3

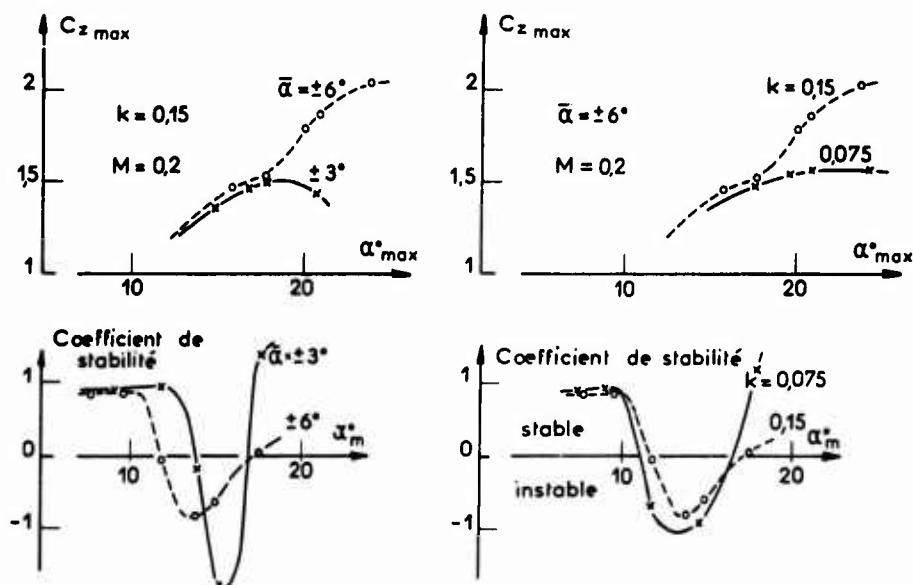


Fig. 5 - INFLUENCE DE LA FRÉQUENCE RÉDUITE ET DE L'AMPLITUDE DES OSCILLATIONS

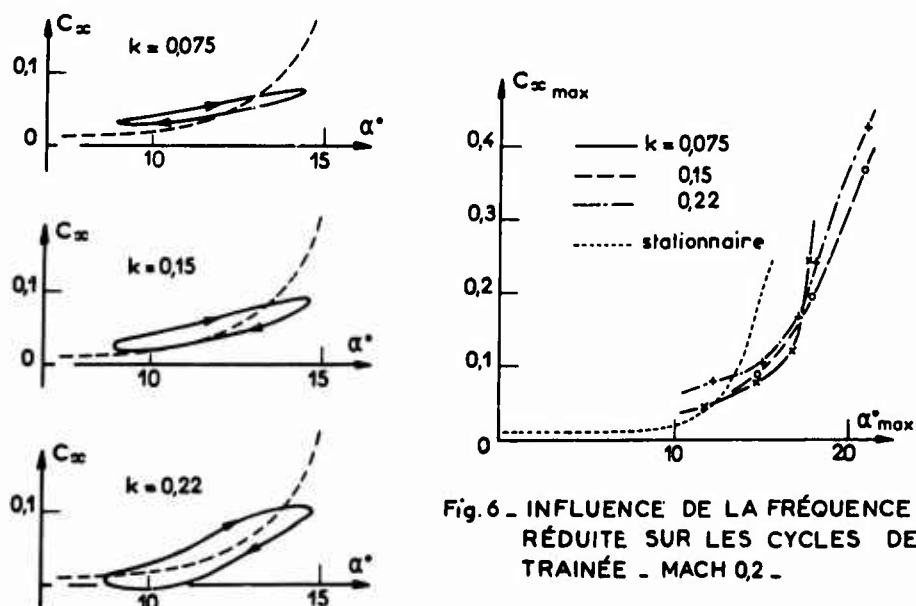


Fig. 6 - INFLUENCE DE LA FRÉQUENCE RÉDUITE SUR LES CYCLES DE TRAÎNÉE - MACH 0,2 -

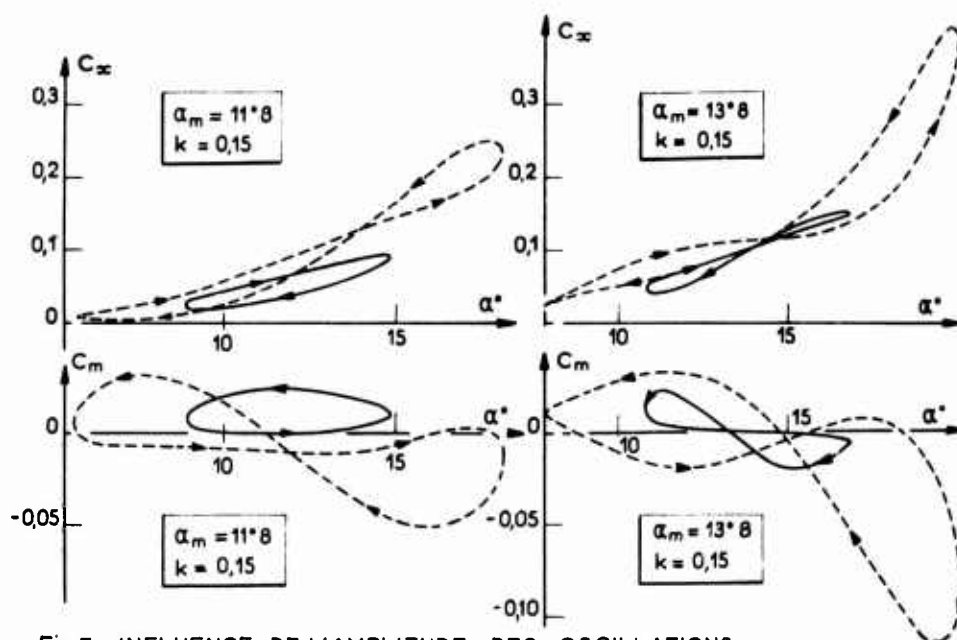
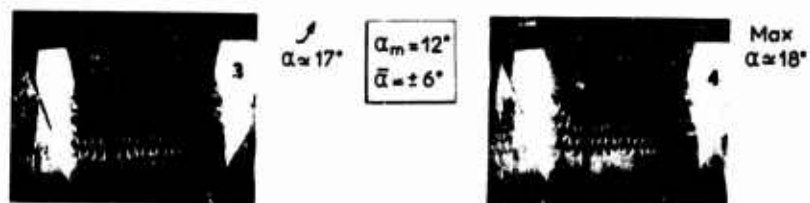
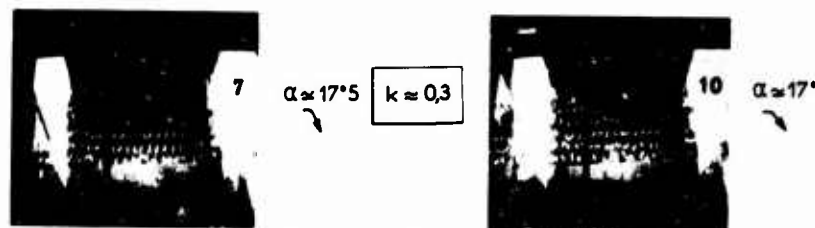


Fig 7. INFLUENCE DE L'AMPLITUDE DES OSCILLATIONS
SUR LES TRAINÉES INSTATIONNAIRES

Incidences croissantes ③ ④



CARACTÈRE TRIDIMENSIONNEL DU DÉCROCHAGE INSTATIONNAIRE



Incidences décroissantes ⑦ ⑩

Fig.8 . VISUALISATIONS DU DÉCROCHAGE INSTATIONNAIRE A M=0,1(Toulouse)

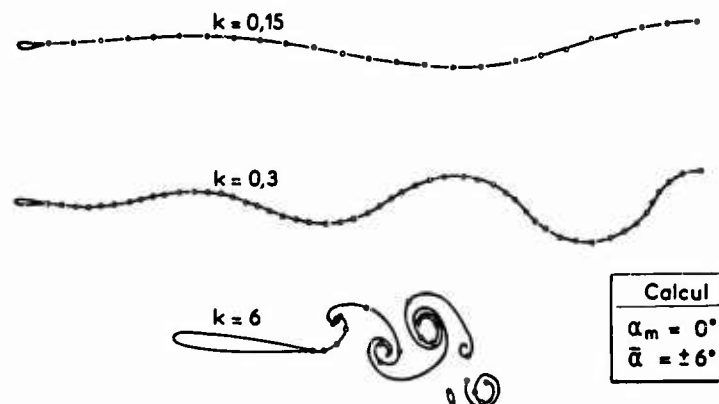


Fig.9. INFLUENCE DE LA FREQUENCE REDUITE SUR LA FORME
DU SILLAGE - CAS NON DECOLLE

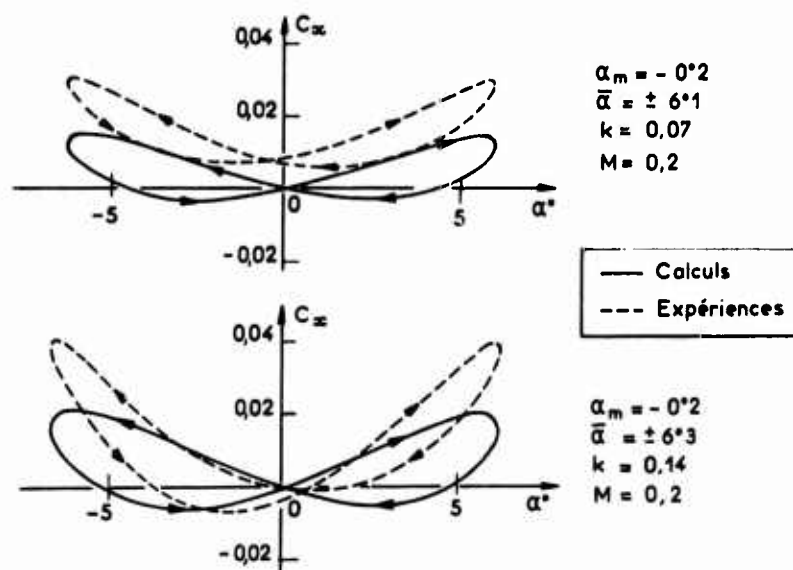


Fig.10. CYCLES DES TRAÎNES - CAS NON DÉCOLLES
INFLUENCE DE LA FRÉQUENCE RÉDUITE

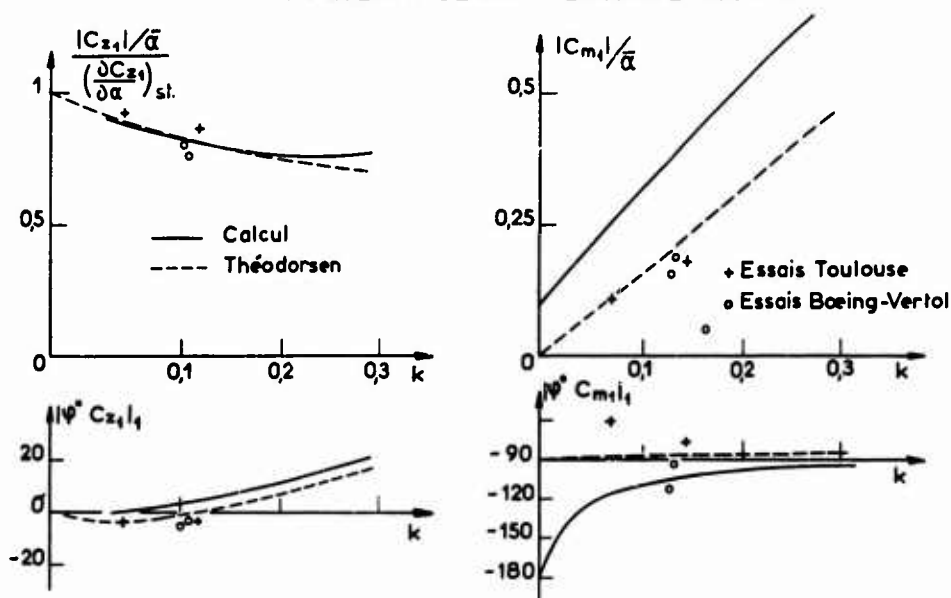


Fig.11. COMPARAISON THÉORIE - EXPÉRIENCES - 1^{er} HARMONIQUE
DES FORCES NORMALES ET MOMENTS DE TANGAGE

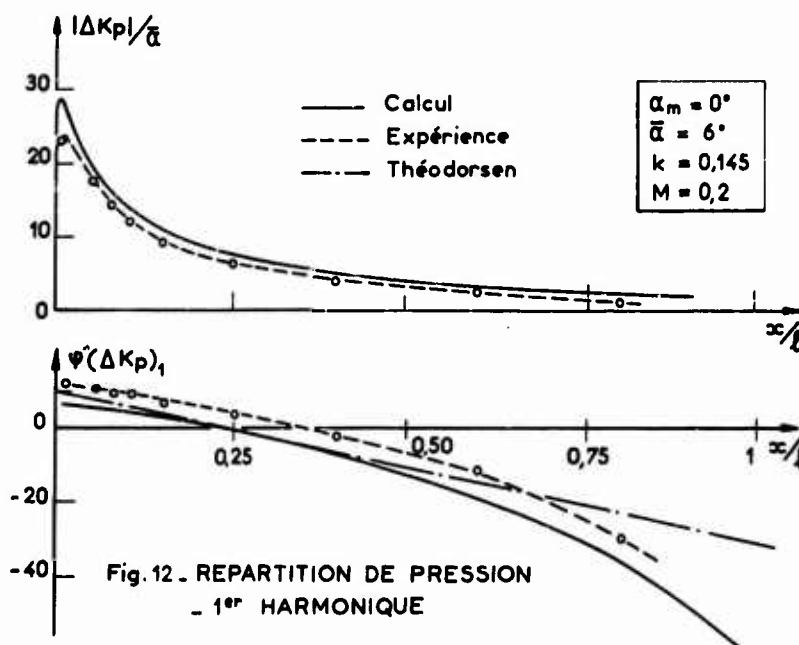


Fig.12. RÉPARTITION DE PRESSION
- 1^{er} HARMONIQUE

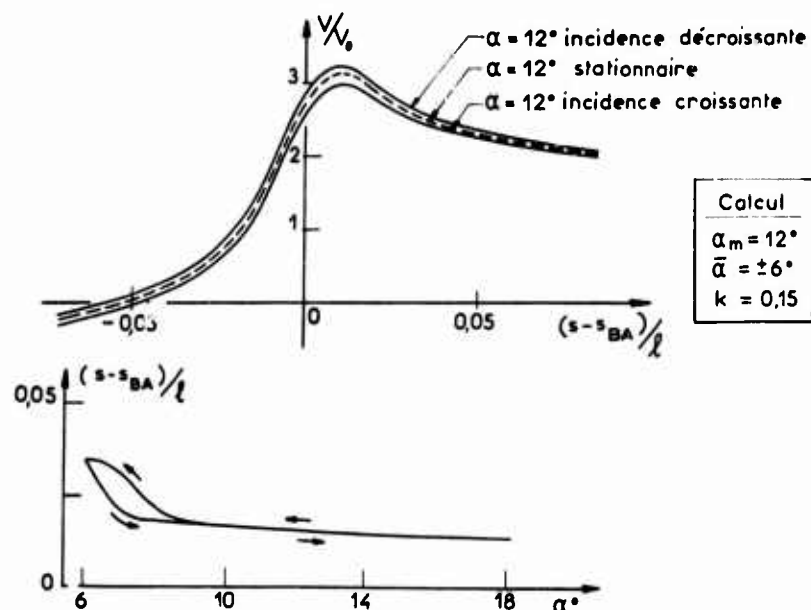


Fig.13. EVOLUTION DE LA REPARTITION DE VITESSE AU BORD D'ATTAQUE DU PROFIL ET DE LA POSITION DU POINT DE DECOLLEMENT

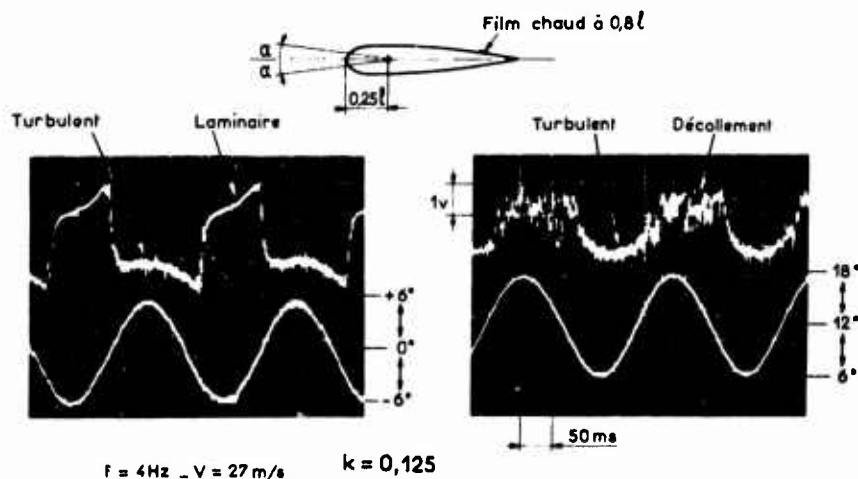


Fig.14. ETUDE DES COUCHES LIMITES INSTATIONNAIRES REPONSES D'UN FILM CHAUD

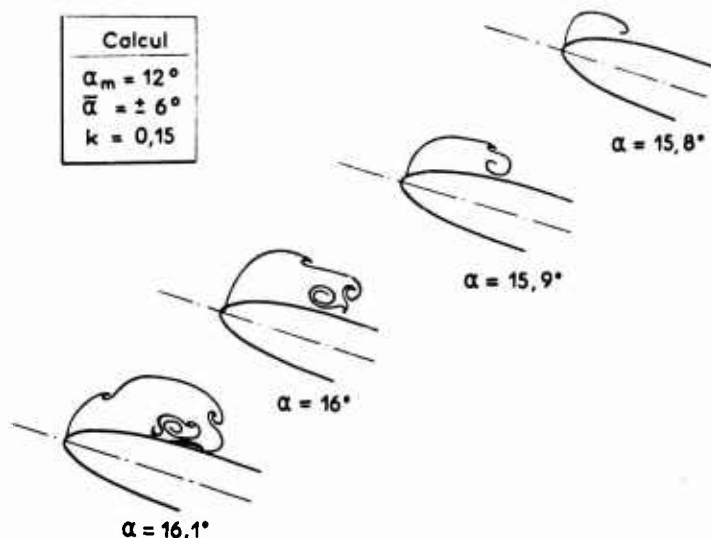


Fig.15. DEVELOPPEMENT DE LA NAPPE TOURBILLONNAIRE DE BORD D'ATTAQUE

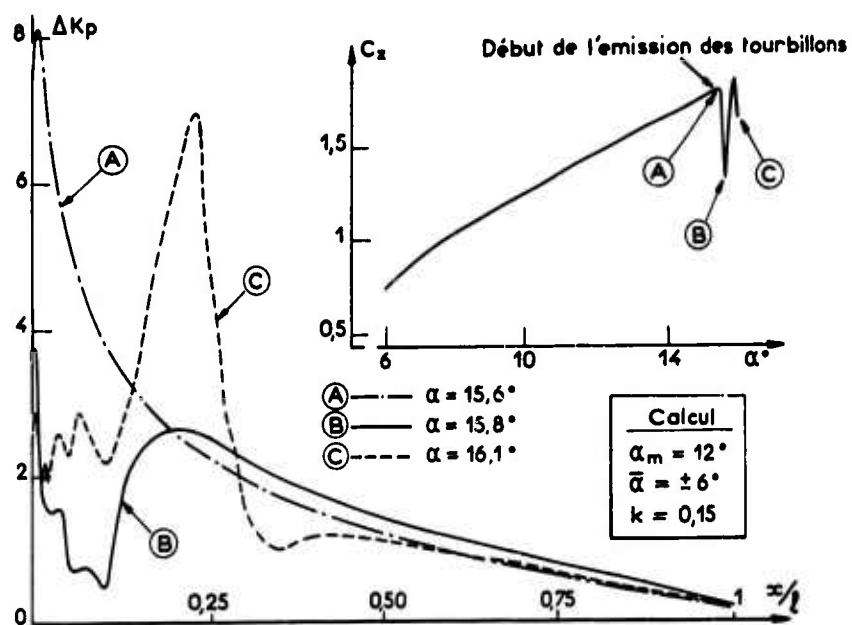


Fig.16. EVOLUTION DES PRESSIONS - CAS DE DECROCHAGE INSTATIONNAIRE

EFFORTS AERODYNAMIQUES SUR UN PROFIL D'AILE ANIME
D'UN MOUVEMENT HARMONIQUE PARALLELE A L'ECOULEMENT
" MOUVEMENT DE TAMIS "

par

J. Valensi⁽¹⁾ et J. Rebont⁽²⁾

Annexe

ANALYSE DES PREMIERS RESULTATS
D'ESSAIS INSTATIONNAIRES EN "TAMIS" EFFECTUES A L'IMFM

par

J. Renaud et G. Vingut
Département Recherches
Division Hélicoptères de l'Aérospatiale
13221 Marseille Cedex 1

(1) J. Valensi : Professeur à l'Université d'Aix-Marseille, Directeur de l'Institut de Mécanique des Fluides

(2) J. Rebont : Ingénieur-Docteur, C.N.R.S.

NOTATIONS

T	traînée instantanée en régime instationnaire
T ^s	traînée en régime stationnaire à la vitesse V _s de la soufflerie
P ^s	portance instantanée en régime instationnaire
P ^s	portance en régime stationnaire à la vitesse V _s de la soufflerie
M ^s	moment de tangage instantané en régime instationnaire
M _s	moment de tangage stationnaire à la vitesse V _s de la soufflerie
V _s	vitesse de l'écoulement non perturbé dans la soufflerie
V	vitesse relative de l'air par rapport au profil $V = V_s - A \Omega \cos \psi$
Ω	pulsation du mouvement de la maquette rd/s
ψ	angle d'azimut du maneton d'entraînement $\psi = \Omega t$
A	amplitude du mouvement d'oscillation
S	surface de référence du profil = C . h
h	hauteur du profil
C	corde du profil

$$C_z = \frac{P_s}{\frac{1}{2} \rho \cdot S \cdot V_s^2} \quad C_x = \frac{T_s}{\frac{1}{2} \rho \cdot S \cdot V_s^2} \quad C_m = \frac{M_s}{\frac{1}{2} \rho \cdot S \cdot C \cdot V_s^2}$$

i	incidence du profil
ρ	masse spécifique de l'air
λ	$\frac{A\Omega}{V_s}$, paramètre d'avancement

$$T_c = \frac{1}{2} \rho \cdot C_x \cdot S \cdot V^2$$

$$P_c = \frac{1}{2} \rho \cdot C_z \cdot S \cdot V^2$$

$$M_c = \frac{1}{2} \rho \cdot C_m \cdot S \cdot V^2$$

EFFORTS AERODYNAMIQUES SUR UN PROFIL D'AILE ANIME
D'UN MOUVEMENT HARMONIQUE PARALLELE A L'ECOULEMENT
" MOUVEMENT DE TAMIS "

J. Valensi et J. Rebont

1. INTRODUCTION

Au cours du vol en translation, le vent relatif autour des pales du rotor subit des variations périodiques en grandeur et direction. De la sorte les forces aérodynamiques qui s'exercent sur les différents éléments de chaque pale, varient avec l'azimut. Or le calcul des forces qui s'exercent sur les pales au cours de leur rotation, est généralement effectué en adoptant pour caractéristiques aérodynamiques (c'est-à-dire pour les coefficients de portance, de moment et de traînée), ceux correspondant à un régime stationnaire, tout en tenant compte bien entendu des variations cycliques du vent relatif.

Dans le but de déterminer l'importance des corrections qu'il conviendrait d'appliquer pour faire un calcul plus précis, on peut imaginer de faire des essais en soufflerie, en simulant tout ou partie des variations du vecteur vitesse relative. C'est ainsi que nous avons été amenés à entreprendre des essais en soufflerie sur un profil d'aile animé d'un mouvement de tamis par rapport au vent, constant en grandeur et direction, de la soufflerie. Dans une première phase, l'étude a porté sur la mesure de la traînée, de la portance et du moment de tangage d'une aile rectangulaire de profil symétrique à différentes incidences et pour différentes valeurs du paramètre d'avancement.

Ces essais ont été effectués dans le cadre d'un programme d'études relatif à l'aérodynamique des rotors d'hélicoptère, financé par le Service Technique de l'Aéronautique, Direction Technique des Constructions Aérospatiales.

2. DESCRIPTION DES DISPOSITIFS DE MESURE

2.1. Dispositif de mesure de la traînée

On pourrait d'abord penser, pour mesurer cette traînée, à rendre la maquette solidaire d'un cadre animé d'un mouvement harmonique forcé, par l'intermédiaire d'une suspension dynamométrique appropriée. Cette suspension devrait alors autoriser de petits déplacements parallèles à la direction de la traînée ; on détecterait donc en même temps la force d'inertie agissant sur le modèle, ce qui rendrait impossible la mesure de la traînée avec une précision acceptable.

En effet, si l'on remarque que d'une part les conditions d'essais conduisent à des accélérations de 10 g et plus, et que d'autre part la masse totale en mouvement, (profil + partie mobile du dynamomètre), ne peut pas être pratiquement inférieure à 500 gr, on voit que les forces d'inertie seraient de l'ordre de 50 N soit 50 fois supérieures environ à la traînée moyenne de la maquette.

C'est pour cette raison que le montage suivant a été adopté.

Le cadre oscillant placé au-dessous de la paroi inférieure de la soufflerie porte un torsiomètre dont l'équipage comprend deux tubes cylindriques verticaux qui traversent librement la paroi inférieure de la soufflerie.

La maquette, constituée par une aile rectangulaire de profil symétrique, est fixée rigidement sur ces tubes de façon que son plan de symétrie coïncide avec le plan des axes des tubes. Le plan de symétrie de l'aile est donc vertical ; l'axe du torsiomètre est par suite perpendiculaire à la vitesse du courant de la soufflerie et au bord d'attaque du profil.

Pour que le mouvement d'oscillation de l'aile ne soit pas gêné par les parois de la soufflerie, son envergure a été limitée à 495 mm, laissant un jeu de 2,5 mm entre le modèle et les parois supérieure et inférieure de la soufflerie. On minimise les échanges possibles à travers l'ouverture de la paroi inférieure, en rendant la pression dans la veine aussi voisine que possible de la pression ambiante.

Un calcul élémentaire montre que pour assurer l'équilibre dynamique de la maquette autour de l'axe du torsiomètre, il suffit à l'aide d'un contrepoids approprié, comme le montre le schéma de la figure 1, de placer le centre de gravité de l'ensemble modèle-suspension sur l'axe de symétrie du torsiomètre (fig. 1-2-3).

Il faut, bien entendu, que la fréquence propre des petits mouvements autour de l'axe de torsion de l'ensemble modèle-suspension par rapport au cadre, soit aussi élevée que possible. La fréquence propre du montage réalisé, égale à 20 HZ, est obtenue en

choisissant une raideur en torsion compatible avec la sensibilité souhaitée pour la mesure de la traînée et une masse de l'ensemble modèle-suspension aussi faible que possible. La maquette a été réalisée en mousse de polyuréthane, les deux tubes supports, en acier inoxydable, de diamètre 16 mm et d'épaisseur 0,6 mm, le bâti, en dural. La masse de l'ensemble s'élève à 500 grs.

Le torsiomètre est fixé sur un chariot qui coulisse sur deux tubes solidaires d'un bâti (fig.4). Le chariot est placé entre quatre ressorts de compression E, calculés pour que la fréquence propre du chariot soit voisine de 5 Hz. Un dispositif à maneton F, se déplaçant dans une lumière G, entraîne le chariot dans un mouvement harmonique forcé à la fréquence choisie. Pour faciliter le démarrage du dispositif, le maneton est monté sur un vérin hydraulique H, qui permet de faire varier l'amplitude du mouvement. Un disque I, solidaire de l'arbre, occulte les rayons lumineux émis par une lampe ; ce disque est percé d'un trou qui fournit un signal lumineux de synchronisation repris par une cellule photoélectrique J.

Les tensions des capteurs sont amplifiées et filtrées à travers un filtre passe bas, du type Butterworth, qui présente les caractéristiques suivantes : fréquence de coupure 5,5 Hz, atténuation, 80 db par octave.

Elles sont analysées dans un moyennneur à 100 voies, synchronisé avec le mouvement d'oscillation. Les 100 valeurs moyennées pendant un temps de 120 sec. sont restituées sur un enregistreur X.Y, qui trace la courbe de la traînée en fonction de la phase du mouvement.

Pour les mesures en régime stationnaire ainsi que pour l'étalonnage, le top de synchronisation du mouvement d'oscillation est remplacé par un top de synchronisation de même fréquence, émis par un oscillateur électronique.

2.2. Dispositif de mesure de la portance et du moment de tangage

Le principe de la mesure et du montage sont semblables à ceux décrits au § 2.1. mais, d'une part, le torsiomètre qui mesure le moment de la portance a son axe G X parallèle à la vitesse V_∞ de la soufflerie (fig. 2) et d'autre part, le torsiomètre qui mesure le moment de tangage a son axe G Y parallèle au bord d'attaque (fig. 3).

3. CARACTERISTIQUE DE LA MAQUETTE

Profil NACA. 0012

Corde = 0,30 m

Hauteur = 0,495 m

4. PROGRAMME D'ESSAIS

Les essais ont été effectués à des incidences comprises entre 0° et 6° pour des vitesses du vent dans la soufflerie comprises entre 10 m/s et 30 m/s et pour deux valeurs de la pulsation du mouvement d'oscillation = 16,5 rad/s, 11,2 rad/s. L'amplitude du mouvement a été prise égale à 0,15 m.

5. RESULTATS

5.1. Traînée

Les résultats sont donnés dans les figures 5 à 12, où l'on a porté d'une part, la traînée enregistrée T rapportée à la traînée en régime stationnaire, à la vitesse du courant de la soufflerie, et d'autre part, la traînée réduite quasi-stationnaire $\frac{T}{T^c}$, calculée à partir du coefficient de traînée en régime stationnaire et de la vitesse relative instantanée de l'air par rapport au modèle. Les valeurs du C_x en régime stationnaire en fonction de l'incidence et pour 3 valeurs différentes du nombre de Reynolds rapporté à la corde sont portées dans la figure 21.

On peut faire les remarques suivantes :

1. la courbe de la traînée périodique mesurée n'est pas sinusoïdale.
2. Cette courbe est toujours plus aplatie que la courbe calculée. La différence entre les deux courbes est plus accentuée pour les valeurs élevées du paramètre d'avancement.
3. Le maximum de l'amplitude de la traînée réduite est en retard sur le mouvement d'entraînement ; le retard est fonction croissante de λ .
4. La traînée moyenne mesurée semble être toujours plus faible que la traînée moyenne calculée.

La figure 22 où l'on a porté en traits interrompus les courbes quasi-linéaires des amplitudes maximales et minimales de la traînée réduite calculée en fonction de λ et les points correspondants aux amplitudes maximales et minimales de la traînée mesurée réduite fonction de λ et de l'incidence, illustre bien la remarque 2 ci-dessus. Les effets instationnaires, toujours présents, s'accroissent lorsque le paramètre d'avancement

cr. it.

5.2. Portance

Les résultats des mesures sont donnés dans les figures 13 à 16 où l'on a porté, d'une part, la portance enregistrée P rapportée à la portance en régime stationnaire à la vitesse du courant de la soufflerie, et d'autre part, la portance réduite quasi-stationnaire $\frac{P_c}{P_s}$, calculée à partir du coefficient de portance en régime stationnaire et de la vitesse relative instantanée de l'air par rapport au modèle.

1. La courbe de la portance réduite mesurée n'est pas sinusoidale.
2. La portance réduite mesurée est en général supérieure à la portance réduite calculée ; l'écart semble être fonction décroissante de l'incidence.
3. Le maximum de l'amplitude de la portance réduite est en retard sur le mouvement d'entraînement. Le retard est fonction croissante de λ .

La figure 23 où l'on a porté en traits interrompus les courbes quasi-linéaires des amplitudes maximales et minimales de la portance réduite calculée en fonction de λ , ainsi que les points correspondants aux amplitudes maximales et minimales de la portance mesurée réduite en fonction de λ et de l'incidence, illustre bien la remarque 2 ci-dessus.

Les effets instationnaires toujours présents s'accroissent, comme il fallait s'y attendre, lorsque λ croît.

5.3. Tangage : Mesure du moment

L'axe de mesure du moment de tangage est placé à la distance 0,343 C du bord d'attaque :

Les résultats des mesures sont donnés dans les figures 17 à 20 où l'on a porté, d'une part, le moment enregistré M , rapporté au moment en régime stationnaire à la vitesse du courant de la soufflerie, et d'autre part, le moment réduit quasi-stationnaire $\frac{M_c}{M_s}$, calculé à partir du coefficient de moment en régime stationnaire et de la vitesse relative instantanée de l'air par rapport au modèle.

On fait les remarques suivantes :

1. La courbe du moment réduit mesuré n'est pas sinusoidale.
2. Le moment réduit mesuré est en moyenne pour $\lambda > 0,10$ inférieur au moment réduit moyen calculé.
3. Le maximum de l'amplitude du moment réduit est en retard sur le mouvement d'entraînement.

On a porté dans la figure 24 en traits interrompus les courbes quasi-linéaires des amplitudes maximales et minimales du moment calculé réduit en fonction de λ ainsi que les points correspondants aux amplitudes maximales et minimales de la portance mesurée, en fonction de λ et de l'incidence.

6. CONCLUSION

Des mesures de traînée, de portance et de moment de tangage relatives à une aile rectangulaire de profil symétrique, ont été effectuées en soufflerie. La soufflerie est à veine fermée de section rectangulaire, l'aile supportée verticalement entre parois est entraînée à l'aide d'une suspension dynamométrique dans un mouvement de translation périodique de va et vient, parallèle à l'axe horizontal de la soufflerie (mouvement dit de tamis).

Les essais ont été effectués dans les conditions suivantes, en vue de déterminer les caractéristiques aérodynamiques de l'aile en mouvement instationnaire : incidence de l'aile variant de 0 à 6° ; vitesse de la soufflerie 10 ms⁻¹ et 20 ms⁻¹ ; paramètre d'avancement $\frac{A\lambda}{V_s}$ variant entre 0 et 0,30.

Le montage réalisé permet des mesures très précises.

La comparaison des caractéristiques aérodynamiques mesurées de l'aile, avec celles que l'on peut calculer en adoptant pour les coefficients C_x , C_z , C_m , ceux mesurés en régime stationnaire, et pour la vitesse de l'air, celle instantanée relative à l'aile, (caractéristiques aérodynamiques quasi-stationnaires), met en évidence des effets instationnaires sensibles, sur les extrêmes d'amplitude et sur le retard par rapport à la sollicitation, en particulier. Ils croissent avec le paramètre d'avancement, mais demeurent faibles jusqu'à $\lambda = 0,3$. Pour λ voisin de 0,3, la finesse de l'aile en mouvement de tamis semble être légèrement supérieure à celle mesurée en régime stationnaire à la même incidence.

De nouvelles mesures sont envisagées pour λ croissant jusqu'à 0,5, qui seront possibles avec une maquette de dimensions plus faibles.

Le Département Recherches de la division Hélicoptères, de la SNIAS de Marignane a effectué une analyse harmonique des résultats exposés ci-dessus ; les observations faites sur le premier harmonique ainsi que la comparaison des résultats obtenus avec ceux des calculs basés sur la théorie de Theodorsen sont données en Annexe.

REFERENCES

1. LIGHTHILL (M.J.)
Response of Laminar Skin Friction and Heat Transfer to Fluctuations in the Stream Velocity. Proc. Roy. Soc. London (1) 224 - 1-23 (1954).
2. LIN (C.C.)
Motion in the Boundary Layer with a Rapidly Oscillating External Flow. Massachusetts Institute of Technology and General Electric Co. June (1953).
3. ROTT and ROSENZWEIG
On the Response of the Laminar Boundary Layer to Small Fluctuations of the Free - Stream Velocity. J. of Aero. Sciences, Vol.27, n°10 (1960).
4. GHOSH (A.)
Contribution à l'étude de la couche limite laminaire instationnaire. Public. Scient. et Tech. du Ministère de l'Air n° 381 (1961).

Annexe

ANALYSE DES PREMIERS RESULTATS D'ESSAIS INSTATIONNAIRES EN "TAMIS" EFFECTUES A L'IMFM

J. Renaud et G. Vingut

1. ANALYSE DES FORCES DE PORTANCE : COMPARAISONS THEORIES LINEARISEES ET ESSAIS

1.1. Une analyse harmonique des efforts aérodynamiques dans les axes vent a été effectuée pour les différents cas d'essais :

- incidence : 0° , 3° , 6°
- fréquence : 11,2 rd/s, 16,5 rd/s
- vitesse soufflerie : 10 m/s, 20 m/s, 30 m/s

Le premier harmonique de la portance expérimentale a été comparé aux résultats de deux théories linéarisées :

- 1°) Théorie pseudo-stationnaire
- 2°) Théorie instationnaire de Theodorsen.

Le mouvement du profil à une incidence i_0 affichée, est représenté comme la superposition de deux mouvements :

- Un mouvement de tamis pur suivant la corde de portance nulle
- Un mouvement de pompage suivant une direction perpendiculaire au précédent.

Le profil étant symétrique, seul le second mouvement donne naissance à des forces de portances instationnaires.

1.2. La comparaison entre les deux théories (pseudo-stationnaire et Theodorsen), est présentée figure 27 où ont été portées en ordonnée les portances données par les deux théories précédentes, ces portances instantanées étant réduites par la portance stationnaire (correspondant à l'incidence affichée i_0 et à la vitesse soufflerie).

Compte tenu des fréquences réduites assez faibles ($\frac{\Omega C}{2V} = 0,126$ pour la figure 27) on vérifie que la théorie pseudo-stationnaire représente correctement le phénomène.

1.3. La comparaison des résultats de ces deux théories avec les valeurs expérimentales, est présentée figure 28.

- On note que les deux théories sont bien représentatives des valeurs expérimentales du premier harmonique des efforts de portance.
- Les déphasages notés sur les planches précédentes entre la valeur totale instantanée de la portance expérimentale et la valeur donnée par la théorie pseudo-stationnaire, sont essentiellement dus à la participation des harmoniques supérieurs.

2. INFLUENCE DES PARAMETRES D'ESSAIS SUR LES EFFORTS INSTATIONNAIRES

2.1. Les résultats d'essais ont été analysés essentiellement sous deux aspects : influence de la fréquence réduite, influence de l'incidence affichée.

Seul, le premier harmonique des efforts aérodynamiques instationnaires a été retenu dans cette comparaison, les harmoniques supérieurs étant trop faibles pour être pris en considération, compte tenu de la précision expérimentale.

C'est ainsi que pour les efforts de traînée, la participation du premier harmonique varie de 10 à 40 % des efforts statiques, alors que celle du deuxième harmonique reste toujours inférieure à 4 %.

2.2. De façon générale, les amplitudes des efforts aérodynamiques (traînée, portance, moment) peuvent être correctement représentées en fonction des deux seuls paramètres : incidence et fréquence réduite.

2.2.1. L'amplitude de la traînée instationnaire est représentée figure 29. On note que :

- cette amplitude augmente avec la fréquence réduite,
- le gradient d'augmentation est d'autant plus fort que l'incidence est grande,
- la participation du premier harmonique est très importante dans la traînée globale.

2.2.2. Les variations de l'amplitude de la portance en fonction de la fréquence réduite et de l'incidence affichée, sont présentées figure 30. Ces amplitudes ont été réduites par les valeurs respectives des portances stationnaires aux incidences aérodynamiques indiquées. On note :

- une augmentation pratiquement linéaire de la portance instationnaire, en fonction de la fréquence réduite,
- un gradient d'autant plus fort que l'incidence aérodynamique est plus élevée.

2.2.3. Les amplitudes des moments instationnaires ont été réduites par les valeurs des moments stationnaires correspondant aux incidences aérodynamiques d'essai. Compte tenu de cette réduction, il s'avère (voir figure 31) qu'une courbe unique permet de représenter l'évolution de l'amplitude du moment en fonction de la fréquence réduite, quelle que soit l'incidence (3° et 6°).

2.3. Les études de stabilité des pales d'hélicoptère montrent qu'en général le flottement est conditionné par le mouvement en trainée des pales.

Il en résulte que l'amortissement aérodynamique lié au mouvement de trainée est d'une importance capitale dans ces problèmes de stabilité.

Les différents cas d'essai de tamis ont été analysés sous cet aspect et la figure 32 donne l'évolution de l'amortissement réduit en fonction de la fréquence réduite, pour les 3 incidences affichées. L'amortissement réduit est ici défini comme le rapport entre le travail effectué par les forces aérodynamiques au cours d'un cycle et un travail de référence : $\pi A T_s$.

On constate que l'amortissement réduit :

- a une valeur importante (de 100 à 200 %)
- croît légèrement avec la fréquence réduite
- reste constamment positif dans le domaine d'essais et contribue par conséquent à une amélioration de la stabilité
- dépend relativement peu de l'incidence.

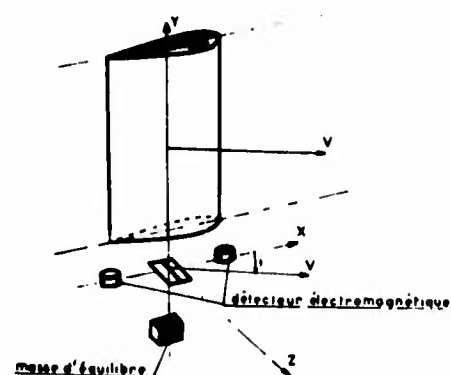


Fig. 1

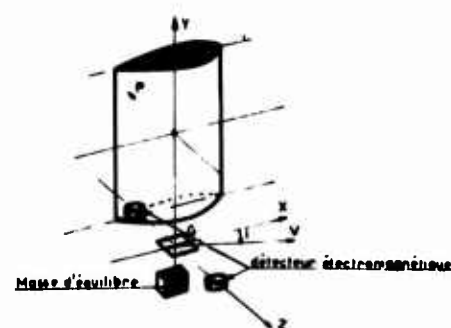


Fig. 2

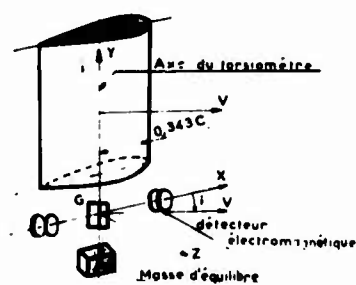


Fig. 3

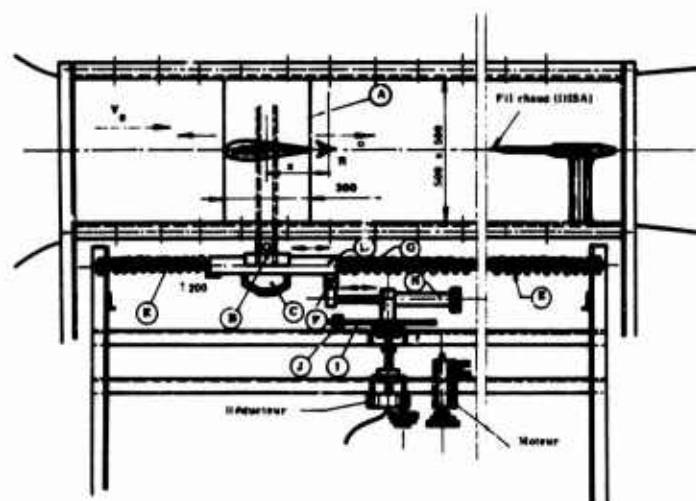


Fig. 4

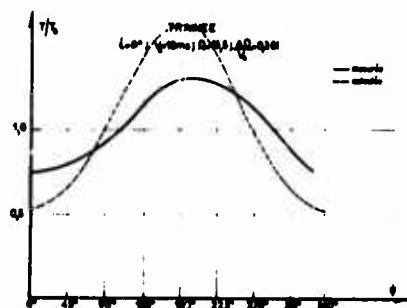


Fig. 5

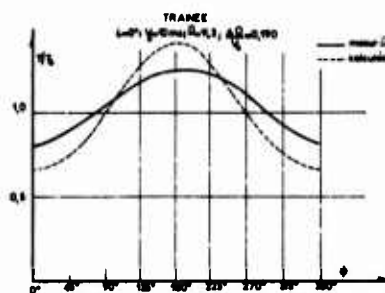


Fig. 6

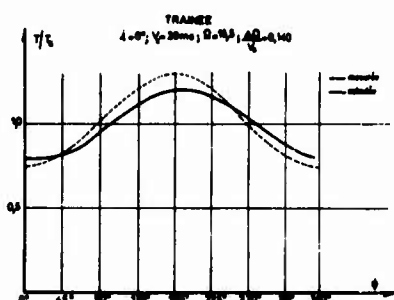


Fig. 7

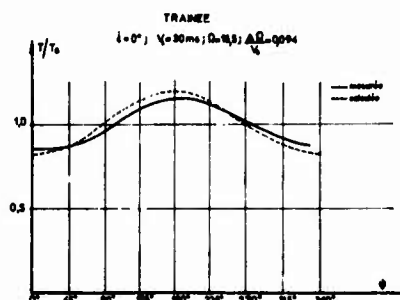


Fig. 8

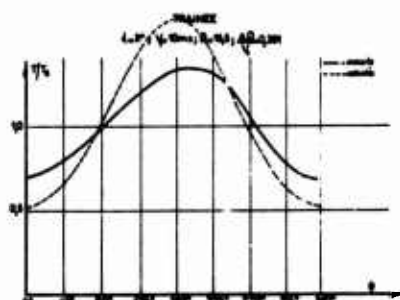


Fig. 9

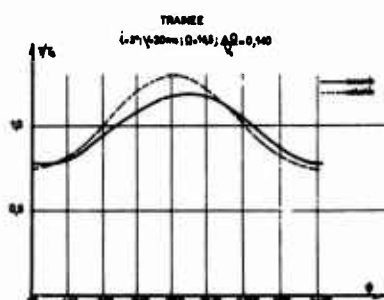


Fig. 10

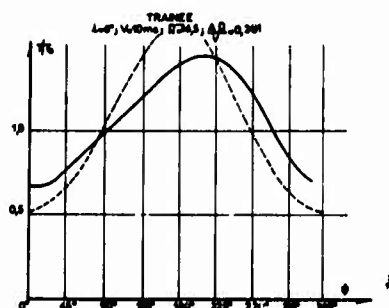


Fig. 11

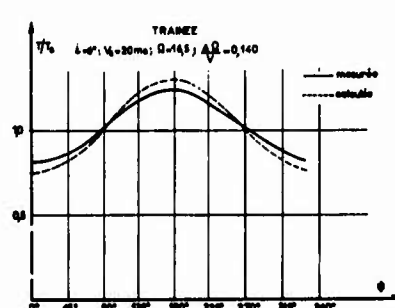


Fig. 12

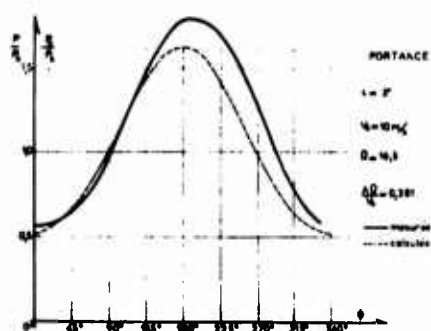


Fig. 13

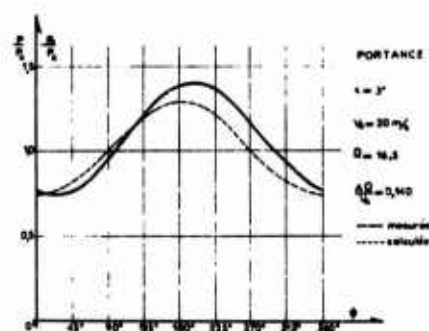


Fig. 14

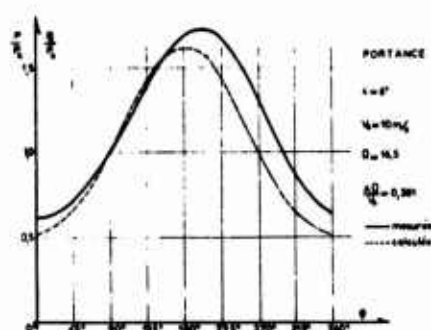


Fig. 15

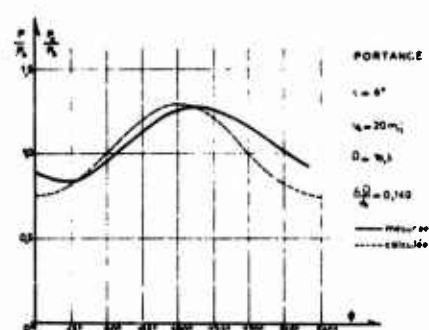


Fig. 16

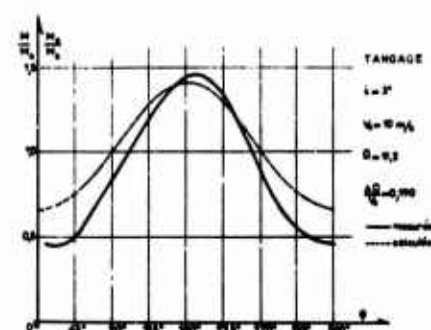


Fig. 17

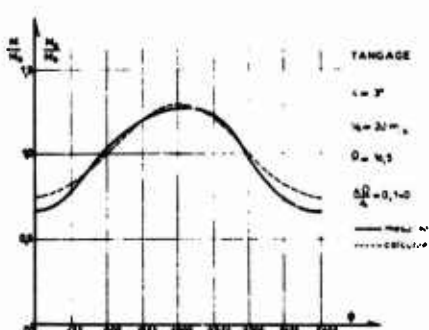


Fig. 18

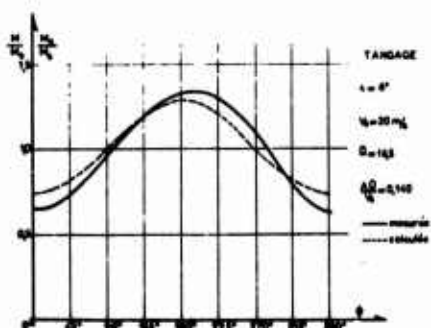


Fig. 19

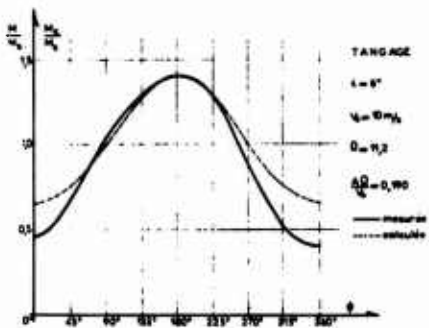


Fig. 20

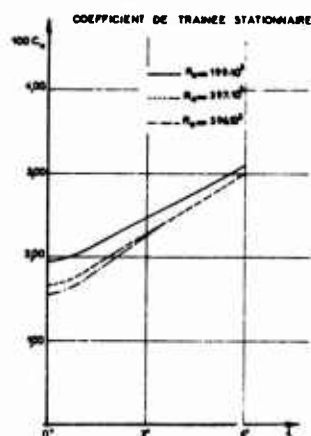


Fig.21

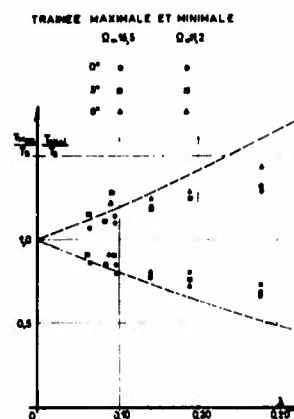


Fig.22

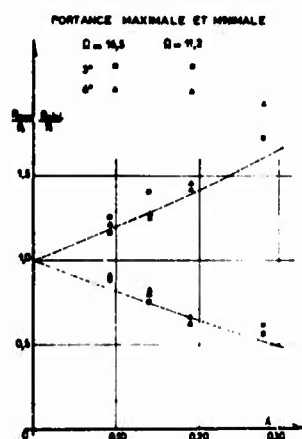


Fig.23

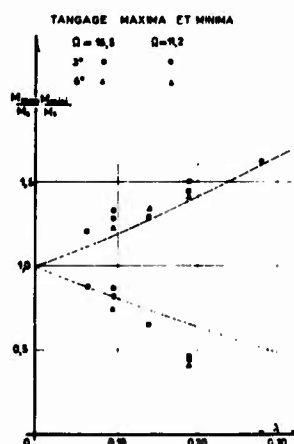


Fig.24

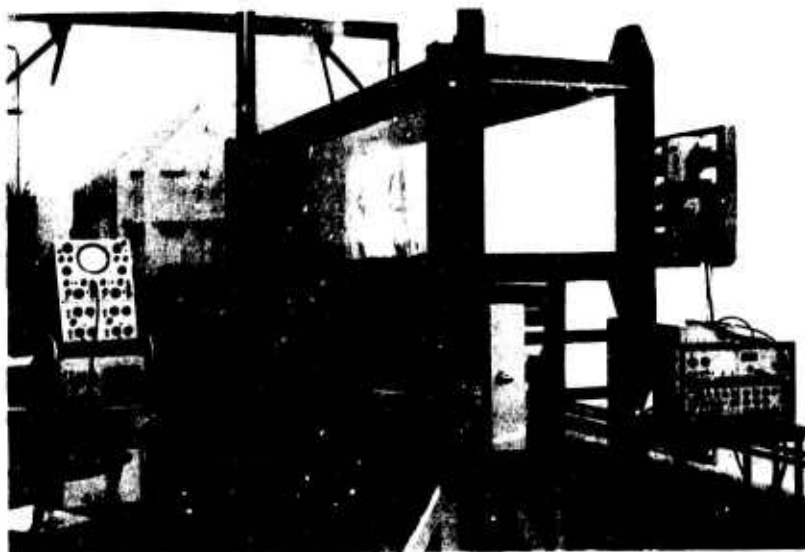


Fig.25
MONTAGE EN SOUFFLERIE

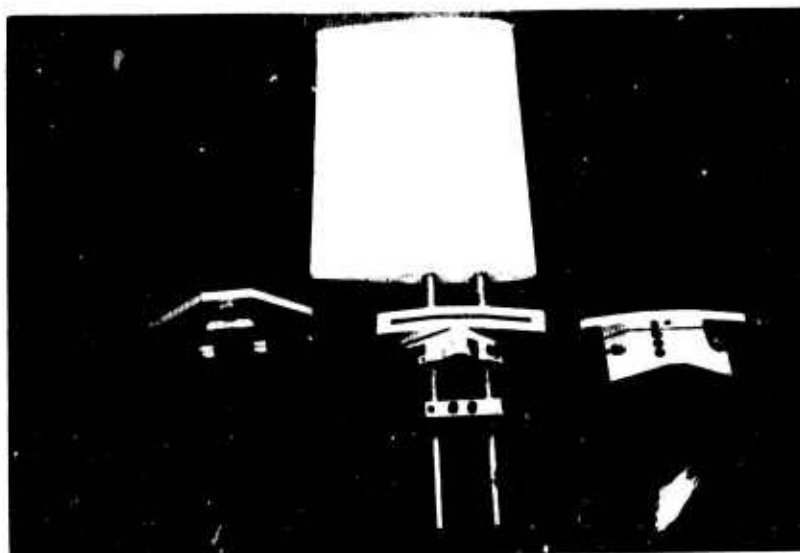


FIG. 26
MAQUETTE MONTÉE SUR LE TORSIOMETRE DE TRAÎNÉE
AVEC SA MASSE D'EQUILIBRAGE
A gauche le torsiomètre de portance
A droite le torsiomètre de tangage

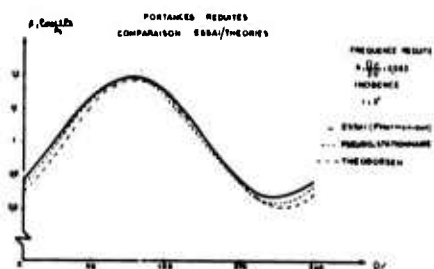


Fig.27

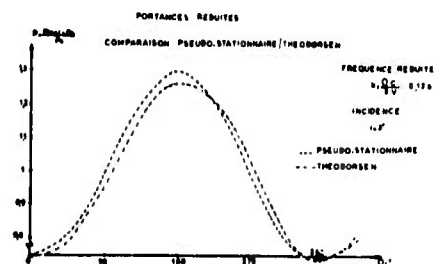


Fig.28

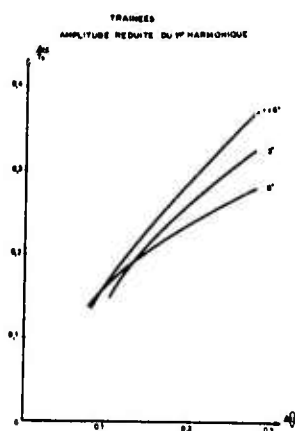


Fig.29

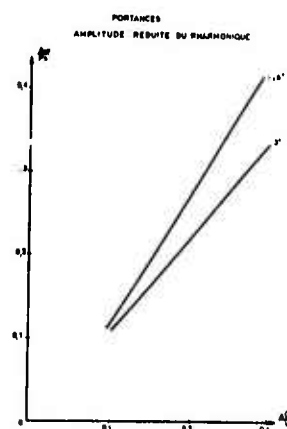


Fig.30

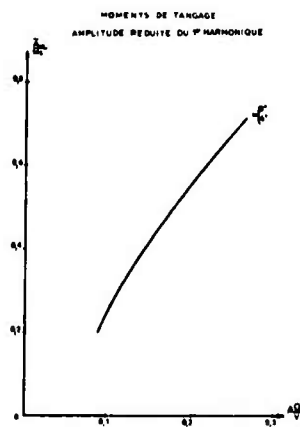


Fig.31

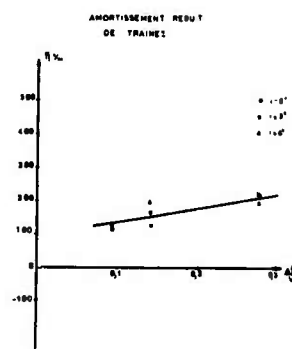


Fig.32

by

Charles E. Hammond**
Langley Directorate
U.S. Army Air Mobility R&D Laboratory
NASA Langley Research Center
Hampton, Virginia

and

G. Alvin Pierce†
Georgia Institute of Technology
Atlanta, Georgia

SUMMARY

An aerodynamic theory is presented which allows the determination of the unsteady aerodynamic loading on a reference section of a helicopter rotor blade in axial or hovering flight under compressible flow conditions. The aerodynamics of the two-dimensional flow model are formulated using a kernel function approach. By introducing the acceleration potential the governing integral equation for the flow and its attendant downwash boundary condition are developed and solved numerically using a pressure mode assumption and a collocation technique. The compressible aerodynamic theory thus developed is compared analytically with two other existing theories, one incompressible and one compressible, and is shown to agree with these theories provided that the appropriate limit is taken so that the flow models agree. The ratio of blade oscillatory frequency to rotor rotational frequency is shown to be the correlation parameter between the two flow models. Differences in the flow models used are shown numerically to cause significant differences in the aerodynamic coefficients for small values of this frequency ratio, but for values of this parameter near unity the aerodynamic coefficients from the three theories are in good agreement. For the case of zero phasing of all rotor blades, two degree of freedom flutter speeds obtained using the two compressible aerodynamic theories exhibit the same order of differences as the aerodynamic coefficients. Incompressible flutter speeds show good agreement.

NOTATION

A_i	pressure series coefficients
a_∞	free stream speed of sound
a	nondimensional location of the reference airfoil elastic axis relative to midchord, measured positive aft
b	semichord length of reference airfoil section
D_n, D_{nq}	distances by which wake airfoils lead the reference airfoil, defined by Equations (33)
$H_0^{(2)}, H_1^{(2)}$	Hankel functions of second kind and zeroth and first order, respectively
h	inflow ratio, nondimensional, $h = h'/b$
h'	vertical spacing between adjacent wake layers, $h' = 2\pi u/q\Omega$
h_{ab}	plunging displacement of elastic axis, positive down
h_c/h	plunge of reference airfoil measured at quarter chord, positive down
i	unit of imaginaries, $i = (-1)^{1/2}$
Im	imaginary part of a complex quantity
K	kernel function of the downwash integral equation, Equation (17)
k	reduced frequency, $k = b\omega/U$
L	aerodynamic lift, positive down
l_h, l_a	aerodynamic lift coefficients due to plunge and pitch, respectively, Equations (32)

* This work was supported by the U.S. Army Research Office-Durham under Contract No. DAHCO4-68-C-0004.

** Aero-Space Technologist.

† Associate Professor.

$\bar{l}_z, \bar{l}_i, \bar{l}_\alpha, \bar{l}_\alpha$	aerodynamic lift coefficients used by Jones and Rao, ¹¹ Equations (35)
M	section Mach number, $M = \Omega r/a_\infty$
M_c/k	aerodynamic pitching moment about the quarter chord, positive nose up
m	frequency ratio, $m = \omega/\Omega$
m_h, m_α	aerodynamic moment coefficients due to plunge and pitch, respectively, Equations (32)
$\bar{m}_z, \bar{m}_i, \bar{m}_\alpha, \bar{m}_\alpha$	aerodynamic moment coefficients used by Jones and Rao, ¹¹ Equations (35)
n	rotor revolution index
p	local pressure
P_∞	free stream pressure
Δp_a	pressure differential across reference airfoil, Equation (9)
Q	total number of blades in rotor
q	blade index for multibladed rotor
Re	real part of complex quantity
r	radial distance of reference airfoil from center of rotation
r_α	nondimensional radius of gyration of the reference airfoil section about elastic axis
t	time variable
U	relative free stream velocity which the reference airfoil experiences, $U = \Omega r$
u	inflow velocity through rotor disk
w	downwash velocity at a general field point in the flow
w_a	downwash velocity at the reference airfoil surface, $w_a = \bar{w}_a e^{i\omega t}$
w', w'', w'''	parameters defined by Equations (6), (14), and (17), respectively
x, z	Cartesian coordinate system; x positive downstream, z positive up
x_α	nondimensional location of reference airfoil center of gravity relative to the elastic axis, measured positive aft
z_a	z-displacement of a point on the midsurface of the reference airfoil, $z_a = \bar{z}_a e^{i\omega t}$
α	angle of attack of reference airfoil, positive nose up
β	$(1 - M^2)^{1/2}$
θ	chordwise coordinate defined by Equation (27)
μ	mass ratio, blade section mass per unit span/ $\rho_\infty b^2$
μ_D	doublet strength/ \bar{U} , i.e., $\bar{U}\mu_D$ = doublet strength
ξ, ζ	doublet coordinates
ρ_∞	free stream density
ϕ	disturbance velocity potential
ψ	acceleration potential
ψ_D	doublet acceleration potential
ψ_q	phase angle by which the motions of the q^{th} blade leads the motions of the reference blade
$\bar{\psi}_s$	parameter defined by Equation (5)
Ω	rotational speed of rotor
ω	blade oscillatory frequency
ω_h	uncoupled natural frequency in bending
ω_α	uncoupled natural frequency in torsion

1. INTRODUCTION

Aeroelastic analyses are essential when designing a vehicle as dynamic as the helicopter. These analyses depend heavily on knowledge of the time-varying forces and moments acting on the aerodynamic surfaces. As fixed wing vehicles have progressed from low subsonic speeds through high subsonic speeds to supersonic speeds and even to hypersonic speeds in the case of missiles and research vehicles, appropriate unsteady aerodynamic theories have been developed to assist in predicting aeroelastic instabilities which might occur. Unfortunately, the state of the art in unsteady helicopter aerodynamics has not progressed as rapidly as that for unsteady fixed wing aerodynamics. This is due in part to the fact that the rotary wing, especially in the forward flight mode, is not as amenable to analysis as its fixed wing counterpart. In dealing with the unsteady flow fields associated with helicopter rotors, the analyses developed for fixed wings must be drastically modified or abandoned altogether as a result of the rotor blade being forced to pass in proximity to its wake on each revolution.

Many of the first attempts to analyze the unsteady rotor blade aerodynamic problem were based on the supposition that the rotor blade could be replaced by an equivalent fixed wing with an appropriate free stream velocity. The potentially important fact that the helicopter blade is forced to pass over its wake was neglected. It might be noted here that this same procedure is currently employed by some in attempting to ascertain the effect of compressibility on the aeroelastic instabilities of rotor blades.

The first significant unsteady approaches to the rotor blade aerodynamic problem which considered the rotor blade to be a separate entity from the fixed wing were made by Loewy,¹ Jones,² and Timman and van de Vooren.³ These investigators in similar but independent studies considered the flow to be incompressible and the rotor was assumed to be operating in axial flight or in a hovering condition. Further, it was assumed that the rotor inflow velocity was low compared to the rotational velocity. With these assumptions it was possible to reduce the complicated three-dimensional rotor flow field to a more manageable two-dimensional flow field. The resulting two-dimensional mathematical model included a reference airfoil together with a complete system of wakes shed by other blades in the rotor as well as the wake shed by the reference blade on previous revolutions. This system of wakes is the one thing which makes the helicopter aerodynamic analysis so much more complicated than the fixed wing aerodynamic problem. Whereas for the fixed wing the wake is assumed to lie in the same plane as the wing, the helicopter rotor wake is blown below the plane of the rotor by the inflow velocity. Determination of the blade loading depends on knowing the location of the wake. Using the two-dimensional approximation to the rotor flow field described above, Loewy¹ was able to show that the two-dimensional loading on the reference airfoil could be written in the same form as the loading on a two-dimensional fixed wing airfoil with the stipulation that Theodorsen's⁴ lift deficiency function be replaced by a modified lift deficiency function applicable to rotor aerodynamics.

In order to determine the importance of the rotor wake a comparison was made, Reference 5, between the flutter speed obtained for a two degree of freedom system using Loewy's¹ aerodynamics and the flutter speed for the same system using Theodorsen's⁴ fixed wing aerodynamics. The results of this study indicated that given the same structural dynamic conditions the flutter speed obtained using Loewy's aerodynamics was generally lower than the flutter speed obtained using Theodorsen's aerodynamics. The implications of this result are that the rotor wake which lies below the reference airfoil exerts a destabilizing influence on the two degree of freedom flutter condition and hence that the use of unsteady fixed wing aerodynamics in rotor blade flutter calculations will lead to unconservative results.

Numerous papers, References 6 - 8 are examples, have been published which deal with the problem of three-dimensional rotary wing aerodynamics. In all these papers the problem of specifying the location of the wake is stressed and the papers have at least one common feature - that of incompressible flow. However, as indicated by Paul⁹ some present-day helicopters operate with tip speeds in the high subsonic speed range. This suggests that compressibility effects should be included in any realistic analysis of helicopter rotor blade loads. Unlike the steady flow case, the transition from incompressible to compressible unsteady flow results cannot be accomplished by simple transformations such as the Prandtl-Glauert transformation. This difficulty follows from the result that in an incompressible fluid a disturbance is propagated at an infinite velocity and thus no time lag occurs between the initiation of a disturbance and its effect at some other point in the flow. However, in a compressible medium a definite time is required for a signal to reach a distant field point so that both a time lag and a change in magnitude result.

In this paper an unsteady aerodynamic theory for helicopter rotors which allows for the compressibility of the fluid medium is presented. The assumptions made by Loewy¹ are employed to reduce the aerodynamic problem to two dimensions. The approach used to obtain the oscillatory loading on a reference airfoil section of the rotor is essentially the same as that used in many fixed wing analyses. The acceleration potential is used in developing an integral relation between the downwash and pressure distribution on the reference airfoil. The integral equation thus obtained, which is the same as Possio's¹⁰ fixed wing integral equation with the addition of a correction term to account for the helicopter wake, is finally solved by collocation for the unknown pressure distribution.

Jones and Rao¹¹ have recently published a similar theory for the unsteady compressible aerodynamic loading on rotor blades. Their theory differs from that developed in the present paper in that a velocity potential approach was used in conjunction with the identical flow model used by Loewy.¹ One of the major conclusions reached in Reference 11 was that the helicopter wake had exactly the same effect on the unsteady aerodynamic blade loading in both compressible and incompressible flows. As will be shown later, this conclusion was a direct consequence of the flow model employed. The flow model used in the present study is a modified version of the two-dimensional model used by Loewy, and Jones and Rao; the modifications being necessary to accommodate the acceleration potential approach.

2. FLOW MODEL

Loewy¹ has given a rather complete discussion of the unsteady flow field associated with a helicopter rotor in hovering or axial flight. The basic flow picture consists of a reference blade and a wake which has been blown below the rotor disk by the inflow velocity through the disk. The customary assumption is that the wake forms a helical surface of vorticity which extends to infinity below the rotor.

By making certain assumptions Loewy was able to argue that the three-dimensional flow field could be reduced to a two-dimensional one. The basic assumption which led to this reduction is that under axial flight and low inflow conditions, only that vorticity which lies in a small azimuth angle on either side of the reference blade significantly affects the loading on that blade. The further assumption of the independence of each radial station allows the further reduction to two-dimensional flow.

The flow picture thus arrived at by Loewy is shown in Figure 1. Note that the flow consists of a reference airfoil section and its immediate trailing wake (both in the same horizontal plane) together with a system of horizontal wake layers lying at regularly spaced intervals below the reference section. These wake layers below the reference airfoil account for the wake which was shed by other blades in the rotor as well as that shed by the reference blade on previous revolutions. The spacing between the layers is determined by the inflow and rotational velocities. The flow model shown in Figure 1 is also the model used by Jones and Rao¹¹ in their compressible flow analysis.

In analyzing the flow model shown in Figure 1 both Loewy and Jones and Rao used a velocity potential approach. In the present paper, on the other hand, the acceleration potential approach which has proved fruitful in fixed wing compressible flow analyses is adopted as the basic method of attacking the problem. The use of the acceleration potential leads to difficulties, however, when one attempts to apply the method to the flow model shown in Figure 1.

In the velocity potential approach the elemental flow solutions from which the overall flow is to be developed must be distributed in the wake as well as on the airfoil itself in order to account for the velocity discontinuity which exists across the wake and across the airfoil. In contrast, the acceleration potential is associated with a pressure discontinuity and thus the elemental flows may be distributed on the airfoil only since no pressure discontinuity is allowed to exist in the wake. With the acceleration potential approach, therefore, it is necessary to introduce a device by which the layers of wake lying below the reference airfoil can be taken into account.

The mathematical model used in this paper is evolved using the following reasoning. Consider first a single bladed rotor and a reference blade section lying a radial distance r from the axis of rotation. As the blade traverses the azimuth it trails a wake which is blown below the blade by the inflow velocity. When the reference section has made one complete revolution it has traveled a distance of $2\pi r$. As the blade makes its second revolution it sees a wake which was shed on the first revolution and which has been displaced downward by the inflow velocity. This wake layer can be thought of as being shed by an airfoil identical to the reference airfoil and which is flying under the reference airfoil and leading it by a distance of $2\pi r$. On the third revolution the reference airfoil sees two layers of wake; the lowermost layer being shed on the first revolution and the upper layer shed on the second revolution. The reference airfoil has now traveled a distance of $4\pi r$ since the wake was shed on the first revolution and a distance of $2\pi r$ since the wake was shed on the second revolution. To account for these wake layers, two airfoils are placed below the reference airfoil; the lowermost one leading the reference airfoil by a distance of $4\pi r$ and the upper one leading the reference airfoil by a distance of $2\pi r$. The vertical spacing of the individual layers is governed by the inflow and rotational velocities and is the same as for Loewy's model in Figure 1. By continuing the above process the entire wake can be represented by a semi-infinite cascade of airfoils regularly spaced below the reference airfoil and leading it by integer multiples of $2\pi r$.

The argument for a multibladed rotor is precisely the same as for a single bladed rotor. The passage of blades other than the reference blade is accounted for by airfoils below the reference airfoil and interspersed between the "wake airfoils" representing previous passages of the reference airfoil. The resulting two-dimensional flow model which is used in the mathematical development is shown in Figure 2.

3. MATHEMATICAL FORMULATION

With the mathematical flow model thus established the problem remains to determine the nonstationary lift and moment on the reference airfoil when it is permitted to oscillate with simple harmonic motion as it moves through a compressible medium. In the following development classical small disturbance assumptions are made so that the governing differential equation for the flow may be taken as the linearized acceleration potential equation

$$\frac{\partial^2 \psi}{\partial x^2} + \frac{\partial^2 \psi}{\partial z^2} - \frac{1}{a_\infty^2} \left[\frac{\partial^2 \psi}{\partial t^2} + 2U \frac{\partial^2 \psi}{\partial t \partial x} + U^2 \frac{\partial^2 \psi}{\partial x^2} \right] = 0 \quad (1)$$

The acceleration potential ψ is related to the disturbance velocity potential ϕ by

$$\psi = \frac{\partial \phi}{\partial t} + U \frac{\partial \phi}{\partial x} \quad (2)$$

and to the pressure at any point in the flow through the equation

$$p - p_\infty = -\rho_\infty \psi \quad (3)$$

The pressure on the reference airfoil is obtained in a manner typical of most linearized aerodynamic analyses. An elementary flow solution is first found for the governing differential Equation (1). The total flow solution is then found by superimposing the elemental flow solutions and satisfying the two boundary conditions for potential flows: (1) All disturbances must vanish at field points far removed from the body, and (2) the flow at the body must follow the body surface.

Since the flow model shown in Figure 2 is simply a semi-infinite cascade of fixed wing airfoils an integral equation will first be developed which relates the downwash at any point (x, z) in the flow to the pressure difference across a single airfoil. The rotary wing effects are then included by determining the downwash at the reference airfoil due to all the "wake airfoils" of Figure 2. In this development the elemental flow solution to Equation (1) is taken as the pulsating line doublet. It is shown in Reference 12 that the acceleration potential for such a line doublet which is pulsating harmonically with a frequency ω and a strength $U_{\mu D}$ is given by

$$\psi_D = U_{\mu D} \frac{\partial \bar{\psi}_s}{\partial z} \quad (4)$$

where

$$\bar{\psi}_s = \frac{1}{4\beta} e^{ikM^2(x-t)/\beta^2 b} H_0^{(2)}(w') e^{i\omega t} \quad (5)$$

$$w' = \frac{kM}{\beta^2} \left[\left(\frac{x-t}{b} \right)^2 + \beta^2 \left(\frac{z-t}{b} \right)^2 \right]^{1/2} \quad (6)$$

Note that the elemental solution satisfies the first boundary condition that all disturbances vanish at points far removed from the body. Therefore, any superposition of these elemental solutions will also satisfy this boundary condition.

These pulsating doublets are next distributed over the chord of an airfoil which is displaced a distance ξ in the z -direction from the origin of the coordinate system and whose chord extends from $x = -b$ to $x = +b$. The acceleration potential for this distribution of doublets becomes

$$\psi = \int_{-b}^b U_{\mu D}(\xi) \frac{\partial}{\partial z} \bar{\psi}_s d\xi \quad (7)$$

It can be shown, using Equation (3), that the doublet strength is related to the pressure difference across the airfoil by

$$\Delta \bar{\phi}_a(x) = -\rho_\infty U_{\mu D}(x) \quad (8)$$

where

$$\Delta \phi_a(x) = p_U - p_L = \Delta \bar{\phi}_a(x) e^{i\omega t} \quad (9)$$

The acceleration potential thus becomes

$$\psi = -\frac{ie^{i\omega t}}{4\rho_\infty \beta} \int_{-b}^b \Delta \bar{\phi}_a(\xi) e^{ikM^2(x-\xi)/\beta^2 b} \frac{\partial}{\partial z} H_0^{(2)}(w') d\xi \quad (10)$$

Now in order to be able to satisfy the second boundary condition on the flow the downwash w at the airfoil must be known. Since the doublets were assumed to be pulsating harmonically with time, the acceleration potential and hence the velocity potential will vary harmonically with time. Thus

$$\begin{aligned} \psi &= \bar{\psi} e^{i\omega t} \\ \phi &= \bar{\phi} e^{i\omega t} \end{aligned}$$

Introducing this harmonic variation into Equation (2)

$$\bar{\psi} = i\omega \bar{\phi} + U \frac{\partial \bar{\phi}}{\partial x} \quad (11)$$

This last equation can be integrated to give

$$\bar{\phi}(x, z) = \frac{1}{U} \int_{-\infty}^x \bar{\psi}(\xi, z) e^{-i\omega(x-\xi)/U} d\xi \quad (12)$$

The downwash is expressed in terms of the velocity potential by

$$v = \frac{\partial \phi}{\partial z}$$

so that in terms of the acceleration potential

$$v(x, z; t) = \frac{e^{i\omega t}}{U} \int_{-\infty}^x \frac{\partial}{\partial z} \bar{\psi}(\xi', z) e^{-i\omega(x-\xi')/U} d\xi' \quad (13)$$

Introducing Equation (10) into Equation (13)

$$v(x, z; t) = - \frac{1e^{i\omega t}}{4\rho_\infty U \beta} \int_{-\infty}^x e^{-i\omega(x-\xi')/U} \int_{-b}^b \Delta \bar{\psi}_a(\xi) \cdot e^{ikM^2(\xi'-\xi)/\beta^2 b} \frac{\partial^2}{\partial z^2} H_0^{(2)}(w'') d\xi' d\xi \quad (14)$$

where

$$w'' = \frac{kM}{\beta^2} \left[\left(\frac{\xi' - \xi}{b} \right)^2 + \beta^2 \left(\frac{z - \xi}{b} \right)^2 \right]^{1/2}$$

The order of integration in Equation (14) can be reversed to give the more familiar form of the equation, namely

$$v(x, z; t) = - \frac{1e^{i\omega t}}{4\rho_\infty U \beta} \int_{-b}^b \Delta \bar{\psi}_a(\xi) e^{-ik(x-\xi)/b} \int_{-\infty}^x e^{ik(\xi'-\xi)/\beta^2 b} \cdot \frac{\partial^2}{\partial z^2} H_0^{(2)}(w'') d\xi' d\xi \quad (15)$$

Manipulation of the interior integral of Equation (15) leads to the kernel for two-dimensional compressible unsteady flow. The resulting downwash equation is

$$v(x, z; t) = - \frac{\omega}{\rho_\infty U^2} e^{i\omega t} \int_{-b}^b \Delta \bar{\psi}_a(\xi) K \left[M, \frac{k(x-\xi)}{b}, \frac{k(z-\xi)}{b} \right] d\xi \quad (16)$$

where the kernel of the equation is given by

$$K \left[M, \frac{k(x-\xi)}{b}, \frac{k(z-\xi)}{b} \right] = \frac{ikM^2}{4\beta^3 w'} \left(\frac{x-\xi}{b} \right) H_1^{(2)}(w') e^{ikM^2(x-\xi)/\beta^2 b} - \frac{1}{4\beta} H_0^{(2)}(w') e^{ikM^2(x-\xi)/\beta^2 b} + \frac{1}{4\beta} \left(\frac{\omega}{U} \right) e^{-ik(x-\xi)/b} \int_{-\infty}^{x-\xi} H_0^{(2)}(w''') e^{ik\xi'/\beta^2 b} d\xi' \quad (17)$$

where

$$w''' = \frac{kM}{\beta^2} \left[\left(\frac{\xi'}{b} \right)^2 + \beta^2 \left(\frac{z-\xi}{b} \right)^2 \right]^{1/2}$$

For complete details of the reduction of the inner integral of Equation (15) to the kernel of Equation (16), see Reference 12.

If $\xi = 0$ is substituted into Equation (16) and the limit is taken as z approaches zero, then the equation becomes Possio's¹⁰ equation for a fixed wing airfoil oscillating in a compressible stream. The kernel in this case becomes

$$K \left[M, \frac{k(x-\xi)}{b}, 0 \right] = \frac{1}{4\beta} \left\{ e^{ikM^2(x-\xi)/\beta^2 b} \left[4M \frac{(x-\xi)}{|x-\xi|} H_1^{(2)} \left(\frac{kM|x-\xi|}{\beta^2 b} \right) - H_0^{(2)} \left(\frac{kM|x-\xi|}{\beta^2 b} \right) \right] + \frac{1}{\beta^2} e^{-ik(x-\xi)/b} \int_{-\infty}^{k(x-\xi)/\beta^2 b} H_0^{(2)}(Mu) e^{iu} du \right\} \quad (18)$$

An excellent discussion of the development of this equation has also been given by Watkins, et al.¹³

Equation (16) may now be used to determine the downwash at the reference airfoil in terms of the pressure distribution on the reference airfoil. This is accomplished by recognizing that Equation (16) is applicable for each airfoil in Figure 2 if a simple transformation of coordinates is made in the case of the "wake airfoils." The limit $z \rightarrow 0$ is then taken to obtain the downwash at the reference airfoil. If it is assumed that the pressure distribution on the q th blade has the same magnitude as that on the reference blade but leads it in time by a phase angle ψ_q , the downwash on the reference airfoil may be written as

$$\begin{aligned}
\bar{v}_a(x) = & -\frac{\omega}{\rho_a U^2} \left\{ \int_{-b}^b \Delta \bar{p}_a(\xi) K \left[M, \frac{k(x-\xi)}{b}, 0 \right] d\xi \right. \\
& + \sum_{n=0}^{\infty} \sum_{q=1}^{Q-1} e^{i\psi_q} \int_{-b}^b \Delta \bar{p}_a(\xi) K \left[M, 2\pi(nQ+q) \frac{m}{q} + \frac{k(x-\xi)}{b}, (nQ+q)kh \right] d\xi \\
& \left. + \sum_{n=1}^{\infty} \int_{-b}^b \Delta \bar{p}_a(\xi) K \left[M, 2n\pi m + \frac{k(x-\xi)}{b}, nQkh \right] d\xi \right\} \quad (19)
\end{aligned}$$

The first integral in Equation (19) is the integral derived by Possio¹⁰ for the two-dimensional fixed wing. The double sum represents the downwash at the reference airfoil caused by previous passages of blades in the rotor other than the reference blade. Finally, the single sum represents the downwash at the reference airfoil due to previous passages of the reference airfoil.

If all blades are assumed to oscillate in-phase, as is the case for "collective" type disturbances, then $\psi_q = 0$ and Equation (19) reduces to

$$\begin{aligned}
\bar{v}_a(x) = & -\frac{\omega}{\rho_a U^2} \left\{ \int_{-b}^b \Delta \bar{p}_a(\xi) K \left[M, \frac{k(x-\xi)}{b}, 0 \right] d\xi \right. \\
& \left. + \sum_{n=1}^{\infty} \int_{-b}^b \Delta \bar{p}_a(\xi) K \left[M, 2n\pi \frac{m}{Q} + \frac{k(x-\xi)}{b}, nkh \right] d\xi \right\} \quad (20)
\end{aligned}$$

It may be noted that this last equation is exactly the same as the downwash expression one would obtain for a single bladed rotor with a frequency ratio m/Q and an inflow ratio h . Thus, with the assumption that all the blades are oscillating in-phase the aerodynamic development for a multibladed rotor can be reduced to the consideration of an equivalent single bladed rotor with

$$\left. \begin{aligned} m_{eq} &= m/Q \\ h_{eq} &= h \end{aligned} \right\} \quad (21)$$

Since this reduction to an equivalent single bladed rotor is possible, all numerical results presented below are for a single bladed rotor.

The downwash at the reference airfoil is specified by the motion of the airfoil. If the displacement of the airfoil is given by z_a then the downwash is given by

$$v_a(x;t) = \frac{\partial z_a}{\partial t} + U \frac{\partial z_a}{\partial x} \quad \text{for } -b \leq x \leq b \quad (22)$$

Assuming simple harmonic motion for the airfoil

$$z_a(x;t) = \bar{z}_a(x) e^{i\omega t} \quad (23)$$

the downwash becomes

$$\bar{v}_a(x) = i\omega \bar{z}_a + U \frac{\partial \bar{z}_a}{\partial x} \quad (24)$$

For an airfoil which is free to pitch about the quarter-chord point and plunge as shown in Figure 3 the displacement of the airfoil may be written as

$$z_a(x;t) = -h_c/l_c - \left(x + \frac{b}{2}\right)\alpha \quad (25)$$

And for simple harmonic motion

$$\begin{aligned} h_c/l_c &= \bar{h} e^{i\omega t} \\ \alpha &= \bar{\alpha} e^{i\omega t} \end{aligned}$$

where \bar{h} and $\bar{\alpha}$ are complex quantities. The downwash thus becomes

$$\frac{\bar{v}_a(x)}{U} = -ik \left(\frac{\bar{h}}{b} \right) - \left[1 + ik \left(\frac{x}{b} + \frac{1}{2} \right) \right] \bar{\alpha} \quad (26)$$

In attempting to solve Equation (20) one notices immediately that the unknown in the equation $\Delta \bar{p}_a(x)$ is contained within the integral and the known quantity $\bar{v}_a(x)$ is on the left-hand side. Since no inversion formula is known for this equation a collocation technique is used. It is first assumed that the pressure distribution may be written in the well-known form

$$\left. \begin{aligned} \Delta \bar{p}_a(\theta) &= A_0 \cot \frac{\theta}{2} + \sum_{j=1}^{\infty} A_j \sin j\theta \\ \cos \theta &= -\frac{x}{b} \end{aligned} \right\} \quad (27)$$

The form of this series is dictated by two considerations: (1) The linearizing assumptions in subsonic small disturbance theory are known to lead to a square root singularity in the pressure distribution at the leading edge, and (2) the Kutta condition must be satisfied at the trailing edge.

With this pressure mode assumption the integral Equation (20) may be solved subject to the boundary condition Equation (26) to yield the unknown coefficients in the pressure series. This is accomplished by truncating the series in Equation (27) after a finite number of terms, substituting the finite series in Equation (20), and performing the necessary integrations. By choosing an equal number of points at which the downwash boundary condition is to be satisfied, a system of algebraic equations is generated which can be solved for the unknown coefficients.

Once the pressure distribution is determined the unsteady lift and moment may be calculated. The lift (positive down) is given by

$$L = \int_{-b}^b (p_U - p_L) dx \quad (28)$$

and the pitching moment about the quarter-chord point (positive nose up) by

$$M_{c/4} = \int_{-b}^b (p_U - p_L) \left(x + \frac{b}{2}\right) dx \quad (29)$$

Since the pressure is assumed to be harmonic in time the lift and moment must also vary harmonically as

$$\begin{aligned} L &= \bar{L} e^{i\omega t} \\ M_{c/4} &= \bar{M}_{c/4} e^{i\omega t} \end{aligned}$$

so that

$$\left. \begin{aligned} \bar{L} &= \int_{-b}^b \Delta \bar{p}_a(x) dx \\ \bar{M}_{c/4} &= \int_{-b}^b \Delta \bar{p}_a(x) \left(x + \frac{b}{2}\right) dx \end{aligned} \right\} \quad (30)$$

Note here that \bar{L} and $\bar{M}_{c/4}$ are complex quantities. Substituting Equations (27) into Equations (30) gives the lift and moment in terms of the pressure series coefficients

$$\left. \begin{aligned} \bar{L} &= \pi b \left(A_0 + \frac{1}{2} A_1 \right) \\ \bar{M}_{c/4} &= \frac{1}{4} \pi b^2 (A_1 - A_2) \end{aligned} \right\} \quad (31)$$

Although the lift and moment depend only on the first three coefficients of the pressure series, this does not mean that only the first three terms of the pressure series need be considered. The values of the first three coefficients of the series will change as more and more collocation points and terms in the series are used and the boundary condition is satisfied more exactly.

For use in a flutter analysis these quantities are written in the usual form employing aerodynamic coefficients, namely

$$\left. \begin{aligned} L &= \pi \rho_{\infty} U^2 b \left[l_h \left(\frac{h}{b} \right)_{c/4} + l_{\alpha} \alpha \right] \\ M_{c/4} &= \pi \rho_{\infty} U^2 b^2 \left[m_h \left(\frac{h}{b} \right)_{c/4} + m_{\alpha} \alpha \right] \end{aligned} \right\} \quad (32)$$

where the aerodynamic coefficients l_h , l_{α} , m_h , and m_{α} are complex quantities that account for the phase lag between the forces and motions.

4. ANALYTICAL COMPARISONS

Before presenting results of the numerical calculations it is of interest to compare the downwash equation developed in the previous section with the downwash equation obtained by Loewy¹ and Jones and Rao¹¹.

This comparison is facilitated by noting that the distances by which the wake airfoils lead the reference airfoil can be written as

$$\left. \begin{aligned} D_{nq} &= 2\pi r \left(n + \frac{q}{Q} \right) \\ D_n &= 2\pi r \end{aligned} \right\} \quad (33)$$

where D_{nq} corresponds to wake airfoils representing previous passages of blades other than the reference blade and D_n corresponds to airfoils representing previous passages of the reference blade. Observe from Figure 2 that if all the wake airfoils are forced to lead the reference airfoil by an infinite distance then the flow model of Figure 2 would be exactly the flow model used by Loewy and Jones and Rao as shown in Figure 1. The analytical comparison of the three theories is accomplished by introducing Equations (33) into the second and third terms of Equation (19) by replacing the appropriate terms in the respective kernels. For the limits $D_{nq} \rightarrow \infty$ and $D_n \rightarrow \infty$ the two flow models agree. It is shown in Reference 12 that this limiting procedure does in fact reduce Equation (19) to the downwash equations obtained by Loewy and Jones and Rao. Thus if the indicated limit of the flow model used in the present paper is taken, then the present aerodynamic theory reduces exactly to the earlier theories of Loewy and Jones and Rao.

This limit taking process in effect causes the wake airfoils to lead the reference airfoil by an infinite distance and presents no real problem in the case of incompressible flow. However, when the flow is considered to be compressible an interesting result occurs. Whereas a disturbance is propagated instantaneously but is attenuated by distance in an incompressible fluid, the speed of propagation is finite in a compressible medium so that both a time lag and a decay in the magnitude of the disturbance result as the disturbance is transmitted through the fluid. When the wake airfoils are at infinity this means that the perturbations in the flow caused by each wake airfoil must travel an infinite distance before reaching the reference airfoil. This in effect means that as far as the reference airfoil is concerned the wakes which are trailed by the wake airfoils are the same as the ones which would occur if the flow were incompressible.

This conclusion of an incompressible wake is one of the major results of Reference 11. That is, Jones and Rao found that the infinite number of wake layers below the reference airfoil as shown in Figure 1 had the same influence on the downwash at the reference airfoil in compressible flow as in incompressible flow.

An incompressible wake is not possible when the flow model of Figure 3 is used. The dependence of the wake term on Mach number is shown explicitly by Equations (17) and (19).

5. DISCUSSION OF RESULTS

It was established in the previous section that in the limit as the wake airfoils of Figure 2 lead the reference airfoil by an infinite distance the downwash equation of this paper agrees with those of Loewy¹ and Jones and Rao.¹¹ This limiting process causes the flow model of Figure 2 to agree with that of Figure 1. For realistic values of the aerodynamic parameters, however, the two flow models cannot be expected to be identical. For this reason a numerical comparison of the three theories is presented in this section.

For the equivalent single bladed rotor the n^{th} wake airfoil of Figure 2 leads the reference airfoil by a distance given by the second of Equations (33). Introducing the reduced frequency and frequency ratio parameters this equation may be written as

$$D_n = 2\pi \frac{mb}{k} \quad (34)$$

From Equation (34) it can be seen that if the frequency ratio m is increased while all the other aerodynamic parameters are held constant, the effect of increasing the distance by which the wake airfoils lead the reference airfoil can be determined. This in turn allows one to determine quantitatively the effect of the two flow models on the aerodynamic coefficients.

This variation of the frequency ratio was made and the results are presented in Figures 4(a) - (d). It should be noted that for ease of comparison the aerodynamic coefficients are plotted in the notation of Reference 11. These coefficients are related to those of Equations (32) by

$$\left. \begin{aligned} \bar{l}_z &= -\text{Re}(l_h) & \bar{m}_z &= \text{Re}(m_h) \\ \bar{l}_z &= -\frac{1}{k} \text{Im}(l_h) & \bar{m}_z &= \frac{1}{k} \text{Im}(m_h) \\ \bar{l}_\alpha &= -\text{Re}(l_\alpha) & \bar{m}_\alpha &= \text{Re}(m_\alpha) \\ \bar{l}_\alpha &= -\frac{1}{k} \text{Im}(l_\alpha) & \bar{m}_\alpha &= \frac{1}{k} \text{Im}(m_\alpha) \end{aligned} \right\} \quad (35)$$

In performing the numerical calculations it was found that approximately 40 terms of the wake series were necessary in most cases to achieve satisfactory convergence of the series. The number of collocation points used were varied from 3 to 10 and it was found that in all cases 3 collocation points were sufficient. It should be noted that the number of collocation points used is independent of the number of terms taken in the wake series.

As can be seen from Figures 4(a) - (d) the agreement between the aerodynamic theories does indeed improve as the frequency ratio m is increased. It is of interest to point out that the aerodynamic theories of Loewy¹ and Jones and Rao¹¹ are cyclic in frequency ratio whereas the theory presented in this

paper is not. That is, for $1 \leq m \leq 2$ the Loewy and Jones and Rao curves would remain exactly as shown in Figures 4(a) - (d) but the curves from the theory presented in this paper would change and should be in better agreement with the other two theories. The significant point about Figures 4(a) - (d) is that they show the results of the two possible mathematical representations of the two-dimensional flow over helicopter blades. As shown in the figures, the differences can be considerable at low values of frequency ratio, but tend to diminish as frequency ratio is increased.

In order to more fully evaluate the differences in the aerodynamic coefficients as shown in Figures 4(a) - (d), a two degree of freedom flutter analysis was conducted. The flutter model is shown in Figure 5. The equations of motion for this system are well known and will not be presented here (see Reference 14 for a derivation). The nondimensional structural parameters which enter the flutter problem are given below along with the values chosen as typical of current helicopter blade designs:

$$\mu = \text{mass ratio} = 80.0$$

$$r_\alpha = \text{radius of gyration} = 0.5$$

$$\omega_h/\omega_\alpha = \text{bending-torsion frequency ratio} = 0.5$$

$$a = \text{pitch axis location} = -0.4$$

$$x_\alpha = \text{c.g. location} = 0.10$$

The flutter speeds obtained from the model shown in Figure 5 using the three aerodynamic theories discussed earlier are plotted in Figure 6 as a function of frequency ratio for an inflow ratio, $h = 2.0$, and Mach numbers of 0.0, 0.6, and 0.8. Note that the flutter trend with Mach number is generally the same as in the fixed wing case, i.e., as Mach number is increased the flutter speed index is decreased. Also apparent is a considerable difference in the flutter results obtained with the two compressible aerodynamic theories discussed, i.e., Jones and Rao¹¹ and the present theory, for frequency ratios less than approximately 0.5. These differences might have been expected from the differences seen in the aerodynamic coefficients. The $M = 0.0$, or incompressible results, on the other hand, are in better agreement. This result indicates that the finite proximity of the wake airfoils in the present theory does not significantly alter the incompressible results but is important in representing the compressible features of the wake.

As a final result, White¹⁵ has recently applied the three aerodynamic theories discussed here in a strip theory fashion to a hovering rotor. Figure 7 taken from Pierce and White's¹⁶ paper presents one flutter point thus obtained compared to an experimental point obtained by Brooks and Baker.¹⁷ The unorthodox behavior of the V-g plot is discussed in detail in References 15 and 16 and will not be discussed further here. Of interest, however, is the close agreement of the flutter point obtained with the aerodynamic theory presented here and the one obtained using Jones and Rao's theory. Note also the close agreement with the experimental point. Another point worth noting with regard to Figure 7 is that the frequency ratio m at flutter was approximately 2.3. At a frequency ratio this high the aerodynamic coefficients of the present study should correspond closely to those calculated by the theory of Reference 11 and thus one would expect the flutter points calculated using the two aerodynamic theories to be in good agreement.

6. CONCLUSIONS

An aerodynamic theory has been presented which allows the determination of the unsteady aerodynamic loading on a reference section of a helicopter rotor blade in axial or hovering flight in subsonic compressible flow. This theory has been compared with similar theories presented by Loewy¹ and Jones and Rao¹¹ and the following conclusions obtained:

1. In the limit as the flow model used in the present paper approaches the flow model used in References 1 and 11, the aerodynamic theory presented here coincides exactly with those theories.
2. The wake obtained in the present theory accounts for compressibility. The incompressible flow wake obtained in Reference 11 was shown to be a direct consequence of the flow model employed.
3. The differences in the flow model used in the present theory and that used in References 1 and 11 causes significant differences in the aerodynamic coefficients calculated for small values of the ratio of blade oscillation frequency to rotational frequency.
4. From the results of an example flutter analysis wherein the same phasing of all rotor blades was assumed, it was concluded that these differences in the aerodynamic coefficients are more important under compressible flow conditions. For zero Mach number the flutter results compared favorably, whereas for higher subsonic Mach numbers the flutter speeds were significantly different when using the present aerodynamic theory as compared to that of Reference 11.
5. The one flutter example cited from Reference 16 indicates that both the theory presented here and that presented in Reference 11 produce flutter results which compare favorably with experimental results when used in a strip theory fashion. The parameters in the case cited were in the range where the two aerodynamic theories are in close agreement.

From the results of this paper one is led to conclude that there are a variety of ways of approximating the flow over rotor blades in hover or axial flight. This paper has sought to point out some of the differences in representations and the consequences of these differences. These different mathematical representations of the helicopter flow field serve as additional evidence of the marked difference between the fluid flow over helicopter blades and that over conventional fixed wings.

REFERENCES

1. Loewy, R. G. A Two Dimensional Approximation to the Unsteady Aerodynamics of Rotary Wings. Journal of the Aerospace Sciences, Vol. 24, No. 2, pp. 81-92, 144 (February 1957).
2. Jones, J. P. The Influence of the Wake on the Flutter and Vibration of Rotor Blades. Aeronautical Quarterly, Vo. IX, pp. 252-286 (1958).
3. Timman, R.
van de Vooren, A. I. Flutter of a Helicopter Rotor Rotating in Its Own Wake. Journal of the Aerospace Sciences, Vol. 24, No. 9, pp. 694-702 (September 1957).
4. Theodorsen, T. General Theory of Aerodynamic Instability and the Mechanism of Flutter. NACA Report 496 (1949).
5. Hammond, C. E. A Parametric Study of Helicopter Rotor Blade Flutter Under Low Inflow Conditions, Using Incompressible Aerodynamics. Georgia Institute of Technology, School of Aerospace Engineering, Student Special Problem (June 1968).
6. Miller, R. H. Theoretical Determination of Rotor Blade Harmonic Airloads. Massachusetts Institute of Technology, Aeroelastic and Structures Research Laboratory, TR 107-2, AD-619048 (August 1964).
7. Ichikawa, T. Linear Aerodynamic Theory of Rotor Blades. Journal of Aircraft, Vol. 4, No. 3, pp. 210-218 (May-June 1967).
8. Landgrebe, A. J. An Analytical Method for Predicting Rotor Wake Geometry. AIAA Paper No. 69-196, Presented at the AIAA/AHS VTOL Research, Design, and Operations Meeting, Georgia Institute of Technology, Atlanta, Georgia (February 17-19, 1969).
9. Paul, W. F. A Self-Excited Rotor Blade Oscillation at High Subsonic Mach Numbers. Journal of the American Helicopter Society, Vol. 14, No. 1, pp. 38-48 (January 1969).
10. Possio, C. L'Azione Aerodinamica sul Profilo Oscillante in un Fluido Compressibile a Velocità Iposonora. L'Aerotecnica, t. XVIII, fasc. 4 (April 1958). (Also available as British Ministry of Aircraft Production R.T.P. Translation 987.)
11. Jones, W. P.
Rao, B. M. Compressibility Effects on Oscillating Rotor Blades in Hovering Flight. AIAA Journal, Vol. 8, No. 2, pp. 321-329 (February 1970).
12. Hammond, C. E. Compressibility Effects in Helicopter Rotor Blade Flutter. Ph.D. Thesis, Georgia Institute of Technology, School of Aerospace Engineering Report GIT-AER-69-4, AD-706243 (December 1969).
13. Watkins, C. E.
Runyan, H. L.
Woolston, D. S. On the Kernel Function of the Integral Equation Relating the Lift and Downwash Distributions of Oscillating Finite Wings in Subsonic Flow. NACA Report 1234 (1955).
14. Bisplinghoff, R. L.
Ashley, H.
Halfman, R. L. Aeroelasticity, Addison-Wesley Publishing Company, Inc., Reading, Massachusetts (1955).
15. White, W. F., Jr. Effect of Compressibility on Three-Dimensional Helicopter Rotor Blade Flutter. Ph.D. Thesis, Georgia Institute of Technology (1972).
16. Pierce, G. A.
White, W. F., Jr. Unsteady Rotor Aerodynamics at Low Inflow and Its Effect on Flutter. Presented at 2nd AIAA Atmospheric Flight Mechanics Conference, Palo Alto, California (September 11-13, 1972).
17. Brooks, G. W.
Baker, J. E. An Experimental Investigation of the Effect of Various Parameters Including Tip Mach Number on the Flutter of Some Model Helicopter Rotor Blades. NACA TN 4005 (September 1958).

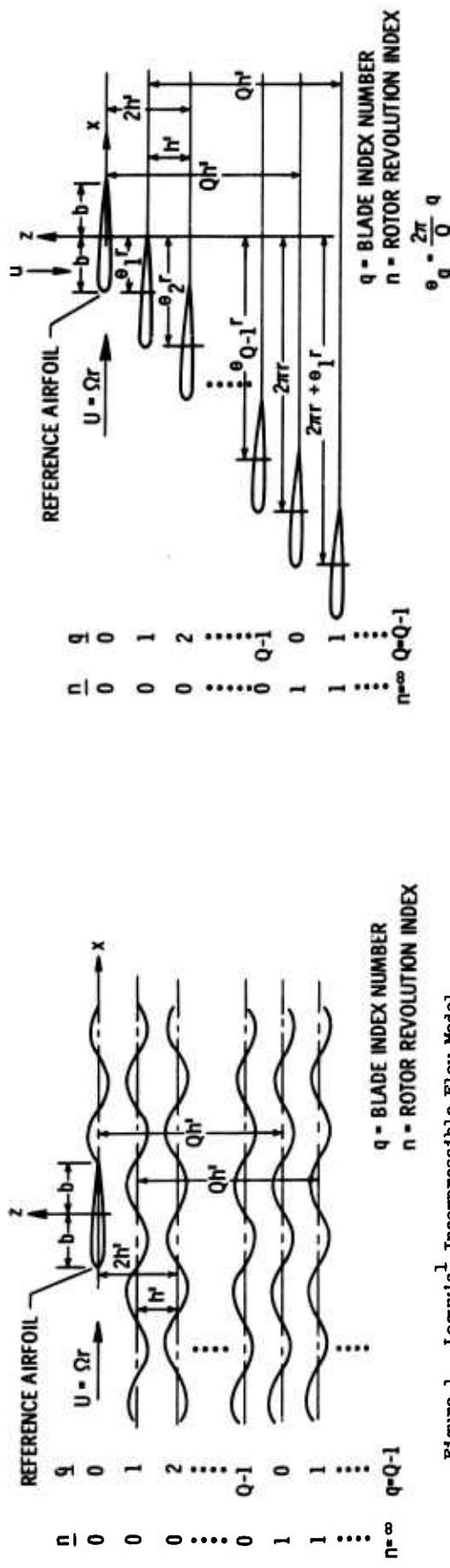


Figure 1. Loewy's¹ Incompressible Flow Model

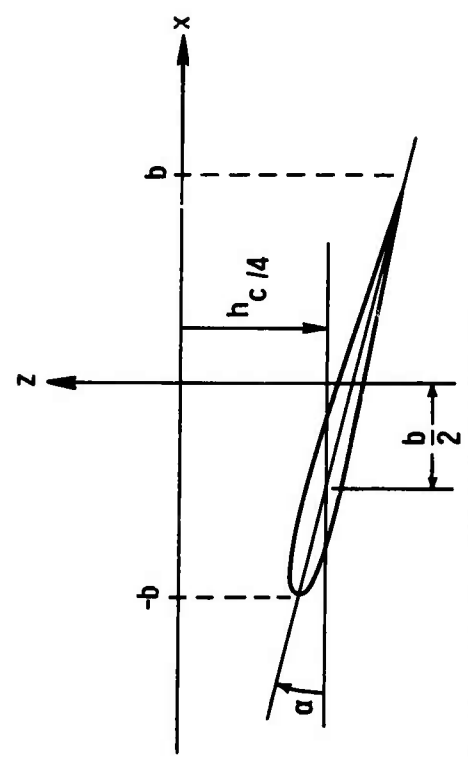


Figure 3. Coordinate System and Assumed Displacements of Reference Airfoil

Figure 2. Compressible Flow Aerodynamic Model for a Multibladed Rotor Showing Notation for Mathematical Analysis

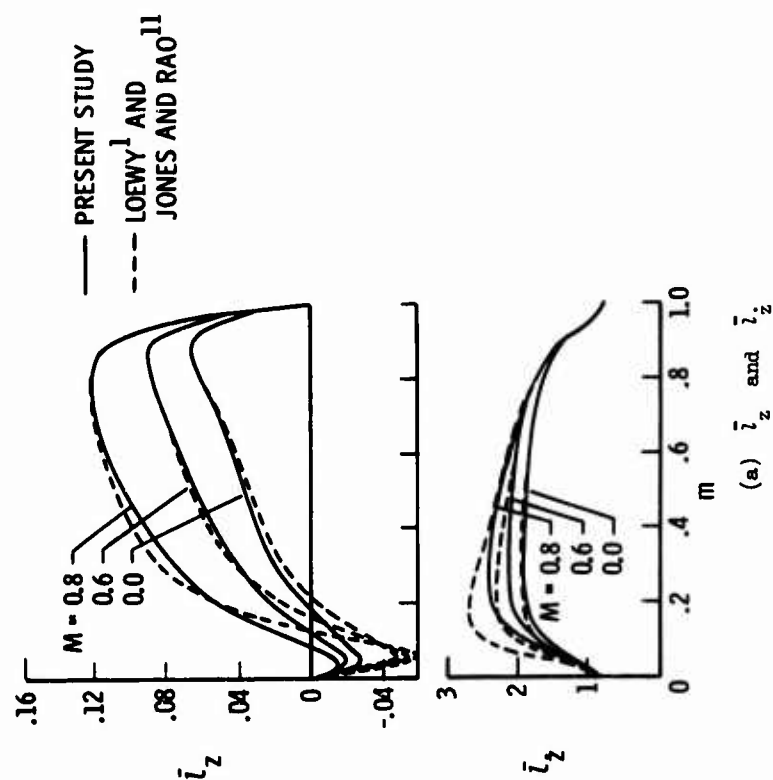
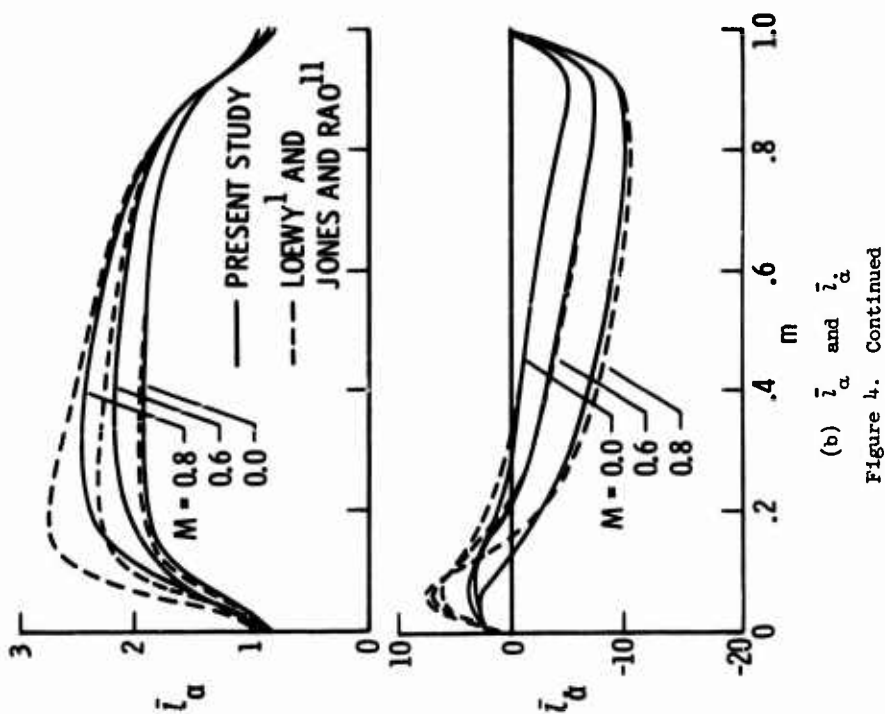


Figure 4. Variation of the Aerodynamic Coefficients with Frequency Ratio ($k = 0.10$, $h = 2.00$)

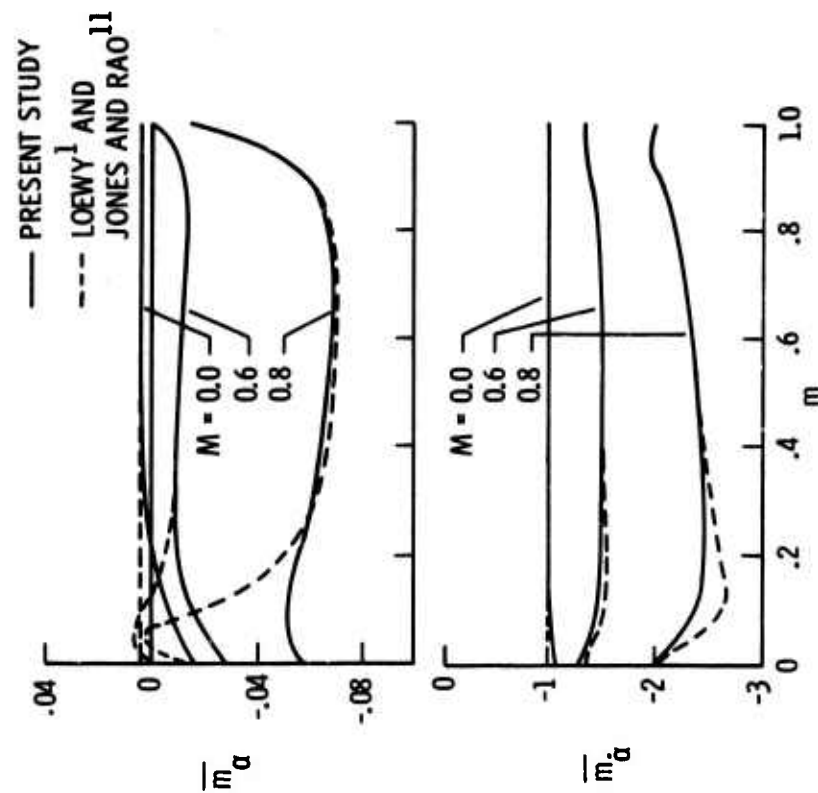
(c) \bar{m}_z and \bar{m}_z

Figure 4. Continued

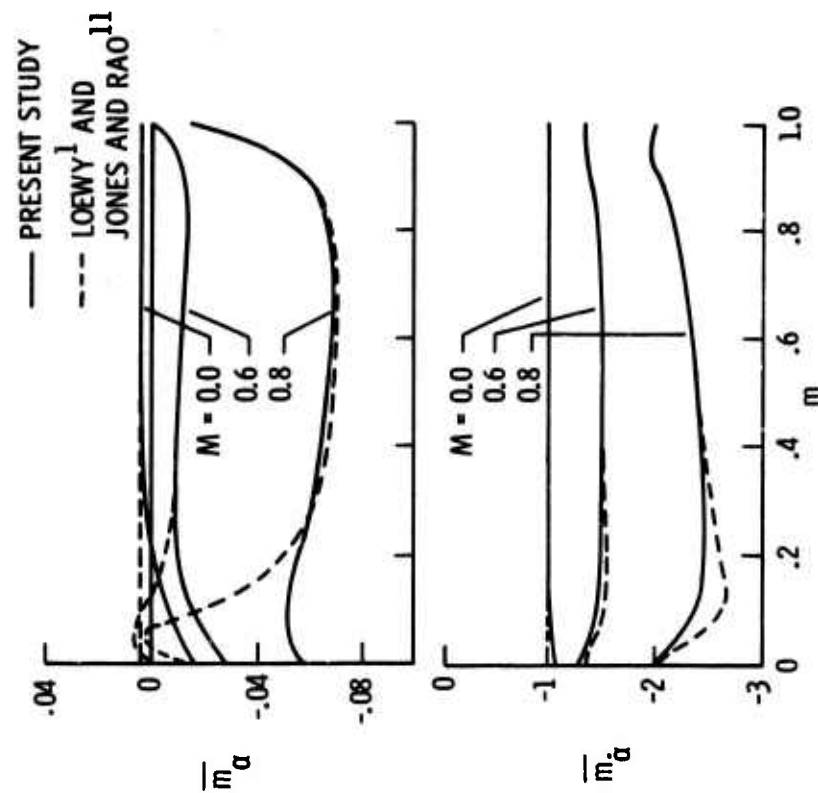
(d) \bar{m}_α and \bar{m}_α

Figure 4. Concluded

SOME ASPECTS OF THE DESIGN OF ROTOR-AIRFOIL SHAPES

by

G. Reichert and Dr. S.N. Wagner
Messerschmitt-Bölkow-Blohm GmbH,
Ottobrunn, Germany

SUMMARY

Analytical studies have shown that performance, stability and control of helicopters can be improved if some characteristics of rotor airfoils could be changed.

Starting from given airfoil shapes the characteristics of these airfoils are idealized by changing lift curve slope, maximum lift boundary and begin of drag divergence. The influences of these changes on the power required, the stability and control of hingeless rotor helicopters are studied. Furthermore, the desirable characteristics of an airfoil or several airfoils of a rotor are defined using these idealized characteristics and analysing common missions of a given helicopter. Similar studies of a larger field of missions and helicopters could lead to new areas of research and development to design advanced profile shapes of helicopters of the future. Several analytical tools for the design of airfoils are discussed.

Wind tunnel measurements up to transonic speeds of several airfoil shapes especially with modified leading and trailing edges show that certain improvements of airfoil characteristics are possible. Test results of rotors having usual and advanced airfoil shapes are included to indicate the progress in the behaviour of rotors with better airfoils.

NOTATIONS

a	local speed of sound	α	angle of attack, degrees
C	chord length	α_0	mean angle of attack, degrees
C_D	drag coefficient	$\Delta\alpha$	amplitude of pitching motion, degrees
C_L, C_z	lift coefficient	Γ	circulation of flow
C_m	pitching moment coefficient	ϵ_0	parameter determining thickness ratio
C_p	pressure coefficient, $\Delta p/q_\infty = (p_1 - p_u)/q_\infty$	Λ	sweep angle
C_p^*	critical pressure coefficient	θ_s	flow direction at the sonic point of the characteristic
H_0	stagnation pressure of free stream	μ	advance ratio or parameter determining profile slope in stagnation point on the nose
k	diffusive damping coefficient or reduced frequency, $\pi fc/V$	ρ	density of air
M	Mach number	ϕ	disturbance velocity potential
M_D	drag divergence Mach number	ψ	azimuth angle of the rotor
M_{xs}	rolling moment around c.g. of helicopter	ω	Prandtl-Meyer angle corresponding to local Mach number
M_{ys}	pitching moment around c.g. of helicopter		
n	load factor		
p	static pressure		
p_∞	static pressure of free stream		
q_∞	dynamic pressure of free stream		
t	profile thickness		
t_D	time to double amplitude		
U	rotational blade tip speed		
U, v_x	horizontal component of velocity		
v, v_y	vertical component of velocity		

The studies have been sponsored in part by the Ministry of Defence of the Federal Republic of Germany

1. INTRODUCTION

With the continuing challenge in performance of modern helicopters, the requirements of their aerodynamic characteristics have increased. As long as pure performance is considered, the main onset of improvement is reduction of parasite drag of a helicopter as a whole. However, the aerodynamic design of the rotor is equally important. The rotor with its aerodynamic behaviour is not only influencing performance, it is, in addition, imposing real aerodynamic limitations to the flight envelope. These limitations are due to Mach number effects at the advancing blade and stall effects at the retreating side, where the main difficulties stem from aeroelastic phenomena.

In the past, the prime design rule was "keep away of these limitations!". Thus, the design boundaries of a rotor blade were relatively conservative: the main goal was to use profiles with nearly zero pitching moments and to bring the important axes of the blade (i.e. control axis, c.g. axis and axis of aerodynamic centre) as close as possible together. Beside a high stall angle and a high critical Mach number, the aerodynamic characteristics of rotor airfoil sections should give low drag throughout the range of low and moderate lifts and moderate drag at high lifts. Most of the conventional airfoils have been developed for use on fixed wing aircraft and are not acceptable for helicopters. The most important exception is the NACA 0012 section, which has already been chosen in the early beginning of the development of helicopters and it has served well so far. If there are no possibilities to improve the situation one has to live with the limitations.

Attempts to improve rotorblade profiles are aggravated by "an aerodynamic situation of exquisite intractability" as Loewy (1) described the situation most strikingly. The flow is extremely complex, the blade is exposed to rapidly changing angles of attack and yaw in combination with rapidly changing velocities. There are regions of high Mach numbers, of stall and of reverse flow. In addition, there are crossflow and unsteady boundary-layer effects. The situation as a whole has been marked by the lack of systematic work, which could be useful in the design work. However, the activities in recent research are most promising.

The importance of helicopter aerodynamics has been well recognized, and the present-day situation including the areas where aerodynamic improvements are most necessary and promising are described in many distinguished papers, see for instance P.F. Yaggy and I.C. Statler (2), J.P. Jones (3), F.X. Wortmann and J.M. Drees (4).

2. INFLUENCE OF AIRFOIL CHARACTERISTICS ON ROTOR BEHAVIOUR

Before an airfoil can be designed one has to know what requirements the new airfoil should meet, and what features are the most desired. The design requirements are primarily fixed by the characteristics of the rotor at high speed conditions including maneuvers. The difficulty is that the design of a rotor is not a classical optimization process but more to find an engineering compromise by trial and error.

Figure 1 illustrates a typical distribution of the section lift coefficient C_L as a function of Mach number. The "section trace curves" are the loci of conditions that would be traced out in each revolution by the blade element section at radius x . These curves describe the operating regime of the different blade elements. The dashed lines combine points with the same rotor azimuth angles. As is well-known, the advancing rotor-blade is operating at low lift up to high subsonic Mach numbers, whereas the retreating blade is working at medium subsonic Mach numbers and high lift values.

In addition, Figure 1 shows two limiting lines, which allow conclusions about the qualification of an airfoil for the investigated mission. The C_{Lmax} -curve describes the maximum C_L -values, which can be reached by the special profile as a function of Mach number including dynamic effects due to oscillating pitch. The closer the section trace curve is approaching the limiting line, the better is the profile utilized in its full C_L -potential at the corresponding section x . The second limiting line ($C_L(M_D)$) of Figure 1 corresponds to the lift coefficient of the drag divergence Mach number. Operation beyond this line causes high drag coefficients and therefore a remarkable increase in power required.

For comparison, Figure 1 also shows the section trace curves for hover condition. There is nearly no change of the operating condition of the profile during one revolution. As far as lift coefficients are concerned, there are no problems as one usually expects, but for highly loaded rotors the blade tip may be operating beyond drag divergence as shown in the figure.

When selecting airfoils for rotorblades, so far simple qualitative comparisons between section shapes were normally made. The profile with the best C_{Lmax} -value at moderate Mach numbers ($M = 0.4 + 0.5$) and with the highest drag divergence Mach number at $C_L = 0$ was preferred. There was no real procedure for weighting the different and opposite characteristics. In order to find a procedure for weighting the different properties of a profile or to find at least more detailed requirements for selection or improvement of blade sections some studies were performed using idealized profile characteristics. Figure 2 shows some typical results of such investigations. As a basis, the section data of the NACA 23012 profile were used with linearly extended lift curves without C_{Lmax} boundaries. The section trace curves in the two diagrams show the conditions for a high speed

level flight (left) and for a maneuver case (right). The C_L -values at the tip of the retreating blade are beyond the boundaries of the actual NACA 23012 profile. Thus the idealized profile shows requirements that are expected from an advanced airfoil. For the selected mission and the assumed rotor and blade geometry the blade sections inside of $x = 0,8$ are operating below C_{Lmax} -boundaries. However, the maneuver flight shows that nearly all blade sections are approaching C_{Lmax} , some of them are even operating beyond the boundaries.

Figure 2 shows also that important parts of the blade are exposed to high drag coefficients. In Figure 3 the situation is more clearly explained by the section trace curves of the drag coefficient at the blade tip. The highest C_D -coefficients occur at the retreating blade, where, however, the dynamic pressure is lower than at the advancing side. The right figure where the C_D -values are weighted by the dynamic pressure shows the fact that in most cases the main contribution to the power required comes from the advancing blade tip.

By studying the flight envelope of a helicopter one can summarize the resulting requirements in one diagram as shown in Figure 4. In the studied case, it turned out that the portion of the blade outside $x = 0,7$ is the important one. The profiles should have high C_{Lmax} -values at Mach numbers between 0,4 and 0,6 as well as a drag divergence boundary shifted to higher Mach numbers. From the left diagram of Figure 4 one can develop the desired curves of C_L and C_D versus α for the different Mach numbers as shown in the diagrams to the right. Of course, the diagrams shown so far are just some ideas for the solution of the whole problem, which needs more systematic research. For instance, the problems are only touched fragmentarily for the mission of one helicopter. Different missions will lead to different requirements, e.g. there are remarkable differences between a high speed and a crane helicopter or a main rotor and a tail rotor. In addition, only the influences of C_L and C_D have been discussed. It is impossible to design a blade profile without taking care of the section moment behaviour. Furthermore, not only some features of the rotor like lift capability or performance characteristics should be investigated but the behaviour of the helicopter as a whole. Figure 5 shows as an example the influence of C_{Lmax} and lift curve slope on the control power and stability characteristics of a helicopter with hingeless rotor system. The left diagram shows that the influence of lift curve slope on the control moments is relatively small compared to the influence of C_{Lmax} . The right diagram shows similar influences on the high speed instability of a hingeless rotor helicopter. A decrease in the lift curve slope and increase in C_{Lmax} will improve this instability. For more detailed information about design problems of hingeless rotor systems see (5).

The informations discussed in this chapter are based on unpublished investigations of references (6) and (7).

3. DESIGN METHODS FOR HELICOPTER AIRFOIL SHAPES

As soon as the desired behaviour of an airfoil is known, i.e. if the desired pressure distribution is given, the contour of the profile has to be determined. This can be done analytically and/or empirically. A well-known analytical procedure to design airfoil shapes is the one by Theodorsen and Garrick (8) that has been used successfully for the development of the newer NACA wing sections, see reference (9). This procedure is based on the theory of conformal mapping, other procedures use the singularity method, e.g. (10) and (11). The left-hand part of Figure 6 shows schematically the concept of the singularity methods: For a given pressure or velocity distribution, the mean line and basic thickness form is calculated by solving numerically some integrals. An improved procedure was developed by R. Eppler (12) and (13), see right-hand part of Figure 6. Using methods of conformal mapping, this procedure allows the calculation of a profile contour when constant pressure distributions over several ranges of the chord length are given. This constant pressure distributions can be related to different angles of attack. The compatibility of the different pressure distributions is obtained by demanding that for any region of the profile contour, the pressure distribution of only one angle of attack is taken to define the profile. The conditions to close the profile are given in analytical form. In addition, the increase of pressure at the upper side of the profile follows a suggestion of F.X. Wortmann (14) to prevent separation of the boundary layer. All these procedures are restricted to incompressible flow. The design of a profile when the pressure distribution in compressible is given causes difficulties, since - even in subcritical flow - the contour is influencing the development of compressible flow around an airfoil. One possibility to solve this problem is to use a design procedure for incompressible flow. After design, the pressure distribution is recalculated from the resulting profile using methods that include compressibility effects, e.g. (15) to (19). The final contour is defined during an iterative process. Figure 7 shows a comparison between experiments and calculated pressure distributions that include a simple compressibility rule. This rule was derived from the compressible and incompressible spiral flow (i.e. a sink-vortex combination):

$$\left(\frac{V}{V_{\infty}}\right)_{\text{compr.}} = \left(\frac{V}{V_{\infty}}\right)_{\text{incompr.}} e^{k \cdot (\tau) + (1-k) g(\tau)}, \quad \tau = \left(\frac{V}{V_{\infty}}\right)^2, \quad k = a + b \cdot C_L$$

It is true, that this compressibility rule is not as accurate as any other rule, that includes the influence of the contour. The advantage is that it can be used in the first design step where the contour is unknown. In addition, the results are satisfactory as shown in Figure 7.

Modern helicopter blades or at least parts of them are usually operating in the transonic flow regime. The problems associated with transonic flow over airfoils have been the subject of an enormous effort of research work over twenty years, see for instance references (20) to (23). The goal of this effort has been the design of airfoils with shockless transonic flow. Although viscous effects play a dominant role in the supercritical flow of interest, one is still forced to decouple the boundary layer and inviscid flows and then seek means to overcome the strong coupling, since the treatment of real flows is further aggravated by the absence of an adequate procedure to treat turbulent boundary layers which encounter severe adverse streamwise pressure gradients such as caused by a shock.

The treatment of the inviscid problem in the physical plane is still difficult enough. The severest problem is the essential nonlinearity of the flow differential equations. Another is the mixed elliptic-hyperbolic character of the equations, where the nonlinearity of the problem precludes an a priori knowledge of the sonic line. Finally, the third difficulty stems from the appearance of embedded shock discontinuities at locations unknown beforehand.

All three difficulties may be circumvented by a transformation of the problem into the hodograph plane. The flow is assumed to be isentropic and the resulting equations become linear, though the flow must be considered in a less familiar u, v space. The second difficulty is largely eliminated since the sonic line is now known and is simply a circle in the hodograph plane. The third difficulty is eliminated by treating only shockless flows. Recent contributions to this method are those of Nieuwland and Boerstoeel, (24) to (26), and Garabedian and Korn, (27) and (28), after Lighthill (29) and Cherry (30) had already made notable contributions to this problem using the Molenbroek transformation. Figure 8 shows a scheme of Nieuwland's and Korn's theory of the flow around quasi-elliptical aerofoil sections. This theory is a method for the transformation of the incompressible potential flow around a lifting ellipse into a compressible potential flow around a lifting quasi-elliptical profile. Though the general approach used by Garabedian and Korn (27) and (28) is similar to that used by Nieuwland and Boerstoeel (24) and (25) in that the nature of the free stream singularity is obtained from the incompressible case, and that the problem of the multivaluedness of the hodograph is resolved in a similar manner, the details beyond this differ significantly in the two methods. Four parameters appear in the basic theory, namely the incidence α of the ellipse in incompressible flow, a term ϵ_0 for the thickness ratio of the ellipse, the circulation Γ of the flow and the free-stream Mach number M_∞ . These four parameters define the symmetric flow, i.e. $\Gamma = 0$. If $\Gamma \neq 0$, these four parameter profiles are not closed. Nieuwland developed a special correction function to make the profiles closed. This function depends also on four parameters, the free-stream Mach number M_∞ , the local Mach number M_c and the local flow angle θ_c at the tail of the closed profile (which appears to be cusped) and a parameter ν determining the profile slope at the nose stagnation point. Thus, seven parameters define the flow around quasi-elliptical airfoils. More details are given in the original papers or in reference (23). A typical result of Nieuwland's method is shown in Figure 9 compared with measurements. The agreement between theory and experiment is remarkably good. A slight waviness in the measured pressures appears in the supersonic region culminating apparently in a weak shock. This waviness is caused by flow perturbations due to model imperfection in the nose region which propagate along Mach waves reflecting back and forth between the sonic line and the airfoil surface. Figure 9 shows also the computed pressure distribution of the finite difference calculation from Magnus and Yoshihara (31) that will be discussed later. Figure 10 shows a typical result of Korn's method compared with the theory of Murman and Cole (33), that will also be discussed later.

The hodograph methods require the assumption of an isentropic flow, but flows with shocks can, in principle, be treated provided the shocks are of the transonic variety, not being excessively strong. The principal difficulty of treating shock waves in the hodograph plane is that as one follows the solution along a streamline, one has to jump from one point in the hodograph to another point connected via a local shock polar as one passes through a shock. These difficulties associated with the occurrence of such gaps in the hodograph plane and the resultant matching required across the gap would discourage the use of the hodograph method despite the linearity of the flow equations. Therefore, these methods are only applicable for shockless flow and lead only to the pressure distribution at the design point, given by the transformation of the incompressible flow around an ellipse. Thus, they cannot be used to calculate steady flows over quasi-elliptical airfoils outside the design point or over prescribed airfoils at prescribed conditions which in general will not be shockless.

For these cases, the flow must directly be considered in the physical plane where the leading equations are nonlinear. They can be solved by numerical methods such as the finite difference method by Magnus and Yoshihara (31) and (32). Here the difficulty of the mixed character of the steady flow equations was circumvented by treating the flow as unsteady. The desired steady flow solution is obtained as the asymptotic flow at large times by imposing proper boundary conditions. In the unsteady form the equations become fully hyperbolic, so that an initial value problem has to be solved which can be done by a finite difference analogue, as shown in Figure 11. Starting from the unsteady continuity equation and the unsteady Euler equations, the flow is assumed to be isentropic. This assumption is based on the fact that for most cases of interest the local entropy additions due to shocks are small. Since the general solutions contain discontinuities in the form of shocks, the usual concept of a solution must be abandoned. In these cases the partial differential equations in Figure 11 become meaningless at the discontinuity since derivatives can no longer be defined. Lax (34) generalized the concept of a solution having given initial values as one which satisfies the requirement that the integral over

all space and time of the differential expression formed from the first equation in Figure 11, multiplied by an arbitrary weighting function, vanishes. This weighting function that is called diffusive damping function and supplementary conditions on the entropy that guarantee the uniqueness of the solution lead to results where the shock waves appear at the proper location when a suitably refined mesh is used through the shock.

The system of partial differential equations is replaced by a system of difference equations by first replacing the continuous x, y, t space by a rectangular lattice of points with the spacing $\Delta x, \Delta y, \Delta t$, see Figure 11. Then the partial derivatives are substituted by partial differences expressed in terms of the values of the dependent variables at the lattice points. For the partial derivatives a modification of the explicit Lax-Wendroff second order differencing scheme is adopted. As an example, a solution of the simple equation $\partial u / \partial t = \partial u / \partial x$ is shown as second equation in Figure 11. Special care must be taken for the region in the vicinity of and on the profile where on the underlying basic rectangular network of points, a sequence of rotated nine point lattice elements has to be imposed. Figure 11 also shows the calculated pattern of expansion and compression waves and the pressure distribution of an airfoil using Yoshihara's method.

In contrast to the unsteady approach Murman and Cole (33) apply the finite difference scheme directly to the steady transonic small perturbation equation. The steady boundary value problem is solved numerically by a finite difference method, where Murman and Cole use a different scheme to represent the derivatives in the subsonic and in the supersonic regions. As in the unsteady procedure, shock waves appear automatically as local steep gradients through the dissipation introduced by the truncation errors. Figure 10 shows the pressure distribution over a quasi-elliptical airfoil as computed by Murman and Krupp (35). Also results for lifting cases have been obtained, see reference (36).

Stager and Lomax (37) have utilized existing experience to develop a procedure that takes advantage of the best of the reported procedures, both in terms of accuracy and computer time. The exact equation of the perturbation potential is used where the independent variables s and n are defined by the orthogonal curvilinear system shown in Figure 12. The s and n coordinates represent, respectively, distances along and normal to the blunt control surface. The boundary value problem is solved by the line relaxation procedure of Murman and Cole using different schemes for the subsonic and supersonic case. The over-relaxation technique is utilized to hasten the convergence guided by the use of interactive graphics. Figure 12 shows an example of a computed pressure distribution compared with experiments and the theory of Magnus and Yoshihara.

There are, of course, several other analytical procedures to calculate the pressure around airfoils in transonic flow (e.g. references (38) to (40)), that cannot be discussed in detail.

The conclusion of this discussion seems to be that one has to combine a good design procedure (e.g. (12)) for incompressible flow, that is improved by adding a simple compressibility rule (e.g. (6) and (7)) with one of the procedures to calculate transonic flow (e.g. (31) to (37)) to an iterative process for the design of airfoils in supercritical flow. In addition, more experiments are necessary to learn more about the physics of transonic flow.

After having discussed the theoretical methods some comments about empirical methods are added. In the design process of rotor airfoil shapes one would like to put the peak of the C_{Lmax} curve versus Mach number at a certain Mach number. Wortmann and Drees (4) have shown that there is a correlation between the pressure at the crest and the Mach number of the peak of C_{Lmax} , see Figure 13. When the absolute value of C_{pcrest} increases at a constant C_L , the maximum in the C_{Lmax} (M_{cr}) curve also shifts to the left in the same way. This result may prove to be a new design concept for section shapes of helicopter blades, if the profiles have a peaky suction loop.

Pearcey (41) developed an empirical method to design supercritical airfoil shapes, after Sinnott and Stuart (42) had shown that the details of the characteristics pattern in the supersonic region of a transonic flow can be determined once the position of the sonic point and the distribution of surface pressures are known. A given section shape can be improved by this method, once the airfoil has been tested and one wants to introduce an extra expansion at the correct upstream point to reduce the shock strength at some given point. A simple property of the characteristics is used to find pairs of connected or "conjugate" points A, B from the observed pressure distribution and surface slope, see diagram in the left-hand top corner of Figure 14. On any given characteristic $\theta_1 - \omega_1 = \theta_2$ or $\theta_2 + \omega_2 = \theta_3$ according to which of the two families it belongs. θ denotes the flow direction, θ_s the flow direction at the sonic point of the characteristic and ω the Prandtl-Meyer angle corresponding to the local Mach number. For a pair of characteristics with the same sonic points $\theta_1 - \omega_1 = \theta_2 + \omega_2$. Thus, for any two points A and B on the surface, that correspond to the same sonic point, an infinitesimal disturbance introduced at A will reach the surface at B with change of sign. The angle ω can be found at all points on the surface from the observed local Mach number (43), and, since θ is also known at the surface, one can plot curves of $\theta + \omega$ and $\theta - \omega$ along the surface as shown in Figure 14 (left-hand corner) and select pairs of conjugate points by drawing horizontal intercepts. Thus, one knows immediately where to modify the surface to reduce the shock strength in the desired downstream position. The danger of a repeated reflection can also be spotted. For more details of the method see (41). On the right-hand side of Figure 14 the shockless pressure distribution of a supercritical airfoil section is shown, that was developed by this procedure.

4. NONSTEADY AND THREE-DIMENSIONAL EFFECTS

As advance ratio of helicopters increases, such factors as compressibility, reversed flow, three-dimensional flow, and blade stall increase both rotor torque and blade flapping motion. To provide a suitable aerodynamic theory one must include the effects of unsteady aerodynamics, three-dimensional flow and blade aeroelasticity. On the other hand, when a section shape is designed for a helicopter blade, steady, two-dimensional flow has to be assumed primarily. But, in a second step, one should also think about the changes of the blade behaviour that are caused by nonsteady, three-dimensional influences.

Figure 15 shows as an example comparisons of dynamic and steady lift curves as measured by J. Liiva et al (44) and predicted by (7). These phenomena have been investigated by many scientists and engineers (e.g. (44) to (50)) and are well-known. The data were obtained for airfoils executing pure sinusoidal pitch motion. Since rotor blades do not normally execute pure sinusoidal motion as they penetrate into the stall regime the question is whether these data can be used for rotor analyses to obtain meaningful results. In a recent paper Carta et al. (49) showed that the blade root torsional moment could be predicted quite accurately as compared to measurements if the available sinusoidal results are converted to a more general nonsinusoidal form in which local section forces and moments are expressed in terms of instantaneous Mach number, angle of attack, an angular velocity and an angular acceleration parameter. In addition, variable inflow distribution over the rotor disc had to be included in the theory to get a good correlation between prediction and experiment.

One of the influences of three-dimensional flow is the effect of yawed flow. Harris (51) developed an empirical approximation for the effects of yawed flow (i.e. radial flow) on the lift coefficient, see Figure 16. The equation used to define the three-dimensional C_L is given as $C_{L(2D)}/\cos\Lambda$, where Λ is the yaw angle. The equation has the restriction that $dC_{L(3D)}/d\alpha$ may not exceed the maximum value of $dC_{L(2D)}/d\alpha$. This means that the effect of yawed flow delays stall to increasingly larger values of C_L with increasingly larger angles of yaw. Figure 16 shows also a comparison of the empirical method with test data (52). While Harris (51) treated the crossflow problem at a more practical level many authors (e.g. (53) to (63)) performed basic research work to study the effects of crossflow and unsteady boundary layer on rotating blades in detail. These influences as far as they are important in this context can be summarized as follows. The chordwise velocity profiles of the boundary layer are very similar in appearance to those that would be expected from ordinary two-dimensional laminar or turbulent boundary layer. The effect of rotation is to delay separation, as shown in Figure 17. The separation line begins to deviate substantially from its two-dimensional value and moves aft at a distance of about six chord lengths from the hub, and near the hub no separation will occur at all. Figure 17 shows also that the crossflow-induced pressure gradients are more effective in delaying separation at small spanwise stations than at large ones. The line labeled "Locus of $\partial p/\partial x = 0$ " separates the regions of favorable pressure gradients from those of unfavorable gradients. For large z , the pressure gradient is favorable near the leading edge of the rotor and then becomes unfavorable past the point of maximum thickness as in two-dimensional flow. Close to the hub, the pressure gradient is favorable over the entire blade. The favorable pressure gradient is a direct result of the crossflow-induced pressure gradient as shown by Dwyer and Mc Croskey (62). However, the non-steady terms which arise as a result of forward flight seem to have an even larger effect than the crossflow derivatives. Also important are Coriolis forces and pressure gradients induced by the potential flow. A large deviation from two-dimensional flow also occurs where the flow approaches separation such as in a laminar separation bubble or in trailing-edge separated flow, or where large external crossflow exist such as in the blade tip region. Within a separation bubble, the centrifugal forces move the fluid outward significantly.

Further remarkable insights into the rotor boundary-layer problem can be obtained from Figure 18. It shows the positions of laminar separation at a distance from hub $z/c = 2.4$ and the locations of transition to turbulence. Dwyer and Mc Croskey (62) found that the latter is essentially independent of three-dimensional effects and Reynolds number for $Re > 5 \times 10^5$ and $\alpha > 0^\circ$, indicating that the chordwise pressure gradients dominate the transition process for these conditions. Another important result is that the chordwise pressure gradients are so strong at large angles of attack that the effects of crossflow and rotation upon the laminar flow are insignificant at this value of z/c since the analytical and experimental results for separation agree well with the two-dimensional calculation for large α . The laminar flow appears to be independent of Reynolds number, see (62) and (64). Finally, Figure 18 shows that the transition process for $\alpha > 60^\circ$ apparently occurs in the free shear layer that develop after laminar separation, and this is followed by turbulent reattachment shortly downstream. At lower angles of attack, transition to turbulence precedes, and therefore precludes laminar separation. The same is true on the lower surface of the airfoil, see reference (62).

Before concluding this chapter a remark should recall a familiar problem to our memory concerning wind tunnel data. Every test engineer knows how difficult it is to measure exactly the things he wants to know and to eliminate all interactions of other effects. For instance, Ericsson and Reding (65) were confronted with such a problem when comparing their theoretical results with measurements. In some cases they found a good agreement between theoretical and experimental results in some cases they did not. Comparing the lift stall characteristics measured by various investigators using two-dimensional wings they found the results of Figure 19. The test geometries obviously influenced the desired two-dimensional character of flow in a more or less strong manner. It seems that one investigator obtains lift curves typical for trailing-edge stall, with lift stall preceding moment stall, whereas other measured curves of the leading-edge typ stall.

5. FEASIBLE MODIFICATIONS OF AIRFOIL SECTION SHAPES

Although research work to develop advanced airfoils for fixed wing aircraft and for rotor blades is in full activity some progress has already been made. Thin-tip blades and blade tip sweep have improved performance and rotor noise remarkably as shown for instance by Spivey (66) and (67), mainly because the formation of shock waves on the advancing blade tip is delayed. The main modifications that were carried out on two-dimensional airfoil shapes are leading-edge design and camber line shape. For helicopter applications it is possible to rule out all camber lines that give large moments $C_{m,c}$. Therefore, only symmetrical airfoils or sections using leading edge (nose droop) camber are acceptable. Figure 20 shows the effect of leading-edge camber on the characteristics of the symmetric Alouette II airfoil as obtained by Poisson-Quinton and de Sievers (68). There is an increase in maximum lift/drag ratio of 27% and an increase in C_{Lmax} of 20%. This gain in lift/drag ratio is particularly interesting to improve rotor performance at a fixed point (hover), since the blade sections then work in the proximity of the maximum lift/drag ratio (e.g. $C_L = 0,7$, $M = 0,65$).

The airfoil tested had also a chord extension of 11,1%. Encouraged by this comparison of cambered and symmetric airfoils a second lesser cambered extension of 5,3% was investigated that had the same radius of the leading edge and the same fairings to the upper surface. The reason for the reduction of extension was to avoid too great a superevelocity on the lower surface of the droop when the section is in the proximity of zero lift (advancing blade tip at high Mach numbers) because of the danger of shock induced separation. These superevelocities of the lower surface, 5 mm behind the leading edge, are plotted in Figure 21. The least extended camber causes lower superevelocities on the lower surface and about the same superevelocities on the upper surface as the 11,1% extended airfoil. Therefore, it is probable that the extension of 5,3% would be less critical than that of 11,1% for the advancing blade around zero lift. Figure 21 shows that the superevelocities on the upper and lower surface in the region of the nose of the cambered (5,3% extension) airfoil are equal and of about the same value as those calculated at zero lift on a symmetric section. Due to the improved C_{Lmax} of the cambered airfoil on the retreating blade it is possible to increase the general lift level on the whole rotor, that is to make the advancing blade operate at positive C_L instead of zero.

The qualitative requirement of getting high C_{Lmax} values at moderate Mach numbers and high drag divergence Mach numbers at low and moderate C_L values can be expressed in a quantitative manner. Figure 22 shows a comparative summary of a number of airfoil families on the basis of C_{Lmax} and M_D characteristics. The NACA laminar flow profiles represented by the 63A OXX family have a poor stall performance that indicates no promise for main rotor applications. The symmetrical 4-digit airfoils that have generally been used come third. The NACA 5-digit family leads to quite an improvement compared to the 4-digit family. The best profiles in this diagram are the profiles developed by the Boeing Vertol Company (69). These airfoil sections were developed on the basis of the NACA 5-digit series by changing the leading edge radius. Applying nose droop camber effectively improves the C_{Lmax} behaviour of symmetric airfoils but can degrade the drag rise behaviour as already mentioned previously. To find a compromise the values of leading-edge radius and leading-edge camber were optimized. This procedure ended up with the improved Boeing-Vertol profiles with the designation for instance V 23010-1,58. The meaning of the first five digits is about the same as of the NACA 5-digit series. However, the camber line of the Vertol profiles can slightly differ from the corresponding NACA mean line. The number after the hyphen is the leading edge radius in percent of chord.

Figure 22 contains also the Boeing Vertol profiles VR-7 and VR-8 that were most recently developed (70). It should be mentioned that these profiles have a peak in the C_{Lmax} versus M curve at $M = 0,5$ and $M = 0,6$ respectively, as shown in Figure 23.

The left diagram of Figure 23 shows the lift capabilities of the airfoils VR-7 and VR-8, the diagrams to the right demonstrate the drag and moment characteristics compared with some other section shapes. These new airfoils produce excellent lift capabilities at high Mach numbers ($M > 0,4$). At high Mach numbers and low C_L 's the V 13006 - 0,7 has the highest M_D and also the lowest C_{D0} , as shown in (70). Airfoils suitable for application on the helicopter rotor are generally leading-edge stall type airfoils that have zero lift pitching moments no greater than -0,04. This pitching moment level is reduced to near zero at the Boeing Vertol sections by deflecting a trailing edge extension with only a small reduction in C_{Lmax} .

Some evidence of the improved hover characteristics of the VR-7 airfoil is shown in Figure 24. These data were obtained on a full scale tail rotor of the BO 105 helicopter and compared with a tail rotor having a NACA 0012 section shape. The improvement in Figure of Merit over the symmetric NACA 0012 section is evident. The C_T/σ range for nearly maximum Figure of Merit is considerably larger for the VR-7 section. Such a behaviour is highly desirable in that the VR-7 section does not incur large penalties in performance when operating at off-design thrust coefficients typical for the demands on a tail rotor during hovering maneuvers. Also clearly demonstrated are the favourable delays in lift and moment stall for the VR-7 airfoil section. Stall conditions are reached by NACA 0012 section at a $C_T/\sigma = 0,12$ which degrades performance. The characteristics of the VR-7 allow reduction of blade area (thereby reducing weight) or, alternatively, of tip speeds (thereby reducing noise).

A similar large increase in tail rotor thrust was obtained by the Hughes Tool Company (71). A tail rotor blade was developed for the Hughes 500 and OH-6 series helicopters which incorporates the NACA 63-415 airfoil. This fully cambered airfoil exhibits very good

stall characteristics at Mach numbers normally associated with tail rotors, see Figure 25. The cambered blade produced an average of 43% more thrust at stall than the symmetric NACA 0012 blade. According to (71) the tail rotor with the NACA 63-415 airfoil produced 35% more thrust at stall than the one with a NACA 0012 airfoil after the data had been corrected to take into account the wider chord of the cambered blade.

Figures 26 and 27 show the characteristics of the original NACA 23012 profile and of two profiles with trailing-edge modifications that were tested up to transonic speeds. The differences between the section with the short tab (5% of chord length) and the one with the long tab (10%) were less important. However, the changes caused by adding a tab to the original profile were beneficial concerning the longitudinal dynamic stability of the BO 105 helicopter, see for instance (72). The modified profiles have - compared with the original NACA 23012 section shape - a slightly larger lift curve slope at moderate Mach number and about the same $dC_L/d\alpha$ at high Mach numbers and a negative dC_m/dC_L curve in both the moderate and high Mach number regime whereas the original profile has a positive dC_m/dC_L at moderate Mach numbers.

One can see that some of the advanced profiles that were discussed in this chapter can already fill up the gap between the actual and desired characteristics of section shapes, as shown in Figure 4.

6. FUTURE PROSPECTS

Further improvements of the characteristics of rotary wing aircraft needs a better understanding and a substantial improvement primarily of the aerodynamics. The large improvements in helicopter techniques up to now did less depend on the progress in aerodynamics but more on a systematic exploitation of other design possibilities. But as the aerodynamic boundaries have been reached the importance of the aerodynamics has been recognized and a directly related effort in research and development has begun. Some advanced airfoils for helicopter rotors are already available, but their full influence on the rotor behaviour has not yet been tested completely. Additional work is needed to further develop the analytical design methods for section shapes, especially in the transonic flight regime, and to understand more exactly the influences of nonsteady, three-dimensional viscous flow effects. Finally, more systematic work is needed to develop suitable evaluation criteria for rotor airfoils starting from the basic helicopter design and its mission requirements.

The basic research work should lead to a better understanding of the physics of flow, and, once this has been accomplished, suitable engineering approximations should be developed to help that the aerodynamics can be regarded as part of the daily work of the design engineer.

7. REFERENCES

1. Loewy, R.G.: "Review of Rotary-Wing V/STOL Dynamic and Aeroelastic Problems". AHS Journal, July 1969, pp. 3-23.
2. Yaggy, P.F. and Statler, I.C.: "Progress in Rotor-Blade Aerodynamics". Presented at the 39th AGARD Flight Mechanics Panel Meeting on "Advanced Rotorcraft", NASA Langley Research Center, 20-23 September 1971, Preprint No. 13.
3. Jones, J.P.: "Rotor Aerodynamics - Retrospect and Prospect". AGARD Conference Proceedings No. 22, September 1967.
4. Wortmann, F.X. and Drees, J.M.: "Design of Airfoils for Rotors". Proceedings of the 3rd CAL/AVLABS Symposium, Buffalo, New York, June 1969.
5. Huber, H.B.: "Some Objectives in Applying Hingeless Rotors to Helicopters and V/STOL Aircrafts". Presented at the AGARD Specialists' Meeting on "The Aerodynamics of Rotary Wings", 13-15 September 1972, Marseille, France, Preprint No. 20.
6. Gehr, S. and Stricker, R.: "Aerodynamische Arbeitsgrundlagen für zukünftige Propeller und Rotoren - Untersuchungen über verbesserte Blattprofile". MBB GmbH, UD TNA D12-23/70, Dezember 1970.
7. Wagner, S., Polz, G. and Stricker, R.: "Aerodynamische Arbeitsgrundlagen für zukünftige Propeller und Rotoren". MBB GmbH, Bericht Nr. UD-75-71, Dezember 1971.
8. Theodorsen, Th. and Garrick, I.E.: "General Potential Theory of Arbitrary Wing Sections". NACA Rept. No. 452, 1933.
9. Abbot, I.H., von Doenhoff, A.E. and Stivers, L.S.: "Summary of Airfoil Data". NACA Rept. No. 824, 1945.
10. Truckenbrodt, E.: "Die Berechnung der Profilform bei vorgegebener Geschwindigkeitsverteilung". Ing.-Arch. Vol. 19 (1951), pp. 365-377.
11. Weber, J.: "Calculation of the Pressure Distribution on the Surface of Thick Cambered

- Wings and the Design of Wings with Given Pressure Distribution". Aeronautical Research Council, R & M No. 3026, 1955.
12. Eppler, R.: "Die Berechnung von Tragflügeln aus der Druckverteilung", Ing.-Arch. Vol. 23 (1955), pp. 436-452.
 13. Eppler, R.: "Direkte Berechnung von Tragflügelprofilen aus der Druckverteilung". Ing.-Arch. Vol. 25 (1957), pp. 32-57.
 14. Wortmann, F.X.: "Ein Beitrag zum Entwurf von Laminarprofilen für Segelflugzeuge und Hubschrauber". Zeitschrift f. Flugwissenschaften, Vol. 3 (1955), pp. 333-. British M.O.S. translation TIL/T A 903.
 15. Wilby, P.J.: "The Calculation of Sub-Critical Pressure Distributions on Symmetrical Aerofoils at Zero Incidence NPL Aero Rep. 1208 (1967).
 16. Lock, R.C., Powell, B.J., Sells, C.C.L., and Wilby, P.G.: "The Prediction of Airfoil Pressure Distributions for Sub-Critical Viscous Flows". AGARD Conference Proceedings No. 35, Transonic Aerodynamics, September 1968.
 17. Labrujere, T.E., Loeve, W. and Slooff, J.W.: "An Approximate Method for the Determination of the Pressure Distribution on Wings in the Lower Critical Speed Range". AGARD Conference Proceedings No. 35, Transonic Aerodynamics, September 1968.
 18. Hess, J. and Smith, A.M.O.: "Calculation of Potential Flow about Arbitrary Bodies". Progress in Aeronautical Sciences, Vol. 8, Pergamon Press 1967, pp. 1-138.
 19. Giesing, J.P.: "Potential Flow about Two-Dimensional Airfoils". Douglas Aircraft Company, Report No. LB 31946, 1965.
 20. Oswatitsch, K. (Editor): "Symposium Transsonicum". IUTAM Symposium, Aachen 1962.
 21. "Transonic Aerodynamics". AGARD Conference Proceedings No. 35, September 1968.
 22. Cole, J.D.: "Twenty Years of Transonic Flow". Boeing Scientific Research Laboratories Document D1-82-0878, July 1969.
 23. Yoshihara, H.: "Some Recent Developments in Planar Inviscid Transonic Airfoil Theory". AGARDograph No. 156, February 1972.
 24. Nieuwland, G.: "Transonic Potential Flow Around a Family of Quasi-Elliptical Aerofoil Sections". NLR Amsterdam, Report TR.T.172, 1967.
 25. Boerstoeel, J.W.: "A Survey of Symmetrical Transonic Potential Flows Around Quasi-Elliptical Aerofoil Sections, NLR Amsterdam, TR.T.136, 1967.
 26. Boerstoeel, J.W. and Uijlenhoet, R.: "Lifting Aerofoils with Supercritical Shockless Flow". Presented at the 7th Congress of the International Council of the Aeronautical Sciences, Roma, Italy, 14-18 September 1970, Paper No. 70-15.
 27. Korn, D.: "Computation of Shock-Free Transonic Flows for Airfoil Design". NYU Report NYO 1480-125, 1969.
 28. Garabedian, P. and Korn, D.: "Numerical Design of Transonic Airfoils". Numerical Solution of Partial Differential Equations, II, Academic Press, 1971.
 29. Lighthill, M.: "The Hodograph Transformation in Transonic Flow". II and III, Proc. R. Soc. London, A-191. 1947.
 30. Cherry, T.: "Flow of a Compressible Fluid About a Cylinder". Proc. R. Soc. London, A-196, 1949.
 31. Magnus, R. and Yoshihara, H.: "Inviscid Supercritical Airfoil Theory". AGARD CP No. 35, 1968.
 32. Magnus, R. and Yoshihara, H.: "Inviscid Transonic Flow Over Airfoils". Presented at the AIAA 8th Aerospace Sciences Meeting, New York, 19-21 January, 1970, AIAA Paper No. 70-47.
 33. Murman, E. and Cole, J.: "Calculation of Plane Steady Transonic Flows". Presented at the AIAA 8th Aerospace Sciences Meeting, New York, 19-21 January, 1970, AIAA Paper No. 70-188.
 34. Lax, P.: "Weak Solutions of Nonlinear Hyperbolic Equations and Their Numerical Computation". Comm. on Pure and Appl. Math. Vol. 7, 1954.
 35. Murman, E. and Krupp, J.: "Solution of the Transonic Potential Equation Using a Mixed Finite Difference System". Lecture Notes Physics, Springer Verlag, 1971
 36. Krupp, J. and Murman, E.: "The Numerical Calculation of Plane Steady Transonic Flows Past Thin Lifting Airfoils". AIAA Preprint No. 71-566, 1971.

37. Steger, J.L. and Lomax, H.: "Numerical Calculation of Transonic Flow about Two-Dimensional Airfoils by Relaxation Procedures". AIAA Preprint No. 71-569, 1971.
38. Spreiter, J.R. and Alksne, A.Y.: "Thin Airfoil Theory Based on Approximate Solution of the Transonic Flow Equation". NACA TN 3970, 1957.
39. Spreiter, J.R. and Stahara, S.S.: "Calculative Techniques for Transonic Flows about Certain Classes of Airfoils and Slender Bodies". NASA-CR 1722, 1971.
40. Nörstrud, H.: "Numerische Lösungen von schallnahen Strömungen um ebene Profile". Technische Hochschule Wien, Dissertation 1968.
41. Pearcey, H.H.: "The Aerodynamic Design of Section Shapes for Swept Wings". Advances in Aeronautical Sciences, Vol. 3, Proceedings of the 2nd International Congress in the Aeronautical Sciences, Zürich 1960. Pergamon Press 1962, pp. 277-322.
42. Sinnott, C.S. and Stuart, C.M.: "An Analysis of the Supersonic Region in a High-Subsonic Flow past an Aerofoil Surface. A.R.C. Rep. 21715, 1960.
43. Rosenhead, L. (Editor): "A Selection of Tables for Use in Calculations of Compressible Airflow". Clarendon Press, Oxford 1952.
44. Liiva, J., Davenport, F.J., Gray, L. and Walton, I.C.: "Two-Dimensional Tests of Airfoils Oscillating Near Stall". USAAVLABS Technical Reports 68-13A, 68-13B, 68-89A and 68-89B. U.S. Army Aviation Material Laboratories, Fort Eustis Virginia, 1968.
45. Ham, N.D.: "Aerodynamic Loading on a Two-Dimensional Airfoil During Dynamic Stall". AIAA Journal, Vol. 6, No. 10, October 1968.
46. Ericsson, L.E. and Reding, J.P.: "Unsteady Airfoil Stall". NASA CR-66787, July 1969. Also: Journal of Aircraft, Vol. 8, No. 8, August 1971, pp. 609-616.
47. Gross, D.W. and Harris, F.D.: "Prediction of Inflight Stalled Airloads from Oscillating Airfoil Data". Presented at the 25th Annual National Forum of the AHS, Washington, D.C., May 1969.
48. Tarzanin Jr. F.J.: "Prediction of Control Loads due to Blade Stall". Presented at the 27th Annual National V/STOL Forum of the AHS, Washington, D.C., May 1971, Preprint No. 513.
49. Carta, F.O., Commerford, G.L. and Carlson, R.G.: "Determination of Airfoil and Rotor Blade Dynamic Stall Response". Presented at the 28th Annual National Forum of the AHS, Washington, D.C., May 1971, Preprint No. 613.
50. Isogai, K.: "An Experimental Study on the Unsteady Behaviour of a Short Bubble on an Airfoil During Dynamic Stall with Special Reference to the Mechanism of the Stall Overshoot Effect". Massachusetts Institute of Technology, Cambridge, Massachusetts 02139, ASRL TR 130-2, June 1970.
51. Harris, F.: "Preliminary Study of Radial Flow Effects on Rotor Blades". Journal of the American Helicopter Society, July 1970.
52. Purser, P. and Spearman, M.: "Wind Tunnel Tests at Low Speed of Swept and Yawed Wings Having Various Plan Forms". NACA TN 2445, December 1951.
53. Himmelskamp, H.: "Profiluntersuchungen an einem umlaufenden Propeller". Mitteilungen des Max-Planck-Instituts, No. 2, Göttingen 1950.
54. Voelkoff, H.R.: "A Preliminary Study of the Effect of a Radial Pressure Gradient on the Boundary Layer of a Rotor Blade". Proceedings of the CAL/USAAVLABS Symposium on Aerodynamic Problems Associated With V/STOL Aircraft, Vol. 3, 1966.
55. Mc Croskey, W.J. and Yaggy, P.F.: "Laminar Boundary Layers on Helicopter Rotors in Forward Flight". AIAA Journal, Vol. 6, No. 10, October 1968.
56. Voelkoff, H.R., Blaser, D.A. and Jones, K.M.: "Boundary-Layer Discontinuity on a Helicopter Rotor Blade in Hovering". AIAA Journal of Aircraft, Vol. 8, No. 2, Feb. 1971.
57. Clark, D.R. and Arnoldi, D.R.: "Rotor Blade Boundary Layer Calculation Programs". USAAVLABS, TR 71-1, March 1971.
58. Mc Croskey, W.J.: "Measurements of Boundary Layer Transition, Separation and Streamline Direction on Rotating Blades". NASA TN D-6321, April 1971.
59. Blaser, D.A. and Voelkoff, H.R.: "Boundary Layer Velocity Profiles on a Helicopter Rotor Blade in Hovering and Forward Flight". Presented at the 28th Annual National Forum of the AHS, Washington, D.C., May 1971, Preprint No. 622.
60. Clark, D.R. and Landgrebe, A.J.: "Wake and Boundary Layer Effects in Helicopter Rotor Aerodynamics". AIAA 4th Fluid and Plasma Dynamics Conference, Palo Alto, 21-23 June, 1971, AIAA Paper No. 71-581.

61. Blaser, D.A.: "An Analytical and Experimental Investigation of Helicopter Rotor Boundary Layers". Ohio State Univ. Ph. D. Dissertation, July 1971.
62. Dwyer, H.A. and Mc Croskey, W.J.: "Crossflow and Unsteady Boundary-Layer Effects on Rotating Blades". AIAA Journal, Vol. 9, No. 8, August 1971.
63. Young, W.H. Jr. and Williams, J.C.III: "The Boundary Layer on Rotating Blades in Forward Flight". AIAA 8th Aerospace Sciences Meeting, New York, 19-21 January, 1970, AIAA Paper No. 70-49.
64. Gault, D.E.: "An Experimental Investigation of Regions of Separated Laminar Flow". NACA TN 3505, 1955.
65. Ericsson, L.E. and Reding, P.J.: "Dynamic Stall Simulation Problems". Journal of Aircraft, Vol. 8, No. 7, July 1971, pp. 579-583.
66. Spivey, R.F.: "Blade Tip Aerodynamics - Profile and Plan Form Effects". Presented at the 24th Annual National Forum of the AHS, Washington, D.C., May 1968.
67. Spivey, W.A. and Morehouse, G.G.: "New Insights into the Design of Swept-Tip Rotor Blades". Presented at the 26th Annual National Forum of the AHS, Washington, D.C., June 1970, Preprint No. 420.
68. Poisson-Quinton, Ph. and de Sievers, A.: "Aerodynamic Study of Helicopter Blade Sections". AGARD Conference Proceedings No. 22 on Fluid Dynamics of Rotor and Fan Supported Aircraft at Subsonic Speeds. Göttingen, September 1967.
69. Davenport, F.J. and Front, J.V.: "Airfoil Sections for Rotor Blades - A Reconsideration". Presented at the 22nd Annual Forum of the AHS, Washington, D.C., May 1966.
70. Benson, R.G., Dadone, L.U., Gormont, R.E. and Kohler, G.R.: "Influence of Airfoils on Stall Flutter Boundaries of Articulated Helicopter Rotors". Presented at the 28th Annual National Forum of the AHS, Washington, D.C., May 1972, Preprint No. 621.
71. Robinson, F.: "Increasing Tail Rotor Thrust and Comments on Other Yaw Control Devices". Journal of the American Helicopter Society, Vol. 15, No. 4, October 1970, pp. 46-52 and Vol. 17, No. 2, April 1972, pp. 67-68.
72. Reichert, G. and Huber, H.: "Influence of Elastic Coupling Effects on the Handling Qualities of a Hingeless Rotor Helicopter". Presented at the AGARD Meeting on "Advanced Rotorcraft". NASA Langley Research Center, September 1971, Paper No. 12.

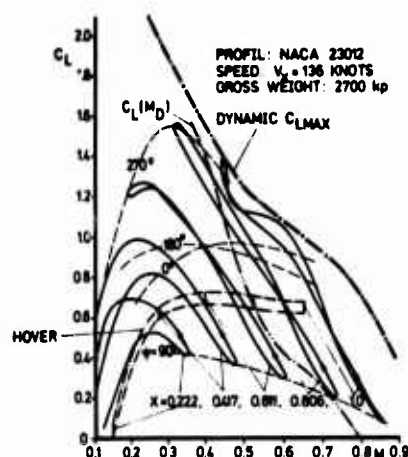


Fig. 1 Distribution of C_L on a Rotor Blade During a Revolution

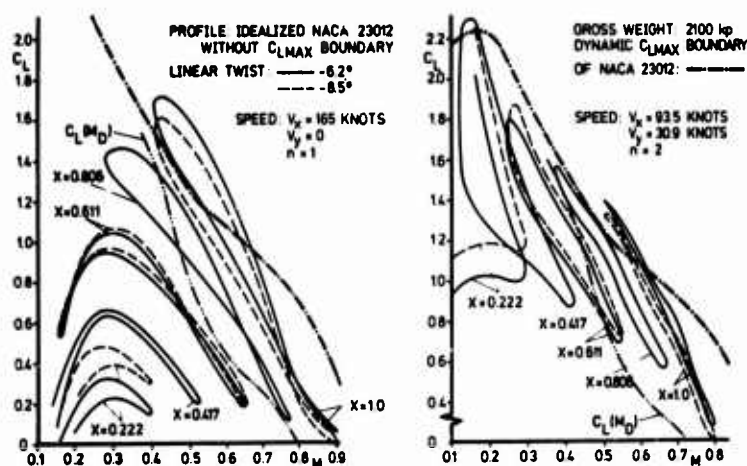


Fig. 2 Distribution of C_L on a Rotor Blade Using Idealized Profile Data

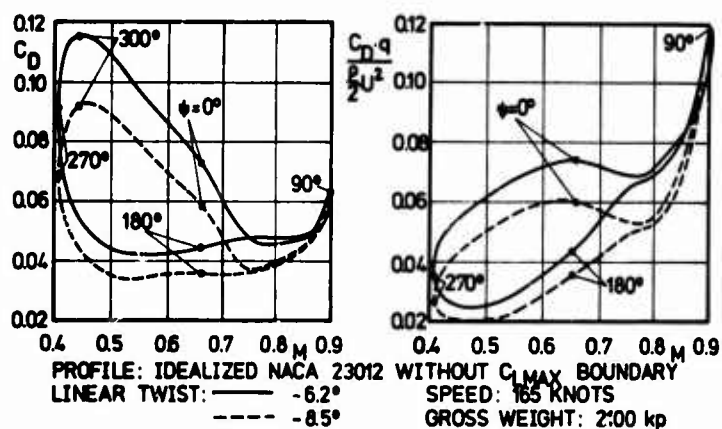


Fig. 3 Distribution of C_D Versus Mach Number of a Blade Tip During One Revolution

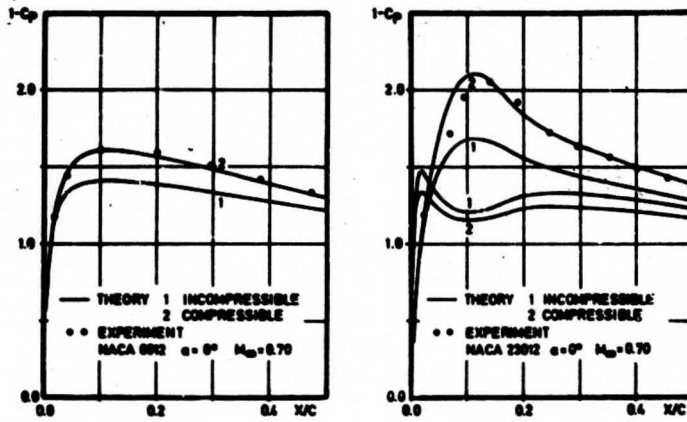


Fig. 7 Comparison of a Simple Compressibility Rule With Experiments

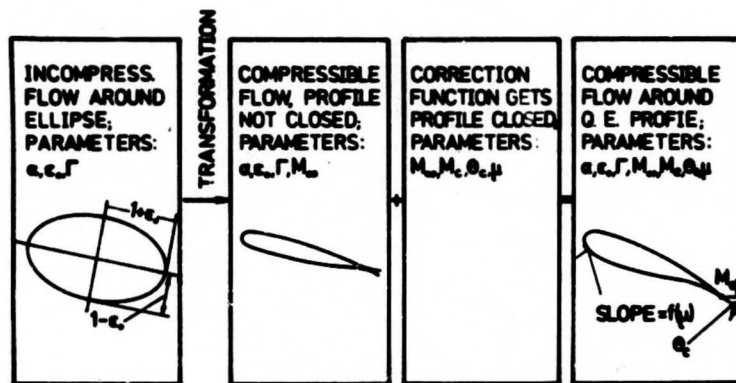


Fig. 8 Scheme of Quasi-Elliptical Profile Theory (Nieuwland and Korn)

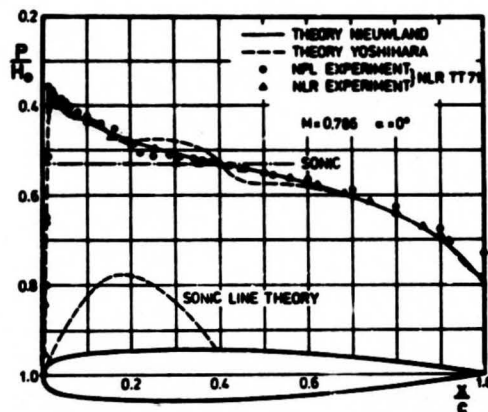


Fig. 9 Quasi-Elliptical Airfoil 0.11-0.77-1.375 (Symmetric Shockless Flow)

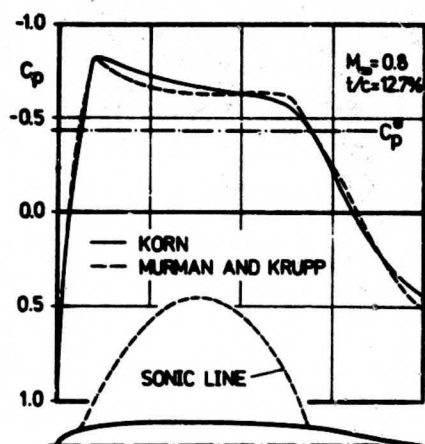


Fig. 10 Pressure Distribution of a Symmetric Airfoil (Korn's Method)

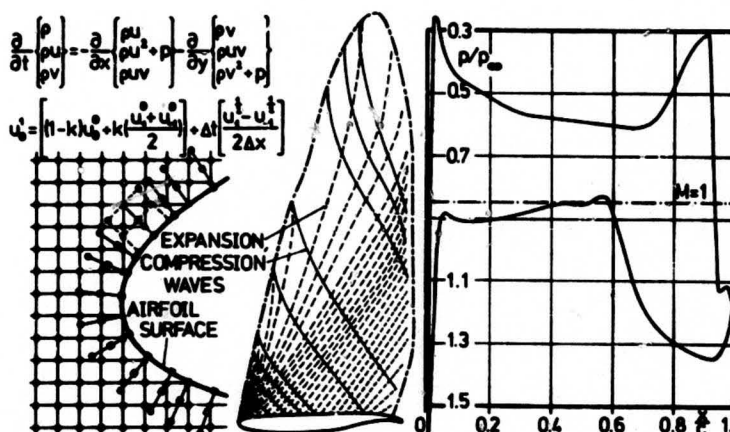


Fig. 11 Lattice Elements, Mach Wave Pattern and Pressure Distribution (Yoshihara)

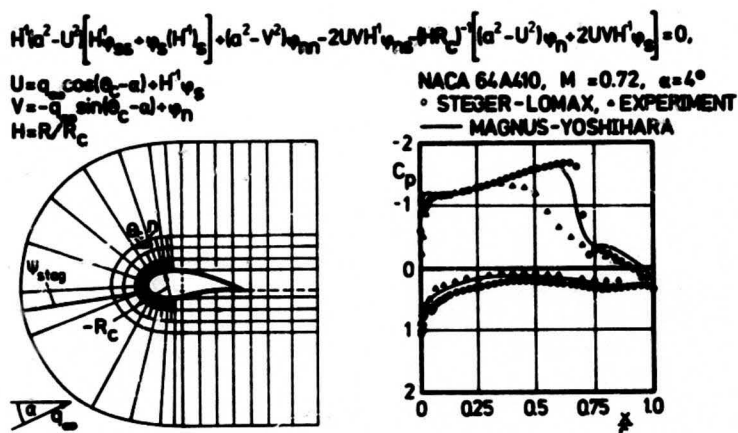


Fig. 12 Coordinate System Used by Steger and Lomax and Example for Pressure Distr.

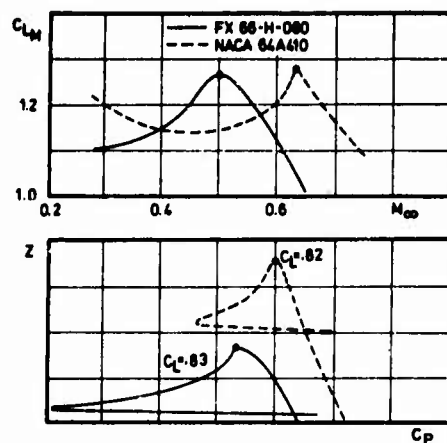


Fig. 13 Correlation Between Pressure at the Crest and Mach Number of the Peak of C_{Lmax}

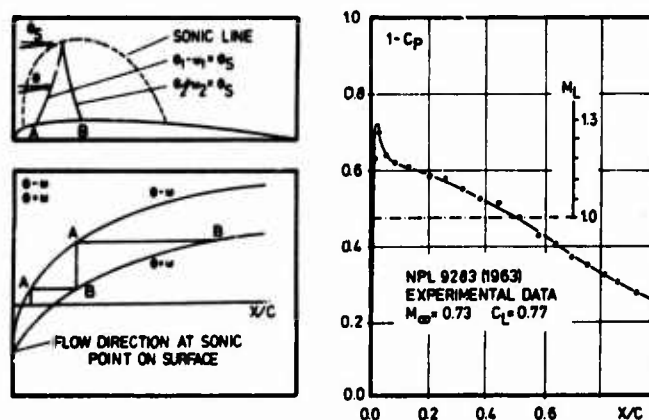


Fig. 14 Shock-Free Flow on an Airfoil Designed Empirically (Pearcey)

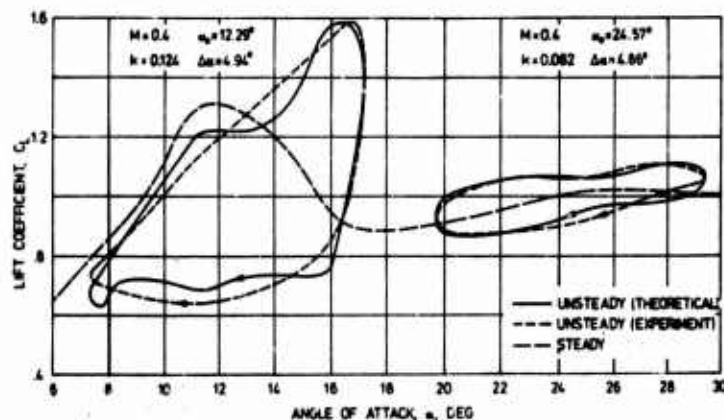


Fig. 15 Static and Dynamic C_L of a V 23012-1.58 Profile Oscillating in Pitch

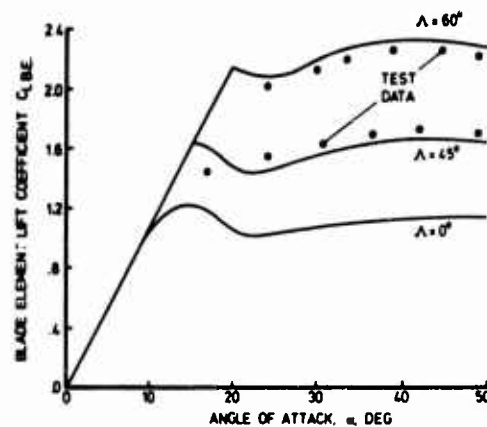


Fig. 16 Engineering Approximation of C_L Accounting for Yawed Flow With $C_{L(3D)} = C_{L(2D)} / \cos \Lambda$

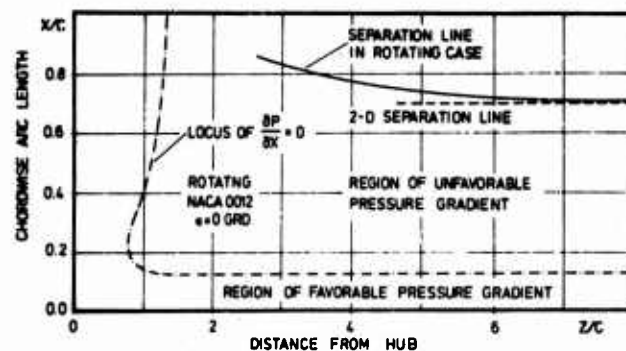


Fig. 17 Effect of Rotation on the Position of Separation for the NACA 0012 Airfoil

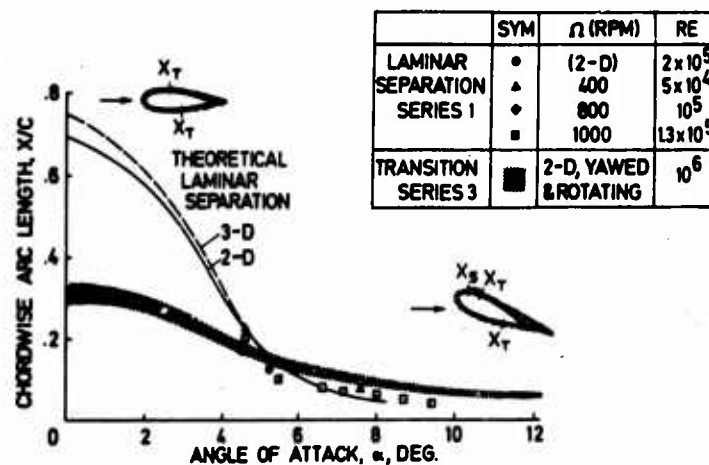


Fig. 18 Separation and Transition on a Rotating NACA 0012 and a Modified 0010 Profile

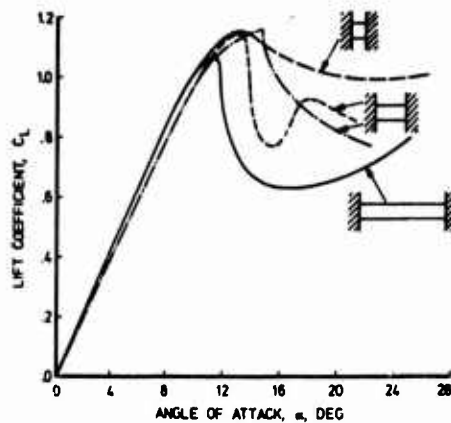


Fig. 19 Two-Dimensional Stall of the NACA-0012 Airfoil Measured by Various Investigations

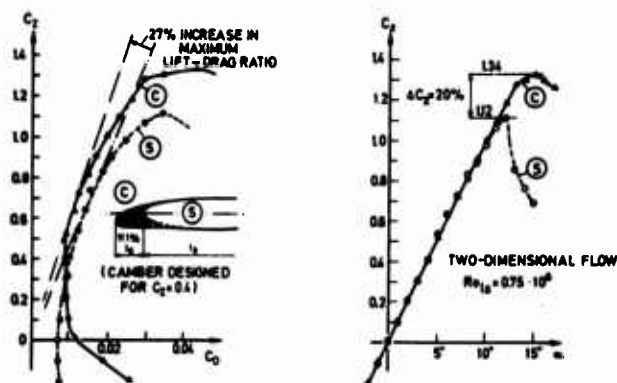


Fig. 20 Effect of Leading-Edge Camber on the Characteristics of an Airfoil

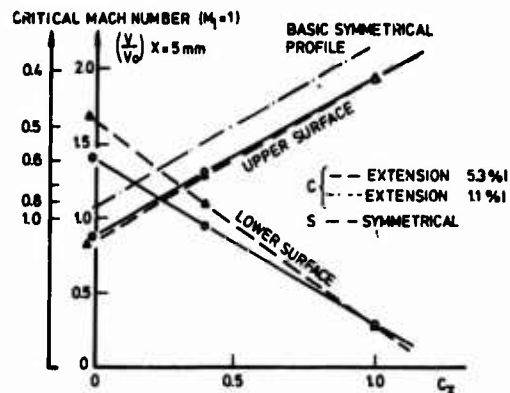


Fig. 21 Theoretical Speeds in the Area of the Cambered Leading Edge

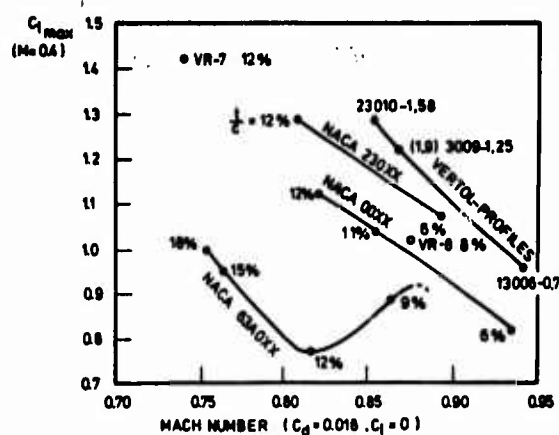


Fig. 22 Summary of Stall and Drag Rise Characteristics for Several Airfoil Families

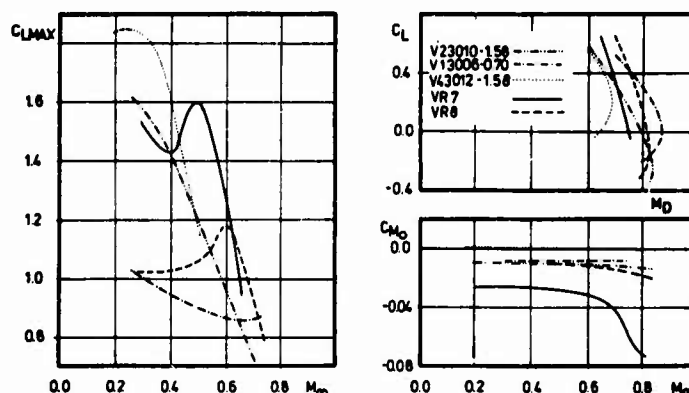


Fig. 23 C_{Lmax} Boundaries, Zero Lift Pitching Moment Levels and Drag Divergence Boundaries

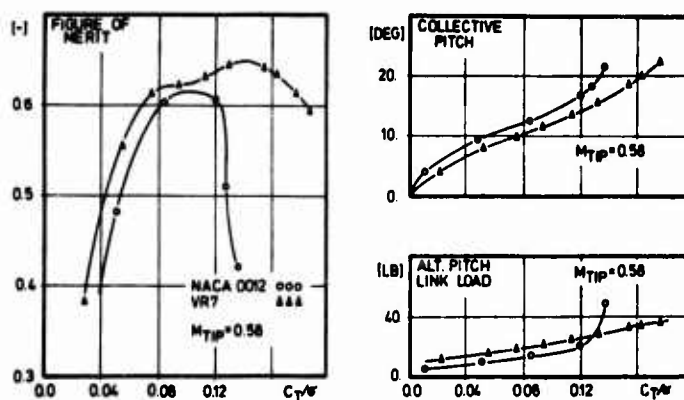


Fig. 24 BO 105 Tail Rotor Hover Test Comparison of NACA-0012 and VR 7 Airfoils

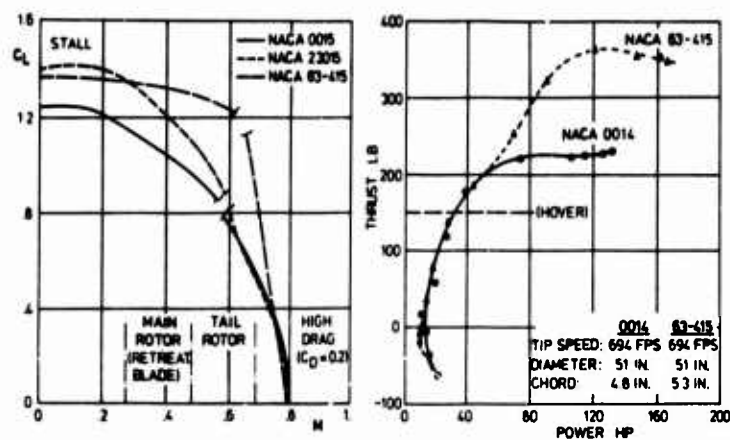


Fig. 25 Thrust of Tail Rotors With Different Profile Shapes

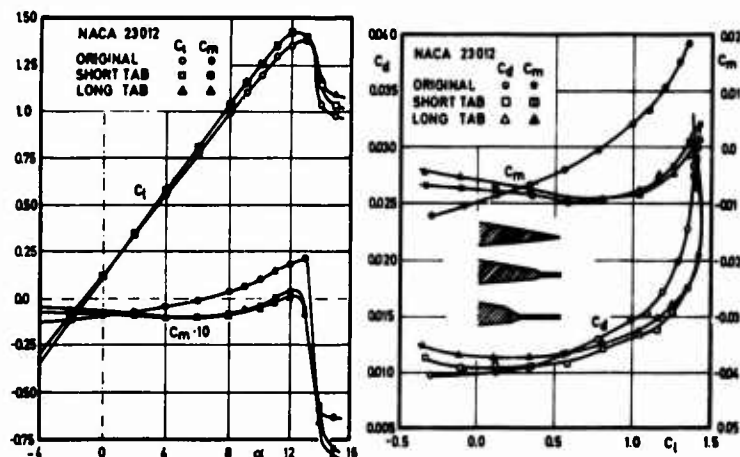


Fig. 26 Effect of Trailing-Edge Modifications on the Characteristics of a NACA 23012 Profile at $M = 0.4$

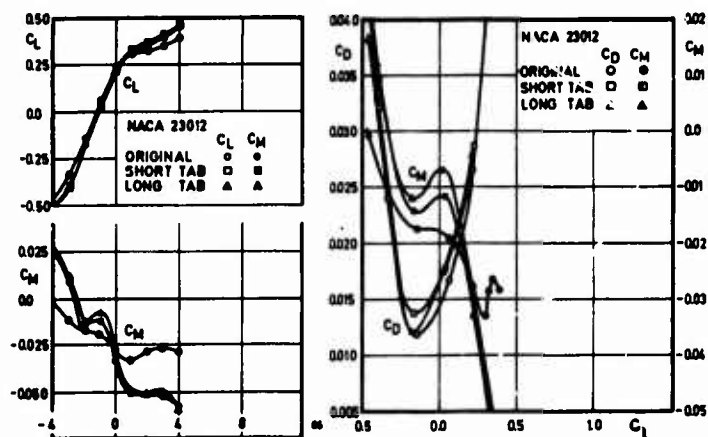


Fig. 27 Effect of Trailing-Edge Modifications on the Characteristics of a NACA 23012 Profile at $M = 0.8$

Prepared Comment on Paper 14

by

F.X.Wortmann

Institut für Aerodynamik und Gasdynamik
der Universität Stuttgart

The paper of Dr Wagner provides a comprehensive survey of the present knowledge of different aspects related to rotor airfoils.

Asked for some comments upon this paper I feel it might be appropriate to make some remarks about my own experience which concentrates more on the design problem. Obviously "the aerodynamic situation of exquisite intractability" needs some simplification to become tractable. In the case of the conventional helicopter rotor the three dimensionality and the unsteadiness of the flow over the blade airfoil are characteristics both important and helpful in understanding the behaviour of the rotor disc. However, with respect to the design problem, fortunately both seem to be of secondary importance. It has long been known and it is also clearly stated in this paper that the most stringent conditions prevail on the advancing blade at high and on the retreating blade at medium subsonic Mach numbers. In both cases the flow on the blades is mostly two dimensional*. It is also unsteady, although improving an airfoil in steady conditions seems to do the same for the unsteady case, at least I do not know of any experience to the contrary. Therefore it is surely justified to consider the design task in the traditional way as a steady and two dimensional problem.

The term "airfoil design" has basically to do with some form of boundary layer control. When the freestream Mach number† approaches higher values the prominent feature of the airfoil flow is the development of local supersonic fields. The best boundary layer control now is to avoid the formation of shocks and to design airfoils for a shockless flow. As mentioned in Dr Wagner's paper there exist several different methods to design shockless airfoils for given boundary conditions, such as prescribed Mach number, airfoil thickness and lift values. These methods are powerful tools in designing an airfoil for one single purpose, for instance for the cruising flight conditions of a fixed wing transport. However, in case of the helicopter airfoil, the design procedure has to be different since the favoured shockless flow should not only be realized in one but in two quite different situations. The airfoil therefore has to be adapted to the double purpose of producing on one hand a shockless flow at low angles of attack and Mach numbers of about 0.85 and on the other hand at high angles of attack and a Mach number of 0.5. At the beginning we are not sure if this challenging task can be done at all.

In this context it might be useful to outline some considerations which narrow the infinity of choices in the direction of a solution for the airfoil of the outer blade of a helicopter rotor.

1. The relative thickness of the airfoil will be in the range of 8–10 per cent. A thicker airfoil will spoil the drag divergence Mach number of the advancing side, whereas a thinner airfoil becomes too sensitive to cover the range of angles of attack (roughly between zero and ten degrees) with reasonable pressure distributions.
2. Along the chord the thickness will be more evenly distributed than usual and hence the rear part of the airfoil becomes relatively thick. This helps to reduce the super velocities for a given maximum thickness and therefore shifts the onset of supersonic flow at low angles of attack to higher free stream Mach numbers.
3. In order to reduce the super velocities at high angles of attack for a given Mach number, the nose region must be cambered and the nose radius should be nearly 1 per cent of the chord. However, this nose droop has to be carefully compromised and should not spoil the high speed characteristics in the very first few per cents of the lower side. The necessity for very low pitching moments eliminates any aftloading. The camber-line therefore is practically flat in this part of the airfoil.
4. In two previous papers [1], [2] I have shown that a velocity peak or higher surface curvature on the upper side at roughly 10 per cent of the chord has a beneficial influence on the $c_{L,max}$ at medium Mach numbers. This is mostly due to a reduced shock strength.

On the other side, the relatively high curvature in this region can also be used at low angles of attack to release a dense fan of expansion waves, which in turn is one of the first requirements to establish a shockless supersonic field downstream of this point. Therefore the curvature on the upper side in the 10 per cent region will be in some sense the key to improving both the maximum lift and the high speed qualities of a helicopter airfoil. In Fig.1 I have summarized these typical features of an advanced helicopter airfoil.

I may conclude my comment by noting that some of these ideas may be improved by replacing the real airfoil by the "fluid" airfoil and that in some cases the unavoidable compromise between partly conflicting requirements may lead to slightly different solutions, but in general the flow environment of a conventional helicopter rotor is so stringent that the future will carve out only one airfoil form which matches the double purpose conditions best.

* At least as long as the stalled condition and the tip vortex interference are excluded.

† Or the angles of attack.

Literature

1. F.X. Wortmann *Design of Airfoils for Rotors*, CAL/AVLABS Symposium 1969, Cornell Aeron. Lab., Buffalo, USA.
2. F.X. Wortmann *Design of Airfoils with High Lift at Low and Medium Mach Numbers*, AGARD Conference Proceedings No. 102, Lisbon 1972, Paper No. 7.

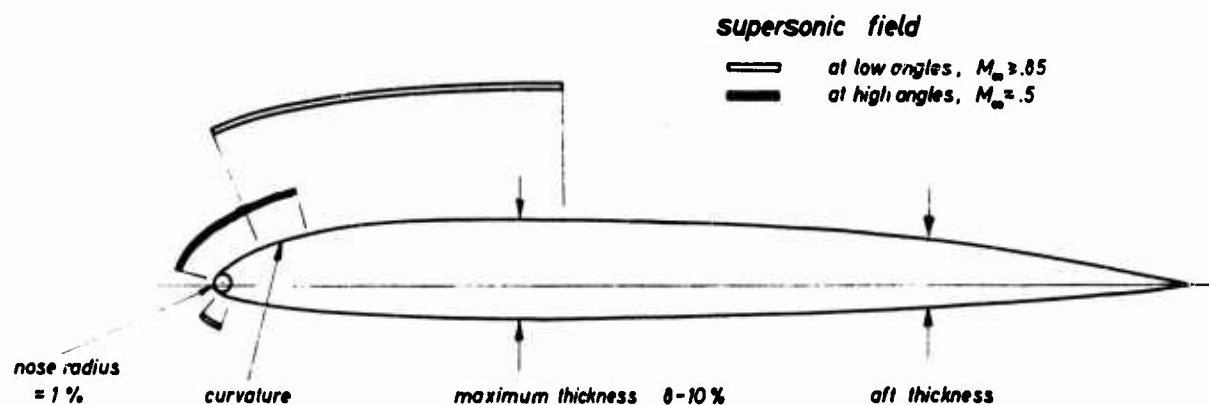


Fig.1 Typical geometric characteristics of a helicopter airfoil

RECENT DEVELOPMENTS IN ROTOR BLADE STALL

by

W. J. McCroskey
U. S. Army Air Mobility R&D Laboratory
Ames Directorate
Moffett Field, California USA 94035

SUMMARY

Considerable progress has been made in recent years in analyzing rotor boundary layers. The basic effects of rotation and crossflow due to forward flight have been identified and found to be insignificant for most cases of practical interest in helicopter aerodynamics. Within the framework of classical thin boundary theory, unsteady viscous effects are also quite small. However, unsteady viscous-inviscid interaction appears to play an important role in retreating blade stall. At high forward speeds, stall on the retreating blade closely resembles dynamic stall on an unsteady two-dimensional airfoil, and the shedding of a vortex-like disturbance from the leading edge of the blade can produce very large transients in the blade element force and moment coefficients.

NOTATION

b	number of blades	α	blade element angle of attack in the chordwise plane
c	chord	α_{SS}, α_{DS}	static and dynamic stall angles, respectively
C_f	skin friction coefficient, $\tau_x / \frac{1}{2} \rho V_0^2$	$\Delta \alpha_{LS}$	increase in α above the static value for laminar separation at $x/c = 0.1$
C_p	pressure coefficient, $(p - p_\infty) / \frac{1}{2} \rho V_i^2$	α_0	mean angle of attack
C_M	blade element pitching moment coefficient based on V_i	α_1	amplitude of sinusoidal oscillation
C_N	blade element normal force coefficient based on V_i	$\dot{\alpha}$	time rate of change of α
$\Delta C_{N_{max}}$	increase in $C_{N_{max}}$ above the static value	β	skew angle of the flow at the wall relative to the flow direction at the outer edge of the boundary layer
C_T/σ	rotor thrust coefficient, $T / \rho b c \Omega^2 R^3$	β_0	undisturbed flow angle relative to the x-axis, $\tan^{-1} \left(\frac{V_1 \cos \psi}{\Omega z + V_1 \sin \psi} \right)$
k	reduced frequency, $\Omega c / 2V_0$	γ	angle between the x-axis and the plane of rotation
M	Mach number based on V_i	θ	blade collective pitch
p	pressure	δ	boundary layer thickness
R	blade radius	μ	advance ratio, $V_1 / \Omega R$
Re_0	Reynolds number, $V_0 x / \nu$	ν	kinematic viscosity
Re_i	Reynolds number, $V_i c / \nu$	ρ	density
t	time	τ_x, τ_z	chordwise and spanwise components of shear stress
u	chordwise velocity in the boundary layer	ψ	rotor blade azimuth
U_e	chordwise velocity at the outer edge of the boundary layer	Ω	angular velocity
v	vertical velocity in the boundary layer		
v_i	induced velocity		
V_0	average chordwise velocity in the flow approaching the blade or airfoil		
V_i	local blade element velocity, $\Omega r + V_1 \sin \psi$		
V_1	translational velocity perpendicular to the axis of rotation		

V_2	translational velocity along the axis of rotation
V_r	radial velocity, $w + u(x/z)$
w	spanwise velocity in the boundary layer
w_e	spanwise velocity at the outer edge of the boundary layer
x	curvilinear chordwise coordinate
y	curvilinear coordinate normal to the airfoil surface
z	spanwise coordinate

1. INTRODUCTION

Helicopters have advanced over the years from aeronautical curiosities to useful and productive aircraft, but retreating blade stall remains a major obstacle to further improving their efficiency and speed in forward flight. Blade stall occurs on the "retreating" side of the rotor disc, where the local aerodynamic angles of attack are forced to large values to compensate for the low blade element velocities, as illustrated in Figures 1 and 2. This stall phenomenon limits the performance of the rotor due to a loss in lift and a rise in drag, and in addition, most helicopters suffer severe vibration and oscillatory loads in the control system due to the large pitching moments that develop in the blades when they stall.

Since stall is a viscous phenomenon, it is logical to inquire how boundary layer flows on rotor blades differ from those on fixed wings. Although numerous investigators have pondered this question over the years, we still do not have a satisfactory theoretical understanding of retreating blade stall. The purpose of this paper is to describe what has been learned about viscous flows on rotor blades, to show why present boundary layer theory fails to predict when stall will occur, and to indicate the directions in which further research should proceed.

Before trying to analyze the boundary layer flow, let us consider briefly the rotor blade element environment. In the hover or axial flow case, the radial and azimuthal variations in the blade element velocities and angles of attack are generally negligible over distances of the order of the blade chord, with the exception of the tip region. However, high speed forward flight can be another story. For example, Fig. 2 shows the operating conditions for a full-scale wind tunnel test [1] simulating a moderately-loaded high speed flight condition of a Sikorsky CH-34 helicopter. For these conditions, the blades operated over a Mach number range from incompressible to transonic flow. The local dynamic pressure, $1/2 \rho V_\infty^2$, varied by more than an order of magnitude, and consequently α and C_N varied over a very wide range. In this particular test, no evidence of stall was observed, even though C_N and α appeared to exceed by significant margins the static stall values obtained in two-dimensional tests [2].

As rotors are pushed to greater thrust levels, the retreating blade angles of attack increase until stall is inevitable. Fig. 3 shows conditions at the 75% radius location for two of the test points reported in References 3 and 4.* The most distinguishing features of the heavily stalled case are the enormous values of C_N and C_M and the fact that "moment stall" precedes "lift stall" by some 25° in azimuth. Furthermore, the retreating blade pressure distributions, Fig. 4, were unlike anything ever observed in static airfoil or hover tests. Rather, they seemed to indicate the formation and shedding of a vortex-like disturbance from the leading edge region, as suggested by Ham and Garelick, [5] followed by large transients in the pressure distribution as this disturbance drifted rearward over the upper surface. As indicated in Fig. 5, the model rotor successively experienced dynamic overshoot of the static stall angle before stall began, followed by vortex shedding and, finally, stall flutter. More detailed descriptions of this phenomenon have been given in References 3-6; the point here is that none of the classical notions about stall on fixed-wing aircraft seem applicable to the helicopter rotor in forward flight.

Since the high speed helicopter rotor blade operates in such a highly unsteady, three-dimensional, and rotating environment, it is not surprising that its aerodynamic characteristics differ considerably from those of fixed wing aircraft. The major questions facing us, then, are (1) how does the structure of the viscous flow on rotating blades differ from that on classical airfoils, and (2) how can the essential features of retreating blade stall be modeled without recourse to an actual helicopter rotor?

2. ROTOR BLADE BOUNDARY LAYER THEORY

In many applications of fluid mechanics, classical thin boundary layer theory provides valuable information concerning skin friction distributions, heat transfer rates, and separation characteristics. However, the general problem of stall on lifting surfaces remains unsolved, even in the relatively simple case of a steady two-dimensional airfoil. Therefore, we should not expect to be able to analyze helicopter retreating blade stall completely within the framework of boundary layer theory. What we can hope for is twofold: first, to derive the predominant parameters and assign relative orders of importance to the various physical effects, and second, to infer something useful about helicopter stall characteristics from the skin friction behavior on rotating blades. From this sort of theoretical understanding, coupled with experimental data, we should be able in the future to empirically model the phenomenon well enough to predict when retreating blade stall will occur, what its consequences will be, and what improvements can be designed into rotor systems.

* A brief description of the model rotor is given in the Appendix.

The boundary layer equations in the coordinate system depicted in Fig. 1 are the following [7-8]:

$$\frac{\partial u}{\partial x} + \frac{\partial v}{\partial y} + \frac{\partial w}{\partial z} = 0 \quad (1)$$

$$\frac{\partial u}{\partial t} + u \frac{\partial u}{\partial x} + v \frac{\partial u}{\partial y} + w \frac{\partial u}{\partial z} - 2\Omega w \cos \gamma = \frac{\partial \tau_x}{\partial y} - \Omega^2 x - \frac{1}{\rho} \frac{\partial p}{\partial x} \quad (2)$$

$$\frac{\partial w}{\partial t} + u \frac{\partial w}{\partial x} + v \frac{\partial w}{\partial y} + w \frac{\partial w}{\partial z} + 2\Omega u \cos \gamma = \frac{\partial \tau_z}{\partial y} - \Omega^2 z - \frac{1}{\rho} \frac{\partial p}{\partial z} \quad (3)$$

where

$$-\frac{1}{\rho} \frac{\partial p}{\partial x} = \frac{\partial U_e}{\partial t} + U_e \frac{\partial U_e}{\partial x} + W_e \frac{\partial U_e}{\partial z} - 2\Omega W_e \cos \gamma + \Omega^2 x \quad (4)$$

Following Ref. 8, it is illuminating to write Eqns. 1 and 2 with the dominant or primary terms on the left hand side and the secondary terms on the right hand side. Then with the aid of Eqn. 4,

$$u \frac{\partial u}{\partial x} + v \frac{\partial u}{\partial y} - \frac{\partial \tau_x}{\partial y} - U_e \frac{\partial U_e}{\partial x} = \underbrace{\frac{\partial}{\partial t}(U_e - u)}_{\text{unsteady}} - \underbrace{2\Omega(W_e - w) \cos \gamma}_{\text{Coriolis}} + \underbrace{(W_e - \frac{wU_e}{U_e}) \frac{\partial U_e}{\partial z} - wU_e \frac{\partial U_e}{\partial z}}_{\text{crossflow momentum flux}} \quad (6)$$

It should be noted that the centrifugal force term does not appear explicitly in Eqn. 6, by virtue of Eqn. 4. Also, the inviscid Coriolis and crossflow momentum flux terms have been combined with the secondary viscous terms. These inviscid terms impress an important effective pressure gradient,

$$W_e \frac{\partial W_e}{\partial x} = -2\Omega W_e + W_e \frac{\partial U_e}{\partial z} \quad (7)$$

on the chordwise momentum equation (see References 7-9).

To a first approximation, the terms on the right side of Eqn. 6 can be considered in effect to play the role of additional chordwise pressure gradients. Thus departures from classical two-dimensional steady boundary layer behavior will be due to unsteady, Coriolis, and spanwise gradient effects. Furthermore, when the sign of these terms is positive, the primary flow will be accelerated, the skin friction will increase, and separation should be delayed. When they are negative, the chordwise flow will be decelerated and separation should occur earlier. Examples of these effects that could delay separation on a helicopter rotor in forward flight are following:

- (1) Increasing angle of attack, e.g., the second and third quadrants. This causes $(U_e - u)$ to increase at a positive rate.
- (2) Increasing local blade element velocity, e.g., the first and fourth quadrants. This also produces a positive rate of change in $(U_e - u)$.
- (3) Crossflow radially inward, e.g., the second and third quadrants. This produces a positive net Coriolis acceleration. Also, the crossflow derivative in the continuity equation couples favorably with the primary flow (see Ref. 8).
- (4) Crossflow radially outward, e.g., the first and fourth quadrants. This produces a positive net spanwise momentum flux.

From these examples, it is clear that a complex competition exists between the several secondary terms, depending upon the azimuthal position of the blade and the detailed u and w velocity profiles. Extrapolating from flat plate studies, McCroskey, et al [7,8] concluded that maximum separation delay would occur in the third quadrant, while Williams and Young [9] found maximum delay at $\psi = 0$ on a Joukowski airfoil. We shall see in Section 3 that both miss the essence of retreating blade stall.

2.1 The Question of Radial Flow

The magnitude and importance of radial flow, or crossflow, has preoccupied rotor aerodynamicists for years. Fogarty's [10] and many subsequent analyses of the laminar hover case have indicated that the centrifugal pumping on a high aspect ratio blade is much less than on the classical von Karman rotating disc, but the notion persists that radial flow is an important factor in rotor blade stall.

2.1.1 Hover or Axial Flow -- Several measurements [11-17] of radial flow are summarized in Table 1. In these cases, the translational velocity is either zero (rotor) or purely axial (propeller), and δ denotes the surface streamline direction relative to circular arcs. The reported results seem to fall into two categories. Except for localized regions of separated flow, high aspect ratio blades exhibit small skew angles and approximately two-dimensional characteristics, whereas large skew angles and anomalous behavior have been observed on blades of marine propeller proportions.

Fig. 6 shows the surface streamline directions that have been predicted by various investigators [8,9,18,19]. The remarkable difference between laminar and turbulent skew angles is due to the fact that near the wall, the much smaller chordwise momentum defect and larger shear stress gradients of turbulent boundary layers make the centrifugal pumping effect much smaller in the turbulent case.

The effect of radial flow on the loci of $\tau_x = 0$, which for rotor applications closely approximates the limiting streamline behavior of three-dimensional separation, is illustrated in Fig. 7 for several types of chordwise pressure distributions [8,9,20]. These laminar results illustrate two important aspects of rotating blades. First, the effects of rotation become more pronounced near the axis of rotation, while the two-dimensional results are approached as z increases. Second, rotational effects on the position of laminar separation are strongly suppressed by increasing chordwise pressure gradients, and they are of no consequence outboard of $z/c \sim 2$ for a rotating blade at large incidence. This has been confirmed in the experiments of Ref. 15 and can be inferred from the data of References 14 and 16.

2.1.2 Forward Flight -- The forward flight case has received less attention than hover, because of the additional complications of unsteady effects. As a result, fewer quantitative estimates of the magnitude and importance of radial flow in forward flight are available.

However, one important facet of radial flow has been established [7-9,20]. In general, crossflow due to the spanwise component of the forward flight velocity, $V_1 \cos \psi$, totally predominates over centrifugal pumping. This is apparent in the radial velocity profiles shown in Fig. 8 for a flat plate blade, and in the measurements [17,22] that have shown the flow directions to be approximately those of the undisturbed streamline, β_0 .

Fig. 9 shows the laminar results of Williams and Young [9] for the variation in the position of $\tau_x = 0$, including both unsteady and radial flow effects. Although Williams and Young chose atypical variations of α vs ψ , the main conclusion that can be drawn from the figure is that, like the hover results in Fig. 7, the position of laminar separation depends much more strongly upon the local instantaneous value of α , and hence upon the local chordwise pressure gradients, than upon radial flow. It is clear that the features of retreating blade stall cannot be explained from these results.

Hicks and Nash [21] neglected unsteady effects and calculated the three-dimensional turbulent boundary layer flow for the rotor conditions shown in Fig. 2. Their quasi-steady results were highly pessimistic on the retreating blade, predicting separation over the whole airfoil when in fact the boundary layer remained attached.

Despite these difficulties, Hicks and Nash were able to demonstrate the effects of radial flow at blade azimuths where α was small, and Fig. 10 shows a typical case. These results demonstrate the competing secondary factors described in the beginning of this section. Near the leading edge, the

inviscid crossflow momentum flux, $W_e \frac{\partial U_e}{\partial x}$ in Eqn. 6, is the largest secondary term and consequently τ_x

is increased over the two-dimensional value. Near the trailing edge, the Coriolis term becomes relatively more important, and τ_x is less than the two-dimensional value. However, the magnitude of the crossflow effects does not seem to be anywhere near the magnitude of stall effects that are suggested by Figures 3-4.

2.2 Unsteady Boundary Layer Effects

From many two-dimensional flat plate studies, it is well known that the magnitude of τ and its phase relative to U_e are strongly affected by unsteady effects. For example, Fig. 11 shows laminar and turbulent results calculated by H. A. Dwyer* for high speed rotor conditions and a very wide chord blade. As in the case of the hover skew angles shown in Fig. 6, the turbulent boundary layer is less sensitive to the secondary effect of unsteady U_e than is the laminar case.

The logical extension from flat plate results is to unsteady airfoils with pressure gradients. In the rotor case, both the blade element velocities and angles of attack vary, as shown in Fig. 3. Accordingly, these two effects are treated separately in Figures 12 and 13. For the sake of studying boundary layer effects alone, the potential flow is taken to be quasi-steady in these two figures. We see that the unsteady viscous effects do affect the position of $\tau_x = 0$, but only at angles of attack well below the stall angle. Therefore, we still do not have an explanation of why retreating blade stall is so different from static stall.

On the other hand, Carta [24] recently proposed that the unsteady potential flow on an oscillating airfoil might contribute to a delay in dynamic stall, due to the attenuation and phase lag of the unsteady chordwise pressure gradients. Accordingly, Fig. 14 shows the change in the position of $\tau_x = 0$ when this effect is taken into account, using the recent unsteady inviscid analysis of Ref. 25. Indeed, much larger unsteady effects are apparent, in comparison with Fig. 13, and the results seem to indicate that an important feature of the problem has been illuminated.

Fig. 15 shows the relative importance of unsteady inviscid and viscous effects on laminar separation on an oscillating airfoil, as a function of the frequency of the oscillation. The unsteady inviscid effect is clearly the predominant one, and the good agreement with measurements** of the position of a laminar separation bubble is encouraging. However, we shall see in Section 3 that dynamic stall is more complicated and cannot be predicted on the same basis.

* Private communication. The turbulent results were obtained using an eddy viscosity model with the steady empirical constants of Cebeci and Smith [23].

** The oscillating airfoil model is described in the Appendix.

2.3 Summary of Boundary Layer Effects

The details of the several analyses of radial flow are interesting in a basic sense, as they give the skew angles and changes in skin friction distributions that occur on rotating blades. However, for cases with realistic chordwise pressure distributions, radial flow does not seem to produce anywhere near the magnitude of effects that are suggested by Figures 3 and 4. Likewise, laminar unsteady viscous effects are very small at angles of attack approaching the stall angle. The flat plate results shown in Fig. 11 suggest that turbulent flows will exhibit even smaller unsteady effects, although this remains to be demonstrated for flows with adverse pressure gradients. However, large effects have been found when the unsteady nature of the potential flow is properly treated. This suggests further consideration should be given to unsteady aerodynamics, and that perhaps there are important interactions between viscous and inviscid effects.

3. DYNAMIC STALL

Several investigators [3,26-29] have indicated that significant improvements in helicopter rotor airloads calculations can be obtained by utilizing two-dimensional unsteady airfoil data. An important link between rotor and unsteady airfoil behavior was provided recently by McCroskey and Fisher [3,4] and is shown in Fig. 16. The figure shows Ham and Garelick's unsteady two-dimensional data [5] superimposed on graphs of model rotor data for nearly identical dimensionless parameters. Open symbols denote unstalled data and the solid symbols stalled conditions. Each symbol on the right hand graph has a corresponding angle of attack symbol on the left hand graph. On both models, the suction near the leading edge began to collapse at $\alpha \sim 19.5^\circ$.

A plot of C_M vs C_N is a sensitive indicator of departures from classical steady airfoil behavior. With this in mind, the striking agreement in Fig. 16 between the model rotor and unsteady airfoil data is remarkable, especially up to the point of complete stall. Beyond this point, the flexible model rotor blade began to flutter, and in the azimuth range $270^\circ < \psi < 360^\circ$, stronger three-dimensional effects and plunging motion of the rotor blade probably produced a significantly different blade-element environment. Nevertheless, the essential features of retreating blade stall seem to be well duplicated by the two-dimensional unsteady airfoil. This is the essential point here, because it indicates that future research efforts can rely more heavily on unsteady airfoil studies. This is obviously a major simplification, and the remainder of this paper deals primarily with oscillating airfoils.

3.1 The Onset of Dynamic Stall

The good agreement between theory and experiment shown in Fig. 15 suggests attempting the same sort of correlation for the onset of dynamic stall, and this is shown in Fig. 17. The stall data [29-32] correspond to "moment stall" angles of attack where nose-down pitching moments increase abruptly; the maximum lift and pitching moment usually occur slightly later [33].

The moment stall delay rises rapidly with increasing frequency to the point where stall occurs at the maximum angle in the cycle, i.e., $\alpha_{ps} = \alpha_0 + \alpha_1$. Also shown in the figure are the angles predicted by the recent analysis of Crimi and Reeves [34]. The two theoretical predictions fall far short of the data, indicating that some sort of unsteady viscous effects that were not present in the laminar separation results, Fig. 15, must be influencing the dynamic stall delay.

The hot wire measurements shown in Fig. 17 indicate that in the present experiment, the inviscid flow began to break down somewhat in advance of moment stall. Fig. 18 shows the signals from the hot wires, pressure transducer, and skin friction gage as the airfoil oscillated in and out of stall. The hot wire at $x/c = 0.75$ indicated some amount of trailing edge separation before stall, but it is interesting to note that all transducers indicate a major change at approximately the same instant.

One of the most interesting aspects of Fig. 18 is that the suction at $x/c = 0.1$ continues to rise, whereas the velocity decreases rapidly after the onset of stall. This means that a viscous-inviscid interaction has begun during which pressure and velocity are not at all related by the usual Bernoulli relation.

The model rotor pressure measurements, Fig. 4, seemed to indicate that during the onset of dynamic stall, a vortex-like disturbance was shed from the leading edge region and grossly distorted the flow field as it passed over the airfoil, as discussed by Ham and Garelick [5] and Philippe [6]. Unfortunately, the oscillating airfoil model had only one pressure transducer, and so this phenomenon could not be observed. The hot wires and skin friction gage indicated fully separated flow, so in this regard, Fig. 18 really raises more questions than it answers.

3.2 Maximum Forces and Moments During Dynamic Stall

The helicopter engineer wants to know how to predict blade airloads during dynamic stall. Several methods are available [27,35,36], but to review them is beyond the present scope or intent. However, it is interesting to inquire what upper limits of force and moment coefficients exist, as these affect performance, blade motion, and vibratory loads.

Fig. 19 shows coefficients from a number of sources [3,4,5,29,30,36,37,38], including rotors and two-dimensional airfoils. The figure is not meant to be all-inclusive; the main point is to indicate the wide range of magnitudes that have been obtained. The oscillating airfoil data are arbitrarily limited to $\alpha_0 \sim \alpha_{ss}$, to $M \leq 0.3$, and to sets of data that include some test points where the airfoil stalled before reaching the maximum angle of attack (solid symbols). Otherwise, the full potential of unsteady aerodynamics was probably not realized.

With the exception of Ham and Garelick's results, the abscissa in Fig. 19 is the nondimensional pitch rate evaluated at the static stall angle. We should not expect this to be a unique correlating

parameter, however, because it does not include any dependence upon the total amplitude of the unsteady motion. For example, an oscillating airfoil will stall at $\alpha_{PS} = \alpha_0 + \alpha_1$ if the amplitude α_1 is small, while it will stall at $\alpha_{PS} < \alpha_0 + \alpha_1$ (although at a greater α_{PS} than before) if α_1 is large. On the other hand, Ham and Garelick's $\dot{\alpha}/v$ evaluated at α_{PS} is inadequate for oscillating airfoils, since they may stall at the top of the cycle, where $\dot{\alpha} = 0$.

Finally, we should note the enormous values of C_N and C_M that sometimes occur. These are not predicted by the empirical models of References 27, 35, and 36, especially the pitching moment coefficients in excess of 0.4.

4. CONCLUDING REMARKS

Considerable progress has been made in recent years in analyzing and understanding rotor blade boundary layers, but so far the mere addition of unsteady, three-dimensional, and rotational terms to classical thin boundary layer theory has failed to explain the primary characteristics of retreating blade stall.

However, the combined information from analyses and experiments indicates that combined viscous and inviscid unsteady effects are important, and much more so than rotational and yawed flow effects. Therefore, it seems that a great deal of valuable information can be obtained from unsteady two-dimensional studies, both theoretical and experimental. Flow visualization and detailed boundary layer measurements during the series of events that comprise dynamic stall are badly needed to guide theoretical unsteady viscous-inviscid interaction studies. In addition, the existing force and moment data, and perhaps new data, need to be analyzed further to establish the parameters that determine the maximum values of C_N and $-C_M$. New tests should concentrate more on the larger amplitudes and lower frequencies that seem to be characteristic of the once-per-rev $\alpha(\psi)$ at extreme operating conditions.

Most of the available rotor data were obtained on conventional fully articulated blades. Therefore, there appears to be a need for some further rotor tests, to see whether the basic fluid dynamic characteristics of retreating blade stall are the same for other rotor types, even though the physical manifestations of stall and practical limitations that arise from stall may be different.

Finally, radically new ideas are needed on the subject of airfoil design for dynamic environments. Most major helicopter manufacturers have now come to accept the concepts of leading edge camber and thin tips to improve static airfoil characteristics, and this generally improves retreating blade stall boundaries as well. But so far, no one has met the challenge of avoiding or softening dynamic stall to any significant degree. Surely there are ways to solve this problem without abandoning the rotor altogether.

5. REFERENCES

1. Rabbott, J. P. Jr.; Lizak, A. A.; and Paglino, V. M. "A Presentation of Measured and Calculated Full Scale Rotor Blade Aerodynamic and Structural Loads," U. S. Army USAAVLABS Technical Report TR 66-31, 1961.
2. Lizak, A. A. "Two-Dimensional Wind-Tunnel Tests of a H-34 Main Rotor Airfoil Section," U. S. Army TREC Technical Report 60-53, 1960.
3. McCroskey, W. J.; and Fisher, R. K. Jr. "Detailed Aerodynamic Measurements on a Model Rotor in the Blade Stall Regime," J. American Helicopter Society, Vol. 17, No. 1, pp. 20-30, 1972.
4. Fisher, R. K. Jr.; Tompkins, J. E.; Bobo, C. J.; and Child, R. F. "An Experimental Investigation of the Helicopter Rotor Blade Airloads on a Model Rotor in the Blade Stall Regime," NASA/US Army AMRDL Contractor Report CR 114424, 1972.
5. Ham, N. D.; and Garelick, M. S. "Dynamic Stall Considerations in Helicopter Rotors," J. American Helicopter Society, Vol. 13, No. 2, 1968, pp. 49-55, 1968.
6. Philippe, J. J. "Le Decrochage Instationnaire d'un Profil," L'Aeronautique et l'Astronautique, Vol. 27, 1971, pp. 51-57.
7. McCroskey, W. J.; and Yaggy, P. F. "Laminar Boundary Layers on Helicopter Rotors in Forward Flight," J. AIAA, Vol. 6, No. 10, pp. 1919-1926, 1968.
8. McCroskey, W. J.; and Dwyer, H. A. "Methods of Analyzing Propeller and Rotor Boundary Layers," NASA SP-228, pp. 473-514, 1969; also J. AIAA, Vol. 9, No. 8, pp. 1498-1505, 1971.
9. Williams, J. C. III; and Young, W. H. Jr. "The Laminar Boundary Layer on a Rotating Blade of Symmetrical Airfoil Shape," U. S. Army USAAVLABS Technical Report 70-64, 1970; also AIAA Paper 70-49, 1970.
10. Fogarty, L. E. "The Laminar Boundary Layer on a Rotating Blade," J. Aero Sci., Vol. 18, No. 4, pp. 247-252, 1951.
11. Himmelskamp, H. "Profiluntersuchungen an einem umlaufenden Propeller" No. 2, Mitteilungen der Max-Planck Inst., Gottengen, 1950.
12. Gutsche, F. "Versuche an umlaufenden Flügelschnitten mit abgerissener Strömung" Jahrb. Schiffbautechn. Gesellschaft Bd. 41, pp. 188-226, 1940.

13. Berry, L. W. "Propeller Boundary Layer Flow and Scale Effect" National Phys. Lab. Ship Division Report SH R12/59, 1959.
14. Tanner, W. H. and Yaggy, P. F. "Experimental Boundary Layer Study on Hovering Rotors" J. American Helicopter Society, Vol. 11, No. 3, pp. 22-37, 1966.
15. McCroskey, W. J. "Measurements of Boundary Layer Transition, Separation, and Streamline Direction on Rotating Blades" NASA TN D-6321, 1971.
16. Velkoff, H. R., Blaser, D. A. and Jones, K. M. "Boundary Layer Discontinuity on a Helicopter Rotor Blade in Hovering" AIAA J. Aircraft, Vol. 8, No. 2, pp. 101-107, 1971.
17. Blaser, D. A. and Velkoff, H. R. "A Preliminary Analytical and Experimental Investigation of Helicopter Rotor Boundary Layers" AIAA Paper 72-38, 1972; also American Helicopter Society Preprint No. 622, 1972.
18. Banks, W. H. H. and Gadd, G. E. "A Preliminary Report on Boundary Layers on Screw Propellers and Simpler Rotating Bodies" National Phys. Lab. Ship Division Report SH R27/62, 1962.
19. McCroskey, W. J., Nash, J. F., and Hicks, J. G. "Turbulent Boundary Layer Flow over a Rotating Flat Plate Blade" J. AIAA Vol. 9, No. 1, pp. 188-189, 1971.
20. Liu, S. W. "The Laminar Boundary Layer Flow on Rotating Cylinders" U. S. Air Force OSR Report TN57-298, 1957.
21. Hicks, J. G. and Nash, J. F. "The Calculation of Three-Dimensional Turbulent Boundary Layers on Helicopter Rotors" NASA Contractor Report CR-1845, 1971.
22. Bowden, T. H. and Shockey, G. A. "A Wind Tunnel Investigation of the Aerodynamic Environment of a Full-Scale Helicopter Rotor in Forward Flight" U. S. Army USAAVLABS Technical Report 70-35, 1970.
23. Cebeci, T., Smith, A. M. O. and Mosinskis, G. "Calculation of Compressible Adiabatic Turbulent Boundary Layers" J. AIAA, Vol. 8, No. 11, pp. 1973-1982, 1970.
24. Carta, F. O. "A Theoretical Study of the Effect of Unsteady Pressure Gradient on Dynamic Stall Delay" AIAA J. Aircraft, Vol. 8, No. 10, pp. 839-841, 1971.
25. McCroskey, W. J. "The Inviscid Flow Field of an Unsteady Airfoil" AIAA Paper 72-681, 1972.
26. Johnson, W. "The Effect of Dynamic Stall on the Response and Airloading of Helicopter Rotor Blades" J. American Helicopter Society, Vol. 14, No. 2, pp. 68-79.
27. Tarzanin, F. J. Jr. "Prediction of Control Loads Due to Blade Stall" J. American Helicopter Society, Vol. 17, No. 2, pp. 33-46, 1972.
28. Bellinger, E. D. "Analytical Investigation of the Effects of Blade Flexibility, Unsteady Aerodynamics, and Variable Inflow on Helicopter Rotor Stall Characteristics" American Helicopter Society Preprint No. 520, 1971.
29. Carta, F. O.; and Niebanck, C. F. "Prediction of Rotor Stability at High Forward Speeds. Vol. III Stall Flutter," U. S. Army USAAVLABS Technical Report 68-18C, 1969.
30. Windsor, R. I. "Measurement of Aerodynamic Forces on an Oscillating Airfoil," U. S. Army USAAVLABS Technical Report 69-98, 1970.
31. Liiva, J.; and Davenport, F. J. "Two Dimensional Tests of Airfoils Oscillating near Stall," U. S. Army USAAVLABS Technical Report 68-13, 1968.
32. Halfman, R. F.; Johnson, H. C.; and Haley, S. M. "Evaluation of High Angle-of-Attack Aerodynamic Derivative Data and Stall-Flutter Prediction Techniques," NACA TN 2533, 1951.
33. Harris, F. D.; and Pruyn, R. R. "Blade Stall - Half Fact, Half Fiction," J. American Helicopter Society, Vol. 13, No. 2, pp. 27-48, 1968.
34. Crimi, P.; and Reeves, B. L. "A Method for Analyzing Dynamic Stall," AIAA Paper No. 72-37, 1972.
35. Arcidiacono, P. J.; Carta, F. O.; Casellini, L. M.; and Elman, H. L. "Investigation of Helicopter Control Loads Induced by Stall Flutter," U. S. Army USAAVLABS Technical Report 70-2, 1970.
36. Ericsson, L. E.; and Reding, J. P. "Analytical Prediction of Dynamic Stall Characteristics," AIAA Paper No. 72-682, 1972.
37. Gray, L.; Liiva, J.; and Davenport, F. J. "Wind Tunnel Tests of Thin Airfoils Oscillating Near Stall," U. S. Army USAAVLABS Technical Report 68-89, 1969.
38. Scheiman, J.; and Kelley, H. L. "Comparison of Flight-Measured Helicopter Rotor-Blade Chordwise Pressure Distributions with Static Two-Dimensional Airfoil Characteristics," NASA TN D-3936, 1967.
39. McCroskey, W. J.; and Durbin, E. J. "Flow Angle and Shear Stress Measurements with Heated Wires and Films," ASME J. of Basic Engr., Vol. 94, Series D, No. 1, pp. 46-52, 1972.

APPENDIX

The model rotor utilized in the McCroskey and Fisher experiment [3] was dynamically representative of one of the main rotors of a Boeing CH-47C helicopter, with blades of 1.18 m span, 0.085 m chord, -9° linear twist, and a modified NACA 23010 airfoil. They were constructed of balsa wood and fiberglass and were instrumented at the 75 percent radius station with absolute pressure transducers and directionally-sensitive heated-film skin friction gages [39].

The pressure measurements utilized 3 mm diam Kulite ultraminiature semiconductor pressure transducers, mounted at 11 chordwise locations on the top of the blade

and 8 locations on the bottom. In addition, a differential pressure transducer was located between orifices at $x/c = 0$ and $x/c = 0.025$ on the lower surface; data from this transducer were used in estimating the local blade-element angles of attack. The pressure transducers were imbedded in silastic rubber beneath 0.1 mm dia. holes, and the skin friction gages were bonded flush on the surface of the blade. More complete discussions of the instrumentation, test procedures, and other data are available in References 3 and 4.

The oscillating airfoil data shown in Figures 15 and 17 were obtained* on a NACA 0012 model of 15.2 cm chord and 30.5 cm span, pitching about $x/c = 0.25$ and tested at $Re_\theta = 3.5 \times 10^5$ and 5×10^5 . The instrumentation consisted of a heated-film skin friction gage [39] and a Kulite pressure transducer at $X = 0.1$, and hot wire anemometers at $X = 0.1, 0.25$, and 0.75 .

The hot wires were normally mounted just outside the boundary layer and used to detect large scale disturbances in the inviscid flow that might be symptomatic of stall. The skin friction gage provided boundary layer transition and separation information. Oil flow visualization at $k = 0$ confirmed the skin friction gage and hot wire indications that transition to turbulence was triggered by a short laminar separation bubble that moved forward over the airfoil as α increased. Therefore, the experiment produced a distinct boundary layer separation event that did not interact significantly with the inviscid flow, in addition to producing the more complicated conditions of stall.

TABLE 1. SUMMARY OF RADIAL FLOW EXPERIMENTS

Reference	Geometry	Boundary Layer State	Skew Angles, β , Upstream of Separation	Remarks
Himmelskamp [11]	propeller $C/R \sim 0.5$	not specified	$5^\circ - 15^\circ$	lift and drag higher than 2-D data
Gutsche [12]	propellers $0.1 < C/R < 0.4$	lam. and turb.	$0 - 20^\circ$	complex separation patterns
Berry [13]	propeller $C/R \sim 0.5$	lam. and turb.	$0 - 30^\circ$	β large for laminar small for turbulent
Tanner & Yaggy [14] McCroskey [15]	rotors $0.1 < C/R < 0.2$	lam. and turb.	$\beta \sim 0$	transition un- affected by rotation
Velkoff et al [16]	rotors $0.1 < C/R < 0.2$	laminar	$\beta \sim 0$	flow visualization; large β within separation bubble
Blaser & Velkoff [17]	rotor $C/R \sim 0.2$	laminar	$5^\circ - 15^\circ$	hot wire data

* The assistance of T. M. Wynn in planning and conducting the experiment is gratefully acknowledged.

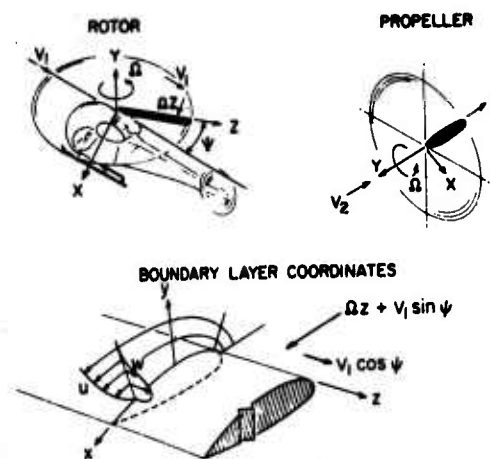


Fig. 1 Coordinate in the rotating system, with V_1 in the plane of the disc and V_2 normal to the disc.

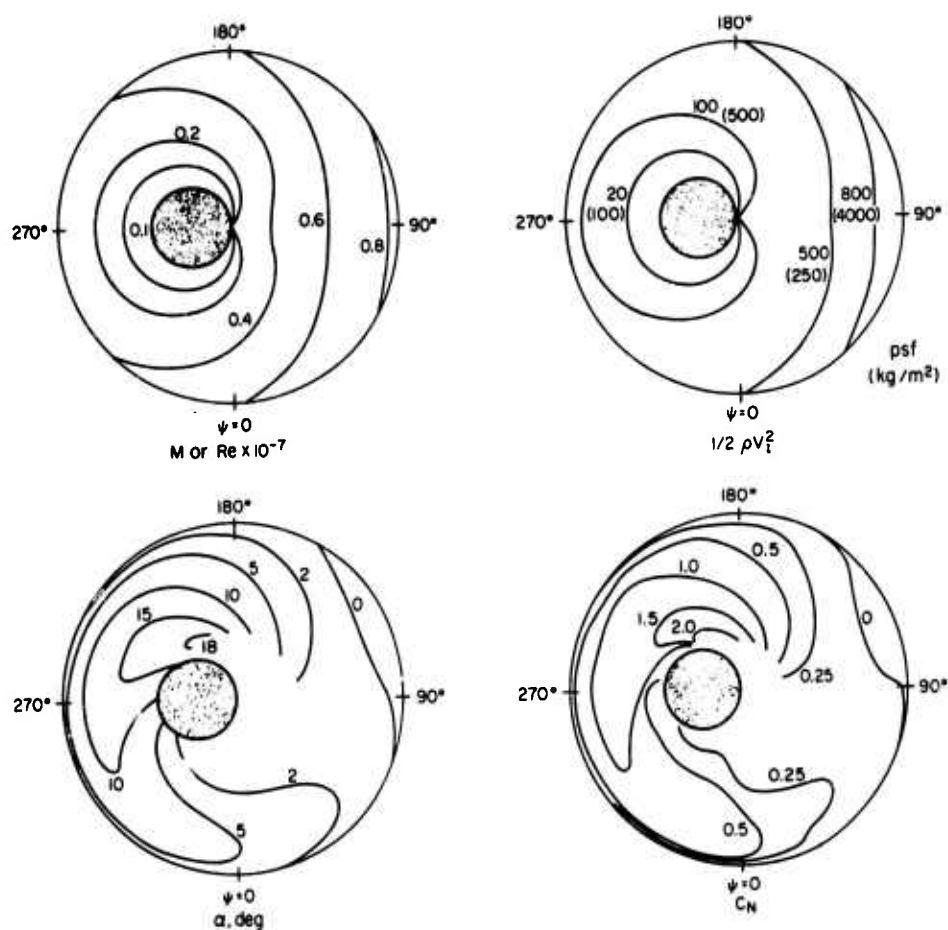


Fig. 2 Representative rotor conditions for high speed flight below stall, based on the measurements of Ref. 1; $\mu = 0.45$, $C_T/\sigma = 0.05$. Static $C_{N_{max}} \sim 1.3$.

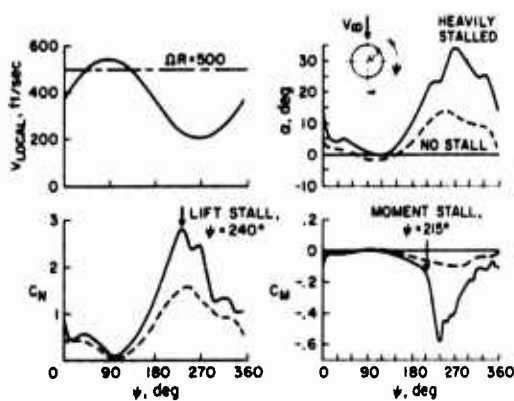


Fig. 3 The blade-element environment and measured airfoil characteristics for the model rotor of Ref. 3; $\mu = 0.35$, $C_T/\sigma = 0.074$ and 0.132 , $z/R = 0.75$. Static $C_{N_{max}} \sim 1.1$.

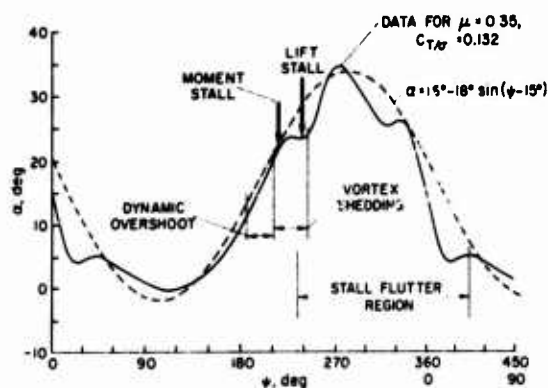


Fig. 5 The variation in angle of attack on the model rotor, showing the sequence of events during retreating blade stall.

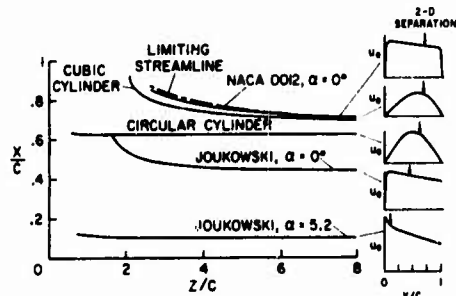


Fig. 7 The effect of rotation on the chordwise position of zero laminar shear stress for rotating blades in hover or axial flow [8,9,20].

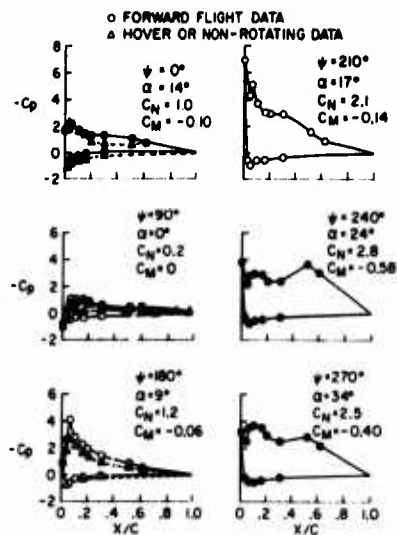


Fig. 4 Measured pressure distributions on the model rotor [3] at $C_T/\sigma = 0.132$. Solid symbols stalled, open symbols unstalled.

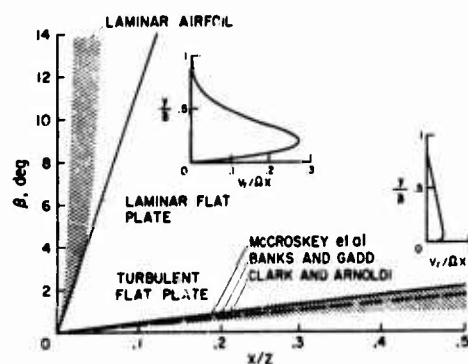


Fig. 6 Surface streamline directions relative circular arcs for rotating blades in hover or axial flow.

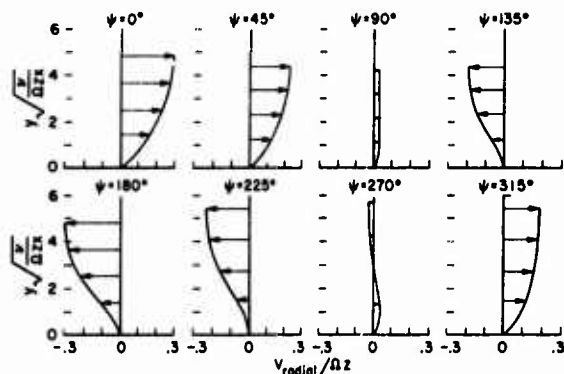


Fig. 8 Radial velocity profiles on a flat plate blade in forward flight; $x/z = 0.1$, $V_1/\Delta z = 0.3$.

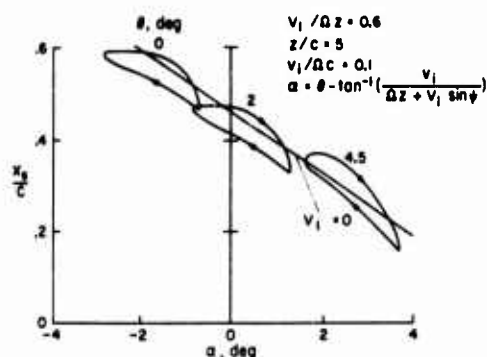


Fig. 9 The variation in the chordwise position of laminar separation on a Joukowski airfoil in forward flight [9].

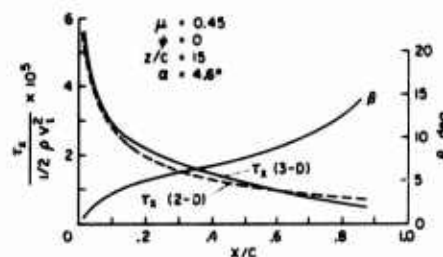


Fig. 10 Quasi-steady results [21] for turbulent shear stress and surface streamline direction at $z/R = 0.75$ for the forward flight conditions of Fig. 2; $\beta_0 = 31^\circ$.

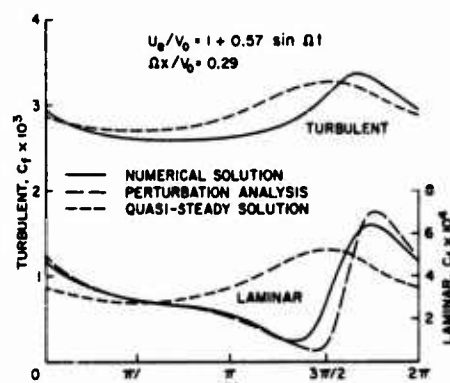


Fig. 11 The effect of an oscillating free stream on flat plate shear stress at $Re_0 = 4 \times 10^6$. (Note the enlarged scale for the laminar case).

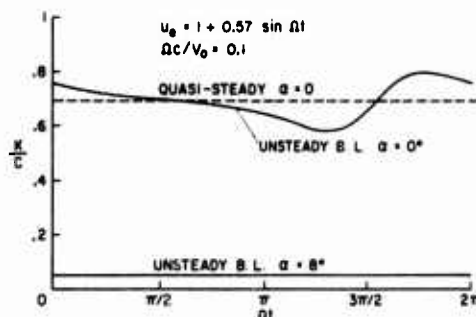


Fig. 12 The effect of oscillating free stream velocity on the position of zero laminar shear stress on a NACA 0012 airfoil.

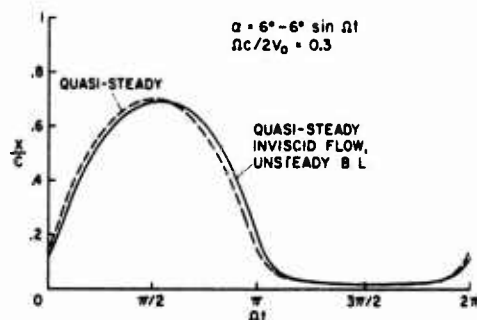


Fig. 13 The effect of oscillating angle of attack on the position of zero laminar shear stress on a NACA 0012 airfoil.

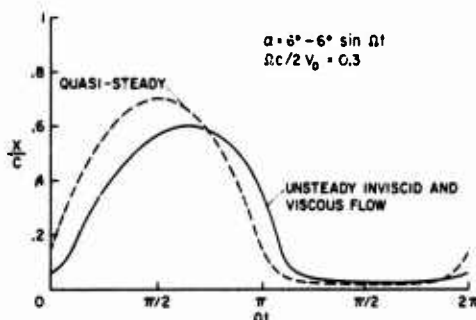


Fig. 14 The effect of oscillating angle of attack on the position of zero laminar shear stress on a NACA 0012 airfoil.

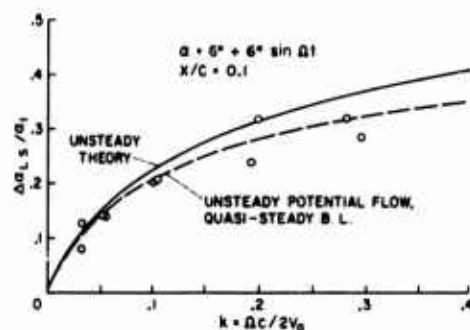


Fig. 15 Comparison of the theoretical and experimental dynamic delay in laminar separation at $x/c = 0.1$ on a NACA 0012 airfoil.

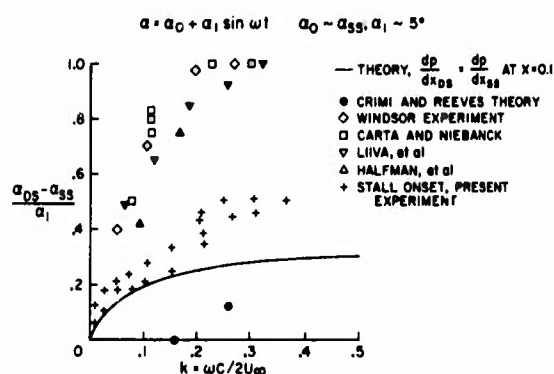


Fig. 17 Theoretical and experimental stall delay on oscillating airfoils. Open symbols denote moment stall data, + denotes initial breakdown of the potential flow.

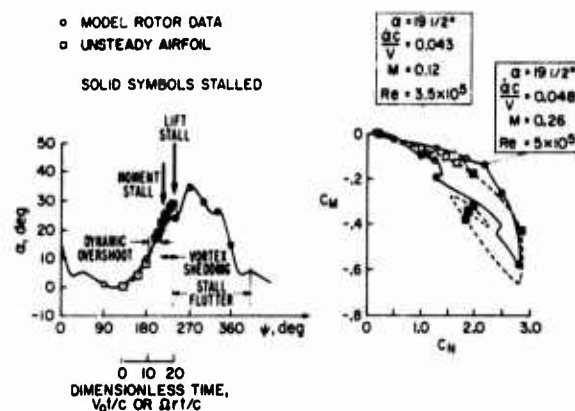


Fig. 16 Correlation of the model rotor data of Ref. 3 with the two-dimensional unsteady airfoil measurements of Ref. 5. Solid symbols stalled, open symbols unstalled.

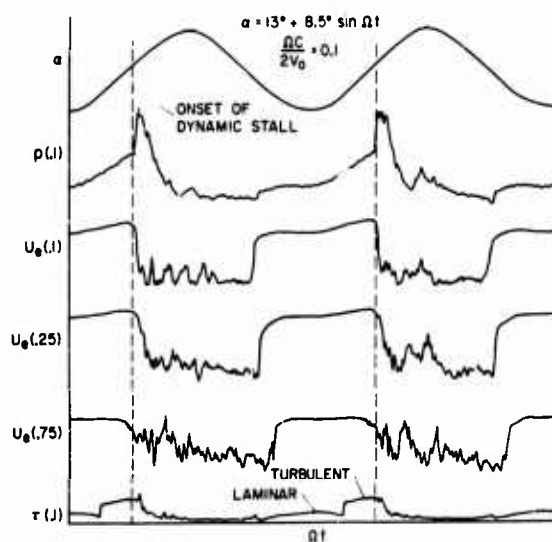


Fig. 18 Pressure transducer, hot wire, and skin friction gage signals obtained on an oscillating NACA 0012 airfoil.

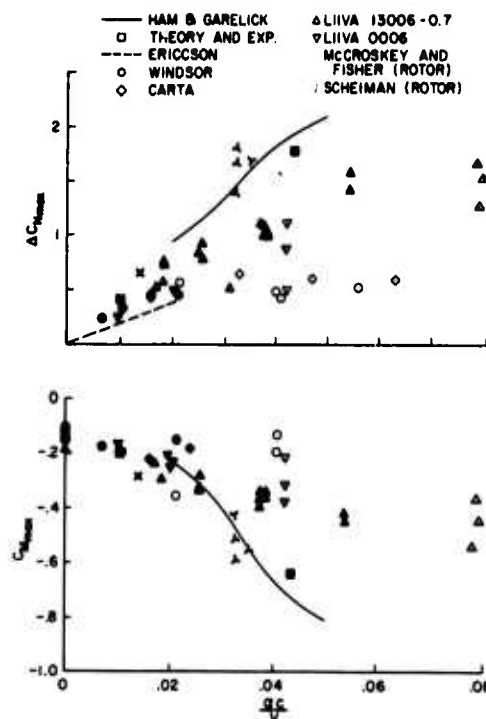


Fig. 19 Maximum normal force and pitching moment coefficients on oscillating airfoils and helicopter rotors.

THE DERIVATION AND VERIFICATION OF A NEW ROTOR PROFILE ON THE BASIS OF FLOW PHENOMENA; AEROFOIL RESEARCH AND FLIGHT TESTS

H. H. Pearcey, P. G. Wilby, M.J. Riley, P. Brotherhood
Aerodynamics Department
Royal Aircraft Establishment, Farnborough, Hants., England

SUMMARY

An account is given of some of the considerations that governed the derivation of new profiles to be incorporated in the design of the rotor blades for the Lynx helicopter at its inception. The changes relative to the NACA 0012 profile were conservative but were chosen to give consistent and significant all-round improvements to the shock-induced limits on the advancing blade, to the retreating-blade thrust limits and to the loading that could be sustained without shock-wave drag in hover.

The conservation applied especially to the stalling characteristics which play such a dominant part in limiting rotor performance but which are so difficult to predict for the rotor environment.

The profiles were derived on the basis of steady flow aerofoil tests, but qualitatively similar improvements have been verified in oscillatory aerofoil tests and in flight. A novel technique, used in the latter tests, is described for measuring pressure distributions along the blade chord and across the blade wake in the region of the rotor tip in flight.

The paper includes a discussion of the flow phenomena observed on the profiles for a wide range of conditions, including flight. This draws attention especially to the crucial part played by local regions of supersonic flow and their consequences for all the limits to rotor performance considered. It suggests that the growth, breakdown and re-establishment of the limiting flows will depend strongly on the combined effects of the simultaneous variations in Mach number and incidence.

SYMBOLS

c	aerofoil chord	V	speed
C_D	drag coefficient	V_{NE}	never exceed speed
C_L	lift coefficient	x	distance along aerofoil chord
C_P	pressure coefficient	x_T	value of x at shock position
C_T	thrust coefficient		
C	net compressive turning angle	α	incidence
E	net expansive turning angle	θ	surface slope
H_0	free stream stagnation pressure	ϕ	flow deflection
M	Mach number	ψ	angle of azimuth
M_L	local Mach number	μ	advance ratio
p	static pressure	σ	rotor solidity
r	distance along blade from hub centre	ω	Prandtl-Meyer angle
R	rotor radius	Ω	angular velocity

1 INTRODUCTION

It is, we believe, fairly well-known¹ that Westland Helicopters Limited are using for the blades of the Lynx rotor new cambered profiles that were derived as part of our continuing programme of aerofoil research (at that time being done at the National Physical Laboratory, Teddington). We now have an opportunity to record not only some of the factors that figured in the derivation of these profiles but also some of the results that have established confidence that they produce the improvements expected of them when exposed to the exacting and complex three-dimensional and periodic environment of the rotor itself.

These latter results include some obtained recently in flight research on a Wessex helicopter at Bedford, as well as some from tests made by Lambourne and his colleagues on oscillating aerofoils. But, by now, of course, we draw most of our confidence from the highly successful way in which the Lynx is proving itself in flight and which is reflected in world speed records that it has already captured. The rotor, including its cambered blades, it evidently performing in the manner that its designers intended.

Quite obviously the research that we shall be describing owes a very great deal by way of stimulus and objectivity to its association with this direct application to the Lynx and to the influence of the Westland design and research teams under Mr. Speechley and Dr. Jones. The fact that the profiles were to be incorporated directly into a new rotor design (with its novel hingeless system and its advanced form of blade construction) was, as we shall see, an overriding consideration in their derivation.

The shapes emerged from an iterative interchange between the aerofoil research at Teddington and the rotor design at Yeovil. For our part, we set out to bring accumulated knowledge of aerofoil design to bear on the aerodynamic problems that were likely to limit rotor performance. Our direct experience had up to then been for fixed wings, and much of it had centred around how to design profiles for which the adverse consequences of separated flow and the shock waves could be delayed in order to allow the processes of generating lift to continue further and further into the domain of increasing incidence and stream Mach number. The fundamental principles had been quite simple - namely, how to develop the lift with the minimum level of velocity on the upper surface of the profile and, then, when these velocities did become high and often locally supersonic, how to decelerate them as smoothly as possible with the minimum

disturbance from shock waves and boundary-layer separations. Obviously these same principles were basic to the rotor problem too.

We felt convinced that, even though the rotor flows were highly three-dimensional and were periodic with azimuthal position, the manner in which many of them developed to the limiting stages of stalling, drag rise and shock-induced separation would be strongly influenced by profile shape.

We were not then by any means so clear about the nature of the profile dependence, nor for that matter of the three-dimensionality or unsteadiness. Nevertheless, we were encouraged by the success that Boeing-Vertol had had with their drooped aerofoil on the Chinook² and by the rotor-flow observations of Tanner³ and others; they had demonstrated that a knowledge of the steady flow on two-dimensional aerofoils was a viable starting point in the design of aerofoils for rotor blades.

Much has transpired in the meantime to confirm this, and many rotors are now being designed with 'advanced' profiles. True, as the characteristics of the three-dimensional flows and unsteady phenomena are progressively exposed by concurrent research they are turning out to be even more complex than expected in certain respects, and more subtle in others. For example, our own flight research illustrates how angles of incidence that are high enough to provoke severe shock-induced separations are often induced in highly localised vortex interactions and, furthermore, reveals that even in 'hover' such phenomena can become strongly periodic - only very slight relative cross winds are required to skew the vortex wake sufficiently to produce this periodicity. Nevertheless, the manner in which the flow reacts to these localised, time-dependent high incidences appears to remain profile-dependent and qualitatively similar to that observed in aerofoil tests.

2 THE BASIS FOR THE DERIVATION OF THE NEW PROFILES

The new profiles represent a reasonably conservative evolutionary change from the standard NACA 0012 profile that has been so widely studied, extensively used, and hence well proven in the rotor environment. This was a prudent and entirely appropriate requirement for profiles that were to be incorporated directly and on the basis of theory into a new rotor design. Since reliance on theory alone would be most at risk for conditions involving blade stall, and since the stalling characteristics so often dictate the limits to performance for one reason or another (e.g. control loads, instabilities, etc.), it seemed especially important to concentrate on the nature of the stall for both steady and oscillatory conditions and for different parts of the Mach number range, and to ensure as far as possible that the basic characteristics exhibited by the NACA 0012 profile were retained for the new profiles.

The present account is based almost exclusively on separated flow phenomena and on how they develop on the old and the new profiles - in steady and in oscillatory aerofoil tests and in flight. We confine ourselves to selected examples appropriate to the advancing blade, retreating-blade stall and hover.

3 AERODYNAMIC LIMITS TO ROTOR PERFORMANCE

From the aerofoil tests, we can define a boundary on the (M, α) plane (Fig.2a) beyond which significant effects of separation, or stall, would be encountered. Byham⁴, following J.P. Jones⁵, has shown that a satisfactory correlation can be obtained between aerofoil results analysed in this way and the aerodynamic limits to rotor performance encountered in flight, Fig.2b. The overall limit to rotor thrust for a given rotor, typically curve DE of Fig.2b, is associated with retreating blade stall and with the profile-related phenomena that determine the corresponding portion DE of the aerofoil separation boundary. The overall limit to forward speed (curve BC of Fig.2b) is associated with the effects of shock-induced separation on the advancing blade and with the profile-related phenomena that determine the corresponding portion BC of the aerofoil boundary.

The limits to the degree to which the blade tips can be loaded in hover are associated with conditions near point A of the separated-flow boundary (Fig.2a).

(The part AB of the separated-flow boundary corresponds to a hypothetical limit to rotor thrust - Fig.2b - that should be achievable if the retreating-blade limit could be removed in order to enable the full potential of the dynamic head to be exploited - as for the ABC concept.)

4 THE NEW PROFILES

It follows from the cautious approach described in section 2 that we shall not be revealing spectacular differences between the characteristics of the new profiles and those of the old. This was not what we were expecting or seeking. Rather, we strove for consistent but significant all-round improvements. We set out to delay the onset of adverse flow phenomena for the whole range of Mach number swept through by elements of the rotor blades.

Fig.3a, for example, illustrates, the consistent improvement in the boundary for separated flow. Fig.3b in turn indicates how such improvements react on the aerodynamic limits to the performance of the Lyrx rotor. The new profiles give a 25 knot increase in the advancing-blade forward-speed limit over what would have been achievable with the NACA 0012 profile on blades and rotor that were identical in every other respect. The simultaneous increase in the retreating-blade thrust limit is 10% for speeds near the maximum.

These improvements stemmed from a combination of leading-edge camber, profile changes at the leading edge, and reduction in thickness. All the changes from NACA 0012 were relatively small and all were contrived to reconcile improvements in one part of the Mach number range with those in others. For conditions associated with the aerodynamic limits of the rotor, local supersonic flow and boundary-layer separation were always involved in some combination or another and in some form or another, but the combination and pattern was different in different parts of the Mach number range. A profile shape that would have given large improvements in any one part of the range would have involved penalties in some other. The new profiles represent a balance in this respect.

5 THE IMPORTANCE OF THE RELATIVE BEHAVIOUR OF THE PROFILES AS DISTINCT FROM ABSOLUTE DATA

One of the main functions intended for the so-called limits estimated from profile data in the manner described by Byham⁴ is to provide a framework for comparison. It would be rash to suggest absolute precision, but this in no way detracts from the validity or from the value of the assessment that they give of the relative properties of the new and old profiles (Fig.3b).

Somewhat similar considerations apply in other ways to many other aspects. Throughout this paper we shall be emphasising the properties of the new profiles relative to those of NACA 0012 rather than any absolute properties.

The aerofoil data can themselves be strongly influenced by several factors, including the effects of Reynolds number, of the position of boundary-layer transition, of wind-tunnel interference and so on. The mere interpretation of what constitutes drag divergence, significant effects of boundary-layer separation, or $C_{L \max}$ even, can introduce significant differences between one set of data and another.

Thus we have throughout used a model of NACA 0012 as a reference datum, in turn in our steady aerofoil tests, in our oscillatory aerofoil tests and in our flight tests (Fig.22). The test conditions for the datum profile were the same as for the new profile in each class of test, but not, unfortunately, the same from one class to the other. In particular, carborundum bands were used to locate transition at the leading-edge for the steady aerofoil tests but not for most of the flight tests. Similarly, the configuration of tunnel walls used for the unsteady tests was different from that used for the steady tests. There were particular reasons for these differences at the time that the tests were made, but now they militate against direct comparisons for any one profile through the steady, unsteady, flight sequence. On the other hand, and as a result of these differences, we have observed the relative behaviour of the new profiles with respect to the old under a variety of conditions. The fact that this relative behaviour remains consistent adds to the confidence in the new profiles. This is especially important for the effects of roughness bands, and of the position of boundary-layer transition, because real uncertainty exists as to what particular conditions are the most appropriate for full scale. Indeed, it seems possible that a range of conditions, and hence a range of stall severity, might be encountered on any given full-scale rotor, depending for example on altitude or on whether there has been a significant degree of erosion at the leading edge.

For present purposes, then, we shall be emphasising the properties of the new profiles relative to NACA 0012, and we shall be using our own data for the latter - we have noted from time to time that sets of data from different sources for this one aerofoil can exhibit differences of about the same order as those due to the profile changes that we are here concerned with. Two new profiles are referred to in this paper, namely RAE(NPL) 9617 and RAE(NPL) 9615, but these differ only in minor respects.

6 ADVANCING BLADE LIMITS

The curves of Fig.3b indicate that the Lynx should have a 25 knot advantage in forward speed attributable to the new profiles. Confidence in this respect runs high as a result of class world speed records already beaten by substantial margins.

The increase in forward speed stems from a delay in the onset of shock-induced boundary-layer separations of the classical type for the low angles of incidence and high values of Mach number appropriate to the tip of the advancing blade.

The type of difference is illustrated by the schlieren photographs reproduced in Fig.4. They were obtained at $M = 0.85$, $\alpha = 0^\circ$, typical of conditions at about 0.95 radius, 90° azimuth angle for the Lynx in forward flight at a speed just a little in excess of that already sustained in its record-breaking runs. For the RAE(NPL) 9617 profile (Fig.4a) the flow has just separated at the feet of the shocks, and is in a state that would probably be just about tolerable in the pertinent transient conditions. However, for the NACA 0012 profile (Fig.4b) the separation is quite severe and would almost certainly cause intolerable consequences - pitching-moment instabilities, for example, for small changes of incidence.

These improvements were associated with a reduction in the level of local supersonic velocities upstream of the shocks which in turn was associated with a reduction in thickness.

This is indicated straightforwardly by the pressure distributions for the upper surfaces of the old and the new profiles (Fig.5a). The supersonic flow accelerates monotonically and in a very similar way for both profiles.

The fact that the local supersonic velocities are everywhere lower for the new profile is a measure of the success with which the droop has been incorporated. The prime purpose of the droop is to delay the retreating-blade stall (see below) by reducing the levels of velocity near the upper-surface leading edge at high incidence. In doing this, though, it would have been all too easy to have introduced high local curvatures and hence more rapid supersonic accelerations aft of the leading edge at low incidence; this pitfall has been avoided.

A second important feature of the shape of the leading-edge droop is illustrated by the changes near the leading edge on the lower surface for the RAE(NPL) 9617 (NACA 0012 is symmetrical, of course) (Fig.5b). The new leading edge successfully generates a 'peaky' type of compression from the high level of velocity that inevitably grows on its underside during the excursions to zero and small negative incidences by the tip sections of the advancing blade.

7 THE STRUCTURE OF LOCAL REGIONS OF SUPERSONIC FLOW

The contrast in Fig.5 between the concurrent monotonic supersonic expansion on the upper surface and peaky expansion/compression/expansion on the lower is but one example of the very wide range of local supersonic flows that a given element of the rotor blade can generate during its normal operating conditions.

The question of supercritical flows thus has to be examined in a light that is very different from that appropriate to the design of profile shapes for fixed wings. For the latter, it is possible to think in terms of one particular 'design condition', to specify margins of usable Mach number and incidence beyond it, and then to optimise shock-free, peaky or 'supercritical' profiles to suit. Although these special aerofoils call for a degree of sophistication in design, the problem of dealing with the local supersonic flow is particularised to a narrow range of conditions. In that sense it is simpler than the corresponding problem for the profiles of helicopter rotors where the excursions into local supersonic flow give rise to such a variety of local velocity distributions.

A further important difference for the rotor is that it becomes essential to consider the cyclic changes in the local supersonic flow in terms of the combined and simultaneous effects of changing Mach number and incidence.

Pearcey and Osborne⁶ introduced a qualitative description of a generalised embedded region of supersonic flow which is useful in the present context in so far as it provides a unifying concept for the wide range of conditions that has to be covered.

Consider the supersonic flow in terms of the flow deflection along streamlines (of which the surface is one) and of the two families of characteristics. The characteristics carry wave-like, infinitesimally small disturbances (Fig.6a). The disturbances on the outgoing characteristics are normally expansive (accelerations) and associated with a convex deflection (Fig.6b). Those on the incoming family are always compressive (decelerations), but also give a convex deflection.

The total convex deflection, $\phi(x)$, between the sonic point and a given downstream point, x , on the same streamlines (the surface say) is then:

$$\phi(x) = E(x) + C(x) , \quad (1)$$

where $E(x)$ and $C(x)$ are respectively the expansive and compressive disturbances, e , c , integrated to the point x .

The angular measure, $\omega(x)$, given by:

$$\omega(x) = E(x) - C(x) , \quad (2)$$

represents the net acceleration from the sonic point. This is the Prandtl-Meyer angle and is related uniquely to the local Mach number and pressure ratio:

$$\omega(x) = f(M_L) = g\left(\frac{p}{p_0}\right) . \quad (3)$$

The local supersonic flows that are implicit in the surface pressure shown in Fig.5 are reproduced in Fig.7 as the graphical representatives of equation (2). Table 1 includes an analysis of the manner in which the turning angle from the forward sonic point to the shock is divided between the cumulative expansive and compressive disturbances. Also shown are the residual values of the net accelerations, $\omega(x_T)$, and the values of local Mach numbers, M_L , that these accelerations represent at the position of the shock.

Table 1

Analysis of local supersonic flows for $M = 0.85$, $\alpha = 0^\circ$
(see Figs.5 and 7)

	$\phi(x_T)$	$E(x_T)$	$C(x_T)$	E/C	$\omega(x_T)$	M_L
NACA 0012 (upper surface)	18.7°	12.8°	5.9°	2.2	6.9°	1.33
RAE(NPL) 9617 (upper surface)	16.1°	10.4°	4.7°	2.2	5.7°	1.28
RAE(NPL) 9617 (lower surface)	28.0°	16.7°	11.3°	1.5	5.4°	1.27

This analysis confirms that the regions of local supersonic flow were similar in structure on the two upper surfaces. In particular, the ratio of expansive disturbances to compressive, E/C , remained the same. The small but crucial reduction in the value of local Mach number at the shock for the new profile can thus be attributed directly to the more rearward location of the forward sonic point in this instance.

For the lower surface, though, the increased compressive effect that is characteristic of peaky flows is clearly indicated. The velocities became supersonic on the under side of the droop and so a larger supersonic turning angle had to be achieved. The extra compressive effect enabled this to be done without increase in shock strength. (It is of interest to note in passing that the ratio of cumulative expansion to compression, E/C , had been reduced from 2.2 to 1.5. The value of this ratio is 1.0 for the ideal, shock-free case. For the chordwise point P , the ratio is as low as 1.2, indicating that the peaky flow would have had its greatest influence at somewhat lower stream Mach numbers when the shock was located in the region of P .)

8 RETREATING-BLADE LIMITS

The so-called natural aerodynamic limits for the Lynx rotor plotted in Fig.3b indicate that the rotor thrust available at forward speeds near the maximum includes an increment of about 10% attributable to the new profiles. The thrust limit is associated with a stall near the tips of the retreating blade.

The corresponding limit for the Wessex III helicopter is shown in Fig.8. The line has been estimated from aerofoil tests on the NACA 0012 profile (used for this rotor) on the basis of the criteria for the onset of severe effects of separation indicated in Fig.2a. The filled symbols are values of V_{NE} established in clearance tests and based on the oscillatory build up in pitch-link loads.

During the derivation of the new profiles, we studied these Wessex retreating-blade limits in order to trace the basic origins of the flow breakdown that is involved and the nature of its profile dependence.

We considered the conditions indicated by the symbol A, which would correspond to an increment in speed of 12 knots over and above V_{NE} at a given all-up weight. Westlands calculated for us the values of (M, α) that would have been attained at local elements of the blade had it been possible to fly at such a condition and assuming for the purpose of the calculations that the flow remained unstalled on the blade. The locus of (M, α) values that would have been traced out in each revolution by the blade element at 0.93 radius is shown in the centre diagram of Fig.9 as the heavy, figure-of-eight line. All the other results reproduced in Fig.9 were obtained on the NACA 0012 profile but in steady-flow aerofoil tests. They therefore represent only simulated flow conditions for the real rotor, but nevertheless present a valid qualitative picture of how the limiting conditions develop on each cycle (and, incidentally, several other features pertinent to the profile-dependence, as we shall discuss later).

The aerofoil results include, on the centre diagram and superimposed on the (M, α) locus for the rotor, the successive boundaries beyond which: (a) the flow is supersonic, (b) the rapid shock-wave drag rise is encountered and, finally, (c) the effects of separated flow become severe ($C_{L \max}$).

The numbers on the locus for the rotor indicate specific azimuthal positions; the appropriate steady-flow surface pressures are shown in the peripheral diagrams. It is immediately clear that the element at 0.93 radius would be encountering stalling conditions for azimuth angles between about 240° and 340° (the precise range will depend on dynamic effects, for example). The inference is then also fairly clear that this was the basic source of the thrust limit on the Wessex rotor.

Two further important points relevant to this limit stand out from Fig.9. These are: (a) that the flow is locally supersonic over a greater or lesser portion of the upper surface for the whole cycle, and (b) that the development of the stall and the subsequent reattachment are both shock-wave dependent and cannot be properly understood without considering the combined effects of incidence and Mach number as they vary simultaneously around the azimuth.

In approaching the critical point 6 ($\psi = 237^\circ$, $M = 0.4$, $\alpha = 10.6^\circ$), the effects of increasing incidence outweigh those of decreasing Mach number; the magnitude of the local supersonic Mach numbers at the leading edge continue to build up to values in excess of 1.4, although the upstream Mach number normal to the blade has fallen to 0.4. It is the shock-induced separation associated with these high local Mach numbers that triggers the stall and the subsequent collapse in the peak suction indicated at point 7 ($\psi = 303^\circ$, $M = 0.4$, $\alpha = 12.6^\circ$).

The reattachment process is influenced and delayed by the adverse effect of increasing Mach number, and a substantial reduction in incidence is necessary - to a value of 8.2° at $M = 0.55$ (point 9) - before an attached flow is again possible, with now a more extensive region of local supersonic flow. We will return in a moment to a fuller interpretation of the basic phenomenon, its profile dependence and other features.

In the meantime, it is helpful to refer to Fig.10 which corresponds exactly to Fig.9 except that the experimental results are now for the new RAE(NPL) 9615 profile. This profile would just have approached the stalling phenomenon just described at the most severe conditions on the loop represented by point 7. The surface pressures of Fig.10 indicate that the leading-edge supersonic flow would not have collapsed and the schlieren photographs of Fig.11 demonstrate the absence of the gross separation exhibited by the NACA 0012 profile for conditions corresponding to point 7.

This comparison highlights the fact that the trigger for the stall with the NACA 0012 profile was a local shock-induced separation in the first few per cent of the chord. This feature is seen in perspective against the results for the new profile for which the local supersonic flow is clearly present, with the maximum local Mach number just touching the critical levels above 1.4. True, the embedded supersonic region and the associated shock are tiny by comparison with those in the more classical transonic flows, but nevertheless the local shock-induced separation remains the trigger for the stall. Furthermore, the key to delaying the stall lies in reducing the rate at which the local supersonic velocities develop at the leading edge of the profile (see below).

A detailed interpretation of this type of stall was presented in Ref.7. This emphasised how, for such conditions on this type of aerofoil, the stalling process involves an interaction between: (i) a shock-induced separation which is provoked at the leading edge as the local supersonic velocities develop with incidence and/or Mach number, and (ii) a subsonic-type, rear separation which had already been growing from the trailing edge (Fig.12). The shock-induced separation, by thickening the upstream boundary layer, accelerates the growth of the rear separation, and, at a critical point of 'bubble burst', triggers a sudden forward jump of the rear separation; the two separated regions link in this process. As the stalling continues, the local supersonic flow at the leading edge collapses.

The results for point 7 in Figs.9, 10 and 11 thus show one example in which the stall has occurred (the old profile) and one (the new profile) in which the level of local supersonic velocity, and hence shock strength, are only just touching the levels that will trigger the stall. The improvement was achieved

by the leading-edge droop which suitably delayed the development of the local supersonic flow for this condition. The type of stall just described is thus dominated by the interplay between the shock-induced phenomena at the leading edge and the subsonic, rear separation. This holds for a range of Mach numbers including those appropriate to hover (see below).

One of the principal aims in deriving the new profiles, bearing in mind that they were to be used directly on the Lynx, was to retain the same balance between the local leading-edge and trailing-edge flows as pertains for the NACA 0012 profile. We felt that this was the best way of ensuring that the stall in the three-dimensional, time-dependent environment of the rotor would not develop vices which were different in nature from those of the much-used NACA 0012 profile and which might as a result nullify the gains shown by the new profile in two-dimensional steady flow. This again is a point to which we shall return.

The stalling phenomenon for point 7 of Fig.9 was in the present context the most critical of the various and varied repercussions of the supersonic flow that grows and decays during each revolution of the rotor blade for conditions represented by Figs.9 and 10.

The processes of growth and decay can perhaps be better seen in their broad perspective in Figs.13 and 14 in which the phenomena are represented with azimuth angle as a continuous variable on the abscissa. It is, however, important to retain clearly in mind in what follows that this presentation of a sequence of steady flow results is only a qualitative simulation of the continuous cyclic changes on a real rotor.

The ordinate in the main diagram is the surface slope, and reductions from 90° (up the page) represent surface flow deflections from the leading edge; these diagrams show the degree of convex turning, $E + C$ (see equation (1)), from the forward sonic point (lower line) to the rear one or, more usually, to the terminating shock wave (upper line). The ordinate in the upper diagrams is the residual Prandtl-Meyer angle ($E - C$) at the end of the supersonic region and therefore a measure of the shock strength (see equations (2) and (3)). An indication of where the shocks cause, first, significant wave drag and, then, separation, is given by the hatching below the abscissae of the upper diagrams. The results are summarised in Table 2 which includes also the analysis of how much of convex turning in the local supersonic flow is achieved by expansive disturbances and how much by compressive ones.

It is instructive to consider first the results for the new profile (Fig.13) because these are unaffected by stall; the growth and decay of the local supersonic flow reflect the more straightforward consequences of the combined and simultaneous variations of incidence and Mach number, with the flow remaining attached throughout the cycle.

It is first of all noteworthy that there are now, in contrast to the NACA 0012 profile, two parts of the cycle (30° to 65° and 165° to 210°) for which the flow is entirely subsonic. The azimuthal regions of supersonic flow thus appear as finite loops.

The smaller loop (65° to 165°), for the advancing blade and embracing points 3 and 4 of Fig.10, represents the classical local supersonic regions that occur away from the leading edge, from about 5% of the chord onwards say, and that were illustrated in Fig.5. For that case, the shock that developed had severe consequences. For the present case the shock waves are relatively innocuous.

The larger loop (210° to 35°), and embracing points 6, 7, 8, 9 and 1 of Fig.10, represents supersonic flows that grow from points very close to the leading edge and includes those that are critical for the retreating blade.

In particular, by point 7, $\psi = 303^\circ$, the forward sonic point has moved to a position that is within 10° in angular coordinate of the leading edge (the stagnation point is of course on the lower surface and significantly further in angular coordinate from the sonic point). For this case (see Table 2) the local supersonic flow turns through a convex angle of 39° at the surface, 24.8° of this being achieved on expansive disturbances and 14.2° on compressive ones. For the residual Prandtl-Meyer angle of 10.6° , representing a local Mach number of 1.46, the separation at the shock just, but only just, touched the critical value that would trigger stall.

From point 7 onwards, through 8 and 9, the forward sonic point moves away from the immediate leading edge as the incidence is reduced. The shock moves rearward though, as a result of the increasing Mach number, and the supersonic turning angles are even higher than before, reaching 58° and 54° , respectively. In spite of these large turning angles, the residual Prandtl-Meyer angles remain at 9° and 8° , respectively, and are thus significantly further from the values that would provoke critical shock-induced separations. The fact that the residual angles are such a small proportion of the total turning angles reflects the fact that the latter are now more evenly divided between expansive and compressive effects. This in turn reflects the degree to which the development of the local supersonic flow has been kept under control by the judicious balancing of local expansive and compressive disturbances.

The differences between this profile and the NACA 0012 can now be studied by reference to Fig.14 and Table 2.

The band of supersonic flow is continuous with azimuth angle for NACA 0012; and the element of the rotor that is under study, namely 0.93 radius, is in drag rise for nearly all of the cycle and in shock-induced stall for a vital part.

We are now in a position to appreciate more clearly how this stall develops and how reattachment occurs.

The conditions critical for shock-induced stall are just reached at point 6 ($\psi = 237^\circ$), when the supersonic turning angle is 37.5° . The residual Prandtl-Meyer angle is 11.1° (local Mach number 1.47), the expansive turning being 24.3° and the compressive turning 13.2° .

* Incidentally, the chordwise scale at the left of the upper diagram indicates that all these developments occur within the first 1% of the chord.

The fact that the extent of local supersonic flow is less than for the new profile for a range of azimuth angle of about 110° from this point on merely reflects the fact that the flow is now stalled, with a severe loss of circulation and a degree of 'collapse' of the local supersonic flow. This, too, is the only significance of the fact that the residual Prandtl-Meyer angles are smaller and the shock waves weaker. To the extent that types of separation can be neatly classified, this one has degenerated into some hybrid form which is not a clear shock-induced one, nor a clear subsonic one. It occurs near the leading edge but is there as a result of the rear separation having moved forward rather than of some specific adverse pressure gradient at the leading edge. The trigger for the degeneration was however the critical shock-induced phenomena present at point 6.

The change that occurs between points 8 and 9, i.e. between $\psi = 340^\circ$ and 355° , is of considerable interest because it includes a regrowth of the fully developed supersonic flow at the leading edge and therefore represents some form of reattachment; it marks the end of the fully stalled region.

At point 9, the flow is still separated locally at the shock, but the severity of this separation is only just touching the limit beyond which the overall circulation would be affected significantly. In other words, an overall flow is now just possible in which the local supersonic flow is fully attached at the leading edge and in which circulation is increased again to the pre-stall value appropriate to this stream Mach number.

Again, as in the development of the stall, it is the simultaneous variation of incidence and Mach number and their combined effects that dominate the 'reattachment' process. In particular, because the effects of increasing Mach number are strongly adverse, attached flow is not possible until the incidence has been reduced to 8.2° (Fig.9).

This is an important point at which to stress again, and strongly, that the results that we have been considering were obtained under steady conditions. The representation against azimuth angle can only be a qualitative simulation of the cyclic changes that will occur on the rotor blade. The real flows will probably differ from these in the precise stage for which the separation occurs, and in how the stall develops. They will almost certainly differ in the manner in which the reattachment occurs. But, nevertheless, it is inescapable that the manner of stalling and reattachment will be dominated by the simultaneous variations of incidence and Mach number, and almost certain that they will in some way be triggered by developments which occur in the local regions of supersonic flow and which are qualitatively similar to those indicated in Figs.12 and 13 - by the movement of the sonic point and by changes in the degree of supersonic turning, for instance. It is in these respects that the dependence on profile shape is most likely to retain its significance in the real rotor environment.

The most relevant advantage of the new profiles for this example can now be seen to be the delay in the growth of the leading-edge supersonic flow in the third and fourth quadrants. As a consequence of this delay, stall is avoided on the new profile and the embedded supersonic flow continues to develop naturally and then to decay again naturally. Furthermore, the development remains fairly well controlled in so far as an effective balance is retained between expansive and compressive disturbances.

9 OSCILLATORY AEROFOIL TESTS

Moore, Lambourne and Woodgate⁸ have checked the properties of the RAE(NPL) 9615 profile relative to that of the NACA 0012 with respect to susceptibility to stall flutter.

Their experiment defined regions of the (M, α) plane in which the aerodynamic damping is negative for pitching oscillations. Representative examples of their results are reproduced in Figs.15 and 16 to illustrate their principal conclusion. This was that the relative properties of the two profiles were the same in oscillatory flow as in steady flow, and therefore that the improvements that the new profile offers in terms of delayed stall (e.g. $C_L \max$) can be used on the rotor without an increased propensity to stall flutter. Thus, in Fig.15, the regions of negative aerodynamic damping are displaced up the page for the new profile by approximately the same amount as are the curves which give the incidence for $C_L \max$ in steady flow*.

The same relative shifts were observed in the presence of leading-edge carborundum bands (Fig.16). It is noteworthy that, in this case, the areas of negative damping are extended very significantly. The carborundum bands were similar to those used for the steady tests and are not unrepresentative of leading-edge roughness sometimes encountered in flight. Again, therefore, confidence is increased that the relative properties of the two profiles will remain similar for a wide range of conditions pertinent to the full-scale rotor in operation, including conditions that can be highly unfavourable to the performance of the blades.

This would seem to support the argument, used earlier, that if the basic nature of the stall on the new profiles was the same in steady flow as for the well-used NACA 0012, then the new profile would not be more susceptible to vices in the real environment than is NACA 0012.

We are fortunate to be able to use some more recent results of Lambourne and his colleagues - and are indebted to them - to illustrate how certain important aspects of the general way in which the aerofoils stall in steady flow carry over to unsteady flow.

Thus Figs.17 and 18 show measurements of surface pressure obtained at 0.95 chord on the upper surface of the NACA 0012 aerofoil for a stream Mach number of 0.4.

The first (Fig.17) shows the variation with increasing incidence in steady flow. The slow fall in pressure (up the page) that starts at about 8° indicates the presence and the progressive development

* Individual curves for the steady aerofoil tests cannot be compared with those given in the other sections of this paper because the tunnel-wall configurations (e.g. number of slots) were different. We rely on directly obtained comparisons between steady flow and unsteady flow, and between one profile and the other for both steady and unsteady flow.

of the subsonic, rear separation to which reference was made earlier. The abrupt divergence for 12° onwards reflects the sudden jump forward that is triggered by the development of the shock-induced phenomena at the leading edge.

The horizontal arrows A and B below the curve indicate the sinusoidal excursions in incidence for which unsteady measurements are shown in Fig.18a and b, respectively. In the first set of these (Fig.18a) the oscillatory excursions took the incidence to 12.4° . In steady flow this would have been just on the point of abrupt divergence, or stall. In oscillatory flow, the pressures vary periodically in a regular manner which suggests that the flow remains in the essentially unstalled regime, with the rear separation fluctuating regularly but relatively mildly in severity.

For the case shown in Fig.18b, the oscillatory excursions took the incidence to 13.1° , now about 1° beyond the point of abrupt divergence for steady flow. The periodic variations now also show an abrupt break from the smooth variation; the fluctuations beyond this point indicate the marked degree of irregularity expected of stalled flow.

Two inferences link these results both with the measurements in steady flow and with the flight measurements to be described later. Firstly, the concept of trailing-edge divergence can be carried over to oscillatory flow and, for the type of stall under consideration at least, it will indicate clearly the critical stage in the development of the stall. Secondly, on the profiles with which we are dealing, the same basic nature of the stall is retained in steady and oscillatory aerofoil tests and in flight; the sudden, leading-edge triggered, 'blow-up' of an already developing near separation is present in all three cases.

10 BLADE TIPS AT HOVER

The new profiles delay the onset of shock-wave drag rise for Mach numbers appropriate to stations near the tip in hover. Fig.19 gives some typical results from the steady aerofoil tests. The improvement of about 0.1 in C_L for a given level of drag corresponds to an increase of about 12 to 15% in the degree to which the blades can be loaded for a given power. This is perhaps not spectacular, and not as large as could be achieved by a peaky section designed specifically for this purpose at the cost of penalties at other conditions; but it is in keeping with the other results illustrated so far and with the objective of achieving consistent and significant all-round improvements.

The surface pressure distributions plotted in Fig.20a and b illustrate that the local supersonic flow now develops over the first 10 to 20% of the upper surface. The developments on the new profile (Fig.20a) are similar to those on NACA 0012 (Fig.20b) but are delayed by about 1° in incidence and are less severe at corresponding incidences. This is reflected in the schlieren photographs reproduced in Fig.21.

The surface pressures illustrate also how the separated flows develop at the higher incidences and hint at the nature of the stall. In the light of what has since been revealed by flight tests (see below) we regret that the aerofoil tests were not taken further into the stall.

Consider first the results for the NACA 0012 profile. The bulge B in the pressure distribution for 7° incidence indicates the characteristic bubble growth for a localised shock-induced separation. The manner in which this exacerbates the rear separation is indicated by the increasing amount by which the pressures near the trailing edge depart from the low incidence values, i.e. by the divergence of trailing-pressure. This is just about detectable at R for 7° and quite pronounced by 8° . By this latter stage, too, the 'stalling' process has begun in which the local supersonic flow collapses under the influence of the interacting shock-induced and rear separations.

For the RAE(NPL) 9615 profile, the bubble, B, is not evident until the incidence reaches 8° , the limit of these tests. The effect on the trailing-edge pressures and the subsequent developments can therefore only be inferred.

11 FLIGHT TESTS

These were made on a Wessex helicopter with a pair of its opposing blades carrying fairings, or gloves, over the outer 12% of their lengths (Fig.22). Both gloves were built up from the basic blade with balsa wood and glass fibre, one to represent the new, RAE(NPL) 9615 profile, and the other to reproduce the basic NACA 0012 profile at the increased chord. Both gloves incorporated pressure tubes for the measurement of time-average pressures and both carried rakes for time-average wake surveys. This technique was chosen to enable the relative properties of the two sections to be assessed simultaneously for the same test conditions and the same three-dimensional, time-dependent environment. It was felt that the time-averaging would be adequate for this purpose for hovering flight, and indeed the sample results shown in Fig.23 reveal the expected delay in the acceleration to local supersonic velocities or the new profile (Fig.23a); for more severe conditions (Fig.23b), the expected reduction in the level of local supersonic flow is demonstrated with the associated reduction in shock-wave drag - as indicated by the reduced spread of pitot-pressure loss in the wake.

During the development of the gloves and their instrumentation, the opportunity arose to incorporate, in the glove with the RAE(NPL) 9615 profile, four miniature pressure transducers to monitor instantaneous pressures or pressure differences at selected chordwise positions. The prime intentions were to evaluate these transducers for the more extensive measurements of instantaneous pressure currently being prepared for flight tests on the same blades and to investigate possible means of indicating local aerodynamic incidence and flow separation. In the event, the instantaneous pressures have helped considerably in several ways. With the aid of a theoretical conceptual model of the blade-tip/vortex intersection they expose the nature of the environment to which the profiles were being exposed; there were in fact large periodic fluctuations in local incidence (see Fig.29). With the aid of the conceptual model of flow separation derived from the aerofoil tests they indicate the manner in which the new profile reacted to this environment; the onset of stall as diagnosed by trailing-edge pressure divergence correlated well with the level of supersonic velocity near the leading edge (Fig.26).

A full report of these techniques and tests is in preparation but it is opportune to include here a brief, preliminary explanation of the three-dimensional, periodic environment created by the rotor and to offer some tentative descriptions of the resulting flow phenomena.

The high loadings near the tip are associated with the incidences induced by the vortices of preceding blades, and our measurements, from 0.90 to 0.96r/R, were made near the crest of a strong radial peak (Fig.27). This is the clue to understanding not only the highly three-dimensional character of the environment to which the profiles were being exposed (there were strong radial gradients in loading as well as in Mach number*, even within the span of the pressure measuring stations) but also the large periodic fluctuations (the magnitude of the instantaneous loading at any given radial station was sensitive to small displacements of the vortex wake).

Simple considerations indicate that the vortex wake can be significantly skewed by quite small translational velocities of the vehicle relative to the wind, which are inevitable even for carefully controlled 'hover' conditions. This means that there is a periodic lateral displacement of the measuring station on a given blade with respect to the vortex from the preceding blade, or, alternatively, that the vortex is displaced periodically with respect to the measuring station. Fig.28 indicates the pattern of the variations in incidence that would be expected from a highly simplified model of this situation. The readings of the instantaneous pressures near the leading edge reflect these variations (Figs.24a and 25a) and indicate that they are indeed quite large.

The absolute scale of incidence should be treated with some caution; it has been derived from a linear calibration obtained in steady aerofoil tests which applies only up to the stall and may not hold for a blade/vortex interaction. Nevertheless, it is adequate as a guide to the range of incidence in a typical cyclic variation. Reference to Fig.20a shows that this range (approximately 5° to 10°) is highly significant in relation to that in which the local supersonic flow develops. Depending on the level of the mean values, the periodic variations are likely to take the local flow into and out of regions of supersonic velocity and drag rise, and even into and out of shock-induced stall.

This is confirmed by the appearance of the tell-tale sudden fall in trailing-edge pressure (trailing-edge pressure divergence⁹), as indicated by the 'blips' at P and Q, for example, in Fig.25b; this is a trace of the pressure difference between the two surfaces at 0.94 chord. This divergence is also clearly indicated at B in Fig.24c and marginally at A. Analysis of several traces (Fig.26) shows that the trailing-edge pressure divergence appears for conditions in which the peak incidence (or leading-edge pressure difference) exceeds a certain critical value. As might be expected, this critical value is higher for the transition free results than for the transition fixed ones**. Beyond the onset of this divergence, for each of the two boundary-layer conditions, the magnitude of the maximum excursion in trailing-edge pressure correlates reasonably well with the maximum value of the peak in leading-edge pressure difference. It should be remembered that, in the stall, the leading-edge suction collapses - and so the maximum value of leading-edge pressure difference is not necessarily a measure of the maximum incidence reached in the excursion. Indeed, for the peak Q of Fig.25a there is a clear suggestion that the pressure difference begins to fall while incidence is still rising; the peak Q in trailing-edge pressure difference indicates that the stall increases in severity well beyond the stage at which the maximum is reached in leading-edge pressure difference (see below).

The correlation with stall onset in the steady aerofoil tests is within 1° of incidence. This is surprisingly good in view of the three-dimensionality and time dependence of the flight environment, and in view of the various possibilities for other experimental errors or differences. The difference is of the same order, for example, as that between transition-free and transition-fixed conditions in flight.

Figs.24c and 25c represent an attempt to analyse the dynamic 'stall' development for the results of Figs.24a, b and 25a, b respectively. The magnitudes of the trailing-edge pressure excursions are plotted as direct functions of the leading-edge pressure difference which will of necessity be treated as an 'independent' variable in following through the loops that are generated in this analysis. It is important to bear in mind, however, that the variations in this quantity are related to the changes in incidence at the station in question and, in turn, that these changes result from spatial (lateral) displacements of the vortex velocity field with respect to the measuring station. This latter point is unlikely to affect the interpretation of the flow phenomena in the early stages of what follows, but we shall return to it towards the end where it clearly could.

Take the transition-free case first. The analysis starts at point O where the incidence is low and the leading-edge flow is subsonic and clearly unstalled. The flow remains unstalled as the leading-edge difference passes through and well beyond the value (about 0.4) corresponding to sonic velocity at the pressure hole in question on the upper surface (0.01 chord). There is a small excursion, A, in trailing-edge pressure at the first peak in incidence (leading-edge pressure difference = 0.6), but some ambiguity exists as to whether or not this indicates an incipient stall at this station. The excursion, B, at the second peak, leaves no ambiguity; but the flow recovers smoothly from the incipient stall, without significant hysteresis.

A similar analysis for the transition-fixed results (Fig.25c) indicates the presence of stalled flow for both the first and second incidence crests, P and Q (Fig.25a). Certain features of the stalling and flow re-establishment processes can be inferred from this limited data and certain questions posed. The main interest in the present context is the bearing that these inferences and questions have on the interpretation of the mean pressures and on the assessment of how the two profilers behave relative to one another in the rotor environment.

* Typically, 0.55 to 0.60.

** It should be stated that most of the flight tests were made without roughness bands. For these, the presence of significant regions of laminar flow was revealed by contrast with a sooty film (from atmospheric pollution) deposited in the turbulent regions. Some tests were made with leading-edge carbide bands similar to those used in the aerofol tests.

The successive excursions in trailing-edge pressure differ mainly in degree. Both start with a divergence from the base line as the value of leading-edge pressure difference exceeds the value, about 0.45, that is critical for the transition-fixed conditions (see Fig.26). It can reasonably be inferred that the severity of the separation is increasing progressively as the trailing-edge pressure continues to fall. Also, it is clear that attached flow has been re-established at both leading-edge and trailing-edge of the particular pressure plotting station in question by the stage at which the line falls sharply from the apex of the loop to the base line.

On following the stall loops in more detail we see that the leading-edge pressure difference at first continues to increase; this implies that the incidence was at first continuing to increase. It is also reasonable to assume that incidence was still increasing around, and to some point beyond, the stationary value in leading-edge pressure difference; this is because we know from aerofoil tests that the leading-edge supersonic velocities begin to collapse as incidence increases into stall for these Mach numbers (see, for example, Fig.9).

We can deduce, however, that incidence almost certainly began to decrease at some point on the loop before the apex was reached; this is because the value of leading-edge pressure difference at which attached flow is re-established corresponds to a significantly lower incidence than is implied by the maximum value of this difference (at least $1\frac{1}{2}^\circ$ lower for loop Q). What we cannot deduce is just where incidence began to fall.

The appearance of significant hysteresis in the loop Q is the stage at which to remind ourselves that the vortex velocity field is being displaced laterally along the blade. As well as, or instead of, stalling hysteresis of the classical type, the loops probably reflect some essentially different aspects implicit in the lateral displacement of the vortex induced flow phenomena. Some of the apparent hysteresis could, for example, be associated with a time lapse for the separated flow to pass clear of the trailing edge of the pressure-measuring station in question.

Finally, it is of some interest to note that the velocity at the upper-surface leading-edge hole that was being used for this exploration remained supersonic for the whole of the first loop P but, for the second loop Q, had fallen to a value just below sonic before 'flow attachment' occurred.

We can now return to the main point of the present exercise, namely the comparison of the two profiles on the basis of time average surface and wake pressures.

It is quite obvious that these pressures will be strongly influenced by the extensive excursions of the type just discussed and especially by the stalling and flow attachment processes. The interpretation of their absolute significance is therefore difficult for the extreme cases. The relative manner in which the two profiles respond to this environment should nevertheless still be reflected in the mean pressures because these were samples simultaneously for the two profiles while each was being subjected to the same cyclic variations. Moreover, the same instrumentation was used.

This deduction is confirmed by the results reproduced in Fig.29 which compare the mean pressures for the two profiles when subjected to the unsteady conditions indicated in the upper diagrams. The main conclusion is that the same relative levels of pressure obtained in steady two-dimensional tests are retained even in the unsteady conditions met in flight. This applies especially and pertinently to the lower level of local supersonic velocity on the new profile and to the correspondingly weaker shock. Our conclusion is strengthened by the fact that the same relative levels were maintained for different forms of cyclic variations of incidence, two of which are shown in Fig.29. These arose from changes in translational velocity alone.

One analysis of the difference between the two profiles is presented in Fig.30, in which the profile drags deduced from mean wake pressures are plotted against lifts integrated from mean surface pressures. These 'polars' bear certain similarities to those shown in Fig.19 for the steady flow aerofoil tests but also certain differences.

The closest similarity occurs for the transition-fixed results (the aerofoil tests were made with transition fixed); the new profile gives the same improvement of about 0.1 in lift coefficient for a given level of drag. A smaller improvement was obtained with transition free.

The main difference lies in the steepness of the drag increase in flight. It is here that the time-averaging technique is likely to have had its strongest influence, because both drag and lift will have varied non-linearly in the extremes of the cyclic incidence variations. The drag will have risen much more steeply and, beyond the stall, the instantaneous lift variations will even change sign. The two non-linear effects will combine to steepen the time-average curves.

A broader perspective of the difference between the two profiles in the rotor environment is provided by the mean surface pressures reproduced in Figs.31 and 32. Each figure shows the pressures at four spanwise stations on each of the two gloves, the upper set in each case being for the new profile and the lower for NACA 0012. The results in Fig.31 were obtained at low altitude and Fig.32 at high altitude with the rotor consequently more heavily loaded and the local tip sections more deeply penetrating the developments of local supersonic flow at the leading edge.

The relative differences between the two profiles are consistent and clear. For corresponding conditions, the developments of the local supersonic flow come later on the new profile and less severely.

There is a quite striking similarity between the broad impression created by Fig.20 (which compares the pressures on the two profiles in two-dimensional steady flow) and that created by Figs.31 and 32 (which compare the mean pressures on the two profiles on the tips of the Wessex rotor in flight).

This similarity applies both to the general shape of the pressure distributions with their local regions of supersonic flow and quite evident shock waves and, especially important in the present context, to the relative magnitudes of the two profiles.

The similarity is all the more striking when one recapitulates what has just been discussed about the environment in which the profiles were being compared in the flight tests. There were significant radial variations in both Mach number and incidence and strong cyclic variations in incidence which in the extreme cases involved dynamic excursions into and out of stall. The profiles evidently responded to these complex changes in qualitatively the same relative way as they did in the steady aerofoil tests.

12 CONCLUDING REMARKS

The new profiles were derived to give consistent and significant all-round improvements to rotor performance - to the shock-induced limits on the advancing blade, to the retreating blade thrust limits and to the loading that could be sustained without shock-wave drag in hover. The changes were conservative, especially with respect to the stalling characteristics; these are the most significant aerodynamic sources of limits to rotor performance, but at the same time, they are the least predictable theoretically - and even conceptually when it comes to the rotor environment. The caution was necessary because the profiles were to be incorporated directly into the Lynx rotor.

The derivation of the profiles was made on the basis of steady flow aerofoil tests, but qualitatively similar improvements have been verified in oscillatory aerofoil tests and in flight. This applies especially to the all important delay in the development of local regions of supersonic flow and in the development of the various stalling phenomena in which shock waves are implicated.

Certain threads run through the discussions of these profile-related stalling phenomena and of the associated reattachment (or flow re-establishment) processes.

The broad fundamental manner in which the stall commences seems to be similar in the steady and oscillatory aerofoil tests and in flight. In particular there is a characteristic divergence of trailing-edge pressure in all cases.

On the other hand, from the very nature of the cyclic variations of incidence and Mach number that are involved, it seems that the way in which attached flow is re-established after stall must differ even in character as between steady and oscillatory aerofoils, as between oscillatory aerofoils and rotors, and as between one type of stall on the rotor (e.g. retreating blade) and another (e.g. vortex-induced tip stall at hover).

One feature that is common to the rotor situations that have been considered is the highly significant implication of the local supersonic flow in both the stalling and the flow re-establishment processes. It must also be highly significant that on the rotor in forward flight there will be simultaneous variations in both Mach number and incidence; the growth, decay and re-establishment of local supersonic flow will almost certainly depend strongly on the combined effects of these simultaneous variations. Herein surely lie the seeds of much fruitful study. The present work suggests that this could be facilitated by rotor tests in which profile shape is a variable; the profile dependence of the phenomena under study would add an extra parameter to help in their resolution.

Acknowledgments

The authors are indebted to Mr. J. Osborne for several valuable contributions to the analysis and interpretation of the flow phenomena. It was he who conceived the instructive presentation used in Figs.13 and 14.

Table 2

ANALYSIS OF THE LOCAL SUPERSONIC FLOWS FOR RESULTS SHOWN IN FIGS.9 AND 10

Point	ψ°	M	α°	$\phi(x_T)^\circ$	$E(x_T)^\circ$	$C(x_T)^\circ$	E/C	$\omega(x_T)^\circ$	M_L
1	10	0.6	5.8	21.8 (47.4)	12.85 (28.65)	8.95 (18.75)	1.44 (1.53)	3.9 (9.9)	1.21 (1.43)
2	42	0.7	1.1	- (9.5)	- (5.15)	- (4.35)	- (1.19)	- (0.8)	- (1.07)
3	112	0.75	1.55	15.3 (26.3)	9.15 (16.4)	6.15 (9.9)	1.49 (1.65)	3.0 (6.5)	1.17 (1.31)
4	155	0.55	3.45	11.8 (22.2)	5.9 (12.7)	5.9 (9.5)	1.00 (1.34)	0 3.2	1.0 (1.19)
5	199	0.5	6.7	- (40.5)	- (22.5)	- (17.95)	- (1.26)	- (4.6)	- (1.24)
6	237	0.4	10.6	16.0 (37.5)	10.85 (24.3)	5.15 (13.2)	2.10 (1.85)	5.7 (11.1)	1.28 (1.47)
7	303	0.4	12.6	39.1 (20.8)*	24.85 (10.7)*	14.25 (10.1)*	1.74	10.6 (0.6)*	1.46 (1.06)*
8	340	0.5	10.1	58.1 (43.4)*	33.6 (24.65)*	24.5 (18.75)*	1.38	9.1 (5.9)*	1.40 (1.29)*
9	355	0.55	8.2	54.4 (59.8)	31.05 (35.95)	23.35 (23.95)	1.33 (1.50)	7.7 12.1	1.35 (1.51)

Values in brackets refer to the NACA 0012 profile (Fig.9); others to the BME (NACA) W-15 profile (Fig.10).

* These values are strongly affected by stall.

REFERENCES

- 1 V.A.B. Rogers, The design of the WG 13. *Roy. Aero. Soc. Rotorcraft Section Symposium*, 13 January 1972. To be published in *Journ. Roy. Aero. Soc.*
- 2 H.N. Stuverude, Operational history and experience with Boeing helicopters. *Journ. American Helicopter Soc.*, Vol.13, No.4 (1968)
- 3 W.H. Tanner, R.M. Wohlfield, New experimental techniques in rotorcraft aerodynamics and their applications. *Journ. American Helicopter Soc.*, Vol.15, No.2 (1972)
- 4 G.M. Byham, A study to investigate the forward flight capabilities of a helicopter rotor. Westland Helicopters Ltd., November 1971
- 5 J.P. Jones, The helicopter rotor. Thirteenth Lanchester Memorial Lecture to the *Roy. Aero. Soc.*, April 1970. To be published in *Journ. Roy. Aero. Soc.*
- 6 H.H. Pearcey, J. Osborne, Some problems and features of transonic aerodynamics. ICAS Paper No.70-14; Seventh Congress of ICAS, September 1970
- 7 J. Osborne, H.H. Pearcey, A type of stall with leading-edge transonic flow and rear separation. AGARD CP No.83, Göttingen (1971)
- 8 A.W. Moore, N.C. Lambourne, L. Woodgate, Comparison between dynamic stability boundaries for the NPL 9615 and NACA 0012 aerofoils pitching about the quarter chord. RAE Technical Report 71163 (1971)
- 9 H.H. Pearcey, D.W. Holder, Simple methods for the prediction of wing buffeting resulting from bubble-type separation. ARC 23884; NPL Aero Report 1024 (1962)



Fig.1 Westland W.53 Lynx

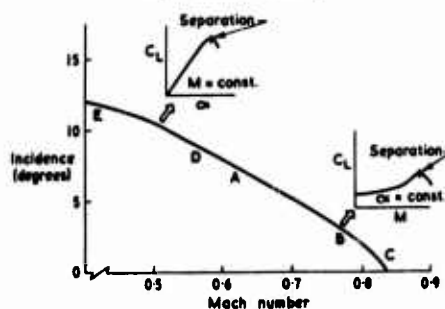
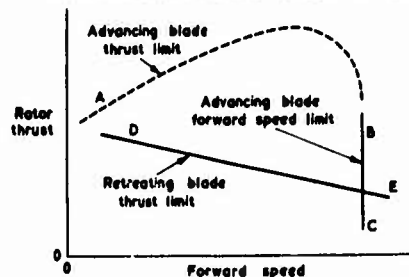
FIG.2(a). Aerofol separation boundary ($C_L \max$)

FIG.2(b). Aerodynamic limits to rotor performance

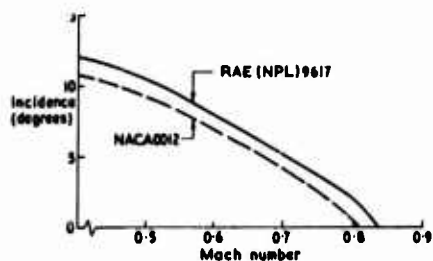


FIG.3(a) Aerofol separation boundaries

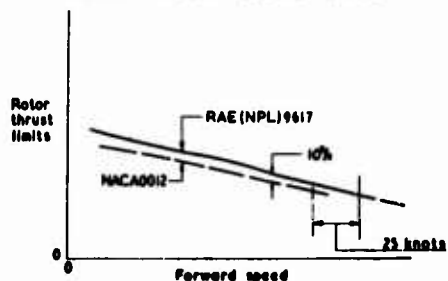


FIG.3(b) Effect of blade profile change on limits to rotor performance (Lynx rotor)



(a) RAE(NPL) 9617



(b) NACA 0012

Fig.4

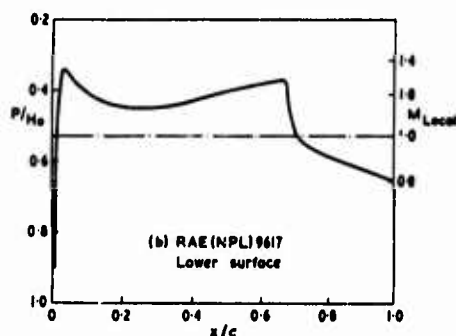
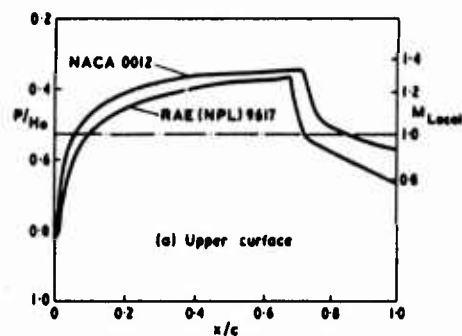
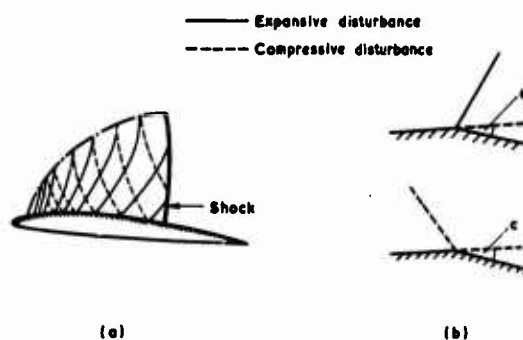
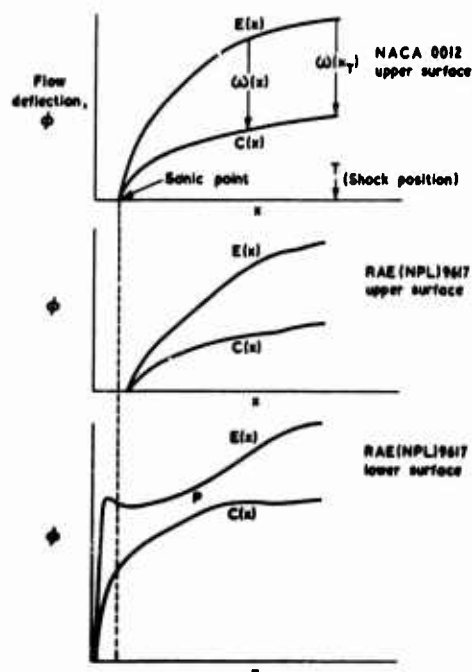
FIG.5. Pressure distributions for NACA 0012 and RAE(NPL)9617 at $M=0.85, \alpha=0^\circ$ 

FIG.6. Disturbances on characteristics and their contributions to convex flow deflection in local supersonic flow

FIG.7. Expansive and compressive flow deflections for the local supersonic regions for $M=0.85, \alpha=0^\circ$ (See Fig.5 and Eqn.3)

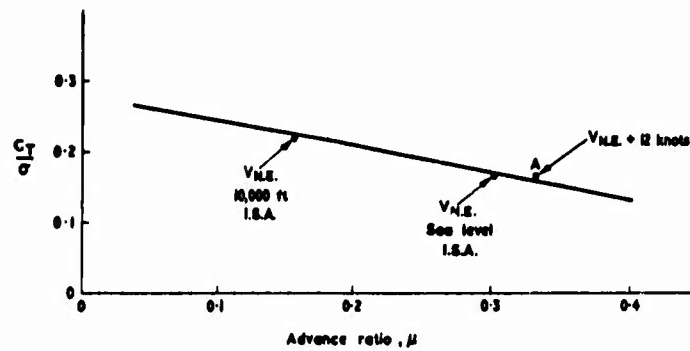


FIG. 8. Retreating-blade thrust limit for the Wessex helicopter

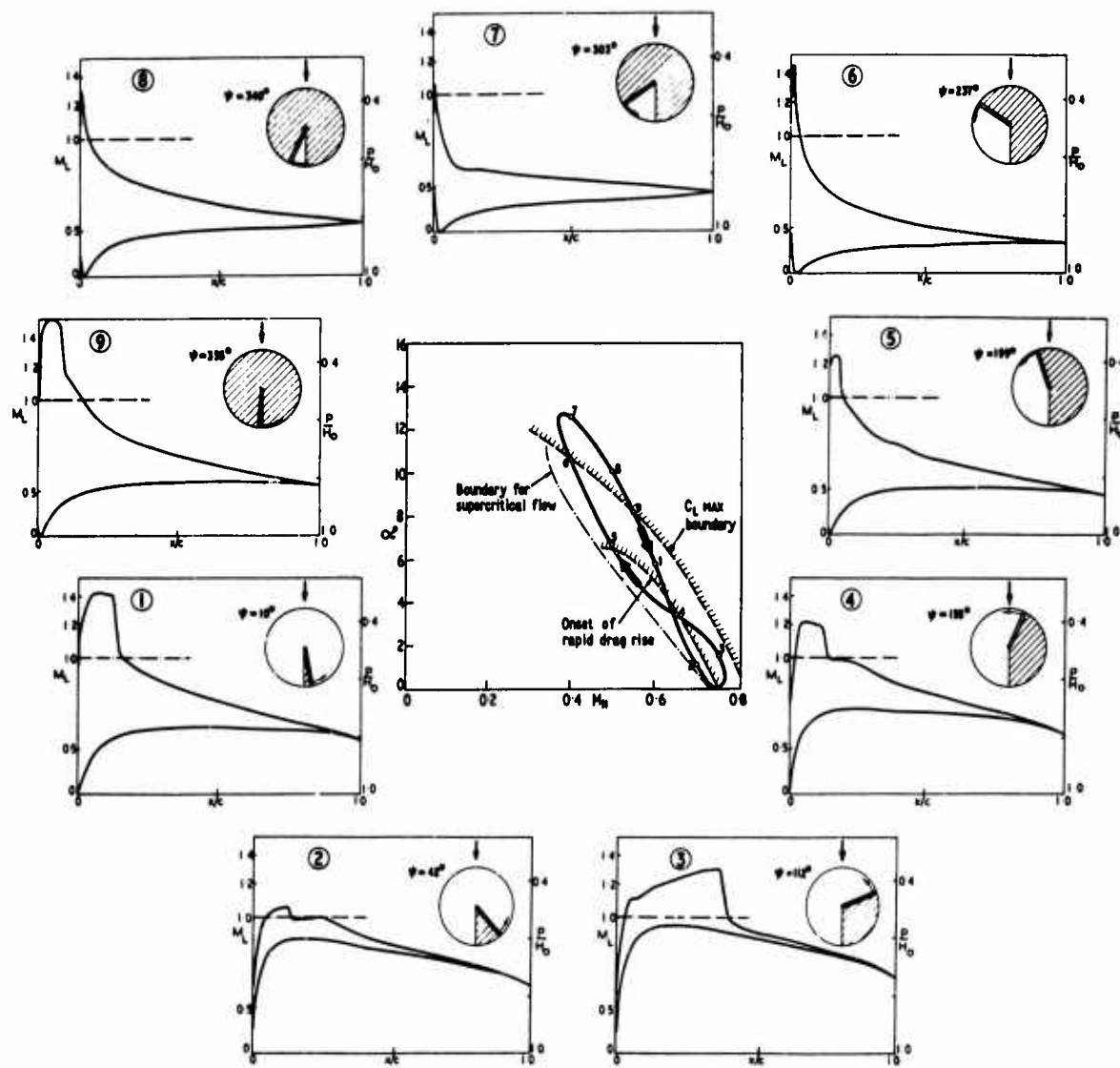


FIG. 9. (Centre diagram)

$M_\infty - \alpha$ locus representing conditions for a rotor blade element at 0.93 radius; Wessex III helicopter at $V_{H.E.} + 12$ knots. Also indicated are measured flow boundaries for NACA 0012 airfoil

(Peripheral diagrams)

Steady flow pressure distributions corresponding to numbered symbols on locus

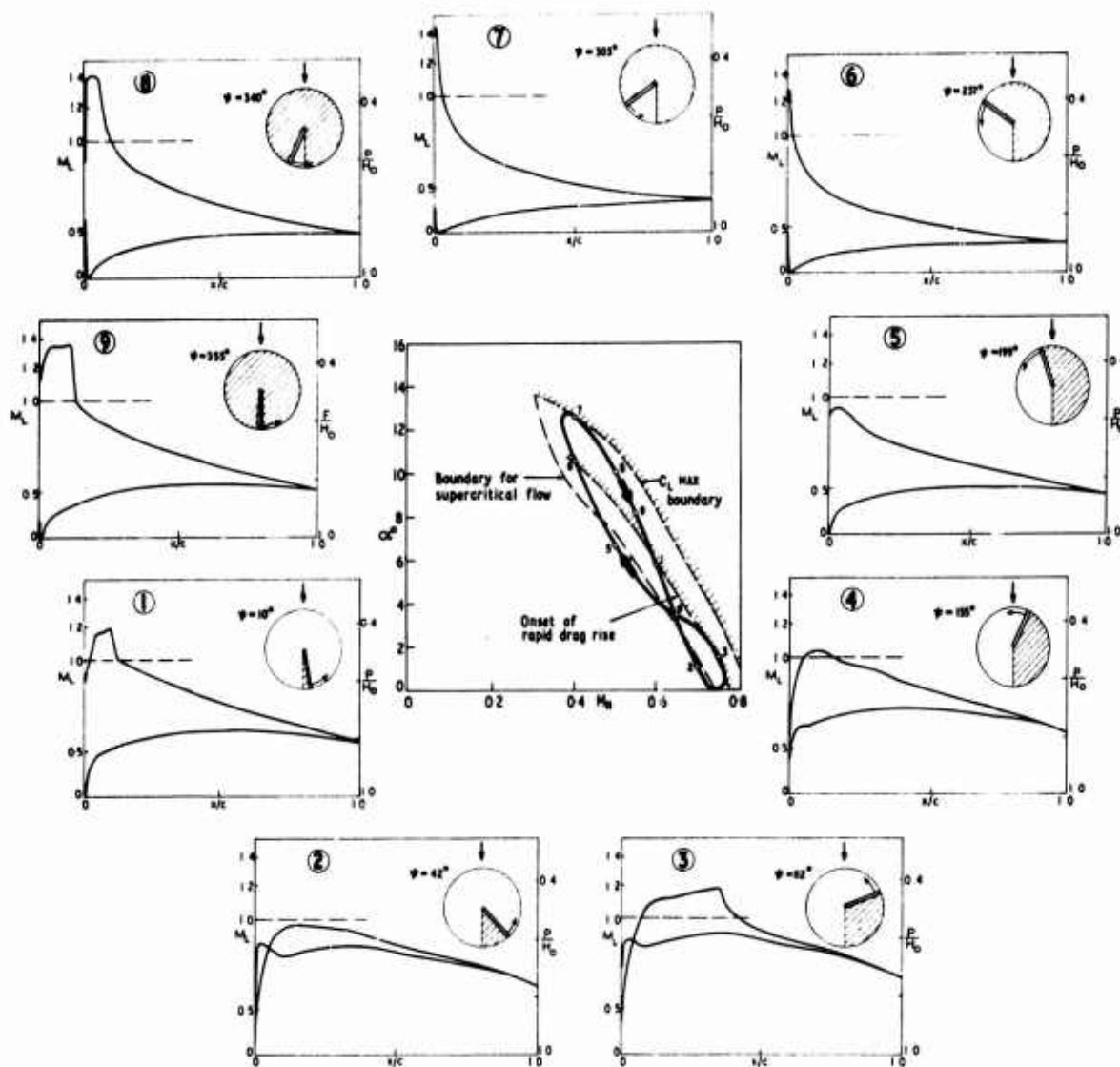


FIG.10. (Centre diagram)

$M_\infty - \alpha$ locus representing conditions for a rotor blade element at 0.93 radius; Wessex III helicopter at $V_{Ht} + 12$ knots. Also indicated are measured flow boundaries for RAE(NPL)9615 aerofoil.

(Peripheral diagrams)

Steady flow pressure distributions corresponding to numbered symbols on locus.

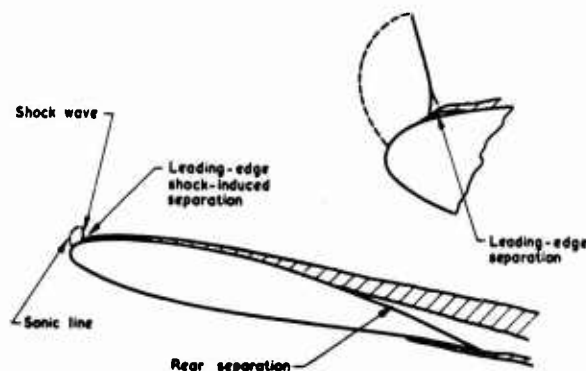


(a) RAE (NPL) 9615



(b) NACA 0012

FIG.11. Comparison of the new and old profiles at conditions encountered near the tip of the retreating blade at its thrust limits; $M = 0.4$, $\alpha = 1$ (Point 7 of Figs. 9 and 10)



The extent of local supersonic flow is typical for conditions encountered on the retreating blade; it would be larger for the blade tips in hover

FIG.12 The leading-edge and trailing-edge separations that interact to provide stall for the profiles studied

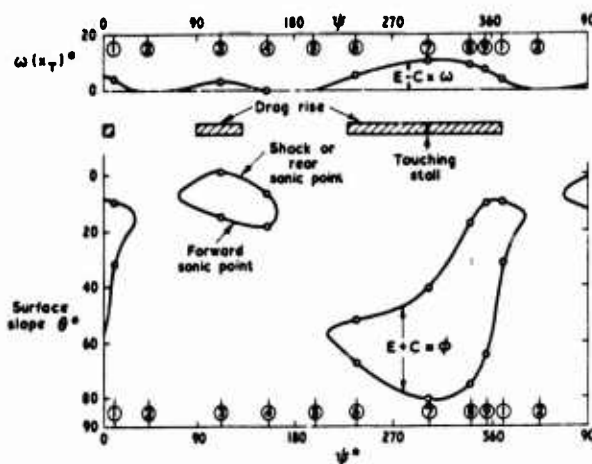


FIG. 13. Analysis of the local supersonic flows represented in Fig. 10; RAE (NPL) 9615 profile

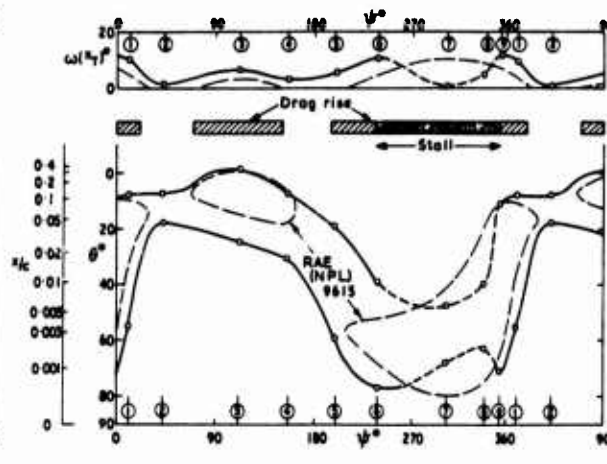


FIG. 14. Analysis of the local supersonic flows represented in Fig. 9; NACA 0012 profile

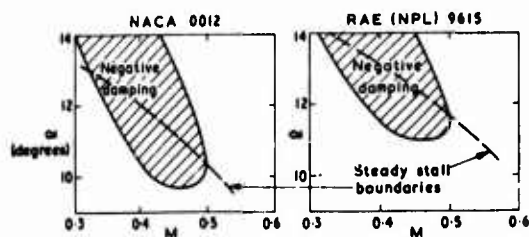


FIG. 15. Comparison of stability boundaries for two profiles

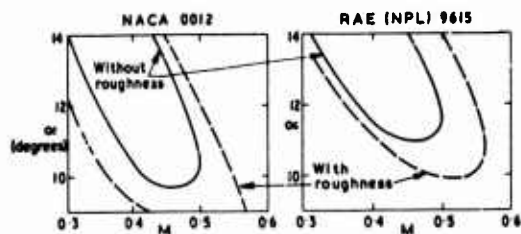


FIG. 16. Effect of leading-edge roughness on stability boundaries

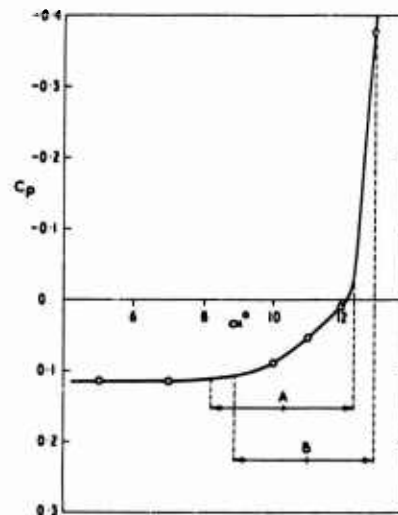
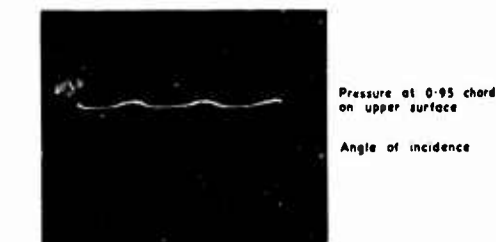
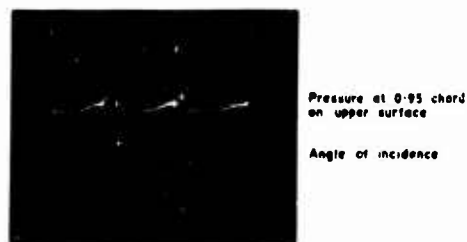


FIG. 17. Incidence-induced divergence of pressure at 0.95 chord on the upper surface of NACA 0012 aerofoil; $M_0 = 0.4$; Steady flow



(a) $\alpha = 10.3^\circ \pm 2.1^\circ$ (see line A of Fig. 17)



(b) $\alpha = 11.6^\circ \pm 2.1^\circ$ (see line B of Fig. 17)

FIG. 18. Pressures near the trailing-edge of the NACA 0012 profile oscillating about a mean angle of incidence near that for stall ($M_\infty = 0.4$; Frequency = 5 cycles/sec.)

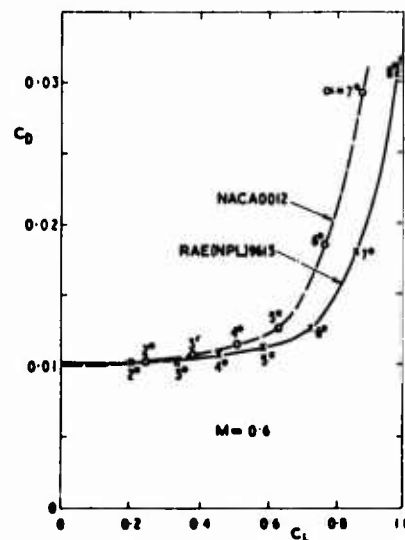


FIG. 19. Comparison of Variations of drag with lift for two aerofoils of $M_0 = 0.6$ (Typical tip Mach number for hover)

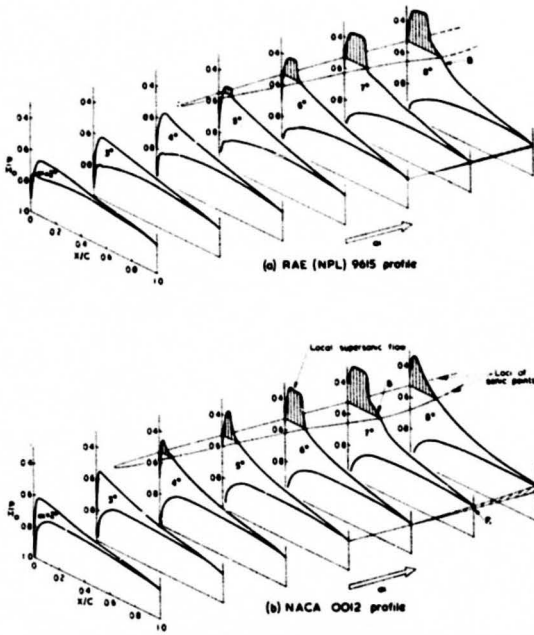


FIG.20. The development of surface pressure distributions with increasing incidence at $M_0 = 0.6$ (Typical tip mach number for hover.)



(a) RAE (NPL) 9615



(b) NACA 0012

FIG.21. Shock waves on two aerofoils at conditions typically encountered near blade tips in hover ($M = 0.6, \alpha = 5.8^\circ$)

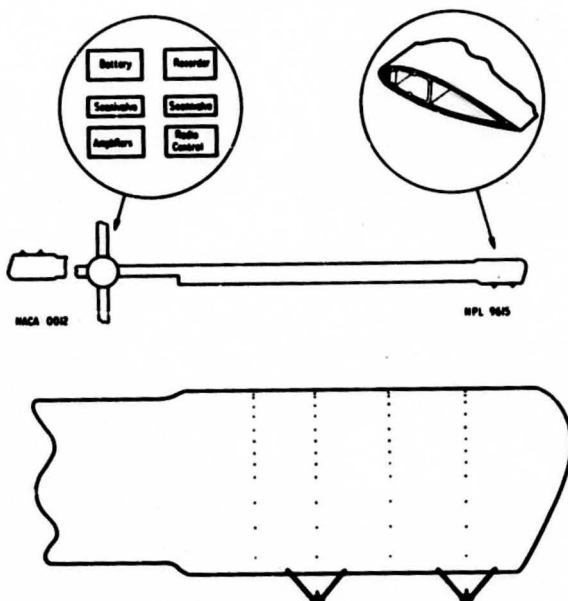


Fig.22 Sketch of the blade modifications to the Wessex helicopter and of the hub-mounted recorder

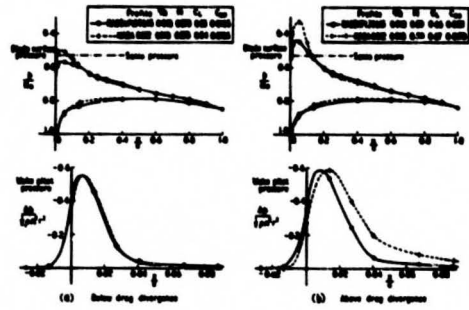


Fig.23 Comparison of mean surface & wake pressures measured simultaneously in hovering flight

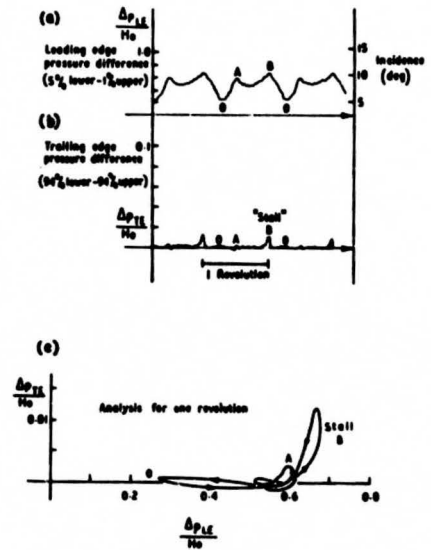
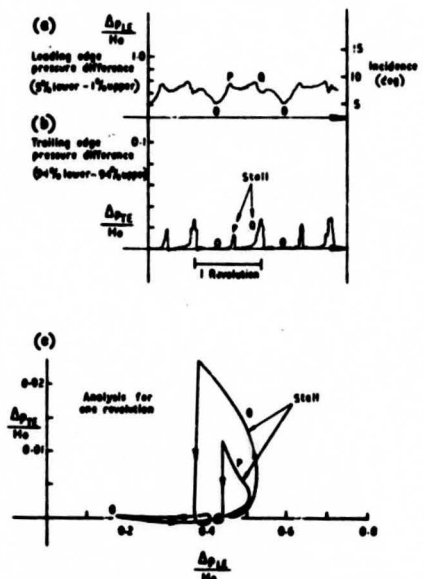


Fig.24 Cyclic variation of instantaneous pressure differences (transition free)



Cyclic variation of instantaneous pressure differences (transition fixed)
Fig.25

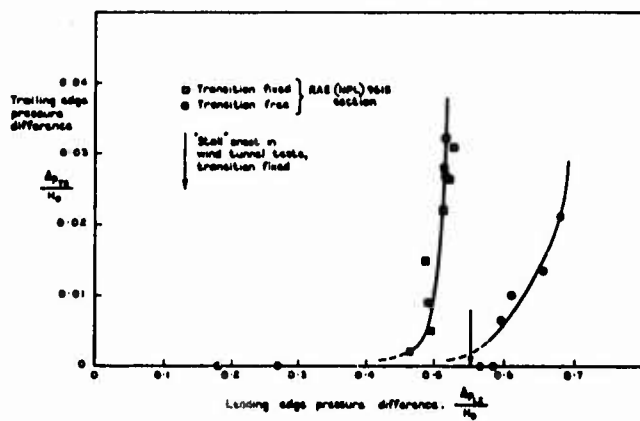


Fig. 26 Stall onset derived from analysis of suction peaks

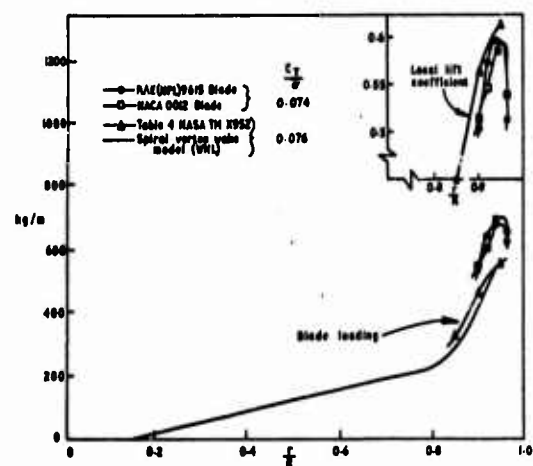


Fig. 27 Mean blade loading measurements showing effect of tip vortex

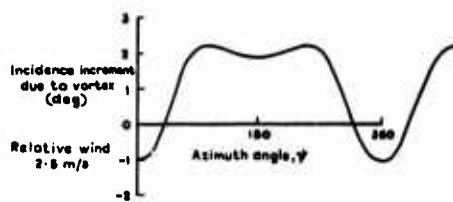
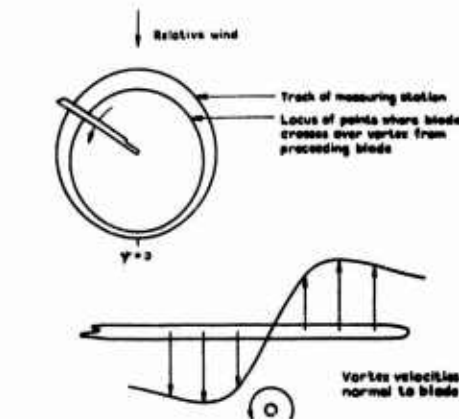


Fig. 28 Line-vortex model of near wake

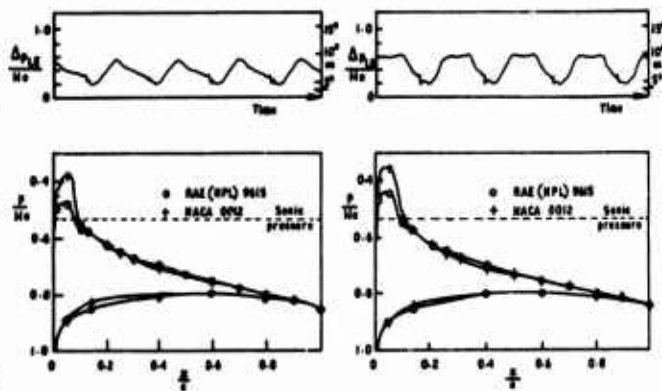


Fig. 29 Mean pressures for two forms of cyclic variation of incidence

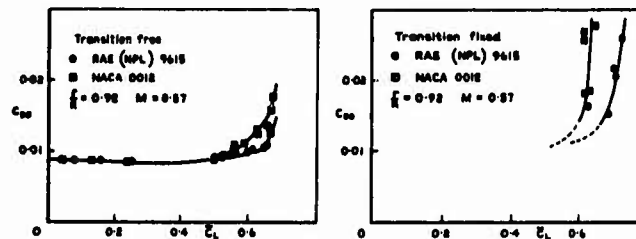


Fig. 30 Lift/drag polars derived from mean pressures

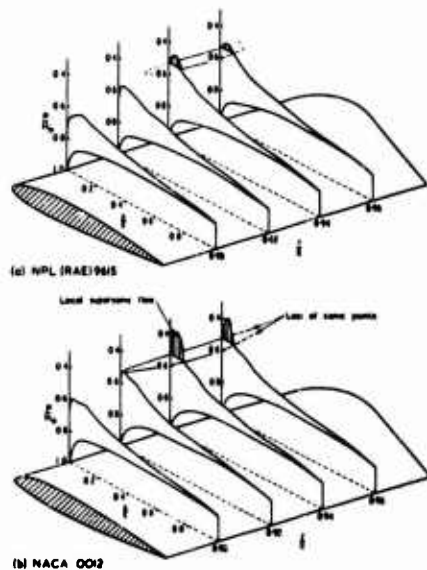


FIG. 31. Pressure distributions on outer portions of two blades with different sections for low altitude hover

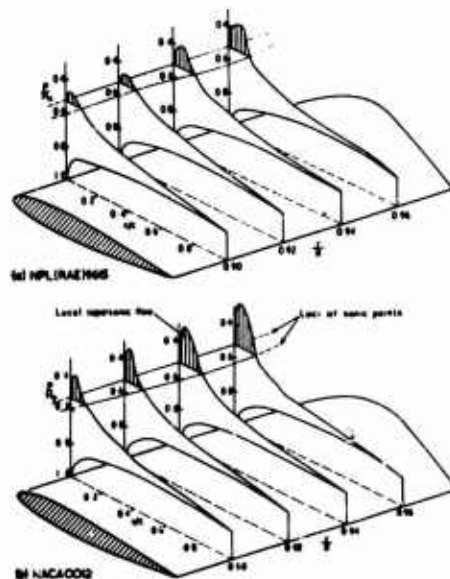


FIG. 32. Pressure distributions on outer portion of two blades with different sections for high altitude hover

THE EFFECT OF PLANFORM SHAPE ON THE TRANSONIC FLOW PAST ROTOR TIPS

by

W. F. Ballhaus and
F. X. Caradonna
U. S. Army Air Mobility R&D Laboratory
Ames Directorate
Moffett Field, California USA 94035

SUMMARY

A numerical relaxation algorithm capable of calculating the transonic inviscid flow about arbitrary planform rotors has been developed. The essential feature of this method is a transformation in which arbitrary planforms are converted to rectangles and all boundary condition problems are transferred to the equation of motion. Preliminary numerical calculations are presented for blades of various sweeps and profiles. It is seen that three-dimensional effects remove sweep effects and can cause shocks which are locally more severe than would occur in less swept or even unswept planforms. The method presents itself as a soon-to-be practical means of checking various rotor configurations before any tests be made.

NOTATION

R	aspect ratio, R/\bar{c}	ΔP	pressure difference across a shock
c	ratio of local chord to \bar{c}	η	transformed spanwise coordinate
\bar{c}	a representative chord value	ξ	transformed chordwise coordinate
C_p	pressure coefficient	ϕ	small disturbance velocity potential
M_T	tip Mach number		
P_1	pressure ahead of shock		
x	\bar{x}/\bar{c} , non-dimensionalized chordwise coordinate	Subscripts	
		2-D	two-dimensional
y	\bar{y}/R , non-dimensionalized spanwise coordinate	0	leading edge
z	$\bar{z} \tau^{1/3}/\bar{c}$, scaled coordinate normal to blade		
$\bar{x}, \bar{y}, \bar{z}$	physical coordinates		

1. INTRODUCTION

The performance of conventional high speed helicopter rotors is severely affected by the large difference in dynamic pressure encountered by the blades on the advancing and retreating sides of the rotor disk. For a given rotor RPM the forward flight velocity is limited by the onset of dynamic stall on the retreating side and adverse transonic effects on the advancing side. Dynamic stall is characterized by severe vibration. It can be alleviated by increasing rotor RPM. The result, however, is to compound the transonic effects on the advancing side where the rotor tip may encounter drag divergence and shock induced separation. Hence, from a purely aerodynamic and performance standpoint, it would be desirable to increase the maximum allowable rotor RPM by minimizing transonic tip effects. One approach to the problem is to vary the rotor tip geometry. Only very approximate methods have been used in such design. The problem is that transonic flow has yielded little to analysis. In addition, there exists, to our knowledge, no reliable pressure data for flow about rotor tips in the transonic regime. However, rotors with various tip planforms have been flown, and improvements in performance and noise have been noted. What is now needed is a reliable means to judge the relative merits of various configurations and improve their design. The numerical simulation of such flows is becoming more attractive due to the increasing speed and capacity of modern computers and the rapidly advancing state of the art in computational fluid mechanics.

Recent renewed interest in transonic aerodynamics has given rise to the development of numerical methods for predicting inviscid transonic flows which include the presence of embedded shock waves. The most efficient techniques at present use relaxation methods to solve finite difference approximations to the governing non-linear small disturbance equation. In the paper of Murman and Cole (Ref 1) it was shown that the use of mixed backward and central differences renders the old relaxation methods quite adequate for calculating two-dimensional transonic flows. By central and backward differencing in the subsonic and supersonic regions respectively, one correctly simulates the physics, i.e., upstream signal propagation in the hyperbolic region is prevented. When this is done, shocks appear quite naturally; no special jump conditions need be specified. Subsequent works have improved on the basic mixed differences method of Murman and Cole (Ref 2,3,4,5). Results have been published which show excellent agreement with experimental data (when corrected for wind tunnel wall and viscous effects) for lifting airfoils with both blunt and sharp leading edges. Work in three dimensions has been limited both by the increased complication of the additional space dimension, and by the increased cost involved. For this reason, three-dimensional

work has been confined to the solution of the inviscid transonic small disturbance equation with linearized boundary conditions. In the work of Ballhaus and Bailey (Ref 7 & 8) solutions were obtained for flows about thin, blunt nose, lifting wings with sweep and taper and about nonlifting wing-cylinder combinations with and without area-ruling. Caradonna and Isom (Ref 6) derived and solved the transonic small disturbance equation for the flow about a thin sharp nose rotor in the hover condition by an extension of the mixed difference relaxation techniques to three dimensions. Calculations for other than rectangular planforms were not attempted, since it is awkward to constantly alter the mesh to fit the planform being tested. A more practical approach was undertaken by Ballhaus and Bailey (Ref 7) who treat swept and tapered fixed wings by transforming the planform shape into a rectangle. Such a procedure is particularly useful in the consideration of blunt nose airfoil sections for which a high density of grid points is required near the leading edge to account for the large gradients there.

The present work is a combination of the algorithms developed in Reference 6 and 7. We consider the simplest problem that maintains the salient features of high speed tip flow. The transonic small disturbance equation for the hover condition is solved for a nonlifting rotor tip of arbitrary planform. The most significant simplification here is the neglecting of viscous effects and unsteadiness in incident Mach number. Calculations include the effects of rotation, nonlinear mixed flow, the spanwise freestream Mach number gradient, and the flow relief as affected by tip geometry.

2. EQUATIONS OF MOTION AND BOUNDARY CONDITIONS

The transonic small disturbance equation for the hover condition derived in Reference 6 can be expressed in the form:

$$\left[\frac{1-M_T^2}{\tau^{2/3}} - (1+\gamma) M_T^2 y \phi_x \right] \phi_{xx} + \phi_{zz} + \frac{1}{R^2 \tau^{2/3}} \phi_{yy} + \frac{M_T^2}{R^2 \tau^{2/3}} [x \phi_x + y \phi_y + 2xy \phi_{xy}] = 0. \quad (1)$$

The pressure coefficient is given by

$$C_F = - \frac{2}{y} \phi_x. \quad (2)$$

The flow tangency condition on the rotor surface is linearized and applied on the wing mean surface

$$\phi_{z,u,1}(x,y,0^+) = y \frac{d}{dx} [f_{u,1}(x,y)] \quad (3)$$

for $0 \leq y \leq 1$, $z = 0$, $x(\text{leading edge}) \leq x \leq x(\text{trailing edge})$.

Elsewhere on the plane $z = 0$, the symmetry condition, $\phi_z = 0$, is enforced. The perturbation potential is set equal to zero on the far field boundaries and two-dimensionality is imposed on the inboard boundary (see Figure 1).

Rotation has two effects, a freestream Mach number gradient and a curvature of the free streamlines. In equation (1) the former effect is accounted for by the first group of terms. The free streamline curvature, represented by the last group of terms in equation (1), has been found to have little effect for moderately high aspect ratios. Therefore, in all that follows these terms are deleted.

In using equation (1) to treat realistic rotors (those with blunt nose leading edges) with non-rectangular planform shapes, difficulties are encountered in establishing a computational grid network. Basically, there are three considerations in constructing the computational grid: (1) economy, i.e. use the minimum amount of mesh points necessary to properly resolve the flow; (2) concentration of grid lines in regions of large velocity gradients, e.g. near stagnation points and in the vicinity of the tip; (3) uniform location of boundaries (leading and trailing edges and tip) between mesh points. Experience has shown that for thin profiles with sharp leading edges, concentrating grid lines near the leading and trailing edges is desirable but not essential. In fact, for rotors with such profiles, satisfactory results can be obtained by superimposing the nonrectangular planform more or less arbitrarily on a predetermined grid system. (The resulting isobar configuration for a flowfield calculated in this manner is shown in Figure 7. Some waviness in the isobars near the leading edge is apparent due to failure to uniformly locate the leading edge boundary between mesh points, but the results are acceptable.) For blunt nose profiles however, grid lines must be concentrated near the leading edge, and boundaries should be uniformly located between mesh points. This can be easily implemented for rectangular planform rotors. However, in solving equation (1) for nonrectangular planforms, these considerations can only be met by: (1) the addition of a prohibitive number of grid lines, or (2) the use of a non-orthogonal grid system coupled with an interpolation scheme. We have chosen rather to use the following coordinate transformation, which transfers the effects of nonrectangular planform geometry from the boundary conditions to the equations of motion (see Figure 2):

$$\xi(x,y) = \frac{x - x_0(y)}{c(y)} \quad (4)$$

$$\eta = y$$

$$z = z$$

The governing small disturbance equation in terms of the new independent variables ξ , η , z is

$$\left[\frac{1-M_T^2}{\tau^{2/3}} - \frac{M_T^2 \eta (1+\gamma)}{c(\eta)} \phi_\xi \right] \frac{\phi_{\xi\xi}}{c(\eta)^2} + \phi_{zz} + \frac{M_T^2}{R^2 \tau^{2/3}} [\phi_{\eta\eta} + 2\xi_\eta \phi_{\xi\eta} + \xi_\eta^2 \phi_{\xi\xi} + \xi_{\eta\eta} \phi_\xi] = 0. \quad (5)$$

The pressure coefficient becomes

$$C_p = - \frac{2\phi_\xi}{nc(\eta)} \quad (6)$$

The boundary condition on the rotor surface is now

$$\phi_{z,u,1}(\xi, \eta, 0^+) = \eta \frac{d}{d\xi} [\phi_{u,1}(\xi, \eta)]$$

and is applied at $0 \leq \xi \leq 1$, $0 \leq \eta \leq 1$, $z = 0$.

Now the ξ - and η -meshes are independent of each other. We are free to concentrate ξ -points near a blunt nose and η -points near regions of radical geometry variation.

3. NUMERICAL ALGORITHM

Finite differences are used to approximate the derivatives of the velocity perturbation potential in equation (5). The derivatives of ϕ with respect to η and z are approximated by centered differences. For the ξ -derivatives, central or backward differences are used depending on whether the sign of the first term in brackets in equation (5) is positive or negative (to maintain stability it was found necessary to

delay backward differencing the term $\frac{M_T^2}{R^2} \frac{1}{\xi^2} \phi_{\xi\xi}$ until the sum of the coefficients of $\phi_{\xi\xi}$ in equation 5 became negative). The resulting nonlinear system of difference equations is solved iteratively by the method of successive overrelaxation. Two aspects of three-dimensional transonic flow computations require further comment - the treatment of shock waves and the treatment of rotor planforms with kinks.

Special care must be taken for rotor planforms with kinked leading and trailing edges because of discontinuities in derivatives with respect to η . Straightforward central differencing to approximate η -derivatives is not permitted across kinks. This problem can be overcome either by using one-sided differences and applying jump conditions or by interpolating across the kink. The latter approach has been found to be more effective.

An essential feature in the construction of relaxation methods for transonic flows is the manner in which local differencing schemes are formulated in the vicinity of shock waves. The important consideration is to avoid, insofar as possible, differencing across embedded shocks. In two-dimensional transonic flows over airfoils, embedded shock waves are nearly normal and hence closely aligned with the Cartesian coordinate system. Thus, central differencing of derivatives in the direction normal to the freestream is naturally restricted to small angles across the shock. The use of central and backward differences for subsonic and supersonic flow regions respectively for the streamwise derivatives also restricts differencing across shocks. Experience has demonstrated that for two-dimensional transonic flows treated in this manner embedded shock waves are resolved with very little smearing. The major problem encountered in an extension of two-dimensional relaxation techniques to three-dimensional transonic flows is the possible presence of shock surfaces that are normal and oblique to the freestream in different regions. Unless by accident the shock surface should coincide with the coordinate system, the principle of no differencing across shock surfaces is extremely difficult to implement while maintaining a stable relaxation algorithm. The differencing scheme used to solve the transformed equation is naturally biased to best capture shock waves that are parallel to the leading edge (for untapered planforms). On the other hand, the differencing scheme of Reference 6 is best suited to capture shock waves that are normal to the freestream direction. Significant smearing is to be expected for shock waves that are severely misaligned with these preferred directions. A technique designed to overcome this difficulty, which has been applied successfully to some simple cases (see Ref 8), is currently under development. A skewed computational molecule is used to avoid differencing across shock surfaces at large angles. Such an additional complication would not be worthwhile for most of the simple swept tips treated in this report, because a straightforward application of the algorithm without skewing resulted in generally satisfactory shock resolution. This point will be mentioned further in conjunction with the discussion of computational results.

4. RESULTS

A series of flows for various swept planforms has been computed. Figures 3 through 5 show the isobar and C_p cross section plots for 12% circular arc profiles at $M_T = .88$ with sweeps of 0° , 15° , and 30° respectively. The 30° sweep case has been computed using both the transformed and untransformed methods, and the results compare well with the exception that the transformed results show some shock smearing near the tip. This is not unexpected since the shock is nearly normal here, which places it at about a 30° angle with the transformed coordinate system. The result of increasing sweep is as one would expect. That is, a progressive weakening of the shock with increasing sweep angle. This is seen in Figure 6 which summarizes the various flow configurations for the circular arc profiles by plotting shock strength as a function of distance from the tip in chords. These shock strengths are calculated using the normal shock relations. Incidentally, in all rotor cases we have computed, the shock has been very nearly normal to the freestream. This is due to the fact that, for the planforms considered, no portion of the transonic flow field is outside of the region of influence of the tip and of a planform kink. On the basis of a comparison of the flows shown in figures 7 and 8, calculated using the untransformed equation, it is seen that, in spite of the shock normality, sweep effects are still quite important. Figure 9 shows a comparison of shock strengths for the flows in figures 7 and 8. Considering the much more drastic leading edge angles in the "paddle" shaped tip, it is surprising that it has stronger shocks than the simply swept tip. An inspection of figures 7 and 8, however, shows that in fact the isobars for the simply swept tip have more sweep in the supersonic expansion region than those of the more complicated shape. The fact

that the isobars, in this latter case are unswept for such an extensive area (essentially the entire supersonic region) is due to the flow relief necessitated by the planform kink. Apparently, while flow relief can be beneficial in reducing shocks it can also be harmful, if it has the effect of eliminating sweep. It is, however, too early to make any general statement on the basis of this evidence as we have not yet obtained solutions for 0012 sections for the paddle type planforms, and this type of variation in profile can make a considerable difference in the sort of results obtained.

Transformation solutions were obtained for the NACA 0012 section with various simply swept planforms (Figures 10 to 12). Here the trend of the flows is quite different from that noted for the circular arc sections. Figure 13 shows that while increasing sweep does improve the situation over much of the rotor, it seems to actually make things worse very near the tip. The shock strengths at the tip for the 30° sweep case should be treated with a little caution as there is some smearing of the shock (we are actually differencing across the shock here at an angle of 30°), and the point at which the shock begins is not obvious. We have used the minimum C_p to compute the shock strength, and it is quite possible that some of the recompression occurring here is isentropic. It does not seem likely however that there is so much isentropic recompression as to radically alter Figure 13. Undoubtedly, this difference in behavior between the NACA 0012 and the circular arc profiles is related to the fact that the former profile has a severe nose expansion and a shock which always occurs much closer to the leading edge than for the latter profile. Naturally, both C_p profiles are shifted upstream at the tip of the swept section. However, the 0012, for lack of space, does so in a much more drastic manner. In fact, an inspection of the isobar sweep in the supersonic tip regions in figures 12 and 5 shows the 0012 flow to be almost completely unswept here while the circular arc flow is not. The large tip shock strength for this case could be explained by the fact that the maximum incident Mach number occurs in the tip region. The loss of sweep effect at the tips of swept wings is well known. Apparently, this is a more serious matter for a rotor, due to the Mach number gradient. The traditional "fix" for a flow such as this would be to fair the tip.

Another interesting effect we have noticed concerns the flow dependence on tip Mach number for identical blades. It was pointed out in Reference 6 that for rectangular blades there was a curious similarity in shock strength variation for different Mach numbers. We have noticed that the same effect holds for non-rectangular planforms. Figures 14 and 15 show the shock strength variation for two non-rectangular planforms with circular arc profiles at various tip Mach numbers. Unfortunately, we have as yet only obtained such comparisons for circular arc profiles, and we cannot say if this is just a quirk of a particular profile or indicative of some as yet undiscovered similarity in the equations.

All the above calculations were performed on an IBM 360/67 computer, and on such a machine they are rather expensive. For a calculation such as shown in Figure 7, in which the untransformed equation was solved, a large mesh (80 x 30 x 10) was necessary. Convergence required about 250 iterations or about two hours of machine time. In the calculations for the NACA 0012, a smaller mesh (64 x 30 x 32) was used. However, the machine time required was similar to the previously mentioned case. That machine time was not reduced in the case with fewer grid points is due primarily to the slower convergence rate resulting from concentrating grid points near the nose of blunt nosed profiles. Another contributing factor is the increased amount of work required to solve the additional terms in the transformed equation.

5. CONCLUDING REMARKS

Preliminary numerical calculations using relaxation techniques have been presented for inviscid transonic flows about thin rotor blades with various planform shapes. Computed solutions indicate the not unexpected result that similar planforms with different profiles can produce radically different flow fields. A rather surprising observation is that highly swept planforms can result in stronger embedded shock waves than less swept or even unswept ones. We expect to be able to make more definite statements concerning the effects of planform on transonic flowfields after a wider variety of cases has been analyzed. To this end, we look forward to the parallel processing capability of the new Illiac IV computer which will soon be operational. Our relaxation method is ideally suited to the Illiac, and the decrease in cost and running time should be considerable. We are currently working to improve our shock capturing technique and to develop the capability of treating rotors with lift.

While only a few cases have been treated thus far, we believe that the solutions obtained indicate that the numerical generation of transonic flowfield data will be a useful tool for improving high speed rotor design.

REFERENCES

1. Murman, E.M., and J. D. Cole, "Calculation of Plane Steady Transonic Flows", AIAA Journal, Vol 9, No. 1, Jan. 1971, pp. 114-121.
2. Krupp, J.A. and E.M. Murman, "The Numerical Calculation of Steady Transonic Flows Past Their Lifting Airfoils and Slender Bodies", AIAA Paper No. 71-566, June 1972.
3. Garabedian, P.R., and D.G. Korn, "Analysis of Transonic Airfoils", Communications on Pure and Applied Mathematics, Vol XXIV, pp. 841-851, 1971.
4. Steger, J.L., and H. Lomax, "Numerical Calculations of Transonic Flow About Two-Dimensional Airfoils by Relaxation Procedures", AIAA Paper No. 71-569, June 1971.
5. Bailey, F.R., "Numerical Calculation of Transonic Flow About Slender Bodies of Revolution", NASA TN D-6582, 1971.
6. Garabedian, P.R., and M.P. Isaac, "Subsonic and Transonic Potential Flow Over Helicopter Rotor Blades", AIAA 10th Aerospace Sciences Meeting, San Diego, CA, Jan. 1972, Pre-print No. 72-39.

7. Ballhaus, W.F., and F.R. Bailey, "Numerical Calculation of Transonic Flow About Swept Wings", AIAA 5th Fluid and Plasma Dynamics Conference in Boston, Mass., June 1972, AIAA Paper No. 72-677.
8. Bailey, F.R., and W.F. Ballhaus, "Relaxation Methods for Transonic Flow About Wing-Cylinder Combinations and Lifting Swept Wings", Proceedings of the 3rd International Conference on Numerical Methods in Fluid Dynamics, Orsay, France, July 1972.

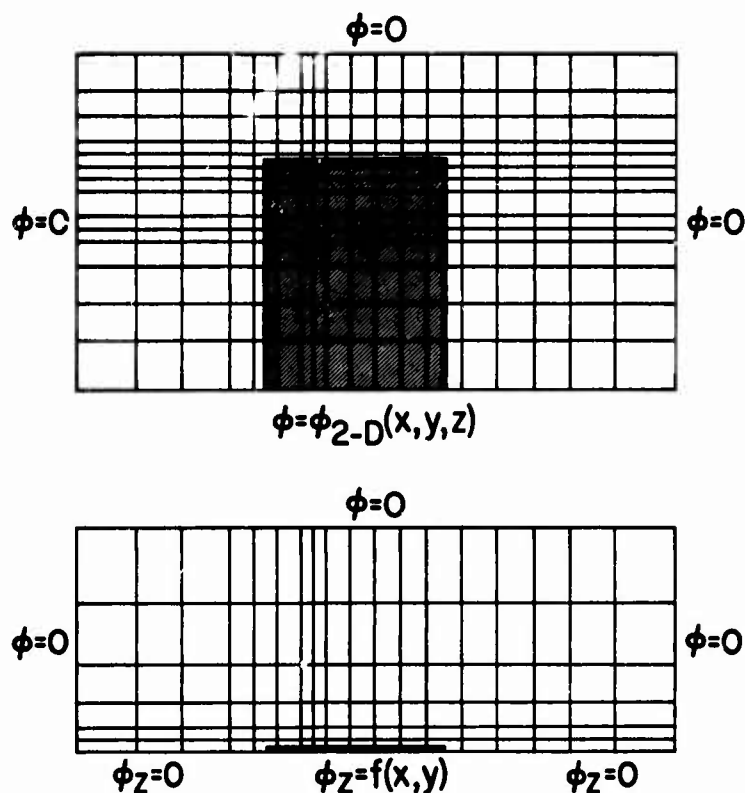


Fig. 1 Boundary Conditions and Computational Grid

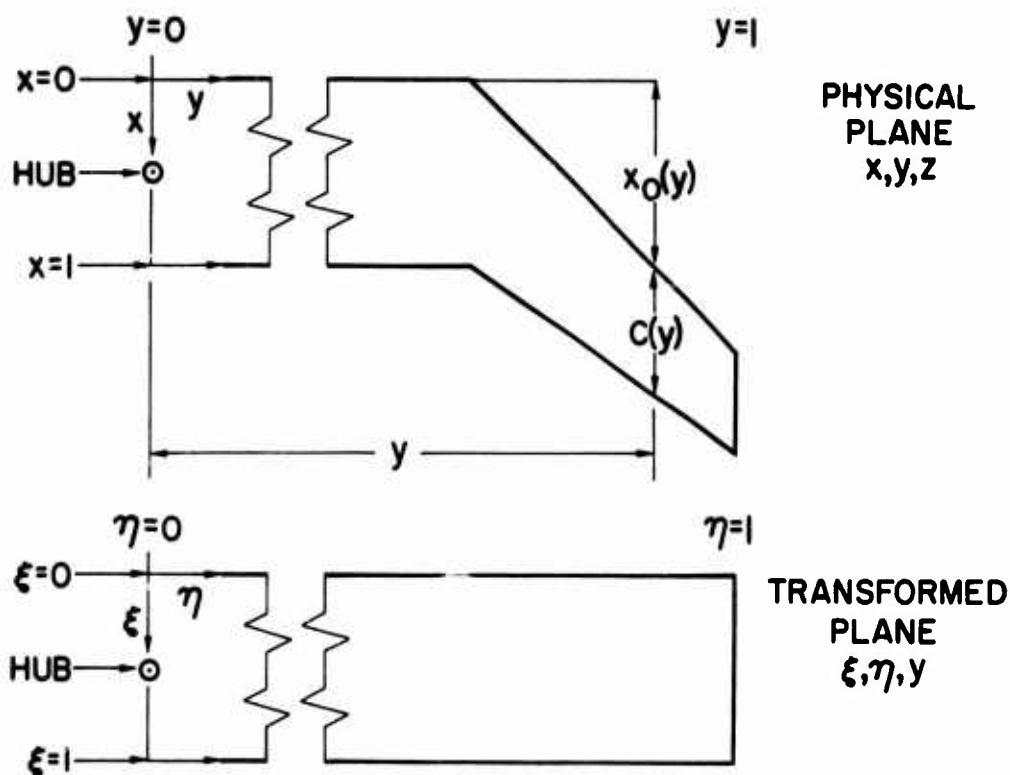


Fig. 2 Rotor Tip Coordinate Systems

12% CIRCULAR ARC PROFILE, NO SWEEP, $M_T = .88$, $R = 15$
 SHADED AREA DENOTES SUPERSONIC REGION

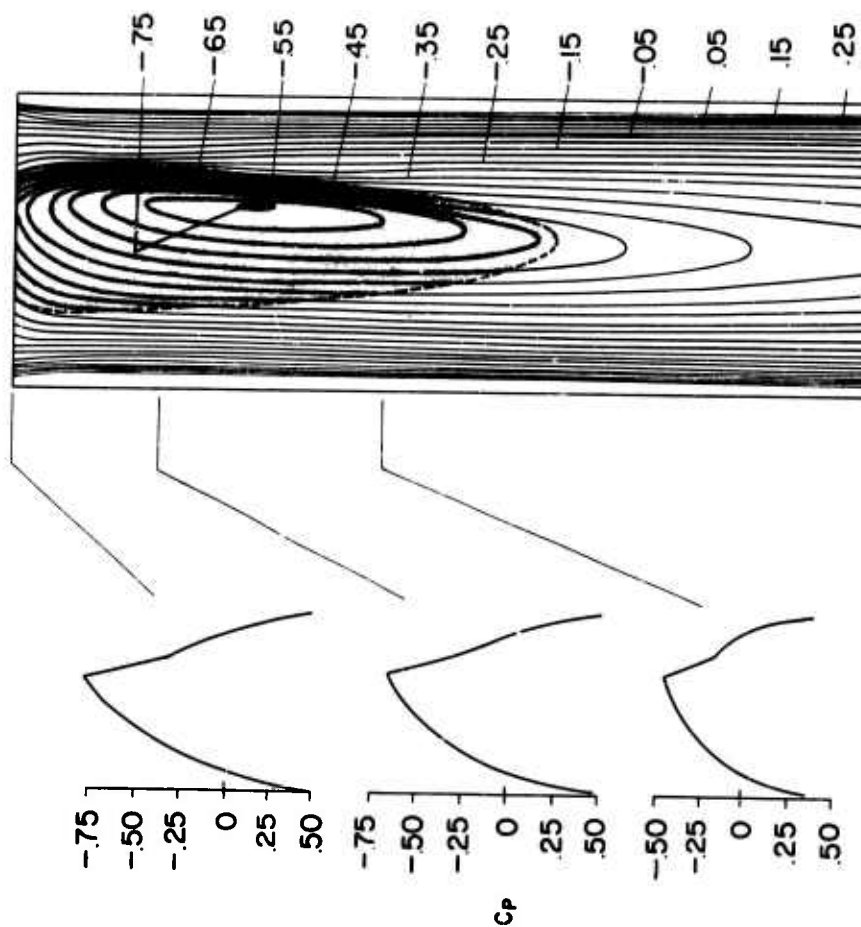


Fig. 3 Calculated Pressure Coefficients on a Rotor Tip

12% CIRCULAR ARC PROFILE, 15° SWEEP, $M_T = .88$, $R = 15$
 SHADED AREA DENOTES SUPERSONIC REGION

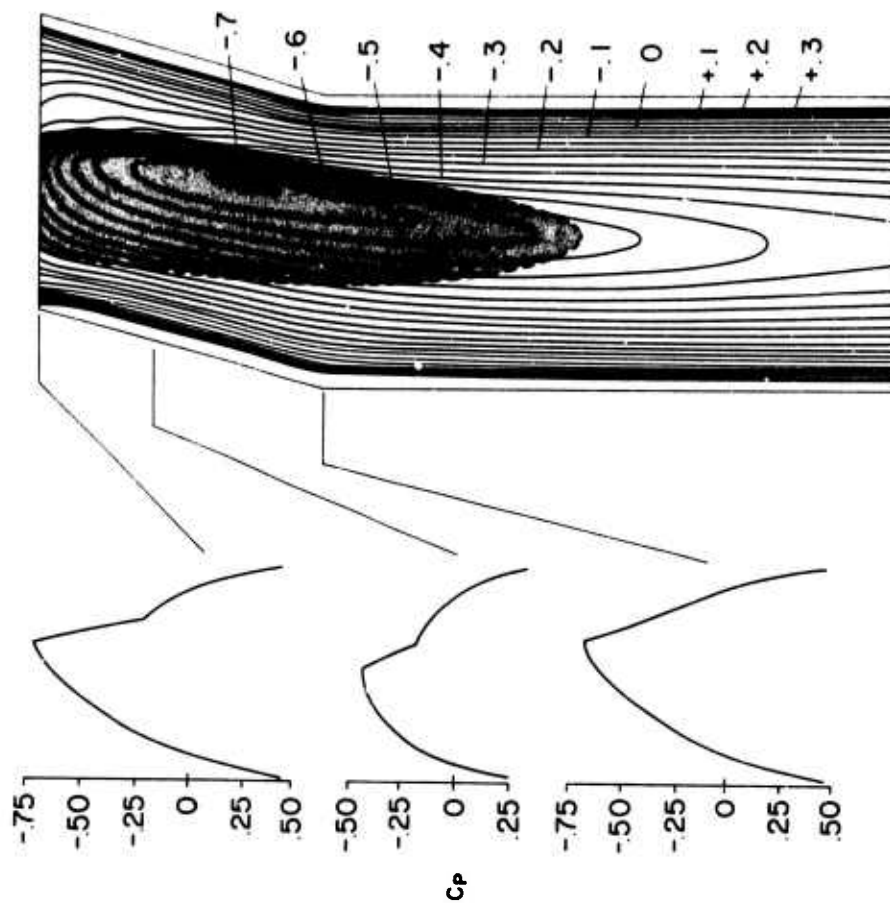


Fig. 4 Calculated Pressure Coefficients on a Rotor Tip

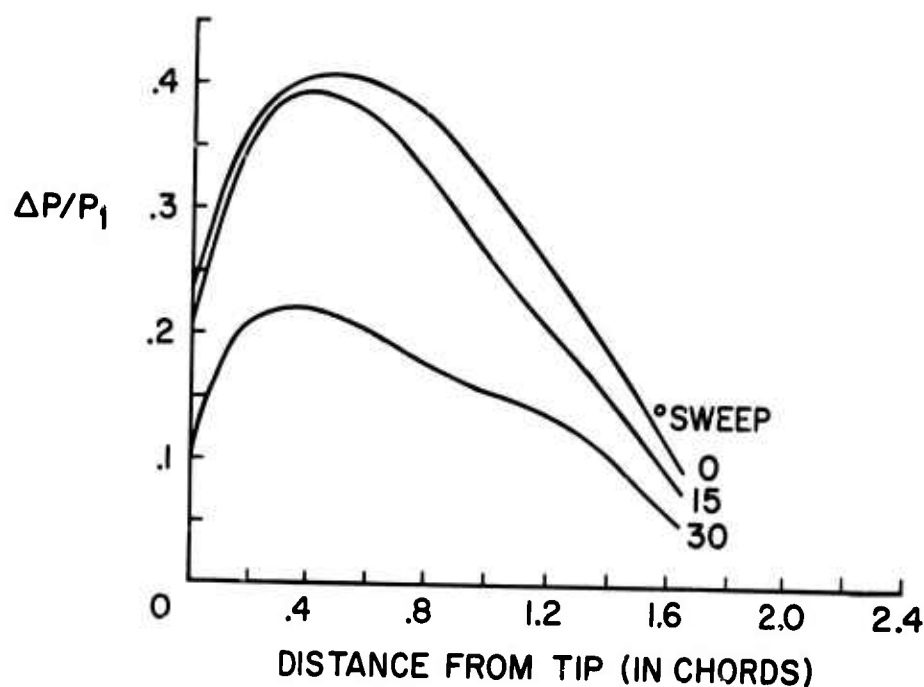


Fig. 6 Effect of Sweep Angle on Shock Strength

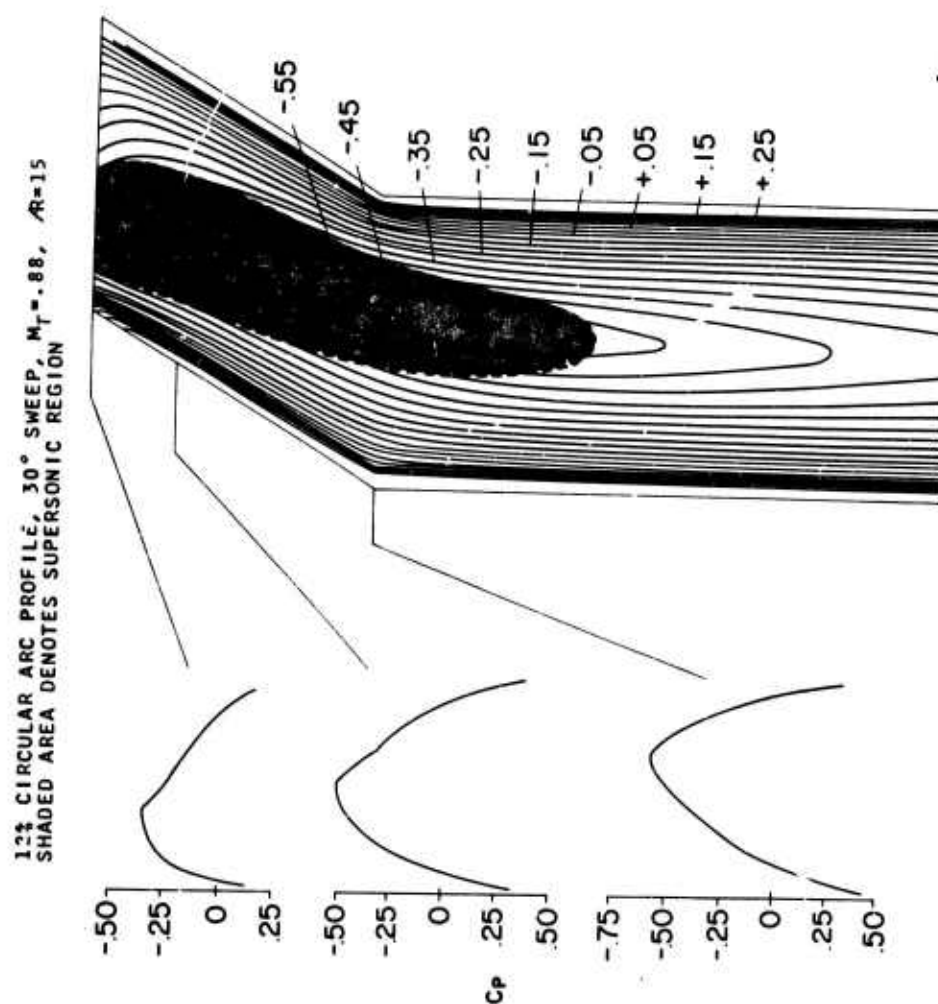


Fig. 5 Calculated Pressure Coefficients on a Rotor Tip

12½ CIRCULAR ARC PROFILE, $M_\infty = .90$, $R = 15$
 SHADED AREA DENOTES SUPERSONIC REGION

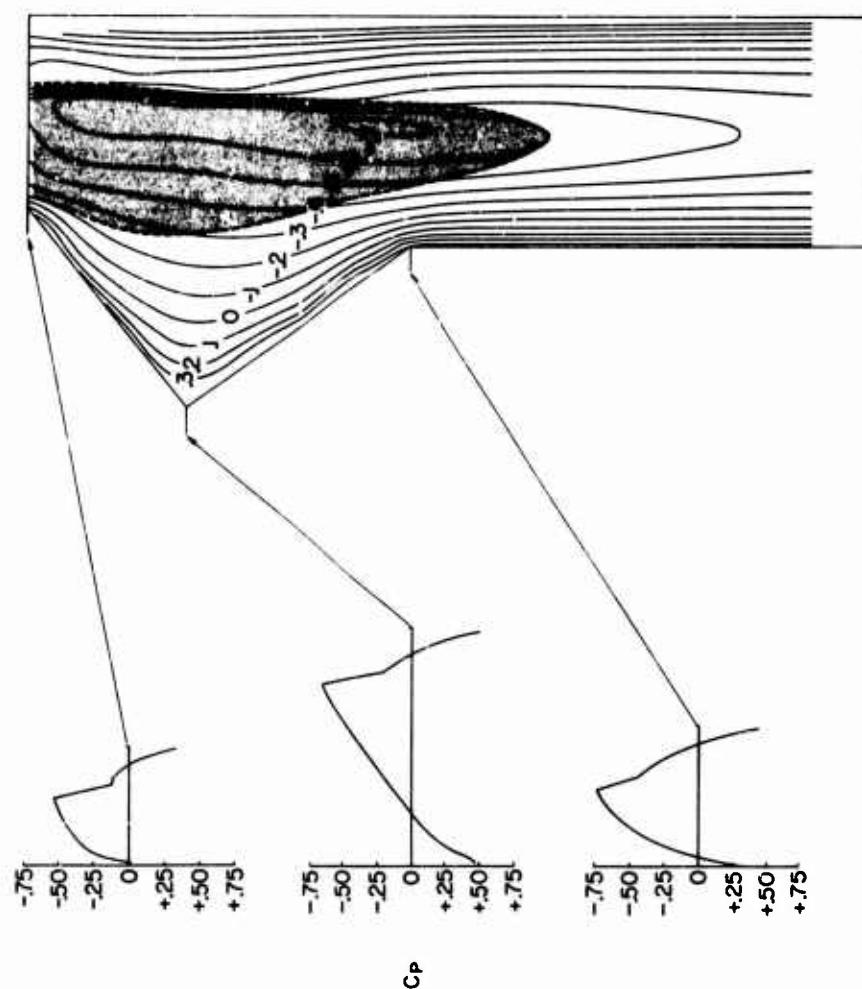


Fig. 7 Calculated Pressure Coefficients on a Rotor Tip

12½ CIRCULAR ARC PROFILE, $M_\infty = .90$, $R = 15$
 SHADED AREA DENOTES SUPERSONIC REGION

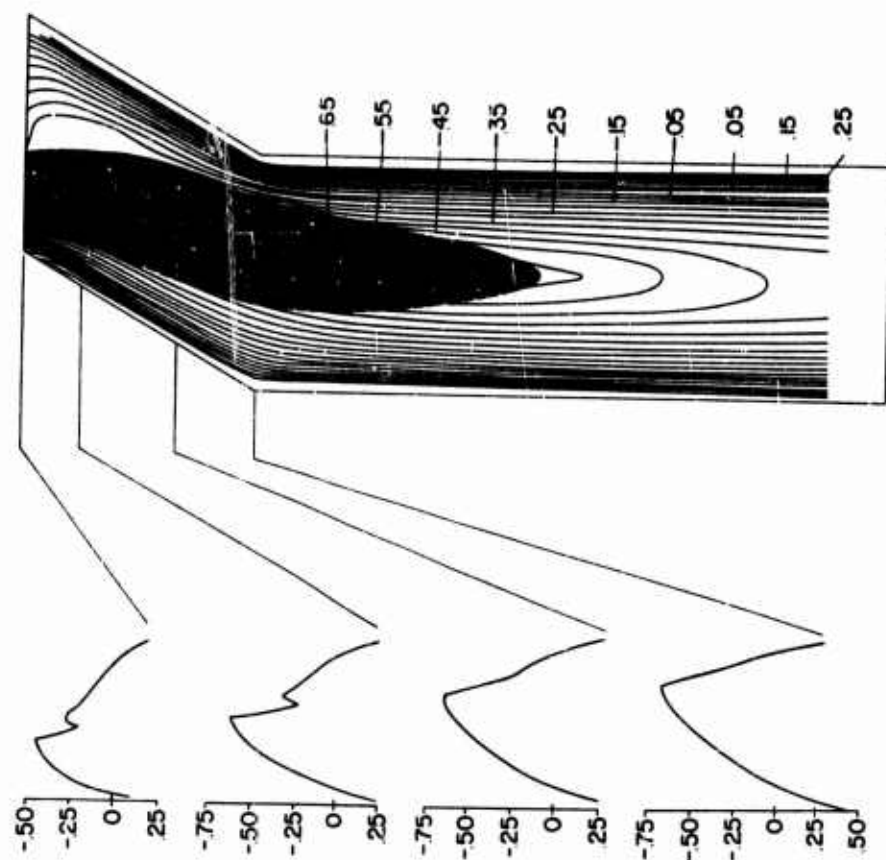


Fig. 8 Calculated Pressure Coefficients on a Rotor Tip

NACA 0012 PROFILE, NO SWEEP, $M_T = .88$, $R = 15$
 SHADED AREA DENOTES SUPERSONIC REGION

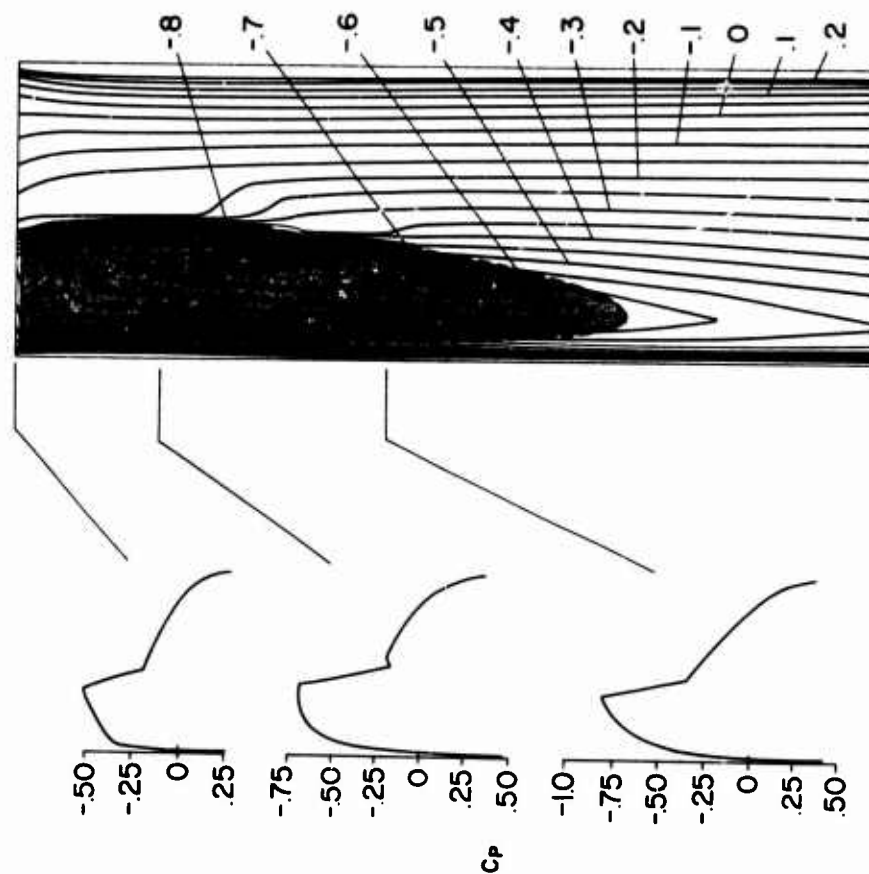


Fig. 10 Calculated Pressure Coefficients on a Rotor Tip

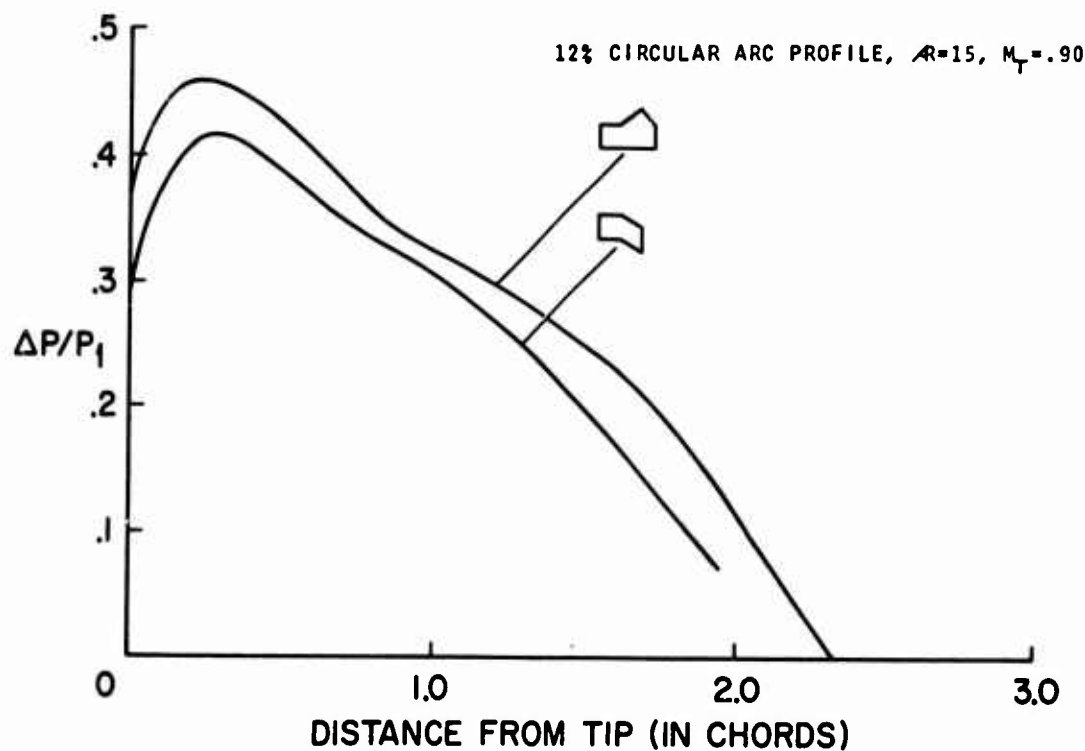


Fig. 9 Effect of Some Planforms on Shock Strength

NACA 0012 PROFILE, 15° SWEEP, $M_{\infty}=0.88$, $R=15$
 SHADED AREA DENOTES SUPERSONIC REGION

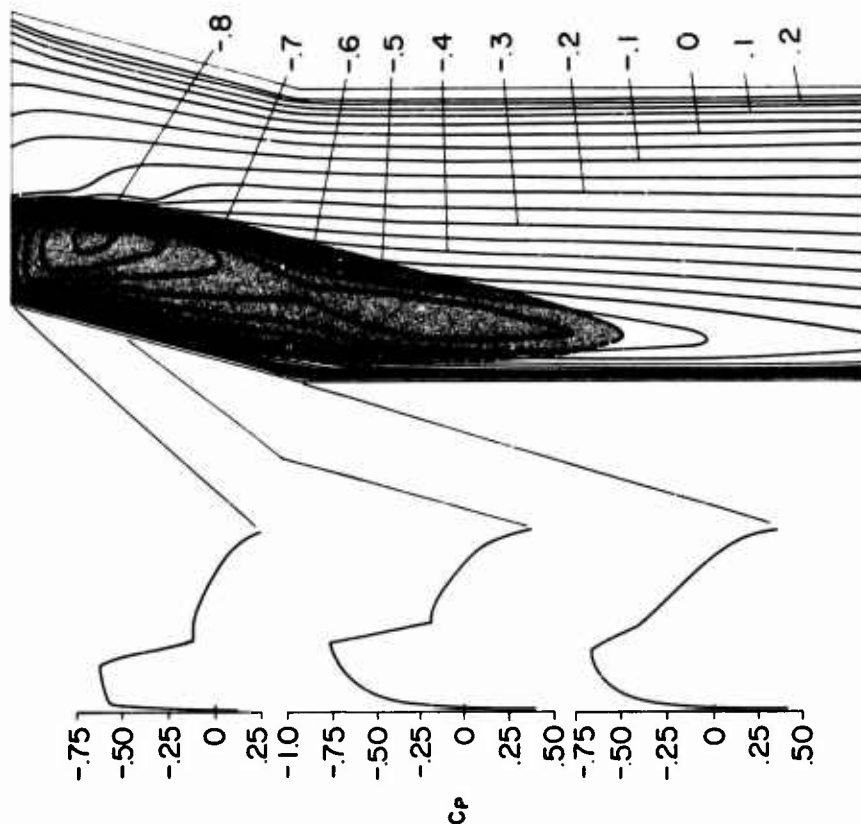


Fig. 11 Calculated Pressure Coefficients on a Rotor Tip

NACA 0012 PROFILE, 30° SWEEP, $M_{\infty}=0.88$, $R=15$
 SHADED AREA DENOTES SUPERSONIC REGION

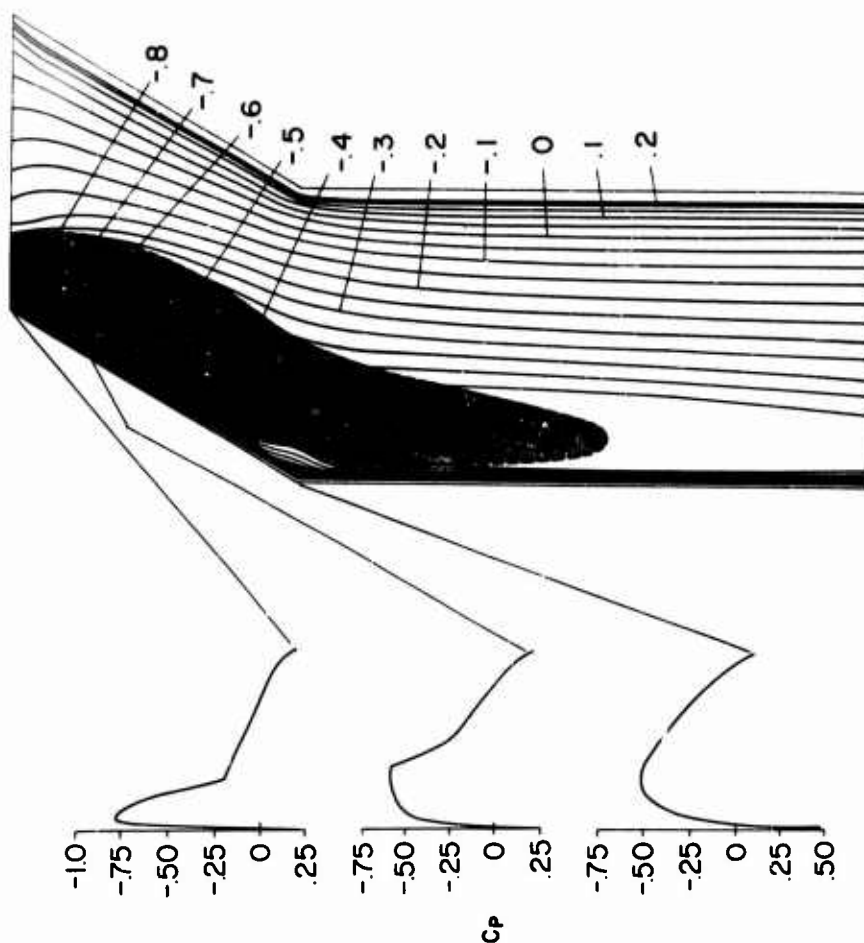


Fig. 12 Calculated Pressure Coefficients on a Rotor Tip

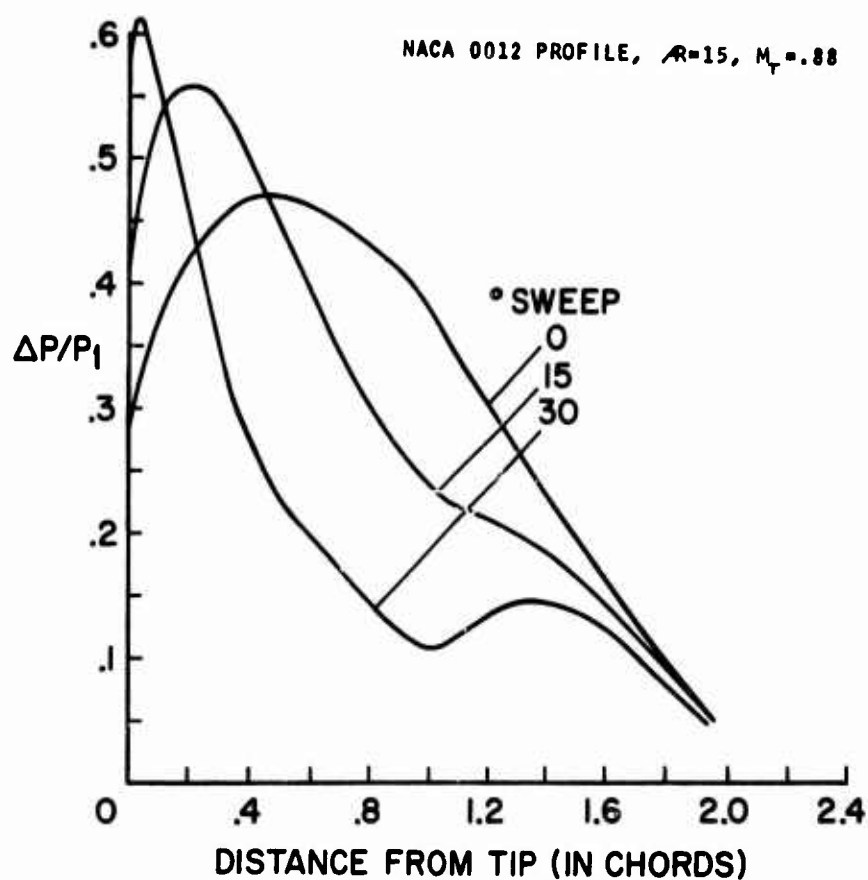


Fig. 13 Effect of Sweep Angle on Shock Strength

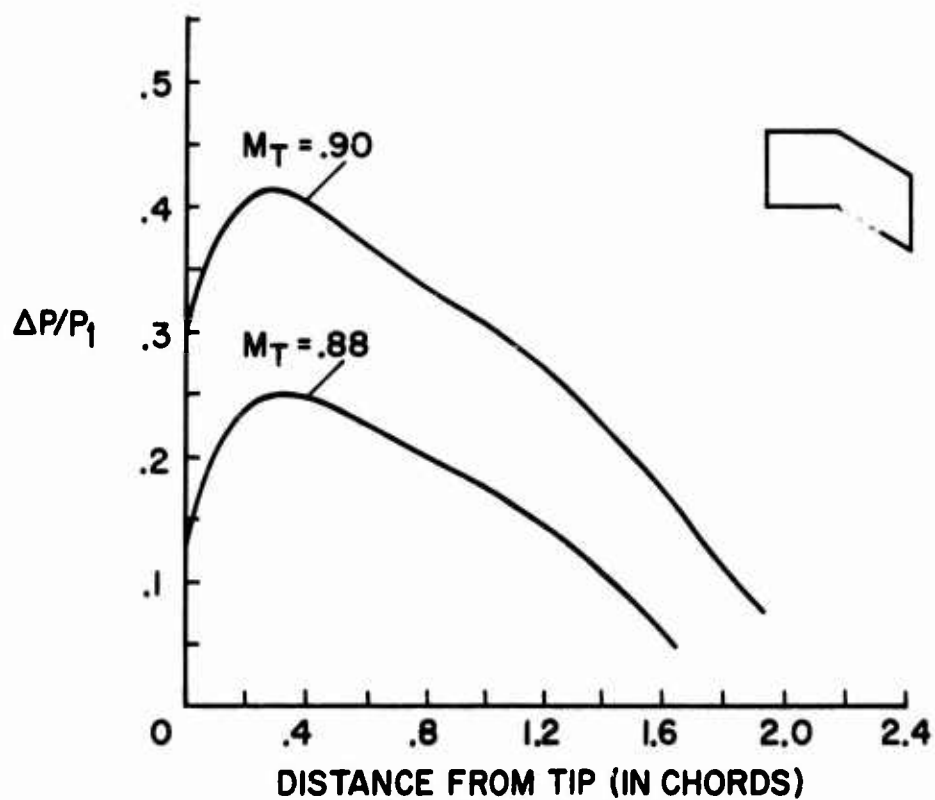


Fig. 14 Effect of Tip Mach Number on Shock Strength

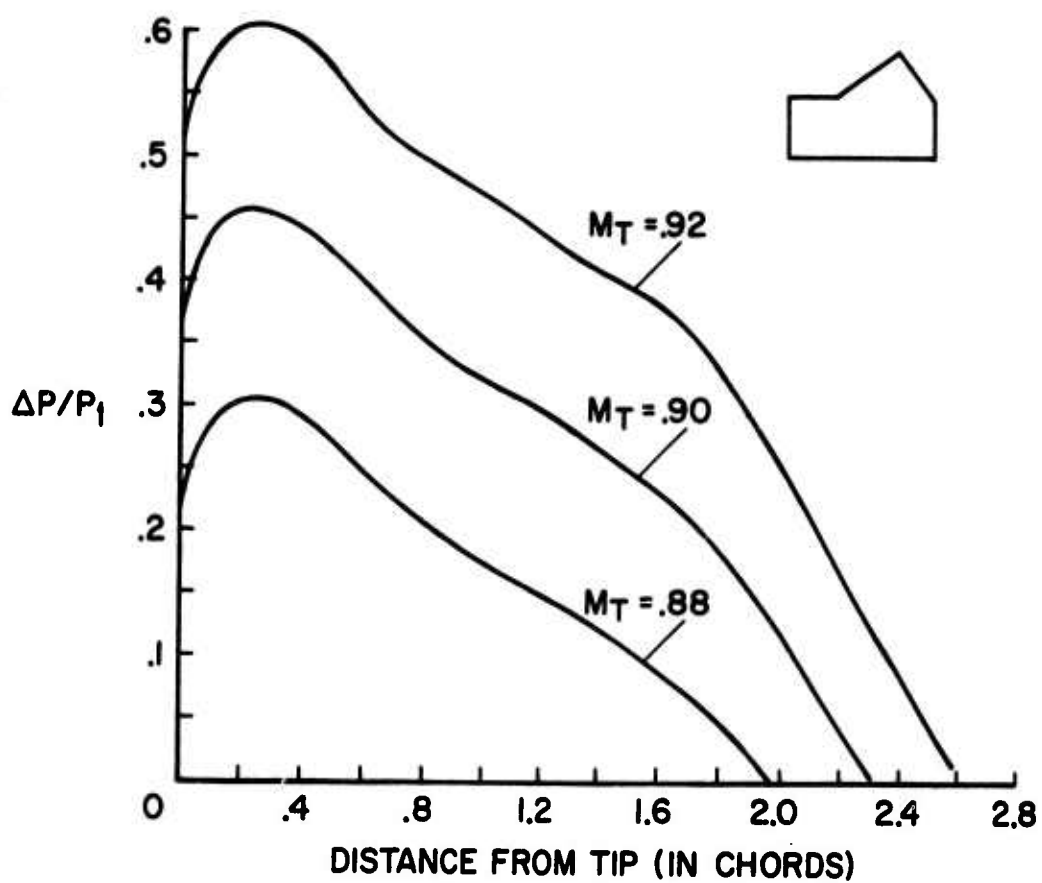


Fig. 15 Effect of Tip Mach Number on Shock Strength

A SUMMARY OF WIND-TUNNEL
RESEARCH ON TILT-ROTORS
FROM HOVER TO CRUISE FLIGHT

by

Ph. POISSON-QUINTON, ONERA^{*}
and W.L. COOK, NASA^{**}

SUMMARY

Within the framework of a cooperative agreement between NASA and ONERA, an experimental research program has been conducted on a series of tilt rotors designed for a range of blades twist in the various wind tunnel facilities of the NASA, ONERA and the USAAMRDL. The facilities include the NASA/Ames 40 x 80-foot Wind Tunnel, ONERA/Modane 8 meter sonic wind tunnel and the USAAMRDL/Ames 7- by 10-foot Wind Tunnel as well as the Air Force static test facility at Wright-Patterson.

The main objective of the experimental program was to obtain precise results about the influence of blades twist and aeroelasticity on tilt rotor performance, from hover to high speed cruise Mach number of about 0.7.

Five aluminium "rigid" rotors with various blade twists, and one fiberglass composite "dynamically scaled" rotor were tested (scaled 13/55th and 5/55th from a typical 55ft tilt rotor aircraft design); global forces on the rotor, local loads and blade torsional deflection measurements were compared with theoretical predictions inside a large Reynolds-Mach envelope. This paper describes some new testing techniques developed for this joint program and gives a brief summary of the main results obtained in the U.S. and French facilities.

NOTATION

C_d	Section drag coefficient
C_l	section lift coefficient
C_T	thrust coefficient, $T_N/\rho n^2 D^4$
C_P	power coefficient, $P/\rho n^3 D^5$
c	blade chord
D	rotor diameter, feet
D_S	spinner drag
FM	figure of merit, $0.798 \frac{C_T^{3/2}}{C_P}$
J	advance ratio, V_o/nD , with $n = \frac{rpm}{60}$
J'	$\frac{V_o \cos \alpha}{nD}$, with α : rotor tilt angle
M	Mach number
P_b	spinner base pressure
P_o	free stream pressure
R	rotor radius
\bar{R}	r/R , local blade station radius ratio
Re	Reynolds number
S_b	spinner base area
T_G	gross thrust
T_N	net thrust, $T_G + D_S$
V_o	free stream velocity
V_t	velocity at blade tip

^{*} Assistant to the Scientific Director for Aeronautics Coordination, ONERA, 92320 CHATILLON FRANCE

^{**} Chief, Advanced Aircraft Programs Office, NASA, Ames Research Center, Moffett-Field, 94035 CALIFORNIA

t	blade section thickness
α	rotor tilt angle
β	rotor blade pitch angle
$\Delta\beta$	blade twist angle, incremental or total
σ	rotor solidity
ρ	density
η	blade efficiency at forward speed.

INTRODUCTION

The tilt-rotor concept is one of the most promising candidates for future VTOL Aircraft because it provides a good compromise in design requirements for both hover and high speed cruise flight ; but two main problems must be carefully studied :

- compromise of geometry for aerodynamic optimization of hover and cruise efficiencies,
- aeroelastic behaviour of the rotor itself, and elastic coupling between rotors and airframe [Réf. 1]

To answer a part of these problems, the Research Program summarized in this paper was initiated by NASA (AMES Research Center, Advanced Aircraft Programs Office) and US Army Aeronautical Research Laboratory with a contract to the Boeing Company, Vertol Division ; the contract objective was to experimentally verify predicted levels of hovering and cruise performance [2] ; this program was conducted as a joint NASA/ONERA effort under an International Cooperative Agreement established in 1968 ; the agreement provided for the use of French and U.S. facilities and for an exchange of the resulting data.

The need for a compromise in the design requirements between hover and cruise flight of a tilt-rotor Aircraft is illustrated in figure 1 :

in hover flight (H), the requirement for efficient performance are high thrust coefficient, high rotational speed (RPM) and small values of blade twist, whereas the requirements for efficient cruise performance (C) are low thrust coefficients, relatively lower RPM, and larger values of blade twist. Typical rotor radial variations of loads and local Mach number for hover (H) and cruise (C) are also given in figure 1, which illustrates the great difference in local lift coefficient and local Mach number for the two conditions of flight.

DESCRIPTION OF TILT ROTORS

The 4 meter (13 foot) diameter rotor models are scaled from a 55-foot diameter design by Boeing-Vertol (low disc loading Tilt Rotor Aircraft, see figure 1).

The 4 m diameter was chosen in order to permit extensive tests in various facilities, including the 40 x 80 ft Ames Tunnel, the AFAPL-USAF test stand, and the ONERA - S₁ Modane sonic 8-meter diameter tunnel. Figures 2 and 3 give the general characteristics of the rotors.

The rotors have a 6-percent thickness at the rotor tip, varying to 10-percent at about 30-percent of the rotor radius. Inboard of 30-percent, due to structural requirements of the smaller 4 m rotor, it was necessary to increase the thickness rapidly to a value of 33-percent thickness at 15-percent radius. This increase in thickness had a negative effect on high speed cruise performance ; however, survey rake measurements were included in the tests to determine the performance loss due to the increased thickness which resulted in a 2 to 3-percent reduction in efficiency at the Mach number range from 0.5 to 0.68. Five semi-rigid rotor designs, each having a different total value of blade twist: 26.6°, 29°, 36°, 40.9° and 44° were tested. The detailed variation of thickness at several radial stations for the rotors and the variation of blade twist for blades D, E and F (44, 36 and 26,6 degrees of twist respectively) are shown in figure 3.

HOVER PERFORMANCE

The calculated variation of local lift coefficient along the blade radius (figure 4a) shows that, with the 44° twisted blades, a large inner part of the rotor penetrates the predicted stall boundaries, whereas the lowest 26.6° twisted blades is far from the separation regime ; this explains the large computed difference in hover efficiency (figure of merit) at the design conditions ($V_{tip} = 230$ m/sec, 6000 ft altitude) shown on figure 4b ; experimental results obtained on these two 13 ft rotors are in good agreement with the predicted (F.M., C_T) trend : the loss in rotor hover performance is about 7-percent at 44° twist compared to 26.6° twist.

The variation of the hover figure of merit measured for the five rotors as a function of their twist from the two test facilities (Ames 40 x 80 ft wind tunnel and U.S. Air Force static test rig) is given on figure 5a for the optimum thrust coefficient $C_T = 0.075$: experimental values are in close agreement with the predicted F.M., and decrease when the blade twist increases.

The variation of figure of merit with rotor blade tip Mach number (figure 5b) and thrust coefficient (figure 5c) indicate a rapid reduction in figure of merit at tip Mach above about 0.8, and a severe reduction in figure of merit occurs at thrust coefficients above about .09, for a given tip Mach number. The data and calculated values indicated that, at design conditions (tip Mach number of 0.67 and thrust coefficient of 0.075) the figure of merit values range from a maximum of about 0.79 for the lower values of twist below 30° to less than 0.72 for values of blade twist greater than 44 degrees.

To illustrate the scale effect, figure 6 presents the variation of figure of merit as a function of thrust coefficient for the 13-foot rotor and for the 5-foot rotor tested by the U.S. Army (AARL Static rig), with the same 36° twist law.

A 5-percent loss in figure of merit with the smaller scale 5-foot diameter rotor at the design C_T can be explained by a Reynolds number effect already evidenced on higher disc loading propellers (see figure 6, profile drag versus Re , and Ref. 1).

The 13-foot rotor falls on the flat part of the curve (F.M., Re) above critical Reynolds number, whereas the 5-diameter rotor (mean Reynolds number of 0.7 million) is on the steep part of the curve. From these curves it would be expected that a 55-diameter rotor would have about 2 percent higher figure of merit than the 13-foot diameter rotor and also that the low disc loading propeller having about 10 to 12 pounds per square foot disc loading would have from 1.5 to 2-percent lower figure of merit than the maximum performance envelope values for higher disc loading propellers.

About hover performance measurements on scaled rotor models, a new method has been recently developed in the ONERA S₁ Modane wind-tunnel, based on an extrapolation to zero speed of the results obtained at very low speed inside the closed test section (figure 7).

For the first time, it was possible to check the validity of this method by comparison with "true" static tests obtained with the same 13 ft rotor on the U.S.A.F./Wright-Field rig: it can be seen in figure 7 that the extrapolated results on power and thrust coefficients obtained at very low values of the advance ratio J in S₁ Modane are in close agreement with those measured on the Special AF/APL static facility; also shown, on the (C_T , J) graph, is the theoretical trend, assuming that C_p and F.M. at low J values are the same as those obtained on a static rig at $J = 0$ (from the relationship:

$$F.M. = \frac{C_T}{C_P} \left(\frac{J}{2} + \sqrt{\left(\frac{J}{2}\right)^2 + \frac{2}{\pi} C_T} \right).$$

To use such low test speed it is necessary:

- to stop the wind-tunnel fans,
- to fit a low permeability screen to the rear of the first diffuser (to reduce the mass flow induced by the rotor inside the return circuit),
- to measure this very low speed with special instrumentation (double-venturi tube).

Finally, the speed was reduced to 2-4 m/sec with the lowest screen porosity, but attained 10-15 m/sec without any screen at the first diffuser exit.

FORWARD SPEED TESTS, RIGID BLADES

Shown in figure 8 is a schematic of the ONERA/Modane 8-meter test facility and the two test rigs used for these investigations wherein one rig is utilized for low speed tests for a large range of tilt angles, 0 to 10-degrees, with a minimum sized after body (this later rig was also used for the previous "quasi-static" tests).

This large tunnel [Réf. 3] has a continuous operating mode with three interchangeable test sections, one of them being mainly used for rotor and propeller, driven by a group of gas turbines (1000 HP); the tunnel is powered by two counter-rotating fans driven by hydraulic turbines (2 x 55000 HP); the stagnation pressure is atmospheric $p_{st} = 0.9$ bar, at the local 3300 ft altitude; the circuit cooling is obtained by air exchange; the test speed can reach Mach 1, but for the purpose of these rotor tests the Mach number was limited to about 0.7.

TILT ROTOR TRANSITION REGIME

One of the goals of the cooperative NASA/ONERA program was to compare the results obtained on the same rotor ($S_R = 12, 5 \text{ m}^2$) inside two very different test section sizes, at Ames ($S_T = 265 \text{ m}^2$) and at Modane ($S_T = 50 \text{ m}^2$), during the transition regime of flight. The effect of tunnel wall on tilt rotor test data, particularly at low speed and high tilt angles, has been the subject of considerable controversy and discussion. The 13-foot diameter rotor was tested in the Ames 40- by 80-foot wind tunnel through a range of tilt angles from 0 to 78° and a range of speeds. The tunnel wall effects of the 13-rotor in the 40- by 80 foot wind tunnel are presumably very small at disc loading of 10 pounds per square foot and at this very low area ratio $S_R/S_T \approx 5\%$. The same rotor 13-foot diameter was tested under the same tilt angle and velocity conditions in the 26-foot or 8-meter wind tunnel wherein the area ratio S_R/S_T is very large: 25%; some investigators have claimed that this ratio would be too great to even consider testing. Nevertheless, the results of these tests in the two wind-tunnels are shown in figure 9: The thrust coefficient as function of the effective advance ratio J^* which is $J \cos \alpha$ (α , angle of tilt) indicates that there is good correlation between the results of the tests in the two wind-tunnels and thus the tunnel wall effects of the 13-foot rotor tested in the ONERA 8-meter wind tunnel are of little significance for research studies of this type of VSTOL propulsion system, at low disc loading. Figure 9 shows that the previous hover tests

in the 40' x 80' Ames tunnel (made with open overhead wind-tunnel doors to minimize from recirculation) give a good extrapolation at $J' = 0$.

CRUISE TESTS

The cruise mode (axial flow) investigation was conducted at the S₁ Modane tunnel on a special axial support system ($D_0 = 0.6$ m) equipped with an internal 6 component balance ; because the axial forces measured on the dynamometer included the drag of the spinner, it was necessary to tare this drag to obtain the "net" thrust in view of comparisons with rotor performance predictions ; Figure 10 explains the two successive methods used for measuring the spinner tare drag :

The first one is based on a spinner base pressure technique : the spinner form drag coefficient was determined from "blades-off" total balance force and base pressure measurements ; during the rotor tests themselves, the total spinner drag D_S was obtained by adding this form drag to the base pressure drag (measured under rotor operating conditions), and then the net thrust was given by $T_N = T_G + D_S$, T_G being the measured gross thrust.

A more satisfactory method was later used where a special balance inside the spinner gives directly its drag with the blades-on and rotating ; a comparison between these two methods seems to indicate that this later method, taking account of the presence of the blades inflow, gives a little larger spinner drag, i.e. a higher cruise efficiency (between 1% and 2%).

This spinner tare drag was found to be a very significant part of the thrust measurements as shown in figure 11 : the gross thrust T_G measured had negative values at Mach numbers above 0.6, where the spinner drag D_S became greater than the blade thrust T_N . All the thrust data shown here have the total spinner drag removed and hence the performance characteristics are for the blades alone and do not include the spinner skin friction or profile drag which would exist on the rotor in flight, whereas the base drag would be part of the total aircraft drag. Also shown in figure 11 are typical advance ratio, J , and thrust coefficient values for a tilt rotor aircraft for a range of Mach numbers from 0.3 to about 0.67 which are used in the following analysis ($V_{tip} = 180$ m/sec, $Z = 10.000$ ft). For all these results from S₁ Modane tunnel, the conventional Glauert wall corrections have been applied (ratio $S_R/S_T = 0.25$), but low levels of thrust loading result in small magnitude of these corrections.

At a cruise Mach number of 0.455, about 290 knots, the radial section lift coefficients and cruise efficiency for blades D and F, 44.0 and 26.6° of twist are shown in figure 12 : although blade F at 26.6° is the best at hover, its section loading is poor and shows approximately one half of the blade (inboard of about 55-percent radial station) with a negative lift which results in a 15-percent lower value of cruise efficiency than for blade D at 44° where positive section lift coefficients exist except over the outboard 10-percent of the radius.

The data in figure 13 are the thrust coefficient and efficiency (*) for a range of advance ratios at two blade angles at each of three Mach number, $M = 0.455$, 0.54 and 0.68. The design thrust coefficient variation with J and the resulting efficiency at each Mach number is also indicated. Because of the low disc loading of the rotor the thrust at maximum efficiency of the rotor is not useable and of no value for the normal cruise operation of tilt rotor aircraft having reasonable levels of drag. As shown in the figure the maximum values of efficiency occur at thrust coefficients and hence power coefficients that are 2 to 4 times higher than required for the aircraft with the higher values occurring at the lower Mach number of 0.455. Utilization of the maximum values of efficiency can only be obtained economically by utilizing rotors or propellers having significantly higher values of disc loading of the order of 250 to 350 daN/m² (50 to 70 pounds per square foot) instead of about 50 daN/m² (10 lb/sq.ft) chosen here.

The data shown in figure 14 summarize the measured cruise efficiency for blades D, E, and F over the Mach number range tested 0.3 to 0.72 and the variation of cruise efficiency with the five differently twisted blades for 0.455 and 0.606 Mach number :

- High Mach number tests ($0.5 < M < 0.72$), i.e. above the rotor design calculation ($M = 0.455$, see Ref. 2), were run to investigate compressibility effects on cruise mode tilt-rotor performance ; figure 14a shows a large decrease of the cruise efficiency above $M = 0.6$ due partly to the large profile thickness (33%) at the blade root (required for structural conditions on these scaled models).

- The blade twist effect (figure 14b) is very important, the best efficiency being obtained with the largest blade twist tested (i.e. an opposite trend than shown in hover) ; the calculated values given here for $M = 0.455$ [Ref. 2] takes into account the measured velocity profile at the disc plane (a small flow acceleration was detected around the "minimum body" in S₁ Modane tunnel) ; the predicted values are higher than those measured, mainly at the lowest blade twist ; for the "E" blade (36° Twist) the experimental cruise efficiency is 0.71 against 0.745 predicted.

To conclude about the need for a compromise between the performances obtained in hover and in cruise modes, figure 15 gives the measured and predicted values of hover figure of merit as a function of the design cruise efficiency at $M = 0.455$. It appears that a blade twist of about 36° ("E" rotor) seems the best compromise for this typical project (F.M. = 0.775, $\eta_{cr} = 0.71$).

(*) The symbols on these graphs are directly reproduced from the automatic plotting of a computer program, which takes account of all the corrections and tares.

FORWARD SPEED TESTS ON AEROELASTICALLY SCALED ROTOR

To study the effect of aeroelasticity on rotor performance, a special 13 foot diameter fiberglass model had been designed and built [Ref. 2] with the optimum twist shown previously (type "E", 36° twist); the main purpose of the tests in the cruise mode was to study the effect of Mach number and loading on "live" twist deformation, and the effect of aeroelasticity on rotor/blade stability. Shown in figure 16 is a sketch of the aeroelastic blades and the photographic torsional blade deformation technique utilized to measure the variation of "live twist" during tests of the rotor. In this method, an ultra high speed photographic flash unit was used to obtain stop action photographs of the back face of one of the rotating blades which was painted with triangular targets at regular spanwise intervals. The angular difference between a pair targets and the blade root reference targets is related to the blade radial twist distribution. A comparison of this measured distribution under forward speed conditions is made with that of the static twist distribution with the blades nonrotating which gives the instantaneous aeroelastic torsional deflection for various radial stations. A comparison for a typical test point is also shown in figure 16 which indicates about a 2 degree torsional deflection near the rotor tip. An interesting aspect of the measurements was that the so called "rigid blades" (built of aluminium) had noticeable blade deformation as shown in figure 17 and that there was a consistent one degree greater twist deformation with the aeroelastic blades than with the "rigid blades" over the entire Mach number and advance ratio, J , range tested as shown in the figure.

The variation of thrust coefficient and efficiency for Mach numbers of 0.455, 0.54 and 0.606 for a range of advance ratios for the aeroelastic blades is compared in figure 18 to the rigid blade data shown previously. Although there is a significant increase in the sharpness of the slope of thrust coefficient variation with advance ratio, the actual cruise efficiency for the cruise Mach numbers is nearly equal to the cruise efficiency with the rigid blades, again indicating a very small twist deformation equivalent to the 1 degree measure. The steepness of the thrust coefficient curve with velocity for the aeroelastic rotor relative to the rigid rotor may be of great concern at the higher Mach numbers due to the potential high sensitivity of thrust to speed and blade angle. This sensitivity made it difficult to control thrust during the wind tunnel tests particularly near values of low or negative thrust where instabilities did occur with the aeroelastic rotor, and prevented testing above a Mach number of 0.606 (the "rigid" rotor was tested to a Mach number of 0.72 with no indication of instability).

A summary curve is shown in figure 19 which compares the measured cruise efficiency for the 36 degree twisted blade rotor for the various rigid and aeroelastic blade rotors tested since 1968 with the calculated cruise efficiency for the same rotor. As can be seen above a Mach number of about 0.45 the test data shows a significant lower cruise efficiency than calculated. At 0.72 Mach number the measured values are of the order of 0.45 whereas calculated is near 0.65. The correlation of the various test data is good in as much as the accuracy of the test data is ± 0.01 in efficiency.

In figure 20 is shown a trace of a specific divergence of rotor loads at a Mach number of 0.63 with the aeroelastic blades that prevented any further tests above a Mach number of 0.606. As can be seen, a rapid and divergent increase in thrust (on the main balance) and in local blade-element torsion and chordwise stress (measured at 23% and 25% R, see figure 21) were measured; a blade flutter occurred prior to the quick stop initiated as these measurements were being monitored. Further analyses on stress data measured on this elastic rotor, taken at 10 degree angle of attack at low Mach number (figure 21), in an effort to better understand the stability problem that was encountered during the tests. But it must be remembered that the Mach number of 0.63 where the instability or flutter occurred is significantly above the anticipated design cruise Mach number of about 0.46 for potential tilt rotor type aircraft being considered.

REFERENCE

- [1] GILLMORE K.B. - Survey of tilt rotor technology development
Agard Meeting on Advanced Rotorcraft NASA/Langley, sept. 1971 - AGARD/F.M.P. Proceeding.
- [2] BOEING-VERTOL Cy- Investigation of the performance of low disc-loading tilt rotors in hovering and cruise flights (NASA contract NAS2-5025) - BOEING/Vertol Division report D160 - 10013 - 1 and 2, March 1971.
- [3] PIERRE M. - Caractéristiques et possibilités de la grande soufflerie sonique de Modane-Avrieux.
ONERA - Note technique n° 134 (1968).

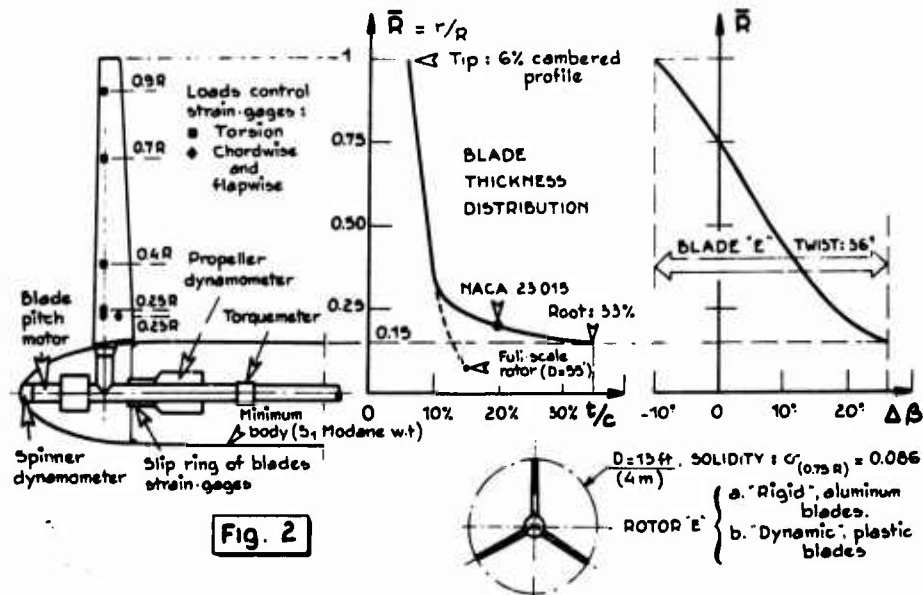
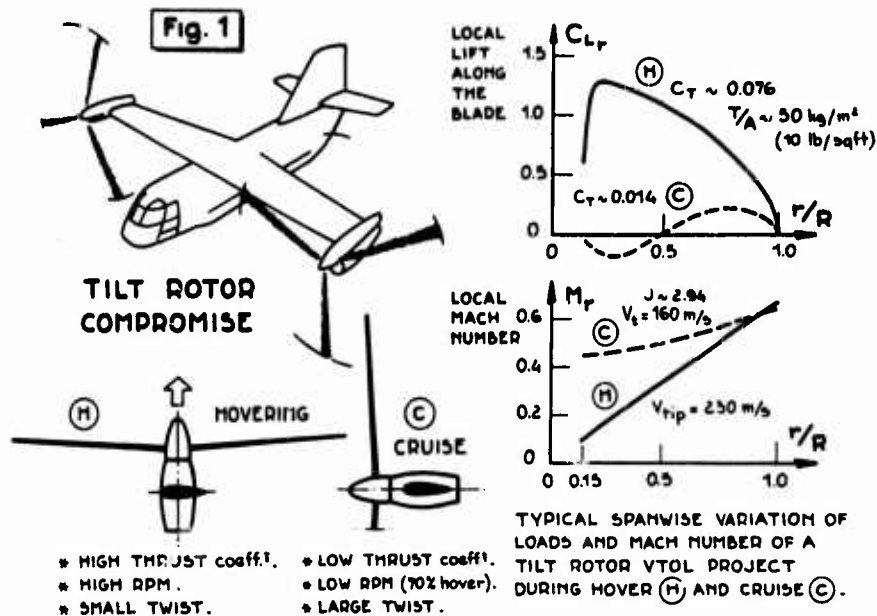


Fig. 3
TILT ROTOR
DIMENSIONAL CHARACTERISTICS

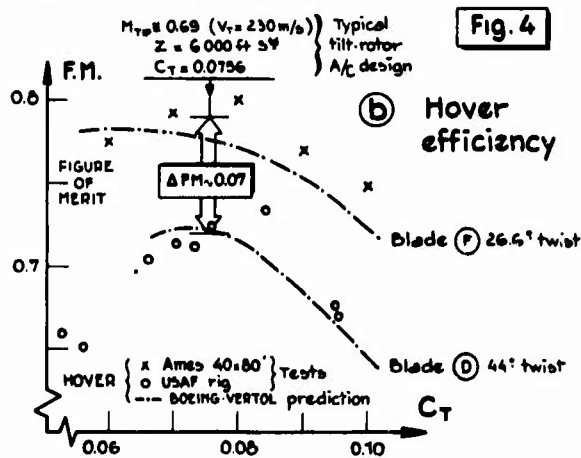
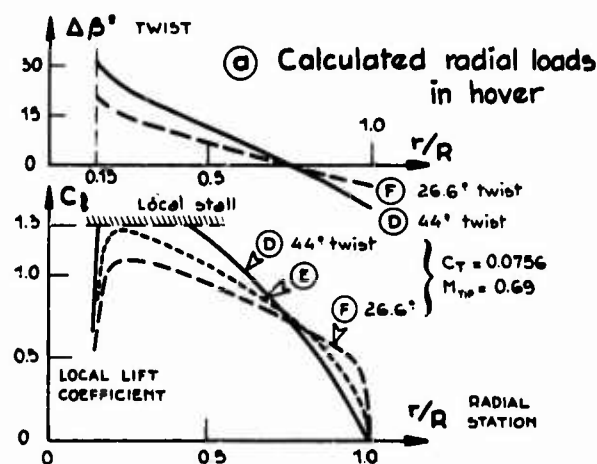
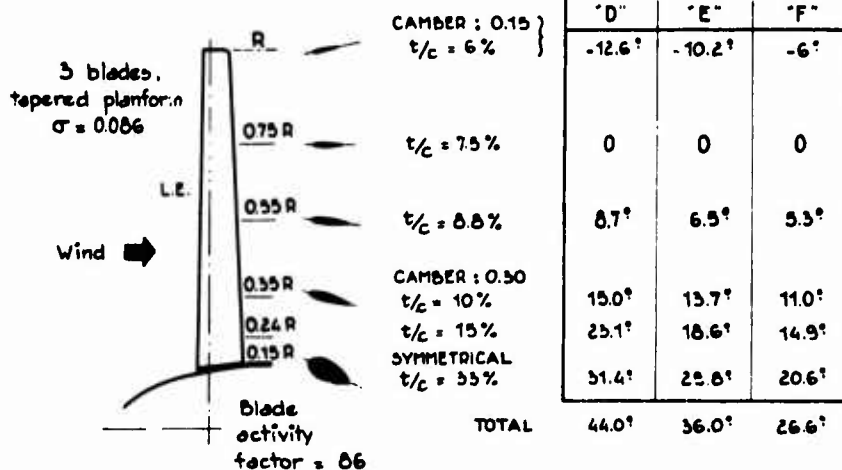


Fig. 5

HOVER, RIGID BLADES $\sim 1/4$ scaled models $D = 15$ ft

Static tests $\left\{ \begin{array}{l} \text{--x-- NASA 40x80 ft W.T.} \\ \text{1968-6- AIR FORCE RIG (Wright-Field, APL).} \end{array} \right.$

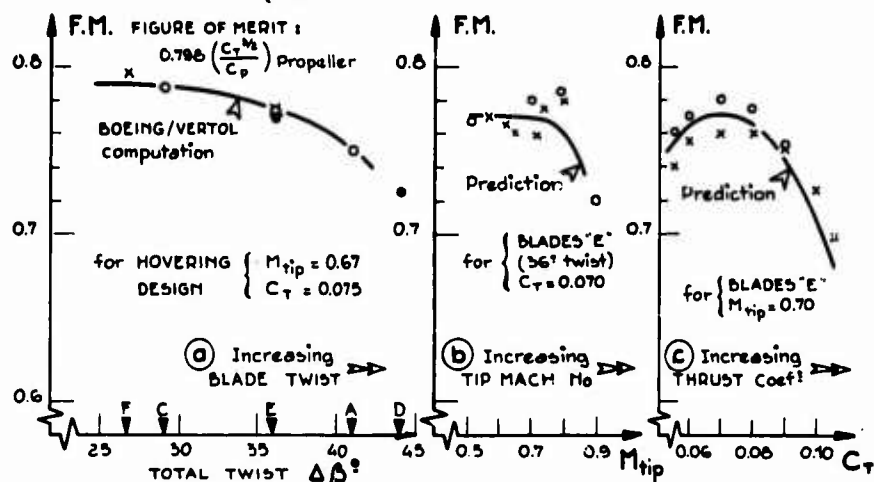
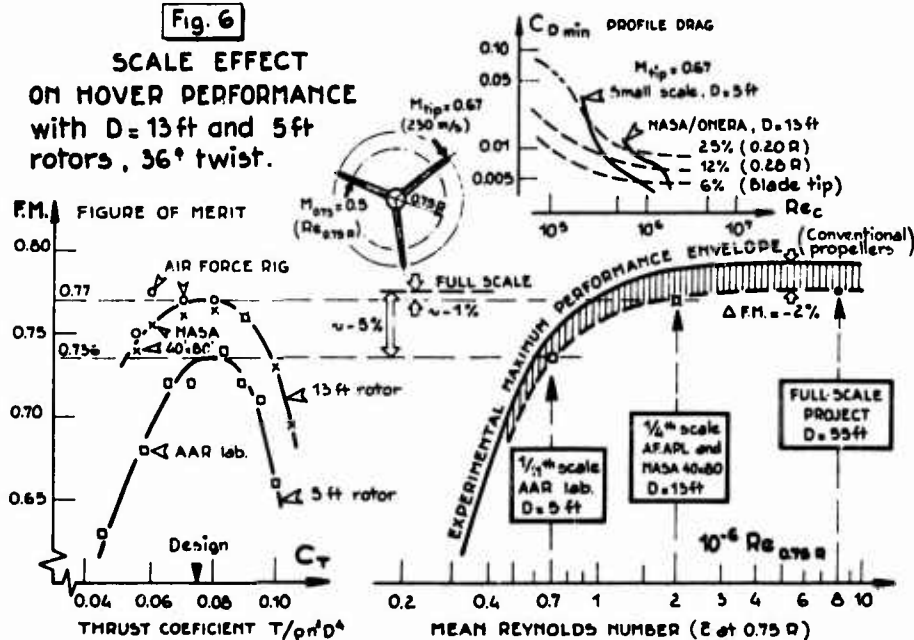


Fig. 6

SCALE EFFECT
ON HOVER PERFORMANCE
with $D = 13$ ft and 5 ft
rotors, 36° twist.

HOVER PERFORMANCE ON A ROTOR
by extrapolation to $J=0$ from wind-tunnel
tests at very low speed.

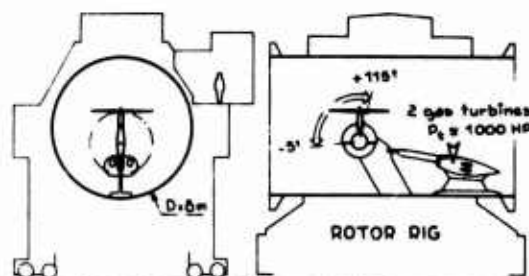
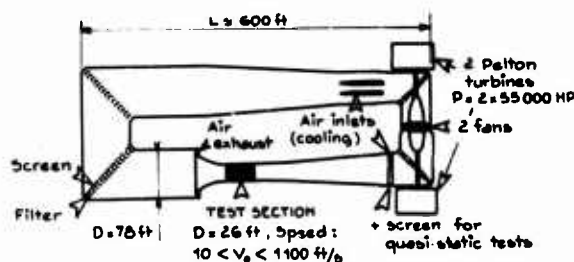
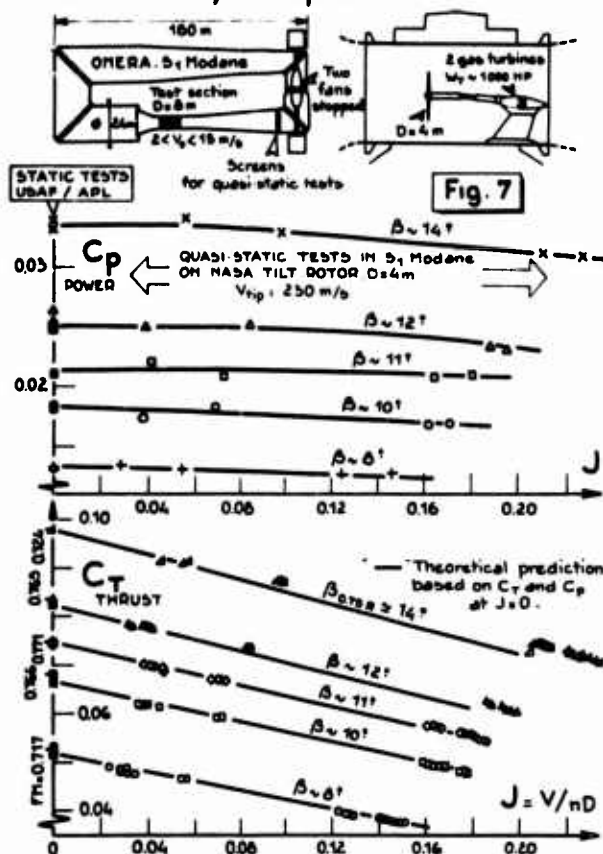


Fig. 8

ONERA TESTS
IN THE SONIC
S₁ WIND-TUNNEL

- * Helicopter rotors.
- * Tilt rotors.
- * V/STOL airframe + propellers.

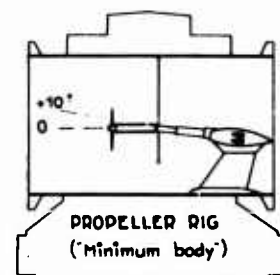


Fig. 9 TILT ROTOR TRANSITION REGIME
with F-13 ft rotor (26.6° twist), $N = 800$ rpm.

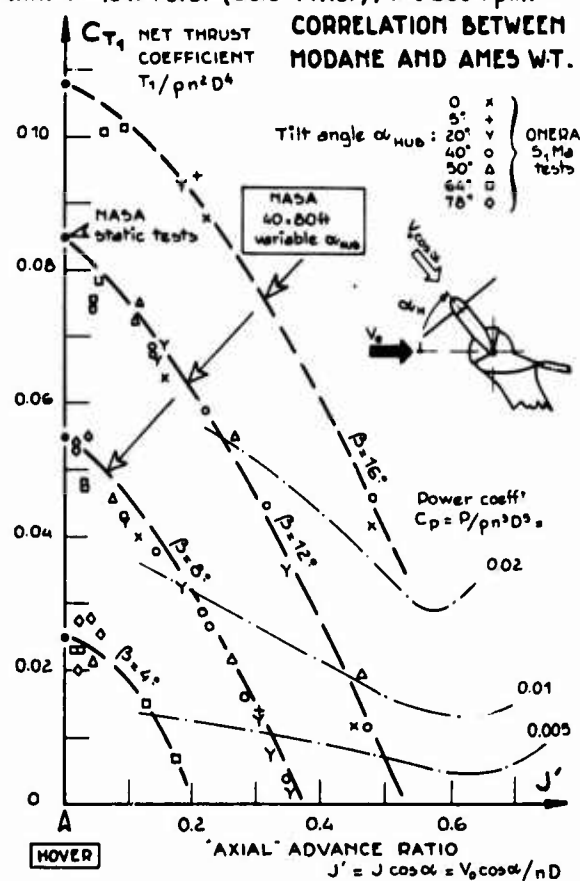
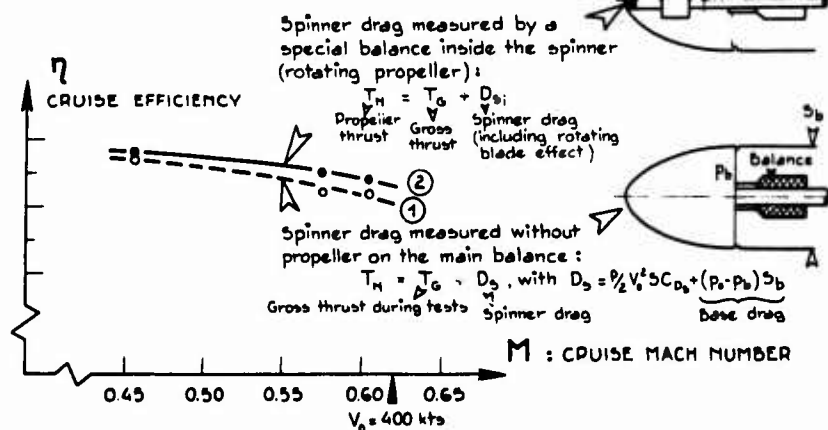
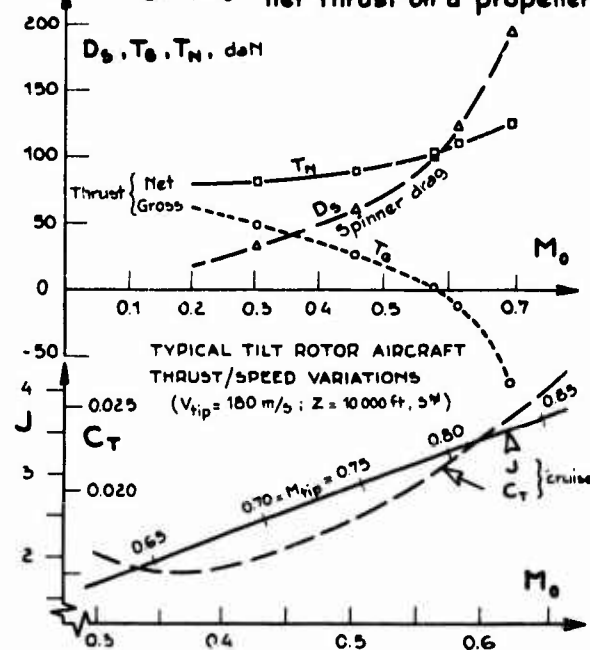
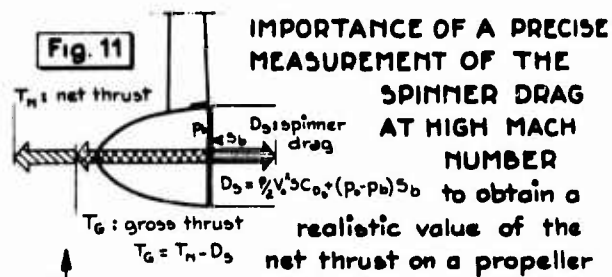


Fig. 10 SPINNER TARE DRAG
IN S₁ MODANE TUNNEL.

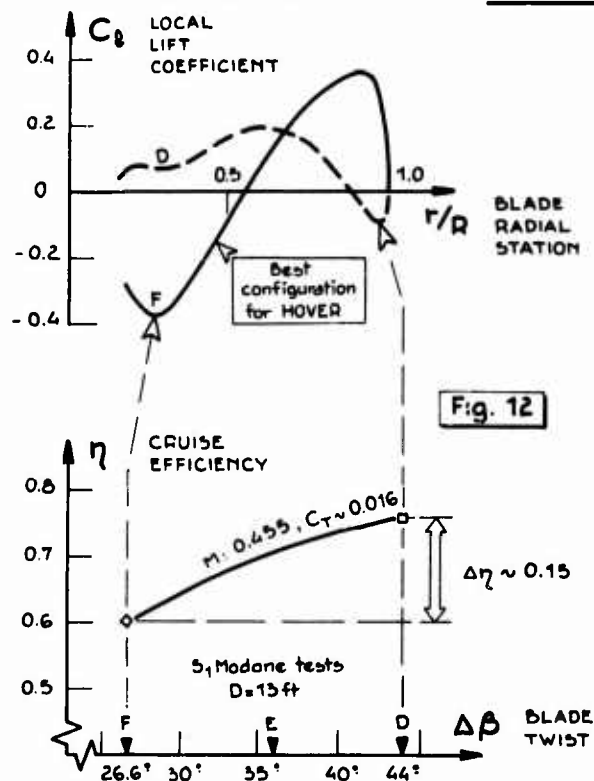
COMPARISON OF TWO SPINNER DRAG MEASUREMENT METHODS:

- ① - WITHOUT PROPELLER
- ② - WITH ROTATING PROPELLER





SPANWISE LOAD DISTRIBUTION ON TILT ROTOR BLADES IN CRUISE.



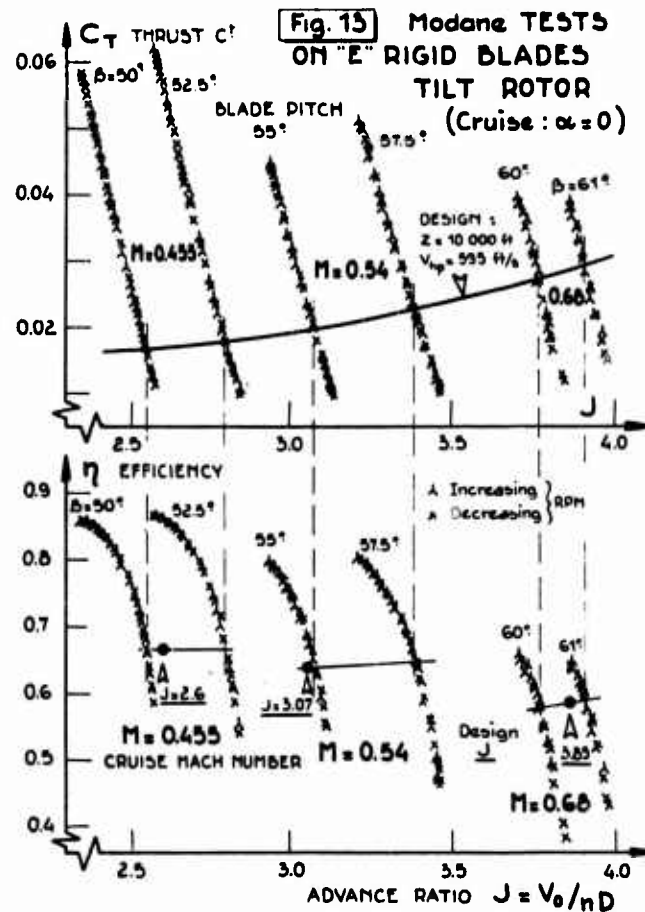


Fig. 14 HIGH SPEED PERFORMANCE OF VARIOUS "RIGID" ROTORS IN S₁ MODANE

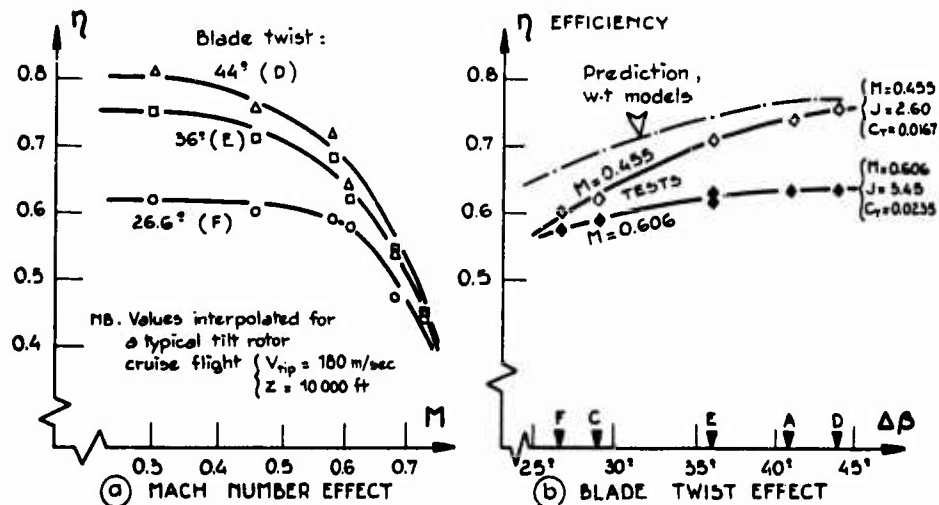
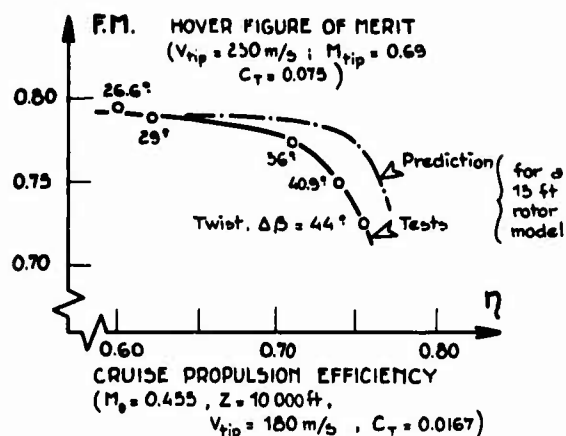
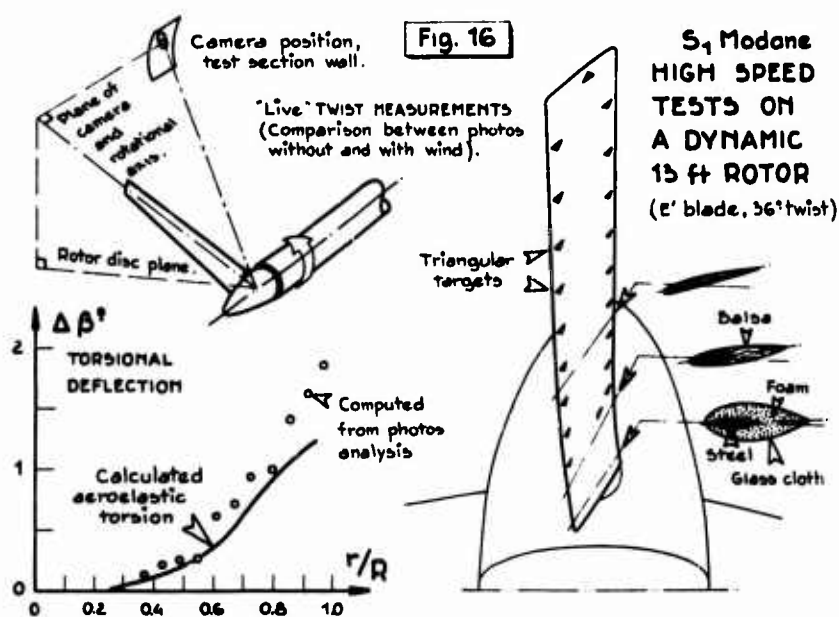


Fig. 15



**SUMMARY OF TYPICAL TILT ROTOR
 PERFORMANCES** obtained from 15 ft
 "rigid" models tested by NASA/USAF
 (HOVER) and ONERA (CRUISE).



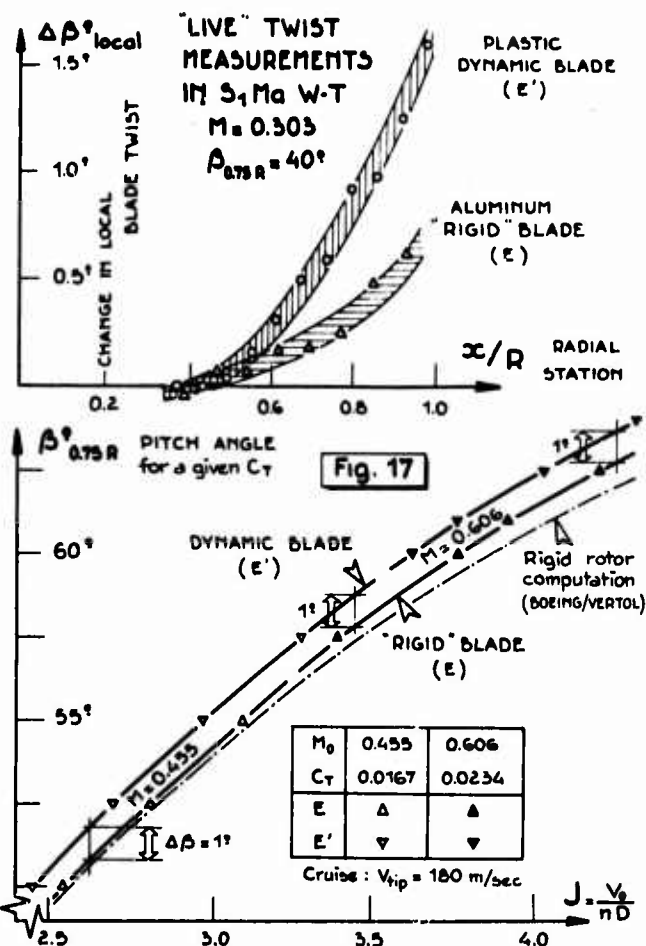


Fig. 18 TESTS ON TWO 36° TWIST TILT ROTORS (Cruise: $\alpha = 0$)
 Influence of blade elasticity

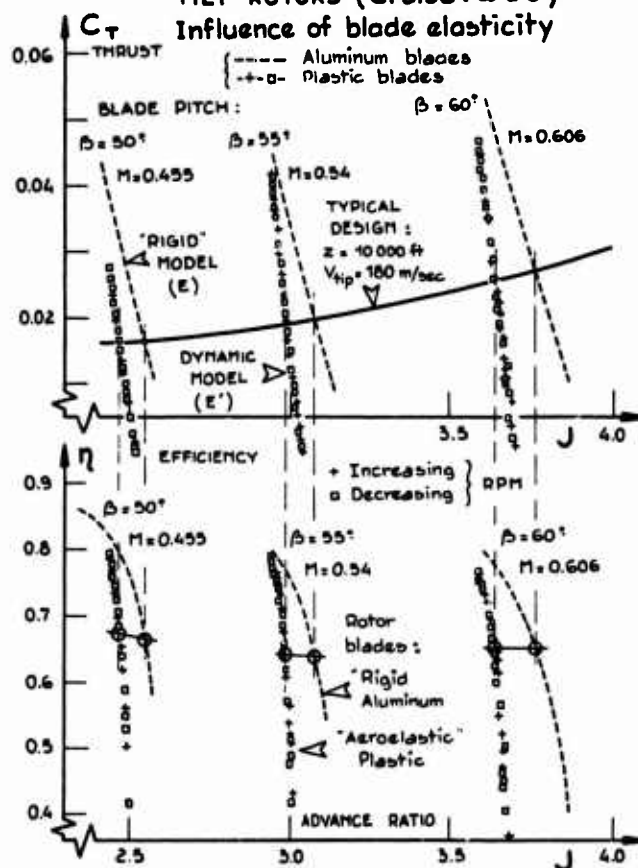


Fig. 19

COMPARISON OF THE MACH NUMBER EFFECT ON CRUISE EFFICIENCY obtained on the "36° twist" rotors in S₁ Modane wind-tunnel.

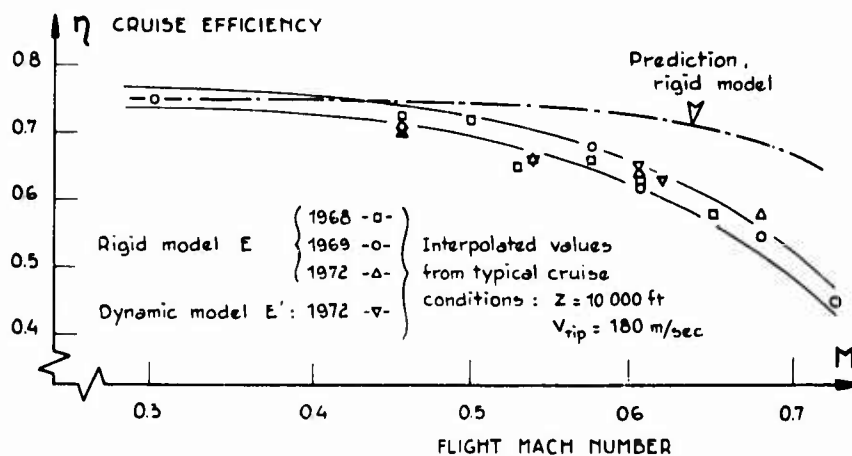


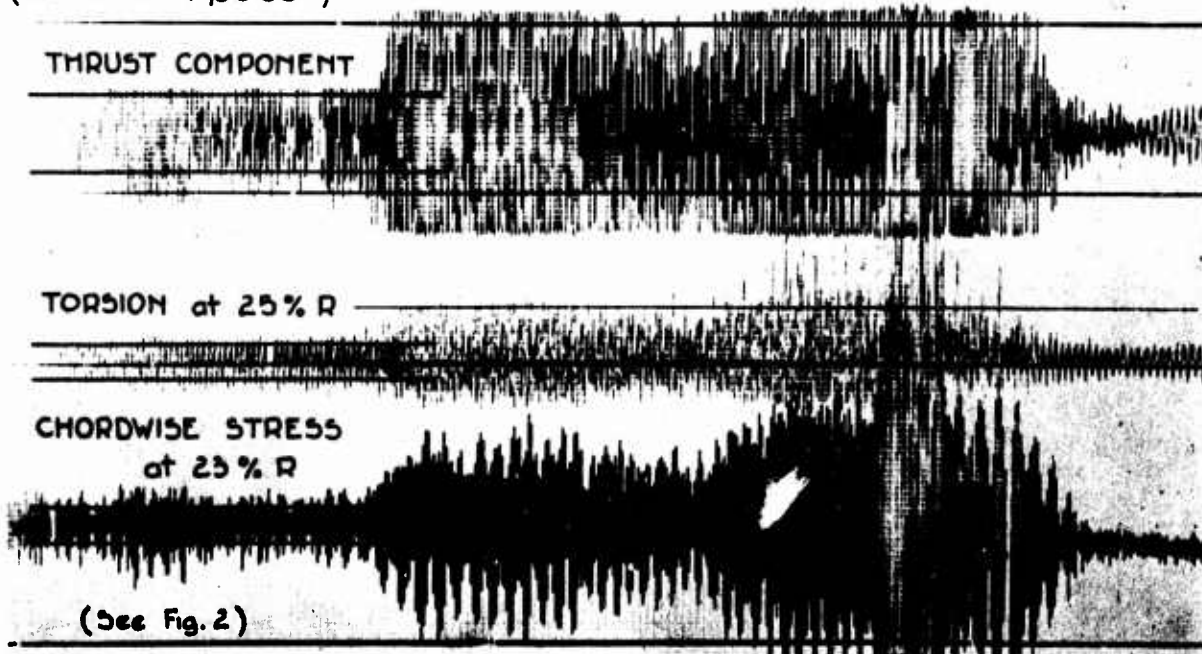
Fig. 20

S₁ Modane. HIGH SPEED TEST ON DYNAMIC ROTOR

M₀ = 0.63 - Divergence on blade loads.

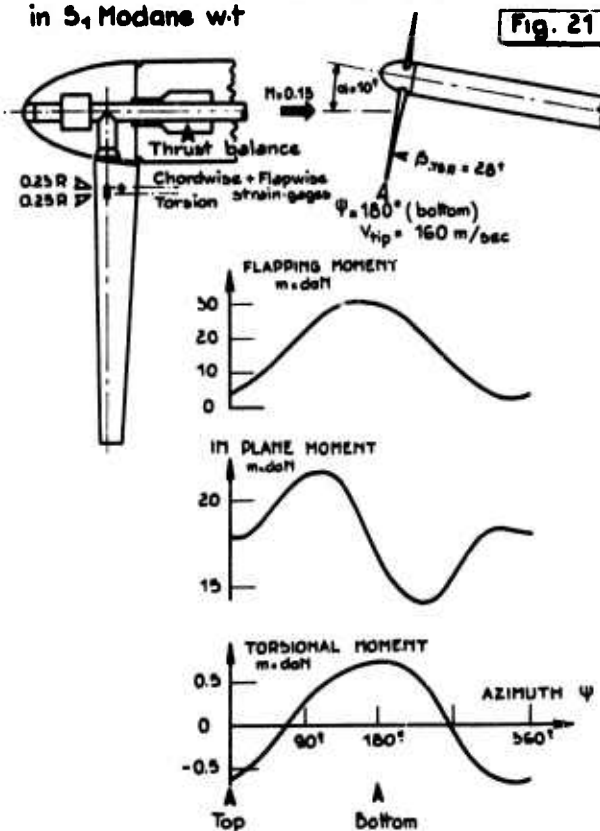
(M = 770 RPM, β = 65°)

1 round mm
→ QUICK STOP



STRESS ANALYSIS ON THE BLADES
OF THE 'AEROELASTIC' ROTOR (E) with $\alpha = 10^\circ$
in S₁ Modane w.t

Fig. 21



RECENT DEVELOPMENTS IN CIRCULATION CONTROL ROTOR TECHNOLOGY

by

Robert Williams
Rotary Wing Division
Aviation and Surface Effects Department
Naval Ship Research and Development Center*
Bethesda, Maryland 20034

SUMMARY

The results of recent research on the historical concept of circulation control applied to rotor blades is presented. A high speed helicopter application is used to illustrate the potential of this rotor for a major breakthrough in the areas of rotor efficiency, parasite drag and weights leading to a large improvement in aircraft productivity. Details of the hover, transition and high speed cruise performance are presented. Some problems of autorotation, vibrations and blade dynamics are also discussed.

LIST OF SYMBOLS

b_a	Amplitude of second harmonic blade pressure control	S	Rotor disc area, ft^2
C_f	Coefficient of radial skin friction	T	Rotor thrust, lb.
C_{LR}	Rotor lift coefficient ($L/\rho S V_{TIP}^2$)	V	Velocity, knots
C_L	Rotor lift coefficient based on freestream dynamic pressure ($\frac{2C_{LR}}{\mu^2}$)	V_{TIP}	Rotational tip speed, ft/sec
D	Parasite drag, lbs.	W	Weight, lb.
f	Flat plate drag area (D/q), ft^2	w/c	Slot height to chord ratio
L	Rotor lift, lbs.	α_s	Rotor shaft angle, deg.
L/D_e	Equivalent lift drag ratio	θ_c	Collective pitch, deg.
M_{TIP}	Advancing tip Mach number	μ	Advance ratio
$P_{T_{max}}$	Maximum compressor output pressure, lb/ft 2	ρ	Density, slugs/ft 3
P_{T_1}	Compressor inlet total pressure, lb/ft 2	σ	Rotor solidity ratio
		ω_n	Natural frequency, radians/sec.

1.0 INTRODUCTION

Under the impetus of U. S. Navy need for improved helicopter capability, the Circulation Control Rotor (CCR) is currently undergoing what may be considered as roughly the fourth evolutionary phase of its development. Its history has in truth been one of international contributions from some of the world's leading aerodynamicists. In its present form (Figure 1) the CCR has retained many of the attributes of the French Blown Flap Rotor [1-3], the U. K. Circulation Control Rotor [4-5], and the U. S. Pure Jet Flap Rotor [6-7]. In addition the CCR has utilized many of the important developments of jet flaps, boundary layer control systems and coanda flows to evolve airfoils suitable for helicopter rotors [8-13]. The major concentration of the present CCR effort at NSRDC has been to develop airfoils which have good overall efficiency over a wide range of lift coefficient and Mach number, where the lift is developed primarily by boundary layer control at small incidence.** The efficient design of the coanda jet region at the trailing edge permits the airfoil to develop high lift coefficients with only ten to twenty percent of the compressor power normally required for a blown flap or jet flap system. Other features include: relatively high thrust recovery, high critical Mach number, maximum lift coefficients near the theoretical limit for attached flow, and the unique property of developing lift independently of both incidence and velocity (with certain constraints). Some possible adverse features include relatively high pitching moments with a variable aerodynamic center, sensitivity to angle of attack, and possible deleterious jet compressibility effects. The airfoils are generally designed for operation near zero angle of attack so that the airfoil shape may be prescribed to achieve good efficiency over the required lift coefficient and Mach number range, subject only to the geometric constraints of the trailing edge design. In general the rotor section requirements are for high lift coefficients and relatively low Mach numbers on the inboard sections and lower lift coefficients and high Mach numbers on the outboard sections. The efficiency considerations then lead to a tapered blade varying from twenty to fifty percent thickness at the root section and ten to fifteen percent at the tip and with the trailing edge design varying from near circular at the root to near elliptical at the tip. The particular geometry selection depends primarily on the maximum speed requirement of the helicopter.

A typical rotor geometry is illustrated in Figure 1 for a single slotted "low speed" concept (less than 200 knots). The thickness and trailing edge curvature are prescribed to give high thrust recovery near the tip region, maximum lift augmentation on inboard sections and good efficiency all along the blade span. For higher speeds than about 200 knots a second slot and air chamber is added on the leading edge as shown in Figure 2. This slot is blown only in the reversed flow region of the retreating side. In this manner the

* Formerly the David Taylor Model Basin

** A recent summary of CC airfoil development and the basic rotor principles has been described at the 1972 American Helicopter Society Meeting and the reader is referred to reference 14 for this background information.

historical problems of retreating blade stall and negative lift are sensibly eliminated. If the rotational speed (RPM) is kept low by use of the high section lift capability, the rotor is aerodynamically capable of achieving speeds in excess of 400 knots with very high efficiencies. Figure 3 illustrates an application of the latter concept to an advanced high speed helicopter having auxiliary propulsion. This high speed rotor represents the fullest exploitation of the aerodynamic potential of the CCR and will be used as an example in this paper. However, it should be noted that several other variants of CCR design are possible which emphasize capabilities other than speed. For example, the control system can be entirely made of simple, non-dynamic components as shown in figure 4, therefore reducing the associated maintenance. Higher harmonic azimuthal variations of blowing can be introduced to reduce helicopter vibrations and alternating blade stresses. The noise levels of rotors can also be significantly reduced by lowering tip speeds and using the greater available lift coefficients. Excellent hover performance may be obtained by distributing slot height to optimize span load distribution. Helicopter load capacity and maneuverability may be enhanced by the greatly increased thrust capability and control power. Blade chord and twist may also be reduced, possibly reducing weight and vibratory stresses. Many of these claims are historical in nature and have been the subject of technical speculation for years. Clearly, some of them are in opposition with each other so that often one is obtained at the expense of another. However, the increased design flexibility can no longer be disputed. Recent model test results at the Aviation and Surface Effects Department of NSRDC (figures 5a, b) and previous tests at the National Gas Turbine Establishment (NGTE) have firmly established their validity. In point of fact the low speed characteristics of the CCR are now sufficiently well in hand that the U. S. Navy has initiated a low speed flight demonstrator program. The major objective of this program is to simplify the rotor hub and controls and improve helicopter readiness, as well as to provide a research vehicle to exploit some of the other features mentioned above. Figure 4 illustrates one of the hub control systems being considered for this demonstrator which has been successfully tested on a seven foot model CCR at NSRDC.*** The system consists of a non-rotating circular cam mounted slightly eccentric to the center of the rotor hub with an air gap between the cam and the blade nozzles. As the blades rotate about the (fixed) circular cam the gap width varies and the air flow is modulated. For a given flight condition the amplitude is determined by raising or lowering the cam while the phasing is obtained by a rotation. At present it appears that the rotor will also require a collective pitch or incidence setting in order to permit autorotation and to give minimum hover power (although on certain designs it may be possible to eliminate this control entirely). It is envisioned that this control would be a simple propeller pitch type of control programmed to vary as a function of flight speed and would not be a primary flight control.

The demonstrator program represents the first of a new generation of helicopters which may include all types from heavy lift to the very high speed version shown in Figure 3. The high speed design will be discussed in detail in this paper because it operates in all the possible flight regimes and as such serves as a good example. Additionally the rotor performance is based on calculations which have been at least partially validated by the test results of the reverse blowing rotor model of Figure 5. Clearly, however, the performance predicted for the high speed design should not be applied arbitrarily to other types which have different design requirements.

The paper is divided into three major sections. The first addresses the general area of high speed helicopter limitations and design and attempts to show the potential of the CCR for achieving a balanced design concept. The second section discusses in some detail the calculated aerodynamic performance of the CCR in hover, cruise and transitional flight. The third section addresses some long standing questions of autorotation, blade dynamics and vibrations at high speeds.

2.0 MAJOR LIMITATIONS OF HIGH SPEED HELICOPTERS

The aerodynamic feasibility of extending rotor borne speeds to 300-400 knots has been essentially demonstrated with experiment and theory by three rotor concepts. These are: the coaxial rotor, characterized by the Advancing Blade Concept [15, 16, 17]; the pitch control rotor characterized by the Reverse Velocity Rotor (RVR) [18, 19]; and the reverse blowing rotor or high speed variant of the Circulation Control Rotor [14, 20, 21]. All three rotor systems operate at high advance ratios ($\mu \approx 1.0$) in a thrust compounded, semi-autorotative condition. All three use (or contemplate using) double ended airfoils with maximum thickness near mid chord in order to efficiently utilize the reversed flow region. In order to reach the high advance ratio condition representative of cruise at 300-400 knots all of the rotors must fly through the difficult $\mu = 0.7$ transition regime where the retreating blade develops little lift due to the low dynamic pressure. The coaxial accomplishes this by contra-rotating the two rotors and essentially neglecting the retreating blade stall; the pitch control rotor by using a second harmonic of pitch control to carry more lift on the front and aft portion of the disc; the CCR by using a second harmonic of cyclic blowing control, high lift airfoils and by the use of simultaneous leading and trailing edge blowing on the retreating side which permits lift to be developed independently of the relative wind direction. Each system incurs performance penalties for the ability to transition and cruise at high speeds. These penalties are primarily in the areas of (1) rotor lifting efficiency, (2) parasite drag and (3) rotor and hub system weights. Significant advances must be made in all three areas before the high speed helicopter can attain productivity levels competitive with other proposed forms of VTOL. The following section illustrates how the CCR may effect improvements in these key areas.

2.1 Rotor Efficiency

Rotor efficiency is customarily measured by hover Figure of Merit (or power loading) and rotor equivalent lift to drag ratio. The latter is given by the generalized equation:

$$(L/D_e)_{\text{ROTOR}} = (L / (\frac{325}{V} (SHP + HP_c) + D_r + D_m))$$

where L is the total lift developed by the rotor at speed V with rotor shaft power SHP, compressor power HP_c , rotor drag D, and momentum drag D_m . The compressor power and intake momentum "ram" drag account for the additional energy penalties of a blown rotor such as the CCR.

*** The development and testing of the model rotor and controls has been conducted under the leadership of Mr. J. B. Wilkerson of the Rotary Wing Division, NSRDC, and will be reported subsequently.

In general, all three of the high speed rotors discussed above cruise near zero shaft power (SHP) in a semi-autorotative condition. The critical factor in determining $(L/D)_{\text{ROTOR}}$ is therefore the rotor drag for conventional types and the rotor drag, momentum drag and compressor power for the CCR. The problem of defining the rotor drag is difficult, both experimentally and theoretically. From an experimental standpoint the rotor hub tares are usually of the same order as the rotor drag itself. Furthermore the superposition method of removing tares is itself very questionable because a rather strong, favorable interference effect may occur. From a theoretical standpoint it is necessary to recognize that the radial component of flow is significant at high advance ratios and the neglect of this term may lead to large errors, particularly in the rotor drag. The impact of this effect on rotor design is to require the minimum solidity ratio possible in order to minimize rotor drag. For the CCR and pitch control rotor the critical solidity design requirement occurs at the transition advance ratio of $\mu = 0.7$ where rotor lift capability is a minimum. For the coaxial the solidity is determined by quite different requirements for vibrations, structure and stiffness. Typically the CCR requires only about sixty percent of the solidity ratio of the "conventional" rotor systems and largely for this reason tends to have significantly higher rotor L/D . In fact its efficiency can actually surpass that of a fixed wing VTOL as shown in Figure 6. It should be noted that the CCR curve shown represents an envelope of rotor designs for different speeds and as such represents no single configuration.

The second efficiency consideration for a high speed helicopter is the hover Figure of Merit. It is well known that any rotor design represents a compromise between the hover efficiency requirement for high blade twist and low solidity and the opposite cruise requirement. This situation may be aggravated with very high speed (300-400 knot) helicopters by the desirability to operate with low hover tip speeds so that at cruise speed the required rotor RPM reduction for compressibility effects may be minimized (dynamic/structural constraint). This requirement in turn leads to hover operation at high thrust coefficients and, if the solidity ratio is low, at high C_{LR}/σ . The conventional high speed rotor system encounters serious difficulty under such conditions because the double ended airfoils have relatively low efficiency. Even if higher solidity ratios are used (with the associated cruise efficiency losses) the basic high speed requirement for zero twist (dynamic/structural constraint) gives rise to large induced power losses. Contrasting with this situation the CCR develops effective aerodynamic twist by varying the slot height and chordwise position along the span. The fundamental efficiency characteristics of the airfoils then lead to excellent hover Figure of Merit over a wide range as shown in Figure 7.

2.2 Effect of Parasite Drag on Overall Efficiency

Figure 8 presents historical data showing the variation of vehicle parasite drag with gross weight. Generally the data can be grouped into aerodynamically "unrefined" helicopters, "clean" helicopters, and fixed wing aircraft (minus wing profile drag). Also it may be noted that the "unrefined" types follow a $f \propto W^2$ law (due to the dominance of separation drag) rather than a $f \propto W^3$ law which the fixed wing aircraft follow. The "clean" types represent either experimental helicopters or recent production types which are at least partially designed for low drag. The "goal" curve represents the drag levels estimated for helicopters equipped with the CCR and designed from the outset for low drag. These latter vehicles would in all probability differ greatly with current rotary wing and even fixed wing design practice. The need for such a radical approach is shown in Figure 9 where the total aircraft equivalent lift drag ratio (range is proportional to this parameter) is plotted against the rotor lifting efficiency for various drag "families" and gross weights. It is immediately clear from these trends that for "clean" types little benefit in aircraft efficiency can be achieved by increasing the rotor lifting efficiency beyond about 10.0. Further improvements can only be accomplished by reducing the parasitic drag, even at a cost in rotor efficiency. Figure 10 presents similar trends but showing the effect of speed and altitude for the "goal" drag of the CCR. In this case the higher lifting system efficiencies still have significant payoff.

The next question is of course how to reduce drag. Some insight may be obtained by studying the origin of helicopter drag. The table below gives a drag breakdown of the CH-53A.

COMPONENT	PERCENTAGE
Basic Fuselage	16
Protuberances, Antennae	6
Main Rotor Pylon & Hub	40
Sponsons/Landing gear	11
Engine/Leakage/Momentum	14
Tail Rotor/Surfaces	13
	<u>100</u>

Surprisingly the basic fuselage contributes only 16 percent of the total drag while the hub and pylon area account for 40 percent! This result is typical of present helicopter designs in the higher weight ranges. It indicates that the major source of drag is basically separated flow in areas of high interference velocities. Figure 11 presents a typical cross sectional area distribution of the CH-53A showing that in the hub-pylon region the area is maximum. Furthermore, because of the separated wake from these components, an effective area magnification factor occurs due to the wake blockage. The result is of course very high interference velocities followed by steep adverse pressure gradients which in turn may lead to further separation. The rather disappointing results with contoured fairings in this region can be explained basically by these two effects. The interacting flow fields of the pylon ramp, pylon, shaft, hub and blade shanks produce a strong diffuser effect which leads to gross separation. This phenomenon is illustrated in Figure 12. In order to achieve significant drag reduction in this region boundary layer control may be incorporated as a "fix" [22]. More fundamentally however, what is needed is (1) to eliminate the peak interference velocities by gross redistribution of cross sectional area and (2) to contour the localized interference regions around the pylon to avoid the sudden deceleration of flow in the boundary layer. The high speed CIRCULATION CONTROL ROTOR offers several interesting possibilities in this regard. First, by using very rigid blades, it promises to greatly reduce the "hump back" requirement of flapping rotors.

The fuselage contour can be quite streamlined with the rotor mounted in close proximity. Second, virtually all the control system may be submerged in the fuselage proper, essentially eliminating a "hub" as such and the associated blockage. Finally, under cruise condition the compressor power requirement becomes relatively small leaving a useful air supply available for suppressing possible localized separation areas (as on the rotor shaft for example).

The other areas of high parasite drag can be approached using the same principle of minimizing interference. Because of the relatively small contribution of the fuselage it appears profitable to make as many components as possible conformal with the basic shape. Stores, landing gear, sponsons and extra fuel tanks fall in this category. Careful integration of the auxiliary propulsion fan, possibly within the basic fuselage, will further reduce interference. Certainly the use of a fan-in-tail or similar low drag device is mandatory in any high speed design.

The helicopter is a unique device from the standpoint of drag. Unlike a fixed wing aircraft it does not require a high fineness ratio fuselage for stability reasons (the optimum fineness ratio without interference is only 3.7); rather, it can obtain its basic stability from the main rotor and tail fan. In effect it has an active control system. Furthermore it has only one major interference surface (the pylon) as opposed to two for the fixed wing aircraft. It is interesting indeed to speculate whether a helicopter designed using a "subsonic area rule" criteria could in fact have lower drag than a fixed wing aircraft. Figure 13 shows an analytical approach to this problem presently underway at NSRDC. The fuselage is mathematically modeled by singularity distributions and the complete inviscid flow field calculated [22, 23]. Streamline paths and pressure distributions are computed and approximate turbulent boundary layer criteria are used to estimate where separation may occur. Problem areas are then redesigned to preclude separation.

2.3 Weight Associated with the Lifting System

As the design speed of VTOL aircraft increases there is a corresponding increase in the empty weight to gross weight ratio. For high speed, 300-400 knot helicopters, the major component weight growth occurs in two areas. The first is the rotor blade/hub/retention and control system weights required to transition through the $\mu = 0.7$ regime and to withstand the stress levels associated with cruise speeds. For the coaxial type system these weights are essentially the second contra-rotating rotor and the very stiff blades needed to avoid excessive rotor spacing and dynamic/aeroelastic instabilities. For the pitch control type the penalty occurs in the greater solidity and two per rev pitch controls needed to maintain rotor lift during transition and also either stiff root retention or tip weights to prevent excessive blade flapping and coning.

In contrast the CCR blade structure lends itself naturally to high speed design by virtue of reduced solidity, a simplified control system and structurally efficient blades. Figure 14 illustrates a high speed, double slotted blade design and also shows a comparison of the inboard section stiffness with a reference OOL2 for the same blade weight and chord. Two possible spar designs are also shown schematically which efficiently close the torsion box while allowing the slot air to flow with minimum duct losses.

The second area of large weight growth in the auxiliary propulsion system and is directly related to the speed and parasitic drag. Here the hub/pylon drag is the crucial distinction between the high speed rotor types. Estimates of the percentage of total drag associated with the hub, pylon, and controls of conventional types range from 35 to 50 percent for the pitch control and coaxial types as compared with only 11 percent for the CCR.

The preceding discussions are summarized in Figure 15 where the empty weight breakdowns for four high speed candidates are summarized. The computations have assumed equal gross weight and limit load factors for a 300 knot aircraft designed for the late 1970's. For the helicopter types the basic parasite drags minus the hub/pylon drags were very close as indicated by the figure. The weights which are attributed to the different lifting systems are indicated separately. The CCR blade weights are based on the coaxial blades (which have similar thickness ratios) and adjusted for the difference in solidity ratio. It was also assumed that the compressor and ducting weight was offset by the transmission weight savings associated with the reduced shaft torque requirement.

Figure 16 summarizes some general trends in empty weight fractions of VTOL aircraft with speed (for equal load factors). It may be seen that the CCR affords the potential for a dramatic change in VTOL weight trends.

2.4 Impact of Limitations on Mission Performance

The preceding sections have addressed the three major performance limitations of high speed helicopters. The significance of these limitations in terms of performance may be conveniently estimated as follows: the payload fraction, PL/GW, is described in terms of the fuel fraction, FW/GW, and empty weight fraction, EW/GW, by

$$\frac{PL}{GW} = 1 - \left(\frac{FW}{GW}\right)_{\text{HOVER}} - \left(\frac{FW}{GW}\right)_{\text{CRUISE}} - \frac{EW}{GW}$$

$$\frac{PL}{GW} \approx 1.0 - \frac{SFC \cdot t \cdot \sqrt{T/S}}{380 \cdot FM} - \frac{SFC}{325 (L/D)_{\text{TOTAL}}} - \frac{EW}{GW}$$

where t represents the "equivalent" hover time at sea level standard (loiter time may be expressed in terms of hover time), R is the total range in nautical miles, and FM is the "total" Figure of Merit of the vehicle including download, tail rotor and other power loss. T/S is the disc loading and SFC represents the mean specific fuel consumption.

Figure 17 presents a typical tradeoff study for a long range ASW type mission. It may be seen that the payload fraction is extremely sensitive to very small changes in empty weight, followed by parasite drag,

and rotor efficiency. These results indicate that the CCR potential for weight reduction should be fully exploited even at the cost of reduced rotor efficiency. For example, a stiff flapwise rotor is preferred to a freely flapping rotor because the potential hub/pylon drag reduction (propulsion and fuel system weight savings) more than offsets the reduction of lifting system efficiency associated with the higher blade thickness ratios (needed for obtaining the stiffness).

3.0 HIGH SPEED CIRCULATION CONTROL ROTOR PERFORMANCE

The basic operation of the CCR has been described in the literature [14] and therefore will not be repeated herein. Rather, some important performance details will be presented of the isolated rotor characteristics in hover, transition, and cruise. The results shown are based on a standard type computer strip theory analysis which includes airfoil section data for each span location as a function of blowing coefficient, angle of attack, freestream Mach number and jet Mach number. The analysis has been modified to include additional calculations of radial skin friction drag, compressor and coriolis horsepower, momentum "ram" drag, and the radial variation of ducting losses in the rotor blade. The latter computation accounts for the various effects of duct area, friction, internal obstructions, heat transfer and temperature variations, centrifugal compression and distributed mass efflux. Generally it is felt that the analysis is conservative for the forward flight calculations and slightly optimistic in hover. The rotor configuration used for these computations is similar to that of Figure 14 with four untwisted blades, aspect ratio 14.3, constant chord and constant slot height. The airfoil shape, slot chordwise position and trailing edge contour vary along the span. It is not, however, considered to be optimum in design, particularly for the low speed regime.

3.1 Modes of Operation of High Speed CCR

The example rotor of this paper is designed to achieve speeds approaching 400 knots. Consequently the maximum rotational tip speeds cannot exceed approximately 350 feet per second in the cruise condition without encountering deleterious compressibility effects. Two avenues are then open to the designer: (1) for best overall aerodynamic efficiency the hover tip speed is maintained around 500-700 feet per second, and then reduced in forward flight, or (2) for minimum dynamic and aeroelastic problems the tip speed is maintained constant around 350 feet per second. This latter approach implies greater solidity (probably 5 blades), increased blade weight and reduced rotor cruise efficiency. However, as discussed in section 2.0 the designer may be able to sacrifice some rotor efficiency without seriously affecting the overall vehicle efficiency.

Considering the case with RPM reduction for the present, Figure 18 shows the various modes of operation of a high speed CCR. Hover and low speed flight are identical with a conventional helicopter or compound. Propulsion is provided by the rotor or by auxiliary means such as a propeller or fan. As the advance ratio reaches $\mu = 0.4$ the reverse blowing and second harmonic blowing controls are turned on to provide maximum lift capability through transition. The aircraft continues to accelerate up to 250 knots in a level attitude where it initiates a fifty percent rotor RPM reduction. The second harmonic control is then turned off and the rotor is flown up to cruise speed. The collective pitch variation is automatically varied with rotor RPM and pitot pressure and becomes zero after the transition maneuver. Figure 18 also shows the variation of rotor and aircraft efficiency over the speed and advance ratio range. An efficiency of eighty percent is assumed for the auxiliary propulsion device and eighty five percent for the compressor. The total and compressor power requirements peak at $\mu = 0.7$ and drop rapidly during RPM reduction to less than half of this value. At the 400 knot cruise speed the ram head total pressure rise is more than sufficient to provide the blowing required.

3.2 Hover Performance

The capability of the CCR to achieve high hover efficiency has been noted previously. Figure 19 shows the span load distributions which can be achieved with the untwisted rotor of this study (Figure 14). The "ideal" loading for minimum induced power as derived from the Lock-Goldstein theory is also shown for comparison. Figure 20 compares the computed downwash distributions and indicates that very close to a constant downwash distribution can be obtained. An empirical correction has been added to the analysis to account for the tip vortex impingement. Figure 21 presents a typical variation of power components in the hover mode and confirms that the induced power is very close to the ideal actuator disc value. The tradeoff in profile, compressor and coriolis power is also shown indicating that the minimum occurs with very low blowing rates and significant angle of attack lift. Figure 22 summarizes the isolated rotor hover performance for the high speed rotor.

3.3 Forward Flight

The variation of rotor lifting system efficiency as a function of speed and advance ratio is presented in Figure 23. The performance shown is nonoptimum but the general trend with advance ratio and disc loading is typical. The trend of increasing efficiency with advance ratio is gradually offset at very high speeds by advancing blade compressibility losses. No three dimensional tip relief has been assumed in this example although this could amount to approximately 0.10 Mach number for the fifteen percent elliptical tip section. The discontinuity in the curves at the transition speed corresponds to the rapid reduction in power required as the rotor RPM is reduced. Figure 24 illustrates the benefit of reducing tip speed further at 400 knots, hence increasing advance ratio and decreasing compressibility losses. A limiting case at $\mu = 200$ is also shown to indicate the upper bound on efficiency. It is evident that stopping the rotor would not result in a substantial improvement in the lift system efficiency. Figure 25 illustrates the potential benefit due to operation at altitude where the radial flow skin friction drag is reduced. In actual applications these higher altitudes would be used to minimize the parasite drag penalty of the fuselage, similar to a fixed wing aircraft.

3.4 Effect of Radial Flow

As previously noted the effect of radial flow on the rotor drag can become very important at high advance ratios. Its effect on torque is usually much less significant because the rotor operates in a semi-autorotative mode. The difference between the classical and radial flow computation is strongly emphasized in Figure 26 where the radial skin friction coefficient is assumed to be $C_f = 0.0$ (classical) and $C_f = 0.0045$ (radial flow). In practice it may be possible to achieve $C_f \approx 0.002$ due to unsteady effects and low Reynolds numbers. For all of the rotor performance examples in this paper a value of $C_f = 0.0045$ has been assumed. The impact of the radial flow results on rotor design is to require the minimum solidity ratio possible consistent with the maximum thrust transition requirements discussed next.

3.5 Transitional Flight

As the rotor accelerates to higher speeds the very high parasite drag forces the rotor to resort to auxiliary thrust and to operate near zero shaft angle. At $\mu = 0.7$ the retreating blade encounters the lowest average dynamic pressure in the flight regime with reverse flow over the inboard 70 percent and forward flow over the outboard 30 percent. This condition represents the critical design point for the CCR which determines the minimum solidity ratio.

Three unique mechanisms are employed on the CCR to permit transition with relatively low solidity. The first is simply the large lift capability of the airfoils but this advantage is somewhat offset by the special contouring of the trailing edge to give low drag at high Mach numbers. The second mechanism is the use of second harmonic cyclic air modulation to heavily load the fore and aft quadrants of the disc while unloading the lateral quadrants. In effect the roll trim problem is reduced while the maximum thrust capability is greatly enhanced. In addition the compressor power consumption is also alleviated by this means. The third mechanism is the unique phenomena of "dual slot blowing" whereby both the leading and trailing edge slots are blown simultaneously (in the mixed flow region of the disc) and lift may be developed with the relative wind coming from either direction. Some interference does occur due to the flow at the leading edge slot, however, airfoil tests to date indicate the phenomena is essentially as described.

Figure 27 shows the maximum lifting capability of the CCR with advance ratio and indicating the advantageous effect of reverse blowing, second harmonic control and a larger slot height to chord ratio ($w/c = 0.003$, also with second harmonic control and reverse blowing). The curve clearly shows that the critical lift condition occurs at $\mu = 0.7$. Translating these results into an actual rotor design at a speed of 250 knots yields a minimum solidity ratio of $\sigma = (T/S)/157$ for the lower slot height design ($w/c = 0.002$). For a design disc loading of $T/S = 10 \text{ lb/ft}^2$ and with a 1.4g maneuver margin the required solidity ratio is only $\sigma = 0.0891$.

Figure 28 shows the effect of solidity ratio on the maximum lifting efficiency at 400 knots. Also shown are design lines for the $\mu = 0.7$ transition condition. This figure depicts the principle design trade off for the high speed CCR. The influence of the larger slot height to chord ratio, cruise altitude, design cruise speed and advancing tip Mach number would also be considered in a final design study. In addition a linearly increasing slot height distribution, blade planform taper and more efficient blowing schedule also appear advantageous so that a significant improvement in maximum rotor efficiency should be possible over the relatively high values of the present example. However, before refining the aerodynamic design much further it is necessary to consider some possible nonaerodynamic constraints which may impact strongly on the design.

4.0 OTHER ASPECTS

In this section some other features of the CCR are described and some potential problems requiring further study are discussed.

4.1 Autorotation

The steady state autorotative performance of the CCR has been analyzed in the low speed mode. The results are presented in Figure 29 for one disc loading. Acceptable rates of descent appear possible down to low ground speeds where the landing transition maneuver would begin. Interestingly a relatively high disc loading of 8.0 psf has a lower rate of descent for the condition studied. The success of CCR autorotation will probably depend heavily on the ability of the compressor to match the rotor requirement through autorotation. At present it is envisioned that this compressor would be installed on the engine shaft ahead of (or integral with) the engine compressor so that it could be driven by the rotor in autorotation and also would reduce the transmission weights by removing power from the turbine shaft. Some means of obtaining variable pressure ratio and mass flow would then have to be incorporated as indicated by the compressor requirements of Figure 29.

4.2 Natural Frequencies and Blade Dynamics

The possibility of torsional instability or divergence caused by relatively high mid chord pitching moments requires the CCR to be very stiff in the torsion mode. In addition the possibility of flapping instability at high advance ratios and the quite separate requirement of a low rotor-fuselage clearance for minimum parasite drag tend to require a stiff rotor in the flapping direction. These constraints are compatible with the natural tendency of the CCR blades to be quite stiff in torsion and bending. For RPM reduction the slope of the bending mode curve can be altered by using coning if resonance is a problem.

The selection of the inplane stiffness is somewhat open to question. It depends on both the bending stiffness (inplane coriolis forces due to flapping) and on the range of RPM reduction. A distinct possibility of inplane resonance exists if the first inplane blade mode crosses the two per rev excitation line (due to the relatively high two per rev aerodynamic forces). To avoid this possibility the blade may have to be quite stiff in this mode also. Figure 30 illustrates a possible choice of frequency placement for the example rotor with a 50 percent RPM reduction. The first inplane mode has been placed above the

two per rev line in order to avoid high stresses during the transition maneuver. Referring to the basic equation for a nonrotating beam with linearly varying properties it can be noted that the inplane natural frequency is given by:

$$\omega_n = (HEt/c)^{0.5} \cdot \left(\frac{n\sigma}{N}\right)$$

where H is a geometric shape factor, E is the elastic modulus, t/c is the root section thickness to chord ratio, σ is the rotor solidity ratio and N is the number of blades. For the high speed CCR of Figure 14 the first term represents a factor of about 2.2 times a conventional rotor while the second term is about 1.4 times so that for the four bladed rotor example of this paper the inplane frequency can be placed sufficiently high without adding unnecessary solidity (as with some hingeless rotors).

4.3 Vibrations

During transition the CCR is heavily loaded on the fore and aft quadrants and essentially unloaded on the lateral quadrants. At high cruise advance ratios the blade encounters a region of essentially zero tangential velocity twice per revolution. These extreme conditions impose high blade loads and bending moments which tend to pass unattenuated to the rotor hub. Figure 31 shows the azimuthal variation of blade loading and hub loads for the four bladed rotor at the two worst vibration conditions. Although these results are only tentative, they do indicate that four blades appear to give acceptable vibration levels. With five blades the oscillating vertical shears are significantly lower.

4.4 Research Recommendations

The CCR appears to hold the potential for a balanced VTOL design which can radically extend the scope and application of the helicopter. Several areas require further definition, however. These include handling qualities, particularly in the areas of gust sensitivity, gyroscopic coupling, phase lags and automatic feedback control systems. The lift independence characteristic of CC airfoils should be studied in the context of reduced vibrations. Higher harmonic azimuthal blowing controls for improved performance and vibration reduction should also be studied. The entire area of blade dynamic and structural design requires detailed study with special attention to the problem of ballistic damage. The unique power requirements of the CCR should be addressed, possibly with advanced fan/shaft engines using supercharged bypass air to supply the blowing requirements.

REFERENCES

1. Dorand, R.: "The Application of the Jet Flap to Helicopter Rotor Control", Journal of the Helicopter Association of Great Britain, Vol. 13, December 1959.
2. Kretz, Marcel and Dubus Claude: "Research Study of a High Speed Helicopter Using the DH 2011 Jet-Flapped Rotor", U. S. Army European Research Office, Contract No. DA-91-591-EUC-3318-3660. Dorand Rpt. DH-2011-A-E3, Jan 1967.
3. McCloud, John L. III, W. T. Evans and James C. Eiggers: "Performance Characteristics of Jet Flap Rotor", NACA SP-116, April 1966.
4. Cheeseman, I. C. and A. R. Seed: "The Application of Circulation Control by Blowing to Helicopter Rotors", Jnl. of the Royal Aeronautical Society, Vol. 71, July 1967.
5. Smith, M. C. G.: "The Aerodynamics of a Circulation-Controlled Rotor", 3rd CAL/AVLABS Symposium on Aerodynamics of Rotary Wing Aircraft, Buffalo, N.Y., June 1969.
6. Yuan, S. W.: "Preliminary Investigation of the Karman-Yuan Helicopter Rotor System", 11th Annual Forum, American Helicopter Society, April 1955.
7. Kuczynski, W. A. and R. B. Lewis II: "Jet Flap Cyclic Twist Feasibility Research Program", Naval Air Systems Command Contract N00019-68-C-0265, Lockheed Report IR 22973, March 1970.
8. I. M. Davidson: "The Jet Flap", Journal of the Royal Aeronautical Society, Vol. 60, January 1956.
9. Malavard, L., Ph. Poisson-Quinton and P. Jousserandot: "Method for Obtaining Increased Lift by Means of a Blowing Jet", Aero Digest, Vol. 73, Sept. 1956.
10. Poisson-Quinton, Ph.: "Idees Nouvelles sur le controle de la couche limite applique aux ailes d'avion", Les Cahiers d'Aerodynamique, No. 3, 1946.
11. Newman, B. G.: "The Prediction of Turbulent Jets and Wall Jets", Canadian Aeronautics and Space Journal, October 1969.
12. Kind, R. J.: "Calculation of the Normal Stress Distribution in a Curved Wall Jet", West Virginia University, Aerospace Engineering TR-18, August 1969.
13. Kind, R. J. and D. J. Maull: "An Experimental Investigation of a Low Speed Circulation Control Airfoil", The Aeronautical Quarterly, Vol. 19, May 1968.
14. Williams, R. M. and E. O. Rogers: "Design Considerations of Circulation Control Rotors", Paper number 603, 28th National Forum of the American Helicopter Society, Wash., D.C., May 1972.
15. Cheney, M. C., Jr.: "The ABC Helicopter", AIAA Paper No. 69-217, Joint AIAA/AHS VTOL Research, Design and Operations Meeting, February 1969.
16. Paglino, V. M.: "Forward Flight Performance of a Coaxial Rigid Rotor", Paper No. 524, 27th Annual Forum of the American Helicopter Society, May 1971.

17. Burgess, R. K.: "Development of the ABC Rotor", Paper No. 504, 27th Annual Forum of the American Helicopter Society, May 1971.
18. Evans, J. R. and others: "Analytical Study of the Reverse Velocity Rotor System", Naval Air Systems Command Contract N00019-69-C-0591, October 1971.
19. "Wind Tunnel Test in the Ames Twelve Foot Pressure Tunnel of the Reverse Velocity Rotor System", (to be published).
20. Seed, A. R.: "A Further Study of Circulation Control Applied to a Helicopter Rotor", National Gas Turbine Establishment, N. T. 659, September 1967.
21. Williams, R. M. and C. L. Bernitt: "Theoretical Performance of a Pure Jet Flap Rotor at High Advance Ratios", NSRDC TN AL-189, December 1970.
22. Linville, James C.: "An Experimental Investigation of High-Speed Rotorcraft Drag", USAAMRDL TR 71-46, February 1972.
23. Hess, J. L. and A. M. O. Smith: "Calculation of Potential Flow About Arbitrary Bodies", Progress in Aeronautical Sciences, Vol. 8, Pergamon Press, New York, 1966.
24. Bauer, A. B., A. M. O. Smith and J. L. Hess: "Potential Flow and Boundary Layer Theory As Design Tools in Aerodynamics", Canadian Aeronautics and Space Journal, February 1970.

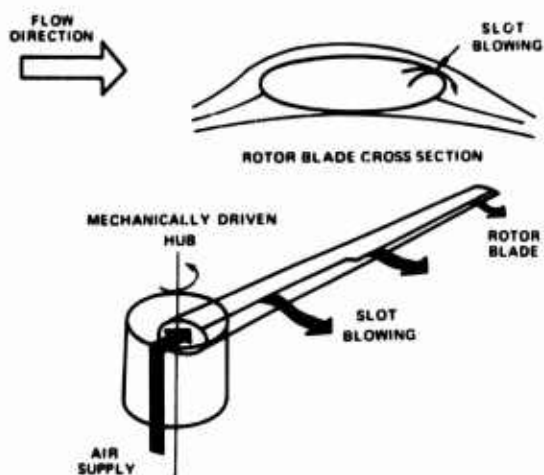


Figure 1 - Basic Concept

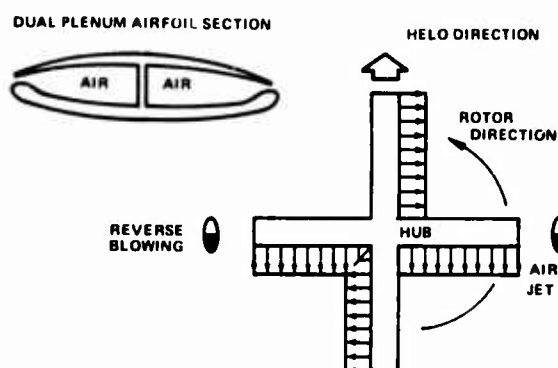


Figure 2 - High Advance Ratio Dual Blowing Concept

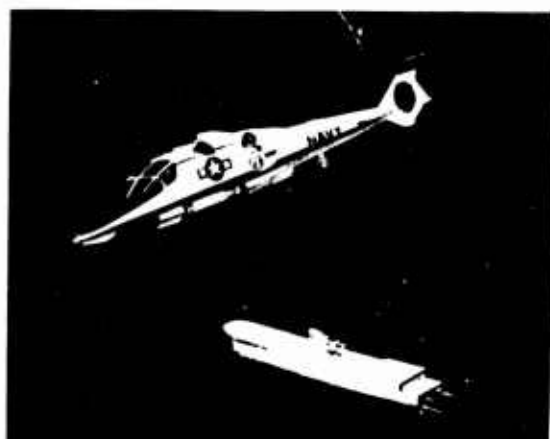


Figure 3 - High Speed Design Concept for ASW Mission

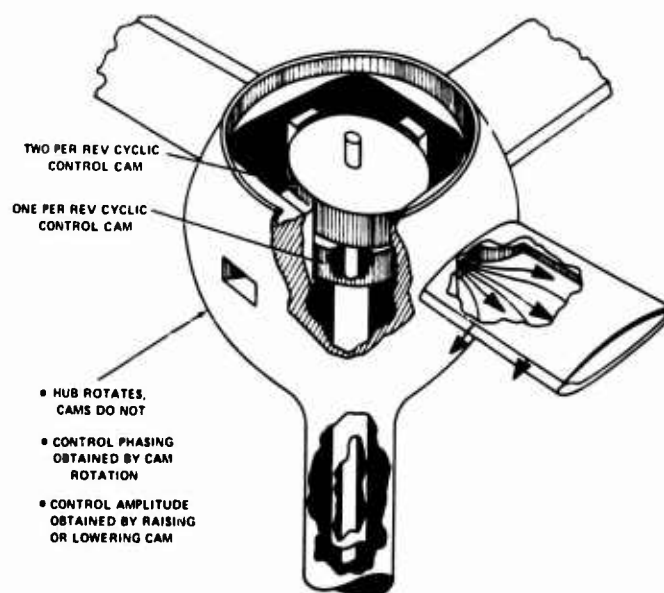


Figure 4 - Example of Hub-Valve Control System



Figure 5a - Low Speed Circulation Control Rotor with Second Harmonic Blowing Control



Figure 5b - High Speed Jet Flap Rotor with Dual Plenum Blowing

Figure 5 - Seven Foot Diameter Blown Model Rotor: Tested in NSRDC 8 x 10 Foot Subsonic Wind Tunnel

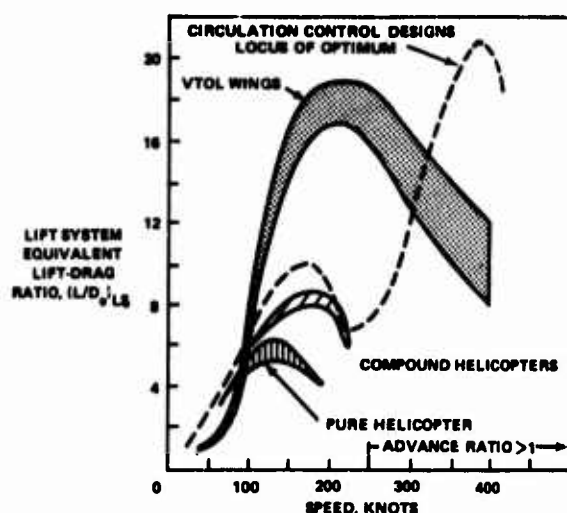


Figure 6 - Trend of Rotor Lifting Efficiency with Speed

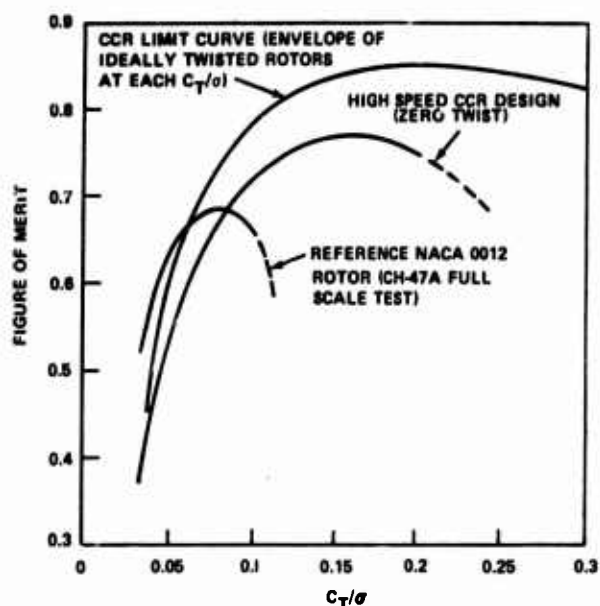


Figure 7 - Hover Efficiency

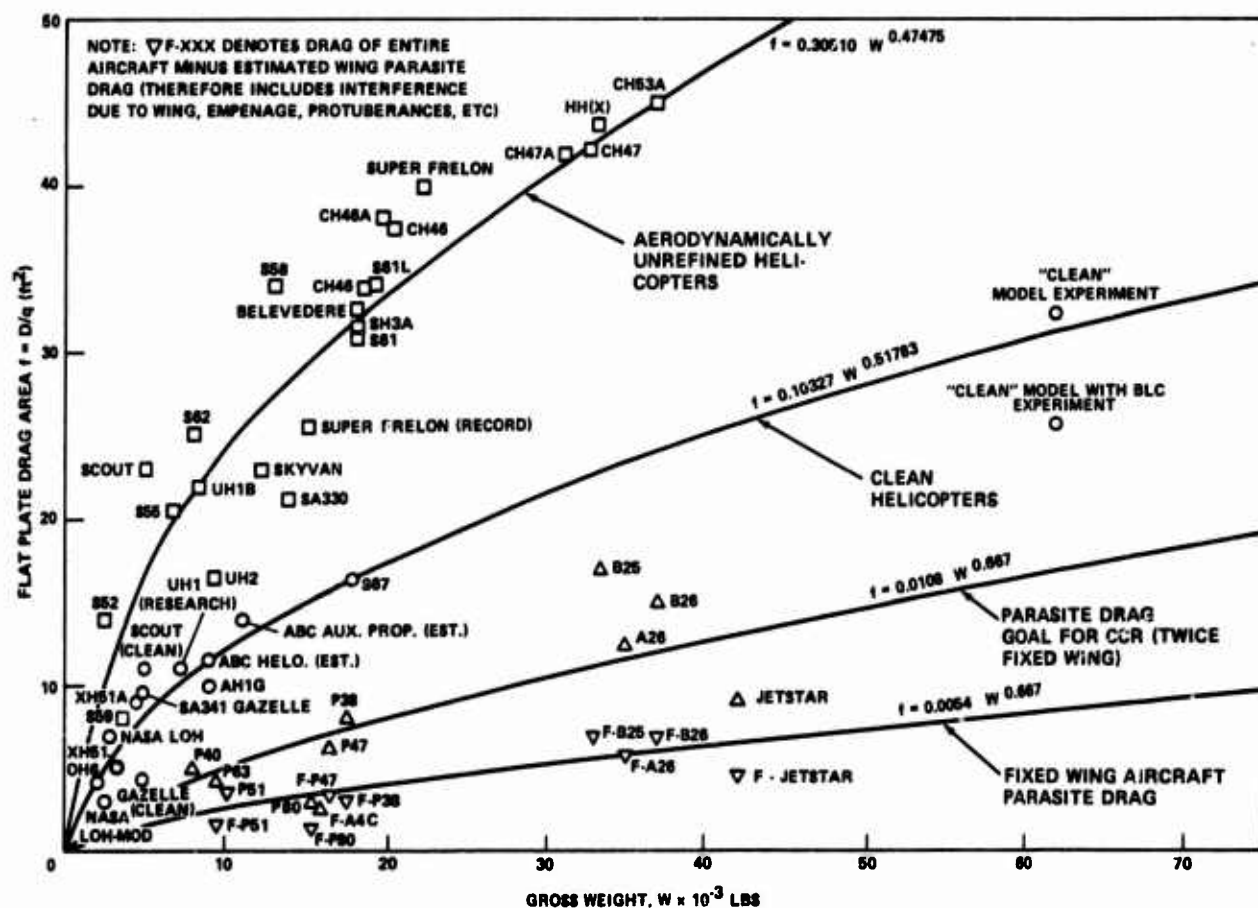


Figure 8 - Parasite Drag Trends of Helicopters and Aircraft

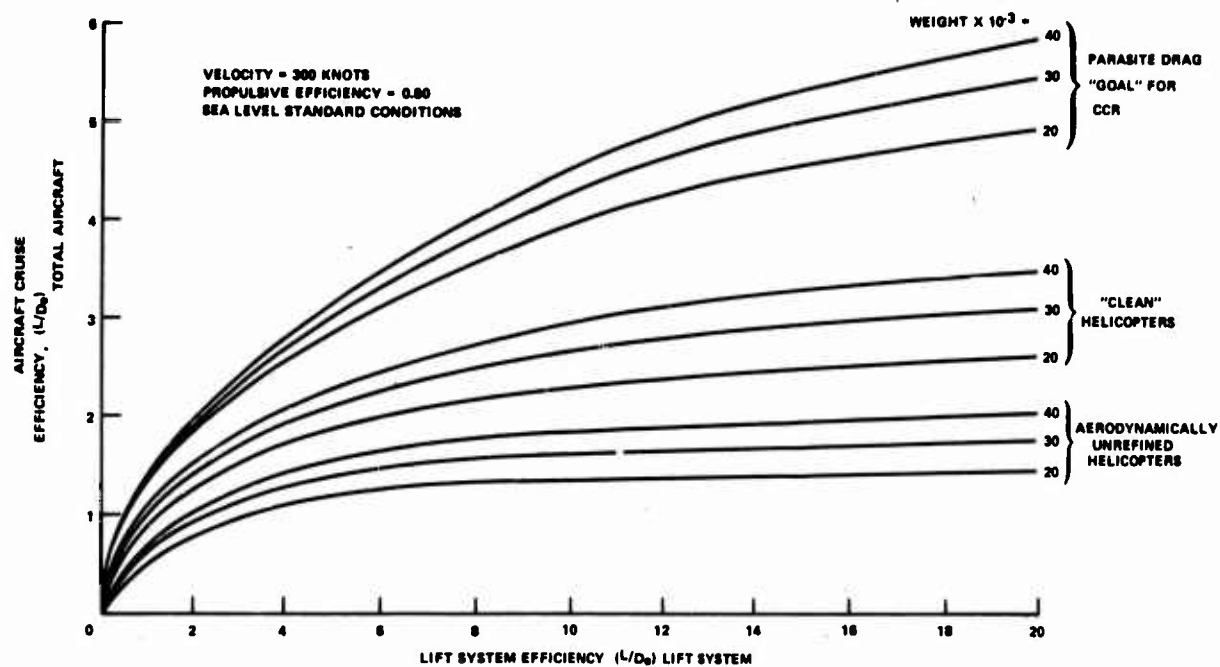


Figure 9 - Effect of Aerodynamic Cleanliness and Weight on Cruise Performance

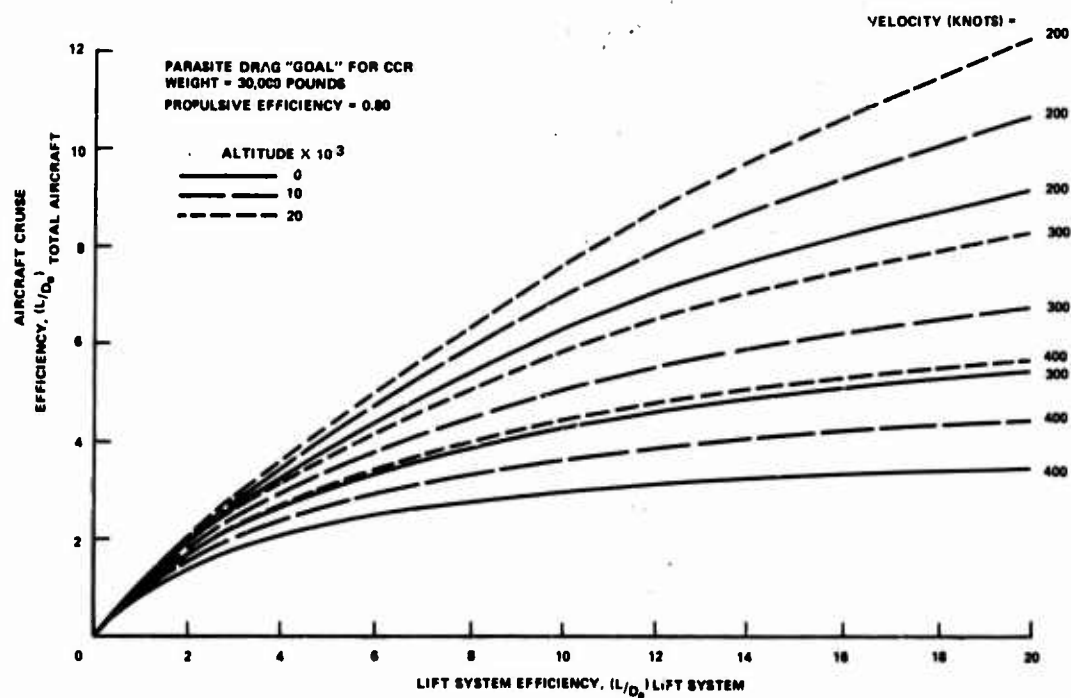


Figure 10 - Effect of Velocity and Altitude on Cruise Performance

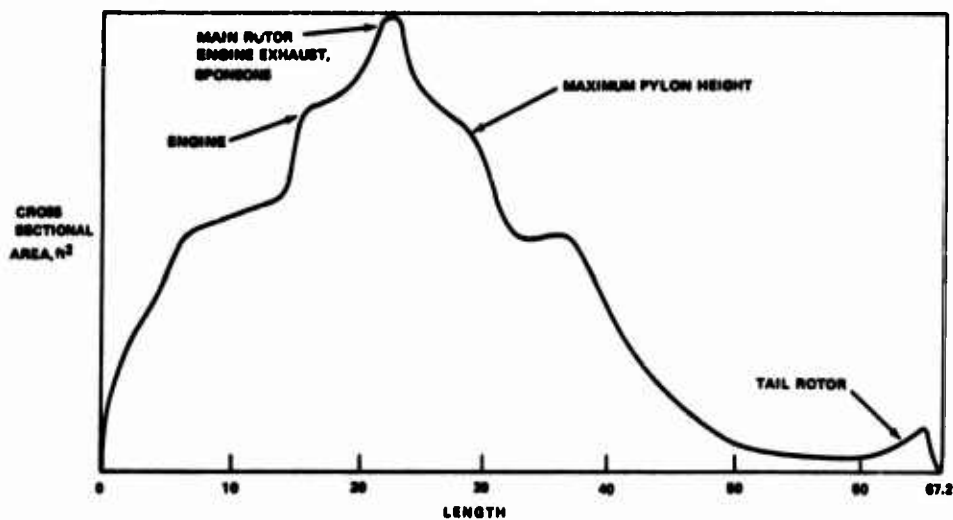


Figure 11 – Cross Sectional Area Distribution of CH-53A

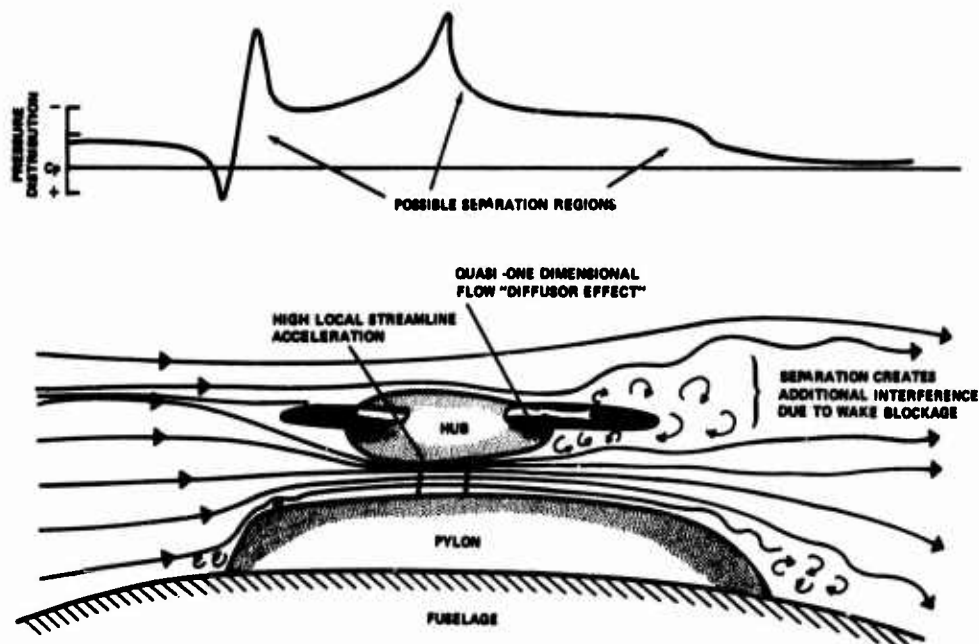


Figure 12 – The Hub-Pylon Interference Problem

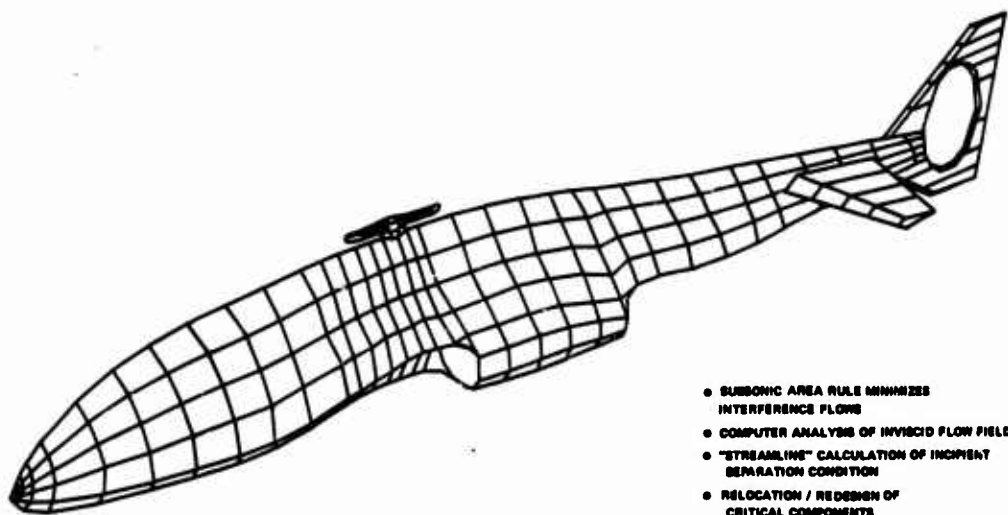


Figure 13 – Analytical Approach to Fuselage Design

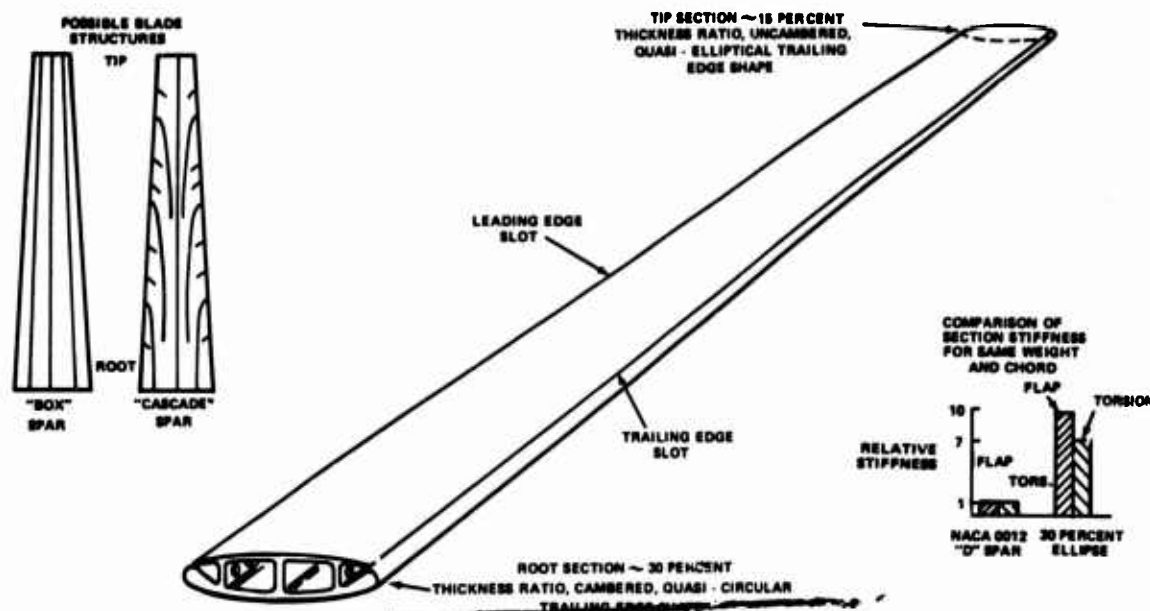


Figure 14 - Typical Dual Plenum Blade Design for High Speed Rotor

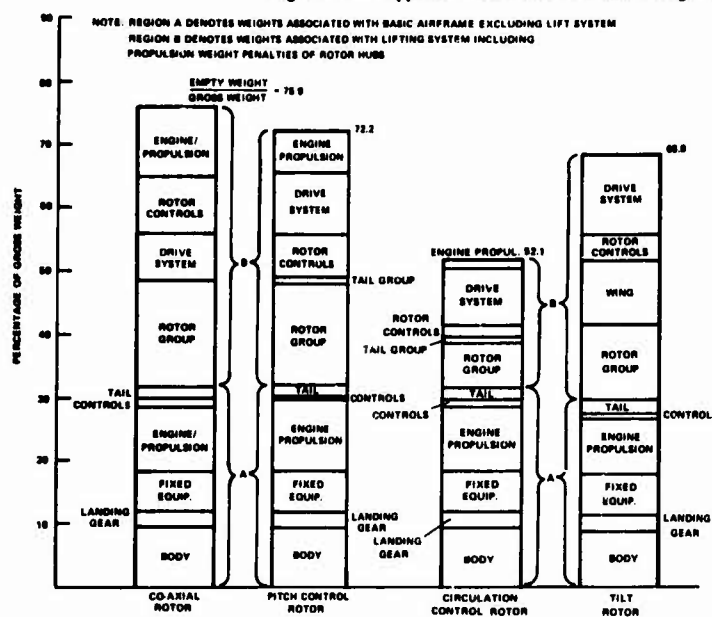


Figure 15 - Impact of Lifting System Efficiency on Vehicle Empty Weight (300-Knot Sea Level Design, 20,000 lb. Gross Weight, 3.0g Limit Load Factor)

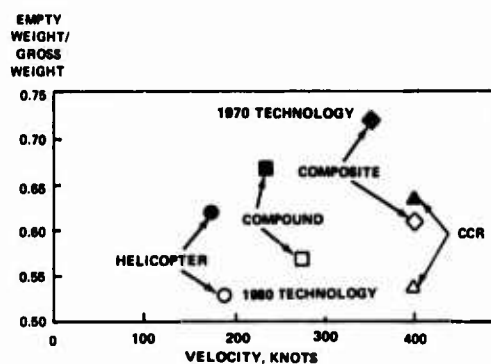


Figure 16 - VTOL Empty Weight Trends with Speed

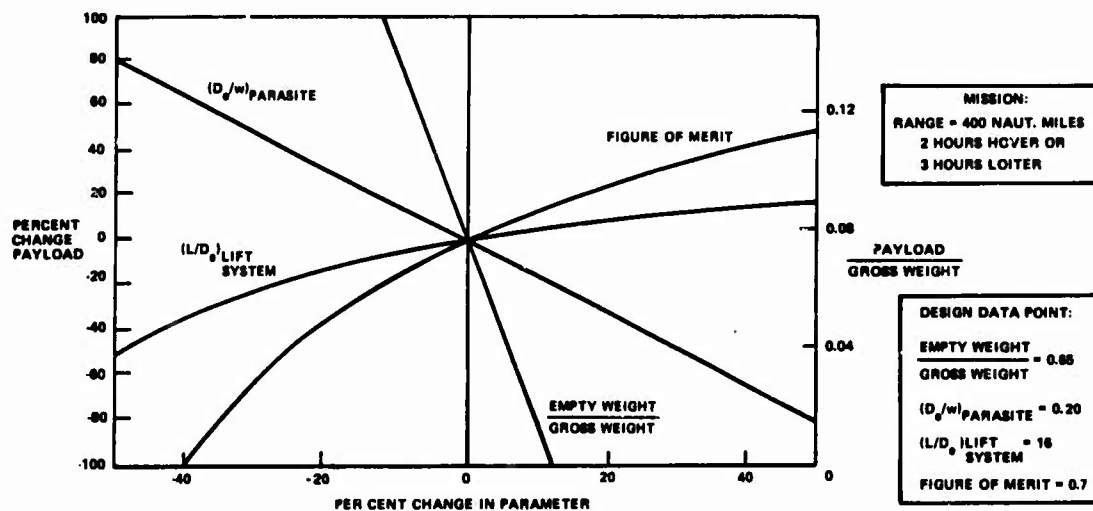


Figure 17 - Sensitivity of Payload to Changes in Design Parameters

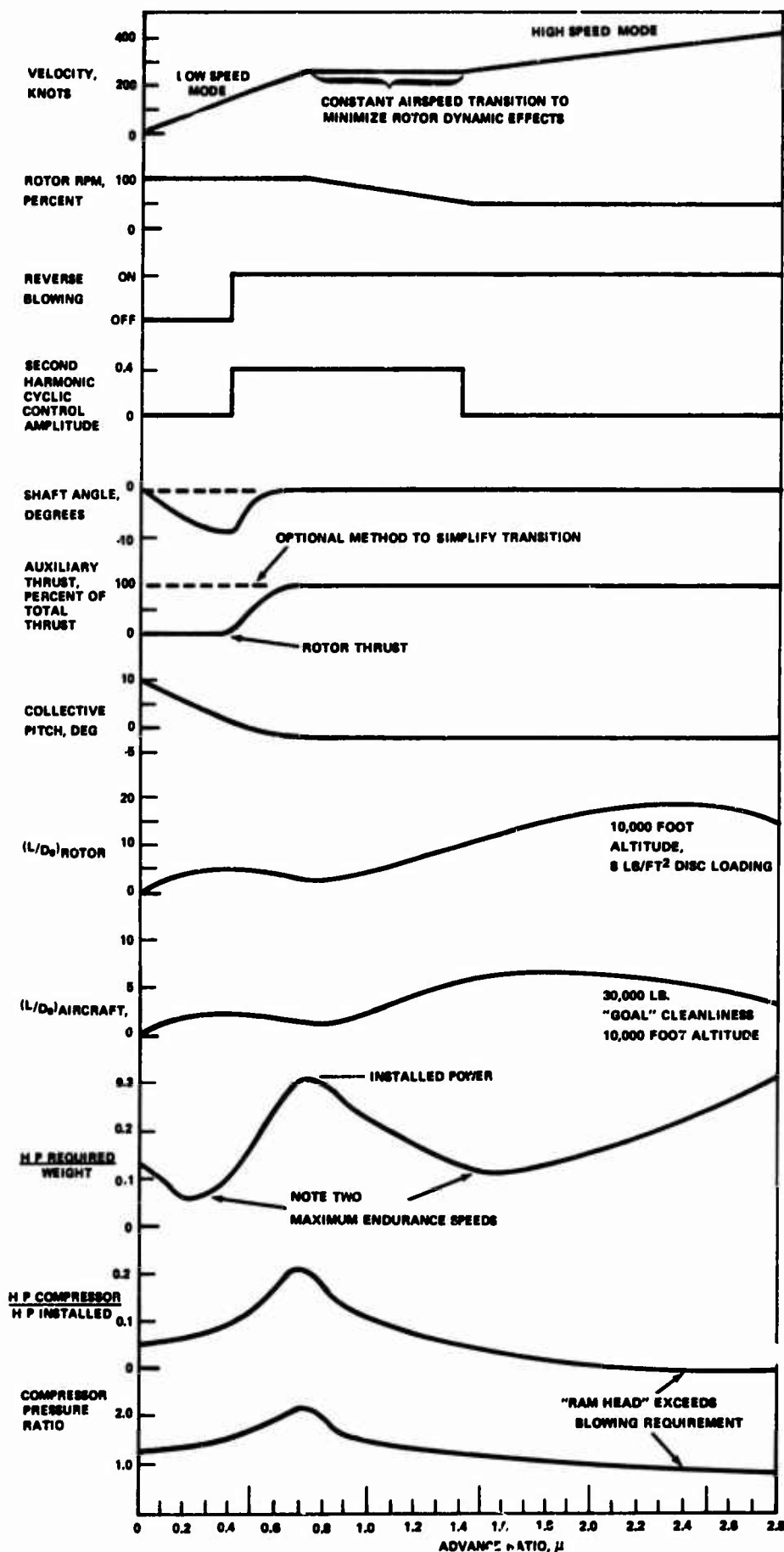


Figure 18 — Typical Modes of Operation of High Speed Circulation Control Rotor Design

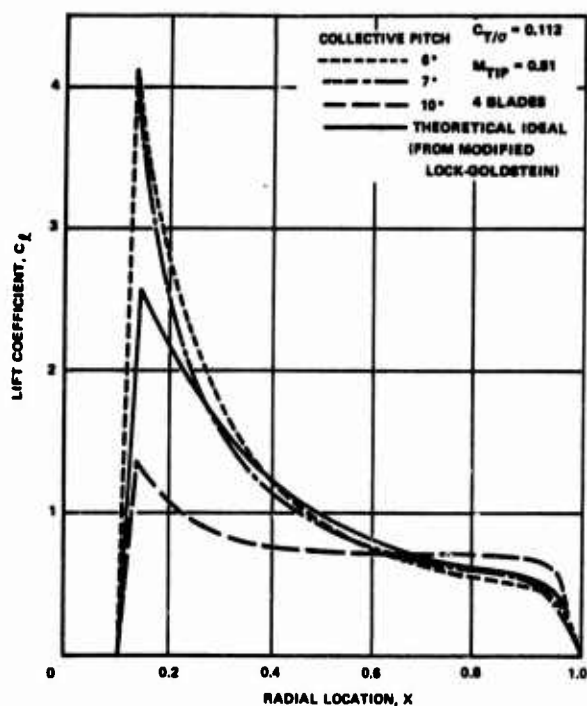


Figure 19 - Variation of Radial Load Distribution with Collective Pitch, $C_T = 0.010$

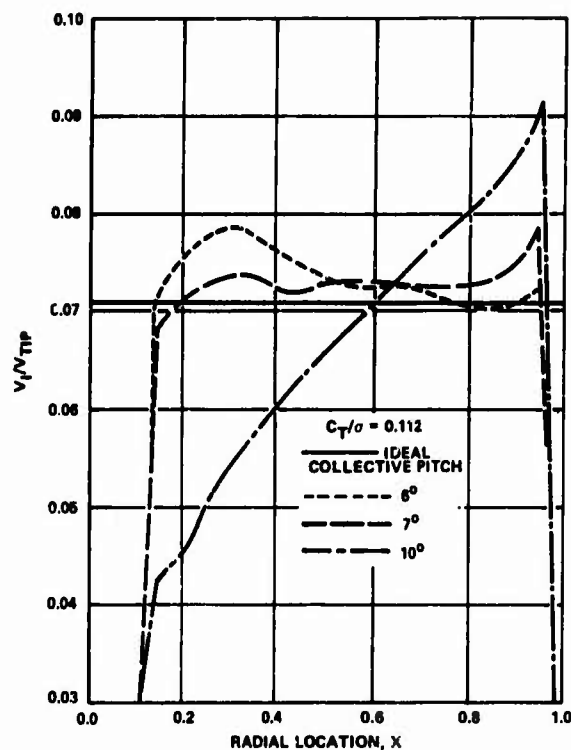


Figure 20 - Calculated Induced Velocity Distribution Corresponding to Lift Distributions of Figure 19

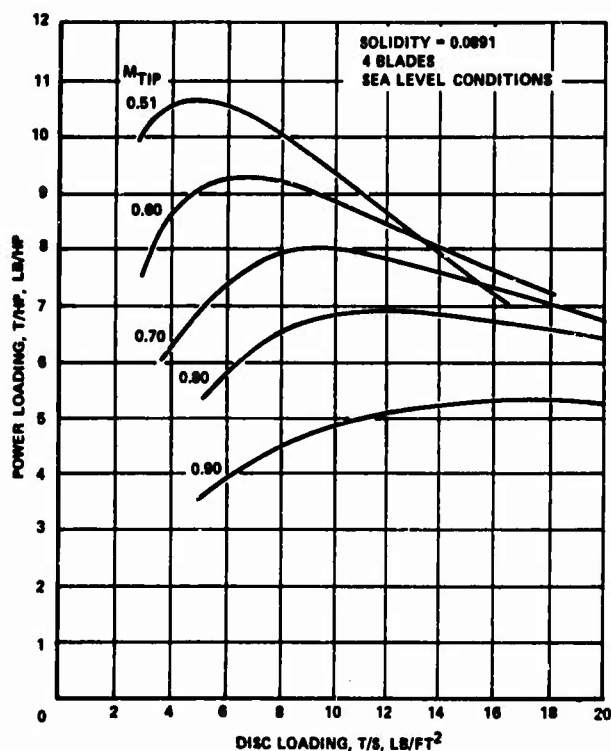


Figure 21 - Variation of Power Loading with Disc Loading and Tip Mach Number

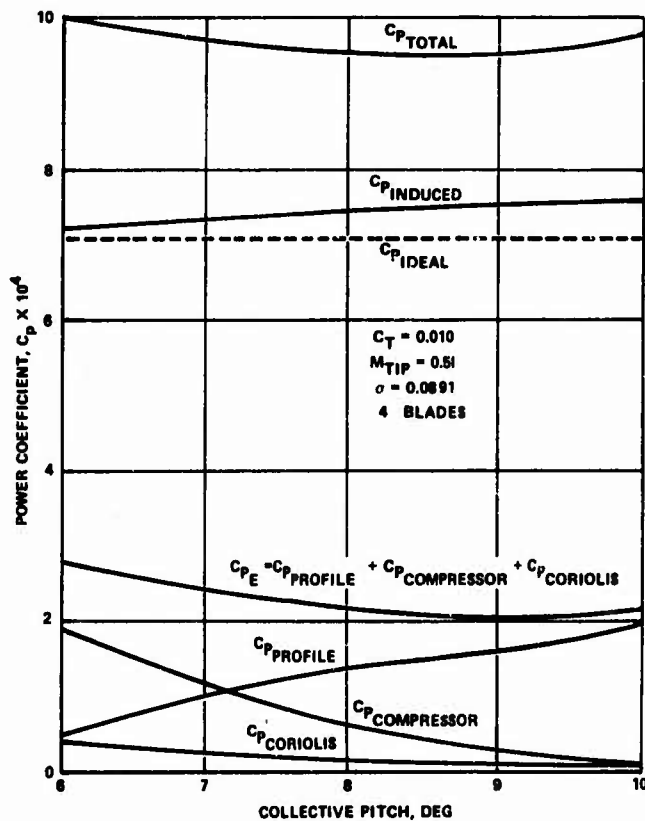


Figure 22 - Variation of Power Components with Collective Pitch, $C_T = 0.010$

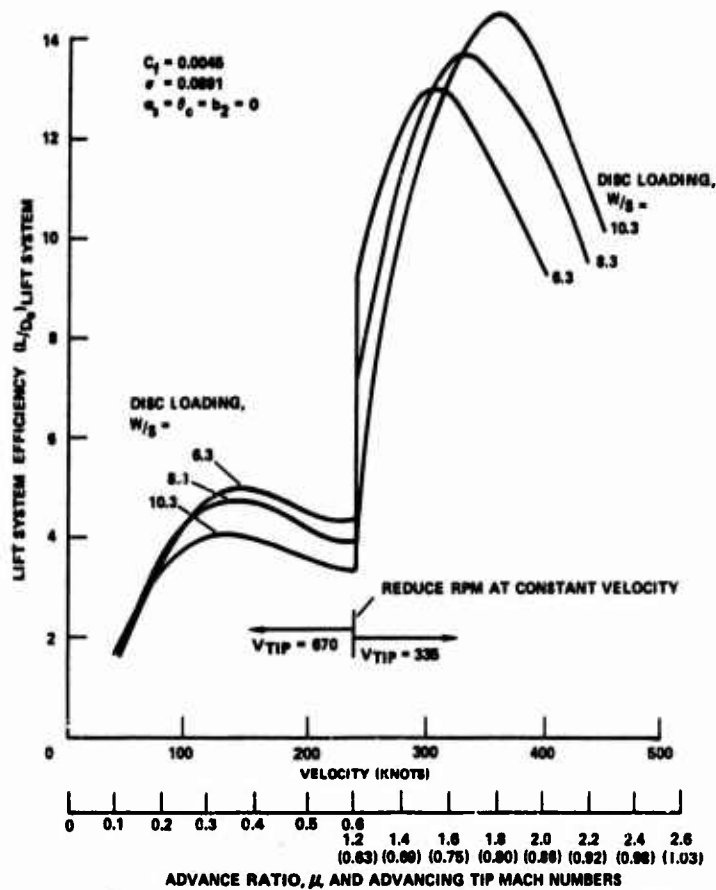


Figure 23 - Typical Variations of Lift System Efficiency with Velocity and Advance Ratio

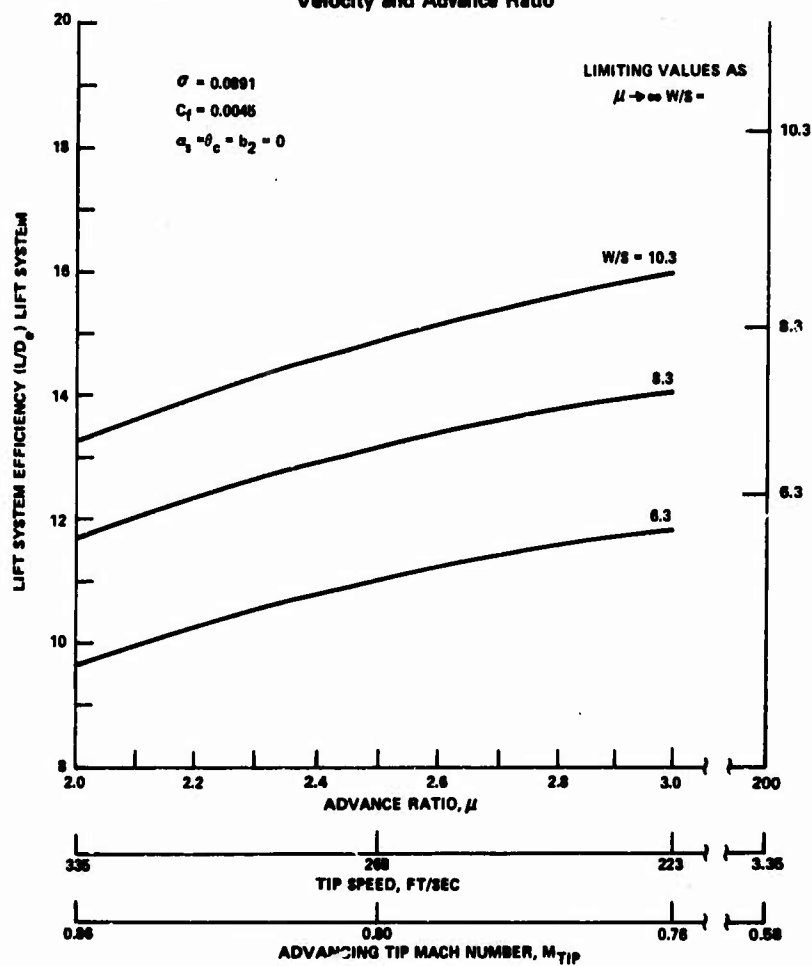


Figure 24 - Effect of Reducing Tip Speed on Rotor Lifting Efficiency at 400 Knots

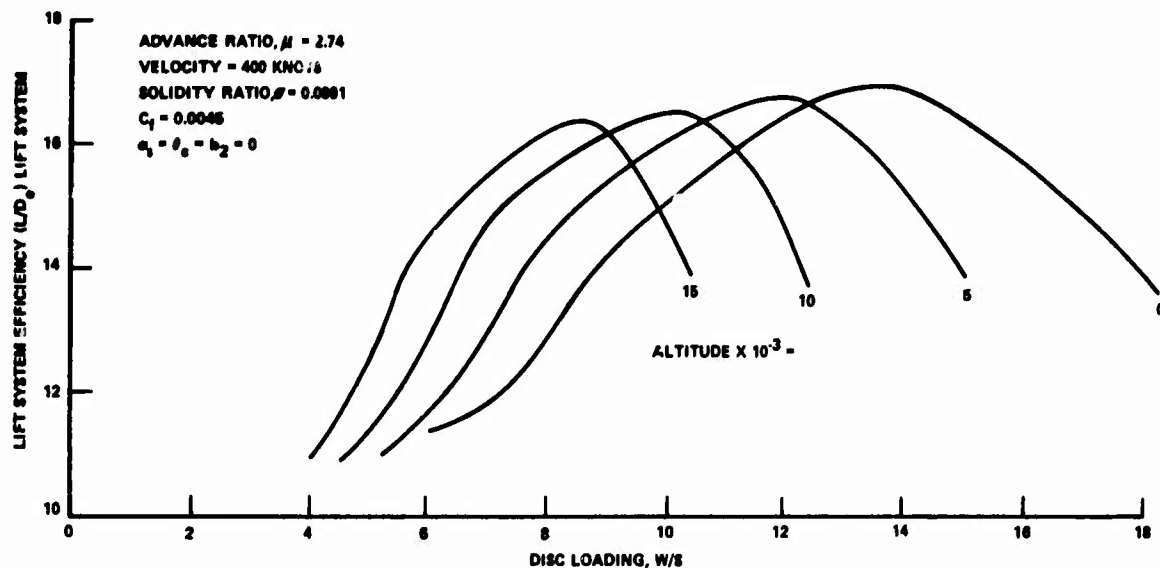


Figure 25 - Effect of Altitude on Lift System Efficiency (Non-Optimized)

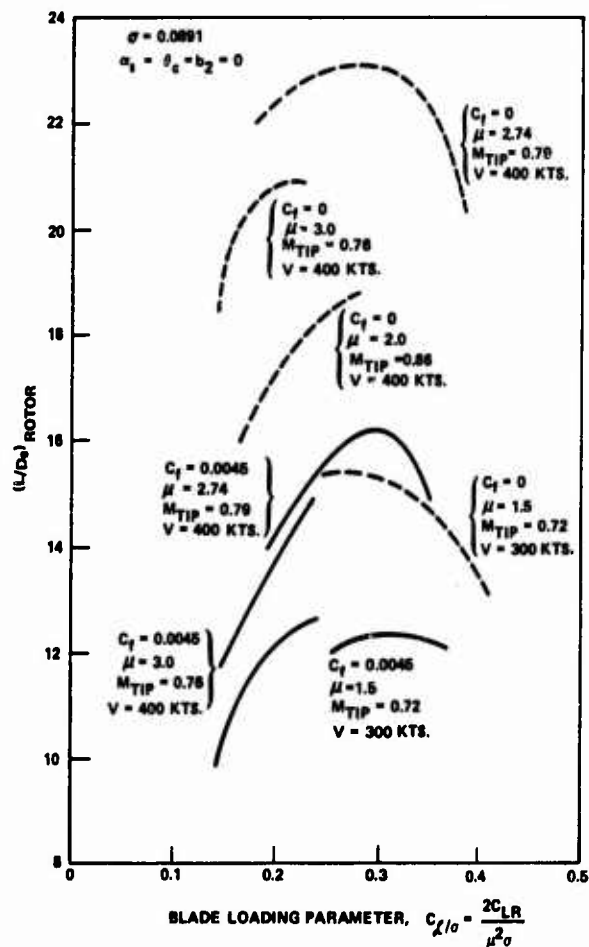


Figure 26 - Effect of Radial Skin Friction Coefficient on Rotor Cruise Efficiency (Non-Optimum; Zero Collective Pitch, Shaft Angle, Second Harmonic)

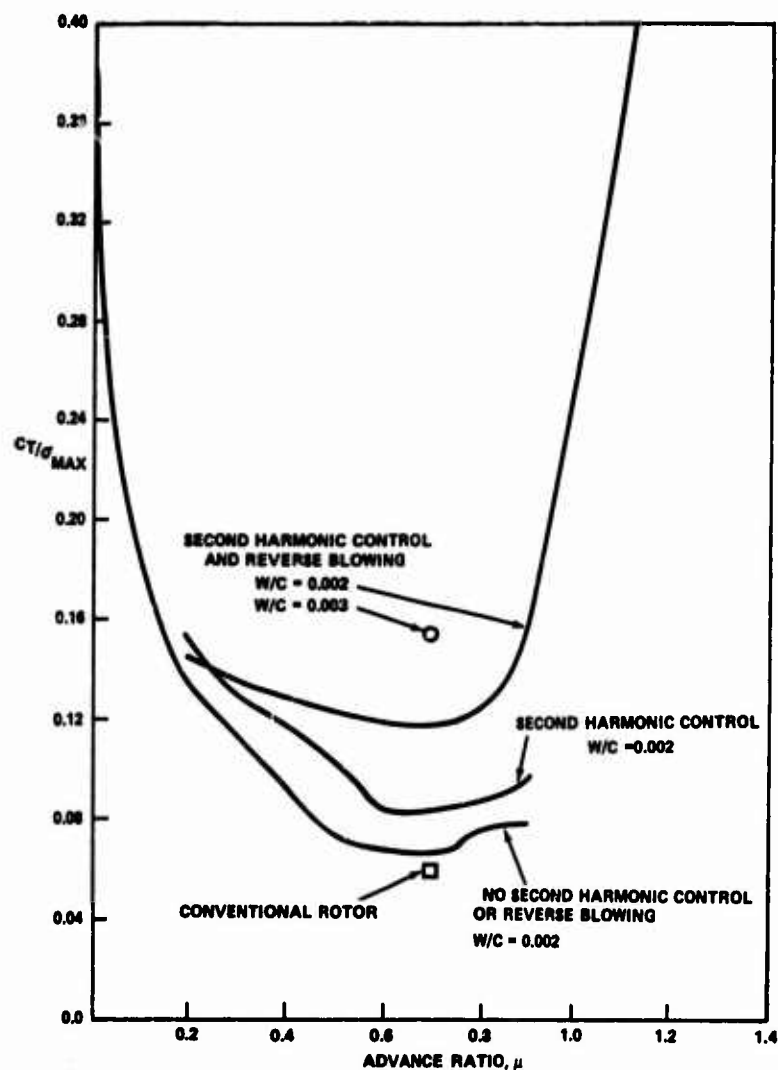
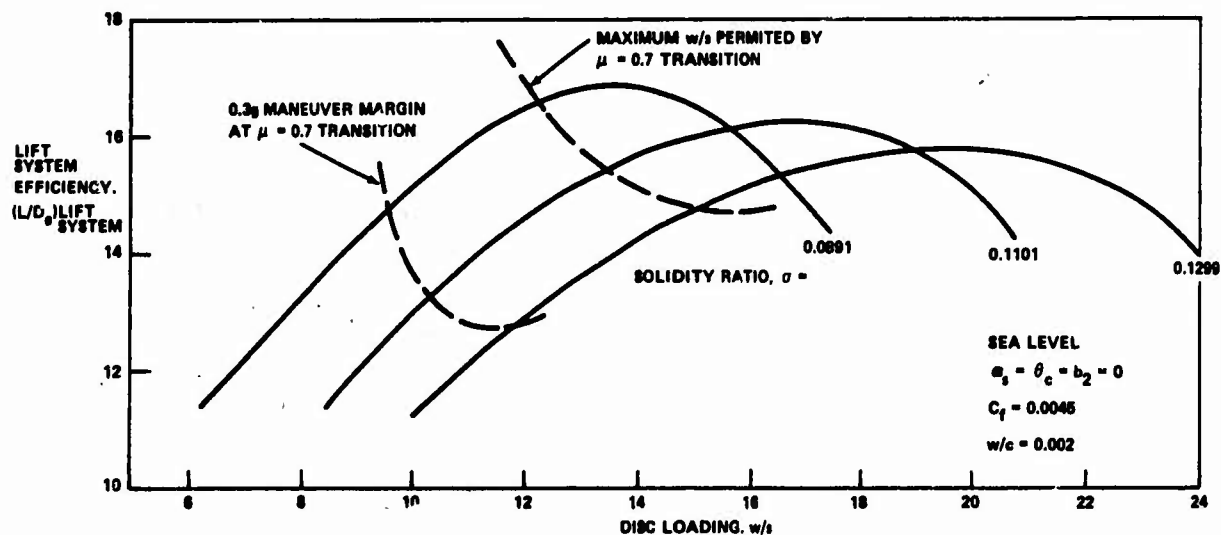


Figure 27 - Maximum Thrust Capability

Figure 28 - Effect of Solidity Ratio on Cruise Performance, $\mu = 2.74$, 400 Knots

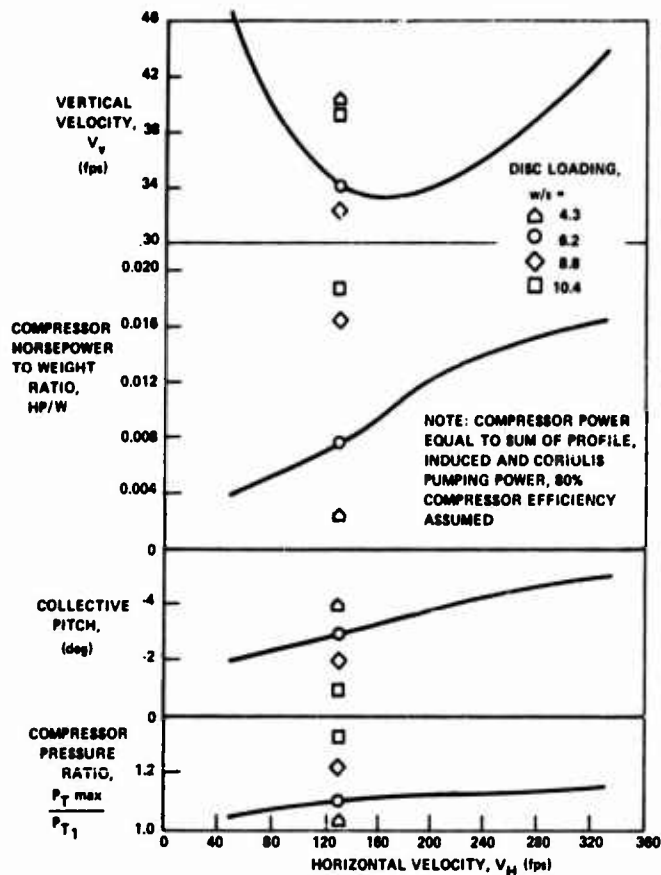


Figure 29 - Steady State Autorotation Characteristics

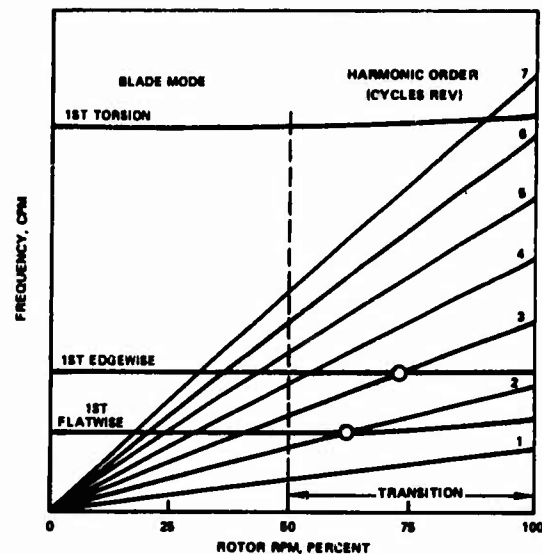
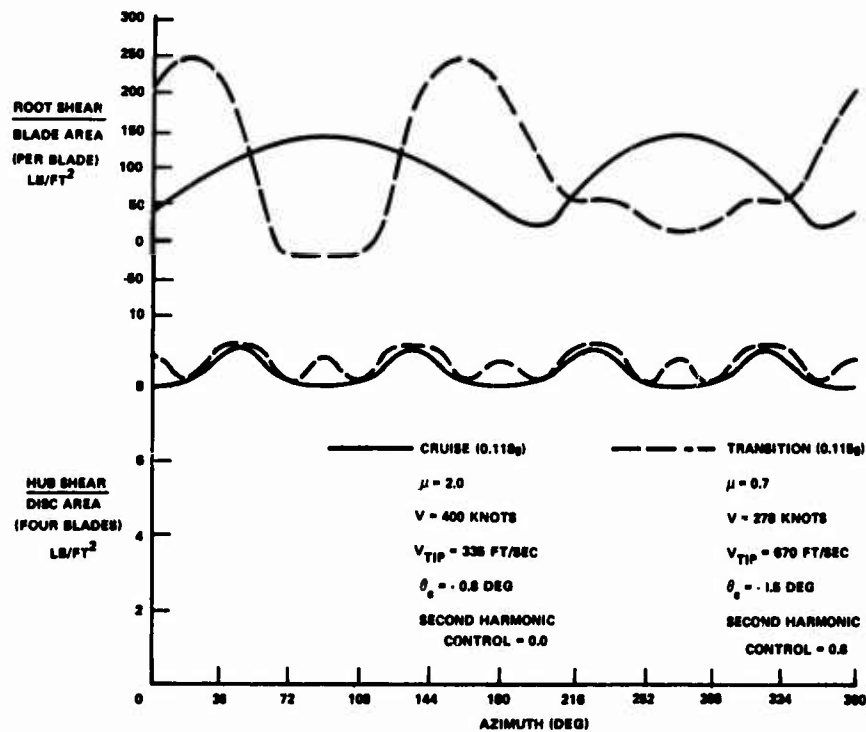


Figure 30 - Rotor Frequency Placement for RPM Reduction

Figure 31 - Rigid Blade Vibratory Shears at Transition and Cruise for Four Bladed Rotor, Disc Loading ≈ 8

SOME OBJECTIVES IN APPLYING HINGELESS ROTORS
TO HELICOPTERS AND V/STOL-AIRCRAFTS

by

H.B. Huber

Messerschmitt-Bölkow-Blohm GmbH
Ottobrunn, Germany

SUMMARY

Some of the aerodynamic, dynamic and aeroelastic problems in rotor design for helicopters and V/STOL-aircrafts will be discussed in this paper. After a short description of the main features of the hingeless rotor concept the most important research and design areas of the system are indicated.

Particular attention must be given to the flapping and inplane stiffness of the blade root section, the aerodynamic and dynamic blade design, the rotor hub geometry and the control system flexibility. The paper will give some insight into the aeroelastic characteristics and will show some important parameter sensitivities.

The analytical and experimental studies include control and flight dynamic characteristics, structural loads, damping behaviour and aeroelastic stability. Analytical results are compared with test data. Based on these results some design criteria are provided and recommendations are made for a successful application of hingeless rotor systems on helicopters and tilting prop/rotor aircrafts.

NOTATIONS

a_s	equivalent hinge offset
a_0, a_1	flapping coefficients
c_δ	equivalent flapping hinge restraint
c_ζ	equivalent lagging hinge restraint
c_θ	blade torsional stiffness
$c_{\theta E}$	control system flexibility
D_ζ	blade lag damping
$D_{\zeta G}$	lag mode damping
$d_{c.g.}$	chordwise center of gravity position
M_δ	blade root flapwise bending moment
M_ζ	blade root inplane bending moment
$M_{\eta x}$	control pitching moment
R	rotor radius
t	time
t_D, t_H	time to double or to half amplitude
T	period
V	air speed
β	flapping angle
β_K	feathering axis precone angle
ζ	lead-lag angle
ζ_K	blade sweep angle
θ_E	torsional deflection of control system
θ_0	collectiv pitch
θ_c	cyclic pitch
δ_1	pitch-lag coupling
δ_3	pitch-flap coupling
Ω	rotor frequency
ω_β	flapping natural frequency
ω_ζ	inplane natural frequency

The studies have been sponsored in part by the Ministry of Defence of the Federal Republic of Germany

1. INTRODUCTION

Over the past years of Vertical-Takeoff- and Landing Aircrafts the low disc loading rotor attained broad acceptance. With increase of physical understanding and improvement of technical facilities new types of rotors are developed and at this the hingeless rotor concept has been favoured in recent years.

Theoretical and experimental investigations have shown that the nonarticulated type of rotor offers advantages and significant improvements in a number of areas. The main advantage of this system can be stated to be the large moment capability which can be transferred to the aircraft. Thus high control power and damping is provided resulting in good handling qualities under all flight conditions. A second reason for selecting hingeless rotors is the simplicity of this system achieved by elimination of hinges, dampers and all sorts of blade stops, for example.

As indicated by analytical studies and test experience, the aerodynamic behaviour is hardly influenced by the type of blade attachment and conventional analysis can be utilized for rotor aerodynamic treatment. From the standpoint of dynamic and aeroelastics, however, the hingeless rotor represents a fairly new concept, and therefore a detailed study of the problems is necessary for a successful application to helicopters and VTOL-aircrafts.

2. BÖLKOW APPLICATION OF HINGELESS ROTORS

Since the beginning of the helicopter activities at the MBB company a variety of rotary wing projects was started. The most famous one, being now in production stage, is the Light-Utility-Helicopter BO 105 with a hingeless type of rotor. This new helicopter system was described in several papers (1, 2) and is well known today. The main objective in rotor design was to get a rotor with improved flying qualities, low maintenance and high blade life. The fact that the rotor system itself didn't need any change since the design phase proves that this work was done successfully (Figure 1).

Naturally, the system was developed further in detail and new effects were investigated on it over the years. There was a tuning of the blades with respect to the main frequencies, a reduction of the hub size by using titanium and a modification of the blades airfoil section. New effects are studied with advanced profile shapes at the tip section and with blades with integrated aeroelastic feedback properties.

In order to provide some physical understanding, a short description of the Bölkow Rotor System will be given. The main components of this rotor (Figure 1) are a very stiff hub and fiberglass rotor blades, which are rigidly attached to short hub arms without flapping and lagging hinges. There is only a feathering hinge fixed to the rigid hub arms. The blade motions are pitching motion at the root, elastic bending in flapwise and chordwise direction and torsional deflections.

Such types of hingeless rotors are sometimes regarded as "rigid" rotors, which would actually behave like a rigid structure. In this respect it must be recognized that in current designs high flexibility is used, especially in the blade root sections. These flexibilities determine the fundamental differences to completely rigid rotors as well as to fully articulated rotors.

Flapping and inplane flexibility are best characterized by the rotating natural frequencies of the blades first bending modes. In the Bölkow Hingeless Rotor System a frequency ratio relative to rotor frequency of about 1.10 to 1.12 is used in flapping direction and a ratio of about 0.6 to 0.7 in inplane direction. The comparable values of a typical articulated rotor are about 1.02 (flapping) and between 0.2 to 0.3 (inplane). It will be shown in this paper that these two values are important characteristics of a rotor system with respect to the flight dynamics, the aeroelastic stability behaviour and the structural loads.

3. REQUIRED RESEARCH AREAS ON HINGELESS ROTORS

As mentioned before, the hingeless rotor system, as it is utilized nowadays is determined by the use of flexibility in the blades. Thus it is far from a conventional hinged blade system and of course far from a "rigid" blade system.

3.1 Technical research areas

The purpose of Figure 2 is to illustrate the most important "research areas" on a non-articulated rotor concept and to summarize some of the problems and effects associated with the main blade properties. As it can be seen, the most interesting blade section is the region of rotorhub and blade root. These areas require particular attention during the layout and design phase.

As it was discussed in several papers (1, 2, 3), the dynamic characteristics of a hingeless rotor helicopter are primarily defined by the flap bending stiffness of the hub and blade root section. The size of the hub and the spanwise blade stiffness and mass

distribution are the determining parameters in this respect. The magnitude of the moments transmitted to the rotor shaft proves to be the most important advantage of the hingeless rotor system, providing an excellent control and damping response and an extensive lift offset range.

A second important layout parameter is the inplane bending stiffness of the blades (Figure 2). It seems to be a question of design philosophy, whether a very stiff subcritical system ($\omega_r > \Omega$), or a supercritical soft inplane system ($\omega_r < \Omega$) is used. In selecting this frequency careful attention must be given to the structural loads and to all sorts of aerodynamic and mechanic lag instabilities, such as flap-lag coupling or ground and air resonance. Relating to these problems the knowledge of the strength behaviour and the damping characteristics of the material is of main importance (5).

A third phase of rotor layout is the blade design. Besides the direct aerodynamic considerations, which are treated usually with respect to performance and mission requirements, specific questions must be regarded, which affect the dynamic behaviour in general. The blade axis positions and the torsional stiffness of the blade are active parameters in this respect (4). In this way further gains in flight characteristics can be made by elastic coupling effects indicating that design work on blade section will be worthwhile, especially for hingeless rotors (4).

The design of hub and blade root attachment and the stiffness of the control system are two more problem areas on the rotor, which must be regarded in the rotor layout. It will be shown in this paper that different hub geometries will result in different coupling effects when control flexibility is present. The effects may be extensive, including flying qualities and even air resonance stability, for example.

3.2 Mathematical model

In order to determine analytically the stability and flight characteristics of a hingeless rotor, a relatively simple blade and rotor model can be used. It is assumed that the articulated blade is replaced by an equivalent offset hinge blade, which is considered as a rigid body with spring restraint and dampers, as shown in Figure 3. This equivalent blade system is an extension of a normal flapping system (1), as it is usually used for pure flapping response studies. This model has additional degrees of freedom in chordwise and torsional directions, it includes

- blade flapwise bending (first mode)
- blade inplane bending (first mode)
- blade twisting (first mode)
- control system flexibility.

Flapping of the blades is the determining degree of freedom and affects the main behaviour of the rotor. Inplane bending is strongly coupled to the flapping motion by Coriolis-forces and is of great influence on the aeroelastic stability. Torsional elastic motions must be included because they act as control inputs, finally control flexibility is a parameter, which affects the coupling of all other blade motions.

Analytical results obtained with this complex aeroelastic model show that hingeless rotors can be simulated well enough for flight dynamics and system stability problems as well as for elastic coupling effects.

4. INFLUENCE OF FLAPPING FREQUENCY

As mentioned before, the main parameter for controllability and stability of a helicopter is the frequency of fundamental flap bending mode. The hingeless blade concept is calculated using conventional hinged-rotor analysis with equivalent offset blade and spring restraint. The influences of these two parameters are shown in Figure 4. Flapping frequency over unit can be obtained by means of hinge offset or structural or artificial blade root restraint. The cantilevered elastic blade of the BO 105 for example results in an equivalent hinge offset of about 15% R and zero or slightly negative hinge restraint.

A third way to influence the flapping response is the use of pitch-flap-coupling (δ_3). Its physical attribute is an "aerodynamic spring" which influences the amplification between angle of attack variations and flapping response. But it must be recognized that the change of flapping frequency with δ_3 -angles is not entirely comparable to real stiffness frequency increase, because there is no change of the specific moments per degree of flap angle. Due to lack of real hinges kinematic δ_3 -coupling can normally not be applied to rigid rotor systems. However, systems with the feathering bearing inboard of the flap and lag flexure are subject to favourable pitch-flap-coupling effects, which are equivalent to kinematic couplings. Therefore, any hub geometry and blade parameter, which results in this type of coupling will influence the dynamics of hingeless rotors.

4.1 Moment capability, trim and control

On helicopters and new types of tilting prop/rotor aircrafts the rotor is used for trimming and controlling the aircraft during transition or even in all flight conditions.

In this respect the principal innovation of hingeless rotor systems is the capability to transmit large moments to the rotor shaft. Figure 5 illustrates the elastic behaviour and the moment capacity of a hingeless rotor over a wide range of blade flapping frequency, including normal articulated rotors and very stiff propellers. It should be noted that the flapping response to cyclic control - on the left part - of a typical hingeless rotor is about the same as the response of a fully articulated rotor ($\omega_g = 1.0$), but is decreasing with higher frequencies. Typical tilting rotors ($\omega_g = 1.2 + 1.4$) and very stiff propellers ($\omega_g = 1.7$) are represented in this case with normal virtual "hinge" offsets and relatively strong root springs. In contrast to the flapping amplitudes the magnitude of the resulting moments at the rotor hub shows a marked increase with flapping stiffness. It is interesting to note that the main increment of control-moment is already obtained at relatively low values of ω_g .

Another effect of cyclic pitch is the side force resulting from the tilt of the rotor disc (δ) and from aerodynamic drag changes. It is shown in this picture that a maximum side force on rotors is obtained with flapping frequency ratios of about 1.2. This is important for hover yaw considerations of tilting prop/rotor aircrafts, where a yawing moment is provided by differential cyclic pitch.

In steady-state flight conditions (Figure 6) the fluctuations in the aerodynamic blade forces during blade revolution are hardly influenced by the flapping frequency of the rotor. The corresponding control angles of the two rotors are fixed by the different flow conditions during the revolution of the rotor blades and by the requirements of trimming the aerodynamic and center of gravity moments of the aircraft. In general, with hingeless rotors it is necessary to reduce the first harmonic flapping motion to limit the moments acting on the helicopter.

In order to illustrate the scope of cyclic requirements for trimmed flight conditions, the longitudinal pitch angles are shown versus airspeed in Figure 7. A helicopter and a tilt wing aircraft with cyclic pitch propellers are selected to show the extreme requirements in this respect. For the helicopter the trim angles are within a range of 6° with a positive static stability over the whole range of normal flight speeds. At the extreme high speed condition (170 knots) longitudinal cyclic angles are required up to 9° , which is about 90% of the control margin of this helicopter. In the right part of the picture the control characteristics of a typical tilt-wing aircraft of about 60,000 pounds gross weight is shown for hover and transition. The reversal in longitudinal stick position is due to the tilt of the wing and is inherent in the nature of such types of aircrafts. But it is of still more interest that a cyclic pitch of less than 2° is sufficient to trim the four propeller aircraft during transition - even with the most unfavourable c.g. position. For additional maneuvers (relating to MIL and AGARD-Requirements) a maximum cyclic of only 5° will be required (5).

4.2 Stability characteristics

Similar to the control moments the stability characteristics of helicopters and tilt-rotor-aircrafts are affected by the flapping stiffness of the blades. It can easily be shown by analysis that the dominating stability parameters are presented by the pitching moment - angle of attack stability and by the rotor damping response. Variations in the flapping frequency will influence these two derivatives in particular (2).

Figure 8 shows the stability characteristics of the hingeless rotor helicopter BO 105 over flight speed. Illustrated are the period and the time to double amplitude of the critical natural helicopter mode with fixed controls. Due to high damping efficiency of the rotor the aircraft is relatively stable in hover and at low flight speeds, becoming more and more unstable at higher speeds.

In this respect it is of interest that the stability characteristics in the high speed range can significantly improve with different blade modifications. The basic stability curve relates to symmetrical blades with O012 profile section. The second curve is obtained with cambered airfoil blades and with a small c.g.-shift at the tip section. The third stability curve relates to the same type of airfoil but with a 5% chordwise overbalance over the whole blade. In the speed range of 100 knots, for example, the time to double amplitude is increased from 4 sec to about 20 sec by using blade 2 and this achievement is further increased by using fully aeroelastic feedback blades. In this way the "speed of equivalent stability" is increased by about 100 knots in the high speed range with proper blade design. It is indicated by these results, that aerodynamic and dynamic blade design work is worthwhile, especially for hingeless rotors.

5. BLADE DESIGN

Another important area of rotor layout is the blade design with respect to the aerodynamic and torsional dynamic qualities. The main problems of rotors at high forward speeds or higher disc loadings are known as classical blade flutter, divergence or dynamic blade stall flutter, resulting from nonsteady aerodynamic effects. These problems are treated by several papers and reports in the last years and nowadays.

In addition to these stability problems there are other aerodynamic and torsional dynamic effects, which are of great influence on the performance and flying qualities. Theoretical investigations and flight test results with the BO 105 helicopter with modi-

fied rotor blades (4) have shown that considerable improvements in performance and flight dynamics can be achieved with proper aerodynamic characteristics and positive elastic effects of the torsionally flexible blades.

Figure 9 shows a comparison of the maneuver-characteristics with two different blade airfoil sections. On the rotor with symmetric 0012-profile section a turn of stick travel over g is reached at the maneuver range of about 1.5 g and the maximum load factor in trimmed flight is limited to 1.9 g . By using unsymmetric profile section the stick instability is postponed and steady load factors up to 2.3 g are obtained. According to the more favourable stall behaviour of these blades the pitch link loads are reduced considerably over the entire speed range and more so in maneuver flights. The results of further investigations show that even the flight characteristics are influenced by the aerodynamic properties of the profile. In this respect a rearward a.c.-position results in an increase of rotor damping and improved stability characteristics. These effects are investigated in more detail in reference (4).

An analysis of the torsional equation of motion indicates (4) that the torsion of rotor blades is further influenced by the relative positions of the blade axes of a.c., c.g., p.a., e.a.. Strong effects are provided especially by the chordwise mass-distribution (c.g.) and it can be shown that a coupling of flapwise bending and torsion of the blade exists, when the blade is unbalanced in chordwise direction.

To illustrate the physical principle of this torsional elastic coupling, the dynamic blade response in flapping and torsional direction to a discrete gust is shown in Figure 10. The rotor is trimmed in this case at a 100 knots flight speed and enters a 35 fps sine-squared vertical gust. The principal feature of the 20% c.g. blade are the torsional motions induced by the flapping motion, acting as stabilizing control inputs. Normal torsional flexibility of the BO 105 blades is considered in this case. The flapping response out of trim condition is reduced by about 40% with a blade of 5% c.g. offset. In fact, this is a very efficient blade integrated feedback system.

Regarding these stabilizing effects of favourable c.g. position, an essential improvement of the stability characteristics can be expected too. Some effects have been indicated in the foregoing chapter. A broad variation of the c.g. position of the blades is shown in Figure 11. The stability increases essentially with forward shift of the c.g. and stable condition will be obtained for this flight condition at about 20% position. This calculation is for normal torsional flexibility again and therefore the improvements seem to be remarkable. There is good correlation of the analysis with flight test data. These data were achieved by adding a concentrated 7-pound weight on the blades leading edge at a 0.7 R spanwise position (Figure 12). With this additional weight an equivalent structural c.g. shift on the total blade of about 2.5% was simulated. These experiments are regarded as a prestep for a test program on the BO 105 with blades of structural positions up to 20%.

6. INPLANE FREQUENCY CONSIDERATIONS

As indicated in Figure 2, another important layout parameter is the chordwise bending stiffness of the rotor blades. Due to the different influence of the centrifugal forces in comparison to the flapping motion, the possible range of inplane frequencies is much more extended. While typical articulated rotors with hinges in flapping and inplane direction lie in a frequency range of $\bar{\omega}_r = 0.2 + 0.3$, hingeless rotor concepts can be handled from 0.3 up to 1.5, depending on the flexibility of the root and the blade section.

In general, there are two principal problem areas which require careful investigation during rotor layout phase. The one is the problem of structural loads and stress levels, the other is the danger of instability of inplane mode oscillations or their coupling with other motions such as body pitch and roll oscillations, called the "classical" ground resonance and the air resonance (6).

6.1 Structural loads

It is indicated by analysis and by flight tests that the build-up of cyclic chordwise blade bending moments occurs mainly in the rotorhub and the blade root with their magnitude depending on the chordwise flexibility in these areas. A variation in oscillatory moments with inplane frequency is shown in Figure 13. Different rotor configurations are calculated with frequency ratios from 0.20 up to 1.30. The lower frequencies are achieved in this case by very small hinge offsets (4% R), the higher frequencies by an offset of about 15% R and increasing inplane springs. In the left part of the picture time histories of the chordwise moments are presented for a cyclic step input in hover. Three typical "soft inplane" frequencies are shown and it is indicated that there is a strong increase in chordwise cyclic loads with increasing inplane stiffness. A summary of the results in the right part shows that the only way to reduce the high cyclic chordwise moments on hingeless rotors is the use of inplane flexibility. So called "soft inplane" rotors with lag frequencies between 0.6 to 0.75 seem to be a good solution in this respect.

During development and test of the BO 105 hingeless rotor the structural loads investigation was always one of the main objectives and the layout procedure was influenced

by these results. The variation in oscillatory flapwise and inplane moments of the today's BO 105 rotor with flight speed is shown in Figure 14. There is only a slight increase in the normal speed range and even at the high speed condition of 170 knots the loads remain below 40% design fatigue limit. The effects of increasing load factors - in the right part - are of normal magnitude too. The agreement between analysis and test results is fairly good, indicating that the equivalent offset method is adequate even for load studies.

6.2 Rotor damping

With inplane frequency considerations another problem must be attentioned, the danger of lead-lag instabilities. Rotors with first inplane frequency below the operating rotor speed are subject to instabilities on ground and in the air, called the ground and air resonance phenomena (6). These instabilities can occur when a body frequency in roll or pitch is close to the blades' inplane natural frequency in the nonrotating system ($\omega - \omega_L$).

One determinative parameter for the stability of the coupled motions is the total damping involved in the system. In general, there are four sources of damping: The blade damping which can be of artificial or structural mode, the aerodynamic damping, the damping involved in the airframe and the damping (or exciting) effects provided by elastic coupling of blade motions.

Since hingeless rotors have normally no possibility of artificial blade damping - and even don't want to have dampers because of simplicity - the question of "material" damping in the blade structure is essential. Therefore in the design of soft inplane ($\omega_L < \Omega$) hingeless rotors there are two decisive questions, namely how much damping is required and how much damping is present. In order to get answers to the damping requirement problem, much theoretical work is necessary involving different ground and air resonance flight conditions.

Figure 15 shows some typical results of a ground resonance study. The analytical model (7) used in this case considers the coupling of the individual blade motions and of the rotor pylon motions. Together with the flapping and inplane motions of the four blades and three translatory and rotational degrees of freedom of the hub, the system consists of 14 nonlinear differential equations. As the airloads are considered individually for each blade, aerodynamic damping is automatically included in calculation. The figure shows the modal damping of the inplane motion as a function of inplane frequency with inherent blade damping as a parameter. The values were obtained by solving the differential equations of motion. As the critical frequency $\omega - \omega_L$ of articulated rotors is much higher than for typical hingeless rotors, more driving energy is present for exciting oscillations. Therefore, on articulated rotors more inherent system damping is necessary to avoid unstable ground and air resonance conditions. As is indicated by Figure 15, the blade damping requirements of the two rotors differ by a factor 5. Similar results are shown in (8).

Up to now the structural loads and stability considerations have resulted in two essential conclusions: The one, in order to get low structural inplane loadings, chordwise flexibility should be used on the blades. The second, in order to avoid mechanical instabilities without artificial dampers, a certain lower limit of inplane stiffness must not be exceeded. It is indicated by these results that the selection and layout of the chordwise stiffness of a hingeless rotor is an optimization process which must be treated in a very thoroughly way. One precondition for doing this successfully is the knowledge of the material's qualities with respect to strength behaviour and damping characteristics. To obtain the answers to these problems, intensive test programs were conducted during the development of the hingeless rotor at the MBB company. It was experienced, for example, that the blades' structural damping depends on a lot of parameters, the most important ones being the way of blade attachment, the centrifugal force and the moment amplitude.

In addition, measurements were made on the helicopter in flight. The objective of these special flight tests was to prove the absence of any lead-lag instability and to measure the damping directly under flight conditions. In the case shown in Figure 16 a continuous roll excitation is made by the pilot by moving the stick periodically lateral with the airresonance frequency of $\Omega - \omega_L$. These "pilot-excited air resonance conditions" were maintained up to 20 sec. In this picture rolling rates of 20°/sec are obtained and the inplane motion is running exactly in its natural frequency. From the recordings after the stop of excitation decay-rates were determined, which allowed conclusions to the blade damping. During these flight tests, which were carried out over the whole speed range with different gross weights and in high altitudes, it was never possible to get into unstable oscillations. The conclusions can be made, that on the BO 105 hingeless rotor blades with a 0.65 inplane frequency ratio the inherent damping in the structure and the blade attachment is sufficient, to avoid any ground and air resonance problems.

7. MECHANICAL HUB VARIATIONS AND CONTROL STIFFNESS

As mentioned before, the feathering axis on hingeless rotors is normally fixed in the hub and the blades are deflected out of this axis. With the "hinge sequence" of feather-flap-lag coupling effects are caused when control flexibility is present. The physical principle is illustrated in Figure 17, showing that the control system dynamic is influenced by the flapping (δ) and inplane (ζ) motion of the blade (4).

7.1 Elastic pitch-flap-coupling

The most common parameters, which can result in this type of coupling, are precone of the feathering axis, blade sweep, flapping and inplane stiffness, blade damping and control system flexibility. It is indicated even by simple trim conditions that the elastic couplings are comparable to pitch-flap-coupling effects. Figure 18 shows some results of a study, illustrating the effective δ_3 -angles obtained at a hover cyclic control condition. The elastic coupling angle is shown as a function of the blade sweep angle. Forward sweep of the blades results in negative δ_3 -angles, rearward sweep in positive δ_3 -angles (negative pitch-flap-coupling). The influence of the control system stiffness proves to be almost linear. Similarly the elastic δ_3 -behaviour of hingeless rotors is influenced by precone of the feathering axis and by the chordwise flexibility of the blades, both changing the blade position relative to the pitch axis (4).

The main effects of a pitch-flap-coupling is a reduction of flapping amplitudes, resulting in improvements of stability and gust behaviour. Two typical results are illustrated in Figure 19, showing the angle of attack stability and the pitch damping moment of an isolated rotor in forward flight. The large destabilizing moments of hingeless rotors, which are increasing with speed, can be reduced by rearward blade sweep and it should be noted that both stability and damping show a trend to the articulated rotor when blade rearward sweep is applied to hingeless rotors.

7.2 Elastic pitch-lag-coupling

In addition to these coupling effects specific interactions between the inplane and pitching motions can be observed at hingeless rotor blades. In order to illustrate these types of coupling, typical variations of elastic blade pitch angle with lag angle are shown in Figure 20. There is indeed an elastic pitch-lag-coupling, as shown by the slope of the curves. In the case of forward sweep blades the coupling becomes negative, aft sweep blades result in a positive coupling. The curves shown in this picture are for a special case of rotor thrust, different curves would be obtained for other flight conditions.

The phenomenon of pitch-lag coupling can be favourable or unfavourable for rotors, depending on the amount and sign of the coupling. A theoretical treatment shows that a coupling in the sense of pitch up with blade lag motion forward has a destabilizing influence on the flap-lag oscillation. In opposite a decrease of pitch as the blade lags forward is stabilizing.

Investigations were done to get more insight into these elastic pitch-lag coupling effects on hingeless rotors. In Figure 21 some results are collected showing the effective pitch-lag coupling factor as a function of collective pitch for rotors with different precone angles. As collective changes, the aerodynamic coning changes and thus the coupling of the pitch-lag motion is affected. Increase of collective pitch results in negative factors (positive pitch-lag-coupling), providing a stabilizing effect on the system stability. Further it can be seen that the precone of the feathering axis will definitely affect the magnitude of this type of coupling. Too high a precone angle will act strongly destabilizing.

Figure 22 shows the lag modal damping over collective pitch, as it was obtained with the analytical model described in the foregoing chapter. The hub freedoms are fixed in this case. Over the total range of collective pitch a minimum of damping is obtained in the low thrust region at about 4° collective. Higher collective pitch setting results in an increase of damping up to a second region of instability with a very rapid damping decay. Investigations of this region show that this form of instability consists of a flap-lag-coupling in the flapping natural frequency. Its physical reason seems to be the increment of aerodynamic drag of the profile at very high thrust conditions.

Another important effect shown in Figure 22 is the influence of precone angle on the lag modal damping. The deterioration of lag damping with high precone angles is evident, showing that a 5° precone hub is acting against the structural damping of the blades. One more conclusion from these results is that rising gross weight of a helicopter with this hingeless system will increase the air resonance stability, because it brings the aerodynamic coning angle above the pitch axis. In contrast, unloading of the rotor will tend to reduce the stability of the system.

Similar effects are provided by other hub parameters, such as blade sweep and control stiffness. A typical result is shown in Figure 23. A completely rigid control stiffness results in a very flat damping curve over collective. As there are no elastic pitch-flap-lag couplings in this case, this curve indicates the effective aerodynamic damping as the difference to the 5% structural damping. In contrast, soft control system results in a very steep damping gradient and will reduce the stability in the lower thrust region.

The results of these investigations are in full agreement with model testing carried out with a BO 105 soft inplane hingeless rotor model (28" rotor diameter) by the Boeing Vertol Company (9). The sensitivity trends are further confirmed by the findings in (10), although the important torsional degree of freedom is not included there.

It seems to be an essential conclusion of these few examples that the hub geometry of hingeless rotors is an active parameter for the aeroelastic behaviour and must be treated very thoroughly in the design phase. This is of main importance not only for helicop-

ter rotors but also for tilting prop/rotors because they are operated over a large pitch range and under different thrust conditions between hover and cruise flight.

8. CONCLUDING REMARKS

Analytical investigations and test experience with hingeless rotors indicate that there are potential advantages in applying this principle to helicopters and V/STOL-aircrafts.

The main feature implying the benefits of this system is the fundamental blade flapwise bending mode, which is determined by the type of hub and blade attachment. The flight dynamic improvements associated with this concept are due to the large moment capacity resulting in outstanding control and stability characteristics.

In addition, the flight dynamics of hingeless rotors are strongly influenced by torsional elastic coupling effects. Improvements of the aerodynamic characteristics and a proper blade design with respect to the chordwise mass distribution will give benefits in the dynamic behaviour of the rotor.

Another design area requiring particular attention is the blade inplane stiffness. It is an active parameter for the structural loading and the stability behaviour of the blades. Stress problems can be resolved by introducing inplane flexibility, but damping and air resonance problems get more important in this case. Thus the selection and layout of the first inplane frequency must be treated very thoroughly.

Finally, the design of the hub geometry must not only consider requirements of steady moments, but must regard dynamic effects too. The placement and precone of the feathering axis, the inplane sweep of the blades and the flexibility of the control system are parameters, which are of main influence on the flight dynamics and the stability characteristics of the blade and the system.

In general, the hingeless rotor concept offers the chance of favourable aeroelastic benefits, which are not present in other rotor systems in this high degree. But - more physical understanding and continuing research seems to be necessary in order to treat this system in the right way.

9. REFERENCES

1. Reichert, G., Oelker, P.: "Handling Qualities with the Bölkow Rigid Rotor System", AHS, 24th Annual National Forum, 1968
2. Reichert, G.: "The Influence of Aeroelasticity on Stability and Control of a Helicopter with a Hingeless Rotor", AGARD CP 46, 1969
3. Huber, H.: "Das Stabilitäts- und Steuerungsverhalten des gelenklosen Rotors System Bölkow", Deutsche Gesellschaft für Luft- und Raumfahrt, DLR-Mitt. 71-12, 1971
4. Reichert, G., Huber, H.: "Influence of Elastic Coupling Effects on the Handling Qualities of a Hingeless Rotor Helicopter", 39th AGARD Flight Mechanics Panel Meeting, Hampton, Virginia, September 1971
5. Huber, H., Weiß, H.: "Moderne Technologien in der Entwicklung von V/STOL-Propellern und Rotoren", Deutsche Gesellschaft für Luft- und Raumfahrt, DLR-Mitt. 71-18, 1971
6. Lytwyn, R.T., Miao, W., Woitsch, W.: "Airborne and Ground Resonance of Hingeless Rotors", AHS, 26th Annual National Forum, 1970
7. Huber, H.: "Berechnung der gekoppelten Bewegungen des Masts und der einzelnen Blätter von Rotoren", Messerschmitt-Bölkow-Blohm GmbH, Bericht DF 92, 1970
8. Richardson, D.A.: "The Application of Hingeless Rotors to Tilting Prop/Rotor Aircraft", AHS, 26th Annual National Forum, 1970
9. Burkam, J.E., Miao, W.: "Exploration of Aeroelastic Stability Boundaries with a Soft In-Plane Hingeless Rotor Model", AHS, 28th Annual National V/STOL Forum, 1972
10. Ormiston, R.A., Hodges, D.H.: "Linear Flap-Lag Dynamics of Hingeless Rotor Blades in Hover", Journal of the American Helicopter Society, April 1972



Fig. 1 Rotorhub and Blade Attachment of the Bölkow Rigid Rotor System

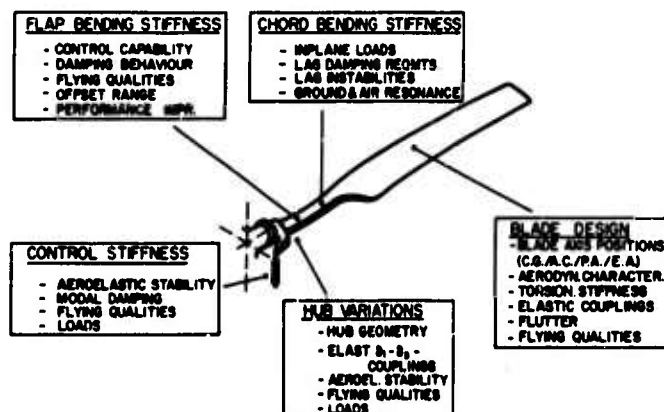


Fig. 2 Dynamic Research Areas on Hingeless Rotors

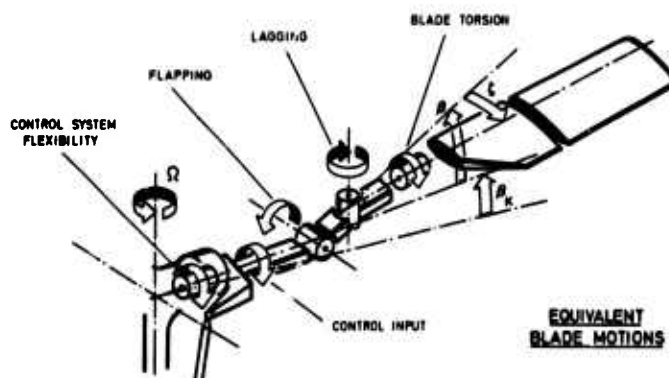


Fig. 3 Analytical Model of Rotor Blade with Elastic Flapping, Lagging and Torsional Degrees of Freedom

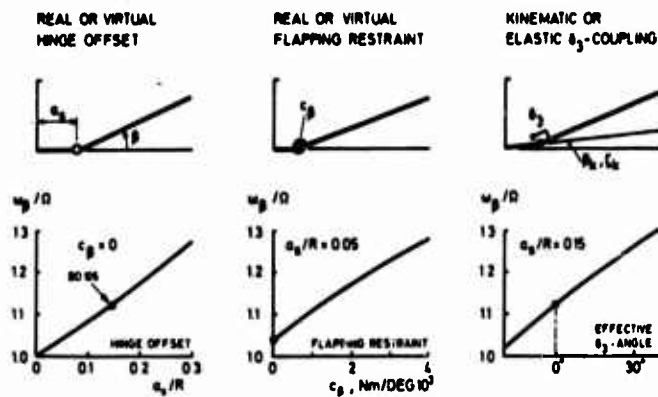


Fig. 4 Basic Influences on Flapping Frequency of Rotor Blades

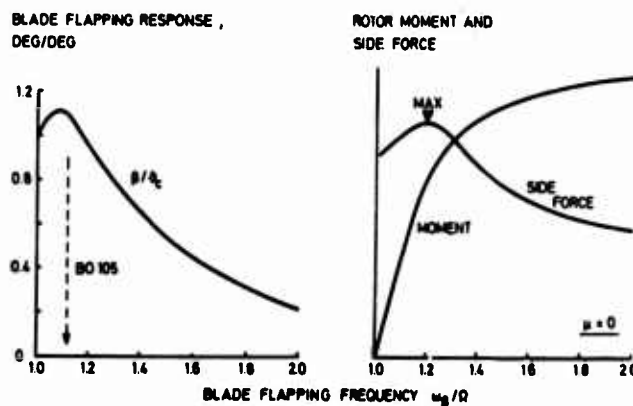


Fig. 5 Blade Flapping, Rotor Forces and Moments Produced by Prop/Rotor Cyclic Pitch in Hover

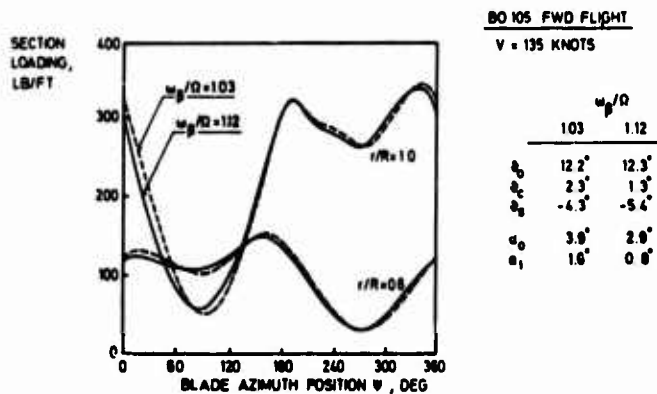


Fig. 6 Azimuthal Blade Section Loading in Trimmed Flight with Different Rotors ($\mu = 0.32$)

LONGITUDINAL CYCLIC PITCH, DEG

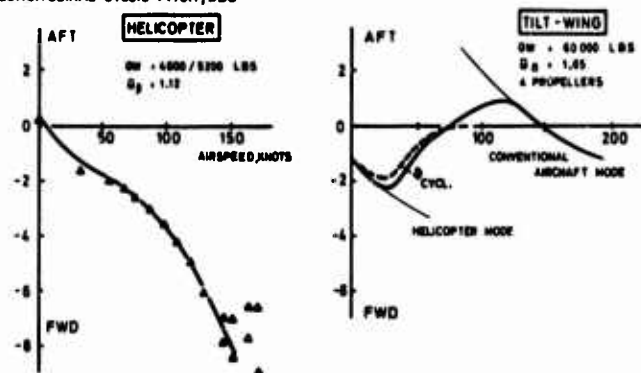
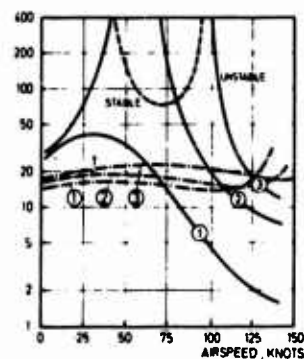


Fig. 7 Longitudinal Cyclic Requirements on a Helicopter and a Tilt-Wing Aircraft

TIME TO DOUBLE
AMPLITUDE,
PERIOD,
SEC



BO 105

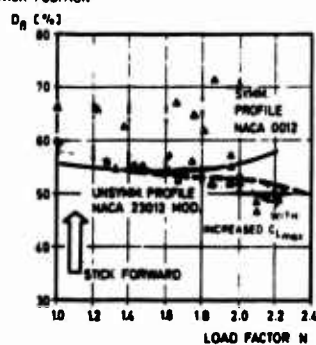
HINGELESS ROTOR

GW = 4400 LBS
 $\mu_s = 3.2$ INCHES
H = 5000 FT

- ① NACA 0012
- ② NACA 23012/SMALL CG VAR
- ③ NACA 23012/5% CG-AC OFFSET

Fig. 8 Effect of Different Blade Modifications on the Inherent Dynamic Stability in Forward Flight

LONGITUDINAL STICK POSITION



BO 105

GW = 2050 lb + 4500 lbs
TAS = 110 Kts
H = 5000 ft

▲ ▲ FLIGHT TEST
— — — ANALYSIS

100% D_0 = 12 in. STICK TRAVEL

Fig. 9 Effect of Different Blade Airfoils on Longitudinal Control and Maneuver-Range

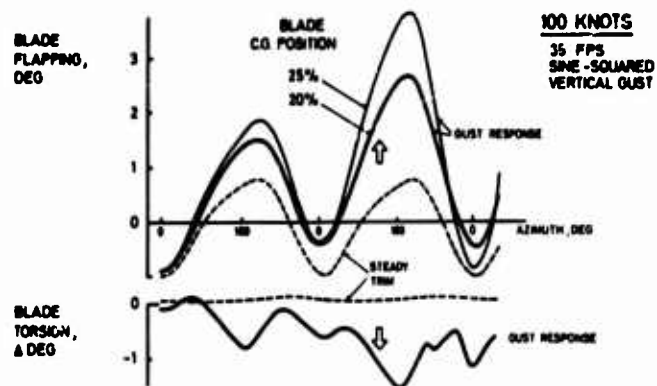


Fig. 10 Influence of Blade C.G.-Position on Blade Gust Response

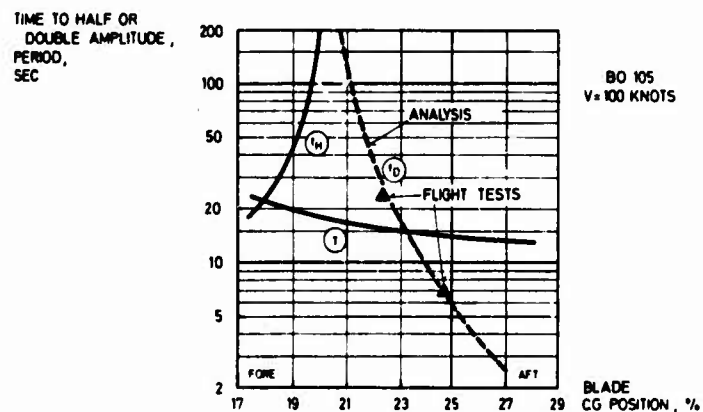


Fig. 11 Effect of Blade C.G.-Position on the Longitudinal Dynamic Stability in Forward Flight



Fig. 12 Experimental Blade with a 7-Pound Weight at Blade Leading Edge on the BO 105

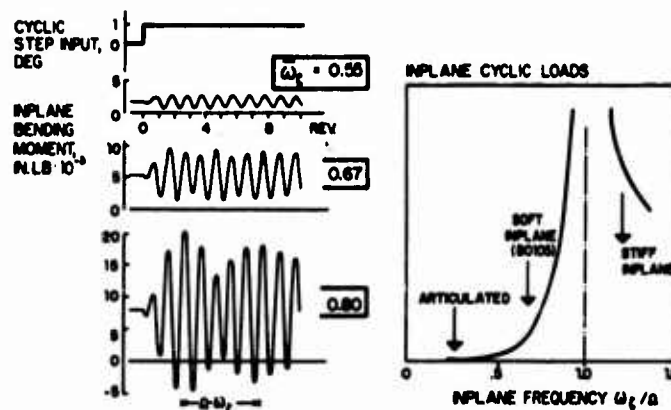


Fig. 13 Effect of Inplane Natural Frequency on Structural Loads

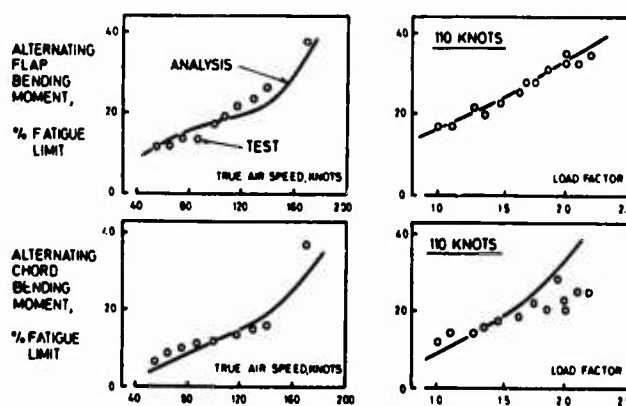


Fig. 14 Blade Loads on the BO 105 Hingeless Rotor in Forward Flight and Maneuvers

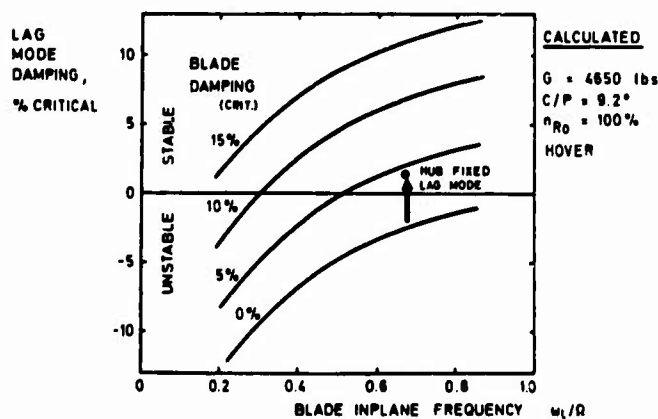


Fig. 15 Effect of Blade Inplane Frequency and Damping on Ground and Air Resonance Stability

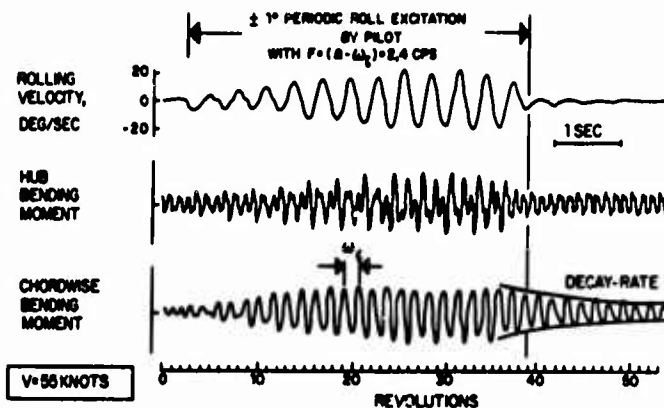


Fig. 16 Time History of an "Excited Air Resonance" by Periodical Roll Excitation (BO 105)

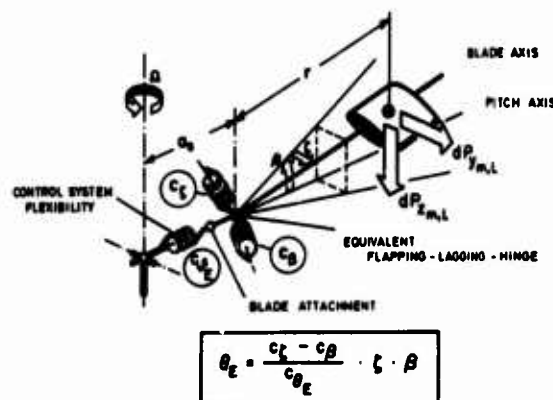


Fig. 17 Principle of the Elastic Pitch-Flap-Lag Coupling on a Hingeless Rotor

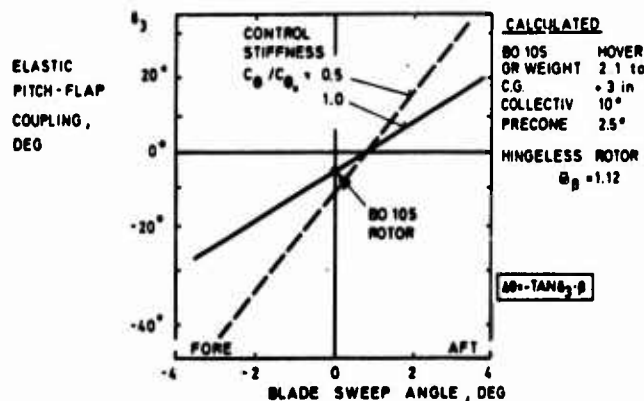


Fig. 18 Effect of Precone on the Elastic Pitch-Flap Coupling in Cyclic Hover Trim Condition

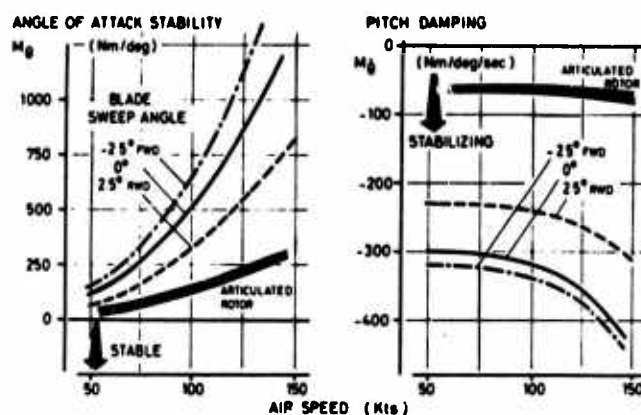


Fig. 19 Effect of Precone on Pitching Moment Derivatives in Forward Flight (Isolated Hingeless Rotor)

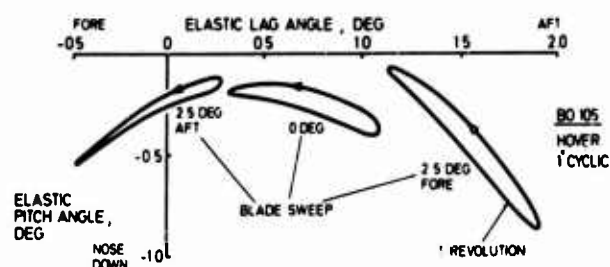


Fig. 20 Sample Cases of Elastic Pitch-Lag Coupling in Cyclic Hover Trim Condition

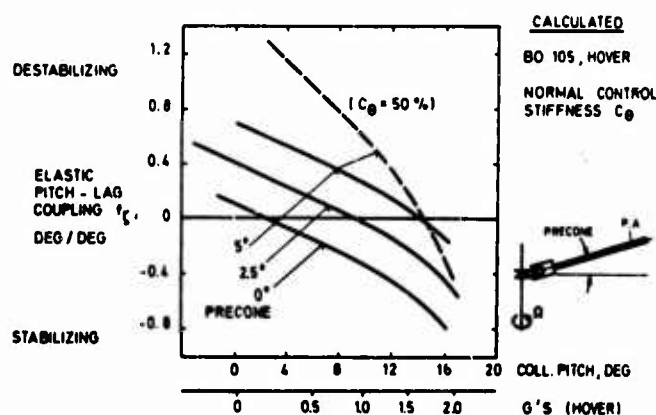


Fig. 21 Effect of Collective Pitch and Precone on the Elastic Pitch-Lag Coupling

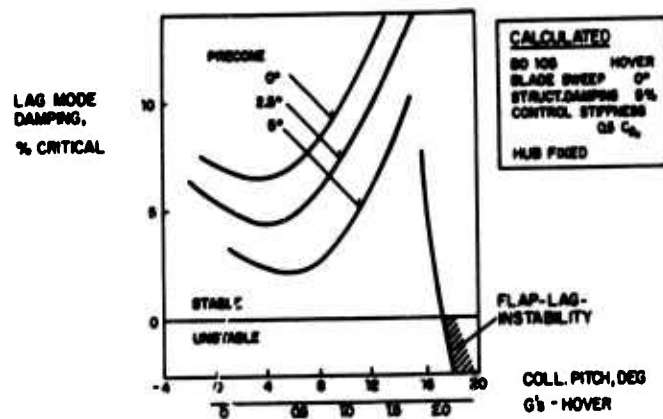


Fig. 22 Effect of Collective Pitch and Precone on the Lag Mode Damping (Air Resonance Stability)

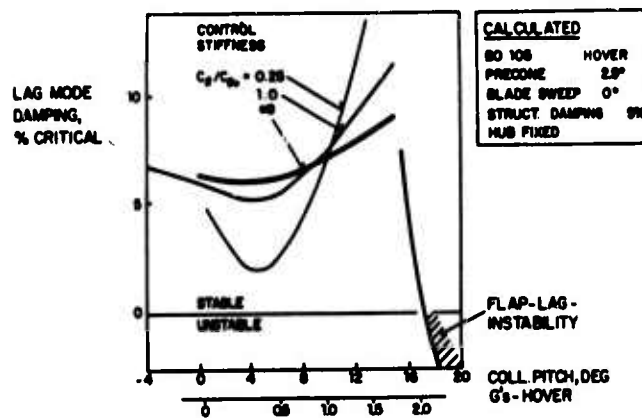


Fig. 23 Effect of Control System Flexibility on the Lag Mode Damping

AERODYNAMICS OF HELICOPTER COMPONENTS OTHER THAN ROTORS

by Dott. Ing. Angelo Bosco
 SIAI Marchetti SpA, Sezione Volo Verticale
 21018 Sesto Calende (Varese), Italy

SUMMARY

Any aircraft design should be based on a selected, but limited, range of missions. A successful aircraft represents compromise between configuration features and between applicable specialties. Rotary-wing aircraft design groups have been slow to adapt these lessons which have been so well explored and demonstrated in the field of fixed-wing aircraft. The SIAI Marchetti SV-20A Winged Helicopter is intended for commercial/utility applications in the second half of the 1970's. Some considerations invoked in defining this configuration are presented. For these missions, the productivity, cruise efficiency, stability, and controllability of a helicopter are all affected by the aerodynamics of the nonrotating components. As a result, the well-developed techniques of fixed-wing subsonic aerodynamics are being applied to the SV-20A design. A break-down wind-tunnel-model is being used to isolate aerodynamic interferences and to confirm aerodynamic analyses. These results are contributing to the SV-20A configuration optimization. They are also being used, together with results from rotor performance analyses, to synthesize the classical "performance, stability, and control" of the complete aircraft. Optimizations such as illustrated, if performed before the aircraft configuration is frozen, should contribute toward a superior product and minimize the time and cost required for the flight test program leading to type certification.

1 INTRODUCTION

Forty-two years have elapsed since the coaxial helicopter built in Italy by Prof. D'Ascanio flew 3000 feet in five minutes, achieved an altitude of 54 feet, and remained aloft for almost nine minutes (Ref. 1).

In the late 40's the first helicopter was certified by the Federal Aviation Agency of the United States. The Bell 47, destined to become one of the most popular in the world, is a good example of the helicopter construction up to this period. The engineering effort put forth to turn a "brain child" into a reliable and useful vehicle, deserves the highest commendation. Concentration during this time was justifiably on the mechanics of flight and development of the rotating and control components. Little or nothing was accomplished toward the aerodynamic sophistication of the nonrotating components.

In the Silvercraft SH4 (Fig. 1-a), built about twenty years after the Bell 47, a certain effort had been made in order to reduce the drag. However in a helicopter of this type, intended mainly for agricultural purpose, the aerodynamic efficiency of the nonrotating components is of secondary importance.

In the helicopter of the 70's, the effort made by the designers to improve aerodynamic efficiency is noticeable. A good example in a pure helicopter is the Agusta 109 Hirundo (Fig. 1-b) with its retractable landing gear, its streamlined fuselage, and its small pylon fairing; all evidence of the effort made to lessen the parasitic drag.

For the helicopters of today and the future, it is shown to be beneficial to promote aerodynamic cleanliness. Proof of this is evident by the prevalence of the very streamlined bodies now being produced for helicopters which utilize high cruising speeds or which require high speeds (Figs. 1-c and 1-d).

Transport helicopters, both in the winged and compound versions with their top speeds between 150 and 220 kts, are in the speed class of the executive turboprop. Now, as has been done and is being done for the executive turboprop, it is becoming more critical to consider aerodynamic effects relative to the helicopter. However, as the drag factor is much higher for a helicopter than for its fixed-wing equivalent, a greater amount of sustained effort will have to be exerted. As the SIAI Marchetti SV-20A winged helicopter (Fig. 1-e) is included in the executive turboprop class, the possible solutions to some of the inherent aerodynamic problems will be treated somewhat subjectively herein. And, because most of the material published to date (Fig. 2) is and has been concerned with the aerodynamic of rotors, this Paper will discuss some of the necessary contributions of the nonrotating elements to be considered relative to compromise and aerodynamic cleanliness.

Today helicopter design is oriented mainly toward production in the following classifications:

Agricultural, Survey, Training
 Heavy Lift
 Observation
 Transport, both Civil and Military
 Attack.

In the overall picture, speed is the most important factor in the last two classes. In the case of the transport helicopters: for the civil helicopter, block speed is of interest; whereas, for the military use, speed may be of interest for possible evasive action or passive defense. For attack helicopters, the speed factor is easily understood.

The need to decrease drag and advance stability, controllability, and maneuverability, concurrently with speed, is obvious.

From what has been stated above it appears very clear that, for at least some types of helicopter, the speed factor is becoming paramount. To increase this speed factor, two of the possibilities are to install more power or to upgrade the aerodynamic efficiency. The ultimate would be to act on both of these elements simultaneously. In the second possibility, the upgrading of aerodynamic efficiency, there are again two main choices; the aerodynamic improvement of the rotating parts or of the nonrotating parts. Improvement of the aerodynamic efficiency of the nonrotating parts means, basically, decreasing the advancing drag. It is intended to show, briefly, herein how some of the problem is being attacked by studies, tests, and analysis of some of the speed/drag factors with appropriate regard for the stability, controllability, maneuverability factors.

In general, a helicopter with little advancing drag is the result of careful aerodynamic consideration of the single parts and of the harmonic fusion of and with the particular structure of the helicopter. This, of course, is necessarily followed by careful checking, testing, and analyzing in order to avoid subsequent dirtying of the aerodynamics during the development of the helicopter itself. Reducing the drag means a reduction of the propulsive force required from the main rotor. In turn, main rotor stall and compressibility effects are delayed with subsequent less aerodynamic load asymmetry on the rotor. Less aerodynamic asymmetry and less load on the main rotor has meant a diminishing of the oscillatory loads on the rotor blades and controls, and lesser apparent vibration in the cockpit/cabin and on the frame (Refs. 2, 3, and 4). Figures 3 and 4 show that both oscillatory loads and vibration are appreciably reduced in the Bell HPH compound helicopter. This reduction was accomplished mostly by the lessening of the required rotor propulsive force, with respect to the basic HPH, by means of the installation of two auxiliary propulsive jet engines. Now that we have defined that better aerodynamic efficiency is indicative of a helicopter which is lighter in weight, simpler, less expensive, more comfortable, and more easily certifiable (Ref. 5), let us examine some of the nonrotating components from the aerodynamic point of view.

2 FUSELAGE

The helicopters of the 50-60's were designed for a speed of about 100 kts. The fuselage was considered mostly as a people container - roughly ovoidal in shape - with an attached tail boom to support the tail rotor. Designers, to reduce the center of gravity (CG) shift, preferred to place the passengers, in a medium size helicopter, in seats up to five abreast. Obviously, the greater number of passengers placed abreast necessitated a greater increase in the frontal area. As the frontal area is one of the main causes of parasitic drag, most any increase of this area will cause a decrease in aerodynamic efficiency. It should then follow that a seating arrangement with as few abreast as possible would be the best solution. This is not necessarily true, because, if carried to an extreme, we may then create the more cumbersome problem of trimming or balancing for CG. Thus we must arrive at one of the many compromises required of a helicopter design engineer; frontal area versus shift in CG. This factor was taken into consideration during the initial design of the SV-20A: by the location of the engines; by reducing the CG shift in that the cabin area is arranged so that the payload can be distributed as equally as possible fore and aft of the main rotor mast; and with forethought as to the aerodynamic optimum of the frontal area for the compromise between aerodynamic efficiency and a profit making payload.

Because forward flight, in most of today's existing helicopters, is at a nose down attitude, there is another advantage in limiting the width of the fuselage. The higher fineness ratio of narrowing (up to the aerodynamic optimum) the width of the fuselage mostly results in a lesser slope when the drag coefficient is plotted against angle of attack. This can also mean a lesser download on the fuselage, when the helicopter is flying nose down, thus adding to aerodynamic efficiency.

3 FAIRING OF ROTATING CONTROLS - TRANSMISSION

While in a low speed helicopter it is convenient to omit the fairing from the rotating control system, both to save the fairing weight and for better accessibility, in a fast helicopter (150 kts and over) it may pay to enclose this system in a streamlined fairing. It is a fact that a two blade teetering rotor has a hub drag substantially less than that of a helicopter with a fully articulated four or more blade rotor. Reference 12 states that from 20 to 50% of the total parasitic drag is created by the main rotor hub. Since either of these percentage figures loom as large drag increments in the design of a helicopter, much effort is and should be expended in this investigation. The design compromise this time must be made between speed and fairing weight plus accessibility.

4 ENGINE NACELLES

In a helicopter, without propulsive assistance for forward flight, an increase in drag will demand a higher propulsive force from the main rotor. As stated before, an increase in propulsive force required from the main rotor has been synonymous with increased oscillating loads and increased vibrations. As engine nacelles contribute to the drag factor it is necessary that strict attention be given to the aerodynamic design of these engine nacelles and a thorough study must be made of the construction and installation details. This study involves close cooperation with the engine manufacturer to determine the best aerodynamically efficient external and internal design for the nacelle/engine ensemble.

In the case of a winged helicopter, with the engine nacelles mounted on the wing away from the fuselage and cabin area, a greater drag increment may be expected. This increased drag, however, may be offset by the advantages of: the minimizing of engine-generated noise and vibration in the cabin area by physical separation; possible relief from snow blockage or ingestion; better pressure recovery as the engine air intake is improved in the absence of the fuselage boundary layer; engine exhaust will not impinge on the vertical tail and tail rotor; engines are physically separated so that damage from a failed engine is very unlikely to affect the remaining engine; improved access for engine installation, maintenance, and overhaul; etc. Enhancement of the growth potential is also a factor to be considered where engines are mounted in nacelles on the wing. This enhancement is especially feasible when basic design consideration provides for possible or probable changes in configuration. Such changes in configuration may be the relatively simple one of a different engine or the more complex one of converting to a compound helicopter by the addition of a propeller. Again compromise, between speed and other considerations, is clearly demonstrated as a necessity in the basic design and plan for the helicopter.

5 LANDING GEAR

In helicopters of smaller dimension, experience has shown that skid type landing gear is highly commendable; not only because it is simpler and lighter in weight but also because it is less expensive as it does not need to be retractable. Streamlining of skid type landing gear usually reduces the drag sufficiently to offset the increased weight (induced drag contribution) necessary for the retractable type landing gear. For example, as recorded for the S.A. 341 Gazelle (Ref. 11): by fairing the skid type landing gear a drag reduction of 2.04 square feet was obtained, whereas with a retractable type landing gear, in the retracted position, a drag reduction of 2.60 square feet only was obtained. This small difference in drag reduction is far outweighed by the facts that skid type landing gear is more reliable and permits safer landings in unprepared areas. As the use of skid type landing gear is one of the outstanding features specific to a smaller helicopter, the compromise is obvious. Tests then only need to be performed to provide data as to the accuracy of the streamlining necessary to obtain the least possible drag for the particular skid landing gear involved.

6 FAIRINGS, SPOILERS, AIR INLETS, PYLON TOP SHIELD, STRAKES, ANTENNAS, DRIP GUARD, RIVETS, ARMAMENT, ETC.

Too much space would be used in this Paper if all of the mentioned components were to be discussed. Moreover, the aerodynamic cleanness of such parts is not the only criterion to be followed in their design, as it is necessary to take into consideration other factors which are sometimes diametrically opposed to such cleanness.

While following the basic concept, of designing external surfaces in such a manner that the airflow around these surfaces be as undisturbed as possible, there are times when it is necessary to renounce a part of the aerodynamic cleanness to alleviate instability phenomena or to prevent vibration, shaking, wake interference, etc. Especially this is true when considering more stringent requirements for or against the truncation of the main rotor pylon fairing, for or against the addition of spoilers, etc. In the case of the main rotor pylon it is apparent that the fairing of the trailing edge is an aerodynamically more clean structure. However, the wake from this fairing was thought to be, in one case, the source of interference problems and by tests, with a truncated pylon fairing, it was shown that this interference could be alleviated. Internal installations or structural consideration may also impose aerodynamic compromises. Again, although there are many others, the truncation of the main rotor pylon will be used as an example as it adds strength to the argument for truncation. For a particular vehicle, a truncated pylon fairing could substantially relieve some of the problems involved in an internal installation of a group of accessory components. Once more it is illustrated that there is much need for forethought, test, and compromise relative to design and aerodynamic cleanliness of rotating components.

7 WING

Intentionally, because their aerodynamic problems are similar, the wing and the horizontal and vertical tail planes are the last to be discussed. Their aerodynamic problems have more influence on the stability, controllability, and maneuverability of the helicopter than all of the other nonrotating components.

In the preceding discussion we have seen that, in forward flight, a rotor less heavily loaded may have some advantage due to a decrease in aerodynamic asymmetry. This decrease in aerodynamic asymmetry is beneficial because of the consequent reduction in oscillating loads, vibration, stall and compressibility effects, etc.

A method to partially unload the rotor during forward flight is to provide the helicopter with a lifting device; namely the wing. The presence of this wing creates design and aerodynamic problems at the same time that it provides the advantages of extra lift and possible better high speed maneuvering capability. Stated below are just a few of the many arguments against the wing and all must be taken into consideration when designing a winged helicopter. In forward flight for the same total lift, the combination of rotor plus wing may have a higher parasitic drag and may have a higher induced drag than the rotor alone configuration. In hovering, the wing negatively affects performance both because of its own weight and because of download effects on the wing generated by downwash from the main rotor. During forward autorotation, if the main rotor has been excessively unloaded by the wing, the RPM will be lowered.

With this lowered or too low RPM, control power is reduced or is insufficient for flight. This loss of control power becomes critical in the presence of gust disturbances, at the point where asymmetrical wing stall may occur, etc. Spoilers may be placed on the wing, to reduce excessive unloading of the main rotor. However, pitch moment problems may result when these spoilers are activated unless their configuration is very carefully designed to reduce or minimize adverse pitch change characteristics.

In spite of these drawbacks, it appears to be advantageous for a fast helicopter to be winged. Today almost all large producers have been and/or are investigating this possibility.

One of the many items of design criterion includes the fact that the wing design is quite dependent on the type of rotor. In general, rigid rotors can be unloaded more than semi rigid or articulated rotors. As this unloading can be from 30 to 90% of the gross weight of the helicopter, a wide band is created with many possibilities for compromise.

Wing flaps are another nonrotating feature to be considered. Because the shift in CG position changes the attitude of the helicopter fuselage in flight, it is necessary that a device be provided to compensate for such shifting. This device may be in the form of a tilting or pivoting wing but the addition of wing flaps to a fixed wing will make it possible to control the wing lift contribution independently of the fuselage attitude.

The addition of a wing, to unload the rotor in forward flight, may decrease control capability. This is especially true in the case of high speed helicopters. To restore the desired control, it appears advisable to add another nonrotating aerodynamic control; the aileron.

Flaps and ailerons thus add two more components to the compromise probabilities and again increase the need for thorough testing and analysis.

8 VERTICAL TAIL

Determination of the position and area of the vertical tail requires consideration of static stability and intrinsic directional stability in case of tail rotor failure. In determining the position of the vertical tail, compromises must be made to allow for the influence of the main rotor wake, the main pylon wake, engine exhaust interference, etc. Almost all of the various problems of the main-rotor/wing are inherent but in a lateral direction. Unloading a tail rotor, by the employment of a cambered vertical tail, reduces the flapping angle and improves fatigue life by the consequent decrease in vibration.

9 HORIZONTAL TAIL PLANE

With the increase in speed of the helicopter, the study of a horizontal tail plane has become more and more a sensitive and important problem. When speed is increased, aerodynamic forces and possible destabilizing moments of the fuselage become quite relevant. Consequent thereto is the increase in importance of the contribution of nonrotating components to longitudinal stabilization and control power margin. As much work is being done on stability augmentation systems (SAS), it will only be mentioned that such a system should definitely be considered wherever, as in the case of the tail plane, the control power margin may be affected.

In the newer helicopters, the necessity of installing a horizontal tail is apparent. It is also apparent that, on a helicopter with a horizontal tail plane, the farther this tail plane is placed aft from the CG the more effective it becomes.

Size and positioning of this horizontal tail are dictated by considerations of stability and of interferences by the main rotor wake. The area of this tail plane is critical. If too small, adequate stability will not be guaranteed. If too large, size alone will create unnecessary parasitic drag and may produce high nose down pitching moments in the case of vertical autorotation. Relative to positioning, it is sometimes advisable to have this horizontal tail always in the main rotor wake. Longitudinal instability could be caused during transition from hover to forward flight if the main rotor wake impinges on the horizontal tail for only a part of the time.

It appears desirable to consider a trimmable horizontal tail plane and/or also provision for this tail plane to be connected to the pitch component of the cyclic control. In forward flight, a trimmable horizontal tail provides a means to control the fuselage attitude independent of the CG position in relation to the rotor and further to control wing/rotor lift sharing. Peripheral advantages may be the reduction in fuselage drag, etc.

Dependent on the compromises, all of these factors may have a beneficial influence on vibrations, oscillatory loads, and helicopter performance. Figures 5 and 6 from Reference 4 show, for a particular case, the influence of the horizontal tail plane incidence on the main rotor loads and on flapping. With the possibility of controlling the fuselage attitude, the control power margin for maneuvering may also be increased.

10 REMARKS

The rate of increase of compromise possibilities and probabilities becomes almost infinite when consideration is given to each new feature that may be added, each feature that may be improved by the development of a new or better item, and then by imposing thereon the whims and fantasies of designer, manufacturer, buyer, and ultimate user. Only a small portion of the picture has been herein portrayed. This portion shows, briefly, that low drag in a helicopter does not come fortuitously from a combination of favorable circumstances, but is the result of careful selection of components to be encompassed in the complete helicopter design.

11 WIND TUNNEL TEST AND ANALYSIS OF THE SV-20A

The first part of this Paper describes, generally, the aerodynamic characteristics of a few nonrotating helicopter components and their influence on helicopter performance.

Now are presented some aerodynamic data obtained from wind tunnel tests performed on the model of the SV-20A. These data can be interesting because the SV-20A configuration includes almost all of the aerodynamic features of which we have previously spoken.

12 MODELS

An initial 1/8 scale model was constructed which, with the appropriate modifications as the SV-20A design progressed, has been tested repeatedly in the subsonic wind tunnels at Università di Pisa and Politecnico di Torino.

As a result of the experience with this 1/8 scale model, a new 3/20 scale breakdown model (Fig. 7) for wind tunnel testing was designed and constructed. Figure 8 shows some of the many components of this model. Specifically it has been designed to facilitate the wind tunnel testing of various combinations of its components.

13 WIND TUNNEL TESTS AND ANALYSIS

The very simple wind tunnel testing technique of talc-kerosene boundary-layer airflow visualization photographs has yielded a surprising amount of information. Figures 9 and 10 show two results of this technique. Figure 9 shows an early main rotor pylon configuration with the maximum thickness relatively far forward. Even at a fuselage pitch attitude or angle of attack of 0° (wing angle of attack of 8°), aerodynamic interference apparently caused by the nearly coincident maximum thicknesses of the fuselage, wing, and main rotor pylon produced a very early inboard wing trailing edge airflow separation. Figure 10 shows a revised configuration. The main rotor pylon shape has been based on the NACA 65-OXX airfoil and the engine nacelle shape has been altered. As shown at two degrees fuselage pitch attitude, the inboard wing airflow separation has been somewhat improved, but still needs further work. It is to be noted that, on both of these airflow visualization photographs, the right side fuselage/wing-trailing-edge junction has only a minimum fillet, whereas the same junction on the left side has an extended fillet built from modeling clay (and not entirely smooth).

The information resulting from simple airflow visualization techniques, as outlined above, is helpful but it does not provide any numbers for lift, drag, pitch moment, etc. for use in further analysis. Therefore, both the 1/8 scale and the 3/20 scale models have been and are being tested to measure these forces and moments.

14 DRAG

The next plots show some of the results of the tests which were made in the wind tunnel at Politecnico di Torino. Figure 12 shows the parasitic drag point for the SV-20A configuration as obtained from wind tunnel tests. This value has been obtained from the plot of C_D versus C_L^2 , as shown in Figure 11, and the extrapolation of the C_L curve to zero. Owing to the particular study of the aerodynamics of the nonrotating components, the equivalent flat plate drag area is somewhat lower than for similar helicopters.

Figure 11 shows another interesting result; the occurrence of complete wing stall at a squared lift coefficient of about 0.9, which means at the fuselage pitch attitude of approximately 7.5° . (The small numbers in the vicinity of the data points on Figure 11 are the nominal fuselage pitch attitude angles in degrees).

The wing trailing edge stall is due to aerodynamic interference, as shown in the visualization photograph (Fig. 10), and it is probably the cause of the discontinuity of the curve at the fuselage attitude of about 4.7° .

The slope of the straight element of the curve is 0.0645. Using this value in calculations for both the aspect and taper ratios, results in a value of $e = 0.68$. Noting the large fuselage, the large nacelles, and the relatively small wing area, this value can be considered a good one because for most airplanes the range is from 0.7 to 0.85.

15 HORIZONTAL TAIL PLANE (SV-20A)

Previously we have spoken about the influence of the horizontal tail plane both on the helicopter intrinsic flight performances (stability, controllability, maneuverability, lift, drag, etc.) and on dynamic loads. It is, therefore, necessary that a precise investigation be made to determine the relative position, area, and setting of the horizontal tail. Figure 13 shows the test results of a particular configuration of the SV-20A with the inverted, highly cambered, horizontal tail plane (NACA 6712). The sign convention is positive for the "nose up" position of this horizontal tail.

Starting with these data and the volume coefficient (Ref. 8), it is possible to calculate the experimental slope of the lift curve, $\frac{dC_L}{d\alpha}$, of the horizontal tail. The results of this calculation were compared with the analytical results, which were derived from the data obtained from the two-dimensional airfoil using the Betz correction for the aspect ratio. Figure 14 is a plot of the ratio of these values and indicates the horizontal tail plane's efficiency. Using this tail plane efficiency correction, it is possible to make good estimates of the effect resulting from changing the geometric characteristics of the horizontal tail plane.

16 DIRECTIONAL STABILITY

Because the wake of the pylon exerts considerable influence on the vertical tail plane efficiency, particular care has been used in the investigation of the directional stability characteristics. In Figures 15 and 16 are plotted some interesting data obtained by testing one of the configurations of the SV-20A helicopter model.

Figure 15 points out the fuselage pitch attitude influence. This configuration, at a pitch attitude equal to 0° , appears directionally unstable over a yaw angle range of about $\pm 4^\circ$; on the contrary, for a pitch attitude of -4° , the stability is about neutral. This is apparently caused by the emergence of at least a part of the vertical tail from the wake of the main rotor pylon. It is found that the horizontal tail, situated relatively far forward from the vertical tail, because of main rotor wake considerations, exerts significant influence on the vertical tail efficiency.

Apparently the downwash effects from the horizontal tail deflect the wake from the main rotor pylon. When this horizontal tail is at -5° (nose down), the main pylon wake is deflected upward to cover a significant portion of the vertical tail thereby reducing the vertical tail plane's contribution to directional stability as shown in Figure 16. When this horizontal tail is at $+5^\circ$ (nose up), the main pylon wake is not deflected as far (permitting at least a part of the vertical tail to be in undisturbed airflow) and the result is a more satisfactory directional stability.

17 CONCLUSION

This paper has presented only some of the more interesting and easy to visualize samples of the wind tunnel data that have been accumulated up to this time. It is realized that the data presented does not represent a completely satisfactory aerodynamic configuration. Studies, therefore, are progressing along these lines and it is expected that further, relatively minor, changes will produce a configuration with optimum aerodynamic cleanliness.

ACKNOWLEDGMENTS

The following organizations have contributed material used in the preparation of this Paper: Agusta SpA; Bell Helicopter Company; The Boeing Company; Douglas Aircraft Company; Lockheed Aircraft Corporation; Sikorsky Aircraft, Division of United Aircraft Corporation; Silvercraft SpA; Università di Pisa, Politecnico di Torino.

Portions of the work presented herein were partially sponsored by the Aeronautics Branch of the European Research Office (ERO) of the United States under \$1.00 Contract DAJA37-72-C-1998.

REFERENCES

- 1 Alfred GESSOW and Garry C. MYERS "Aerodynamics of the Helicopter". Frederick Unger Publishing Co. - 1967 Ed.
- 2 J. F. VAN WYCKHOUSE and W. L. CRESAP - Trecom Technical Report 64-61: "High Performance Helicopter Program - Summary Report, Phase II" - October 1964
- 3 Walter G. C. SONNEBORN - USAAVLABS Technical Report 71-2: "High Mach Number/High Advance Ratio Flight Test Program with the High-Performance UH-1 Compound Helicopter" - February 1971
- 4 T. T. KAPLITA - USAAMRDL Technical Report 71-55: "Investigation of the Stabilator on the S-67 Aircraft" - October 1971

- 5 MIL-H-8501A - Amendment I - 3 April 1962: "Helicopter Flying and Ground Handling Qualities; General Requirements for".
- 6 Sighard F. HOERNER - "Fluid-Dynamic Drag". Published by the Author, 1965
- 7 Alan POPE and John J. HARPER - "Low-Speed Wind Tunnel Testing". John Wiley and Sons - Ed. 1966
- 8 Courtland D. PERKINS and Robert E. HAGE "Airplane Performance Stability and Control". John Wiley and Sons - Ed. 1956
- 9 "Caratteristiche Aerodinamiche di Ali. Risultati della Galleria a Densità Variabile N.A.C.A." Editoriale Aeronautica, 1938
- 10 Carlo FERRARI, Giovanni JARRE, Silvio NOCILLA "Centro di Studio per le Dinamiche dei Fluidi, Torino - Attrezzature Sperimentali". Roma, C.N.R., 1963
- 11 Rene MOUILLE "The World Speed Records of the SA. 341 Gazelle". American Helicopter Society, 28th Annual Forum, Washington, D. C. - May 1972
- 12 Paul YAGGY "Pure and Compound Helicopters" - AGARDograph 126, May 1968.
- 13 Prof. Ing. Corrado CASCI and Dott. Ing. Emilio BIANCHI "New Trends for High Speed Helicopter Propulsion." AGARD-NATO June 1968 Ottawa, Canada.



FIG.1-a SILVERCRAFT SH-4

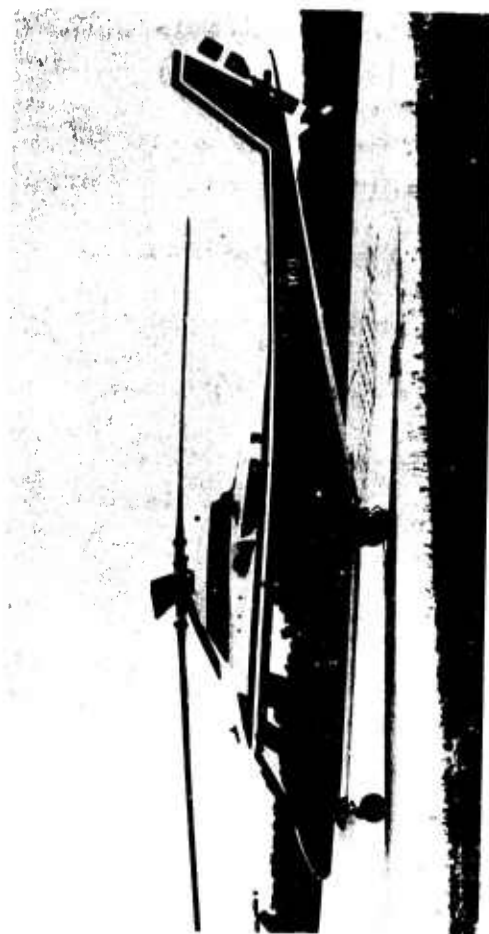


FIG.1-b AGUSTA A109 HIRUNDO



FIG.1-c SIKORSKY S-67 BLACKHAWK

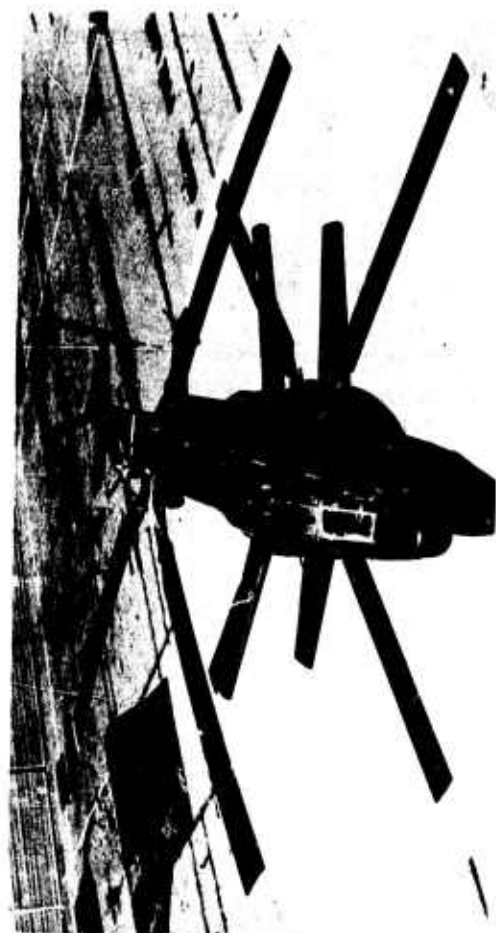


FIG.1-d LOCKHEED AH-56A CHEYENNE

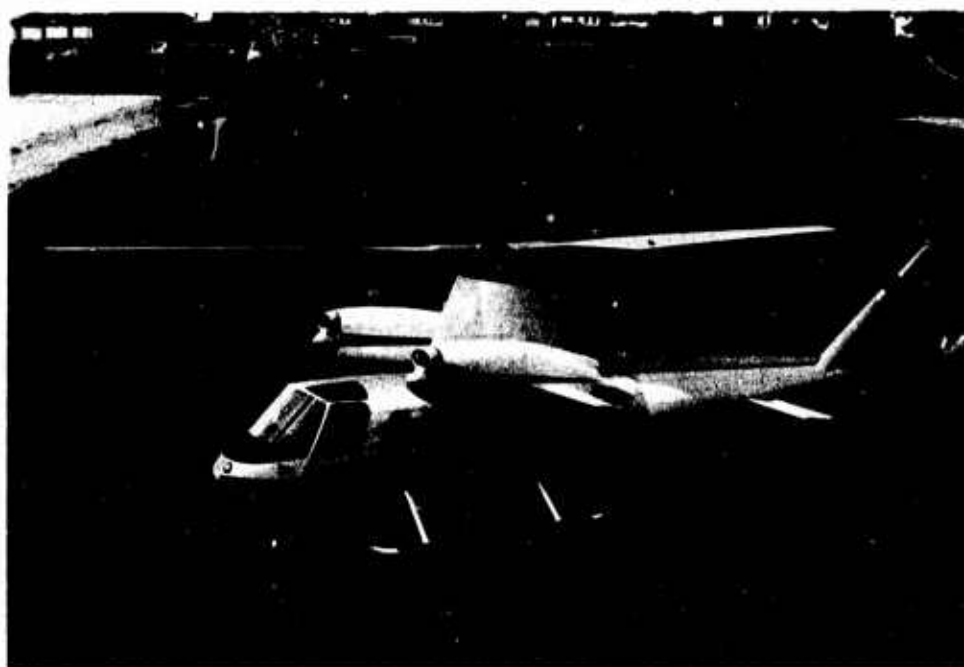
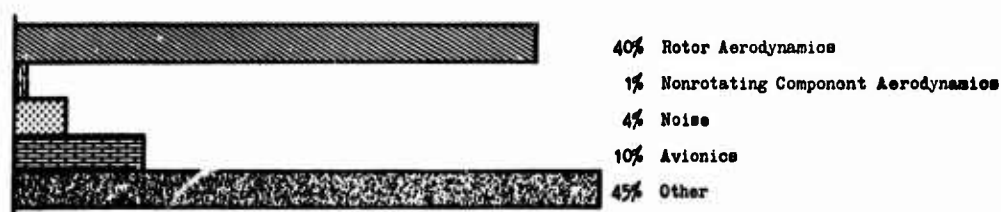


FIG.1-e SIAI MARCHETTI SV 20



Journal of the American Helicopter Society, 1965-1972



28th Annual American Helicopter Society Technical Forum, 1972



IAA and STAR Indexes, 1965-1972

FIG. 2 EMPHASIS ON AERODYNAMIC SPECIALTIES IN ROTARY WING TECHNICAL LITERATURE

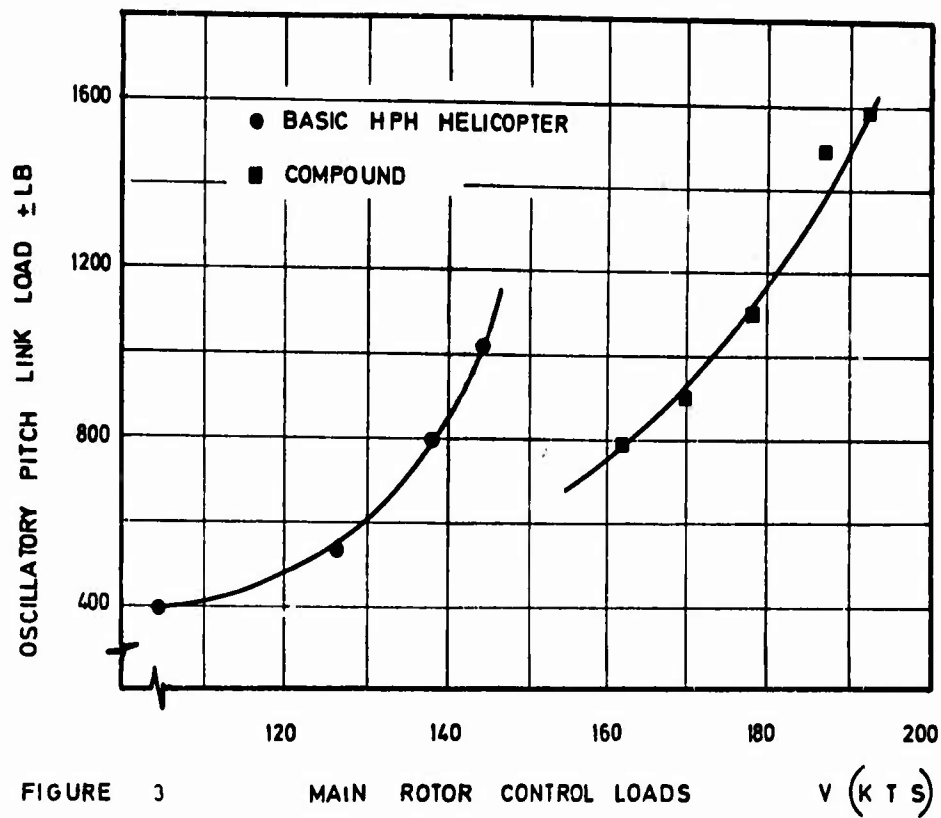


FIGURE 3 MAIN ROTOR CONTROL LOADS V (KTS)

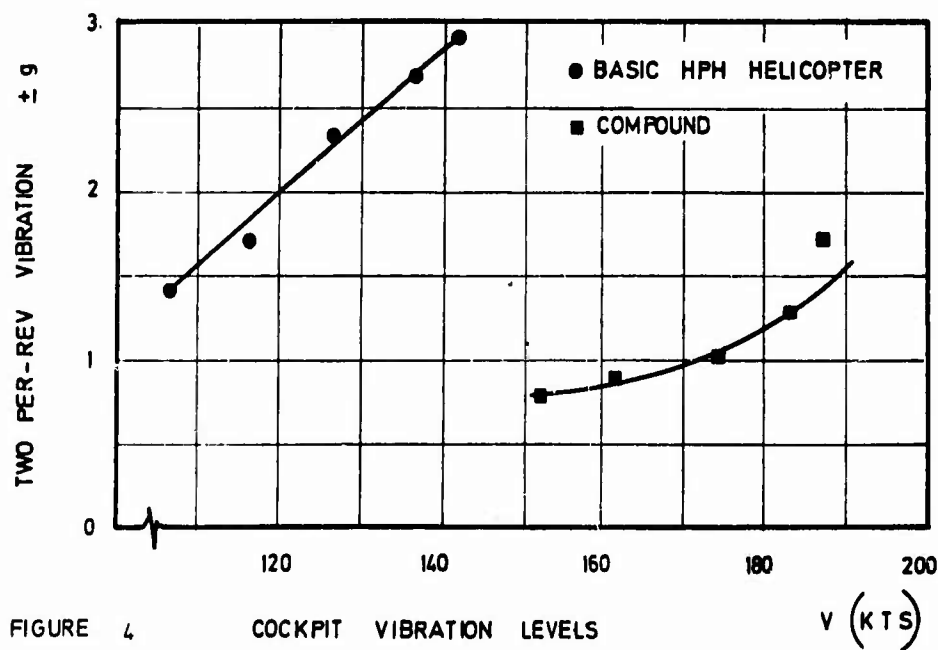


FIGURE 4 COCKPIT VIBRATION LEVELS V (KTS)

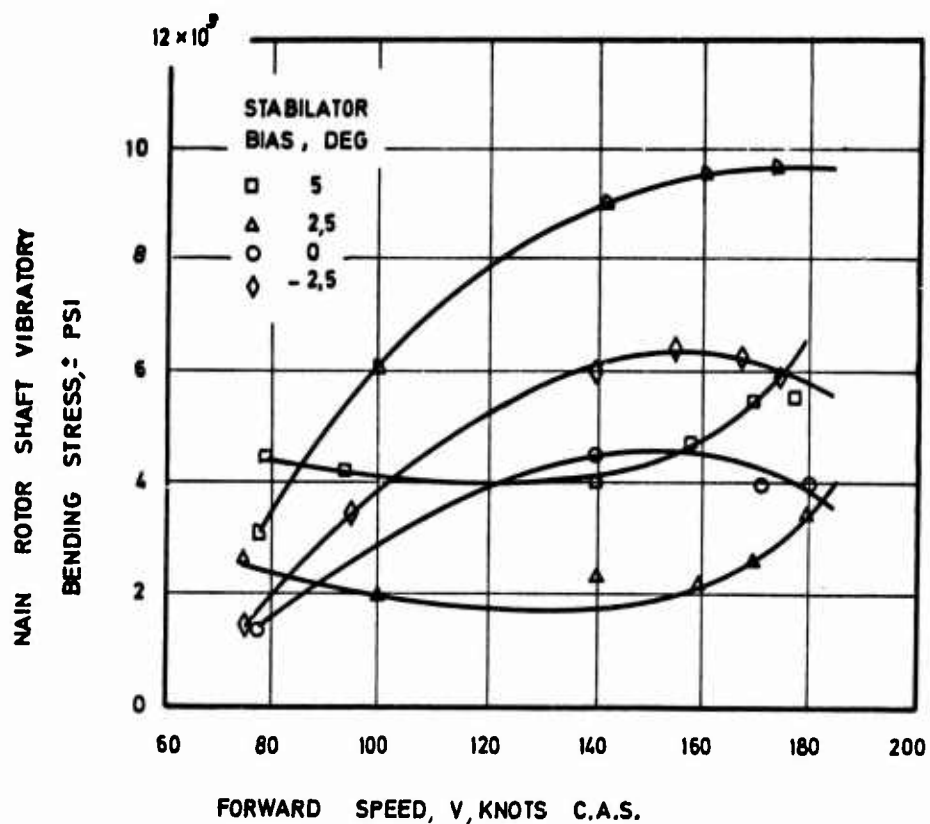


FIGURE 5 MAIN ROTOR SHAFT BENDING STRESS

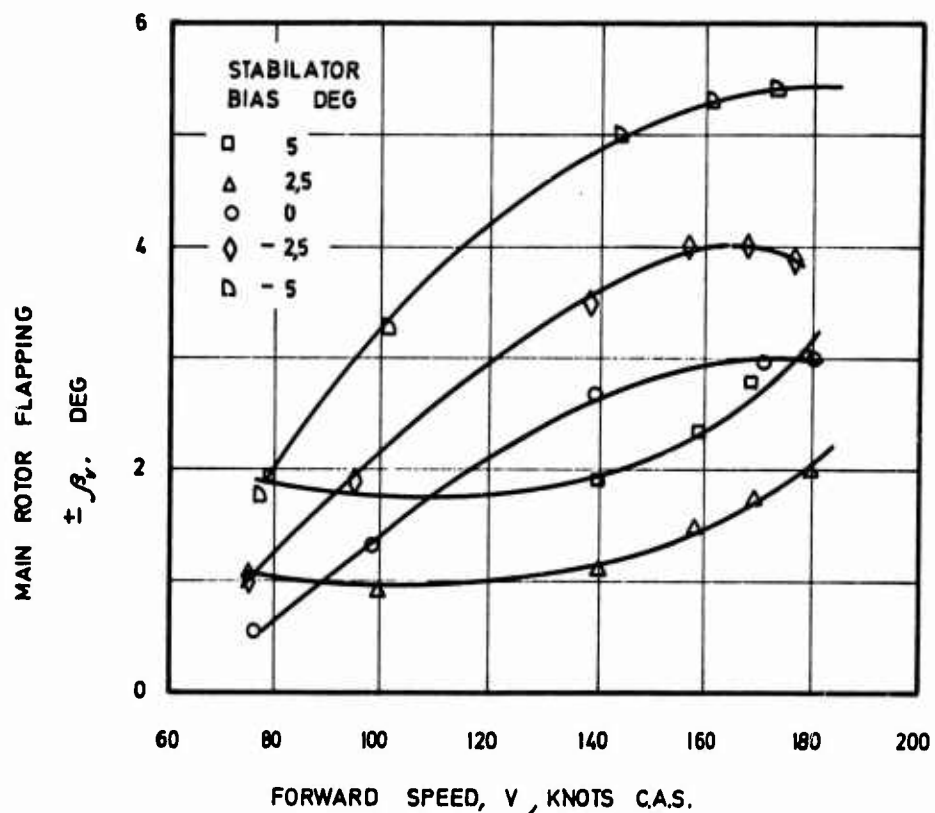


FIGURE 6 MAIN ROTOR FLAPPING ANGLE



FIG. 7 SV 20 HELICOPTER 3/20 SCALE MODEL

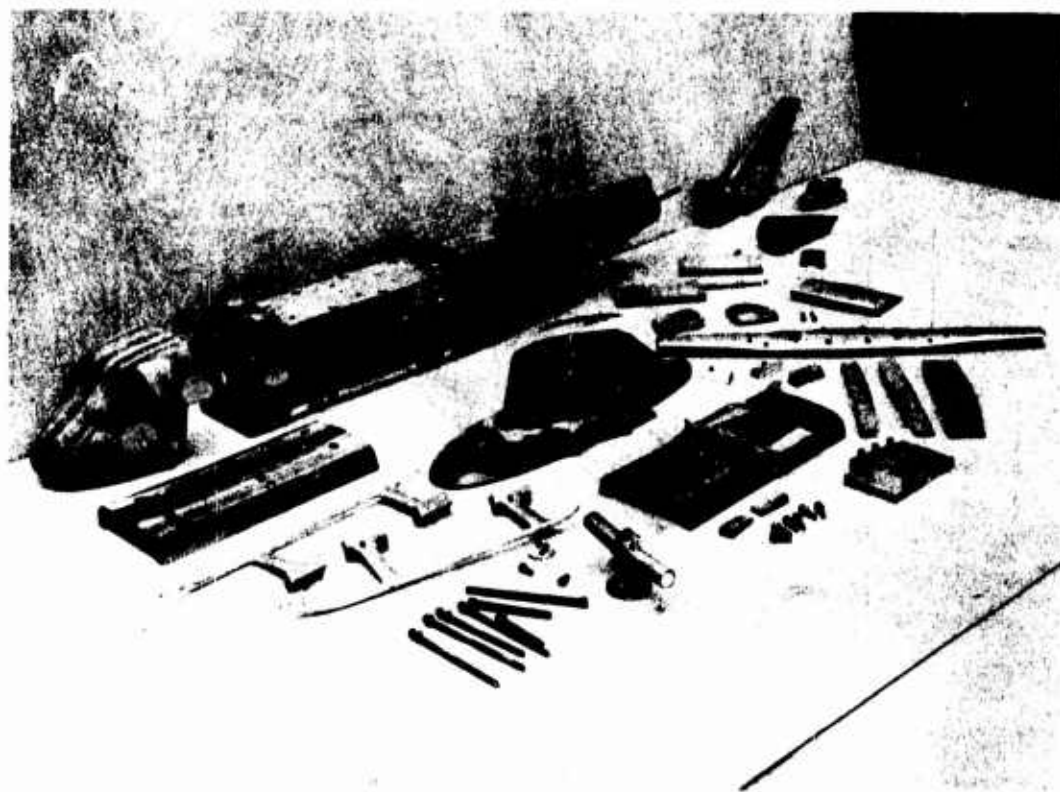


FIG. 8 SV 20 HELICOPTER 3/20 SCALE BREAK-DOWN MODEL COMPONENTS

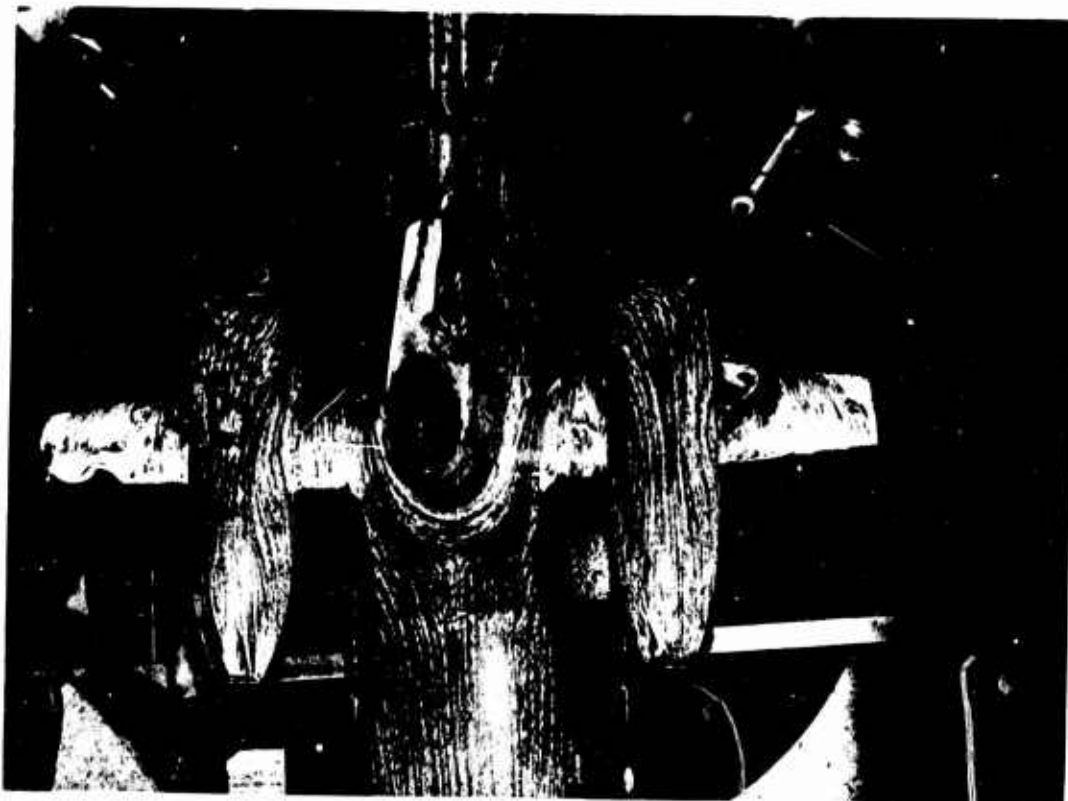


FIG. 9 SV 20A EARLY CONFIGURATION

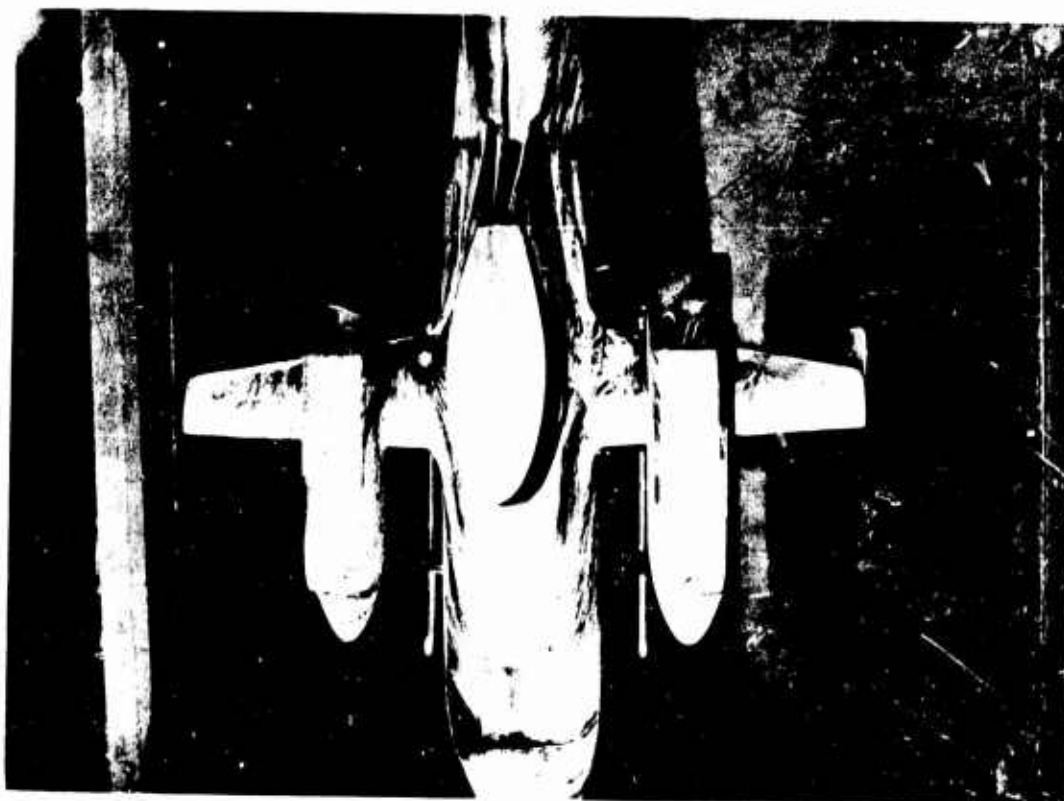


FIG. 10 SV 20A REVISED CONFIGURURATION

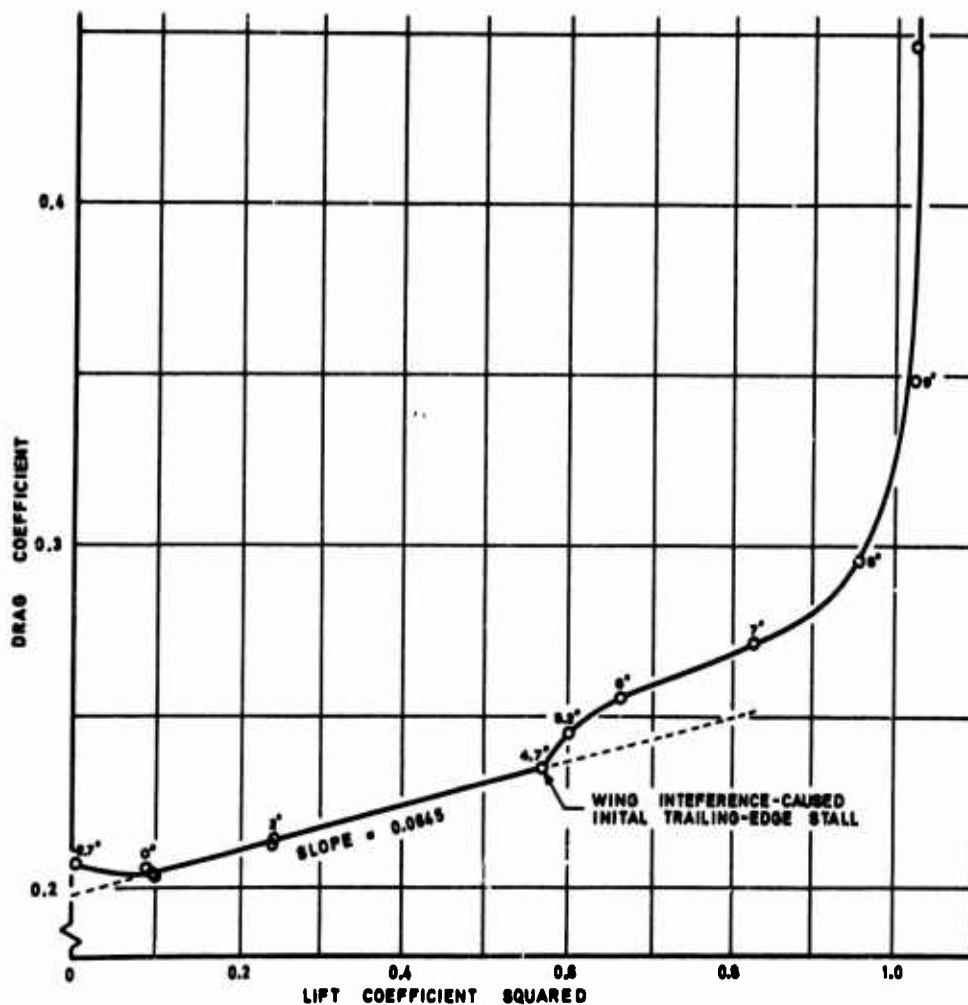


FIGURE 11

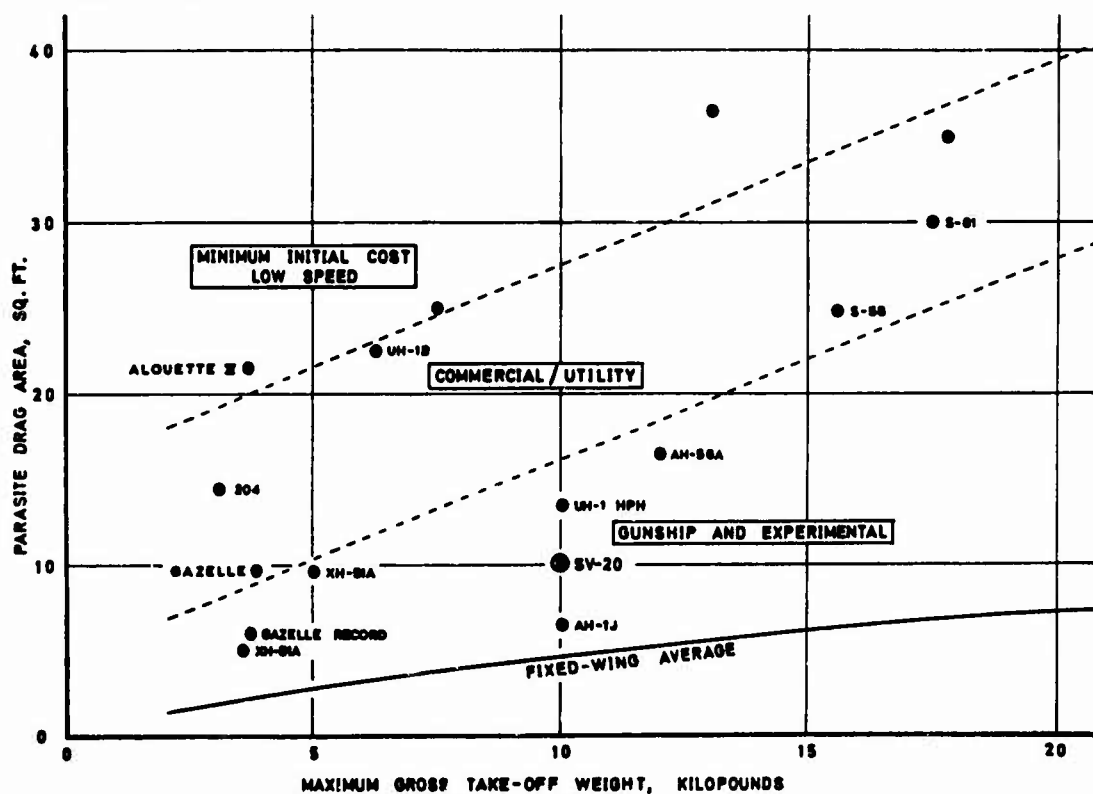


FIGURE 12

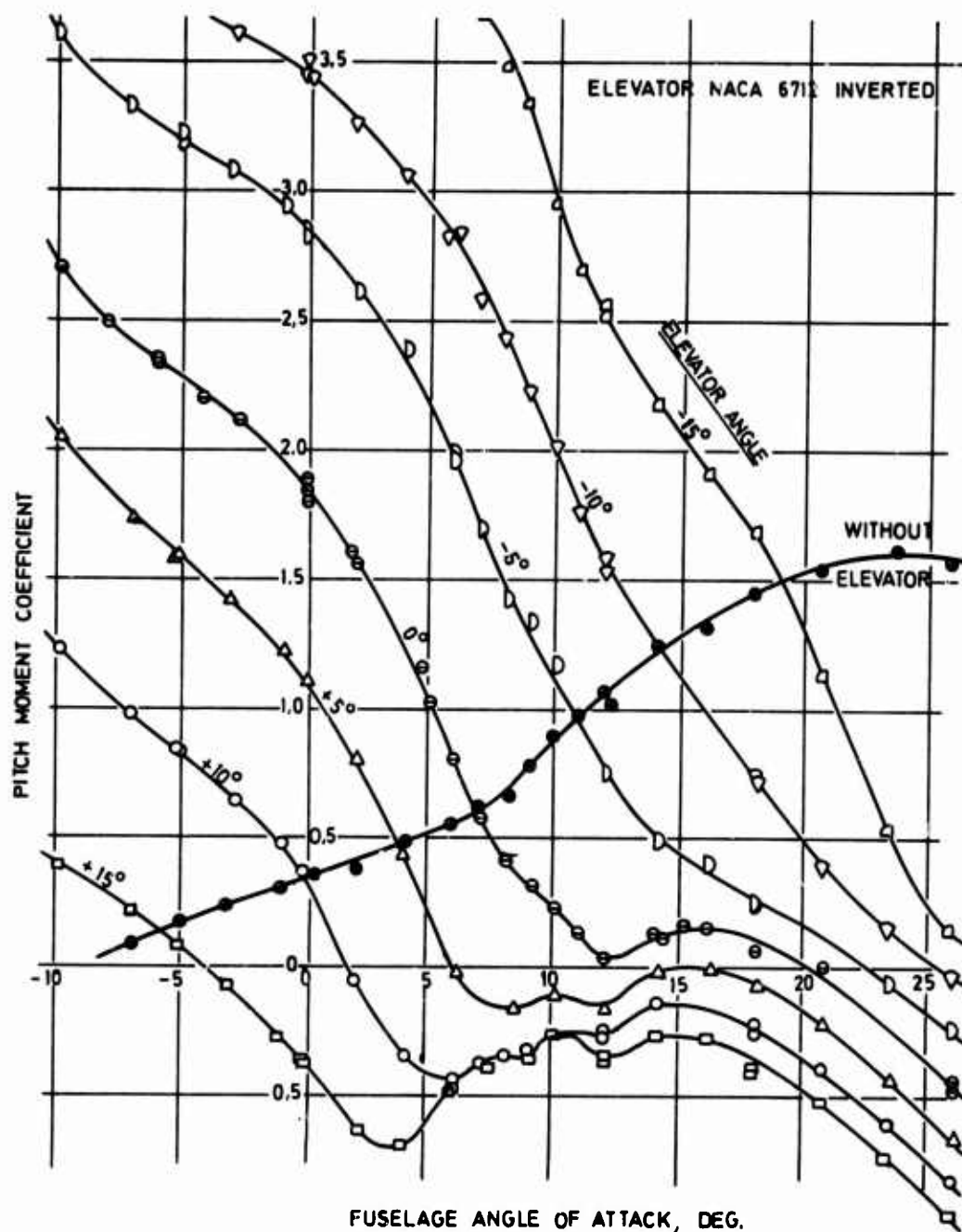


FIGURE 13 PITCH MOMENT COEFFICIENT VS. FUSELAGE ANGLE OF ATTACK

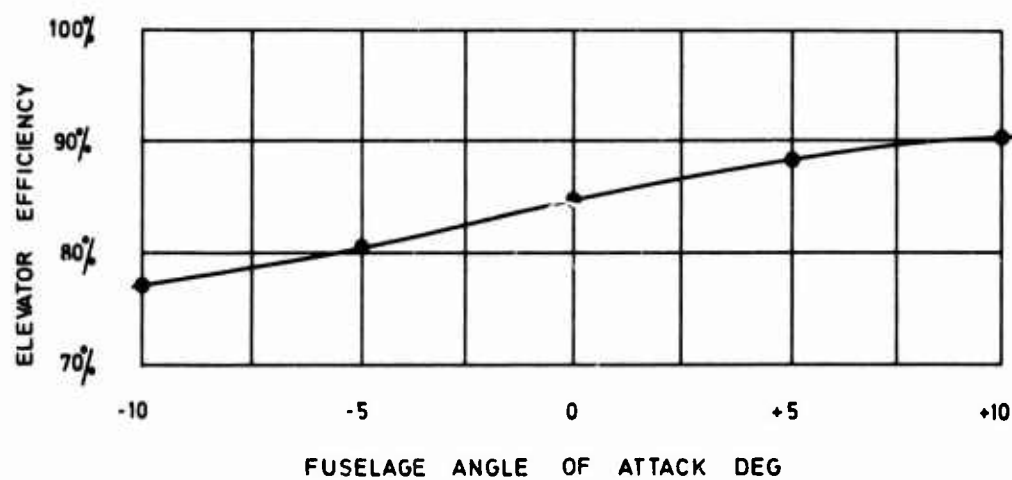


FIGURE 14 ELEVATOR EFFICIENCY VS. FUSELAGE ANGLE OF ATTACK

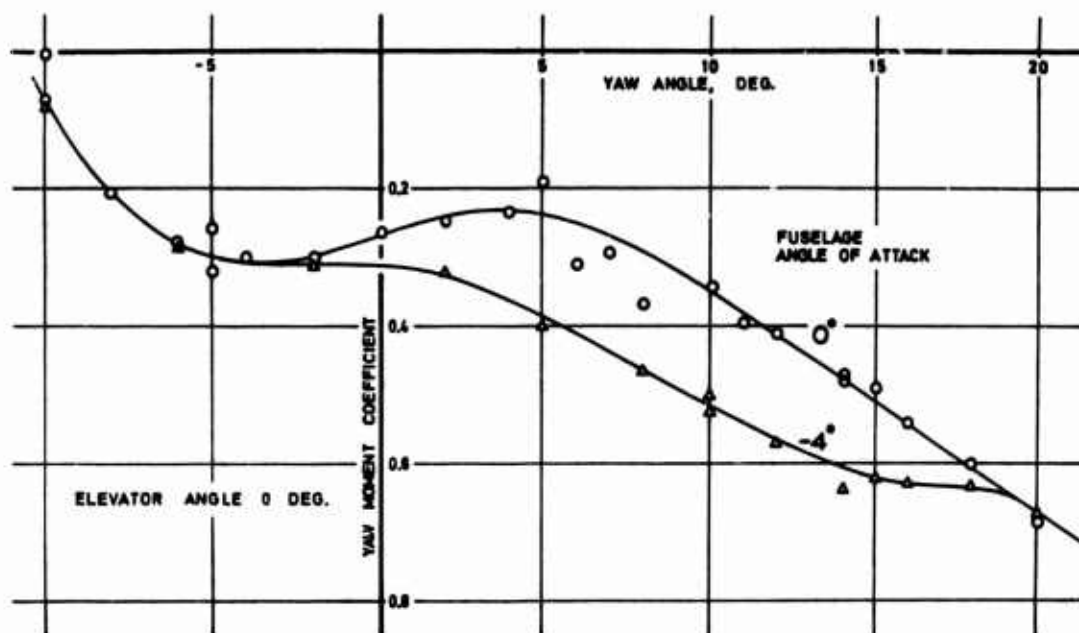


FIGURE 15 YAW MOMENT COEFFICIENT VS. YAW ANGLE FOR
DIFFERENT FUSELAGE ANGLES OF ATTACK

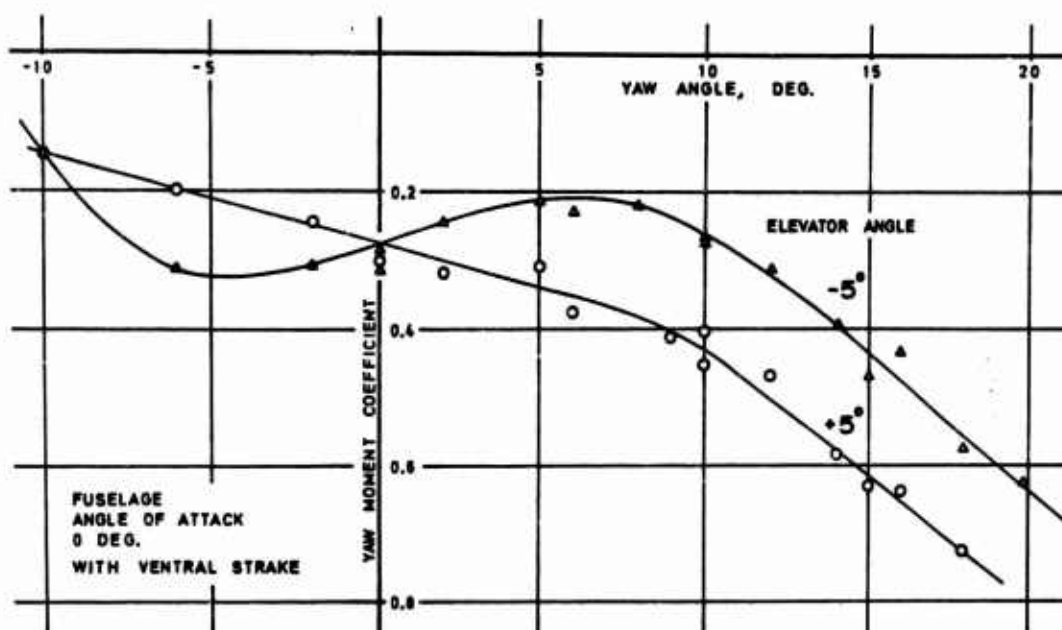


FIGURE 16 YAW MOMENT COEFFICIENT VS. YAW ANGLE FOR DIFFERENT
ELEVATOR ANGLES

FUNDAMENTAL CONSIDERATIONS OF NOISE RADIATION BY

ROTARY WINGS*

by

Martin V. Lowson,
Loughborough University of Technology,
Leicestershire, England.

SUMMARY

The paper commences with an historical review of progress in understanding of rotor noise. Initial work was principally on propellers, but has many obvious applications to noise from rotary wings. Current understanding of rotor noise radiation is then reviewed in some detail. The principal noise sources appear to be: discrete frequency due to distorted inflow, low frequency broadband due to turbulent inflow, and high frequency broadband due to tip effects. On a helicopter rotor each of these sources seems to be intimately connected with the shed vortex wakes. Tip modifications offer one method for controlling the effects. The implications for the designer are discussed. Rotor subjective noise levels appear to obey a velocity to the eighth power law, independent of thrust. Experiments to rectify some of the present deficiencies in knowledge are suggested.

1. INTRODUCTION

1.1 The first studies

The earliest demonstration of sound from a rotating source appears to have been performed by Mach¹. The apparatus is described by Rayleigh², with his customary lucidity, as follows: "It consists of a tube six feet (183cm) in length, capable of turning about an axis at its centre. At one end is placed a small whistle or reed which is blown by wind forced along the axis of the tube. An observer situated in the plane of rotation hears a note of fluctuating pitch, but if he places himself in the prolongation of the axis of rotation the sound becomes steady". The effect is due to the modulated Doppler shift in observed frequency at off-axis positions. Frequency modulation of a rotating source is a fundamental property, and has many significant implications for rotor noise as will be shown.

Sound radiation from rotating sources was solely a laboratory curiosity for many years, until the advent of propeller powered aircraft. It then became apparent that a rotating propeller was a source of significant noise radiation. This had immediate military relevance because of the possibility of acoustic detection and location of aircraft, and in Britain a special experimental station was set up at Butley, Suffolk, for noise studies³. Acoustic measuring apparatus available in 1917 was crude. The most advanced form of analysis was made via measurements of groove depth on a phonograph recording. From this Fourier analysis was in principle possible, but little spectral data was published. However, these shortcomings necessitated more active reliance on intelligent subjective observation and reported results of tests³ correctly define features which were still a matter of controversy fifty years later. Perhaps there is an important moral here.

Two of these features were the minimum of propeller noise observed on axis, and the major difference between ground and flight tests at nominally equivalent conditions. This latter point is often overlooked even today. Much reported data on propeller noise taken on ground rigs is irrelevant to noise in flight. For helicopter rotors the problem is less acute, and ground data is probably more representative, but considerable care in extrapolation will always be necessary.

Theoretical work on the propeller noise problem was also undertaken. Lynam and Webb⁴ considered the propeller as a ring of sources and sinks, and properly evaluated the retarded time integral to give a solution in terms of Bessel functions. However their basic model of the propeller was equivalent to an axial dipole and necessarily led to the prediction of zero sound in the rotor disc plane, completely contrary to experimental findings. They therefore removed the sinks to infinity, and the rotating source results, although physically rather meaningless, at least resembled experimental trends. Bryan's⁵ approach was more fundamental, and he did indicate the solutions for dipoles oriented in each of the three major directions, but he avoided explicitly modelling the propeller.

In the inter-war years interest in propeller noise reduced. The official attitude appears to have been that, quoting from Reference 3, "The problem of silencing an aircraft in flight was one of such difficulty that substantial progress was unlikely". The author went on to make a plea for improved instrumentation, and indeed it appears that only now do we at last have sufficiently good instruments and analysis methods to permit a full understanding of rotor noise sources.

* This work was partially supported by joint contracts from the National Gas Turbine Establishment and the National Aeronautics and Space Administration.

British work concentrated on internal noise problems in aircraft, for, to quote from Davis⁷ in 1932, "It is common knowledge that until comparatively recently the noise in the cabins of aircraft was so extreme that for many persons it constituted the chief deterrent to air travel. Conversation was wholly impossible, and often wads of cotton wool were issued to passengers to enable them to obtain some slight - but welcome - relief from the pandemonium of sounds, and to protect them in some measure from the period of perceptible deafness which followed an excursion by air". Possibly the same remarks apply to certain rotor powered craft today, but, in general, the achievement of acoustic science so far has been to remove the noise problem from the interior of aircraft and to impose it instead on the community at large.

Some valuable experimental work on propeller noise was reported by Kemp⁸ and Paris⁹. They both found that the sound showed a marked peak just behind the rotor disc. Paris attempted to explain this by combining the single and double source hypotheses from Lynam and Webb's work. This arbitrary assumption was quite close to the truth, but the problem of modelling the boundary conditions for the propeller was still not solved correctly. This remained the case until 1936, when Gutin¹⁰ produced his now classic paper, identifying the forces on the rotor as dipole acoustic sources. The result used was based on a formula in Lamb's Hydrodynamics¹¹, a book which must have been familiar to the earlier workers. By combining terms proportional to both thrust and drag (torque), Gutin predicted sound with a maximum behind the disc and a non-zero level in the disc plane, in agreement with experimental trends. Furthermore the theoretical value for the overall level of noise radiation was encouragingly close to experiment. Thus Gutin's model of noise radiation by the action of rotating steady forces on the propeller became widely accepted, and the discrete frequency noise due to the steady forces alone acting on a rotor is now often known as 'Gutin' noise.

The second major component of noise from a rotor is broad band in nature. The first experiments relevant to this source were performed by Stowell and Deming¹² who measured the noise from rotating cylindrical rods. Cylinders in a uniform flow radiate Aeolian tone noise due to the action of their Karman vortex street, and Stowell and Deming found that the noise radiation from the rotating cylinders was within a frequency range compatible with the expected variation of Strouhal frequency over the road. Fuller experiments were reported by Yudin¹³. He analysed the noise from several rotating shapes, and also presented a theoretical analysis. This followed Gutin in modelling the fluctuating forces on the rods as dipoles. Yudin found that the sound power was given by an equation of the form

$$W = K \frac{\rho}{a_0^3} S V_T^6 \quad (1)$$

where W is acoustic power
 ρ is density
 a_0 is speed of sound
 S is profile area
 V_T is tip velocity
 and K is an empirical constant

Yudin found that a wide variety of profiles, including both aerofoils and circular cylinders, obeyed this general law, differing only in their value of the empirical constant K . Essentially equivalent formulae are in use today for prediction, as will be discussed later. Further experiments along similar lines were later reported by Von Wittern¹¹. These are of interest because they are the first to demonstrate the Doppler broadening of the broadband noise spectrum at the higher rotational speeds on a rotor. This is as expected after the first experiments of Mach¹.

Thus, at the end of the second war work, principally in Russia and England, had laid a foundation for the understanding of the noise from rotating sources. In addition a substantial amount of information was available from abortive German work aimed at acoustic location of aircraft¹⁵. But comparatively little experimental work had been performed on noise from full scale propellers. This deficiency was soon remedied in America, when a series of systematic acoustic experiments on far field sound radiation commenced at NACA Langley. This data provided the basis of our knowledge of rotor noise today. A series of reports were produced, for example References 16-21. Much of the presented data suffer from one obvious drawback. They were taken on a stationary propeller. However, the propellers were mounted in a clear area and acoustic data were only taken during calm air conditions. Wind can have a major effect. Hicks and Hubbard¹⁶ record that "measurements taken on a day when gusts were approximately 20 m.p.h. showed sound pressure variations of approximately 15 decibels". Other experimenters have not been so careful either in their choice of rig location, or of test conditions.

Data from the early tests were presented principally in terms of overall sound pressure level at the position of maximum noise. The Gutin theory gives fairly acceptable results for such points, at least for tip Mach numbers greater than about 0.6. But at lower tip Mach numbers the Gutin theory systematically underestimates even the overall noise level, especially for rotors with high blade numbers. This discrepancy was explained as "the contribution from the oscillating disturbances in the flow around the propeller blade"¹⁶. The concept that turbulence interacting with the blade can give rise to a significant broad band noise spectrum is undoubtedly correct. Unfortunately, the physical model taken for this noise was based on the earlier experiments on rotating rods, discussed above. Consequently, this original rather general concept of vortex noise was re-interpreted as a noise specifically due to trailing edge vortex shedding. This is rather misleading.

The original experiments involved rotating cylinders in their own wake, forcing a response at the wake frequency. It is noteworthy that Yudin's results show how the noise radiated by a flat plate actually reduces compared to the zero incidence case when the plate is at 10° incidence. In the latter case, the blades would not pass through their own wake. The importance of this was demonstrated as early as 1924 in a paper by G.I. Taylor²² based on observations on a toasting fork. The fork was observed to radiate far more noise when moved rapidly through the air with the prong plane held parallel to the motion than with the prong plane at right angles to the motion. In the first case each prong is bathed in the wake of its leader, while in the latter case each prong can react independently. This clearly shows the relative significance of self-induced and external turbulence.

The first paper specifically oriented towards helicopter rotor noise was also the result of work of the NACA Langley group. Hubbard and Maglieri's paper²¹ contains much significant information, and their principal results are shown here as Figure 1. This shows several important features of rotor noise. Firstly, the noise increases rapidly with tip speed. Secondly, it can increase markedly as the blade approaches stall, (solid symbols on Figure 1). Thirdly, the noise levels can also increase at low rotor incidences. Thus a minimum in rotor noise occurs in the intermediate operating range of the rotor. This is of obvious interest to the designer. Hubbard and Maglieri found the sound at high speeds for low rotor incidences to be particularly intense. Today this would be known as blade slap. It is obviously directly related to the wake interaction effects demonstrated by the experiments of Yudin and Taylor.

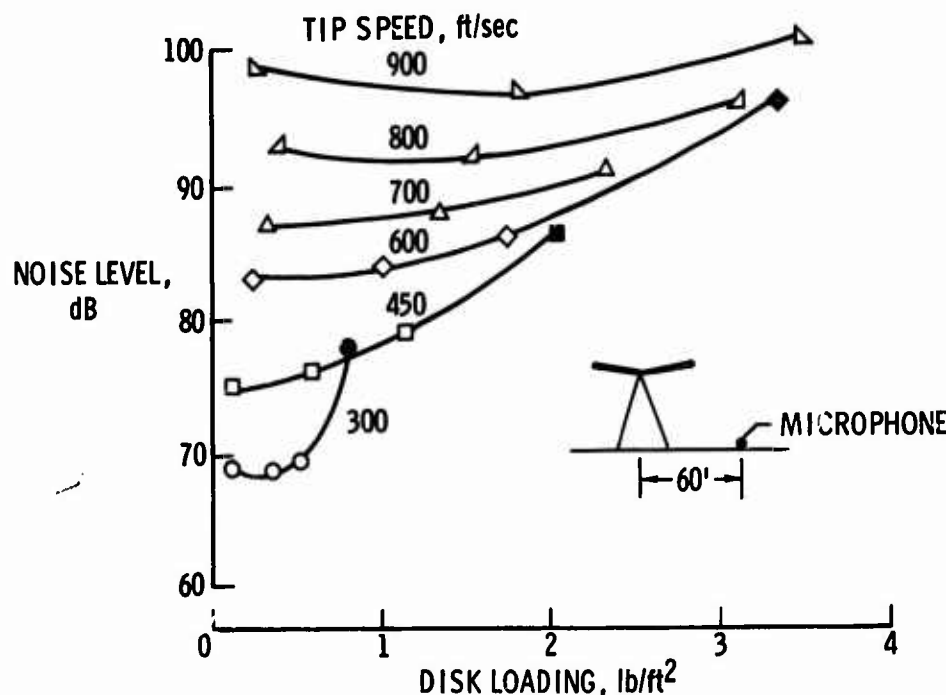


Figure 1: Rotor noise levels after Hubbard and Maglieri²¹

Comparison of the then existing theory with the helicopter noise data gives mixed results. For prediction of overall levels near the plane of the rotor disc the Gutin theory for the rotational noise, supported by a vortex noise formula at the lower rotational speeds is generally acceptable. Unfortunately, more detailed predictions are required for subjective ratings, including definition of the frequency spectrum. In the early experimental work on propellers spectral measurements were tedious, and only limited results from the wave analyser were usually presented. These showed that the Gutin formula systematically underestimated the noise level at the higher frequencies, especially for low tip speeds or many bladed propellers. One further discrepancy was also clear. The Gutin theory predicts zero discrete frequency noise on the rotor axis. However, significant discrete frequency levels are inevitably measured on the axis.

All these problems became especially acute for helicopter noise. The fundamental

frequency for a helicopter rotor is normally below the range of hearing so that it is only the higher harmonics which are important. The rotors normally operate at moderate tip speeds, and near axis locations have far more practical significance. Vortex noise concepts cannot explain all these problems, and it became clear that, in some important respect the theory was incomplete. A significant improvement was necessary to allow understanding of helicopter noise predictions. A vital clue could have been found from the work of Kemp⁸ in 1932. He found that sound just behind the propeller disc (where the Gutin noise is at its maximum) was comparatively steady in level. But he also found substantial fluctuations in level near the axis and for the higher harmonics; that is, for just those conditions where the Gutin theory is inadequate. Gutin considered the noise resulting from steady loads only. This suggests that the key to all the problems is the action of the fluctuating loads.

2. THE BASIS OF PRESENT UNDERSTANDING

2.1 Effects of non-uniformity

The possible significance of unsteady load components was recognised by many workers and was, indeed, the motivation behind the original vortex noise concepts. But their explicit inclusion in a rotating source theory has only occurred recently²³⁻²⁵. The first work applying these ideas to rotor noise was that of Schlegel, King and Mull²³ who numerically evaluated the retarded time integrals of the unsteady source functions. Computer time and accuracy were their main problems. Shortly thereafter Lowson and Ollerhead²⁴ and Wright²⁵ gave analytic solutions for the noise as the summation of an infinite series of Bessel functions. The actual result is as follows, based on equation 11 of Reference 26.

$$c_n = \frac{i n \Omega}{2 \pi a_0 r} \sum_{\lambda} (-i)^{n-\lambda} \left[\frac{x T_{\lambda}}{r_1} - \frac{(n-\lambda)}{n m} D_{\lambda} \right] J_{n-\lambda} \left(\frac{n m y}{r_1} \right) \quad (2)$$

where c_n is the magnitude of the sound in the n^{th} harmonic
 Ω is the rotational speed in radians/second
 a_0 is the speed of sound
 r_1 is the distance from rotor hub to observer
 T_{λ}, D_{λ} are the harmonic components of axial and circumferential force on the rotor.

This result allowed much further insight into the underlying acoustic source mechanisms and justifies further discussion.

The non-uniform inflow into the disc is Fourier analysed into a series of "modes". Each mode is a steady sinusoidal distortion pattern around the disc, which causes a sinusoidal force fluctuation at the rotor. Thus each mode causes a fluctuating force of different frequency on the rotor disc. On the axis of the rotor each frequency is heard directly, but off the axis the modulated Doppler frequency shift reported by Mach causes a large number of acoustic frequencies to result from each single mode input. Thus it is found that away from this axis each mode is an effective sound generator over a range of harmonic frequencies. Inverting this argument it is seen that each sound harmonic results from contributions from a limited number of modes. Figure 2 taken from Ref. 24 shows the effect for a particular sound harmonic $mB=16$ where m is the harmonic order and B is the blade number. It will be observed that the contribution to this harmonic drops away very rapidly outside a central range over which the efficiency is essentially constant. The range of distortion modes which are important for each sound harmonic is shown in Figure 3, also from Ref. 24.

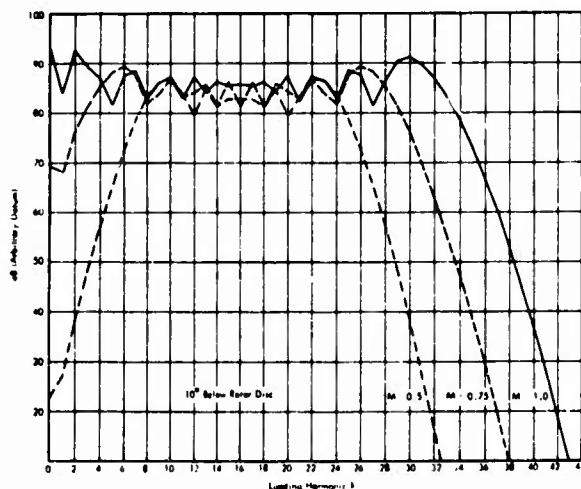


Figure 2: Contribution of higher harmonics to rotor noise²⁴

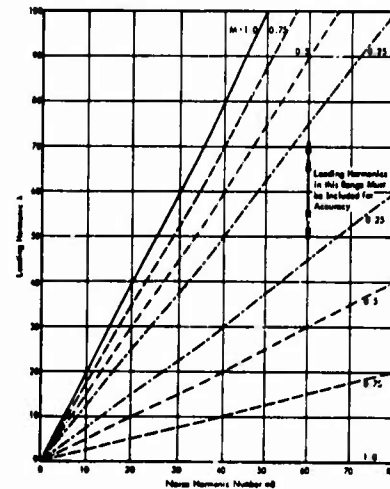


Figure 3: Range of effective contribution of loading harmonics to sound radiation²⁴

On the rotor axis, where there is no Doppler shift, there is a one to one relation between input modes and output harmonics. Equation (2) takes a particularly simple form for this case reducing to

$$c_n = \frac{in\Omega T_n}{2\pi a_0 r_1} \quad (3)$$

In addition, sound harmonics which are not integral multiples of the blade passing frequency cancel out identically, so that only every B^{th} mode (for a B bladed rotor) contributes to the on-axis noise.

Equation (3) has important implications in experiment, for measurements of the on-axis sound radiation will be directly related to fluctuating forces on the rotor disc. Thus the levels of these forces can be inferred from the on-axis acoustics. It seems that on-axis measurements can be used to some extent as acoustic diagnosis of the rotor unsteady aerodynamics. Once the fluctuating force field is known the whole rotor noise field can be calculated by equation (2), as shown for instance by Barry and Moore²⁷. Thus, the on-axis point becomes the prime location for acoustic measuring instruments for any test.

Now the steady loads correspond to the zeroth order mode. Going back to Figure 2, this can be seen to have very minimal contribution to the higher harmonic case given here. Indeed the steady load contribution at $M=0.5$ is seen to be about 60dB down on the contribution in the central range. Thus the direct contribution of Gutin noise, or of any steady rotating acoustic source, to subjective levels of a low speed rotor is very small. For the case shown a high order mode with intensity of only one millionth of the steady (that is, an amplitude of one thousandth of the steady) will have an equal acoustic effect. Thus the enormous acoustic efficiency of the higher order modes more than compensates for their small source strength. It can be seen that very minor levels of fluctuation in the aerodynamic input to the rotor can give rise to very large levels of high harmonic acoustic output from the rotor. The increase of noise level by 15dB due to a 20 m.p.h. wind reported by Hicks and Hubbard¹⁶ is immediately explained by these arguments.

The theory successfully explains the source of rotor noise observed at both high frequencies and low tip speeds. Furthermore, the unsteady sources can be seen to radiate on the rotor axis. Thus, virtually all the disagreements between Gutin's steady force theory and experiment are resolved simultaneously. In addition, theory demonstrates unequivocally that the rotor noise subjective levels can be controlled directly by minimisation of all unsteady inflow into the rotor.

Unfortunately, the theory does not allow immediate prediction of the rotor noise. The input loading data for the Gutin theory was simply thrust and torque, which will be known for any rotor. But predictions using the unsteady theory require a knowledge of the miniscule levels of loadings in all the higher modes. On-axis acoustic measurements are a direct source of this information. However, this knowledge is unlikely to be available at the design stage except in special cases. Alternative methods for predicting these higher order modal levels must therefore be sought.

Lowson and Ollerhead²⁴ used extrapolated empirical fits based on data for the aerodynamic loadings on a helicopter rotor. It is an open question how representative these results may be, and they are obviously inappropriate in many cases. Nevertheless, they do form the basis for a prediction method and some comparisons between Lowson and Ollerhead's predictions and measured acoustical data are shown in Figure 4.

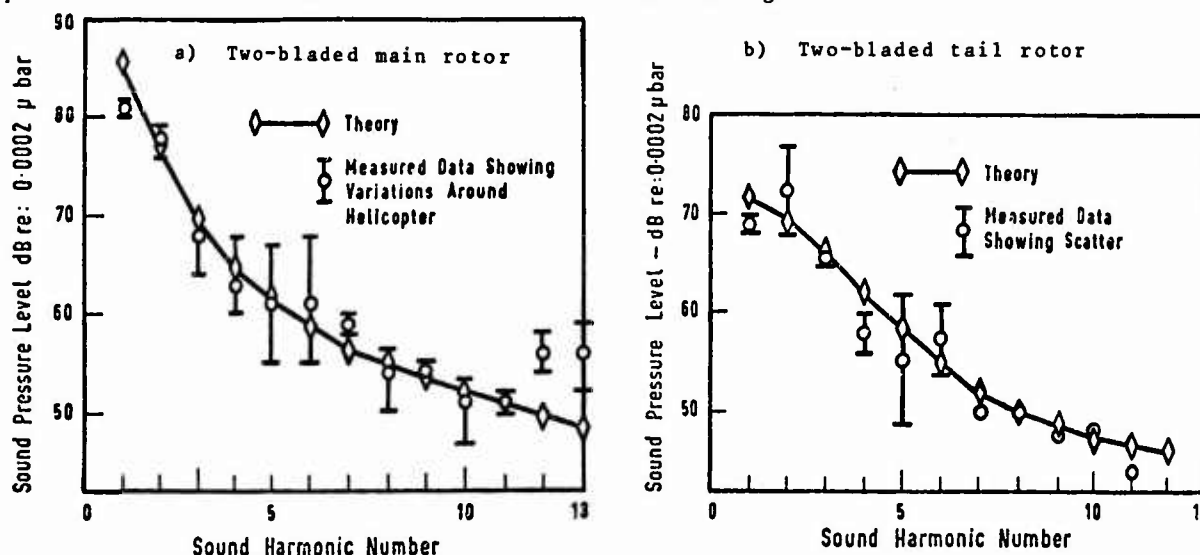


Figure 4: Theory and experiment for noise from a light helicopter⁵⁷

An explicit assumption in this prediction was that of random phase for the input modes. This assumption appears to be in fair agreement with experiment, and allows the theory to adopt a simpler, phase independent form, giving an axisymmetric sound field around the rotor. The noise output of systematic azimuthal events such as vortex intersection would not be satisfactorily predicted by this form of the theory, but for most cases the random phase assumption gives a significant improvement in computational time and ease of interpretation. In general terms, basic understanding of the discrete frequency radiation from a rotor is now fairly complete.

2.2 Broad band noise

The general concepts underlying the discrete frequency radiation by rotor apply equally well to the broad band case. Random source fluctuations on the blade will generate broad band noise, with a Doppler broadened spectrum due to the rotation. Theoretical calculations can be made following this idea (see Refs. 24, 28, 36, 42). In practice, it is very difficult to draw a clear distinction between discrete frequency and broad band noise. Several workers (e.g. Refs. 24, 29) showed how much of the region of the rotor noise spectrum which appeared to be broad band in nature from early tests in fact contained substantial contributions from the higher harmonics of the blade passing frequency. Categorising sound in this region as either broad band or discrete frequency is difficult. An experiment which does show the classes clearly was reported by Leverton²⁹, and his results are reproduced here as Figure 5. This shows analysis of measurements taken on a

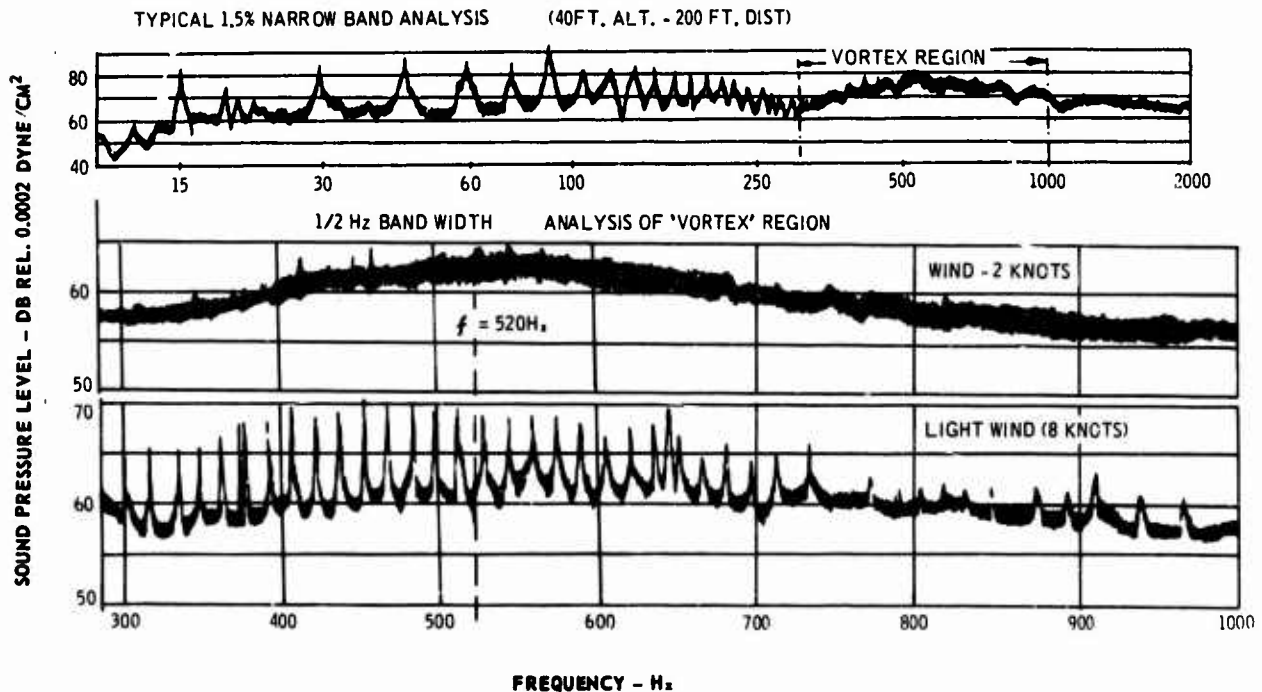


Figure 5: Narrowband analysis of helicopter noise - Hovering Wessex - from Leverton²⁹

rotor under conditions of calm, and slight wind. It can be seen that for calm conditions no harmonics are observable, whereas a slight wind immediately results in the presence of discrete frequencies. Furthermore, the underlying broad band level in the slight wind case is unchanged. These experiments therefore demonstrate the existence of a genuine broad band background noise radiation from a rotor. However, the fundamental question is the source of the random fluctuations. As has been discussed, early work was oriented towards a trailing edge vortex mechanism as a fundamental source. The first paper to explicitly contradict this concept was produced by Kramer³⁰ in 1953. He applied both trailing edge suction and blowing to a propeller, and was unable to detect any change in level. This is a powerful argument against any possible trailing edge effects. Kramer proposed that inflow turbulence to a rotor was the dominant source.

Several source mechanisms are possible. Calculations of the noise of various possible broad band acoustic sources are reasonably straightforward, and were presented by Sharland³¹. In Table 1 a slightly modified set of results is given based on the work of Ref. 32. The equations given refer to three sources. Firstly, inflow turbulence, as has been discussed; secondly, sound due to direct radiation by the random fluctuating pressures acting on the blade due to its turbulent boundary layer; and thirdly, sound due to action of a tip vortex over the extreme outer part of the blade.

Source	Typical Level	Typical Frequency
1. Turbulent Input	$p^2 = 2.5 \times 10^{-3} \rho_0^2 a_0^4 M_T^6 \left(\frac{u_{rms}}{V_T} \right)^2 \frac{S}{r^2}$	as turbulence
2. Attached Boundary Layer	$p^2 = 1.5 \times 10^{-9} \rho_0^2 a_0^4 M_T^6 \frac{S}{r^2}$	$f = 20V_T/c$
3. Tip Radiation	$p^2 = 4 \times 10^{-8} \rho_0^2 a_0^4 M_T^6 \frac{S}{r^2}$	$f = 6V_T/c$

Table 1: Parameters of Broad Band Noise Sources

First of all the effect of external turbulence will be examined. The key experiment in this area was performed by Sharland (Ref 31) who measured the noise radiated by a small plate in the turbulent air stream of a jet. The results are shown in Figure 6. Sharland also estimated the noise using a formula almost identical to equation 1 in Table 1, and obtained good agreement, as shown in Figure 6. Sharland used established measurements of the turbulent flow parameters in a jet, which should be acceptably accurate for this case. He also measured the noise radiated by a plate in the laminar flow portion of the jet. The results show almost 20dB less sound radiation, thus confirming the significance of external compared to self-generated turbulence.

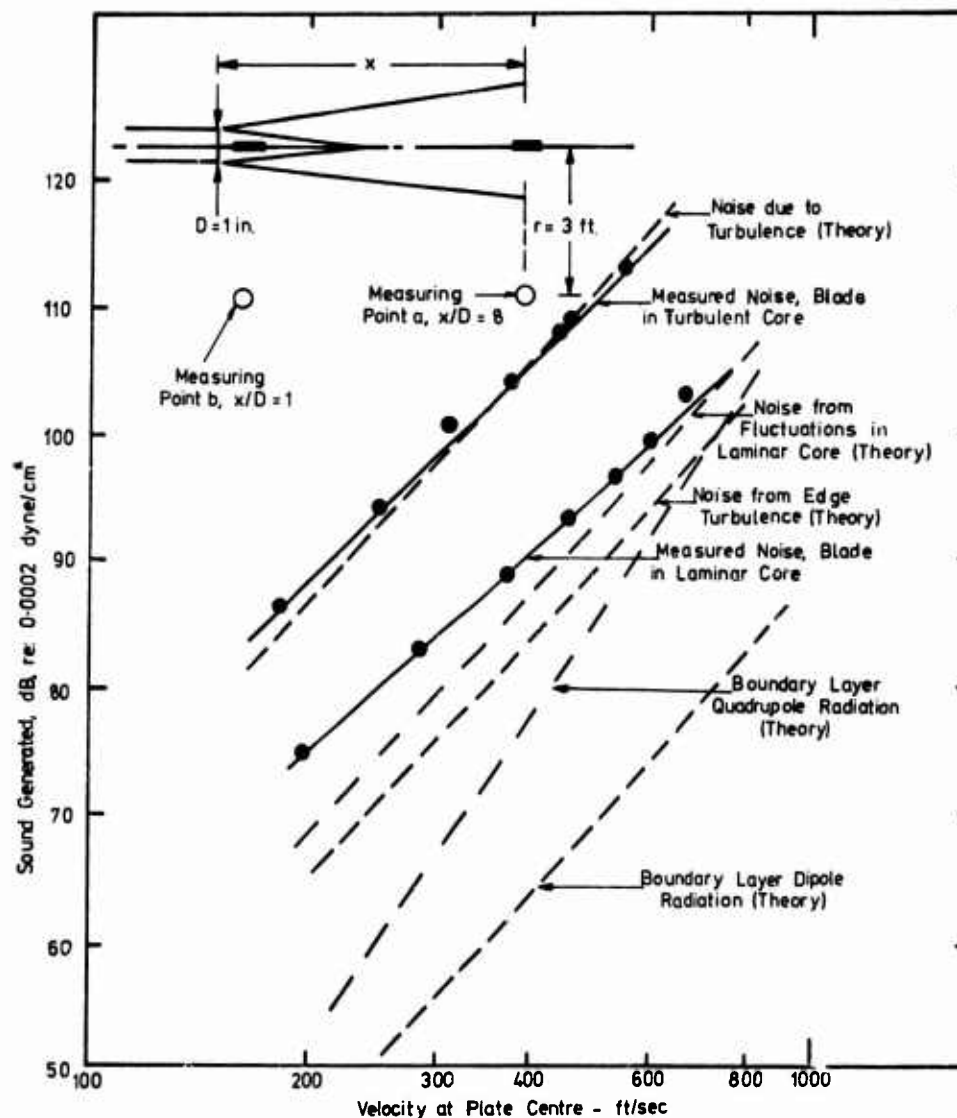


Figure 6: Noise radiation from a plate in an airstream - after Sharland³¹

However, detailed interpretation of these "laminar" results is far more difficult. Sharland did estimate the effect of the shear layer turbulence over the part of the plate projecting outside the laminar core, as shown in Figure 6. However he did not consider the possibility of fluctuations within the core itself. Even if the jet exit flow was entirely turbulence-free, recent research has shown how a distinct fluctuating field exists in the core even quite close to the exit. Data taken by Tu³⁵ and others has shown that the cross-stream component of turbulence will be of order 0.1U at the downstream location used by Sharland, but as high as 0.012U at the core location. These latter levels are quite sufficient to explain Sharland's acoustic radiation in the "laminar" case as shown in Figure 6. Thus it seems probable that Sharland's "laminar flow" data is also effective for an external turbulence case.

In addition to externally induced sources on the blade, typically inflow turbulence, there is the possibility of self-induced sources, for instance the trailing edge effects discussed above. Kramer's experiments are a powerful experimental argument against the reality of trailing edge vortex noise mechanisms. The results of two further relevant studies, unfortunately as yet unpublished, have been kindly communicated to the author by Davis, and by Foley. Both these workers attempted to repeat Sharland's experiments, with a plate in a two-dimensional channel, but with the precaution of removing the turbulent shear layer which passes over the parts of the plate nearest the wall. Davis removed the boundary layers by suction, and Foley mounted his plate just after a substantial contraction, so that

the boundary layer was very thin. Both workers were unable to detect any effect of the presence or absence of the plate on the broad band noise radiation, and inferred that actual levels of noise radiated by a plate in an undisturbed flow must be an order of magnitude below those found by Sharland for the laminar case. Thus it must be concluded that the trailing edge vortex mechanism is not of practical significance.

The data used for the existing correlation of broad band noise is based on helicopters, which undoubtedly undergo wake interactions. Even given this, the data can be used to argue a U^8 law at work rather than a U^6 , as is discussed in Ref. 32. Other self-induced effects on the blades are of interest. As is shown by Table 1 and Figure 6, the sound levels resulting from the direct radiation of noise from a uniform blade boundary layer are very small. Furthermore, Table 1 shows how the typical frequencies will be extremely high, and outside the range of practical interest. This comment applies to radiation from attached uniform boundary layers. As discussed in Ref. 32, the effect of non-uniformity, and of possible transition or separation phenomena on the blade, could be important. Perhaps the most significant of the possible self-induced sources is due to the flow at the blade tips. At angle of attack the tip flow is generally in the form of a concentrated vortex which springs from the forward part of the tip and passes back over the top surface. Some data on this has been given recently by Hoffman and Velkoff³⁴. Experiments on delta wings have demonstrated that significant levels of pressure fluctuations can occur in this case, and based on this data a crude estimate can be made of possible tip noise level³², as given in Table 1.

It is clearly of interest to be able to predict both the discrete and the broad band components of the rotor noise. As shown by Figure 5, the distinction between the two is difficult, and discrete frequency components, at least, are affected by the wind. It is clear that the discrete frequency noise does result from the non-uniform inflow to the rotor and this in turn appears to be a function of detail rotor geometry. Broad band noise, where turbulence is the cause, is possibly a little less affected by details. It has been examined by an empirical correlation of data along lines very similar to those suggested by Widnall³⁵. Her correlation included results from a wide range of helicopter tests, but the data frequently included the full noise radiation and not simply the broad band noise component alone. The correlation shown here in Figure 7 features data which includes some attempt to remove the discrete frequency contribution. It is therefore intended to give broad band rotor noise only. It also has the advantage of being non-dimensional. Most of the data points shown are from Schlegel's work²³, which only included contributions above 150Hz. This was helicopter test tower data. Also shown are some recent data from the work of Brown and Ollerhead³⁶ on noise from a propeller at a stand. Their levels were found by subtracting all observed frequency peaks from the signal. One point from Hubbard and Maglieri's work is shown, this is based on the spectrum given in their paper together with comments received personally from H.H. Hubbard. Only the integrated contribution of the noise above 160Hz is shown for this.

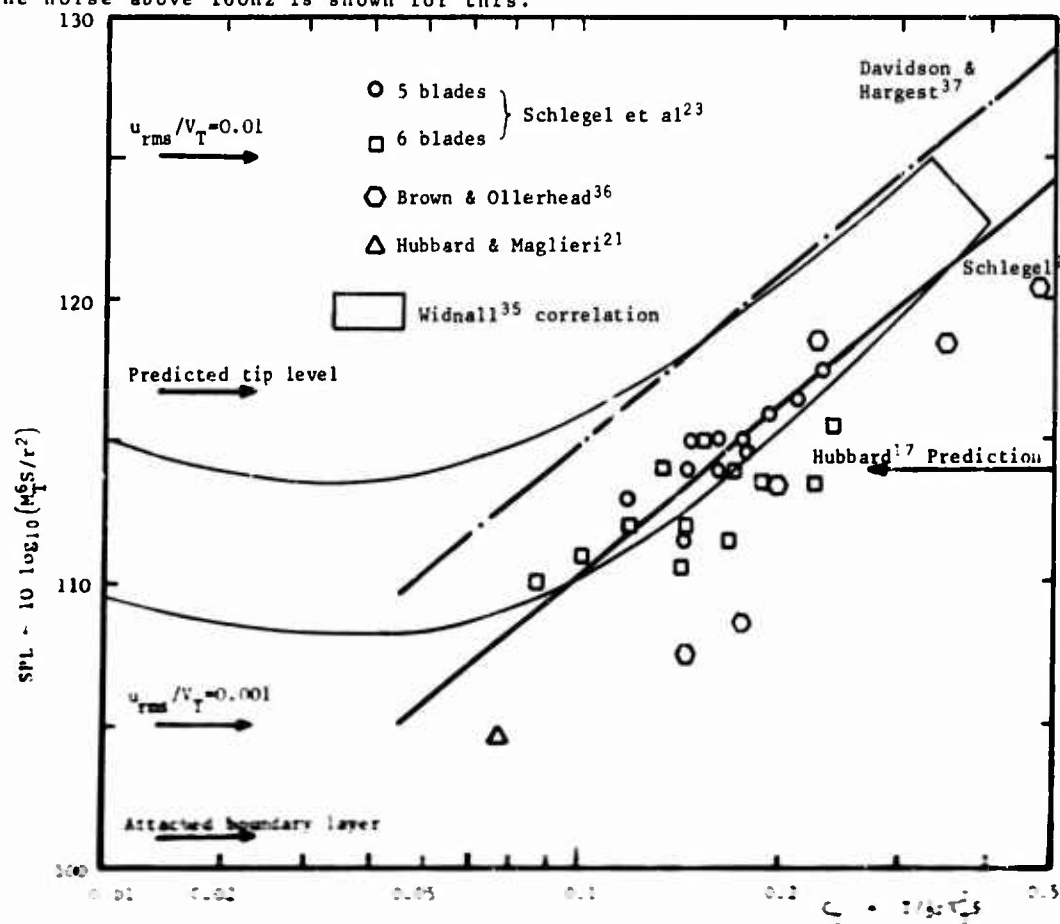


Figure 7: A correlation of broad band noise

Also shown are prediction formulae due to Hubbard, and to Schlegel. Not surprisingly, Schlegel's empirical formula matches his own data well. But it is also in acceptable agreement with the other data plotted. Thus it appears that this formula does give a reasonable prediction of broad band levels. Further work along equivalent lines has been reported by Davidson and Hargest³⁷. Their prediction curve is based on sound analysis of noise from a helicopter in free flight, but the number of data points apparently used is rather small. It is supported by test results on a rotor tower which was almost certainly atypical, with large levels of recirculation. Davidson and Hargest's formula contains a large directional term, and their numerical values must be reduced by 10dB to allow direct comparison with Schlegel. A further 3dB reduction is allowed to account for their "mean peak" level prediction. Even so their prediction curve is 4.5dB up on Schlegel's, as shown in Figure 7. The Davidson and Hargest prediction for broad band noise alone is sometimes higher than measurements for the full helicopter. Thus it is thought to be somewhat overconservative. On the other hand, it should be noted that the data on Figure 7 comes entirely from rig tests and could therefore be suspect. Further systematic tests on full scale helicopters, allowing systematic analysis of broad band noise, are clearly highly desirable.

Also shown on Figure 7 are theoretical predictions based on the formulae of Table 1. It is noteworthy that a turbulence level of as little as 0.1% is sufficient to produce broad band noise levels of the order of those measured. Figure 7 also shows how predicted levels due to direct blade boundary layer radiation are inadequate to explain observed noise levels, but the tip noise radiation formula given does indicate levels of the same order as those observed in practice. This empirical evidence is, at least, not in disagreement with the idea that inflow turbulence and tip radiation are the principal sources of broad band noise radiation by rotors.

2.3 Other source mechanisms

To this point the paper has concentrated on sound radiation by fluctuating force (dipole) mechanisms on the blades. As early as 1938 Deming³⁸ showed the possible effects of blade thickness in producing noise. Although the existence of thickness noise sources is now universally recognised, in most work on rotor noise they are conveniently neglected. Little basis has been given for this, but, in fact, the comparative level of the thickness noise source can be calculated directly. As first stated explicitly by Lighthill³⁹, for "compact" sources when the acoustic wavelength is greater than the blade chord, the thickness noise source reduces to an equivalent dipole of strength $\rho V \dot{V}$ where V is the blade volume and \dot{V} the local acceleration. This is very similar to the model proposed by Lynam and Webb in 1919.

Now the force terms have dipole strengths equal to the magnitude of the forces acting. In the rotor case acceleration is U^2/R and the force in the chord direction is the drag $\frac{1}{2}\rho U^2 S C_D$, so that the ratio of thickness to torque noise is $2t/RC_D$ where t is the mean blade thickness and C_D includes any backward orientation of the thrust. The ratio will normally be very small. Thus, theory suggests that thickness noise can be neglected at moderate rotor speeds and radiation frequencies. For high frequencies or at speeds approaching sonic the compactness condition breaks down so that possible noise effects of thickness must again be taken into consideration. Lyon⁴⁰ has recently considered this.

A further source of possible radiation from the blade is the stress system around it. Lighthill's general theory of aerodynamic noise⁴¹ demonstrated the possible significance of fluctuating stresses as quadrupole sources of sound in 1952, but it was not until 1969 that Ffowcs Williams and Hawkins⁴² pointed out that the fluctuating stress system on a rotating blade must also radiate. The key features of sound radiation from any rotating source are governed by Mach's modulated Doppler frequency shift, and Figure 3 will therefore apply to all sources equally. Thus distinction between the various forms of source is not easy. Any simple theoretical model suggests that a feature of stress (quadrupole) radiation would be a U^8 dependence. There is some evidence of this (see Ref. 32) but not enough to be convincing. Direct estimation of quadrupole source strength is difficult. Most simple models tried by the writer seem to result in logarithmically singular integrals, and further theoretical study is required. On the other hand, the fluctuating force (dipole) source strengths can be calculated straightforwardly, and predicted results agree with virtually all the experimental information available. Thus, at the present time, any real significance of fluctuating stress sources is not demonstrated, but the difficulty of early workers in properly modelling the blade boundary conditions is far from being fully clarified.

Ffowcs Williams and Hall⁴³ and others have extended the basic quadrupole source concept to include the possible effects of blade trailing edges. They find that diffraction around the trailing edge can give large increments in acoustic efficiency so that the U^8 law goes over to a U^5 law. Several objections can be made to their theoretical model - notably, no account of boundary layer velocity gradient at the trailing edge and non-inclusion of the Kutta condition. Equally, no experimental evidence supporting the theory exists. Nevertheless the possible significance of trailing edge actions on blade noise radiation remains a question of considerable theoretical and experimental interest. The effects of blade motion are also a possible source of noise, but the effects can be shown to be comparatively small. A general theory for point forces in motion⁴⁴ shows that the dominant thrust term only radiates as a result of the acceleration of the rotor, proportional to $\dot{U}^2 R$. Blade motion effects will therefore only be significant overall if the acceleration in question is larger than $\dot{U}^2 R$, which is extremely unlikely for a helicopter rotor. It is the rotor force fluctuations associated with any blade motion that will be the dominant source in any practical situation. The insignificance of blade motion effects was also shown by direct computation in the report of Lousser and Ollerhead⁴⁵.

Finally, it must be emphasised that any unsteady source on the rotor is only important if tip Mach numbers are low (roughly < 0.7). For high tip Mach numbers the direct radiation by the steady rotating sources becomes very efficient, as shown by Figure 2. In this context steady sources would include steady thickness or stress contributions in addition to the steady force (Gutin) terms previously discussed. However, when rotor noise is a problem, low tip Mach numbers must be chosen, so that the unsteady sources will usually dominate practical rotor noise control considerations.

2.4 Some recent experiments

The key to the theoretical studies has been the concept that the unsteady aerodynamic input to the rotor causes its acoustic output. Thus a low speed rotor may be regarded simply as a machine for converting inflow variations into noise. From this viewpoint each rotor will have a unique aero-acoustic transfer function which defines its effectiveness as a noise generator. Recent experiments³² at Loughborough University of Technology have attempted to measure this. Experimental definition of the aero-acoustic transfer function requires simultaneous measurement of source strengths and noise. As has been discussed, the immediate source of noise is the fluctuating force system on the rotor. Measurement of this is difficult, and was not attempted in the tests, although some success has been reported in recent work by Heller and Widnall⁴⁴. The fluctuating forces are, in turn, caused by the unsteady inflow. This can be measured straightforwardly and this approach was chosen in the present tests. The disadvantage of the technique is that the fluctuating forces on the blades must be evaluated theoretically but this is outweighed by the advantages of experimental convenience. Furthermore the results may be of direct practical value for noise prediction since estimates of unsteady inflow levels to a rotor may be available at the design stage.

The experiments were performed on a small (0.66m dia.) open fan, leading details of which are given in Table 2. The inflow variation was measured using a rotating hot wire, mounted on the hub of the rotor. Circumferential variations of the inflow were thus recorded as time variations at the rotating hot wire, and spectral analysis of the signal gave the levels of the aerodynamic input modes directly. Acoustic output was measured on axis where the one to one relation of output to input applies (equation 3). Subtraction of the relevant aerodynamic input levels from the acoustic output levels thus gave a direct estimate of the aero-acoustic transfer function. This is shown in Figure 8.

Number of blades	= 2, 7 or 14
Hub diameter	= 0.24m
Rotor disc diameter	= 0.66m
Blade chord at tip	= 0.064m
Blade chord at root	= 0.085m
Maximum blade thickness at tip	= 0.003m
Blade tip angles	= $5^\circ, 10^\circ, 15^\circ, 20^\circ$
Blade root angles	= $25^\circ, 30^\circ, 35^\circ, 40^\circ$
Speed range between 0 and 3000rpm	approximately
D.C. motor of 7.5kW	
$\frac{1}{2}$ " B&K microphone position	- variable on 2.14m radius
	from fan centre
Hot wire location	- 0.26m from axis, 0.02m from blade leading edge

Table 2: Rig Parameters

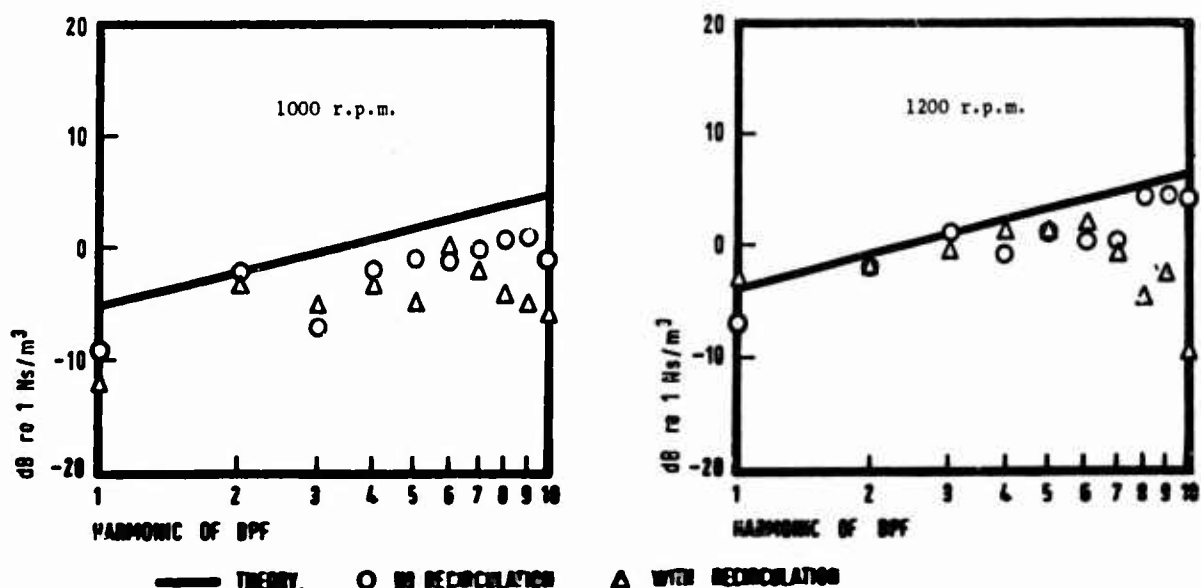


Figure 8: Aero-acoustic transfer functions³²

Two different inflow conditions are shown. The fan was mounted in an anechoic chamber, and normally operated in a recirculating condition, giving one set of data points. However, the recirculation took some time (3-5 secs) to build up to its full value. Thus at the start of each run different flow conditions prevailed, and data for this initial case are also shown. Both the acoustics and aerodynamics of these two cases are very different. But if the basic concept is correct, the aeroacoustic transfer function should be the same. This is verified by Figure 8 within experimental accuracy, at least for the low harmonics of the noise. A theoretical curve is also shown. This is based on equation 3, with the relation of unsteady aerodynamics to the unsteady forces being estimated from the theory of Sears⁴⁵. Agreement between theory and experiment is also good, both for trends and for absolute levels.

At the highest harmonics some discrepancies appear for the recirculating case. This is thought to be the result of increased levels of turbulent inflow and is currently the subject of further study. A comparison of broad band noise with turbulent inflow was also made for the 1200 r.p.m. case with clipped blades (see also below). Both aerodynamic and acoustic broad band levels were estimated from integrations of the measured spectra with discrete frequency peaks removed. The root mean square turbulent input level measured by the rotating hot wire was 0.556 m/sec. The broad band acoustic level may then be predicted to be 70 dB via equation 1 of Table 1. The measured level for this one case so far studied was also 70 dB. Thus theory gives very acceptable predictions of level for both the discrete frequency and broad band parts of the rotor noise radiation, showing a dominant effect of rotor inflow on noise.

Further experiments showed that the high frequency component of the noise was strongly affected by tip condition. The measured effect of tip shape is shown on Figure 9. It can be seen that clipping the trailing edge of the blade reduced noise at the higher frequencies by over 10 dB. The reduction observed is consistent with the idea advanced earlier that separated vortex flow over the tips is a significant source of noise.

Thus from these experiments it may be concluded that there were three principal sources of noise from the rotor tested

1. Discrete frequency noise, governed by inflow distortion
2. Low frequency broad band noise governed by inflow turbulence
3. High frequency broad band noise governed by the blade tips.

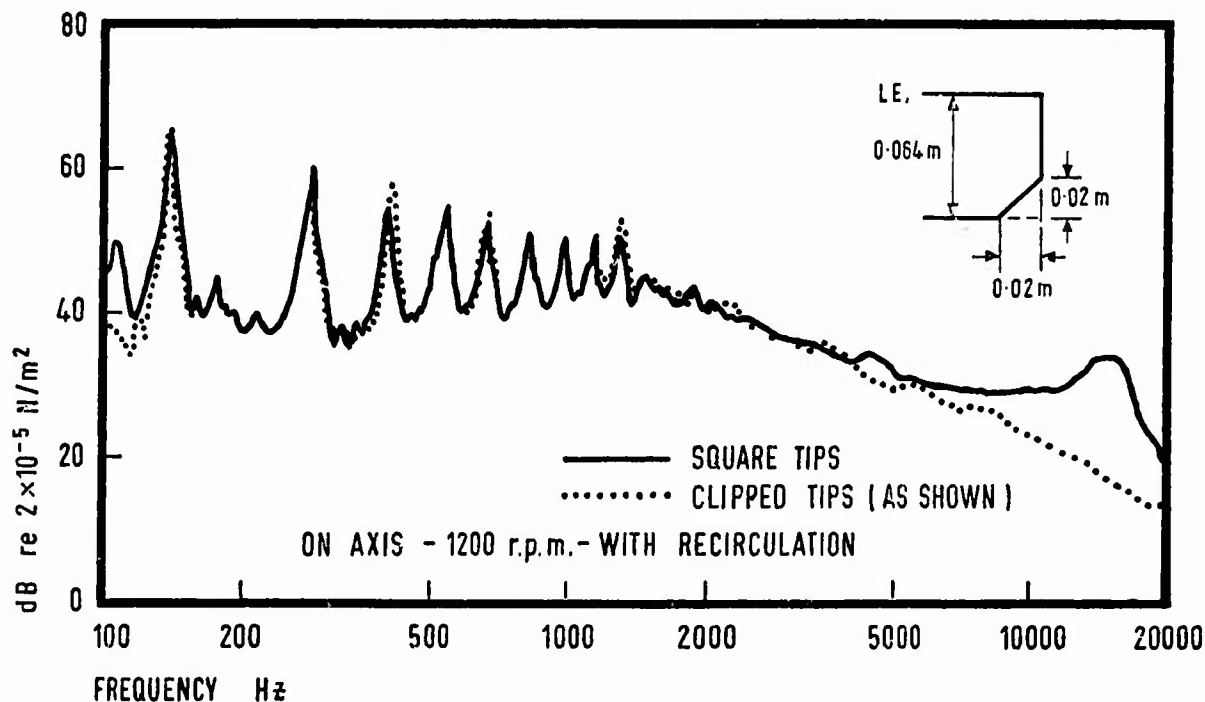


Figure 9: Effect of tip shape on fan noise spectra³²

3. APPLICATIONS TO NOISE CONTROL

3.1 Effect of design parameters

In attempting to minimise noise from a rotor, or indeed, from any acoustic source, the comparative insensitivity of the ear to changes in a level necessitates fundamental reconsideration of the optimum approach. The problem is illustrated by Table 3. It can be observed that a factor of 2 change in intensity at 3 dB is barely distinguishable subjectively. Successful noise control measures will require reductions by a factor of perhaps 10. It therefore becomes clear that a conventional design optimisation approach in which parameters are varied by perhaps 25% has little possibility of achieving the

Factor change in intensity	dB value	Subjective effect
2	3	Barely distinguishable
4	6	Noticeable
16	12	Pronounced

Table 3: Effect of changes in acoustic intensity

desired noise reduction goals. Indeed once design layout is complete the acoustic output is largely determined, and noise reductions after that point in time will not generally be possible unless there was a fundamental acoustic problem in the original design. An alternative way of looking at the problem is to consider that a typical helicopter uses around 1 MW of power, and only emits around 1kW as sound. Thus it is already 99.9% efficient at being quiet and will be difficult to improve to the 99.99% quietness necessary to make a useful noise reduction. In fact helicopter rotors are unusually noise sensitive to detail modifications. Nevertheless, the general ideas above still have considerable force, and it is important to consider overall acoustic goals from the outset.

Some general laws for rotors can be specified. Equation 2 shows that the discrete frequency radiation is governed by disc loading, while equation 1 and Table 1 suggest that the broad band noise is governed by blade loading. Thus at the low blade loadings characteristic of a helicopter rotor broad band noise would be more important. This concept is discussed in more detail in Reference 46. For design purposes, an idea of trends of noise with the principal design parameters is of interest, and some general arguments may be put forward for this.

It is the subjective response to rotor noise which is nearly always of concern, and this response depends not only on the level of the sound but also its frequency. The typical response curves for the human ear are shown in Figure 10. These correspond to the A and D frequency weighting scales which are based on extensive laboratory testing. The 'A' scale is perhaps the more widely used while the 'D' scale represents current estimates of response more closely. Each scale very roughly follows a frequency squared law at low frequencies, as shown in Figure 10. For the present purposes the detail differences between the scales are not of importance, and attention will be focused on the effect of the frequency squared variation, which should be appropriate to the noise from helicopter rotors.

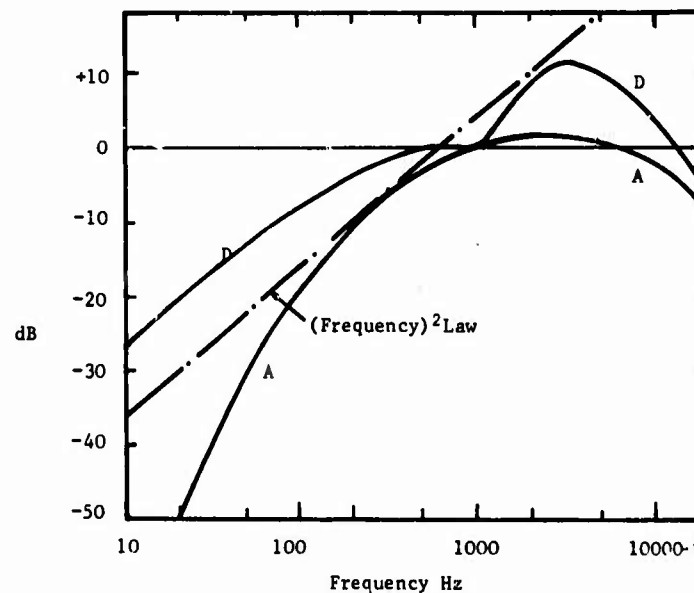


Figure 10: Frequency weighting curves for subjective response

Now, as shown by Schlegel et al²³, for a helicopter rotor, the physical levels of sound intensity vary roughly as

$$p^2 \sim U^2 T^2 / S \sim T^3 / S^2$$

and the typical frequency squared varies as

$$f^2 \sim U^2 / l^2 \sim T / l^2 S$$

where l is a typical length (say equal to $S^{0.5}$).

In each case the velocity has been eliminated by using the relation $T \sim U^2 S$. Thus the perceived noise levels measured in any unit will typically vary as

$$L_{PN} \sim f^2 p^2 \sim \frac{T^4}{S^3} \sim \frac{T^4}{l^6} \sim U^6$$

Thus the perceived sound levels are a strong function of disc loading. Although demonstrated here for the broad band case, the general features of the results apply equally to the discrete frequency components. The arguments have interesting consequences. Firstly, it will be seen that rotors of any scale are predicted to sound as loud as each other provided disc loading (or velocity) is the same. It therefore appears that some empirical design predictions of noise from large thrust rotors may have been over-conservative, and also that a scale model rotor will sound as loud as the real thing. Secondly, it will be seen that increase of scale at constant thrust has a major benefit on noise. This is equivalent to a reduction in velocity. For either parameter the variation is as the (\pm) eighth power.

These arguments are based on very rough power law approximations both to the sound intensity laws and to the subjective response. More detailed examination has therefore been carried out on a general rotor noise prediction programme at Loughborough University of Technology. The programme includes both a full discrete frequency calculation based on equation 2 and a broad band noise calculation based on the empirical results of Figure 7, and includes many additional detail features which will not be discussed here. This programme will be described in a later document. Results shown here are given in PNdB⁴⁷, which is a more elaborate subjective response scale essentially equivalent to the frequency weighting curves of Figure 10.

Two results are shown here. Figure 11 gives the effect of variation of scale for a two-bladed rotor at a constant disc loading of 4 lb/ft² (191 N/m²). Non uniformities in the curve are caused by non-linearities in the PNdB function, especially the low frequency cut-off. Nevertheless, over a scale range of 20:1 PNdB levels vary by less than ± 3 dB from the mean value. Note that thrust would vary by 400:1 over this range.

Figure 12 demonstrates the effect of variation of scale at a constant thrust of 10,000 lb (4550 kg). A dramatic reduction in noise ensues as scale is increased or tip velocities reduced roughly as the eighth power predicted. At higher Mach numbers the reduction is even more pronounced. Choice of large size low tip speed rotors must impose many problems on the designer, but it is hoped that this curve will suggest that these problems justify study in order to minimise rotor noise output.

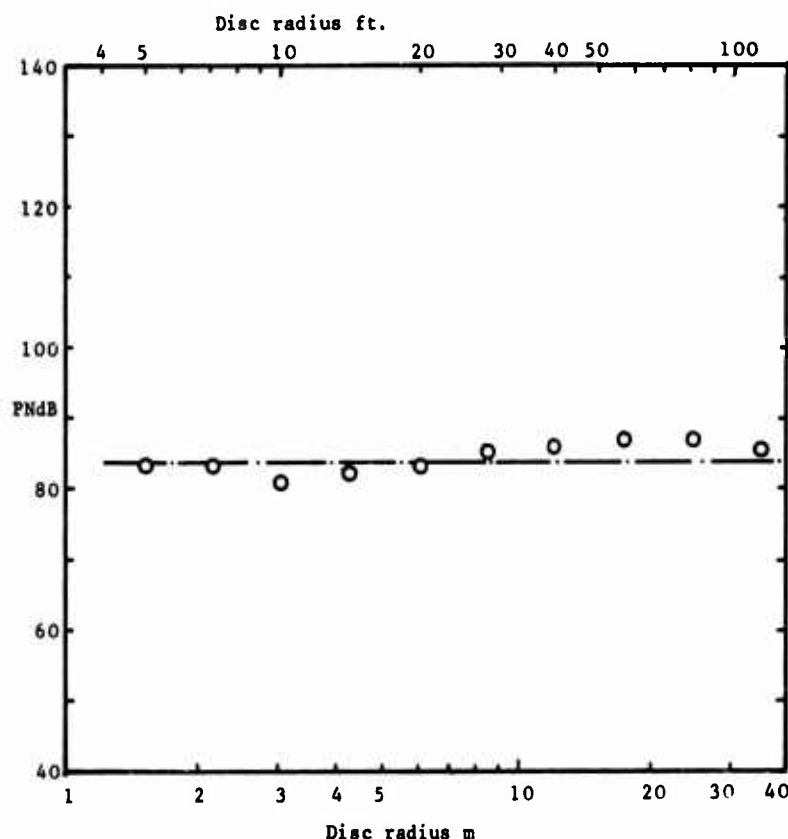


Figure 11: PNdB vs Scale for constant disc loading

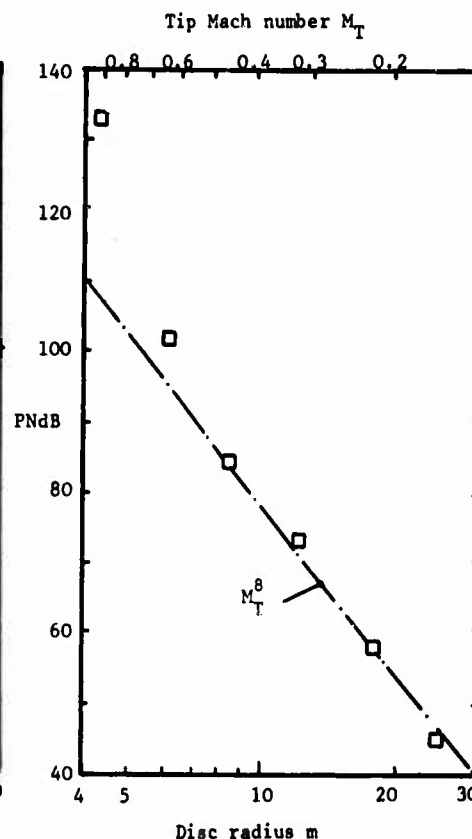


Figure 12: PNdB vs Scale for constant thrust

3.2 Detail improvements

For helicopter rotors there appears to be some genuine hope that detail variations can have useful effects on noise. As has been discussed, there appear to be three main sources of noise from a rotor: inflow distortion, inflow turbulence and tip effects. On a rotor each of these is fundamentally controlled by the rotor vortex system. This may well be sensitive to detail modifications.

Jones⁴⁸ and others have demonstrated how the tip vortex from a helicopter rotor can actually move upwards as it moves away from the blade, and frequently passes above the following blade. Direct interaction of a blade with a vortex is a known cause of blade slap as discussed by Leverton⁴³ and, more recently, by Widnall⁵⁰. Blade slap will not be considered in any detail here since it is an excessive noise, unlikely to be tolerated when noise is a problem. Also it appears that it can be substantially controlled by operating procedures. However, there can be little doubt that more moderate blade vortex interactions are a prime cause of noise problems, so that the rotor noise problem can perhaps be regarded as a problem in mild blade slap.

The noise radiation is reduced by reducing the aerodynamic fluctuations. This involves minimising vortex strength and maximising its distance from the following blade. Several workers have reported attempts to reduce vortex strength^{51,52}, normally via tip modifications. These have had mixed success when applied to flight hardware. On the other hand, there has been comparatively little attempt to reduce noise by increasing blade-vortex separation. Calculation of shed vortex paths should, in principle, be possible, and some success has been reported⁴⁸. Close to the blade the vortex paths must be a strong function of the loading distribution, and it should be possible to find loading distributions which maximise vortex separation from the following blade, particularly for multibladed rotors. Equally the rate of roll-up of the vortex must also be a function of blade loading. Thus renewed attack on the rotor vortex wake problem from the noise viewpoint appears to have useful potential.

When considering vortex wakes it is important also to consider non-ideal conditions such as that of wind and unfavourable manoeuvres. The increase in noise level due to wind is well documented, but comparatively little substantive data is available. Most useful existing rotor noise data have been carefully taken under calm conditions. However, it is clear that reduction of rotor noise under ideal conditions may result in comparatively little benefit for practical rotorcraft operating in a real atmosphere. Reduction of the wind induced rotor noise level is a major problem facing the designer, and fuller data on this is certainly desirable.

Much of the existing work on rotor noise control has concentrated on tip modifications^{23,51,53}, and benefits of over 6dB are often reported. On the other hand, these benefits are not always found in flight, or in repeat tests at other centres. Leverton⁵⁴ for instance found an increase in noise for most tip modifications tested. It has been argued here, via Figure 9, that the tip effects are specific to the high frequencies. Strouhal scaling these results up to a helicopter suggests that the effect will be centred around 2000Hz.

From tower tests on a rotor, Leverton⁵⁵ has defined a second broad band hump in this region. In the author's opinion this hump is due to tip effects, and represents the modulated swishing sound observed on helicopters. In this context it is noteworthy that experiments by Schlegel²³ on trapezoidal tips reduced the depth of modulation of the broad band noise as well as the absolute levels. Maximum modulation might be expected from tip sources when Doppler changes in frequency, and in near field amplitude, would be at a maximum. Further experiments on a wide range of tips have recently been reported by Leverton⁵⁶. Variations of level of up to 15dB due to tip modifications are found, but the optimum tip is a function of rotor r.p.m., and a strong function of blade pitch. Noise benefit was also found to be a strong function of pitch in the recent tests at Loughborough³².

Leverton's recent results show little benefit of a clipped trailing edge, in contrast to that shown in Figure 9. This may be due to the relatively thick (12%) sections used in his tests compared to the thinner (5%) sections of Figure 9.

The one clear conclusion from all these studies is that tip shape does have a major effect on rotor noise. The reasons for the effect must lie in the varying structures of the shed vortex from each tip. Systematic understanding of this does not exist, and represents an obvious area of profitable research. Meanwhile it is clear that rotor noise control programmes must include empirical evaluation of various tip shapes, preferably at full scale.

A major source of subjective annoyance from helicopters is the tail rotor. The general considerations for rotor noise radiation apply equally to tail rotor noise. The tail rotor typically operates in inflow which is badly distorted by the proximity of the tail boom and by the action of the main rotor. This must result in severe increases of noise level, and the design modifications necessary to improve the situation are apparent. A longer tail boom should add little to helicopter weight, and give a useful noise benefit. From the noise point of view alone a canted front anti-torque rotor would be preferable, but presumably this would not be acceptable on operational grounds. Note that the asymmetry caused by forward flight of the rotor would not directly generate significant noise loads. This is because the asymmetry causes a first order input mode at the rotor which is of extreme inefficiency, as shown by Figure 2.

A final consideration is the effect of blade number. Tower tests normally demonstrate lower levels of noise for high blade numbers. The effect is probably due to the increased disc loading producing increased rotor downwash. This carries the vortex wakes clear of the following blades before significant roll-up can occur. However, theory shows that, at a constant (low) disc loading, a reduced number of blades should give reduced noise. This is because with fewer blades each must be larger in chord. Increased cancellation of fluctuating pressures will then occur over the blade surface. Sears⁴⁵ theory indicates a reduction in level of 3dB for every doubling of chord. Blade number tests normally involve differing numbers of the same blades and would not demonstrate this effect. Indeed an increase in broad band level would occur for fewer blades at the same overall thrust because of the increased blade loading (see Figure 7). Experiments directly evaluating blade chord effects are required to test this concept. A further advantage of such tests would be the possibility of examining the Strouhal scaling of the broad band noise usually assumed.

4. CONCLUSIONS

From the historical survey two morals can perhaps be drawn. Firstly, that the intelligent human observer can produce information of considerable value without complicated instruments. Secondly, that ground rig tests are a poor substitute for full scale data. The principal theoretical difficulty in the early work was the correct choice of boundary conditions to represent the acoustic source on the blade. This difficulty persists to the present day, now in the guise of the dipole/quadrupole source model for the noise.

However, as a result of experimental, theoretical, and empirical work the fundamental causes of rotor radiation are reasonably clear. They are

1. Discrete frequency noise, due to distorted inflow
2. Low frequency broad band noise, due to turbulent inflow
3. High frequency broad band noise due to the tips.

Except for high speed rotors ($M_T > 0.7$) the Gutin noise radiated by the steady forces on the rotors is not of subjective importance. Also it appears that any trailing edge vortex noise generation mechanisms are of minor significance.

Thus rotor noise control is simply a matter of minimising distorted and turbulent inflow, and empirically finding an optimum tip. Similarly noise prediction requires specification of the distorted and turbulent inflow to the rotor. The problem therefore passes from the acoustician to the aerodynamicist. Unfortunately the steady aerodynamics problems involved are extremely complex. However, they centre around the shed vortex structure, and there is some prospect that improved understanding of this is possible. In general terms, subjective levels of rotor noise are shown to depend on blade loading to the fourth power or velocity to the eighth. This shows that rotors of equal blade loading will have roughly equal subjective noise levels at any scale, and that there is substantial benefit to be gained from a low tip speed large scale rotor.

The key to future rotor noise control appears to lie in the understanding gained by careful experiments. There are several areas of uncertainty at present which justify study. Detailed correlation of ground and flight tests does not yet seem to have been performed. The noise effects of characteristic manoeuvres and of typical wind levels are not fully known, and may limit the possibilities for rotor noise reduction on real aircraft. The benefit of increased blade chord predicted theoretically also justifies some experimental study. Possibilities for noise control seem to centre around a full understanding of the shed vortex wake. Both experimental and theoretical approaches to this problem would be valuable. The most obvious area for study is the effect of tip shape, and blade loading distribution, on the wakes and noise of a rotor.

REFERENCES

1. Mach E. Pogg Ann Vol 112, p 66, 1861, and Vol 116, p 333, 1868
2. Rayleigh, Lord "The Theory of Sound", 2nd Ed. Dover, N.Y., 1945
3. Director of Research "The Sounds of Aeroplanes", A.R.C., R & M 694, October 1920
4. Lynam E.J.H. and Webb H.A. "The emission of sound by airscrews" A.R.C. R & M 624, March 1919
5. Bryan G.H. "The acoustics of moving sources with application to airscrews" A.R.C. R & M 684, March 1919
6. Hart M.D. "The aeroplane as a source of sound" A.R.C. R & M 1310, May 1929
7. Davis A.H. "Silencing aircraft", A.R.C. R & M 1542, September 1932
8. Kemp C.F.B. "Some properties of the sound emitted by air screws" Proc. Phys. Soc. Vol 44, pp 151-165, 1932
9. Paris E.T. "A note on the sound generated by a rotating airscrew" Phil. Mag. Vol 13, No 82, pp 99-111, 1932 (see also Phil. Mag. Vol 16, p 60, 1933)
10. Gutin L. Ya "On the sound field of a rotating propeller" from Phys. Zeit Sowjet Band A, heft 1, pp 57-71, 1936, Translated as NACA TM-1195, October 1948 (see also J. Applied Physics, Leningrad, Vol 6, pp 899-909, 1936, in A.R.C. Rep 3114, 1946)

11. Lamb H. "Hydrodynamics", 6th Edn, Dover, N.Y., 1945.
12. Stowell E.Z., and Deming A.F. "Vortex noise from rotating cylindrical rods", NACA, TN 519, 1936
13. Yudin E.Y. "On the vortex sound from rotating rods", Zh. Tekh. Fiz. Vol 14, No. 9, p 561, 1944, Translated as NACA TM 1139, March 1947
14. Von Wittern W.W. "The relation between vortex noise and wind resistance", CADO Tech. Data Digest, Vol 16, pp 20-23, September 1951
15. Billing H. Modern aeronautical acoustics, A.V.A. Monographs R 1-3, Reports and Translations 960, 1947
16. Hicks C.W. and Hubbard H.H. Comparison of sound emission for two-blade, four-blade and seven-blade propellers, NACA TN 1354, July 1947
17. Hubbard H.H. and Regier A.A. "Propeller-loudness charts for light aeroplanes", MACH TN 1358, 1947
18. Hubbard H.H. "Sound from dual-rotating and multiple single rotating propellers" NACA TN 1654, 1948
19. Hubbard H.H. and Regier A.A. Free-space oscillating pressures near the tip of rotating propellers, NACA Report 996, 1950
20. Hubbard H.H. "Propeller-noise charts for transport airplanes", NACA TN 2968, June 1953
21. Hubbard H.H. and Maglieri D.J. "Noise characteristics of helicopter rotors at tip speeds up to 900 feet per second", J. Acoust. Soc. Amer., Vol 32, pp 1105-1107, September 1960
22. Taylor G.I. "The singing of wires in a wind", Nature, Vol 63, P 536, 1924
23. Schlegel R.G., King R.J. and Mull H.R., "Helicopter rotor noise generation and propagation", USA AVLABS Tech. Rep. 66-4, October 1966
24. Lawson M.V. and Ollerhead J.B. "A theoretical study of helicopter rotor noise" J. Sound Vib., Vol 9, pp 197-222, March 1969 (see also USA AVLABS TR 68-60)
25. Wright S.E. Sound radiation from a lifting rotor generated by asymmetric disc loading, J. Sound Vib., Vol 9, pp 223-240, 1969
26. Lawson M.V. "Theoretical analysis of compressor noise", J. Acoust. Soc. Amer., Vol 47, No 1 (Pt 2), pp 371-385, (see also NASA CR 1287)
27. Barry B. and Moore C.J. Subsonic fan noise, J. Sound Vib., Vol 17, pp 207-220, 1971
28. Tanna H.K. and Morfey C.L. "Sound radiation from point sources in circular motion", J. Sound Vib., Vol 16, pp 337-348, June 1971
29. Leverton J.W. "Noise of rotorcraft", Westland Aircraft, RP 365, March 1969
30. Kramer M. "The aerodynamic profile as acoustic noise generator", J. Aero. Sci., Vol 20, p 280-282, 296, April 1953
31. Sharland I.J. "Sources of noise in axial flow fans", J. Sound Vib., Vol 1, No 3, pp 302-322, 1964
32. Lawson M.V., Whatmore A., and Whitfield C.E. "Source mechanisms for rotor noise radiation", Loughborough University of Technology Rep. TT 7202, March 1972
33. Tu B.J. "Experimental investigation of turbulent velocities in a subsonic circular jet", Wyle Laboratories WR 70-2, February 1970
34. Hoffman J.D. and Velkoff H.R. "Vortex flow over helicopter rotor tips", J. Aircraft, Vol 8, pp 739-740, September 1971
35. Widnall S.E. "A correlation of vortex noise data from helicopter main rotors" J. Aircraft, Vol 6, No 3, pp 279-281, May-June, 1969
36. Brown D. and Ollerhead J.B. Propeller noise at low tip speeds, US Air Force Aero Propulsion Laboratory, AFAPL-TR-71-55, 1971
37. Davidson I.M. and Hargest T.G. "Helicopter noise", J. Roy. Aero. Soc., Vol 69, pp 325-336, May 1965
38. Deming A.F. Noise from propellers with symmetrical sections at zero blade angle I NACA TN 605, 1937, II NACA TN 679, 1938
39. Lighthill M.J. "Sound generated aerodynamically, Bakerian Lecture 1961", Proc. Roy. Soc. (London) A, Vol 267, pp 147-182, 1962
40. Lyon R.H. "Radiation of noise by aerofoils that accelerate near the speed of sound", J. Acoust. Soc. Amer., Vol 49, pp 894-905, March 1971
41. Lighthill M.J. "On sound generated aerodynamically - I: General Theory", Proc. Roy. Soc., A, Vol 211, pp 564-587, 1952
42. Ffowcs-Williams J.E. and Hawkings D.L. Theory relating to the noise of rotating machinery, J. Sound Vib., Vol 10, No 1, pp 10-21, 1969
43. Ffowcs-Williams J.E. and Hall L.H. Aerodynamic sound due to a source near a half-plane, J. Fluid Mech., Vol 40, pp 657-670, 1970

44. Heller H. and Widnall S.E. The role of fluctuating forces in the generation of compressor noise, NASA CR 2012, 1972
45. Sears W.R. Some aspects of non-stationary airfoil theory and its practical application, J. Aero. Sci., Vol 8, pp 104-108, 1940
46. Lowson M.V. "Noise radiation from V/STOL Aircraft", Paper 72-22, ICAS Meeting, Amsterdam, 1972
47. I.S.O. Recommendation R507, "Procedure for describing aircraft noise around an airport", 2nd Ed. 1970
48. Jones J.P. "Rotor aerodynamics, retrospect and prospect", Paper I AGARD Adv Rep 13, September, 1967
49. Leverton J.W. and Taylor F.W. "Helicopter blade slap", J. Sound Vib., Vol 5, pp 50-80, January 1967
50. Widnall S.E. "Helicopter noise due to blade-vortex interaction", J. Acoust. Soc. Amer., Vol 50, p 354, July 1971
51. Spencer R.H. et al "Tip vortex core thickening for application to helicopter noise reduction", Vertol Division, The Boeing Co., USA AVLABS Technical Report 66-1, September 1966
52. Spivey W.A. and Morehouse "New insights in the design of swept tip rotor blades", 26th Forum of Am. Hel. Soc., 1970
53. Hickey D.H. "Some developments in noise reduction in ducted propellers and fans", pp 104-119, in Rep. FAA No. 69-1, January 1969
54. Leverton J.W. "The sound of rotorcraft", The Aeronautical Journal, Vol 75, pp 385-397, June 1971
55. Leverton J.W. "Helicopter noise" in AGARD Conf. Proc. No. 31, June 1968
56. Pollard J.S. and Leverton J.W. "Effect of blade tip planform on the noise and aerodynamics of a helicopter rotor", Westland Helicopters, RP 414, April 1972
57. Ollerhead J.B. and Lowson M.V. "Problems of helicopter noise estimation and reduction", AIAA Paper 69-195, February 1969
58. Lowson M.V. "The sound field for singularities in motion", Proc. Roy. Soc., A, Vol 286, pp 559, 1965

APPENDIX: SUPPLEMENTARY BIBLIOGRAPHY OF EARLIER WORK ON PROPELLER NOISE

1. Fage A "An experimental study of the vibrations in the blades and shaft of an airscrew", Proc. Roy. Soc. A, Vol 107, pp 451-469, 1925
2. Stowell E.L. and Deming A.F. Noise from two-blade propellers, NACA TR 526, 1935
3. Ernsthausen W. The source of propeller noise, NACA TM 825, May 1937
4. London A. Principles, practice and progress of noise reduction in airplanes, NACA TN 748, January 1940
5. Deming A.F. Propeller rotation noise due to torque and thrust, NACA TN 747, 1940
6. Ernsthausen W. "Der Einfluss aerodynamischer Eigenschaften auf Schallfeld und Strahlungsleistung eine Luftschraube" Akustische Zeit, pp 245-261, July 1941
7. Shirokov M.F. The sound of a moving aeroplane propeller, Comptes Rendus Acad.Sci. URSS, Vol XLIX, No 8, 1945
8. Theodorsen T. and Regier A.A. "The problem of noise reduction with reference to light airplanes", NACA TN 1145, 1946
9. Fleming N. The silencing of aircraft, Journal of the Royal Aeronautical Soc., No 50, 1946
10. Stüper J. and Ginzel I. Airscrews, AVA Monographs H4.4-4.7, Reports and Translations 913, 1947
11. Hubbard H.H. "Sound measurements for five shrouded propellers at static conditions" NACA TN 2024, April 1950
12. Ernsthausen E.W. "Der rotierende Tragflügel als Strahlungsproblem", Z.A.M.M., pp 20-35, January/February 1951
13. Hubbard H.H. and Lassiter L.W. Sound from a two-blade propeller at supersonic tip speeds, NACA Report 1079, 1952
14. Von Gierke H.E. Physical characteristics of aircraft noise sources, Journal of the Acoustical Society of America, Vol 25, No 3, May 1953
15. Regier A.A. and Hubbard H.H. Status of research on propeller noise and its reduction, Journal of the Acoustical Society of America, Vol 25, No 3, May 1953
16. Garrick I.E. and Watkins C.E. A theoretical study of the effect of forward speed on the free-space sound pressure field around propellers, NACA TN 3018, October 1953

17. Arnoldi R.A. "Propeller noise at compressible forward flight velocities", United Aircraft Corp, M-12610-2, 1953
18. Hubbard H.H. and Lassiter L.W. "Oscillating pressures near a static pusher propeller at tip Mach numbers up to 1.2⁰ with special reference to the effects of the presence of the wing", NACA TN3202, July 1954
19. Diprose K.V. "Some propeller noise calculations showing the effect of thickness and planform" R.A.E. Tech. Note M.S.19, January 1955
20. Kurbjun M.C. "Noise survey of a 10-foot four-blade turbine-driven propeller under static conditions" NACA TN 3422, 1955
21. Arnoldi R.A. "Propeller noise caused by blade thickness", United Aircraft Corp., Rep. R-0896-1 (see also Rep R-0896-2), 1956
22. Watkins C.E. and Durling B.J. "A method for calculation of free-space sound pressures near a propeller in flight, including considerations of the chordwise blade loading" NACA TN 3809, November 1956
23. Kurbjun M.C. "Noise survey of a full-scale supersonic turbine-driven propeller under static conditions" NACA TN 4059, July 1957
24. Dodd K.N. and Roper G.M. "A deuce programme for propeller noise calculations", RAE TN M.S. 45, January 1958
25. Kurbjun M.C. and Vogeley A.W. "Measurements of free-space oscillating pressures near propellers at flight Mach numbers to 0.72", NACA Rep 1377, 1958
26. Kurbjun M.C. "Noise survey under static conditions of a turbine driven transonic propeller with an advance ratio of 4.0", NASA Memo 4-18-592, May 1959

WAKE CHARACTERISTICS OF A TWO-DIMENSIONAL ASYMMETRIC AEROFOIL

by

*Ibrahim Kavrak, Ph.D.
Boğaziçi University
Istanbul
Turkey

SUMMARY

To gain insight into the process by which dipole noise is generated by the turbulent wake behind an aerof il, the characteristics of the wake are investigated and compared to the drag and lift coefficients as well as to the noise radiated. It is concluded from the results that both the drag coefficient and the generated noise are closely related to the turbulent shear in the separated flow region. The maximum velocity defect $(U - u_{min})/U$ is shown to be an important parameter which affects both the performance and the noise intensity. The investigation was concerned only with the two-dimensional flow field.

SOMMAIRE

Pour mieux comprendre le processus par lequel le bruit bipolaire est produit par le sillage turbulent derrière une aile, les caractéristiques du sillage sont examinées et comparées aux coefficients de traînée et de levée et au bruit produit. D'après les résultats on a conclu que le coefficient de traînée et le bruit produit sont en relation étroite avec le cisaillement turbulent dans le champ de l'écoulement séparé. La vitesse déficitaire maximum $(U - u_{min})/U$ est montrée d'être un paramètre important affectant à la fois le performance et l'intensité du bruit. La recherche était limitée seulement à un champ d'écoulement bi-dimensionnel.

NOTATION

a	Sonic velocity	\bar{U}	mean velocity in the wake
b	distance to half value of maximum velocity defect	u	temporal mean velocity at a point
C_D	drag coefficient	x_i	coordinates ($i = 1, 2, 3$)
C_L	lift coefficient	Y	non-dimensional transverse distance
$C(R)$	correlation function	y	transverse distance
$K_{1,2,3}$	constants	Z	span length
L	length of separated flow	α	angle of incidence
n	frequency	α_0	flow deflection angle for $\alpha = 0^\circ$
P	sound pressure level	δ	half wake thickness
p	fluctuating pressure amplitude	ϕ	function of
q	non-dimensional velocity	ξ	maximum velocity defect
r	distance of observer from source	λ	wavelength
S	surface over which sources are correlated	ρ	fluid density
t	time	σ	a constant in the velocity profile.
U	mainstream flow velocity		

1. INTRODUCTION

The problem of broad band - or vortex - noise has long been recognized as an important factor in the design of rotary wings. The advances in manufacturing methods will make possible the use of large propellers of low rotational speeds with low rotational sound intensity, but of high tip velocities with relatively high vortex noise intensity. In such a case, the dominant source will probably be vortex noise.

It is now well established that for subsonic speeds the quadrupole field due to turbulence in the wake of an object is a much weaker source compared with the dipole field stemming from the fluctuating forces caused by vortex shedding at the trailing edge. The knowledge that vortex noise is caused by fluctuating forces may provide an adequate explanation for the dipolar nature of the noise, but does not provide for a insight into the basic cause of the noise, i.e. how the fluctuating forces are set-up in the first place.

This investigation is, therefore, mainly concerned with the mechanism of vortex noise generation, and its relation to the performance characteristics of a two-dimensional aerofoil. In particular the generated noise is related to the velocity profiles in the wake and the drag and lift coefficients. A maximum velocity defect parameter $(U - u_{min})/U$ has been defined and it is shown that the drag coefficient as well as the generated noise are functions of this parameter. In view of the wide application of variable pitch propellers and also because of the importance of stall, variations in the wake properties with angle of incidence were studied.

2. PROCEDURE

The aerofoil used in this investigation was an asymmetric high-lift section of 100 mm chord length and of 10% thickness, designated NGTE 10C4 30C50. During the experiments the range of incidence angles was -10° - $+35^\circ$, and the range of Reynolds numbers based on chord length was 4×10^4 - 2×10^5 . The sequence of the work followed was:

* Member of the Faculty of Engineering.

- a) Visual observation of the wake geometry in a water channel. The separated flow region and the turbulent wake were made visible by the hydrogen bubble technique and sequential photographs of the wake were obtained¹.
- b) Velocity profiles in the wake of the aerofoil in a wind tunnel. The transverse distribution of the temporal mean velocity in the wake was measured, using a pitot-static tube with a total pressure hole of 0.75 mm diameter.
- c) Lift and drag coefficient determination. The aerofoil blade was attached to the arm of a balance which could measure the horizontal and vertical components of the force acting on the blade, corresponding to the drag and lift forces.
- d) Fluctuating pressure in the wake. Both transverse and longitudinal distributions of the fluctuating pressure were obtained, using a miniature pressure transducer of maximum thickness 0.90 mm^{2,3}.
- e) Sound pressure level measurements. Four blades were attached to the periphery of a 1.20 m diameter disc in such a way that their spans were parallel to the axis of rotation of the disc. The radiated noise was measured by means of a microphone placed along the axis, equidistant from all blades.

3. VELOCITY PROFILES IN THE WAKE

It can be shown from the equation of motion that the velocity distribution in the wake of an aerofoil, assuming a constant eddy viscosity and neglecting the fluctuating components of velocity in the x and y directions, is represented approximately by⁴,

$$\frac{U - u}{U - u_{\min}} = \exp \{-\sigma(y/b)^2\} \quad (1)$$

where U is the mainstream velocity, u is the velocity at y ($y = 0$ at the centre of the wake), and b is the position of half the maximum velocity defect, $(U - u_{\min})/2$, measured from the centre.

Eq (1) can also be written as;

$$\frac{U - u}{U} = \xi \exp\{-\sigma(y/b)^2\} \quad (2)$$

where

$$\xi = \frac{U - u_{\min}}{U}$$

Both σ and ξ have to be determined experimentally, and correspond to the empirical constants in the profiles given by Betz, Reichardt and Schlichting⁵. The flow downstream of the aerofoil is deflected by an angle α_0 due to the camber of the aerofoil. The reference co-ordinate axes are therefore rotated by α_0 so that the

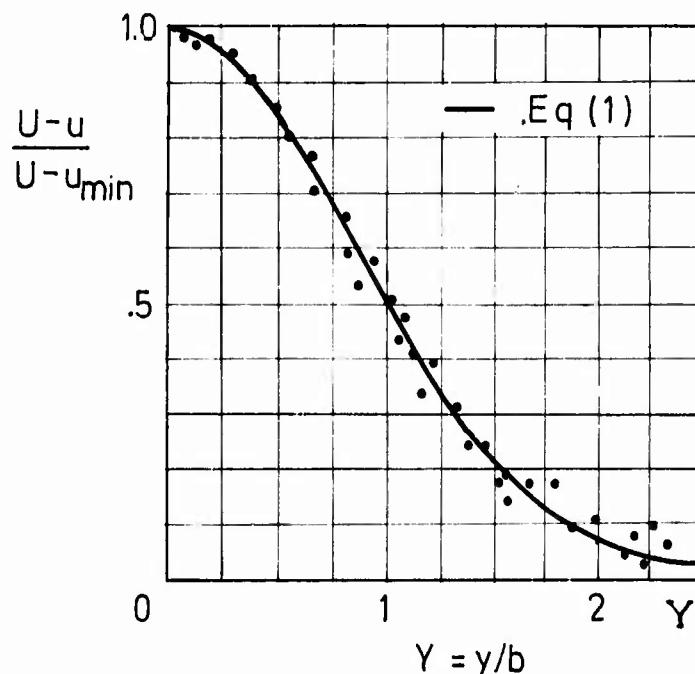


Fig.1 Non-dimensional velocity profile in the wake of an aerofoil.

x-axis approximately coincides with the centre of the wake. This modification simplifies the mathematical representation of the velocity and pressure distributions. Eq (1) and the results of experiments have been plotted non-dimensionally in Fig.1. The value of σ is found to be very nearly 0.7. Although U is a constant, ξ in Eq (2) is not, and in general is a function of the Reynolds number and the angle of incidence. The variation in ξ is given in Fig.2 together with δ , the half wake width, which is the distance from the centre of the wake to the point where $u = 0.99 U$. The half wake width is also approximately equal to $0.3b$.

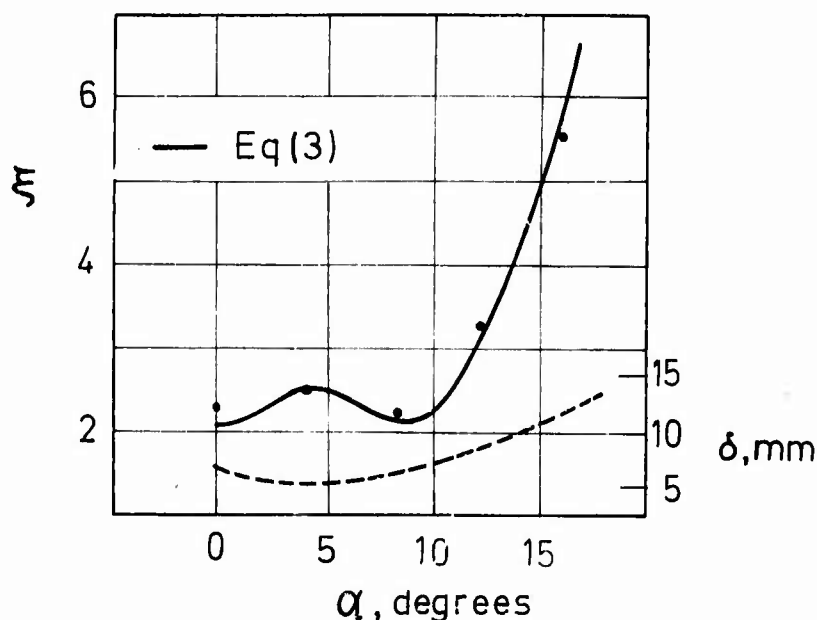


Fig.2 Variation of half wake width δ , and maximum velocity defect ξ with angle of incidence.

The maximum velocity defect can be expressed by the fitted equation

$$\xi = \phi(Re) \left[\exp \left\{ -0.2 \left(\frac{\alpha - \alpha_0}{2} \right)^2 \right\} + 0.02(\alpha - \alpha_0)^2 \right] \quad (3)$$

where α is the angle of incidence in degrees, and $\alpha_0 = 4^\circ$.

The validity of the expressions for the velocity profile and the maximum velocity defect were tested by comparing the measured drag coefficient of the aerofoil for various angles of incidence with that calculated from the above expressions

$$C_D = \frac{2}{t} \int_0^\delta \left\{ \frac{u}{U} - \left(\frac{u}{U} \right)^2 \right\} dy \quad (4)$$

where t is the blade thickness, and

$$\frac{u}{U} = 1 - \xi \exp[-\sigma(y/b)^2] \quad (5)$$

Both the computed and experimental values of the drag coefficient are shown in Fig.3 together with the lift coefficient for the same aerofoil.

The close agreement between the two sets of results confirms the validity of the velocity profile and maximum velocity defect expressions. Also seen is the drop in the lift coefficient with an increase in the maximum velocity defect, or, the drag coefficient. It is therefore clear that the maximum velocity defect is indicative of the performance of the aerofoil section. The physical explanation is that the sudden increase in the maximum velocity defect indicates the moving of the position of separation to a point near the leading edge of the blade, causing a depreciation in the circulation around the aerofoil resulting in a drop in the lift coefficient.

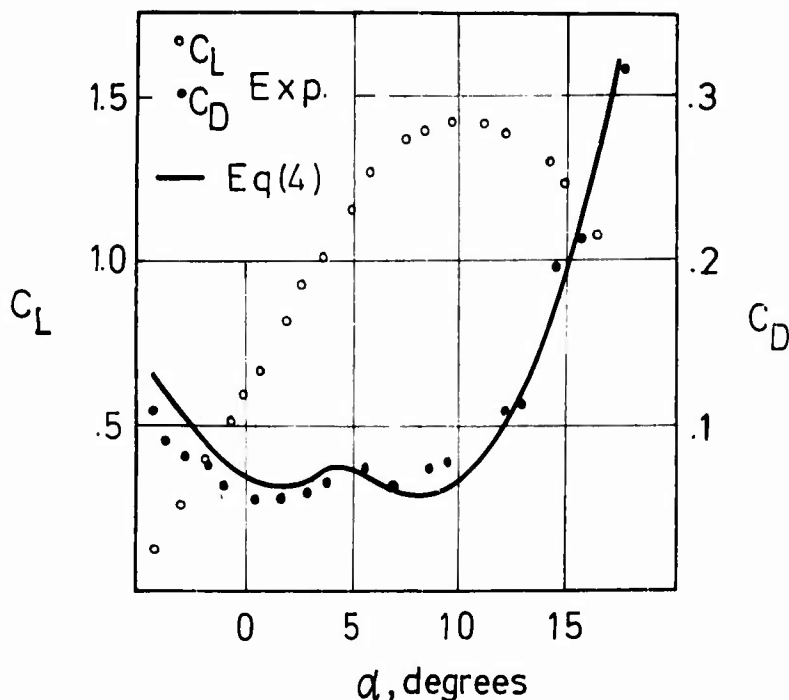


Fig.3 Lift and drag coefficients as functions of the angle of incidence.

4. PRESSURE FLUCTUATIONS IN THE WAKE

The wake downstream of the aerofoil is substantially composed of vortices mixing violently while being swept with the influence of the main flow. Some of the energy contained in the vortices is dissipated as heat, while the rest is radiated as sound.

It has been shown by Townsend⁶ that there is a strong correlation between the rate of shear and the fluctuating velocity and pressure in the wake. The gradient of the mean velocity in the wake as found from Eq (2) is

$$\frac{\partial u}{\partial y} = 2\sigma U \xi (y/b^2) \exp\{-\sigma(y/b)^2\} \quad (6)$$

or, in non-dimensional form,

$$\frac{\partial q}{\partial Y} = 2\sigma \xi Y \exp(-\sigma Y^2) \quad (7)$$

where q and Y are non-dimensional velocity u/U and non-dimensional transverse distance y/b , respectively. Since the mean amplitude of the fluctuating pressure p is proportional to $\partial q / \partial Y$, then,

$$p = K_1 \xi Y \exp(-\sigma Y^2) \quad (8)$$

or, in non-dimensional form:

$$\frac{\partial q / \partial Y}{(\partial q / \partial Y)_{\max}} = \frac{p}{p_{\max}} = K_2 \xi Y \exp(-\sigma Y^2) \quad (9)$$

where K_1 and K_2 are constants.

Eq (9) is given in Fig.4 together with the measured values of the fluctuating pressure, as obtained by the miniature transducer. The position of p_{\max} corresponds fairly well to the position of maximum shear rate, as expected. The measured values of p are greater than those predicted by theory. This is hardly surprising since the transducer measures the local fluctuating pressure, plus that radiated from nearby sources, as it is practically impossible to isolate one part of the wake from another. One correction that can be made to the theory is to include the contribution by the pressure radiation field of p_{\max} , knowing that in the near field the pressure amplitude varies with the inverse square of the distance. This is also given in Fig.4 shown with dashed lines.

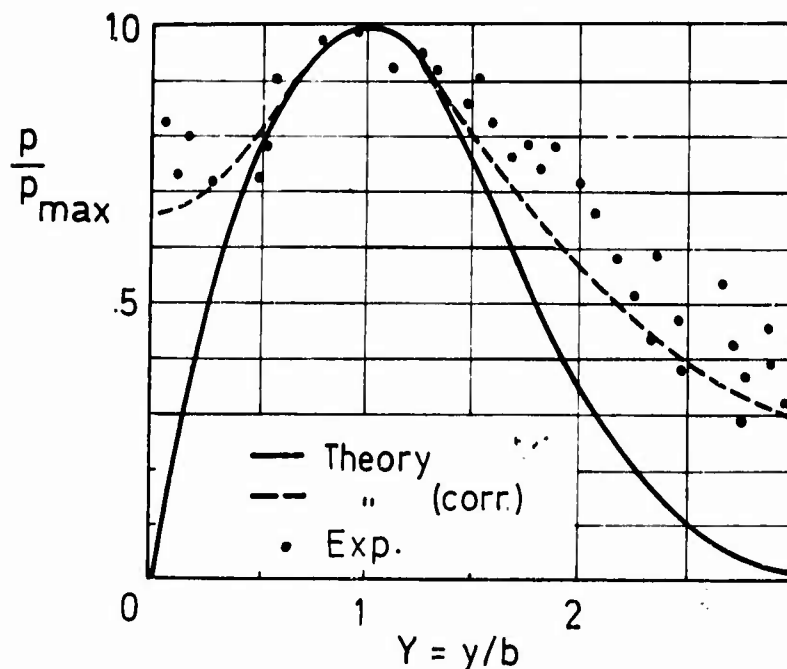


Fig.4 Transverse variation of fluctuating pressure in the wake of an aerofoil.

The above result indicates that the shear rate and the fluctuating pressure are correlated. In order to verify this, the maximum fluctuating pressure amplitude was measured for various values of the incidence angle, similar to the maximum velocity defect determination. The pressure transducer was moved across the wake until the maximum value was obtained for a given angle of incidence. The process was repeated for the whole range of the incidence angle, while the upstream velocity was held constant throughout the experiment. Fig.5 shows the variation of the non-dimensional fluctuating pressure $p_{max}/(1/2 \rho U^2)$ with angle of incidence, measured at several Reynolds numbers, together with

$$\frac{p_{max}}{(1/2)\rho U^2} = \phi(Re)Y \exp(-\sigma Y^2) [\exp\{-0.05(\alpha - \alpha_0)^2\} + 0.02(\alpha - \alpha_0)^2] \quad (10)$$

where $\phi(Re)$ is a function describing the variation with Reynolds Number.

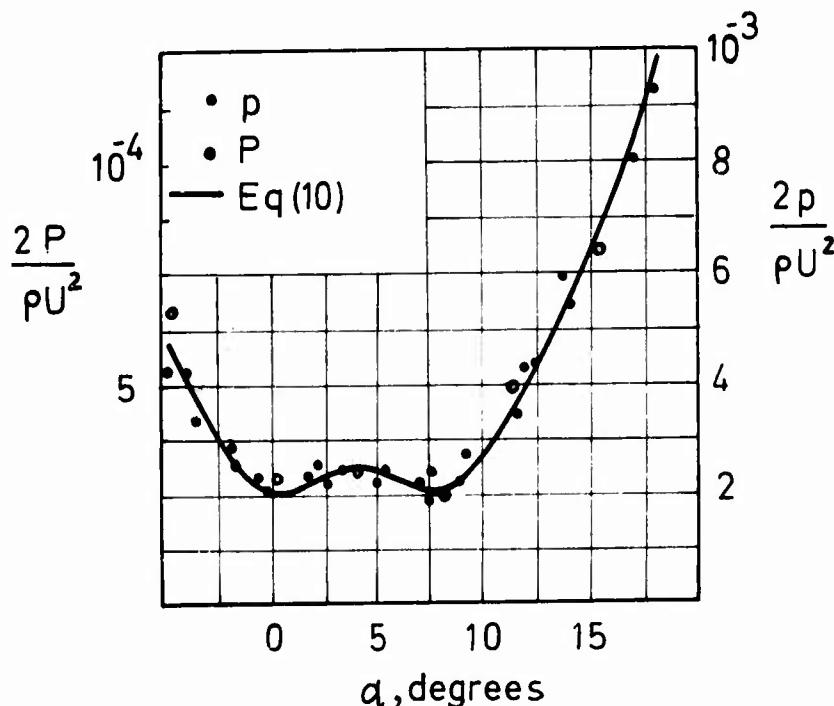


Fig.5 Fluctuating pressure p and sound pressure level P as functions of the angle of incidence.

5. NOISE FROM A SET OF AEROFOILS

The sound pressure P at a distance r from a dipole source, as found from the wave equation is

$$P = -\frac{1}{4\pi r} \int_S \frac{\partial F_1}{\partial x_1} ds \quad (11)$$

where F_1 is the dipole strength density and S is the surface over which the sources are integrated. $\partial F_1/\partial x_1$ must be evaluated at the retarded time $t - r/a$ since the sound wave takes a time r/a to reach an observer distant r from the source. For the aerofoil section used, the area S is the area on the blade surface over which the flow is separated. Therefore, the integral becomes

$$P = -\frac{1}{4\pi r} \int_0^L \int_0^Z \frac{\partial F_1}{\partial x_1} dZ dL \quad (12)$$

where Z is the span width and L is the distance from the trailing edge to the position of separation. Since the flow is assumed to be two-dimensional

$$P = -\frac{Z}{4\pi r} \int_0^L \frac{\partial F_1}{\partial x_1} dL \quad (13)$$

or

$$P = -\frac{Z}{4\pi r} \int_0^L c(R) \frac{\partial F_1}{\partial x_1} dL \quad (14)$$

where $c(R)$ is a correlation factor which is assumed to be a function of the angle of incidence and the Reynolds Number.

The vortices produced at the separated flow region and responsible for the dipole noise are not cast off regularly like, say, the Karman vortex street, but are highly irregular. Experiments with this aerofoil have shown that the non-dimensional vortex shedding frequency (Strouhal number) $n(2\delta)/U$ varies between 0.19 and 0.20, where n is the fundamental vortex shedding frequency and (2δ) is the wake width behind the aerofoil⁷.

Assuming that the vortices move with the mean velocity in the wake, the wavelength of the pressure is

$$\lambda = \frac{\bar{U}}{u} \quad \text{or} \quad \lambda = \frac{1}{n\delta} \int_0^\delta u dv \quad (15)$$

and substituting the value for the frequency n

$$\lambda \approx \frac{10}{U} \int_0^\delta u dy \quad (16)$$

also

$$\lambda \approx 10(\bar{U}/U)$$

where \bar{U} is the mean velocity.

The ratio \bar{U}/U changes between 0.82 and 0.75 for angle of incidence varying between 0° and 20° . Therefore, the wavelength corresponding to the fundamental frequency is approximately 200 mm over the range of α considered. On the other hand, the length L of the separated zone is smaller than 100 mm, the chord length.

It can be said, then, that since the wavelength of the pressure is greater than twice the distance over which it is acting, there is no change in the correlation of the dipole sources at the surface of the aerofoil while the angle of incidence is varied. Consequently, the sound pressure level of the fundamental frequency at the point r changes proportionally to the strength density p of the dipole source.

The sound pressure level P was measured by the microphone placed at the axial position of the rotating disc set-up mentioned earlier. The results are given non-dimensionally as $P/(1/2 \rho U^2)$ against the angle of incidence in Fig.5. It can be seen that the amplitude of the radiated noise changes in a way similar to that of the maximum velocity defect, again indicating the influence of the shear rate.

As further evidence for the cause of the noise, spectrographs of the fluctuating pressure and the generated noise were compared. It was found that the spectrographs are highly similar for the same values of the Reynolds number and the incidence angle. A typical spectrograph of the pressure is given in Fig.6.

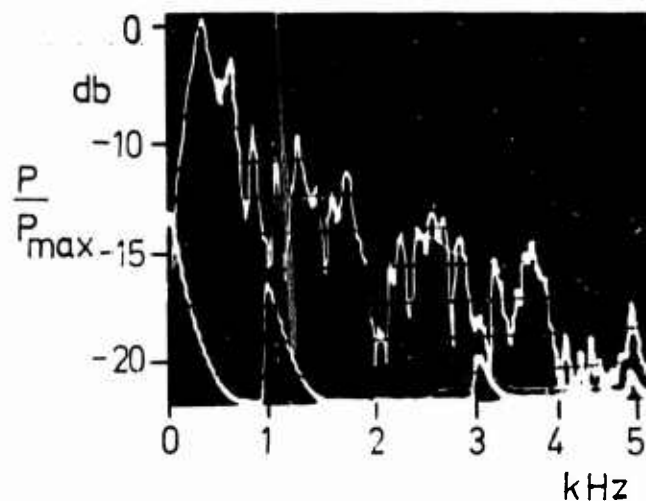


Fig.6 Spectrograph of the pressure in the wake.

6. CONCLUSIONS

It can be concluded from this investigation that

$$\begin{aligned} C_D &= \phi_1(\xi) \\ P &= \phi_2(\xi) \\ P &= \phi_3(\xi) \end{aligned}$$

These results have interesting implications. For example, the angle of incidence for minimum drag coefficient coincides with that for minimum noise generation. On the other hand, the steep increase in the noise level and the drag coefficient is followed by stall and the associated drop in the lift coefficient. The practical aspects of the results are even more interesting in that both the noise and the drag coefficient are dependent on the maximum velocity defect, which may lead to considerable reductions in experimentation with aerofoils.

7. REFERENCES

1. I. Kavrak, Boğaziçi Univ. Research Cent. Publ., Series 101, 1972.
2. B.S. Massey, I. Kavrak, J. Sci. Instr., V.43, Aug. 1966, 569-571.
3. I. Kavrak, Rev. Sci. Instr., V.41, No.5, May 1970, 628-631.
4. Y. Mori, Bull. Jap. Soc. Mech. Eng., V.3, 1959, 463-469.
5. H. Schlichting, Boundary Layer Theory, 4. Ed., New York, McGraw-Hill, 1960, 600-613.
6. A.A. Townsend, The Structure of Turbulent Shear Flow, Cambridge, Cambridge Univ. Press, 1956.
7. I. Kavrak, Proc. XI. Yug. Congr. Rat. Appl. Mech., V.11, Part 9, June 1972.

MESURES DE BRUIT D'HELICOPTERES EN VOL

par

Fernand d'AMBRA et Jean-Pierre DEDIEU
Ingénieurs à l'AEROSPATIALE
Division HELICOPTERES
13221 MARSEILLE CEDEX 1 FRANCE

et

Alain JULIENNE
Ingénieur à l'OFFICE NATIONAL d'ETUDES et de RECHERCHES AEROSPATIALES
92 CHATILLON FRANCE

RESUME

Une campagne de mesures de bruit a été faite en septembre 1971 sur plusieurs hélicoptères. Les essais, préparés en étroite collaboration avec l'ONERA, avaient pour but d'étudier le bruit de plusieurs hélicoptères dans différents cas de vols.

Pour satisfaire les objectifs de cette campagne, des techniques originales ont été utilisées et notamment un relevé de trajectoire par un système de trajectographie à l'horloge. Les dépouillements des survols sont du type "Certification acoustique des avions". Les résultats sont ramenés à des conditions standard de trajectoire et d'atmosphère dans différentes unités. Une étude de dispersion a été faite sur les niveaux maximaux et les résultats sont donnés avec un intervalle de confiance statistique. Le système de trajectographie a permis également de dater les spectres acoustiques et d'obtenir les directivités en vol des appareils complets et de quelques sources particulières.

SUMMARY

Noise measurements have been performed on several helicopters in September 1971. These tests, prepared in close connection with ONERA, were aimed toward a complete survey of helicopters internal and external noise levels in several flight conditions.

In order to satisfy the objectives of these tests, original techniques were used, in particular through precise time measuring trajectography equipment.

Data analysis of flyover tests follows conventional aircrafts acoustical certification procedure. Test results are corrected to duplicate nominal flight path and standard atmosphere conditions in several noise units.

A statistical analysis of maximum noise levels has been performed and results are presented with their confidence level.

The use of the trajectography equipment grants in addition the exact timing of acoustical spectra from which directivity patterns of noise radiated from the complete aircraft in flight and from particular noise sources can be obtained.

1. INTRODUCTION

Le bruit des avions préoccupe depuis de nombreuses années les Services Officiels et les Constructeurs, par suite de l'accroissement du trafic aérien et de la taille des appareils. En cherchant à s'introduire sur le marché civil, les hélicoptères posent à leur tour un problème de nuisance, l'intérêt de telles machines étant de pouvoir évoluer au sein même des agglomérations. Après avoir élaboré des normes acoustiques pour les avions futurs, les organismes de Certification s'intéressent maintenant aux appareils du type STOL, VTOL.

Aidée par les ministères des Transports et des Armées, la Société Nationale Industrielle Aérospatiale a entrepris un programme général d'études dans le but de réduire le bruit de ses hélicoptères. Cherchant dans un premier stade à mieux connaître les problèmes de mesure et d'analyse, ainsi que les mécanismes de génération de ces bruits, elle a réalisé, en collaboration avec l'OFFICE NATIONAL d'ETUDES et de RECHERCHES AEROSPATIALES, une importante campagne de mesures en septembre 1971 sur le terrain de La Fare-les-Oliviers, près de MARIGNANE.

Les essais ont permis d'étudier le bruit extérieur et intérieur de quatre hélicoptères dans différents cas de vols : survols, atterrissages, décollages, stationnaires. L'utilisation de chaînes de mesures télécommandées synchronisées avec un système de trajectographie, a permis d'obtenir les diagrammes de rayonnement instantanés au sol.

Après une description du matériel et des méthodes de dépouillement employées, les premiers résultats, relatifs aux survols du SA 340 sont donnés dans ce papier.

2. ORGANISATION GENERALE DES ESSAIS

Les essais ont porté essentiellement sur deux appareils, un SA 330 et un SA 340, de masses maximales respectives 6 400 kg et 1 700 kg. Quelques mesures seulement ont été faites pour deux autres appareils du type SA 316 et SA 319.

Les survols étaient effectués à 50, 100 et 150 m d'altitude pour deux vitesses différentes : vitesse de croisière économique et vitesse à puissance minimale. Chaque cas de vol était triplé pour pouvoir donner une plus grande confiance aux résultats de mesures.

.../...

Pour les atterrissages - décollages, deux pentes étaient retenues : une pente classique d'environ 10° et une pente faible du type atterrissage I. L. S. Les stationnaires étaient effectués à 10 m, 30 m, 100 m et 150 m, dans deux directions opposées.

La figure n° 1 donne un schéma de l'implantation à douze points de mesures, qui était retenue pour les mesures de bruit des survols et d'atterrissages - décollages. Chacun de ces points était équipé d'une station autonome de mesure (voir chapitre 3).

Pour les vols stationnaires, la plupart de ces stations étaient conservées, mais l'implantation était complétée par onze points de mesures, disposés sur un cercle de 50 m de rayon et reliés à un enregistreur multipiste. (Figure n° 2)

Les hélicoptères étaient également équipés de microphones à l'intérieur de la cabine et à l'extérieur près des sources prépondérantes de bruit : entrée d'air et éjection des moteurs, mécanique et rotors. Les enregistrements étaient faits sur magnétophone multipiste embarqué, synchronisé avec le magnétophone multipiste au sol.

Cette disposition de microphones sert à identifier les différentes sources de bruit en vol et d'en connaître la part relative dans le bruit global dans différents azimuts autour de l'appareil en stationnaire.

Enfin, un relevé continu de température, pression, degré hygrométrique et de vitesse du vent, était fait sur le terrain, dans le but de corrections ultérieures des résultats obtenus.

3. MATERIEL DE MESURE DE BRUIT

Au cours d'une campagne de mesures de ce type, de nombreuses évolutions sont effectuées, amenant un volume considérable de données à traiter. Il est donc indispensable, pour une exploitation rapide des mesures, de rendre automatiques à la fois les prises de son et les analyses et dépouillements.

Le matériel utilisé pendant ces essais a été développé par l'Office National d'Etudes et de Recherches Aérospatiales et par la Société Nationale d'Etude et de Construction de Moteurs d'Aviation. Il a déjà fait l'objet d'une communication au dixième Congrès International Aéronautique organisé par l'A. F. I. T. Aé (Réf. 1).

Son but est de faciliter les enregistrements sonores en des points multiples lors des essais de survol ou de point fixe et de préparer les bandes magnétiques analogiques en vue de leur dépouillement ultérieur par analyse en temps réel et traitement numérique du signal.

Nous n'en rappellerons que le principe général de fonctionnement. La figure n° 3 représente le schéma d'utilisation de cet appareillage.

Un émetteur d'ordres, constitué d'une horloge à diapason donne des ordres de mise en marche et d'arrêt pour les enregistreurs et des ordres séquentiels pour la synchronisation. Ces ordres, sous forme de tops ou trains d'ondes composés de deux signaux sinusoïdaux, modulent en fréquence un émetteur CSF.

Une sortie logique des signaux de synchronisation autorise un recalage dans le temps, avec le système de trajectographie.

Côté réception, la boîte logique reçoit d'un récepteur CSF les signaux basse fréquence qui, après décodage et temporisation vont donner naissance aux tops définitifs, normalisés pour le dépouillement automatique et qui sont insérés sur la bande magnétique dans le signal microphonique.

Cette boîte reçoit également, venant d'un adaptateur pour microphone à capacité (BRUEL et KJAER 1/2 pouce), les signaux microphoniques dont le niveau convenable peut être réglé par bonds de 10 déciBels.

Les enregistreurs utilisés sont des magnétophones monopiste du type NAGRA.

La figure n° 4 donne une vue d'une station de mesure.

4. RELEVÉ DES TRAJECTOIRES

Les trajectoires des hélicoptères ont été relevées à l'aide d'un système prototype de trajectographie à l'horloge développé par l'ONERA (Réf. 2). Le principe est basé sur la mesure des distances du mobile à un certain nombre de stations au sol, par comparaison d'un signal émis sous le contrôle d'une horloge embarquée à un signal homologue produit au sol sous le contrôle d'une horloge locale.

Les horloges équipant le mobile et les différents postes sont constituées par des oscillateurs très stables associés à des générateurs d'échelles de temps. Les échelles de temps utilisées sont constituées par des impulsions brèves à une récurrence donnée (10 Hz par exemple).

Dans le mobile, une commande d'émetteur fournit, à partir de l'échelle de temps notée H_M , des impulsions codées à un émetteur. Les signaux modulent une fréquence porteuse et les impulsions émises sont reçues au sol dans les différentes stations (3 au minimum).

Chaque station est équipée d'un récepteur et d'un décodeur qui restituent l'échelle de temps transmise H'_M .

Les échelles de temps restituées H'_M sont transmises par câbles vers un poste central qui comporte une horloge fournissant une échelle de temps H_B . Un dispositif de chronométrie détermine la position de chaque échelle de temps transmise H'_M par rapport à l'échelle de temps locale H_B .

Ces mesures permettent d'accéder aux temps de propagation de l'échelle de temps H_M entre le mobile et les différentes stations. On obtient ainsi les distances radiales à partir desquelles il est possible de calculer un point de trajectoire en coordonnées appropriées. La figure n° 5 présente le schéma de fonctionnement de ce système. La figure n° 6 montre le matériel embarqué dans l'hélicoptère.

.../...

Dans le dispositif utilisé, les distances entre les bases sont voisines du kilomètre, ce qui permet de relever les trajectoires des hélicoptères sur plusieurs kilomètres.

Les résultats sont donnés, soit en temps réel sous forme de distances radiales, soit en différé, après traitement sur ordinateur, sous forme de coordonnées X, Y, Z, dans le système d'axes de la figure n° 1, choisi pour l'ensemble des essais.

Une mesure brute permet de localiser un point de la trajectoire dans un cube d'environ 4 m d'arête. Par ailleurs, la présence d'horloges dans le mobile et les bases permet de dater des enregistrements autres que ceux de la trajectographie, par exemple les enregistrements de bruit.

Les figures n° 7 et n° 8 montrent le principe de la synchronisation utilisée pendant les essais de La Fare-les-Oliviers. Pour les survols, les tops de repérage des enregistrements de bruit sont datés par l'horloge de la station de trajectographie. Pour les vols stationnaires, les horloges sol et appareil pilotaient des codeurs de temps chargés d'inscrire l'heure sur les enregistreurs multipistes.

5. DEPOUILLEMENTS

Nombreuses sont les analyses que l'on peut effectuer sur les enregistrements d'une telle campagne : bruit global, analyse 1/3 d'octave ou analyse à bande étroite.

Nous ne parlerons ici que des dépouillements 1/3 d'octave qui ont été faits dans le cas des survols. La procédure d'analyse retenue a été celle de la certification acoustique des avions, conformément aux normes existantes. Un spectre 1/3 d'octave est donné chaque 500 ms sur lesquelles 495 ms sont consacrées à l'analyse et 5 ms au calcul. Ces analyses ont été faites à l'ONERA sur un analyseur Général Radio 1921 couplé à un calculateur CII 10020 (Réf. 1).

Ces spectres 1/3 d'octave sont corrigés d'après la courbe de réponse de la chaîne d'enregistrement et sont transmis à la SNIAS sous la forme de bandes magnétiques numériques. Là, un programme de calcul permet d'obtenir, pour un point donné, le niveau sonore global chaque 0,5 s, exprimé dans différentes unités : dBlin, dBA, dBD, PNdB, TPNdB. Pour un survol complet on peut également donner le niveau en E PNdB.

Ces résultats sont relatifs aux mesures réellement faites sur le terrain. En tenant compte des mesures de trajectographie, il est possible de ramener les résultats relatifs à un vol réel à ceux d'un vol fictif parfaitement rectiligne à l'altitude demandée. Pour cela, il faut calculer la position retardée de l'hélicoptère, c'est-à-dire la position qu'il occupait au moment où il a émis le son sur lequel on cherche à appliquer une correction de niveau. La position d'émission étant connue, le spectre est corrigé en fonction de l'absorption atmosphérique correspondant à l'écart entre la position réelle et la position théorique. Les mêmes calculs de niveaux globaux que pour les mesures directes sont effectués à partir des spectres ainsi corrigés.

Pour opérer les corrections atmosphériques, il est nécessaire de faire intervenir les caractéristiques atmosphériques, température et degré hygrométrique, observées pendant la mesure. Il est possible de ramener toutes les mesures à une atmosphère moyenne du jour de mesure.

Compte tenu de ces diverses corrections de trajectoire et d'atmosphère, il a été possible d'améliorer l'écart type sur des lots de mesures de même nature (d'environ 0,2 à 0,3 dB).

La figure n° 9 donne l'organigramme général du traitement numérique qui a été fait à partir des enregistrements magnétiques.

6. PREMIERS RESULTATS RELATIFS AUX SURVOLS DU SA 340

Tous les niveaux sonores qui sont donnés dans les paragraphes suivants sont corrigés :

- de la courbe de réponse de la chaîne de mesure
- des imperfections de trajectoire
- des fluctuations des conditions atmosphériques d'un essai à un autre, les conditions moyennes retenues étant $T = 25^{\circ}\text{C}$, $H = 34\%$

Faute d'unité bien définie pour le bruit des hélicoptères, tous les résultats sont exprimés dans les différentes unités usuelles.

6.1. Evolution du niveau global pendant le passage de l'appareil

Sur les planches 10, 11, 12 et 13, ont été tracées les évolutions du niveau global (en dBlin, dBA et PNdB) en fonction du temps, pour deux cas de vol à 50 m d'altitude.

Que ce soit sous trace ou latéralement à 100 m, il est intéressant de comparer les évolutions dans les différentes unités et pour les deux cas de vitesse d'avancement. Les variations relatives entre les différentes unités rendent en effet bien compte de l'évolution du spectre de bruit.

En approche, à 250 km/h, il y a un bruit important du rotor principal qui se traduit par un fort niveau en dBlin. Ce n'est que 2 ou 3 secondes avant le passage à la verticale que le niveau en PNdB devient plus important par suite de la participation des autres sources de bruit telles que le rotor arrière ou le moteur. La courbe d'évolution en dBA a la même allure avec une différence générale d'environ 13 dB.

Dans tous les cas, après le passage à la verticale, la décroissance est du même type dans toutes les unités, preuve qu'à l'arrière de l'appareil le bruit du rotor principal n'est plus très important par rapport aux autres sources. Nous retrouverons ces résultats sur les diagrammes de directivité.

6.2. Niveaux maximaux

La disposition des microphones permet d'avoir 7 points répartis sur 800 m le long d'une ligne perpendiculaire à la trace au sol du survol (400 m de part et d'autre).

.../...

Les points de mesure disposés sur une même parallèle au survol doivent donner les mêmes niveaux décalés dans le temps. Comme de plus les vols sont triplés, on obtient jusqu'à 12 mesures du même niveau de bruit sous trace et 9 mesures pour le bruit latéral à 100 m.

Les niveaux maximaux ont été relevés pour tous les vols et tous les points de mesure. Une étude de normalité et d'élimination de points aberrants a été faite pour chaque lot de mesures. On arrive ainsi à des écarts type de 1 dB environ et des intervalles de confiance à 90 % pour la valeur moyenne de 0,6 dB environ.

Seul le phénomène de "blade slap" vient parfois perturber ces mesures en augmentant leur dispersion. Les niveaux maximaux moyens sont portés sur les figures 14 et 15.

6.3. Champs sonores au sol

Dans les cas de vols où la dispersion sur les niveaux maximaux (sous trace par exemple) est faible, on peut faire l'hypothèse que l'hélicoptère entraîne avec lui un champ sonore constant.

Il est alors possible d'utiliser conjointement les résultats d'acoustique et de trajectographie pour restituer avec un assez grand nombre de points le champ sonore au sol (voir figures 16 et 17).

On peut également obtenir les diagrammes de directivité de l'hélicoptère en vol. Ces diagrammes ont été tracés pour une distance constante à l'appareil de 250 m (voir figures n° 18 et 19). Ces mêmes diagrammes de directivité peuvent être faits dans les mêmes conditions pour des bandes de fréquences particulières : on obtient alors les directivités des différentes sources (figure 20).

Il faut noter que ces diagrammes sont ceux des bandes 1/3 d'octave contenant les fréquences caractéristiques des sources considérées. Dans ce cas, les sources sont le rotor principal, le rotor arrière caréné et le compresseur du moteur dont les fréquences fondamentales sont respectivement 18 Hz, 1250 Hz et 8000 Hz.

Pour le rotor principal, les trois premiers harmoniques ont été pris en compte.

Ces diagrammes appellent quelques commentaires :

- quelles que soient les unités employées et quel que soit l'azimut choisi, les niveaux sonores sont plus élevés à grande vitesse d'avancement.
- il y a d'importantes variations de directivité en dBlin (donc essentiellement rotor principal) entre les vols à 250 km/h et 125 km/h.
- les directivités sont assez différentes également suivant les unités choisies. En dBlin on a une forte directivité vers l'avant. Les dBA et PNdB donnent, à un écart général près, la même directivité avec des niveaux maximaux latéralement.

Ceci s'explique aisément à l'aide de la figure 20, montrant les directivités par source.

7. CONCLUSION

Une étude détaillée des problèmes de bruit d'hélicoptères doit passer, dans un premier temps, par le stade des mesures. La campagne de La Fare-les-Oliviers aura permis, grâce à l'utilisation de matériel spécialement étudié pour les mesures de bruits aéronautiques, d'amener un grand nombre d'informations intéressantes.

Outre la connaissance des niveaux sonores des appareils, une campagne de ce type permet d'obtenir, moyennant un important traitement numérique :

- des éléments précieux pour effectuer des recoupements avec les différentes théories existantes
- une meilleure connaissance des phénomènes acoustiques particuliers aux hélicoptères

Références

1. Méthodes de mesure et d'analyse du bruit des avions en vol, par F. AUZOLLE et J. HAY
Aéronautique et Astronautique n° 33, 1972 - 1 - Pages 17 à 28.
2. Time frequency localization system applied to acoustic certification of aircraft, by Jean BESSON and Jean BOILLOT - A.I.A.A. Guidance and control conference STANFORD University - August 14-16, 1972.

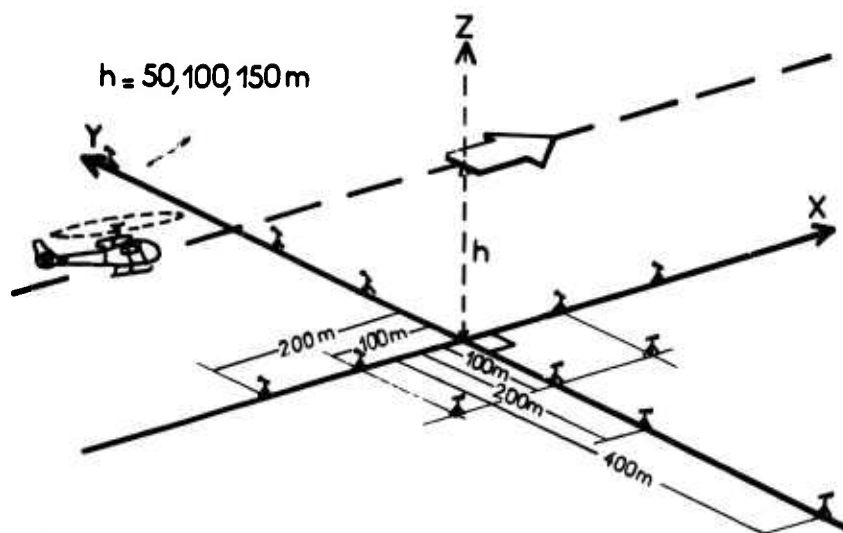


Fig 1 Implantation des microphones
pour les mesures de bruit de survol.

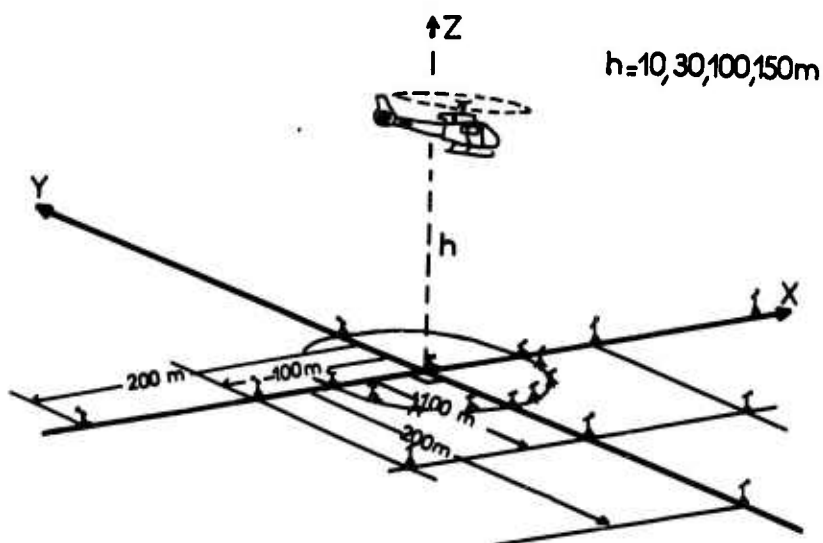


Fig 2 Implantation des microphones pour
les mesures de bruit en stationnaire.

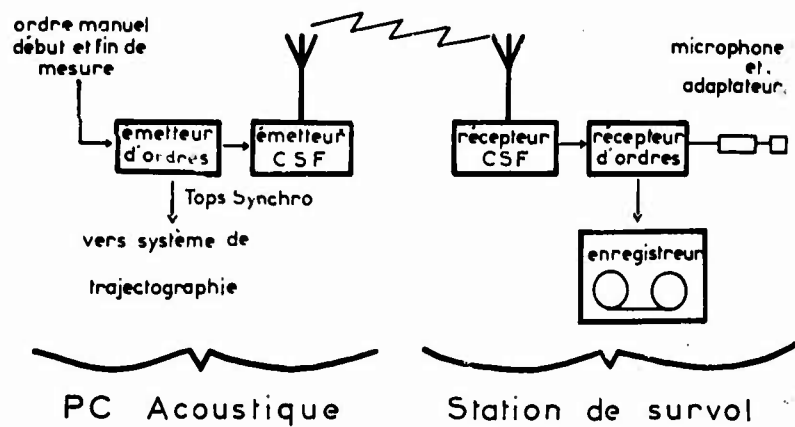


Figure 3 : Schéma de principe du matériel de mesure de bruit.



Figure 4 : VUE D'UNE STATION DE MESURE

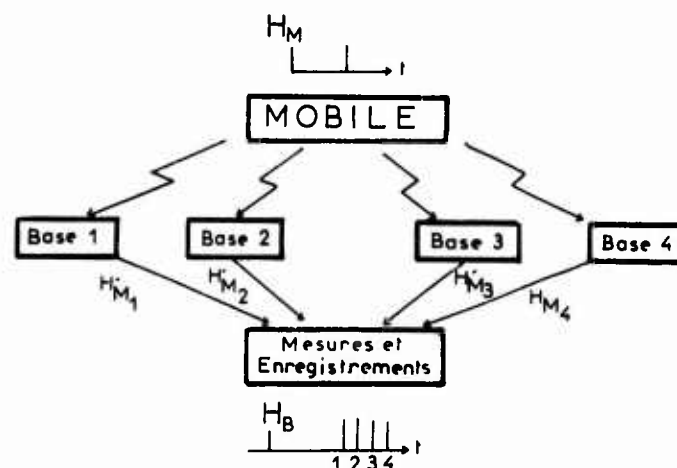


Figure 5 : Schéma de Fonctionnement du système de trajectographie à l'horloge

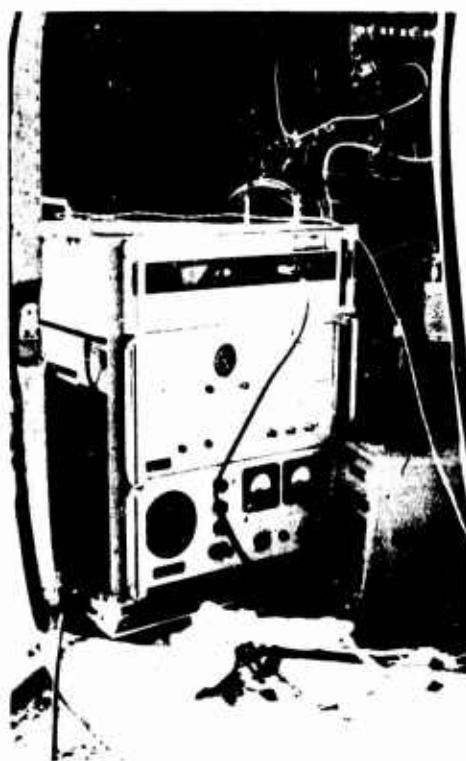
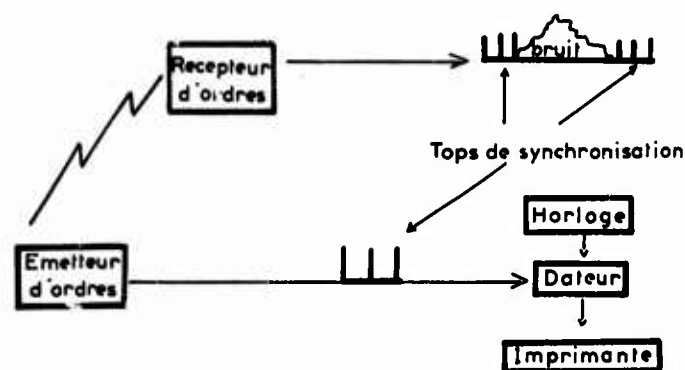
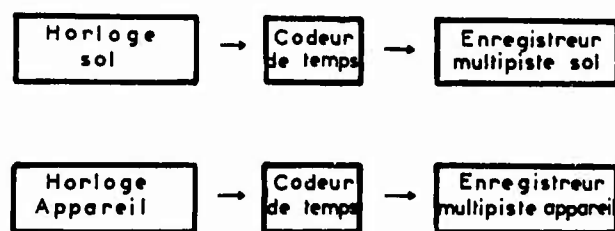


Figure 6 : VUE DE L'EQUIPEMENT DE TRAJECTOGRAPHIE A BORD DE L'HELICOPTERE



SURVOLS

Figure 7 : Synchronisation des mesures acoustiques et des mesures de trajectographie



STATIONNAIRES

Figure 8 : Synchronisation des mesures acoustiques et des mesures de trajectographie

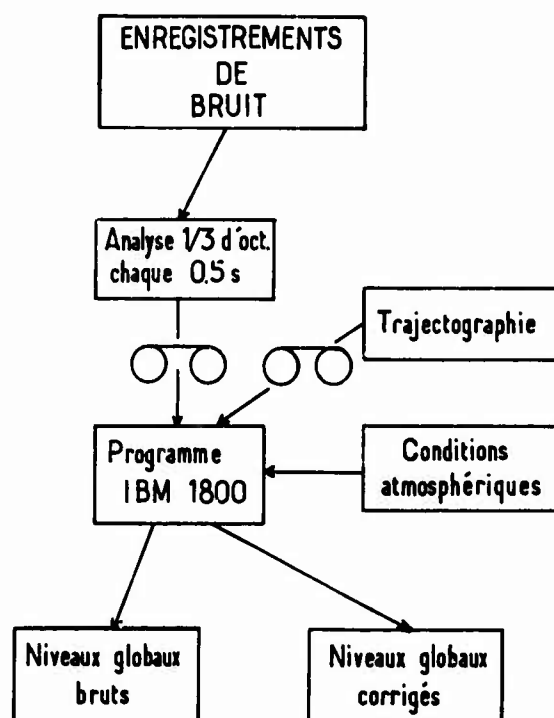


Fig 9 : Organigramme des dépouillements

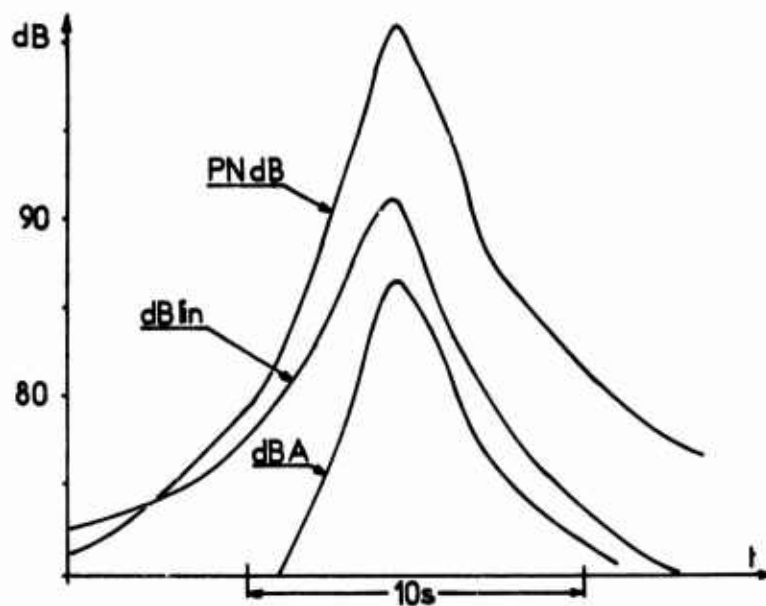


Fig 10 : Survol (50m, 125 km/h) - Mesure sous trace

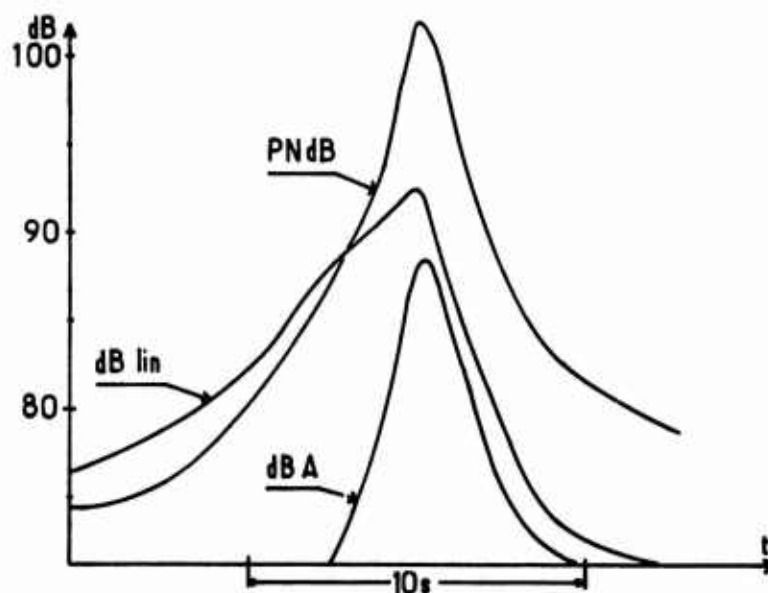


Fig 11 : Survol (50m, 250 km/h) - Mesure sous trace

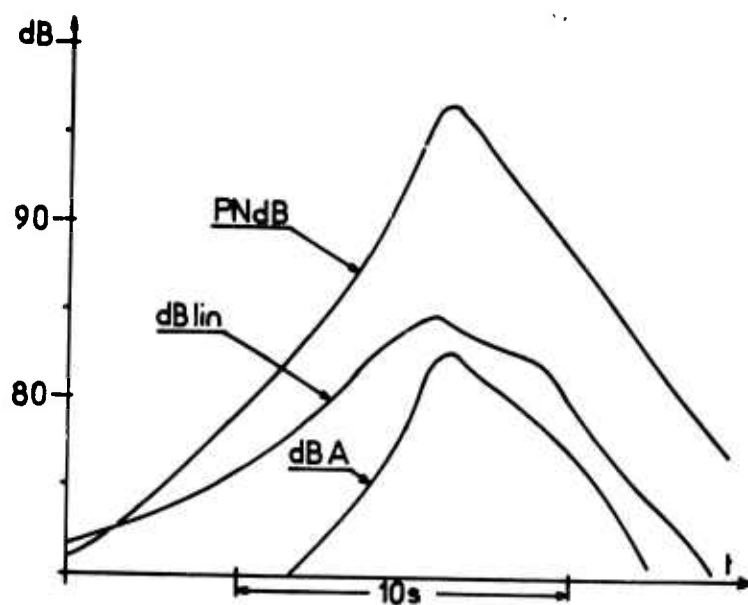


Fig 12: Survol (50m, 125km/h) - Mesure 100m en latéral

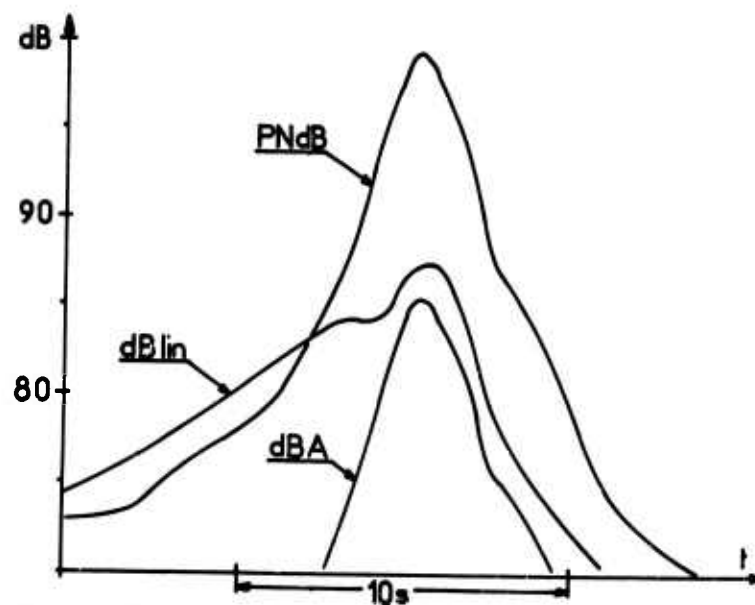


Fig 13: Survol (50m, 250km/h) - Mesure 100m en latéral

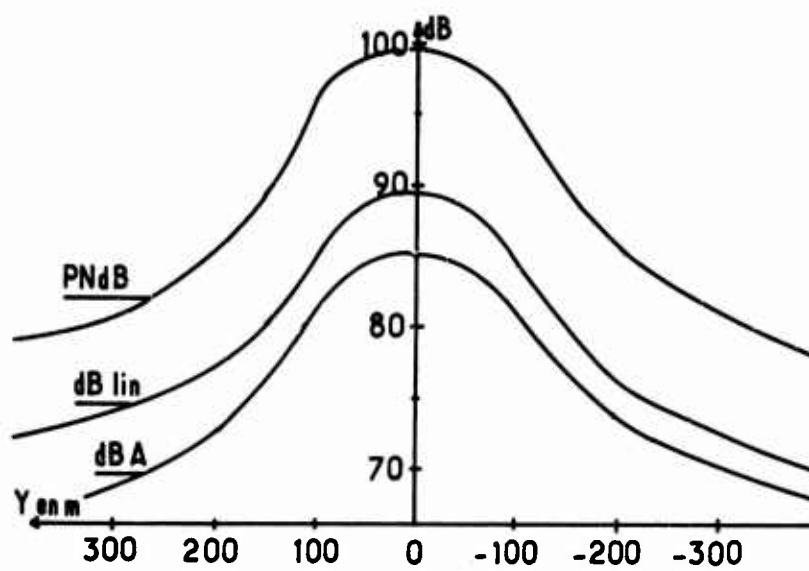


Fig 14 : Niveaux max. en survol (50 m, 125 km/h)

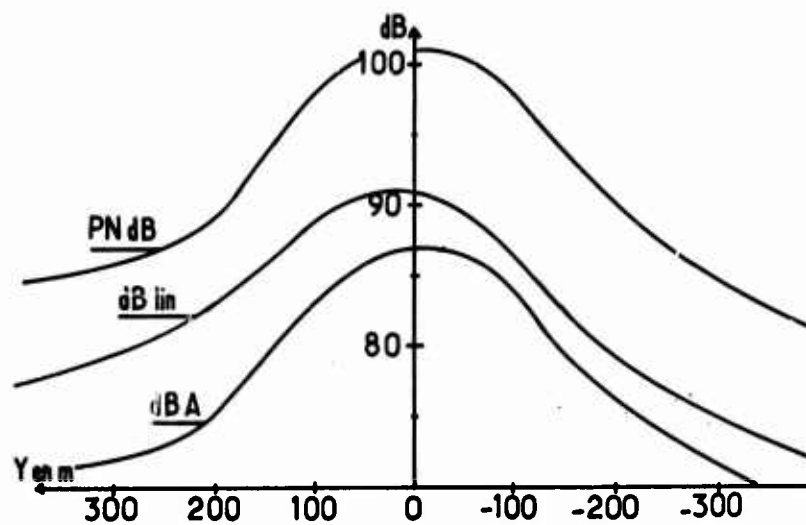


Fig 15 : Niveaux max. en survol (50 m, 250 km/h)

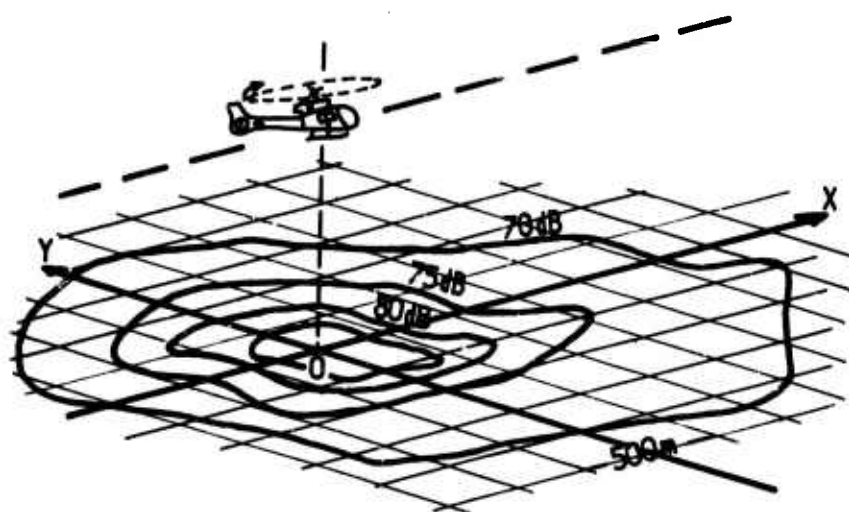


Fig 16 : Bruit au sol en dB lin (survol 50m, 125 km/h)

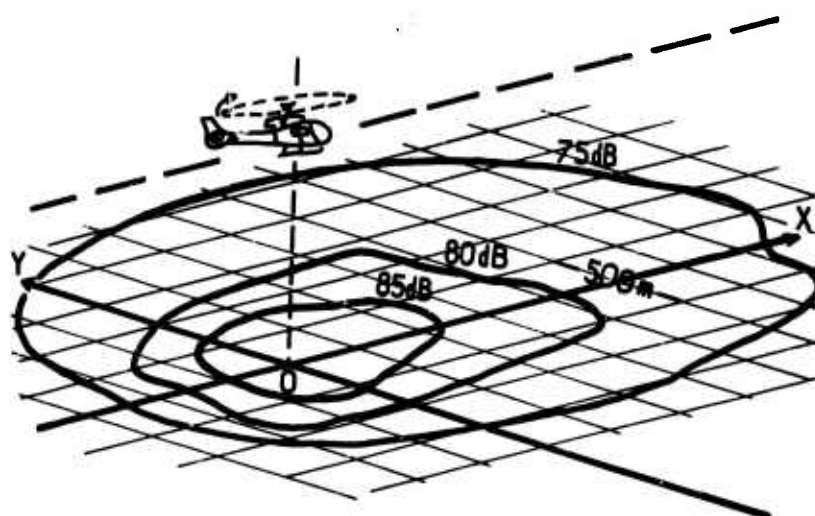


Fig 17 : Bruit au sol (survol 50m, 250 km/h) en dB lin.

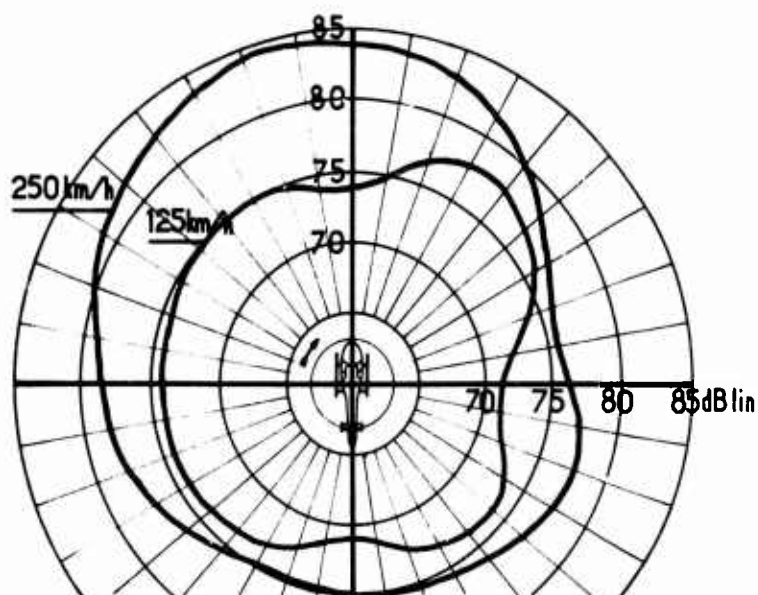


Fig 18 : Diagramme de directivité à 250m (survols à 50m)

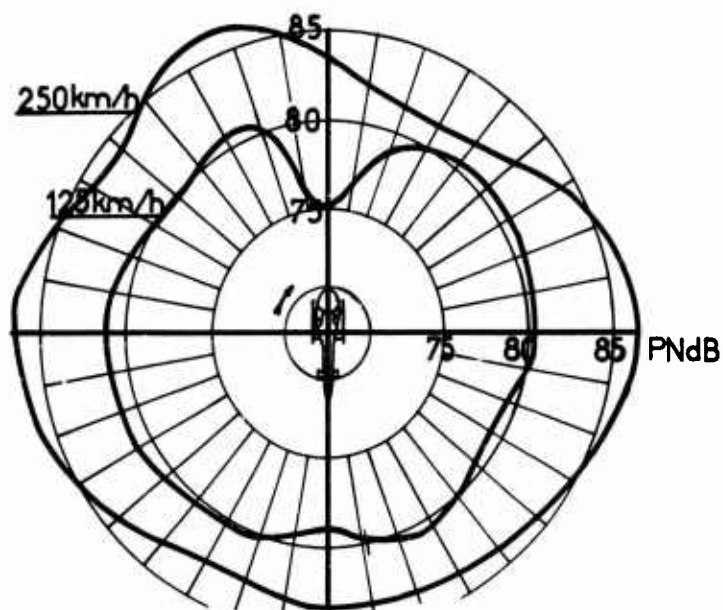


Fig 19 : Diagramme de directivité à 250m (survols à 50m)

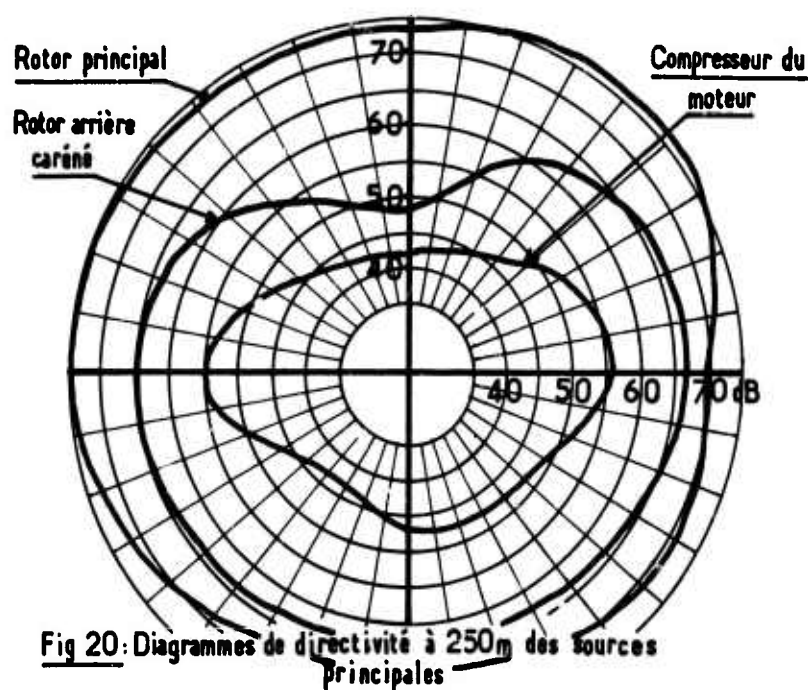


Fig 20: Diagrammes de directivité à 250m des sources principales

THE NOISE CHARACTERISTICS OF A LARGE "CLEAN" ROTOR

John W. Leverton
Head of Applied Acoustics
Westland Helicopters Limited
Yeovil, Somerset,
England

Part-Time Lecturer
Institute of Sound and Vibration Research
University of Southampton
Southampton,
England

Summary

A 2 bladed 56 ft. diameter rotor was run on a tower in an inverted mode so that the problem of recirculation and the difficulties of measuring noise directivity characteristics could be overcome. This paper outlines the analysis procedure used and presents the detailed results obtained. From a practical point of view rotor noise can be considered to consist of rotational or discrete frequency noise, low frequency broadband noise and high frequency broadband noise. The spectrum characteristics and the directivity patterns of each of these sources have been examined as a function of the blade tip speed, the total rotor thrust and the measurement angle relative to the rotor disc plane. The trends associated with the overall noise, which is dependent on the relative magnitude of the individual sources, have also been studied. These results have been compared, where possible, with the trends given by theoretical and semi-empirical prediction methods. Time history traces are also included; these show that even under ideal conditions rotor noise is impulsive in nature.

Résumé

On a fait tourner un rotor bipale de 17 m de diamètre au banc dans un mode inversé de façon à pouvoir surmonter le problème de recirculation et les difficultés relatives à la mesure des caractéristiques de directivité du bruit. La présente étude décrit dans ses grandes lignes l'analyse qui a été menée et en fournit les résultats détaillés. Du point de vue pratique, on peut estimer que le bruit du rotor se décompose en bruit rotationnel ou à fréquence discrète, en bruit à basse fréquence à large bande et en bruit à haute fréquence à large bande. Les caractéristiques spectrales et les diagrammes de directivité de chacune de ces sources ont été examinés en fonction de la vitesse en bout de pale, de la poussée totale du rotor et de l'angle de mesure relatif au plan du disque rotor. Les indications provenant du bruit global, lequel est fonction de l'importance relative des sources individuelles, ont également été étudiées. On a, dans la mesure du possible, comparé les résultats obtenus, avec les indications fournies par les méthodes de prévision théoriques et semi-empiriques. On a également tenu compte des indications accumulées dans le temps, et, il ressort de ces dernières que même dans des conditions idéales, le bruit du rotor présente un caractère très irrégulier.

1. INTRODUCTION

The understanding of rotor noise and the development of reliable prediction methods have been restricted by the lack of accurate and detailed experimental test data. In the past full scale testing has generally been carried out using either hovering helicopters, where the "noise" is a combination of main rotor, tail rotor and engine noise, or low whirl towers which are subject to ground effects and considerable flow recirculation. Occasionally high whirl towers have been used but due to the problem of mounting microphones etc, measurements appear to have been limited to one or two isolated positions. The majority of these tests have been conducted on an 'ad hoc' basis with the result that the range of test conditions on one particular configuration has usually been very limited and, because of the test layout, directivity measurements have not been possible. It also appears from a study of previous investigations, that severe limitations have been imposed on the analysis because 'off-the-shelf' noise instrumentation was simply coupled together without detailed thought being given to the practical problems involved.

To overcome these restrictions, and in particular the recirculation effects, a rotor was run on a tower in an "up-side-down" mode so that the flow from the rotor was directed upwards. To allow the directivity characteristics of the noise to be assessed a balloon supported microphone was used, together with a ground microphone array, so that measurements could be obtained on an arc at a distance of approximately 5 rotor diameters. Other microphones were positioned so that the near field noise characteristics and limited information on the attenuation of noise with distance could be assessed. A special set of recording instrumentation was designed and an analysing system was developed so that detailed narrowband analysis could be performed. The main series of tests were conducted using a 2 bladed rotor and measurements were, in general, only made when the wind speed was 2 knots or less. Thus the rotor was run in as near as possible ideal "clean" conditions. Flow visualisation tests (using smoke) were conducted to study the aerodynamic environment and these confirmed that the flow through the rotor was for all practical purposes steady and, except for the "ceiling effect" caused by the ground, the wake shapes were as expected for a hovering rotor. Similar flow visualisation studies were carried out using a single bladed rotor and, largely as a result of the stable nature of the wake, it has been possible to measure the structure of the tip vortex using a 'hot wire' anemometer (1).

The main emphasis of this 'clean' rotor study was placed on determining the noise characteristics of a 2 bladed 56 ft. diameter S55 helicopter rotor. This paper outlines the specific rotor noise sources of interest on this rotor and presents the results of the initial analysis programme.

2. ROTOR NOISE SOURCES

The noise produced by a rotor is a combination of the sounds generated by a number of individual source mechanisms. From a practical viewpoint rotor noise can be considered to consist of rotational or discrete frequency noise and broadband noise. Experimentally it is usual to define all the acoustic energy which does not show up as "peaks" on a very narrowband spectrum analysis (where the filter bandwidth is much less than the rotational frequency) as broadband noise. Although it was known that broadband noise extended over a very wide frequency region, it was thought that its spectrum was dominated by a 'peak' of energy in the 250-500Hz range at a frequency dependent on a Strouhal relationship. This study has shown that this is not the case and that in the region traditionally associated with broadband or "vortex" noise, the noise is comprised of both rotational noise components and broadband noise components. The improved measurement and analysis techniques used for this investigation have also shown that around 4kHz there is a previously undetected narrowband "hump" of random noise. Since the results for these two main broadband noise regions exhibit distinctive and well defined characteristics, they have been termed for convenience as low frequency broadband noise and high frequency broadband noise.

3. TEST PROGRAMME/INSTRUMENTATION

A diagrammatic representation of the test layout and instrumentation is shown in figure 1. The whirl tower, which is capable of being run in either direction, was fitted with a modified hub so that the blades could be run inverted. The rotor disc plane-to-ground clearance was 19 ft (5.8 m) and the ground in the vicinity of the tower was essentially flat.

The Hi-Pass filter was incorporated in the system to improve the effective signal-to-noise ratio when studying broadband noise and the Data Signal Monitoring Unit was designed to prevent overloading or underloading of the recorded signal. The FM tape recorder (AMPEX FR1300) was used to collect general data from all the microphones, while at the positions at which high signal-to-noise ratios were required recordings were also made on Nagra Direct AM Tape Recorders. For the rotational noise studies low frequency PZT microphones were used. Full details of this recording system, including the special instrumentation developed for this investigation are described in reference 2. Precise checks of "internal equipment noise" and detailed calibrations were made: these showed that with the system illustrated in figure 1 high quality recordings with signal-to-noise ratios far in excess of those normally associated with recorded signals were obtained (2).

For analysis a facility based on a Spectral Dynamics SD 101 analogue analyser was developed (2). This allows analysis with filter bandwidths of 1.5Hz, 2Hz, 5Hz, 10Hz, 20Hz and 100Hz to be obtained and plotted on long traces - for ease of reading - to a linear or logarithmic frequency base. With this facility "filtered (2Hz)-signal-to-noise-ratios" of 80dB were obtainable.

For the tests described in this paper a 2 bladed S55 rotor was used. The parameters of this rotor are summarised in Table 1 and the range of test conditions detailed in Table 2. As indicated, measurements were made over a tip speed range of 408 ft/sec (124.5m/sec) to 758 ft/sec (231 m/sec) and the total thrust was varied between zero and 5000 lbs. (2265Kg).

4. ANALYSIS PROGRAMME

Analyses of selected conditions have been carried out for all the recording positions on the 250 ft. radius illustrated in Figure 1. Except in the case of the directivity studies where information from all microphones is of interest, the initial aim was to study the characteristics directly below the rotor (B5) and in the rotor disc plane (F9). The results obtained at position B5 were, however, affected in many cases by cancellation effects and the character of the spectrum obtained from recordings made at F9 appeared to have been influenced by ground reflections. Thus the results given in this paper are based, in general, on measurements taken at B4 (75° below the rotor disc) and F7 (11.5° below the rotor disc) which are both free from ground effects. In determining the directivity patterns very detailed analyses of the recordings made at B5 and F9 have been made and, where necessary, allowances and corrections applied to the results. The values given in the paper are, therefore, as near as possible representative of results which would be obtained under 'free field' conditions.

The three main sources - rotational noise, low frequency broadband noise and high frequency broadband noise - all have distinctive and well defined characteristics. These have been examined as a function of the blade tip speed, the total rotor thrust and the measurement angle relative to the rotor disc plane. The trends associated with the overall noise, which is dependent on the relative magnitude of the individual sources, have also been studied.

5. ROTOR NOISE - GENERAL CHARACTERISTICS

Typical narrowband analysis results are shown in figure 2. Indicated on these traces are the three sources of interest together with their appropriate frequency ranges. Below 200Hz the spectrum is dominated by rotational noise which shows up as a series of "peaks" which are harmonically related to the blade passing frequency. Above 1.5kHz the spectrum is random in nature and, as can be seen from the figure, a "hump" of broadband energy occurs in the 4kHz region. This is most significant at the low lift/low tip speed conditions when it is subjectively very noticeable. In the region 150Hz to 1.5kHz both rotational noise and broadband noise are present. At the low lift/low speed conditions the broadband noise controls the spectrum, while at high lift/high speed both sources are equally important. Increases in tip speed (at fixed thrust) produce considerable increases in the level of the higher harmonic rotational noise, while increases in thrust (at constant tip speed) only nominally raise the rotational noise content. This supports the general observations that rotor noise is more sensitive to variations in tip speed than changes in thrust.

6. LOW FREQUENCY BROADBAND NOISE

6.1. Analysis procedure

As explained previously the broadband region is often a combination of broadband noise and discrete frequency noise as illustrated in figure 2. It is necessary, therefore, to study this region in detail before the level of the broadband noise can be determined. The approach used by the author involves analysing this region of the spectrum with several different bandwidth filters. When a very narrowband filter, say 2Hz, is used the spectrum is dominated by the discrete frequency "peaks" and the broadband noise forms the "troughs" or general base level. As the filter bandwidth is increased the broadband noise increases in amplitude while the "peaks" remain at essentially the same level. If this process is continued a stage is reached at which the spectrum level is solely a function of the broadband energy. When this is the case the spectrum details are unfortunately lost since the filter bandwidth is very wide. It is necessary, therefore, to select a filter bandwidth which gives a fairly accurate measure of the broadband energy, while at the same time, allowing the spectrum characteristics to be obtained. For this particular investigation it was found that a 20Hz bandwidth filter was suitable.

Typical 20Hz bandwidth results are shown in figure 3. A study of these results suggests that, although there is some indication of a 'hump' or peak, the well defined peak referred to by other investigators seems to be largely a result of the analysis methods used. Since there were no well defined characteristics, it was necessary to establish an "analysis model" before meaningful results could be obtained. A review of the results indicated that the method shown in figure 4 was appropriate. This is based on a log frequency scale and the SPL variation has a 'flat' portion and a constant dB/octave 'fall-off' portion with the latter extending over a range of two octaves. There is some indication of a fall-off in level at low frequencies, but it is not possible to define the nature of this since the noise appears to fluctuate considerably with time and to be a combination of amplitude varying discrete frequency noise and broadband noise. It is impossible to determine the centre frequency of the broadband noise "flat" and thus the "breakpoint" shown in figure 4 is of interest since it allows the frequency dependency of this noise to be studied.

A comparison of the analysis model, with the results reproduced in figure 3 shows that this model is a fair representation of the spectrum over the complete frequency range of interest.

6.2. Variation with thrust

Typical results for the low frequency broadband noise are shown in figure 5. The 'flat' sound pressure level (see figure 4) is plotted as a function of total blade thrust for the high and low tip speed conditions. Results presented are for microphones F7 and B4 which are 11.5° and 75° below the rotor disc plane respectively. It will be noted that "thrust" is presented on a log base and that the zero thrust results have been added for completeness. These results show that the noise exhibits two trends, one which decreases slightly with thrust and the other which increases at a rate of approximately T^2 . It will be observed that the "change-over point" is dependent on blade tip speed and the angle relative to the rotor disc plane. The T^2 law is the one which is usually associated with broadband noise (3,4), but to date there does not appear to be any theoretical explanation for the decrease in SPL which follows a $T^{-1/2}$ law as thrust is initially increased from zero.

It was thought that the increase in levels at high thrust may have been influenced by rotational noise components, but detailed narrowband analysis confirmed that the levels measured are those associated with broadband noise. If a single line had to be drawn through the experimental points then any law from T^0 to T^2 could have been obtained. This is the usual approach and could explain some of the discrepancies which exist between the results of different investigations. It is also of interest to note that these results show very similar trends to the generalized results compiled by Widnall (5), but in this case a curve was used instead of the 'two law' approach shown in figure 5.

6.3. Variation with velocity

The variation of the 'flat' SPL with velocity, at constant thrust, is shown in figure 6. It will be observed that the trends are less precise than those associated with the thrust variations. Near the rotor plane (microphone B4) the noise follows a V^0 law at low thrust. At high thrust the increase in level is less, except at high tip speeds when it again appears to follow a V^0 law. Below the rotor disc the variation of SPL with tip speed is nearer to a V^0 law. These values are contrary to the results of other investigators who have suggested that when thrust is held constant broadband noise varies as $V^{2(3,4)}$ or $V^{2.7(6)}$.

6.4. Frequency characteristics

As explained previously it is not possible to detect a "peak" or locate a centre frequency of the "flat" SPL. In an attempt to overcome this limitation the "break point frequency" (fig.4) has been plotted as a function of rotor speed as indicated on fig. 7. Near the rotor plane the frequency of the 'break point' is for all practical purposes independent of rotor speed and thrust. Below the rotor there appears, however, to be some difference between the high thrust and low thrust conditions. As shown on the figure the variation of "break point" frequency is more pronounced with rotor speed at high thrust than at low thrust. It is usual to assume that the broadband noise centre frequency is given by a Strouhal Number relationship which is directly proportional to the blade tip speed. Although this relationship seems to give the approximate frequency at which the maximum broadband energy occurs, the variations in "break point" frequency are independent of tip speed, except under the rotor at high thrust. This aspect obviously needs further examination since Wilkes (7) also found that the broadband noise "peak" was insensitive to tip speed.

6.5. Directivity

The directivity characteristics of the low frequency broadband noise for the conditions at the upper and lower limits of the thrust and tip speed ranges are shown in figure 8. In addition to the 'flat' SPL derived from the 20Hz analysis, the figure also shows 'peak' $\frac{1}{3}$ octave band, dBA and OASPL (dB(LIN)) values. The 'peak' $\frac{1}{3}$ octave band is typically the 315Hz band and is essentially a measure of low frequency broadband noise combined with rotational noise.

The results show the general dipole (figure of eight) shape with the minimum noise on the rotor disc plane. A "dip" in the SPL occurs directly below the rotor at high blade loading. This "dip" of about 5dB is for all practical purposes independent of the blade tip speed. The possibility that this "dip" is a result of cancellation effects directly above the rotor has been investigated and detailed analysis suggests that this is not the cause.

The directivity pattern and the absolute levels agree fairly well with those proposed by Davidson & Hargest (4) at high thrust/high tip speed conditions except in the rotor disc plane where the predicted value is zero, and under the rotor where a "dip" occurs in the measured levels. The shapes developed from theoretical considerations by Morfey & Tanna (6) also agree well with those shown in figure 8.

7. HIGH FREQUENCY BROADBAND NOISE

7.1. Analysis procedure

For the study of the high frequency broadband noise, 20Hz bandwidth analysis (figure 2) and 100Hz bandwidth analysis (figure 3) were used. Except for increased spectral details obtained with a 20Hz bandwidth filter there appeared to be little advantage in using this filter, so in order to reduce the analysis time the main emphasis was placed on 100Hz bandwidth analysis. In this context it should be noted that when analysing high frequencies, a 100Hz filter is essentially a narrowband filter. From traces of the type illustrated in figure 3, the 'hump' SPL and 'hump' frequency were determined.

7.2. Variation with thrust

The variation of the high frequency broadband noise 'hump' SPL with thrust for two tip speeds at two microphone locations is shown in figure 9. The thrust is plotted on a log-scale and, as in the case of the low frequency broadband noise, the zero thrust value is also shown. It will be observed that over the complete test range the SPL decreases with increasing thrust and follows a similar slope to the "initial portion" of the low frequency broadband noise results illustrated in figure 5. There is at the present time no explanation for this characteristic, which corresponds approximately to a $T^{-1/2}$ variation.

7.3. Variation with velocity

The velocity dependency of the high frequency broadband 'hump' is shown in figure 10 for a range of thrust conditions at two microphone locations. Except for the 14CRPM case recorded at microphone B4, the SPL values at both microphone positions follow very closely a V^4 law.

7.4. Frequency characteristics

The frequencies of the high frequency broadband noise 'hump' have been plotted against rotor speed as shown in figure 11. At B4 (75° below the rotor disc) the frequency f_H is independent of thrust and directly related to the tip speed, V_T , by the relationship $f_H = 6.5 V_T$ Hz. This "line" has been superimposed on the results for F7 (11.5° below rotor disc) and as can be seen the scatter is greater than at B4 and the 'zero thrust results' are all to one side of the mean. These results show that the 'hump' frequency is directly related to the tip speed and thus it can be considered to be dependent on a Strouhal type relationship on similar lines to that often quoted for low frequency broadband noise. In this case, however, the "peak frequency" is approximately 10 times higher than that associated with the low frequency broadband noise.

7.5. Directivity

The directivity characteristics for the high frequency broadband 'hump' are shown in figure 12 for four test conditions. This noise source takes on a completely different form to that of the low frequency broadband noise shown in figure 8. It appears that in this case the directivity pattern is comprised of two lobes which are centred on the rotor disc plane and rotor axis respectively. As indicated on figure 12 the 'minimum level' occurs at an angle of about 30° from the rotor disc and although the levels vary with conditions the general shape remains constant.

8. ROTATIONAL NOISE

8.1. Analysis procedure

Rotational noise is analysed using either 1.5Hz, 2Hz or 1% bandwidth analysers and a typical series of results obtained using a 2Hz bandwidth filter is shown in figure 2. These results were obtained using a Spectral Dynamics Analogue Analyser and although in the example shown the filter bandwidth is changed at 200Hz, the normal procedure is to analyse using the 2Hz filter up to 500Hz when studying rotational noise. The results shown in figure 2 were derived from Nagra tape recordings which effectively have a lower frequency 'out-off' at 20Hz. Thus study of the fundamental and low frequency harmonics is precluded. Use of the FM tape recorders and low frequency microphones F12 and F13 (figure 1) mean that recordings are available with low frequency limits of 2Hz but to date the main emphasis has been placed on the Nagra tape recordings.

The rotational noise study is at present in its preliminary stages and since the results are based on only a limited number of analyses they must be taken as tentative. The initial nature of this rotational noise study has precluded any investigation of the variation of the harmonic noise levels with thrust or velocity.

8.2. Harmonic content

The traces in figure 2 obtained from microphone F7 (11.5° below the rotor disc) show a rotational noise harmonic content which is representative of all positions between F7 and B3 (11.5° to 60°). In the rotor disc plane (F9) and at angles greater than 75° to rotor disc, the harmonics are less well defined even at high thrust/high tip speed conditions. As can be seen from figure 2 the rotational noise spectrum shows considerable variation with operating conditions and the scatter of individual harmonics about a "mean" is relatively large. The general "fall-off" is, however, small and on average the "mean" decay rate is between 0.5dB and 1dB per harmonic for the first 10 or so harmonics. An exception to this is at microphone F9 (in the rotor disc plane) where there is typically a 15dB difference in level between the 3rd and 9th harmonic. Above the 10th harmonic, however, they tend to "flatten out" and the spectrum takes on a form similar to those at other locations. It was originally thought that rotational noise decayed rapidly in amplitude above the 15th to 20th harmonic and that for all practical purposes higher frequency harmonics were non-existent. Narrowband analysis has shown, however, that over 50 blade passing harmonics can often be detected. The second and bottom traces on figure 2 represent such conditions and although this presentation is not suited to a study of rotational noise, harmonics in the region of 4000Hz can be seen. It is clear therefore, even from this initial analysis that the rapid "fall-off" in the level of harmonics with increasing frequency suggested by some investigators is incorrect.

8.3. Directivity

As mentioned previously there is a large scatter about a mean and thus directivity plots of individual harmonics fail to reveal any clear trend. To overcome this difficulty the measurements have been averaged over successive bands of harmonics to give the results shown in figure 13. At the microphones near the rotor disc plane, ground reflection effects combined with the random nature of the rotational noise 'peaks' has prevented any meaningful results being obtained at low lift/low tip speed conditions.

At angles of 30° and greater, the directivity characteristics are very similar to those of the low frequency broadband noise given in figure 8. Again there is a "dip" under the rotor at high thrust; this is independent of tip speed and disappears at low thrust. In the rotor disc plane the lower frequency harmonics exhibit maximum levels, while the high harmonics take on a distribution very similar to the broadband noise.

These results have been compared to the Lawson & Ollerhead method (9) and a semi-empirical approach developed by the author. The former method predicts quite well the directivity pattern, but vastly underestimates the important higher harmonics. The semi-empirical solution, which is not intended to take into account any angular variations, predicts fairly accurately the high order harmonics, while at the same time over estimating slightly the lower frequency harmonics.

9. OVERALL NOISE

9.1. Analysis procedure

The overall characteristics have been studied in terms of OASPL (dB.LIN) and dBA measurements. The majority of the analysis to date has been made from 'DIRECT-AM' (Nagra) tape recordings so the effective frequency range is 20Hz to 17kHz. Thus the fundamental note and the first few blade passing harmonics, which occur at frequencies below 20Hz, have been excluded. A comparison of a selection of these results with those obtained from the FM tape recordings - frequency range 2Hz to 20kHz - has shown, however, that the error on OASPL is for all practical purposes zero.

The overall noise level is dependent on the relative magnitude of the three individual sources and thus the most dominant source controls the overall characteristics. Although it is expected that the trends associated with the individual sources are similar on all rotors, it is thought that the relative amplitude of each source is a function of the particular blade configuration under investigation. Thus the overall noise characteristics are most likely only applicable to the rotor under consideration.

9.2. Variation with thrust

The overall noise SPL follows the same general pattern as that shown for the low frequency broadband noise in figure 5, with the SPL being on average 15dB higher than those for the 'flat' SPL. Thus as in the case of the low frequency broadband noise there is initially a decrease in level as the thrust is increased from zero. Eventually a "changeover condition" is reached, which is a function of tip speed and angle to the rotor disc plane, when the OASPL increases with increasing thrust. The thrust law of this latter portion varies between the T^2 associated with the low frequency broadband noise (figure 5) and T^3 depending on the test condition and measuring location. It is thought that this more rapid T^3 variation of SPL with thrust is due to the influence of rotational noise, particularly since it occurs at high thrust/high tip speed, but this aspect has not been investigated in detail. These results do, however, indicate that the general overall prediction formulae which are based on T or T^2 can lead to significant errors (9,4).

9.3. Variation with velocity

Again the characteristics are very similar to those of the low frequency broadband noise shown in figure 6 with the generalised laws for the OASPL being in order of V^6 at B4 (75° below the rotor disc) and V^8 at F7 (11.5° below the rotor disc). These results differ from the normally accepted formulae for estimating overall rotor noise levels, which have velocity dependencies varying from V^2 to V^6 .

9.4. Directivity

The OASPL and dBA directivity characteristics are shown on figure 8. It will be observed that in general the pattern follows closely that of the low frequency broadband noise also shown on figure 8. At low speed/zero lift condition there is an increase in noise at an angle of 27° from the rotor disc which is due to the rise in the rotational noise harmonics which occur in the low frequency broadband noise region. At high lift (3050 lbs)/low speed the overall noise exhibits a maximum at about 60° to the rotor disc; it is not clear why this occurs but it appears to be associated with high level low order rotational noise. It will be noted that although the 'flat SPL' is unaffected by this noise, the 'peak' $\frac{1}{3}$ octave band and the OASPL exhibit a similar trend. The dBA value, which is relatively insensitive to low frequency noise, smooths out this effect and follows more closely the 'flat' SPL.

Near the rotor disc plane there is a departure of the OASPL, and to some extent the dBA values, from the low frequency broadband characteristics. This is due to the influence of the low frequency rotational noise which is relatively high in magnitude, particularly at high tip speeds, as indicated in figure 13. It will also be observed that the "dip" under the rotor is present at high thrust and that the high frequency broadband noise directivity characteristic (figure 12) has no effect on that of the OASPL.

10. THE IMPULSIVE NATURE OF ROTOR NOISE

The sound of a main rotor is impulsive even when blade slap is non-existent, but the extent of this has rarely been established. The harmonic content of a narrowband analysis is indicative of the impulsiveness of the time history of the signal, since the more harmonics the "sharper" the impulse. It is, however, extremely difficult from a narrowband analysis presentation to judge the true impulsive nature of the signal. One method of rating the impulsive content is the difference between the "peak" pressure level in dB and the RMS overall sound pressure level.

Some representative time histories, recorded at microphone F7 (11.5° below the rotor disc) are shown in figure 14. For the four conditions shown the 'peak'-to-RMS values are, from top to bottom traces, 13dB, 22dB, 20dB and 22dB respectively. These results support the observation made previously that changes in tip speed have a greater influence on the noise than changes in thrust. These results are also of interest since they are higher than similar results obtained from recordings made at the same position for a rotor operating in the conventional manner and subjected to flow recirculation effects (10). This aspect has not been studied in detail, but it would appear that the broadband noise which has a major influence on the OASPL is significantly lower on the "clean" rotor, while the 'peak' levels are only a few dB lower.

The subjective impression of impulsive noise is dependent on the 'sharpness' or rate of pressure rise, as well as the 'peak'-to-RMS value. Thus although time histories of the type shown in figure 14 can be used to give an indication of the subjective impression, the available methods for rating the noise are not really adequate since they do not give a measure of loudness or annoyance.

11. CONCLUDING REMARKS

The results presented in this paper were derived from the analysis of several different series of tests which were carried out over a period of 18 months. Each particular test series was formulated so that one specific aspect, for instance the variation of noise levels with thrust, could be studied in isolation. To allow a comparison to be made between the various series of tests a number of identical conditions were included in each of the individual test programmes. The magnitude of the scatter between results obtained from nominally the same conditions has not been fully established, but it would appear to be in the order of ± 2 dB. Thus the values given on the various figures for the same test condition can differ by a few dB.

The preliminary investigations reported in this paper have shown that rotor noise contains, from an experimental point of view, three distinct and well defined sources. These are rotational or discrete frequency noise, low frequency broadband noise and high frequency broadband noise. The results also illustrate that the overall noise characteristics are dependent on the relative magnitude of these three noise sources. It is also clear from this study that many of the accepted theoretical and semi-empirical models as well as the prediction methods relating to broadband and overall rotor noise are suspect. It is hoped that the next stage of the analysis will clarify this situation and allow, at least, accurate empirical formulae for each source to be derived. In addition to the velocity, thrust and blade dependencies the aim is to establish the directivity factors for each source.

12. ACKNOWLEDGEMENT

The investigation reported in this paper was carried out under a Ministry of Defence Contract.

The author wishes to thank colleagues in the Westland Applied Acoustics Group for their help in preparation of this paper. The author is also particularly grateful to members of the Westland Research Experimental Department, who under the direction of Mr. T.R. Ives, were responsible for the test work and analysis of data. Views expressed in this paper are those of the author.

REFERENCES

1. COOK, C.V. Structure of the Rotor Blade Vortex. AGARD "Aerodynamics of Rotary Wings". Proceedings Paper 3, September 1972.
2. IVES, T.R. & LEVERTON, J.W. Measurement and Analysis of Rotor/Propeller Noise. Westland Helicopters Limited Research Paper 407, September 1971.
3. SCHLEGEL, R., KING, R. & MULL, H. Helicopter Rotor Noise Generation and Propagation. USAAVLABS Tech. Report 66-4, 1966.
4. DAVIDSON, I.M. & HARGEST, T.J. Helicopter Noise. Journal of the Royal Aeronautical Society. Vol. 69, May 1965.
5. WIDNALL, S.E. A Correlation of Vortex Noise Data from Helicopter Main Rotors. AIAA Journal. Vol. 6, May-June 1969.
6. GODDARD, J.O. & STUCKEY, T.J. Investigation and Prediction of Helicopter Rotor Noise. Westland Helicopters Limited. Report No. AAD. 4/1. November 1964.
7. WILKES, L.H. Noise Research on Helicopter Rotors. Westland Helicopters Limited. Research Paper R.P. 349. January 1968.
8. MORFEY, C.L. & TANNA, H.K. Sound Radiation from a Point Force in Circular Motion. J. of Sound & Vib. 15(3), 325-351. 1971.
9. LOWSON, M.V. & OLLERHEAD, J.B. Studies of Helicopter Rotor Noise. USAAVLABS Tech. Report 68-60. 1968.
10. LEVERTON, J.W. The Sound of Rotorcraft. Journal of the Royal Aeronautical Society. Vol. 75, June 1971.

TABLE 1 - ROTOR BLADE PARAMETERS

Type	855	
No. of (N)	2	
Radius (R)	27.85ft.	8.5m
Chord (c)	16.4ins.	416.5mm
Area (NoR)	76.2ft ²	7.08m ²
Section	NACA 0012	
Twist	8°	

TABLE 2 - TEST PROGRAMME

TABLE 2.1 - TEST CONDITIONS

ROTOR SPEED RPM	TOTAL THRUST - lbs									
	0	700	875	1125	1450	1850	2375	3050	3900	5000
140	0	0.046		0.075	0.096	0.123				
160	0	0.036	0.045	0.057	0.074	0.094	0.121	0.155	0.20+	
180	0	0.028		0.047		0.077	0.095	0.126		
205	0	0.022	0.027	0.035	0.045	0.057	0.074	0.094	0.121	0.154
230	0	0.017		0.028		0.046		0.075	0.096	0.123
260	0	0.014	0.017	0.022	0.028	0.036	0.046	0.059	0.075	0.096

} C_{LT}
VALUES

(+ THRUST AVAILABLE LIMITED TO 3650/3700 lbs)

$$C_{LT} = \frac{C_T}{S} = \frac{T}{\frac{1}{2} V_T^2 \rho N c R} \quad \text{where: } C_T = \text{thrust coefficient, } S = \text{rotor solidity} = \frac{N c R}{4 \pi R^2}, T = \text{Total Thrust}$$

ρ = density of air, V_T = tip speed, N = No. of Blades, c = Blade chord, R = Blade Radius

Note: Mean Lift Coefficient $\bar{C}_L = 3 C_{LT}$

TABLE 2.2 - ESTIMATED THRUST COMPONENTS AT 'ZERO' THRUST

	ROTOR SPEED - RPM					
	140	160	180	205	230	260
+ve & -ve LIFT COMPONENTS lbs.	55	71	90	117	147	188

TABLE 2.3 - ROTOR SPEEDS

ROTOR RPM	TIP SPEED		MACH NO.
	ft/sec.	m/sec.	
140	408	124.5	0.37
160	466	142	0.42
180	525	160	0.47
205	598	182	0.54
230	670	204	0.60
260	758	231	0.68

TABLE 2.4 - THRUST SETTINGS

TOTAL THRUST		DISC LOADING		BLADE LOADING	
lbs	Kg	lb/ft ²	Kg/ft ²	lbs/ft ²	Kg/ft ²
0	0	0	0	0	0
700	315	2.86	14.0	9.2	45.0
875	394	3.57	17.45	11.5	56.85
1125	506	4.6	22.5	14.75	72.1
1450	653	5.93	29.0	19.0	92.95
1850	833	7.56	37.0	24.25	118.5
2375	1068	9.7	47.4	31.1	152.0
3050	1375	12.45	60.8	40.0	195.5
3900	1755	15.92	76.9	51.1	250.0
5000	2250	20.4	99.9	65.55	320.5

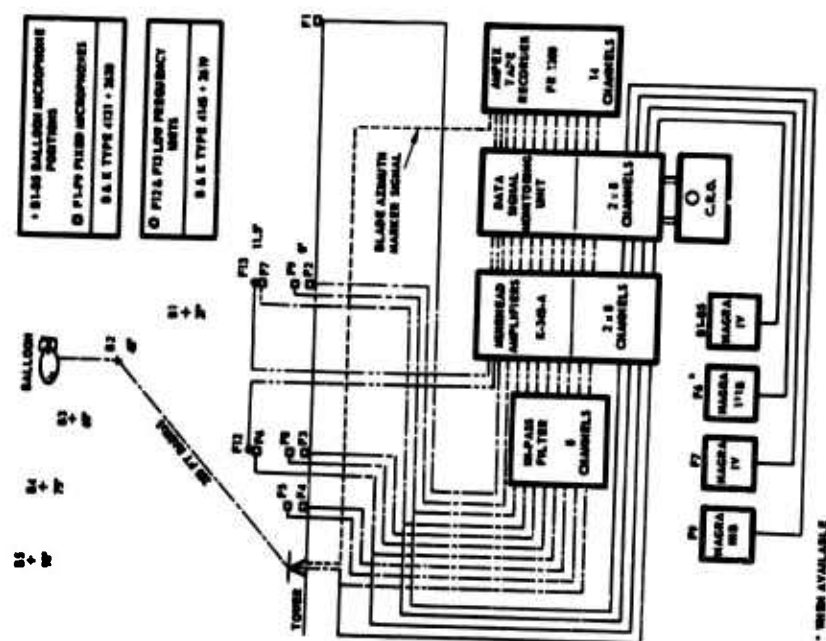


FIG. 1. TOWER RECORDING SYSTEM

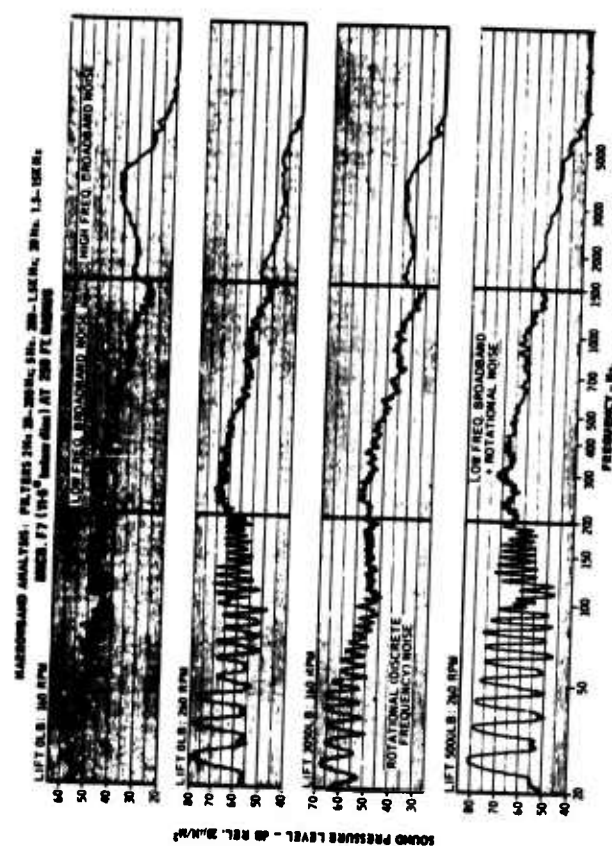


FIG. 2. ROTOR NOISE SPECTRA

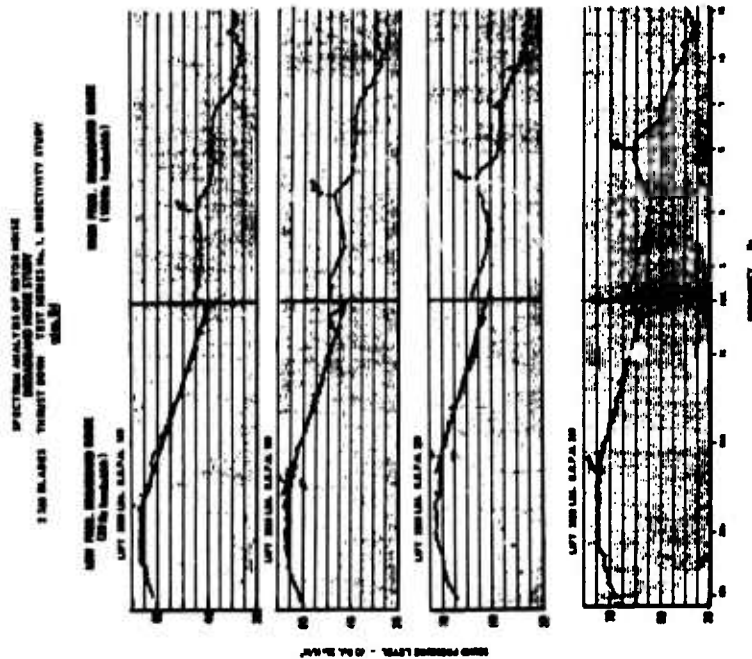


FIG. 3. BROADBAND NOISE SPECTRA

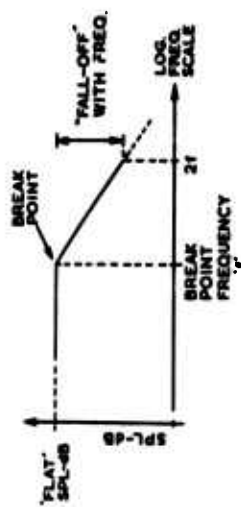


FIG. 4.

LOW FREQUENCY BROADBAND NOISE: ANALYSIS MODEL

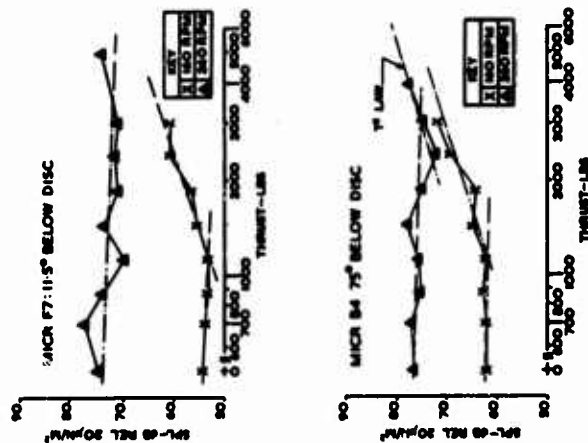


FIG. 5. LOW FREQUENCY BROADBAND NOISE:
'FLAT' SPL v THRUST

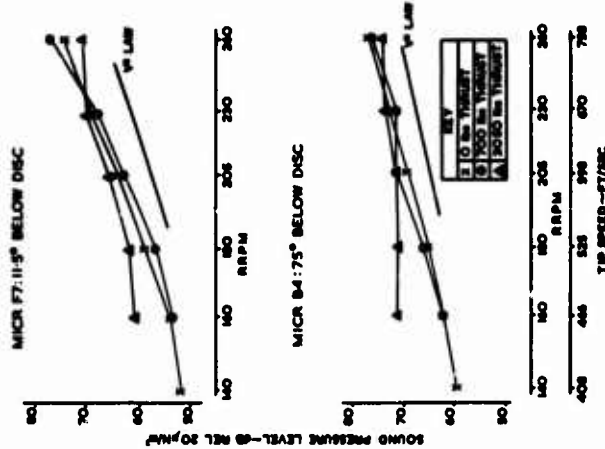


FIG. 6. LOW FREQUENCY BROADBAND NOISE:
'FLAT' SPL v TIP SPEED

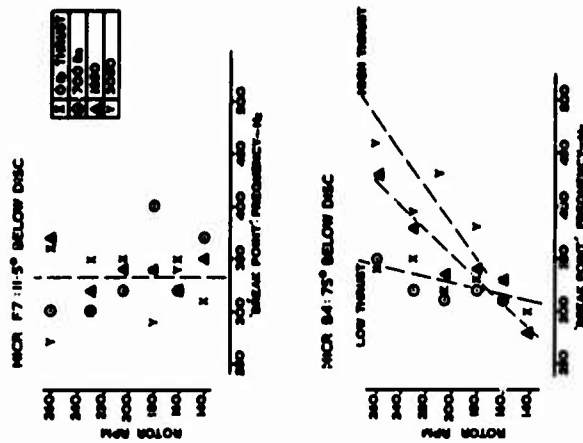


FIG. 7. LOW FREQUENCY BROADBAND NOISE:
'BREAK POINT' FREQ. v RPM

2 BLADED (5.55) ROTOR at 250 ft radius - SERIES I

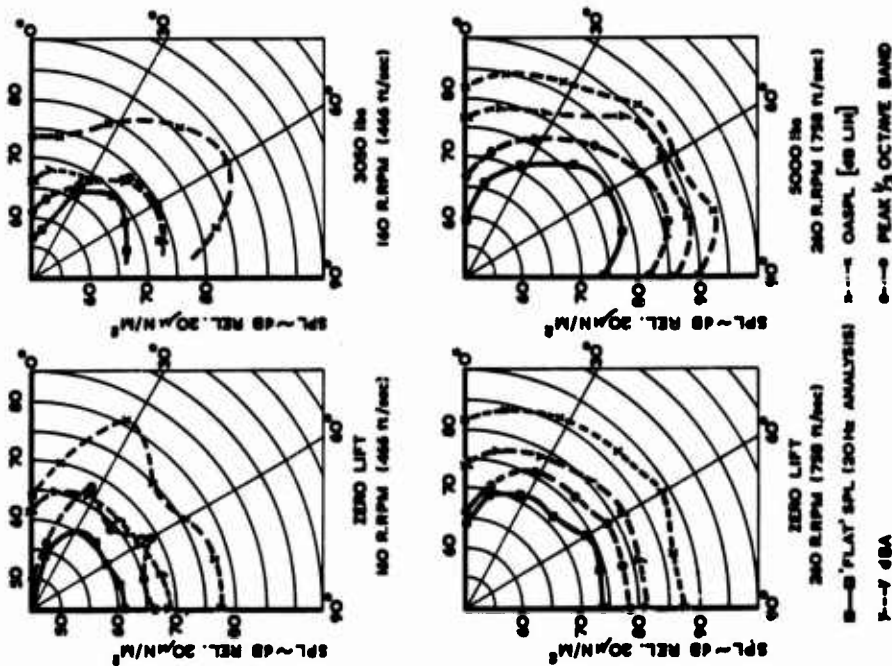


FIG. 8.

OVERALL NOISE AND LOW FREQUENCY BROADBAND NOISE DIRECTIVITY

REV	1	2	3	4	5	6	7	8	9	10
1	1	1	1	1	1	1	1	1	1	1
2	1	1	1	1	1	1	1	1	1	1
3	1	1	1	1	1	1	1	1	1	1
4	1	1	1	1	1	1	1	1	1	1
5	1	1	1	1	1	1	1	1	1	1
6	1	1	1	1	1	1	1	1	1	1
7	1	1	1	1	1	1	1	1	1	1
8	1	1	1	1	1	1	1	1	1	1
9	1	1	1	1	1	1	1	1	1	1
10	1	1	1	1	1	1	1	1	1	1

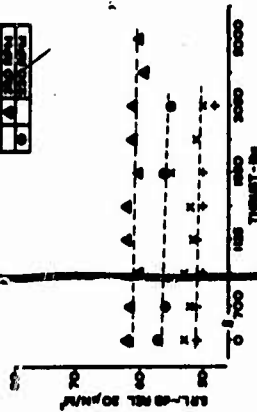


FIG. 9. HIGH FREQUENCY BROADBAND NOISE:

"PUMP" SPL v THRUST

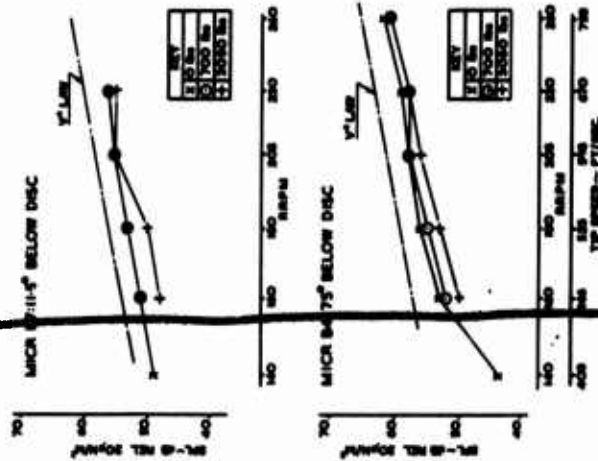


FIG. 10. HIGH FREQUENCY BROADBAND NOISE:

"PUMP" SPL v RPM

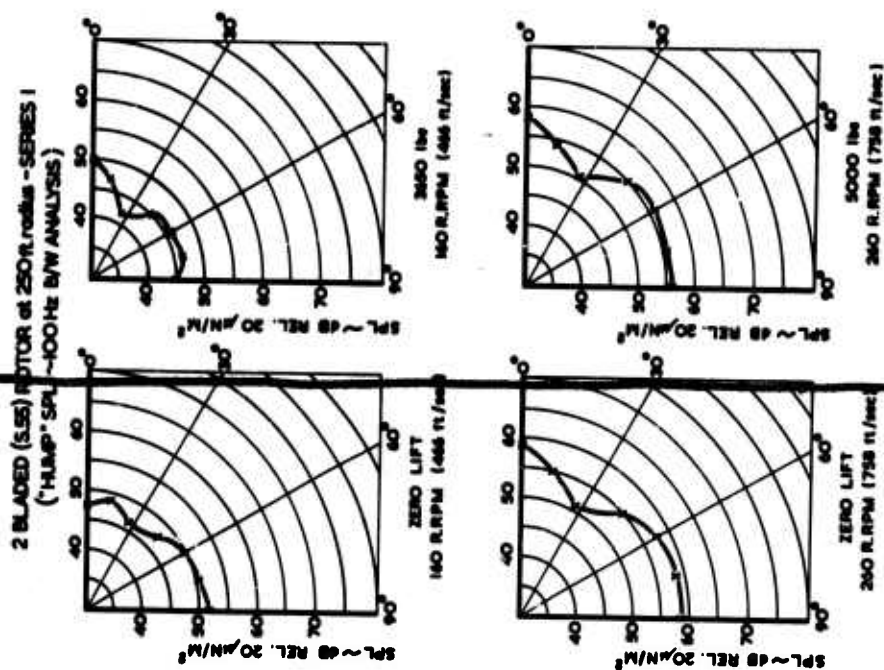
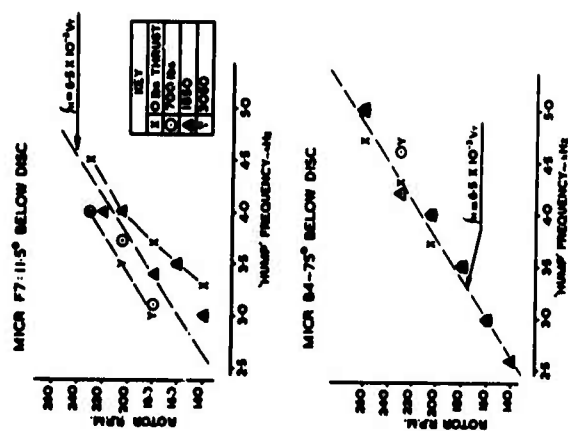


FIG. 12. HIGH FREQUENCY BROADBAND NOISE DIRECTIVITY

FIG. 11. HIGH FREQUENCY BROADBAND NOISE:
'HUMP' FREQ. v RPM

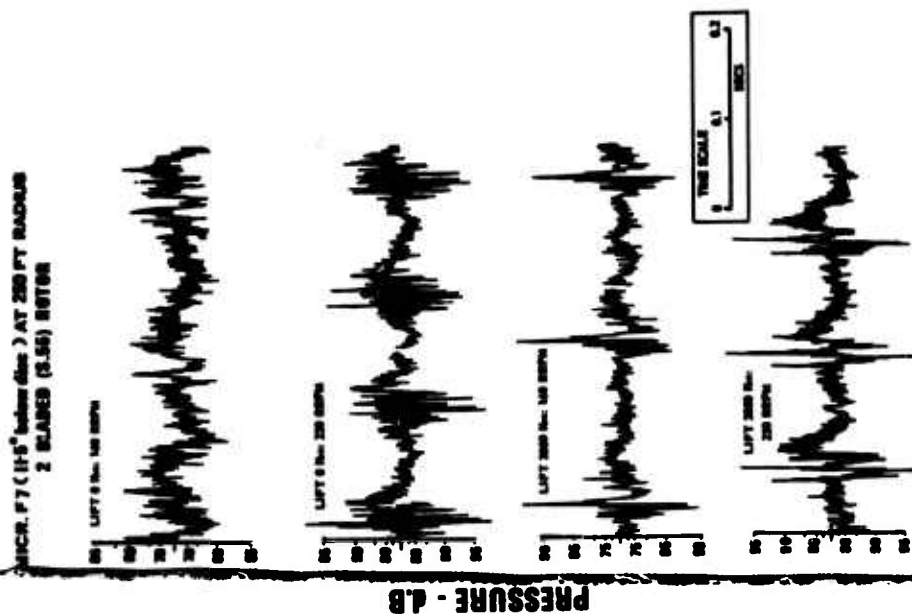


FIG. 14. ROTOR NOISE TIME HISTORIES

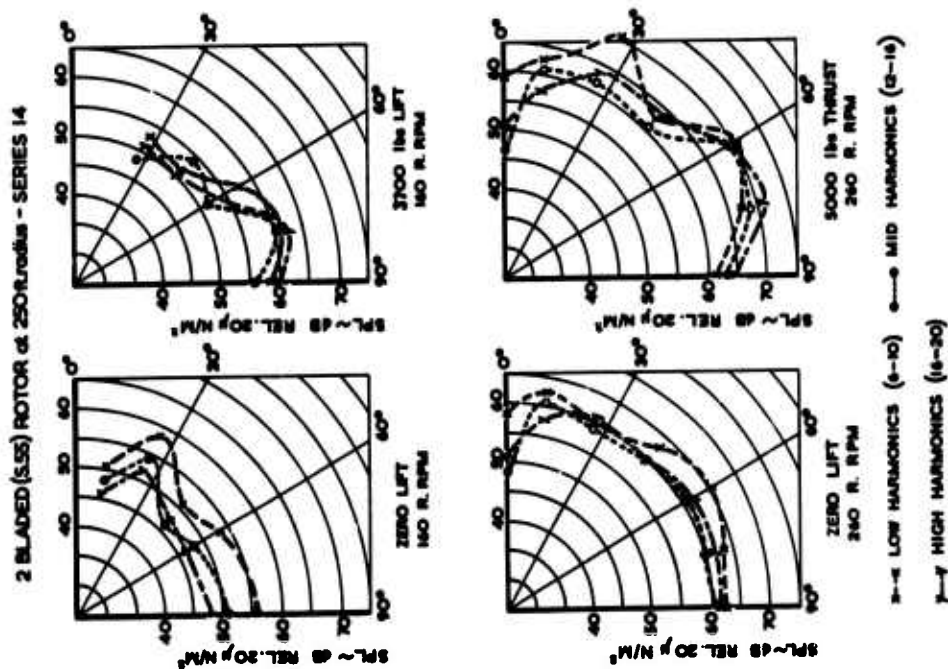


FIG. 13. ROTATIONAL NOISE DIRECTIVITY

APPENDIX A

DISCUSSIONS

~~following presentation of papers at the~~
Meeting reported in these Conference Proceedings.

This report has been transcribed from forms completed by the questioners and authors during discussion. Although almost complete, it has not been possible to include quite all the discussion. We apologise to speakers whose contribution is not recorded.

Discussion of Paper 1
"Rotor wakes – Key to Performance Prediction"
 presented by M.C.Cheney

Dr Stepniewski: What is the influence of compressibility (tip Mach number) on the structure of the wake performance of the rotor?

Mr Cheney: For model scale tests at $M = 0.6$ (and lower) no important influence of Mach number on wake structure was observed. Effect of tip speed on performance for values tested are generally of secondary importance although specific data can be obtained from USAAMRDL Tech.Rep 71-24.

Mr Drees: This was a very good survey of state of the art experience. I have three comments

1. By including wake instabilities of hovering wake and assuming vortex decay, the induced velocity is calculated low, thus making correlation with flight tests worse than with use of momentum theory.
2. At high tip Mach numbers schlieren tests indicate that tip vortex is eliminated altogether.
3. We agree that vortex interference with 2 bladed rotors is minimal, and momentum theory holds quite well.

Mr Cheney: Replies to your comments are as follows

1. Our initial results indicate vortex decay and instabilities occur sufficiently below the rotors as not to seriously effect the aerodynamics at the blades.
2. We have not tested at Mach numbers above about 0.6 and therefore cannot verify or dispute this comment.
3. Vortex interference may *not* be minimal if blade chords of two-bladed rotors become very high (so as to give total blade areas equivalent to those of 6 bladed rotors).

Mr Kretz:

1. The tests have been done on small models and full-size rotors: what scale effect exists between these results? What is the Reynolds – Number influence and more generally, what are the similarity conditions?
2. The transients such as flares, constitute important load conditions. Do you intend to study and analyse them?

Mr Cheney:

1. Controlled flow visualization tests have *not* been conducted full scale at UAC. Wake geometry results obtained from models (at full scale tip speeds but at much reduced Reynolds numbers) and used to predict full scale performance give good results. Reynolds number effects at low values are not significant however; details can be obtained from USAAMRDL Tech.Rep. 71-24.
2. Such studies are planned and initial work is underway to determine the effect of ambient winds on wake/rotor interaction.

Discussion of Paper 2
"An Actuator Disc Theory for Rotor Wake Induced Velocities"
 presented by R.A.Ormiston

Mr Fradenburgh: The paper presents examples for constant radial circulation strength. The usual case for a helicopter is non-constant radial circulation. Would author comment on difficulty of incorporating this in theory for reasonably accurate determination of induced velocities?

A second comment is that, for a rotor that is laterally balanced (zero rolling moment), the angular momentum of the downwash about the longitudinal axis must also be zero. Does the method described give this result automatically for zero rolling moment cases?

Mr Ormiston: The method described is intended to treat the general case of both radial and azimuthal variations of the bound circulation, although numerical examples are given only for the uniform circulation distribution. In the general case, the circulation would be expressed as a double Fourier series in two variables, radius and azimuth, where the radial harmonics of loading would be analogous to the spanwise loading harmonics of classical fixed-wing

lifting-line theory. The harmonic balance solution would proceed as outlined, although additional loading coefficients due to the radial harmonics of circulation would be obtained. With an appropriate choice of radial loading functions, (satisfying the zero loading boundary condition at the rotor center and perimeter) as few as two radial harmonics should be adequate. Although this would double the number of unknown circulation coefficients, this is acceptable because the computations involve only simultaneous algebraic equations.

If the wake vorticity is complete and consistent with the bound circulation distribution, then the rolling moment of the rotor must be equal to the rate of increase of angular momentum (about an axis in the direction of flight) in the wake. For the example of uniform circulation distribution shown, a rolling moment exists which is consistent with the induced velocity obtained from superposition of the vorticity components γ_l and γ_r . For a zero rolling moment circulation distribution the angular momentum would be zero.

Mr Ettore: According to the Biot - Savart law, when the distance from the vortex approaches zero, the induced velocity tends to infinity. How did you account for that? Did you limit the (maximum allowable) induced velocity? If yes, what is that limit value?

Mr Ormiston: One of the reasons for using the actuator disc formulation is that the circulation loading distribution, and the trailing and shed wake vorticity are all continuous functions. Thus the difficulties associated with singularities of finite strength vortices are avoided. Other methods using finite vortex element wake representations often do require arbitrary limitations on maximum induced velocity near vortex elements. (The root vortex and infinite perimeter velocities in the numerical example are only due to the uniform bound circulation distribution, which cannot exist physically since the loading must vanish at the rotor center and perimeter. Practical results must be based on valid loading distributions).

Dr Jones: I should like to ask in which way the method you describe is different to that of Mangler? I understand that you have extended the analysis to include blade motion etc. but the idea of using an actuator disk with prescribed loading distributions is the same.

Mr Ormiston: The idea of obtaining rotor downwash distributions (called downwash influence functions in the paper) corresponding to specified loading distributions for an actuator disc is not different from Mangler's theory. The present paper, however, addresses the general problem which requires a consistent solution for rotor circulation, blade motion, and rotor downwash by simultaneously solving the equations representing each of these physical variables. In this context, Mangler's theory represents a part (admittedly the most difficult) of the total problem.

A more fundamental difference exists however, and that is the method of obtaining the downwash for a prescribed loading. Mangler's method is based on obtaining solutions for a potential function satisfying Laplace's equation where the specified pressure loading (not the circulation loading) is equal to the discontinuity in potential across the disc. The induced velocities are then obtained by integrating the gradient of this potential function. It may be noted that induced velocities associated with the rotor torque are not included.

In the present method the wake vorticity is determined directly from the various bound circulation functions according to the Helmholtz theorem and integrated with the Biot-Savart law for the downwash. The induced velocity associated with the rotor torque is not excluded since all wake vorticity elements are retained.

Mr Williams: Can this method eventually be employed as a set of influence functions for various circulation distributions so that it reduces to a simple set of algebraic equations? How much additional effort will be required, (if so).

Mr Ormiston: Yes, this is the intent of the present method. Before useful rotor calculations can be performed, however, further downwash influence functions must be obtained for a series of bound circulation distributions, although this is relatively straightforward as shown in the paper.

Mr Kreiz:

- (a) What is the domain of applicability of the method proposed? As far as μ , M , etc. are concerned.
- (b) What is the computer time for one rotor configuration analysis?
- (c) Are experimental verifications feasible to verify the 4 components mentioned in the paper.

Mr Ormiston: For the flat planar wake, the permissible advance ratio range would extend down to about 0.15. For lower advance ratios or very high thrust, a skewed cylindrical wake would be required although correspondingly more influence functions would be required. At very low speeds even the skewed cylindrical wake would be invalid. The theory is entirely incompressible but for typical helicopters and even high speed compound helicopters this should not be a serious restriction.

Computer time requirements will be very low, since only simultaneous linear algebraic equations need be solved. This would be practical even on small computers.

Experimental verification of each of the four downwash components would probably not be possible because they would be superimposed together in an actual experiment. In principle it might be possible to identify the components which have a different functional dependence on advance ratio but this would probably not be very practical. Experimental verification of the theory, by direct downwash measurement would be very useful however. The best way would be to compute the total downwash from all loading distributions and compare directly with time averaged measurements obtained in the rotor disc plane. This is a very difficult experimental problem, but it may become feasible with laser techniques.

Mr Drees: Could free wake effects be included?

Mr Ormiston: The present theory is inherently based on a prescribed wake geometry which is valid for certain operating conditions. It is probably not practical to incorporate free wake effects without losing the advantages of superposition of the downwash influence functions or requiring iterative calculations which are characteristic of all existing finite vortex element free wake methods. However, a free wake theory for an actuator disc with continuous wake could be envisioned where the spatial position of the wake would be described analytically by a suitable infinite series. Then it might be possible to include the wake position in a non-iterative simultaneous solution of all the relevant equations, i.e. circulation, blade motion, downwash, and wake position.

Dr Küchemann: Since the wake is assumed to be planar and since the treatment is quasi-steady, why should it not be possible to consider blade elements as wings which change their angle of sweep during rotation? In that case, existing theories could be used to calculate the loadings along the blade as well as along the chord. What is the point in developing a new theory?

Mr Ormiston: In essence there is nothing really new in this theory because it is simply an extension of classical lifting line theory to rotary wings. The main departure from previous work is to extend the elementary actuator disc concept to a general solution which satisfies all the rotor variables consistently and simultaneously. However, the initial assumptions must be made carefully in order that the theoretical development can then proceed in a fully rigorous manner without additional ad hoc approximations. The most fundamental assumption is that the infinite bladed actuator disc is required when lifting line theory is used. Otherwise the unsteady shed wake deposited by each blade in a finite bladed rotor will induce downwash which is singular at each lifting line and which requires an arbitrary truncation of the sheet near the blade. A rigorous solution for a time dependent shed wake can only be obtained with an unsteady lifting surface theory. With an infinite number of blades this difficulty does not arise because the shed wake is continuous both in front of and behind the blade.

However, the actuator disc also implies that the unsteady influences of the near shed wake are lost because as the number of blades becomes infinite, the blade chord vanishes in the limit and the reduced frequency k also vanishes. Thus the complex Theodorsen lift deficiency function $C(k)$ reduces to 1.0. Again this is consistent with simple lifting-line theory.

It should be noted that the term quasi-steady takes on a slightly different meaning for the actuator disc than for fixed wings. In the latter, quasi-steady implies the shed wake is entirely neglected, but for the rotor this is not true. Only the unsteady influence of the near shed wake is lost, but the important downwash distribution at the disc due to the shed wake is retained. For the purposes of low frequency rotor response this contribution will be most significant.

These comments should help to explain why the use of existing fixed wing theory at various sweep angles would at best yield only an approximate solution. (However, this may be suitable for some purposes and has been treated by Willmer and Woodley). For instance the spiral wake trajectory would not be present nor would the isolated swept wings experience mutual self induction unless this was included. Also, since the loading would be time varying, unsteady wing theory would be required.

Discussion of Paper 3 "The Structure of the Rotor Blade Tip Vortex" presented by C.V.Cook

Mr Cheney: The film showed the tip vortex traveling above the rotor before being washed down stream. This is somewhat misleading and I believe is caused by operating the rotor in the inverted position. In so doing an inverse ground effect is produced which creates a steady velocity parallel to the ground moving inwards towards the hub. This combined with the blade coning, produces the unconventional vortex geometry shown in the film.

Mr Cook: Inverting the rotor on a whirl tower and making it thrust downward *does* change the relative position of the tip vortex to the following blade compared with the conventional rotor thrusting upward. However, this arrangement was deliberate as it positioned the vortex below the rotor, making the velocity profile far easier to measure. It also produced a flow that was far steadier than operation in the conventional mode. The success of the experiment relied on a consistent passage of the tip vortex across the disc, operation in the normal mode would produce an unacceptable amount of unsteadiness.

Mr Fradenburgh: The paper seems to equate vortex "age" with azimuth angle of the rotor blade. Research conducted by Sikorsky Aircraft, under NASA Langley sponsorship, indicated that the absolute time in seconds, rather than the number of chord lengths down stream, determines vortex tangential velocity and core size (Paper presented by Messrs. Roske, Maffitt, and Ward at AHS Annual National Forum, May 1972). Did the author run different rotor RPM values to distinguish between absolute time and blade azimuth angle?

Mr Cook: I agree that it is the absolute time that determines the decay of the tangential velocity and core size, rather than the azimuth angle.

The changing vortex characteristics were presented in terms of azimuth angle primarily to indicate the structure of the vortex that the following blade might experience.

The only tip speed condition examined was the 600 ft/sec case, although it is hoped to extend the study in the future.

Mr Lambourne: Since it seems likely that the tip vortex is originally generated by the separation of flow going from lower to upper surface at the tip of the blade, it might be expected that the character and size of the *viscous* core would be dependent on the details of the tip geometry. Had this possibility been examined by experiments?

Mr Cook: The blade tip used in the experiment was the standard S55 type. I would agree that the character and size of the vortex core would be affected by the tip geometry, but this was not the primary aim of the study.

An investigation of the effects of tip shape on the tip vortex structure has recently been attempted at Southampton University using a small model rotor.

Mr Drees: Tip shape, according to Bell helicopter tests, has a large effect on viscous core strength:

- (a) Elliptical shape — strong core
- (b) Tapered shape — weak core

Also:

- (a) High bladeloads — core disappears soon in comparison with light blade loading.
- (b) High RPM reduces core life also.

Mr Cook: I agree that a large number of factors can affect the structure of the tip vortex; this experiment was not intended to study variations, but rather devised as an exploratory exercise to indicate the feasibility of measuring the tip vortex issuing from a full scale rotor using a hot wire anemometer.

Discussion of Paper 7 "Aerodynamic Factors Influencing Overall Hover Performance" presented by E.A.Fradenburgh

Mr Kretz: What theory has been used in the figure giving comparison for cut-off conditions between tests and analysis?

Mr Fradenburgh: There were three theories used in the comparison shown in Figure 8 of the paper. These calculations, described in Reference 8 of the paper, were as follows:

- (a) a prescribed wake calculation, using wake geometry parameters previously established from flow photography of conventional rotors,
- (b) a prescribed wake calculation using wake geometry parameters established from flow photographs of the large cut-out rotor (this improved correlation only slightly) and

(c) a simple blade element - momentum hover performance calculation.

Mr Tilenius: Did you look into the effect of the cut-outs on autorotation degradation of the rotor?

Mr Fradenburgh: This was not a part of the investigation described; however more recent tests of another model have indicated that there is no appreciable degradation of autorotative characteristics due to large cut-out.

Mr Drees: Does non linear tip twist have adverse effects at high speed? How much twist was used?

Mr Fradenburgh: Any blade twist, including tip twist, tends to cause blade vibratory stresses at high speed. However the effects of the tip twist have not caused any problems to date. We use a twist increment near the tips of the order of two degrees. It is necessary only to use enough twist to reduce the angle of attack of the critical region below the stall angle. We do not attempt to achieve the theoretical optimum load distribution near the tips in all cases; eliminating the stalled region is the most important thing.

Mr Riley: Mr Fradenburgh has explained how a change in blade twist can be applied near the tip to alleviate the effects of blade stall in the hover. He has emphasised how near-hover conditions are most important from a performance point of view. Since the high loading peak oscillates radially along the blade in these conditions, would a more gradual variation of incidence not be better suited to the real conditions?

Mr Fradenburgh: We have not investigated variations in the rate at which the twist change is built into the blade - this might very well be something that should be tried. However, measurements of pressure on the surface of the blade near the leading edge, used as a measure of local angle of attack, indicate that the angles of attack in the critical region are reduced in a beneficial manner under conditions of wind as well as under conditions of no wind, for the geometry we are using at the present time.

Paper No. 8
"The Rotor in Axial Flow"
presented by H.F.Zimmer

A discussion comment by Professor A.Naumann

A short historical remark may be added to the interesting paper of Mr Zimmer. About 30 years ago in the Aerodynamisches Institut der Techn. Hochschule Aachen, I measured thrust and torque coefficients (k_s , k_d resp) of model airscrews in a wide range of advance ratios^{1,2}. These measurements covered the so called vortex ring state and the turbulence state too, the flow pattern of which are schematically sketched in Figure 1.

The vortex ring state usually occurs at small negative advance ratios λ_R ; if this state coincides with the flow separation (e.g. at small negative blade angles), the superposition of these two critical states leads to very strong vibrations of the airscrew blades; partially they caused the fracture of the blades.

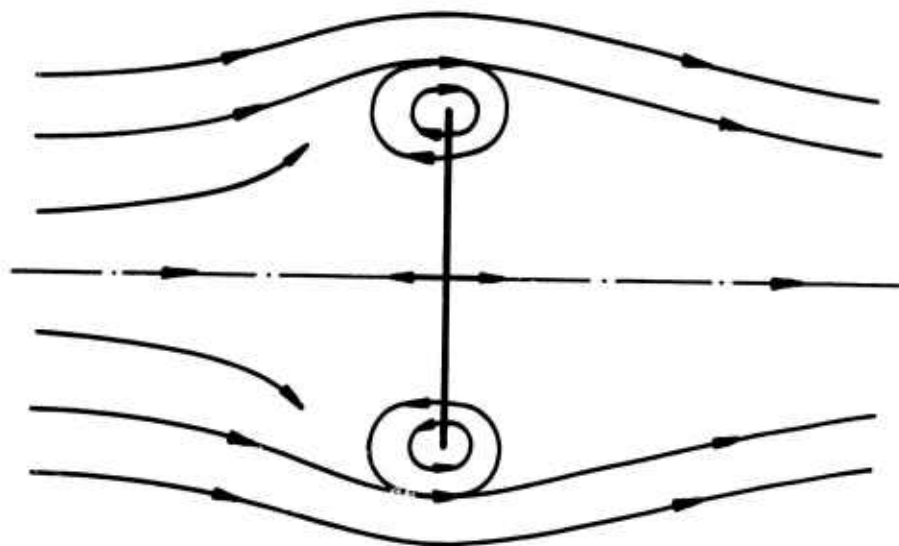
Starting from the vortex ring state at a certain increase of the flight speed, the turbulence state occurs; the oncoming air is laterally forced away by the opposite flow produced by the airscrew itself; the flow pattern becomes similar to that past a solid disc, where an (unstable) vortex ring street is shedded.

At very small incidence angles of the blades against the rotor plane the vortex ring state is restricted to a narrow λ_R region; at higher negative angles it occurs at small positive λ_R values, at which a small negative thrust can coincide with a high positive torque.

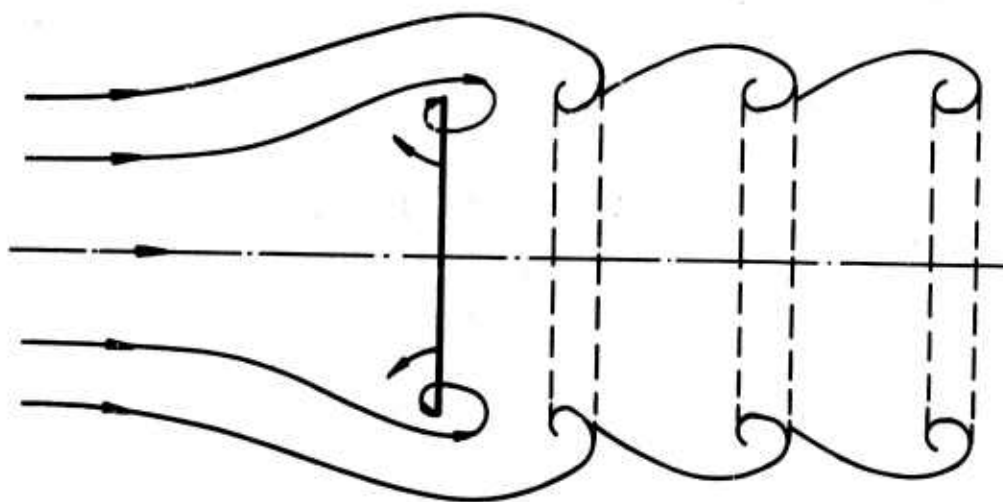
The results are dependent on the form of the blades; they could be gained with several propellers of different blade forms and blade numbers. One example is shown in Figure 2 and 3; the thrust coefficients k_s and torque coefficients k_d are plotted against the advance ratio λ_R for a two bladed airscrew.

REFERENCES

1. A.Naumann, Luftschraubenmessungen im Wirbelring- und Turbulenzgebiet. Technische Berichte Vol.9 (1942) S. 27-35.
2. A.Naumann, Luftschrauben im Bremsbereich Jahrb. 1940 Deutsche Luftfahrtforschung I S. 745 ff.



vortex ring state



turbulence state

Figure 1

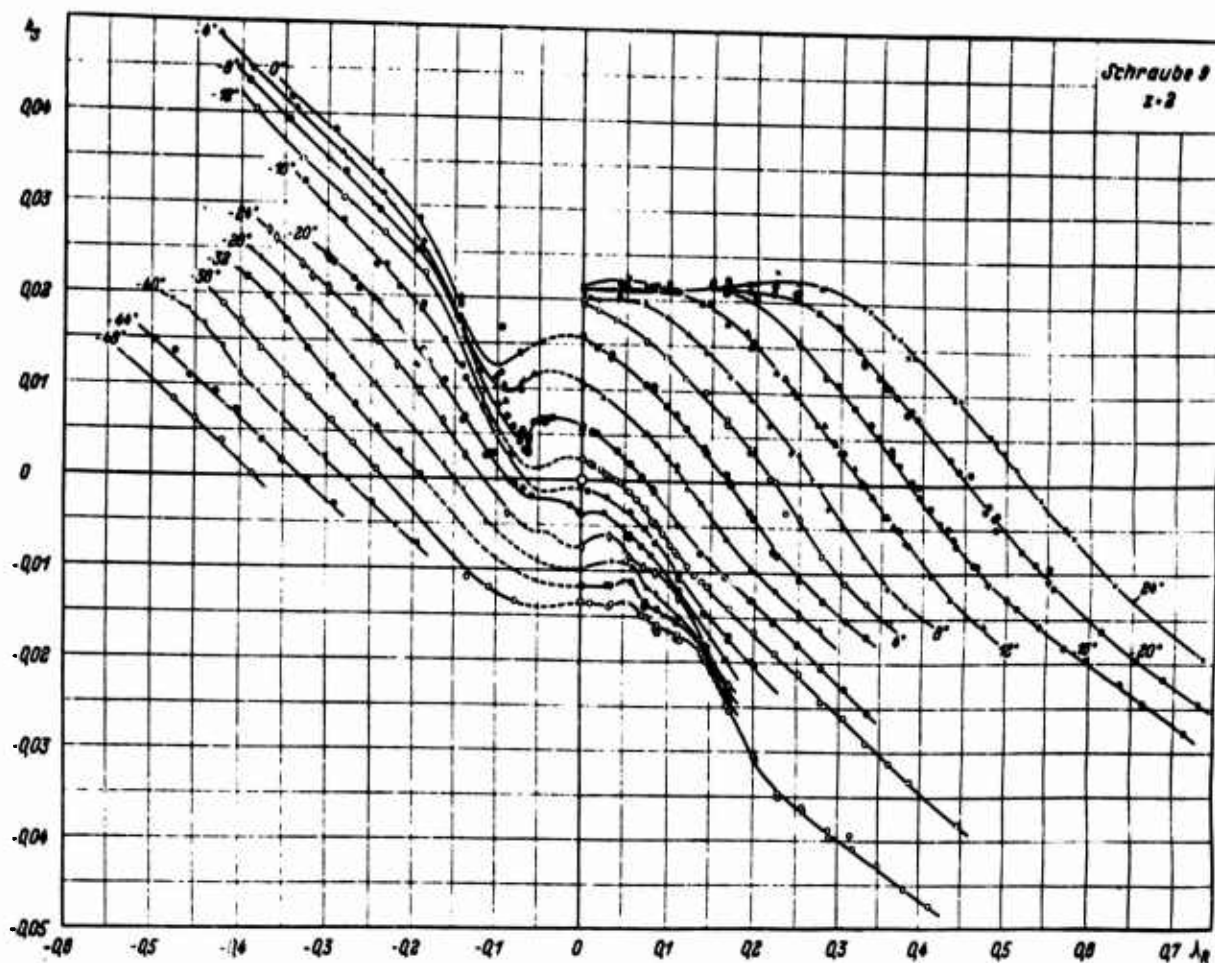


Fig.2 Thrust coefficient

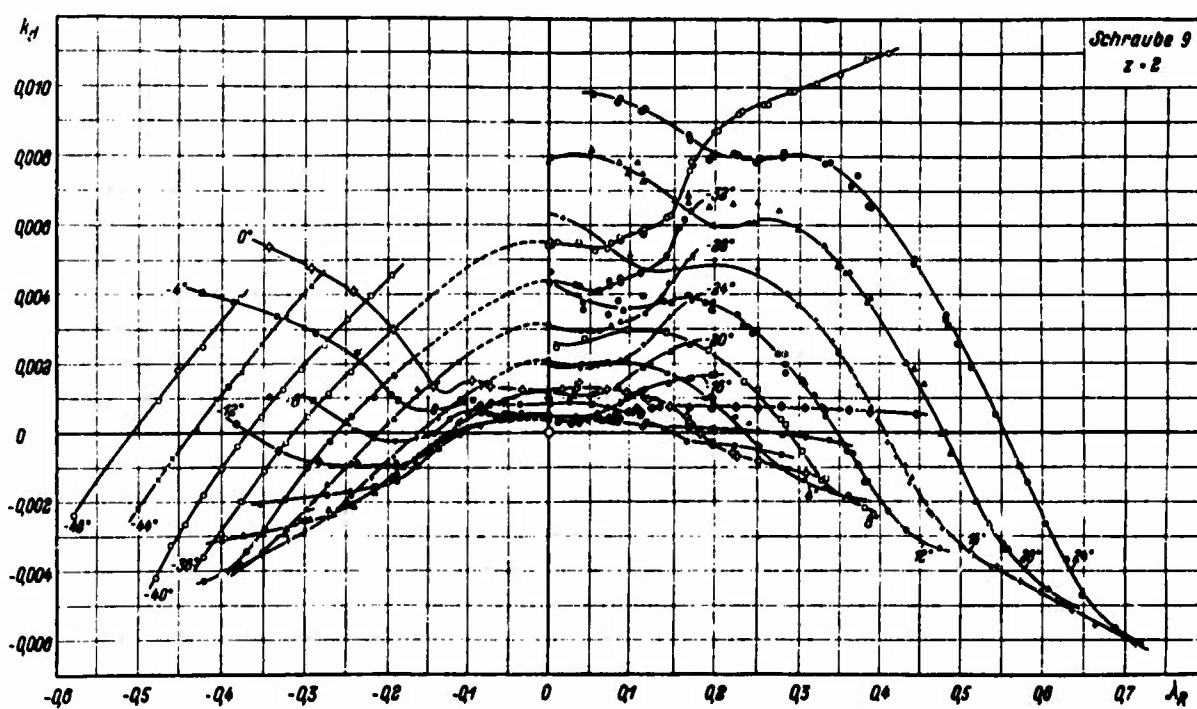


Fig.3 Torque coefficient

Discussion of Paper 9
"The Development of an Efficient Hovering Propeller/Rotor
Performance Prediction Method
presented by D.C.Gilmore

Mr Kretz: Is your analytical model sensitive to this planform, more particularly, to the tip shape?

Mr Gilmore: Not normally since we use planform in the calculation of local lift and drag once the velocity field is known. Performance predicted would only be sensitive if the tip shape extended inboard of the tip by a large amount.

Mr Ormiston: Referring to Figure 22 in the written version of the paper, could you comment on the reasons for the large variation in figure of merit due to core size?

Mr Gilmore: The necessity for large core size in the inboard and outboard sheets arises for two reasons.

1. The location of control points on the lifting line (which are situated at the shedding location of the trailing vortices).
2. The use of the solenoidal assumption during calculation of the inboard sheet strength is prone to instability which is effectively damped out with a large (or $1/10$ blade radius) core size. We recognise that use of such core sizes is not physically real, but it serves to allow the method to give useful results until appropriate modifications can be made.

Discussion of Paper 10
"A Summary of Current Research in Rotor Unsteady Aerodynamics
with Emphasis on work at Langley Research Center"
presented by J.F.Ward and W.H.Young Jr

Dr Jones: I sympathise with Dr Johnson's request for a better basic research programme but it is most important to have in mind the likely value of the results to helicopter designers.

For instance the concept of an improved model for the dynamic stall must depend upon a better knowledge of mechanisms of separation — a subject which has occupied aerodynamists for a century. It is to be expected that further progress in this area will be shown.

In the paper, and on occasions in the meeting, there have been several examples of Schlieren pictures of rotor flows. Is there any example which shows shock waves extending beyond the blade tip? Some 35 years ago Dr W.F.Hilton showed shadowgraphs with shockwaves extending well beyond the blade tip at $M = 0.85$ or so.

Mr Ward: I do not remember seeing any Schlieren photos showing shock waves extending beyond the blade tip. However, in most of the photos I recall the Schlieren orientation was not suited to the detection of this type of shock.

Prof.Ham: Much dynamic stall research is devoted to the accumulation of empirical data rather than the achievement of basic understanding.

Mr Caradonna: Concerning Dr Jones question: on the basis of numerical calculations, shocks definitely do seem to extend out beyond the blade tip.

Prof.Küchemann: It seems that it is proposed to deal with the problems of dynamic stall first for the case of two-dimensional aerofoils, assuming the types of bubble separation to be the same as in steady flows. I should like to ask whether you have any reason to suppose that such flow models will apply in the real case of time-dependent separated three-dimensional flows over rotating blades.

Prof.Ham: Concerning Dr Küchemann's comment, the three-dimensional rotor dynamic stall data of McCroskey agrees closely with the two dimensional unsteady airfoil data of Ham. This suggests the applicability of two-dimensional data to the three-dimensional case.

Mr Young: Our investigations are not limited to separation bubble type separation. They include the trailing edge separation in the analysis. For the present, models of two-dimensional dynamic stall seem sufficiently complex. Eventually the inclusion of three-dimensional and compressible effects must be considered.

Mr Lambourne: Although Mr Ward had stressed that "lift stall" and "moment stall" were to be reported as separate events, would he agree that they were related events resulting from the same cause - separation?

Was it likely that compressibility would have to be included in the modelling of dynamic stall in order to get agreement with reality and whether shock wave effects were also present even at the lower Mach numbers of the retreating blade?

Mr Ward: It is agreed that, while "lift stall" and "moment stall" are seen by the blade as separate events, both events are the result of a single flow separation event. In addition it appears that compressibility will have to be included in the dynamic stall modelling even for the lower Mach number range on the retreating blade. The high angles of attack and inflow velocities induced by the unsteady wake, including blade/vortex interaction, suggest that unsteady compressibility effects must be studied.

Prof. Young: I was interested in the diagram (Fig.14) showing the effect of change in tip shape on the strength of the tip vortex. This rather re-inforces a general impression that I have, which as a layman in helicopter aerodynamics I have hesitated to put forward before, that in the various theories that have been developed for providing rotor characteristics there has been too great a concentration on the tip vortex, dramatic as it is, to the relative neglect of the rest of the trailing-vortex system in the blade wake. It seems that small changes in the blade planform shape can, by modifying the loading distribution near the tip, result in significant changes in the tip vortex strength near the rotor disc. If this is so it might be of importance in rotor design, and I would welcome the comments of the authors on this point.

Mr Ward: Alleviation of the intensity of the tip vortex will indeed have an effect on rotor design. Some of the more serious rotor problems, such as trailing vortex induced tip stall in hover, rotor blade "slop" noise and rotor blade impulsive loading can be alleviated. Once some of these problems are under control the rotor can then be improved from a performance standpoint by utilizing optimum planform, twist and airfoil distributions.

Mr Johnson: The attention to the tip vortex influences seems to be justified now as the greatest source of loads, vibration, noise, and other problems. If the efforts to dissipate or decrease the vortex strength are successful, there will probably then be a swing of attention to the other elements of the vortex wake.

Mr Williams: With limited resources there should be a balance of effort into

- (1) prediction and understanding of phenomena
- (2) alleviating or avoiding the phenomena altogether.

In particular I would offer a caution that we do not overemphasize the predictive capability at the expense of research into methods of avoiding the phenomena. For example the use of rotor tip air injection to alleviate or completely disperse the vortex may nullify the tip roll-up phenomena; also high lift may alleviate dynamic stall or advancing tip Mach number.

Mr Kretz: There has been an impressive effort to gain an understanding of the unsteady aerodynamic phenomena. The question is what means, positive and active are envisaged to control these effects. The variable geometry rotor is one of them and mass injection has been mentioned. Are other means under investigation? More particularly are feed back inputs, as active means, being studied?

Mr Ward: Active feed back control of unsteady aerodynamic phenomena are under study. Fluidic control systems are being applied to control local blade section lift through sensing upper surface pressure in the airfoil midchord region and controlling jet flap deflection angle. Other methods of blade modal control are under study including servo-tabs, electro-magnetic shakers installed in the rotor blade, and direct control by servo-actuators installed in the blade pitch control linkage.

Mr Young: I would like to thank Dr Ham, as a potential flow expert, for his endorsement of the Navier-Stokes solutions.

Discussion of Paper 11

"Calcul et Mesure des Forces Aerodynamiques sur un
Profil Oscillant, avec et sans Décrochage
presented by J.J.Philippe and M.Sagner

Mr Lambourne: M.Philippe had referred to work at the RAE on dynamic stall. In this work oscillatory measurements had been made on an aerofoil for Mach numbers between 0.35 and 0.5, which to some extent complemented the range covered by M.Philippe. Briefly, the general conclusions were that for these higher Mach Numbers the hysteresis loops for lift and moment became thinner as Mach number increased. The lift "dynamic overshoot" decreased and certainly by $M = 0.5$ the overshoot had practically disappeared. These changes were, perhaps not surprisingly, accompanied by a reduction in the region of negative pitching damping at higher Mach number. The measurements at the RAE had also included instantaneous pressure distributions across the chord of the aerofoil. The time histories following the onset of separation exhibited a randomness which meant that the behaviour after separation occurred was not the same for each cycle. I am very impressed by the calculated results shown in Figure 16 because these show remarkable similarity to some of my measurements. I have a question regarding the method of calculation. Is there an element of randomness in the calculation process or does the method produce a unique pressure time-history which is identical for each every cycle?

M.Souquet: le Calcul, dont les résultats font l'objet de la Figure 16, ne représente qu'une portion de cycle (environ 1/6) après la première apparition d'un décollement. Si on recommence un calcul avec les mêmes données initiales, on retrouve les mêmes résultats aux erreurs près, liées aux problèmes d'arrondi et de troncature inhérents aux calculs digitaux. Toutefois il est impossible d'affirmer que, lorsqu'on effectuera des calculs sur plusieurs cycles successifs, on ne verra pas se manifester une instabilité qui créera des différences aléatoires ou périodiques entre cycles.

Les seuls termes aléatoires introduits dans le calcul sont les erreurs d'arrondi et de troncature du calculateur. Si deux calculs consécutifs sont effectués avec les mêmes conditions initiales et le même processus de traitement on retrouve le même résultat à quelques différences mineures près.

M.Philippe: De nombreuses expériences ont déjà mis en évidence le fait que, cycles après cycles, l'incidence de début de décollement ou celle du recollement n'est pas exactement identique (je pense notamment aux travaux de Liiva et DAVENPORT) Ceci conduit d'ailleurs à moyenniser les résultats ou un certain nombre de cycles pour fournir des valeurs disponibles des composants aléatoires dues à certains phénomènes liés au décrochage instationnaire.

M.Lecarme:

- (a) La trainée instationnaire peut avoir une grande importance sur la sécurité des rotors; en effet quand on fait décrocher un rotor les vibrations de trainée des pales augmentent généralement peu, mais si l'on persiste (en augmentant le pas général) il arrive souvent que l'on observe une divergence brutale de ces vibrations de trainée, la trainée instationnaire peut jouer un rôle dans ce phénomène.
- (b) Au-delà des paramètres d'avancement de l'ordre de 0,3 à 0,4 l'attaque oblique joue un très grand rôle notamment dans le dépassement du coefficient de portance maximum (dans les zones non contaminées par le cercle d'inversion).

M.Philippe: I agree.

Mr Kretz: Quelle est la signification des tracés dans la figure 15?

M.Sagner: Etant donné que la nappe tourbillonnaire, liée au décollement de bord d'attaque est représentée par une émission de tourbillons discrets, émission qui débute au moment où les conditions d'éclatement du bulbe sont créées, les traces montrées sur la Figure 15 représentant à l'instant correspondant à l'incidence portée sur la figure, le lieu géométrique de tous les tourbillons émis par ce processus entre l'instant de début d'émission (temps correspondant à 15°) et les instants correspondant aux différentes incidences mentionnées.

Discussion of Paper 13
"A Compressible Unsteady Aerodynamic Theory
for Helicopter Rotors"
 presented by C.E.Hammond

Prof.Ham: What is the effect of compressibility on "wake-excited" flutter?

Mr Hammond: The purpose of the numerical study was to determine the effect of the various parameters, including Mach number, on the flutter speed. No effort was made to isolate the "wake-excited" flutter condition and study it individually. In all the cases examined, however, the effect of compressibility was to lower the flutter speed.

Mr Zwaan: The success of your method and those of Loewy, Jones and Rao depends heavily on the supposition that only the parts of the wakes very near to the reference aerofoil contribute to the aerodynamic forces. If I make in this respect a distinction between near-field and far-field disturbances, the differences between your results and those of Loewy, Jones and Rao seem to stem from different treatments of the far-field disturbances. Have you made an attempt to assess the relative importance of the near-field and far-field disturbances, e.g. numerically, in order to get an impression to which extent the outer field may be modified, thus simplifying the problems?

Mr Hammond: The only effort which has been made in this respect is the variation of the frequency ratio parameter which is presented in the paper and which was covered in the presentation. This variation shows essentially the effect of increasing the upstream length of the wake layers and it was found that this did have a marked effect up to a certain point. Beyond a frequency ratio of 0.5 it was found that the results of this paper and those of Loewy, Jones and Rao were in very close agreement. Thus there is a point beyond which the wake can be represented as layers of vorticity having infinite length. This representation simplifies the analysis and reduces the computation time.

M.Costes: A l'ONERA j'emploie la même théorie compressible linéarisée avec un sillage en nappe hélicoidale pour le calcul des efforts aérodynamiques sur un rotor d'hélicoptère. Les effets tridimensionnels sont donc inclus. Dans les cas de vols que nous avons étudié (rapport d'avancement = 0,3), l'influence des zones de sillage proches de la pale intéressée, c'est à dire celles que vous considerez dans votre article, est d'environ les 80% de l'influence totale.

J'ai maintenant une question à poser. Vous utilisez cette méthode tridimensionnelle compressible pour retrouver les résultats d'une expérience de flottement. Avez-vous envisagé une comparaison entre la théorie et l'expérience pour les portances aérodynamiques sur les pales d'un rotor d'hélicoptère?

Votre travail a aussi le grand mérite de montrer tout l'intérêt que l'on peut avoir à utiliser une méthode qui tient compte de manière rigoureuse des effets de compressibilité; même si cette méthode est plus difficile à mettre en oeuvre que celle qui consiste à faire un calcul incompressible, puis à appliquer une correction comme celle de Prandtl.

Mr Hammond: I am familiar with Mr Costes' work at ONERA. The aerodynamic theory which he employs is quite elegant and gives good correlation with experimentally measured results.

In response to your question, we have not made any comparisons of our computed aerodynamic forces and moments with experimental values. This could be done easily, of course, since the chord-wise pressure distribution and section lift and moment are results of the computations. The original impetus for developing the aerodynamic theory was, however, to determine the effect of compressibility on the flutter speed of rotary wings and at present this is the only use which has been made of the theory.

Discussion of Paper 14
"Some Aspects of the Design of Rotor Airfoil Shapes"
 presented by S.Wagner

Mr Wagner: First of all I would like to thank Professor Wortmann for his prepared comment. I agree that the most important part of the profile that influences the flow significantly is the region around the leading edge. In addition, it should be possible to choose a curvature on the upper side of the profile close to the leading-edge radius that meets the requirements of transonic flow (advancing blade) and high lift conditions (retreating blade).

Mr Sloof: In your presentation you quite correctly mentioned the hodograph method as a potential tool to be used in the design of rotor airfoils. I think I should mention that, as part of a NASA contract, we are presently studying the possibility of using Nieuwlands hodograph method to generate airfoils that are suitable for application in the outboard section of a helicopter rotor. We found, that by adding two extra series to the solutions of the hodograph equations that lead to the so called quasi-elliptical airfoils, we were able to generate shock-free sections for the high Mach number low C_L condition, that at the same time exhibit the kind of leading edge droop that is required for a high C_L max at moderate Mach numbers. From these analytical studies it appeared to us that a key feature to the compatibility of the multiple design requirements for helicopter airfoils is indeed the curvature distribution on the front part of the upper surface. Thus, in this respect, as well as in others, the airfoils that the hodograph method is providing us with closely follow the general description of the "optimized rotor airfoil" just given by Dr Wortman.

Mr Wagner: Thank you for this interesting comment.

Mr Wilby: First I would like to stress the importance of pitching moment in the design of a rotor blade section, particularly the requirement for zero pitching moment at zero lift and high subsonic Mach number. If this requirement is to be met, then viscous effects must be accounted for in any computations of the theoretical pressure distributions. Existing methods can deal with this situation for subcritical conditions and at the RAE we have been able to design aerofoils with reflex camber to compensate for the nose-down pitching moment produced by nose droop.

I was interested to see the results presented by Dr Wagner for aerofoils modified at the trailing-edge to represent the tab formed by full scale manufacturing techniques. We have carried out similar tests at the RAE and found much the same results, a considerable change in pitching moment characteristics being observed. If two-dimensional aerofoils are being tested to obtain data to feed into a rotor performance computer program in order to assess the performance of a particular project, then it is important to test the shape of blade section that actually appears on the final real rotor blade.

My last comments concern the contribution from Prof. Wortmann. He suggests that one can reconcile the design features for high C_L max: at low speed with those for high drag-rise Mach number at low C_L in a design that incorporates a region of high curvature on the upper surface of the profile at about 10 to 15% chord. I feel that there must always be a penalty to pay at some conditions for a region of high curvature, and in this case it could well be at conditions appropriate to the blade tip in hover, where the shock would form just to the rear of the high curvature region. In these circumstances the high curvature would produce local expansions that would result in a stronger shock.

Mr Wagner: It is good to hear that you got similar results of experiments with modified trailing edges.

Mr Eppler: The method given by the authors would very easily allow us to compute airfoils from given pressure distribution in the incompressible case. If these pressure distributions are given at different stations at different angles of blade. If the pressure distribution is not only given at different stations at different lift coefficients, but also at different Mach numbers, different compressibility reductions are obtained. Therefore a method for airfoil computation was developed, in which the shape can be given in one part, and pressure distribution in the other. I hope that this method together with new compressibility reductions will help to get the optimum shape for helicopters.

Mr Drees: In addition to high C_L max and high M_{DD} the optimisation of L/D for hover conditions should be added as one of the most important requirements.

Mr Wagner: I agree. Figure 20 of this paper shows that a droop of leading edge improves not only C_L max but also L/D.

Discussion of Paper 16
 "The Derivation and Verification of a New Rotor Profile on the Basis of
 Flow Phenomena Aerofoil Research and Flight Tests"
 presented by P.G.Wilby

Mr Williams: Please comment on the use of a drag rake for flow measurements (accuracy, unsteady effects etc.)

Mr Wilby: The wake measurements may be interpreted in a two-dimensional sense to give a direct comparison of the two profiles, when the well established corrections for static pressure may be applied to give accurate drag values. In a wider sense, the validity of a strictly two-dimensional interpretation of the wakes must be questioned, and the rake measurements themselves have now helped in building up the detailed picture of the blade tip environment provided by these pressure measurements.

Discussion of Paper 17

"The Effect of Planform Shape on the Transonic Flow past Rotor Tips" presented by F.X.Caradonna

Mr Drees: This was a very nice paper. In practice gains of 15% power reduction are shown. The critical azimuth position is not 90 degrees but about 130. The tip vortex has to be included.

Mr Caradonna: The large power reduction you mention is gratifying. As we have seen, our calculations show the possibility of considerable shock strength reductions with geometry variation. However, we have also seen that planform and profile variations can have some rather unexpected effects and I wouldn't be surprised if you have seen some surprisingly small power reductions for some of the planforms you have tried.

You are quite correct concerning the probable location of the worst transonic effects. A swept back tip is effectively less swept in this region. Furthermore, the incident Mach number is still considerable at this point. And, as we have seen, a blunt nosed airfoil can be strongly affected by moderate sweep changes.

Concerning the treatment of tip vortices, for the low lift, advancing side, I anticipate that vortex roll up is no problem, as this will probably occur sufficiently far downstream as to have little effect. A greater concern is the tip vortex and vortex sheet from the previous blade and we hope that the wake analysis people can provide us with good information. When a previous tip vortex comes too close to the blade, the small disturbance approximation will surely have to be abandoned. For calculation of highly lifting flows the tip roll up can occur immediately and the treatment of this situation is by no means clear.

Discussion of Paper 18

"Wind Tunnel Tests of a Tilt Rotor from Hovering to Fast Cruise" presented by W.L.Cook

Mr Williams: This is only a comment. In our work at NSRDC about 1968 we obtained very similar results at the optimum blade twist for hover-cruise compromise; I believe for your disc loading range it was about 37° .

We then studied higher disc loading, for Navy missions (higher speed, smaller blade stowage area. We found that BLC on the inboard leading edge was effective in allowing maximum twist for cruise and also good Figure of Merit.

Discussion of Paper 19

"Recent Developments in Circulation Control Rotor Technology" presented by R.M.Williams

Mr Lecarme: En cas de panne de compresseur l'autorotation du rotor est-elle possible et peut-elle assurer la sécurité de l'appareil.

Mr Williams: Loss of all compressors may be catastrophic although there is some indication from theory that the centrifugal compression may be of help. Normally the compressor is connected by the transmission to the rotor.

Mr Kretz: May I congratulate the author for this excellent presentation of the impressive effort done by the Navy on CC rotor. Working on similar lines we have found most of the results cited.

There is a question I wish to ask: what is the blade loading envisaged for the CC rotor?

Moreover, may I add that centrifugal effects add to maintain circulation control in autorotative flight.

Mr Williams: Thank you for your comment. The blade loading is high, of the order of 150 lb/ft². The pressure ratio required during autorotation is about 1.1 to 1.2 so that your results on blown rotors may well apply to our case.

Mr Reichert: You need a different control system for hovering and for cruise. Does this impose mechanical complexity and additional weight?

Mr Williams: The same system is used. The cams are merely lowered to remove the cyclic variation.

Discussion of Paper 20
"Some Objectives in Applying Hingeless Rotors to Helicopters
and V/STOL Aircraft"
presented by H. Huber

Mr Cheney: This paper described excellent work. I have these questions to ask.

1. What is percent normal RPM when $\left(\frac{\omega}{\Omega}\right)$ in plane = 1.0?
2. What is percent normal RPM when RPM is coincident with aircraft roll frequency and describe what occurs during run-up at this frequency?
3. How far does RPM drop at power failure?
4. Does BO 105 have skid landing gear?

Mr Huber:

1. The section point of inplane frequency with 1Ω , when reducing the rotor RPM is at about 58% normal RPM.
2. The aircraft roll natural frequency is about 30% of normal RPM. Flight tests were done with periodic stick excitation by pilot by moving the stick laterally at just this frequency. There was of course an increase of lag oscillations (at the air resonance frequency), but the oscillations were highly damped, i.e. the whole system is stable.
3. At power failure the rotor RPM drops to a minimal 75-80% at the moment of ground contact at collective flare during autorotation landing and then reduces further. There are no stress problems at the 58% condition.
4. Yes, the BO 105 has skid landing gear.

Mr Ormiston:

1. It is very evident in the results of this paper that aerodynamic phenomena are of particular importance for hingeless rotors, both in regard to rotor blade dynamics and stability and in regard to fuselage motion dynamics and flying qualities. These aerodynamic effects are in many respects of greater relative importance for hingeless rotors than for articulated rotors which may not be as yet fully appreciated by rotary wing aerodynamicists.
2. Are the effects of airfoil variations in Figure 8 due primarily to aerodynamic effects or rather to the influence of blade center of gravity variations?

Mr Huber:

1. I am in full agreement with your comment about the increasing importance of aerodynamic and aerolastic effects on hingeless types of rotors. The reason is that all effects which influence the rotor blade dynamics will be increased in their effect because of the large moment arms of the system. Hingeless rotors show very sharp reactions to all aerodynamic inputs and neglect of this or wrong aerodynamic treatment will result in incorrect calculations. In this respect the hingeless rotor can be said to be a "non-forgiving" rotor.
2. The effects of airfoil modifications (fig.8) are partly due to aerodynamic effects and partly due to c.g. variation. Curve (3) can be said to be mainly influenced by the large c.g. shifts.

Mr Zwaan:

1. What type of structural damping did you apply in your calculation model (hysteresis or velocity-dependent); I can imagine that the type differs for the blade structure and the control mechanism.
2. Furthermore, did you perform ground resonance tests in order to check your calculation model before flight testing?

Mr Huber:

1. In our calculation model there is now included a velocity-dependent structural damping. But as soon as we know more about the structural damping behaviour (from running damping tests), we will include the effects.
2. Yes, we did very extensive ground and air resonance tests with the new type of soft inplane rotor. The correlation with calculation results was very good.

Mr Kretz:

1. What is the value of the damping in the in-plane direction?
2. Is it purely structural, without any artificial device?

Mr Huber:

1. Structural in-plane damping depends on some parameters, such as inplane moments, blade lift and centrifugal force. On average the damping can be said to be about 2-4% critical.
2. On the Bo 105 rotor there is no artificial damping device. Damping is entirely by structural damping and damping effects in the blade attachment device.

Discussion of Paper 22
"Fundamental Considerations of Noise Radiation by Rotary Wings"
presented by M.V.Lowson

Mr Kretz:

1. Do you envisage use of the effects of boundary layer and circulation control and air injection at the tip, to reduce the noise signature.
2. Do you intend to employ means other than I have just mentioned, to reduce or modify the noise spectrum?

Dr Lowson: I have not looked specifically at possible effects of boundary layer control. The acoustic effects due to any change of force resulting from this could, of course, be calculated by the theories presented. I am personally rather doubtful if any noise benefit would result. There are certainly additional noise sources due to the intense shear layers resulting from boundary layer control jets, and due to the rotating mass output. Mass injection at the tips has been proposed as a noise reduction method, and is supposed to act via reduction or elimination of the tip vortex. I have not been able to read the original paper on this proposal, but at present am unconvinced of its effectiveness. The most promising noise control approach to date appears to be via tip modifications, and understanding of the reasons for their effects seems likely to pay valuable dividends.

Mr Schmitz: It has been shown that higher order loading harmonics can be efficient radiators of sound. However, measured higher order loading harmonics is lacking along with definite proof that this higher harmonic data is in fact random. Thus how do we conclusively prove that rotational noise is entirely governed by "miniscule variations" in blade loading? What we have shown is that it *may* be an important source of noise. Further experimental measurements of actual detailed pressure variations along the blade appear necessary.

Dr Lowson: The tests reported here go as far as a harmonic order of 70. I feel the present results do verify the theory at moderate harmonic orders, and inference of accuracy at higher orders seems acceptable, particularly since there is no counter-evidence. In my view the theory is now sufficiently well verified that acoustic measurements may be used to *predict* pressure fluctuation levels with reasonable confidence. It is clearly going to be impossible to prove this or any theory conclusively for all harmonics, as this would require a complete carpeting of the rotor blade with transducers. Thus the principal value of detail pressure measurements seems to be in understanding local aerodynamic effects, for instance at the tips or during vortex intersection.

Melle Merle: Nous étudions en laboratoire la rencontre d'une onde de choc et d'un tourbillon et l'onde sonore qui en résulte. Le conférencier a-t-il étudié ce problème?

Dr Lowson: We have not studied shock/vortex interaction. Although this is a problem of considerable general interest I am somewhat doubtful about its relevance to the helicopter noise problem.

Discussion of Paper 23
"Wake Characteristics of a Two-Dimensional Asymmetric Aerofoil"
 presented by I.Kavrak

Mr McCroskey: Would you characterize the boundary layer and wake as "turbulent"? Is the velocity defect low (Eqn. 1), for laminar or turbulent flow? The spectrograph of fluctuating pressure level shows very discrete frequencies.

I think you have studied an interesting but complex regime in Reynolds number which is neither completely laminar nor fully-developed turbulent. It would be interesting to determine to what extent the results extend to lower and higher Reynolds numbers.

Mr Kavrak: For this particular aerofoil, flow separation takes place very close to the leading edge. Both the boundary layer and the wake contain turbulence of a special character, which is certainly not fully-developed. As is evident from the spectrograph of the fluctuating pressure, it does show periodicity with a large harmonic content. The wavelength of the fundamental is given by Equation 15. The velocity defect law (Eqn. 1) is for such turbulent wakes; in fact, in most any turbulent wake some scale effect exists.

The range of Reynolds numbers covered was between 4×10^4 and 2×10^5 . The spectrograph of Figure 6 is typical of this range, that is, the characteristics of the spectra in that range were nearly identical with each other. A mathematical model of the waveform for the fluctuating pressure has been given in Reference 7, where it was shown that the model was applicable over a range of Reynolds numbers. I agree, however, that it would be interesting to determine the applicability of both the velocity defect law and the waveform model at higher Reynolds numbers.

Discussion of Paper 25
"The Noise Characteristics of a Large 'Clean' Rotor"
 by J.W.Leverton, presented by C.V.Cook

Dr M.V.Lowson replied to discussion in Mr Leverton's absence

Dr Lowson: I guess I am standing here in my role as consultant to Westland Aircraft, although I should make it clear that the preceding paper is entirely the work of John Leverton. Before answering any points I would like to make three comments.

1. It was very interesting to find that Leverton has classified Rotor Noise into the same three categories as myself, that is discrete frequency, low frequency broad band, and high frequency broad band. The general agreement arrived at quite independently in entirely different tests seems to be a powerful argument in favour of this three component model. Many of the general trends of Leverton's results are also rather similar to those obtained at Loughborough. One significant difference is the effect of thrust on the high frequency noise. The tests at Loughborough University showed this source to be strongly affected by tip incidence or in other words, by thrust.

(Written comment by Mr Leverton: "The three-source approach was originally adopted by myself following model tests at ISVR in 1967/68 and confirmed in full scale tests at WHL when I joined them in 1969/70. Even so it should be stated that, except for Dr Lowson's recent work at Loughborough, this approach does not appear to have been used by any other investigators")

2. The Direct application of the empirical loading models developed by John Ollenhead and myself in our earlier papers does not give results in agreement with the discrete frequency levels measured by Leverton. It seems that each family of rotors requires different empirical loading information to establish the discrete frequency levels theoretically.
3. It does appear that blade loadings used by Leverton were rather lower than would normally be used on a helicopter. This can be seen by reference to the C_{LT} values given in his Table 1. At the higher levels of blade loading his results do appear to follow the accepted T^2 law, and it would appear that his data follows the general trends suggested by Widnall as also presented in my own paper at this conference.

Mr Schmitz: Please comment on the possibility of vortex interactions in the experiment. What acoustic differences from a rotor hovering out of ground effect are expected?

Dr Lawson: The Loughborough experiments were carried out on a seven-bladed fan. Immediate vortex intersections seem unlikely, and are not suggested by either the acoustic or aerodynamic measurements. The tests were on a flow with gross recirculation not typical of a hovering rotor. However, the noise generation mechanisms would be expected to be very similar, particularly when considered via an aero-acoustic transfer function approach.

Mr Cook: The vortex paths of this 2 bladed rotor operating in the inverted position were studied in a similar manner to that described in Paper No. 3 (The Structure of the Rotor Blade-Tip Vortex) of these proceedings. Flow visualisation using smoke showed that the tip vortex moved above the plane of the disc until the following blade passed, then it was swept into the wake in a manner similar to that observed on the single bladed case. The blade does not, therefore, intersect a tip vortex.

The details of the steady loading on the blade are however slightly different from those of an isolated rotor in the immediate vicinity of the tip vortex from the preceeding blade. The effect of the ground is to move the vortex above the disc whereas it is possible that, in the absence of any obstruction, the vortex from the preceeding blade would lie in or below the tip path plane. However, this change in position does not have the dramatic effect on the blade loading that might at first be expected. The fact that the vortex is above the blade does not change the sense (or sign) of the downwash, only the radial component of the induced velocity changes in sign. The blade loading in the vicinity of the vortex would not therefore change materially due to the vortex being above the blade, only the relative distance of the vortex from the blade would effect the loading in the immediate vicinity to any extent.

Additional Comments

by

Mr J.W.Leverton

The sound generated by a rotor is a function of the blade loading and obviously changes in the spanwise distribution and the position of the tip vortex will have an affect on the noise. Taking into account the comment given above, however, it is thought that these effects would be small and have more influence on the absolute amplitude rather than on the trends/characteristics discussed in this paper. The results presented have been compared to those obtained from the same two bladed rotor operating on the same whirl tower in the conventional manner and with model rotor results. All these rotors exhibit similar trends but the scatter of results is, in general, larger when the rotors are run the "correct way up". This is considered to be due to the effects of recirculation. Comparison of the two sets of full scale rotor results shows that, although the level of the "broadband noise" is lower on the "clean rotor", the level of the first 15/20 rotational noise harmonics appear to be about the same order. Except for these differences the two rotors show the same type of dependancy with changing thrust, tip speed etc. It is reasonable to assume, therefore, in the context of this paper that the influence of the "ceiling effect" is small.

With regards the point on a "hovering out of ground effect rotor", intuitively the levels would be expected to be nominally lower, but again based on the evidence the parameters appropriate to the various noise sources would be expected to be the same.

APPENDIX B

**TRANSCRIPT OF THE TAPE OF THE ROUND TABLE DISCUSSION
HELD AFTER THE PRESENTATION OF PAPERS**

Mr P.F.YAGGY (Chairman)	Director US Army Aeronautical Laboratory Moffett Field California 94035
Professor N. HAM	Associate Professor Massachusetts Institute of Technology Cambridge, Massachusetts 02139
Mr G. REICHERT	Messerschmitt Bolkow Blohm GmbH Helicopter Division 8 Munchen 80
Dr J.P. JONES	Research Director Westland Helicopter Ltd Yeovil Somerset, England
Professor J. VALENSI	Directeur de l'Institut de Mécanique des Fluides Université d'Aix-Marseille 1 rue Honnorat 13003 Marseille

TRANSCRIPT OF THE TAPE OF THE ROUND TABLE DISCUSSION HELD AFTER THE PRESENTATION OF PAPERS

Mr Yaggy: We began the Meeting by talking about rotor wakes, and then we had a session which looked at the rotor in hover and high advance ratio, unsteady air loads, and then the rotor airfoil design. All of these were purposefully integrated to show the complex picture, in the fluid dynamics sense, that occurs in the rotorcraft. One of the problems which arises of course is that of coupling all of these various investigations in various areas into a meaningful analysis which will improve both the design characteristics in terms of productivity and efficiency, and the various factors which were covered in the session on rotor configurations, and also to solve many of the problems that arise in the rotorcraft from the dynamic experience.

It is quite obvious when one investigates the characteristics of the rotorcraft, and projects its use in the future, that if it is to accomplish a greater capability than it has to date, it will be necessary that it provide several factors. For the civil situation it must obviously be more efficient, it must be able to operate out to reasonable ranges of say 100 to 200 miles or perhaps 250 - 300 kilometers. It must be necessary that it operate to a reasonable time factor, that it provide good ride quality, and that it be able to do all this in a cost-effective manner, which means, of course, that it must be a durable machine with considerable reliability and reduced maintenance cost. In the military application these factors pertain, as do others, particularly the reduction in detection, the subject we have just discussed on noise, and again the ability to live in a hostile environment.

These improvements will not be achieved unless we are able to put together all the various factors in the fundamental areas of discipline which we have been discussing.

One does not have to look very far to realize that rotorcraft have developed somewhat empirically. In most situations a trial and error method, rather than a scientific approach in an orderly fashion was used. Also, one would not have to look very far to realize that the barrel from which we have extracted this empiricism is empty, there is no more. So, if we are to realize the purposes of this discussion, in which we have reviewed the potential and future of rotorcraft, we must allot priorities to the various factors which have arisen, so that we can apply our resources to those of high priority with prospect of good payoff, and then move on in an orderly fashion to the next series of events. It would occur to us, if we look at the findings that we have to date, that in many instances we cannot quantify them adequately, even to know what their potential is. In many instances where we have applied classical methods and have arrived at what we consider to be ideal values, there are things which are arising at this time which would make us question whether they really are the ideal value. Consequently, it would be our hope that from this group of specialists and these presentations which we have had, there would be some direction for future research effort, and there would be some thought as to what our priorities might be. So, perhaps in this roundtable discussion, some opinions and expressions regarding this can be had. We may leave then, with some indication as to what we collectively feel is the proper approach to the future research effort.

Professor Ham: Since my overall impression of the meeting will be expressed more formally in the evaluation, I would like to restrict my comments to something quite specific, namely, the question of blade-vortex interaction. As we have seen in these three days, this is a most important subject, not only in calculating those unsteady air loads which determine the fatigue life of the structure, the vibration level of the aircraft, but also having a profound influence on the noise generated by rotary wing devices. Since, if you show a Professor a blackboard, he must use it, I will move over here. What I am proposing to do is to discuss some research that has been going on at MIT, very briefly.

This research started about 3 years ago, initially sponsored by Langley Research Center of NASA and more currently, by the Army Research Office in Durham. To go through this rather quickly, what we have is a model with a single rotating blade (there is a counter-weight, but I will not draw that), then we generate upstream in the wind tunnel a vortex from a wing, mounted vertically in the tunnel. We let this blade see the vortex by sweeping around over it. Then we have eight pressure transducers at the $3/4$ radius station measuring differential pressure. At the same time, we have looked theoretically at the distribution of airloading on the blade considered as a lifting surface. Drawing the other view, there is the blade in edge view and there is the vortex, down below. Just to idealize the loading generated in this situation, it looks something like that. The first thing I would like to mention that comes about in such a situation is that, in the near vicinity of the blade vortex pair, the center of pressure can shift substantially from the $1/4$ chord point. Now that we are worrying so much about highly

loaded rotors in hover with the vortices moving in in the tip region and staying close to the rotor blades for a good period of time, it is possible that there are some twisting effects generated, especially in the vicinity of the tip. The next thing of interest is that if you look at this vortex-induced loading, there will be counter vortices generated as a result of the loading induced by the vortex on the blade. These would appear in the simple picture as counter vortices opposing the rotation of the primary vortex. In our rather long-term investigation of calculation of the unsteady airloads on rotors, we have found that after a vortex has seen a blade it seems to get weak and tired, so that if another blade sees this same vortex, the vortex strength has apparently weakened. Possibly the reason for that is a rolling up of these three vortices in this idealized picture to form one weaker vortex. The final thing I wanted to mention on this subject was what appears to be a dynamic stall induced during close blade vortex interaction. If you take the peak differential pressure Δp non-dimensionalized by dynamic pressure at the station where the pressure transducers signal and take the peak value, call it the peak positive and this the peak negative, plot that experimentally against vortex spacing in numbers of chord length. This is the distance h . Then that experimental pressure expressed in this manner will look like that, and when compared with our full lifting surface theory, when the vortex gets closer than about $1/2$ chord to the blade, we no longer correlate with the theory. The other aspect is that this is of the order of about 0.5 which is not a high non-dimensional pressure at all. It corresponds to an angle of attack like 1 or 2° , so you would not expect separation problems. In the last month we succeeded in visualizing separations during this process by mounting a camera which looked at the blade as it rotated, putting smoke out of a T-shaped probe in this vicinity. We have seen evidence visually of both leading edge and trailing edge separation of the flow over the blade surface. There is a lot more to this airloads problem than we have yet put into our theoretical work.

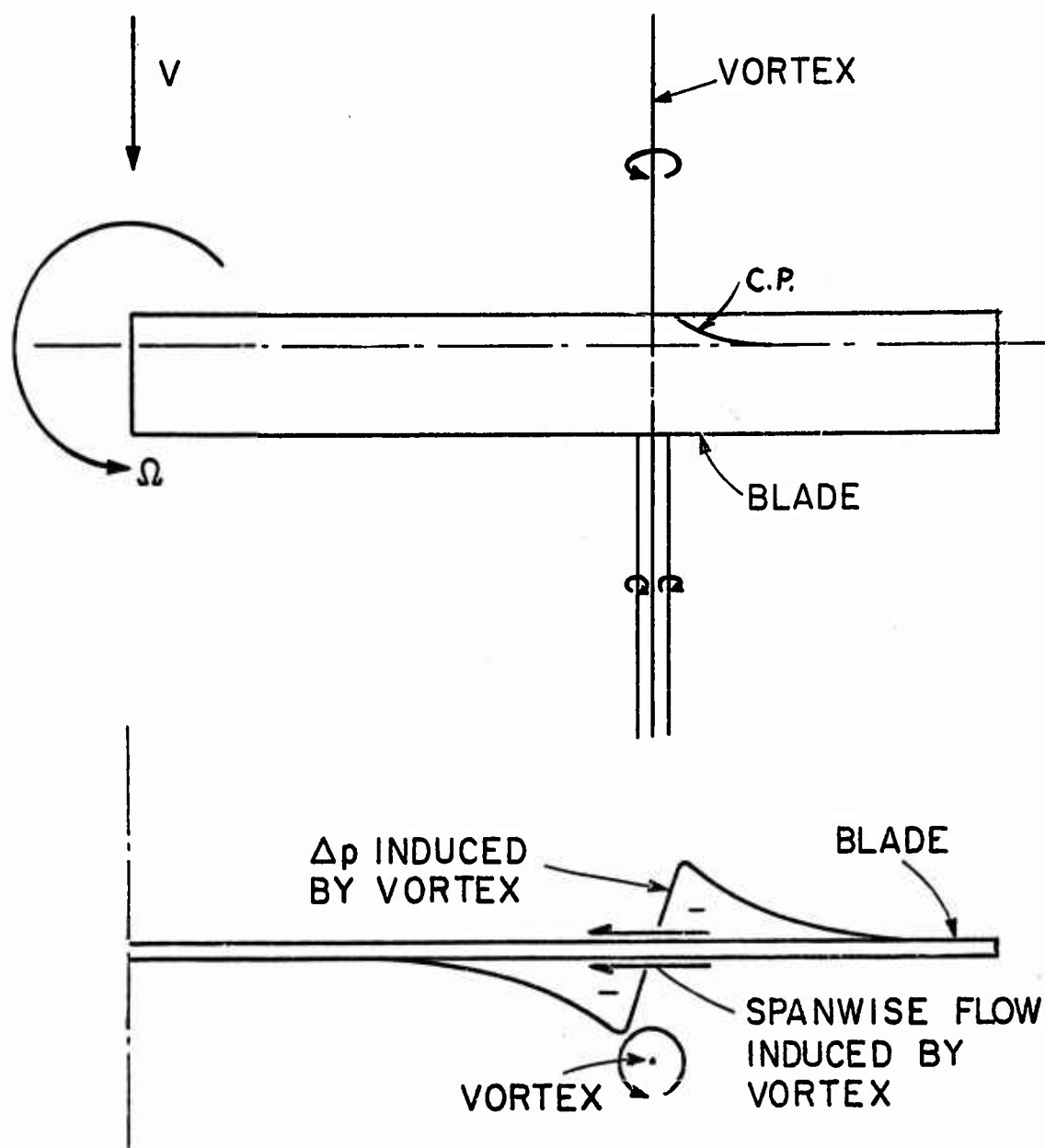


Fig.1 Blade-vortex interaction

Mr Reichert: I would like to make a more general comment. In my opinion, the large improvement in helicopter techniques up to now has depended less on progress in aerodynamics, and more on the systematic exploitation of other design possibilities and a better understanding of some dynamic and structural conditions. But, as the real aerodynamic boundaries have been reached, aerodynamics became more important and a directly related effort in research is a consequence. For the helicopter engineer the question arises "can this new research, in the sense of basic research, be helpful for design work within the near future?". It is my feeling that for the next design the engineer will have to live with the tools of today. Therefore, we should divide the problem into short term and long-term programs. For the next designs we can only get some improvement by improved semi-empirical methods. As a long-term program, we should do basic research, but we should keep in mind that new theories will be of technical value only when engineering applications, which are not too sophisticated and complex can be found afterwards. In my opinion, the main areas for research should be rotor unsteady airloads, including stall, and rotor airfoils. The situation as it exists at the moment forces the helicopter engineer to be conservative and progress is in small steps. He will keep as close as possible to the region of his experience, and he will use theoretical tools more or less as means for interpolation and extrapolation. We should do more, if we want further progress in helicopter technique with improvement at high speed, but we also need better understanding for necessary improvements within the limitations of today — in areas, for instance, like noise or aerodynamically induced vibrations, mainly in the transition region.

Dr Jones: I have one comment to make first of all about the conference itself. I have a feeling that helicopter aerodynamics has come of age, even if only because it is now recognized by a fluid motion panel as being a subject worthy of study. To have noise accepted also as an aerodynamic problem, instead of an engineering problem, is a big step forward. There are many things one could say about the conference, but we all want to arrive at some kind of conclusion, and I would like to make a point about the blade-vortex interaction. This has been the subject of study for a long time, and intensively so, to my knowledge, for over 12 years. It is now a standard design tool; by no means precise, but it is a standard design tool. We have taken the greatest advantage in the hover as we discussed earlier this week, and there are reasons for thinking that in forward flight, it is not really very important at all. Indeed, on a vibration problem which we had to deal with just recently at high speed, it was the uniform inflow and not the variations in the inflow which mattered. One can go on thinking of examples of this kind for some time. Therefore, my recommendation really would be that we should pay much less attention to blade-vortex interaction in future. There are many other areas which need investigation, such as airfoils, and there, I think we should consider also the possibility of raised tip speeds. If we are to increase the efficiency of rotors, both structurally and aerodynamically, I think we shall have to raise tip speeds. This will in itself tend to reduce the retreating blade stall problem, but, of course, it will make the advancing blade problem rather more difficult. On the other hand, I think that techniques available to us from general aerodynamics for dealing with the advancing blade are better than the ones available to us for dealing with the non-steady stall on the retreating blade. Especially as all one is doing is working to get a little bit of extra for nothing on the retreating blade. I would recommend, personally, increased study of tip speed effects.

There are many other aerodynamic problems which are of great interest to the helicopter designer. For instance, normally the aircraft flies slightly nose down to get propulsive force, and this means, since the body is a low aspect ratio wing with a negative angle of attack, that separation vortices are leaving the body and producing quite a substantial downward lift and, of course, a very annoying nose-down pitching moment which has to be got rid of at the tail. This also produces a downward lift. These effects are much greater than effects of variations in the efficiency of the rotor. So there are many areas to which we could turn our attention.

Professor Valensi: I will speak rather as an aerodynamicist and will say a few words about the discussion I had already with my friend Mr. Hirsch, with whom I used to work. I will concentrate my comments mainly on aspects concerning the prediction of the aerodynamic characteristics of the rotor. The first sessions concerned rotor wakes. From what we heard, their precise configuration in hovering is nowadays the subject of advanced investigation, particularly thanks to the numerical computers available.

Most of the authors have focussed their attention on the tip vortex, as responsible for the greater part of the induced flow. As a matter of fact the tip vortex is the most spectacular feature of the wake. However, it constitutes only a part of the wake as Professor Young pointed out. It must be stressed that the tip vortex is not a vortex in the mathematical sense, but rather a locus of concentrated vorticity diffusing in time and space. Consequently, it would seem appropriate to introduce viscous effects in the analysis. On the other hand, as has been shown by different authors, the tip vortex is influenced in intensity and configuration by the shape of the blade tip. These observations suggest the possibility of looking for an optimal shape of the tip.

Obviously, the configuration of the wake can be noticeably influenced by the fuselage and other components of the craft. Dr Jones has just pointed out the effect of the incidence of the fuselage. This aspect needs more investigation.

In Session 3 very interesting correlations between theory and experiment were presented concerning the aerofoil in unsteady motion, pitching and drag. Most important from our point of view, are the attempts to extend these investigations, theoretical and experimental, in the stall region when boundary layer behaviour is to be considered. This is a necessary introduction, a first step, to the study of three-dimensional cases which must be tackled afterwards.

My third comment concerns the shape of the section of the blade in compressibility effects. We have been much impressed by the potential of the new method of calculation, as applied to the determination of the three-dimensional flow around wings in the transonic regime. We should now be able to predict rotor characteristics which it is most important to know. It seems consequently necessary to push forward such investigations in order to advance our understanding of the phenomena.

In conclusion, I would like to recall the words of our distinguished President at the meeting last year in Langley Field, "Research in the area of rotor aerodynamics should include the accommodation of data to demonstrate the effects of camber, twist, number of blades, aspect ratio, variable geometry, Mach number on forward flight-rotor performance, and the associated characteristics of the wake geometry." From the papers which have been presented here, it seems that we are now in a position to predict these different effects to a good approximation by calculation, so long as the transonic regime is not considered. It seems to me, from all the papers presented, that a much better understanding of the involved mechanism of the airflow through the rotor and the interference with the fuselage and the ground must be achieved by good basic research.

Mr Yaggy: As Professor Valensi has just noted, this is not the first time that we have considered the conglomeration of problems which face us. I do not think it will be the last. As we have ascertained thus far from the comments from the table, there is some disparity of opinion as yet on which way we ought to go. I would suggest that this is somewhat inherent in those who made the comments, since two of them are basic researchers and two of the others are production people. Therefore, I think we have this problem. Perhaps you have some thought at this time that you would like to share with us from the floor. Would someone like to enter into the roundtable?

Prof. Küchemann: I should like to make one brief remark of a general nature. If you ask me which is the problem that is really sticking out most to an outsider, not a helicopter man, then I would say it is the problem of vibrations. This must affect the aerodynamic design, the structural design, and the systems design to a very high degree. It must affect the first cost of the helicopter and the maintenance costs, and so this is really a serious problem. Most of these vibrations, as far as I can make out, are aerodynamically excited. There is here a real job for the aerodynamicist: to reduce or to eliminate the sources of vibration. I am always saying that if you want to solve problems, you ought to practice the art of the soluble. One should not try to undertake something which cannot be done with the tools we have. If one is thinking of dealing with the vibration sources in a theoretical way, then this seems extremely difficult to me; if we really wanted to treat the three-dimensional rotating blade properly with all these unsteady flows, I would not expect that a complete theoretical solution would be in sight. But, on the other hand, I think some special problems could now well be tackled on the theoretical side. One I would suggest is the question of tip vortices, which kept on coming up, even when considering noise. As shown by some of the very beautiful photographs and films we have seen, these are things which can be described by the classical vortex theory model, where one deals with a continuous sheet that rolls up along the edges. I think that the time has come when one can give up making these very much simplified models of cores and lines and things that "age" or "weaken." One could attempt to use a sheet model and fulfil the boundary conditions properly and use a computer. It is a three-dimensional problem, of course, but I think that that is one of the problems theoretical people could now tackle with some hope of success. If I say that there will be many, many problems where a theoretical solution is not in sight, then the question arises as to how one gets the answers, which we do need, after all, even if we proceed in small steps, as has been suggested. There I am a bit surprised that this question has not been brought up more forcefully at the meeting. I would have expected that the helicopter people, the designers in particular, would have got up one by one and would have said that now, especially since the empirical barrel is empty, we want more tests in windtunnels, such as those we heard about in the Ames 40ft by 80ft tunnel and in the S1 tunnel at Modane. We want more tests done of that kind, we want more special rigs. I would have expected that they would have cried out for some new large tunnel where one can test much larger models which are representative of full-scale construction, and where Mach-number effects and Reynolds-number effects can really be investigated in some detail. As an outsider, I am rather surprised that this question has never been raised; i.e., what kind of tools do we need if we want to solve the problems which are facing us?

Mr Yaggy: I have one comment before we move on, and that is that I think that it is surprising that that did not happen. I can only feel that perhaps we do not have as large a representation of designers as we have of fundamental aerodynamicists in our midst, and that is probably the reason. Many of you, perhaps, are aware that Prof. Küchemann chairs the group on large-scale wind tunnel studies for the AGARD at the present time, and there is, from other quarters, a very large pressure for larger tunnels to test and get more validating information for the methodology which is being developed. I would not want you to leave Prof. Küchemann thinking that there still is not such a

demand, because there is. Perhaps a point that is not coming out very strongly is that the methodology which is being developed and which we have seen to a large extent, must ultimately be verified. I think this was the heart of Dr Johnson's comments on Mr Ward's paper, that if we are not able to understand and comprehend the models that we place on the computer, we cannot expect to get very far. The physical scientific aspects of those models must be understood. Otherwise, the operations which we go through may be producing some form of an answer, but we have no confidence in the validity of that answer. This can only be done in what really ought to be termed full-cyclic research, where first the methodology is developed, or vice-versa; the methodology is developed as a result of experiment or verified therein. This is the only way that one can approach with confidence the aspects which we hope to develop regarding a low-risk design factor. I think sometimes we tend to forget that the purpose of developing the fundamental aerodynamics and dynamics is the ultimate development of design techniques which can be applied with confidence to increase the capability of the vehicle under consideration. One of the reasons we introduced the section on configurations was that, as we often say, the aerodynamicist and dynamicists must live in the real world. I think sometimes we tend to forget that and the comment which Dr Küchemann has made in this regard is well taken. Vibration is perhaps one of the greatest deterrents to the greater use of rotorcraft. This can only be solved adequately in the fundamental sense by removing the exciting factor, and not by taking it out with dampers and all kinds of things of that sort as we have in the past.

Monsieur Souslez-Lariviere: Je vais essayer de répondre à M Yaggy, Mr. Jones et Mr Lashka dont j'ai noté l'intervention. De toute façon, je réponds également au Dr Küchemann puisqu'ici, je représente une industrie qui, fabriquant des hélicoptères et vivant de leur vente, a peut-être un point de vue beaucoup plus pratique que d'autres personnes qui s'occupent davantage de faire progresser la science des rotors. J'ai noté d'abord, dans ce que M Yaggy a dit, que l'empirisme était terminé en matière d'hélicoptères. Je suis partiellement d'accord avec cela. J'ai exposé tout cet historique des hélicoptères et des voilures tournantes et j'ai montré combien l'empirisme a été important.

Les hélicoptères actuels ont été essentiellement fabriqués par des mécaniciens et par des gens qui faisaient voler l'hélicoptère un peu en dépit de toutes les lois aérodynamiques. Je ne crois pas que cette sorte d'empirisme soit terminée, et je crois qu'il prévaudra encore beaucoup durant de nombreuses années. Par contre, il est certain que nous devons de plus en plus nous pencher sur les phénomènes aérodynamiques qui sont liés, et que l'aérodynamique aura dans l'avenir une part beaucoup plus importante que par le passé dans le progrès des machines. Le second point, d'ailleurs, c'est celui que M.Lashka a évoqué. Il n'est pas raisonnable, je pense, d'étudier au point de vue théorique des dispositions qui ne sont pas réalisables. On ne peut pas réaliser et faire voler n'importe quoi pour les raisons que vous connaissez: les hélicoptères sont des machines compliquées, difficiles à rendre fiables. Par conséquent, tous ces points de vue du réalisateur doivent rester très présents à l'esprit de tous et le choix du sujet à étudier au point de vue aérodynamique doit quand même tenir compte très étroitement de ce qui est réalisable et de ce qui ne l'est pas.

Enfin, pour répondre au Dr Jones, le troisième point est un point de détail, mais je ne peux pas être d'accord avec son idée qui consiste à chercher à progresser en augmentant les vitesses périphériques. Je pense au contraire que la tendance au cours des années futures, sera de diminuer ces vitesses périphériques. D'abord, si on augmente la vitesse, on augmente le Mach; or on est tout à fait limité entre le Mach de pale avançante à 0.85 actuellement et Mach 0.95 par exemple; on ne peut vraiment presque rien gagner, et augmenter la vitesse périphérique obligerait à diminuer la vitesse de l'hélicoptère. En outre, la vitesse périphérique joue sur la traînée du profil, sur le bruit, toutes sortes de choses qui sont contraires. Donc, la tendance de ce côté là me semble être beaucoup plus vers une diminution des vitesses périphériques et vers une plus grande concentration d'efforts sur la pale reculante et tous les phénomènes d'hypersustentation que l'on pourrait trouver. Il y a eu beaucoup d'exemples cités sur les possibilités d'hypersustentation de la pale reculante. Nous sommes actuellement à un C_z de l'ordre de deux avec les phénomènes instationnaires, mais très en-dessous de ce qui va élever les performances de l'avion. Par conséquent, là, je crois que c'est dans l'autre sens qu'il faudrait agir.

Mr Yaggy: Yes, I agree that perhaps that comment that the empirical barrel is dry should be viewed as a comparative one; I think it may be a little more bare than we think. I did not mean to confuse engineering development in that sense with empiricism. I think engineering development in that sense will be with us always, as a proper tool of the designer. I was thinking more of what we call a cut-and-paste or cut-and-try methodology, rather than something based on a fundamental knowledge of the scientific phenomena involved. Perhaps some of the other members of the panel would like to respond to the comments which were made.

Dr Jones: Apart from the tip speed, I am sure we can get along comfortably.

Mr Reichert: Can I made one short comment about why we do not want very large wind tunnels. If there were enough money, I would say that we would like these large tunnels, but full-scale rotors need nearly complete development and so cannot be a model for development. I think that from fight testing we have a lot of

experience with large, full-scale rotors. The problem of translating these experiences to new development is the same. You need similarity rules and so on. This is the problem with smaller models also.

Mr Yaggy: Yes, I think if we go back to that area again, part of the studies that we have made in the wind tunnel requirements indicate that for all types of aircraft, fixed wing as well as rotary wing, the ability to test vehicles or their model representations at large-scale has saved not only a considerable amount of investment in flight hardware, but also human life. This is a result of identifying areas of difficulty such as instabilities which are of primary concern to the rotor designer, and thus making possible many programs which probably otherwise would not have been pursued because of the risk of catastrophic occurrences. Your point is well taken as to the cost, but I think that one has to evaluate the cost honestly in terms of those aspects which are actually cost savings or cost avoidance. That is not an easy thing to convince people of, and I am sure that Prof. Küchemann is well aware of that at this time.

Mr Wilby RAE Farnborough: Personally, I think that a large wind tunnel is probably essential even from the research aspect, if one is really going to get to the bottom of the vibrational problems on a rotor. I think one of the major causes of vibration must be the retreating blade stall problem, the dynamic stall. This has been studied two-dimensionally in wind tunnels at constant Mach number. But, is this really going to tell us the truth about what is happening on the real rotor? Well, of course, the Mach number that the blade experiences is varied throughout one revolution, and we have seen that the Mach number can change quite a lot between the angle of azimuth at which separation onset occurs and the azimuth at which reattachment occurs. There can be a considerable change in Mach number and this involves a considerable change in the angle of attack for which one can maintain attached flow. I think one must simulate the correct variation of Mach number, as well as the correct variation of incidence in order to really understand this problem of the retreating blade. If one throws in the Reynolds number as well, then this is calling for quite a large rotor and quite a large wind tunnel.

Monsieur Hirsch, Aerospatiale: On parle toujours beaucoup évidemment de pales reculantes, mais peut-être faut-il aussi parler de convertibles. Pour eux en particulier, le problème de la pale reculante et peut-être aussi le problème de la vitesse périphérique se posent de manière moins aigue. Si on arrive à ce moment là, à une bonne compatibilité entre les conditions d'"hovering" d'une part et les conditions de croisière, il nous semble actuellement qu'il deviendra possible à assez brefs délais de concevoir des convertibles, ayant en même temps que les vertus de decollage vertical, celles des STOL, actuellement en projet, c'est-à-dire, capable de voler aux alentours de 750 kilomètres à l'heure.

Dr Stepniewski: Gentlemen, it appears to me that here we are suffering from the general disease of our time: lots of analysis and not enough synthesis. It appears to me that we tend to know more and more about less and less. As I have been listening to all the presentations of aerodynamic problems, I expected that somebody would finally come out and say that if you apply all the knowledge that has been presented here, then such and such progress in the overall performance may be expected in the future.

Let's look at the helicopter. The classical helicopter in forward motion is probably one of the least efficient vehicles that ever existed. Nevertheless, because of its completely unique hovering and vertical flight capabilities, it is generally accepted, but its forward flight deficiencies still remain the Achilles heel of that configuration. It is logical, hence, to ask the following questions: With all the beautiful aerodynamic knowledge now acquired, what kind of progress can we make in L/D of the aircraft as a whole? Is it a hopeless problem, or can we move somewhere? If we cannot make any progress in L/D, it means that the sphere of application of the helicopter will probably remain more or less the same as it is at present and of course, what we should do in that case is to concentrate our R&D efforts on other than aerodynamic problems: vibration, maintenance and so on. If, on the hand, it is possible to make progress in L/D of the helicopter then, of course, immediately the whole field of its applications could be expanded and more effort in aerodynamics would be required. Is there such a possibility? This is my first question. If not then perhaps just as Mr Hirsch mentioned before, we should look into some other configurations that have almost equally good, or at least acceptable, hovering capabilities, but with much better forward flight characteristics than the classical helicopter. This is a very basic question that should be answered. I am really addressing it to the panel members who are connected with aerodynamics and I ask, "How much progress is expected in the future in the L/D of the rotor and of the helicopter as a whole?"

Dr Jones: I think you are in as good a position as anyone to answer that. Where can the gains come? Where can the gains in L/D come? I do not think there is much to come from the rotor itself, except possibly in the reduction of the drag of the hub and so on. Therefore, I would suspect if there is any change in overall L/D it will come from the fuselage, or perhaps from some different rotor configuration. There is not a great deal to come, I think that we know that. Then the question is, what is the advantage of going very much faster in helicopters?

Mr Yaggy: Faster than what?

Dr Jones: Faster than we go now, which is 150 - 200 knots.

Mr Yaggy: Perhaps not faster, but farther on a gallon of fuel.

There is a great deal to be gained from an increase in efficiency of this sort. That is really what I was alluding to earlier. You talk about not being able to improve the L/D of the rotor as a whole, but I saw immediately that you stepped on Mr Williams' foot when you said that, because he thinks, and perhaps has demonstrated at least partially, that there is a potential of perhaps considerable increase in the L/D of a rotor. This is the thing that we should be careful of, because there are perhaps areas that we have not even quantified as yet which may give us significant advance or potential for advance. We must not close our eyes to that. What we come to is a kind of decision on the proportion of effort we should give to the intensification of research in the fundamental sense and how much we should give to the evolution of design parameters which will allow a better design at this point of time. That is perhaps something that we will not answer today, but I think we should keep it continually before us. Did we answer the question? I do not think we did, obviously. Dr Stefnewski did not think we could when he asked it.

Dr Stepniewski: That is one question that I try to answer in my mind quite often. Probably because it sits there all the time, I am asking it aloud: What kind of progress can really be made in classical helicopter, or whether the classical helicopters are already almost at the end of their natural evolution. If this is so, then of course, we are on the curve of diminishing returns, and thus, we may spend a lot of money and effort in order to make very little real progress. Perhaps now is the time to redirect our efforts. On the other hand, when we try to look at all other attempts at VTOL that have been made in the past, it looks as though the helicopter always has so many advantages that even compounding (which at one time, looked like a good way to improve the performance of the helicopter) becomes less attractive because it introduces immediately many more problems and many more penalties.

Another question that often comes to my mind is how we can expand the field of application of helicopters. When you start to think of the civilian application which, in principle, appears to contain wide possibilities, then the question is whether we need an improvement in L/D in order to go into the commercial and especially the transportation field, or whether by lowering the cost in general, and improving both flying and riding qualities, you can make helicopters more attractive to the potential operators, as well as the traveling public. But regardless of the outcome of the other questions, you would face a hard constraint of noise, which may be in conflict with such desires as improving the gross weight-to-payload ratio, etc. For instance, Dr Jones mentioned before that increasing the tip speed would be very attractive to every designer because it would immediately start to decrease the structural weight, but what about the probable increase in the noise level? Even the advanced helicopters are considered too noisy for acceptance by residential communities.

Admittedly, here are all of these conflicting aspects, and the question now is in which direction to go with research. Probably, that is exactly what Mr Yaggy would like to know: what would be a proper balance of the effort level in applied research for classical helicopters, study of new configurations, and of course, basic research? Unfortunately, we are probably still not in a position to answer these questions. My personal opinion is that as far as L/D of the helicopters are concerned, we cannot expect too much progress in configurations based on classical rotors. In order to overcome that barrier, new rotor concepts are required. In this respect, I would again like to ask Bob Williams to say something about it.

Mr Yaggy: While Mr Williams is deciding to volunteer, of course, some of the configurations that you have seen have been directed in that way. The tilt rotor obviously is a mechanism for accomplishing this. Before I give Bob a chance to speak, though, I would like to point out a couple of things. You recall the calculations which were made by Frank Harris. They indicate that as far as the blade is concerned, there is a tremendous potential for increase in L/D except for the fact that such things as the requirement for varying twist distribution with forward flight and things of this sort prevent our really achieving it. That is what Bob Williams is looking at, to try to overcome some of these factors. I think that the other factor that should be kept in mind is the one you mentioned, the empty weight fraction and the potential of new materials in the structural aspects of the aircraft, particularly in the rotor itself, possibly giving the ability to design a cleaner hub and perhaps a better hub-pylon juncture. We might do a far better job in that respect. So, there seems to be considerable potential in those areas for an improvement. I do not think we ought to be terribly pessimistic. I think that there is a real opportunity if we can find a mechanism for doing it. Perhaps it calls for innovation rather than for the dog-work of orderly development in that sense. I think that is what makes it hard to decide what we ought to do in the fundamental research area. Perhaps you are right that we are over the break point of the curve. There must be a continual decision as to how much of the rather expensive fundamental research should be done in large computer efforts and things of that sort, considering what the payoff will be. Some means for quantifying that is required, but it is also extremely elusive.

Mr Williams - US Navy: I see the orientation of the meeting starting from a group of aerodynamicists, which we are primarily, and now being evolved more along the direction of design, where we are talking about integrating the aerodynamics of the rotor and the fuselage. We are also bringing out weight. After all, in terms of performance and productivity, this is the name of the game. It is the overall L/D, and it is that empty weight fraction. I think perhaps we are putting our finger on a general area of integration of design. Perhaps we have extracted from the "classical" rotor blade the last few percent out of its performance. Figures of merit are getting pretty high on rotors. L/Ds are pretty good now. However, look at the fuselage. Even after the "cleaning up" of helicopter fuselages which has come about in recent years, they are still filthy. Aerodynamically, they are filthy. Why? Largely because of the interference flows around the hub pylon region, which are aggravated by the fact that we have flapping rotors and we have to put these things so far up in the air. We have to build a mound to set them on. So, maybe we need to rethink this and consider going to stiffer systems. I am not just pushing for the CCR concept, but in general, rotor systems need to be married to the fuselage, to give something we can consider as an overall system. Then addressing the areas of difficulty in the junction, a very difficult separation problem exists there. We do not at present have the analytical tools available to us to calculate the difficult flow in this region. We just close our eyes and say, well, there are going to be a few things sticking out in the air stream, but it is too difficult to analyze. Maybe we need to study that area more. Those were my basic comments. I believe, of course, the circulation control rotor is the eventual solution. It would use an untwisted blade. It does have a possibility of introducing air into the forming tip vortex and eliminating the vortex. This has now been demonstrated by experiment. It has a number of other very exciting possibilities, and I think that it should certainly be pursued.

I had one other comment, in the area of communications. This is my first meeting of this type and in talking with people from different countries, I found that, for example, the proceedings of the last American Helicopter Society Meeting had not yet found their way to many of the participants of this meeting. Furthermore, in talking with individuals from various countries, there seem to be difficulties in relations between government and industry and feeding information back and forth, particularly from one industry to another. This is a natural problem which is to be expected, but a lot of this work is government funded, and I think the results of R and D work should be available for exchange between individual companies; this should certainly be so in the United States.

Mr Yaggy: You would have to talk to the State Department about that. The reason we sponsor this sort of conference with AGARD is for the purposes that you have mentioned, to get this international dissemination of information.

Mr Williams: As a final word, I would like to say that I was very impressed by the overall level of technical sophistication. I think that rotary wing aerodynamics have really reached a stage of maturity at this meeting.

Mr Yaggy: I think that it was interesting and it should be noted that some of the work presented was of a type that is often overlooked. That is, a fundamental investigation of the effects of various configurations, configuration buildup and configuration component testing of this sort. It is a type of effort that we have tried to get under way for some time, so far without success, but there needs to be a systematic investigation of variation in components such as pylon shapes, pylon size, pylon height, the location of the various other ancillary equipment on the aircraft, and the effect of the rotor wake on these various parts of the vehicle. This is something that has not been done and can be very systematically accomplished. It was done many years ago for a fixed wing aircraft. We can think back to the many different types of configurations which were evident in the early days of fixed wing and find that they finally settled on a monocoque, generally low wing, configuration as being the most efficient. Very seldom does one build anything other than that. Yet, you can find any number of configurations in rotorcraft, and one does not really know whether there is even an optimum configuration. One would suspect that there might be. Therefore, we would seem to be quite far behind in that respect.

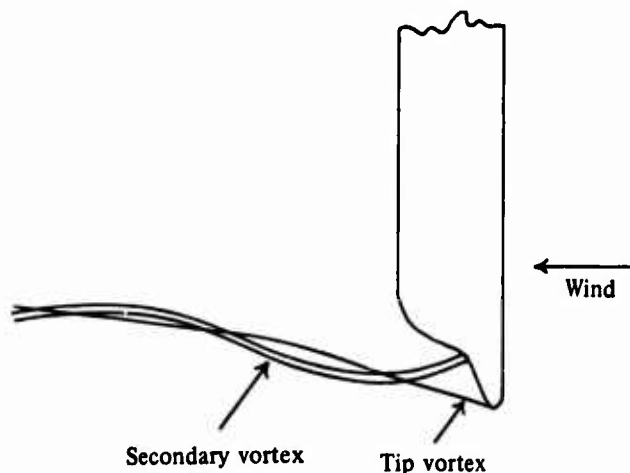
Dr Jones: I would like to say something about body drag, that is fuselage drag in particular - interference and so on. This gives one sure way of cutting down the aircraft vibration, because the drag of the fuselage has to be overcome by putting more thrust into the rotor. This has quite a serious effect on the vibration. Particularly as vibration is something which has a threshold. It is not noticeable below a certain level, and then it suddenly becomes very noticeable. Nobody has mentioned tail rotors. They are a bane to all designers. We know very little about tail rotors. We know very little of the environment in which they work and the loads which come on them. I do not think we have anything like the same kind of design rules or design patterns of thinking for tail rotors that we have for main rotors.

Mr Yaggy: One might say concerning tail rotors, if they are as you say, the bane of everyone's existence, you can not say that no one has thought of them. It is certainly an example of at least trying to make a more acceptable installation. Of course, Sikorsky, with their advancing blade concept would hope to rid themselves of a tail rotor entirely. The tandem designers might take you to task, saying that they have put the tail rotor to much better use. So there are several configurations in that respect. However, it certainly needs to have considerable thought given

to it. There was one other comment that I forgot to make earlier. I would like to make it now. It was regarding the necessity for wind tunnel testing and I think it was Mr Wilby who made the comment about the ability to integrate these results and to find them meaningful in terms of the prediction of what actually takes place in flight. I was not sure whether you were speaking at that time in terms of full rotor investigations. I presume you were, that is of a full rotor in the wind tunnel. In that sense, I realize this is a problem. The fundamental difference between operating in the wind tunnel and operating in flight is that you are on a seismic base in the wind tunnel and you do not have the body dynamics, nor do you have the relieving aspects of the body motion in this sense. This has usually been found to be of a conservative influence. The results that you get from a wind tunnel in terms of air loads and vibratory inputs, and so forth, generally are conservative when you take the vehicle to flight. As was mentioned by Mr Ward, in the United States we are going to build, at least so I hope, a rotor research aircraft which we will be able to mount also in the wind tunnel and get some verification of these various factors. This again points out the importance of having a wind tunnel of such a size that one can make that type of comparison. Perhaps you might want to comment further to this.

Mr Wilby, RAE: Can I come back to the point I was trying to make earlier? Perhaps I did not make myself quite clear. What I was trying to get at was that one can study certain aspects of unsteady aerodynamics, dynamic stall, using a two-dimensional model in a wind tunnel and having a constant free stream. One can also study various effects of Mach number in steady flow conditions using a fairly simple wind tunnel model. What is really happening on a rotor is the combination of these two effects and this can only be really fully simulated on a large rotor model; it is not until we get a large rotor model that we really will know how these two effects combine and control the vibrations that actually happen on a helicopter.

Professor Valensi: If I have understood correctly, there is some thought that it would be possible by changing the shape of the tip of the blades, to suppress the vortex. I do not think that this is possible because the circulation round the blade sections at the tip has to go somewhere. What you can do is to influence the shape of the vortex immediately behind the rotor. I will go to the blackboard: I have myself, a long time ago, in 1938 or so, investigated the influence of the shape of the tip, not of a blade, but of a wing, on the configuration of the tip vortex. We had something like that.



Then, if you look at the configuration of the vortex, you see first, quite well defined, a tip vortex shedding from the very tip of the wing. This vortex takes away the circulation from the last sections of the tip. There is another more diffused vortex shedding from the inflexion point of the wing (plan view), which is twisted round the first one. I was surprised to see in some of the pictures concerning a rotor blade tip of a similar shape, that there was no appearance of any vortex. It is because the Schlieren method used to visualize the vortex is probably not sensitive enough. It must be pointed out also that Schlieren pictures give only a projection of the phenomenon and not the phenomenon itself, as smoke visualisation shows. With such a blade tip the vortex cannot be suppressed and in any case there is no way of suppressing the vortex by changing the shape of the tip. What you can change is the configuration of the vortex, near the blade.

Mr Ward - NASA Langley: Basically, I would agree that the total circulation is still there in the tip region. The tip shape that we are both discussing does in fact have separation at the very tip end. What seems to have been done here is to spread the core of the vortex out to a much larger and more diffuse core. Still, the total circulation in the tip region is probably unchanged. This is difficult to determine accurately from surveys of the diffuse core. The major effect is a substantial reduction of the maximum tangential velocities.

Mr Yaggy: I would like to pose a question to the two panel members from the production area. If you were to have a choice between an increase in L/D in the general sense, that is to be able to take a vehicle to higher speeds, or if you were to have the choice of a reduced vibratory load input, which would you rather have?

Mr Reichert: It all depends. You should find the best compromise for given operational requirements.

Mr Yaggy: You merely enforce the argument that helicopters evolve empirically. That is exactly what happens, but it is a trade-off, I understand.

Dr Jones: It means that we have a different set of rules for a different design. I think that for a civil aircraft where an interspeed gain is only 10 knots and the vibration reduction was 0.1g, clearly you would take the vibration.

Mr Yaggy: Yes, but let us face up to the other fact that if you were able to reduce the vibratory loads, you could probably reduce the weight of the vehicle and its complexity and in so doing you could probably get the additional speed.

Dr Jones: Perhaps, I am not sure how much weight we carry around.

Professor Young: This last remark brings us back to what Dr Küchemann said earlier, that vibration is clearly one of the most important problems of the helicopter. I would like to ask the experts whether there are understood factors in helicopter design which make for high vibration and conversely factors which make for low vibration. My own guess, as an aerodynamicist is, that you ought to seek out those points and areas where flow separation is likely. I suspect the fuselage, as Dr Jones remarked, where much flow separation occurs. Helicopter fuselages seem to have rather crude shapes, possibly for very good reasons, unfaired lumps being used to support the rotors, and it is possible that such flow separations can quite easily be reduced or even removed. Coming back to the rotor blade, I would suggest that an investigation of the shape of the pinform in the region of tip, as has been remarked earlier, might well produce considerable reductions in both the buildup in the boundary layer in that region and in the type of pressure gradient that blades are being subjected to by the incipient vortices that have started from other blades. Thus, it seems likely that quite small changes in design may result in considerable improvements. It seems to me that the question that you put, Mr Chairman, might be a false one, in the sense that suppression of separation in suitable places can lead to both an increase in L/D and reduction of vibration levels. The helicopter has unavoidable sources of vibration; it has rotating lifting surfaces whose lifting history is changing cyclically, and as such, they must obviously produce vibration effects. I suspect however that there are also avoidable sources of vibration, and here I would say, instead of *cherchez la femme*, *cherchez the separation*. I think that we will then find room for considerable improvement. Additionally, there are the developments we have been hearing about such as circulation control rotors; these may produce in the long run quite considerable improvements in performance and flexibility.

Mr Yaggy: Yes, the question was intentionally loaded, you are right. But, I think too often that we overlook that very fundamental aspect of what you mentioned. That is, the improvement is bound to be an improvement in both areas. The reason I asked the question is that, generally speaking, in the vehicles we have today, we cannot use their full speed potential simply because of the vibratory input. At least, if it is used, it can only be used for a very short period of time, because human tolerance will not permit its longer utilization. Therefore, it would seem that we might be wiser to be putting our efforts into those things which would make the current vehicle capable of all of its inherent capabilities in operation, rather than to be striving for a higher forward speed or things of that sort. This is the point I was trying controversially perhaps to make, and to elucidate.

Mr Williams: If you consider what the sources of vibration are, we have the once per revolution variation of velocity about the disc which is fundamental. The only way you can get around that is to take the thing so fast that it does not see the difference; that is, very high advance ratio operation, or very, very low advance ratio operation. Anywhere in between you are stuck with that fundamental problem, if the lift depends on the velocity squared. Secondly, you have the inflow variations about the disc due to the development of lift, and these are largely due to the tip vortex. Here we might ask if we can do anything about that. There is sufficient evidence to date to show that you can do something about it. The tip vortex being the primary contributor, but also the inboard vortices, the root vortex is something that we have not really considered. I do not understand how big a problem it is, but I assume it has some influence. The third contributor is the pitching moments. This is made up of a whole series of things, including the airfoil angle-of-incidence. We have pitching blades now. That can be eliminated, possibly. Twist — there may be a very favorable effect by eliminating twist. You do not lose much in L/D and I think some people have looked at this. Camber — we are going into advanced airfoils and adding camber and adding pitching

moment. There is a tendency to add pitching moment. We are trying to pick up L/D, but at the expense of pitching moment, and we have to be very careful in the airfoil design, not to add this pitching moment, particularly at the high Mach numbers when we start having shocks on the airfoil. I think this problem can be approached by looking at all these different sources and asking what research areas can be developed to eliminate some of these sources?

Monsieur Philippe, ONERA: Pour des projets futurs, on a souvent besoin d'un certain nombre de données pour prévoir les performances du rotor par exemple. Un travail d'Harris et Pruyer a montré que l'on doit tenir compte de deux effets: — effet tridimensionnel dû à l'effet de flèche — et effet instationnaire, dont les contributions respectives sont relativement égales. Dans ce congrès, on a parlé assez longuement des effets instationnaires. Je pense qu'ils sont effectivement importants mais qu'en est-il de l'effet de flèche? J'en ai peu entendu parler. Doit-on considérer qu'on dispose actuellement d'informations assez complètes dans ce domaine?

Mr Ward: I would like to go back to the subject of tip speed again for a comment or two. I sense an implied consensus among the group that there is a rotor tip Mach number limit. I would suggest that we should not overlook the possibilities of operating with transonic and supersonic transient Mach number excursions on the advancing blade tip to achieve increased forward speeds. Very little research has been done on this problem. However, current work with advanced supercritical airfoils, tip shapes and rotor noise investigations may lead the way to higher tip Mach numbers. We should be careful not to discard the possibilities here — the payoff could be significant. In this regard I would like to endorse Dr Jones' earlier comments about looking at increased rotor tip speeds.

Mr Yaggy: In summary, it is obvious that there is still some disparity of opinion as to where we should go, and I think that this is a healthy situation, because we must keep an open mind about the direction in which we pursue these matters. I think we would also agree that there is considerable potential. It would be well for us, however, to keep in mind that, while we have specialized in the fields of aerodynamics and to some extent dynamics in this conference, as fundamental areas for improving rotor technology, and therefore rotor capability, these are certainly not the only factors in the design of helicopters. There are very strong advances that will be coming as a result of the introduction of new materials. As the introduction of the turbine engine in the past was a significant step forward in both the consideration of specific fuel consumption and specific weight, it would appear that the most logical step forward in the near future will be in the area of better and lighter materials. But it is a rather damning commentary that advances in helicopters have resulted primarily, in the past, from propulsion improvements, and look likely in the near future to come from structures and materials improvements, while we do not really get a significant gain in the aerodynamic sense. Perhaps that is the challenge with which we should leave this conference. We are striving to find mechanisms which will give much improved aerodynamic characteristics, if they exist, if they do not, we must say so, defining the physical laws which lead to that conclusion, and go on to the other areas Dr Stufniewski has referred to, perfecting the device to its maximum capability and getting on with other matters. With that challenge I think that we can close, I trust that you agree with me that this has been a most productive conference and I am sure that we will return, not only with renewed enthusiasm, but perhaps with a clearer vision of the problems that lie before us.

APPENDIX C

**A SELECTION OF
AGARD PUBLICATIONS IN RECENT YEARS**

**A SELECTION OF
AGARD PUBLICATIONS IN RECENT YEARS**

**CATEGORY I - PUBLISHED BY TECHNIVISION SERVICES AND
PURCHASABLE FROM BOOKSELLERS OR FROM:-**

Technical Press Ltd
112 Westbourne Grove
London W.2
England

Hans Heinrich Petersen
Postfach 265
Borsteler Chausee 85
2000 Hamburg 61
West Germany

Circa Publications Inc.
415 Fifth Avenue
Pelham
New York 10803, USA

Diffusione Edizioni Anglo-Americaine
Via Lima
00198 Rome
Italy

1969

AGARDograph 120 **Supersonic turbo-jet propulsion systems and components**
Edited by J.Chauvin, August 1969.

1970

AGARDograph 115 **Wind effects on launch vehicles**
By E.D.Geissler, February 1970.

AGARDograph 130 **Measurement techniques in heat transfer**
By E.R.G.Eckert and R.J.Goldstein, November 1970.

Conference **New experimental techniques in propulsion and energetics research**
Proceedings 38 Edited by D.Andrews and J.Surugue, October 1970.

**CATEGORY II - NOT ON COMMERCIAL SALE - FOR
AVAILABILITY SEE BACK COVER**

1965

Report 514 **The production of intense shear layers by vortex stretching and convection**
By J.T.Stuart, May 1965. (Report prepared for the AGARD Specialists' Meeting on
"Recent developments in boundary layer research", May 1965.)

AGARDograph 91 **The theory of high speed guns**
By A.E.Seigel, May 1965.

AGARDograph 97 **Recent developments in boundary layer research**
(in four parts) AGARD Specialists' Meeting, Naples, May 1965.

- AGARDograph 102** **Supersonic inlets**
By Ione D.V.Faro, May 1965.
- AGARDograph 103** **Aerodynamics of power plant installation**
AGARD Specialists' Meeting, Tullahoma, October 1965.
- 1966**
- Report 525** **The pitot probe in low-density hypersonic flow**
By S.A.Schaaf, January 1966.
- Report 526** **Laminar incompressible leading and trailing edge flows and the near wake rear stagnation point**
By Sheldon Weinbaum, May 1966.
- Report 539** **Changes in the flow at the base of a bluff body due to a disturbance in its wake**
By R.Hawkins and E.G.Trevett, May 1966.
- Report 542** **Transonic stability of fin and drag stabilized projectiles**
By B.Cheers, May 1966.
- Report 548** **Separated flows**
(Round Table Discussion), Edited by J.J.Ginoux, May 1966.
- Report 550** **A new special solution to the complete problem of the internal ballistics of guns**
By C.K.Thornhill, 1966.
- Report 551** **A review of some recent progress in understanding catastrophic yaw**
By J.D.Nicolaides, 1966.
- AGARDograph 109** **Subsonic wind tunnel wall corrections**
By Gardner, Acum and Maskell, 1966.
- AGARDograph 112** **Molecular beams for rarefied gasdynamic research**
By J.B.French, 1966.
- AGARDograph 113** **Freeflight testing in high speed wind tunnels**
By B.Dayman, Jr, 1966.
- Conference Proceedings 4** **Separated flows**
(two parts and one supplement) Specialists' Meeting, Rhode-Saint-Genèse (VKI), May 1966.
- Conference Proceedings 10** **The fluid dynamic aspects of ballistics**
Specialists' Meeting, Mulhouse, September 1966.
- Conference Proceedings 12** **Recent advances in aerothermochemistry**
(in two parts) 7th AGARD Colloquium sponsored by PEP and FDP, Oslo, May 1966.
- 1967**
- Report 558** **Experimental methods in wind tunnels and water tunnels, with special emphasis on the hot-wire anemometer**
By K.Wieghardt and J.Kux, 1967.
- Advisory Report 13** **Aspects of V/STOL aircraft development**
(This report consists of three papers presented during the joint session of the AGARD FDP and FMP held in Göttingen, September 1967.)
- AGARDograph 98** **Graphical methods in aerothermodynamics**
By O.Lutz and G.Stoffers, November 1967.
- AGARDograph 117** **Behaviour of supercritical nozzles under three-dimensional oscillatory conditions**
By L.Crocco and W.A.Sirignano, 1967.

- AGARDograph 119** **Thermo-molecular pressure effects in tubes and at orifices**
By M.Kinslow and G.D.Arney, Jr, 1967.
- AGARDograph 121** **Techniques for measurement of dynamic stability derivatives in ground test facilities**
By C.J.Schueler, L.K.Ward and A.E.Hodapp, Jr, 1967.
- AGARDograph 124** **Nonequilibrium effects in supersonic-nozzle flows**
By J.Gordon Hall and C.E.Treanor, 1967.
- Conference Proceedings 19** **Fluid physics of hypersonic wakes**
(in two parts) Specialists' Meeting, Fort Collins, Colorado, May 1967.
- Conference Proceedings 22** **Fluid dynamics of rotor and fan supported aircraft at subsonic speeds**
Specialists' Meeting, Göttingen, September 1967.
- Conference Proceedings 22 - S 4** As above - with supplement
- 1968**
- AGARDograph 132** **The electron beam fluorescence technique**
By E.P.Muntz, 1968.
- Conference Proceedings 30** **Hypersonic boundary layers and flow fields**
Specialists' Meeting, London, May 1968.
- Conference Proceedings 30 Suppl.** Supplement to the above.
- Conference Proceedings 35** **Transonic aerodynamics**
Specialists' Meeting, Paris, September 1968.
- Conference Proceedings 35 Suppl.** Supplement to the above.
- 1969**
- Advisory Report 17** **Technical Evaluation Report on AGARD Specialists' Meeting on Transonic aerodynamics**
By D.Küchemann, April 1969.
- AGARDograph 134** **A portfolio of stability characteristics of incompressible boundary layers**
By H.J.Obrenski, M.V.Morkovin and M.Landahl, 1969.
- AGARDograph 135** **Fluidic controls systems for aerospace propulsion**
Edited by R.J.Reilly, September 1969.
- AGARDograph 137** **Tables of inviscid supersonic flow about circular cones at incidence $\gamma = 1,4$**
(in two parts) By D.J.Jones, November 1969.
- Conference Proceedings 42** **Aircraft engine noise and sonic boom**
Joint Meeting of the Fluid Dynamics and Propulsion and Energetics Panels, held in Saint-Louis, France, May 1969.
- Conference Proceedings 48** **The aerodynamics of atmospheric shear flow**
Specialists' Meeting, Munich, September 1969.
- 1970**
- Report 575** **Test cases for numerical methods in transonic flows**
By R.C.Lock, 1970.
- Advisory Report 22** **Aircraft engine noise and sonic boom***
By W.R.Sears. (Technical Evaluation Report on AGARD FDP and PEP Joint Meeting on "Aircraft engine noise and sonic boom".) January 1970.

*See also Advisory Report 26 by J.O.Powers and M.Pianko, June 1970. AR26 has the same title as AR22 but was produced by the Propulsion and Energetics Panel of AGARD and deals primarily with engine noise.

- Advisory Report 24 **The aerodynamics of atmospheric shear flows**
By J.E.Cermak and B.W.Marschner, May 1970. (Technical Evaluation Report on AGARD Specialists' Meeting on "The aerodynamics of atmospheric shear flows".)
- Advisory Report 30 **Blood circulation and respiratory flow**
By J.F.Gross and K.Gersten, December 1970. (Technical Evaluation Report on AGARD Specialists' Meeting on the above subject.)
- AGARDograph 138 **Ballistic range technology**
By T.N.Canning, November 1970.
- AGARDograph 144 **Engineering analysis of non-Newtonian fluids**
By D.C.Bogue and J.L.White, July 1970.
- AGARDograph 145 **Wind tunnel pressure measurement techniques**
By D.S.Bynum, R.L.Ledford and W.E.Smotherman, December 1970.
- AGARDograph 146 **The numerical solution of partial differential equations governing convection**
By H.Lomax, P.Kutler and F.B.Fuller, November 1970.
- AGARDograph 147 **Non-reacting and chemically reacting viscous flows over a hyperboloid at hypersonic condition**
Edited by C.H.Lewis. (M.Van Dyke, J.C.Adams, F.G.Blottner, A.M.O.Smith, R.T.Davis and G.L.Keltner were contributors.) November 1970.
- Conference Proceedings 60 **Numerical methods for viscous flows**
By R.C.Lock, November 1970. (Abstracts of papers presented at a Seminar held by the FDP of AGARD at the NPL, Teddington, UK, 18-21 September 1967.)
- Conference Proceedings 62 **Preliminary design aspects of military aircraft**
March 1970, AGARD Flight Mechanics Panel Meeting held in The Hague, The Netherlands, September 1969.
- Conference Proceedings 65 **Fluid dynamics of blood circulation and respiratory flow**
Specialists' Meeting, Naples, May 1970.
- Conference Proceedings 71 **Aerodynamic interference**
Specialists' Meeting, Silver Spring, Maryland, USA, September 1970.
- 1971**
- Report 588 **Aerodynamic testing at high Reynolds numbers and transonic speeds**
By D.Küchemann, 1971.
- Advisory Report 34 **Aerodynamic interference**
By D.J.Peake, May 1971. (Technical Evaluation Report of the Specialists' Meeting on "Aerodynamic interference", September 1970.)
- Advisory Report 35 **Report of the high Reynolds number wind tunnel study group of the Fluid Dynamics Panel**
April 1971
- Advisory Report 36 **Report of the AGARD Ad Hoc Committee on Engine-airplane interference and wall corrections in transonic wind tunnel tests**
Edited by A.Ferri, F.Jaarsma and R.Monti, August 1971.
- Advisory Report 37 **Facilities and techniques for aerodynamic testing at transonic speeds and high Reynolds number**
By R.C.Pankhurst, October 1971. (Technical Evaluation Report on Specialists' Meeting held in Göttingen, Germany, April 1971.)
- AGARDograph 137 (third volume) **Tables of inviscid supersonic flow about circular cones at incidence, $\gamma = 1.4$**
Part III, by D.J.Jones, December 1971.

- AGARDograph 148 **Heat transfer in rocket engines**
by H.Ziebland and R.C.Parkinson, September 1971.
- Conference
Proceedings 83 **Facilities and techniques for aerodynamic testing at transonic speeds and high Reynolds number**
August 1971. Specialists' Meeting held in Göttingen, Germany, April 1971.
- Conference
Proceedings 91 **Inlets and nozzles for aerospace engines**
December 1971. Meeting held in Sandefjord, Norway, September 1971.
- 1972
- Report 598 **Experiments on management of free-stream turbulence.**
By R.I.Loehrke and N.M.Nagib, September 1972.
- Report 603 **Aerodynamic test simulation: Lessons from the past and future prospects**
Ed. J.Lukasiewicz, December 1972.
- AGARDograph 156 **Planar inviscid transonic airfoil theory**
By H.Yoshihara, February 1972.
- AGARDograph 161 **Ablation**
by H.Hurwicz, K.M.Kratsch and J.E.Rogan, March 1972.
- AGARDograph 163 **Supersonic ejectors**
Ed. J.J.Ginoux, November 1972.
- AGARDograph 164 **Boundary layer effects in turbomachines**
Ed. J.Surugue, December 1972.
- Conference
Proceedings 93 **Turbulent shear flows**
January 1972. Specialists' Meeting held in London, England, September 1971.
- Conference
Proceedings 102 **Fluid dynamics of aircraft stalling**
November 1972, Specialists' Meeting held in Lisbon, Portugal, April 1972.
- Advisory Report 46 **Turbulent shear flows**
By R.Michel, July 1972 (Technical Evaluation Report of the Specialists Meeting on "Turbulent Shear Flows", September 1971).
- Advisory Report 49 **Fluid dynamics of aircraft stalling**
By R.C.Pankhurst (Technical Evaluation Report on Fluid Dynamics Panel Specialist's Meeting), November 1972.
- Advisory Report 50 **Energetics for Aircraft auxiliary power systems**
by R.H.Johnson, C.E.Oberly and R.E.Quigley, Jr (Technical Evaluation Report on 39th Propulsion and Energetics Panel Meeting), November 1972.
- Lecture Series LS42 **Aerodynamic problems of hypersonic vehicles. (Two volumes)**
Ed. R.C.Pankhurst, July 1972.
- Lecture Series LS48 **Numerical methods in Fluid dynamics**
Ed. J.J.Smolderen, May 1972
- Lecture Series LS49 **Laser technology in aerodynamic measurements**
Ed. R.C.Pankhurst, March 1972.
- Lecture Series LS53 **Airframe/engine integration**
May 1972.